# PROCEEDINGS
# OF THE
# OCEAN DRILLING
# PROGRAM

## INITIAL REPORTS

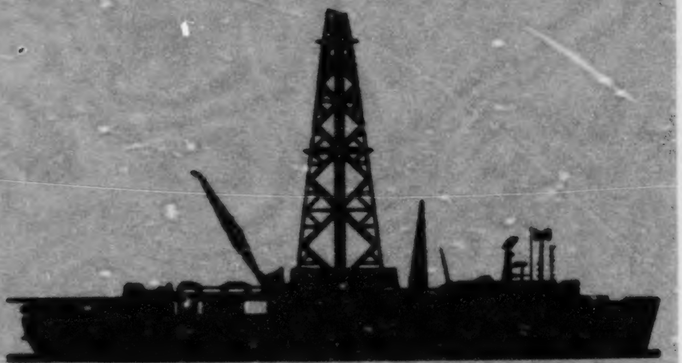

VOLUME 129
20 November 1989—18 January 1990

NATIONAL SCIENCE FOUNDATION

JOINT OCEANOGRAPHIC INSTITUTIONS, INC.

129

DRILLING LOCATION

| LEG | LOCATION | REP | SITES |
|---|---|---|---|
| 100 | Gulf of Mexico | E | 625A-625C |
| 101 | Bahamas | E | 626-636 |
| 102 | Bermuda Rise | E | 418 |
| 103 | Galacia Margin | E | 637-641 |
| 104 | Norwegian Sea | E | 642-644 |
| 105 | Baffin Bay | E | 645-647 |
| 106 | Mid-Atlantic Range | E | 648-649 |
| 107 | Tyrhenian Sea | E | 650-656 |
| 108 | Eastern Tropical Atlantic | E | 657-668 |
| 109 | Mid-Atlantis Range | E | 669-670,395,648 |
| 110 | Northern Barbados Ridge | E | 671-676 |
| 111 | Costa Rica Rift | G | 677-678,504B |
| 112 | Peru Continental Margin | G | 679-688 |
| 113 | Weddel Sea, Antarctica | E | 689-697 |
| 114 | Subantarctica South Atlantic | E | 698-704 |
| 115 | Mascarene Plateau | G | 705-716 |
| 116 | Distal Bengal Fan | G | 717-719 |
| 117 | Oman Margin | G | 720-731 |
| 118 | Southwest Indian Ridge | G | 732-735 |
| 119 | Kerguelen Plateau-Prydz Bay | E | 736-746 |
| 120 | Central Kerguelen Plateau | E | 747-751 |
| 121 | Broken Ridge & Ninetyeast Ridge | G | 752-758 |
| 122 | Exmouth Plateau | G | 759-764 |
| 123 | Argo Abyssal Plain | G | 765-766 |
| 124 | Celebes & Sulu Seas | G | 767-771 |
| 124E | Philippine | G | 772-777 |
| 125 | Bonin / Mariana Region | G | 778-786 |
| 126 | Bonin Arc-Trench System | G | 787-793 |
| 127 | Japan Sea | G | 794-797 |
| 128 | Japan Sea | G | 794,798-799 |
| 129 | Old Pacific Crust | G | 800-802 |

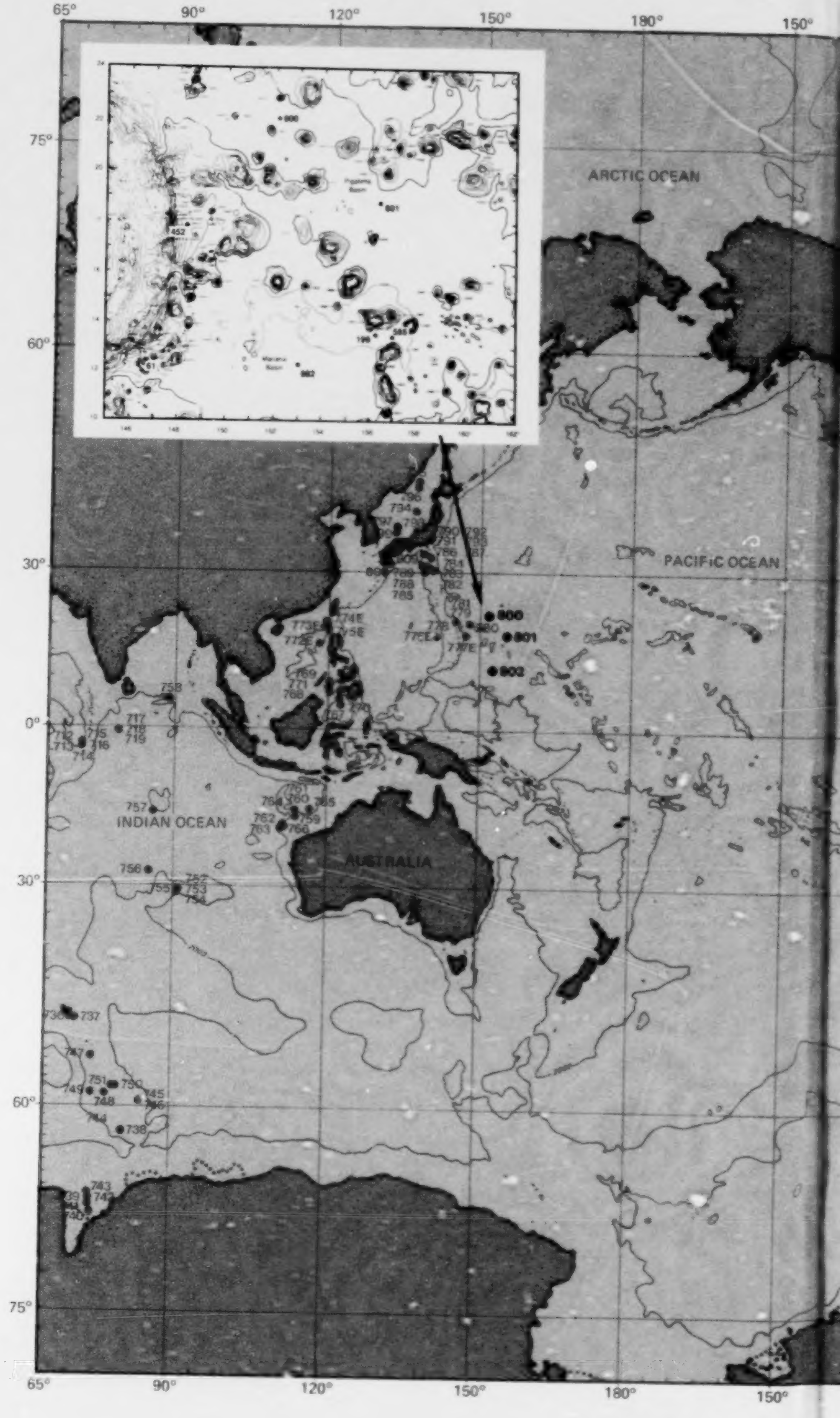

65°
90°
120°
150°
180°
150°
75°
60°
30°
0°
ARCTIC OCEAN
PACIFIC OCEAN
INDIAN OCEAN
AUSTRALIA
800
801
802
452
Pigafetta Basin
Mariana Basin

ORAGE

East Coast Repository
Gulf Coast Repository

NS 1.38/2:

OCEAN DRILLIN

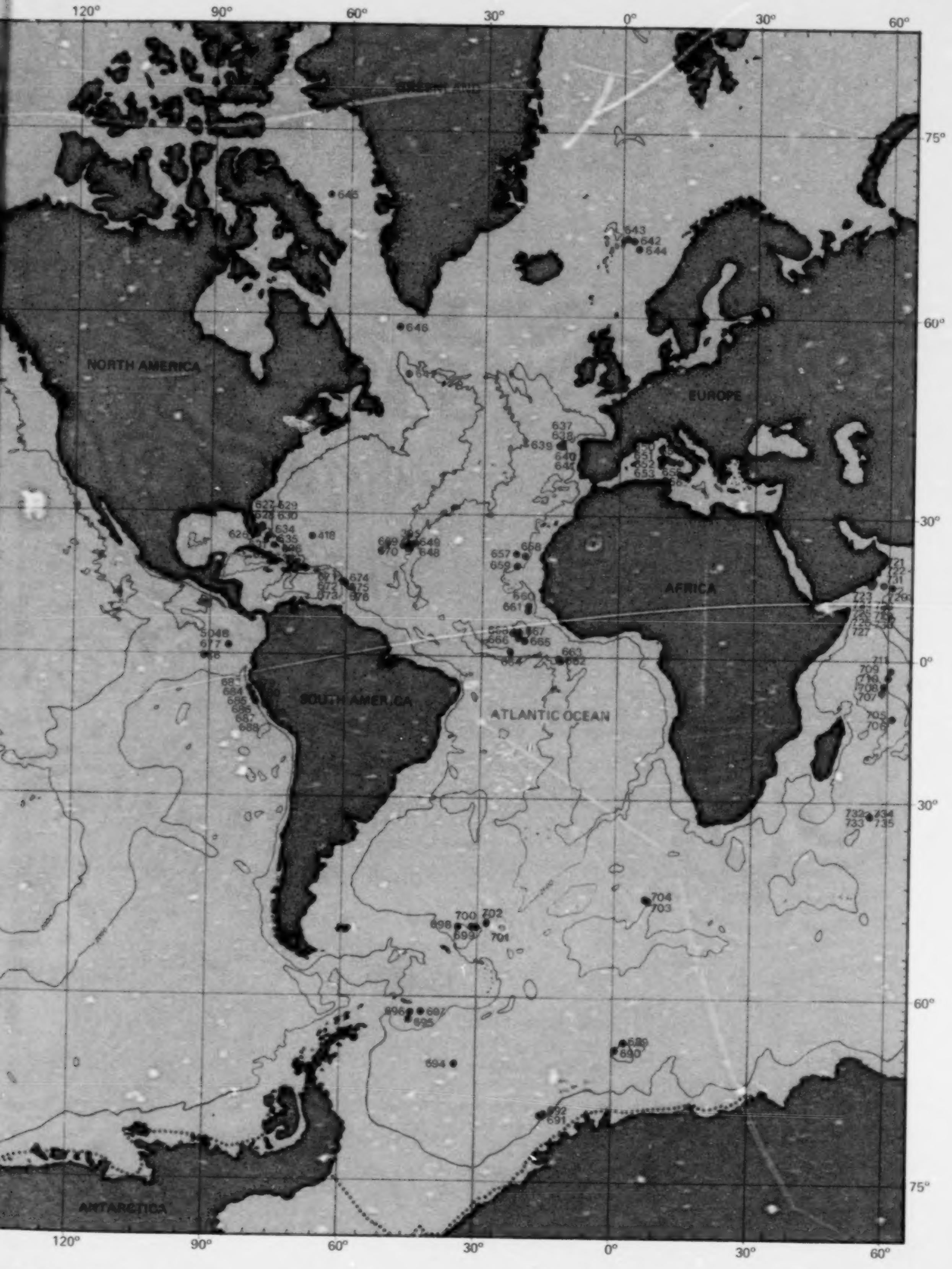
120°
90°
60°
30°
0°
30°
60°
75°
60°
30°
0°
30°
60°
75°
NORTH AMERICA
EUROPE
AFRICA
SOUTH AMERICA
ATLANTIC OCEAN
ANTARCTICA
645
646
643
642
644
637
638
639
640
641
650
651
652
653
627
629
628
630
626
634
635
418
669
670
395
649
648
657
658
659
671
672
673
674
675
676
660
661
663
664
665
666
667
662
5046
677
683
684
685
686
687
688
721
722
731
723
727
711
709
710
708
707
705
706
732
733
734
735
704
703
698
699
700
701
702
696
697
695
694
689
690
692
691

G PROGRAM

# PROCEEDINGS OF THE OCEAN DRILLING PROGRAM

## VOLUME 129
## INITIAL REPORTS

## OLD PACIFIC CRUST

Covering Leg 129 of the cruises of the Drilling Vessel *JOIDES Resolution*,
Apra Harbor, Guam, to Apra Harbor, Guam, Sites 800–802,
20 November 1989–18 January 1990

Yves P. Lancelot, Roger Larson, Andrew Fisher,
Lewis Abrams, Richard Behl, William H. Busch, Gordon Cameron, Paterno R. Castillo,
James M. Covington, Gabriele Dürr, Elisabetta Erba, Peter A. Floyd, Christian France-Lanord,
Ernst H. Hauser, Susan M. Karl, Anne-Marie Karpoff, Atsushi Matsuoka, Alain Molinie,
James G. Ogg, A.R.M. Salimullah, Maureen Steiner, Brian P. Wallick, Winton Wightman
*Shipboard Scientists*

Andrew Fisher
*Shipboard Staff Scientist*

Prepared by the
OCEAN DRILLING PROGRAM
TEXAS A&M UNIVERSITY

Lona Haskins Dearmont
*Volume Editor*

in cooperation with the
NATIONAL SCIENCE FOUNDATION
and
JOINT OCEANOGRAPHIC INSTITUTIONS, INC.

This publication was prepared by the Ocean Drilling Program, Texas A&M University, as an account of work performed under the international Ocean Drilling Program, which is managed by Joint Oceanographic Institutions, Inc., under contract with the National Science Foundation. Funding for the program was provided by the following agencies at the time of this cruise:

Canada/Australia Consortium for the Ocean Drilling Program, Department of Energy, Mines and Resources (Canada) and Department of Primary Industries and Energy (Australia)

Deutsche Forschungsgemeinschaft (Federal Republic of Germany)

European Science Foundation Consortium for the Ocean Drilling Program (Belgium, Denmark, Finland, Iceland, Italy, Greece, the Netherlands, Norway, Spain, Sweden, Switzerland, and Turkey)

Institut Français de Recherche pour l'Exploitation de la Mer (France)

National Science Foundation (United States)

Natural Environment Research Council (United Kingdom)

University of Tokyo, Ocean Research Institute (Japan)

Any opinions, findings, and conclusions or recommendations expressed in this publication are those of the author(s) and do not necessarily reflect the views of the National Science Foundation, the participating agencies, Joint Oceanographic Institutions, Inc., Texas A&M University, or Texas A&M Research Foundation.

It is recommended that reference to the whole or to part of this volume be made in one of the following forms, as appropriate:

Lancelot, Y., Larson, R., et al. 1990. *Proc. ODP, Init. Repts.*, 129: College Station, TX (Ocean Drilling Program).

Shipboard Scientific Party, 1990. Site 800. *In* Lancelot, Y., Larson, R., et al., *Proc. ODP, Init. Repts.*, 129: College Station, TX (Ocean Drilling Program), 33–89.

## Effective Publication Dates of ODP *Proceedings*

According to the International Code of Zoological Nomenclature, the date of publication of a work and of a contained name or statement affecting nomenclature is the date on which the publication was mailed to subscribers, placed on sale, or when the whole edition is distributed free of charge, mailed to institutions and individuals to whom free copies are distributed. The mailing date, *not the printed date*, is the correct one.

The mailing dates of recent *Proceedings of the Ocean Drilling Program* are as follows:

Volume 126 (*Initial Reports*): August 1990
Volume 127 (*Initial Reports*): September 1990
Volume 128 (*Initial Reports*): September 1990
Volume 113 (*Scientific Results*): July 1990
Volume 115 (*Scientific Results*): September 1990
Volume 116 (*Scientific Results*): September 1990

## Distribution

Copies of this publication may be obtained from Publications Distribution Center, Ocean Drilling Program, 1000 Discovery Drive, College Station, Texas 77845-9547. Orders for copies will require advance payment. See current ODP publication list for price and availability of this publication.

**Printed December 1990**

ISSN 0884-5883
Library of Congress 87-655-674

---

The paper used in this publication meets the minimum requirements of American National Standard for Information Sciences–Permanence of Paper for Printed Library Materials, ANSI Z39.48-1984∞ ™

# Foreword

## By the National Science Foundation

The scientists of the Ocean Drilling Program (ODP) have embarked on what could prove to be one of the most important earth science initiatives of the decade—an initiative rivaling in scope and impact the exploration of the frontiers of outer space. The program explores our planet's last frontier—the Earth's structure and history as it is revealed beneath the oceans. The scope of the program's scientific goals excites the imagination, challenges the intellect, and enhances the spirit of cooperation among peoples in countries around the world.

Between 1872 and 1876, HMS *Challenger* undertook the world's first major oceanographic expedition. That expedition greatly expanded man's knowledge of the world's oceans and revolutionized our ideas about planet Earth. From 1968 to 1983, another ship named *Challenger* logged more than 375,000 miles on 96 voyages across every ocean for the Deep Sea Drilling Project (DSDP), operated by Scripps Institution of Oceanography. Among the project's many remarkable discoveries were the confirmation of seafloor spreading and the establishment of the relative youth of the seafloor, thus verifying the dynamic and changing nature of the Earth's crust.

Today, the Ocean Drilling Program, which began in 1983, brings new resources to bear on scientific ocean drilling. A new drillship is in operation—the *JOIDES Resolution*—one of the world's most modern and best equipped drillships with enhanced capability for drilling and coring in polar areas and rough weather, expanded laboratory space, facilities for more scientists, and a major drill-hole logging program. The name of the ship was derived from the international scientific partnership that directs the program—the Joint Oceanographic Institutions for Deep Earth Sampling (JOIDES)—and from the flagship of Captain Cook's second voyage to the Pacific Ocean in the late 18th century. Texas A&M University is responsible for science operations in the program, and Lamont-Doherty Geological Observatory is responsible for the logging program.

The Ocean Drilling Program truly has international participation. In 1975, the International Phase of Ocean Drilling began with member nations—the U.S.A., U.S.S.R., Federal Republic of Germany, Japan, United Kingdom, and France—all providing funds and scientific guidance for the project. Today, ODP partners include the U.S.A., the Canada/Australia Consortium for the Ocean Drilling Program, France, the Federal Republic of Germany, Japan, the United Kingdom, and the European Science Foundation, which represents Sweden, Finland, Norway, Iceland, Denmark, Belgium, the Netherlands, Spain, Switzerland, Italy, Greece, and Turkey. The National Science Foundation, with funds contributed by the United States and international partners, supports the scientific operations and planning for the ODP through a contract with Joint Oceanographic Institutions, Inc. (JOI).

The information gained by the program leads to a better understanding of the Earth and its dynamic processes. Drilled sediment cores and logs reveal clues to past climatic history and tie into parallel studies of paleoclimates from glacial ice cores drilled on the continents. Understanding these sediment cores will enable scientists to complete the map of major geologically active regions of the Earth, and to identify processes that lead to dynamic change such as earthquakes, volcanic eruptions, and mountain and continental growth. We are far from being able to predict such changes accurately now; but with the new tools and understanding, the accuracy of such predictions can be improved. This better understanding of the Earth's system(s) will allow us to identify regions of potential mineral and energy resource development, an issue of worldwide human interest. The Ocean Drilling Program is not in itself aimed at finding resources, but the knowledge of the Earth's processes that is gained through such a basic research program will inevitably provide pieces of information required for such resource discovery and exploitation.

The program is fully under way in its aim to further the understanding of the Earth's dynamic systems. People of our planet will benefit directly and indirectly from this research in both their daily living and work activities. This multinational endeavor will perhaps foster other cooperative efforts in science or among societies. The Ocean Drilling Program has distinguished ancestors in the original *Resolution* and *Challenger* expeditions and the Deep Sea Drilling Project. The National Science Foundation is proud to be playing a leading role in this program, and we are looking forward to significant and innovative science for many years to come.

Erich Bloch
Director
National Science Foundation

Washington, D.C.

# Foreword

**By Joint Oceanographic Institutions, Inc.**

This volume presents results from the Ocean Drilling Program (ODP), where scientists use a specially equipped ocean drilling ship to sample and measure the properties of the submerged part of the Earth's crust. These data are then synthesized with other information to yield new insights into earth processes.

These results address the scientific goals of the program, which include providing a global description of geological and geophysical structures and materials, studying in detail areas of major geophysical activity such as mid-ocean ridges and the associated hydrothermal circulations, and studying passive and active continental margins. In addition, the ODP data support the study of sea-level and ocean-circulation changes, the effects of the Earth's orbital variations on climate, and the study of processes and mechanisms of evolution from the biological records in the cores which are recovered from drilling.

The Ocean Drilling Program is a partnership of scientists and governments. Overall scientific policy and management guidance is provided by Joint Oceanographic Institutions for Deep Earth Sampling (JOIDES), which consists of committees and panels made up of representatives of the participating institutions and other scientific and engineering experts. The JOIDES Executive Committee (EXCOM) provides general oversight; the JOIDES Planning Committee (PCOM) is the focal point for all scientific planning for the ODP and is key to the scientific success of the program.

The PCOM has a network of panels and working groups which screen drilling proposals, evaluate instrumentation and measurement techniques, and assess geophysical survey data and other safety and siting information. PCOM uses the recommendations of these panels and committees to select drilling targets, to specify the major scientific objectives of each two-month drilling segment or leg, and to provide the science operator with nominations for co-chief scientists. The science operator, Texas A&M University, in turn is responsible for planning the detailed ship's operations, actual drilling schedules, and final scientific rosters, which are developed in close cooperation with PCOM and the cognizant panels.

Many of the scientific goals can be met only with new technology. Thus the program has identified engineering goals, which include the ability to start a hole and to core on bare rock at mid-ocean ridge sites, to drill in high-temperature and corrosive regions typical of hydrothermal areas, and to core in high latitudes with minimum interference from high seas and sea ice. To meet these needs, the program operates a specially equipped drillship, the *JOIDES Resolution*, which contains laboratories and equipment that are state-of-the-art, and carries a major new logging program.

The ship, registered as SEDCO/BP 471 after her owners and her length in feet (144 meters), is 70 feet (21 meters) wide, and has a displacement of 16,595 long tons. Her derrick towers 200 feet (61 meters) above the waterline, and a computer-controlled dynamic-positioning system stabilizes the ship over a specific location while drilling in water depths up to 27,000 feet (8230 meters). The drilling system collects cores from beneath the seafloor with a derrick and drawworks that can handle 30,000 feet (9144 meters) of drill pipe. More than 12,000 square feet (1115 square meters) of space distributed throughout the ship is devoted to scientific laboratories and equipment. The ship sails with a scientific and technical crew of 50 and a ship's crew of 65.

Logging is a major part of the overall operation. The program provides a full suite of geochemical and geophysical measurements for every hole deeper than 1300 feet (400 meters). For each such hole, there are lowerings of basic oil-industry tools: nuclear, sonic, and electrical. In addition, a borehole televiewer is available for imaging the well-bore wall, a 12-channel logging tool provides accurate velocity and elastic property measurements as well as sonic waveforms for spectral analysis of energy propagation near the well bore, and a vertical seismic profiler records reflectors from below the total depth of the hole.

Texas A&M University serves as science operator for the Ocean Drilling Program. In this capacity, they operate and staff the drillship to collect cores from JOIDES-designated sites from around the world. The science operator also ensures that adequate scientific analyses are performed on the cores by maintaining the shipboard scientific laboratories and by providing logistical and technical support for shipboard scientific teams. Onshore, Texas A&M manages scientific activities after each leg, is curator for the cores, distributes samples, and coordinates the editing and publication of the scientific results. Lamont-Doherty Geological Observatory (LDGO) of Columbia University manages the program's logging operations, which include processing the data and provision of assistance to scientists in data analysis. The ODP Data Bank, a repository for geophysical data, is also managed by LDGO. Core samples from ODP and the previous Deep Sea Drilling Project are stored for future investigation at three sites: ODP Pacific and Indian Ocean cores at Texas A&M University, ODP and DSDP Atlantic and Antarctic cores at Lamont-Doherty Geological Observatory, and DSDP Pacific and Indian Ocean cores at Scripps Institution of Oceanography.

International oversight and coordination are provided by the ODP Council, a governmental consultative body of partner country representatives, chaired by the United States, which periodically reviews the general progress of the program and discusses financial plans and other management issues. Joint Oceanographic Institutions, Inc., a nonprofit consortium of U.S. oceanographic institutions, serves as the National Science Foundation's prime contractor and manages the ODP. JOI is responsible for seeing that the scientific objectives and plans are translated into scientific operations consistent with JOIDES recommendations and budgetary constraints.

Scientific achievements of the ODP already include new data on early seafloor spreading and how continents separate and their margins evolve. We have new insight into glacial cycles and the fluctuations of currents throughout geological time. Technical achievements include the first bare-rock coring, and logging data more accurate and complete than ever before. JOI is pleased to have played a facilitating role in the Ocean Drilling Program.

James Baker

D. James Baker
President
Joint Oceanographic Institutions, Inc.

Washington, D.C.

# OCEAN DRILLING PROGRAM

## MEMBER ORGANIZATIONS OF THE JOINT OCEANOGRAPHIC INSTITUTIONS FOR DEEP EARTH SAMPLING (JOIDES):

University of California at San Diego, Scripps Institution of Oceanography

Columbia University, Lamont-Doherty Geological Observatory

University of Hawaii, Hawaii Institute of Geophysics

University of Miami, Rosenstiel School of Marine and Atmospheric Science

Oregon State University, College of Oceanography

University of Rhode Island, Graduate School of Oceanography

Texas A&M University, College of Geosciences

University of Texas at Austin, Institute for Geophysics

University of Washington, College of Ocean and Fishery Sciences

Woods Hole Oceanographic Institution

Canada/Australia Consortium for the Ocean Drilling Program, Department of Energy, Mines and Resources (Canada) and Department of Primary Industries and Energy (Australia)

European Science Foundation Consortium for Ocean Drilling, Belgium, Denmark, Finland, Iceland, Italy, Greece, the Netherlands, Norway, Spain, Sweden, Switzerland, and Turkey

Federal Republic of Germany, Bundesanstalt für Geowissenschaften und Rohstoffe

France, Institut Français de Recherche pour l'Exploitation de la Mer

Japan, University of Tokyo, Ocean Research Institute

United Kingdom, Natural Environment Research Council

## PRIME CONTRACTOR

Joint Oceanographic Institutions, Inc.
Washington, D.C.

Thomas E. Pyle
Director, Ocean Drilling Programs

## OPERATING INSTITUTION

College of Geosciences
Texas A&M University
College Station, Texas

Melvin Friedman
Principal Investigator

## OCEAN DRILLING PROGRAM

Philip D. Rabinowitz
Director

Timothy J.G. Francis
Deputy Director

Richard G. McPherson
Administrator

Audrey W. Meyer, Manager
Science Operations

Barry W. Harding, Manager
Engineering and Drilling Operations

Russell B. Merrill, Curator and Manager
Science Services

Robert E. Olivas, Manager
Technical and Logistics Support

## LOGGING OPERATOR

Borehole Research Group
Lamont-Doherty Geological Observatory
Columbia University
Palisades, New York

Roger N. Anderson, Head

# PARTICIPANTS ABOARD *JOIDES RESOLUTION* FOR LEG 129*

Yves P. Lancelot
Co-Chief Scientist
*Université Pierre et Marie Curie*
*4 Place Jussieu, Tour 26*
*75252 Paris Cedex 05*
*France*

Roger Larson
Co-Chief Scientist
*Graduate School of Oceanography*
*University of Rhode Island*
*Narragansett, Rhode Island 02882-1197*

Andrew Fisher
ODP Staff Scientist/Logging Scientist
*Ocean Drilling Program*
*Texas A&M University*
*1000 Discovery Drive*
*College Station, Texas 77845-9547*

Lewis Abrams
Logging Scientist/Seismologist
*Graduate School of Oceanography*
*University of Rhode Island*
*Narragansett, Rhode Island 02882-1197*

Richard Behl
Sedimentologist
*Earth Sciences Board of Studies*
*Applied Sciences Building*
*University of California, Santa Cruz*
*Santa Cruz, California 95064*

William H. Busch
Physical Properties Specialist
*Department of Geology and Geophysics*
*University of New Orleans*
*New Orleans, Louisiana 70148*

Gordon Cameron
Physical Properties Specialist
*44½ Ochterloney Street*
*Dartmouth, Nova Scotia B2Y 1B9*
*Canada*

Paterno R. Castillo
Igneous Petrologist
*Division of Marine Geology and Geophysics*
*Rosenstiel School of Marine and Atmospheric Science*
*University of Miami*
*4600 Rickenbacker Causeway*
*Miami, Florida 33149-1098*

James M. Covington
Paleontologist (nannofossils)
*Department of Geology*
*Florida State University*
*Tallahassee, Florida 32306*

Gabriele Dürr
Paleontologist (palynomorphs/dinoflagellates)
*Institut für Geologie und Paläontologie*
*Universität Tübingen*
*Sigwartstrasse 10*
*D-7400 Tübingen*
*Federal Republic of Germany*

Elisabetta Erba
Paleontologist (nannofossils)
*Dipartimento di Scienze della Terra*
*Universitá degli Studi di Milano*
*Via Mangiagalli 34*
*I-20129 Milano*
*Italy*

Peter A. Floyd
Igneous Petrologist
*Department of Geology*
*University of Keele*
*Keele, Staffordshire ST5 5BG*
*United Kingdom*

Christian France-Lanord
Igneous Petrologist/Geochemist
*Centre de Recherches Pétrographiques et Géochemiques*
*B.P. 20*
*54501 Vandoeuvre Cedex*
*France*

Ernst H. Hauser
Paleontologist (foraminifers)
*Institut für Paläontologie und Geologie*
*Universität München*
*Richard-Wagner-Strasse 10*
*D-8000 München 2*
*Federal Republic of Germany*

Susan M. Karl
Sedimentologist
*Branch of Alaskan Geology*
*U.S. Geological Survey*
*4200 University Drive*
*Anchorage, Alaska 99508-4667*

Anne-Marie Karpoff
Sedimentologist
*Institut de Géologie*
*Université Louis Pasteur*
*1 rue Blessig*
*67084 Strasbourg Cedex*
*France*

---

*Addresses at time of cruise.

Atsushi Matsuoka
Paleontologist (radiolarians)
*Faculty of General Education*
*Department of Earth Sciences*
*Niigata University*
*Niigata 950-21*
*Japan*

Alain Molinie
LDGO Logging Scientist
*Borehole Research Group*
*Lamont-Doherty Geological Observatory*
*Columbia University*
*Palisades, New York 10964*

James G. Ogg
Sedimentologist
*Department of Earth and Atmospheric Sciences*
*Purdue University*
*West Lafayette, Indiana 47907*

A.R.M. Salimullah
Sedimentologist
*Geology Department*
*University of Southampton*
*Southampton SO9 5NH*
*United Kingdom*

Maureen Steiner
Paleomagnetist
*Department of Geology and Geophysics*
*University of Wyoming*
*P.O. Box 3006*
*University Station*
*Laramie, Wyoming 82071*

Brian P. Wallick
Paleomagnetist
*Department of Earth and Atmospheric Sciences*
*Purdue University*
*West Lafayette, Indiana 47907*

Winton Wightman
Paleontologist (foraminifers)
*Centre for Marine Geology*
*Dalhousie University*
*Halifax, Nova Scotia B3H 3J5*
*Canada*

## SEDCO OFFICIALS

Captain Anthony ("Tom") Ribbens
Master of the Drilling Vessel
*Underseas Drilling, Inc.*
*707 Texas Avenue South*
*Suite 103D*
*College Station, Texas 77840-1917*

Jack Tarbutton
Drilling Superintendent
*Underseas Drilling, Inc.*
*707 Texas Avenue South*
*Suite 103D*
*College Station, Texas 77840-1917*

### ODP ENGINEERING AND OPERATIONS PERSONNEL

| | |
|---|---|
| Glen N. Foss | Operations Superintendent |
| Patrick Thompson | Special Tools Engineer |

### ODP TECHNICAL AND LOGISTICS PERSONNEL

| | |
|---|---|
| Daniel Bontempo | Marine Technician |
| Jim Briggs | Electronics Technician |
| Scott Chaffey | Chemistry Technician |
| Jo Claesgens | Yeoperson |
| Valerie Clark | Chemistry Technician |
| Joe DeMorett | Marine Technician |
| Susan Erb | Marine Technician |
| David Erickson | Electronics Technician |
| Edwin Garrett | Computer Systems Manager |
| Brad Julson | Laboratory Officer |
| Kazushi ("Kuro") Kuroki | Marine Technician |
| Kathe Lighty | Marine Technician |
| John H. Miller | Curatorial Representative |
| Michael Moore | Marine Technician |
| Joan Perry | Marine Technician |
| Joe Powers | Assistant Laboratory Officer |
| John Tenison | Photographer |
| Lisa Tirey | Graphics Illustrator |

## Ocean Drilling Program Publications Staff

*Publications Supervisor*
William D. Rose

*Chief Editor*
Norman J. Stewart

*Editors*
Eva M. Barbu
Lona Haskins Dearmont
Sondra K. Stewart
William R. Winkler

*Chief Production Editor*
Jennifer Pattison Hall

*Production Editors*
Janna Abel
Jaime A. Gracia (this volume)

*Publications Coordinator*
Janalisa Braziel Soltis

*Assistant Publications Coordinator*
Jill Mutschler-Fontenot

*Hole Summary Coordinator*
Laura Hammond Young

*Publications Distribution Specialist*
Fabiola Muñoz Byrne

*Senior Photographer*
John W. Beck

*Photographer*
Roy T. Davis

*Chief Illustrator*
Deborah Partain

*Illustrators*
Michelle Curtis
Linda C. De Leon
Garnet D. Gaither
Cynthia M. Mullican

*Compositor*
Mary Elizabeth Betz

*Production Assistants*
Gudelia ("Gigi") Delgado
Lisa L. Tirey

# TABLE OF CONTENTS

## VOLUME 129—INITIAL REPORTS

Acknowledgments . . . . . . . . . . . . . . . . . . . . . . . . . . . . . . . . . . . . . . . . . . . . 1

### SECTION 1: INTRODUCTION

1. Explanatory Notes . . . . . . . . . . . . . . . . . . . . . . . . . . . . . . . . . . . . . . 5
Shipboard Scientific Party

### SECTION 2: SITE REPORTS

2. Site 800 . . . . . . . . . . . . . . . . . . . . . . . . . . . . . . . . . . . . . . . . . 33
Shipboard Scientific Party

3. Site 801 . . . . . . . . . . . . . . . . . . . . . . . . . . . . . . . . . . . . . . . . . 91
Shipboard Scientific Party

4. Site 802 . . . . . . . . . . . . . . . . . . . . . . . . . . . . . . . . . . . . . . . . . 171
Shipboard Scientific Party

### SECTION 3: CORES

Core description forms and core photographs for:

Site 800 . . . . . . . . . . . . . . . . . . . . . . . . . . . . . . . . . . . . . . . . . 247

Site 801 . . . . . . . . . . . . . . . . . . . . . . . . . . . . . . . . . . . . . . . . . 303

Site 802 . . . . . . . . . . . . . . . . . . . . . . . . . . . . . . . . . . . . . . . . . 419

### SECTION 4: POLICY

JOIDES Advisory Groups . . . . . . . . . . . . . . . . . . . . . . . . . . . . . . . . . 483

Sample-distribution Policy . . . . . . . . . . . . . . . . . . . . . . . . . . . . . . . . 487

### BACK-POCKET MICROFICHE

Formation microscanner images for Leg 129 (fiche 1–10):

Hole 800A: Main log, 51–136 mbsf
Main log, 123–228 mbsf
Main log, 211–313 mbsf
Repeat interval, 71–136 mbsf
Hole 801B: Pass 1/Pass 2, 95–265 mbsf
Pass 1/Pass 2, 255–462 mbsf
Hole 802A: Main log, 112–300 mbsf

"The deep basin of the western Pacific still holds as its secret the earliest records remaining of the history of the Pacific basin. . . . Ultimately, another serious attempt must be made to solve these immensely important problems . . . held on, and in, the oldest oceanic crust."
B. C. Heezen (1973)

# ACKNOWLEDGMENTS

Leg 129 marks the culmination of a very long search for the oldest rocks of the Pacific Ocean. That search began over 20 years ago and involved a long series of proposals, geophysical surveys, committee fights, beer talks, dreams, drilling cruises, successes, failures, frustrations, and faith. A great number of individuals, institutions, special interest lobbies, ship crews, technicians, and scientists took part in the adventure. Some of us were involved almost from the beginning; others came and went. All contributed, however, and we feel privileged to have been there, finally, at the right place and time to "cash in" for such a large community.

The main force behind this project was of course in the various JOIDES panels and especially the Ocean Paleoenvironment Panel in the 1970's, and its successor the Sediment and Ocean History Panel (now the Ocean History Panel). FUSOD, COSOD I, and COSOD II conferences helped keep the dream alive. Finally, the JOIDES Planning Committee showed constant support during all these years, dedicating all or parts of DSDP Legs 6, 7, 17, 20, 32, 33, 60, 61, and 89 of the *Glomar Challenger* to the search for the origins of the Pacific plate.

We are especially indebted to those who actually got "out there" on the drilling vessel and came back either empty-handed or loaded with fascinating unexpected discoveries that brought more questions than answers. Our very special thoughts naturally go to Bruce C. Heezen who did not live to see the ultimate success, after having invested so much of his time and passion in the search. Many of our friends and colleagues, who at one time or another got directly involved with the project, joined forces in the "Old Pacific Club," and refused to give up even after repeated frustrating experiences. E. L. Winterer, S. O. Schlanger, R. Moberly, I. Premoli-Silva, W. Sliter, D. Bukry, R. G. Douglas, and H. P. Foreman are especially persistent members of this club that is led by Ralph Moberly, who sailed on five of the above legs and spent nearly a year on the *Glomar Challenger* drilling in the Mesozoic Pacific.

In the most recent years prior to Leg 129, multichannel seismic surveys played a major role in the definition of new strategies and the discovery of the most promising drilling targets. T. S. Shipley (who claims that he is not *really* a seismologist, but who is certainly better at it than any of us) was behind most of it, especially the last cruise of the *Fred H. Moore* that brought back enough evidence to convince the various JOIDES panels and committees. The combination of the results of the FM35-12 cruise of the *Fred H. Moore* and of the MESOPAC II cruise of the *Le Suroit*, which both had their share of adventures, set the final stage before the actual drilling could take place. We thank the crews, technicians, and fellow scientists who shared our excitement and frustrations during these surveys. Without their cooperation Leg 129 would never have happened.

Drilling operations on the *JOIDES Resolution* exceeded our expectations thanks to the experience of the ODP operations engineers and technicians under Glen Foss, operations superintendent, and Brad Julson, laboratory officer. Our very special thanks go to the SEDCO/FOREX engineers, technicians, and drillers led by "Jack" Tarbutton, as well as to the entire ship's crew under Captain Tom Ribbens.

Finally, we thank all the ODP staff at Texas A&M University for their help before, during, and after the cruise. Their expertise ranged from critical suggestions for scientific crew selection to photocopying. Their diligence and good humor contributed especially to making the documentation of Leg 129 both relatively error free and enjoyable.

# SECTION 1: INTRODUCTION

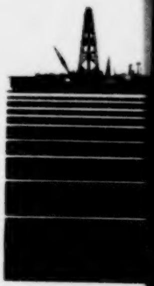

Lancelot, Y., Larson, R. L., et al., 1990
*Proceedings of the Ocean Drilling Program, Initial Reports*, Vol. 129

# 1. EXPLANATORY NOTES[1]

Shipboard Scientific Party[2]

In this chapter, we have assembled information that will help the reader understand the basis for our preliminary conclusions and also help the interested investigator select samples for further analysis. This information concerns only shipboard operations and analyses described in the site chapters in the *Initial Reports* volume of the Leg 129 *Proceedings of the Ocean Drilling Program*. Methods used by various investigators for shore-based analysis of Leg 129 data will be detailed in the individual scientific contributions published in the *Scientific Results* volume.

## AUTHORSHIP OF SITE CHAPTERS

The separate sections of the site chapters were written by the following shipboard scientists (authors are listed in alphabetical order, no seniority is necessarily implied):

Site Summary (Lancelot, Larson)
Background and Objectives (Lancelot, Larson)
Operations (Lancelot, Larson)
Sedimentology and Lithostratigraphy (Behl, Karl, Karpoff, Ogg, Salimulah)
Biostratigraphy (Covington, Durr, Erba, Hauser, Matsuoka, Wightman)
Paleomagnetics (Steiner, Wallick)
Inorganic Geochemistry (France-Lanord)
Igneous Petrology (Castillo, Floyd, France-Lanord)
Physical Properties (Busch, Cameron)
Downhole Measurements (Abrams, Fisher, Molinie)
Site Geophysics and Seismic Stratigraphy (Abrams, Lancelot, Larson)
Conclusions (Lancelot, Larson)
Appendix (Shipboard Scientific Party)

Following the text of each site chapter are summary downhole logs. Core descriptions ("barrel sheets" and igneous rock visual core descriptions) and photographs of each core appear in Section 3, near the back of this volume.

## DEFINITIONS

### Conventional Use of Time and Time-Rock Units

The subdivisions of epochs/series into *early, middle, late,* or *lower, middle, upper* have no real formal standing in stratigraphy. The subdivision of lithostratigraphic (rock), chronostratigraphic (time-rock), and geochronologic (time) units is defined as follows throughout this volume.

#### Lithostratigraphic Units

For rock units, the terms *lower, middle,* and *upper* describe sections of rocks subdivided on the basis of superposition, without any implication of time-partitioning.

#### Chronostratigraphic Units

These units imply bodies of strata formed during specific intervals of geologic time. According to convention they are subdivided using the terms *lower, middle,* and *upper*. The basis of formal time-rock units are stages, each of which has (or should have) a stratotype, a standard section with which other sections can be compared. Stages are conventionally grouped together into the subunits that subdivide the series. When referring to the entire subdivision of the series, the terms Lower, Middle, and Upper are capitalized by convention. The lowercase forms, lower, middle, and upper, refer only to a portion of the subunit or its equivalent, or instead imply informal usage.

#### Geochronologic Units

When speaking of time, age, or of sections in the temporal sense, the terms *early, middle,* and *late* are used for subdivision. The basis of the formal geochronologic units are ages (time equivalent of stages). Like stages, ages grouped together form the time subunits that subdivide epochs. When referring to the entire subunit, the terms Early, Middle, and Late are capitalized, but not when only a part of the subunit, or an informal sense is implied. However, such combinations as early Early, middle Early, late Early, etc., are used to refer to older, medial, or younger parts of the entire subunit.

#### Use of Ma vs. m.y.

*Ma* is equivalent to and replaces m.y.B.P. (million years Before Present), e.g., 35–40 Ma. The abbreviation *m.y.* is still used in sentences such as, "...for five m.y. in the early Miocene."

## DRILLING CHARACTERISTICS

Information concerning sedimentary stratification in uncored or unrecovered intervals may be inferred from seismic data, wireline-logging results, and from an examination of the behavior of the drill string as observed and recorded on the drilling platform. Typically, the harder a layer, the slower and more difficult it is to penetrate. A number of other factors may determine the rate of penetration, so it is not always possible to relate the drilling time directly to the hardness of the layers. Bit weight and revolutions per minute, recorded on the drilling recorder, also influence the penetration rate.

## DRILLING DEFORMATION

When cores are split, many show signs of significant sediment disturbance, including the concave-downward appearance of originally horizontal bands, haphazard mixing of lumps of different lithologies (mainly at the tops of cores), and the near-fluid state of some sediments recovered from tens to hundreds of meters below the seafloor. Core deformation probably occurs during cutting, retrieval (with accompanying changes in pressure and temperature), and core handling on deck. A detailed discussion of slump-like drilling disturbance is given in the "Core Description" section of this chapter.

---

[1] Lancelot, Y., Larson, R. L., et al., 1990. *Proc. ODP, Init. Repts.*, 129: College Station, TX (Ocean Drilling Program).

[2] Shipboard Scientific Party is as given in the list of participants preceding the contents.

## SHIPBOARD SCIENTIFIC PROCEDURES

### Numbering of Sites, Holes, Cores, and Samples

Ocean Drilling Program (ODP) drill sites are numbered consecutively and refer to one or more holes drilled while the ship was positioned over one acoustic beacon. Multiple holes may be drilled at a single site by pulling the drill pipe above the seafloor (out of the hole), moving the ship some distance from the previous hole, and then drilling another hole.

For all ODP drill sites, a letter suffix distinguishes each hole drilled at the same site. For example, the first hole drilled is assigned the site number modified by the suffix A, the second hole takes the site number and suffix B, and so forth. Note that this procedure differs slightly from that used by the Deep Sea Drilling Project (DSDP) (Sites 1 through 624), but prevents ambiguity between site- and hole-number designations. It is important to distinguish among holes drilled at a site, because recovered sediments or rocks from different holes usually do not come from equivalent positions in the stratigraphic column.

The cored interval is measured in meters below seafloor (mbsf). The depth interval assigned to an individual core begins with the depth below the seafloor that the coring operation began, and extends to the depth that the coring operation ended (see Fig. 1). For example, each coring interval is generally up to 9.5 m long, which is the length of a core barrel. Coring intervals may be shorter and may not necessarily be adjacent if separated by drilled intervals. In soft sediments, the drill string can be "washed ahead" with the core barrel in place, without recovering sediments. This is achieved by pumping water down the pipe at high pressure to wash the sediment out of the way of the bit and up the space between the drill pipe and the wall of the hole. If thin, hard, rock layers are present, then it is possible to get "spotty" sampling of these resistant layers within the washed interval, and thus to have a cored interval greater than 9.5 m. In drilling hard rock, a center bit may replace the core barrel if it is necessary to drill without core recovery.

Cores taken from a hole are numbered serially from the top of the hole downward. Core numbers and their associated cored intervals (in mbsf) usually are unique in a given hole. This may not be true, however, if an interval must be cored twice because of caving of cuttings or other hole problems. Maximum full recovery for a single core is 9.5 m of rock or sediment contained in a plastic liner (6.6-cm internal diameter) plus about 0.2 m (without a plastic liner) in the core catcher (Fig. 2). The core catcher is a device at the bottom of the core barrel which prevents the core from sliding out when the barrel is being retrieved from the hole. In certain situations (e.g., when coring gas-charged sediments that expand while being brought on deck) recovery may exceed the 9.5-m maximum.

A recovered core is divided into 1.5-m sections that are numbered serially from the top (Fig. 2). When full recovery is obtained, the sections are numbered from 1 through 7, with the last section possibly being shorter than 1.5 m (rarely, an unusually long core may require more than 7 sections). When less than full recovery is obtained, there will be as many sections as needed to accommodate the length of the core recovered. For example, 4 m of core would be divided into two 1.5-m sections and one 1-m section. If cores are fragmented (recovery less than 100%), sections are numbered serially and intervening sections are noted as void, whether shipboard scientists believe that the fragments were contigu-

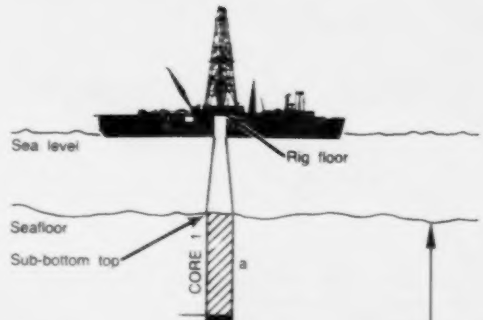

BOTTOM FELT: distance from rig floor to seafloor

TOTAL DEPTH: distance from rig floor to bottom of hole (sub-bottom bottom)

PENETRATION: distance from seafloor to bottom of hole (sub-bottom bottom)

NUMBER OF CORES: total of all cores recorded, including cores with no recovery

TOTAL LENGTH OF CORED SECTION: distance from sub-bottom top to sub-bottom bottom minus drilled (but not cored) areas in between

TOTAL CORE RECOVERED: total from adding a, b, c, and d in diagram

CORE RECOVERY (%): equals TOTAL CORE RECOVERED divided by TOTAL LENGTH OF CORED SECTION times 100

Figure 1. Coring and depth intervals.

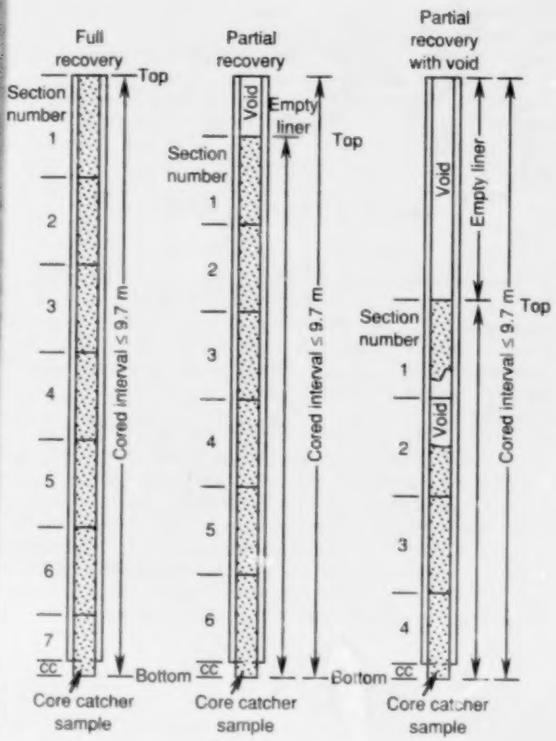

Figure 2. Examples of numbered core sections.

ous *in situ* or not. In rare cases, a section less than 1.5 m may be cut in order to preserve features of interest (e.g., lithological contacts).

By convention, material recovered from the core catcher is placed below the last section when the core is described, and labeled core catcher (CC); in sedimentary cores, it is treated as a separate section. The core catcher is placed at the top of the cored interval in cases where material is only recovered in the core catcher. However, information supplied by the drillers or by other sources may allow for more precise interpretation as to the correct position of core catcher material within an incompletely recovered cored interval.

Igneous rock cores are also cut into 1.5-m sections that are numbered serially; each piece of rock is then assigned a number. Fragments of a single piece are assigned a single number, and individual fragments are identified alphabetically. The core-catcher sample is placed at the bottom of the last section and is treated as part of the last section rather than as a separate piece. Scientists completing visual core descriptions describe each lithologic unit, noting core and section boundaries only as physical reference points.

When, as is usually the case, the recovered core is shorter than the cored interval, the top of the core is equated with the top of the cored interval by convention, in order to achieve consistency in handling analytical data derived from the cores. Samples removed from the cores are designated by distance measured in centimeters from the top of the section to the top and bottom of each sample removed from that section. In curated hard-rock sections, sturdy plastic spacers are placed between pieces that do not fit together in order to protect them from damage in transit and in storage. Therefore, the centimeter interval noted for a hard-rock sample has no direct relationship to that sample's depth within the cored interval, but is only a physical reference to the location of the sample within the curated core.

A full identification number for a sample consists of the following information: leg, site, hole, core number, core type, section number, piece number (for hard rock), and interval in centimeters measured from the top of section. For example, a sample identification of "129-800A-25R-1, 10-12 cm" represents a sample removed from the interval between 10 and 12 cm below the top of Section 1, Core 25 (R designates that this core was taken during rotary drilling) of Hole 800A during Leg 129.

All ODP core and sample identifiers indicate core type. The following abbreviations are used: R = rotary core barrel (RCB); H = hydraulic piston core (HPC; also referred to as APC, or advanced hydraulic piston core); P = pressure core barrel; X = extended core barrel (XCB); B = drill-bit recovery; C = center-bit recovery; I = *in-situ* water sample; S = sidewall sample; W = wash-core recovery; and M = miscellaneous material. On Leg 129, only RCB cores were recovered.

## Core Handling

### *Sediments*

As soon as a core is retrieved on deck, a sample is taken from the core catcher and given to the paleontological laboratory for an initial age assessment. The core is then placed on the long horizontal rack, and gas samples may be taken by piercing the core liner and withdrawing gas into a vacuum tube. Voids within the core are sought as sites for gas sampling. Some of the gas samples are stored for shore-based study, but others are analyzed immediately as part of the shipboard safety and pollution prevention program. Next, the core is marked into section lengths, each section is labeled, and the core is cut into sections. Interstitial-water (IW), organic geochemistry (OG), and physical properties (PP) samples are then taken. In addition, some headspace gas samples (HS) are scraped from the ends of cut sections on the catwalk and sealed in glass vials for light hydrocarbon analysis. Each section is then sealed at the top and bottom by gluing on color-coded plastic caps: blue to identify the top of a section and clear for the bottom. A yellow cap is placed on the section ends from which a whole-round sample has been removed. The caps are usually attached to the liner by coating the end liner and the inside rim of the cap with acetone, and then the caps are taped to the liners.

The cores are then carried into the laboratory, where the sections are again labeled using an engraver to permanently mark the full designation of the section. The length of the core in each section and the core-catcher sample are measured to the nearest centimeter, and this information is logged into the shipboard core-log database program.

Whole-round sections from APC and XCB cores are normally run through the multisensor track (MST). The MST includes the GRAPE (gamma-ray attenuation porosity evaluator) and *P*-wave logger devices, which measure bulk density, porosity, and sonic velocity, and also includes a meter which determines the volume magnetic susceptibility. As all material collected during Leg 129 was rotary-cored, the sediments were far too disturbed for testing with the standard MST. Individual samples removed from split cores were subjected to a 2-min GRAPE count, as described in the "Physical Properties" section (this chapter). After the core has equilibrated to room temperature (approximately 3 hr), thermal conductivity measurements are performed on relatively soft sediments, and the cores are split.

Cores of soft material are split lengthwise into *working* and *archive* halves. The softer cores are split with a wire or saw, depending on the degree of induration. Harder cores are split with a band saw or diamond saw. The wire-cut cores are split from the bottom to top, so investigators should be aware that older material could have been transported up the core on the split face of each section.

The working half of the core is sampled for both shipboard and shore-based laboratory studies. Each extracted sample is logged into the sampling computer database program by the location and the name of the investigator receiving the sample. Records of all removed samples are kept by the curator at ODP headquarters. The extracted samples are sealed in plastic vials or bags and labeled. Samples are routinely taken for shipboard physical properties analysis and subsequently used for determining calcium carbonate ($CaCO_3$) (coulometric analysis) and organic carbon (CNS elemental analyzer,) and the data are reported in the site chapters.

The archive half is described visually. Smear slides are made from samples taken from the archive half, and are supplemented by thin sections and X-ray-diffraction (XRD) samples taken from the working half. Most archive sections are run through the cryogenic magnetometer. The archive half is then photographed with both black-and-white and color film, a whole core at a time. Close-up photographs (black-and-white) are taken of particular features for illustrations in the summary of each site, as requested by scientists.

Both halves of the core are then put into labeled plastic tubes, sealed, and transferred to cold-storage space aboard the drilling vessel. At the end of the leg, the cores are transferred from the ship in refrigerated airfreight containers to cold storage at the Gulf Coast Repository at the Ocean Drilling Program, Texas A&M University, College Station, Texas.

#### *Igneous and Metamorphic Rocks*

Igneous and metamorphic rock cores are handled differently from sedimentary cores. Once on deck, the core catcher is placed at the bottom of the core liner and total core recovery is calculated by shunting the rock pieces together and measuring to the nearest centimeter. The core is then cut into 1.5-m-long sections and transferred to the lab.

The contents of each section are transferred into 1.5-m-long sections of split core liner, where the bottom of oriented pieces (i.e., pieces that clearly could not have rotated top to bottom about a horizontal axis in the liner) are marked with a red wax pencil. This is to ensure that orientation is not lost during the splitting and labeling process. The core is then split into archive and working halves. A plastic spacer is used to separate individual pieces and/or reconstructed groups of pieces in the core liner. These spacers may represent a substantial interval of no recovery. Each piece is numbered sequentially from the top of each section, beginning with number 1; reconstructed groups of pieces are assigned the same number, but are lettered consecutively. Pieces are labeled only on external surfaces. If the piece is oriented, an arrow is added to the label pointing to the top of the section.

The working half of the hard-rock core is then sampled for shipboard laboratory studies. Records of all samples are kept by the curator at ODP headquarters. Minicore samples are routinely taken for physical properties and magnetic studies. Some of these samples are later subdivided for thin-sectioning, so that as many measurements as possible are made on the same pieces of rock. At least one minicore is taken per lithological unit when recovery permits, generally from the freshest areas of core. Additional thin sections and XRD samples are selected from areas of particular interest. Samples for shore-based studies are selected in a sampling party held after drilling has ended.

The archive half is described visually, then photographed with both black-and-white and color film, one core at a time. Both halves of the core are then shrink-wrapped in plastic to prevent rock pieces from vibrating out of sequence during transit, put into labeled plastic tubes, sealed, and transferred to cold-storage space aboard the drilling vessel.

## VISUAL CORE DESCRIPTION

### Sediment "Barrel Sheets"

The core description forms (Fig. 3), or "barrel sheets," summarize the data obtained during shipboard analysis of each sediment core. The following discussion explains the ODP conventions used in compiling each part of the core-description forms and the exceptions to these procedures adopted by the Leg 129 scientific party.

### Sediments and Volcaniclastic Deposits

Shipboard sedimentologists were responsible for visual core logging, smear slide analyses, and thin-section descriptions of sedimentary and volcaniclastic material. Mineral composition data, determined by X-ray diffraction, were used to augment the visual core descriptions. Data on biostratigraphy (age), geochemistry ($CaCO_3$, $C_{org}$), magnetics, and physical properties (wet-bulk density and porosity), were integrated with the sedimentological information.

### Core Designation

Cores are designated using leg, site, hole, core number, and core type as discussed in a preceding section (see "Numbering of Sites, Holes, Cores, and Samples" section, this chapter). The cored interval is specified in terms of meters below sea level (mbsl) and meters below seafloor (mbsf). On the basis of drill-pipe measurements (DPM), reported by the SEDCO coring technician and the ODP operations superintendent, depths are corrected for the height of the rig floor dual elevator stool above sea level to give true water depth and correct mbsl.

### Graphic Lithology Column

The lithology of the material recovered is represented on the core description forms, by a single symbol or by two or more symbols (see Fig. 4). Where an interval of sediment or sedimentary rock is a mixture, the constituent categories are separated by a solid vertical line, with each category represented by its own symbol. In an interval composed of two or more sediment types that have quite different composition, such as thin-bedded and highly variegated sediments, the average relative abundances of the constituents are represented graphically by dashed lines that vertically divide the interval into appropriate fractions as described above.

The graphic lithology column only shows the composition of layers or intervals exceeding 10 cm in thickness. Information on finer-scale lithologic variations is included in the VCD (visual core description) forms available from ODP upon request.

Where sedimentary material was intercalated with igneous rocks, the igneous petrologists described the igneous section and recorded results under "Hard Rock Core Description Forms." These are referred to on the sedimentary barrel sheets as "see igneous rock description."

### Sedimentary Structures

In sediment cores, natural structures and structures created by the coring process can be difficult to distinguish. Natural structures observed are indicated in the "Sedimenta-

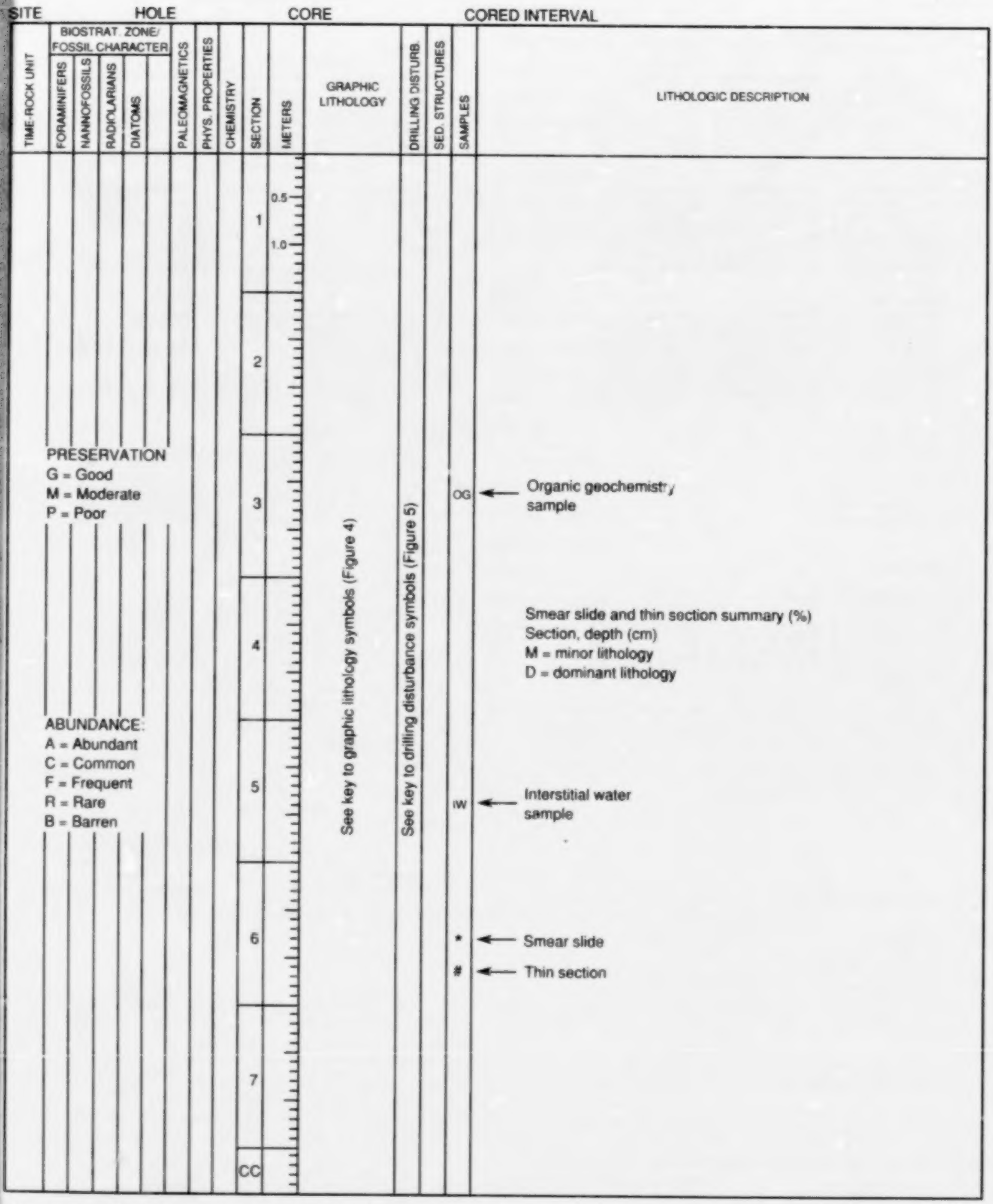
SITE
HOLE
CORE
CORED INTERVAL
TIME-ROCK UNIT
BIOSTRAT. ZONE/ FOSSIL CHARACTER
FORAMINIFERS
NANNOFOSSILS
RADIOLARIANS
DIATOMS
PALEOMAGNETICS
PHYS. PROPERTIES
CHEMISTRY
SECTION
METERS
GRAPHIC LITHOLOGY
DRILLING DISTURB.
SED. STRUCTURES
SAMPLES
LITHOLOGIC DESCRIPTION
0.5
1.0
1
2
3
4
5
6
7
CC
OG
IW
*
#

PRESERVATION
G = Good
M = Moderate
P = Poor

ABUNDANCE:
A = Abundant
C = Common
F = Frequent
R = Rare
B = Barren

See key to graphic lithology symbols (Figure 4)

See key to drilling disturbance symbols (Figure 5)

Organic geochemistry sample

Smear slide and thin section summary (%)
Section, depth (cm)
M = minor lithology
D = dominant lithology

Interstitial water sample

Smear slide

Thin section

Figure 3. Core description form ("barrel sheet") used for sediments and sedimentary rocks.

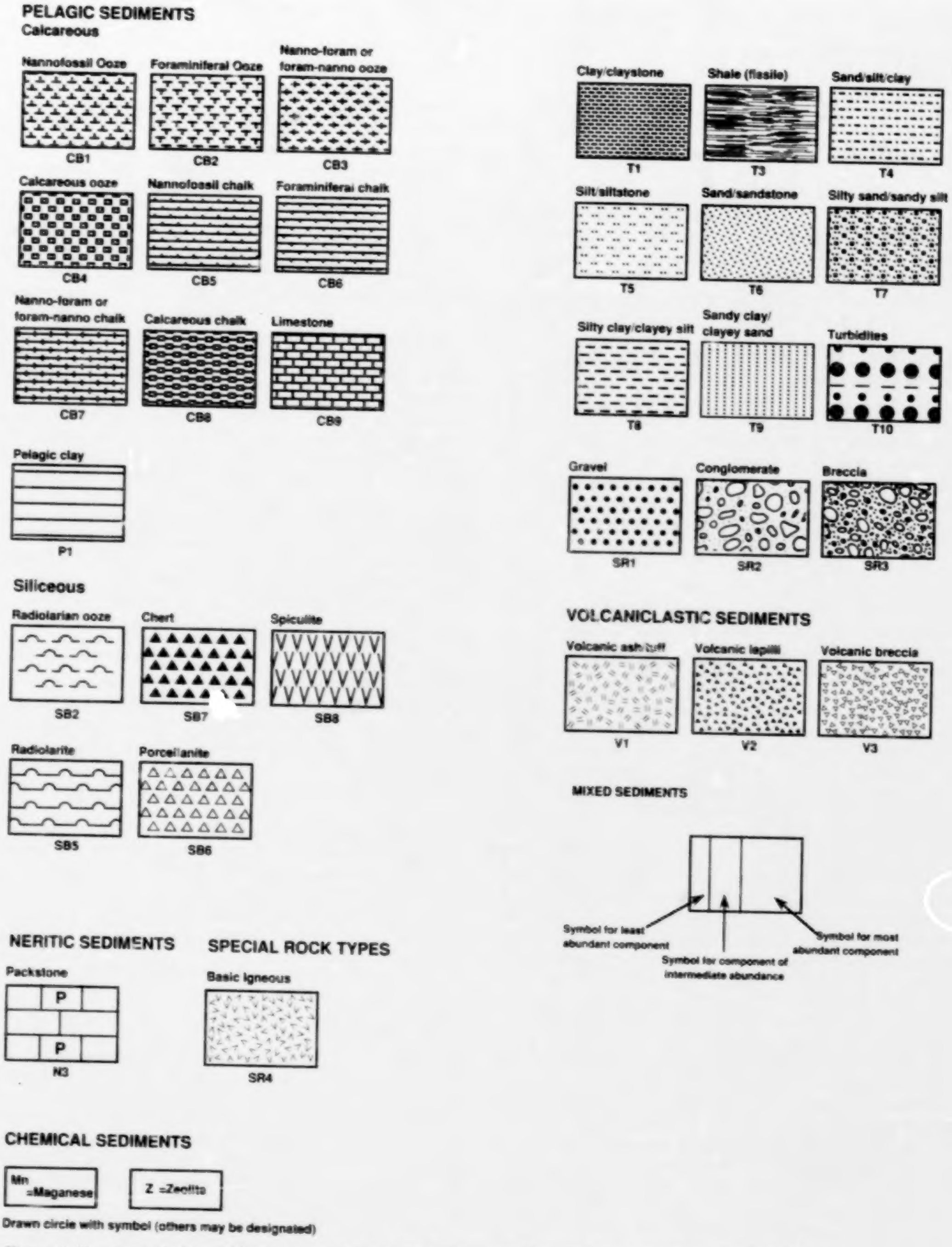
PELAGIC SEDIMENTS
Calcareous
Nannofossil Ooze
Foraminiferal Ooze
Nanno-foram or foram-nanno ooze
CB1
CB2
CB3
Calcareous ooze
Nannofossil chalk
Foraminiferal chalk
CB4
CB5
CB6
Nanno-foram or foram-nanno chalk
Calcareous chalk
Limestone
CB7
CB8
CB9
Pelagic clay
P1
Siliceous
Radiolarian ooze
Chert
Spiculite
SB2
SB7
SB8
Radiolarite
Porcellanite
SB5
SB6
Clay/claystone
Shale (fissile)
Sand/silt/clay
T1
T3
T4
Silt/siltstone
Sand/sandstone
Silty sand/sandy silt
T5
T6
T7
Silty clay/clayey silt
Sandy clay/ clayey sand
Turbidites
T8
T9
T10
Gravel
Conglomerate
Breccia
SR1
SR2
SR3
VOLCANICLASTIC SEDIMENTS
Volcanic ash/tuff
Volcanic lapilli
Volcanic breccia
V1
V2
V3
MIXED SEDIMENTS
Symbol for least abundant component
Symbol for component of intermediate abundance
Symbol for most abundant component
NERITIC SEDIMENTS
Packstone
P
P
N3
SPECIAL ROCK TYPES
Basic Igneous
SR4
CHEMICAL SEDIMENTS
Mn =Maganese
Z =Zeolite
Drawn circle with symbol (others may be designated)

Figure 4. Key to symbols used in the "graphic lithology" column on the core description form shown in Figure 3.

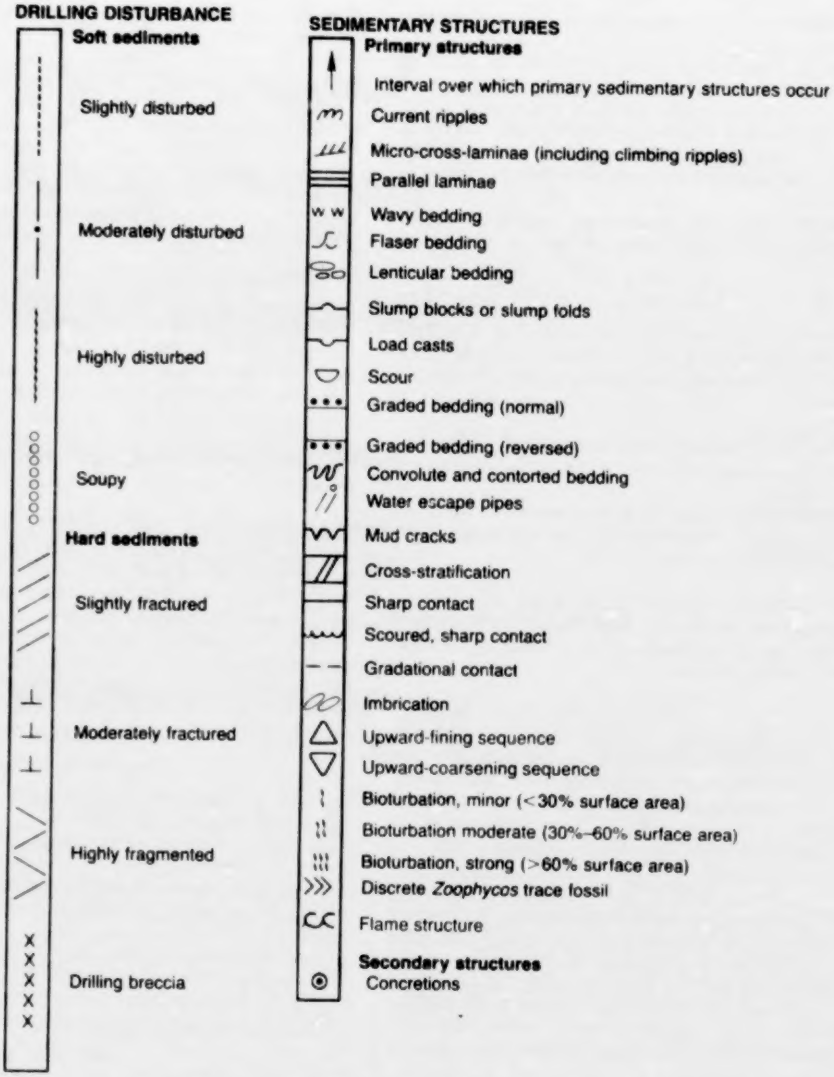
DRILLING DISTURBANCE
Soft sediments
Slightly disturbed
Moderately disturbed
Highly disturbed
Soupy
Hard sediments
Slightly fractured
Moderately fractured
Highly fragmented
Drilling breccia
SEDIMENTARY STRUCTURES
Primary structures
Interval over which primary sedimentary structures occur
Current ripples
Micro-cross-laminae (including climbing ripples)
Parallel laminae
Wavy bedding
Flaser bedding
Lenticular bedding
Slump blocks or slump folds
Load casts
Scour
Graded bedding (normal)
Graded bedding (reversed)
Convolute and contorted bedding
Water escape pipes
Mud cracks
Cross-stratification
Sharp contact
Scoured, sharp contact
Gradational contact
Imbrication
Upward-fining sequence
Upward-coarsening sequence
Bioturbation, minor (<30% surface area)
Bioturbation moderate (30%–60% surface area)
Bioturbation, strong (>60% surface area)
Discrete Zoophycos trace fossil
Flame structure
Secondary structures
Concretions

Figure 5. Symbols used for drilling disturbance and sedimentary structures on core description forms shown in Figure 3.

Structure" column of the core description form. The nbols used to describe the primary biogenic and physical imentary structures, and secondary structures such as rofaults, dewatering veinlets, and mineral-filled fractures, given in Figure 5. Two new symbols were added to the al key. A wavy line indicates the presence of flame ictures, which are common in turbidites. Triangles with erent heights represent turbidite beds fining upwards.

### Sediment Disturbance

This is illustrated in the "Drilling Disturbance" column on core description form (using the symbols in Fig. 5). Blank ons indicate a lack of drilling disturbance. Drilling disturbance is recognized for soft and firm sediments using these categories:

1. Slightly deformed: Bedding contacts are slightly bent.
2. Moderately deformed: Bedding contacts have undergone extreme bowing.
3. Highly deformed: Bedding is completely disturbed, sometimes showing symmetrical diapir-like or flow structures.
4. Soupy: Intervals are water-saturated and have lost all aspects of original bedding.

The degree of fracturing in indurated sediments and igneous rocks is described using the following categories:

1. Slightly fractured: Core pieces are in place and contain little drilling slurry or breccia;

2. Moderately fragmented: Core pieces are in place or partly displaced, but original orientation is preserved or recognizable (drilling slurry may surround fragments);

3. Highly fragmented: Pieces are from the interval cored and probably in correct stratigraphic sequence (although they may not represent the entire section), but original orientation is completely lost;

4. Drilling breccia: Core pieces have lost their original orientation and stratigraphic position and may be mixed with drilling slurry.

### Induration

The criteria used to determine the induration of pelagic sediments found during Leg 129 are those of Gealy et al. (1971). These criteria are subjective and provide three classes for pelagic oozes:

1. Soft: Sediments that have little strength and are readily deformed under the finger or broad blade of the spatula are termed oozes or clay.

2. Firm: Partly lithified pelagic sediments as oozes or clays are readily deformed under the fingernail of the edge of a spatula blade.

3. Hard: Nonfriable, cemented rocks.

The suffix "-stone" is added to the name of cemented rocks (e.g., limestone, claystone). Hard siliceous sedimentary rocks are called chert or porcellanite (see "Sediment Classification" section, this chapter).

### Color

Colors were determined by comparison with Munsell soil-color charts. Colors were determined immediately after the cores were split because redox-associated color changes may occur when deep-sea sediments are exposed to the atmosphere. Information on core colors is given in the text of the "Lithologic Description" on the core description forms.

### Samples

The position of samples taken from each core for shipboard analysis is indicated in the "Samples" column on the core description form (Fig. 3). The symbol "*" indicates the location of smear slide samples, and the symbol "#" indicates the location of thin-section samples. The notations IW and OG designate the location of samples for whole-round interstitial water geochemistry and frozen organic geochemistry, respectively.

### Smear Slide Summary

A table summarizing data from smear slides and thin sections appears on each core-barrel description form. The table includes information on the sample location, whether the sample represents a dominant ("D") or a minor ("M") lithology in the core, and the estimated percentages of sand, silt, and clay, together with all identified components. Note that smear slide analyses tend to underestimate the abundance of foraminifers and volcaniclastic-detrital material because these larger grains are difficult to incorporate into the smear.

### Lithologic Description–Text

The lithologic description that appears on each core description form (barrel sheet) consists of two parts: (1) a heading that lists all the major sediment types (see "Sediment Classification" section, this chapter) observed in the core; and (2) a more detailed description of these sediments, including data on color, location in the core, significant features, etc. Descriptions and locations of thin, interbedded, or minor lithologies are included in the text.

### Paleontological Data

Microfossil abundance, preservation, and zone assignment appear on the core description form under the heading "Biostrat. Zone/Fossil Character." The chronostratigraphic unit, as recognized on the basis of paleontological results, is shown in the "Time-Rock Unit" column. Detailed information on the zonations and terms used to report abundance and preservation is presented in the "Biostratigraphy" section (this chapter).

### Paleomagnetic, Physical Property, and Chemical Data

Columns are provided on the core description form to record paleomagnetic results (normal, reversed, or unknown polarity, shown as "N," "R," or "?," respectively), physical properties values (wet-bulk density and porosity), and chemical data (percentages of $CaCO_3$ determined with the coulometrics analyzer). Additional information on shipboard procedures for collecting these types of data appears in the "Paleomagnetics," "Physical Properties," and "Organic Geochemistry" sections (this chapter).

## SEDIMENT CLASSIFICATION

The standard DSDP/ODP sediment classification scheme (Supko et al., 1978, with some amendments, was used during Leg 129. Because of the abundance of cherts and porcellanites, extended comments are included on the identification of siliceous sedimentary rocks. A summary of the lithologic classification scheme is shown in Figures 6 through 8. The major component of a sediment type is always listed last in the name, and qualifiers are used as long as the components are present with greater than 25% in smear slides.

### Biogenic Sediments

Biogenic sediments are distinguished by biogenic carbonate or/and biogenic silica contents in excess of 30%.

1. Pelagic biogenic oozes contain more than 60% of biogenic components such a nannofossils, foraminifers, radiolarians, diatoms, or silicoflagellates, and are then named appropriately (i.e., siliceous ooze, nannofossil ooze, radiolarian chalk).

2. Transitional biogenic sediments contain 30%–60% biogenic components and more than 40% silt or clay. Sediment names for these materials contain appropriate modifiers (i.e., clayey calcareous ooze or silty limestone).

### Pelagic Clays

Pelagic clays which contain less than 30% biogenic components are mainly composed of "residual" pelagic material that accumulated at very slow rates. The various fine-grained components of pelagic clays formed during erosion or nondeposition of biogenic phases include: detrital clay minerals and quartz deposited through eolian transport, authigenic silicates such as clay minerals and zeolites, abundant iron oxides as small aggregates mixed with clays, micronodules of iron and manganese oxides, volcanogenic components (glass, basaltic minerals, palagonite), fish remains, and cosmic particles.

### Classification of Siliceous Deposits

Hard sedimentary rocks found during Leg 129 are mainly chert, porcellanite, and limestone. Chert and porcellanite are field terms based on easily observable physical properties; these names are *not* strictly dependent on mineralogy. Cherts and porcellanites can each be composed of either diagenetic quartz (microcrystalline, cryptocrystalline, or chalcedonic varieties) or opal-CT (opal-cristobalite/tridymite). Chert has a

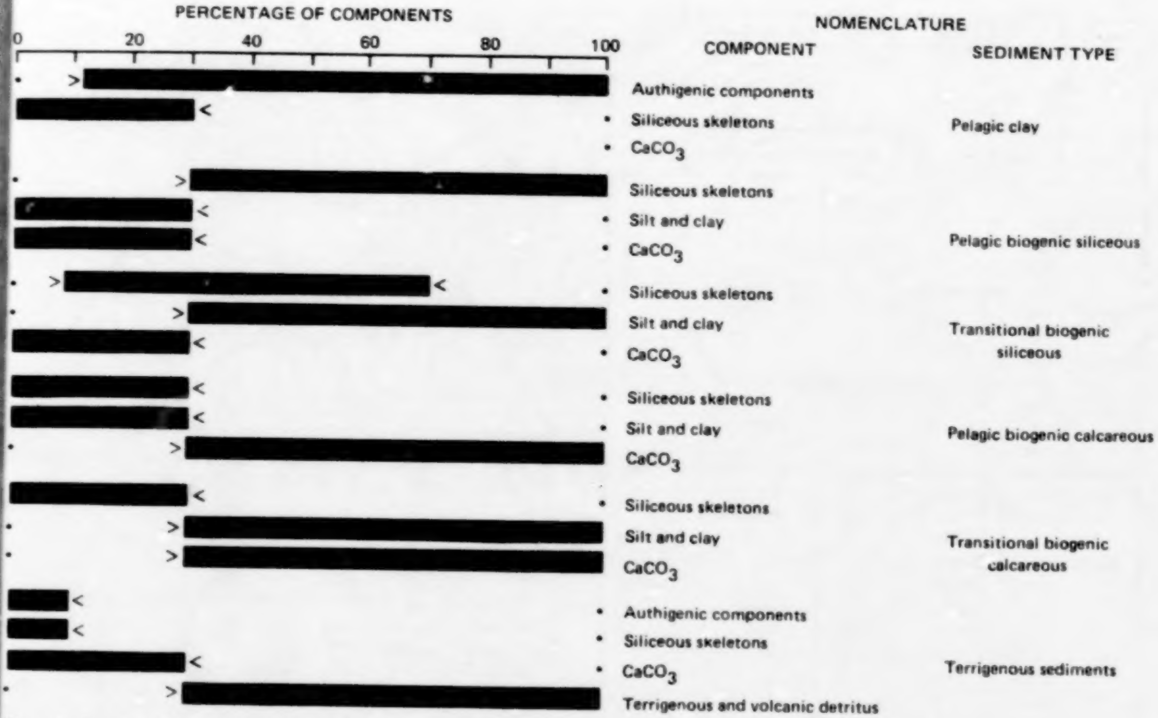

Figure 6. Summary chart of lithologic classification for oceanic sediments used during Leg 129.

glassy to waxy luster, smooth fracture surface, conchoidal fracture, and hardness near 6.3–7.0. Porcellanite has a dull luster, matte to rough surface texture, blocky fracture, and hardness near 4.0–5.5.

Wood- and plastic-handled probes with steel needle tips were used to discriminate between these two lithologies. The steel usually has a hardness of about 5.5–6.0. When a streak of metal was left on a sample scraped with a medium-light stroke, the sediment was named chert. If the sample was gouged by the probe, it was called porcellanite.

Although Leg 129 sedimentologists classified these rocks on their physical properties on the core description form, the principal control on these properties is the ratio of silica/clay (Isaacs, 1982). A ratio of 8:1 or higher is typically needed for a siliceous rock to display cherty characteristics; facies with a ratio less than 8:1 will be a porcellanite or siliceous mudstone (e.g., clayey chert, clayey siliceous ooze, clayey radiolarite). The calcite component has much less effect than clay on the physical characteristics of diagenetic siliceous rocks; a rock with a ratio of 4:1 of silica:calcite may still be chert-like, having a vitreous luster and smooth, conchoidal fracture.

### Turbidites

Deposits with graded bedding and locally sharp, scoured bases, cross and planar laminations, and flame structures were described as turbidites. This lithology includes sandstones, siltstones, and claystones (often volcaniclastic) according to the standard grain-size categories and textural classification described earlier (Figs. 6 through 8). A new symbol (T10) was established in the core description form for the normally graded interlayered sand-, silt-, and/or claystones deposited as turbidite beds less than 50 cm thick (Fig. 4).

### Volcanogenic Sediments

Volcanogenic rocks were described according to the textural and compositional schemes of Schmid (1981) and Fisher and Schminke (1984). The textural groups are (1) volcanic breccia or agglomerate, greater than 64 mm, (2) volcanic lapillistone or lapilli tuff, 2–64 mm, and (3) volcanic tuff, or ash if unlithified, less than 2 mm in diameter. Tuffs may be composed of various proportions of as vitric (glass), crystal, or lithic particles.

### Thickness of Lithologic Units

Thickness of lithologic units defined in the sites reports included unrecovered intervals and were extended downcore until the lithology assigned to the next unit was reached. For example, if only 2 cm of brown clay was recovered in Core 129-800A-1R (0–9.4 mbsf), and the uppermost sediments in the next core contained material assigned to a second unit, then Unit I-Brown Clay would be assigned a thickness of 9.4 m.

## BIOSTRATIGRAPHY

The Leg 129 paleontologists chose the following chronostratigraphy for use during the cruise: the time scale of Berggren et al. (1985a, 1985b) for the Cenozoic and the chronostratigraphy and geochronology of Kent and Gradstein (1985), with modifications, for the Early Cretaceous and the Jurassic (Fig. 9).

Preliminary age assignments made on Leg 129 were based mainly on core-catcher samples. Samples from within the cores were examined when fossils were rare or when the need for more a refined age determination seemed necessary. Sample position, abundance, preservation, and age were recorded for each fossil

| MILLIMETERS | | µm | PHI (Ø) | WENTWORTH SIZE CLASS | |
|---|---|---|---|---|---|
| | | | -20 | | |
| | 4096 | | -12 | Boulder (-8 to -12 Ø) | |
| | 1024 | | -10 | | |
| | 256 | | -8 | | |
| | 64 | | -6 | Cobble (-6 to -8 Ø) | |
| | 16 | | -4 | Pebble (-2 to -6 Ø) | GRAVEL |
| | 4 | | -2 | | |
| | 3.36 | | -1.75 | | |
| | 2.83 | | -1.5 | Granule | |
| | 2.38 | | -1.25 | | |
| | 2.00 | | -1.0 | | |
| | 1.68 | | -0.75 | | |
| | 1.41 | | -0.5 | Very coarse sand | |
| | 1.19 | | -0.25 | | |
| | 1.00 | | 0.0 | | |
| | 0.84 | | 0.25 | | |
| | 0.71 | | 0.5 | Coarse sand | |
| | 0.59 | | 0.75 | | |
| 1/2 | 0.50 | 500 | 1.0 | | |
| | 0.42 | 420 | 1.25 | | |
| | 0.35 | 350 | 1.5 | Medium sand | SAND |
| | 0.30 | 300 | 1.75 | | |
| 1/4 | 0.25 | 250 | 2.0 | | |
| | 0.210 | 210 | 2.25 | | |
| | 0.177 | 177 | 2.5 | Fine sand | |
| | 0.149 | 149 | 2.75 | | |
| 1/8 | 0.125 | 125 | 3.0 | | |
| | 0.105 | 105 | 3.25 | | |
| | 0.088 | 88 | 3.5 | Very fine sand | |
| | 0.074 | 74 | 3.75 | | |
| 1/16 | 0.0625 | 63 | 4.0 | | |
| | 0.053 | 53 | 4.25 | | |
| | 0.044 | 44 | 4.5 | Coarse silt | |
| | 0.037 | 37 | 4.75 | | |
| 1/32 | 0.031 | 31 | 5.0 | | |
| 1/64 | 0.0156 | 15.6 | 6.0 | Medium silt | |
| 1/128 | 0.0078 | 7.8 | 7.0 | Fine silt | |
| 1/256 | 0.0039 | 3.9 | 8.0 | Very fine silt | MUD |
| | 0.0020 | 2.0 | 9.0 | | |
| | 0.00098 | 0.98 | 10.0 | Clay | |
| | 0.00049 | 0.49 | 11.0 | | |
| | 0.00024 | 0.24 | 12.0 | | |
| | 0.00012 | 0.12 | 13.0 | | |
| | 0.00006 | 0.06 | 14.0 | | |

Figure 7. Grain-size categories used for classification of volcanogenic and pelagic sediments (from Wentworth, 1922).

group on core description sheets during examination of each sample, and subsequently combined onto barrel sheets.

## Calcareous Nannofossils

### Zonation

#### *Cenozoic Zonation*

Cenozoic calcareous nannofossil zonation applied during Leg 129 included the schemes of Martini (1971) and Okada and Bukry (1980), both regarded as standard. Calibration of nannofossil zonation with geochronology follows Berggren et al. (1985a, 1985b).

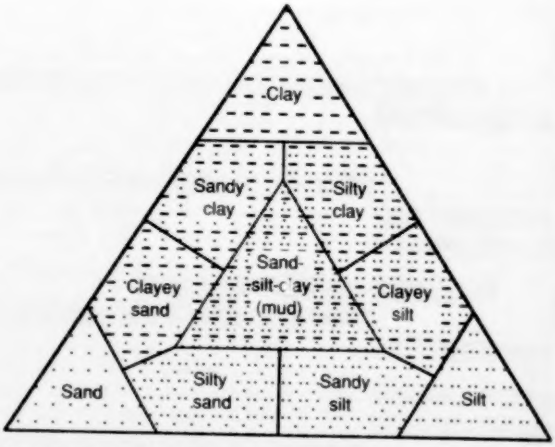

Figure 8. Triangular diagram showing classification scheme used for sedimentary rocks on Leg 129 (after Shepard, 1954).

#### *Mesozoic Zonation*

The zonations of Sissingh (1977), Roth (1978), and Thierstein (1976) used in conjunction with the Kent and Gradstein (1985) time scale were applied to Cretaceous sediments (Fig. 9).

For the Early Cretaceous-Late Jurassic interval, modifications proposed by Bralower (1987) and Bralower et al. (1989), who directly calibrated nannofossil events with magnetic anomalies, were adopted.

### Methods

#### *Abundance*

Total assemblage abundance and species abundances for each sample were estimated by smear slide examination using a light-polarizing microscope at 1250× magnification. A letter code was assigned to represent these abundances and presented in the core description forms ("barrel sheets") as follows:

For total abundance, V = very abundant (>50% of the fine fraction), A = abundant (30% to 50% of the fine fraction), C = common (12% to 30% of the fine fraction), F = few (2% to 12% of the fine fraction), R = rare (<2% of the fine fraction), and B = barren.

For species estimates, V = very abundant (more than 10 specimens per field of view), A = abundant (1–10 specimens per field of view), C = common (1 specimen per 2 to 10 fields of view), F = few (1 specimen per 11 to 100 fields of view), and R = rare (1 specimen per 101 to 1000 fields of view).

#### *Preservation*

Preservation was estimated by the degree of etching and/or overgrowth of calcareous nannofossils. A letter code was assigned as follows: E = excellent (no evidence of overgrowth or etching), G = good (slight overgrowth and/or etching; nannofossils retained the diagnostic characteristics and could therefore be taxonomically differentiated), M = moderate (overgrowth and/or etching partially altered the ultrastructure of nannofossils but diagnostic features were preserved), and P = poor (overgrowth, etching and/or fragmentation highly altered most nannofossils; only a few could be identified).

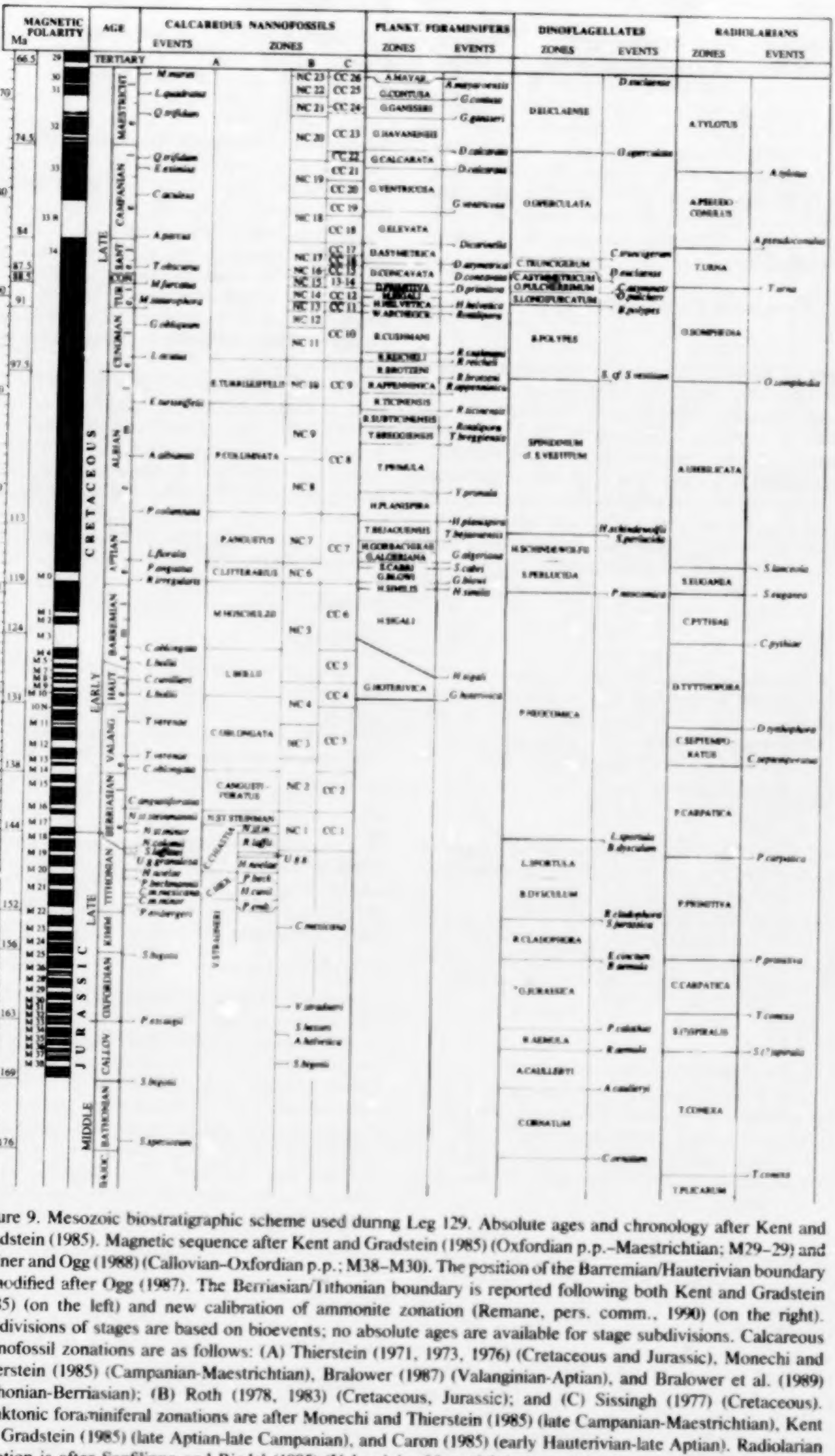

Figure 9. Mesozoic biostratigraphic scheme used during Leg 129. Absolute ages and chronology after Kent and Gradstein (1985). Magnetic sequence after Kent and Gradstein (1985) (Oxfordian p.p.–Maestrichtian; M29–29) and Steiner and Ogg (1988) (Callovian–Oxfordian p.p.; M38–M30). The position of the Barremian/Hauterivian boundary is modified after Ogg (1987). The Berriasian/Tithonian boundary is reported following both Kent and Gradstein (1985) (on the left) and new calibration of ammonite zonation (Remane, pers. comm., 1990) (on the right). Subdivisions of stages are based on bioevents; no absolute ages are available for stage subdivisions. Calcareous nannofossil zonations are as follows: (A) Thierstein (1971, 1973, 1976) (Cretaceous and Jurassic), Monechi and Thierstein (1985) (Campanian-Maestrichtian), Bralower (1987) (Valanginian-Aptian), and Bralower et al. (1989) (Tithonian-Berriasian); (B) Roth (1978, 1983) (Cretaceous, Jurassic); and (C) Sissingh (1977) (Cretaceous). Planktonic foraminiferal zonations are after Monechi and Thierstein (1985) (late Campanian-Maestrichtian), Kent and Gradstein (1985) (late Aptian-late Campanian), and Caron (1985) (early Hauterivian-late Aptian). Radiolarian zonation is after Sanfilippo and Riedel (1985) (Valanginian-Maestrichtian), modifications of Matsuoka and Yao (1985, 1986) (Bajocian-early Valanginian). Dinoflagellate zonation is after Williams (1977).

*Sample Preparation*

Smear slides were prepared for all samples, and investigated with a light-polarizing microscope using transmitted light, phase contrast, and cross-polarized light. Sample preparation was kept simple in order to retain the original nannofossil assemblages. No centrifuge or ultrasonics were applied. A small quantity of sediment was smeared onto a cover glass with a drop of water using a flat toothpick. The suspension was immediately dried on a hotplate. The cover glass was then permanently mounted on a glass slide using optical adhesive and exposed to ultraviolet light for a minimum of 15 min to cure the mounting medium.

## Planktonic Foraminifers

### Zonation

The zonations of Blow (1969) and Bolli and Saunders (1985) were used for the Neogene. Berggren and Miller's (1988), Bolli and Saunder's (1985), and Toumarkine and Luterbacher's (1985) zonations were used for the Paleogene. For the Cretaceous the zonations reported by Caron (1985), Kent and Gradstein (1985), and Monechi and Thierstein (1985) were followed. Calibration of planktonic foraminiferal zonation with chronostratigraphy and geochronology followed Berggren et al. (1985a, 1985b) for the Cenozoic and Kent and Gradstein (1985) for the Cretaceous (Fig. 9).

### Methods

*Abundance*

Foraminiferal abundance for each sample as reported in the core description forms ("barrel sheets") was based on the following percentage scales: A = abundant (>20% of the picked sample), C = common (10%–20% of the picked sample), F = few (2%–10% of the picked sample), R = rare (<2% of picked sample), and B = barren.

*Preservation*

The following terms were used to describe the state of foraminiferal preservation: E = excellent (specimens complete with well preserved fine detail), G = good (some specimens fractured or distorted but with good preservation of fine detail), M = moderate (specimens fractured or distorted, and lacking some fine detail), and P = poor (specimens fractured or distorted, fine detail absent or overgrown).

*Sample Preparation*

Samples of approximately 20 $cm^3$ were processed for foraminifers by kiln-drying the samples and treating with a 1% Calgon solution. Samples were then wet-sieved through a 38-$\mu$m screen and oven-dried. Residues were divided as necessary with a microsplitter and hand-picked for all foraminifers greater than 38 $\mu$m in size. Specimens were mounted in 64 cell reference slides.

## Radiolarians

### Zonation

*Cenozoic Zonation*

Radiolarian zonal assignments of Cenozoic samples were based on the tropical zonation of Riedel and Sanfilippo (1978) and subsequent modification in Sanfilippo et al. (1985). Calibration of this zonation with chronostratigraphy and geochronology follows Berggren et al. (1985a, 1985b).

*Mesozoic Zonation*

Figures 9 and 10 show the radiolarian zonation scheme adopted during Leg 129 for Middle Jurassic to Cretaceous sediments and the calibration with the geochronology of Kent and Gradstein (1985). The zonation of Sanfilippo and Riedel (1985) was applied to the Cretaceous sediments except for the Berriasian and early Valanginian. For the Middle Jurassic to early Valanginian interval, the radiolarian zonation of Matsuoka and Yao (1985, 1986) was adopted with modifications. The lowermost Cretaceous *Pseudodictyomitra carpatica* Zone is here defined as an interval zone, although it was originally defined as an assemblage zone (Matsuoka and Yao, 1985). Its base and top are limited by the first occurrences of *P. carpatica* and *Cecrops septemporatus*, respectively. The top of the uppermost Jurassic *Pseudodictyomitra primitiva* Zone is defined by the first occurrence of *P. carpatica*.

Age determinations of sediments for the Middle Jurassic to early Valanginian interval are tentative because radiolarian zones of this interval are not sufficiently dated by other age diagnostic fossils. Age assignments of sediments depended largely on correlation of Matsuoka and Yao's zonation with Baumgartner's (1984, 1987) zonation. His zonation was based primarily on his research of Atlantic and Mediterranean Tethys regions where radiolarian-bearing sequences contain other age diagnostic fossils.

### Methods

*Abundance*

Total abundance of radiolarians was estimated on strewn slides of sieved acid residues. Abundance was recorded on the core description forms ("barrel sheets") as follows: A = abundant (>1000 radiolarians per slide), C = common (101–1000 radiolarians per slide), F = few (11–100 radiolarians per slide), R = rare (1–10 radiolarians per slide), and B = barren.

*Preservation*

Preservation of radiolarian tests in strewn slides was defined as follows: G = good (no or little signs of dissolution and/or fragmentation), M = moderate (dissolution and/or fragmentation evidently observed, but not heavy), and P = poor (dissolution and/or fragmentation effect).

*Sample Preparation*

Strewn slides were prepared and examined for each core catcher and occasionally from other stratigraphic intervals as well. Unconsolidated sediment samples were boiled in Calgon for 5–20 min. Consolidated samples were disaggregated using 5% hydrofluoric acid (HF) for 12–24 hr. The time of treatment varied depending on the degree of induration of the sediments. Carbonate-rich samples were first decalcified in 10% hydrochloric acid (HCl). The samples were sieved and the >46-$\mu$m fraction was examined. The residues, including radiolarian tests, were mounted in Norland Optical Adhesive or Entellan New according to the refractive index of the tests.

## Palynomorphs

### Zonation

At present no standard dinoflagellate zonation is available for the Mesozoic and Cenozoic of the Pacific. Ages are mainly based on the dinoflagellate zonation scheme of Williams (1977). The zones of Williams (1977) are based on range zones, concurrent zones, and well-defined acme zones (Hedberg, 1976). The adopted zonation is correlated to the geochronol-

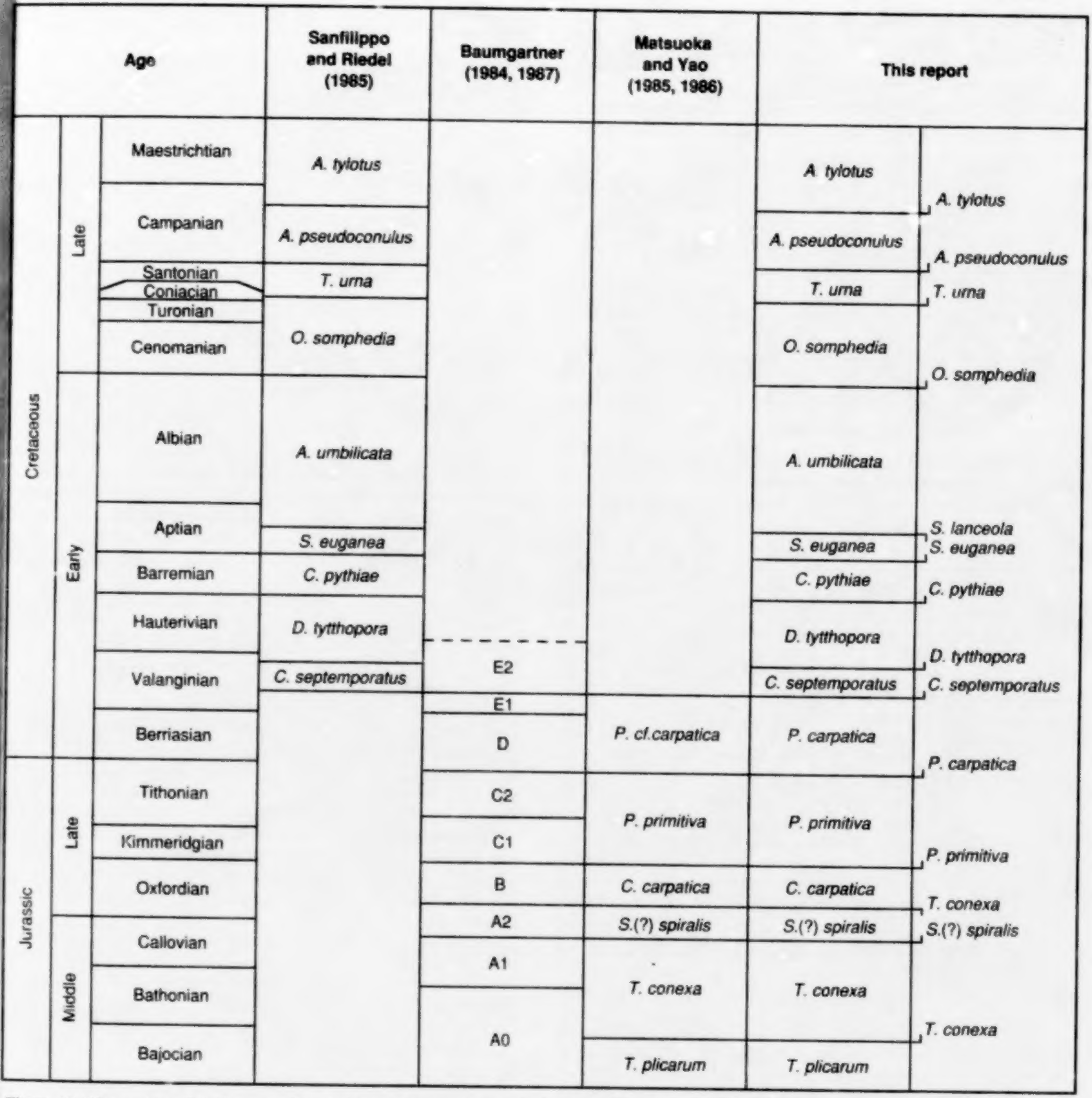
Age
Sanfilippo and Riedel (1985)
Baumgartner (1984, 1987)
Matsuoka and Yao (1985, 1986)
This report
Cretaceous
Late
Early
Jurassic
Late
Middle
Maestrichtian
Campanian
Santonian
Coniacian
Turonian
Cenomanian
Albian
Aptian
Barremian
Hauterivian
Valanginian
Berriasian
Tithonian
Kimmeridgian
Oxfordian
Callovian
Bathonian
Bajocian
A. tylotus
A. pseudoconulus
T. urna
O. somphedia
A. umbilicata
S. euganea
C. pythiae
D. tytthopora
C. septemporatus
E2
E1
D
C2
C1
B
A2
A1
A0
P. cf.carpatica
P. primitiva
C. carpatica
S.(?) spiralis
T. conexa
T. plicarum
A. tylotus
A. pseudoconulus
T. urna
O. somphedia
A. umbilicata
S. euganea
C. pythiae
D. tytthopora
C. septemporatus
P. carpatica
P. primitiva
C. carpatica
S.(?) spiralis
T. conexa
T. plicarum
A. tylotus
A. pseudoconulus
T. urna
O. somphedia
S. lanceola
S. euganea
C. pythiae
D. tytthopora
C. septemporatus
P. carpatica
P. primitiva
T. conexa
S.(?) spiralis
T. conexa

Figure 10. Mesozoic radiolarian zonation and age assignment used during Leg 129. The zonation of Matsuoka and Yao (1985, 1986) was not originally assigned to stages.

ogy of Berggren et al. (1985a, 1985b) for the Cenozoic and to the time scale of Kent and Gradstein (1985) for the Mesozoic (Fig. 9).

### Methods

#### Abundance

The abundance of palynomorphs per slide was registered in the core description forms ("barrel sheets") as follows: A = abundant (>1000), C = common (100–1000), F = few (10–100), and R = rare (1–10).

#### Preservation

Palynomorph preservation was reported as follows: G = good (>75% undamaged specimens, i.e., oxidized, broken, or folded), M = moderate (25%–75% undamaged specimens), and P = poor (<25% undamaged specimens).

#### Sample Preparation

The samples were treated with 35% HCl and sieved through a 17-$\mu$m sieve to remove fine sand and clay. After sieving the residue was put in a watch glass. Rotation of the watch glass concentrated the palynomorphs in the upper and middle part of the solution, where they could be extracted with a pipette. In addition, cherts were treated with 40% HF to dissolve the silicates and then sieved through a 10-μm mesh. Samples were mounted with glycerine jelly.

## PALEOMAGNETISM

Measurements of natural remanent magnetization (NRM) and volume magnetic susceptibility ($K_a$) were performed aboard ship. Progressive demagnetization was undertaken to obtain the characteristic remanent magnetization (ChRM) of the rocks. Aboard ship, alternating field (AF) demagnetization was the only practical method for examining ChRM because of the time factor; the automated AF demagnetization and measurement equipment embodied in the pass-through magnetometer system aboard ship allows a rapid examination of all core material as it is recovered. Most recovered core was measured in this manner, but consequently, no time was left for discrete sampling and demagnetization.

### Instruments

A 2G Enterprises (Model 760R) 3-axis, pass-through cryogenic rock magnetometer was available for measurement of remanence aboard the *JOIDES Resolution* during Leg 129. AF demagnetization equipment (Model 2G600) capable of alternating fields up to 25 mT is integrated with the cryogenic magnetometer. Communications between cryogenic sensors, the AF degaussing system, and the drive motor moving the core were linked through a FASTCOM4 multiserial communications board in an IBM PC AT-compatible computer; all devices and actual measurements of core were controlled by a modified version of the Rhode Island University BASIC program. Leg 129 modifications to this program included superconducting quantum interference devices (SQUID) control commands such that the magnetometer could operate at the 1× scale with flux counting for sediments and 100× for basalts. The spinner magnetometer was not used during Leg 129.

The sensors in the cryogenic magnetometer measure magnetization over an interval of approximately 20 cm. Each axis has a slightly different response curve. The widths of the sensor regions are such that up to 150 $cm^3$ of core contributes to the sensor response at any measurement instant. The large volume of core material within the sense region permits determination of remanence for even weakly magnetized samples despite the relatively high background noise related to the motion of the ship.

### Sediments

Remanence measurements of sediments were performed by passing archive-half sections through the cryogenic magnetometer. In cores where recovery consisted of discrete fragments, these fragments were taped in the magnetometer tray with bedding planes perpendicular to the magnetometer's "z" axis; to compensate for the size of the sense region, samples were separated by 10 cm. Depending on the lithology, measurements were taken at 2-, 3-, or 5-cm spacings. The AF strengths used also depended on lithology; generally, most core segments were demagnetized to 15 mT.

### Basalts

Basalts from Leg 129 were measured in much the same fashion as the sediments. Basalt cores generally were run as whole sections. The excessive weight of the whole sections occasionally required that they be divided into two (or three) parts and run separately; this required individual pieces to be taped into the magnetometer tray, spaced apart as described for the chert fragment measurements. More detailed AF demagnetization steps were used for the basalts than for the sedimentary rocks, again generally concluding with 15 mT.

### Magnetic Susceptibility Measurements

Magnetic susceptibility was measured for Sites 801 and 802. A Bartington Instruments magnetic susceptibility meter (model M.S.1) with an M.S.1/CX 80-mm whole-core sensor loop set at 0.47 kHz (range 1) was used for sediment measurements. The susceptibility meter is on-line with the GRAPE and *P*-wave logger on the MST. Igneous rock susceptibility was measured using the type MS1B sensor unit. Whole cores were measured, prior to splitting. Only those cores having sufficient volume recovery were run.

## INORGANIC GEOCHEMISTRY

### Interstitial Water Sampling and Chemistry

Shipboard interstitial water analyses were performed on 5- to 10-cm-long whole-round sections that were cut from the core immediately after it arrived on deck. Interstitial waters were obtained by squeezing using a titanium and stainless steel piston modified after Manheim and Sayles (1974). Before squeezing, the core surfaces were carefully scraped with a spatula to remove the potentially contaminated exterior of the sample. Then the core was placed into the piston and squeezed using a hydraulic press at pressure up to 240 MPa. The water was collected in a plastic syringe and filtered through a 0.2-μm disposable filter.

Interstitial water samples were routinely analyzed for *alkalinity, pH, and salinity and for chlorine (Cl), sulfate* ($SO_4$), calcium (Ca), and silicon (Si) concentrations using the analytical technique described in Gieskes and Peretsman (1986). Magnesium (Mg), potassium (K), manganese (Mn), and strontium (Sr) concentrations were measured via atomic absorption. Most measurements were calibrated on the International Association of Physical Sciences Organizations (IAPSO) standard seawater. Results are expressed in milli- or micromole per liter of solution, taking 1.024 $g/cm^3$ for the density of sample water. Sodium concentrations were calculated by charge balance ($Na^*$); the difference between calculated salinity using $Na^*$ data and measured salinity never exceeds 3%. Chemical data are reported in tables in each site chapter in this volume. Sub-bottom depths given have been rounded to the nearest meter.

Alkalinity and pH were determined using a Metrohm autotitrator with a Brinkmann combination pH electrode. Alkalinity reproducibility is better than 5%; data are given in millimoles of acid equivalent per liter.

Salinity was determined using a Goldberg optical hand refractometer measuring the total dissolved solids. Values are given in weight per mil.

Chlorinity was measured by silver nitrate titration of 0.1 mL of sample diluted in 5 mL of deionized water using potassium chromate as an indicator. Reproducibility on the IAPSO standard is better than ±0.6%.

Sulfate concentration was measured by ion chromatography. Samples of 0.1 mL diluted to 50 mL with deionized water were used. Reproducibility on different dilutions of the IAPSO standard is better than ±2%.

Calcium was determined by titration of a 0.5-mL sample with EGTA using GHA as an indicator. Near the endpoint, the Ca-GHA complex was extracted into a layer of butanol to enhance the precision. No correction was made for Sr that is included in the results. Reproducibility is ±0.7% on the IAPSO standard.

Silica was determined by production of silicomolybdate complex and its reduction to give a blue color on a 0.1-mL sample. Absorption was measured at 812 nanometers. Reproducibility is ±3%.

Atomic absorption measurements were done with a Varian SpectrAA-20 spectrophotometer to determine Mg, Mn, K, and Sr concentrations. All measurements were done in absorption mode using an oxidizing air-acetylene flame.

Magnesium was analyzed on 1:1,000 to 1:10,000 solutions of the samples. Lanthanum trichloride (10,000 ppm) was used as a realizing agent in the sample solution and in the standards. Reproducibility varies from ±0.5% at 54 mmol/L concentration to ±2% at 5 mmol/L concentration.

Potassium was determined on 1:100 to 1:500 sample solutions with 1,000 ppm cesium chloride as ionization suppressor. Reproducibility is ±3%.

Strontium concentrations were measured on 1:10 to 1:50 solutions of the samples. Lanthanum trichloride (10,000 ppm) was used as a realizing agent in the sample solution and in the standards. Reproducibility is better than ±2%.

Manganese concentrations were analyzed on 1:5 solutions of the samples without releasing agent. Reproducibility is better than ±2%.

### Carbonate, Organic Carbon, and Sulfur Content Determinations

Samples of both sediment and basaltic crust were analyzed aboard ship for inorganic carbon, total carbon, and sulfur. Analyses are presented in the "Sedimentology" and "Igneous Petrology" sections of the site chapters in this volume. Sediment $CaCO_3$ data are reported on the core description forms ("barrel sheets"). Measurements were done on most of the samples used for physical properties measurements, on samples of the interstitial water squeeze-cake, and on some additional samples. All samples were about 10 $cm^3$ in size and were freeze-dried prior to powdering. Samples were weighed with a Cahn 29 Automatic Electrobalance, which averages a total of 50 weight measurements to compensate for ship heave. Organic carbon is calculated as the difference between total carbon and inorganic carbon. Results are expressed in weight percent (wt%). Inorganic carbon is expressed in wt% equivalent of $CaCO_3$.

Total inorganic carbon concentrations were obtained using a coulometric 5011 Coulometer equipped with a system 140 carbonate carbon analyzer. About 60 mg of each sample was reacted in 2-ml 2N HCl solution; the liberated $CO_2$ was carried into a coulometric cell where it reacted in a monoethanolamine solution with a colorimetric indicator. The change in absorbance was monitored by a photocell. Frequent blank and standard runs indicated a relative error of ±1%.

Total carbon and sulfur content were determined using a CNS Carlo Erba analyzer NA 1500. Vanadium pentoxide was added to a sample of about 30 mg in a tin container, which was flash-combusted at more than 2000°C in an oxygen atmosphere. The oxidized species were driven by a helium flux through (1) an oxidation catalyst, (2) a copper reduction reactor to remove $O_2$ and transform $SO_x$ into $SO_2$, (3) a Mg perchlorate filter to remove $H_2O$, (4) a chromatographic column to separates the different gases, and (5) a thermal conductivity detector to measure the concentrations of gases. Blanks, standards, and duplicates give a reproducibility of ±1% and ±0.02% as a limit detection level.

## PHYSICAL PROPERTIES

Shipboard measurement of physical properties provides information that aids characterization of lithologic units, allows verification of downhole geophysical logging results, and provides constraints on interpretation of seismic reflection and other geophysical data. Furthermore, these data are used in paleoceanographic interpretation of sedimentary units, heat-flow calculations, and determination of the mechanical state of sediments and rocks.

Physical properties measurements made on cores recovered during Leg 129 included index properties, compressional-wave velocity, and thermal conductivity. Samples were chosen to be representative of the core or section as a whole, and were taken in areas of least disturbance. Sample selection and spacing depended on the core recovery and the thickness and homogeneity of the recovered sequences. All measurements were conducted on discrete samples taken from split cores, with the exception of thermal conductivity measurements of soft sediments that were made at discrete intervals in whole-round core sections. Continuous measurements of wet-bulk density and compressional-wave velocity, provided by the gamma-ray attenuation porosity evaluator (GRAPE) and IOS compressional-wave core logger (*P*-wave logger) incorporated in the multisensor track, were not made because sediments and rocks typically did not completely fill core liners, or, in the recovery of soft sediments, because the cores were too highly disturbed by rotary coring.

### Compressional-Wave Velocity

Compressional-wave velocity measurements were taken on discrete samples that were sufficiently competent to provide adequate signal strength. All velocity measurements were made at atmospheric pressure and involved the determination of the traveltime of a 500-kHz compressional wave through a measured thickness of sample, using a Hamilton Frame Velocimeter and Tektronix DC 5010 counter/timer system. Samples of soft sediment were taken with a parallel-sided sampling tool or carefully cut from the cores. A double-bladed diamond saw was used to cut samples from lithified sediments and basement rocks. Sample thickness was measured directly from the velocimeter-frame lead screw. Zero traveltimes for the velocity transducers were estimated by linear regression of traveltime vs. distance for a series of aluminum and lucite standards. Filtered seawater was used to improve the acoustic contact between the sample and the transducers. Estimated accuracy of the velocity measurements is ±2% (Boyce, 1976). Compressional-wave velocity was measured for both vertical (perpendicular to bedding) and horizontal (parallel to bedding) propagation directions for all samples that were large enough and sufficiently indurated to be cut perpendicular to bedding with the double-bladed saw. Velocity anisotropy was calculated from the vertical velocity ($Vv$) and horizontal velocity ($Vh$) values following the expression of Carlson and Christensen (1979), where anisotropy (A) is given as the ratio of velocity difference to mean velocity, expressed as a percentage:

$$A = 200(Vh - Vv)/(Vh + Vv). \quad (1)$$

Igneous rocks were treated differently than sedimentary rocks. The curatorial procedures required for igneous rocks involvedrying the samples, which may increase measured velocities by as much as 8% (Hay et al., 1984). Samples cut from the cores were placed in sea water for several hours prior to velocity and index properties measurements in an attempt to resaturate the rock sand minimize the drying-induced error.

### Index Properties

Index properties (bulk density, grain density, water content, and porosity) were calculated from measurements of wet and dry weights and dry volume. Wet-bulk density was also determined using the GRAPE special 2-min count technique (Boyce, 1976). Samples of approximately 10 $cm^3$ were taken for gravimetric determination of index properties. Soft sediment samples were placed in precalibrated aluminum containers prior to weight and volume measurements. Index properties measurements for lithified sediment and basement rock samples were made using sample cubes cut for velocity determinations. The calibrated aluminum containers were not used for weight and volume measurements for the cubes because these samples were larger than the containers. Sample weights were determined aboard ship to a precision of ±0.01 g using a Scitech electronic balance. These measurements were repeatable within ±0.04 g. Wet and dry volumes were determined using a Quantachrome helium-displacement Penta-Pycnometer. Volumes of soft sediment samples were determined using the pycnometer's small sample chamber inserts, whereas volumes for the cube samples were determined in the large-capacity chambers. At Sites 800 and 801, a 70-$cm^3$ displacement volume was added to the chambers to reduce the empty volume and associated measurement error. Volumes of cube samples from Site 802 were measured using inserts fabricated to more closely match the dimensions of the cubes and displace a greater volume in the large-capacity chambers. The Quantachrome pycnometer measures volumes to an approximate precision of $10^{-4}$ $cm^3$. Measurements were typically repeatable to ±0.05 $cm^3$ using the small chamber inserts and ±0.05–0.10 $cm^3$ using the large-capacity chambers. Use of the inserts designed for cube samples improved the accuracy of volume determinations for the cubes. Dry weight and volume measurements were obtained after the samples were oven-dried at 105°C for 24 hr and allowed to cool in a desiccator. All weight and volume measurements were performed in triplicate and averaged to obtain the values used in calculating index properties. A salt correction assuming 35 ppt interstitial fluid salinity was applied to density and porosity computations as per Hamilton (1971).

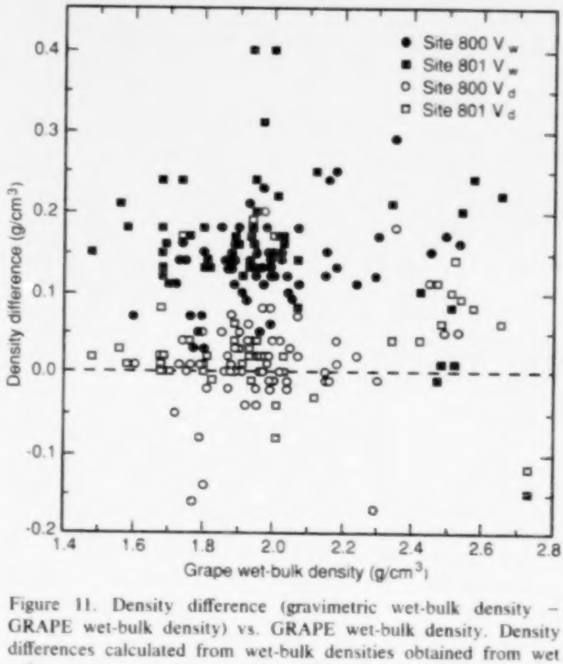

Figure 11. Density difference (gravimetric wet-bulk density − GRAPE wet-bulk density) vs. GRAPE wet-bulk density. Density differences calculated from wet-bulk densities obtained from wet volume measurements are represented by filled circles and squares. Density differences calculated from estimates of wet volume derived from dry volume, dry weight, and wet weight measurements are represented by open circles and squares.

Wet-bulk density was also determined using the GRAPE special 2-min count technique as described by Boyce (1976). The GRAPE measurements were made perpendicular to bedding on half-round samples cut from the cores using the double-bladed saw. All counts for the samples and accompanying air (background) counts were made in duplicate and averaged. Grain density values from gravimetric measurements were used to correct the wet-bulk density determined by the GRAPE for deviation of the grain density of the sample from that of quartz. The precision estimated for this technique is ±1.5% (Boyce, 1976). Wet-bulk density values determined by the 2-min GRAPE technique were used to estimate porosity of samples for which gravimetric measurements were not made. Porosity ($\varphi$) was estimated by assuming a value for grain density ($\delta s$) and using the relationship:

$$\varphi = (\delta s - \delta bw)/(\delta s - \delta f) \tag{2}$$

where $\delta bw$ is wet-bulk density determined by the GRAPE and $\delta f$ is interstitial fluid density, which is assumed to equal 1.024 g/$cm^3$.

Determination of wet-bulk density by gravimetric techniques was initially based on measurement of wet weight ($Ww$) and wet volume ($Vw$) and calculated using the relationship:

$$\delta bw = Ww/Vw. \tag{3}$$

Comparison of the wet-bulk density calculated using equation 3 with that determined by the GRAPE 2-min technique revealed that gravimetric determinations were consistently higher than GRAPE measurements (Fig. 11). The difference between wet-bulk densities determined by the two methods was resolved to be a result of anomalously low wet volume measurements. This source of error was indicated by samples for which the measured wet volume was less than the dry volume and situations in which the calculated wet-bulk density was greater than the grain density. Because of the wet volume measurement errors the calculation of wet-bulk density was changed to include an estimate of wet volume derived from dry volume ($Vd$), wet weight, and dry weight ($Wd$) measurements according to the relationship:

$$Vw = Vd + (Ww - Wd)/\delta f \tag{4}$$

where $\delta f$ is the density of evaporated water and assumed to equal 1. The dry volume, $Vd$, includes both the volume of the sediment or rock constituents and the volume of salt remaining in the sample upon drying. Wet-bulk densities calculated using the above relationship more nearly approximate those obtained using the GRAPE (Fig. 11).

Dry volume measurement errors were encountered in measurements of low porosity cherts and igneous rocks. These errors were manifested as anomalously high dry volumes and low grain densities. The errors were overcome by crushing samples, determining the grain density of the powdered samples, and using the grain density and water content to estimate the dry volume and by increasing the helium purge time for the pycnometer from 2 min to 4 min.

### Thermal Conductivity

The thermal conductivity measurement techniques used during Leg 129 are described by Von Herzen and Maxwell

(1959) and Vacquier (1985). Measurements were made with a Thermcon-85 unit, and all data are reported in units of W/m · K. The estimated error in the measurements is about 5%–10%. All data were corrected for *in-situ* pressure and temperature (Ratcliffe, 1960), assuming hydrostatic pressure and a conductive thermal gradient of about 35°C/km.

### *Soft Sediment "Full-space" Measurements*

To reduce background thermal transients, cores were allowed to equilibrate in their liners until the sediments reached a temperature near that in the lab. A needle probe was inserted in every other section, through holes drilled through the liners. New thermal conductivity software, introduced during Leg 129, allowed the user to monitor sample temperatures (using the thermistors in the needle probes) without applying a current to the heater wires. The actual test sequence can then be delayed until after the background temperature drift in all samples has been reduced to some arbitrary level (in this case 0.04°C/min). Once the samples are fully equilibrated, the heater circuit is closed and the temperature rise of the probes is recorded. Thermal conductivity is calculated from the rate of temperature rise in the probe while a heater current is flowing.

After the heater has been on for about 60 s, the needle probe response is very close to that of a line source with a constant heat generation per unit length. We always used the time interval of 60 to 240 s after the heater was turned on. The temperature rise in the probe should vary logarithmically with time as:

$$T(t) = (q/4\pi k)\ln(t) + \text{const.} \qquad (5)$$

where $k$ is the thermal conductivity, $T$ and $t$ are the temperature and time, respectively, and $q$ is the heat generated per unit length of the probe. From equation 5, the thermal conductivity is derived from the slope of temperature vs. the logarithm of time. When the sediment became too firm to allow easy insertion of the probe, we tested half-round samples, as described below.

### *Hard Rock "Half-space" Measurements*

Thermal conductivity measurements on lithified sediments and rocks were conducted on split cores using the half-space technique (Vacquier, 1985). With this method a rock sample with one flat surface is placed on top of a needle probe that is embedded along the surface of a slab of low conductivity material. The flat surface of the sample is polished with sandpaper to minimize pockets of water or air and thus to assure good contact with the slab containing the needle probe. EE&G thermal conducting compound was also used to improve the thermal contact between the slab and the sample. The sample and needle are immersed in a water bath to maintain a uniform temperature, to avoid cooling by evaporation, and to keep the sample saturated. The data reduction procedure for the half-space method is exactly the same as for the full-space method except that the data must be corrected to account for the geometry of the experiment.

**Table 1. Half-space thermal conductivity standards.**

| Probe | Black rubber | Red rubber | Fused rubber | Macor |
|---|---|---|---|---|
| 1 | 0.340 ± 0.004 | 0.508 ± 0.013 | 0.693 ± 0.018 | 0.825 ± 0.026 |
| 4 | 0.305 ± 0.004 | 0.478 ± 0.009 | 0.661 ± 0.017 | 0.794 ± 0.024 |
| 9 | 0.333 ± 0.005 | 0.520 ± 0.009 | 0.725 ± 0.015 | 0.864 ± 0.008 |
| 211 | 0.315 ± 0.004 | 0.496 ± 0.024 | 0.679 ± 0.018 | 0.838 ± 0.029 |

The original ODP half-space water bath was constructed (on Leg 106) out of a standard thermal conductivity needle probe, a block of epoxy, and a plastic wash basin. The epoxy block was fixed to the bottom of the basin, and the probe was inserted through a hole cut in the side of the basin so that the needle fit in a groove on the top of the epoxy block. The upper surface of the needle was exposed so that the probe would be sandwiched between the sample and the epoxy block. During the early part of Leg 129 we built a larger bath with three probes and epoxy bases so that several samples could be tested at one time.

Because the geometry of the half-space experiment is not perfect (i.e., the needle is never positioned exactly between the sample and epoxy, the sample is not semi-infinite, there is never an ideal thermal contact, the EE&G thermal compound is a heat sink), each block/needle pair was separately calibrated over fixed time intervals. We chose an interval of 60–240 s because (1) before 60 s the temperature vs. log (time) data rarely vary linearly, and (2) after about 240 s the thermal front from the heated needle tends to "feel" the edge of the smaller, more conductive samples. We conducted several hundred experiments with 4 standards in full-space and half-space configurations to establish an empirical relationship between the two (Table 1 Fig. 12). The standard with the highest conductivity, macor, has a conductivity of about 1.61 W/m · K, which is lower than the conductivities of some of the samples. Sample conductivities greater than 1.61 W/m · K thus required that we extrapolate past the range of the standards; these measurements probably have the highest errors.

The following full-space conductivities were determined for each standard (± standard deviation) in full-space configuration using a time interval of 60–240 s: black rubber = 0.544 ± 0.015 W/m · K ($n$ = 8), red rubber = 0.967 ± 0.048 ($n$ = 27), fused silica = 1.536 ± 0.055 W/m · K ($n$ = 28), macor = 1.752 ± 0.058 ($n$ = 27). The fused silica and macor values are both higher than determined elsewhere (1.38 and 1.61 W/m · K, Vaquier, 1985; Shipboard Scientific Party, 1989; M. Langseth, pers. comm., 1989; A. Fisher, unpubl. data), possibly because we were forced to use a lot of the EE&G thermally conductive compound to assure a good contact between the needle and the standards. The excess compound probably acted as a heat sink, simulating unrealistically high conductivities in the full-space tests with fused silica and macor. We did not have this problem with the rubber standards because these materials tend to grip the needles.

We converted half-space values to full-space conductivities by using a least-squares best-fit of the data to derive a linear equation of the form: full-space conductivity = A + B (half-space conductivity). Previously determined full-space conductivities for fused silica and macor were used in these regressions.

## IGNEOUS ROCKS

### Core Curation and Shipboard Sampling

Igneous rocks are split into archive and working halves using a rock saw with a diamond blade. The petrologists decide on the orientation of each cut so as to preserve unique features and/or expose important structures. The archive half is described, and samples for shipboard and shore-based analyses are removed from the working half. Each piece is numbered sequentially from the top of each section, beginning with the number 1. Pieces that can be fitted together (like a

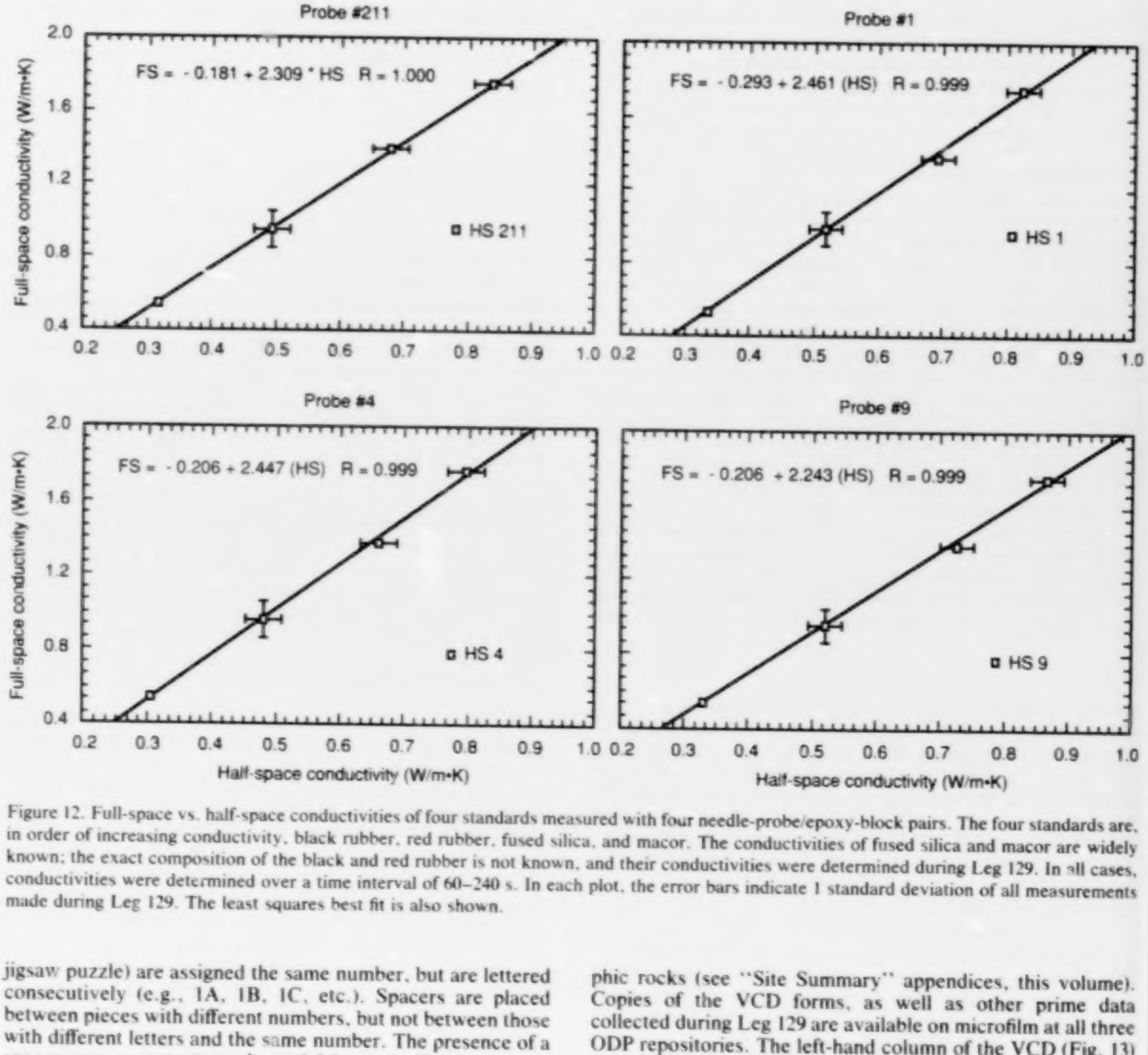

Figure 12. Full-space vs. half-space conductivities of four standards measured with four needle-probe/epoxy-block pairs. The four standards are, in order of increasing conductivity, black rubber, red rubber, fused silica, and macor. The conductivities of fused silica and macor are widely known; the exact composition of the black and red rubber is not known, and their conductivities were determined during Leg 129. In all cases, conductivities were determined over a time interval of 60–240 s. In each plot, the error bars indicate 1 standard deviation of all measurements made during Leg 129. The least squares best fit is also shown.

jigsaw puzzle) are assigned the same number, but are lettered consecutively (e.g., 1A, 1B, 1C, etc.). Spacers are placed between pieces with different numbers, but not between those with different letters and the same number. The presence of a spacer may represent a substantial interval of no recovery. Whenever the original unsplit piece is sufficiently large that the top and bottom can be distinguished before removal from the core liner (i.e., the piece could not have rotated about a horizontal axis in the liner during drilling), a red wax cross is marked on the base of each piece.

Before the rock is dry, sampling is carried out for shipboard physical properties, magnetics, XRD, and thin-section studies. Minicores are taken from the working half and stored in seawater prior to physical properties measurements. Nondestructive measurements of magnetic susceptibility and sometimes thermal conductivity are made on the archive half of the core. The archive half is next described in detail on the VCD form and finally photographed before storage.

## Visual Core Descriptions

Hard rocks sampled from the basement are graphically represented on VCD forms specific to igneous and metamorphic rocks (see "Site Summary" appendices, this volume). Copies of the VCD forms, as well as other prime data collected during Leg 129 are available on microfilm at all three ODP repositories. The left-hand column of the VCD (Fig. 13) is a graphical representation of the archive half. A horizontal line across the entire width of this column denotes a plastic spacer glued between rock pieces inside the liner. The number of each piece is also recorded, with oriented pieces indicated by the presence of an upward-pointing arrow to the right of the relevant piece. Shipboard samples and studies are indicated in the "shipboard studies" column, using the following notation: XRD = X-ray diffraction analysis, PM = magnetic measurements, TSB = thin-section billet, and PP = physical properties measurement.

When cores are described, checklists of macroscopic features are used to ensure consistent and complete descriptions, one for fine- and medium-grained extrusives and dikes, and another for plutonic rocks. The VCD form for fine- and medium-grained igneous rocks requires the following information:

1. The leg, site, hole, core number and type, and section number.

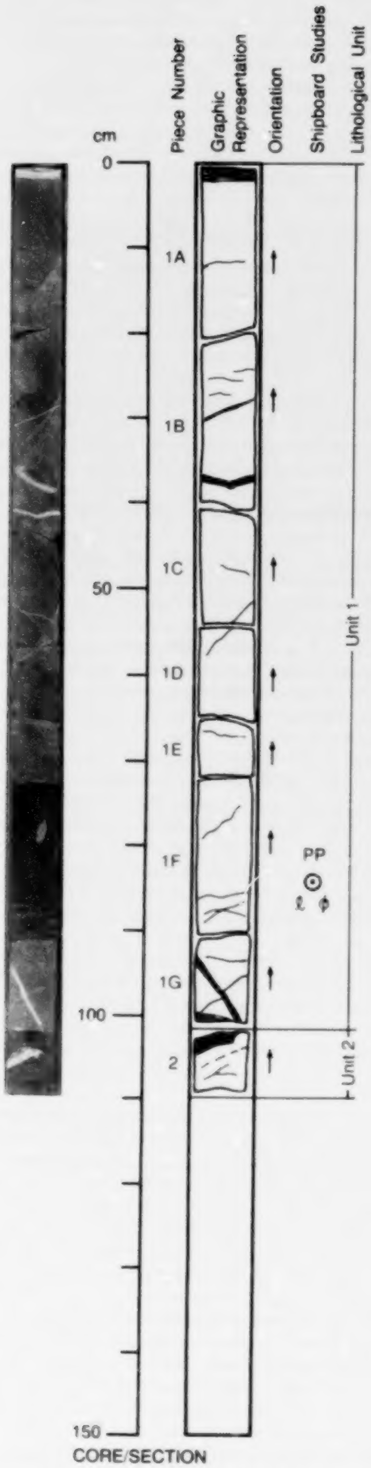

### 129-801C-1R-3

### UNIT 1: APHYRIC MICRODOLERITE GRADING TO SPARSELY PLAGIOCLASE PHYRIC BASALT

### Pieces 1A-1G

**CONTACTS:** Not actually observed, but grain-size fines towards the bottom (cut by veinlet).
**PHENOCRYSTS:**
Plagioclase - 1%; c.1.0; euhedral/subhedral laths, altered to white and green clays.
**GROUNDMASS:** Holocrystalline to hypocrystalline, particularly at bottom. Medium to fine grained, fining towards the bottom.
**VESICLES:** None observed.
**COLOR:** White fine-speckled black (N2)
**STRUCTURE:** Massive, perhaps base of sill or flow.
**ALTERATION:** Moderate. Plagioclase replaced by whitish and greenish clays, some with Fe-hydroxide staining. Generally greenish matrix. Whitish leucoxene associated with relict opaques. Carbonate present along grain boundaries. Short, whitish veinlets present in some areas.
**VEINS/FRACTURES:** 10%; 0.2-13 mm; 0-90 degrees; wide veins (0-45 orientation) and narrow veins (0-90 orinetation), both infilled with carbonate and greenish clays. Veinlets often branching and cross-cutting.
**ADDITIONAL COMMENTS:** Generally finer grained than Sections 1 and 2 and fining steadily towards the base.

### UNIT 2: SPARSELY PLAGIOCLASE-OLIVINE MICROPHYRIC BASALT

### Piece 2

**CONTACTS:** Not actually observed. Well preserved, devitrified glassy margin in contact with veinlet at margin. Glassy rim zone grades downwards to a cryptocrystalline bottom. 45 degree inclination.
**PHENOCRYSTS:**
Plagioclase - 1%; <1; Subhedral/euhedral; mostly altered to carbonate.
Olivine - trace; <1; Subhedral/euhedral (hopper crystal morphology).
**GROUNDMASS:** Ranges from (a) devitrified glassy rim, (b) transition zone consisting of glass mesostasis and spherulites, (c) spherulite zone, and (d) cryptocrystalline zone with plenty of feathery and plumose variolites. Plagioclase microlites present in transition zone downwards.
**VESICLES:** None observed.
**COLOR:** Brownish gray top (5Y 5/1) to dark gray bottom (N5).
**STRUCTURE:** Inclined; glassy margin of a pillow or thin flow.
**ALTERATION:** Moderate. Plagioclase phenocrysts and microlites mostly altered to carbonate; olivine phenocrysts pseudomorphed by whitish clay. Glass is devitrified, spherulites and glass interstices altered to brown clays.
**VEINS/FRACTURES:** 15%; 1-80 mm; irregular; most are subparallel to glassy rim, but rest are irregular; generally branching and cross-cutting. Infilled with carbonate +/- green clays. No halos observed.
**ADDITIONAL COMMENTS:** Typical quenched margin to a flow.

Figure 13. Example of a completed VCD form for igneous rocks.

2. A graphic representation of the core, including the rock piece numbers and positions of shipboard samples.
3. Lithologic unit boundaries, based on criteria such as the occurrence of glassy and quenched margins, trends of marked grain-size variation, and changes in petrographic type and phenocryst assemblages.

The following checklist is used for fine- and medium-grained igneous rocks. For each lithologic unit defined, note the following:

1. UNIT number (consecutive downhole), including numbers of top and bottom pieces in unit.
2. ROCK NAME (to be filled in later).
3. CONTACT TYPE. Intrusive, discordant, depositional, etc. Note the dip of the contact.
4. PHENOCRYSTS. Determine if homogeneous or heterogeneous through unit. For each phenocryst phase, list the abundance (%), average size (in mm), shape, degree of alteration (%), type and secondary phases, and any other comments.

Now fill in ROCK NAME (item 2 above.)

5. GROUNDMASS TEXTURE. Glassy, microcrystalline, fine-grained (<1 mm), medium-grained (1–5 mm). Note any relative grain-size changes within unit from piece to piece.
6. COLOR (dry).
7. VESICLES. Size, shape, percentage, distribution, and nature of any fillings. Collect similar data for miaroles (vugs).
8. STRUCTURE. Massive, pillowed, thin or sheet-like, brecciated.
9. ALTERATION. Type, form, distribution, and degree, from fresh (<2% alteration present) to slightly altered (2%–10%), moderately altered (10%–40%), highly altered (40%–80%), very highly altered (80%–95%), and completely altered (95%–100%).
10. VEINS/FRACTURES. Type, width, orientation, percent present, and nature of infillings.

Finally, any other comments may be added, including continuity of the unit within the core and interrelationship between units. When the VCD form is complete and agreed upon by the igneous petrologists, the same information is then recorded in the VAX computer database HARVI. Each record is checked by the database program for consistency and printed in a format which can be directly pasted onto the final VCD record for subsequent curatorial handling.

Igneous rocks are classified mainly on the basis of mineralogy and texture. Basalts (fine-grained) and dolerites (medium-grained) are termed aphyric if lacking phenocrysts or if they amount to <1% of the rock. If porphyritic the rock may be sparsely phyric (phenocryst content of 1%–2%), moderately phyric (2%–10%) or highly phyric (>10%). Estimates of phenocryst proportions are based on those visible with a hand lens or binocular microscope of about 10× power. Basaltic rocks may be further classified by phenocryst type: a moderately plagioclase-olivine phyric basalt contains 2%–10% total phenocrysts, most of which are plagioclase with lesser amounts of olivine.

### Thin-Section Descriptions

Thin-section billets of basaltic rocks recovered during Leg 129 were examined to help define unit boundaries indicated on the VCD forms and to confirm the identity of petrographic groups and/or alteration products. At least one thin-section was made of each unit where sufficient rock was available.

Petrographic descriptions together with estimates of the various mineral phases (both primary and secondary) are made on the igneous thin-section description forms, which are also entered up in the VAX computer database HRTHIN. Modal abundances were also determined for selected representative samples by point counting.

The mineralogical and textural effects of interaction between seawater and basement rocks was also described in thin-section, together with the nature of secondary phases infilling vesicles, fractures, and veins. Identification of secondary phases such as clays and zeolites were augmented, in some cases, by XRD.

### X-ray Diffraction Analysis

A Philips ADP 3720 X-ray diffractometer was used for the XRD analysis of unknown, generally secondary mineral phases in sedimentary and igneous rocks. Instrument conditions were as follows: CuK$\alpha$ radiation with nickel filter, 40 kV, 35 mA, goniometer scan from 2° to 50° $2\theta$, step size = 0.02°, count time = 2 s.

Samples were prepared by grinding in an agate pestle and mortar until reduced to a very fine powder. The resulting diffractograms were interpreted with the help of a computerized search and match routine using JCPDS powder files.

## DOWNHOLE MEASUREMENTS

### Tool Strings

The purpose of downhole logging is to directly determine the properties of *in-situ* formations adjacent to the borehole wall. After coring is completed in a hole, a tool string is lowered downhole on a coaxial cable, with each of several tools in the tool string continuously monitoring some property of the adjacent borehole. Of the dozens of different tool strings in common use in the petroleum industry, three Schlumberger combinations were selected for use on Leg 129: the quad combination (LSS, NGT, HLDT, and DIL), the geochemical combination (NGT, GST, and ACT), and the Schlumberger formation microscanner combination (FMS, NGT, and GPIT). In addition, the Schlumberger well seismic tool (WST) was run at Site 802. We also included the Lamont temperature tool (TLT) on the quad and geochemical combination strings. The FMS images are presented on microfiche in the back of this volume. Summary log figures appear at the end of each site chapter.

### Log Types

A brief description of logging tools run during Leg 129 is given in the following section. A detailed description of logging tool principles and applications is provided in Schlumberger (1972) and Serra (1984).

#### *Dual Induction Resistivity Log (DIL)*

The DIL is a resistivity logging device that provides measurements of spontaneous potential (SP) and three resistivity values, each with a different depth of investigation: ILD (deep induction), ILM (medium induction), and SFLU (shallow, spherically focused resistivity). Because the solid constituents are orders of magnitude more resistive than the pore fluids in most rocks, resistivity is controlled mainly by the amount and connectivity of the porosity and the conductivity of the pore fluids.

Spontaneous potential is a measure of the streaming potential generated by the differences between borehole and pore-fluid electrical properties, from which both membrane and liquid junction potentials result from the differences in ion mobility in the formation and drilling fluids. The induction sonde consists of a series of transmitter coils excited by a high-frequency (25 kHz) sinusoidal current and a series of detector coils. In a nonconducting medium, the electromagnetic field induced in the detector coils by the transmitting coils is balanced between coil pairs. In a conducting medium, the magnetic field produced by currents induced in the surrounding material induces additional currents in the receivers, changing the amplitude and phase of the total induced current. The depth of investigation is between 0.5 and 5 m, and the vertical resolution about 1.5 m.

The resistivities measured with the induction log are quite accurate for low (less than 100 ohm-m) values, but for more resistive formations it reads too low by as much as 50%–70%. In these rocks the focused resistivity log produces more reliable results. The SFLU consists of a transmitter coil and a series of focusing coils that force current into the formation laterally, away from the borehole. Without these field-shaping coils, current would tend to be conducted exclusively within the borehole. The SFLU provides a direct measurement of formation resistivity about 1 m from the well bore, with a vertical resolution of about 0.6 m.

### *Long-Spaced Sonic Tool (LSS)*

The LSS tool is designed to measure the elastic compressional-wave velocity of the formation surrounding the borehole. In essence, the sonic tool can be thought of as a miniature seismic-refraction experiment carried out within the ylindrical borehole. A source fires acoustic energy that is ransmitted into the borehole fluid. When the wavefront mpinges on the borehole wall, a refracted compressional wave is generated. If the formation shear velocity is higher han the acoustic velocity of the fluid, a refracted shear wave vill also be generated. The refracted waves travel along the orehole wall, reradiating energy into the fluid. Energy arrives t receivers on the logging tool at a time linearly proportional o their offset from the source. Formation elastic-wave veloc- ties thus can be determined from the difference between the rrival times at two receivers a known distance apart.

The LSS sonde uses two acoustic transmitters spaced 2 ft part and two receivers also spaced 2 ft apart and located 8 ft bove the transmitters. This arrangement provides four ource-receiver offsets of 8, 10, and 12 ft. Compensation for orehole irregularities and the inclination of the tool to the ole axis is achieved by averaging the first transit-time reading vith a second reading obtained after the sonde has been aised a fixed distance along the borehole. The LSS tool ecords the full waveform for each source-receiver pair, in ddition to automatically determining its arrival time. The SS is centered in the borehole by the arms of a mechanical aliper (MCD) tool placed immediately above the LSS. The ICD is used only for this purpose, while borehole measure- ents are made with the more accurate caliper on the HLDT ool.

Compressional sonic velocity is one of the primary elastic roperties measured during logging. The product of velocity nd density (impedance) is useful in computing synthetic eismograms for time-depth ties of seismic reflectors.

### *atural Gamma-Ray Tool (NGT)*

The NGT utilizes a sodium iodide detector to determine the pectral content of naturally occurring radiation. The entire pectrum is transmitted to the surface, and the energy arriving five preselected windows is measured by the surface ectronics. The concentrations of potassium, uranium, and orium are determined by analysis of the energy in the five ands. The spectral gamma log is commonly referred to as a UT (K, U, and Th) log. The concentration of thorium in ppm determined directly, whereas the concentrations of uranium ppm and potassium in wt% are determined by a stripping chnique.

The relative proportions of K, Th, and U are controlled by the mineralogy, clay content, and alteration history. Clay type is determined from the relative abundances of thorium and potassium, the primary radioactive elements in clay. Uranium is commonly associated with organic matter in carbonates. The vertical resolution of the tool is about 0.25 m.

### *Lithodensity Tool (HLDT)*

The HLDT contains a chemical source ($^{137}$Ce) of 0.66-MeV gamma rays. The two detectors measure the flux of transmitted gamma rays in a series of energy windows to determine density (RHOB) and photoelectric factor (PEF). A measure of tool performance based on the energy distribution at the near and far receivers (DRHO) is also provided. Gamma rays with energies less than 1.01 MeV interact with atoms in the formation by Compton scattering and via the photoelectric effect. Compton scattering is an elastic collision by which energy is transferred between the gamma ray and electron in the formation. This interaction forms the basis of the density measurement. In effect, the HLDT measures electron density directly, and formation density is determined using the fact that the atomic weight is approximately twice the atomic number in most rock-forming elements. At low energies (below about 0.06 MeV) gamma rays are subject to absorption via the photoelectric effect. One of the energy windows on the far detector is tuned to measure this effect, and the measurement is inverted to obtain the PEF determination. Because this measurement is almost independent of porosity it can be used directly as a matrix lithology indicator.

The depth of investigation of the lithodensity tool depends on the density of the rock: the higher the density, the lower the penetration. In porous and permeable formations the density tool does not read deeper than 0.16 m. The vertical resolution is about 0.3 m. The caliper arms on the HLDT that force the tool against the borehole wall are also used to measure borehole size. These measurements are primarily used to indicate bad parts of the hole, where other logs may read inaccurately, and to correct the responses of those logs sensitive to less severe variations in hole size. The caliper response can also be indicative of lithology. For instance, in zones with swelling clays, hole constrictions are observed where the caliper reads less than the bit size. In addition, as hole conditions in general are a consequence of rock properties, variations in hole size may correlate with lithologic changes.

### *Gamma Spectrometry Tool (GST)*

The GST consists of a pulsed source of 14-MeV neutrons and a gamma-ray scintillation detector. A surface computer performs spectral analysis of gamma rays resulting from the interactions of neutrons emitted by the source with atomic nuclei in the formation. Characteristic sets of gamma rays from six elements dominate the spectrum, permitting calculation of six elemental yields: calcium, silica, iron, chlorine, hydrogen, and sulfur. As the normalized sum of their abundance is always one, values do not reflect the actual elemental composition. Instead, ratios of these yields are commonly used in interpreting the lithology, porosity, and salinity of the formation fluid.

### *Aluminum Clay Tool (ACT)*

Aluminum abundance as measured by the ACT is determined by neutron-induced (cf. chemical source) late gamma-ray spectrometry. By placing sodium iodide detectors both above and below the neutron source, contributions from natural gamma-ray activity can be removed. Calibration to elemental wt% is performed by taking irradiated core samples of known volume and density and measuring their gamma-ray output while placed in a jig attached to the logging tool (generally after logging).

### *General Purpose Inclinometer Tool (GPIT)*

This tool determines the hole azimuth and deviation and the vector components of the magnetic field. Although it is not oriented gyroscopically, the GPIT can accurately measure the magnetic field inclination. The device also monitors vertical and horizontal accelerations applied to the logging probe and thus can be used to determine the effects of ship heave on the logging run.

### *Lamont Temperature Tool (TLT)*

The TLT is self-contained and can be attached to any of the sensor combinations. Data from two thermistors and a pressure transducer are collected every 0.5–5.0 s and stored within the tool. Once the *in-situ* measurement is completed the data are transferred to a shipboard computer for analysis. The fast-response thermistor, though low in accuracy, is able to detect small abrupt temperature excursions caused by fluid flow from the formation. The slow-response thermistor has a high accuracy and can be used to estimate the temperature gradient. Data are recorded as a function of time, with conversion to depth based on the pressure transducer (or preferably, based on simultaneous recording by Schlumberger of both depth and time).

### *Formation Microscanner Tool (FMS)*

The formation microscanner produces high-resolution borehole images from electrical conductivity measurements (Ekstrom et al., 1986; Pezard and Luthi, 1988). Its application as used in the petroleum oil industry since 1986 has been precluded in ODP because of constraints imposed by the internal diameter (4.125 in.[3]) of the drill pipe. A modified sensor was consequently developed by Schlumberger for ODP and first deployed during Leg 126. The FMS has a vertical resolution of approximately 1 cm, but a detection threshold for conductive features of the order of microns. This fine-scale detection ability (raw data points are recorded every 2.5 mm) allows for the detailed study of subsurface structures.

In contrast, typical conventional downhole measurements are averaged over 150 mm; thus the sampling rate of the FMS is 60 times larger than most other logging devices. The FMS has four orthogonal pads which are pressed against the borehole wall. In the original version developed by Schlumberger, two adjacent pads each carry an array of 27 closely spaced electrodes, from which two electrical images are derived. The electrode currents probe the conductivity of the rock to a depth of a few cm into the borehole wall, responding to variations in physical and chemical properties of the rock such as porosity and surface conduction. The series of conductivity traces are displayed side-by-side and coded into an image in which black represents the most conductive values and white the most resistive ones. The new ODP sensor was designed in such a way that four images of 16 traces each are recorded simultaneously. In addition, the resolution of the images is improved due to the smaller size of the electrode array.

Once the data have been acquired in the borehole, the images are processed on a devoted workstation to allow for on-site comparison with the cores. In the future, a graphic analysis software will be installed on the ship using a Macintosh II color workstation in order to perform such basic analysis as the interactive mapping of geological features. Possible applications of the FMS-derived images include: detailed correlation of coring and logging depths, orientation of cores, mapping of fractures, faults, foliations, and formation structures, and the analysis of depositional environments (with information on transport direction, structure of the pore space, nature of contacts, and depositional sequences). The formation microscanner also provides precise measurements of borehole diameter in two orthogonal directions. In an isotropic, linearly elastic rock subjected to an anisotropic stress field, breakouts form along the borehole wall as a result of compressive stress concentrations exceeding the strength of the rock. Under these conditions, the breakout orientation develops in the direction of the least principal horizontal stress. It has been previously demonstrated that stress orientations deduced from rock breakouts are consistent with other independent indicators (Bell and Gough, 1979; Zoback et al., 1988).

### *Well Seismic Tool (WST)*

Vertical seismic profiles are typically run with a surface sound source and receivers (geophones) such as the WST down the hole. At each receiver location, multiple shots are taken to allow stacking for noise reduction. During Leg 129 at Site 802, several problems were encountered with both the tool and the surface equipment, permitting only several shots to be recorded.

### Log Analysis

During logging, incoming data were observed in real time on a monitor oscilloscope and simultaneously recorded on digital tape in the Schlumberger logging unit. After logging, this tape was copied from 800 to 1600 bpi on the shipboard VAX computer system. The 1600 bpi tape was then read by the Masscomp computer system in the downhole logging laboratory aboard ship and reformatted to a FLIC format compatible with the "Terralog" log-interpretation software package. Rather than being a "black box," Terralog is an interactive system consisting of many log manipulation and plot options. Thus, the log analysis and interpretation varied in duration and procedure for each site. Log display and preliminary interpretation were carried out aboard ship; further analysis and interpretation were undertaken after the cruise, using a companion system in the Borehole Research Laboratory of Lamont-Doherty Geological Observatory. Logs are presented at the end of individual site chapters in a series of summary diagrams.

## SITE GEOPHYSICS AND SEISMIC STRATIGRAPHY

Site selection for Leg 129 was based on the multichannel seismic (MCS) surveys conducted aboard the *Fred H. Moore* during the FM35-12 expedition (November-December 1987) and aboard *Le Suroit* during the MESOPAC II expedition (August-September 1989). Underway geophysical data were collected as we approached all sites and provided the correlations with principal MCS sections needed to position the ship at preferred locations. Instrumentation on board included precision echo-sounders, a magnetometer, a seismic reflection acquisition system, and satellite navigation systems.

### Navigation

Navigation data were collected on the bridge and in the underway geophysics laboratory using a Magnavox MX1107 satellite navigation system (SATNAV), which accesses both transit and global positioning system (GPS) satellites. Positions were recorded on magnetic tape and paper records every 2 min during non-seismic transits and every 14 s (i.e., every shotpoint) during seismic operations. Routine collection of navigation data includes recording course and speed data by HIGHRES, the shipboard seismic data acquisition software package. The more accurate GPS fixes were available for 12 to 14 hr each day when at least three satellites were accessible.

When possible, site approach surveys were carried out during times of GPS coverage (see "Operations" sections in each site chapter for details). The final site locations are an average of all SATNAV positions collected while on location. The ship's track for Leg 129 was generated from satellite navigation course and speed information using the SMOOTH program aboard the *JOIDES Resolution*.

### Bathymetry

Bathymetric data were recorded with both 3.5- and 12-kHz echo-sounder systems. The signals were displayed on two Raytheon recorders with 1-s sweeps (750 m/sweep). The quality of these records was quite poor during the full speed (9 kt) transit from Guam, principally due to ship motion and noise as we headed northeast into 25 kt winds and the resulting rough seas. However, during our final approach to Site 800 and subsequent Sites 801 and 802, at approximately 6.5 kt the 3.5-kHz system provided excellent records that assisted in site location. During subsequent full-speed transits (between Sites 800 and 801, and Sites 801 and 802) these echo-sounder systems provided good quality records.

### Magnetics

Total intensity measurements of the Earth's magnetic field were obtained with a Geometrics 801 proton precession magnetometer towed approximately 400 m astern. The data were recorded continuously on a graphic recorder and in the header record of seismic tapes, once per shot. The magnetometer was not operational during the first few days of the cruise, but was operational during the approach to all three site locations and intervening transits.

### Seismic Reflection Acquisition and Processing

Single-channel seismic reflection (SCS) data collected during the final approach to all site locations were recorded using the following equipment and parameters. The seismic source consisted of two synchronized 80-in.$^3$ water guns operating at 1900 psi at a repetition rate of 14 s. The guns were towed approximately 25 m behind the ship and 14 m apart. Reflections were recorded with a teledyne "high speed" streamer with a 100-m-long active section containing 60 hydrophones, a 15-m-long "stretch" section, and a 488-m lead section. The head of the streamer was positioned approximately 503 m behind the ship. The water guns and streamer were towed at estimated depths of 7–8 m and 10–12 m, respectively. Raw data were filtered (25–250 Hz) and recorded with a 6- or 7-s delay for 5 s on 1600 bpi magnetic tape in SEGY format, at a 1-msec sampling interval. The one exception to this occurred during the approach to Site 801 when an error in setting the deep-water delay resulted in inadequate data coverage (only .5 s two-way traveltime below seafloor was recorded). This problem was rectified and a short post-site survey successfully obtained adequate SCS coverage across Site 801. Upon playback of the digital SCS record across Site 801, another acquisition problem was recognized; all the data appeared to be clipped. The most likely explanation for this is that the input gain was set too high, so that the system digitizer was overdriven with voltages in excess of 5 V. The streamer signal was also passed through amplifiers and band-pass filters (20–150 Hz, 30–150 Hz) for real-time display on two EDO 550 dry-paper analog recorders set with a 4 s sweep.

The seismic system employs a super-micro 561 Masscomp computer to record, process, and display data. Although time-consuming, the shipboard processing package (SIOSEIS) proved useful in providing large-scale plots of windowed data for interpretation, including comparisons with synthetic seismograms derived from logging data (see "Downhole Measurements" sections, "Site 800" and "Site 802" chapters, this volume).

### Site Surveys

The FM35-12 expedition collected over 3900 km of MCS data using a 2819-in.$^3$ air-gun array seismic source and a 3.3-km-long, 96-channel receiving streamer (Abrams et al., 1988). Refraction data collected by seven long-range sonobuoys were also digitally recorded during this regional survey. The MESOPAC II MCS survey focused on potential drilling targets first identified on FM35-12, as well as investigated the northern Pigafetta Basin within the oldest portion of the M-sequence lineation pattern. The MESOPAC II expedition also recorded approximately 3900 km of MCS data using six 80-in.$^3$ water guns during vertical incident profiling and two 1000-in.$^3$ air guns while digitally recording refraction data from six long-range sonobuoys. Seismic signals were received by a 2.7-km-long, 96-channel streamer. The MESOPAC II expedition also acquired high quality 3.5-kHz records used as a final constraint on site location. The MCS vertical incidence data recorded with both large volume air-gun and water-gun sources, along with refraction data from long-range sonobuoys, provided the best possible constraints for locating potential drill sites.

### Sonobuoy Analysis

In an effort to further define the seismic structure of the East Mariana and Pigafetta basins, we have analyzed reflection and refraction data collected simultaneously with MCS using long-range sonobuoys. The combination of vertical incidence MCS data and wide angle reflection/refraction data from sonobuoys provide the best possible estimate of subbottom structure (short of drilling) in these two basins. Major emphases in this area of the Pacific, where oceanic crust is unusually smooth and/or overlain by draping diagenetic or volcanic intrusive horizons, are the identification of a crust/sediment interface and, secondarily, determination of crustal velocity structure.

The sonobuoy T/X data from both FM35-12 and MESOPAC II were inverted to a layered isovelocity vs. depth model using the tau-*p* method of Diebold and Stoffa (1981). At the time of Leg 129, only analog records of the MESOPAC II sonobuoys were available; the following processing and analyses involving digital manipulation apply only to FM35-12 sonobuoys. The isovelocity model was used as a starting point for interactive one-dimensional ray tracing, which allowed for vertical velocity gradients and iterative real-time comparison of modeled vs. observed T/X data. Absolute amplitudes were not modeled, but relative amplitudes were used to qualitatively access velocity gradients and to locate critical points on mantle arrivals. The primary limitations of this modeling are (1) the assumption of one-dimensionality and (2) the nonuniqueness of any "best fit" model, particularly the inherent ambiguity between variations in layer thickness and velocity in modeling traveltime. The assumption of one-dimensionality appears justified in this area where the seafloor is essentially flat (±15 m) over the 40- to 50-km range of these buoys, and except for FM35-12 sonobuoy 23, the highest amplitude sub-bottom reflections are also flat-lying (<10° dip). There are some buoys, however, that are disturbed by out-of-plane effects. Direct wave arrivals were used to calculate ranges assuming a D-wave channel velocity of 1.54 km/s estimated from CTD measurements made during the FM35-12 cruise. Changes in the D-wave slope, indicating a change in distance/shot (assuming constant $V_W$), were apparent on some sonobuoy records; and these variations in range were included in our modeling. Sonobuoy data were not used to derive sediment velocities (i.e., velocities between the seafloor and the first refraction). Sediment velocities were based on velocity analysis of four contiguous CDP gathers from the 3.3 km-long, 96-channel streamer. Sediment velocities derived from MCS velocity analysis ranged from 1.6 to 3.0 km/s, usually increasing with depth. This range in velocities is similar to velocities derived from T2/X2 sonobuoy solutions in the northwest Pacific and those measured during DSDP Legs 20, 32, and 89 (Heezen, MacGregor, et al., 1973; Larson, Moberly, et al., 1975; Moberly, Schlanger, et al., 1986). Only one or two of the highest amplitude reflectors were matched by velocity contrasts in the model, and sediments were divided into isovelocity layers even though it is recognized that velocity gradients may also occur.

The depth to the crust/sediment interface depends on the overlying velocity structure and was chosen based on the depth to the first refracted arrivals. Often precritical refracted arrivals were observed within the near vertical reflections and traced to their tangency to a sub-bottom reflection. These continuously curved refractions are indicative of velocity gradients. Wide angle reflection events from the Moho were also modeled; the curvature of these events was constrained by the overlying velocity structure, whereas the underlying mantle velocity was constrained by the our choice of critical point location. The slope of a line drawn tangent to this reflection can also give an estimate of mantle velocity.

## REFERENCES

Abrams, L. J., Larson, R. L., Shipley, T., and Lancelot, Y., 1988. Cretaceous volcanic sequences and Jurassic(?) crust in the western Pacific. *Trans. Am. Geophys. Union*, 69:1442.

Baumgartner, P. O., 1984. A Middle Jurassic–Early Cretaceous low-latitude radiolarian zonation based on Unitary Associations and age of Tethyan radiolarites. *Eclogae Geol. Helv.*, 77(3):729–837.

———, 1987. Age and genesis of Tethyan Jurassic Radiolarite. *Eclogae Geol. Helv.*, 80(3):831–879.

Bell, J. S., and Gough, D. I., 1979. Northeast-southwest compressive stress in Alberta: evidence from oil wells. *Earth Planet. Sci. Lett.*, 45:475–482.

Berggren, W. A., and Miller, K. G., 1988. Paleogene tropical planktonic foraminiferal biostratigraphy and magnetobiochronology. *Micropaleontology*, 34(4):362–380.

Berggren, W. A., Kent, D. V., and Flynn, J. J., 1985a. Paleogene geochronology and chronostratigraphy. *In* Snelling, N. J. (Ed.), *Geochronology and the Geologic Time Scale:* Geol. Soc. London Mem., 10:141–195.

Berggren, W. A., Kent, D. V., and van Couvering, J. A., 1985b. Neogene geochronology and chronostratigraphy. *In* Snelling, N. J. (Ed.), *Geochronology and the Geologic Time Scale:* Geol. Soc. London Mem., 10:211–260.

Blow, W. H., 1969. Late middle Eocene to Recent planktonic foraminiferal biostratigraphy. *In* Brönnimann, P., and Renz, H. H. (Eds.), *Proc. 1st Intl. Conf. Planktonic Microfossils:* Leiden (E. J. Brill), 199–241.

Bolli, H. M., and Saunders, J. B., 1985. Oligocene to Holocene low latitude planktic foraminifera. *In* Bolli, H. M., Saunders, J. B., and Perch-Nielsen, K. (Eds.), *Plankton Stratigraphy:* Cambridge (Cambridge Univ. Press), 155–262.

Boyce, R. E., 1976. Definitions and laboratory determination of compressional sound velocity parameters and wet-water content, wet-bulk density and porosity parameters by gravimetric and gamma-ray attenuation techniques. *In* Schlanger, S. O., Jackson, E. D., et al., *Init. Repts. DSDP*, 33: Washington (U.S. Govt. Printing Office), 931–958.

Bralower, T. J., 1987. Valanginian to Aptian calcareous nannofossil stratigraphy and correlation with the upper M-sequence magnetic anomalies. *Mar. Micropaleont.*, 11:293–310.

Bralower, T. J., Monechi, S., and Thierstein, H. R., 1989. Calcareous nannofossil zonation of the Jurassic-Cretaceous boundary interval and correlation with the geomagnetic polarity timescale. *Mar. Micropaleont.*, 14:153–235.

Bukry, D., 1973. Low-latitude coccolith biostratigraphic zonation. *In* Edgar, N. T., Saunders, J. B., et al., *Init. Repts. DSDP*, 15: Washington (U.S. Govt. Printing Office), 685–703.

———, 1975. Coccolith and silicoflagellate stratigraphy, northwestern Pacific Ocean, Deep Sea Drilling Project, Leg 32. *In* Larson, R. L., Moberly, R., et al., *Init. Repts. DSDP*, 32: Washington (U.S. Govt. Printing Office), 677–701.

Carlson, R. L., and Christensen, N. L., 1979. Velocity anisotropy in semi-indurated calcareous deep-sea sediments. *J. Geophys. Res.*, 84:205–211.

Caron, M., 1985. Cretaceous planktic foraminifera. *In* Bolli, H. M., Saunders, J. B., and Perch-Nielsen, K. (Eds.), *Plankton Stratigraphy:* Cambridge (Cambridge Univ. Press), 17–86.

Diebold, J., and Stoffa, P., 1981. The traveltime equation, tau-*p* mapping, and inversion of common-midpoint data. *Geophysics*, 46:238–254.

Ekstrom, M. P., Dahan, C. A., Chen, M. Y., Lloyd, P. M., and Rossi, D. J., 1986. Formation imaging with microelectrical scanning arrays. *Trans. 27th Ann. Logging Symp., Soc. of Prof. Well Log Analysts*, Paper BB.

Fischer, R. V. and Schminke H. V., 1984. *Pyroclastic Rocks:* Berlin (Springer-Verlag).

Gealy, E. L., Winterer, E. L., and Moberly, R., 1971. Methods, conventions, and general observation. *In* Winterer, E. L., Riedel, W. R., et al., *Init. Repts. DSDP*, 7: Washington (U.S. Govt. Printing Office), 9–26.

Gieskes, J. M. and Peretsman, G., 1986. Water chemistry procedures aboard *JOIDES Resolution:* Some comments. *ODP Tech. Note*, 5.

Hamilton, E. L., 1971. Prediction of *in-situ* acoustic and elastic properties of marine sediments. *Geophysics*, 36:266–284.

Hay, W. W., Sibuet, J.-C., et al., 1984. Introduction and explanatory notes, Deep Sea Drilling Project Leg 75. *In* Hay, W. W., Sibuet, J.-C., et al., *Init. Repts. DSDP*, 75 (Pt. 1): Washington (U.S. Govt. Printing Office), 3–25.

Hedberg, H. D., 1976. *International Stratigraphic Guide:* New York (Wiley, New York).

Heezen, B. C., MacGregor, I. D., et al., 1973. *Init. Repts. DSDP*, 20: Washington (U.S. Govt. Printing Office).

Isaacs, C. M., 1982. Influence of rock composition on kinetics of silica phase changes in the Monterey Formation, Santa Barbara area, California. *Geology*, 10:304–308.

Kent, D. V., and Gradstein, F. M., 1985. A Cretaceous and Jurassic geochronology. *Geol. Soc. Am. Bull.*, 96:1419–1427.

Larson, R. L., Moberly, R., et al., 1975. *Init. Repts. DSDP*, 32: Washington (U.S. Govt. Printing Office).

Manheim, F. T., and Sayles, F. L., 1974. Composition and origin of interstitial water of marine sediments based on deep sea drilled cores. In Goldberg, E. D. (Ed.), *The Sea* (Vol. 5): New York (Wiley Interscience), 527–568.

Martini, E., 1971. Standard Tertiary and Quaternary calcareous nannoplankton zonation. *In* Farinacci, A. (Ed.), *Proc. 2nd Planktonic Conf.*, Rome (Ed. Tecnoscienza), 739–785.

Matsuoka, A., and Yao, S., 1985. Latest Jurassic radiolarians from the Torinosu Group in Southwest Japan. *J. Geosci., Osaka City Univ.*, 28:125–145.

———, 1986. A newly proposed radiolarian zonation for the Jurassic of Japan. *Mar. Micropaleont.*, 11:91–106.

Moberly, R., Schlanger, S. O. et al., 1986. *Init. Repts. DSDP*, 89: Washington (U.S. Govt. Printing Office).

Monechi, S., and Thierstein, H. R., 1985. Late Cretaceous-Eocene nannofossil and magnetostratigraphy correlations near Gubbio, Italy. *Mar. Micropaleont.*, 9:419–440.

Ogg, J. G., 1987. Early Cretaceous and Tithonian magnetostratigraphy of the Galicia margin (Ocean Drilling Program Leg 103). *In* Boillot, G., Winterer, E. L., et al., *Proc. ODP, Sci. Results*, 103: College Station, TX (Ocean Drilling Program), 659–682.

Okada, H., and Bukry, D., 1980. Supplementary modification and introduction of code numbers to the low-latitude coccolith biostratigraphic zonation (Bukry, 1973; 1975). *Mar. Micropaleont.*, 5:321–325.

Pezard, P. A., and Luthi, S. M., 1988. Borehole electrical images in the basement of the Cajon Pass scientific drill hole, California: fracture identification and tectonic implications. *Geophys. Res. Lett.*, 15:1017–1020.

Ratcliffe, E. H., 1960. The thermal conductivities of ocean sediments. *J. Geophys. Res.*, 65:1535–1541.

Riedel, W. R., and Sanfilippo, A., 1978. Stratigraphy and evolution of tropical Cenozoic radiolarians. *Micropaleontology*, 24:61–96.

Roth, P. H., 1978. Cretaceous nannoplankton biostratigraphy and oceanography of the northwestern Atlantic Ocean. *In* Benson, W. E., Sheridan, R. E., et al., *Init. Repts. DSDP*, 44: Washington (U.S. Govt. Printing Office), 731–759.

———, 1983. Jurassic and Lower Cretaceous calcareous nannofossils in the Western North Atlantic (Site 534): Biostratigraphy, preservation, and some observations on biogeography and paleoceanography. *In* Sheridan, R. E., Gradstein, F. M., et al., *Init. Repts. DSDP*, 76: Washington (U.S. Govt. Printing Office), 587–621.

Sanfilippo, A., and Riedel, W. R., 1985. Cretaceous radiolaria. *In* Bolli, H. M., Saunders, J. B., and Perch-Nielsen, K. (Eds.), *Plankton Stratigraphy:* Cambridge (Cambridge Univ. Press), 573–630.

Sanfilippo, A., Westberg-Smith, M. J., and Riedel, W. R., 1985. Cenozoic radiolaria. *In* Bolli, H. M., Saunders, J. B., and Perch-Nielsen, K. (Eds.), *Plankton Stratigraphy:* Cambridge (Cambridge Univ. Press), 631–712

Schlumberger, Inc., 1972. *Log Interpretation* (Vol. 1): New York (Schlumberger).

Schmid, R., 1981. Descriptive nomenclature and clarification of pyroclastic deposits and fragments: recommendations of the IUGS Subcommission on the Systematics of Igneous Rocks. *Geology*, 9:41–43.

Serra, O., 1984. *Fundamentals of Well Log Interpretation:* Amsterdam (Elsevier).

Shepard, F. P., 1954. Nomenclature based on sand-silt-clay ratios. *J. Sediment. Petrol.*, 24:151–158.

Shipboard Scientific Party, 1989. Introduction and explanatory notes. *In* Robinson, P. T., Von Herzen, R., et al., *Proc. ODP, Init. Repts.*, 118: College Station, TX (Ocean Drilling Program).

Sissingh, W., 1977. Biostratigraphy of Cretaceous calcareous nannoplankton. *Geol. Mijnbouw*, 56(1):37-65.

Steiner, M. B., and Ogg, J. G., 1988. Early and Middle Jurassic magnetic polarity time scale. *In* Rocha, B. (Ed.), *Proc. 2nd Int. Jurassic Stratigraphy Symp.*, Lisbon, Sept. 14–18, 1987 (Geol. Surv. Denmark).

Supko, P., Ross, D. A., and Neprochnov, Y. P., 1978, Introduction and explanatory notes, Leg 42B, Deep Sea Drilling Project. *In* Ross, D. A., Neprochnov, Y., P., et al., *Init. Repts. DSDP*, 42, Pt. 2: Washington (U.S. Govt. Printing Office), 3–15.

Thierstein, H. R., 1976. Mesozoic calcareous nannoplankton biostratigraphy of marine sediments. *Mar. Micropaleont.*, 1:325-362.

———, 1973. Lower Cretaceous calcareous nannoplankton biostratigraphy. *Abh. Geol. Bundesenst. (Austria)*, 29:1–52.

———, 1971. Tentative Lower Cretaceous nannoplankton zonation. *Eclogae Geol. Helv.*, 64:459–488.

Toumarkine, M., and Luterbacher, H., 1985. Paleocene and Eocene planktic foraminifera. *In* Bolli, H. M., Saunders, J. B., and Perch-Nielsen, K. (Eds.), *Plankton Stratigraphy:* Cambridge (Cambridge Univ. Press), 87–154.

Vaquier, V., 1985. The measurement of thermal conductivity of solids with a transient linear heat source on the plane surface of a poorly conducting body. *Earth Planet. Sci. Lett.*, 74:275–279.

Von Herzen, R. P., and Maxwell, A. E., 1959. The measurements of thermal conductivity of deep-sea sediments by a needle probe method. *J. Geophys. Res.*, 64:1557–1563.

Wentworth, C. K., 1922. A scale of grade and class terms of clastic sediments, *J. Geol.*, 30:377–390.

Williams, G. L., 1977. Dinocysts: their paleontology, biostratigraphy and paleoecology. *In* Ramsay, A.T.S. (Ed.), *Oceanic Micropalaeontology*, 2:1231–1325.

Zoback, M. D., Zoback, M. L., Mount, V. S., Suppe, J., Eaton, J. P., Healy, J. H., Oppenheimer, D., Reasenberg, P., Jones, L., Raleigh, C. B., Wong, I. G., Scotti, 0., and Wentworth, C., 1988. New evidence on the state of stress of the San Andreas Fault, *Science*, 238:1105–1111.

**Ms 129A-101**

# SECTION 2: SITE REPORTS

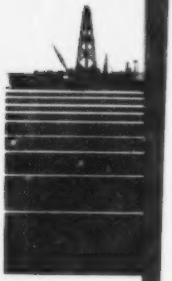

Lancelot, Y., Larson, R. L., et al., 1990
*Proceedings of the Ocean Drilling Program, Initial Reports*, Vol. 129

# 2. SITE 800[1]

Shipboard Scientific Party[2]

## HOLE 800A

**Date occupied:** 25 November 1989

**Date departed:** 5 December 1989

**Time on hole:** 9 days, 19 hr, 45 min

**Position:** 21°55.38'N, 152°19.37'E

**Bottom felt (rig floor; m, drill-pipe measurement):** 5697.0

**Distance between rig floor and sea level (m):** 11.00

**Water depth (drill-pipe measurement from sea level, m):** 5686.0

**Total depth (rig floor; m):** 6241.40

**Penetration (m):** 544.40

**Number of cores (including cores with no recovery):** 61

**Total length of cored section (m):** 544.40

**Total core recovered (m):** 150.73

**Core recovery (%):** 27

**Oldest sediment cored:**
Depth (mbsf): 498.10
Nature: chert
Earliest age: Berriasian
Latest age: Valanginian

**Basement:**
Depth (mbsf): 498.10
Nature: Basalt

**Principal results:** Site 800 is located in the northern Pigafetta Basin on magnetic anomaly lineation M33, 40 miles northeast of Himu Seamount. Its presumed basement age is Jurassic, based on an extrapolation of the Japanese magnetic lineation pattern that is contained in the same spreading compartment to the northwest. Hole 800A consists of the following stratigraphic sequence:

0–38 mbsf: Tertiary to Upper Campanian zeolitic brown clay.

38–78 mbsf: Upper Campanian to Turonian red cherts and porcellanites corresponding to the top of the reverberant layer on seismic records.

78–229 mbsf: Cenomanian to Lower Albian grey chert and silicified limestone with increasing amounts of silicified limestone downsection, grading into nannofossil chalk at the base of the sequence.

229–450 mbsf: Aptian volcaniclastics, well indurated and possibly emanating from Himu Seamount 40 miles to the southwest that is radiometrically dated at 120 m.y. (Aptian-Barremian), with occasional included radiolarites. The volcaniclastics contain spectacular turbidite and debris flow features, including graded beds, cross bedding, tear-up structures, and penecontemporaneous deformation obvious even to geophysical investigators.

450–498 mbsf: Hauterivian to Berriasian laminated claystones, red with occasional black banding and green reduction halos. Hard red chert at the base of the sequence.

500–545 mbsf: Dolerite, massive, aphyric, medium-grained, holocrystalline with no observed internal cooling unit boundaries. The dolerite is marginally finer grained at the top and contains no macroscopically observable glass or palagonite. Large, elongate clinopyroxene crystals are present throughout, and the material is relatively fresh and unweathered except for the top 1 m. The top of this unit corresponds to a flat, high-amplitude seismic reflector that is essentially acoustic basement in this area.

Drilling was terminated at 545 mbsf due to a tight spot in the hole at 350 mbsf that was probably caused by swelling clays in the volcaniclastic section. A summary of coring statistics is presented in Table 1. Logging with standard tools was conducted in three runs from 45 to about 300 mbsf.

## BACKGROUND AND OBJECTIVES

The correlation of the M1 to M22 Mesozoic magnetic anomaly sequence in the Pacific by Larson and Chase (1972) indicated that the oldest ocean crust beneath the Pacific Basin is centered in the far western Pacific Ocean. Hilde (1973) and Hilde et al. (1976, 1977) extended these correlations to M26, and predicted that the point of origin of the Pacific plate lies within the triangle found at the Leg 129 drill sites (800, 801, and 802), and is of Middle to Early Jurassic age. Cande et al. (1978) extended these Pacific magnetic lineation correlations to M29, and Handschumacher and Kroenke (1978) recognized some version of the same lineations. These correlations were further extended to M38 by Handschumacher and Gettrust (1985).

Site 800 (proposed site PIG-1) was drilled in the northwestern region of the Pigafetta Basin (Fig. 1), in an area where magnetic anomalies believed to correspond with the M-series were mapped recently by Handschumacher and Gettrust (1985), Tamaki et al. (1987), Handschumacher et al. (1988), and Nakanishi et al. (1989). These anomalies are well defined in this area and extend from M25 to the northwest through M37 to the southeast. Because we follow Tamaki et al.'s (1987) suggestion that Handschumacher et al. (1988) miscorrelated M29 from its original definition in Cande et al. (1978), our M-series numbers are always one less than in Handschumacher et al. (1988) for anomalies older than M29.

Site 800 lies on anomaly M33 (Figs. 2 and 3), in an area where multichannel seismic profiles (including refraction data) obtained aboard the *Le Suroit* during the MESOPAC II cruise in August 1989 (see "Site Geophysics and Seismic Stratigraphy" section, this chapter) indicated that the basement might be reached relatively easily, as there is no evidence of substantial accumulation of Cretaceous volcanogenic sediments or hard rocks within the sediment section. The total sediment thickness was estimated to be about 550 m based on seismic velocities obtained from a refraction sonobuoy launched nearby during MESOPAC II.

The final choice for the location of this site was also determined by the thickness of soft sediment lying above the top of the "opaque layer" (Houtz and Ludwig, 1979) which was correlated regionally with Upper Cretaceous cherts that result from diagenetic alteration of siliceous organisms accumulated during the transit of this area beneath the equatorial zone of high productivity. A minimum of about 35 m of soft sediment above the hard chert is generally considered necessary to provide support for the bottom-hole assembly before any substantial weight can be applied to the drill bit. At Site

---

[1] Lancelot, Y., Larson, R. L., et al., 1990. *Proc. ODP, Init. Repts.*, 129: College Station, TX (Ocean Drilling Program).

[2] Shipboard Scientific Party is as given in the list of participants preceding the contents.

Table 1. Coring summary for Site 800.

| Core | Date (1989) | Time (UTC) | Depth (mbsf) | Length cored (m) | Length recovered (m) | Recovery (%) |
|---|---|---|---|---|---|---|
| 129-800A- | | | | | | |
| 1R | 26 November | 1545 | 0.0–1.0 | 1.0 | 0.32 | 32.0 |
| 2R | 26 November | 1950 | 1.0–10.6 | 9.6 | 0.01 | 0.1 |
| 3R | 26 November | 2055 | 10.6–20.2 | 9.6 | 2.03 | 21.1 |
| 4R | 26 November | 2200 | 20.2–29.9 | 9.7 | 5.07 | 52.2 |
| 5R | 26 November | 2305 | 29.9–39.6 | 9.7 | 0.39 | 4.0 |
| 6R | 27 November | 0030 | 39.6–49.2 | 9.6 | 0.51 | 5.3 |
| 7R | 27 November | 0210 | 49.2–58.9 | 9.7 | 0.53 | 5.5 |
| 8R | 27 November | 0350 | 58.9–68.5 | 9.6 | 0.70 | 7.3 |
| 9R | 27 November | 0525 | 68.5–78.2 | 9.7 | 0.34 | 3.5 |
| 10R | 27 November | 0715 | 78.2–87.8 | 9.6 | 0.57 | 5.9 |
| 11R | 27 November | 0845 | 87.8–97.3 | 9.5 | 0.71 | 7.5 |
| 12R | 27 November | 1035 | 97.3–106.8 | 9.5 | 0.32 | 3.4 |
| 13R | 27 November | 1230 | 106.8–116.2 | 9.4 | 0.57 | 6.1 |
| 14R | 27 November | 1430 | 116.2–125.4 | 9.2 | 1.03 | 11.2 |
| 15R | 27 November | 1610 | 125.4–134.9 | 9.5 | 0.16 | 1.7 |
| 16R | 27 November | 1805 | 134.9–144.2 | 9.3 | 0.24 | 2.6 |
| 17R | 27 November | 2025 | 144.2–153.7 | 9.5 | 0.65 | 6.8 |
| 18R | 27 November | 2245 | 153.7–162.9 | 9.2 | 1.31 | 14.2 |
| 19R | 28 November | 0050 | 162.9–172.4 | 9.5 | 0.77 | 8.1 |
| 20R | 28 November | 0320 | 172.4–181.3 | 8.9 | 0.40 | 4.5 |
| 21R | 28 November | 0720 | 181.3–191.0 | 9.7 | 1.59 | 16.4 |
| 22R | 28 November | 1005 | 191.0–200.5 | 9.5 | 0.67 | 7.1 |
| 23R | 28 November | 1255 | 200.5–209.9 | 9.4 | 0.92 | 9.8 |
| 24R | 28 November | 1620 | 209.9–219.3 | 9.4 | 1.00 | 10.6 |
| 25R | 28 November | 1830 | 219.3–228.6 | 9.3 | 0.41 | 4.4 |
| 26R | 28 November | 2040 | 228.6–238.0 | 9.4 | 4.41 | 46.9 |
| 27R | 28 November | 2250 | 238.0–247.2 | 9.2 | 2.19 | 23.8 |
| 28R | 29 November | 0050 | 247.2–256.5 | 9.3 | 7.23 | 77.7 |
| 29R | 29 November | 0310 | 256.5–265.9 | 9.4 | 4.41 | 46.9 |
| 30R | 29 November | 0525 | 265.9–272.0 | 6.1 | 3.18 | 52.1 |
| 31R | 29 November | 0735 | 272.0–278.1 | 6.1 | 3.54 | 58.0 |
| 32R | 29 November | 1140 | 278.1–287.5 | 9.4 | 2.84 | 30.2 |
| 33R | 29 November | 1450 | 287.5–297.0 | 9.5 | 9.12 | 96.0 |
| 34R | 29 November | 1655 | 297.0–306.4 | 9.4 | 6.92 | 73.6 |
| 35R | 29 November | 1850 | 306.4–315.9 | 9.5 | 4.37 | 46.0 |
| 36R | 29 November | 2100 | 315.9–325.1 | 9.2 | 7.81 | 84.9 |
| 37R | 29 November | 2250 | 325.1–334.5 | 9.4 | 3.10 | 33.0 |
| 38R | 30 November | 0040 | 334.5–343.8 | 9.3 | 1.90 | 20.4 |
| 39R | 30 November | 0250 | 343.8–353.1 | 9.3 | 5.58 | 60.0 |
| 40R | 30 November | 0500 | 353.1–362.5 | 9.4 | 1.52 | 16.2 |
| 41R | 30 November | 0650 | 362.5–368.6 | 6.1 | 2.02 | 33.1 |
| 42R | 30 November | 0840 | 368.6–374.7 | 6.1 | 1.69 | 27.7 |
| 43R | 30 November | 1315 | 374.7–383.7 | 9.0 | 1.28 | 14.2 |
| 44R | 30 November | 1515 | 383.7–393.1 | 9.4 | 2.52 | 26.8 |
| 45R | 30 November | 1725 | 393.1–402.5 | 9.4 | 5.27 | 56.0 |
| 46R | 30 November | 2125 | 402.5–411.9 | 9.4 | 5.34 | 56.8 |
| 47R | 30 November | 2345 | 411.9–421.4 | 9.5 | 5.22 | 54.9 |
| 48R | 30 November | 0215 | 421.4–430.9 | 9.5 | 8.22 | 86.5 |
| 49R | 01 November | 0450 | 430.9–440.2 | 9.3 | 5.42 | 58.3 |
| 50R | 01 November | 0740 | 440.2–449.6 | 9.4 | 3.55 | 37.7 |
| 51R | 01 November | 0950 | 449.6–458.8 | 9.2 | 1.68 | 18.2 |
| 52R | 01 November | 1200 | 458.8–464.9 | 6.1 | 3.53 | 57.8 |
| 53R | 01 November | 1420 | 464.9–471.0 | 6.1 | 2.27 | 37.2 |
| 54R | 01 December | 1915 | 471.0–479.1 | 8.1 | 2.88 | 35.5 |
| 55R | 01 December | 2200 | 479.1–488.5 | 9.4 | 3.00 | 31.9 |
| 56R | 01 December | 0105 | 488.5–498.0 | 9.5 | 0.36 | 3.8 |
| 57R | 01 December | 0555 | 498.0–507.2 | 9.2 | 1.94 | 21.1 |
| 58R | 02 December | 1030 | 507.2–516.6 | 9.4 | 3.55 | 37.7 |
| 59R | 02 December | 1425 | 516.6–525.9 | 9.3 | 0.22 | 2.4 |
| 60R | 02 December | 1810 | 525.9–535.3 | 9.4 | 1.12 | 11.9 |
| 61R | 03 December | 0020 | 535.3–544.4 | 9.1 | 0.31 | 3.4 |
| Coring totals | | | | 544.4 | 150.73 | 27.7 |

800 the thickness of the soft sediment layer believed to correspond with post-Cenomanian deposits was estimated at about 51 m, based on 3.5-kHz profiles from the MESOPAC II survey as well as those obtained aboard the *JOIDES Resolution* during the approach to the site (see "Site Geophysics and Seismic Stratigraphy" section, this chapter).

The specific objectives for this site were (1) to determine if the lowermost sediment layers and basement could be reached with a single bit hole, and (2) to obtain as complete a section as possible down to the presumed Jurassic sediments and basement. We planned to drill a pilot hole at Site 800 to be followed by drilling another hole to the southeast, within the Jurassic quiet zone (JQZ), before deciding if and where a multiple reentry site with extensive casing would offer the best opportunity to sample the oldest sediment and achieve substantial penetration into the basement. Site 800, representing the youngest end of a transect across the oldest portion of the Mesozoic magnetic anomalies, was also considered of particular interest in the attempt to calibrate the age of these anomalies.

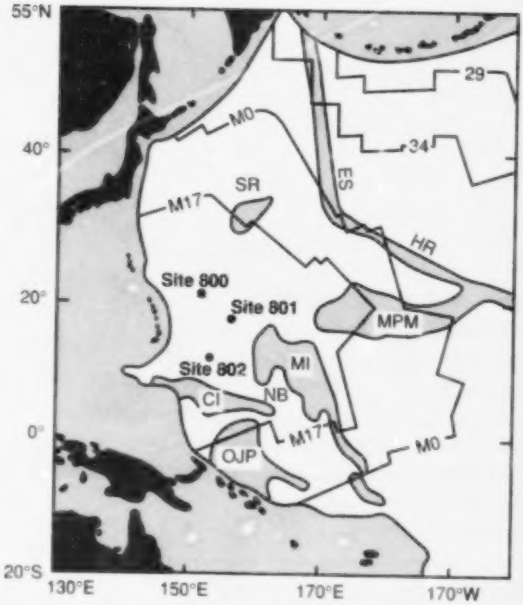

Figure 1. Location of Leg 129 Sites 800, 801, and 802. Bedrock isochrons are determined from magnetic anomaly lineation mapping on the Pacific plate (after Larson et al., 1985) and superimposed on groups of islands, atolls, and guyots in the western Pacific Ocean. (Feature abbreviations are as follows: Caroline Islands (CI), Ontong Java Plateau (OJP), Marshall Islands (MI), Nauru Basin (NB), Mid-Pacific Mountains (MPM), Shatsky Rise (SR), Hawaiian Ridge (HR), and Emperor Seamounts (ES). Jagged contours represent magnetic lineations and unshaded areas represent normal Pacific oceanic crust. Shaded areas represent volcanic edifices with thickened crustal sections, as well as the younger areas beyond the Pacific subduction zones.

An interpretation of the regional seismic stratigraphy combined with what is known from the history of plate motion during the Mesozoic (Lancelot and Larson, 1975; Lancelot, 1978) allowed us to predict that the sediment section would consist of a very thin cover of soft pelagic brown clay resting on a series of chert layers of Late to middle Cretaceous age. The lower part of the section was believed to consist of clay and limestones of Early Cretaceous age, possibly underlain by another series of cherts and/or limestones of Late Jurassic age, and finally by basaltic basement.

## OPERATIONS

### Approach to the Site

We approached Site 800 from the peak of Himu Seamount on course 52.5° at 6 kt, shooting a seismic line with two 80-in.$^3$ water guns (Fig. 4). Our target was a point at 0740 hr

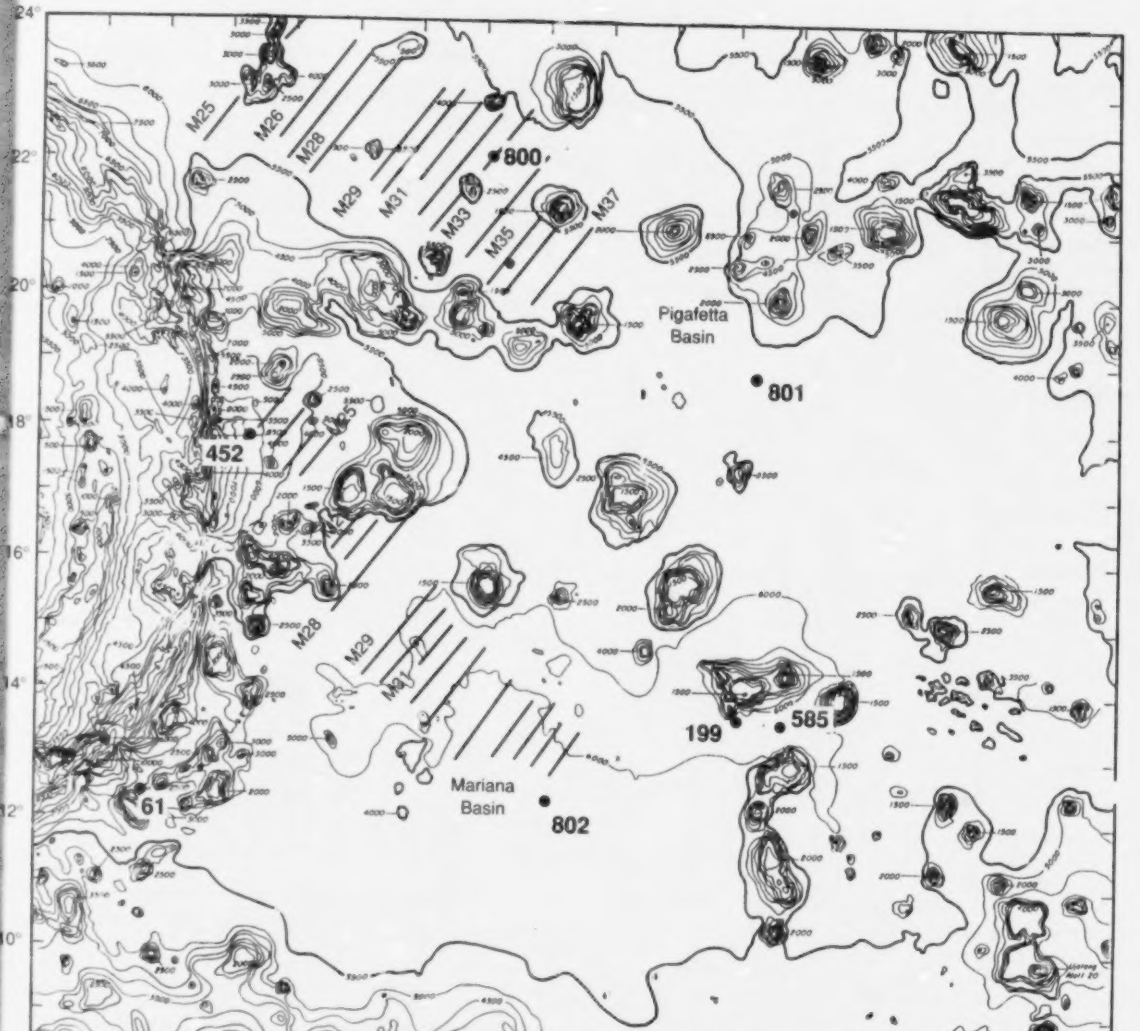

Figure 2. Bathymetry (in meters) of the central western Pacific (M. Angell and C. Brenner, pers. comm., 1990) with location of drill sites. Magnetic anomalies modified from Handschumacher and Gettrust (1985), Tamaki et al. (1987), and Handschumacher et al. (1988).

(Universal Time Coordinated, UTC), 21 August 1989, on MESOPAC II line 3 that trends at about a 45° angle to our approach direction. At 1244 hr, 25 November 1989, when we were still 1.5 miles south of the MESOPAC II target, the water gun and 3.5-kHz records showed a very clear seismic picture (see Figs. 40 and 41, "Site Geophysics and Seismic Stratigraphy," this chapter) comparable or superior to the MESOPAC II profile. We launched the beacon at that location (21°55.408'N, 152°19.386'E, which is slightly different from the final site position). We then continued on a constant heading to cross MESOPAC II line 3 at our original target location where the seismic picture was about the same. We proceeded 2.8 miles beyond the MESOPAC II line where we changed course to 167° and ran 4.3 miles, crossing MESOPAC II again to a point where we could run parallel to MESOPAC II and over the beacon drop site. We changed course to 283° and ran an 8.7-mile line that passed 0.3 mile south of the beacon drop site and trended parallel to MESOPAC II line 3. We then retrieved the seismic gear and returned to the beacon location.

Our first line shows a very clear reflector at 500 ms that extends continuously for 3 miles. The beacon drop site is nearly centered in the middle of the extent of the reflector. The last (cross-strike) line shows that this reflector marks the basement of a narrow basin, with the beacon drop site close to the west basin wall. However, the beacon drop site is also on the deepest location of the basement reflector, and thus probably is close to the optimum location for Site 800.

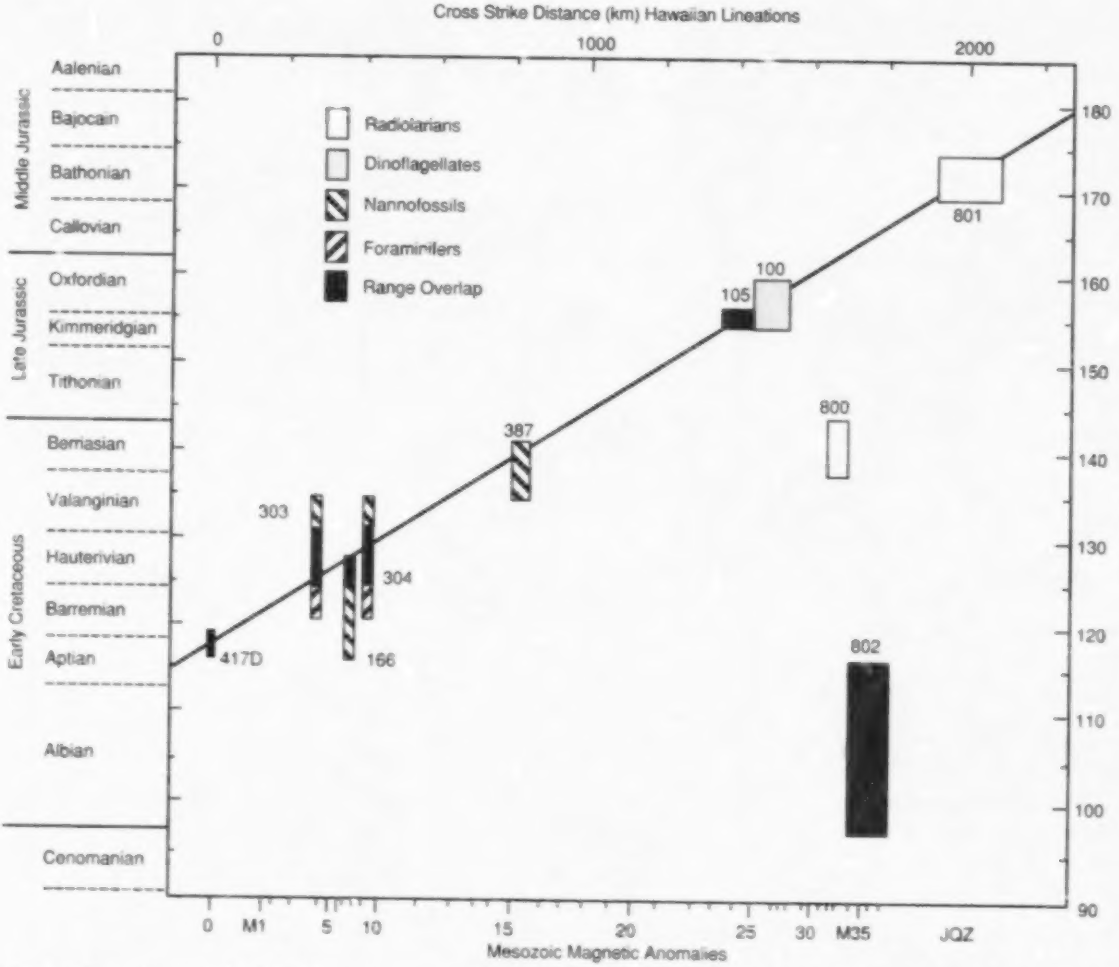

Figure 3. Time calibration plot of the Mesozoic anomalies M0 to M37 and the preceding magnetic quiet zone (JQZ). Magnetic anomalies plotted as cross-strike distance across the Hawaiian lineations for M0 to M25. Anomalies M25 to M37 are normalized to that parameter after Handschumacher et al. (1988). Geologic time scale and radiometric ages are from Harland et al. (1982), as modified by Kent and Gradstein (1985) at the Tithonian/Kimmeridgian boundary. Diagonal line indicates a predicted time scale constrained prior to Leg 129 that closely fits the calibration points. Oldest paleontologic ages in various DSDP holes (numbered) are shown as rectangles. Vertical lengths of rectangles show paleontological age ranges from DSDP *Initial Reports*, except for 100 (Zotto et al., 1987) and 105 (Gradstein and Sheridan, 1983). Horizontal lengths show magnetic age ranges from Larson and Hilde (1975) for DSDP Sites 303, 304, 166, 100, and 105, and DSDP *Initial Reports* for Sites 387 and 417D. Age ranges from Sites 800, 801, and 802 are also shown.

## Hole 800A

A bottom-hole assembly (BHA) 154 m long was made up almost completely of 8¼-in. drill collars with a 3-m-long set of Hydrolex jars at 115 m. Total BHA weight was 65,000 lb with 47,000 lb below the jars. A Rock Bit International C4 coring bit was chosen to lead our assault on the Jurassic. This bit consisted of four roller cones with short chisel teeth, tungsten carbide inserts, sealed journal bearings, and inlaid hard metal armor to retard shirt-tail wear.

The corrected seafloor precision depth recorder (PDR) depth at Site 800 is 5697 m to the rig floor. A core was taken from 5693 m of measured drill pipe to account for a theoretical 11 m of pipe stretch. This core was all water. The string was lowered 5 m and the next core taken (Core 129-800A-1R) contained 0.32 m of brown clay. The mud line was established at 5697 m of measured drill pipe, exactly equal to the corrected PDR depth.

As this was a potential reentry site, we next conducted a jet-in test to determine the length of casing that could be washed in. Resistance was met at 38 mbsf, and 40 strokes per min (spm) of pump pressure only produced an additional 2 m of penetration. We concluded that 38 m of conductor casing is the maximum that could be washed in at this location.

Core 129-800A-2R then was taken from 1.0 to 10.6 mbsf. Only a core-catcher sample and a clean core liner were recovered, casting some doubt on our previous mud-line determination. We proceeded to recover a medium to poor

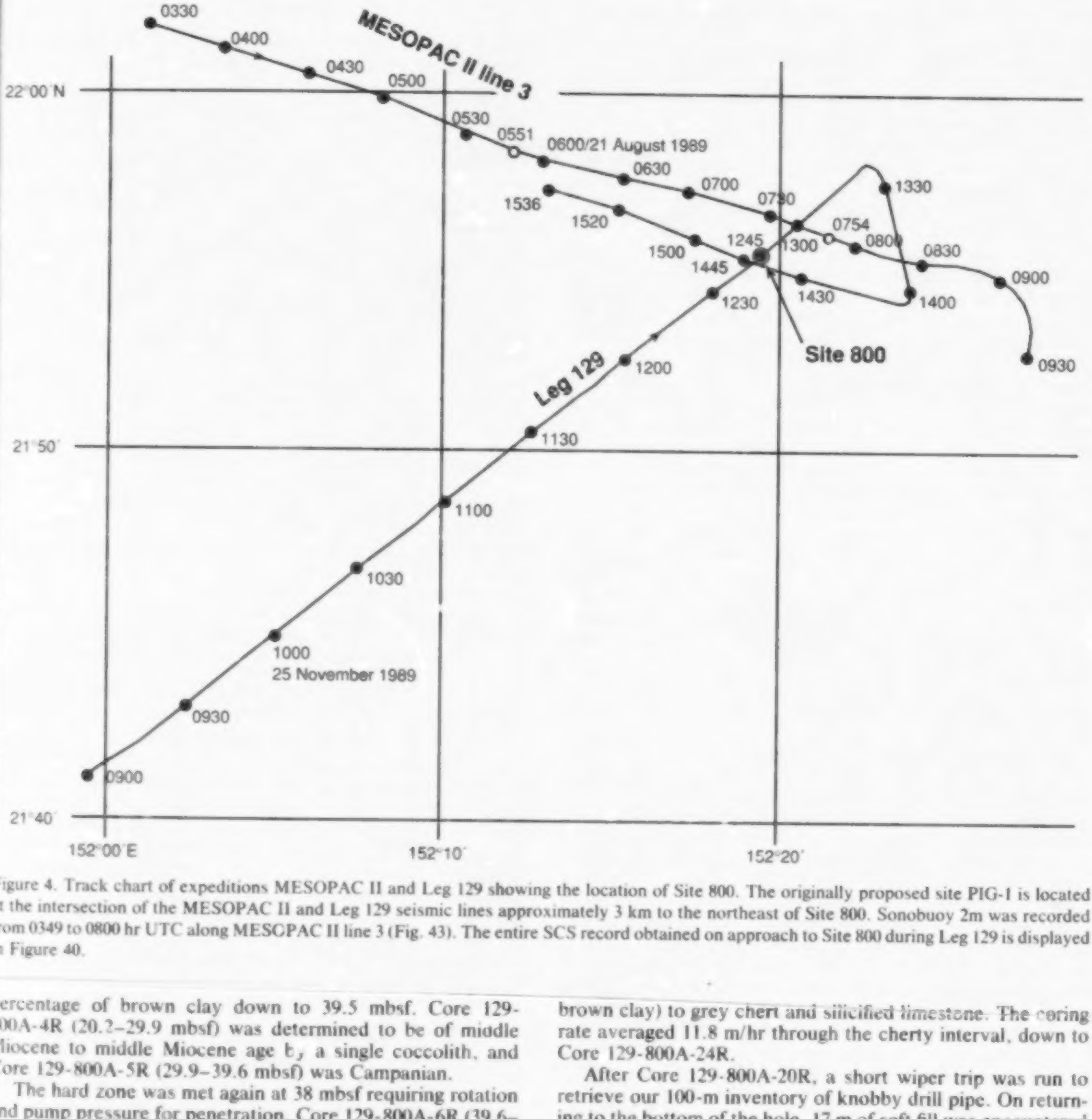

Figure 4. Track chart of expeditions MESOPAC II and Leg 129 showing the location of Site 800. The originally proposed site PIG-1 is located at the intersection of the MESOPAC II and Leg 129 seismic lines approximately 3 km to the northeast of Site 800. Sonobuoy 2m was recorded from 0349 to 0800 hr UTC along MESOPAC II line 3 (Fig. 43). The entire SCS record obtained on approach to Site 800 during Leg 129 is displayed in Figure 40.

percentage of brown clay down to 39.5 mbsf. Core 129-800A-4R (20.2–29.9 mbsf) was determined to be of middle Pliocene to middle Miocene age by a single coccolith, and Core 129-800A-5R (29.9–39.6 mbsf) was Campanian.

The hard zone was met again at 38 mbsf requiring rotation and pump pressure for penetration. Core 129-800A-6R (39.6–49.2 mbsf) and the immediately subsequent cores proved to be red, banded porcellanites and cherts with recovery averaging 5%–10%. Cores required about 30 min to cut with 15,000 to 20,000 lb of bit weight and 20–40 spm of pump pressure. A minor amount of drill string torquing was experienced. The good weather and heave compensator provided a relatively constant weight on bit that made penetration relatively routine. Coring continued in this fashion, although the porcellanites hardened into true cherts, requiring more bit weight and cutting time. Cores 129-800A-10R to -16R were cut with 20,000 to 25,000 lb of weight on bit, 40 spm of pump, and 40–50 rotations per minute (rpm). They each required 40–45 min of cutting time. After Core 129-800A-10R, 15 barrels of mud were pumped into the hole after every third core. The recovered cherts graded down section from red (recrystallized brown clay) to grey chert and silicified limestone. The coring rate averaged 11.8 m/hr through the cherty interval, down to Core 129-800A-24R.

After Core 129-800A-20R, a short wiper trip was run to retrieve our 100-m inventory of knobby drill pipe. On returning to the bottom of the hole, 17 m of soft fill was encountered and cutting torque increased significantly. Starting with Core 129-800A-25R, the cutting rate increased and cutting torque decreased as the formation changed from cherts and silicified limestones to indurated and slightly silicified claystones with occasional volcanic ash.

Recovery on Core 129-800A-26R was nearly 50%, up from 5%–10% in the chert sequence. The hole remained clean (no torque with the bit off the hole bottom) and the bit cutting structure was still intact, as the claystone was recovered as full-gauge core (diameter = 2.28 in.). Beginning with Core 129-800A-26R, we cored through, and recovered a substantial percentage of, a thick section of well-cemented, fine- to medium-grained volcaniclastic turbidites, probably shed from Himu Seamount 40 miles to the southwest. The volcaniclastics contain occasional, deep-water pelagic sediments that are uniformly Aptian in age (as is Himu Seamount) down through Core 129-800A-50R. The coring rate averaged about 20 m/hr through this sequence. Wiper/knobby trips were run after Cores 129-800A-31R and -42R. A drift survey after Core 129-800A-39R measured 3° of hole inclination off vertical.

Cores 129-800A-51R to -55R recovered relatively soft, red claystone that caused some torquing problems of the drill string. Several sweeps of mud were run to combat the problem, and a knobby/wiper trip was run after Core 129-800A-53R.

Coring was relatively rapid until the last 2 m of Core 129-800A-56R, when a very hard formation was encountered. This proved to be hard, red chert in Core 129-800A-56R and the top of Core 129-800A-57R. The bottom of Core 129-800A-57R and the succeeding cores proved to be basaltic dolerite that cored smoothly at the rate of 3–4 m/hr. The basalt was jammed off in Core 129-800A-57R by a deformed, plastic core liner, so we decided to core without liners in the basalt section after that. The hole held up well until the end of Core 129-800A-61R, when it was difficult to pick up the bit off the bottom of the hole. It was decided to run a knobby/wiper trip prematurely to ream out the hole. After laying down the knobby pipe and several stands of regular drill pipe, the drilling line was also slipped, cut, and reterminated. After the wiper trip it was impossible to return to the bottom of the hole, due to a tight spot at 350 mbsf. Apparently the large percentage of clay in the volcaniclastic turbidites was swelling and seizing the BHA. Several attempts to ream through the tight spot were not successful, and we abandoned our attempts to core ahead in this hole. It required several attempts to release the bit for logging at 335 mbsf, probably due to volcaniclastic debris plugging the bit release mechanism.

Standard logging in this hole was conducted in three runs: the quad combination consisting of caliper, natural gamma ray, dual induction, long-spaced sonic, temperature, and lithodensity tools; the geochemical string consisting of induced-gamma, aluminum clay, neutron, and natural gamma ray tools; and the formation microscanner (FMS) consisting of FMS and natural gamma-ray tools. At the start of the quad combination run, it was discovered that the wireline heave compensator was inoperative despite a service call from its designer during the Singapore yardwork. We were not able to make repairs during the logging period and operated without the compensator in relatively calm seas. All logs were run up to 45 mbsf. The quad combination bottomed at 294 mbsf, the geochemical string at 315 mbsf, and the FMS at 214 mbsf. Logging took a total of 28 hr, after which we pulled out of the hole and proceeded to proposed site PIG-3A at 1103 hr UTC on 5 December 1989.

## LITHOSTRATIGRAPHY AND SEDIMENTOLOGY

The stratigraphic sequence penetrated at Site 800 consists predominantly of pelagic clays, cherts and porcellanites, limestones, volcaniclastic claystones, siltstones, and sandstones. On the basis of the distribution of these lithologies, the sedimentary column between 0 and 498.1 mbsf has been divided from top to bottom into five lithologic units: a pelagic brown clay unit, a brown porcellanite and chert unit, a gray siliceous limestone and chert unit, a volcaniclastic turbidites unit, and a siliceous and pelagic clay unit. Intrusive dolerite sills that contain minor amounts of sediment were recovered between 498.1 and 544.5 mbsf and are described as Unit VI. The main lithologic facies, mineralogical composition, and depositional trends are shown in Figure 5.

### Lithologic Units

#### *Unit I. Cores 129-800A-1R to -6R (0 to 38.0 mbsf): Pelagic Brown Clay; Pliocene to Upper Cretaceous*

Unit I, 38 m thick, consists of soft- and fine-grained pelagic brown clay. Its homogeneous character is probably related to the high degree of drilling disturbance. The pelagic clay is composed of clay aggregates and abundant iron oxide globules and granules which are similar to those occurring in deep-sea pelagic clay of abyssal plains and often described as RSO's (''red-brown semi-opaque objects,'' Yeats, Hart, et al., 1976). Sediment colors range from a very dark reddish brown in the highest four cores (129-800A-1R to -4R) to lighter hues as yellowish brown in the lowest core, 129-800A-5R. Detrital phases, represented by quartz and scarce feldspar are more abundant in the surface deposits, whereas the zeolites (phillipsite) increase in the lower part of the unit.

The possible ages of this sequence are derived from scarce foraminifer, nannofossil, and radiolarian populations, and range from middle Pliocene to middle Miocene in the upper dark brown deposits (Cores 129-800A-1R to -4R) to late Campanian in the lower, lighter deposits from Core 129-800A-5R. A long hiatus probably ranged from the Late Cretaceous to middle Miocene. The very low sedimentation rate for this unit, estimated to be lower than 0.5 m/m.y., is typical of pelagic deep-sea brown clays, deposited below the carbonate compensation depth (CCD). This facies is well represented in the entire deep northern Pacific Ocean.

On top of the subsequent core (129-800A-6R) at 39.6 mbsf, a 10-cm-thick layer of light brown clay occurs, which is probably uphole contamination from drilling operations.

#### *Unit II. Cores 129-800A-6R to -9R (38 to 78.2 mbsf): Brown Porcellanite and Cherts; Campanian to Turonian*

Unit II, 40.2 m thick but poorly recovered, is predominantly composed of porcellanites in gradational transition to cherts at various scales. The porcellanite and chert are very dark brown to brown in reddish and yellowish hues. Patches of chert cut across millimeter-scale laminations in the porcellanite (Fig. 6). Porcellanite prevails in the upper part of the unit and radiolarian cherts become more abundant downward. A zeolitic claystone occurs in interval 129-800A-8R-1, 35–40 cm. The main mineralogical composition of this facies consists of variable amounts of quartz and opal-CT.

Radiolarians provide late Campanian to early Campanian and Turonian ages. Therefore, the sedimentation rate of this sequence is estimated to be <2 m/m.y., a relatively low rate.

#### *Unit III. Cores 129-800A-10R to -25R (78.2 to 228.6 mbsf): Gray Siliceous Limestones and Cherts; Albian-Cenomanian*

A major change in color, from the reddish and yellowish brown cherts of Unit II to olive gray and gray cherts and porcellanites determines the top of Unit III. This unit, 150.4 m thick, consists of cherts and siliceous limestones. The cherts contain radiolarians filled with opal and chalcedony; some are pyrite-replaced (Core 129-800A-10R). The texture is aphanitic, with a waxy luster and smooth, conchoidal fracture. In the upper part of the unit, the limestone layers are locally replaced by cross-cutting chert, with variable degrees of silicification (Fig. 7). The discontinuous laminations are often deformed and show slight bioturbation. Siliceous limestone becomes more abundant, as an interlayered major lithology, in Cores 129-800A-13R through -22R (Figs. 8 and 9A). Rare thin layers of soft micrite with nannofossils occur within Core 129-800A-17R. Foraminiferal fauna are mainly redeposited (see ''Biostratigraphy'' section, this chapter). At 181.4 mbsf (Core 129-800A-21R), the siliceous limestone and nannofossil

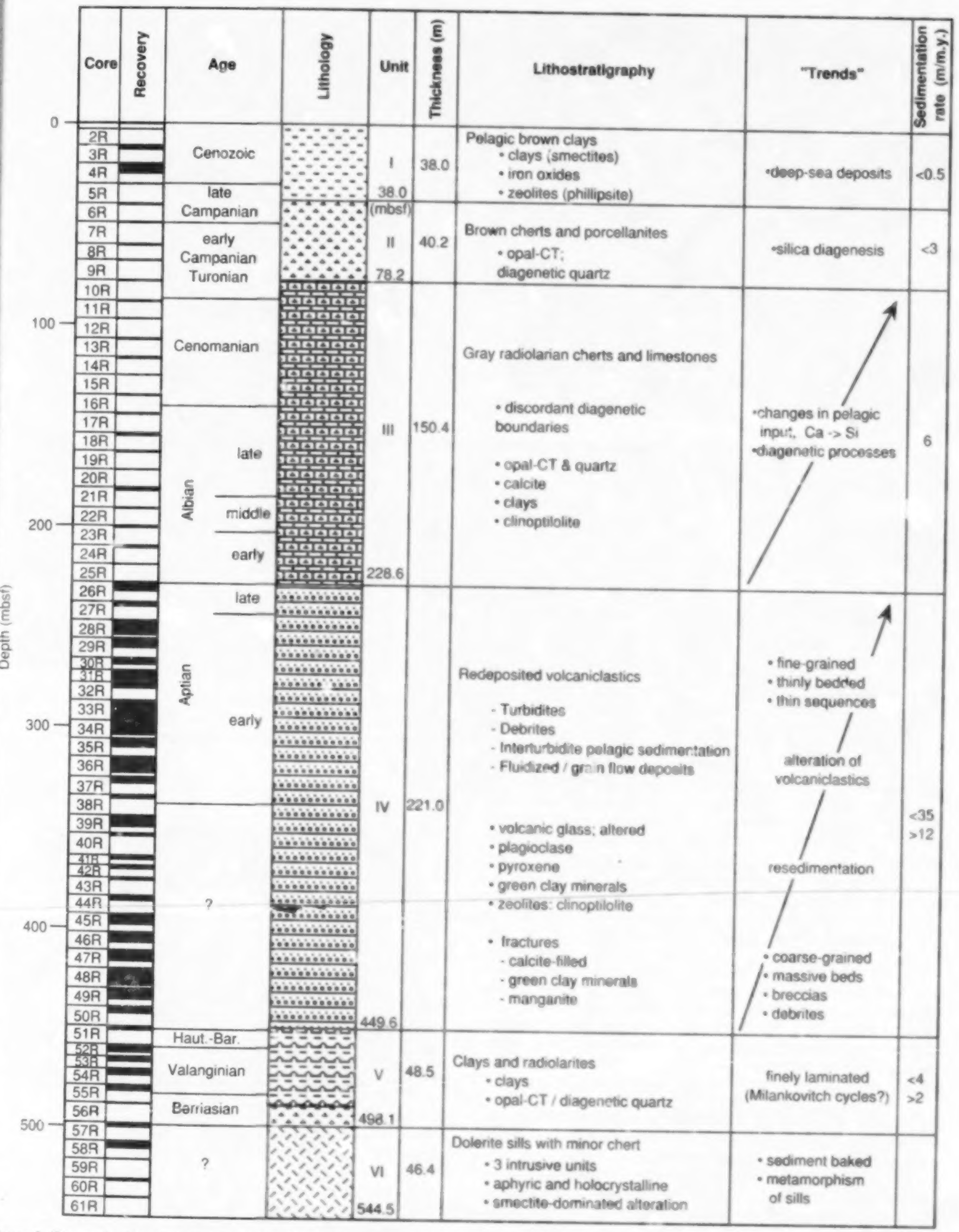
Core
Recovery
Age
Lithology
Unit
Thickness (m)
Lithostratigraphy
"Trends"
Sedimentation rate (m/m.y.)
Depth (mbsf)
0
100
200
300
400
500
2R
3R
4R
5R
6R
7R
8R
9R
10R
11R
12R
13R
14R
15R
16R
17R
18R
19R
20R
21R
22R
23R
24R
25R
26R
27R
28R
29R
30R
31R
32R
33R
34R
35R
36R
37R
38R
39R
40R
41R
42R
43R
44R
45R
46R
47R
48R
49R
50R
51R
52R
53R
54R
55R
56R
57R
58R
59R
60R
61R
Cenozoic
late Campanian
early Campanian Turonian
Cenomanian
Albian
late
middle
early
Aptian
late
early
?
Haut.-Bar.
Valanginian
Barriasian
?
I
38.0
38.0 (mbsf)
II
40.2
78.2
III
150.4
228.6
IV
221.0
449.6
V
48.5
498.1
VI
46.4
544.5
Pelagic brown clays
• clays (smectites)
• iron oxides
• zeolites (phillipsite)
•deep-sea deposits
<0.5
Brown cherts and porcellanites
• opal-CT;
diagenetic quartz
•silica diagenesis
<3
Gray radiolarian cherts and limestones
• discordant diagenetic boundaries
• opal-CT & quartz
• calcite
• clays
• clinoptilolite
•changes in pelagic input, Ca -> Si
•diagenetic processes
6
Redeposited volcaniclastics
- Turbidites
- Debrites
- Interturbidite pelagic sedimentation
- Fluidized / grain flow deposits
• volcanic glass; altered
• plagioclase
• pyroxene
• green clay minerals
• zeolites: clinoptilolite
• fractures
- calcite-filled
- green clay minerals
- manganite
• fine-grained
• thinly bedded
• thin sequences
alteration of volcaniclastics
resedimentation
• coarse-grained
• massive beds
• breccias
• debrites
<35
>12
Clays and radiolarites
• clays
• opal-CT / diagenetic quartz
finely laminated (Milankovitch cycles?)
<4
>2
Dolerite sills with minor chert
• 3 intrusive units
• aphyric and holocrystalline
• smectite-dominated alteration
• sediment baked
• metamorphism of sills

Figure 5. Composite lithologic units at Hole 800A and summary of the main mineralogical composition and sedimentary trends established for each unit.

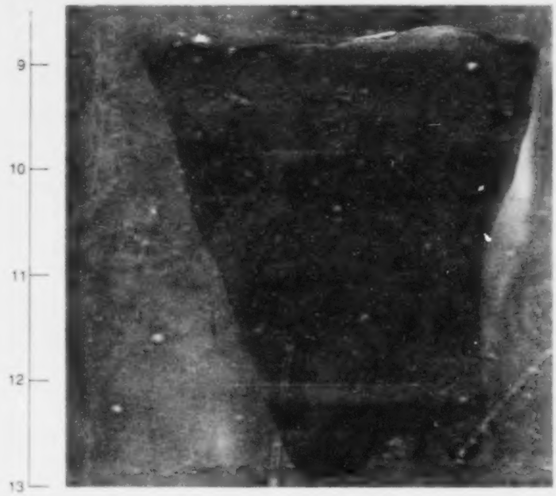

Figure 6. Sample 129-800A-9R-1, 9–13 cm, from Unit II. Porcellanite (light reddish brown, 5YR 6/4) with thin planar bedding and local replacement by chert.

chalk are microlaminated. Variations in grain size which form the laminations are related to the abundance of radiolarians and to the degree of dissolution and cementation of the siliceous microfossils. The gradational transitions between the limestone or porcellanite and chert, as nodules or layers, are well established by thin-section observations (Fig. 9B, -C). In the lower part of the unit (Cores 129-800A-22R through -25R), a few volcanic clasts and clinoptilolite zeolite were detected (in smear slides, thin sections, and XRD). The volcaniclastic input within the base of the silicified limestone, expressed as fine-grained clasts and glass, establishes a transitional zone between the siliceous limestone and chert and the underlying volcaniclastic deposits (Unit IV).

The main mineral composition of the sediment from Unit III, determined by XRD analyses, ranges from prevalent quartz and opal-CT contents in the upper part of the unit (Cores 129-800A-10R to -17R), to higher calcite (Core 129-800A-22R), followed by higher clay contents in the lower levels (Cores 129-800A-23R to -25R).

Nannofossils as well as radiolarian assemblages indicate an age of Cenomanian for the top of the unit and early Albian for Cores 129-800A-21R to -25R (see "Biostratigraphy" section, this chapter). Thus, the mean sedimentation rate estimated for the whole Unit III is approximately 6 m/m.y. A possibly lower sedimentation rate is suspected in the lowest part of the unit, from Cores 129-800A-21R-2 through -25R (182.5–228.6 mbsf), because it is entirely middle to early Albian in age. A possible hiatus occurs between these Albian deposits and the underlying Aptian sediments.

### *Unit IV. Cores 129-800A-26R to -50R (228.6 to 449.6 mbsf): Redeposited Volcaniclastic Sandstone to Claystone; Aptian*

Unit IV consists of a 221-m-thick sequence of interbedded clays and claystones, silty clays, silty sandstones, and sandstones, mainly redeposited ash, and tuff with scarce biogenic phases. This unit is described as volcaniclastic turbidites and redeposited volcaniclastic sandstone. Several intervals are distinguished on the basis of the grain size, the thickness of the upward-fining beds, and carbonate content which were

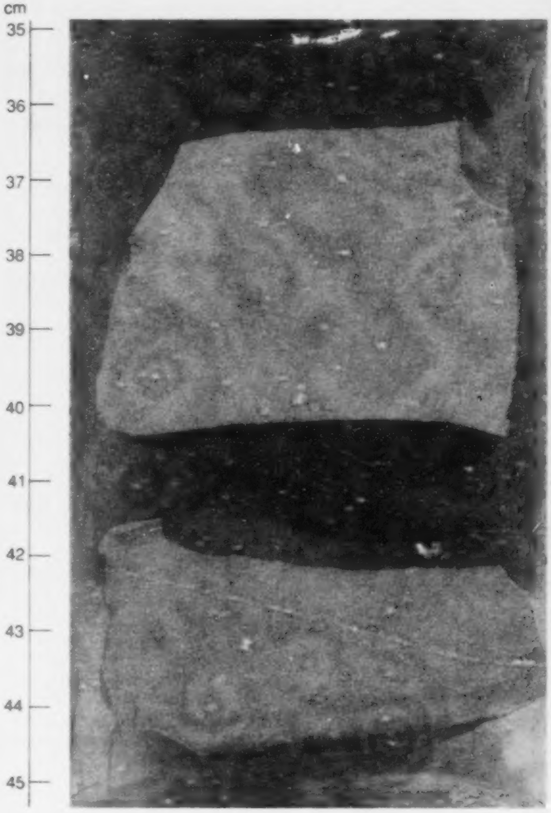

Figure 7. Interval 129-800A-13R-1, 35–45 cm, from Unit III. Limestone (light gray, 5Y5/1) with dark chert intervals about 3 cm thick. Porcellanite rims fringe the lower chertification zone (medium gray).

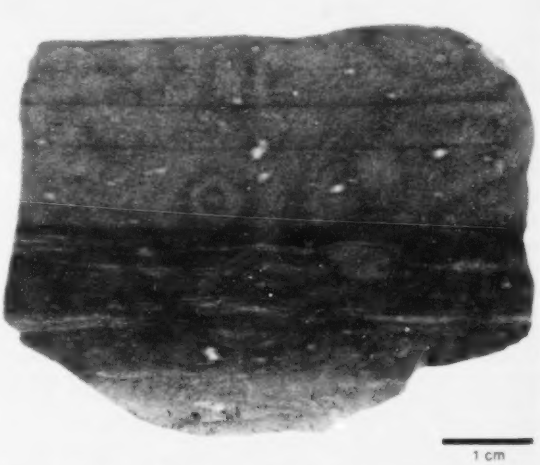

Figure 8. Interval 129-800A-14R-1, 51–55 cm, from Unit III. Siliceous limestone, fine-grained, with wavy planar laminations and compacted possible bioturbation features.

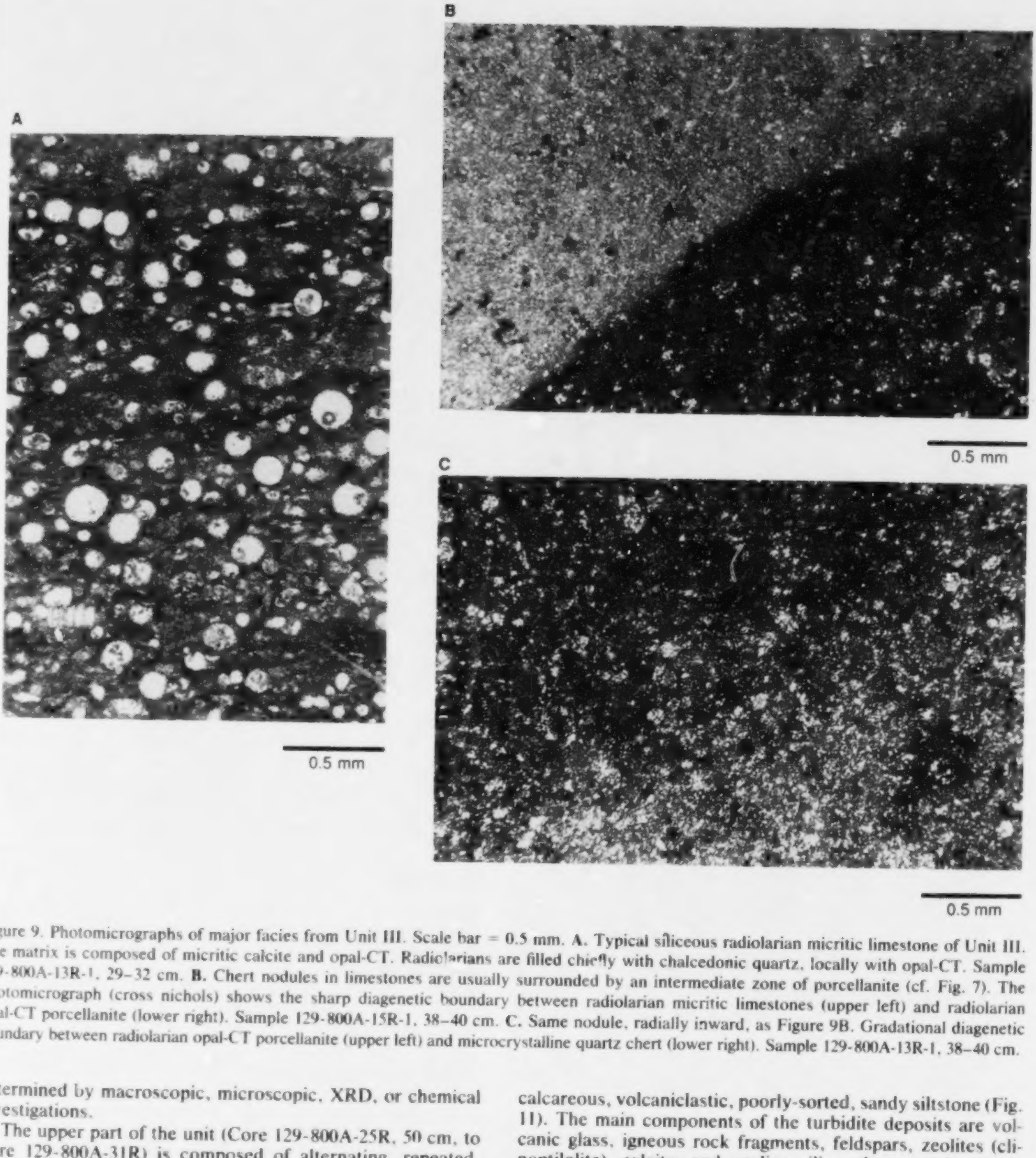

Figure 9. Photomicrographs of major facies from Unit III. Scale bar = 0.5 mm. **A.** Typical siliceous radiolarian micritic limestone of Unit III. The matrix is composed of micritic calcite and opal-CT. Radiolarians are filled chiefly with chalcedonic quartz, locally with opal-CT. Sample 129-800A-13R-1, 29–32 cm. **B.** Chert nodules in limestones are usually surrounded by an intermediate zone of porcellanite (cf. Fig. 7). The photomicrograph (cross nichols) shows the sharp diagenetic boundary between radiolarian micritic limestones (upper left) and radiolarian opal-CT porcellanite (lower right). Sample 129-800A-15R-1, 38–40 cm. **C.** Same nodule, radially inward, as Figure 9B. Gradational diagenetic boundary between radiolarian opal-CT porcellanite (upper left) and microcrystalline quartz chert (lower right). Sample 129-800A-13R-1, 38–40 cm.

determined by macroscopic, microscopic, XRD, or chemical investigations.

The upper part of the unit (Core 129-800A-25R, 50 cm, to Core 129-800A-31R) is composed of alternating, repeated, upward-fining beds of dark bluish to greenish grays. The thicknesses of these individual beds average about 50 cm (Figs. 10 and 11). In this part of the unit volcaniclastic siltstones grade upward to claystones that contain less than 10% radiolarians and scarce nannofossils. The graded beds are finely laminated, with load casts and convolute layers, and cross or planar laminations. Rare fractures are quartz-filled. Some of the turbidite beds grade upwards to olive brown radiolarian pelagic claystone with local bioturbation features (Fig. 12). Some turbidite beds begin with a thin horizon of calcareous, volcaniclastic, poorly-sorted, sandy siltstone (Fig. 11). The main components of the turbidite deposits are volcanic glass, igneous rock fragments, feldspars, zeolites (clinoptilolite), calcite, and opaline silica; the ground mass is made up of green clay minerals.

From Core 129-800A-32R through -38R the graded beds become coarser and thicker, consisting of gray gritstone to fine-grained sandstones, and to reddish brown claystones or clayey radiolarites. Calcareous claystone increases below Core 129-800A-36R. Several intervals show reversely graded bedding. Ripple laminations, cross laminations, and calcite veins are the main sedimentary and structural features. Reduction fronts often extend from the gray-green sharp base of turbidites beds downward into the underlying reddish brown

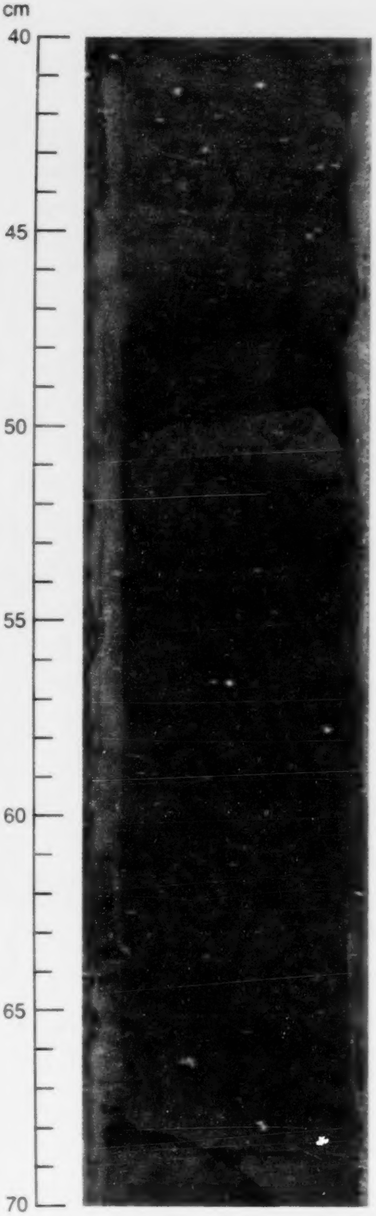

Figure 10. Typical, small, fine-grained, fining-upward turbidite bed of volcaniclastics ranging from dark gray (N4) sandy siltstone to lighter blue-green (5BG 5/1) claystone. This lithology comprises mainly the uppermost part of the Unit IV. Interval 129-800A-26R-3, 40–70 cm.

claystones. The turbidites increase in thickness to approximately 0.8–1 m. The main composition of the deposits is the same as the overlying fine-grained beds, but with higher calcium carbonate contents. The calcareous sandstone recovered in Core 129-800A-32R-1, 80–125 cm, contains up to 50% red algae fragments (Fig. 12C, -D). In the surrounding area of Site 800, similar calcareous compounds were described by Witman et al. (1986) and Haggerty and Premoli-Silva (1986). These fragments are also similar to the debris studied by McKenzie et al. (1980, and references therein) on northwestern Pacific seamounts and attributed to the "coral-algal facies" from low latitudes. In interval 129-800A-38R-1, 25–40 cm, numerous large fractures are filled by very a well-crystallized manganese hydroxide, identified as manganite (MnOOH). Dendrites are also abundant on fracture surfaces.

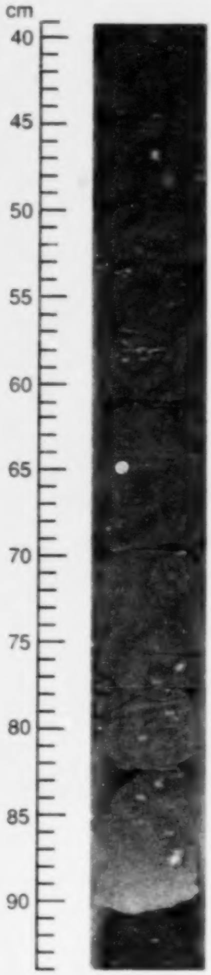

Figure 11. Within the upper part of Unit IV, some turbidite beds are made up of poorly sorted, yellowish gray (5Y 8/1) calcareous siltstone to light greenish gray (5GY 7/1) laminar volcaniclastic and clayey beds. The composition of the basal sand is calcareous microfossils, inorganic calcite, and volcaniclastic fragments. Interval 129-800A-28R-3, 40–90 cm.

From Core 129-800A-39R through -46R, the prevalent lithologies are volcaniclastic sandstones, claystones, and poorly sorted sandstone breccia, with less frequent claystone horizons than above. The breccia facies shows numerous clasts of finely laminated claystone or radiolarite, poorly sorted sandstone and some volcanic rock fragments; trains of clasts are randomly oriented and some may represent debris flows (Fig. 13). The finest claystones and radiolarites contain

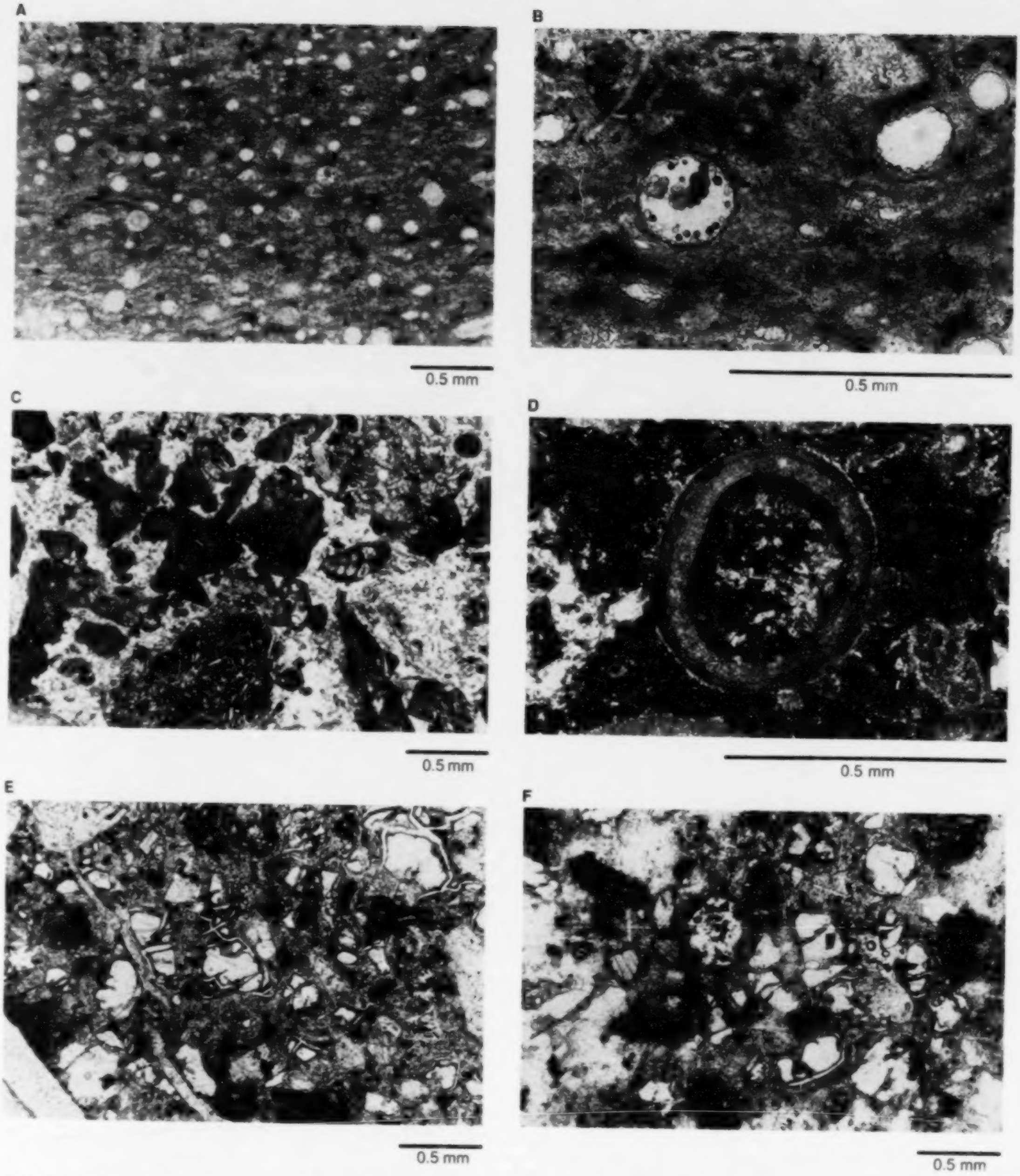

igure 12. Photomicrographs of the major sedimentary facies from Unit IV. Scale bar = 0.5 mm. **A.** Background pelagic sedimentation between he redepositional events is mainly radiolarian-rich. The facies is typical radiolarian opal-CT porcellanite with a clay and opal-CT matrix. Sample 29-800A-30R-1, 34–37 cm. **B.** Close-up from previous thin section. Radiolarians tests are replaced by opal-CT and partially filled by opal-CT epispheres. The clear remainder of radiolarian internal tests are filled with chalcedony. Sample 129-800A-30R-1, 34–37 cm. **C.** Calcareous olcaniclastic turbidite beds (cf. Fig. 11) contain abundant biogenic components. The fragments of foraminifers and micritized red algae are ssociated with ooids and volcaniclasts. Scattered fragments of *Orbitolinidae* foraminifers in other parts in the thin section are typical, middle retaceous neritic forms. Sample 129-800A-32R-1, 117–118 cm. **D.** Ooid nucleated on volcaniclast, and a foraminifer similar to *Bolivinopsis* sp. n calcareous volcaniclastic turbidites. Same sample as Figure 12C. Cross nichols. **E.** Volcaniclastic sandstone turbidites with prevalent volcanic lass, igneous rock fragments, clinopyroxene, and calcite. Sample 129-800A-37R-2, 123–128 cm. **F.** Volcaniclastic, medium-grained, dusky green G 3/2) sandstone turbidites are composed mostly of microphyric glass fragments replaced by clays, plagioclase, clinopyroxene clasts, black chylite, iron-oxides, clay minerals, and secondary calcite. Sample 129-800A-47R-2, 64–67 cm.

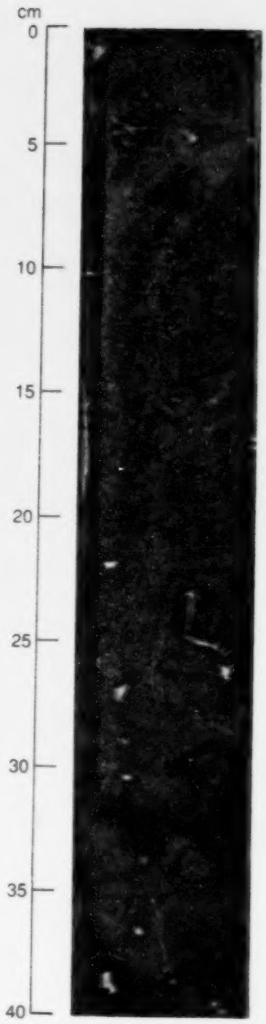

Figure 13. Lower part of lithologic Unit IV. The basal horizon of the thicker turbidite beds are often composed of a breccia of reddish brown (5YR 4/4) claystone clasts within a greenish gray (5G 5/1), sandy, volcaniclastic matrix. The clasts are angular to sub-rounded, 0.2–1.5 cm in size, and without preferential orientation. The distribution suggests a debris flow deposit. Interval 129-800A-2R-1, 0–40 cm.

up to 50% radiolarians. Several generations of fractures occur. Some horizons are oxidized, resulting in medium gray and grayish red hues. The bulk mineralogy of the facies consists of quartz, feldspar, and clay minerals and few iron oxides. The fracture fillings are mainly calcite and/or dark green clay minerals such as palygorskite. The volcaniclastic sandy horizons are composed of unvesiculated glass often altered to clays, pyroxene clasts, and very few trachylite fragments within a clayey matrix (Fig. 12E, -F).

The lowest part of Unit IV (Cores 129-800A-47R to -50R) is a massive, dusky green, sandy volcaniclastic deposit containing igneous rock fragments, claystone fragments, and prevalent fresh volcanic glass shards; the latter are scarcely and locally palagonitized. Breccia horizons are frequent, and numerous redox fronts are expressed by sharp variation in colors ranging from green to brown. The clay-filled fractures are also more frequent. At interval 129-800A-48R-5, 107–118 cm, a calcareous sandstone contains moderately sorted carbonate grains within a clay matrix.

The calcareous microfauna found within the turbidite deposits of Unit IV indicate an early to late Aptian age for the upper part of the unit (Core 129-800A-25R to -37R) and a high sedimentation rate of 12–35 m/m.y. is estimated from the ages of the under- and overlying sediments (Fig. 5). A hiatus possibly occurred during the Barremian, probably reflecting the drastic change in energy between the volcaniclastic deposits (Unit IV) and the underlying siliceous sediments (Unit V).

### *Unit V. Core 129-800A-51R to Section 129-800A-57R-1, 10 cm (449.6 to 498.1 mbsf): Clayey Radiolarites to Siliceous Claystones; Valanginian-Barremian*

A distinct change in lithology distinguishes Unit V from the previous volcaniclastic and turbiditic deposits. This unit, 48.5 m thick, consists of microlaminated clayey radiolarites and siliceous claystones (Fig. 14). The sediment displays scarce green reduced zones in the mostly dark red to light red alternating beds. The mean thickness of the regularly alternating light-colored radiolarite (up to 85% radiolarians) and red claystone layers is about 6 cm. The mineralogical composition consists of varying concentrations of silica and clay minerals, with small amounts of feldspar (XRD). Frequent thin coatings of manganese oxide cut across or follow the laminations (Core 129-800A-53R to -54R). Bioturbation is common throughout the unit. Common, thin, silica-filled fractures cross-cut the layers in the lowest part of unit (Core 129-800A-55R). Within the interval from Core 129-800A-56R to interval 129-800A-57R-1, 0–10 cm, a grayish brown chert bed, with subtle laminations, directly overlies the first recovered igneous rocks.

Radiolarian assemblages indicate Hauterivian-Barremian to Berriasian ages. The sedimentation rate of the whole sequence of clays and radiolarites is estimated to be 2–4 m/m.y.; this sedimentation rate is low compared to average recent biogenic pelagic sedimentation rates of 5–10 m/m.y.

### *Unit VI. Section 129-800A-57R-1, 10 cm, to Core 129-800A-61R (498.1 to 544.5 mbsf): Dolerite Sills and Cherts; Berriasian*

Unit VI, the lowest lithologic unit recovered at Site 800, is composed of igneous rocks with one thin, interlayered chert horizon. The igneous rocks are described as intrusive dolerite sills (see "Igneous Petrology" section, this chapter). The dolerite is aphyric, non-vesicular, hyalocrystalline, and divided into three sub-units based on macrotextural variations and the presence of a chert sedimentary interlayer. All dolerite units are moderately to highly altered, dominated by secondary smectites, iron oxides, and carbonate, together with minor proportions of sericite, chlorite, celadonite, zeolite, actinolite, and biotite.

The interlayered sediments at interval 129-800A-58R, 30–45 cm, consist of dark reddish brown chert and radiolarite. They exhibit thin laminations similar to that of the chert layer above the dolerite (Core 129-800A-56R).

## Thin-Section and XRD Data from Sedimentary Rocks

Detailed descriptions of 79 thin sections were used to estimate the various major and minor lithologies and have been incorporated into the above lithologic descriptions. XRD analyses from 38 samples (see "Explanatory Notes" chapter, this volume) from both the dominant or minor lithologies

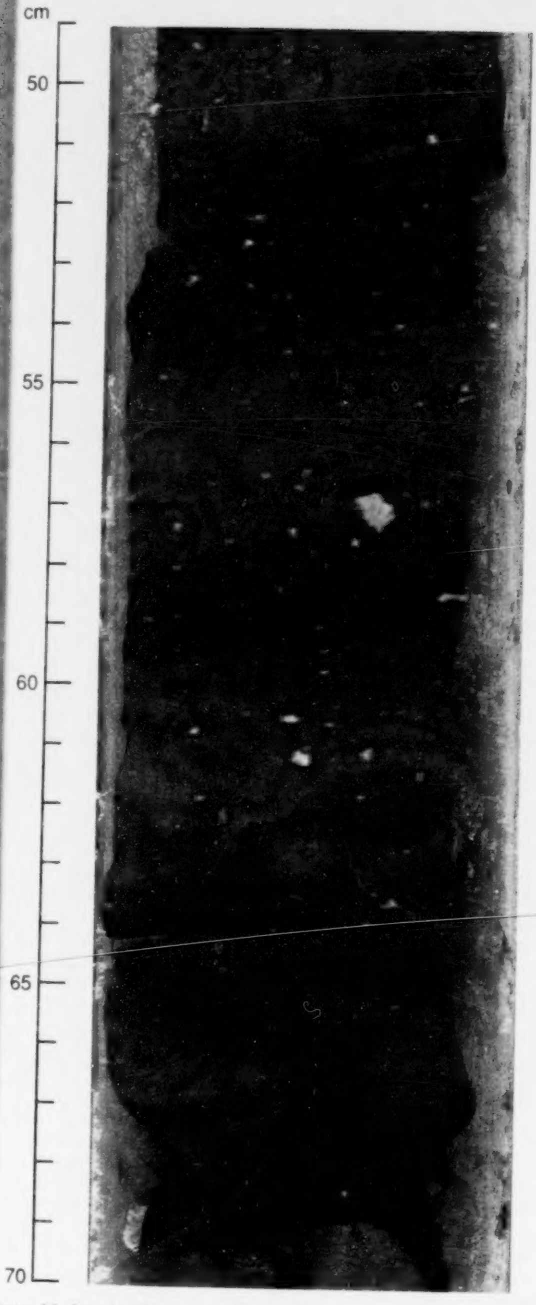

Figure 14. Interbedded, microlaminated, clayey radiolarites (lighter ayers as brown, 7.5YR 4.5/2–5/5) and siliceous claystones (dark rown layers, 7.5YR 3/1) form lithologic Unit V. The frequent thin fractures are silica-filled. The microlaminations are delineated by lack manganese oxide concentrations. Interval 129-800A-55R-2, 0–70 cm.

encountered in the various facies were selected to distinguish the relative mineralogic abundances and trends of these sediments, and to attempt the determination of specific features such as fracture fillings or thin lamination. Several trends can be observed in these data:

1. The nature of the zeolites. Phillipsite is present in the soft pelagic brown clay facies (Unit I), in clinoptilolite in the siliceous limestones (Unit III), and in the volcaniclastic turbidites and sandstones (Unit IV). The occurrence of these secondary silicates appears related to diagenetic processes.

2. Downhole increase in calcite and clay mineral contents, in the lowest part of Unit III. These variations in calcite and clay contents are inferred to represent a gradual change in biogenic input and an increasing silicification through diagenetic processes.

3. Composition of the sandstone and claystone layers in the turbiditic deposits (Unit IV). Higher plagioclase and pyroxene contents are found in the former, and higher clay minerals and clinoptilolite contents in the latter. The XRD data, limited to the peak values files ranging from between 2° to 40° $2\theta$, is not sufficient for the determination of specific clay minerals.

4. Barite occurs in some sampled intervals, such as the lowest part of the pelagic brown clays and interbedded claystones within the porcellanite and chert of Unit II. The widespread occurrence of barium-rich phases in pelagic deposits is often related to early diagenetic evolution of biogenic silica (dissolution-recrystallization processes).

### Carbonate Contents

Carbonate content data from selected samples were obtained following the method described in the "Explanatory Notes" chapter (this volume). Results are given in Table 2 and represented in Figure 15.

The calcium carbonate contents are very low, as expected, in the pelagic brown clay and underlying brown chert, and in the basal siliceous deposits (Units I, II, and V).

The sediments from Units III and IV contain variable amounts of calcium carbonate related to the primary nature of the lithologic facies and their subsequent diagenetic evolution. Thus, in Unit III, the interlayering and transitions between limestones, siliceous limestones, and cherts are well-documented. For example, a progressive downward increase of carbonate content from limestone to underlying chert is established from the data of Cores 129-800A-14R to -17R (Table 2). The higher contents (>80%) are reached in samples from chalk and limestone horizons within Cores 129-800A-19R and -20R. The main trend in this unit, composed predominantly of biogenic deposits, is a slight decrease in the number of carbonate layers and overall carbonate content from bottom to top.

The redeposited volcaniclastics forming Unit IV contain very little calcium carbonate (<10%), except for a few horizons occurring in the middle of the sequence (Cores 129-800A-32R and -33R), where the turbidite beds are coarse-grained. The carbonates are described mainly as reworked shallow-water biogenic fragments. Within turbidite beds, the coarser layers show higher calcium carbonate content than the overlying claystone layers. Fine-grained claystone horizons (i.e., interval 129-800A-39R-2, 41–43 cm) show relatively high calcite content, corresponding to the occurrence of numerous fracture fillings.

### Sedimentological Implications

The lithological and mineralogical description of the successive lithologic units allow us to define major trends in the sedimentary history of Site 800 (Fig. 5) in relation to the

Table 2. Carbon carbonate, expressed as $CaCO_3$, organic carbon, and sulfur contents of sediments from Hole 800A.

| Core, section, interval (cm) | Depth (mbsf) | $CaCO_3$ (wt%) | Organic carbon (wt%) | Sulfur (wt%) | Lithology |
|---|---|---|---|---|---|
| 129-800A- | | | | | |
| 3R-1, 82–85 | 11.42 | 0.3 | 0.03 | 0.10 | Pelagic clay |
| 4R-1, 115–118 | 21.35 | 0.4 | 0.04 | 0.12 | Pelagic clay |
| 4R-2, 25–30 | 21.95 | 0.6 | 0.21 | 0.09 | Pelagic clay |
| 4R-3, 58–60 | 23.78 | 0.5 | 0.02 | 0.11 | Pelagic clay |
| 6R-1, 35–37 | 39.95 | 0.1 | | | Pelagic clay |
| 8R-1, 35–36 | 59.25 | 0.1 | 0.09 | 0.02 | Chert |
| 8R-1, 36–37 | 59.26 | 0.2 | 0.14 | 0.01 | Chert |
| 8R-1, 37–38 | 59.27 | 0.1 | 0.05 | l.d. | Chert |
| 8R-1, 56–57 | 59.46 | 0.1 | 0.05 | 0.01 | Chert |
| 9R-1, 9–12 | 68.59 | 0.1 | | | Chert |
| 10R-1, 7–8 | 78.27 | l.d. | 0.04 | 0.58 | Chert |
| 10R-1, 32–34 | 78.52 | 0.1 | | | Chert |
| 12R-1, 21–25 | 97.51 | 18.2 | 0.14 | l.d. | Siliceous limestone |
| 13R-1, 62–64 | 107.42 | 31.7 | | | Siliceous limestone |
| 14R-1, 1–3 | 116.21 | 0.2 | | | Chert |
| 14R-1, 92–93 | 117.12 | 0.2 | 0.09 | 0.01 | Chert |
| 15R-1, 36–38 | 125.76 | 27.3 | 0.08 | l.d. | Siliceous limestone |
| 16R-1, 45–46 | 135.35 | 21.2 | 0.07 | l.d. | Siliceous limestone |
| 17R-1, 47–49 | 144.67 | 37.2 | | | Siliceous limestone |
| 17R-1, 63–64 | 144.83 | 23.3 | 0.18 | l.d. | Siliceous limestone |
| 18R-1, 88–9 | 154.58 | 0.1 | 0.13 | l.d. | Chert |
| 18R-1, 104–105 | 154.74 | 49.3 | 0.21 | l.d. | Limestone |
| 18R-1, 128–1130 | 154.98 | 0.1 | | | Chert |
| 19R-1, 23–25 | 163.13 | 29.4 | | | Siliceous limestone |
| 19R-1, 52–53 | 163.42 | 88.1 | 0.53 | l.d. | Limestone |
| 21R-1, 1–2 | 181.31 | 0.4 | | | Chert |
| 21R-1, 135–137 | 182.65 | 81.7 | | | Limestone |
| 22R-1, 22–23 | 191.22 | 86.8 | | | Limestone |
| 22R-1, 25–27 | 191.25 | 44.6 | | | Limestone |
| 23R-1, 18–20 | 200.68 | 8.4 | | | Silicified limestone |
| 23R-1, 53–55 | 201.03 | 44.1 | | | Limestone |
| 23R-1, 68–69 | 201.18 | 0.4 | | | Chert |
| 23R-1, 90–91 | 201.40 | 21.1 | | | Silicified limestone |
| 24R-1, 86–87 | 210.76 | 13.6 | | | Silicified limestone |
| 24R-1, 120–122 | 211.10 | 22.5 | | | Silicified limestone |
| 25R-1, 11–12 | 219.41 | 19.1 | | | Silicified limestone |
| 25R-1, 31–33 | 219.61 | 0.3 | | | Chert |
| 26R-1, 114–115 | 229.74 | 5.8 | 0.12 | l.d. | Volcanic turbidite, fine |
| 26R-2, 140–148 | 231.50 | 5.3 | 0.05 | l.d. | Volcanic turbidite, fine |
| 26R-3, 54–56 | 232.14 | 1.4 | | | Volcanic turbidite, fine |
| 26R-CC, 10–12 | 232.84 | 0.5 | | | Volcanic turbidite, medium |
| 27R-1, 16–18 | 238.16 | 4.1 | | | Volcanic turbidite, fine |
| 27R-1, 97–99 | 238.97 | 0.3 | 0.04 | l.d. | Volcanic turbidite, fine |
| 27R-1, 140–150 | 239.40 | 2.0 | 0.01 | l.d. | Volcanic turbidite, medium |
| 28R-1, 19–20 | 247.39 | 4.2 | 0.07 | l.d. | Volcanic turbidite, medium |
| 28R-1, 33–35 | 247.53 | 6.6 | | | Volcanic turbidite, medium |
| 28R-2, 55–56 | 249.25 | 0.6 | | | Volcanic turbidite, medium |
| 28R-3, 106–108 | 251.26 | 0.9 | | | Volcanic turbidite, fine |
| 29R-2, 29–31 | 258.29 | 2.4 | | | Volcanic turbidite, fine |
| 30R-2, 102–104 | 268.42 | 0.6 | | | Volcanic turbidite, medium |
| 30R-2, 107–117 | 268.47 | 1.0 | | | Volcanic turbidite, fine |
| 31R-1, 50–52 | 272.50 | 2.1 | | | Volcanic turbidite, fine |
| 32R-1, 103–105 | 279.13 | 49.6 | | | Volcanic turbidite, coarse |
| 33R-1, 27–35 | 287.77 | 11.6 | | | Volcanic turbidite, fine |
| 33R-3, 74–76 | 291.24 | 18.4 | | | Volcanic turbidite, coarse |
| 33R-5, 12–14 | 293.62 | 4.2 | | | Volcanic turbidite, coarse |
| 33R-6, 60–70 | 295.60 | 8.2 | l.d. | l.d. | Volcanic turbidite, coarse |
| 34R-3, 15–17 | 300.15 | 5.9 | | | Volcanic turbidite, medium |
| 35R-3, 36–38 | 309.76 | 0.3 | | | Volcanic turbidite, medium |
| 36R-1, 63–65 | 316.53 | 6.6 | | | Volcanic turbidite, coarse |
| 36R-3, 76–78 | 319.66 | 5.3 | | | Volcanic turbidite, fine |
| 37R-2, 0–10 | 326.60 | 0.7 | 0.01 | l.d. | Volcanic turbidite, fine |
| 37R-2, 115–116 | 327.75 | 5.0 | 0.14 | l.d. | Volcanic turbidite, coarse |
| 38R-1, 112–114 | 335.62 | 2.1 | | | Volcanic turbidite, fine |
| 39R-2, 41–43 | 345.71 | 14.8 | | | Volcanic turbidite, fine |
| 40R-1, 39–41 | 353.49 | 2.4 | | | Volcanic turbidite, medium |
| 41R-1, 19–21 | 362.69 | 0.9 | | | Volcanic turbidite, fine |
| 41R-2, 0–10 | 364.00 | 1.2 | 0.08 | 0.03 | Volcanic turbidite, fine |
| 42R-1, 53–55 | 369.13 | 0.5 | | | Volcanic turbidite, fine |
| 43R-1, 106–108 | 375.76 | 0.6 | | | Volcanic turbidite, coarse |
| 44R-1, 123–126 | 384.93 | 0.7 | | | Volcanic turbidite, medium |
| 45R-1, 85–87 | 393.95 | 1.9 | | | Volcanic turbidite, medium |
| 46R-1, 78–80 | 403.28 | 0.2 | | | Volcanic turbidite, fine |
| 47R-1, 89–91 | 412.79 | 1.3 | | | Volcanic turbidite, medium |
| 48R-4, 21–23 | 426.11 | 1.2 | | | Volcanic turbidite, medium |
| 49R-1, 35–37 | 431.25 | 0.5 | | | Volcanic turbidite, fine |
| 49R-2, 140–150 | 433.80 | 0.2 | 0.07 | 0.03 | Volcanic turbidite, fine |
| 50R-1, 81–83 | 441.01 | 0.5 | | | Volcanic turbidite, fine |
| 51R-1, 71–73 | 450.31 | 0.2 | | | Volcanic turbidite, fine |
| 52R-2, 118–120 | 461.48 | 0.2 | | | Volcanic turbidite, fine |
| 53R-1, 128–130 | 466.18 | 0.1 | | | Volcanic turbidite, medium |
| 54R-2, 0–12 | 472.50 | 0.2 | | | Clay radiolarite |
| 54R-2, 57–59 | 473.07 | 0.2 | | | Radiolarite |
| 55R-2, 62–64 | 481.22 | 0.2 | | | Clay radiolarite |

Note: l.d. = less than detection level.

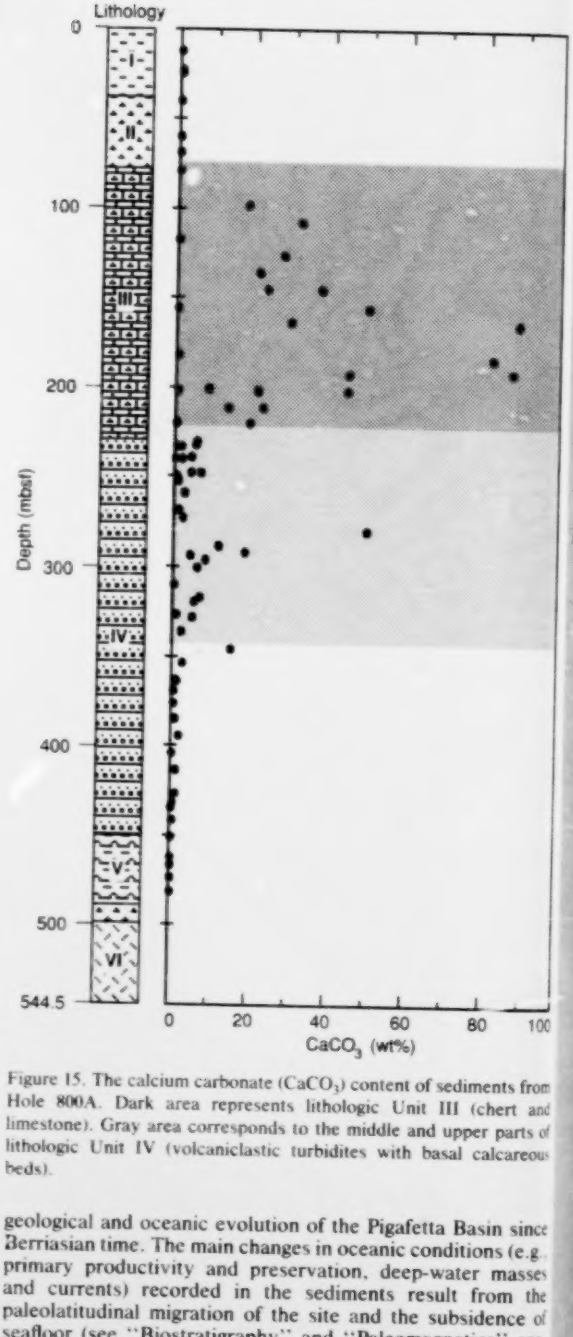

Figure 15. The calcium carbonate ($CaCO_3$) content of sediments from Hole 800A. Dark area represents lithologic Unit III (chert and limestone). Gray area corresponds to the middle and upper parts of lithologic Unit IV (volcaniclastic turbidites with basal calcareous beds).

geological and oceanic evolution of the Pigafetta Basin since Berriasian time. The main changes in oceanic conditions (e.g., primary productivity and preservation, deep-water masses and currents) recorded in the sediments result from the paleolatitudinal migration of the site and the subsidence of seafloor (see "Biostratigraphy" and "Paleomagnetics" sections, this chapter).

### *The Intrusive Event and Early Cretaceous Sedimentation (Berriasian-Barremian)*

Above and within the intrusive dolerites between 498.1 and 449.6 mbsf, the sediments are siliceous and consist mainly of radiolarian claystones and radiolarites. Thermal diagenetic effects of the intruded sill on the sediments may have induced the formation of red chert with well-preserved laminations (Unit VI at 507.5 mbsf). Siliceous biogenic deposits, sometimes baked or metamorphosed by the setting of igneous rocks, are common. The epochs of siliceous sedimentation are also often contemporaneous with episodes of fast oceanic spreading, volcanism, and consequent global transgressions (Garrison, 1974; Jenkyns, 1978; Jenkyns and Winterer, 1982).

Lithologic Unit V (449.6–498.1 mbsf), which overlies the dolerites, consists of alternated red radiolarites and claystones beds showing an apparent cyclicity. Based on the low sedimentation rate of this facies (about 2 m/m.y.), the average rhythmicity is about 40 k.y., a period clearly compatible with Milankovitch-type cycles. The worldwide formation of pelagic alternations during the Early Cretaceous is generally attributed to global climatic pulses (Berger et al., 1984). In the northwestern Pacific such deposits were described by Ferry and Schaaf (1982). Even if such rhythmic deposits are mostly described in calcareous sediments (alternations of limestones, marls, and clays), siliceous deposits at Site 800 may have recorded fluctuations in productivity that resulted in rhythmic deposition of biogenic siliceous phases at depths below a contemporaneous CCD, within an oxidizing bottom environment. The slight influence of the underlying volcanics is expressed in the lower part of these deposits by the diagenetic remobilization of various components expressed as manganese oxide coatings and abundant thin, silica-filled fractures.

### *Aptian Volcanic Event*

During terminal Barremian times, Site 800 experienced an intense volcaniclastic deposition event which seems to have abruptly interrupted and diluted the biosiliceous sedimentation. The volcaniclastic material was redeposited mostly as turbidite beds in a thick "sequence" of about 221 m (449.6 to 228.6 mbsf, Unit IV). Successive types of turbidites, differentiated by thickness, grain size, and composition, record the relative variations of intensities of volcaniclastic or/and pelagic inputs, and the environment conditions of the deep sea.

The lower volcaniclastic deposits are coarse-grained, form massive beds, and contain grain flows, breccia, and debrites (449.6–343.8 mbsf). The deposits are free of calcareous biogenic phases but the fracture fillings are often calcitic within the more volcanogenic layers. Thus, the biogenic contribution is mostly siliceous, in continuity with the previous deposits, and better represented in the finer clayey beds that also show upward-migrating oxidation fronts. Alteration and authigenetic processes within volcanogenic deposits form a green clay minerals matrix and fracture filling. This type of deposit reflects: (1) a high level of volcanic activity producing material which reacts intensively with seawater, (2) the proximal location of the site to the volcanic source, and (3) the oxidizing bottom conditions allowing preservation of biogenic phases and development of red top beds during quiet episodes between intermittent setting of volcaniclastic flows.

The overlying turbidites, from 343.8 to 278.1 mbsf, have mostly the same characteristics, with a slight decrease in thickness and grain size in some beds. The main change is in the calcareous input; carbonate phases are mainly shallow-water debris. This deposition interval could result from the degradation, under high energy conditions, of the top and shallow slopes of the nearby, still active seamounts. The intense erosion processes of such shallow-water volcanogenic and biogenic facies may occur during abrupt tectonic events of seamount subsidence (e.g., Jackson, Koizumi, et al., 1980, and references therein).

The uppermost interval of turbidites (top of Unit IV, 278.1–228.6 mbsf) corresponds to the final stage of the large volcaniclastic sedimentary event. The turbidite beds become thinner, finer-grained, and finer-laminated. The facies grades up to more siliceous and somewhat calcareous biogenic deposits. Carbonate content is low, reflecting limited pelagic input (nannofossils). The time span between the deposition of successive turbidite beds allows the development of well-oxidized horizons with abundant bioturbation features. Thus, migration of the site into an area of high primary productivity may have provided an adequate environment for the formation of clayey siliceous pelagic sediments mixed with the final stage of volcaniclastic redeposition.

The volcaniclastic and pelagic sequence with its characteristic high sedimentation rate provides a complete record of a middle Cretaceous volcanic event in a deep basin. This volcanic activity, which resulted in the edification of major volcanic plateaus and numerous seamounts in the northwestern Pacific, occurred throughout the Pacific Ocean (Larson and Schlanger, 1981; Moberly, Schlanger, et al., 1986).

### *Albian-Cenomanian Biogenic Sedimentation*

After the volcanic event, sedimentation was dominated by the siliceous and calcareous biogenic contribution (lithologic Unit III, 228.6–78.2 mbsf). The sedimentary transition is gradational and the remobilization of volcanogenic phases is common in the lower levels of the gray radiolarian chert and limestone. The main trends in this lithologic unit are the progressively upward increase in calcareous biogenic input within the lowermost horizons (228.6–162.9 mbsf), followed by a gradational decrease in the calcium carbonate content (162.9–78.2 mbsf). The deposits seem to reflect the oceanic environment when the site reached subequatorial paleolatitudes, characterized by nutrient-rich surface water masses yielding high primary productivity, a weakly reducing deep-water environment, and a sufficiently high sedimentation rate, favoring preservation of biogenic phases. Diagenesis then silicified limestones and chertified radiolarian oozes, creating of a full range of various lithologies between chalks and cherts. The evolution of siliceous biogenic oozes and formation of cherts, and the role of various amounts of clays and carbonate, as well as the role of time in the mineralogical composition of cherts, have been discussed by Lancelot (1973), Wise and Weaver (1974), Kastner et al. (1977), and Pisciotto (1981) and references therein.

### *Siliceous Sedimentation During the Late Cretaceous*

During Turonian to late Campanian times, sedimentation was predominantly siliceous, with a relatively low sedimentation rate. The diagenetic transformation of clayey siliceous oozes leads to the formation of iron-rich, red porcellanite and cherts (lithologic Unit II, 78.2–38.0 mbsf). The conditions of deposition show a slight change from the previous gray cherts with more oxidizing bottom conditions. Similar Upper Cretaceous red cherts are widespread in the northwestern Pacific Ocean (Thiede, Vallier, et al., 1981; Pisciotto, 1981).

### *Pelagic Brown Clay Deposition from the Latest Cretaceous to the Cenozoic and Quaternary*

The uppermost deposits (0–38 mbsf, lithologic Unit I) are pelagic brown clay similar to that described in the recent deep ocean basins. A drastic change in sedimentation outlines the transition between cherts and clays in the late Campanian. The clay facies results from the nondeposition and/or dissolution of biogenic compounds at depths below the CCD. The CCD depth was about 3500 m during the early Tertiary and deepened near the end of the Eocene down to an average depth of about 4500 m (Hay, 1988). The average sedimentation rate of such deposits is very low and enhances early diagenetic processes expressed by authigenesis of clays, iron oxides, and zeolites. A possible hiatus separates the lowest and lighter-colored Campanian pelagic clay from the Cenozoic brown clay. Because biostratigraphy is not very precise in the condensed deposits, it is not possible to preclude the occurrence of successive hiatuses during the whole period. Long hiatuses, particularly during the Paleocene, across the Eocene-Oligocene boundary, and during Miocene, are widespread in the northern Pacific Ocean (Karpoff, 1989, and references therein).

## BIOSTRATIGRAPHY

A sequence of sediments was recovered from 58 rotary-drilled cores dated as possibly Miocene-Pliocene to Berriasian-Valanginian, based on their microfossil content. A hiatus is suspected at the base of Core 129-800A-4R, from which core-catcher sediments were tentatively dated as middle Miocene to middle Pliocene. Core recovery was generally less than 30% although in some instances it was as high as 96%. Core-catcher samples were examined for radiolarians, foraminifers, palynomorphs, and calcareous nannofossils. Other samples from within the cores were examined when core catchers yielded few or no microfossils.

The cores were dated using three groups: calcareous nannofossils, radiolarians, and foraminifers. The calcareous nannofossils are most abundant and useful in the middle Cretaceous sediments. Radiolarians are the most persistent group but their stratigraphic utility at this site is limited to the Neocomian and Upper Cretaceous intervals. Although foraminifers occur sporadically through the cores, they corroborate ages determined by calcareous nannofossils and radiolarians. A summary of the biostratigraphy of Site 800 is presented in Figure 16.

Our interpretation of a general abyssal paleoenvironment, with deposition below the CCD, is attested by a high abundance of radiolarians throughout the cores, sparsity of calcareous nannofossils, virtual absence of planktonic foraminifers, and presence of agglutinated benthic foraminifers. Redeposited larger foraminifers signify proximity to shallow-marine (photic zone) paleoenvironments and transportation and reworking by turbidity currents. Palynomorphs were not observed in samples examined thus far, although amorphous organic matter was encountered in some intervals.

Preliminary data regarding the abundance of calcareous nannofossil and radiolarians are reported in Figure 17 against ages, lithostratigraphy, and paleolatitude. Radiolarians occur abundantly through the Mesozoic except for the Aptian to Barremian(?) interval corresponding to the southernmost location of this site with respect to the equator, as suggested by paleomagnetic data. Highest nannofossil abundance was observed in the Cenomanian to Albian interval, whereas during the Aptian nannofossils are sporadic and rare to few.

### Calcareous Nannofossils

No age-diagnostic nannofossils were observed from Cores 129-800A-1R through -5R, except for a single specimen of *Reticulofenestra pseudoumbilica* in Sample 129-800A-4R-CC. If this is reliable, then Core 129-800A-4R is middle Miocene to middle Pliocene in age. We hesitate to place much confidence in an age determination from a single specimen from otherwise barren cores. No other Cenozoic age determinations were made at this site.

The first evidence of Cretaceous sediments was found in Sample 129-800A-6R-1, 3–4 cm. Two specimens of *Watznaueria barnesae* were encountered in this sample but accompanied by a badly overgrown discoaster. As discoasters are confined to the Cenozoic and *Watznaueria* is confined to the Mesozoic, the former must be considered contamination or the latter considered reworking. Other fossil groups indicate that this sample is Cretaceous in age, so we consider the discoaster contamination and, consequently, also consider this sample Cretaceous in age.

All subsequent samples examined are barren of nannofossils until Sample 129-800A-11R-1, 11–23 cm. This sample contains rare specimens of *Cruciellipsis chiastia*, *Lithastrinus floralis*, *Rucinolithus terebrodentarius*, *Prediscosphaera columnata*, *Eiffellithus turriseiffelii*, and several other less diagnostic species. We assign this sample to the *E. turriseiffelii* Zone of Thierstein (1973, 1976), Zone NC10 of Roth (1978), and Zone CC9 of Sissingh (1977), based on the presence of *E. turriseiffelii* and the absence of *Lithraphidites acutus*, *Microrhabdulus decoratus*, or any other younger nannofossil markers.

Nannofossils remain few to common in abundance and the assemblage is basically unchanged down to the middle of Core 129-800A-16R, where well-preserved, abundant nannofossils occur. A form closely resembling *Lithraphidites alatus* was observed in that core and consistently downhole until Sample 129-800A-19R-CC. While not mentioned in zonal schemes used here, *L. alatus* ranges from the top of Sissingh's Zone CC9 down to the middle of Zone CC8 on the generalized range chart of Perch-Nielsen (1985, p. 374). If this datum proves reliable, this sequence of cores should be no older than middle Albian. *Rucinolithus irregularis* was first observed in the above sequence from Sample 129-800A-16R-CC. Although the last occurrence of *R. irregularis* is not used as a datum in the zonal schemes adopted here, the species has the last occurrence during the late Albian according to Perch-Nielsen's (1985, p. 342) range chart. This allows us to place the Cenomanian/Albian boundary within Core 129-800A-16R.

*E. turriseiffelii* was observed down to Section 129-800A-21R-2, 3 cm, and we place the lower limit of the *E. turriseiffelii*/NC10/CC9 Zone within Section 129-800A-21R-2, which is slightly younger than the upper/middle Albian boundary.

The persistent occurrence of *P. columnata* down to Sample 129-800A-24R-1, 86–87 cm, allows determination of the boundary between the *P. columnata*/NC8-NC9/CC8 and *P. angustus*/NC7 zones. We use here *P. columnata* as emended by Manivit et al. (1977), referring to both the species and the zonal names. The *P. columnata*/*P. angustus* zonal boundary is placed within Core 129-800A-24R, below the sample mentioned above.

*Tranolithus orionatus* is not used in the adopted zonal schemes but its first occurrence is reported in the middle Albian by Perch-Nielsen (1979, 1985). On the basis of the distribution of this taxon, the middle/lower Albian boundary is assigned between Sample 129-800A-23R-1, 21–22 cm, and Sample 129-800A-23R-1, 77–78 cm.

Sediments between Samples 129-800A-24R-CC and -27R-1, 111 cm, contain common nannofossils which include *L. floralis* and *P. angustus*, but not *P. columnata*. We consequently assign these samples to the upper Aptian *P. angustus* Zone of Thierstein (1971, 1973, 1976) and Zone NC7 of Roth (1978).

The Albian/Aptian boundary cannot be determined on the basis of nannofossil events. This boundary is reported within the upper part of the *P. angustus* Zone (Thierstein, 1971, 1973, 1976) and Zone NC7 (Roth, 1978). In the drilled sequence it could coincide with the boundary between lithostratigraphic Unit III and Unit IV, at 228.6 mbsf (see "Lithostratigraphy" section, this chapter). Consequently, a hiatus should not be ruled out at this interval.

The lower boundary of the *P. angustus*/Zone NC7 coincides with the upper/lower Aptian boundary; therefore, we believe this boundary lies within Core 129-800A-27R.

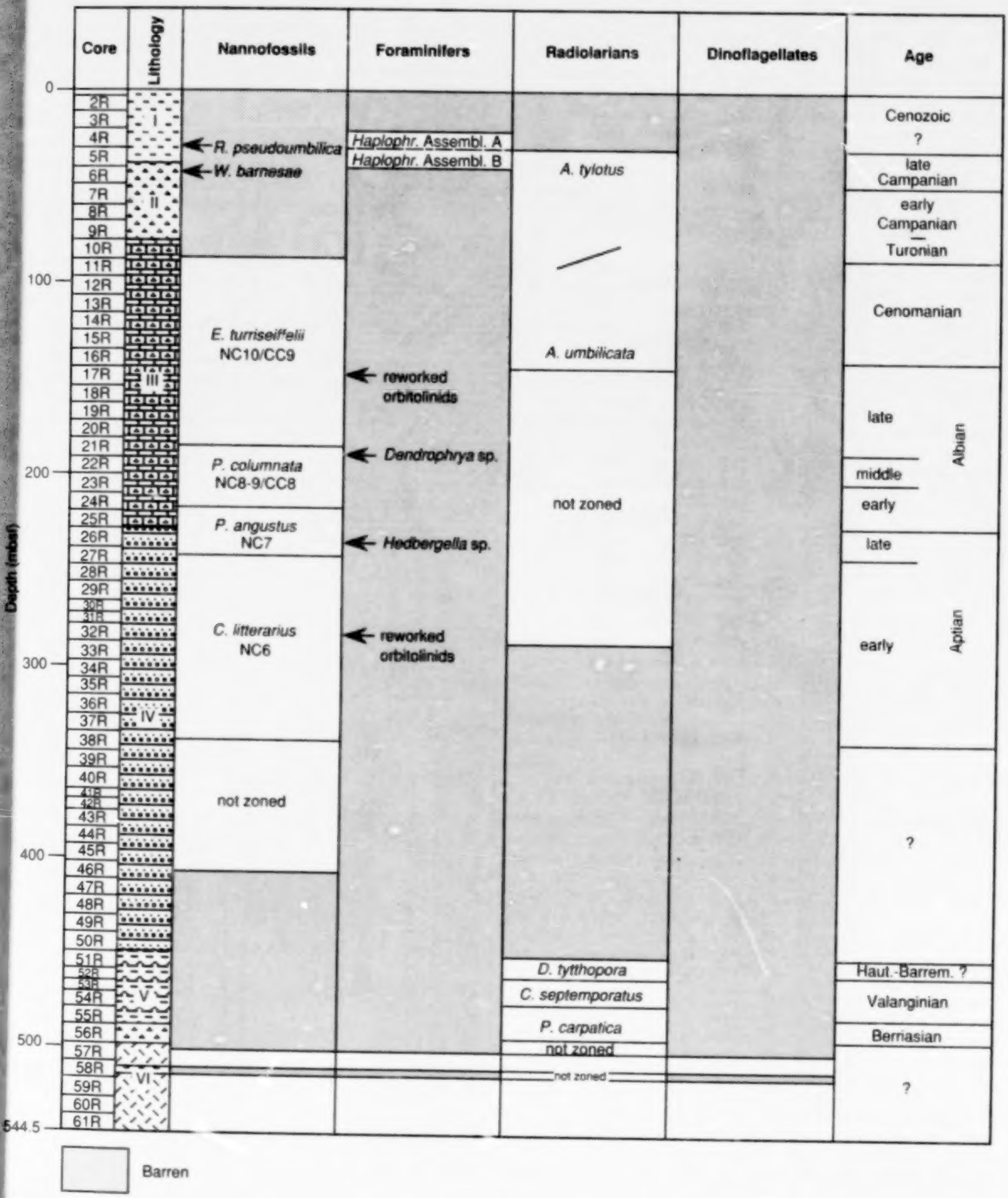

igure 16. Summary of the biostratigraphy for Hole 800A.

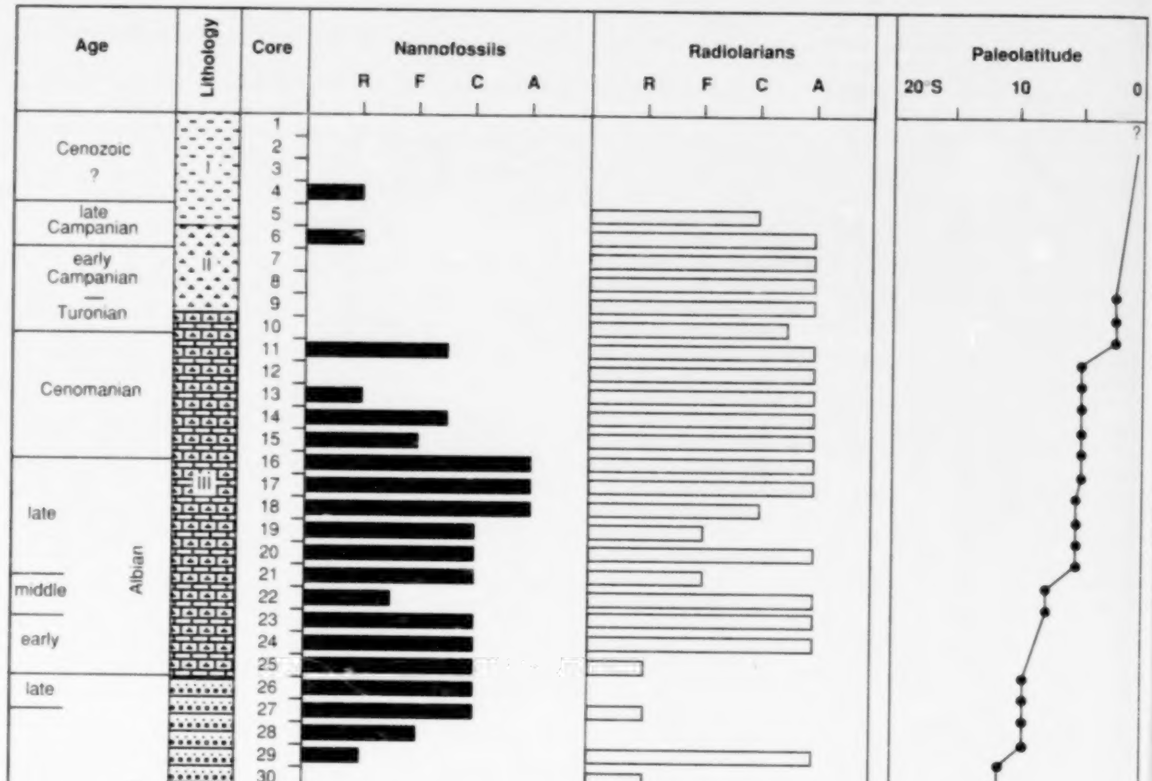

Figure 17. Abundance of calcareous nannofossils and radiolarians plotted against age, paleolatitude, and lithostratigraphy. Relative abundance is denoted as follows: rare (R), few (F), common (C), and abundant (A). (See "Explanatory Notes" chapter, this volume, for further discussion of abundance parameters.)

Sample 129-800A-26R-1, 103 cm, contains our first observance of *Assipetra infracretacea*. Although not mentioned in zonal definitions, Perch-Nielsen (1985) reports the range of this species as Valanginian to Aptian, which confirms our assignment of that sample within the Aptian.

The abundance of nannofossils for the subsequent cores fluctuates from barren to few, with preservation remaining poor. *R. irregularis* was observed as low as the bottom of Section 129-800A-38R-1, confirming that the age of that core is no older than the lower Aptian *C. litterarius* Zone of Thierstein (1971, 1973, 1976) and Zone NC6 of Roth (1978).

A range chart of important species used as markers in the Aptian-Cenomanian interval at this site is presented in Figure 18.

No more age-diagnostic nannofossils were encountered in the remainder of these cores, and the last nannofossil observed, *W. barnesae*, was in Sample 129-800A-46R-1, 91–92 cm.

### Foraminifers

Only four of the 56 core-catcher samples recovered from Hole 800A contain foraminifers, which are present in moderate abundances and are sometimes well preserved. Additional samples were processed for foraminifers from the relevant cores.

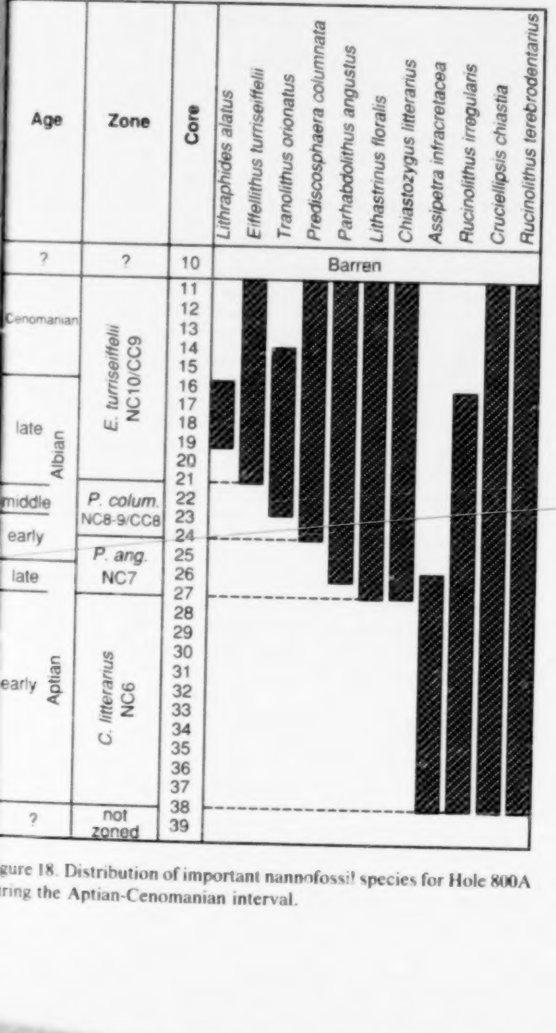

gure 18. Distribution of important nannofossil species for Hole 800A ring the Aptian-Cenomanian interval.

The core catcher from Core 129-800A-4R and four additional samples, 129-800A-4R-1, 72–74 cm; -4R-3, 30–32 cm; -4R-3, 96–98 cm; and -4R-4, 27–29 cm, contain low-diversity (benthic) agglutinated foraminifers that we informally refer to as *Haplophragmoides* Assemblage A. This assemblage is dominated by a possible new species of *Haplophragmoides*, as well as *Paratrochamminoides* sp., *Pseudobolivina munda*, and *Bolivinopsis parvissimus* in low abundances. The latter two species have previously been described from Deep Sea Drilling Project (DSDP) sites, where they are reported to be Late Cretaceous, Santonian to Campanian in age (e.g., Krasheninnikov, 1971). Depending on the reliability of the nannofossil evidence, the stratigraphic range of these species may be extended into the Cenozoic, middle Miocene to middle Pliocene.

Sample 129-800A-5R-CC contains a more diverse agglutinated foraminiferal assemblage that we refer to as *Haplophragmoides* Assemblage B. The majority of these species so far have been described only from the Pacific (DSDP Site 198). The species *Haplophragmoides multicamerata*, *H. fraudulentus*, *H. pervagalus*, *H. biumbilicata*, *H. perexplicatus*, *H. parvus*, *H. brevialus*, and *Praecystammina globigeriniformis* have previously been assigned a Late Cretaceous, Santonian to Campanian age (Krasheninnikov, 1971), and a similar age is attributed to this interval in Hole 800A. *Hormosina ovulum* is also present in this interval but is reported to be a long-ranging form, from Hauterivian (Lower Cretaceous) to Thanetian (Paleocene), according to Geroch and Nowak (1983). Presence of the radiolaria *Dictyomitra koslovae* in this sample indicates a late Campanian age. The very fine-grained and delicate nature of the agglutinated foraminiferal tests in these samples is characteristic of foraminifers from abyssal paleoenvironments.

The sedimentologic thin-section Sample 129-800A-17R-1, 44–46 cm, contains rare, reworked, smaller calcareous benthic foraminifers, but these are not identifiable. Reworked larger benthic foraminifers tentatively identified as *Orbitolina* sp., but lacking diagnostic internal specific characters, are also present in this thin section. Thin sections from Core 129-800A-18R also contain rare reworked benthic foraminifers.

The core-catcher samples from Cores 129-800A-6R to -20R are barren of foraminifers. Sample 129-800A-21R-CC contains abundant primitive tubular agglutinated foraminifers identified as *Dendrophrya* sp. and *Rhabdammina* sp. Both of these forms, however, are long-ranging and neither are age-diagnostic, but their presence has interesting paleoenvironmental implications. Recent studies in the Panama Basin (Kaminski et al., 1988a) have shown that *Dendrophrya* lives in an epifaunal habitat with the abundance of specimens falling sharply beneath the flocculent (nephloid) surface layer, the form being absent 5 cm below the surface. Schroeder (1986) has shown the presence of high concentrations of primitive tubular foraminifers in turbidite layers of the Nares Abyssal Plain. Kaminski et al. (1988b) report a redeposited *Dendrophrya* assemblage from turbidite clays of the lower Lizard Springs Formation of Trinidad. It is expected (Kaminski et al., 1988b) that concentrations of *Dendrophrya* would be seen in the "d" layer of the Bouma turbidite sequence, following erosion of flocculent surface sediments by turbidity currents and subsequent deposition of the entrained turbidite component. From the concentration of primitive tubular agglutinated foraminifers in Hole 800A, a similar mechanism is envisaged. The absence of multichambered or other foraminifers supports the argument of redeposition.

Samples 129-800A-22R-CC to 129-800A-25R-CC are barren of foraminifers. Minute planktonic foraminifers that may belong to the genus *Hedbergella* are seen in the 38- to 63-μm sieve fraction from Sample 129-800A-26R-1, 98–100 cm. These could not be positively identified due to small size and poor preservation. *Hedbergella* is the dominant Early Cretaceous planktonic foraminifer in the Barremian and Aptian, which would be in accordance with the Aptian age given for the calcareous nannofossils. The very small size of the form in Hole 800A may indicate that specimens are juveniles, although the possibility that it represents dwarfism in less than optimum conditions (high silica content of the seawater) cannot be excluded.

Rarity of planktonic foraminifers and their restriction to the fine (silt) fraction of the sediments together with the calcareous nannofossils points toward preferential preservation of the microplankton, perhaps through ingestion and redeposition via fish fecal pellets in an otherwise non-carbonate environment. Absence of benthic agglutinated foraminifers may be due to dilution through high sedimentation rates.

A sedimentologic thin section, Sample 129-800-32R-1, 117–118 cm, contains orbitolinid foraminifers, echinoderm, and algae fragments, which indicate redeposition from shallow-water environments. The sediments in this interval are dated by nannofossils as early Aptian.

### Radiolarians

In addition to the 56 core-catcher samples, 19 additional samples from Cores 129-800A-50R to -58R were investigated. Cores 129-800A-1R to -4R are barren of radiolarians. No Cenozoic radiolarians were obtained from this site.

Samples 129-800A-5R-CC to -16R-CC yielded abundant but poorly preserved radiolarians. Only robust and morphologically characteristic species such as *Dictyomitra koslovae*, *Dictyomitra formosa* and *Pseudodictyomitra pseudomacrocephala* were identified at the species level. These assemblages indicate a late Albian to late Campanian age (upper *Acaeniotyle umbilicata* Zone to lower *Amphipyndax tylotus* Zone). It is difficult to draw any zonal boundaries in this interval because of the lack of zone diagnostic radiolarians. *D. koslovae* was observed in Samples 129-800A-5R-CC and -6R-CC, indicating late Campanian age.

In Samples 129-800A-17R-CC to -32R-CC, common to abundant but poorly preserved radiolarians are present. Cryptocephalic and cryptothoracic nassellarians are common. The poor preservation does not permit zonal assignment. Samples 129-800A-33R-CC to -50R-CC are barren of radiolarians.

Radiolarite and underlying chert samples of Cores 129-800A-51R to -57R contain abundant radiolarian tests. All samples except for Samples 129-800A-56R-CC; -57R-1, 3–7 cm; and -57R-1, 5–8 cm, yield poorly to moderately preserved radiolarians that permit zonal division of this interval. Radiolarians from the three lowermost samples are very poorly preserved because of contact metamorphism from the underlying dolerite sills. In this interval, *Pseudodictyomitra carpatica*, *Thanarla pulchra*, *Sphaerostylus lanceola*, and *Acanthocircus dicranacanthos* commonly occur. These species generally characterize Neocomian sediments. A single specimen of *Dibolachras tytthopora* was observed in Sample 129-800A-52R-1, 57–59 cm. Therefore, the lower limit of the *D. tytthopora* Zone should be situated below that sample. *Archaeodictyomitra lacrimula* appears in Sample 129-800A-52R-2, 49–51 cm, and was found in three samples above the first occurrence. *Cecropus septemporatus* first occurs in Sample 129-800A-54R-2, 50–52 cm, and last occurs in Sample 129-800A-52R-CC. The first occurrence of *C. septemporatus* defines the base of the *C. septemporatus* Zone. The order of the first occurrence of the above-mentioned three species is consistent with range charts presented by Schaaf (1984) and Sanfilippo and Riedel (1985). The interval from the Sample 129-800A-51R-1, 30–31 cm, to Sample 129-800A-56R-1, 5–7 cm, is biostratigraphically subdivided into three parts: *D. tytthopora* Zone, *C. septemporatus* Zone, and *Pseudodictyomitra carpatica* Zone in descending order. It is difficult to assign ages to these zones because ranges of key species are quite different among authors. However, the first occurrence of *C. septemporatus* is regarded as being within the Valanginian by several authors (e.g., Schaaf, 1984; Sanfilippo and Riedel, 1985; Baumgartner, 1984, 1987). Radiolarians restricted to pre-Cretaceous ages are absent in this interval.

Sample 129-800A-58R-1, 45–48 cm, is chert that is intercalated within the dolerite sills. It contains common radiolarian tests but because of its extremely poor preservation, it is not assigned an age.

### Palynomorphs

Cores 129-800A-1R through -57R are barren of palynomorphs. Samples 129-800A-7R-CC to 129-800A-9R-CC contain abundant amorphous organic matter, but no determinable palynomorphs.

### Sedimentation Rates

Figure 19 shows the sedimentation rates for Site 800, as determined on the basis of nannofossil and radiolarian biostratigraphy.

## PALEOMAGNETICS

### Methods

All measurements were made with the whole-core cryogenic magnetometer. Cores 129-800A-1R through -5R were completely homogenized by the rotary coring process and thus were not measured. Beginning with Core 129-800A-6R, discrete core fragments, most often pieces of chert, were selected from the recovered core and placed in the sample holder with a 10-cm space between pieces; the pieces were taped into position with bedding planes oriented as nearly perpendicular to the magnetometer "z" axis as possible. Selection of samples was based primarily on large size and visibility of bedding traces. Measurements were then made utilizing a 1-cm sampling interval and a radius that approximated the average radius of the group of fragments within each measurement group. This method of measurement was used through Core 129-800A-22R and allowed magnetic measurements to be obtained in a sedimentary interval where recovery was low and represented by only fragments of chert and porcellanite.

Measurements of continuous cores were begun at Section 129-800A-23R-1 and continued through Core 129-800A-60R. Measurement intervals were chosen on the basis of (1) recovery, (2) lithology, and (3) the expected reversal frequency. Thus, a sampling interval of 2 cm was chosen in areas of low recovery, 3 cm for cores with continuous recovery, 5 cm for the high sedimentation rate sequence of the volcaniclastics, and 2 cm for Cores 129-800A-51R through -55R because of the high reversal frequency of the Berriasian-Barremian time interval.

Alternating field (AF) demagnetization of whole cores was varied in the number of steps and peak-field intensity, based on lithology and expected reversal frequency. Maximum AF demagnetization levels averaged approximately 10 mT but ranged from 8 to 20 mT. Lower fields were used for gray and white sediments in which the magnetic carrier seemed to be magnetite or a similarly low coercivity mineral. Demagnetization to 20 mT was used for the red-colored Berriasian-Barremian radiolarite and clay (Cores 129-800A-51R through

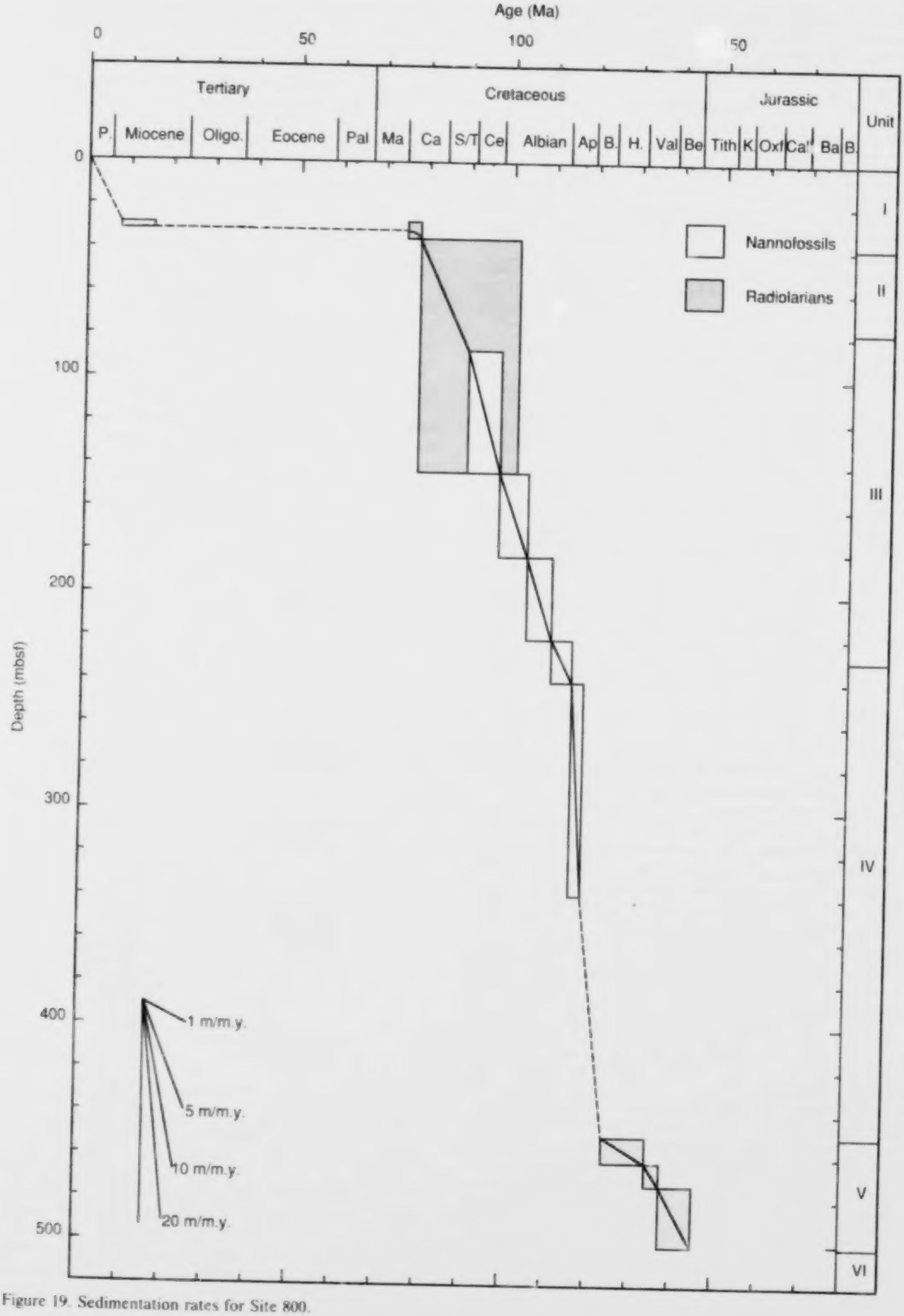

Figure 19. Sedimentation rates for Site 800.

-56R) and for reddish segments of volcaniclastic turbidites, both of which appeared from the red color and demagnetization responses to have higher coercivity remanence components.

### Magnetostratigraphy

Definitive magnetostratigraphy at Site 800 was hampered by a combination low recovery rate for much of the hole, particularly in the Upper Cretaceous section, and the paucity of paleontological fauna at critical stratigraphic horizons such as the Maestrichtian/Campanian/Santonian boundaries and Aptian/Barremian/Hauterivian boundaries (see "Biostratigraphy" section, this chapter). Moreover, much of the recovery was occupied by an Aptian (hence normal polarity) volcaniclastic turbidite sequence; therefore, a large segment of the recovered record is a record of geologic events of probable short duration.

Site 800 is located at modern low latitudes, and was located at low paleolatitudes during the deposition of its sedimentary section. As a result, determination of polarity from unoriented drill cores can be difficult, because at low latitudes secular variation is high and thereby undermines the use of inclination data alone. Another difficulty in polarity determination is always the possibility of inversion of core fragments during preparation. Polarity was determined by large relative changes in declination during demagnetization (exceeding approximately 45°) combined with changes in the sign of inclination. In determining a polarity change, more consideration was given to large changes in declination than to inclination sign changes, because secular variation can readily change the sign of low-latitude inclinations but large shifts in declination during demagnetization are most likely due to the removal of the normal present-field component from a reversed characteristic magnetization. It should be remembered, however, that lack of change in declination (in an interval of significant inclination change) may be due to the presence of an unremoved overprint. This is of special concern in the lower part of this section where the red color and high coercivities suggest that hematite or iron hydroxides are a significant magnetic remanence carrier.

The youngest observed reversed interval occurs in Section 129-800A-7R-1 and is based on a single chert sample. The identification of the radiolarian *Dictyomitra koslovae* in Cores 129-800A-5R through -6R suggests that Section 129-800A-7R-1 may be as young as upper Campanian. However, the presence of reversed polarity in this core suggests that it was deposited during geomagnetic polarity interval 33R, therefore indicating an early Campanian age. Normal polarity was obtained in the lower part of this core and in many subsequent cores, suggesting a record of interval 34, the Cretaceous long normal interval, and therefore implying that the lowest part of the core is earliest Campanian to Santonian age.

No polarity changes were observed in the fragments measured from Cores 129-800A-8R through -22R, nor in the continuous core measurements of Cores 129-800A-23R through -50R. Their ages place them within the long normal polarity interval of the Cretaceous (see Fig. 5). Lithology changes markedly at Core 129-800A-51R, from volcaniclastics to finely laminated clays and radiolarites (Fig. 5), and remains that lithology to the end of the sedimentary section (through Core 129-800A-55R). Cores 129-800A-51R through -55R have been determined by radiolarian zonation to range in age from Barremian-Hauterivian(?) to Berriasian (see "Biostratigraphy" section, this chapter). Reversals were observed frequently in this part of the section, beginning in Core 129-800A-52, and continuing through Core 129-800A-55R. Reversals were not observed in Core 129-800A-51R, although this may be an artifact of its lithology; it has a large percentage of orange-colored radiolarite as compared to succeeding cores which are alternating orange and brown color. The orange color was observed to be correlated with higher coercivities; hence, it is possible that instead of being normal polarity, Core 129-800A-51R sediments simply may not be effectively demagnetized by the limited AF treatment. Shore-based thermal demagnetization will test this possibility. Even though reversals are observed throughout Cores 129-800A-52R through -55R, incomplete recovery and lack of more complete biostratigraphic zonation preclude polarity chron identification. Figure 20 shows the polarity reversals observed for the lower part of Hole 800, along with the biostratigraphic age assignments.

### Paleolatitude

An important goal of Leg 129 is to decipher the motion of the Pacific plate for the Late Jurassic through the Late Cretaceous. The preliminary data from Site 800 can be used to estimate paleolatitude and, although limited in scope because of the limited demagnetization, offer some insight as to the amount of plate motion that has occurred. The problems encountered in determining polarity applied to the estimation of paleolatitudes as well. In addition, the AF demagnetization treatment of Site 800 sediments did not allow determination of stable endpoints because of the limited field strengths of the whole-core magnetometer assembly. Also, it was clear that

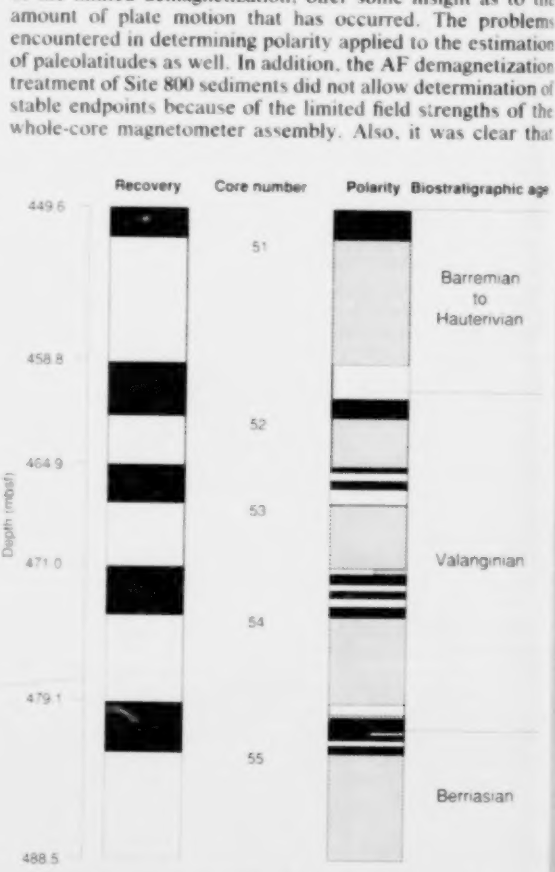

Figure 20. Summary of magnetic polarity for the Lower Cretaceous strata of Cores 129-800A-51R through -55R. Left-hand bar chart indicates interval recovery (black). Black and white bars in polarity column indicate normal and reversed polarities, respectively. Half bars represent a single sample or one with questionable polarity. Ages are from radiolarian zonation (see "Biostratigraphy" section, this chapter).

**Table 3. Inclinations and mean paleolatitudes for selected intervals as described in the text.**

| Core, section, interval (cm) | Mean inclination (°) | No. of samples | Latitude | $\alpha_{95}$ | $\alpha_{63}$ |
|---|---|---|---|---|---|
| 129-800A- | | | | | |
| 8R-1, 0–5 | −6.0 | | | | |
| 8R-1, 27–32 | −2.3 | | | | |
| 8R-1, 35–40 | −3.8 | | | | |
| 8R-1, 40–45 | −1.4 | | | | |
| 8R-1, 47–50 | −1.8 | | | | |
| 8R-1, 60–63 | −4.8 | | | | |
| 8R-1, 70–77 | −4.0 | | | | |
| 8R-CC, 7–13 | −3.5 | | | | |
| 8R-CC, 15–21 | −2.1 | | | | |
| 8R-CC, 28–31 | −10.6 | | | | |
| 9R-1, 8–13 | −3.1 | | | | |
| 9R-1, 13–19 | −8.2 | | | | |
| 9R-1, 24–29 | −1.0 | | | | |
| 9R-1, 34–42 | −12.9 | | | | |
| 10R-1, 30–36 | −4.6 | | | | |
| 10R-1, 56–63 | −9.8 | | | | |
| | | 16 | −2.5 | 1.68 | 0.98 |
| 11R-1, 11–23 | −4.9 | | | | |
| 11R-1, 28–35 | −6.1 | | | | |
| 11R-1, 49–55 | −13.5 | | | | |
| 13R-1, 29–32 | −16.4 | | | | |
| 13R-1, 35–41 | −11.6 | | | | |
| 13R-1, 51–57 | −8.2 | | | | |
| 14R-1, 51–55 | −15.3 | | | | |
| 14R-1, 107–112 | −8.3 | | | | |
| 15R-1, 11–14 | −3.7 | | | | |
| 16R-1, 47–52 | −12.2 | | | | |
| | | 10 | −5.1 | 2.88 | 1.67 |
| 17R-1, 44–54 | −7.4 | | | | |
| 17R-1, 68–72 | −16.4 | | | | |
| 17R-1, 80–83 | −1.9 | | | | |
| 18R-1, 1–6 | −10.6 | | | | |
| 18R-1, 30–36 | −11.1 | | | | |
| 18R-1, 76–84 | −10.9 | | | | |
| 18R-1, 124–132 | −13.5 | | | | |
| 19R-1, 1–6 | −6.8 | | | | |
| 19R-1, 36–43 | −9.3 | | | | |
| 19R-1, 68–80 | −18.2 | | | | |
| 20R-1, 29–39 | −12.3 | | | | |
| | | 11 | −5.5 | 2.77 | 1.61 |
| 21R-1, 72–78 | −20.6 | | | | |
| 21R-1, 87–99 | −17.2 | | | | |
| 21R-1, 144–150 | −14.4 | | | | |
| 21R-2, 0–6 | −15.1 | | | | |
| 22R-1, 47–52 | −12.8 | | | | |
| 22R-1, 52–58 | −16.4 | | | | |
| 22R-1, 58–64 | −9.9 | | | | |
| | | 7 | −7.8 | 3.02 | 1.75 |
| 24R-1, 117–126 | −5.1 | | | | |
| 25R-1, 41–47 | −11.8 | | | | |
| 26R-2, 20–30 | −14.3 | | | | |
| 26R-2, 57–77 | −8.9 | | | | |
| 26R-3, 49–68 | −20.0 | | | | |
| 27R-1, 95–107 | −23.5 | | | | |
| 28R-1, 45–75 | −33.2 | | | | |
| 28R-2, 15–25 | −15.7 | | | | |
| 28R-3, 0–13 | −22.4 | | | | |
| 28R-4, 15–30 | −24.5 | | | | |
| 28R-4, 70–90 | −22.0 | | | | |
| | | 11 | −9.5 | 5.22 | 3.03 |
| 29R-1, 0–20 | −18.0 | | | | |
| 29R-1, 95–130 | −25.5 | | | | |
| 29R-2, 77–100 | −21.0 | | | | |
| 29R-3, 19–37 | −16.0 | | | | |
| 31R-2, 22–50 | −26.5 | | | | |
| 31R-2, 80–115 | −24.2 | | | | |
| | | 6 | −11.4 | 4.69 | 2.72 |
| 32R-2, 0–20 | −24.4 | | | | |
| 33R-1, 10–25 | −20.0 | | | | |
| 33R-1, 25–150 | −33.5 | | | | |
| 33R-2, 15–85 | −31.4 | | | | |
| 33R-2, 95–140 | −28.8 | | | | |
| 33R-3, 0–30 | −24.0 | | | | |
| 33R-3, 30–50 | −22.0 | | | | |
| 33R-3, 130–150 | −27.0 | | | | |
| 33R-4, 15–62 | −32.8 | | | | |
| 33R-4, 105–140 | −25.4 | | | | |
| 33R-5, 15–45 | −23.8 | | | | |
| 33R-5, 105–145 | −29.5 | | | | |
| 33R-7, 35–75 | −29.7 | | | | |
| 34R-1, 95–125 | −29.2 | | | | |
| 34R-2, 80–130 | −25.9 | | | | |
| 34R-3, 135–150 | −25.9 | | | | |
| 34R-4, 0–40 | −25.9 | | | | |
| 34R-4, 50–67 | −25.7 | | | | |
| 34R-4, 70–100 | −27.1 | | | | |
| 34R-4, 105–150 | −25.9 | | | | |
| 34R-5, 30–75 | −21.6 | | | | |
| | | 21 | −14.1 | 1.67 | 0.97 |
| 35R-1, 0–150 | −22.6 | | | | |
| 35R-2, 0–80 | −25.2 | | | | |
| 35R-2, 90–150 | −29.5 | | | | |
| 35R-3, 0–20 | −26.3 | | | | |
| 35R-3, 20–40 | −27.8 | | | | |
| 36R-2, 80–110 | −31.3 | | | | |
| 36R-3, 30–70 | −25.5 | | | | |
| 36R-4, 70–120 | −22.2 | | | | |
| 36R-5, 30–50 | −22.7 | | | | |
| 36R-5, 80–100 | −28.1 | | | | |
| 37R-1, 45–115 | −29.3 | | | | |
| | | 11 | −14.0 | 2.15 | 1.25 |
| 40R-1, 30–45 | −28.7 | | | | |
| 40R-1, 85–100 | −36.7 | | | | |
| 40R-1, 105–125 | −37.9 | | | | |
| 44R-2, 0–25 | −16.2 | | | | |
| | | 4 | −16.3 | 24.79 | 14.38 |
| 45R-1, 55–145 | −21.4 | | | | |
| 45R-2, 0–150 | −21.4 | | | | |
| 45R-3, 0–140 | −21.5 | | | | |
| 46R-2, 80–130 | −24.7 | | | | |
| 48R-1, 60–110 | −26.9 | | | | |
| 48R-6, 0–20 | −18.4 | | | | |
| | | 6 | −11.7 | 3.28 | 1.90 |

sediments with red coloration, particularly in Cores 129-800A-51R through -55R, contained high-coercivity minerals and were not completely demagnetized with the AF technique.

Paleolatitude data were obtained from all core fragments exhibiting magnetic stability (Cores 129-800A-8R through -23R) and from all portions within the continuous recovery in which pieces were at least 15 cm long. An additional constraint was to use only those portions of the continuous recovery that contained an interval of at least 10 cm over which declination was uniform at the maximum AF demagnetization step, a characteristic used to assure homogeneity of the magnetic signature. This latter restriction eliminated much of the information from the lower part of the hole.

All magnetic measurements within each acceptable core segment were averaged, excluding 3–5 cm at each end of the interval. These averages were grouped loosely by a combination of age and data quantity. The true mean inclinations, variances, and corresponding paleolatitudes of each group were computed using the method of Kono (1980), a method developed specifically for analysis of azimuthally unoriented cores. The results of this analysis are summarized in Table 3, and are plotted against age in Figure 21. It should be noted that relatively steep (15°) bedding plane dips were observed in the Aptian volcaniclastic turbidites (Cores 129-800A-26R through -50R). Furthermore, Hole 800A also deviates from vertical by up to 3°. Neither of these factors has been removed from these preliminary shipboard paleolatitude results.

The data from Site 800 indicate northward drift from at least Core 129-800A-44R onward, and suggest that a change

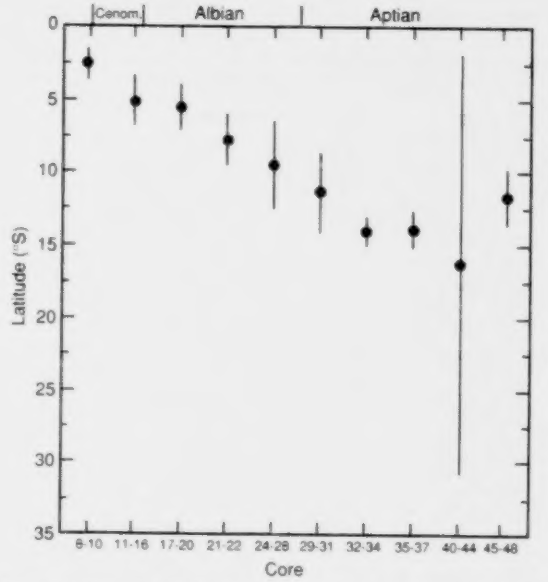

Figure 21. Mean paleolatitudes for core groups (as described in the text). Error bars represent standard deviation values ($\alpha_{63}$; see Table 3).

from southward drift to northward drift occurs between the Hauterivian-Barremian and the early Aptian. This inference is remarkably consistent with the results of a study of Leg 32 basalts, in which Larson and Lowrie (1975) also postulated that a change in direction from southward to northward drift of the Pacific plate occurred during the Early Cretaceous. While the inflection point in the paleolatitudes (Fig. 21) is indicated by only a single point, preliminary work with Cores 129-800A-50R through -55R suggests a continuation of this trend.

## Dolerite Magnetization

Cores 129-800A-57R through -60R were demagnetized with alternating fields of 4, 8, and 12 mT; core sections showing high coercivity of magnetization were demagnetized at 16 mT. The inclination values of the sills in the following discussion are subject to some uncertainty, as the horizontal reference is unknown, and the immediately overlying sediments display dips of up to 33°. The dolerite recovery was divided into three sill units on the basis of grain size and texture (see "Igneous Petrology" section, this chapter). The top of the upper sill (sill 1) is orange in color, suggesting significant oxidation. Sill 1 changes to a gray color in its lowest part (the lower part of Section 129-800A-57R-2). In addition to this oxidation, petrographic studies identified an additional, pervasive, low-grade metamorphism in the gray portions of sills 1, 2, and 3, which varied from a generation of large amounts of secondary clays to a greater alteration which generated lower greenschist facies minerals (see "Igneous Petrology" section, this chapter).

The intensity of natural remanent magnetization (NRM) was comparatively low for igneous material, averaging about 5 by $10^1$ mA/m in the least altered dolerite, 1 by $10^2$ mA/m in the most metamorphosed material (greenschist facies), and 2 by $10^1$ mA/m in the most oxidized top portion of sill 1. NRM inclinations varied from 20° to +60°. Because the three different levels of alteration in these rocks are reflected in the magnetic behavior, the magnetic characteristics will be discussed according to alteration state.

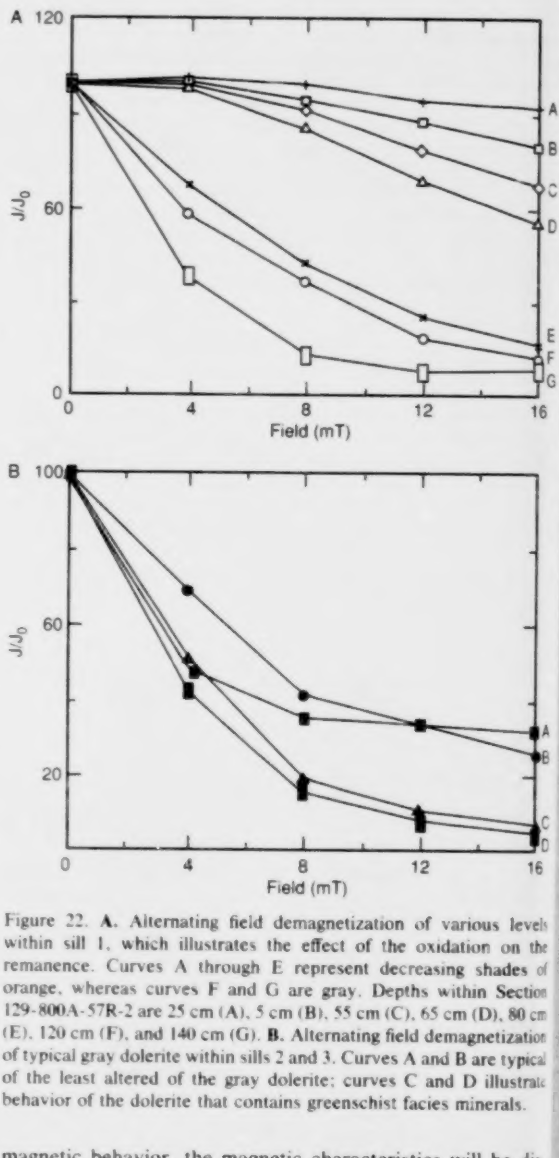

Figure 22. **A.** Alternating field demagnetization of various levels within sill 1, which illustrates the effect of the oxidation on the remanence. Curves A through E represent decreasing shades of orange, whereas curves F and G are gray. Depths within Section 129-800A-57R-2 are 25 cm (A), 5 cm (B), 55 cm (C), 65 cm (D), 80 cm (E), 120 cm (F), and 140 cm (G). **B.** Alternating field demagnetization of typical gray dolerite within sills 2 and 3. Curves A and B are typical of the least altered of the gray dolerite; curves C and D illustrate behavior of the dolerite that contains greenschist facies minerals.

The most prominent result of magnetic measurements in the dolerites is that the orange oxidized material at the top of sill 1 is clearly different from the underlying gray dolerites, both in polarity and response to AF demagnetization. Figure 22A shows demagnetization responses within sill 1; the distinctly orange dolerite displays behaviors depicted by curves A though E, while F and G represent the gray portion of sill 1. Median destructive fields (MDF) of much greater than 16 mT characterize the orange dolerite of sill 1 whereas MDF's of 3–6 mT characterize the gray dolerite of all three sills (e.g., curves F and G in Fig. 22A and all curves in Fig. 22B).

The inclination of the orange dolerite is negative, indicating normal polarity in the Southern Hemisphere, whereas inclinations in the gray dolerite vary from shallow to steeply positive values, indicating reversed polarity. The most heavily orange-colored dolerite has the steepest negative inclinations, approximately 21° after demagnetization to 16 mT. The inclinations decrease downcore uniformly and change to shallow, then steeper, positive values; the change coincides with the gradational change from orange to gray color (Fig. 23).

The least altered dolerite, found in Core 129-800A-60R (lower part of sill 3), has positive inclinations (after demagnetization to 16 mT) of about +42°. However, these are not yet trending to the origin on orthogonal axes plots. If the observed trends are continued, inclinations of about +30° might be inferred. Sill 2, although represented by only 27 cm of recovery, also displays steeply positive inclinations, approximately +50° after demagnetization to 12 mT. Inclinations within the upper part of sill 3 vary from shallow negative to shallow positive, with demagnetization responses reminiscent of the behavior of the oxidized top of sill 1. The polarity of this top part of sill 3 (Sections 129-800A-58R-1 and -58R-2) is generally normal with two intervals of reversed polarity (positive inclinations) interspersed.

Two slightly different AF demagnetization behaviors were noted in the gray dolerite of sills 1, 2, and 3. These differences appear to correspond to the alteration differences between the extensive clay production and appearance of lower greenschist facies minerals. Those areas identified as lower greenschist facies, e.g., Sections 129-800A-58R-1 and -58R-2, have lesser MDF's (curves C and D of Fig. 22B) than the least altered material (curves A and B of Fig. 22B). The lower greenschist grade regions also have normal polarity in contrast to the reversed polarity of the least altered dolerite, suggesting that if the reversed polarity is primary, this alteration also occurred at a later time than intrusion.

In summary, the sills appear to have been emplaced in a time of reversed polarity and were later altered in a time or times of normal polarity. The sills were intruded just below Berriasian sediments (see "Biostratigraphy" section, this chapter) and there is no indication that their reversed polarity magnetization is not a primary magnetization. Because the very thick volcanogenic turbidite sediments uphole are Aptian in age, and because one might expect that the intrusive emplacement was related to the extrusive activity giving rise to the volcaniclastic sediments of the turbidites, the age of the sill emplacement is likely to have been in a reversed interval closely preceding or succeeding Aptian time. This would suggest intrusion during M0 to M3 time (earliest Aptian-Barremian-late Hauterivian), or during anomaly 33R time (early Campanian). The proximity in age of the reversed interval in earliest Aptian time (M0) to the Aptian age of volcaniclastic sediment pile favors this Early Cretaceous age as the time of intrusion.

## INORGANIC GEOCHEMISTRY

Eight interstitial water samples were squeezed from sediment cores recovered in Hole 800A. The first sample belongs to lithologic Unit I (brown clay); the others were collected in lithologic Unit IV (volcaniclastic turbidites) and Unit V (brown claystone). Unfortunately, it was impossible to sample water from chert and silicified limestone of the lithologic Unit III, because of both the lithology and the scarce recovery. Chemical analyses are summarized in Table 4 and presented in Figures 24 and 25. Except for the first sample, 10 to 20 cm$^3$ of water were extracted from 10-cm-long, whole-round core samples. No evidence of pollution by drilling fluids (seawater or mud, Table 4) was found from a combination of analytical results.

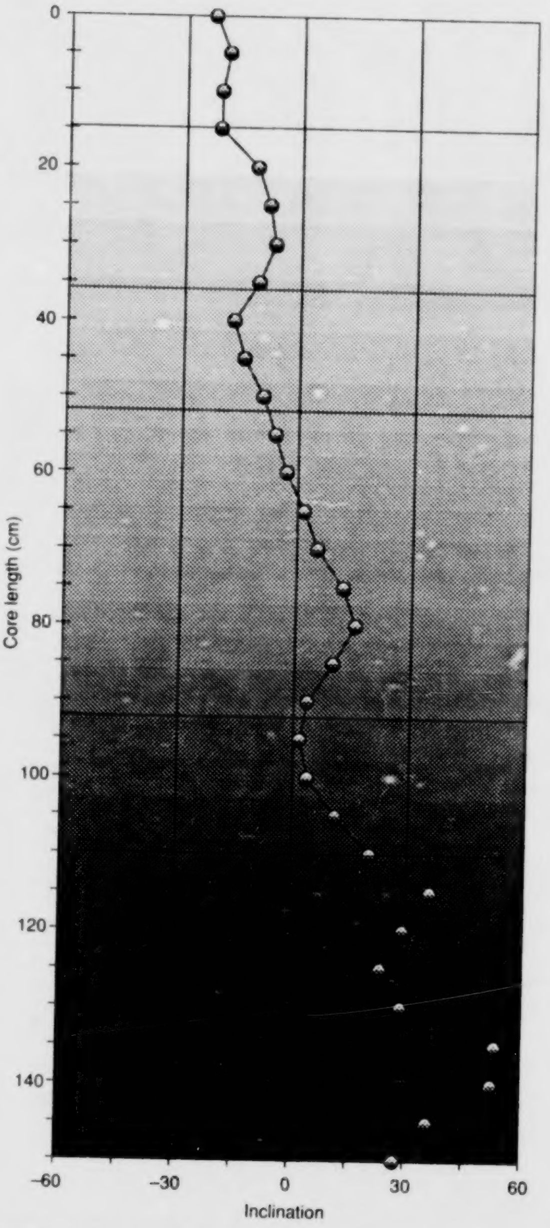

Figure 23. Inclination variations within sill 1, illustrating the correlation between orange color and inclination change. The sill in Section 129-800A-57R-2 is orange down to 110 cm, becoming gradually lighter from top to bottom; below 110 cm only gray dolerite is present. This color gradation is schematically illustrated by the background shading in the diagram. The lines indicate the positions of distinct oxidation fronts within the orange dolerite.

**Table 4. Chemical composition of interstitial water extracted from sediments in Hole 800A, surface seawater, and water extracted from drilling mud.**

| Core, section, interval (cm) | Depth (mbsf)[a] | Alkalinity (meq/L) | Cl (mmol/L) | $SO_4$ (mmol/L) | pH | Salinity (‰) | Ca (mmol/L) | Mg (mmol/L) | K (mmol/L) | Na* (mmol/L) | Mn (μmol/L) |
|---|---|---|---|---|---|---|---|---|---|---|---|
| 129-800A- | | | | | | | | | | | |
| 4R-2, 25–30 | 22 | 2.3 | 568.9 | 25.8 | 7.5 | 36.2 | 10.5 | 53.1 | 11.8 | 480 | 1.8 |
| 26R-2, 140–148 | 232 | 0.5 | 537.2 | 17.6 | 8.2 | 33.8 | 56.0 | 9.2 | 2.8 | 436 | 86.7 |
| 27R-1, 140–150 | 239 | 0.5 | 527.3 | 14.5 | 8.1 | 33.0 | 58.3 | 8.2 | 1.8 | 417 | 57.8 |
| 33R-6, 60–70 | 296 | 0.6 | 530.3 | 14.0 | 7.8 | 33.5 | 58.2 | 6.7 | 1.4 | 426 | 33.1 |
| 37R-2, 0–10 | 327 | 1.2 | 554.1 | 16.4 | 8.1 | 35.0 | 54.7 | 13.7 | 1.9 | 444 | 49.2 |
| 41R-2, 0–10 | 364 | 0.6 | 531.3 | 11.1 | 7.1 | 32.2 | 57.3 | 8.0 | 1.6 | 420 | 38.1 |
| 49R-2, 140–150 | 434 | 0.7 | 531.3 | 12.3 | 7.1 | 33.0 | 59.2 | 10.6 | 1.3 | 411 | 18.3 |
| 54R-2, 0–12 | 473 | 0.6 | 554.1 | 13.2 | 8.2 | 33.7 | 60.8 | 11.7 | 2.0 | 429 | 6.3 |
| Surface seawater | | 2.2 | 562.0 | 28.1 | 8.0 | 35.0 | 10.4 | 53.5 | 11.2 | 480 | l.d. |
| Water from drilling mud | | 0.6 | 256.8 | 14.4 | 8.4 | 15.8 | 8.7 | 7.4 | 4.3 | 249 | <3.0 |

Note: Na* is calculated by charge balance; n.d. = not determined; l.d. = less than detection level.

[a] Sub-bottom depth rounded to nearest meter.

### Results

Concentrations of all major constituents except calcium show roughly the same depth profiles with different amplitudes (Figs. 24 and 25). For sodium, magnesium, potassium, chlorine, sulfate, and alkalinity, concentrations at 22 mbsf are close to seawater concentrations. Between 232 and 473 mbsf (in lithologic Unit IV), the concentrations of these species are reduced. The extent of the depletion depends on the chemical species. Potassium, magnesium, and alkalinity are reduced to 10%–30% of their values in seawater, sulfate to 40%–50%, sodium to about 85%, and chlorine to 94%. One sample at 327 mbsf appears systematically less depleted than the others; qualitatively, it contains fewer clay minerals than the other samples from this lithology. Finally, at 472 mbsf (in lithologic Unit V), the concentrations of these species increase to varying extents. These general trends are reflected by the depth profile of salinity, which decreases from a seawater value (36‰) at 22 mbsf to 32.2‰–33.8‰ between 232 and 473 mbsf, with the exception of the sample at 327 mbsf. The behavior of calcium is the opposite of the other major constituents. Below 232 mbsf, calcium concentration increases to about 560% to its value in seawater.

Strontium and silicon are enriched with respect to seawater at 22 mbsf and reach 321 and 546 μmol/L, respectively, at 240 mbsf. Strontium moderately increases to 356 μmol/L at 473 mbsf. In contrast, silicon concentrations decrease sharply between 240 and 296 mbsf to 200 μmol/L. Manganese concentrations are similar to seawater at 22 mbsf, then increase to 86 μmol/L at 232 mbsf, and decrease gradually to 6 μmol/L at 473 mbsf.

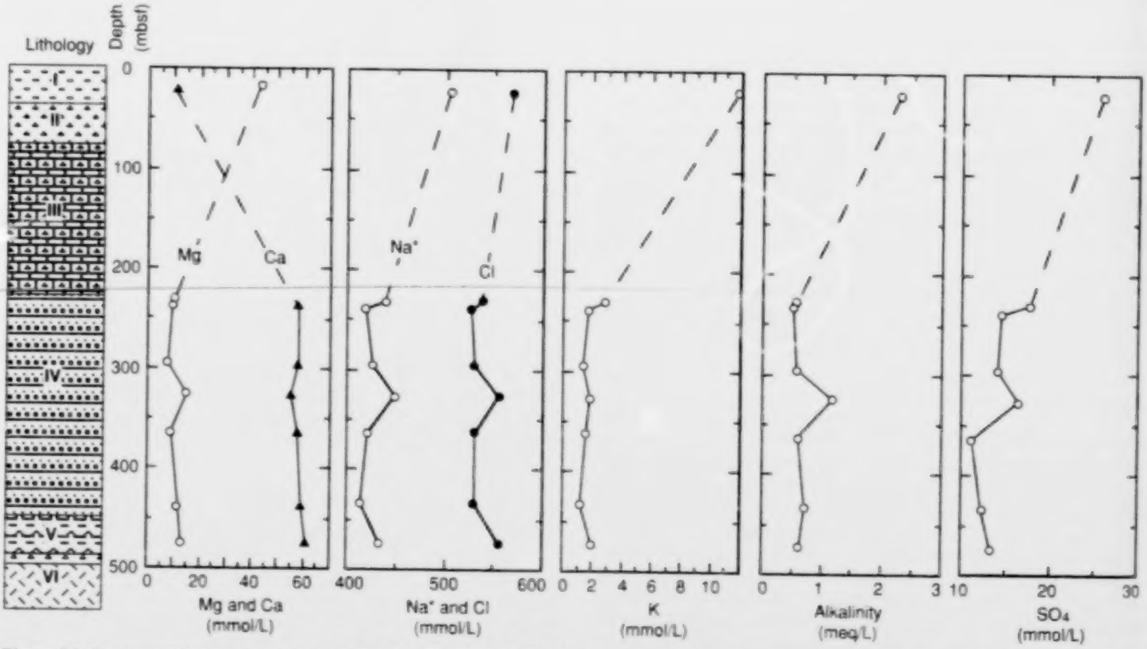

Figure 24. Concentration vs. depth profiles for Mg, Ca, Na*, Cl, K, alkalinity, and $SO_4$ in interstitial water extracted from sediments in Hole 800A. The lithostratigraphic column refers to the lithologic units defined in the "Lithostratigraphy and Sedimentology" section (this chapter). Unit I = brown clay, Unit II = red chert and porcelanite, Unit III = silicified limestone and chert, Unit IV = volcaniclastic turbidites, Unit V = brown claystone, and Unit VI = aphyric basalt.

**Table 4 (continued).**

| Si (μmol/L) | Sr (μmol/L) | Lithology |
|---|---|---|
| 377 | 89 | Pelagic brown clay |
| n.d. | 321 | Volcanic turbidite |
| 546 | 321 | Volcanic turbidite |
| 206 | 274 | Volcanic claystone |
| 193 | n.d. | Volcanic turbidite |
| 185 | 362 | Volcanic sandstone |
| 158 | 345 | Volcanic siltstone |
| 231 | 356 | Radiolarian claystone |
| 11 | 49 | |
| 17 | — | |

## Concentration Gradients

The shapes of the concentration gradients of the major ions (Fig. 24) are characterized by a break below the cherts of lithologic Unit III and then by nearly constant concentrations in the underlying volcaniclastic turbidites. The break is certainly due to the presence of the chert, which acts as a very efficient barrier to diffusional communication. This is a consequence of the low porosity (10% to 30%) and low water content (5% to 15%) of the cherts (see "Physical Properties" section, this chapter). A similar effect of a lithological barrier was described previously and attributed to the occurrence of cherts over volcaniclastic units (e.g., DSDP Sites 315 and 317: Gieskes, 1976; DSDP Site 462: Gieskes and Johnson, 1981). The question is whether the chlorine, magnesium, sodium, potassium, and calcium concentration changes occur in lithologic Unit III or in the underlying sediments. In the absence of fluid samples from lithologic Unit III or above, it is difficult to give direct arguments. However, the reactions most probably occur in the volcaniclastic turbidites because the observed chemical variations are typical of the alteration of volcanic material. Similar conclusions were reached at DSDP Sites 317 and 462 based on diffusion gradients above the cherts (Gieskes, 1976; Gieskes and Johnson, 1981).

## Chlorinity

The chloride ion is considered conservative in marine sediments because there are generally no significant sinks or sources present (e.g., Sayles and Manheim, 1975). Four of the five samples from Unit IV were depleted by about 6% with respect to seawater. Such a depletion is due either to dilution by low-chlorinity water or to uptake of chloride in solid phases during alteration. Chloride uptake by serpentine has been documented elsewhere (Miura et al., 1981), however, serpentine is uncommon in this unit. Dilution by low-salinity water could be related to several processes:

1. Pollution by drilling fluids or during squeezing. Mud injected episodically while drilling contains low-chlorinity water (Table 4, analysis of water extracted from mud) and hence could dilute interstitial water. This cause can be ruled out because (1) no mud was injected during drilling of Core 129-800A-49R and during the three previous cores, and (2) the calcium content of the mud water is 10 mmol/L; hence, pollution would induce a calcium decrease whereas a slight increase is observed. During handling of the sample, pollution is very unlikely because only seawater is in contact with the sample.

2. Dehydration related to diagenetic reactions such as degradation of organic matter or the smectite to illite reaction. These reactions are not important in this context. Only the opal-A/opal-CT/quartz transformation is likely to release water, but this reaction produces only a small amount.

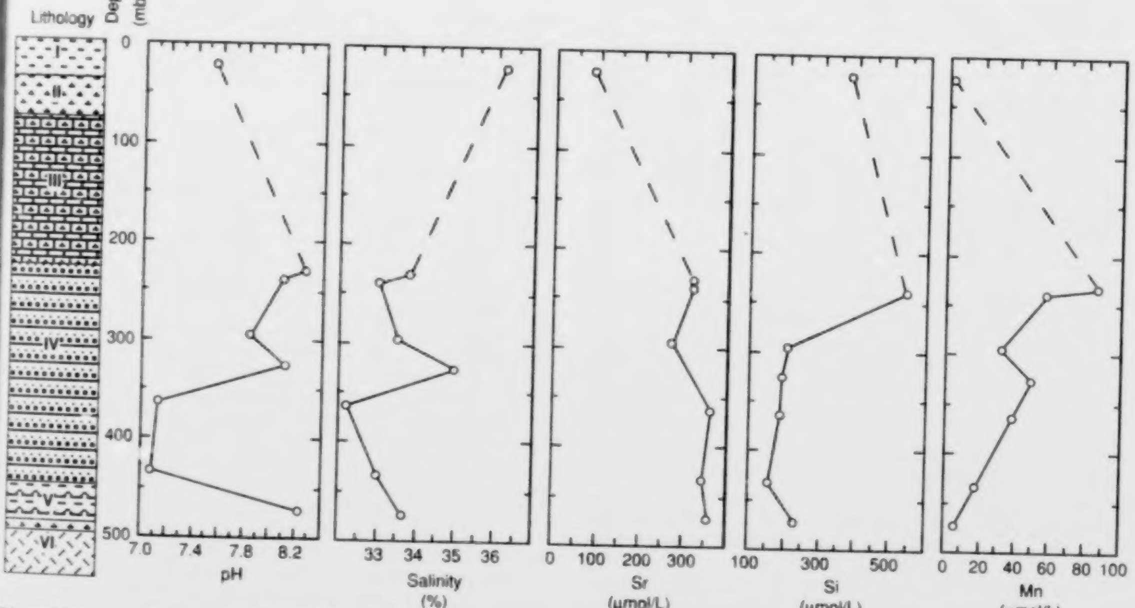

Figure 25. Profiles of depth vs. pH, salinity, and Sr, Si, and Mn concentrations in interstitial water extracted from sediments in Hole 800A. The lithostratigraphic column refers to the lithologic units defined in the "Lithostratigraphy and Sedimentology" section (this chapter). Unit I = brown clay, Unit II = red chert and porcelanite, Unit III = silicified limestone and chert, Unit IV = volcaniclastic turbidites, Unit V = brown claystone, and Unit VI = aphyric basalt.

3. Ultrafiltration process in which chloride ions are retained in a clay-rich formation, producing low-chlorinity water that could percolate in the sampled area. The abundance of clay minerals in Unit IV and below is too low to generate fresh water by membrane filtration.

4. Dewatering of smectite-type minerals. This remains the more probable explanation, but needs to be supported by mineralogical data. The only direct argument in favor of this process is the observation that the only sample from Unit IV that is not rich in clay minerals is also the least depleted in chloride (Sample 129-800A-37R-2, 0–10 cm; 554 mmol/L). The dewatering would certainly occur during the compaction of the sediments. The alternative is that interlayer water is released during squeezing, but this would happen for all squeezed smectite-rich sediments, which is not the case. Dewatering of hydrous minerals was proposed to explain low chlorinity values in Legs 116 (Shipboard Scientific Party, 1989), 123 (Shipboard Scientific Party, 1990a), and 125 (Shipboard Scientific Party, 1990b).

### Calcium, Magnesium, Potassium, and Sodium

A calcium increase associated with magnesium and potassium depletion is well known and documented in numerous DSDP-ODP reports. It is attributed to either the effect of alteration of basaltic basement or to diagenetic reactions with the sediment itself. In Hole 800A, the absence of a concentration gradient from 232 to 473 mbsf (top of Unit IV to basement) indicates that it is the alteration of these volcaniclastic turbidites that releases calcium and uptakes magnesium and potassium, probably during the formation of authigenic smectite and zeolite. The exact reactions responsible for these variations must be further documented on the basis of detailed mineralogical and geochemical studies of the sediments. However, the consistent presence of green clays, which could be either celadonite, glauconite, or saponite (see "Lithostratigraphy and Sedimentology" section, this chapter) is certainly a sink for magnesium. Clinoptilolite, also common in Unit IV, may have taken up potassium. Less common in interstitial water is a sodium depletion. Mineralogical investigations are necessary to identify which phase could uptake sodium in the sediment, but the most likely sink is the formation of zeolites. In Cores 129-800-27R and -49R, the absolute sink in sodium reaches 80 mmol/L or 60 mmol/L if it is corrected for a possible dilution. This depletion is about 2 times that of magnesium; therefore, the reaction(s) involving sodium should be important.

### Silica

Below the Unit III, silica concentrations decrease abruptly from 546 $\mu$mol/L at 240 mbsf to 206 $\mu$mol/L at 296 mbsf. The high concentration at 239.40 mbsf is probably due to the proximity of the cherts of Unit III and the sink in silicon may be related to the formation of authigenic clays and zeolites.

### Manganese

The progressive decrease in manganese observed from 232 to 473 mbsf (top of Unit IV to the Unit V) reflects the observed increase of manganese oxide minerals in veins (see "Lithostratigraphy and Sedimentology" section, this chapter) toward the bottom and the oxidizing conditions in Unit V.

### Conclusion

Interstitial water compositions in sediments recovered from Hole 800A are controlled by three main factors: (1) the presence of the cherts in Unit III which act as a diffusional barrier; (2) the diagenetic and alteration reactions in the volcaniclastics of Unit IV which deplete the water in sodium, magnesium, potassium, and silicon, and release calcium; and (3) the compaction that probably enhances release of interlayer water from smectite-type clays in Unit IV. It is possible that this is observed in this site because the low porosity of Unit III prevents diffusion to erase such concentration gradient.

## PHYSICAL PROPERTIES

Determination of physical properties of sediments and rocks recovered at Site 800 was based only on measurements using discrete samples. Continuous measurements provided by the gamma-ray attenuation porosity evaluator (GRAPE) and compressional-wave (*P*-wave) logger were not obtained because sediments and rocks typically did not completely fill core liners, or in the recovery of soft sediments, the cores were too highly disturbed. Physical properties measured on discrete samples are listed in Table 5 and include index properties (wet-bulk density, porosity, water content, and grain density), compressional-wave velocity, and thermal conductivity. All techniques and equipment used in making the measurements are described in the "Explanatory Notes" chapter (this volume). Differences in the properties of the various lithologies encountered at Site 800 can be identified in the physical properties data. However, because of the low recovery rate and low sampling frequency, trends in physical properties variation within the lithologic units are not well defined.

### Index Properties

Variations in index properties among the six lithologic units identified at Site 800 are described in the following section in terms of porosity, wet-bulk density, and grain density. Water content varies directly with porosity. Values for water content are listed in Table 5 and plotted in Figure 26. Wet-bulk density was determined by gravimetric and 2-min GRAPE techniques. The values cited are those of the gravimetric analyses, unless otherwise specified. Grain density was determined for all samples using solid "chunks" and for a limited number of powdered samples (Table 5). Analyses of powdered samples are believed to be the more accurate determinations at this site.

Pelagic brown clays of lithologic Unit I (0–38.0 mbsf) were sampled for index properties in Cores 129-800-3R and -4R. The pelagic clays were highly disturbed by rotary coring, and measured values of porosity and wet-bulk density, which average 81.0% and 1.34 g/cm$^3$, respectively, should be viewed with caution. Grain density averages 2.65 g/cm$^3$ for the pelagic clays.

The porcellanites and cherts of lithologic Unit II (38.0–78.2 mbsf) display downsection trends of decreasing porosity and increasing wet-bulk density and grain density (Fig. 26). The grain density of these opal-rich sediments is low, ranging from 2.32 to 2.34 g/cm$^3$. The increase in grain density with depth combined with the downsection decrease in porosity from 25.7% to 22.2% produces an increase in wet-bulk density of 2.00 to 2.05 g/cm$^3$ with depth.

Trends of decreasing porosity and increasing wet-bulk density and grain density that characterize Unit II continue in the uppermost part of lithologic Unit III (78.2–228.6 mbsf). The trends for porosity and wet-bulk density are reversed at 88.84 mbsf, at which depth values for porosity and wet-bulk density are 10.0% and 2.30 g/cm$^3$, respectively (Table 5). The increase in grain density continues to 97.40 mbsf, where it is 2.47 g/cm$^3$. Below 108 mbsf in Unit II the variability in grain density increases in response to fluctuations in calcium carbonate concentration (see "Lithostratigraphy and Sedimentology" section, this chapter). Grain density and calcium

Table 5. Physical properties summary for Site 800.

| Core, section, interval (cm) | Depth (mbsf) | Wet-bulk density | | Grain density[a] (g/cm³) | Porosity (%) | Water content (%) | Vertical velocity (m/s) | Horizontal velocity (m/s) | Velocity anisotropy (%) | Thermal conductivity (W/m · K) | Remarks |
|---|---|---|---|---|---|---|---|---|---|---|---|
| | | Gravimetric (g/cm³) | GRAPE (g/cm³) | | | | | | | | |
| 129-800A- | | | | | | | | | | | |
| 3R-1, 82–85 | 11.42 | 1.30 | | 2.62 | 82.8 | 64.8 | 1481 | | | 0.91 | Pelagic clay |
| 3R-2, 20 | 12.30 | | | | | | | | | 0.93 | Pelagic clay |
| 4R-1, 115–118 | 21.35 | 1.34 | | 2.67 | 81.1 | 61.8 | | | | 0.87 | Pelagic clay |
| 4R-3, 58–60 | 23.78 | 1.37 | | 2.66 | 79.0 | 58.8 | 1460 | | | 0.91 | Pelagic clay |
| 6R-1, 35–37 | 39.95 | 2.00 | | 2.01(2.34) | 25.7 | 13.1 | 3412 | 3713 | 8.4 | | Porcellanite |
| 8R-1, 2–4 | 58.92 | 1.96 | | 2.16(2.32) | 27.5 | 14.2 | 3032 | 3196 | 5.3 | | Chert |
| 9R-1, 10–12 | 68.60 | 2.05 | | 2.21(2.34) | 22.2 | 11.0 | 3229 | | | | Chert |
| 10R-1, 32–34 | 78.52 | 2.09 | 2.07 | 2.15(2.37) | 21.1 | 10.3 | 3459 | 3561 | 2.9 | 1.81 | Radiolarian chert and porcellanite |
| 11R-1, 104–106 | 88.84 | 2.30 | 2.27 | 2.22(2.44) | 10.0 | 4.4 | 4276 | 4539 | 6.0 | 1.85 | Chert |
| 12R-1, 10–12 | 97.40 | 2.26 | 2.21 | 2.30(2.47) | 14.3 | 6.4 | 3838 | 4184 | 8.6 | 2.09 | Siliceous limestone |
| 13R-1, 62–64 | 107.42 | 2.22 | 2.18 | 2.29(2.47) | 17.1 | 7.8 | 3628 | 3669 | 1.1 | | Siliceous limestone |
| 14R-1, 1–3 | 116.21 | 2.02 | 2.02 | 2.39 | 27.0 | 13.6 | 2954 | 3164 | 6.9 | 1.44 | Siliceous limestone |
| 15R-1, 36–38 | 125.76 | 2.41 | 2.40 | 2.36(2.52) | 7.0 | 3.0 | 4823 | 5100 | 5.6 | | Siliceous limestone |
| 16R-1, 30–32 | 135.20 | 2.17 | 1.97 | 2.10(2.43) | 18.4 | 8.6 | 3458 | 3523 | 1.9 | | Siliceous limestone |
| 17R-1, 47–49 | 144.67 | 2.26 | 2.24 | 2.28(2.51) | 16.5 | 7.4 | 3651 | 3690 | 1.1 | 1.65 | Porcellaneous limestone |
| 18R-1, 127–129 | 154.87 | 1.91 | 1.95 | 2.37 | 34.3 | 18.3 | 2533 | 2535 | 0.1 | 1.04 | Porcellanite |
| 19R-1, 23–25 | 163.13 | 1.99 | 2.00 | 2.47 | 33.5 | 17.1 | 2467 | 2569 | 4.1 | 1.63 | Siliceous radiolarian limestone |
| 21R-1, 65 | 181.95 | | | | | | | | | 0.94 | Nannofossil chalk |
| 21R-1, 135–137 | 182.65 | 2.08 | 2.05 | 2.69 | 36.9 | 18.1 | 2083 | 2150 | 3.2 | 1.53 | Nannofossil chalk |
| 22R-1, 25–27 | 191.25 | 2.14 | 2.15 | 2.51 | 24.9 | 11.8 | 2967 | 2907 | −2.0 | 1.48 | Siliceous limestone |
| 23R-1, 53–56 | 201.03 | 2.15 | 2.16 | 2.45 | 21.3 | 10.1 | 3281 | 3375 | 2.8 | 1.78 | Siliceous limestone |
| 24R-1, 120–122 | 211.10 | 2.12 | 2.29 | 2.27 | 12.2 | 5.9 | 4119 | 4335 | 5.1 | 0.89 | Siliceous limestone |
| 25R-1, 42–44 | 219.72 | 1.92 | 1.89 | 2.48 | 38.3 | 20.3 | 2379 | 2662 | 11.2 | | Radiolarite |
| 26R-1, 126–128 | 229.86 | 1.96 | 1.96 | 2.66 | 42.9 | 22.3 | 2039 | 2236 | 9.2 | 0.86 | Volcaniclastic silty sandstone |
| 26R-3, 54–56 | 232.14 | 2.00 | 1.98 | 2.84 | 46.2 | 23.5 | 2380 | 2420 | 1.7 | 1.16 | Volcaniclastic sandstone |
| 27R-1, 16–18 | 238.16 | 1.91 | 1.91 | 2.70 | 47.4 | 25.3 | 1911 | 2079 | 8.4 | 1.30 | Silty claystone |
| 28R-1, 33–35 | 247.53 | 1.88 | 1.88 | 2.84 | 52.8 | 28.6 | 1792 | 1899 | 5.8 | 0.97 | Volcaniclastic siltstone |
| 28R-3, 70 | 250.90 | | | | | | | | | 1.02 | Clayey siltstone |
| 28R-3, 73–85 | 250.93 | 1.88 | 1.92 | 2.64 | 47.2 | 25.6 | 1822 | 1927 | 5.6 | 1.04 | Clayey siltstone |
| 28R-5, 76–78 | 253.96 | 1.77 | 1.76 | 2.80 | 58.2 | 33.5 | 1773 | 1882 | 6.0 | | Silty claystone |
| 29R-2, 29–31 | 258.29 | 1.80 | 1.79 | 2.74 | 54.7 | 30.9 | 1787 | 1857 | 3.8 | | Clayey siltstone |
| 29R-3, 69–71 | 260.19 | 1.95 | 1.88 | 2.54 | 39.2 | 20.5 | 2235 | 2431 | 8.4 | | Volcaniclastic sandstone |
| 30R-1, 42–44 | 266.32 | 1.99 | 1.93 | 2.47 | 33.6 | 17.2 | 2735 | 3438 | 22.8 | | Volcaniclastic clayey siltstone |
| 30R-2, 102–104 | 268.42 | 1.98 | 1.96 | 2.55 | 37.7 | 19.4 | 2401 | 2609 | 8.3 | 1.51 | Porcellanite |
| 31R-1, 53–55 | 272.53 | 1.89 | 1.88 | 2.56 | 44.0 | 23.8 | 2166 | 2333 | 7.4 | 0.99 | Clayey siltstone |
| 31R-2, 34–36 | 273.84 | 2.06 | 2.02 | 2.87 | 43.9 | 21.7 | 2554 | 2569 | 0.6 | 1.32 | Volcaniclastic sandstone |
| 31R-2, 120 | 274.70 | | | | | | | | | 1.05 | Volcaniclastic sandstone |
| 32R-1, 101–103 | 279.11 | 2.14 | 2.07 | 2.68 | 32.5 | 15.4 | 2655 | 2676 | 0.8 | 1.42 | Volcaniclastic sandstone |
| 33R-1, 29–31 | 287.79 | 1.79 | 1.81 | 2.66 | 53.0 | 30.1 | 1844 | 1922 | 4.1 | 0.77 | Volcaniclastic siltstone |
| 33R-3, 73–75 | 291.23 | 2.29 | 2.30 | 2.82 | 29.6 | 13.2 | 3049 | 3110 | 2.0 | 0.66 | Volcaniclastic sandstone |
| 33R-5, 12–14 | 293.62 | 2.19 | 2.18 | 2.75 | 32.5 | 15.1 | 3107 | 3009 | −3.2 | 0.85 | Volcaniclastic sandstone |
| 34R-1, 60–62 | 297.60 | 2.15 | 2.15 | 2.76 | 35.2 | 16.7 | 2783 | 2794 | 0.4 | 1.27 | Volcaniclastic sandstone |
| 34R-3, 115–117 | 301.15 | 1.80 | 1.79 | 2.82 | 57.1 | 32.4 | 1749 | 1819 | 3.9 | 1.35 | Silty claystone |
| 35R-1, 47–49 | 306.87 | 1.89 | 1.89 | 2.72 | 49.3 | 26.6 | 1909 | 1991 | 4.2 | 1.43 | Volcaniclastic silty claystone |
| 35R-3, 36–38 | 309.76 | 1.75 | 1.75 | 2.69 | 56.3 | 32.7 | 2038 | 2070 | 1.6 | 1.28 | Volcaniclastic sandstone |
| 36R-1, 63–65 | 316.53 | 2.02 | 2.04 | 2.78 | 43.3 | 21.8 | 2563 | 2540 | −0.9 | 1.26 | Volcaniclastic sandstone |
| 36R-3, 76–78 | 319.66 | 1.71 | 1.79 | 2.50 | 53.9 | 32.1 | 1822 | 1913 | 4.9 | 1.26 | Volcaniclastic clayey siltstone |
| 37R-1, 46–48 | 325.56 | 1.89 | 1.87 | 2.80 | 51.2 | 27.6 | 2275 | 2259 | −0.7 | 1.26 | Volcaniclastic sandstone |
| 38R-1, 112–114 | 335.62 | 1.61 | 1.77 | 2.26 | 52.8 | 33.4 | 1772 | 1804 | 1.8 | 1.20 | Claystone |
| 39R-2, 41–43 | 345.71 | 1.66 | 1.80 | 2.37 | 52.6 | 32.2 | 1759 | 1842 | 4.6 | 1.08 | Volcaniclastic silty-claystone |
| 39R-3, 64–66 | 347.44 | 1.67 | 1.72 | 2.63 | 59.7 | 36.4 | 1856 | 1841 | −0.8 | 1.22 | Volcaniclastic sandstone |
| 40R-1, 39–41 | 353.49 | 2.04 | 2.00 | 2.86 | 44.9 | 22.4 | 2491 | 2503 | 0.5 | 1.05 | Silty claystone |
| 41R-1, 20–22 | 362.70 | 1.97 | 1.95 | 2.85 | 48.5 | 25.2 | 2253 | 2239 | −0.6 | 1.22 | Sandstone breccia |
| 42R-1, 53–55 | 369.13 | 1.78 | 1.74 | 2.75 | 56.5 | 32.4 | 1951 | 2043 | 4.6 | | Claystone breccia |
| 43R-1, 105–107 | 375.75 | 1.74 | 1.73 | 2.70 | 57.4 | 33.6 | 1965 | 1979 | 0.7 | 0.84 | Claystone breccia |
| 44R-1, 124–126 | 384.94 | 1.99 | 1.98 | 2.77 | 44.9 | 23.0 | 2375 | 2386 | 0.5 | 1.21 | Volcaniclastic sandstone |
| 45R-1, 85–87 | 393.95 | 1.97 | 1.97 | 2.74 | 44.9 | 23.2 | 2545 | 2534 | −0.4 | 1.03 | Volcaniclastic sandstone |
| 46R-1, 78–80 | 403.28 | 2.05 | 1.97 | 2.79 | 41.8 | 20.7 | 2023 | 1908 | −5.9 | 1.62 | Radiolarian claystone |
| 46R-3, 43–45 | 205.93 | 1.85 | 1.80 | 2.77 | 52.7 | 29.0 | 2058 | 2109 | 2.4 | 1.26 | Silty breccia |
| 47R-1, 89–90 | 412.79 | 1.93 | 1.95 | 2.75 | 47.8 | 25.3 | 2340 | 2268 | −3.1 | 1.25 | Volcaniclastic sandstone |
| 47R-3, 79–81 | 415.69 | 1.97 | 1.99 | 2.82 | 47.5 | 24.6 | 2321 | 2348 | 1.2 | 1.25 | Volcaniclastic sandstone |
| 48R-1, 7–9 | 421.47 | 2.03 | 2.04 | 2.73 | 41.5 | 20.8 | 2681 | 2664 | −0.6 | 1.25 | Volcaniclastic sandstone |
| 48R-4, 21–23 | 426.11 | 2.09 | 2.07 | 2.80 | 40.2 | 19.6 | 2698 | 2640 | −2.2 | 1.34 | Volcaniclastic sandstone |
| 48R-5, 147–149 | 428.87 | 1.95 | 1.90 | 2.78 | 47.5 | 24.8 | 2124 | 2184 | 2.8 | 1.24 | Sandy siltstone |
| 49R-1, 35–37 | 431.25 | 1.85 | 1.87 | 2.77 | 53.1 | 29.3 | 2027 | 2076 | 2.4 | 1.14 | Volcaniclastic sandstone |
| 49R-4, 43–45 | 435.83 | 1.86 | 1.86 | 2.75 | 51.9 | 28.5 | 2212 | 2194 | −0.8 | 1.23 | Volcaniclastic sandstone |
| 50R-1, 81–83 | 441.01 | 1.61 | 1.60 | 2.70 | 65.0 | 41.1 | 1668 | 1708 | 2.4 | 1.20 | Volcaniclastic silt-claystone |
| 50R-3, 18–20 | 443.38 | 2.01 | 1.99 | 2.79 | 44.4 | 22.5 | 2496 | 2464 | −1.3 | 1.28 | Volcaniclastic sandstone |
| 51R-1, 71–73 | 450.31 | 2.07 | 1.99 | 2.66 | 36.1 | 17.7 | 2301 | 2443 | 6.0 | | Siliceous claystone |
| 52R-2, 118–120 | 461.48 | 1.97 | 1.93 | 2.68 | 43.2 | 22.4 | 1962 | 1945 | −0.9 | 1.56 | Clay radiolarite |
| 53R-1, 128–130 | 466.18 | 1.98 | 1.99 | 2.59 | 38.8 | 19.9 | 2102 | 2157 | 2.6 | 1.58 | Clayey radiolarite |
| 54R-2, 57–59 | 473.07 | 1.93 | 1.89 | 2.69 | 45.7 | 24.0 | 1882 | 1980 | 5.1 | 1.65 | Radiolarian claystone |
| 55R-2, 62–64 | 481.22 | 1.90 | 1.85 | 2.65 | 46.0 | 24.6 | 1890 | 1898 | 0.4 | 1.68 | Radiolarian claystone |
| 56R-1, 38–40 | 488.88 | 2.56 | 2.45 | 2.46(2.63) | 4.2 | 1.7 | 5296 | 5419 | 2.3 | | Chert |
| 57R-1, 22–24 | 498.22 | 2.53 | 2.35 | 2.73(2.78) | 14.1 | 5.7 | 4025 | 3963 | −1.6 | 1.68 | Dolerite |
| 57R-2, 87–89 | 499.37 | | 2.48 | | 15.6[b] | | 4542 | 4496 | −1.0 | 1.81 | Dolerite |
| 57R-2, 98–100 | 499.48 | 2.54 | 2.49 | 2.72(2.72) | 10.8 | 4.3 | 4656 | 4514 | −3.1 | 1.92 | Dolerite |
| 58R-1, 49–51 | 507.69 | | 2.54 | | 12.2[b] | | 4658 | 4564 | −2.0 | 1.65 | Dolerite |
| 59R-1, 7–9 | 516.67 | | 2.57 | | 10.6[b] | | 4646 | 4576 | −1.5 | 1.61 | Dolerite |
| 60R-1, 44–46 | 526.34 | | 2.53 | | 12.7[b] | | 4279 | 4417 | 3.2 | 1.70 | Dolerite |
| 60R-1, 69–71 | 526.59 | 2.58 | 2.53 | 2.76(2.79) | 11.9 | 4.7 | 4442 | 4219 | −5.1 | 1.77 | Dolerite |

[a] Values in parentheses were determined using powdered samples.

[b] Porosity determined from GRAPE wet-bulk density.

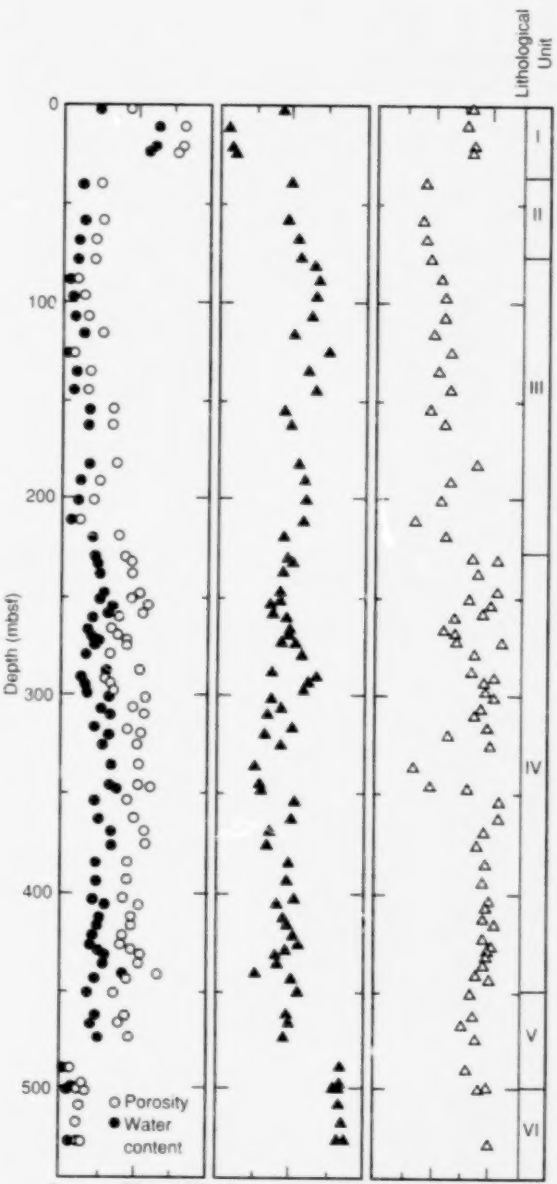

Figure 26. Index properties (porosity, water content, wet-bulk density, and grain density) vs. depth for Hole 800A.

carbonate concentration vary directly in this interval. The downsection increase in calcium carbonate concentration and change in composition from chert to siliceous limestone in Unit II (see "Lithostratigraphy and Sedimentology" section, this chapter) are reflected by increasing porosity and grain density with depth, below 89 mbsf (Fig. 26). Maxima in porosity (36.9%) and grain density (2.69 g/cm$^3$) occur at 182.65 mbsf and coincide with a carbonate concentration maximum (82%). Below this depth, porosity and grain density decrease rapidly to values of 12.2% and 2.27 g/cm$^3$, respectively, at 211.10 mbsf. Decreasing porosity and grain density between 183 and 211 mbsf coincide with an increase in silica concentration, indicated on geochemical logs (see "Downhole Measurements" section, this chapter). The covariance of porosity and grain density in Unit III has opposing effects on wet-bulk density, and wet-bulk density varies irregularly between 1.91 and 2.30 g/cm$^3$ (Fig. 26). Below 211.10 mbsf sharp increases in porosity and grain density and a decrease in wet-bulk density characterize the transition zone between lithologic Units III and IV. At 219.7 mbsf the respective values for porosity, grain density, and wet-bulk density are 38.3%, 2.48 g/cm$^3$, and 1.92 g/cm$^3$.

Highly variable porosity, wet-bulk density, and grain density characterize the volcaniclastic sediments of lithologic Unit IV (228.6–449.6 mbsf) (Fig. 26). Variability of the index properties in part is related to sampling both coarse-grained rocks (sandstones and breccias) and fine-grained rocks (siltstones and claystones); however, variation in properties within these two general rock types is also large. Porosity of the fine-grained rocks ranges from 33.6% to 65.0%, whereas porosity of the coarse-grained volcaniclastic rocks varies between 29.6% and 56.3%. Variation in wet-bulk density is of similar scale (Fig. 26), and values range from 1.61 to 2.29 g/cm$^3$. Grain density displays large variations in the upper part of Unit IV, between 228.6 and 362.7 mbsf, with values ranging from 2.26 to 2.86 g/cm$^3$ (Fig. 26). Between 362.7 mbsf and the base of Unit IV, grain density is more closely clustered about an average value of 2.76 g/cm$^3$.

Claystones and radiolarites of Unit V (449.6–498.1 mbsf) are characterized by a more regular increase in porosity and decrease in wet-bulk density with depth. Grain density is nearly constant at 2.65 g/cm$^3$. In Unit V porosity increases downsection from 36.1% at 450.31 mbsf to 46.0% at 481.22 mbsf (Fig. 26). Over this interval wet-bulk density decreases from 1.99 to 1.85 g/cm$^3$. The lowermost sample from Unit V, at 488.88 mbsf, is chert, which is characterized by properties distinctly different from those of the other rocks in Unit V. The porosity of the chert is 4.2%, its grain density is 2.63 g/cm$^3$, and its wet-bulk density is 2.56 g/cm$^3$.

Dolerites of lithologic Unit VI (498.1–544.5 mbsf) are characterized by little variation in physical properties. Index property measurements were based on gravimetric and 2-min GRAPE analyses for three samples and 2-min GRAPE analyses only on an additional four samples. Porosities of rocks analyzed only with the GRAPE were estimated from the GRAPE wet-bulk density as outlined in the "Explanatory Notes" chapter (this volume). An average grain density of 2.75 g/cm$^3$ was assumed for these calculations. Porosity of the dolerites is high, ranging from 10.6% to 15.6%. The highest porosity values are from Section 129-800-57R-1, which is contained in the oxidized interval of the upper flow unit within Unit VI. Wet-bulk density of the dolerites varies between 2.35 and 2.58 g/cm$^3$, and grain density of these rocks ranges from 2.72 to 2.79 g/cm$^3$. Low values of wet-bulk density 2.35 to 2.48 g/cm$^3$ characterize the upper flow unit of Unit VI.

## Compressional-Wave Velocity

At Site 800, compressional-wave velocities were measured in both vertical and horizontal propagation directions. Velocity anisotropy was calculated as the difference between the horizontal and vertical velocities divided by the average velocity (see "Explanatory Notes" chapter, this volume). Large variations are present in the velocity data set. Despite the wide variation, trends that correspond to changes in physical properties and lithology can be recognized. Unless otherwise noted, the velocity values cited are for measurements made in the vertical direction.

Compressional-wave velocity was measured for two samples of questionably intact pelagic clay of Unit I (Table 5). The average of the measurements is 1470 m/s, less than the velocity of sound in seawater. This anomalous situation is not unusual for deep-sea sediments at shallow burial depths (Hamilton, 1974).

In lithologic Unit II velocity varies roughly directly with wet-bulk density and increases downsection to a local maxima of 4276 m/s in chert at 88.84 mbsf, near the top of Unit III (Fig. 27). Below 88.84 mbsf sonic velocity is highly variable in Unit III, varying roughly inversely with carbonate concentration. A velocity maxima of 4823 m/s occurs in siliceous limestone at 125.76 mbsf. Below this depth, velocity rapidly decreases to 2083 m/s in nannofossil chalk at 182.65 mbsf and subsequently increases downsection to 4119 m/s in siliceous limestone at 211.10 mbsf. The rapid increase in velocity between 183 and 211 mbsf correlates with a rapid decrease in grain density (Fig. 26) and increase in silica, as indicated by silica geochemical logs (see "Downhole Measurements" section, this chapter). The decrease in velocity at the base of Unit III coincides with an increase in grain density (Fig. 26). Velocity anisotropy for sediments and rocks of Units II and III ranges from 2.0% to 11.2% (Table 5). Anisotropy is high at the top of Unit II (8.4%) and at 97.40 mbsf in Unit III (8.6%). The general trend in anisotropy for Units II and III is a broad downsection decrease in anisotropy (Fig. 27), although the highest anisotropy (11.2%) was measured for a radiolarite sample near the base of Unit III, at 219.72 mbsf. High-velocity anisotropy in the radiolarite is associated with well-defined parallel lamination that characterizes these rocks.

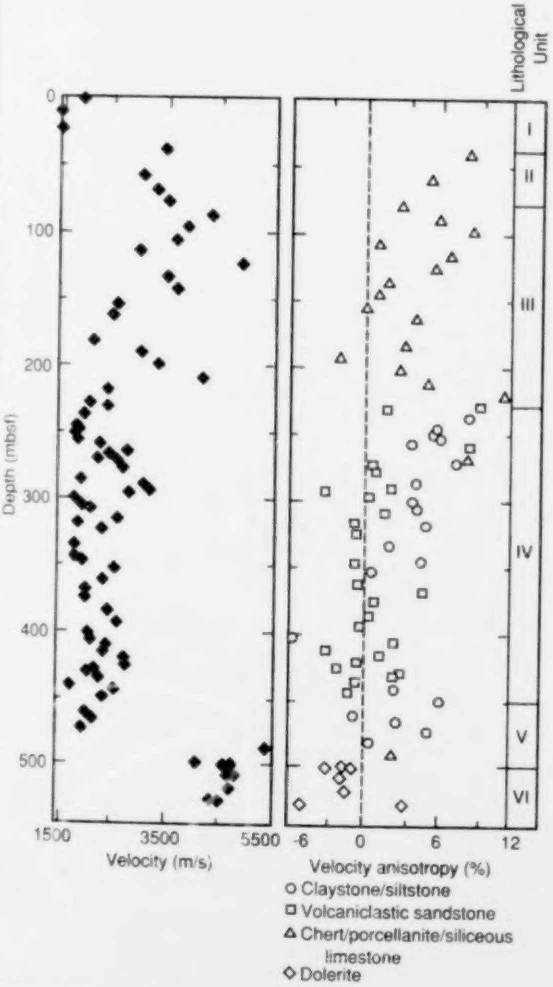

Figure 27. Compressional-wave velocity (measured perpendicular to bedding) and velocity anisotropy vs. depth for Hole 800A. Velocity anisotropy profile is coded according to sediment and rock type.

Lithologic Unit IV is characterized by distinct differences in the velocity of coarse-grained rocks (sandstones and breccias) and fine-grained rocks (siltstones and claystones) that comprise the unit. Velocity of the sandstones and breccias ranges from 1856 to 3107 m/s and averages 2371 m/s. Velocity of the siltstones and claystones of Unit IV ranges from 1668 to 2735 m/s and averages 1946 m/s. Well-defined trends in velocity variation with depth are not apparent in Unit IV (Fig. 27). Velocity anisotropy of rocks of Unit IV varies as a function of lithology. Fine-grained rocks typically display higher anisotropy than coarse-grained rocks in this interval (Fig. 27). Anisotropy of the claystones and siltstones ranges from 5.9% to 22.8% and is characterized by a general decrease downsection. Anisotropy of the sandstones and breccias ranges from 3.2% to 9.2%, with most values clustered near zero.

The claystones and radiolarites of lithologic Unit V display a regular decrease in velocity with depth from 2443 m/s at 450.31 mbsf to 1898 m/s at 481.22 mbsf (Fig. 27). This downsection decrease in velocity correlates with a downsection decrease in wet-bulk density in Unit V (Fig. 26). The chert in the lowermost part of Unit V is characterized by high wet-bulk density (2.56 g/cm$^3$) and the highest velocity measured at Site 800 (5296 m/s). Rocks of Unit V display a wide range in velocity anisotropy, from 0.9% to 6%, and no regular pattern in anisotropy variation.

The dolerites of Unit VI are characterized by little variation in compressional-wave velocity with depth (Fig. 27). Sonic velocity in these rocks ranges from 4025 to 4646 m/s (Table 5). The lowest velocity occurs in the oxidized interval at the top of Unit VI. All but one of the dolerite samples are characterized by higher vertical velocity than horizontal velocity. Velocity anisotropy in these rocks averages 1.6%.

The different sediment and rock types recovered at Site 800 show consistent relationships between wet-bulk density and compressional-wave velocity. The overall pattern is that of increasing velocity with increasing wet-bulk density (Fig. 28). However, the relationship between bulk density and velocity differs with differing lithologies. The lithologic grouping consisting of clays, claystones, siltstones, and radiolarite claystones displays the lowest velocities and the lowest velocity/density gradient (Fig. 28). The field represented by volcaniclastic sandstones and breccias on the crossplot of wet-bulk density and velocity overlaps that of the fine-grained sediments and rocks, but is characterized overall by higher velocities and a higher velocity/density gradient. Siliceous sediments encompass a wide area on the density-velocity crossplot. The variety of sediments included in this grouping, porcellanite, chert, and siliceous limestone, may account in part for the spread in the data. The siliceous sediments are characterized by velocities higher than those of other rocks at equivalent densities and the highest velocity/density gradient, a pattern consistent with previous studies of velocity-density

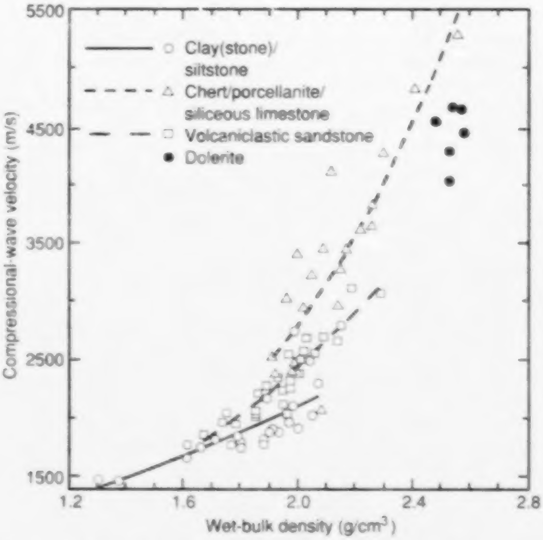

Figure 28. Wet-bulk density vs. compressional-wave velocity (measured perpendicular to bedding) for Hole 800A, coded according to sediment and rock type. Lines are best-fit exponential curves through the data.

relationships in deep-sea sediments (Hamilton, 1978). Density and velocity data for the dolerites do not define a clear relationship between the two parameters. However, velocities displayed by the dolerites are approximately equal to those predicted for oceanic basalts by empirical relations between bulk density and compressional-wave velocity established by Christensen and Salisbury (1975) for measurements made on oceanic basalts at 0.5 kbars effective pressure.

### Thermal Conductivity

Thermal conductivity was measured for both sediments and rocks recovered at Site 800. The conductivity of soft sediments was measured by a heated needle probe inserted in the sediment. Conductivity of lithified sediments and basement rocks was measured by a heated needle probe sandwiched between the sample and a slab of low-conducting material. Details for both procedures for measuring thermal conductivity are described in the "Explanatory Notes" chapter (this volume). Fewer measurements of thermal conductivity were made than measurements of other physical properties because the rock fragments recovered were frequently too small to use with the needle probe technique.

General differences in thermal conductivity can be identified among the different lithologies recovered at Site 800 (Fig. 29). Pelagic clays of Unit I are characterized by a low and nearly constant conductivity averaging 0.90 W/m · K. Poor recovery precluded conductivity measurements for Unit II rocks. Silica-rich rocks of Unit III are characterized by high conductivity. The thermal conductivity of siliceous limestone at 97.40 mbsf is 2.09 W/m · K, the highest conductivity measured at Site 800 (Table 5). Thermal conductivity values for Unit III are highly variable, but the general trend is that of decreasing conductivity downsection. Thermal conductivity is also highly variable in the upper part of lithologic Unit IV, ranging from 0.66 to 1.51 W/m · K between the top of the unit and 300 mbsf. In this interval values less than 0.90 W/m · K are suspect either as a consequence of poor sample quality or

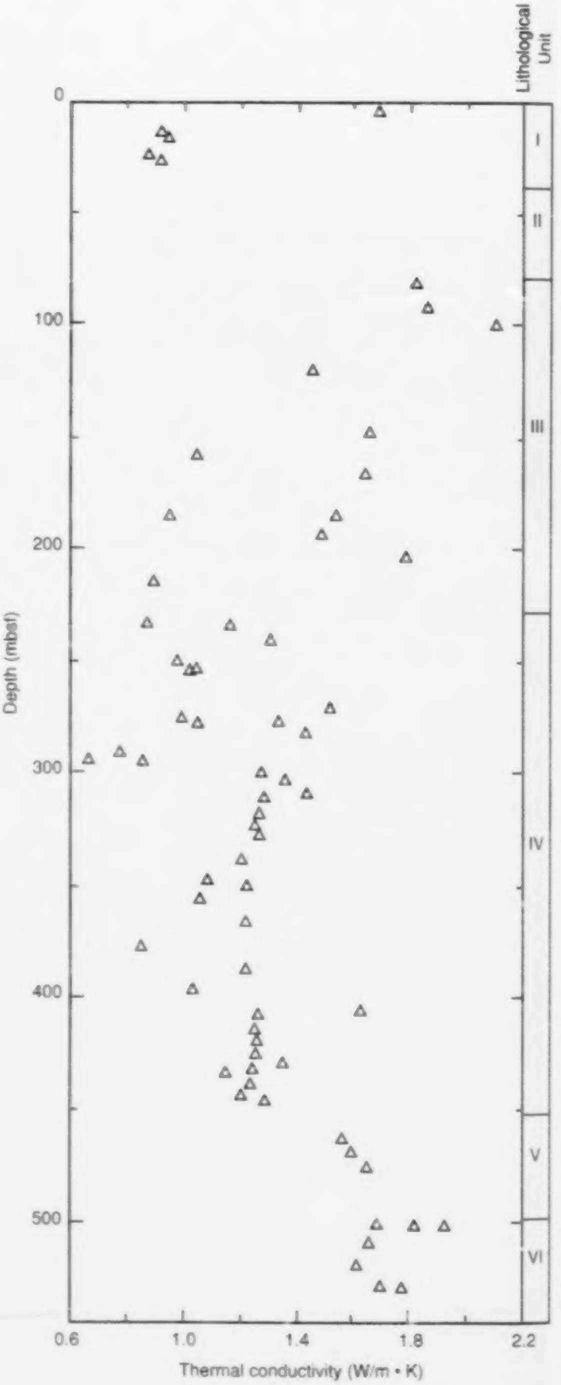

Figure 29. Thermal conductivity vs. depth for Hole 800A.

poor contact between the sample and needle. Below 300 mbsf in Unit IV most of the conductivity measurements fall in a relatively narrow range between 1.20 and 1.40 W/m · K. Thermal conductivity of the claystones and radiolarites of Unit V is markedly higher than that of the volcaniclastic rocks of Unit VI (Fig. 29). Unit V is also characterized by a steady increase in conductivity with depth, from 1.56 to 1.68 W/m · K. Thermal conductivity values measured for the dolerites of Unit VI range from 1.61 to 1.92 W/m · K (Table 5) and average 1.73 W/m · K. The largest variation in conductivity occurs in the altered rocks of the upper flow unit in Unit VI. The average conductivity for Unit VI rocks is slightly less than that reported for basalts from Hole 395A, 1.80 W/m · K (Hyndman et al., 1984) and Hole 648B, 1.77 W/m · K (Detrick et al., 1988). Porosities for basalts from these two holes, however, are less, averaging between 5% and 10%.

The combined sediment and rock conductivity data for Site 800 exhibit a moderately strong inverse relationship between porosity and thermal conductivity (Fig. 30). Figure 30 also illustrates potentially spurious conductivity measurements. Data in the field bounded by conductivities between 0.6 and 1.0 W/m · K and porosities between 10% and 60% fall markedly off the trend defined by the rest of the data and may represent inaccurate conductivity measurements.

## IGNEOUS PETROLOGY

One of the hard-rock objectives of Leg 129 at Site 800 was to reach oceanic basement formed at magnetic anomaly M33 (~160 Ma) in the Pacific. Although a series of dolerites was penetrated at the base of Hole 800A, these rocks were not considered to represent "normal" ocean crust, because they (1) occurred just below sediments of lowermost Cretaceous age (~140 Ma), and (2) were interpreted to be intrusive sills rather than submarine lavas, as might be reasonably anticipated for true crust. We were also unable to determine their chemical signature relative to normal-type, mid-ocean ridge basalt (N-MORB) due to the nonoperation of the XRF spectrometer on board. Sills intruded into Cretaceous sediments were also encountered in the Nauru Basin during Leg 129 (Hole 462), and were considered to be probably Aptian-Albian in age (Schlanger and Moberly, 1986). No chemical analyses are available to compare the two groups of intrusives, but preliminary data for the Hole 800A sills suggest they may be older than the Nauru sills and are petrographically distinct.

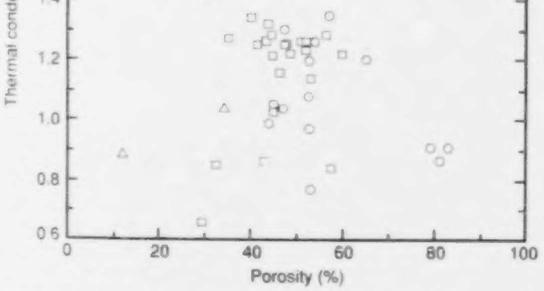

Figure 30. Porosity vs. thermal conductivity for Hole 800A, coded according to sediment and rock type.

### Lithology

Five cores (129-800A-57 through -61), representing about 12% recovery overall, sampled just over 7 m of dolerites. Although in gross terms the lithology is similar throughout, and actual contacts were not visible, three separate units within the dolerites were recognized on the basis of (1) a sedimentary interlayer, (2) systematic grain-size variations, and (3) macroscopic textural variations. Bearing in mind that a considerable amount of core is missing, the actual observed extent of each unit is shown in Table 6.

The contact between Unit 1 and the cherty sediments above (Fig. 31) is inferred from the upward-decreasing grain size and increasing degree of oxidation of the dolerite, as well as its more granular texture. The boundary between Units 1 and 2 is probably represented by slightly oxidized, dolerite drilling rubble at the base of Section 129-800A-57R-3 and indicates that a section of core is probably missing at this point. Red chert with silicified cream-colored and pale brown, laminated siltstones (at interval 129-800A-58R-1, 27–43 cm) marks the boundary between Units 2 and 3 (Fig. 32). The indurated and bleached nature of the sediment interlayer suggests that it had been thermally heated by intrusions. This feature, together with the relatively coarse texture of the dolerites, provides evidence for the sill-like nature of the igneous body. Sedimentary features allow the sediments to be directly compared with unaltered, laminated, brown and red siltstones and mudstones higher in the sequence just above the dolerites.

### Petrography

In general terms, all the massive dolerites are medium-grained, aphyric, and largely holocrystalline, with very minor, glassy mesostasis (a few percent). Small, open miaroles (commonly 1 mm in diameter), lined with the terminations of plagioclase crystals or sometimes partly infilled with carbonate or clays, are randomly developed throughout.

The dolerites differ macroscopically and display three main textural variants:

1. Finer-grained, granular, equidimensional matrix (grains commonly <1 mm long), characteristic of the chilled facies at the top of Unit 1. In view of the reduced grain size this chilled zone is strictly a basalt, rather than a dolerite.
2. Medium-grained, hypidiomorphic-granular matrix (grains 1–2 mm in length) exhibiting black, stubby, and elongate prisms of pyroxene with white and green (clay-altered) plagioclase laths; featured in Unit 2.
3. Medium-grained, hypidiomorphic-granular matrix (grains commonly 1–5 mm in length), but characterized by long, straight (more rarely curved), skeletal-looking, black pyroxene crystals (5–15 mm long). The pyroxene may form

**Table 6. Extent of sill units recognized in Hole 800A.**

| Unit no. | Interval | | Sample thickness (cm) |
|---|---|---|---|
| | Top | Bottom | |
| 1 | 129-800A-57R-1, 13 cm | 129-800A-57R-3, 41 cm | 192 |
| 2 | 129-800A-58R-1, 0 cm | 129-800A-58R-1, 27 cm | 27 |
| 3 | 129-800A-58R-1, 43 cm | 129-800A-61R-1, 31 cm | 489 |

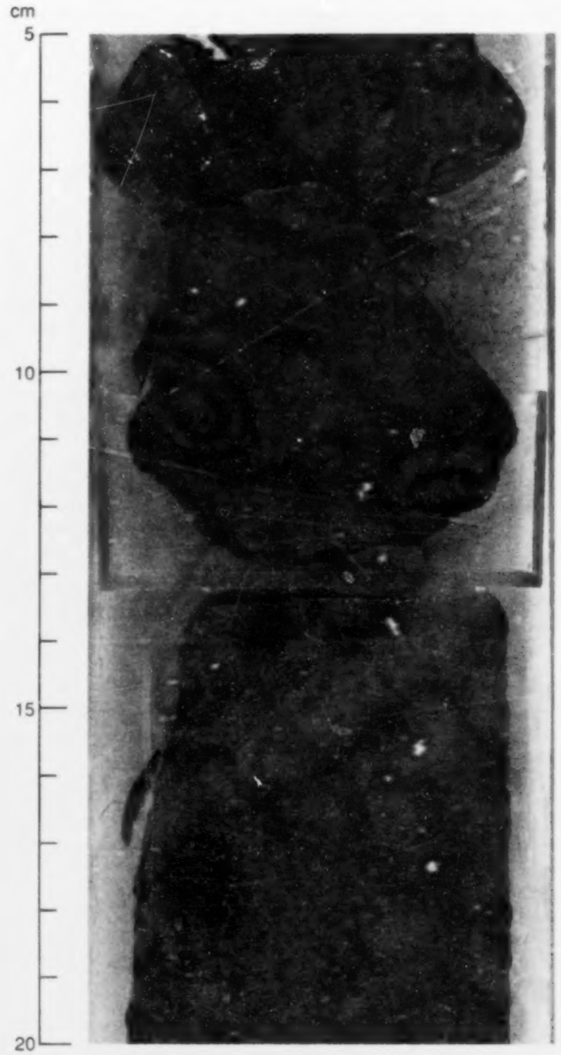

Figure 31. Photograph of the contact between dolerite Unit 1 and chert rubble in Section 129-800A-57R-1, 13 cm. Although much of the contact facies is missing, the dolerite is fine-grained, largely holocrystalline, and gradually increases in grain size down the unit. This section of dolerite also exhibits progressive oxidation toward the assumed contact.

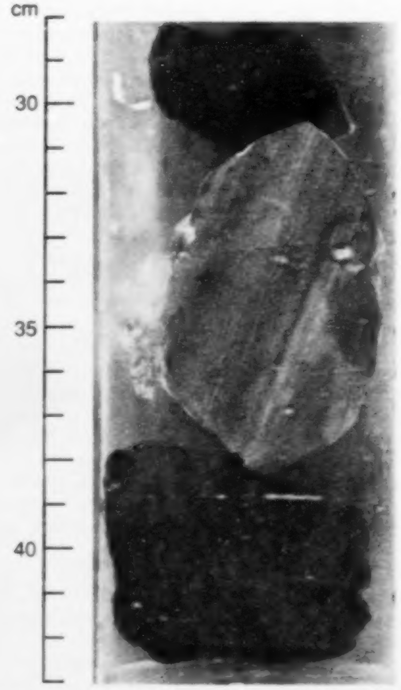

Figure 32. Photograph showing the baked chert and silicified siltstone interlayer between dolerite Units 2 and 3 within interval 129-800A-58R-1, 28–43 cm. The actual contacts between the lithologies were not recovered. The well-preserved lamination in the central siltstone block can be matched with unaltered, sedimentary material above the dolerites.

crude radiate groups composed of 2 to 4 individual crystals. These long crystals are most pronounced in altered zones of Unit 3 where they stand out against a pale green clay matrix (Fig. 33). The actual length and thickness of the black pyroxenes may vary in a random fashion through this unit.

Thin-section examination of samples from Units 1 and 3 (Table 7) confirms that the dolerites are aphyric and generally medium-grained with a hypidiomorphic-granular texture containing no or minor mesostasis (1%–2%). The clinopyroxene is invariably a pink pleochroic titanaugite and suggests the dolerites have alkaline affinities. All are moderately to highly altered (see below) such that only plagioclase remains as an abundant, primary phase (40%–55%), whereas clinopyroxene and titanomagnetite may be totally replaced or remain as volumetrically reduced relicts (maximum fresh clinopyroxene content was on the order of 10%). Some petrographic features of the dolerites are illustrated in Figure 34. A brief description of the more important primary characteristics obtained from thin-section study follows.

### *Unit 1*

Unit 1 shows a gradual increase in the grain size of primary plagioclase ($An_{55-60}$) from <1.0 mm (commonly 0.4–0.6 mm) to 1.0–1.5 mm towards the bottom of the unit. Secondary materials (see below) occupy the spaces between the plagioclase laths which may show Carlsbad, and more rarely, polysynthetic twinning. Zoning within the plagioclase is suggested by the cores often being replaced, whereas the rims are clear.

### *Units 2 and 3*

Units 2 and 3 are dominated by primary plagioclase laths (0.5–5.0 mm in length) showing a range of composition from $An_{35-70}$, with more sodic values, probably representing secondary alteration. Most plagioclases are zoned with altered cores. Clinopyroxene (titanaugite) occurs both as anhedral grains or more commonly as elongate, subhedral prisms normally varying from 0.4 to 4.0 mm (longer prisms are seen in hand specimens). The macroscopic, skeletal-like form is due to variable alteration and replacement of the elongate

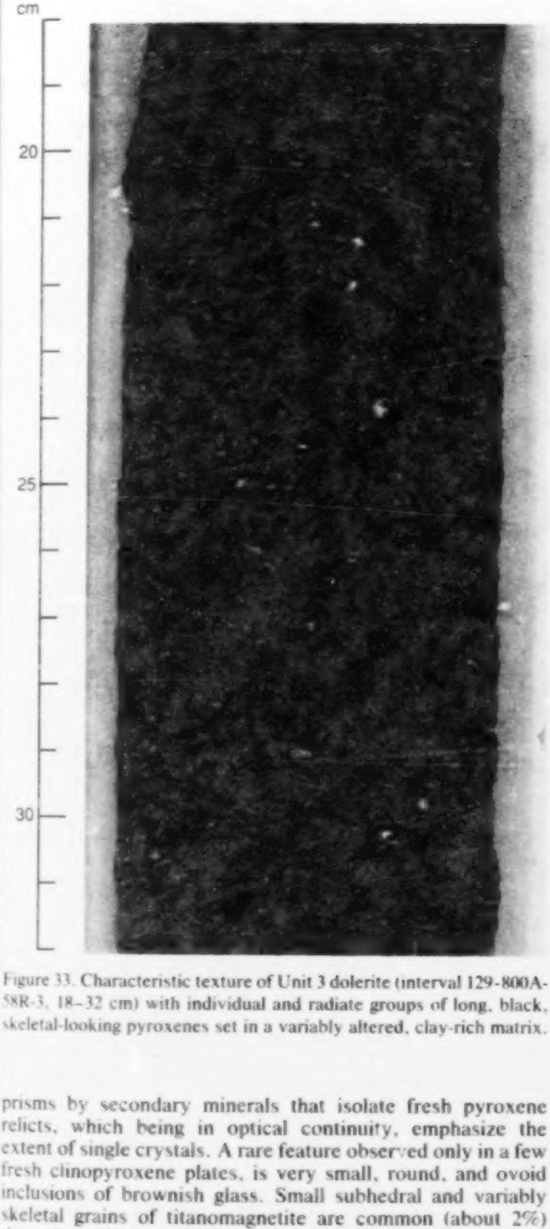

Figure 33. Characteristic texture of Unit 3 dolerite (interval 129-800A-58R-3, 18–32 cm) with individual and radiate groups of long, black, skeletal-looking pyroxenes set in a variably altered, clay-rich matrix.

prisms by secondary minerals that isolate fresh pyroxene relicts, which being in optical continuity, emphasize the extent of single crystals. A rare feature observed only in a few fresh clinopyroxene plates, is very small, round, and ovoid inclusions of brownish glass. Small subhedral and variably skeletal grains of titanomagnetite are common (about 2%) throughout both units, together with ubiquitous secondary pyrite, and show variable alteration depending on their proximity to the Unit 2/Unit 3 contact. The only other primary minerals observed are occasional, small apatite crystals. Some highly altered, angular-shaped zones between plagioclase laths have been interpreted as being originally glassy mesostasis, although the proportion is very low (a few percent) in these essentially holocrystalline rocks.

### Alteration

The dolerites are moderately to highly altered (generally 20%–55%) due mainly to variable oxidation, clay development, carbonate, and other secondary minerals in minor proportions. Variation in the degree of alteration is seen at two core positions:

1. The top of Unit 1 (interval 129-800A-57R-1, 13–55 cm) is the most oxidized (as shown by hematite and a hydrated, iron-oxide, limonitic stain) with the degree of alteration decreasing downward from the assumed contact. The presence of an oxidized zone here implies alteration due to the downward percolation of oxygenated seawater, probably soon after consolidation of the sill. However, magnetic studies indicate that this section of core has a superimposed normal polarity (and small inclination) that is different from the rest of the fresher dolerite below which exhibits a reversed polarization throughout and a high inclination (+50°). This suggests that oxidation was a later phenomenon, possibly in response to a subsequent intrusion, or later volcanic activity that raised the ambient temperature of this zone.
2. The top of Unit 3 (Section 129-800A-58R-1) does not show much of an increase in the degree of alteration (30%) to the rest of the unit below, but a number of alteration domains composed of specific secondary phyllosilicates, as well as the presence of higher-grade amphibole and biotite, characterize this core section (see below). Magnetically, this zone (down to about Section 129-800A-58R-2, 80 cm; see "Paleomagnetics" section, this chapter) has a low inclination of 0°–10°, which steadily increases down the core and also reinforces the notion that Unit 3 is distinct from Unit 2 above which has a strong positive inclination (+50°).

Unit 1 is characterized by the presence of deep, red hematite almost totally replacing magnetite and pyrite, and with brown, limonitic stains covering clays and along mineral boundaries. Pale green, smectitic clays replace both pyroxene and plagioclase and together with carbonate and limonite, may sometimes totally replace plagioclase laths. Lower down in this unit, replacement takes the form of alteration domains typified by specific secondary minerals or assemblages. Three domains are recognized, comprising sericite and some carbonate (replacing plagioclase), opaque and brown smectites, and dark green chlorite (both replacing pyroxene). Throughout the altered matrix are colorless, acicular crystals of a zeolite (phillipsite?), although the proportion is low (about 1%). Of particular interest is the presence of biotite and traces of actinolite, both of which are restricted to the smectite- and chlorite-rich domains (see below).

Units 2 and 3 show similar alteration features to the lower portion of Unit 1 with abundant brownish smectites (20%–40%) and minor proportions of chlorite, carbonate, and zeolite. The most significant development at the top of Unit 3 (Sections 129-800A-58R-1 and -58R-2) is the presence of pleochroic, colorless to dull pale green actinolite and strongly pleochroic, pale yellow to red-brown biotite (about 5% and 1%, respectively). Both are secondary and, due to their generally unaltered nature and porphyroblastic growth within and across smectite and chlorite domains, have most probably formed later than the main, clay-rich alteration. In only a single recorded case do actinolite fibers replace a fresh, clinopyroxene crystal as a uralitic fringe. Lower down in the core, the proportion of actinolite rapidly drops, although the content of biotite, often seen as flakes, now independent of the actinolite, is maintained (2%–3%). Biotite may also nucleate on magnetite or grow within the interspaces of skeletal magnetite crystals. Occasionally it may be partly replaced by a bright, blue-green pleochroic "clay" which is tentatively identified as either smectite-chlorite or, more likely, celadonite.

Table 7. Approximate proportions (visual estimate) of primary and secondary phases in dolerites at the base of Hole 800A.

| Core, section, interval (cm) | 129-800A-57R-1, 20–22 | 129-800A-57R-2, 89–91 | 129-800A-58R-1, 46–47 | 129-800A-59R-1, 3–4 | 129-800A-60R-1, 43–44 | 129-800A-60R-1, 71–74 |
|---|---|---|---|---|---|---|
| Piece | 1 | 1E | 2A | 1A | 1B | 2 |
| *Primary minerals (%)* | | | | | | |
| Plagioclase | 40 | 40 | 55 | 50 | 45 | 40 |
| Clinopyroxene | 0 | 0 | 10 | 10 | 5 | 5 |
| Magnetite | 0 | 2 | 2 | 2 | 1 | 2 |
| Apatite | 0 | tr | 0 | 0 | tr | tr |
| Spinel | 0 | 0 | 0 | 0 | tr | 0 |
| Mesostasis | 0 | 0 | pr | pr | 0 | 0 |
| *Secondary minerals (%)* | | | | | | |
| Smectitic clays | 42 | 10 | 10 | 20 | 38 | 40 |
| Celadonite(?) | 0 | 0 | 1 | 5 | 3 | 4 |
| Carbonate | 3 | 5 | 0 | 5 | tr | tr |
| Sericite | 0 | 20 | 0 | 0 | 0 | 0 |
| Zeolite | 0 | 1 | 2 | 1 | 2 | 1 |
| Chlorite | tr | 18 | 11 | tr | 2 | 2 |
| Hematite | 9 | 0 | 0 | 0 | 0 | 1 |
| Pyrite | 2 | 3 | 3 | 4 | 2 | 2 |
| Actinolite | 0 | tr | 5 | 1 | tr | tr |
| Biotite | 4 | 1 | 1 | 2 | 2 | 3 |

Note: tr = trace constituent; pr = present.

In conclusion, the dolerites exhibit four alteration stages:

1. Initial development of smectitic clays, chlorite, sericite, and possibly zeolite. This mineral assemblage is typical of low-grade submarine alteration in the zeolite facies.
2. Oxidation probably followed stage 1 as clays are often iron stained. Also, carbonate appeared at a later stage relative to the clays, although it may span the oxidation phase as calcite and unaltered pyrite are seen as veinlets cutting all units.
3. Development of secondary actinolite and biotite. This implies a higher grade of alteration than stage 1, within the lower part of the greenschist facies.
4. Celadonite(?) alteration of biotite indicates relatively low grades of alteration again after stage 3.

A tentative explanation for the lower greenschist facies event, which is mainly recorded at the top of Unit 3, is the thermal effect of a subsequent intrusive sill, such as now represented by Unit 2.

### Fractures and Veins

Thin (~1 mm wide), horizontal, and oblique (40° dip) veinlets occur spasmodically throughout the dolerites and are commonly filled with calcite (with or without pyrite) and rarer, dark green, saponitic(?) clay. Pyrite and calcite are also relatively common in the dolerite matrix. Alteration haloes or zones associated with the veinlets are not present.

### Geochemistry

No geochemical analysis for major oxides or trace elements was achieved at Hole 800A. As part of the inorganic geochemistry program on the sediments, the dolerites were analyzed for carbon and sulfur (Table 8) and show high $CaCO_3$ values that correspond to concentrations of secondary calcite within the core.

### Summary of Main Features

1. The only igneous rock lithology encountered in Hole 800A was a massive, aphyric, largely holocrystalline, slightly miarolitic alkali dolerite that was characterized by the presence of macroscopic, elongate, black pyroxene crystals.
2. Three dolerite units are recognized on the basis of textural variation and the presence of a sedimentary interlayer between Units 2 and 3.
3. The dolerites are moderately to highly altered, with the presence of ubiquitous green and brown smectitic clays, hydrated iron oxides, calcite, and pyrite, and lesser amounts of chlorite, sericite, and possibly celadonite. Apart from the above low-grade alteration assemblages, the presence of later secondary actinolite and biotite indicates a low greenschist facies event possibly caused by the emplacement of a subsequent, adjacent sill.

## DOWNHOLE MEASUREMENTS

### Operations

On 3 December 1989, after reaching a total depth (TD) of 544.5 mbsf, pipe was drawn up to 312 mbsf during a short wiper trip. The pipe was unable to penetrate below 335 mbsf on the run back to TD and at this point it was decided to prepare what was left of the hole for logging. The bit was dropped (with great difficulty) at 335 mbsf and the hole was filled with mud at an effective concentration of 2.5% KCl above that of seawater. The last circulation into Hole 800A was at 1845 hr UTC on 3 December. Logging operations began at Site 800 at 2025 hr on 3 December 1989 and were completed at 0015 hr on 5 December, corresponding to a total logging time of 28 hr (Table 9). The pipe was pulled to 70 mbsf for the beginning of each logging run and raised to approximately 50 mbsf while logging up hole.

The quad combination tool string (see "Downhole Measurements" section, "Explanatory Notes" chapter) included, from top to bottom, telemetry, long-spaced sonic, lithodensity, natural gamma-ray spectrometry, and dual induction resistivity tools, in addition to the Lamont temperature logging tool (TLT). These tools were rigged at 2145 hr on 3 December, creating a tool string 30.72 m long. At 0100 hr, this string was run down to 28 m above the mud line and held stationary for 3 min to obtain a bottom-water calibration point for the TLT. The depth to the end of pipe as recorded on this logging run was within .6 m of that calculated by the driller. As logging continued downhole it was reported that the wireline heave compensator (WHC) was not operating. The WHC was reportedly repaired in Singapore during dry dock prior to Leg 129 but was untested under full tensional load until the first logging run at Site 800. Down-going logging data were only acquired to 142 mbsf due to a hard disk failure in the recording

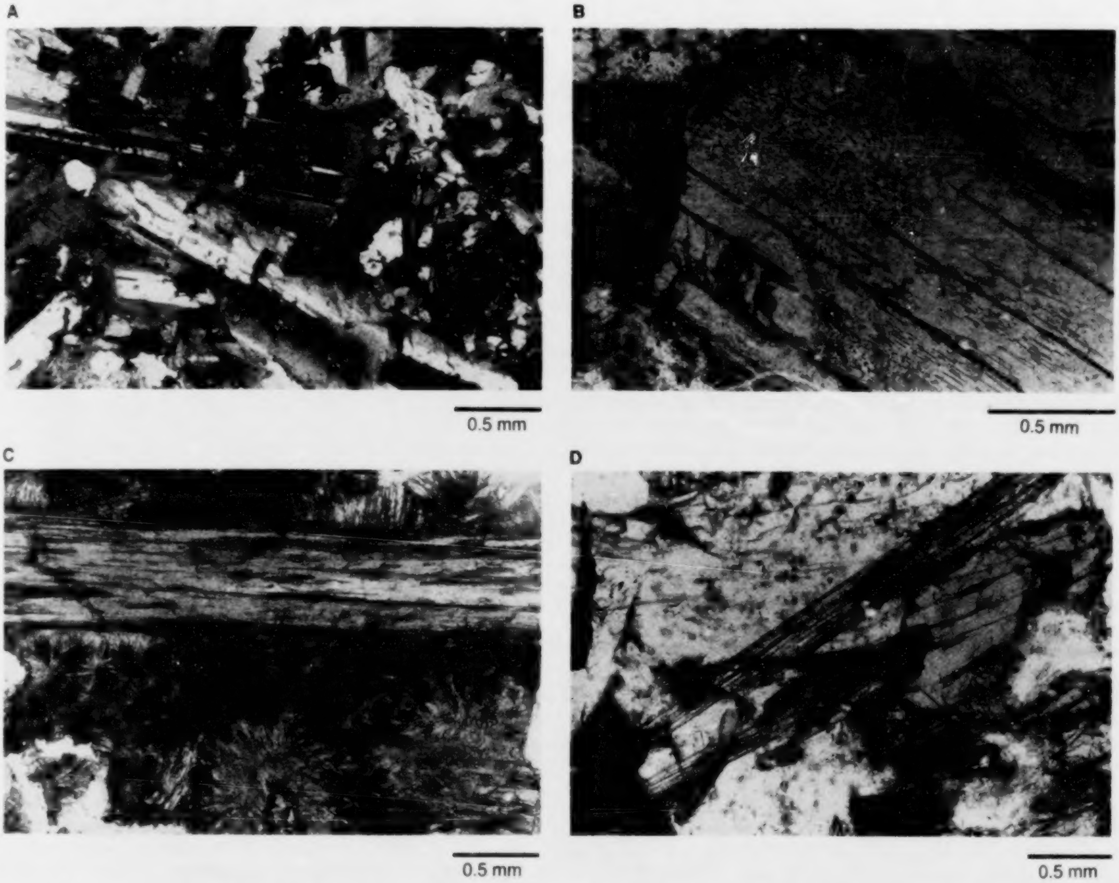

Figure 34. Photomicrographs illustrating some characteristic petrographic dolerites from Hole 800A. Scale bar = 0.5 mm. **A.** Zoned, twinned plagioclase laths with altered cores. Sample 129-800A-59R-1, 3–4 cm (crossed polars). **B.** Cloud of minute glass inclusions within clinopyroxene crystal. Sample 129-800A-60R-1, 43–44 cm (plane polarized light). **C.** Large, unaltered actinolite prism growing across groups of radiate smectite fibers. Sample 129-800A-58R-1, 46–47 cm (plane polarized light). **D.** Acicular zeolite fibers. Sample 129-800A-60R-1, 71–74 cm (plane polarized light).

unit. The tool string continued downhole until a bridge was encountered at 313.1 mbsf. Logging data were recorded successfully on a backup system as the tool string moved uphole at 300 m/hr from 312.3 to 50.6 mbsf (Fig. 35) with a repeat section taken from 312.3 to 222.2 mbsf. The bottom of pipe was encountered at approximately 50 mbsf and another bottom-water temperature calibration point for the TLT was obtained inside the pipe at 28 m above the mud line. The quad combination string was returned to the rig floor at 0600 hr on 4 December. The TLT was then taken from the rig floor to the downhole measurements lab, opened, and hard-wired to the Masscomp computer to download the recorded temperature/time measurements. The second of two TLT's was taken down to the rig floor and attached to the end of the geochemical combination tool string.

The geochemical tool string (see "Downhole Measurements" section, "Explanatory Notes" chapter, this volume), which included telemetry, natural gamma-ray spectrometry, aluminum clay, induced gamma-ray spectrometry, and Lamont temperature tools, was rigged at 0845 hr on 4 December creating a tool string 18.13 m long. This tool combination was lowered down the pipe and held stationary for 3 min at 28 m above the mud line to obtain a bottom-water calibration point for the TLT. The tool string encountered the bridge at 313.1 mbsf and logging data were recorded from 313.1 mbsf up into pipe at 43.12 mbsf as the tool string moved uphole at 200 m/hr (Fig. 36). A repeat logging run beginning at 244.2 mbsf was attempted but the neutron generator portion of the gamma-ray spectrometry tool failed. Another bottom-water temperature calibration point for the TLT was obtained inside the pipe at 28 m above the mud line and the geochemical logging run was completed at 1552 hr on 4 December.

The final tool combination run at Site 800 was the formation microscanner (FMS) (see "Downhole Measurements" section, "Explanatory Notes" chapter), which included telemetry, natural gamma-ray spectrometry, and the FMS tools (but no TLT). This tool string was rigged and in the hole at 1700 hr on 4 December. FMS data were recorded uphole at 260 m/hr from 312.3 to 50.6 mbsf with no problems. The final logging run ended at 0015 hr on 5 December with all tools off

Table 8. Carbon and sulfur analyses for dolerites at the base of Hole 800A.

| Core, section, interval (cm) | Depth (mbsf) | $CaCO_3$ (wt%) | $C_{org}$ (wt%) | S (wt%) | Comment |
|---|---|---|---|---|---|
| 129-800A- | | | | | |
| 57R-1, 17–24 | 498.17 | 3.0 | 0.00 | 0.02 | Oxidized zone |
| 57R-2, 86–91 | 499.36 | 3.2 | 0.02 | 0.20 | Calcite-pyrite vein |
| 58R-1, 47–51 | 507.67 | 0.4 | 0.00 | 0.04 | Miarolitic |
| 58R-2, 32–37 | 508.85 | 1.6 | 0.00 | 0.10 | Calcite replacement |
| 58R-2, 106–110 | 509.59 | 0.2 | 0.00 | 0.04 | |
| 59R-1, 4–9 | 516.64 | 1.1 | 0.00 | 0.06 | |
| 60R-1, 44–46 | 526.34 | 0.2 | 0.00 | 0.10 | Miarolitic |
| 60R-1, 69–74 | 526.59 | 0.2 | 0.00 | 0.00 | |

Table 9. Actual time schedule (UTC) for logging operations at Hole 800A, including a listing of the tools used during each logging run.

| Tool string | Time | Procedure |
|---|---|---|
| Quad combination (TCCB—LSS—HLDT—NGT—DIL—TLT) | RIH, 2145 hr UTC 3 December 1989<br>POOH, 0600 hr UTC, 4 December 1989 | Log down to 13 mbsf. Run down to 312.3 mbsf (312.3 mbsf), log up to 50.6 mbsf. Run down to 312.3 mbsf, log up to 222.2 mbsf. |
| Geochemical combination (TCCB—NGT—ACT—GST—TLT) | RIH, 0845 hr UTC<br>POOH, 15.52 hr UTC | Run down to 313.1, log up to 43.12 mbsf. |
| Formation microscanner (FMS—TCCB—NGT) | RIH, 1700 hr UTC<br>POOH, 0015 hr UTC, 5 December 1989 | Run down to 312.3 mbsf, log up to 50.6 mbsf. |

Note: Total logging time = 28 hr (includes rig-up and final rig-down of tool strings). Abbreviations are as follows: TCCB = telemetry tool; LSS = long-spaced sonic tool; FMS = formation microscanner; HLDT = lithodensity tool; TLT = Lamont temperature tool; DIL = dual induction tool; ACT = aluminium clay tool; GST = induced gamma-ray spectrometry tool; NGT = natural gamma-ray spectrometry tool; RIH = Run in to hole; POOH = Pull out of hole.

of the wireline and secured on deck. Logging depths recorded during the quad combination run were shifted to match drill-string depths (and thus coring depths). Subsequent logging runs were shifted relative to the quad combination using the natural gamma-ray log. The geochemical combination log was shifted upwards by 3 m and the FMS log was not shifted.

Summary log figures appear at the end of this chapter. The FMS images are presented on microfiche in the back of this volume.

### Log Quality

The logs are generally of good quality (Figs. 35, 36, 37, and "Summary Log" following this chapter). The raw sonic data, however, required significant shipboard processing and editing to create a useful sonic log (Figs. 35 and 38). The data recorded from the induced gamma-ray spectrometry tool require post-cruise processing; references made to silicon, calcium, and iron are therefore only broadly qualitative. In contrast, the natural gamma-ray spectrometry tool produces reliable values for the concentration of potassium, thorium, and uranium and the aluminum clay log is generally little improved through post-cruise processing. The quad combination and geochemical logs are not obviously affected by ship's heave. The small degree of elasticity within the wireline summed over its extreme length (6000 m) may have acted to slightly decouple these logging tools from the heave of the ship. The ship's heave did adversely affect the raw FMS records, but these data would require significant shore-based image-processing to achieve an interpretable record even without these adverse effects.

### Logging Units

Five logging units were identified in Hole 800A (Figs. 35 to 37) based on log response and analyses of recovered cores, but are not to be confused with the lithologic units defined earlier (see "Lithostratigraphy and Sedimentology" section, this chapter). The boundaries between adjacent logging units were placed at significant inflection points resulting from simultaneous variations on at least several of the logs illustrated in Figures 35 and 36. These units display consistent log responses or distinct overall trends.

Core recovery was poor throughout most of the logging interval (less than 10%) and only fragments of the most indurated portions of the formation were actually recovered. The lithologies for unrecovered intervals have been inferred from the logs based on the broad assumption that the logging tools respond to varying proportions of the primary constituents in samples actually recovered (e.g., biogenic silica, carbonate, pelagic clay, and volcanogenic clay) and to their relative porosity.

#### *Logging Unit 1 (50.6–78 mbsf)*

Logging Unit 1 is distinguished by covarying resistivity and total gamma-ray responses. This unit contains both the highest resistivity values (6–9 ohm-m) obtained in Hole 800A as well as extended high values of total gamma-ray (80 API), which are apparently due to a high uranium concentration (4.4–4.7 ppm). High values of uranium/thorium are often associated with increases in organic material (Fertl, 1979). The highest uranium/thorium ratios occur between 50.6 and 68 mbsf. Indeed, samples from Sections 129-800A-7R-CC and 129-800A-9R-CC (49.2–58.9 mbsf and 68.5–78.2 mbsf) contained abundant organic material (see "Lithostratigraphy and Sedimentology" section, this chapter). Logging Unit 1 is also characterized by high silicon and low calcium contents. The lower boundary of logging Unit 1 at 72–78 mbsf is marked by abrupt, simultaneous, local minima in velocity (1.9 km/s), resistivity (1 ohm-m), density (1.75 g/cm$^3$), uranium/thorium, and silicon, along with local maxima in total gamma-ray (79 API), aluminum (.35 wet wt%), and iron. These variations are juxtaposed against local minima/maxima in the opposite sense for all logs including a jump to higher calcium values from 78 to 81 mbsf. The inflection point for this sinusoidal variation in logs occurs at 78 mbsf and is chosen as the base of logging Unit 1. The high resistivity values, reflecting low porosity, together with the high relative silicon values, suggest that the chert and porcellanite recovered in this section accurately reflect the most indurated portion of this formation. The high total gamma-ray count and the high uranium/thorium ratio suggest that this formation may include a less indurated clay matrix containing an elevated concentration of organic matter. The logging response at the lower boundary of logging Unit 1 argues strongly for a volcanic clay-rich, chert-poor layer at approximately 75 mbsf, immediately overlying a more indurated, less porous layer containing silica and relatively more carbonate beginning at approximately 78 mbsf. The logging data correlate well with lithofacies unit II ("Lithostratigraphy and Sedimentology" section, this chapter) with the base of logging Unit 1 and lithofacies Unit II coinciding exactly.

#### *Logging Unit 2a (78–142 mbsf)*

Logging Unit 2a is characterized by relatively low sonic velocities (1.7–2.2 km/s), low resistivities (1–2 ohm-m), initially high total gamma-ray (55–70 API) decreasing to 25 API from 107 to 127 mbsf, and a relatively high calcium/silicon ratio that increases with depth and reaches a maximum in logging Unit 2b.

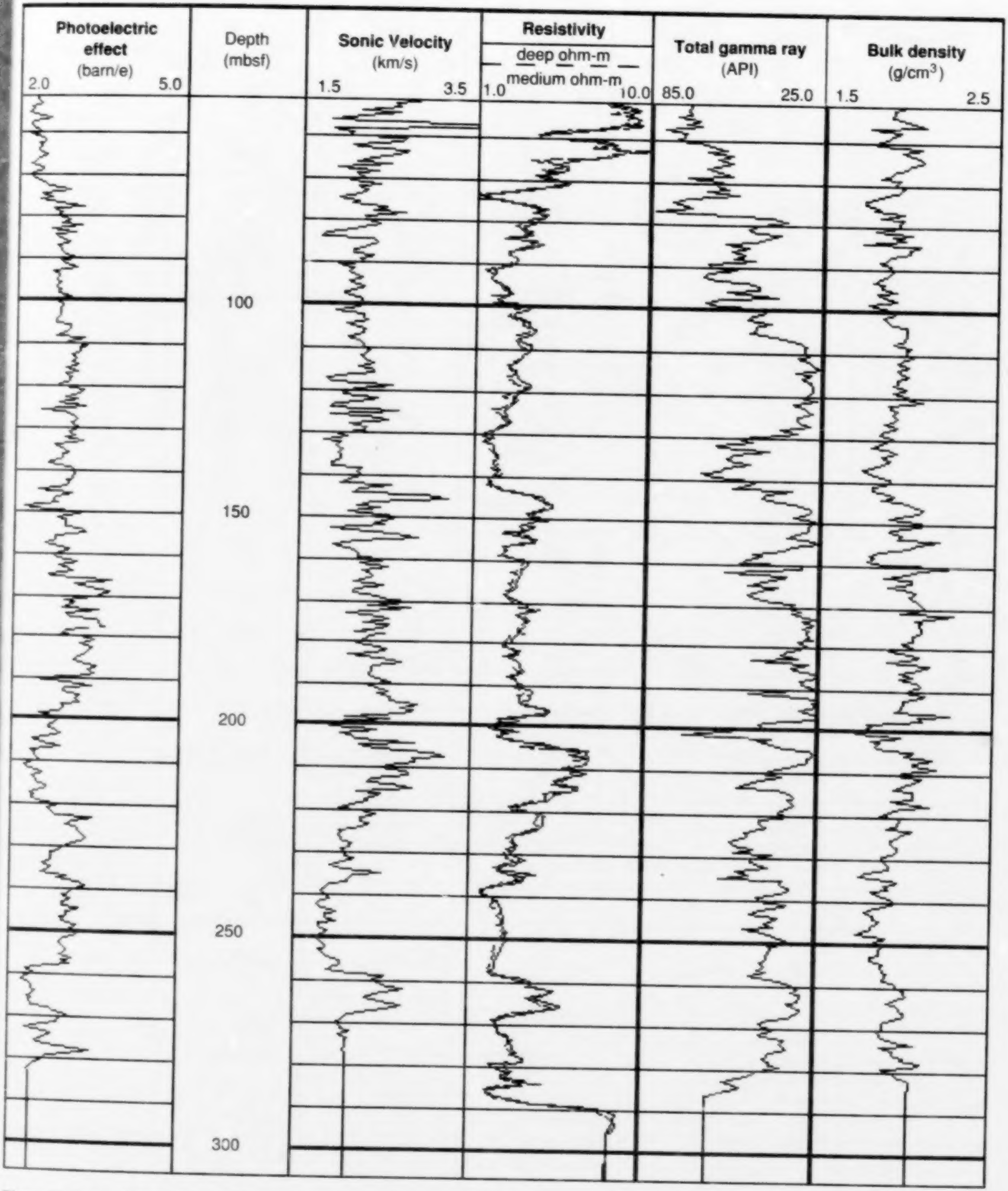

Figure 35. Selected downhole logs from the quad combination tool string for the interval 50.6 to 306.2 mbsf in Hole 800A: photoelectric effect, sonic velocity, resistivity, total gamma ray, and bulk density. Sonic velocity, resistivity, and density reflect the porosity of the formation and, therefore, the degree of lithification or cementation (e.g., chert vs. radiolarite).

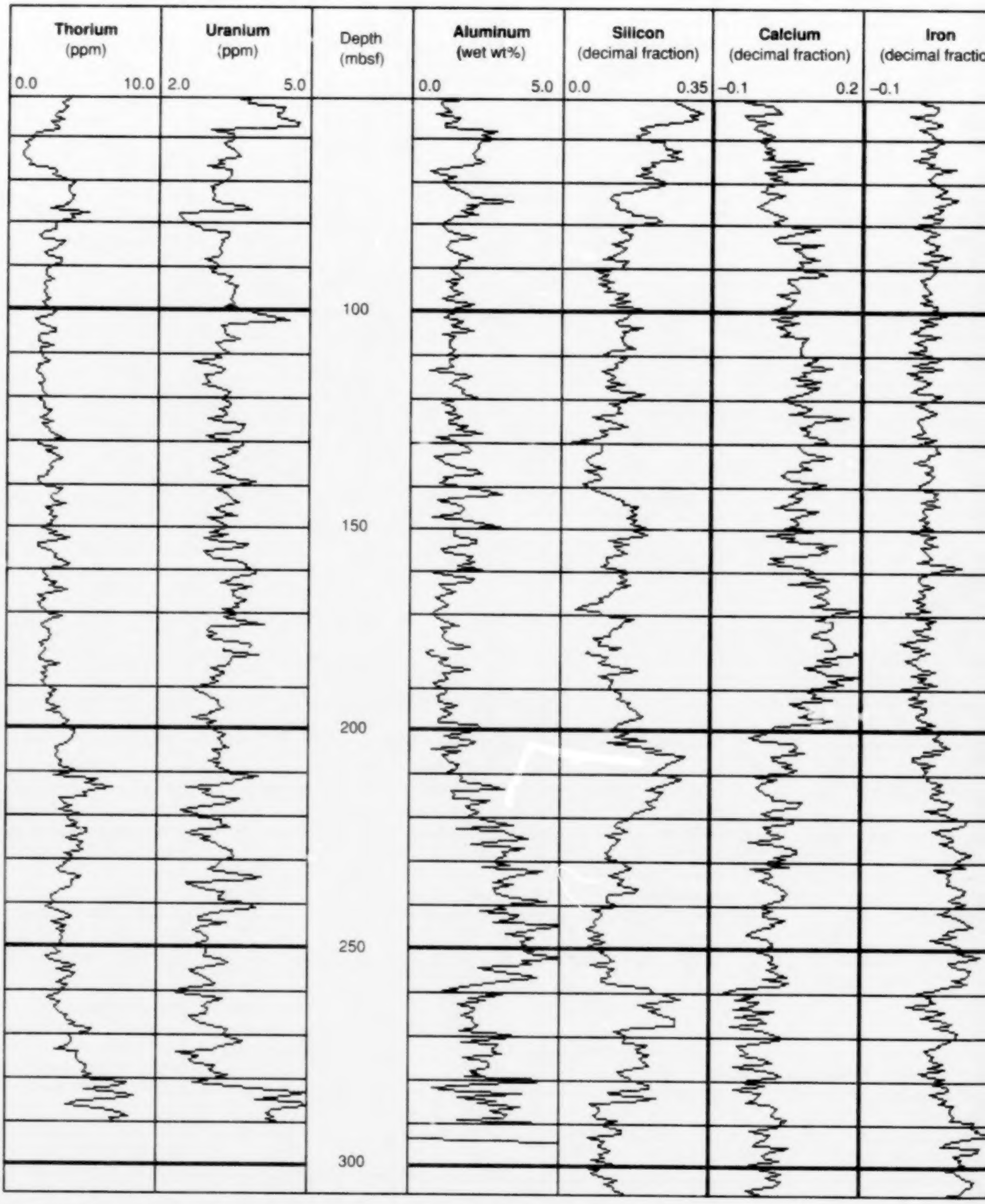

Figure 36. Selected downhole logs from the geochemical combination tool string for the interval from 50.6 to 306.2 mbsf in Hole 800A: thori uranium, aluminum, silicon, calcium, and iron. The relative abundances of these elements serve to identify the primary constituents distinguish the major lithologies recovered at Hole 800A (e.g., biogenic silica and carbonate, pelagic clay, and volcanogenic material, inclu clay).

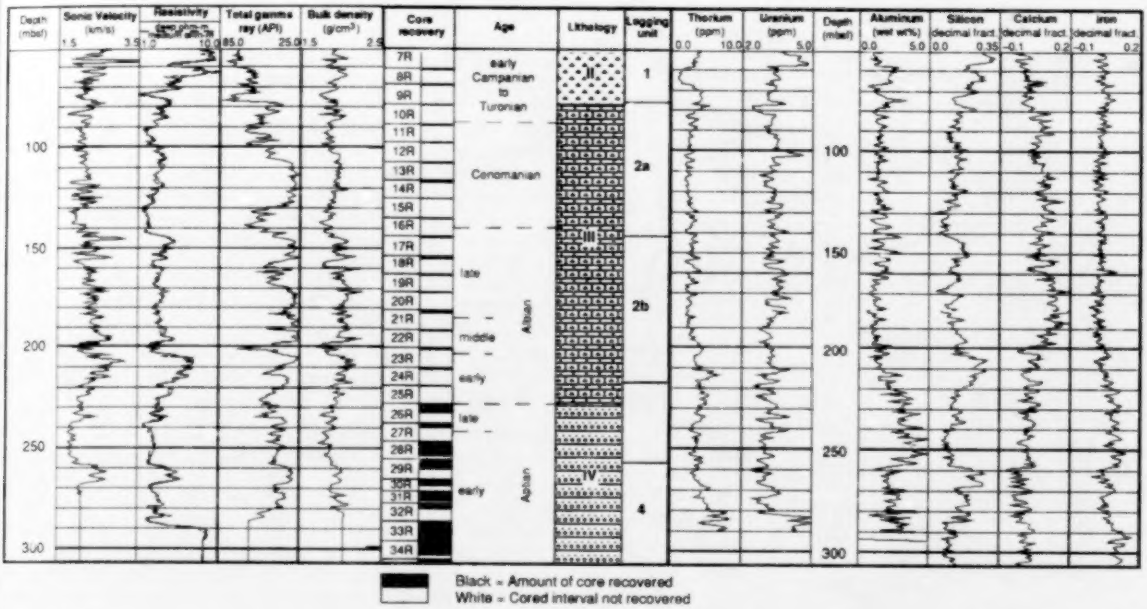

Figure 37. Summary compilation of downhole logs, intervals of core recovery, lithology, and downhole logging units at Hole 800A. Lithologic units are based on coring results (see "Lithostratigraphy and Sedimentology" section, this chapter).

This type of logging response corresponds well with the lithologies and trends observed for lithofacies Unit III ("Lithostratigraphy and Sedimentology" section, this chapter), but the average formation velocity as well as the low resistivity and high total gamma-ray emphasize that less indurated, higher porosity, clay-rich intervals must make up the unrecovered majority of this section. The lower boundary of logging Unit 2a is again an inflection point created by a sinusoidal variation observed on several logs. The boundary is marked by local minima in velocity (1.9 km/s), resistivity (.5 ohm-m), density (1.75 g/cm³) and silicon with a relative maximum in total gamma-ray (67 API) juxtaposed against maxima/minima for all these logs, including the introduction of a local maximum in calcium. This logging boundary occurs from 131 to 151 mbsf and may be interpreted as a change from a clay-rich chalk to a massive, silicified limestone bed at approximately 142 mbsf.

### *Logging Unit 2b (142–219 mbsf)*

Logging Unit 2b is characterized by high velocities (2.1–3.1 km/s), resistivities (1.5–3.0 ohm-m), and densities (1.9–2.3 g/cm³), and low gamma-ray (25 API). This logging unit is also distinguished by the highest calcium/silicon ratios obtained within the entire logged interval.

The logging response observed in Unit 2b indicates an overall decrease in clay content and increase in carbonate content compared to the overlying unit, with restricted zones that are clay-rich and carbonate-poor (e.g., at 157 mbsf). These results correspond well with the lithologic trends observed in the cores (lithologic Unit III). The lower boundary of logging Unit 2b is distinguished by another sinusoidal variation observed on all logs from 198 to 219 mbsf. The boundary is marked by local minima in velocity (1.7 km/s), resistivity (.5 ohm-m), density (1.7 g/cm³), silicon, and calcium, and local maxima in total gamma-ray (73 API), iron, and aluminum immediately juxtaposed against maxima/minima in these logs, including an overall shift to lower calcium and higher silicon values. This logging response is probably due to a clay-rich interval of volcanic origin (high aluminum and iron, low silicon) overlying an interval with low clay content dominated by chert rather than silicified limestone. The bottom portion of this logging unit from 198 to 219 mbsf corresponds to the transitional zone at the base of lithofacies Unit III ("Lithostratigraphy and Sedimentology" section, this chapter), where volcanogenic clays are interbedded with chert.

### *Logging Unit 3 (219–258 mbsf)*

Logging Unit 3 is characterized by simultaneous trends of increasing aluminum and iron content and decreasing silicon content with depth along with an overall shift towards low calcium. This interval is also marked by decreasing velocity (2.2 to 1.7 km/s) and resistivity (5 to .5 ohm-m) with variable total gamma-ray counts.

Logging Unit 3 corresponds to lithologic Unit IV and illustrates the transition from nonvolcanogenic lithologies to a sequence dominated by volcanogenic material. The lower boundary of logging Unit 3 is marked by a sharp increase in velocity (1.9 to 2.7 km/s), resistivity (.5 to 3.5 ohm-m), and silicon content along with a sharp decrease in aluminum, iron, and total gamma-ray count. The lowest values of calcium observed in Hole 800A also begin at this level (near 258 mbsf). An interval dominated by chert or a silica-rich sand with a virtual absence of volcanogenic clays is inferred from the logging response that defines the base of Unit 3.

### *Logging Unit 4 (258–312 mbsf)*

Logging Unit 4 begins at 258 mbsf and terminates at the TD for logging operations at Site 800. This unit is characterized by the lowest calcium values observed in Hole 800A, variable but elevated aluminum and iron content, and a trend toward a lower silicon content with depth. Logging Unit 4 also corre-

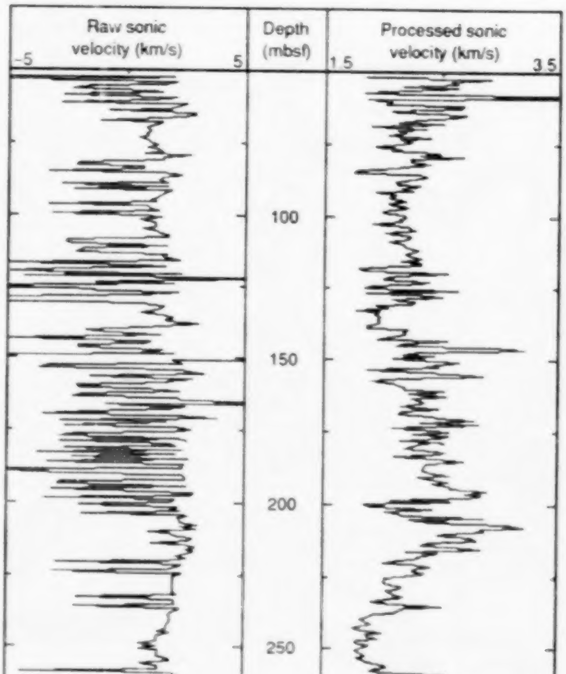

Figure 38. Comparison of observed "raw" and processed velocity logs for Hole 800A. The velocity spike (processed log) at 58 mbsf is an artifact. Covariation of the processed sonic log with resistivity, gamma ray, and bulk density logs (Fig. 35) indicates that a useful velocity log was produced.

sponds to lithofacies Unit IV and is interpreted as a zone dominated by volcanogenic material grading upward into a zone containing greater amounts of biogenic silica. A rapid change from high silicon to low silicon content is matched by the disappearance of radiolarians below approximately 285 mbsf (see "Biostratigraphy" section, this chapter).

## Synthetic Seismogram

A synthetic seismogram was computed for Site 800 to accurately tie the drilled sequence in the hole to seismic reflection data over the site (Fig. 39). The seismogram covers the interval from 50.6 to 306.2 mbsf, approximately 7.576 to 7.804 s two-way traveltime (twt).

The unprocessed sonic velocity log at Hole 800A (Fig. 38) is dominated by very high and/or low values corresponding to cycle skipping, especially in the uppermost 175 mbsf. The sonic log-processing software aboard the *JOIDES Resolution* allowed us to set a window of possible velocity values and then recalculate a new log using only the traveltime data that result in velocities within the chosen window. We chose a minimum-maximum window of 1.69 to 5.1 km/s. The processed sonic log (Fig. 38) was used in combination with the raw-bulk density log to calculate reflection coefficients that were convolved with the source wavelet to produce a synthetic seismogram. The synthetic seismogram was shifted to the proper two-way traveltime on the seismic profile by matching the reflection created by the first chert encountered at this site. The synthetic seismogram (Fig. 39) is compared with the single-channel seismic (SCS) line shot on approach to Site 800. The major reflectors apparent on the synthetic seismogram are correlated with the seismic 10-trace mix and seismic reflection profile. Improved synthetic seismograms will be produced following shore-based processing, including incorporation of physical properties data, repicking of traveltimes and the use of improved source wavelets.

A few general interpretations of the rocks comprising a portion of the sedimentary section at Site 800 have been made by extrapolating the downhole logging results onto the seismic profile. A further description of the correlation between seismic stratigraphy and lithostratigraphy is given in the "Site Geophysics and Seismic Stratigraphy" section, this chapter (see Fig. 40).

### *Seismic Intervals*

1. 7.512 to 7.572 s twt: This uppermost zone corresponds to lithofacies Unit I. The seismically transparent nature indicates a relatively homogenous interval with no significant impedance contrasts. The first reflector on the SCS profile is due to the impedance contrast at the sediment/water interface and is followed 24 ms later by another high-amplitude event that is part of the source wavelet and does not represent a separate impedance contrast. The thickness of this unit is most accurately determined with the 3.5-kHz profiler at 60 ms (see Fig. 41, "Site Geophysics and Seismic Stratigraphy" section, this chapter).

2. Logging Unit 1, 7.572 to 7.608 s twt (average velocity = 2.2 km/s): The sharp velocity/porosity contrasts of chert and interbedded, clay-rich zones of lithofacies Unit II create the two moderate-amplitude, flat-lying reflectors that bound lithofacies Unit II.

3. Logging Unit 2a, 7.608 to 7.664 s twt (average velocity = 2.29 km/s): This interval contains discontinuous, moderate-amplitude reflections and more continuous, high-amplitude events, both of which are the result of velocity-density contrasts between clay-rich zones and silicified limestone/chert-dominated intervals of lithofacies Unit III. A single, very high amplitude reflector observed on the synthetic seismogram at approximately 7.66 s twt is produced by a high-velocity/low-porosity interval at 142 mbsf, which is interpreted to be a zone of silicified limestone (see logging Units 2a to 2b). This reflector corresponds to a very low amplitude event on the 10-trace mix; however, the seismic reflection profile shows that this event varies dramatically in amplitude across Site 800, perhaps indicating lateral variation in silicification within this carbonate/clay sequence.

4. Logging Unit 2b, 7.664 to 7.716 s twt (average velocity = 2.96 km/s): This interval contains slightly higher amplitude and more continuous flat-lying reflections. The high carbonate, low clay content inferred for the unrecovered section of this interval from both logs and cores apparently creates a low-porosity matrix that results in the high-interval velocity.

5. Logging Units 3 and 4, 7.716 to 7.804 s twt (average velocity = 2.00 km/s): This interval is characterized by the highest amplitude and most continuous reflections observed within the logged interval. This sequence of flat-lying reflections corresponds to the volcanogenic turbidites of the upper portion of lithofacies Unit IV ("Lithostratigraphy and Sedimentology" section, this chapter). This section is dominated by volcanogenic silt and clay (low silicon/aluminum ratio), resulting in a low-interval velocity of 1.77 km/s interspersed with intervals of elevated silica (e.g., the boundary of logging Units 3 and 4).

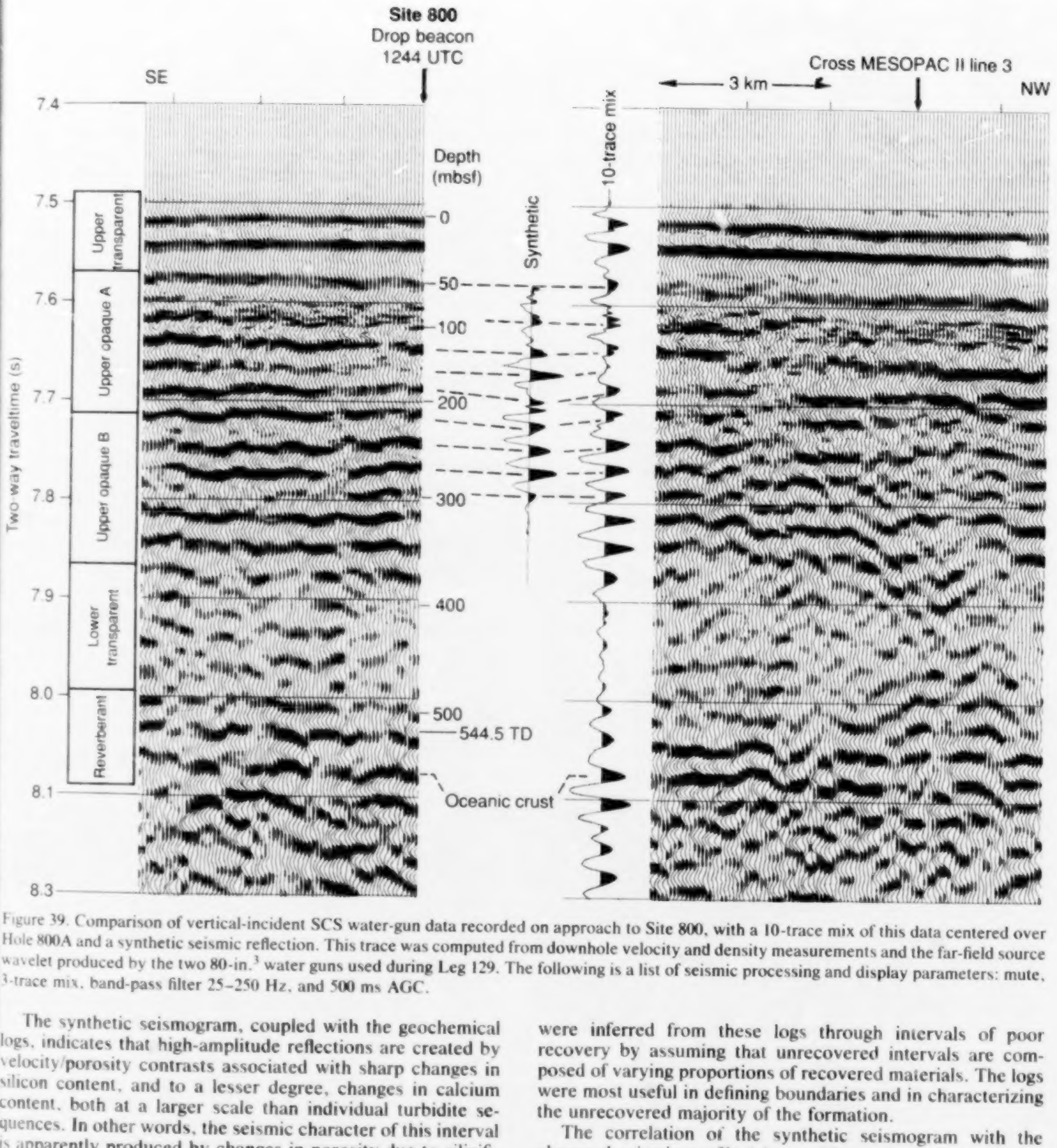

Figure 39. Comparison of vertical-incident SCS water-gun data recorded on approach to Site 800, with a 10-trace mix of this data centered over Hole 800A and a synthetic seismic reflection. This trace was computed from downhole velocity and density measurements and the far-field source wavelet produced by the two $80\text{-in.}^3$ water guns used during Leg 129. The following is a list of seismic processing and display parameters: mute, 3-trace mix, band-pass filter 25–250 Hz, and 500 ms AGC.

The synthetic seismogram, coupled with the geochemical logs, indicates that high-amplitude reflections are created by velocity/porosity contrasts associated with sharp changes in silicon content, and to a lesser degree, changes in calcium content, both at a larger scale than individual turbidite sequences. In other words, the seismic character of this interval is apparently produced by changes in porosity due to silicification along primary bedding structures observed within turbidites. This observation may explain the relatively transparent seismic character of the lowermost volcanic turbidite sequence, which is barren of both microfossils (the sources for excess silica and carbonate) and any dominant bedding structures ("Sedimentology and Lithostratigraphy" and "Biostratigraphy" sections, this chapter).

### Summary

A suite of eight different downhole logs were successfully recorded at Site 800, resulting in the identification of five distinct logging units. Compositional trends and boundaries were inferred from these logs through intervals of poor recovery by assuming that unrecovered intervals are composed of varying proportions of recovered materials. The logs were most useful in defining boundaries and in characterizing the unrecovered majority of the formation.

The correlation of the synthetic seismogram with the observed seismic profile (along with geochemical logs) indicates that diagenetic horizons along primary bedding structures rather than the primary structures themselves create the large impedance contrasts that control the character of the seismic image.

## SITE GEOPHYSICS AND SEISMIC STRATIGRAPHY

### Site Geophysics

Site selection for Leg 129 was based on the multichannel seismic (MCS) surveys described in the "Explanatory Notes" chapter (this volume). Underway geophysical data were collected as we approached all sites. These data provided the

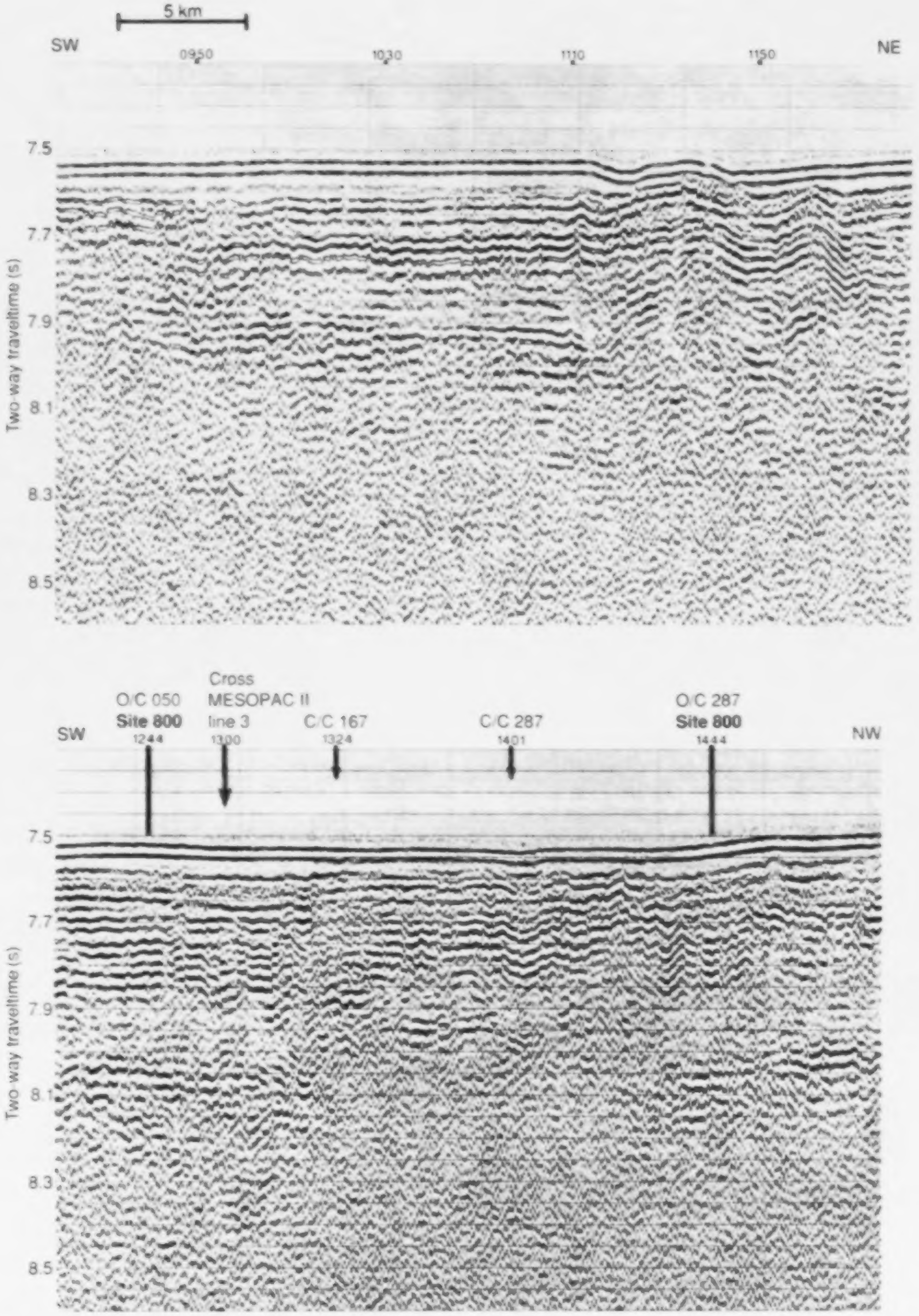

Figure 40. The entire SCS profile (two 80-in.$^3$ water guns) obtained on approach to Site 800 (1244 hr UTC, 25 November 1989) during Leg 129. This SCS profile crosses MESOPAC II line 3 (see Fig. 43) at 1300 hr, where proposed site PIG-1 was originally located. This SCS profile recrosses Site 800 at 1444 hr on a nearly orthogonal path. High velocity basement (sills) and total depth at Site 800 lie at 8.004 and 8.024 s twt, respectively. The SCS data were processed and displayed with the following parameters: water velocity F/k migration, mute, 2-trace mix, band-pass filter 30–100 Hz, and 500 ms AGC. Vertical exaggeration is approximately 22× at 1.5 km/s.

correlations with principal MCS sections needed in order to position the ship at preferred locations.

Site 800 (proposed site PIG-1) in the northern Pigafetta Basin is located near the intersection of lines 1 and 3 of an MCS survey obtained during the MESOPAC II expedition aboard *Le Suroit* in August-September 1989. Because Leg 129 began less than 3 months after the *Le Suroit* cruise, only single-channel records of both water-gun and air-gun data, as well as sonobuoy refraction data, obtained during MESOPAC II were used to locate proposed site PIG-1. The site was specifically located at 0740 hr UTC 21 August 1989 along an air-gun (two 1000-in.$^3$) portion of MESOPAC II profile 3, which includes the area sampled by sonobuoy 2m (see Fig. 4 and "Background and Objectives" section, this chapter). The only other seismic data in the area are a few widely spaced, single-channel, air-gun analog profiles (e.g., C1205, V3312, V3214, and V3012).

SCS reflection and 3.5- and 12-kHz profiling were conducted during the approach of the *JOIDES Resolution* to Site 800 (see "Operations" section, this chapter, for detailed approach plan). The actual site is located on this SCS water-gun profile at 1244 hr UTC, 25 November 1989 (Fig. 40), approximately 3 km southwest of the intersection of Leg 129's SCS and MESOPAC II's line 3 (proposed site PIG-1 location).

The water-gun (two 80-in.$^3$) data collected by the *JOIDES Resolution* and the air-gun (two 1000 in.$^3$) data of MESOPAC II are corroborative and, together with 3.5-kHz data, provided the following seismic criteria for locating Site 800:

1. The relatively thick (60–65 ms), transparent layer over acoustic basement, imaged with an excellent 3.5-kHz record (Fig. 41), indicated that enough soft sediment was present over the first cherts to provide lateral support for the drill string during spud-in.
2. A high-amplitude reflection imaged at .50 to .55 s below seafloor (bsf) corresponds to the onset of velocities characteristic of oceanic crust as recorded on sonobuoy 2m (MESOPAC II), indicating that approximately 500 to 600 m of sediment overlie oceanic crust in this area.
3. This basement reflection shallows in areas surrounding the site and, therefore, this location offered a thicker, lower sediment section without putting basement out of reach of a single-bit hole.

### Seismic Stratigraphy

The acoustic stratigraphy of large portions of the western Pacific consists of four units originally defined by Ewing et al., (1968): (1) an upper transparent layer, (2) an upper opaque layer, (3) a lower transparent layer, and (4) acoustic basement. These seismic facies descriptions were made from observations of SCS analog air-gun profiles. Acoustic basement has been characterized by the presence of a prominent zone of flat-lying ("smooth"), high-amplitude, closely spaced reflections referred to as "horizon B" by Ewing et al. (1968), the "deep opaque layer" by Heezen, et al. (1973), and as the "reverberant layer" by Houtz et al. (1970) and Houtz and Ludwig (1979). It is now recognized that the reverberant nature of acoustic basement in such profiles is usually the result of a trailing bubble pulse oscillation reflecting from a single, high-impedance boundary (Shipley et al., 1983). This characteristic of the air-gun source is now routinely compensated for through the use of tuned air-gun arrays and deconvolution techniques. The use of water guns in these surveys provides a much more implosive and bubble pulse-free source signature that provides a high-resolution record with little processing effort (Hutchinson and Detrick, 1984).

Although modern acquisition and processing techniques have allowed a more detailed and quantitative assessment of the stratigraphic units originally proposed by Ewing et al. (1968) (especially acoustic basement), these units can still serve to describe the general seismic character of the Pigafetta Basin.

The lowermost sequence, known as the "reverberant layer," is composed of closely spaced, high-amplitude, continuous reflections that directly overlie a less continuous, more diffractive surface. This sequence extends over a 100-ms interval from 492 ms to approximately 600 ms bsf (8–8.1 s twt) (Figs. 40, 42, and 43). Immediately overlying this interval is the "lower transparent" layer, which is characterized by low-amplitude, widely spaced, discontinuous reflections that extend from 372 to 492 ms bsf (7.884–8.004 s twt). This interval appears to thin to under 100 ms in thickness within 6 km to either side of Site 800 along the intersecting SCS profiles recorded during the approach (see 1210 hr and 1315 hr, Fig. 40). The deepening of basement resulting in this locally thickened, lower transparent sequence is also observed on MESOPAC II line 3, locating this site in a somewhat elongate structural basin. The lower transparent layer is bounded on top by another distinct sequence of closely spaced, moderate- to high-amplitude reflections that are traceable for over 50 km. This interval extends from 60 to 372 ms bsf (7.572–7.884 s twt) and is identified as the "upper opaque" sequence. The upper opaque zone can be divided into two units: (A) 60 to 204 ms bsf and (B) 204 to 372 ms bsf. The lower sequence, from 204 to 372 ms bsf (upper opaque B), is composed of parallel, continuous, high-amplitude reflections. The upper opaque zone, from 204 up to 60 ms bsf (upper opaque A), displays somewhat more discontinuous, lower amplitude reflections with the uppermost reflectors in the sequence exhibiting localized pinch-outs, in addition to a possible truncation of reflectors marking an unconformity between the upper opaque and upper transparent sequences.

The "upper transparent zone" as envisioned by Ewing et al. (1968) is very much attenuated in the Pigafetta Basin and extends from 0 to approximately 60 ms bsf (7.512–7.572 s twt) at Site 800. This interval is best displayed on the 3.5-kHz record obtained during Leg 129 (Fig. 41) and during MESOPAC II, but is also apparent on SCS records. These four seismic facies are essentially identical on the SCS of both Leg 129 and MESOPAC II.

### Correlation between Seismic Stratigraphy and Lithology at Site 800

Figure 42 summarizes the seismic reflection record and correlates this record with lithologic and logging observations and measurements obtained at Site 800.

The lithofacies significance of the "reverberant layer" or "acoustic basement" had never been determined for the Pigafetta Basin before Leg 129. Houtz and Ludwig (1979) completed an extensive review of the areal extent, thickness, and velocity of this seismic facies and demonstrated that the reverberant layer in the Pacific can be produced by the impedance contrasts between sediments and volcanic sills or flows (e.g., DSDP Site 462 in the Nauru Basin), by volcanogenic turbidites (e.g., DSDP Site 585 in the East Mariana Basin) and, in some cases, the sediment oceanic crust in areas of particularly smooth crust. A firm understanding of seismic source and display characteristics is necessary to interpret a zone of closely spaced reflections as the result of multiple impedance contrasts (true layering) or simply a single, high-impedance boundary. The physical significance of the reverberant layer, and therefore its utility as a seismic-stratigraphic

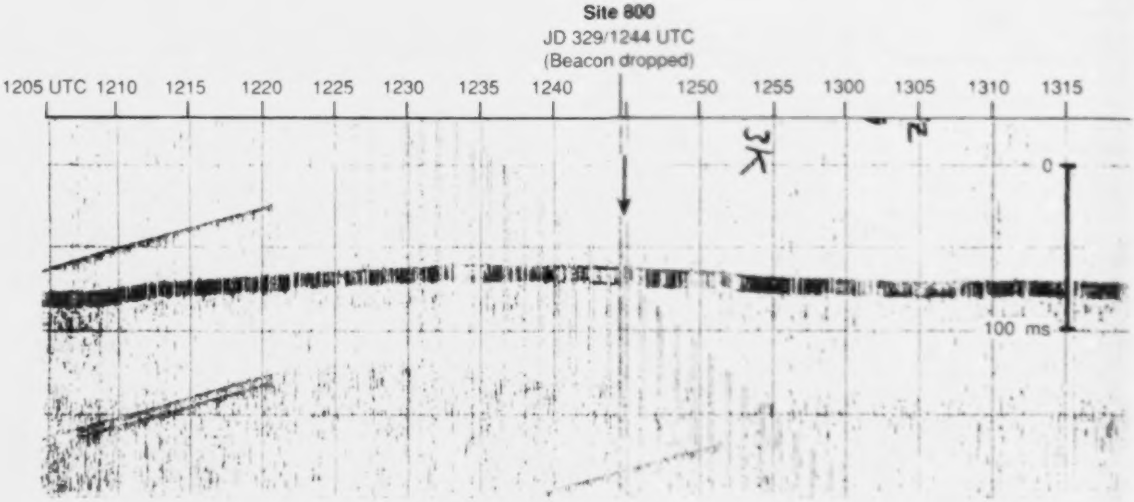

Figure 41. The 3.5-kHz record collected on approach to Site 800 (beacon drop) during Leg 129. Acoustic basement on this record marks the top of the first chert and indicates 0 to 65 ms of pelagic clay. This record displays a slightly thicker transparent layer than that observed on SCS profiles. The 60 ms reported for the thickness of the upper transparent seismic facies was measured from an enlarged 10-trace mix of the SCS record.

correlation unit, can now be better determined (Shipley et al., 1983).

The reverberant layer at Site 800 is created by a massive chert overlying a series of dolerite sills (see "Igneous Petrology" section, this chapter). The physical nature of these closely spaced reflections is primarily due to source characteristics and not on any real layering. This seismic facies is interpreted to result primarily from a single-impedance contrast between the radiolarite clays and the top of chert overlying dolerite sills at 498 mbsf. However, a second impedance contrast at 552 ms bsf (8.07–8.1 s twt) apparently creates a more diffractive reflection, which is interpreted as the top of oceanic crust. The top of the massive chert creates a very uniform, smooth reflecting surface and the high-velocity material directly overlying basement acts to reduce basement relief on time-section displays. This type of smooth, flat-lying, high-velocity horizon is characteristic of much of the Pigafetta Basin and the majority of the East Mariana Basin (Abrams et al., 1988). The deeper diffractive reflection marks the top of a rougher, less uniform surface interpreted as the top of oceanic crust. If this diffractive reflection does represent the top of oceanic crust, some lower velocity material must exist between it and the dolerite sills. An estimate of 133 m for the maximum thickness of sills over basement has been made by assuming the dolerite sills extend all the way to this reflection with a constant velocity of 4.46 km/s (see "Physical Properties" section, this chapter). Sonobuoy data correctly indicated that high velocities (4.8 km/s) begin at the clay/dolerite sill interface but were unable to resolve the differences in velocity and velocity gradients that could distinguish normal oceanic crust from oceanic crust with such a thin overburden of igneous material.

The lower transparent layer correlates with the thin (48.5 m) pelagic sequence of clay and radiolarite sand and the poorly bedded brecciated debris flows between 498 and 343 mbsf (see "Lithostratigraphy and Sedimentology" section, this chapter). This interval is also characterized by an absence of radiolarians and nannofossils. The discontinuous, widely spaced, low-amplitude reflections in this interval indicate that no large, laterally continuous impedance contrasts are present, and it is inferred that the lack of diagenetic or well-cemented horizons focused along well-developed bedding structures is responsible for the seismically transparent nature of this layer.

The transition from brecciated, poorly bedded debris flows to coarse-grained, bedded turbidites, along with the appearance of nannofossils at approximately 343 mbsf, correlates to a change from lower transparent to upper opaque seismic facies. The lowermost section of the opaque zone (upper opaque B), which is characterized by the highest amplitude, most continuous reflections, changes to lower amplitude, continuous to more discontinuous events upsection within the upper opaque A zone. The subtle change in seismic character that divides the upper opaque seismic facies is clearly correlated to the transition from redeposited volcanogenic material with intervals of high silicon content (about 219 to 300 mbsf) to a sequence of pelagic carbonate and silica-rich sediments (between 78 and 219 mbsf). The most discontinuous, diffuse reflections are associated with the clay/porcellanite/chert sequence between 38 and 78 mbsf.

The transparent nature of the uppermost 60 ms (upper transparent layer) indicates a relatively homogenous interval containing no significant impedance contrasts and is correlated to pelagic brown clay (0–38 mbsf).

The correlation of seismic facies with lithofacies is most strongly constrained within the interval logged at Site 800, which lies entirely within the upper opaque layer. It is apparent from correlations with the synthetic seismogram (Fig. 43) that high-amplitude reflections are associated with intervals of elevated silica content, high velocity, resistivity, and density, and low total gamma-ray count (see "Downhole Measurements" section, this chapter). The reflection events in this interval (50–307 mbsf) are interpreted to be caused by impedance contrasts created by diagenetic or well-cemented horizons interbedded with clay- and chalk-dominated intervals. Reflections are highest in amplitude and most contin-

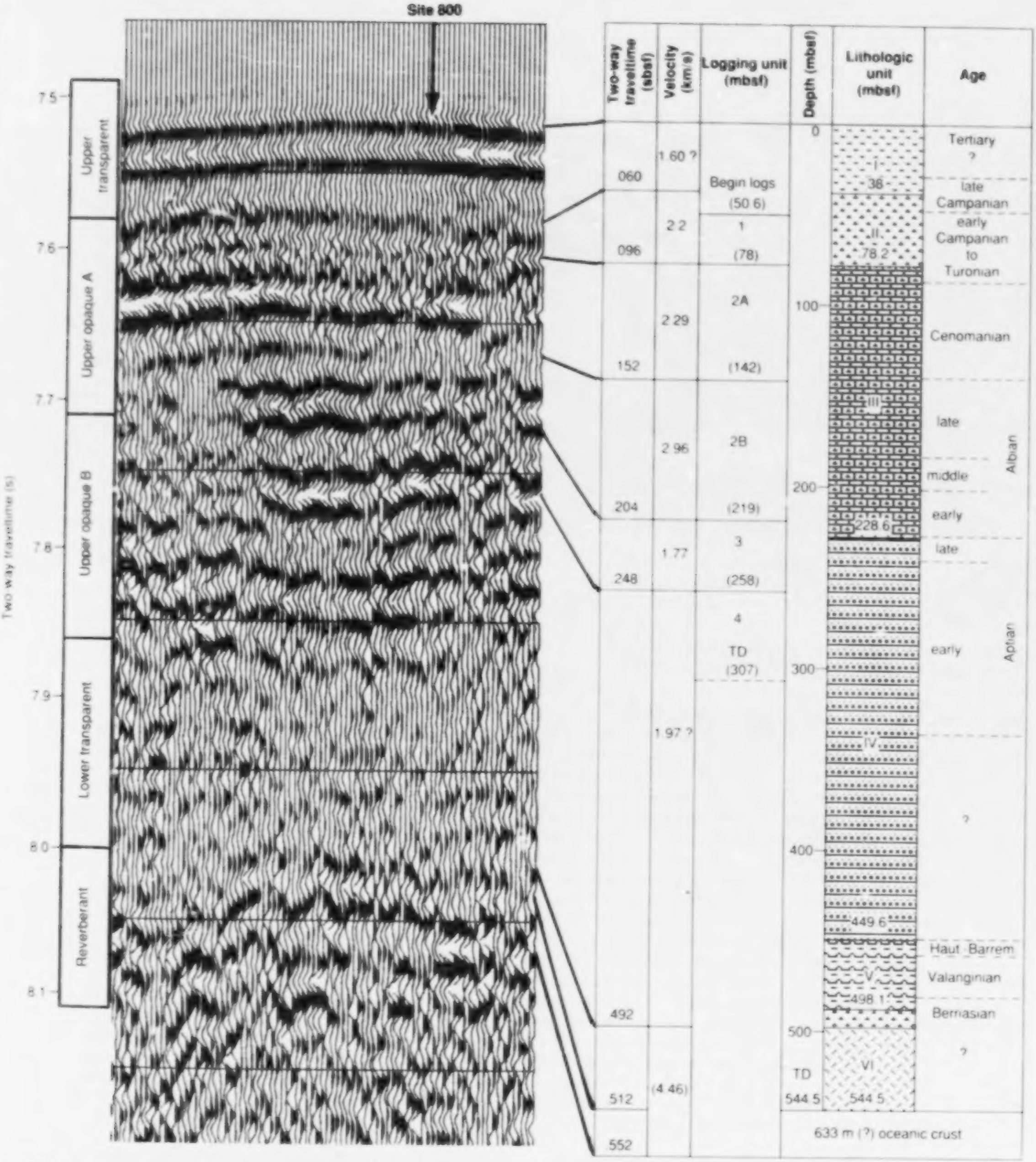

Figure 42. Summary of seismic stratigraphy at Site 800 showing correlations with logging units, ages, and depths. These correlations should only be considered as best estimates until further constraints are provided by improved synthetic seismograms (see Fig. 39). The velocity calculated for lithologic Unit I, assuming that the first sub-seafloor reflection at 60 ms bsf is the first chert at 38 mbsf, is 1.27 km/s. A more reasonable velocity of 1.6 km/s is assumed, resulting in a thickness of 48 m of pelagic clay (Unit I). The 10-m discrepancy in thickness derived from drill-string length vs. that predicted by the 3.5-kHz record is discussed in the "Operations" section, "Site 801" chapter. The 2.2-km/s velocity corresponds to the interval 38 to 78 mbsf. The 4.46-km/s velocity given for the dolerite sills is an average from physical properties measurements. This SCS water-gun record is displayed with a vertical exaggeration of 33× at 1.5 km/s with the same parameters described in Figure 40.

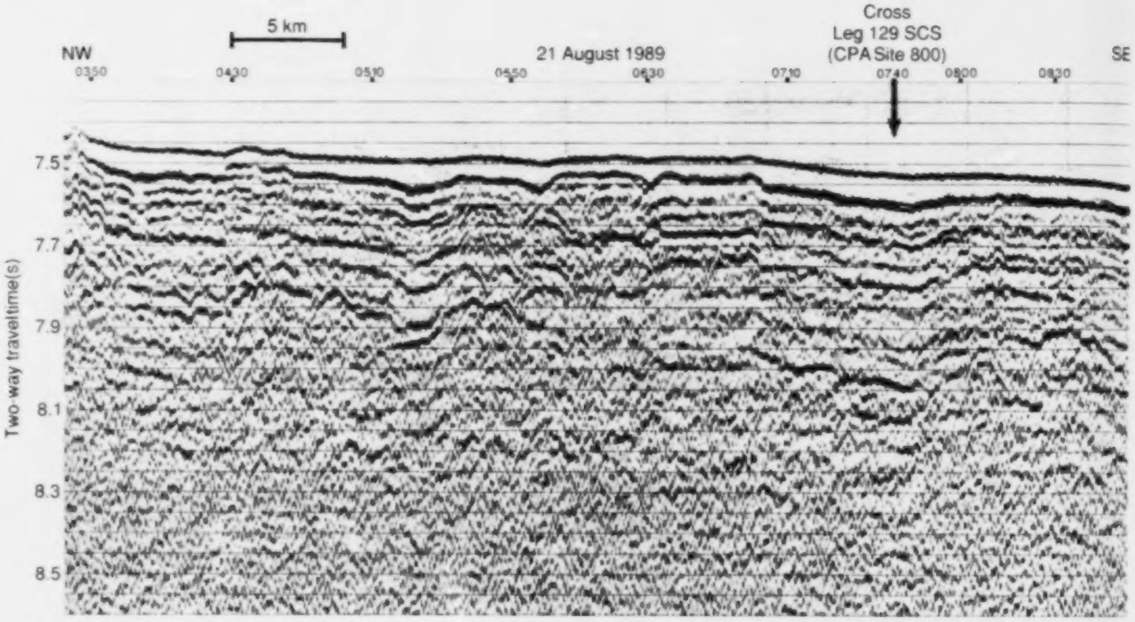

Figure 43. MESOPAC II line 3 SCS record (two 1000-in.$^3$ air guns) showing intersection with the SCS approach profile collected during Leg 129, 3 km northeast of Site 800. Sonobuoy 2m was recorded along this profile from 0349 to 0800 hr UTC and indicates that high-velocity basement begins at 8.025–8.050 s twt at the closest point of approach (CPA) to Site 800. The relief of the basement reflection along this flow-line profile indicates that original abyssal hill morphology is not completely muted by thick sequences of sills or flows. This near-channel record was processed and displayed with the following parameters: shot edit, mute, predictive deconvolution, band-pass filter 8–40 Hz, and 500 ms AGC. Vertical exaggeration is approximately 25× at 1.5 km/s.

uous within the well-developed, graded turbidite beds between 228 and 343 mbsf and become lower in amplitude and more variable in continuity within the pelagic carbonate-silica interval between 38 and 228 mbsf. These observations indicate that within the fine-grained, thinly bedded turbidites, redeposited silica can be focused along well-developed bedding structures creating continuous, high-amplitude reflections, and alternatively, that silica redeposition is less focused, creating more diffuse reflecting horizons in the intervals of less robust bedding structure above. Within the logged interval the common factor for creating reflections is low porosity associated with excess silica. Unfortunately, the logged interval at Site 800 did not reach significantly below the fine-grained, thinly bedded turbidites that extend to 278 mbsf, and so we cannot determine if the continuous reflections below this interval are due solely to primary structure of the coarser grained, thicker turbidite beds interbedded with less indurated clay/claystone, or if excess silica also plays a role in the creation of these reflectors.

## SUMMARY AND CONCLUSIONS

### Introduction (Jurassic Hopes and Cretaceous Fears)

The first site drilled on Leg 129 was considered an important test of our hypothesis that Jurassic crust and sediment were within reach in the Pigafetta Basin. The results of this single-bit pilot hole were to set the pace for the rest of the leg. If Jurassic rocks were indeed present at this site, located in an area where magnetic anomaly identification was indisputable, we were confident that we would be able to find even older rocks at the next site, within the Jurassic quiet zone. The section was thin enough to be cored quickly and we expected to reach the top of the Mesozoic within a few tens of meters of penetration. Below that level, if Upper Cretaceous cherts would not hamper operations too much, drilling through the entire sediment section was only a matter of a few days. The image of the basement on the seismic profiles was certainly not as clear as we would have liked for a first attempt, but other conditions were so encouraging that we were optimistic about the outcome.

The upper part of the section corresponds exactly to what we expected to find: equatorial cherts of Late Cretaceous age overlying Albian pelagic sediments. The composition of these sediments, partly silicified but still calcareous, yielded relatively good biostratigraphic control and their moderate rates of accumulation were an indication that most of the Mesozoic section that we had hoped for was indeed present at this site. The first cores recovered that contained some redeposited volcaniclastics of Aptian age were not really a surprise because a large seamount of that age (Himu) was only some tens of miles away. The shallow-water nature of these sediments indicates that they are more probably derived from Golden Dragon Guyot about 100 miles to the southeast, or from a larger, unnamed guyot slightly farther away to the northeast. Recovering more of the same facies core after core was not really alarming since we were steadily getting back in time, and reaching the lower Aptian told us that we could be out of the volcanogenic deposits soon. Basement was getting closer with each core, however, and volcaniclastics were also becoming coarser grained toward the base of the section, indicating higher rates of sedimentation that began to cloud our optimistic predictions. Relief came with siliceous claystones and radiolarites of Hauterivian-Barremian age. It looked as if we had seen most of the ever-feared middle Cretaceous sediments and were again in pelagic deposits well down into the Lower Cretaceous. Within a few tens of meters, however, medium-grained dolerites were encountered. Before we even had a confirmation of the age of the overlying sediments we knew that we had not reached the Jurassic crust. The igneous rocks were clearly intrusive and soon we learned that the oldest sediments were of Berriasian age and that we had just missed the Jurassic.

Although the main objective for this site was not achieved, drilling at Site 800 nevertheless yielded interesting results pertaining to the Mesozoic evolution of the western Pacific. These results mostly concern the history of the middle Cretaceous volcanic events and the motion of the Pacific plate since the earliest Cretaceous. In addition this site provided enough background information to better understand the geophysical characteristics of the Pigafetta Basin and plan our strategy for the remainder of the cruise.

## Basement Problems

We are convinced that the lowermost layers cored at this site do not represent the oceanic crust. They consist of dolerites of a clearly intrusive nature, injected in sediments that post-date the magnetic anomalies. We believe that the true basement corresponding to the top of the oceanic crust cannot be very far below the top of the dolerite sills because the flat acoustic basement observed in the area lies at a depth of 8.05 s twt. This depth is compatible with the theoretical depth of Upper Jurassic crust, so that a thick accumulation of volcanic rocks or sediments sandwiched between the sills and the top of the oceanic crust is unlikely. Because the oldest sediment reached at this site is of earliest Cretaceous age (Berriasian), an age that predates all of the volcanic events recorded in the Nauru Basin, as well as on the numerous seamounts dredged in the western Pacific, it is likely that the intrusives here could be related to, and contemporaneous with, these events. The actual age and exact depth of the oceanic basement at Site 800 remain a mystery, but it appears probable, in hindsight, after having reached the Jurassic crust at Site 801, 290 nm to the southeast, that Site 800 is indeed underlain by crust of Oxfordian age, as predicted from the magnetic anomalies and basement depth.

## Cretaceous Volcanic Events

Hard rock and sediments recovered at this site document a major pulse of volcanic activity during the Cretaceous. The igneous intrusives are probably related to that activity, although their age remains unknown until it is determined by radiometric methods. The sediments have also recorded that pulse in a series of thick, redeposited, volcaniclastic turbidites that account for about half of the section cored at this site. These sediments attest to the construction of volcanic edifices that must have reached close to the sea surface some time during the Aptian. The lower part of the turbidite interval is poorly dated, but the first sequences were deposited on top of Hauterivian-Barremian pelagic sediments. The sedimentary structures observed in this interval seem to indicate that the rate of sedimentation, or at least the distance from the sources of the redeposited material has decreased steadily with time. Most, if not all, of the volcanic "pulse" coincides with the entire Aptian stage. This site has again documented in detail what appears to be one of the dominant geological features of the western Pacific: widespread, vigorous volcanic activity during the Aptian. It is expressed here in the construction of volcanic edifices large enough to have reached close to the surface, or even to have been emergent at times, and it is possible that the intrusives found at the base of Hole 800A correspond to the same event. In any case, these two distinct expressions of intraplate volcanism are now documented over an area covering several millions of square kilometers.

## History of Plate Motion

Site 800 provides a new set of data which, when combined with results from the other sites drilled during Leg 129, should be very useful for the study of the motion of the Pacific plate during the Mesozoic. An estimate of the successive paleolatitudes of the site was obtained from paleomagnetic data, and the distribution of various sediment facies in time provides additional independent clues for the determination of the time at which the site crossed the equator.

The reconstruction of the history of Pacific plate motion has been attempted through various models relying on different sets of references such as hotspot traces, paleolatitude estimates from seamounts or magnetic anomalies, sediment record of equatorial crossings, and combinations of these approaches. Despite discrepancies between the different models, the general trend of the history of plate motion is relatively well established for the period ranging from the Late Cretaceous to the Holocene. The older record, however, is still subject to major uncertainties. The few sites that have reached Lower Cretaceous sediments have provided enough information to indicate that the Pacific plate motion had a major northward component since at least as early as the Valanginian (Lancelot and Larson, 1975; Lancelot, 1978). Larson and Lowrie (1975) suggested that during at least the earliest Cretaceous and possibly the Late Jurassic, the plate moved from north to south so that it may actually have crossed the equator twice.

Paleomagnetic data from Site 800 confirm that the motion of the Pacific plate had a monotonic northward component at least from the early Aptian through the Cenomanian, and that indeed the plate moved from north to south prior to that time. The shift from southward to northward motion appears to have occurred between the Hauterivian-Barremian and the early Aptian. These findings show a good agreement with the biogenic component of the sediment record. The time when the site was in the vicinity of the high productivity, equatorial zone is well documented by a relative increase in the abundance of silica of biogenic origin in the sediments. This increase is recorded by a peak in the abundance of radiolarians, the presence of chert, and the amount of silicon detected by the geochemical logging tool. Carbonate sedimentation exhibits trends that supplement the information provided by silica. Calcareous nannofossils show a marked increase in quantity from the late Aptian through the Cenomanian. The combined influences of the production of carbonate in the surface waters and the dissolution at depth will have to be studied in more detail before a model of equatorial CCD evolution for this period can be established. The older equatorial crossing has not been documented at this site by paleolatitude estimates from paleomagnetic measurements because the core samples from the older sediments recovered near the base of the hole were not judged entirely suitable for shipboard analysis. The silica content of the sediment, however, indicates that Site 800 was close to the equator during Berriasian-Valanginian times.

## REFERENCES

Abrams, L. J., Larson, R. L., Shipley, T., and Lancelot, Y., 1988. Cretaceous volcanic sequences and Jurassic(?) crust in the western Pacific. *Trans. Am. Geophys. Union*, 69:1442.

Baumgartner, P. O., 1984. A middle Jurassic-Early Cretaceous low-latitude radiolarian zonation based on Unitary Associations and age of Tethyan radiolarites. *Eclogae Geol. Helv.*, 77:729–837.

Baumgartner, P. O., 1987. Age and genesis of Tethyan Jurassic Radiolarites. *Eclogae Geol. Helv.*, 80:831–879.

Berger, A., Imbrie, J., Hays, J., Kukla, G., and Saltzman, B., 1984. *Milankovitch and Climate* (Pt. 1): NATO ASI Ser., Ser. C, 126.

Cande, S. C., Larson, R. L., and LaBrecque, J. L., 1978. Magnetic lineations in the western Pacific Jurassic Quiet Zone. *Earth Planet. Sci. Lett.*, 41:433–440.

Christensen, N. L., and Salisbury, M. H., 1975. Structure and constitution of the lower oceanic crust. *Rev. Geophys. Space Phys.*, 13:57–86.

Detrick, R., Honnorez, J., Bryan, W. B., Juteau, T., et al., 1988. *Proc. ODP, Init. Repts.*, 106/109: College Station, TX (Ocean Drilling Program).

Ewing, J., Ewing, M., Aitken, T., and Ludwig, W. J., 1968. North Pacific sediment layers measured by seismic profiling. *In* Drake, C. L., and Hart, P. J. (Eds.), *The Crust and Upper Mantle of the Pacific Area.* Am. Geophys. Union. Monogr., 12:147–173.

Ferry, S., and Schaaf, A., 1982. Early Cretaceous environment at Deep Sea Drilling Project Site 463 (Mid Pacific Mountains) with reference to the Vocontian Trough (French Subalpine Ranges). *In* Thiede, J., Vallier, T. L., et al., *Init. Repts. DSDP*, 62: Washington (U. S. Govt. Printing Office), 669–682.

Fertl, H. H., 1979. *Gamma Ray Spectral Data Assists in Complex Formation Evaluation:* Houston (Dresser-Atlas).

Garrison, E. D., 1974. Radiolarian cherts, pelagic limestones and igneous rocks in eugeosynclinal assemblages. *In* Hsü, K. J., and Jenkyns, H. C. (Eds.), *Pelagic Sediments on Land and Under the Sea.* Spec. Publ. Int. Assoc. Sedimentol., 1:367–399.

Geroch, S., and Nowak, W., 1983. Proposal of zonation for the late Tithonian-Late Eocene, based upon arenaceous foraminifera from the Outer Carpathians, Poland. *In* Oertli, H. J. (Ed.), *Benthos '83:* 2nd Int. Symp. on Benthic Foraminifera (Pau), 225–239.

Gieskes, J. M., 1976. Interstitial water studies, Leg 33. *In* Schlanger, S. O., Jackson, E. D., et al., *Init. Repts. DSDP*, 33: Washington (U.S. Govt. Printing Office), 563–570.

Gieskes, J. M., and Johnson, J., 1981. Interstitial water studies, Leg 61. *In* Larson, R. L., Schlanger, S. O., et al., *Init. Repts. DSDP*, 61: Washington (U.S. Govt. Printing Office), 603–605.

Gradstein, F. M., and Sheridan, R. E., 1983. On the Jurassic Atlantic Ocean and a synthesis of results of DSDP Leg 76. *In* Sheridan, R. E., Gradstein, F. M., et al., *Init. Repts. DSDP*, 76: Washington (U.S. Govt. Printing Office), 913–943.

Haggerty, J. A., and Premoli-Silva, I., 1986. Ooids and shallow-water debris in Aptian-Albian sediments from the East Mariana Basin, Deep Sea Drilling Project Site 585: implications for the environment of formation of ooids. *In* Moberly, R., Schlanger, S. O., et al., *Init. Repts. DSDP*, 89: Washington (U.S. Govt. Printing Office), 399–412.

Hamilton, E. L., 1974. Prediction of deep-sea sediment properties: state of the art. *In* Inderbitzen, A. L. (Ed.), *Deep-Sea Sediments: Physical and Mechanical Properties:* New York (Plenum), 1–44.

———, 1978. Sound velocity-density relations in sea-floor sediments and rocks. *J. Acoust. Soc. Am.*, 63:366–377.

Handschumacher, D. W., and Gettrust, J. F., 1985. Mixed polarity model for the Jurassic "Quiet Zones": new oceanic evidence of frequent pre-M25 reversals. *Eos*, 66:867.

Handschumacher, D. W., and Kroenke, L., 1978. An extended time scale of Mesozoic geomagnetic reversals. *Eos*, 59:266.

Handschumacher, D. W., Sager, W. W., Hilde, T.W.C., and Bracey, D. R., 1988. Pre Cretaceous tectonic evolution of the Pacific Plate and extension of the geomagnetic polarity reversal time scale with implications for the origin of the Jurassic "Quiet Zone." *Tectonophysics*, 155:365–380.

Harland, W. B., Cox, A. V., Llewellyn, P. G., Pickton, C.A.G., Smith, D. G., and Walters, R., 1982. *A Geologic Time Scale:* Cambridge (Cambridge Univ. Press).

Hay, W. W., 1988. Paleoceanography: a review for the GSA Centennial. *Geol. Soc. Am. Bull.*, 100:1934–1956.

Heezen, B. C., MacGregor, I. D., and DSDP Leg 20 Scientific Party, 1973. Mesozoic chalks beneath the Caroline abyssal plain: DSDP Site 199. *In* Heezen, B. C., MacGregor, I. D., et al., *Init. Repts. DSDP*, 20: Washington (U.S. Govt Printing Office), 65–85.

Hilde, T.W.C., 1973. Mesozoic seafloor spreading in the North Pacific [D.Sc. thesis]. Univ. of Tokyo, Tokyo, Japan.

Hilde, T.W.C., Isezaki, N., and Wageman, J. M., 1976. Mesozoic seafloor spreading in the North Pacific. *In* Sutton, G. H., Manghnani, M. H., and Moberly, R. (Eds.), *The Geophysics of the Pacific Ocean Basin and its Margins.* AGU Geophys. Monogr. Ser., 19:205–226.

Hilde, T.W.C., Uyeda, S., and Kroenke, L., 1977. Evolution of the western Pacific and its margins. *Tectonophysics*, 38:145–166.

Houtz, R. E., Ewing, J., and Buhl, P., 1970. Seismic data from sonobuoy stations in the northern and equatorial Pacific. *J. Geophys. Res.*, 75:5093–5111.

Houtz, R. E., and Ludwig, W. J., 1979. Distribution of reverberant subbottom layers in the southwest Pacific Basin. *J. Geophys. Res.*, 84:3497–3504.

Hutchinson, D. R., and Detrick, R. S., 1984. Water gun vs. air gun: a comparison. *Mar. Geophys. Res.*, 6:295–310.

Hyndman, R. D., Christensen, N. I., and Drury, M. J., 1984. The physical properties of basalt core samples from Deep Sea Drilling Project Leg 78B, Hole 395A. *In* Hyndman, R. D., Salisbury, M. H., et al., *Init. Repts. DSDP*, 78B: Washington (U.S. Govt. Printing Office), 801–810.

Jackson E. D., Koizumi, I., et al., 1980. *Init. Repts. DSDP*, 55 Washington (U.S. Govt. Printing Office).

Jenkyns, H. C., 1978. Pelagic environments. *In* Reading, H. G. (Ed.), *Sedimentary Environments and Facies:* Oxford (Blackwell), 314-370.

Jenkyns, H. C., and Winterer, E. L., 1982. Palaeoceanography of Mesozoic ribbon radiolarites. *Earth Planet. Sci. Lett.*, 60:351-375.

Kaminski, M. A., Gradstein, F. M., Berggren, W. A., Geroch, S., and Beckmann, J. P., 1988a. Agglutinated foraminiferal assemblages from Trinidad. Taxonomy, stratigraphy and paleobathymetry. *Abh. Geol. Bundensanst. Austria*, 41:155–227.

Kaminski, M. A., Grassle, J. F., and Whitlatch, R. B., 1988b. Life history and recolonization among agglutinated foraminifera in the Panama Basin. *Abh. Geol. Bundensanst. Austria*, 41:229-243.

Karpoff, A. M., 1989. Les faciès pélagiques condensés cénozoiques des océans Pacifique et Atlantique: témoins des grandes crises géodynamiques [Thèse Doc. ès Sci.], Univ. Louis Pasteur, Strasbourg.

Kastner, M., Keene, J. B., and Gieskes, J. M., 1977. Diagenesis of siliceous oozes. I. Chemical controls on rate of opal-A to opal-CT transformation - an experimental study. *Geochim. Cosmochim. Acta*, 41:1041–1059.

Kent, D. V., and Gradstein, F. M., 1985. A Cretaceous and Jurassic geochronology. *Geol. Soc. Am. Bull.*, 96:1419–1427.

Kono, M., 1980. Statistics of paleomagnetic inclination data. *J. Geophys. Res.*, 85:3878–3882.

Krasheninnikov, V. A., 1971. Cretaceous benthonic foraminifera: DSDP Leg 20. *In* Heezen, B. C., MacGregor, I. D., et al, *Init. Repts. DSDP*, 20: Washington (U.S. Govt. Printing Office), 205-213.

Lancelot, Y., 1973. Chert and silica diagenesis in sediments from the central Pacific. *In* Winterer, E. L., Ewing, J. I., et al. *Init. Repts. DSDP*, 17: Washington (U.S. Govt. Printing Office), 377–405.

———, 1978. Evolution sedimentaire et tectonique de la plaque Pacifique. *Mem. Soc. Geol. France*, Nelle Ser., 134.

Lancelot, Y., and Larson, R. L., 1975. Sedimentary and tectonic evolution of the northwestern Pacific. *In* Larson, R. L., Moberly, R., et al., *Init. Repts. DSDP*, 32: Washington (U.S. Govt. Printing Office), 945–957.

Larson, R. L., and Chase, C. G., 1972. Late Mesozoic evolution of the western Pacific Ocean. *Geol. Soc. Am. Bull.*, 83:3627–3644.

Larson, R. L., and Hilde, T.W.C., 1975. A revised time scale of magnetic reversals for the Early Cretaceous and Late Jurassic. *J. Geophys. Res.*, 80:2586–2594.

Larson, R. L., and Lowrie, W., 1975. Paleomagnetic evidence for motion of the Pacific plate from Leg 32 basalts and magneticanomalies. *In* Larson, R. L., and Moberly, R., et al., *Init. Repts. DSDP*, 32: Washington (U.S. Govt. Printing Office), 571–577.

Larson, R. L., and Schlanger, S. E., 1981. Geological evolution of the Nauru Basin, and regional implications. *In* Larson, R. L., Schlanger, S. E., et al., *Init. Repts. DSDP*, 61: Washington (U.S. Govt. Printing Office), 841–862.

Larson, R. L., Pitman, W. C., Golovchenko, X., Cande, S. C., Dewey, J. F., Haxby, W. F., and LaBrecque, J. L., 1985. *The Bedrock Geology of the World:* New York (W. H. Freeman).

Manivit, H., Perch-Nielsen, K., Prins, B., and Verbeek, J. W., 1977. Mid Cretaceous calcareous nannofossil biostratigraphy. *Proc. K. Ned. Akad. Wet., Ser. B: Palaeontol., Geol., Phys., Chem.*, 8:169–191.

McKenzie, J. A., Bernoulli, D., and Schlanger, S. O., 1980. Shallow-water carbonate sediments from the Emperor Seamounts: their diagenesis and paleogeographic significance. *In* Jackson, E. D., Koizumi, I., et al., *Init. Repts. DSDP*, 55: Washington (U.S. Govt. Printing Office), 415–455.

Miura, Y., Rucklidge, J. C., and Nord, G. L., Jr., 1981. The occurrence of chlorine in serpentine minerals. *Contrib. Miner. Petrol.*, 76:17–23.

Moberly, R., Schlanger, S. O., et al., 1986. *Init. Repts. DSDP*, 89: Washington (U.S. Govt. Printing Office).

Nakanashi, M., Tamaki, K., and Kobayashi, K., 1989. Mesozoic magnetic anomaly lineations and seafloor spreading history of the northwestern Pacific. *J. Geophys. Res.*, 94:15437–15462.

Perch-Nielsen, K., 1979. Calcareous nannofossils from the Cretaceous between the North Sea and the Mediterranean. *In* Wiedmann, J. (Ed.), *Aspekte der Kreide Europas*. Int. Union Geol. Sci., Ser. A, 6:223–272.

———, 1985. Mesozoic calcareous nannofossils. *In* Bolli, H. M., Saunders, J. B., and Perch-Nielsen, K. (Eds.), *Plankton Stratigraphy:* Cambridge (Cambridge Univ. Press), 329–426.

Pisciotto, K. A., 1981. Distribution, thermal histories, isotopic compositions, and reflection characteristics of siliceous rocks recovered by the Deep Sea Drilling Project. *In* Warme, J. E., Douglas, R. G., and Winterer, E. L. (Eds.), *The Deep Sea Drilling Project: A Decade of Progress*. SEPM Spec. Publ., 32:129–148.

Roth, P. H., 1978. Cretaceous nannoplankton biostratigraphy and oceanography of the northwestern Atlantic Ocean. *In* Benson, W. E., Sheridan, R. E., et al., *Init. Repts. DSDP*, 44: Washington (U.S. Govt. Printing Office), 731–759.

Sanfilippo, A., and Riedel, W. R., 1985. Cretaceous radiolaria. *In* Bolli, H. M., Saunders, J. B., and Perch-Nielsen, K. (Eds.), *Plankton Stratigraphy:* Cambridge (Cambridge Univ. Press), 573–630.

Sayles, F. L., and Manheim, F. T., 1975. Interstitial solutions and diagenesis in deeply buried marine sediments: results from the Deep Sea Drilling Project. *Geochim. Cosmochim. Acta*, 39:103–127.

Schaaf, A., 1984. Les radiolaires du Cretace inferieur et moyen: biologie, systematique biochronologie et paleoenvironement. [These Doc. es Sci.], Univ. Louis Pasteur, Strasbourg.

Schlanger, S. O., and Moberly, R., 1986. Sedimentary and volcanic history: East Mariana Basin and Nauru Basin. *In* Moberly, R., Schlanger, S. O., et al., *Init. Repts. DSDP*, 89: Washington (U.S. Govt. Printing Office), 653–678.

Schroeder, C. J., 1986. Deep-water arenaceous foraminifera in the Northwest Atlantic Ocean. *Can. Tech. Rept. Hydrogr. Ocean Sci.*, 71:1–191.

Shipboard Scientific Party, 1989. Site 717: Bengal Fan. *In* Cochran, J. R., Stow, D.A.V., et al., *Proc. ODP, Init. Repts.*, 116: College Station, TX (Ocean Drilling Program), 45–90.

Shipboard Scientific Party, 1990a. Site 765. *In* Gradstein, F. M., Ludden, J. N., et al., *Proc. ODP, Init. Repts.*, 123: College Station, TX (Ocean Drilling Program), 63–267.

Shipboard Scientific Party, 1990b. Site 780. *In* Fryer, P., Pierce, J., et al., *Proc. ODP, Init. Repts.*, 125: College Station, TX (Ocean Drilling Program).

Shipley, T. H., Whitman, J. M., Dunnebier, F. K., and Peterson, L. D., 1983. Seismic stratigraphy and sedimentation history of the East Mariana Basin, Western Pacific. *Earth Planet. Sci. Lett.*, 64:257–275.

Sissingh, W., 1977. Biostratigraphy of Cretaceous calcareous nannoplankton. *Geol. Mijnbouw*, 56:37–65.

Steinberg, M., 1981. Biosiliceous sedimentation, radiolarite periods and silica budget fluctuations. *In* Int. Geol. Congr., 26th, Ocean Symp., (Paris 1980). *Oceanol. Acta*, 149–154.

Tamaki, K., Nakanishi, M., Sayanagi, K., and Kobayashi, K., 1987. Jurassic magnetic lineations of the western Pacific Ocean and the origin of the Pacific plate. *Eos*, 68:1493.

Thiede, J., Vallier, T. L., et al., 1981. *Init. Repts. DSDP*, 62: Washington (U.S. Govt. Printing Office).

Thierstein, H. R., 1971. Tentative Lower Cretaceous nannoplankton zonation. *Eclogae Geol. Helv.*, 64:459–488.

———, 1973. Lower Cretaceous calcareous nannoplankton biostratigraphy. *Abh. Geol. Bundesanst. Austria*, 29:1–52.

———, 1976. Mesozoic calcareous nannoplankton biostratigraphy of marine sediments. *Mar. Micropaleontol.*, 1:325–362.

Wise, S. W., Jr., and Weaver, F. M., 1974. Chertification of oceanic sediments. *In* Hsü, K. J., and Jenkyns, H. C. (Eds.), *Pelagic Sediments: on Land and under the Sea*. Spec. Publ. Int. Assoc. Sedimentol., 1:301–326.

Witmann, J. M., Baltuck, M., Haggerty, J. A., and Dean, W., 1986. Turbidite sedimentology and history of the East Mariana Basin. *In* Moberly, R., Schlanger, S. O., et al., *Init. Repts. DSDP*, 89: Washington (U.S. Govt. Printing Office), 365–387.

Yeats, R. S., Hart, S. R., et al., 1976. *Init. Repts. DSDP*, 34: Washington (U.S. Govt. Printing Office).

Zotto, M., Drugg, W. S., and Habib, D., 1987. Kimmeridgian dinoflagellate stratigraphy in the Southwestern North Atlantic. *Micropaleontology*, 33:193–213.

**Ms 129A-102**

**NOTE: All core description forms ("barrel sheets") and core photographs have been printed on coated paper and bound as Section 3, near the back of the book, beginning on page 247.**

Hole 800A: Resistivity-Sonic-Gamma Ray Log Summary

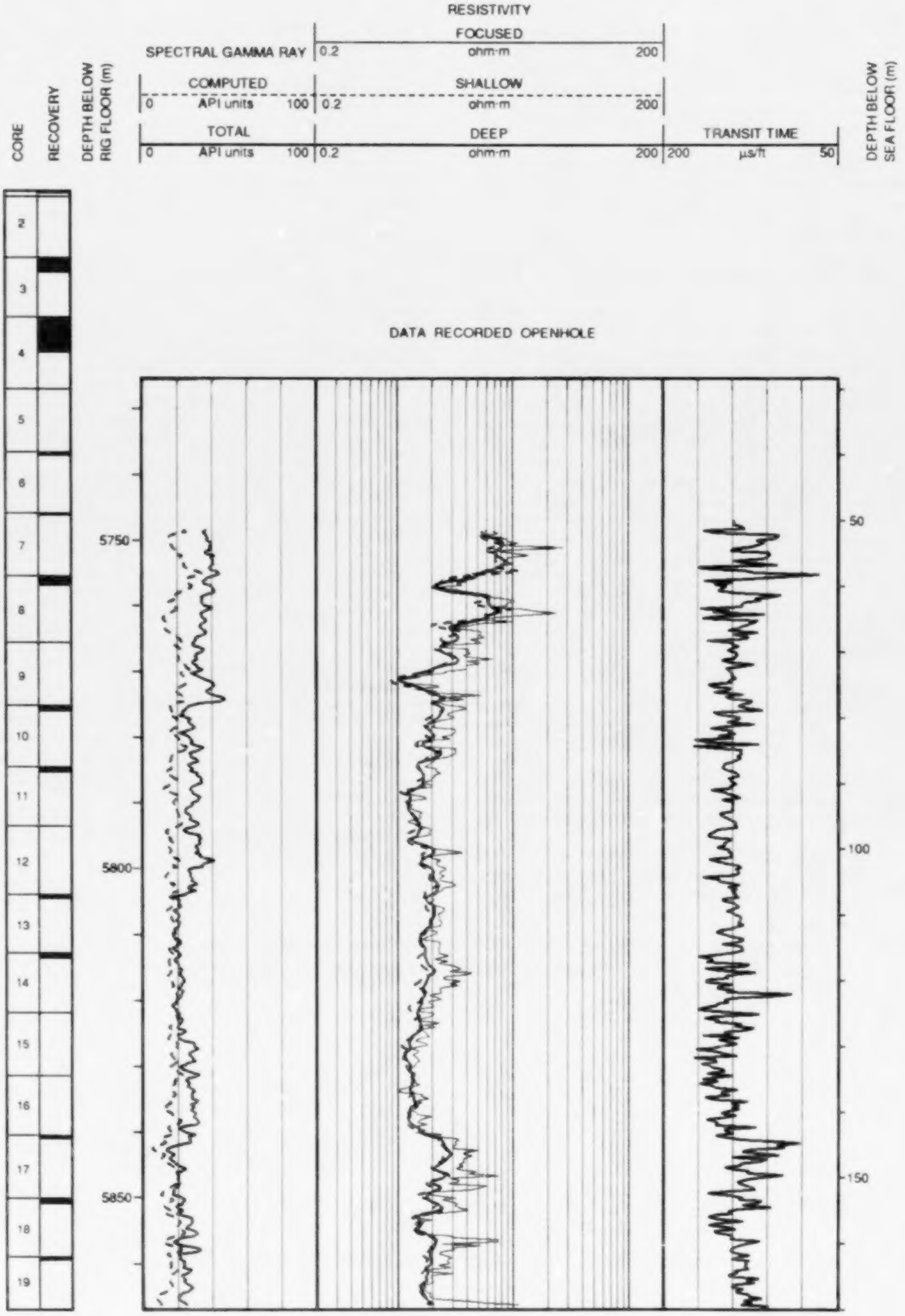

Hole 800A: Resistivity-Sonic-Gamma Ray Log Summary (continued)

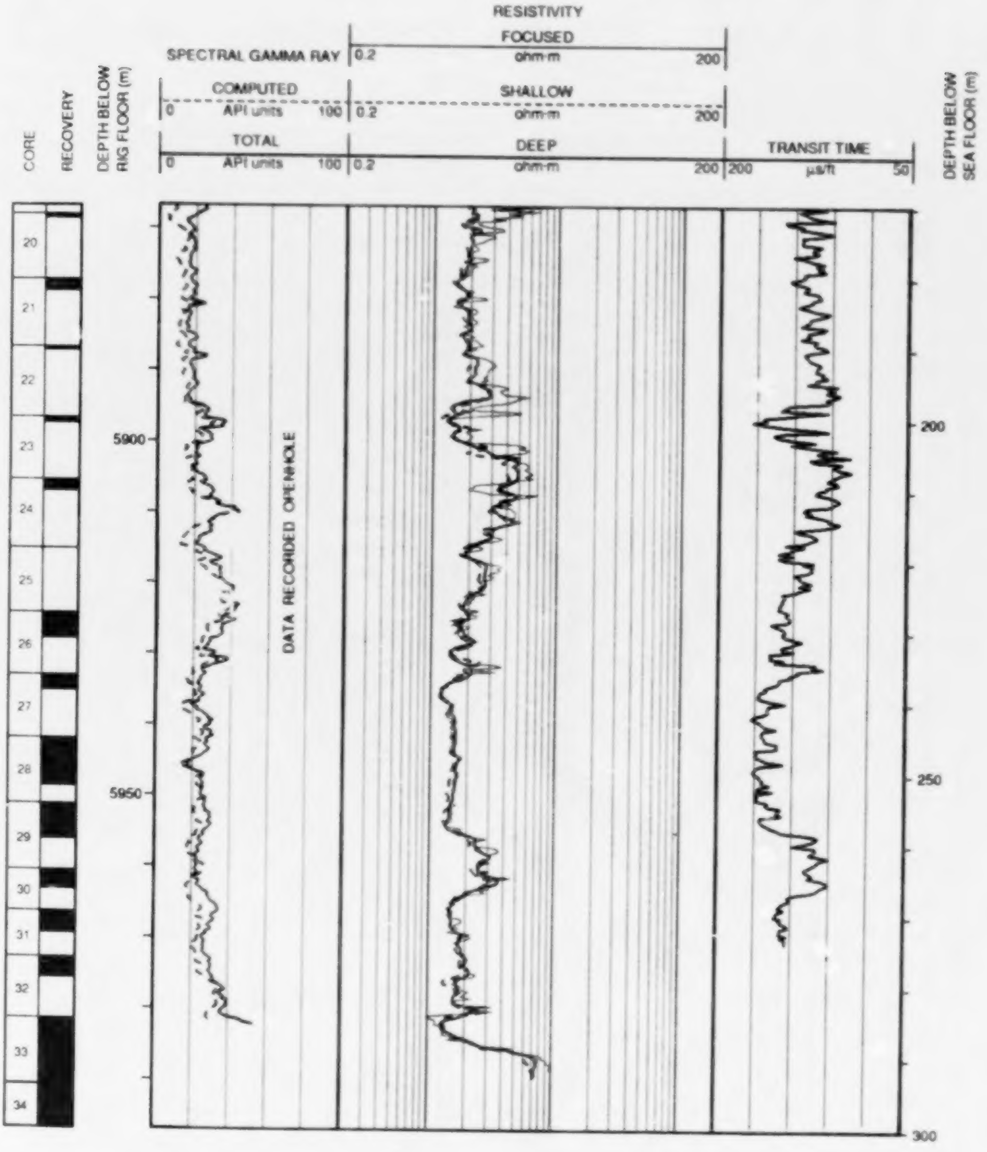

Hole 800A: Density-Caliper-Gamma Ray Log Summary

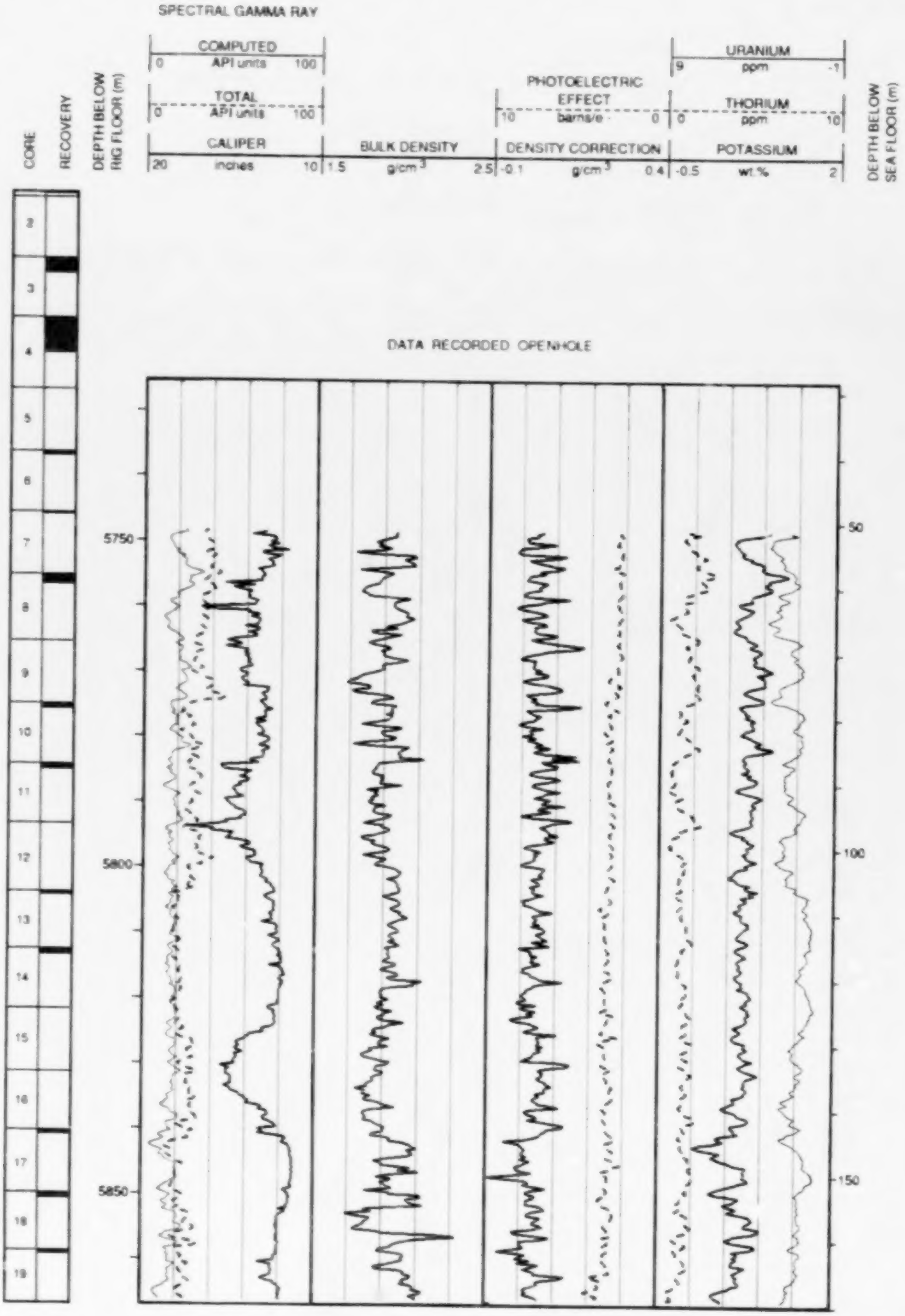

Hole 800A: Density-Caliper-Gamma Ray Log Summary (continued)

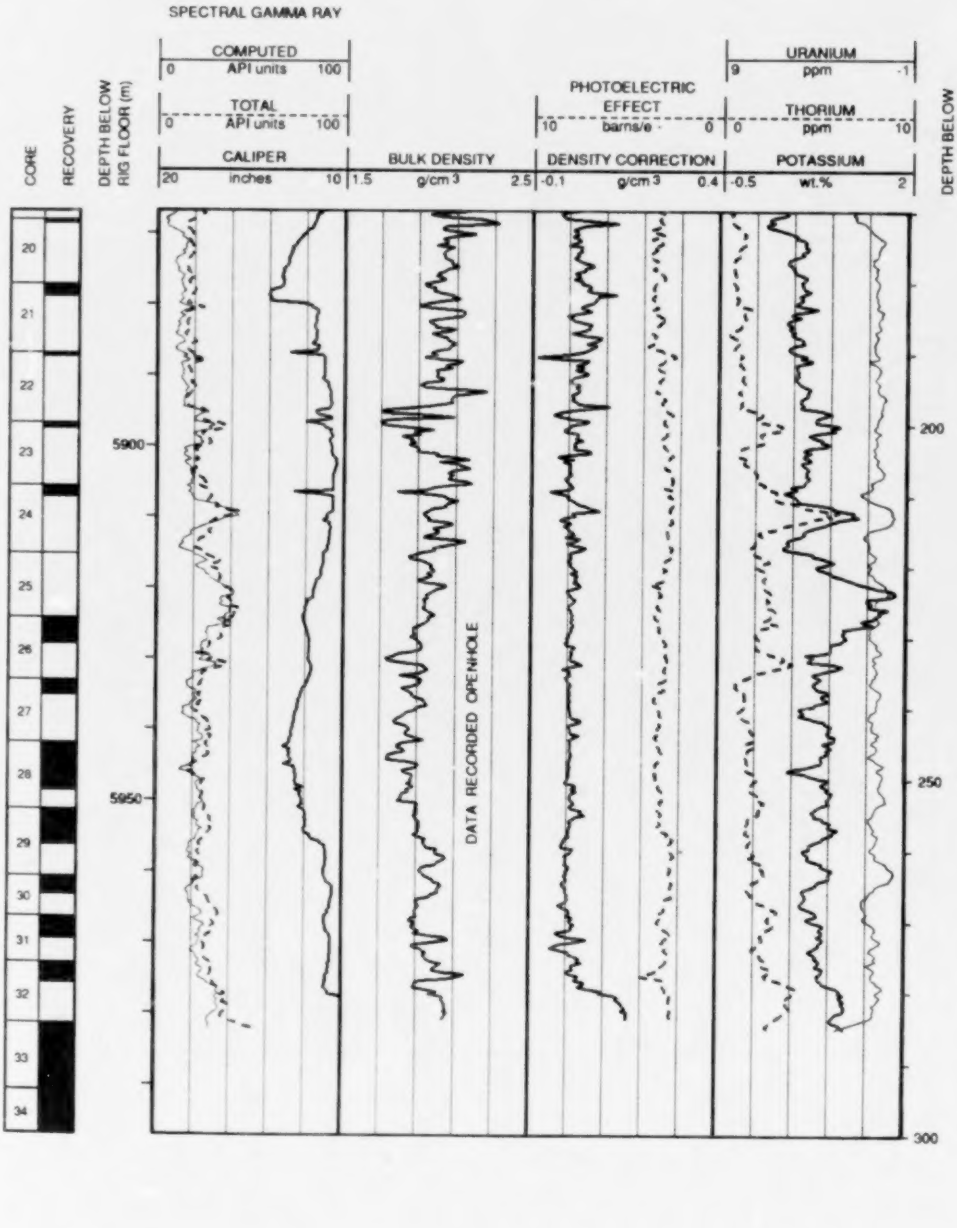

## Hole 800A: Geochemical Log Summary

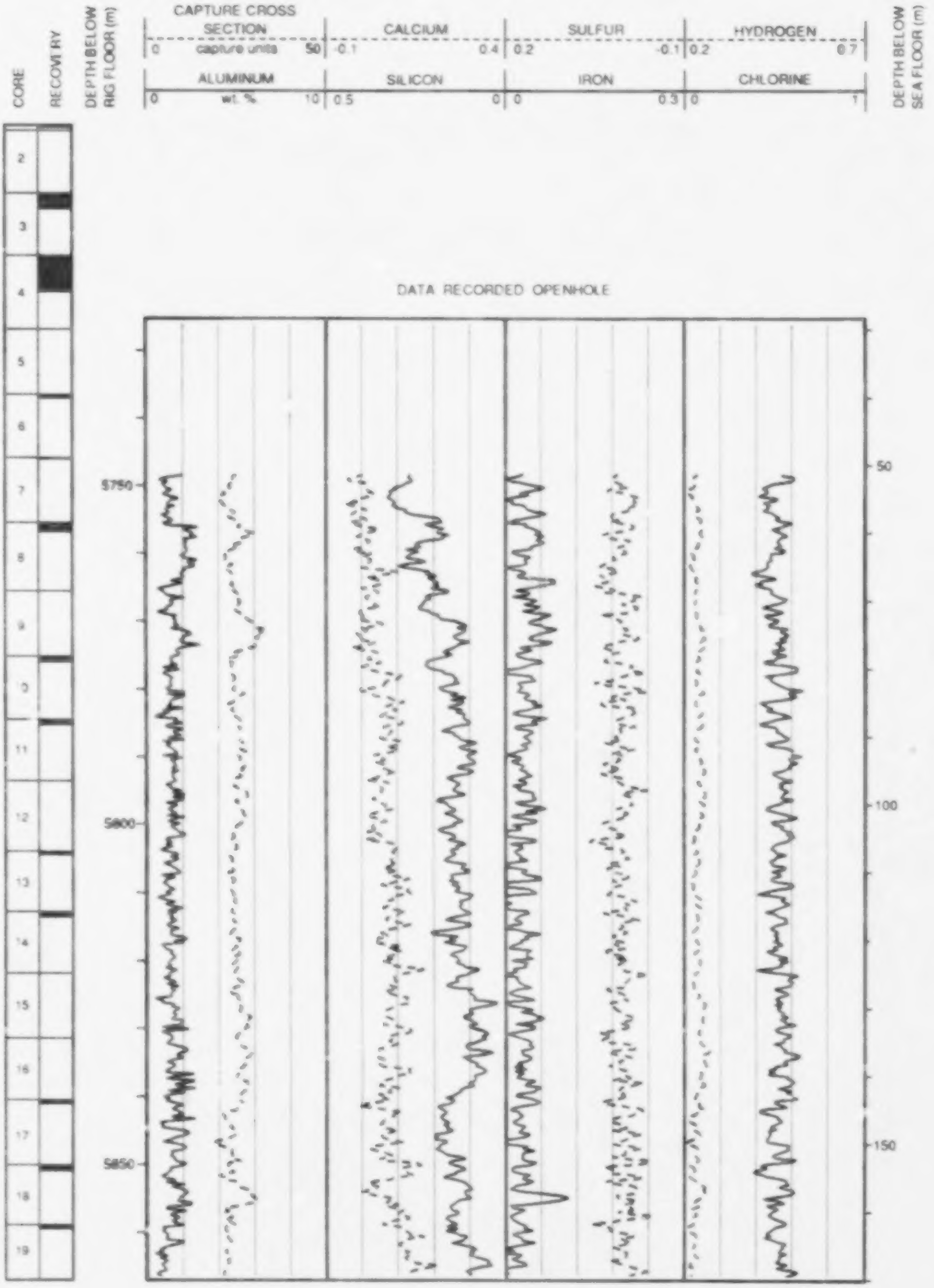

## Hole 800A: Geochemical Log Summary (continued)

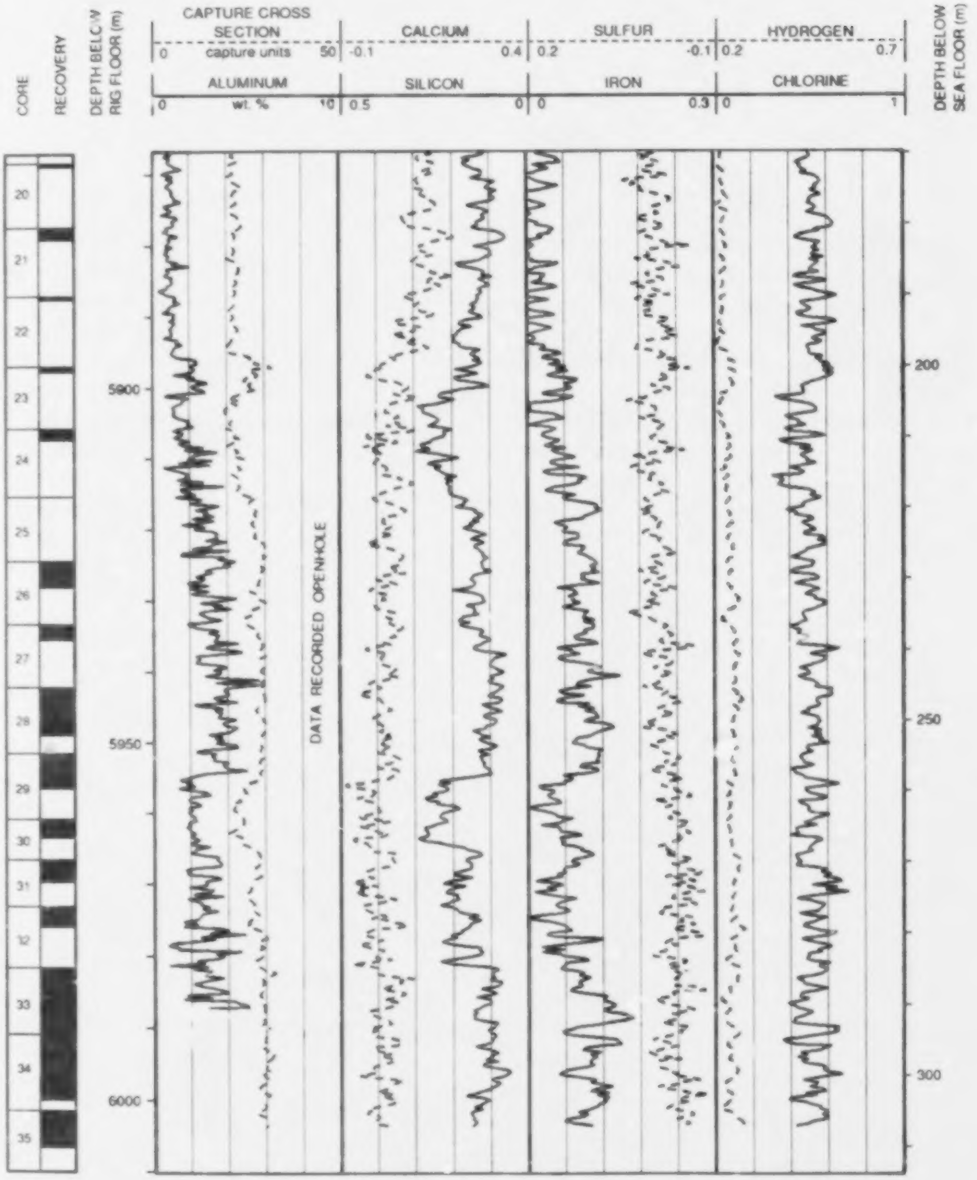

Lancelot, Y., Larson, R. L., et al., 1990
*Proceedings of the Ocean Drilling Program, Initial Reports*, Vol. 129

# 3. SITE 801[1]

Shipboard Scientific Party[2]

## HOLE 801A

**Date occupied:** 6 December 1989

**Date departed:** 9 December 1989

**Time on hole:** 2 days, 10 hr, 00 min

**Position:** 18°38.568′N, 156°21.57′E

**Bottom felt (rig floor, m; drill-pipe measurement):** 5685.0

**Distance between rig floor and sea level (m):** 11.20

**Water depth (drill-pipe measurement from sea level, m):** 5673.8

**Total depth (rig floor; m):** 5879.00

**Penetration (m):** 194.0

**Number of cores (including cores with no recovery):** 20

**Total length of cored section (m):** 186.0

**Total core recovered (m):** 31.49

**Core recovery (%):** 16

**Oldest sediment cored:**
  Depth (mbsf): 194.0
  Nature: Radiolarian claystone
  Age: Cenomanian

## HOLE 801B

**Date occupied:** 9 December 1989

**Date departed:** 17 December 1989

**Time on hole:** 7 days, 8 hr, 45 min

**Position:** 18°38.52′N, 156°21.582′E

**Bottom felt (rig floor; m; drill-pipe measurement):** 5685.0

**Distance between rig floor and sea level (m):** 11.20

**Water depth (drill-pipe measurement from sea level, m):** 5673.8

**Total depth (rig floor; m):** 6196.20

**Penetration (m):** 511.20

**Number of cores (including cores with no recovery):** 44

**Total length of cored section (m):** 317.20

**Total core recovered (m):** 59.17

**Core recovery (%):** 18

**Oldest sediment cored:**
  Depth (mbsf): 511.20
  Nature: Calcareous silicified tuff and radiolarian metasiltstone
  Earliest age: Callovian-Bathonian
  Latest age: Oxfordian

**Basement:**
  Depth (mbsf): 461.6
  Nature: Basalt

## HOLE 801C

**Date occupied:** 18 December 1989

**Date departed:** 16 January 1990

**Time on hole:** 16 days, 2 hr, 00 min

**Position:** 18°38.538′N, 156°21.588′E

**Bottom felt (rig floor; m; drill-pipe measurement):** 5685.0

**Distance between rig floor and sea level (m):** 11.00

**Water depth (drill-pipe measurement from sea level, m):** 5674.0

**Total depth (rig floor; m):** 6279.30

**Penetration (m):** 594.30

**Number of cores (including cores with no recovery):** 12

**Total length of cored section (m):** 100.60

**Total core recovered (m):** 60.60

**Core recovery (%):** 60

**Basement:**
  Depth (mbsf): 493.7
  Nature: Basalt

**Comments:** Revisited site for fishing and reentry.

**Principal Results:** This is the first Deep Sea Drilling Project/Ocean Drilling Program (DSDP/ODP) drill site ever to recover Jurassic-age sediments and oceanic crust from the Pacific plate or Pacific Ocean Basin. Site 801 is located in the central Pigafetta Basin on a magnetic quiet zone southeast of, and presumably older than, the M25–M37 magnetic lineation sequence. Holes 801A, 801B, and 801C consist of the following stratigraphic sequence:

8.0–64.0 mbsf: Tertiary to Campanian brown pelagic clay.

64.0–126.5 mbsf: Campanian to Turonian brown chert and porcellanite.

126.5–318.3 mbsf: Cenomanian and Albian volcaniclastic turbidites with minor radiolarite near the base.

318.3–442.9 mbsf: Lower Cretaceous (Valanginian) to Upper Jurassic (Oxfordian) brown radiolarite with dark brown chert and abundant manganese.

442.9–461.6 mbsf: Middle Jurassic (Callovian-Bathonian) umber-colored radiolarite and claystone with strong hematite enrichment, probably indicative of hydrothermal activity during or just after deposition. The oldest dated sediment is interbedded with the basalts in the underlying unit at 473 m where the *Tricolocapsa conexa* zone of Matsuoka and Yao (1986) has been identified. This radiolarian assemblage is the same as the basal radiolarian sequence of DSDP Site 534 that has been recalibrated by Baumgartner (1987) to lie at the Callovian/Bathonian boundary, ~170 Ma. No carbonate in this ridge-crest, equatorial-paleolatitude sedimentary facies suggests that the Late/Middle Jurassic superocean was characterized by extremely low carbonate production and/or preservation.

461.6–590.9 mbsf: Middle Jurassic basement. Interbedded basaltic thin flows, possibly some thin sills, and silicified claystone are at the top of the sequence. Pillow basalts begin at 495 mbsf that exhibit concave pillow structures with chilled margins, variolitic textures, and microcrystalline interiors. A remarkable hydrothermal concretion occurs between 522 and 531 mbsf that is chrome yellow and silica cemented. It is underlain by pillow basalts that are extremely altered directly beneath the hydrothermal deposit, and become less altered towards the bottom of the hole. A summary of coring statistics is present in Table 1.

---

[1] Lancelot, Y., Larson, R. L., et al., 1990. *Proc. ODP, Init. Repts.*, 129: College Station, TX (Ocean Drilling Program).

[2] Shipboard Scientific Party is as given in the list of participants preceding the contents.

Standard logging was completed, including a repeat formation microscanner run with the wireline heave compensator operating, from 56 to about 460 mbsf.

## BACKGROUND AND OBJECTIVES

Site 801 (proposed site PIG-3A) is located within the so-called "Jurassic magnetic quiet zone" in the central part of the Pigafetta Basin, approximately 150 nautical miles (nmi) southeast of the last well-defined magnetic anomaly (M37) (Figs. 1 and 2). The main objective at this site was to recover Jurassic sediment and oceanic crust that might be the oldest in the Pacific Ocean and possibly in the world ocean.

The main reason for interest in Jurassic sediments from the Pacific is that they chronicle the paleoenvironment of the Jurassic superocean, which covered two-thirds of the Earth at that time, but for which we have no direct record. The only samples of pelagic "deep-sea" Jurassic sediments come from the fold belts surrounding the Tethys paleo-ocean and from DSDP sites in the proto-Atlantic, both of which correspond to relatively restricted marine conditions mostly from continental margin environments.

Previous attempts to recover Jurassic sediments in the Pacific prior to Leg 129 all have failed in cherts or extraordinarily thick lava flows, sills, or volcaniclastics of middle to Late Cretaceous age that proved impossible to penetrate (DSDP Site 461 in the Nauru Basin and Site 585 in the East Mariana Basin). The most recent attempt was the previous site on Leg 129 (Site 800), where again volcanic rocks of probable Early Cretaceous age were found above the top of the oceanic crust, as inferred from seismic data. The oldest sediments that we recovered at that site, before encountering a series of thick dolerite sills, were claystones of Berriasian age, and although that discovery was indeed a disappointment, it did not seriously alter our hopes to find the Jurassic basement in the Pigafetta Basin. The results from the sonobuoys in the area of Site 801, as well as the much clearer image of the acoustic basement on reflection profiles, were very encouraging in that respect. Furthermore, since the acoustic basement at Site 801 was visible near 8.0 to 8.1 seconds two-way traveltime (s twt), chances appeared good that this reflector would coincide with the top of the oceanic crust because that depth is approximately the level at which crust of Jurassic age is expected (approximately 6200 mbsl).

The lowermost reflector observed on both the multichannel seismic profile from the MESOPAC II cruise (see "Site Geophysics and Seismic Stratigraphy" section, this chapter) and the single-channel profile recorded while approaching the site lies at approximately 8.0 s twt beneath sea level. Its exhibits a "hummocky" character that strongly suggests its correspondence to the top of seismic layer 2. Based on this observation, the total sediment thickness at Site 801 was estimated at about 460 m assuming an average sound velocity of about 2.0 km/s for the whole sedimentary section, a value derived both from site survey data (sonobuoys from MESOPAC II and *Fred H. Moore* 35-12 cruises) and from drilling results from Site 800.

A simple, straightforward extrapolation of ages and spreading rates of the magnetic anomalies observed in the northwestern part of the Pigafetta Basin (M20–M25), predicts the basement to be of Middle to Late Jurassic age at Site 801 (Fig. 3). The sediment section was believed to consist mostly of pelagic deposits, although chances remained good to encounter volcaniclastic turbidites again since the seismic interval corresponding to these sediments could be traced all the way

**Table 1. Coring summary for Site 801.**

| Core | Date | Time | Depth (mbsf) | Length cored (m) | Length recovered (m) | Recovery (%) |
|---|---|---|---|---|---|---|
| 129-801A- | | | | | | |
| 1R[a] | 7 Dec 1989 | 1145 | 14.5 | 6.5 | 1.30 | 20.0 |
| 2R | 7 Dec | 1545 | 20.4 | 5.9 | 0.50 | 8.5 |
| 3R | 7 Dec | 1645 | 30.0 | 9.6 | 5.29 | 55.1 |
| 4R | 7 Dec | 2025 | 39.6 | 9.6 | 2.45 | 25.5 |
| 5R | 7 Dec | 2125 | 49.3 | 9.7 | 8.50 | 87.6 |
| 6R | 8 Dec | 0020 | 59.0 | 9.7 | 0.02 | 0.2 |
| 7R | 8 Dec | 0210 | 68.6 | 9.6 | 5.15 | 53.6 |
| 8R | 8 Dec | 0400 | 78.2 | 9.6 | 0.27 | 2.8 |
| 9R | 8 Dec | 0545 | 87.5 | 9.3 | 0.16 | 1.7 |
| 10R | 8 Dec | 0735 | 97.1 | 9.6 | 0.42 | 4.4 |
| 11R | 8 Dec | 0920 | 106.8 | 9.7 | 0.17 | 1.8 |
| 12R | 8 Dec | 1115 | 116.5 | 9.7 | 0.22 | 2.3 |
| 13R | 8 Dec | 1320 | 126.2 | 9.7 | 0.35 | 3.6 |
| 14R | 8 Dec | 1520 | 135.9 | 9.7 | 0.63 | 6.5 |
| 15R | 8 Dec | 1720 | 145.6 | 9.7 | 0.42 | 4.3 |
| 16R | 8 Dec | 1940 | 155.2 | 9.6 | 1.59 | 16.5 |
| 17R | 8 Dec | 2130 | 165.0 | 9.8 | 0.74 | 7.6 |
| 18R | 8 Dec | 2350 | 174.7 | 9.7 | 1.69 | 17.4 |
| 19R | 9 Dec | 0205 | 184.4 | 9.7 | 1.25 | 12.9 |
| 20R | 9 Dec | 0450 | 194.0 | 9.6 | 0.37 | 3.9 |
| | | Coring totals | | 186.0 | 31.49 | 16.9 |
| 129-801B- | | | | | | |
| 1R | 10 Dec | 0320 | 203.5 | 9.5 | 6.45 | 67.9 |
| 2R | 10 Dec | 0610 | 212.9 | 9.4 | 1.31 | 13.9 |
| 3R | 10 Dec | 0830 | 222.3 | 9.4 | 1.29 | 13.7 |
| 4R | 10 Dec | 1025 | 231.7 | 9.4 | 0.44 | 4.7 |
| 5R | 10 Dec | 1315 | 241.3 | 9.6 | 4.01 | 41.8 |
| 6R | 10 Dec | 1500 | 251.0 | 9.7 | 5.67 | 58.4 |
| 7R | 10 Dec | 1655 | 260.7 | 9.7 | 1.21 | 12.5 |
| 8R | 10 Dec | 1845 | 270.3 | 9.6 | 7.92 | 82.5 |
| 9R | 10 Dec | 2040 | 280.0 | 9.7 | 0.01 | 0.1 |
| 10R | 10 Dec | 2250 | 289.7 | 9.7 | 0.75 | 7.7 |
| 11R | 11 Dec | 0055 | 299.3 | 9.6 | 0.19 | 2.0 |
| 12R | 11 Dec | 0305 | 309.0 | 9.7 | 0.86 | 8.9 |
| 13R | 11 Dec | 0600 | 318.3 | 9.3 | 1.17 | 12.6 |
| 14R | 11 Dec | 0815 | 327.7 | 9.4 | 0.49 | 5.2 |
| 15R | 11 Dec | 1030 | 337.2 | 9.5 | 0.12 | 1.3 |
| 16R | 11 Dec | 1245 | 346.6 | 9.4 | 0.49 | 5.2 |
| 17R | 11 Dec | 1520 | 355.8 | 9.2 | 0.38 | 4.1 |
| 18R | 11 Dec | 1730 | 365.3 | 9.5 | 0.46 | 4.8 |
| 19R | 11 Dec | 1920 | 374.5 | 9.2 | 0.25 | 2.7 |
| 20R | 11 Dec | 2135 | 383.7 | 9.2 | 0.29 | 3.2 |
| 21R | 12 Dec | 0005 | 389.8 | 6.1 | 0.21 | 3.4 |
| 22R | 12 Dec | 0215 | 395.9 | 6.1 | 0.05 | 0.8 |
| 23R | 12 Dec | 0620 | 400.6 | 4.7 | 0.16 | 3.4 |
| 24R | 12 Dec | 0825 | 405.2 | 4.6 | 0.68 | 14.8 |
| 25R | 12 Dec | 1025 | 410.0 | 4.8 | 0.62 | 12.9 |
| 26R | 12 Dec | 1230 | 414.7 | 4.7 | 0.10 | 2.1 |
| 27R | 12 Dec | 1425 | 419.4 | 4.7 | 1.02 | 21.7 |
| 28R | 12 Dec | 1625 | 424.2 | 4.8 | 0.11 | 2.3 |
| 29R | 12 Dec | 1815 | 428.9 | 4.7 | 0.14 | 3.0 |
| 30R | 12 Dec | 2000 | 433.6 | 4.7 | 0.16 | 3.4 |
| 31R | 12 Dec | 2155 | 438.2 | 4.6 | 0.28 | 6.1 |
| 32R | 12 Dec | 2340 | 442.8 | 4.6 | 0.07 | 1.5 |
| 33R | 13 Dec | 0115 | 447.6 | 4.8 | 2.18 | 45.4 |
| 34R | 13 Dec | 0325 | 452.3 | 4.7 | 0.72 | 15.3 |
| 35R | 13 Dec | 0515 | 456.9 | 4.6 | 3.43 | 74.5 |
| 36R | 13 Dec | 0710 | 461.5 | 4.6 | 0.06 | 1.3 |
| 37R | 13 Dec | 0930 | 466.1 | 4.6 | 0.58 | 12.6 |
| 38R | 13 Dec | 1205 | 470.7 | 4.6 | 0.20 | 4.4 |
| 39R | 13 Dec | 1425 | 476.9 | 6.2 | 0.29 | 4.7 |
| 40R | 13 Dec | 1845 | 483.0 | 6.1 | 0.94 | 15.4 |
| 41R | 13 Dec | 2355 | 487.6 | 4.6 | 2.66 | 57.8 |
| 42R | 14 Dec | 0305 | 492.2 | 4.6 | 2.39 | 51.9 |
| 43R | 14 Dec | 0905 | 501.7 | 9.5 | 5.00 | 52.6 |
| 44R | 14 Dec | 1625 | 511.2 | 9.5 | 3.36 | 35.3 |
| | | Coring totals | | 317.2 | 59.17 | 18.7 |
| 129-801C- | | | | | | |
| 1R | 9 Jan 1990 | 1145 | 511.0 | 9.3 | 7.43 | 79.9 |
| 2R | 9 Jan | 1835 | 520.2 | 9.2 | 6.69 | 72.7 |
| 3R | 9 Jan | 2200 | 529.7 | 9.5 | 0.95 | 10.0 |
| 4R | 10 Jan | 0100 | 539.2 | 9.5 | 2.42 | 25.5 |
| 5R | 10 Jan | 0607 | 548.5 | 9.3 | 6.36 | 68.4 |
| 6R | 10 Jan | 1615 | 558.1 | 9.6 | 6.52 | 67.9 |
| 7R | 11 Jan | 0005 | 567.5 | 9.4 | 5.87 | 62.4 |
| 8R | 11 Jan | 0830 | 571.2 | 3.7 | 2.22 | 60.0 |
| 9R | 14 Jan | 1300 | 577.0 | 5.8 | 5.83 | 100.0 |
| 10R | 14 Jan | 2050 | 585.9 | 8.9 | 8.42 | 94.6 |
| 11R | 15 Jan | 0320 | 595.3 | 9.4 | 4.25 | 45.2 |
| 12R | 15 Jan | 1830 | 602.3 | 7.0 | 3.64 | 52.0 |
| | | Coring totals | | 100.6 | 60.60 | 60.2 |

[a] Top of Core 129-801A-1R is 8 mbsf.

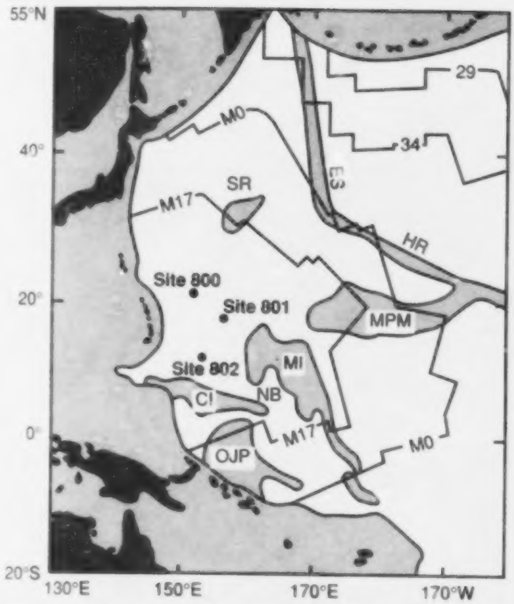

Figure 1. Location of Site 801. Bedrock isochrons are determined from magnetic anomaly lineation mapping on the Pacific plate (after Larson et al., 1985) and superimposed on groups of islands, atolls, and guyots in the western Pacific Ocean. Feature abbreviations are as follows: Caroline Islands (CI), Ontong Java Plateau (OJP), Marshall Islands (MI), Nauru Basin (NB), Mid-Pacific Mountains (MPM), Shatshy Rise (SR), Hawaiian Ridge (HR), and Emperor Seamounts (ES). Jagged contours represent normal Pacific oceanic crust. Shaded areas represent volcanic edifices with thickened crustal sections as well as younger areas beyond the Pacific subduction zones.

through the Pigafetta Basin from Site 800 to Site 801. Abundant chert was also expected at this site both in the upper and in the lower parts of the sediment column, corresponding to two successive crossings of the equatorial zone. The youngest of these crossings is believed to have occurred, from south to north, during the Late Cretaceous (Lancelot and Larson, 1975; Lancelot, 1978) and should correspond with abundant deposition of biogenic silica, later diagenetically altered into chert and/or porcellanite. These layers are probably responsible for the uppermost strong reflector observed at about 60 milliseconds below seafloor (ms bsf), both on the 3.5-kHz and water-gun seismic profiles.

The results from drilling at Site 800 have confirmed that the motion of the Pacific plate was such that the spreading ridge that generated the seafloor of the Pigafetta Basin was probably located north of the equator prior to the earliest Cretaceous, accounting for the oldest equatorial crossing from north to south, as suggested by Larson and Lowrie (1975). If productivity at the equator was comparable to what is observed for the subsequent times, this older equatorial crossing would certainly have been also characterized by abundant deposition of silica. The lowermost part of the sediment section was thus expected to be composed of chert and possibly limestone, depending on the level of the carbonate compensation depth (CCD) at the time. These deposits could be responsible for the rather strong regional reflector observed on most seismic profiles just above the horizon that we interpret as the top of the oceanic crust.

In summary, because of (1) the location of Site 801 on seafloor presumably older than the M30–M37 magnetic lineation sequence, (2) the "hummocky" character of the acoustic basement, and (3) comparison with results obtained from drilling at Sites 307 and 800, this site appeared to offer the best chance to sample Jurassic sediments and the underlying oceanic crust and hence to achieve the primary objectives of Leg 129.

If indeed the results from the single-bit pilot hole confirmed our hopes, then the site obviously would become the first choice for a major attempt at deep basement penetration with reentry. The plan, therefore, was to continuously core the pilot hole to basement, obtain a complete suite of logs in the sediment section, drill and case another hole into basement, and try to reach at least 100 to 150 m into the oceanic crust in the reentry hole. After logging the lower part of the hole and running a packer/permeability test into the crust, we intended to leave a clean-cased hole, open for future downhole experiments, as well as for further penetration into what is believed to be the oldest crust of the world ocean.

## OPERATIONS

### Approach to the Site

We approached Site 801 from the northwest on a course of 127°, parallel to MESOPAC II line 6, at 6 knots (kt), shooting a seismic line with two 80-in.$^3$ water guns (Fig. 4). Our target was a point at 0600 hr (Universal Time Coordinated, or UTC), 26 August 1989, on MESOPAC II line 10 that is perpendicular to our approach direction. At 1600 hr UTC, 6 December 1989, we crossed MESOPAC II line 6 at the target location (18°38.5′N, 154°211.6′E) and launched a beacon over a very clear seismic target on the system of the *JOIDES Resolution* corresponding exactly to MESOPAC II lines 6 and 10 (see Figs. 51, 52, and 53, "Site Geophysics and Seismic Stratigraphy," this chapter). We continued this profile on this heading until 1655 hr, when we retrieved the seismic gear, returned to the beacon location, and discovered the beacon was inoperable. Having no global positioning system (GPS) available for navigation, we hove to, acquired a transit satellite fix, and dead-reckoned back to the original drop site to deploy a second beacon, which was also a dud. This procedure was repeated again, and we finally placed a working beacon on bottom, but GPS eventually proved its location to be 1180 m south of the intended drill site. An 1180-m offset from this beacon provided marginal positioning in calm weather, so we dropped a fourth beacon at the drill site just prior to spudding into the seafloor.

### Hole 801A

The bottom-hole assembly (BHA) for Hole 801A was identical to that for Hole 800A (see "Operations" section, "Site 800" chapter, this volume). The depth to the rig floor, measured by precision depth recorder, was 5696 m. The first mud-line coring attempt was at 5698 m, and provided a core liner completely covered with soupy brown clay. We raised the bit 8 m and recovered a completely clean and empty core liner. We lowered the bit to 5699 m and recovered 6 m of soupy brown clay, establishing the mud line at 5693 m below the rig floor. A jet-in test from this depth met slight resistance at 35 mbsf and a hard layer that could not be washed through at 53 mbsf. These sub-bottom depths are about 10 m too shallow when compared with reflector depths on the 3.5-kHz records. This discrepancy was also present at Sites 800 and 307 in similar geologic environments. It might be explained by an extremely soupy seafloor that would reflect 3.5-kHz sound, but whose sediment would not be retained by the core catcher or adhere to the plastic core liner. This speculation was confirmed at Hole 801C by TV observation

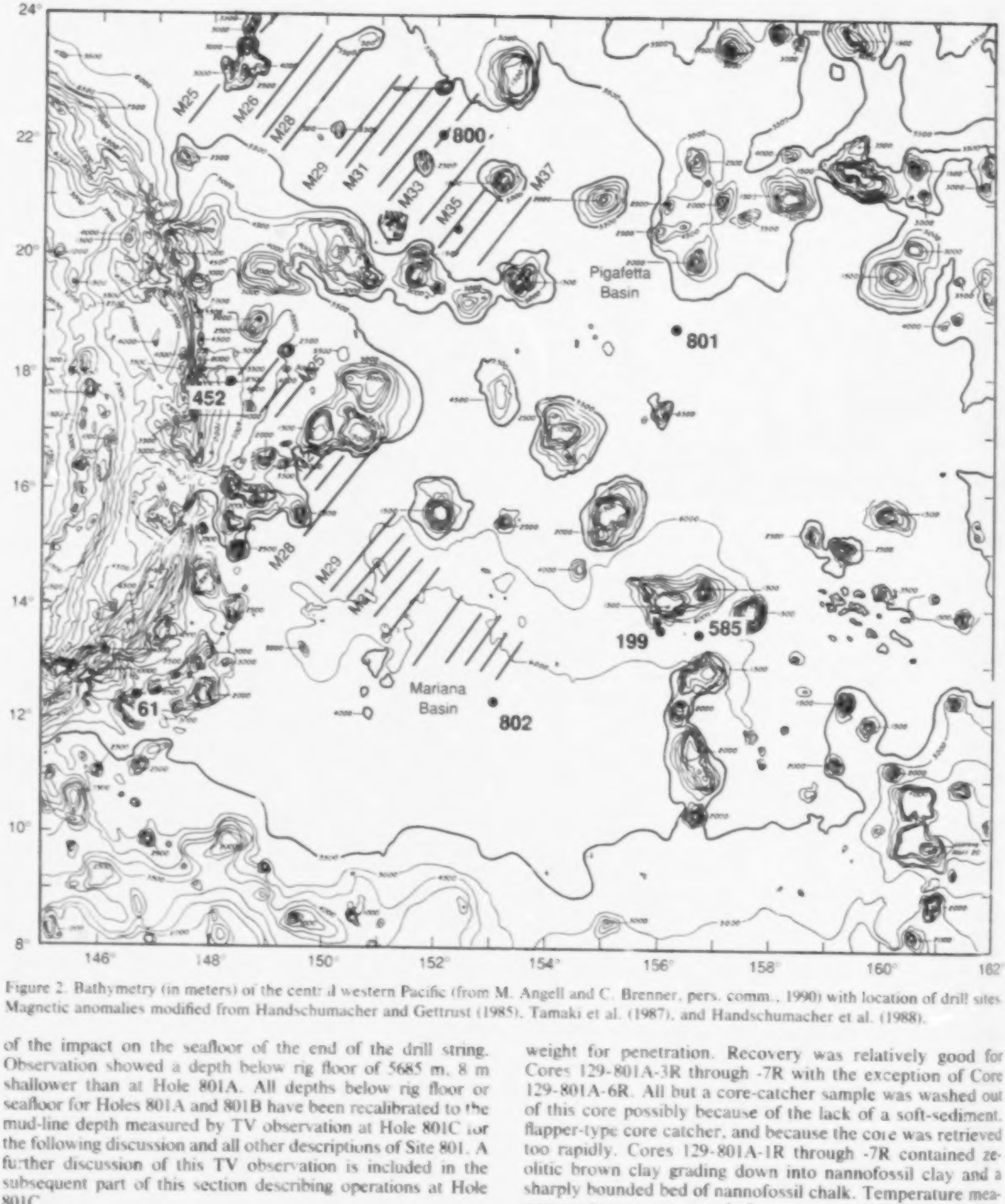

Figure 2. Bathymetry (in meters) of the central western Pacific (from M. Angell and C. Brenner, pers. comm., 1990) with location of drill sites. Magnetic anomalies modified from Handschumacher and Gettrust (1985), Tamaki et al. (1987), and Handschumacher et al. (1988).

of the impact on the seafloor of the end of the drill string. Observation showed a depth below rig floor of 5685 m, 8 m shallower than at Hole 801A. All depths below rig floor or seafloor for Holes 801A and 801B have been recalibrated to the mud-line depth measured by TV observation at Hole 801C for the following discussion and all other descriptions of Site 801. A further discussion of this TV observation is included in the subsequent part of this section describing operations at Hole 801C.

Coring proceeded without pumping or rotation for Cores 129-801A-1R through -6R. The hard layer at 61 mbsf (listed at 53 in the previous paragraph, but now corrected by the addition of 8 m as discussed above) proved to be red chert in Core 129-801A-7R and required moderate pumping and bit weight for penetration. Recovery was relatively good for Cores 129-801A-3R through -7R with the exception of Core 129-801A-6R. All but a core-catcher sample was washed out of this core possibly because of the lack of a soft-sediment, flapper-type core catcher, and because the core was retrieved too rapidly. Cores 129-801A-1R through -7R contained zeolitic brown clay grading down into nannofossil clay and a sharply bounded bed of nannofossil chalk. Temperature measurements were attempted after recovery of Cores 129-801A-3R and -5R. Both attempts were unsuccessful owing to a faulty thermistor.

Coring continued in cherts from Cores 129-801A-7R through -13R. The bit then met a sequence of claystones and mudstones with interbedded turbidites containing mainly volcaniclastic de-

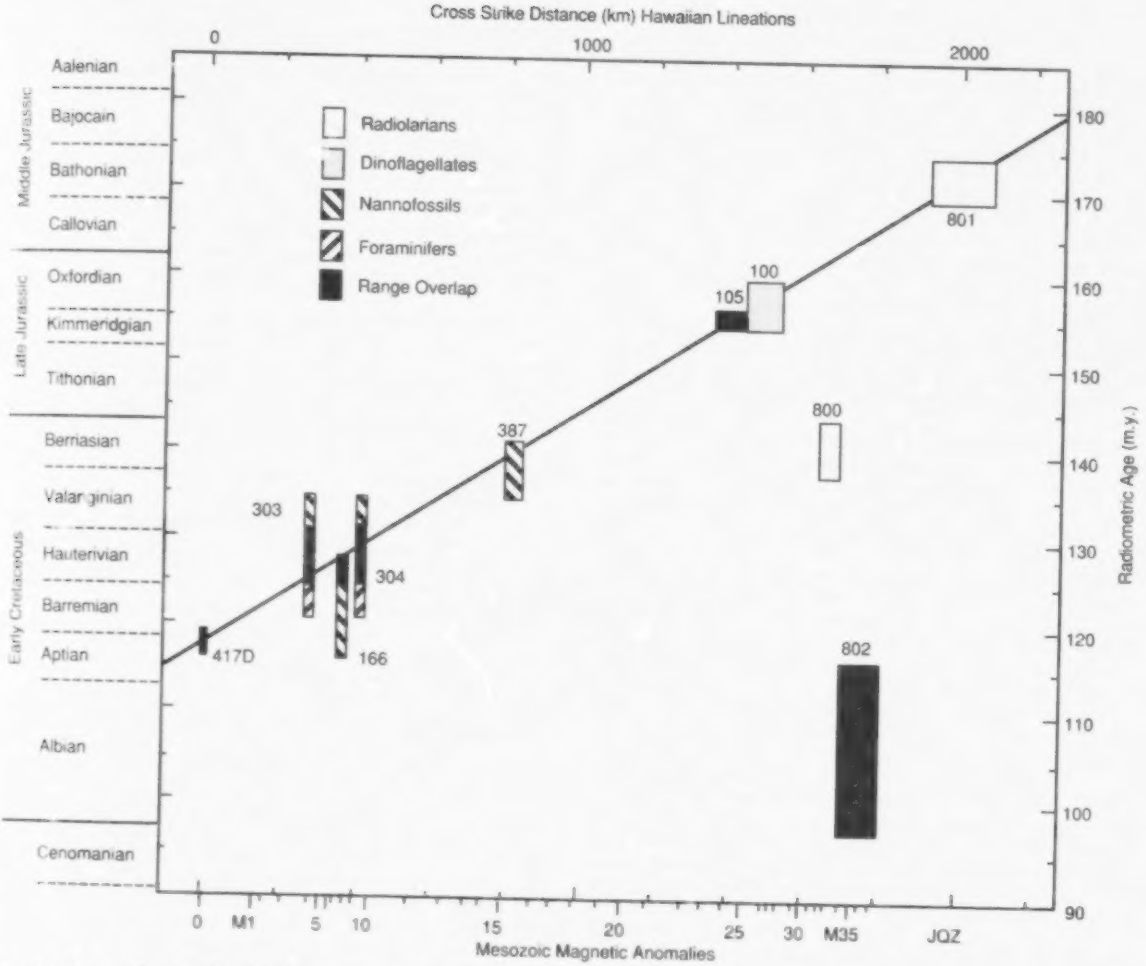

Figure 3. Time calibration plot of the Mesozoic anomalies M0 to M37 and the preceding Jurassic magnetic quiet zone (JQZ). Magnetic anomalies are plotted as cross-strike distance across the Hawaiian lineations for M0 to M25. Anomalies M25 to M37 are normalized to that parameter after Handschumacher et al. (1988). Geologic time scale and radiometric ages are from Harland et al. (1982), as modified by Kent and Gradstein (1985) at the Tithonian/Kimmeridgian boundary. Diagonal line indicates a predicted time scale constrained prior to Leg 129 that closely fits the calibration points. Oldest paleontologic ages in various DSDP holes (numbered) are shown as rectangles. Vertical lengths of rectangles show paleontological age ranges from DSDP *Initial Reports*, except for 100 (Zotto et al., 1987) and 105 (Gradstein and Sheridan, 1983). Horizontal lengths show magnetic age ranges from Larson and Hilde (1975) for DSDP Sites 303, 304, 166, 100, and 105, and from DSDP *Initial Reports* for Sites 387 and 417D. Age ranges from Sites 800, 801, and 802 are also shown.

hrs. Hole inclination surveys were taken after Cores 129-801A-16R, -18R, and -19R, with the first two showing 8° of deviation from the vertical at the bottom of the hole. This was further verified on the last inclination survey that also showed the drill pipe vertical above the mud line. Most of this excessive hole deviation probably occurred at the top of the chert sequence at 61 mbsf, either due to the bit glancing off the edge of a chert ledge or to excessive weight on bit (15,000 lb) when first penetrating the cherts.

We decided to terminate this hole after Core 129-801A-20R due to the hole deviation, offset a short distance, and spud-in Hole 801B with the same bit and BHA.

## Hole 801B

We pulled the bit approximately 20 m above the mud line and offset from Hole 801A 15 m east and 46 m south. Hole 801B was spudded at 0945 hr UTC, 9 December 1989, and drilled to the total depth of Hole 801A (194.0 m), where we measured 2.5° of hole inclination and proceeded to core ahead. It took almost an identical amount of rotating time (10 hr) to redrill this interval as it had taken in the same interval in Hole 801A.

At 194 mbsf we began continuous coring in the middle Cretaceous volcaniclastic sequence that we had recovered

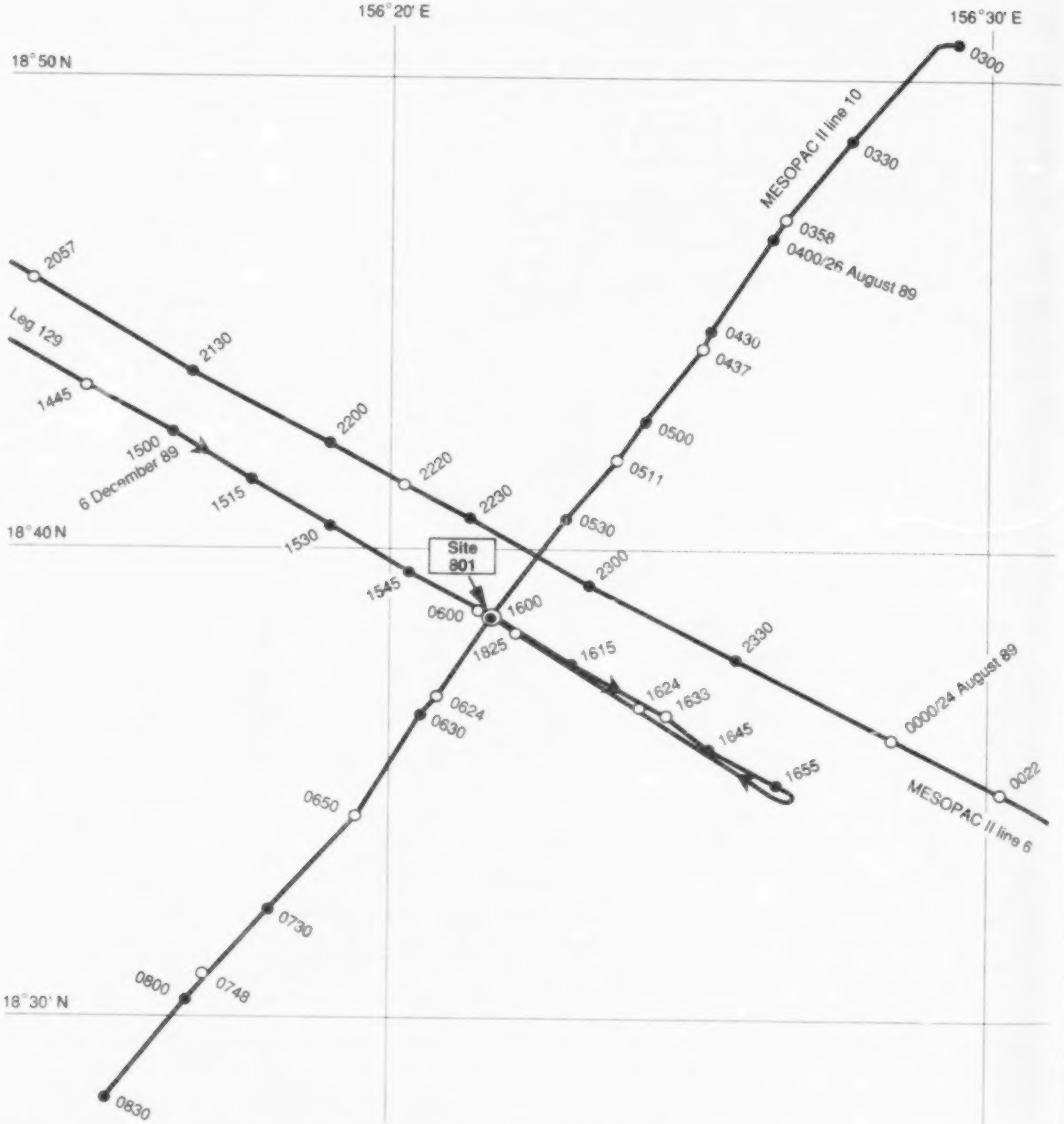
156°20' E
156°30' E
18°50 N
18°40 N
18°30' N
MESOPAC II line 10
MESOPAC II line 6
Leg 129
0300
0330
0358
0400/26 August 89
0430
0437
0500
0511
0530
0600
0624
0630
0650
0730
0748
0800
0830
2057
2130
2200
2220
2230
2300
2330
0000/24 August 89
0022
1445
1500
6 December 89
1515
1530
1545
1600
1615
1624
1633
1645
1655
1825
Site
801

Figure 4. Track chart of the expeditions MESOPAC II and Leg 129 showing the location of Site 801. Note that the Leg 129 track shown here is the initial approach to Site 801, whereas that shown in Figure 51 in the "Site Geophysics and Seismic Stratigraphy" section (this chapter) is a reshoot line run essentially coincident with the approach track after Hole 801B was completed.

from the bottom 63 m of Hole 801A. We continued in this sequence to 280 mbsf for a total thickness of 149 m of volcaniclastics. Below 280 mbsf we encountered 34 m of mixed volcaniclastics and chert from Cores 129-801B-10R through -13R, where we encountered 2 m of extremely hard drilling that correlates with a prominent seismic reflector at 300 ms twt. None of the material believed to be responsible for this reflector was recovered. Below this level (315 mbsf) we recovered only minor amounts of chert for 128 m down through Core 129-801B-32R at 443 mbsf. Half-cores were pulled from the lower portion of this interval in an effort to increase recovery. From 443 to 461 mbsf we recovered a much greater percentage of iron-enriched, umber-colored radiolarite in Cores 129-801B-33R through -36R. Basalt was then encountered interbedded with chert from 461 to 483 mbsf in Cores 129-801B-37R through -40R. Essentially solid basalt was encountered from there to the bottom of the hole at 511 mbsf, although a minor amount of baked claystone was recovered in the lowest core (Core 129-801B-44R).

This entire coring operation was conducted with no hole problems of any consequence with the exception of extremely low recovery in the chert sequence. We terminated the hole so that the sedimentary sequence could be logged while the hole was in good condition, and with the expectation of setting a reentry cone and casing to basalt at a short offset distance for an attempt at deeper penetration into basement. At total depth the bit had 55 hr of wear with no core gauge or torquing problems. However, the penetration rate in basalt had slowed to less than 2 m/hr, suggesting that the cutting structure was wearing out.

A complete wiper trip was made and mud was pumped in preparation for logging. The bit was then dropped at the bottom of the hole and the pipe bottom raised to 70 mbsf. Standard logging was conducted using exactly the same tool strings as at Hole 800A. All logs were run up to 64 mbsf, which is just below the top of the upper chert sequence. The quad combination logs bottomed at 474 mbsf, the geochemical string at 482 mbsf, and the formation microscanner (FMS) at 456 mbsf. The FMS log was run twice in the hope that the second run would be slightly rotated relative to the first, which was indeed the case. The wireline heave compensator was operational for both of the FMS runs, but not for the other runs. Logging took a total of 26 hr, after which we pulled out of the hole and began to assemble reentry hardware for Hole 801C.

## Hole 801C

We assembled a full-sized reentry cone with fixed sonar reflectors, floating sonar reflectors on 2-m-long tethers, and a fixed acoustic beacon, all for relocation purposes, and latched in 51.13 m of 16-in. conductor casing at approximately 0130 hr on 17 December 1989. The base of the conductor casing was intended to land 1 or 2 m above the top of the upper chert sequence. The drill pipe and BHA were terminated with a 14¾-in. standard oil field drill bit with no coring capability for rapid penetration through the sedimentary sequence. This entire apparatus was lowered away through the moon pool directly after latch-in of the conductor casing. Spud-in was achieved with the drilling vessel offset 20 m north of Hole 801B. The casing washed in easily to 44 mbsf where considerable pumping was required to achieve further penetration. Penetration ceased at 51 mbsf, essentially equivalent to the length of the conductor casing.

After unlatching, we proceeded to drill a casing hole through the remainder of the sedimentary section into solid basalt to a total depth of 491 mbsf. This should have provided an adequate casing seat for the main casing string, and 20 m of overlap section with the previous hole. We experienced moderate torque conditions during this drilling operation and were stuck temporarily after the hole was about half completed. Hole conditions improved when basalt was reached and most of the chert cuttings had been flushed from the hole. After drilling, a wiper trip was run to the base of the conductor casing and the hole was swept with mud. Rotation was required to regain the bottom of the hole, so it was decided to fill the lower portion of the hole with high-viscosity mud in an effort to prevent further fill. The drill string was tripped to the rig floor, and the bit was recovered intact. Two cones had undergone initial bearing failure and the third had suffered serious shirt-tail wear. About 30% of the cutting teeth were badly abraded or missing from extended drilling through chert gravel.

An 11¾-in. casing string, 479 m long, with one 3-m-long slip joint, was made up and run in. The cone was located easily with the TV camera, and less certainly with the scanning sonar. The cone was easily reentered and the casing string run into the hole without obstruction until about 25 m above the latch-in depth. Pumping and multiple raising and lowering of the pipe gained 5 m towards the bottom of the hole where a ledge that we could not pass, probably near the top of basement, was encountered. The top drive was picked up and the drill string rotated slowly to the right in an attempt to "screw past" this ledge without disconnecting the casing string at the lefthand disconnect thread. While the drill string was rotated, the casing disconnect joint was observed on the TV camera in order to verify that the casing string was also rotating with the drill pipe. The ledge was passed while allowing a maximum of about 60,000 lb to come off the total drill-string weight. We then continued to lower the drill string for an additional 5 to 10 m and to rotate it slowly with about the same weight fluctuations until the TV cable parted about 15 m below the drilling vessel with the casing shoe about 10 m from the latch-in depth.

The TV cable had most probably become wrapped around the drill pipe during lowering because its compass was seen to rotate at least 4 times during this operation. Rotation of the drill pipe may have caused additional wraps to be taken around the pipe; however, the camera was not observed to rotate during this operation. A more likely scenario is that rotating the drill string caused the previously acquired wraps to be tightened around the drill pipe so that it could not be lowered without eventually breaking the TV cable. In hindsight, it appears that the TV cable was indeed holding back the drill-string lowering, because the casing lowered much more easily into the casing seat immediately after the cable broke. It is likely that a significant fraction of the weight loss observed on the drill-pipe weight indicator prior to the cable break was the result of tension on the TV cable, which has a breaking strength of 30,000 lb.

The casing latched into the cone with the casing shoe at about 481 mbsf. This was well into the basalt which was first observed in the pilot hole 20 m away at 461 mbsf. The casing was disconnected easily by allowing the cone to support the casing string weight (120,000 lb) while rotating the drill pipe 10 turns to the right. We then cemented the casing into place and pulled out of the hole.

The pipe was brought on deck free of any junked TV cable or the TV camera frame itself. Since the wire broke when the pipe was still in the hole, we assumed that the camera fell into the cone and was still there, with 5600 m or more of camera wire attached to it. Because the spare camera flooded and was not reparable, we could not conduct the relatively simple fishing job of removing this junk from the cone until we obtained another video camera. Thus, we conducted a short post-site survey and got underway for East Mariana Basin proposed site EMB-2A, while contacting ODP headquarters to request resupply with another video system.

After successfully coring Site 802 (proposed site EMB-2A) and receiving a new TV camera by tug boat transfer, we returned to Hole 801C to fish for the lost TV system and to core ahead into the Jurassic basement. We approached the site without operating the seismic system, and acquired two weak but operational beacons when we hove to. One of these was the beacon mounted on the reentry cone, so its position was fixed. We dropped a new beacon for a stronger signal in the windy weather, detorqued the new TV cable, magnafluxed the BHA, and ran in the pipe. When the cone was viewed with the TV, we observed that it was free of all parts of the lost TV system. On orders from ODP headquarters we then spent the next 9 hr searching for the lost system in the vicinity of the cone. The camera frame itself was never spotted, but we thought we recognized the camera wire on several occasions. In three attempts to snag the wire with our fishing tool (a double-pronged fish hook designed to lock onto the camera frame), we lowered the pipe about 1 m into the mud and then offset away from the cone, "plowing" a furrow across the target area. Although we stirred up a lot of mud, we were unsuccessful in hooking onto the TV camera wire or frame. We did document the ability of a "steering jet" bored into the side of the fishing tool sub to offset the drill pipe when water was pumped through the jet with the mud pumps. After determining that it was futile to continue this exercise, we recovered the operational TV camera and the drill string in preparation for a reentry attempt with a coring bit in place.

We also documented a mud-line depth below the rig floor of 5685 m by direct observation with the TV camera of the impact on the seafloor with the fishing tool at the end of the drill pipe. This is 8 m shallower than the mud-line depth documented earlier at Hole 801A by the level of the uppermost mud smeared on the core liner of the uppermost core. Although Holes 801A and 801C are physically separated by about 30 m, our survey of the immediate area around the reentry cone indicates that the seafloor is essentially horizontal. Thus, we concluded that the mud-line depth at Holes 801A and 801B is also 5685 m below rig floor, substantiating our earlier speculation that the extremely soupy seafloor is not retained on the core liner at the seafloor level itself. Only when (in this case) 8 m of penetration had been accomplished was mud retained on the core liner. This discrepancy has been corrected throughout the Leg 129 reports by calibrating all depths below rig floor or sea level to the depth observed with the TV camera at Hole 801C.

The BHA for coring at Hole 801C was the same as that used at Holes 801A and 801B, with the addition of three stabilizers within 25 m of its base to help maintain the bit in place at the bottom of the hole, and a Rock Bit International C4 bit as the coring tool. The BHA was made up and run in to just above the seafloor, and the TV camera/scanning sonar was lowered on the exterior camera frame. The reentry cone was just coming into view on both of these instruments when they stopped working simultaneously with dead shorts to both tools. We retrieved the system after suffering some initial trepidation that we had lost a second camera frame and the attached instruments. Instead, we discovered a flooded cable connector as the cause of the malfunction. With the cable connector repaired, but the scanning sonar still on deck because of an additional electronic problem, we relowered the TV system alone on the camera frame. Reentry was eventually accomplished this time after 4 hr of efforts to minutely offset the drilling vessel in the presence of gusting 30- to 40-kt winds.

Coring proceeded without serious delays, and with the best percentage of basement recovery for the leg due to the massive and/or weathered nature of the basalts. The weather did not improve, with the winds continuing in the presence of two distinct swells forming an interference pattern that resulted in large (10°) rolls during the coring process. This, plus the large dynamic loads, large heave-compensator stroke, and marginal acoustic conditions, placed us at the use limits of several systems at once.

Core 129-801C-7R was cut at a rate of only 1.5 m/hr, and Core 129-801C-8R was cutting at less than 1 m/hr when the bit locked with a large amount of torque after 35 hr of bit life. The bit was retrieved and discovered to have lost three of its four cones, along with the shanks attached to two of the cones (Fig. 5). The hole was thus junked with about 10 kg of steel and tungsten carbide in at least three large pieces. Opinions varied as to the cause of the failure. We noted that large portions of the tungsten carbide that had made up the middle stabilizer were missing, suggesting that the bit wore out prematurely as a result of excess grinding on fragments of the missing stabilizer. This is supported by the condition of the remaining, and eventually recovered, bit cones that had all their cutting teeth nearly worn off. We also noted that one of the shank "sockets" was much more badly worn than the other, suggesting that its weld had fractured early. It had eventually fallen off and taken the rest of the lost material with it. Although the exact causes of the specific failure(s) are unknown, they are almost certainly related to the rough weather conditions we experienced during coring. The 35- to 40-kt winds, and in particular the 4- to 5-m swells, undoubtedly caused large fluctuations in weight on bit, which eventually resulted in premature failures. The lesson for future drillers is that coring during rough weather in a basalt formation will almost certainly reduce bit life by more than 50%.

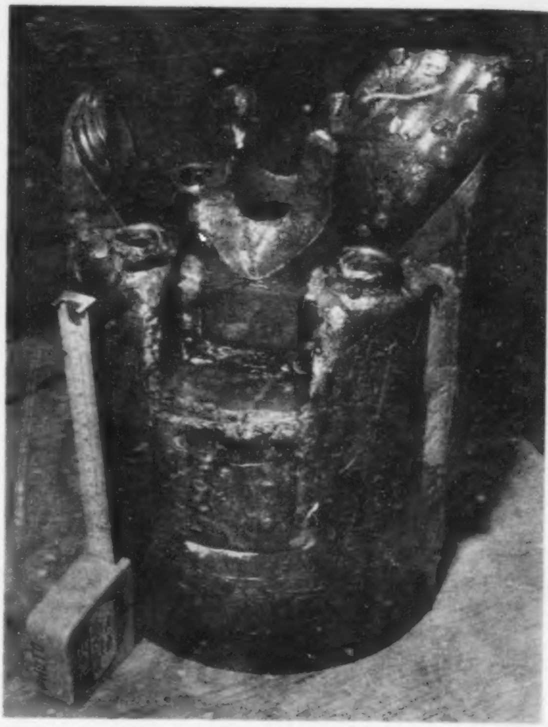

Figure 5. Broken bit used in Hole 801C. All the missing junk metal was recovered in subsequent fishing operations.

We decided to make one fishing run in an attempt to pick up the lost fragments. We employed a recirculating junk basket that allows circulation water to be diverted out of the bit sub and reverse-circulated up into the throat of the junk basket in order to pick up the junk. We ran in this assembly and after considerable effort regained the bottom of the hole, where we rotated with light bit weight and circulated both water and mud for about 1 hr. Amazingly, when the BHA was brought on deck, all three of the main broken parts were recovered, one cone/shank inside the junk basket and the other cone/shank and cone wedged tightly into its throat. We lacked only one small piece of throat-guide metal from the broken bit, and decided that would not impede subsequent coring operations.

We assembled a coring BHA, this time without the stabilizers, with a re-bearinged, F-99-CK, button-toothed coring bit, originally of Smith manufacture, that was equipped with a "boot basket" at the bit sub to trap remaining small metal parts. The drill string was run in and reentry was made without incident, and without the extreme wind conditions present at previous reentries. Coring proceeded at a slow rate of penetration but with excellent recovery. This bit run was terminated by the end of the leg with 18.5 hr of bit life. The recovered bit had broken teeth and two leaking bearing seals. The throat-guide metal from the broken bit was recovered in the boot basket, so the hole was left entirely clean for deepening on future expeditions.

## LITHOSTRATIGRAPHY AND SEDIMENTOLOGY

### Lithostratigraphy

The sedimentary section recovered at Site 801 is divided into six lithologic units based on composition, color, and presence of volcanics (Fig. 6; Table 2).

Unit I (8.0–63.8 mbsf, Cenozoic and Upper Cretaceous) is composed of pelagic clay and is subdivided into two subunits according to color. Subunit IA (8.0–41.0 mbsf, Tertiary) is dark reddish brown clay and Subunit IB (41.0–63.8 mbsf, Maestrichtian-Campanian?) is brown clay with light-colored streaks.

Unit II (63.8–126.5 mbsf, Campanian-Cenomanian) is predominantly composed of brown chert and porcellanite.

Unit III (126.5–318.3 mbsf, Cenomanian-Albian) consists of volcaniclastic turbidites with minor pelagic intervals.

Unit IV (318.3–442.9 mbsf, Valanginian-Oxfordian) consists of brown radiolarite with dark brown chert and is subdivided into two subunits according to clay content; Subunit IVA (318.3–400.6 mbsf, Valanginian-upper Tithonian) is brown radiolarite and Subunit IVB (400.6–442.9 mbsf, upper Tithonian-Oxfordian) is brown, clayey radiolarite.

Unit V (442.9–461.6 mbsf, Callovian-Bathonian) consists of alternating red radiolarite and claystone.

Unit VI (461.6–590.9 mbsf, Callovian-Bathonian) consists of basaltic sills and pillows with interbedded, silicified claystone.

Placement of the boundaries of these major lithologic units, which were generally based upon low rates of core recovery, is supported by analysis of geochemical logs from Hole 801B.

#### *Unit I. Core 129-801A-1R to Section 129-801A-7R-4, 29 cm (8.0–63.8 mbsf): Brown Pelagic Clay; Cenozoic to Maestrichtian-Campanian?*

This unit is composed of pelagic clay with different colorations. Age-diagnostic microfossils are generally lacking. The rotary coring has completely obliterated any original sedimentary structures of the soft deposits.

#### *Subunit IA. Dark Reddish Brown Pelagic Clay with Zeolites; Tertiary (Core 129-801A-1R to Section 129-801A-5R-2, 0 cm; 8.0–41.0 mbsf)*

Subunit IA extends 33 m from the first recovery at 8 mbsf to the top of underlying lighter-colored Subunit IB. This dark reddish brown, ferruginous pelagic clay contains some silt-sized globules or aggregates of iron oxyhydroxides, and zeolite (phillipsite), minor quantities of micronodules, quartz silt and rare benthic foraminifers. This facies is typical of condensed sediments deposited below the CCD.

The dark reddish brown color is derived from an abundance of fine, silt- to clay-sized globules or aggregates of iron oxyhydroxides (20%–45% of the sediment as estimated from smear slides). These semi-opaque, isotropic, or weakly birefringent dark red particles, described by Yeats, Hart, et al. (1976) as "red brown semi-opaque objects" or "RSO's," are common at other deep Pacific sites. The co-occurrence of zeolites with numerous iron oxyhydroxides indicates an intense early diagenetic process during periods of low sedimentation rates (Karpoff, 1989, and references therein).

Pale yellow to light olive brown nannofossil ooze intervals occur in the lower portion of this subunit (Sections 129-801A-4R-2 to 129-801A-5R-1). The mixed assemblages of late Paleocene and Late Cretaceous nannofossils, and the sharp contacts of pelagic clay with the layers of calcareous ooze, suggest that the layers represent redeposition events.

#### *Subunit IB. Brown Pelagic Clay with Light-colored Streaks; Paleocene-Campanian (Sections 129-801A-5R-2, 0 cm, to 129-801A-7R-4, 29 cm; 41.0–63.8 mbsf)*

Subunit IB is distinguished by lighter color, a much lower abundance of the iron oxyhydroxides aggregates, and by a generally lower abundance of zeolites. At Site 800, a similar change in the color of the pelagic clay coincides with a hiatus between Tertiary and Campanian deposits (see "Lithostratigraphy and Sedimentology" section, "Site 800" chapter, this volume). At Site 801, the uppermost portion of this subunit contains nannofossils of late Paleocene age (lower part of Core 129-801A-5R) and there are inadequate biostratigraphic data to identify a possible hiatus between the Tertiary and Cretaceous.

The pelagic clay is brown to dark reddish gray with streaks, mottles, and thin bands of reddish yellow to light yellow and is composed of clay with variable abundances of zeolites (traces to 20%) and iron oxyhydroxides aggregates (3%–5%) and with minor amounts of micronodules, radiolarian fragments, and quartz silt. The main composition difference between the brown and the light-colored streaks is the concentration of aggregates and micronodules. In the basal portion of this subunit (Section 129-801A-7R-3 and upper Section 129-801A-7R-4), there are several bands of brown radiolarian clay which progressively increase in thickness from 2 to 15 cm. These beds contain 40%–50% radiolarians and mark a transition to the underlying Unit II, which consists of brown chert and porcellanite.

#### ***Unit II. Sections 129-801A-7R-4, 29 cm, to 129-801A-14R-1, 35 cm (63.8–126.5 mbsf): Brown Chert and Porcellanite; Campanian-Cenomanian***

The sediments recovered from Unit II consist of pieces of brown radiolarian chert with porcellanite. No core from this 62.7-m-thick unit recovered more than 5% of its drilled interval; therefore, the following characterization of Unit II probably applies only to the more resistant beds.

The radiolarian chert and porcellanite are generally moderate brown to light brown, commonly with darker laminations. Several pieces display a variable degree of chertification with alternating bands of lighter-colored chert and darker-colored porcellanite (Fig. 7). Textures range from planar laminated to moderately bioturbated. Fracture surfaces commonly have manganese oxide fillings or dendrites. Chalcedony- or opal-CT-filled radiolarians and siliceous spines range in abundance from 20%–35% in thin sections and occur in a matrix made of micro- to cryptocrystalline silica, along with variable amounts of clay (Fig. 8).

Except for the lower transition zone to the underlying lithologic Unit III, Unit II is non-calcareous. Also recovered were light brown to dusky brown claystone (Cores 129-801A-8R to -11R), and light brownish gray calcareous radiolarian porcellanite (silicified clayey limestone; Core 129-801A-13R), which is 20% chalcedony-filled radiolarians, spines, and sponge spicules in a mixed matrix of micrite, clay, and silica.

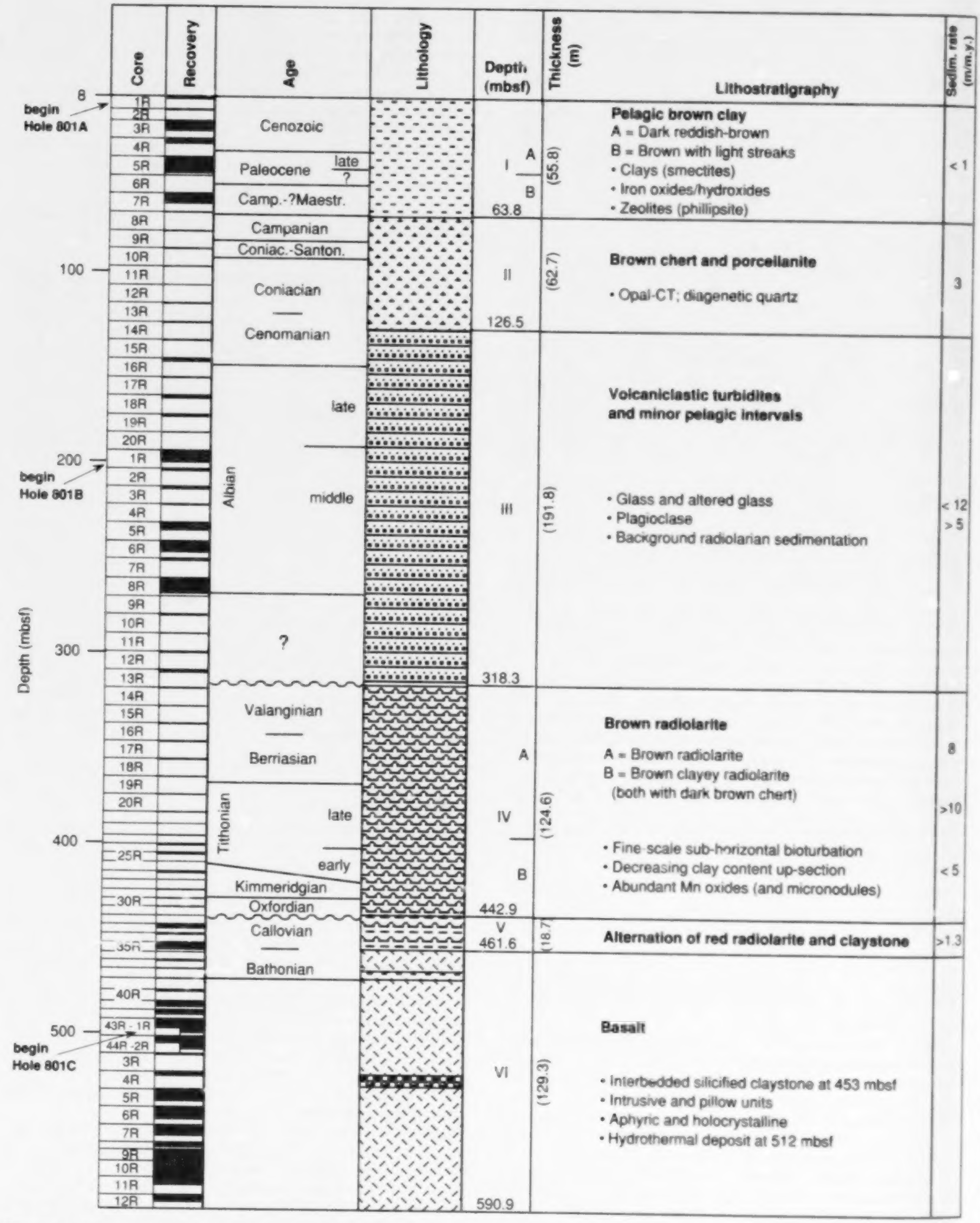
Core
Recovery
Age
Lithology
Depth (mbsf)
Thickness (m)
Lithostratigraphy
Sedim. rate (m/m.y.)
Depth (mbsf)
8
100
200
300
400
500
begin Hole 801A
begin Hole 801B
begin Hole 801C
1R
2R
3R
4R
5R
6R
7R
8R
9R
10R
11R
12R
13R
14R
15R
16R
17R
18R
19R
20R
1R
2R
3R
4R
5R
6R
7R
8R
9R
10R
11R
12R
13R
14R
15R
16R
17R
18R
19R
20R
25R
30R
35R
40R
43R - 1R
44R - 2R
3R
4R
5R
6R
7R
9R
10R
11R
12R
Cenozoic
Paleocene
late
?
Camp.-?Maestr.
Campanian
Coniac.-Santon.
Coniacian
Cenomanian
Albian
late
middle
?
Valanginian
Berriasian
Tithonian
late
early
Kimmeridgian
Oxfordian
Callovian
Bathonian
I
A
B
63.8
(55.8)
Pelagic brown clay
A = Dark reddish-brown
B = Brown with light streaks
• Clays (smectites)
• Iron oxides/hydroxides
• Zeolites (phillipsite)
< 1
II
126.5
(62.7)
Brown chert and porcellanite
• Opal-CT; diagenetic quartz
3
III
318.3
(191.8)
Volcaniclastic turbidites and minor pelagic intervals
• Glass and altered glass
• Plagioclase
• Background radiolarian sedimentation
< 12
> 5
A
IV
B
442.9
(124.6)
Brown radiolarite
A = Brown radiolarite
B = Brown clayey radiolarite (both with dark brown chert)
• Fine-scale sub-horizontal bioturbation
• Decreasing clay content up-section
• Abundant Mn oxides (and micronodules)
8
>10
< 5
V
461.6
(18.7)
Alternation of red radiolarite and claystone
>1.3
VI
590.9
(129.3)
Basalt
• Interbedded silicified claystone at 453 mbsf
• Intrusive and pillow units
• Aphyric and holocrystalline
• Hydrothermal deposit at 512 mbsf

Figure 6. Lithostratigraphy of Site 801. (Note: No recovery from 0 to 8 mbsf. Total depth is 5675 mbsl.)

These minor lithologies may be representative of poorly recovered, less competent beds.

Two trends mark a gradual transition to the underlying lithologic Unit III (volcaniclastic turbidites). First, the color of the radiolarian porcellanite changes downward from brown to gray near the top of Section 129-801A-13R-1 (116.5 mbsf), and the underlying clayey radiolarian porcellanites become progressively grayer and slightly greener with increasing abundance of interbedded volcaniclastic turbidites. Second, the abundance of calcareous beds increase downward. Core 129-801A-13R includes a piece of calcareous radiolarian porcellanite (silicified limestone), and Cores 129-801A-14R and -15R include pieces of tuffaceous nannofossil claystone and chalk with a Cenomanian nannofossil assemblage. Within this transition zone, the boundary between Units II and III was set arbitrarily as the top of the highest recovered turbidite, a piece of a feldspathic radiolarian volcaniclastic turbidite of sandy texture (Sample 129-801A-14R-1, 35–37 cm).

#### *Unit III. Sections 129-801A-14R-1, 35 cm, to 129-801B-14R-1, 0 cm (126.5–318.3 mbsf): Volcaniclastic Turbidites with Minor Pelagic Intervals; Cenomanian-Albian*

This 191.8-m-thick unit consists of volcaniclastic turbidites with scattered pelagic beds of radiolarian claystone to radiolarite, radiolarian porcellanite and chert, and nannofossil claystone to chalk. The relative abundance of turbidites and pelagic interbeds varies considerably downcore. The initiation and termination of the turbidite input appears to be gradational; the top of Unit III was set at the top of the highest volcaniclastic turbidite (Core 129-801A-14R) and the base was set at the bottom of the lowest volcaniclastic deposit (between Cores 129-801B-13R and -14R).

The deposits are dark greenish gray to medium bluish gray beds, which darken and fine upward and range from sandstone to claystone in texture. Turbidite beds in cores with good recovery display typical sequences that include basal scour, graded sediments, scattered rip-up clasts, ripple- and cross-laminations, lower bed planar lamination, and bioturbation in their uppermost portions. Consequently, sections of similar volcaniclastic sandstone to claystone are interpreted as incomplete recovery of turbidites beds.

The recovered turbidite series displays a peak in bed thickness (5 m), grain size (coarse-sand), rip-up clast concentration, and rate of accumulation (debris or fluidized flow vs. turbidite flow) in the interval from 165 to 214 mbsf (Cores 129-801A-18R to 129-801B-1R). This section of the unit includes the most "proximal" turbidite facies observed (Fig. 9). Thin sections from these highest energy turbidites contain minor amounts of red algae and echinoderm fragments, implying contributions from shallow-water sources.

The volcaniclastic turbidites are composed of glass and volcanic fragments, feldspar, pyroxene, smectites, and other clay minerals with minor iron oxides, zeolites, quartz, secondary calcite, and accessory minerals (Fig. 10). Some of the volcanic glass has been altered or palagonitized and some of these sandstones now have a clayey matrix, a precursor to a greywacke texture. The finer-grained upper layers also contain rare radiolarians, foraminifers, and nannofossils. Cores 129-801A-18R and 129-801B-5R contain calcitic sandstones with abundant calcite-replaced and -filled radiolarians, in places defining discrete through cross-laminations within the otherwise volcaniclastic sandstone. A bed of black, well-sorted sandstone in Core 129-801A-16R may represent a coarse ash-tuff deposit.

Pelagic interbeds within the uppermost four cores of the turbidite unit (Cores 129-801A-14R through -18R, 126–165 mbsf) consist mainly of grayish olive to dark gray clayey radiolarite to radiolarian porcellanite, and of dusky green to gray nannofossil claystone to tuffaceous nannofossil chalk. Fine-grained pelagic intervals through Core 129-801A-20R are finely laminated or display irregular, discontinuous laminations and weak bioturbation. Pelagic interbeds are less common in the central portion of the volcaniclastic unit (Cores 129-801A-18R through 129-801B-9R, 165–280 mbsf) and consist of pieces of dark gray chert (Core 129-801B-6R) or thin, olive gray layers of radiolarite (Core 129-801B-8R).

The four lowest cores of Unit III (Cores 129-801B-10R to -13R, 280–318 mbsf) comprise a transition zone to the underlying brown radiolarite of Unit IV. The poorly recovered sediments of Cores 129-801B-10R and -11R consist of pieces of calcareous claystone and radiolarite without volcaniclastic beds. Core 129-801B-12R is mainly fine-grained volcaniclastic turbidites. Core 129-801B-13R consists of closely spaced, 2-cm-thick, fine-grained "distal" siltstone/claystone turbidites interbedded with millimetric layers of pelagic radiolarian claystone (Fig. 11).

#### *Unit IV. Sections 129-801B-14R-1, 0 cm, to 129-801B-33R-1, 10 cm (318.3–442.9 mbsf): Brown Radiolarite; Valanginian-Oxfordian*

The Upper Jurassic and Lower Cretaceous strata of this unit consist of 125 m of brown radiolarite with scattered dark brown chert or porcellanite bands or nodules. With the exception of rare nannofossils in Cores 129-801B-25R and -26R, this siliceous facies lacks a calcareous component. The unit is subdivided into an upper, clay-poor radiolarite with abundant chert (Subunit IVA) and a lower, clay-rich radiolarite with lesser amounts of chert (Subunit IVB).

#### *Subunit IVA. Brown Radiolarite with Abundant Dark Brown Chert; Valanginian-Upper Tithonian (Sections 129-801B-14R-1, 0 cm, to 129-801B-24R-1, 0 cm; 318.3–400.6 mbsf)*

Subunit IVA consists of 81 m of brown radiolarite with abundant porcellanite and chert. Recovery was less than 5% for all cores; therefore, the following description is probably biased toward the relatively resistant lithologies. A downcore increase in the proportion of hard chert to radiolarite also corresponded to decreased core recovery.

The radiolarite is characterized by varied shades of brown from tan to dusky yellowish brown to very dark gray. Ferromanganiferous oxyhydroxides occur as spotted deposits on most natural fractures, as discontinuous microlaminations within the radiolarite and as tiny black flecks. Precipitation of manganese oxide along some fractures preceded quartz or opal fracture-filling. The radiolarite generally displays a finely laminated texture, but the discontinuous or elongate, flaser nature of these laminations suggest that they may be caused by compacted, subhorizontal bioturbation (Fig. 12). Some of the recovered pieces within Cores 129-801B-16R through -18R have a vague rhythmic banding of clay content, color darkness, radiolarian abundance, and/or degree of silicification at intervals of approximately 5 cm (Fig. 12). The poor recovery precludes identification of cyclicity, such as that observed in the coeval Lower Cretaceous radiolarite unit at Site 800 (see "Lithostratigraphy and Sedimentology" section, "Site 800" chapter, this volume).

Porcellanite or chert occurs within the radiolarite as bands of preferential silicification (Fig. 12A) or less commonly as cross-cutting nodules (Fig. 12B). These bands or nodules are dusky yellowish brown to very dark grayish brown and darker than the host radiolarite. Some pieces display tan or reddish brown mottles, thin lenses, or discoloration near fractures. Some light-colored layers in chert show many hollow radio-

**Table 2. Lithofacies of cores from Holes 801A, 801B, and 801C.**

| Core | Depth (mbsf) | Length cored (m) | Length recovered (m) | Lithology | Age |
|---|---|---|---|---|---|
| Unit I—Brown pelagic clay | | | | | |
| Subunit IA—Dark brown pelagic clay; 129-801A-1R-1, 0 cm; 8 mbsf; uppermost recovered sediment | | | | | |
| Hole 801A | | | | | |
| 1R | 8.0–14.5 | 6.5 | 1.30 | Pelagic clay with zeolites | |
| 2R | 14.5–20.4 | 5.9 | 0.50 | Pelagic clay with zeolites | ?Cenozoic |
| 3R | 20.4–30.0 | 9.6 | 5.29 | Pelagic clay with zeolites | |
| 4R | 30.0–39.6 | 9.6 | 2.45 | Pelagic clay and minor nannofossil ooze | late Paleocene |
| 5R | 39.6–49.3 | 9.7 | 8.50 | Pelagic clay and minor nannofossil ooze | Paleocene |
| Subunit IB—Brown clay with light streaks; 129-801A-5R-2, 0 cm; 41.6 mbsf | | | | | |
| 6R | 49.3–59.0 | 9.7 | 0.02 | Pelagic clay | |
| 7R | 59.0–68.6 | 9.6 | 5.15 | Pelagic clay with zeolites | ?Maestrichtian-Campanian |
| Unit II—Brown chert and porcellanite; 129-801A-7R-4, 29 cm; 63.8 mbsf; highest chert | | | | | |
| 8R | 68.6–78.2 | 9.6 | 0.27 | Chert, porcellanite | |
| 9R | 78.2–87.5 | 9.3 | 0.16 | Chert | Campanian |
| 10R | 87.5–97.1 | 9.6 | 0.42 | Porcellanite, chert | Coniacian-Santonian |
| 11R | 97.1–106.8 | 9.7 | 0.17 | Chert, porcellanite | |
| 12R | 106.8–116.5 | 9.7 | 0.22 | Chert, porcellanite | |
| 13R | 116.5–126.2 | 9.7 | 0.35 | Calcareous porcellanite | |
| | | | | Transition zone: gray cherts, below 13R-1, 2.5 cm; 116.5 mbsf | Cenomanian-Coniacian |
| 14R | 126.2–135.9 | 9.7 | 0.63 | Porcellanite, minor volcaniclastic sandstone | |
| Unit III—Volcaniclastic turbidites and pelagic intervals; 124-801A-14R-1, 35 cm; 126.5 mbsf; uppermost volcaniclastic turbidite | | | | | |
| 15R | 135.9–145.6 | 9.7 | 0.42 | Volcaniclastic sandstone, porcellanite | |
| 16R | 145.6–155.2 | 9.6 | 1.59 | Volcaniclastic sandstone to claystone | |
| 17R | 155.2–165.0 | 9.8 | 0.74 | Clayey radiolarite, calcareous claystone | |
| 18R | 165.0–174.7 | 9.7 | 1.69 | Volcaniclastic sandstone | upper Albian |
| 19R | 174.7–184.4 | 9.7 | 1.25 | Volcaniclastic siltstone | |
| 20R | 184.4–194.0 | 9.6 | 0.37 | Silty radiolarian claystone | |
| Hole 801B | | | | | |
| 1R | 194.0–203.5 | 9.5 | 6.45 | Volcaniclastic sandstone and silty claystone | |
| 2R | 203.5–212.9 | 9.4 | 1.31 | Volcaniclastic silty sandstone | |
| 3R | 212.9–222.3 | 9.4 | 1.29 | Volcaniclastic silty sandstone and clayey siltstone | |
| 4R | 222.3–231.7 | 9.4 | 0.44 | Volcaniclastic sandy claystone and sandstone | |
| 5R | 231.7–241.3 | 9.6 | 4.01 | Volcaniclastic claystone and turbidites | |
| 6R | 241.3–251.0 | 9.7 | 5.67 | Volcaniclastic turbidites | |
| 7R | 251.0–260.7 | 9.7 | 1.21 | Volcaniclastic claystone and turbidites | middle Albian |
| 8R | 260.7–270.3 | 9.6 | 7.92 | Volcaniclastic turbidites | |
| Transition zone | | | | | |
| 10R | 280.0–289.7 | 9.7 | 0.75 | Calcareous claystone, radiolarite | |
| 11R | 289.7–299.3 | 9.6 | 0.19 | Radiolarite, porcellanite | |
| 12R | 299.3–309.0 | 9.7 | 0.86 | Volcaniclastic turbidites, radiolarite and chert | |
| 13R | 309.0–318.3 | 9.3 | 1.17 | Volcaniclastic turbidites, radiolarian claystone | |
| Unit IV—Brown radiolarite | | | | | |
| Subunit IVA—Brown radiolarite with dark chert; 129-801B-14R-1, 0 cm; 318.3 mbsf; top of radiolarite prevalence | | | | | |
| 14R | 318.3–327.7 | 9.4 | 0.49 | Clayey radiolarite, procellanite | |
| 15R | 327.7–337.2 | 9.5 | 0.12 | Radiolarite to chert | |
| 16R | 337.2–346.6 | 9.4 | 0.49 | Chert, radiolarite | |
| 17R | 346.6–355.8 | 9.2 | 0.38 | Radiolarite, chert | Valanginian-Berriasian |
| 18R | 355.8–365.3 | 9.5 | 0.46 | Radiolarite, chert | |
| 19R | 365.3–374.5 | 9.2 | 0.25 | Radiolarite, chert | |
| 20R | 374.5–383.7 | 9.2 | 0.29 | Chert, radiolarite | |
| 21R | 383.7–389.8 | 6.1 | 0.21 | Chert | |
| 22R | 389.8–395.9 | 6.1 | 0.05 | Chert | |
| 23R | 395.9–400.6 | 4.7 | 0.16 | Chert, porcellanite | |
| Subunit IVB—"Woody" brown clayey radiolarite and chert; 129-801B-24R-1, 0 cm; 400.6 mbsf; highest dominance of clayey radiolarite | | | | | upper Tithonian |
| 24R | 400.6–405.2 | 4.6 | 0.68 | Clayey radiolarte, chert | |
| 25R | 405.2–410.0 | 4.8 | 0.62 | Clayey radiolarite, chert | |
| 26R | 410.0–414.7 | 4.7 | 0.10 | Clayey radiolarite, chert | |
| 27R | 414.7–419.4 | 4.7 | 1.02 | Chert, clayey radiolarite | lower Tithonian |
| 28R | 419.4–424.2 | 4.8 | 0.11 | Chert, clayey radiolarite | |
| 29R | 424.2–428.9 | 4.7 | 0.14 | Chert, clayey radiolarite | |
| 30R | 428.9–433.6 | 4.7 | 0.16 | Chert, clayey radiolarite | Kimmeridgian |
| 31R | 433.6–438.2 | 4.6 | 0.28 | Chert, clayey radiolarite | |
| 32R | 438.2–442.8 | 4.6 | 0.07 | Brown clayey radiolarite | Oxfordian |
| Unit V—Alternations of red radiolarite and claystone; 129-801B-33R-1, 10 cm; 442.9 mbsf; highest red coloration | | | | | |
| 33R | 442.8–447.6 | 4.8 | 2.18 | Red radiolarite, claystone | Callovian |

Table 2 (continued).

| Core | Depth (mbsf) | Length cored (m) | Length recovered (m) | Lithology | Age |
|---|---|---|---|---|---|
| 34R | 447.6–452.3 | 4.7 | 0.72 | Claystone, red radiolarite | Callovian-Bathonian |
| 35R | 452.3–456.9 | 4.6 | 3.43 | Claystone, red radiolarite | |
| 36R | 456.9–461.5 | 4.6 | 0.06 | Red radiolarite, claystone | |
| Unit VI—Interbedded basalt and silicified claystone: 122-801B-37R-1, 7 cm; 461.6 mbsf; highest brecciated chert | | | | | |
| 37R | 461.5–466.1 | 4.6 | 0.58 | Brecciated chert, basalt | |
| 38R | 466.1–470.7 | 4.6 | 0.20 | Basalt, brecciated chert | |
| 39R | 470.7–476.9 | 6.2 | 0.29 | Basalt, chertified radiolarian claystone | |
| 40R | 476.9–483.0 | 6.1 | 0.94 | Basalt | |
| 41R | 483.0–487.6 | 4.6 | 2.66 | Basalt | |
| 42R | 487.6–492.2 | 4.6 | 2.39 | Basalt | |
| 43R | 492.2–501.7 | 9.5 | 5.00 | Basalt, limestone fragment | |
| 44R | 501.7–511.2 | 9.5 | 3.36 | Basalt, claystone | |
| Hole 801C | | | | | |
| 1R | 493.7–503.0 | 9.3 | 7.43 | Basalt | |
| 2R | 503.0–512.2 | 9.2 | 6.69 | Basalt | |
| 3R | 512.2–521.7 | 9.5 | 0.95 | Basalt | |
| 4R | 521.7–531.2 | 9.5 | 2.42 | Silica and iron hydrothermal deposit | |
| 5R | 531.2–540.5 | 9.3 | 6.36 | Basalt, minor calcareous claystone | |
| 6R | 540.5–550.1 | 9.6 | 6.52 | Basalt, minor calcareous claystone | |
| 7R | 550.1–559.5 | 9.4 | 5.87 | Basalt | |
| 8R | 559.5–563.2 | 3.7 | 2.22 | Basalt, minor metalliferous claystone | |
| 9R | 563.2–569.0 | 5.8 | 5.83 | Basalt, minor siliceous claystone | |
| 10R | 569.0–577.9 | 8.9 | 8.42 | Basalt | |
| 11R | 577.9–587.3 | 9.4 | 4.25 | Basalt | |
| 12R | 587.3–594.3 | 7.0 | 3.64 | Basalt | |

larian molds, in contrast to the chalcedony-filled radiolarians common in the darker chert or radiolarite.

Thin-section analyses reveal that the radiolarite, chert, porcellanite, and radiolarian claystone differ only in the relative proportions of the main components: radiolarians, silica, clay, and iron-manganese oxides. Layers of radiolarians are alternately grain- or matrix-supported, making up 10%–60% of the bulk lithology. These radiolarians, usually completely replaced by microcrystalline quartz or chalcedony, are difficult to distinguish from the matrix, which is composed of iron-manganese oxides, clay, and silica. Silica does not include opal-CT below Core 129-801B-20R. Radiolarians and rare foraminifers are often sites of precipitation of oxides (Fig. 13). Interstitial iron-manganese oxides comprise 5%–20% of most thin sections.

Brecciation of chert progressively intensifies from Cores 129-801B-16R through -21R, then becomes less important in Core 129-801B-22R and below. Most fractures in this interval are filled by one or more generations of macroquartz or chalcedony; drusy, quartz-lined, open voids, up to 3 by 8 mm, occur in Cores 129-801B-20R and -21R (Fig. 14). In some breccias, fragments of siliceous radiolarite are separated from adjacent chert with similar texture by the quartz-filled fractures, suggesting that the brecciation and quartz-filling of resulting fractures occurred prior to full chertification, differentially affecting the rates of silicification of each piece.

### *Subunit IVB: Brown Clayey Radiolarite; Upper Tithonian-Oxfordian (Sections 129-801B-24R-1, 0 cm, to 129-801B-33R-1, 10 cm; 400.6–442.9 mbsf)*

The lowermost 42 m of Unit IV consist of a brown clayey radiolarite with approximately equal amounts of clay and radiolarians. The contact between Subunits IVA and IVB was placed at the top of the highest core in clayey radiolarite was recovered (Core 129-801B-24R). The estimated average clay content of Subunit IVB is 40%–50% vs. 10%–20% in Subunit IVA. The transition between clay-rich and clay-poor strata appears to be sharp in the cores. The recovery of this subunit was enhanced by a combination of a decrease in the size of each core (4.7 m/core vs. 9.4 m/core for overlying units), and by a lesser amount of chert.

The clayey radiolarite is dark brown, mottled or banded by light yellowish brown to pink. The mottling commonly cuts across burrows and laminations and is probably due to mobilization and differential staining by iron-manganese oxyhydroxides (Fig. 15A). Slightly lighter-colored bands seem to be richer in radiolarians, whereas darker-colored bands seem to be richer in clay and minor amounts of volcanic glass. Most radiolarians are filled by microquartz (Fig. 16), with calcite-filled radiolarian casts present in Core 129-801B-29R.

Manganese micronodules, 1–2 mm in diameter, which occur scattered in the radiolarite or in clusters subparallel to the laminated fabric, are less common in the chert. However, the presence of micronodules in porcellanite and chert indicates that their formation partially predates silicification. Oxides also occur as black flecks or streaks, as replacement of microfossil tests, and as dendritic spots on fractures (Fig. 15A).

The clayey radiolarite has a distinctive "woody" texture of subhorizontal streaks, discontinuous planar to irregular laminations and thin, elongate lenses (Fig. 15A). This texture could be the result of subhorizontal burrows and bioturbation that underwent considerable and differential compaction. Continuous laminations are much less common.

Chert or radiolarian porcellanite occurs as secondary lenses within the clayey radiolarite, or was recovered as separate pieces (Fig. 15B). The chert is typically very dark brown, commonly with reddish brown coloration in layers, lenses, burrows, mottles, and adjacent to fractures. Quartz-filled fractures display multiple generations of silica precipitation and locally influence the degree of oxidation of the host rock (Cores 129-801B-27R to -30R). A higher abundance of chert relative to clayey radiolarite in the lower half of Subunit IVB may be an artifact of recovery.

In Core 129-801B-27R (414.7 mbsf) and below, the recovered blocks have an apparent dip of 10°, increasing to 30° in

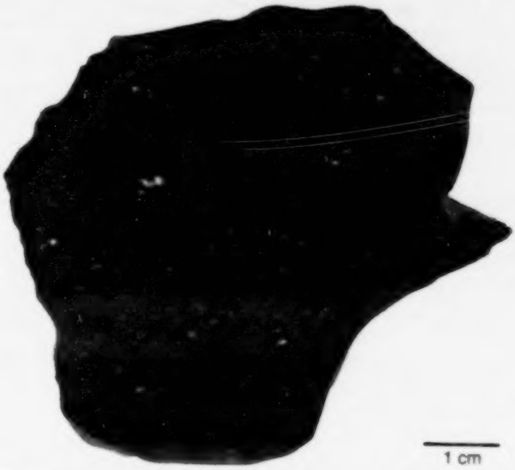

Figure 7. Brown radiolarian porcellanite with bands of lighter-colored chert typical of lithologic Unit II (Campanian-Cenomanian). Moderate bioturbation. Interval 129-801A-10R-1, 8–15 cm.

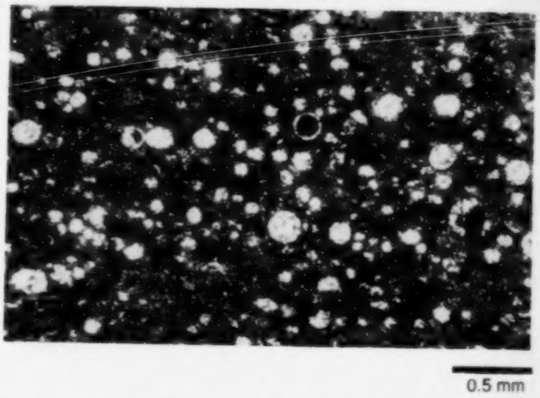

Figure 8. Photomicrograph of radiolarian porcellanite typical of lithologic Unit II, Campanian-Cenomanian. Radiolarians are commonly infilled with opal-CT or chalcedony. Crossed nicols. Sample 129-801A-13R-1, 18–20 cm.

Core 129-801B-33R. This apparent dip exceeds the measured 2¼° deviation of the drilling from vertical, indicating that the strata have a moderate tectonic or depositional dip.

### *Unit V. Sections 129-801B-33R-1, 10 cm, to 129-801B-37R-1, 7 cm (442.9–461.6 mbsf): Alternations of Red Radiolarite and Claystone; Callovian-Bathonian*

The lowest major sedimentary unit at Site 801 consists of 18 m of red, interbedded radiolarite and claystone. The boundary between Units IV and V was placed at the highest appearance of red coloration. This color boundary, which appears as a sharp contrast in a piece of radiolarite in the uppermost portion of Core 129-801B-33R, also corresponds to a change in degree of lithification.

Alternations of radiolarite and claystone average about 5 cm, but have irregular spacing. Contacts between the two lithologies are generally sharp (Fig. 17). However, thin sections show that the boundaries are gradual on a millimeter scale, suggesting that the lithologic variations reflect changes in primary sedimentation deposition or the intensity of winnowing, rather than redeposition events (Fig. 18).

Radiolarite layers are generally yellowish red to brick red, silty in texture, vaguely laminated to weakly bioturbated, and contain intervals with anastomosing clay-rich seams or lenses of partial silicification (Fig. 17). Claystone layers are slightly darker red with respect to adjacent radiolarite bands, and are featureless to moderately bioturbated. They lack the distinctive "woody" texture of Unit IV.

Several types of alteration features are common in both lithologies. Reduction mottles (patches of light greenish gray to white) cut across layering and bioturbation, occur adjacent to some fractures, or are present as elongate lenses parallel to bedding. Zones of diffuse brownish yellow are adjacent to some fractures. White, translucent, silica-lined fractures are common whereas manganese oxides coat rare fractures, and are much less common than in overlying Unit IV. Pieces of varicolored chert and breccia were recovered only in the uppermost portion of Core 129-801B-34R, and probably represent contamination from strata uphole.

The bedding has an apparent dip of 27°–30° (pieces of Core 129-801B-33R) and one large intact block in Core 129-801B-35R (at 99–110 cm) has an apparent dip of 60°.

The base of this unit was placed above the uppermost reddish brown chert, representative of silicified sediments interbedded with basalts, at Core 129-801B-37R, 7 cm. The uppermost sediment piece of Core 129-801B-37R is a pink radiolarite with brown porcellanite, similar to the "woody" textured, brown radiolarite of Subunit IVB. However, its Callovian-Bathonian radiolarian assemblage (see "Biostratigraphy" section, this chapter), suggests that this pink radiolarite may represent a lithology which was not recovered in the 4.6-m interval spanned by Core 129-801B-36R. Regardless, the division of Site 801 into lithologic units must rely on the actual recovered sediments; therefore, the very distinct lithologic change between radiolarite and underlying chert near the top of Core 129-801B-37R is used as the base of Unit V.

### *Unit VI. Sections 129-801B-37R-1, 7 cm, to 129-801B-44R-3, 47 cm, and Cores 129-801C-1R to 129-801C-12R (461.6–590.9 mbsf): Interbedded Basalt and Silicified Claystone (Chert); Callovian-Bathonian*

The lowermost 133 m drilled at Site 801 consist of fine-grained basalt and microdolerite flows and sills (see "Igneous Petrology" section, this chapter), interbedded with red to brown chert and metasediments.

Above the highest recovered basalts (Section 129-801B-37R-1), and also occurring as probable cavings at the top of Core 129-801B-38R, are fragments of silica-cemented and -replaced claystone breccia, approaching chert in hardness (Fig. 19). The reddish brown claystone is intensely crackle brecciated, such that in places the pieces would fit back together (Fig. 20A, -B). Drusy quartz fills most of the fractures between clasts, but some open voids exist. Brecciation probably occurred during rapid dewatering or fluid injection associated with the heating of soft clay by the adjacent basalt. Similar breccia pieces occur at the tops of Cores 129-801B-40R and -41R. These may be contamination from the same breccia zone of Core 129-801B-37R.

Interflow sediments in Core 129-801B-39R consist mainly of dark brown chert with grayer mottles and dark, silicified radiolarite (Fig. 20C, -D). Faint burrow-mottling is marked by silica-filled radiolarians.

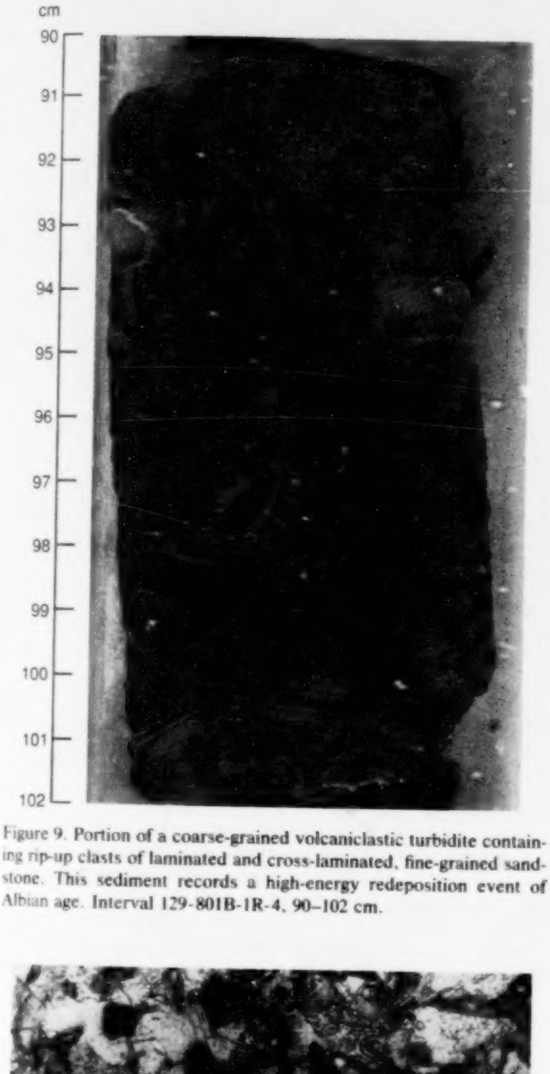

Figure 9. Portion of a coarse-grained volcaniclastic turbidite containing rip-up clasts of laminated and cross-laminated, fine-grained sandstone. This sediment records a high-energy redeposition event of Albian age. Interval 129-801B-1R-4, 90–102 cm.

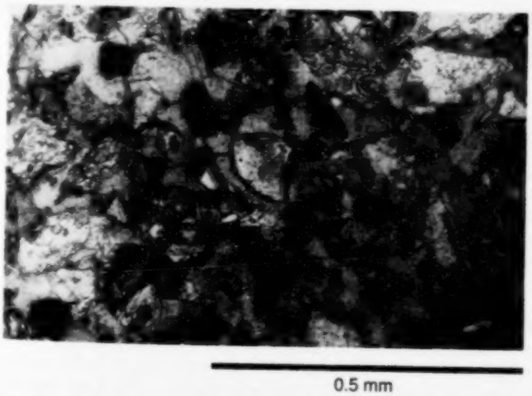

Figure 10. Photomicrograph of volcaniclastic sandstone (lithologic Unit III) with volcanic glass and igneous fragments with minor feldspar, opaques and oxides, pyroxene, and calcite. Crossed nicols. Sample 129-801A-19R-1, 1–4 cm.

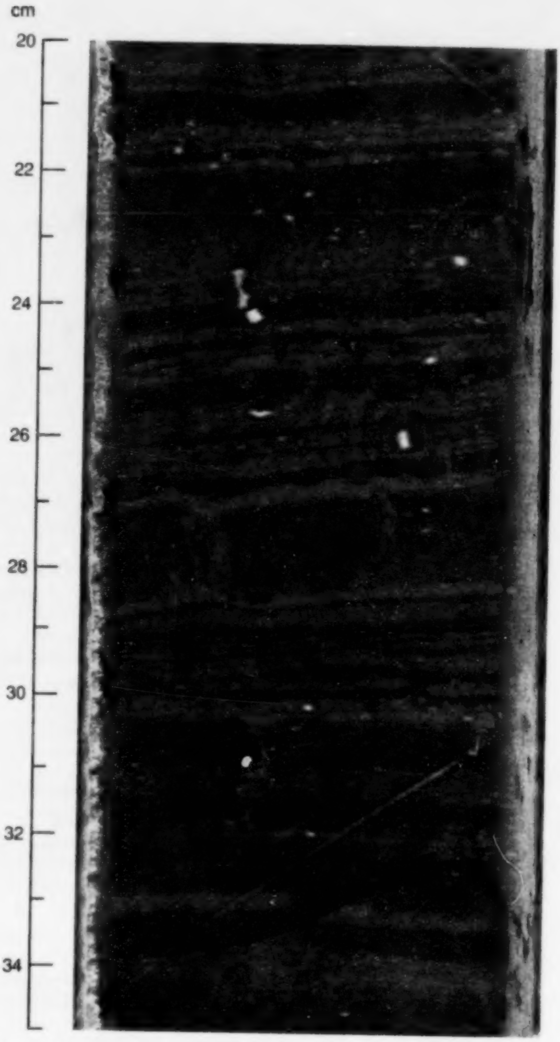

Figure 11. Fine-grained, fining-upward volcaniclastic turbidites (base of lithologic Unit III; middle Cretaceous) consisting mainly of altered volcanic glass and igneous rock fragments, interbedded with lighter-colored radiolarian claystone containing rare nannofossils. Interval 129-801B-13R-1, 20–35 cm.

Recrystallized limestone occurs between basalt flows in interval 129-801B-43R-3, 76–81 cm (Fig. 20E). Irregular pods of gray crystalline calcite are in a matrix of relatively porous white calcite. The piece contains rare nannofossils and very small (<0.3 mm) patches of lapilli partially replaced by calcite.

Between the basalt pillows in Cores 129-801B-40R to -44R are 1- to 5-cm-thick beds of red claystone. Core 129-801B-44R also contains volcaniclastic metasediments with recrystallized microfossils(?) overlain by iron-rich radiolarian metasiltstone (Fig. 20F).

Core 129-801C-4R consists of a yellow hydrothermal deposit of iron hydroxide (goethite) associated with silica. Thin-section observations indicate a multi-stage diagenetic history as yellow iron hydroxide deposits grew outward as radially

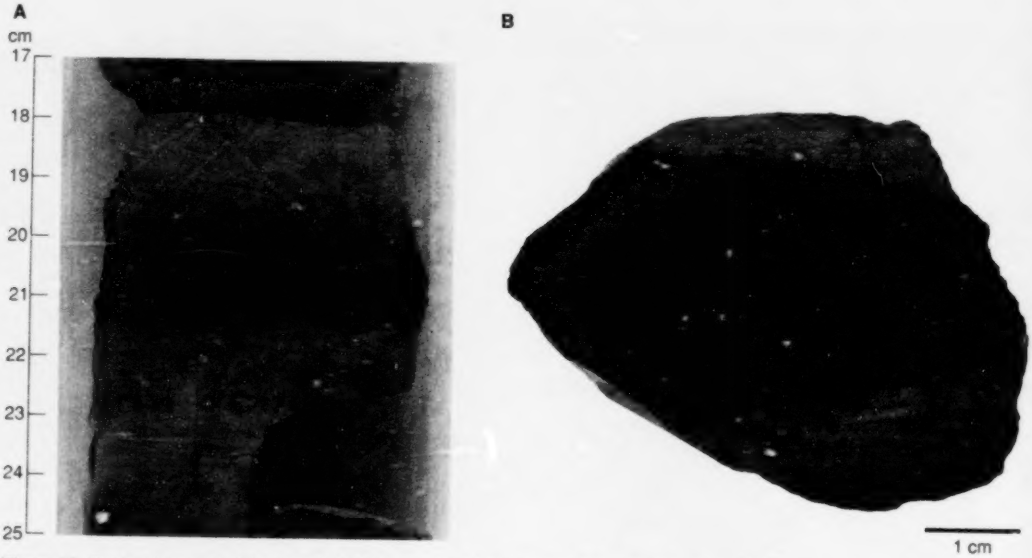

Figure 12. Typical brown radiolarite and dark brown chert of lithologic Subunit IVA. **A.** Radiolarite with discontinuous streaks and wispy, elongate flaser laminations subparallel to bedding that may be partially caused by compaction of fine subhorizontal bioturbation. Black streaks and spots are concentrations of iron-manganese oxides; dark layer in middle of center piece is silicified to chert. Note light-colored reduction mottles. Interval 129-801B-18R-1, 17–25 cm (Berriasian-Valanginian). **B.** Progressive chertification with radiolarite. An irregular, thin zone of lighter-colored porcellanite is between the dark brown chert and the outer radiolarite. Interval 129-801B-17R-1, 29–33 cm (Berriasian-Valanginian).

fibrous, coalescing, botryoidal masses, commonly zoned, then divided into platelets, followed by partial replacement by triple-junctioned quartz crystals. Larger quartz crystals fill secondary veins that traverse the deposit.

Red calcareous claystone, siliceous claystone, and chert occur between basalt flows throughout the lower portion of Hole 801C, with thicker intervals having depositional contacts to chill margins of basalt pillows recovered in intervals 129-801C-5R-4, 8–31 cm, and 129-801C-8R, 17–32 cm.

### Carbonate Analyses

The percentage of carbonate remains very low throughout all these sedimentary facies (Table 3, Fig. 21). The few exceptions consist of rare nannofossils chalk beds in Unit II and some volcaniclastic turbidites beds of Unit III which contain shallow-water carbonate debris or nannofossils.

### Sedimentation History of Site 801

The recovered sedimentary record of Site 801, when integrated with geophysical data on the motion and subsidence of this portion of the Pacific plate and with sedimentary facies data from nearby DSDP and ODP sites, provides a preliminary synthesis of the main features of its sedimentation history.

From the paleomagnetic data for Site 801 (see "Paleomagnetics" section, this chapter), the estimated paleolatitudes imply that the site was within or near the zone of equatorial divergence and upwelling during most of its Mesozoic history.

#### *Callovian-Bathonian to Basal Oxfordian: The Interflow Sediments and Hydrothermal Deposit, and the Red Radiolarite and Claystone*

During the formation of the basal igneous complex, various deposits were trapped between pillows or thin sheet flows of aphyric basalt and underwent significant recrystallization. The metasediments include silicified red claystone and radiolarian claystone, recrystallized gray limestone, and reddish calcareous and silicified tuff (Fig. 20). Hydrothermal processes produced an interval of at least 3 m of yellow siliceous iron oxyhydroxide deposit (Core 129-801C-4R).

The occurrence of calcareous layers and scarce nannofossils suggests either that the ridge site was above the CCD or that peculiar conditions of local chemistry enabled pockets of calcareous sediments to be preserved.

The biogenic siliceous and clayey sediments have a high content of metal oxides as hematite. The lowest silicified claystone breccia above the basalt (Section 129-801B-37R-1) probably resulted from rapid dewatering or fluid injection associated with the emplacement of the adjacent basalt.

Callovian-Bathonian sediments (Unit V) consist of red, hematite-rich alternations of claystone and radiolarite with an average repetition at intervals of approximately 5 cm (Fig. 17). A minimum sedimentation rate of 1.3 m/m.y. for this unit can be calculated assuming that sedimentation extended continuously through the Bathonian and Callovian. This implies that the alternations have a maximum average duration of 38,000 yr. The distinct radiolarian concentration and sharp contacts between the radiolarite and claystone layers are similar to radiolarian sand horizons observed in the Callovian of Atlantic Site 534 (Ogg et al., 1983) and in the upper Cenomanian of Atlantic Sites 386 and 387 (McCave, 1979). Three main hypotheses have been suggested to explain the contrast between these layers at Atlantic occurrences: (1) episodic blooms of high radiolarian productivity, (2) radiolarian-rich redeposition events, and (3) bottom-current winnowing and concentration of radiolarians followed by differential silica dissolution between radiolarian-enriched and -depleted layers. According to a thin-

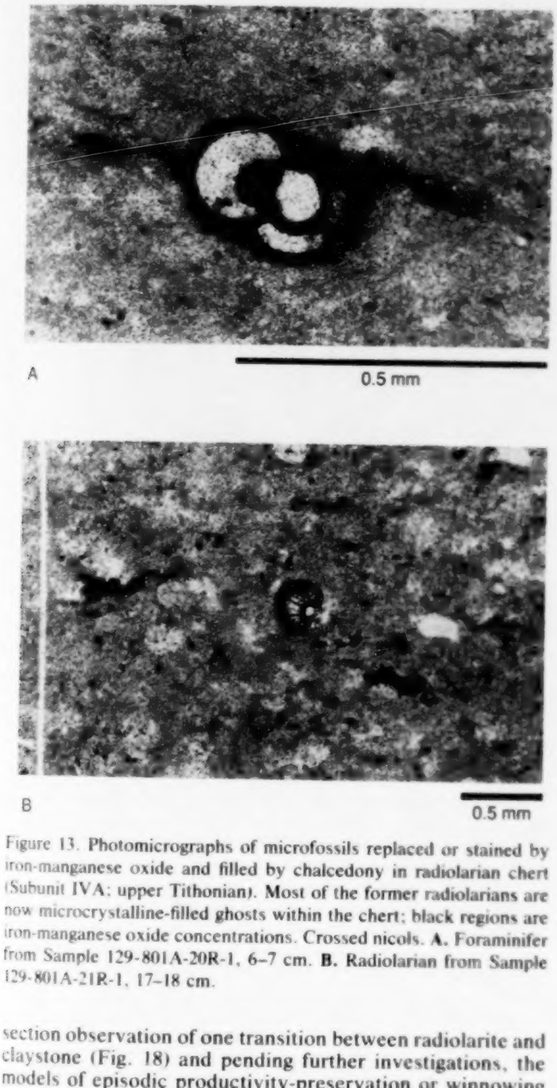

Figure 13. Photomicrographs of microfossils replaced or stained by iron-manganese oxide and filled by chalcedony in radiolarian chert (Subunit IVA; upper Tithonian). Most of the former radiolarians are now microcrystalline-filled ghosts within the chert; black regions are iron-manganese oxide concentrations. Crossed nicols. **A.** Foraminifer from Sample 129-801A-20R-1, 6–7 cm. **B.** Radiolarian from Sample 129-801A-21R-1, 17–18 cm.

section observation of one transition between radiolarite and claystone (Fig. 18) and pending further investigations, the models of episodic productivity-preservation or winnowing of radiolarians are favored.

Hematite enrichment of the Callovian strata may result from the combined effect of well-oxygenated bottom waters and the proximity of the site to the effluent of metal-rich hydrothermal waters produced at the active spreading ridge (Boström and Peterson, 1965; Bonatti, 1981). Localized reduction mottles post-date oxidation of the sediment that occurred at the surface. Low sedimentation rates and proximity to the ridge axis contributed to the iron and manganese enrichment of these sediments.

#### *The Callovian-Oxfordian Boundary*

The distinct lithologic boundary between the Callovian red radiolarite and claystone (Unit V) and the Oxfordian brown clayey radiolarite (Unit IVB) is probably a hiatus or a condensed section marked by: (1) a distinct upward color change from red to brown with corresponding enrichment in oxides, (2) a change in style of sedimentation from alternating layers to a more homogeneous clayey radiolarite, (3) a change in average apparent dip of bedding from about 30° in Callovian-Bathonian strata to about 10° in Upper Jurassic strata, and (4) a gap in radiolarian zones. The change in apparent dip suggests that tectonic tilting may have occurred. Worldwide, the contact between Oxfordian and Callovian marine sediments is commonly a hiatus, with upper Callovian and/or lower Oxfordian sediments being absent or extremely condensed. The presence of a hiatus between Callovian-Bathonian and Oxfordian at Site 801 may also be a manifestation of the general global events demarcating the Middle/Late Jurassic boundary, and not solely a local tectonic coincidence.

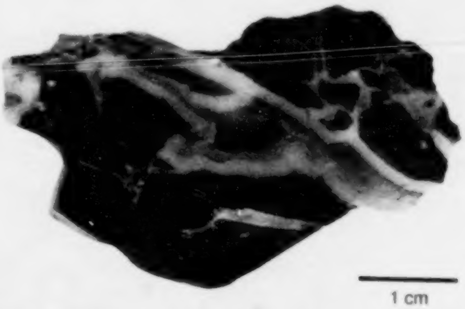

Figure 14. Brecciated radiolarian chert from the lower part of Subunit IVA (upper Tithonian). Fractures in the dark brown chert are completely filled with multiple generations of quartz; an open void is lined by drusy quartz. Siliceous radiolarite is separated from adjacent chert with similar texture. Sample 129-801B-21R-1, 19–22 cm.

### ***Oxfordian to Valanginian: The Brown Radiolarite Deposition and Diagenesis***

#### *Depositional Environment and Change of Sedimentation of the Siliceous and Clayey Facies*

Variations on the scale of several centimeters occur in the relative radiolarian concentration, in the development of porcellanite or chert, and in the character of the quasi-laminated texture. These small-scale variations suggest the possibility of periodic changes in siliceous productivity; however, recovery was inadequate to unequivocally demonstrate cyclicity, such as that described in coeval sediments at nearby sites: the Berriasian-Valanginian of Site 800 (see "Lithostratigraphy" section, "Site 800" chapter, this volume) and in the Lower Cretaceous limestones at Site 167 on Magellan Plateau (Winterer, Ewing, et al., 1973; Cotillon, 1984, 1985).

The less silicified radiolarites generally exhibit a streaky, discontinuous-laminated, "woody" texture, which is interpreted as the result of compaction of sub-horizontal bioturbation. Less distorted bioturbation occurs in some intervals. No definite evidence either of low-oxygen bottom water or of bottom-current activity was noted, which suggests that deposition was on a quiet, but oxygenated, seafloor.

Within the brown radiolarite sequence (Unit IV) the relative abundance of radiolarians increases upward, reaching a maximum in the upper Tithonian sediments. The Oxfordian-lower Tithonian clayey radiolarite (Subunit IVB) implies an average sedimentation rate of less than 5 m/m.y. In contrast, the thickened upper Tithonian-Valanginian radiolarite (Subunit IVA) has an apparent sedimentation rate of about 8 m/m.y. (Fig. 24). In between, the upper Tithonian,

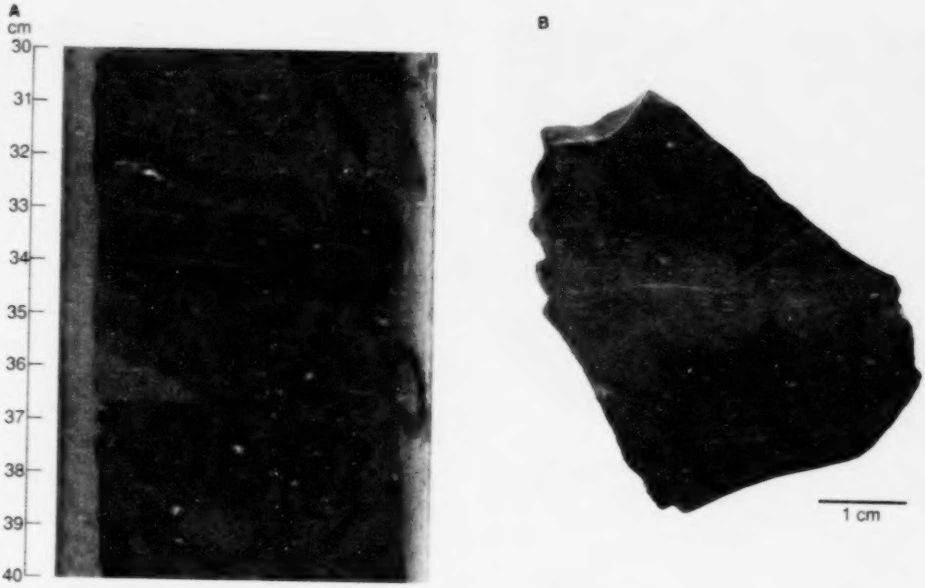

Figure 15. Typical clayey radiolarite and radiolarian chert of lithologic Subunit IVB. **A.** Clayey radiolarite. Discontinuous streaks and wispy, elongate flaser laminations subparallel to bedding may be partially caused by compaction of fine subhorizontal bioturbation. Black spots and streaks are concentration of iron-manganese oxide; reduction mottling is also present. Interval 129-801B-27R-1, 30–40 cm (lower Tithonian). **B.** Radiolarian chert formed by silicification of clayey radiolarite. The dark brown chert has weak bioturbation to wispy laminations, black spots of concentrated iron-manganese oxide, and a reduction mottle of reddish brown in the center. Interval 129-801B-28R-1, 10–14 cm (Kimmeridgian-lower Tithonian).

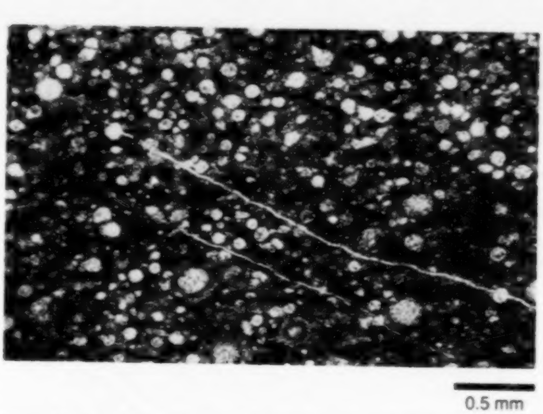

Figure 16. Photomicrograph of typical clayey radiolarite from lithologic Subunit IVB. Radiolarians are chalcedony-filled and commonly coated with iron-manganese oxide. Plain light. Scale bar is 0.5 mm. From sample 129-801B-23R-CC, 1–4 cm (middle Tithonian).

more siliceous sediments record a higher sedimentation rate of about 10 m/m.y. or greater (Cores 129-801B-20R through -23R). Silica abundance and the silicon/aluminum ratio, as measured by the geochemical logging of the site, attains a distinctive peak in this interval (370–395 mbsf) (Fig. 47). The increase in silica content also correlates with an assemblage of sparse nannofossils indicative of high fertility in the lowest upper Tithonian strata of Site 801 (see "Biostratigraphy" section, this chapter). The change between lower Tithonian clayey radiolarite and upper Tithonian radiolarite and chert is sharp in both the recovered sediments and in the geochemical logs; this sudden transition marks the boundary between Subunits IVB and IVA.

The upper Tithonian burst in radiolarian abundance can be partially explained by the near-equatorial position of the site (see "Paleomagnetics" section, this chapter); the equatorial current system is a likely area for preferential radiolarite deposition throughout the Mesozoic (Lancelot and Larson, 1975; Lancelot, 1978; Baumgartner, 1987).

The upward decrease in the abundance of radiolarians relative to clay in Berriasian through Valanginian strata (upper Subunit IVA) probably reflects a slow decline in radiolarian productivity and preservation due to the steady southward drift of the site from the equatorial high-fertility zone.

### *Diagenetic and Deformation Features*

Primary textural differences of the facies have been enhanced by later diagenesis, especially by dissolution and reprecipitation of silica. In some intervals, radiolarians have been silica-infilled in the darker, partially silicified layers and left as molds in the adjacent, more porous, light-colored layers. Most of the dark brown chert occurs as bands parallel to bedding, but discordant diagenetic boundaries are also common (Fig. 12B).

Fracturing of the chert beds and the associated formation of quartz-lined voids decrease uphole from Cores 129-801B-22R to -16R, suggesting that early chertification of the radiolarian-enriched mid-Tithonian strata resulted in horizons susceptible to later brittle deformation (Fig. 14). The early-formed quartz fillings of some fractures served as permeability barriers and resulted in isolated "compartments" in the

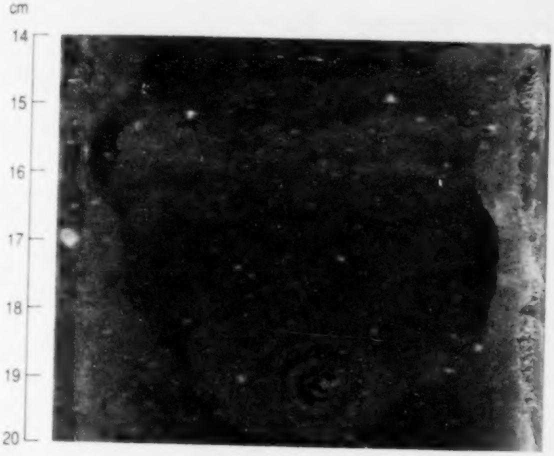

Figure 17. Alternating red radiolarite and claystone of lithologic Unit V. Central block has a dark band of radiolarian-poor claystone between two lighter-colored bands of concentrated radiolarians. Upper radiolarite band displays flaser or lenticular structures of radiolarian concentrations between discontinuous, wavy, clay-rich laminations. Interval 129-801B-33R-1, 14–20 cm (Callovian).

radiolarite which experienced different degrees of chertification.

The brown radiolarite of Unit IV has abundant brown staining and black micronodules, fracture coatings, and internal flecks of oxides (Figs. 12 and 15). In mottles where brown coloration is absent, the sediment is reddish, indicating the continued presence of iron oxide. Some of the micronodules appear to have begun as manganiferous replacement or coatings of biogenic tests (Figs. 13 and 16). Growth of micronodules preceded silicification as indicated by their occurrence within chert nodules of probable low permeability. The high abundance of manganese in Unit IV, in contrast to the underlying red claystone and radiolarite of Callovian-Bathonian Unit V, may be the result of post-burial, slow, upward

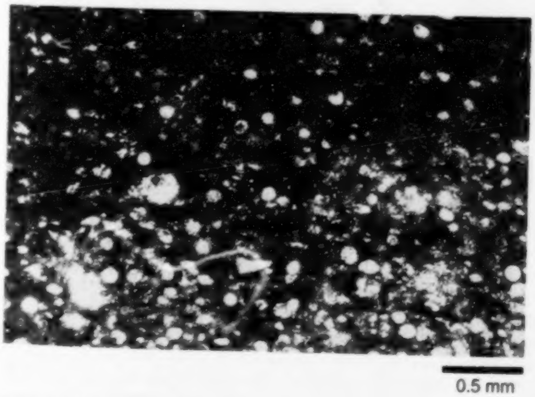

Figure 18. Photomicrograph of a transition between a radiolarite band and a claystone band in lithologic Unit V. In this thin section, the transition is narrow, but not abrupt. The claystone and the radiolarite are rich in hematite. Plain light. Scale bar is 0.5 mm. Sample 129-801B-35R-1, 62–65 cm (Callovian).

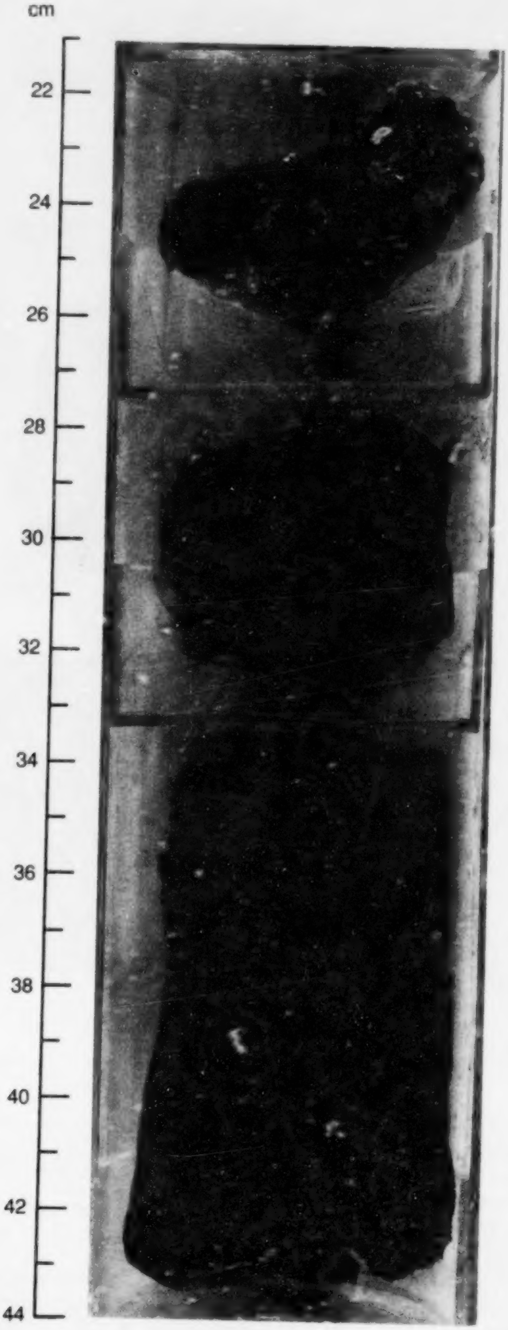

Figure 19. Uppermost recovered flow or thin-sill aphyric basalt underlying brecciated chert. Top of basalt has a fine-grained chill margin, but actual sediment/basalt contact was not recovered. Interval 129-801B-37R-1, 22–43 cm. (Callovian-Bathonian).

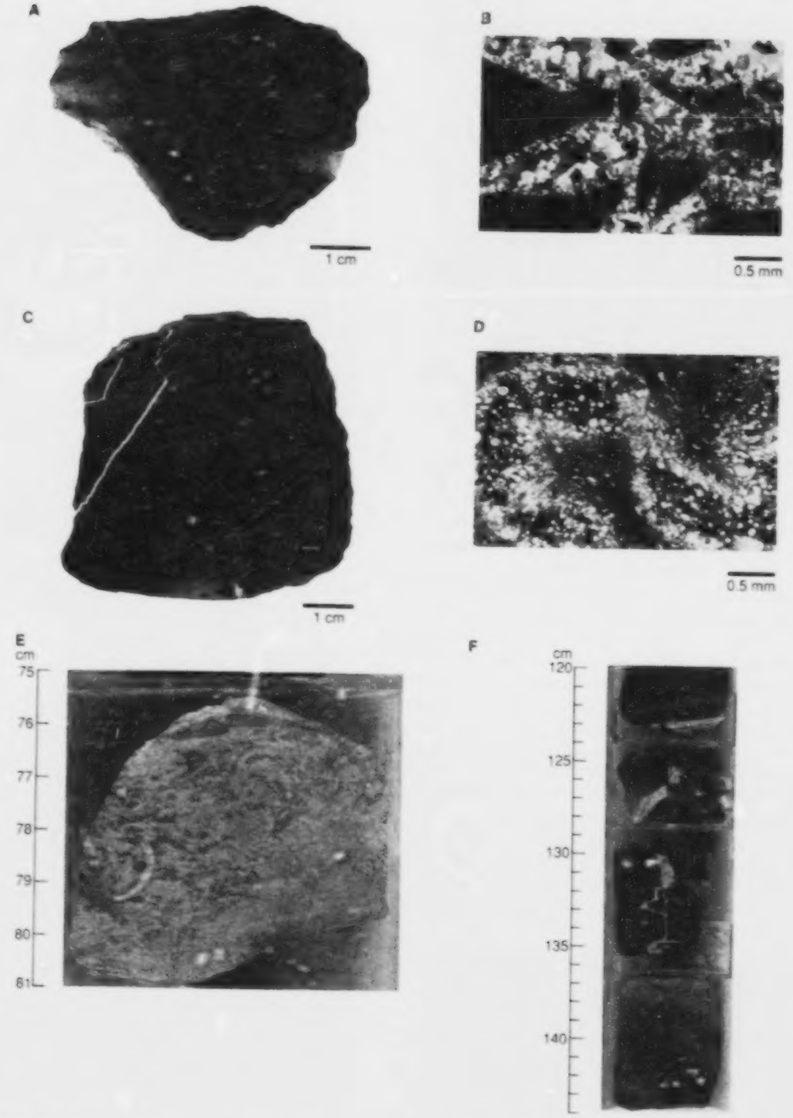

Figure 20. Representative lithologies of basal and interpillow sediments, the oldest sediments recovered from the Pacific plate (Callovian-Bathonian). **A.** Reddish brown chert crackle breccia. Brecciation occurred in soft clay, by rapid dehydration or fluid injection associated with heating by the adjacent basalt, which is suggested by quartz-filled fractures that have curved, non-parallel surfaces that taper into the host siliceous claystone with a feathery or horsetail appearance. Interval 129-801B-37R-1, 11–16 cm. Centimeter scale bar is parallel to bedding. **B.** Photomicrograph of reddish brown chert breccia similar to (A). Metalliferous siliceous claystone clasts are separated by quartz-filled fracture fillings. Crossed nicols. Sample 129-801B-38R-1, 4–7 cm. **C.** Interflow silicified radiolarite. Radiolarite is dark reddish gray with moderate bioturbation. Radiolarians are replaced by opaque white silica, making some burrow-fillings clearly evident. Darker area on the left is more silicified. Interval 129-801B-39R-1, 27–32 cm. **D.** Photomicrograph of silicified radiolarite similar to (B). Silica-filled radiolarians are most abundant or best preserved within the burrow-fillings. Interburrow sediment is a metalliferous claystone with radiolarians. Plain light. Sample 129-801B-39R-1, 15–16 cm. **E.** Interflow gray limestone. Irregular pods of darker gray, densely crystalline calcite are contained within a matrix of more porous calcite in a fabric which may represent disruption or injection. Interval 129-801B-43R-3, 75–81 cm. **F.** Interflow reddish gray, calcareous, silicified tuff (two lowest pieces) that is depositionally overlain by dark reddish brown, bioturbated, radiolarian metasiltstone (second piece from top). Calcareous, silicified tuff has a finely laminated, aphanitic groundmass; the upper piece contains 1- to 3-mm calcareous ovoids with coarser, crystalline calcite centers, which are possibly biogenic tests. Radiolarian metasiltstone has a cryptocrystalline to microcrystalline siliceous matrix containing ghosts of radiolarians and rich in iron-manganese oxides. Interval 129-801B-44R-1, 120–144 cm.

Table 3. Carbonate, organic carbon, and sulfur content of samples from Site 801.

| Core, section, interval (cm) | Depth (mbsf) | $CaCO_3$ (wt%) | $C_{org}$ (wt%) | S (wt%) | Lithology |
|---|---|---|---|---|---|
| 129-801A- | | | | | |
| 4R-1, 76–78 | 30.76 | 0.5 | 8.50 | | Pelagic clay |
| 5R-1, 74–76 | 40.34 | 73.9 | | | Nannofossil ooze |
| 5R-5, 57–58 | 46.17 | 0.2 | | | Pelagic clay |
| 5R-5, 74–76 | 46.34 | 0.4 | | | Pelagic clay |
| 7R-1, 75–77 | 59.75 | 0.2 | | | Pelagic clay |
| 7R-CC, 11–13 | 64.06 | 0.2 | | | Chert |
| 9R-1, 17–19 | 78.37 | 0.1 | | | Chert |
| 12R-1, 0–2 | 106.80 | 0.1 | | | Chert, porcellanite |
| 13R-1, 13–15 | 116.63 | 5.4 | | | Calcareous porcellanite |
| 14R-1, 51–53 | 126.71 | 0.2 | | | Radiolarian porcellanite |
| 15R-1, 10–12 | 136.00 | 1.2 | | | Volcaniclastic sandstone |
| 16R-1, 44–46 | 146.04 | 2.8 | | | Volcaniclastic sandstone |
| 17R-1, 64–66 | 155.84 | 0.2 | | | Chert with porcellanite |
| 18R-1, 49–51 | 165.49 | 3.4 | | | Volcaniclastic sandstone |
| 19R-1, 33–35 | 175.03 | 7.7 | | | Volcaniclastic calcareous claystone |
| 20R-1, 15–17 | 184.55 | 0.2 | | | Radiolarian claystone |
| 129-801B- | | | | | |
| 1R-1, 60–62 | 194.60 | 0.2 | | | Radiolarian silty claystone |
| 1R-3, 81–83 | 197.81 | 3.2 | | | Volcaniclastic sandstone |
| 2R-1, 92–94 | 204.42 | 1.2 | | | Volcaniclastic silty sandstone |
| 3R-1, 76–79 | 213.66 | 0.3 | | | Volcaniclastic silty sandstone |
| 3R-1, 79–81 | 213.69 | 1.1 | | | Volcaniclastic silty sandstone |
| 3R-CC, 0–2 | 214.06 | 1.2 | | | Volcaniclastic silty sandstone |
| 4R-1, 17–19 | 222.47 | 3.7 | | | Volcaniclastic clayey sandstone |
| 5R-2, 0–10 | 233.20 | 4.3 | | | Volcaniclastic silty claystone |
| 5R-2, 145–147 | 234.65 | 15.2 | | | Calcareous volcaniclastic sandstone |
| 6R-4, 10–12 | 245.90 | 2.3 | | | Volcaniclastic clayey siltstone |
| 7R-1, 3–5 | 251.03 | 15.5 | | | Calcareous volcaniclastic claystone |
| 8R-3, 115–125 | 264.85 | 4.0 | | | Volcaniclastic silty claystone |
| 8R-4, 126–128 | 266.46 | 2.8 | | | Volcaniclastic silty claystone |
| 10R-1, 22–24 | 280.22 | 0.1 | | | Calcareous claystone |
| 10R-1, 29–31 | 280.29 | 5.7 | | | Calcareous siltstone |
| 11R-1, 21–23 | 289.91 | 0.2 | | | Clayey radiolarite |
| 12R-1, 13–17 | 299.43 | 0.6 | | | Volcaniclastic turbidite |
| 13R-1, 46–51 | 309.46 | 1.4 | | | Volcaniclastic turbidite |
| 14R-1, 15–24 | 318.45 | 0.2 | | | Clayey radiolarite |
| 16R-1, 30–32 | 337.50 | 0.4 | | | Radiolarite |
| 17R-1, 1–3 | 346.61 | 0.2 | | | Radiolarite |
| 18R-1, 17–19 | 355.97 | 0.3 | | | Radiolarite |
| 19R-1, 26–28 | 365.56 | 0.2 | | | Radiolarian chert |
| 20R-1, 21–23 | 374.71 | 0.2 | | | Radiolarian chert |
| 21R-1, 10–12 | 383.80 | 0.1 | | | Radiolarian chert |
| 23R-CC, 13–15 | 396.03 | 0.1 | | | Radiolarian chert |
| 25R-1, 41–43 | 405.61 | 0.2 | | | Radiolarite with chert |
| 27R-1, 37–39 | 415.07 | 0.2 | | | Clayey radiolarite with chert |
| 31R-1, 25–27 | 433.85 | 0.2 | | | Radiolarian chert |
| 33R-1, 55–57 | 443.35 | 0.2 | | | Clayey radiolarite |
| 35R-1, 131–133 | 453.61 | 0.2 | | | Radiolarite |
| 37R-1, 54–56 | 462.04 | 0.4 | 0.0 | 0.1 | Basalt |
| 37R-1, 66–71 | 462.16 | 0.5 | | | Basalt |
| 38R-1, 22–25 | 466.32 | 1.9 | | | Basalt |
| 39R-1, 9–11 | 470.79 | 0.4 | | | Basalt |
| 40R-1, 20–23 | 477.10 | 0.2 | | | Basalt |
| 40R-1, 38–40 | 477.28 | 1.7 | 0.0 | 0.1 | Basalt |
| 40R-1, 85–91 | 477.75 | 9.1 | | | Basalt |
| 41R-1, 26–31 | 483.26 | 6.8 | | | Basalt |
| 41R-1, 95–97 | 485.45 | 8.2 | 0.0 | 0.0 | Basalt |
| 42R-2, 93–95 | 489.98 | 1.2 | 0.0 | 0.1 | Basalt |
| 43R-1, 42–44 | 492.62 | 2.0 | 0.0 | 0.0 | Basalt |
| 43R-3, 119–121 | 496.17 | 23.0 | 0.1 | 0.0 | Basalt |
| 44R-1, 52–54 | 502.22 | 8.8 | 0.0 | 0.0 | Basalt |

diffusion of reduced manganese into overlying Upper Jurassic strata, which had sufficiently oxidizing conditions for the manganese to reprecipitate. A similar model of upward diffusion of manganese and precipitation at the sediment surface explains the formation of manganese-rich nodules and segregation between iron and manganese oxides during early diagenesis of pelagic sediments (Lynn and Bonatti, 1965; Tsunogai and Kusakabe, 1982; Karpoff, 1989, and references therein).

Underlying lower Tithonian and Kimmeridgian strata (Cores 129-801B-24R through -27R) have apparent dips of 5°–10°, in contrast to the relatively horizontal strata of upper Tithonian and higher, in which the apparent dip is indistinguishable from the 2°–3° deviation of the drill string from vertical. The simultaneous upward decrease in the clay content in Core 129-801B-24R (boundary between Subunits IVB and IVA, which is also sharply delimited on the geochemical logs) and in the apparent dip of bedding suggests the possibil-

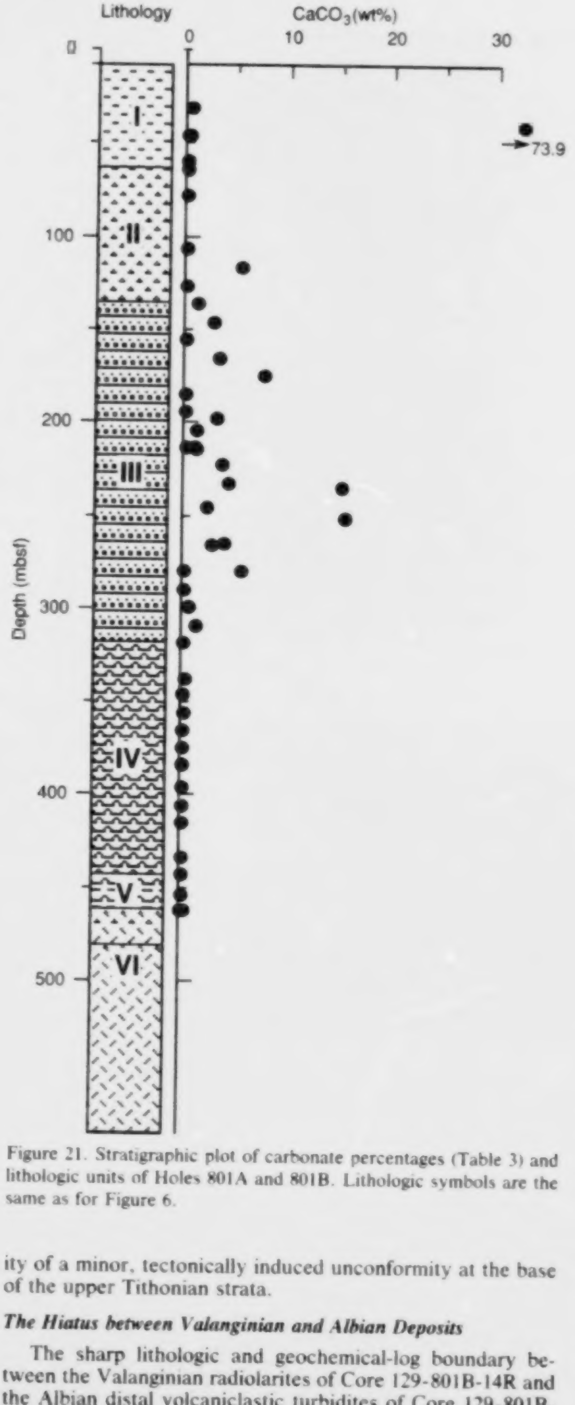

Figure 21. Stratigraphic plot of carbonate percentages (Table 3) and lithologic units of Holes 801A and 801B. Lithologic symbols are the same as for Figure 6.

ity of a minor, tectonically induced unconformity at the base of the upper Tithonian strata.

### *The Hiatus between Valanginian and Albian Deposits*

The sharp lithologic and geochemical-log boundary between the Valanginian radiolarites of Core 129-801B-14R and the Albian distal volcaniclastic turbidites of Core 129-801B-13R (318 mbsf; Unit III) is either a hiatus or condensed interval in sedimentation. A hiatus within this same age span is also suspected at nearby Site 800 (see "Paleomagnetics" and "Biostratigraphy" sections, "Site 800" chapter, this volume).

### *Aptian-Cenomanian: The Origin and Pulses of the Volcaniclastic Turbidites and Associated Pelagic Sediments*

The first pulse of volcaniclastic input is recorded at Site 801 as distal, fine-grained turbidites interbedded with radiolarian claystone (Cores 129-801B-13R and -12R). This initial herald of local seamount formation had not been precisely dated at the time of preparation of this report. The lack of magnetic reversals suggests an Aptian age (see "Paleomagnetics" section, this chapter). After an interval of siliceous pelagic sedimentation (Cores 129-801-11R and -10R), a second sustained pulse of volcaniclastic input began in the middle Albian with thick fine-grained turbidites.

Despite their apparent source in seamounts located over 100 km from the site, individual volcaniclastic turbidite beds at Site 801 exceed 4 m in thickness and can approach a debris flow texture in their abundance of rip-up clasts. The seamounts which were the source of these turbidites had built up to neritic depths by the late Albian, as shown by occurrence of fragments of red algae and echinoderms.

Pelagic intervals occur mainly as minor interbeds between turbidites, except for a brief, pelagic-dominated interval during the upper Albian (Cores 129-801A-20R to -17R). The pelagic facies primarily range from nannofossil-bearing siliceous clay to radiolarian ooze.

A third pulse of volcaniclastic turbidites and tuffaceous beds of latest Albian and Cenomanian age (Cores 129-801A-17R to -14R) completed the volcanic sequence.

At Site 800, the Albian and Cenomanian is represented by 150 m of siliceous limestone, a lithology virtually absent at Site 801. Many of the Albian-Cenomanian pelagic interbeds at Site 801 contain minor amounts of nannofossils and carbonate, but clay and radiolarians remain the dominant components. Site 801 was 3° farther south from the paleoequator and perhaps slightly deeper; hence, it may have received and preserved less calcareous input. However, such effects would seem relatively insignificant considering the 5°–10° of northward drift of the Pacific plate through this time interval (see "Paleomagnetic" section, this chapter). Other alternate explanations include locally enhanced carbonate productivity associated with proximity of seamounts, erosional removal of carbonate strata, and post-burial dissolution; however, our favored explanation is that the low carbonate content of Albian-Cenomanian deposits at Site 801 reflects the geographic variation of a redeposited facies. Albian to Cenomanian radiolarian-rich limestones at Sites 800 and 802 are largely muddy turbidites (see "Lithostratigraphy and Sedimentology" sections, "Site 800" and "Site 802" chapters, this volume). At Sites 800 and 801, the change from calcareous-bearing pelagic sediment to noncalcareous radiolarian cherts and porcellanites occurs approximately during Turonian time, suggesting a regional rise in the CCD.

### *Cenomanian to Campanian: Brown Chert and Porcellanite*

There was very poor recovery of the Upper Cretaceous brown chert and porcellanite Unit II. Those recovered facies probably represent some of the more silicified layers within a host radiolarian clay. This interpretation of the *in-situ* unrecovered lithology is supported by the common occurrence of "rinds" of lighter brown siliceous claystone on the some edges of the tumbled chert fragments, by the recovery of some pieces of softer clayey radiolarian porcellanite (e.g., within Core 129-801A-10R), and by the interbedded radiolarite and claystone character of the upper portion of this unit (lower Core 129-801A-7R).

Although some chert or porcellanite fragments display minor bioturbation, most of the sediment retains an original banding undisrupted by bioturbation. The brown to reddish coloration, probably related to iron-manganese oxides, suggests that the bottom waters were oxidizing, but that either oxygen or nutrient levels were not conducive to an abundance of bottom life. The primary compositional differences, such as relative content of minor amounts of clay, partially controlled the chertification processes (Lancelot, 1973) and result in thin bands of porcellanite in the chert.

The decrease in radiolarian content of the sediments at the end of the Campanian, and the corresponding termination of the chert-rich Unit II, may represent the passage of Site 801 into the low-fertility waters of the North Pacific gyre. Brown pelagic clay deposition completes the Mesozoic sedimentation history of Site 801. There is a probable hiatus between Campanian-Maestrichtian and Paleocene sediments, as occurs at other nearby sites.

The brown pelagic clay of the latest Cretaceous and Tertiary are typical deep-sea clay deposits formed below the CCD, such as those described in deep basins from Pacific and Atlantic realm. Some redepositional events, expressed as calcareous ooze layers, are recorded in the deep Pigafetta Basin.

### Main Aspects of Mesozoic Sedimentation

Several main aspects of the sedimentation at Site 801 in the deep Pigafetta Basin can be established from the preliminary lithologic observations.

Mesozoic pelagic sedimentation at Site 801 was dominated by radiolarians and clay. The siliceous deposits were dominant, with high sedimentation rates during the late Tithonian-early Berriasian and the Cenomanian-Campanian, coincident with times of equatorial paleolatitudes. Jurassic and Cretaceous pelagic sediments preserved on circum-Pacific terrains consist mainly of ribbon radiolarite cherts (e.g., Baumgartner, 1987). In contrast, sediments recovered at Site 801 and other Pacific Mesozoic sites have never displayed such sharply bedded and cherty ribbon radiolarites.

Calcareous biogenic phases are rare components of Mesozoic sediments at Site 801. At DSDP Sites 303 and 304, about 21° north of the Site 801, Lower Cretaceous basal calcareous sediments were recovered. Therefore, during the Early Cretaceous the CCD could be estimated to lie between the paleodepths of Sites 801, 303, and 304, between 3.5 and 4.5 km. The scarce nannofossils suggest high-fertility surface conditions during the Jurassic (see "Biostratigraphy" section, this chapter), although calcareous nannoplankton were probably not an important component of near-equatorial sedimentation. Pelagic limestones are scarce in the Atlantic and western Tethys basins below the Upper Tithonian (Bernoulli, 1972; Lancelot et al., 1972) and in circum-Pacific terrains younger than Upper Cretaceous (Baumgartner, 1987). Siliceous epochs are often contemporaneous with periods of fast oceanic spreading and volcanism (Garrison, 1974; Adachi et al., 1986). The absence of a calcareous sequence of Callovian through Kimmeridgian age at Site 801 may be the result of selectively siliceous, high surface-productivity, rather than a shallow CCD.

Mesozoic pelagic deposits at Site 801 are weakly to moderately bioturbated, devoid of organic carbon, and rich in iron oxide. This character is quite comparable to most other sites drilled in the deep Pacific, and indicates continually oxygenated bottom waters during the Cretaceous.

The basal and interpillow sediments at Site 801 have been affected to varying degrees by hydrothermalism and thermal effects accompanying emplacement of the basalt flows. The iron, manganese, and even silica-rich deposits from this hydrothermal activity at the nearby spreading ridge axis may be compared to metalliferous deposits described in the Tethyan realm at the Oman and Cyprus ophiolites (e.g., Karpoff et al., 1988, and references therein).

## BIOSTRATIGRAPHY

Sediment was cored in two holes (801A and 801B) at this site. Twenty rotary cores were taken from Hole 801A, and a sequence of sediments was recovered and dated as latest Paleocene to late Albian. In contrast to the Santonian-Campanian to late Tertiary hiatus suspected at Site 800, continuous sedimentation is believed to have taken place from the Late Cretaceous to the early Tertiary at Site 801, although the exact position of the Cretaceous/Tertiary (K/T) boundary in the hole could not be determined because of insufficient core recovery.

Hole 801B was drilled in response to an 8° deviation of the drill string at the bottom of Hole 801A, and was washed down to the depth at which Hole 801A was terminated. The sediments recovered from 44 rotary cores in Hole 801B are dated as middle Albian to Bathonian. Core-catcher samples were routinely analyzed for calcareous nannofossils, foraminifers, radiolarians, and palynomorphs, and where necessary, additional samples from within the cores were also examined for these microfossils.

Radiolarians are the most abundant and persistent group throughout the cored sequence, whereas the distribution of calcareous nannofossils is sporadic and their abundance is usually lower. Planktonic foraminifers occur rarely in the sequence, and benthic foraminifers are of low to moderate abundance in the Campanian to Paleocene pelagic clay. Amorphous organic matter was found at some levels, but dinoflagellate cysts were absent.

Cores from Holes 801A and 801B were dated using calcareous nannofossils, foraminifers and radiolarians. The calcareous nannofossils provide useful datums in the Tertiary and middle Cretaceous, and the presence of single specimens in two deeper cores in Hole 801B are in agreement with Jurassic ages determined by radiolarians. The agglutinated foraminifers allow approximate determination of the Late Cretaceous and early Tertiary from their occurrence in Site 800. The planktonic foraminifers, although rare and only moderately well preserved, provide middle Cretaceous ages. Radiolarians are poorly preserved in the Cretaceous intervals, although late Albian to Campanian biozones may be recognized, supported by evidence from planktonic foraminifers. The radiolarians also provide detailed stratigraphic resolution of the Lower Cretaceous and Middle Jurassic intervals and indicate a possible hiatus in the early Oxfordian. A summary of the biostratigraphy of Site 801 is provided in Figure 22.

The paleoenvironment of Site 801 is interpreted as abyssal with deposition below the calcium carbonate compensation depth during the late Cenomanian through early Tertiary, based primarily on the presence of deep-water agglutinated foraminifer assemblages. It is hard to speculate on the paleobathymetry for the Albian through Bathonian interval at this site since sedimentation rates, likely affected by changing paleolatitude, volcanism, and gravity flows, will have had an important influence on the abundance trends of the nannofossils and radiolarians.

### Calcareous Nannofossils

Forty-one core-catcher and 50 additional samples from Site 801 were investigated. Nannofossil distribution is very uneven (Fig. 23). Total abundance fluctuates from barren to very abundant, and preservation varies from poor to good. Diver-

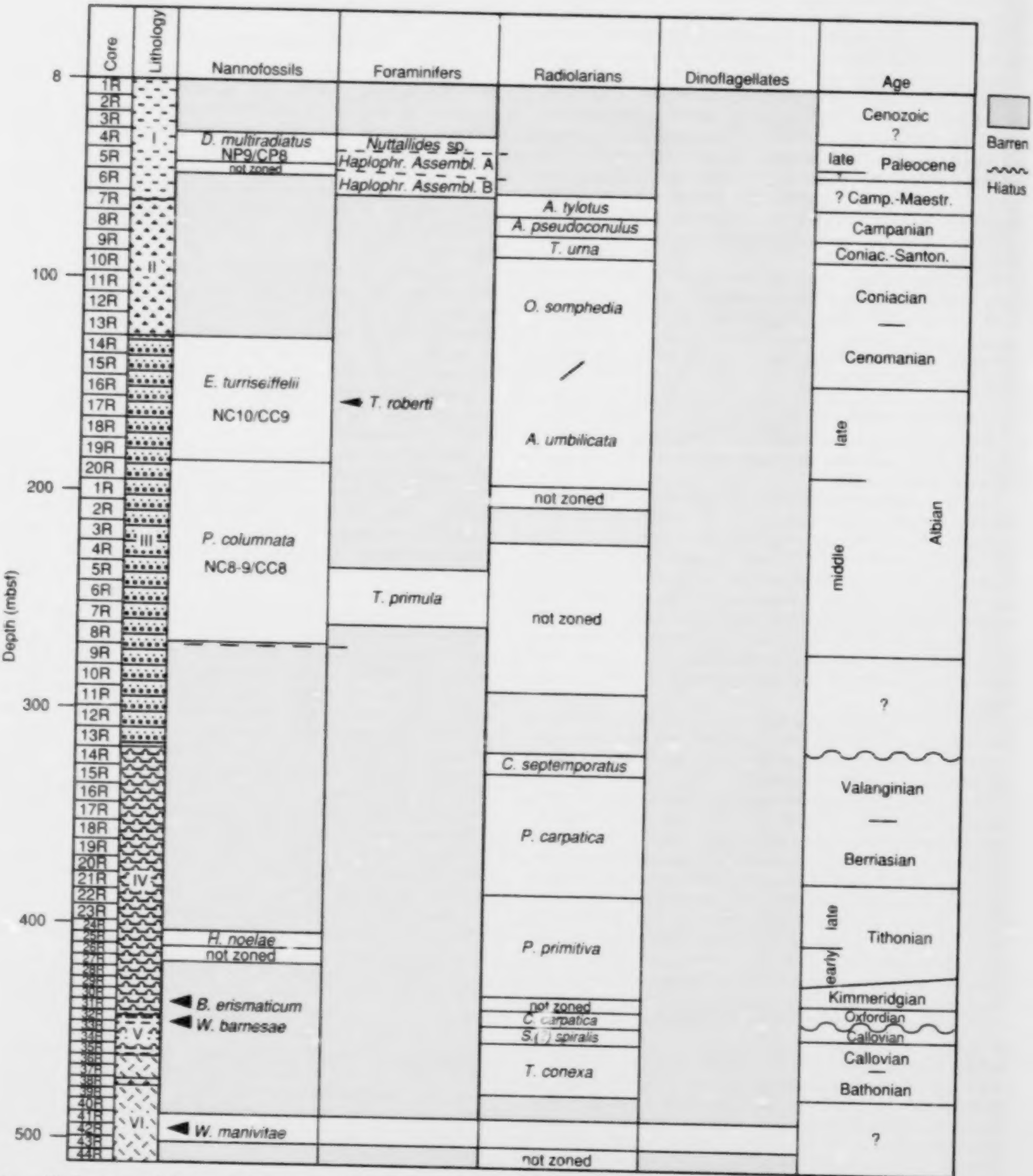

Figure 22. Summary of the biostratigraphy for Holes 801A and 801B. (Note: No recovery between 0 and 8 mbsf.)

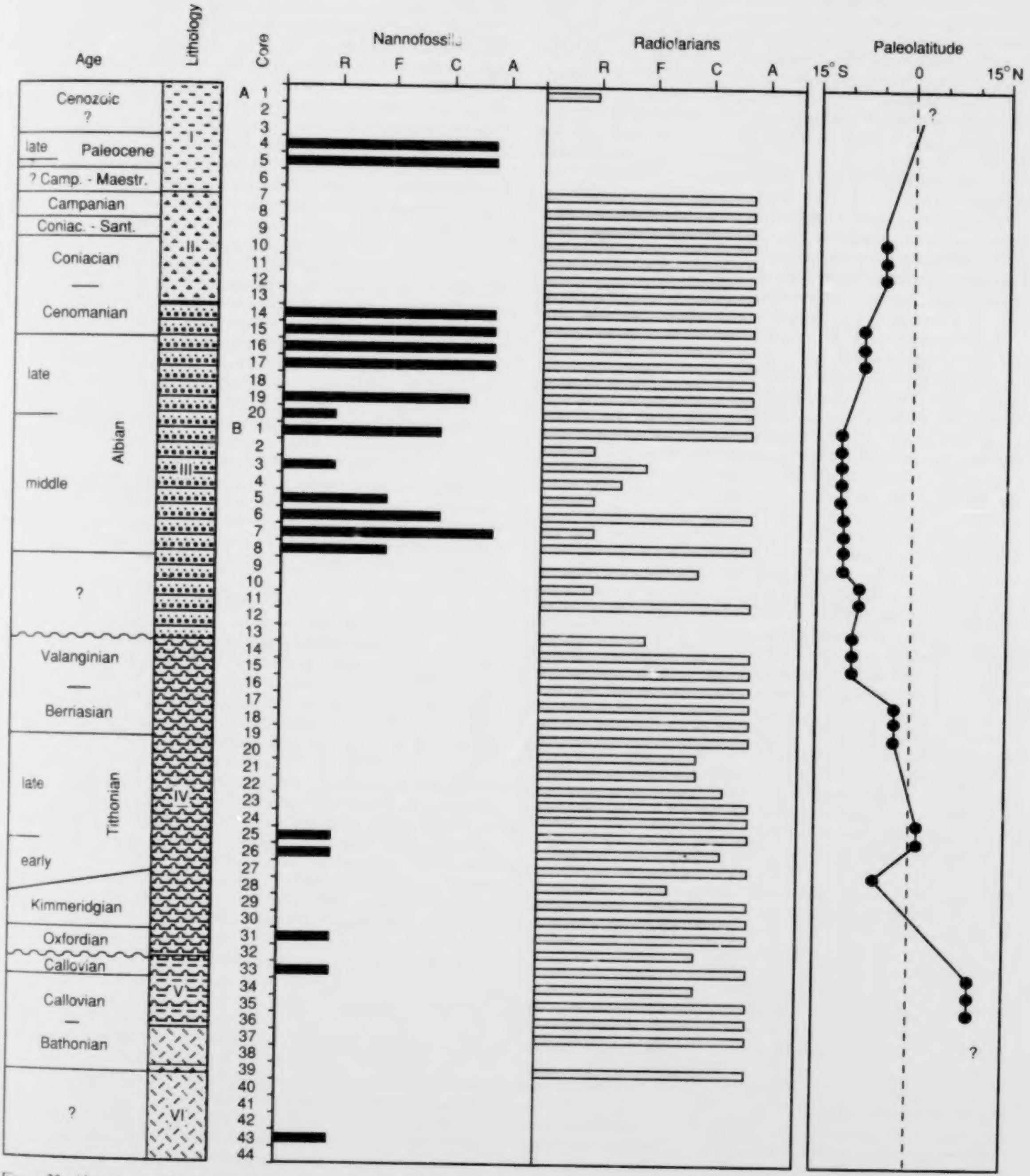

Figure 23. Abundance of calcareous nannofossils and radiolarians plotted against age, lithostratigraphy, and paleolatitude in Holes 801A and 801B. Relative abundance is denoted as follows: rare (R), few (F), common (C), and abundant (A). See "Explanatory Notes" chapter (this volume) for further discussion of abundance parameters.

sity (number of species) is usually proportional to total abundance, reaching maxima in the Cenomanian-uppermost Albian and lower middle Albian sediments.

Cores 129-801A-1R to -3R are barren of calcareous nannofossils. Samples between Sections 129-801A-4R-CC and 129-801A-5R-1, 28 cm, contain an abundant and moderately preserved mixture of nannofloras which range in age from latest Campanian to latest Paleocene. The Paleocene assemblage is characterized by abundant *Fasciculithus* spp. and *Fasciculithus tympaniformis*, common *Discoaster multiradiatus*, and rare *Heliolithus kleinpellii*, while the age-diagnostic Cretaceous species include common to few *Ceratolithoides aculeus*, *Micula decussata*, *M. murus*, *Quadrum sissinghii*, *Q. trifidum*, and *Aspidolithus parcus constrictus*. No species of *Tribrachiatus* were encountered but *D. multiradiatus* was abundant in some samples, so we assign this interval to the latest Paleocene *D. multiradiatus* (NP9) Zone of Martini (1971). The core catcher of Core 129-801A-5R contains rare Paleocene nannofossils, including *Coccolithus* sp. and *Fasciculithus tympaniformis*.

All samples examined from the core catcher of Core 129-801A-6R to the core catcher of Core 129-801A-13R are barren of nannofossils. Sample 129-801A-14R-1, 62–63 cm, contains common, moderately preserved Cretaceous nannofossils. The occurrence of the diagnostic species *Eiffellithus turriseiffelii*, *Prediscosphaera columnata*, *Cruciellipsis chiastia*, *Axopodorhabdus albianus*, and *Lithraphidites alatus* allows determination of the upper Albian-Cenomanian *E. turriseiffelii* Zone of Thierstein (1971, 1973, 1976), Zone NC10 of Roth (1978), and Zone CC9 of Sissingh (1977). The absence of *Microrhabdulus decoratus*, *Lithraphidites acutus* and any younger taxa, and the occurrence of *C. chiastia* corroborate the zonal and age assignment.

This nannofloral assemblage remains unchanged down to Sample 129-801A-19R-CC where we placed the lower limit of the *E. turriseiffelii*/NC10/CC9 Zone. The absence of *Rucinolithus irregularis* throughout this interval prevents determination by nannofossils of the Albian/Cenomanian boundary, which was recognized on the basis of planktonic foraminifers. The upper/middle Albian boundary is slightly older than the base of the *E. turriseiffelii*/NC10/CC9 Zone.

Subsequent samples down to Core 129-801A-20R contain only rare, non-diagnostic nannofossils.

As mentioned in the introduction of this chapter, Hole 801B was washed down to the approximate depth that Hole 801A was terminated. Sample 129-801B-1R-1, 30–31 cm, contains only rare, non-diagnostic nannofossils, whereas in Sample 129-801B-1R-1, 59–60 cm, a common, diverse assemblage was observed. The occurrence of *P. columnata* and the absence of *E. turriseiffelii* indicate the Albian *P. columnata* Zone of Thierstein (1971, 1973, 1976), Zones NC8–NC9 of Roth (1978), and Zone CC8 of Sissingh (1977).

The abundance of nannofossils in the interval between Sections 129-801B-1R-CC and 129-801B-4R-CC fluctuates from barren to rare and only non-diagnostic taxa were encountered.

Sections 129-801B-5R-1, 75 cm, through 129-801B-8R-CC contain frequent to common, diverse nannofossils. The assemblage is composed of *P. columnata*, *C. chiastia*, *Lithastrinus floralis*, *Parhabdolithus angustus*, *Rucinolithus terebrodentarius*, and *R. irregularis*, along with several other less diagnostic species. We assigned this interval to the Albian *P. columnata* Zone of Thierstein (1971, 1973, 1976), Zones NC8–NC9 of Roth (1978), and Zone CC8 of Sissingh (1977). The persistent occurrence of *Tranolithus orionatus* throughout this zone indicates a middle Albian age (Perch-Nielsen, 1985). This age assignment is corroborated by planktonic foraminiferal data.

No more calcareous nannofossils were observed in the remainder of the sedimentary section (Cores 129-801B-9R to -43R), with the exception of five samples. Sample 129-801B-25R-CC contains a diverse nannoflora despite the low total abundance. Rare *Polycostella beckmannii*, *Hexalithus noelae*, *Umbria granulosa minor*, *Cyclagelosphaera margerelii*, *Watznaueria barnesae*, *Watznaueria communis*, *Watznaueria manivitae*, *Zygodiscus erectus*, *Biscutum constans*, *Discorhabdus rotatorius*, *Vagalapilla stradneri*, *Rucinolithus* sp., *Cretarhabdus* sp., *Paleopontosphaera* sp., and *Parhabdolithus* sp. were observed. Although we are conscious that a zonal assignment based on a single sample from otherwise barren cores is difficult to substantiate, we tentatively assign this sample to the middle Tithonian *Hexalithus noelae* Subzone of Bralower et al. (1989).

In Sample 129-801B-26R-CC rare nannofossils occur. They include *W. barnesae*, *W. manivitae*, *B. constans*, *C. margerelii*, *Cretarhabdus* sp., and *P. beckmannii*. The latter taxon is a marker species restricted to the late early to late Tithonian.

Sample 129-801B-31R-CC contains a single specimen of *Biscutum erismaticum*. This species was first described from the Oxfordian of the Falkland Plateau (Wise and Wind, 1976), but its range has subsequently been extended back to the Toarcian (Perch-Nielsen, 1985). Rare specimens of the non-diagnostic species *Watznaueria barnesae* were observed in Sample 129-801B-33R-1, 58 cm.

The lowermost nannofossils observed from Hole 801B, two specimens of *W. manivitae*, were encountered in Sample 129-801B-43R-3, 80–81 cm, from claystones entrapped within pillow lavas of Unit VI (see "Lithostratigraphy and Sedimentology" section, this chapter).

### Foraminifers

Twelve core-catcher samples and nine additional samples within the cores were examined in Hole 801A. Only 14 core-catcher samples could be examined for foraminifers in Hole 801B since the lithology was predominantly chert. Of the 35 samples investigated, 10 contain assemblages of foraminifers. Four of the foraminiferal assemblages display good preservation, and specimen abundance is within the range of "few" to "common." The remaining foraminiferal assemblages show poor to moderate preservation, and are of low abundance ("rare" to "few" categories).

Foraminifers are absent from Samples 129-801A-1R-CC through 129-801A-3R-CC. The core catcher from Core 129-801A-4R contains one specimen of *Recurvoides* sp. and several very small specimens (about 100 µm) of the calcareous benthic genus *Nuttallides*. Specimens are similar to *Nuttallides truempyi* except for their small size. The species *Nuttallides truempyi*, regarded as having had a cosmopolitan distribution throughout its Campanian to late Eocene range, is believed to be a lower bathyal to abyssal paleobathymetric indicator (Morkhoven et al., 1986). On the basis of the associated nannofossils, the foraminiferal assemblage in Sample 129-801A-4R-CC is assigned an upper Paleocene age.

Good recovery in Core 129-801A-5R allowed investigation of four additional samples. Sample 129-801A-5R-1, 83–87 cm, contains a low-diversity assemblage of finely agglutinated foraminifers that roughly correspond to those seen in the *Haplophragmoides* Assemblage A at Site 800, and include the following forms: *Haplophragmoides* sp., *Paratrochamminoides* sp., *Praecystammina globigerinaeformis*, *Bolivinopsis parvissimus*, and *Recurvoides deflexiformis*. Samples 129-801A-5R-3, 59–61 cm, 129-801A-5R-5, 41–46 cm, and 129-801A-5R-5, 76–78 cm, are characterized by an increase in the abundance of primitive tubular agglutinated foraminifers and a corresponding decrease in abundance of the coiled forms typical of the *Haplophragmoides* Assemblage A. Specimens from Sample 129-801A-5R-CC are dominated by primitive tubular foraminifers. Core 129-801A-5R is assigned to the Paleocene on the basis of associated nannofossils.

The core catcher from Core 129-801A-6R contains a more diverse assemblage of foraminifers that correspond well to those seen in the *Haplophragmoides* Assemblage B of Site 800. This assemblage is principally characterized and distinguished from *Haplophragmoides* Assemblage A by more numerous species of *Haplophragmoides* (for example, *Haplophragmoides multicamerata*, *H. fraudulentus*, *H. constrictus*, and *H. pervagatus*), and is assigned to the Upper Cretaceous on the basis of the age of this assemblage at Site 800. The presence of Campanian radiolarians in Core 129-801A-7R suggests a Campanian or younger age for Core 129-801A-6R.

The implication of the biostratigraphy outlined above is that the K/T boundary lies within Core 129-801A-6R. The nature of the deep-water benthic foraminiferal assemblages is of interest to proponents of the widely reported extinctions seen among other fossil groups at the K/T boundary. A number of scientists argue that deep-water benthic foraminifers may have been little, if at all, affected by the K/T boundary "event" and its associated faunal extinctions. Moullade et al. (1988), on the other hand, observe a significant faunal break in deep-water foraminifers coinciding with the K/T boundary in the North Atlantic Plantagenet formation where the Paleocene foraminiferal assemblages are impoverished in comparison to those of the Upper Cretaceous. A similar trend is observed in our sequences. Additionally, the vertical change from an astrorhizid-dominated foraminiferal assemblage in Section 129-801A-5R-CC to a more diverse assemblage higher in the pelagic clay could be evidence of recolonization of the seafloor following an event that disrupted the community structure. Alternatively, such assemblages could result from hydrodynamic sorting by bottom-water or turbidity currents as was suggested for the astrorhizid-dominated assemblage of Core 129-800A-27R. Because of poor recovery from this interval, however, we are unable to investigate the effects of the so called K/T boundary "event" on the deep marine benthic foraminifers of the Pigafetta Basin in more detail.

Sample 129-801A-7R-1, 124–129 cm, contains a foraminiferal assemblage similar to that referred to as the *Haplophragmoides* Assemblage B of Site 800, but differing by the presence of abundant *Praecystammina globigerinaeformis*. The latter species seems to be of stratigraphic value in high latitude abyssal assemblages in the Atlantic Ocean (Moullade et al., 1988), where it is reported to have a last occurrence datum near the Coniacian/Santonian. In lower latitudes, on the other hand, it has also been reported from abyssal assemblages of the uppermost Cretaceous (Hemleben and Troester, 1984). Rare finds of *Praecystammina globigerinaeformis* in Paleocene sediments in Hole 801A extends the range of this species to the lowermost Tertiary in abyssal assemblages of low latitudes. Gradstein et al. (1988) observed a very similar form, which they determined as *Cystammina* aff. *globigeriniformis*, in bathyal Paleocene wells of the central North Sea. A planned comparison of our specimens with those from the North Sea may resolve any taxonomic difficulties with these forms.

Samples 129-801A-7R-2, 51–53 cm, 129-801A-7R-2, 94–99 cm, and 129-801A-7R-3, 134–139 cm, contain only a few specimens of the *Haplophragmoides* Assemblage B species. The sparsity of foraminifers in these samples may be partly the result of the dilution effect of the increasingly abundant radiolarians seen downhole.

Core-catcher samples from Cores 129-801A-7R to -15R are barren of foraminifers. Sample 129-801A-16R-CC contains the planktonic foraminifers *Ticinella roberti*, *Globigerinelloides bentonensis*, and *Hedbergella delrioensis* in low abundance and of poor to moderate preservation. The presence of *Ticinella roberti* allows the sample to be dated as upper Albian, as the last occurrence of this species is found within the lower *Rotalipora appenninica* Zone (uppermost Albian) of Caron (1985).

The core-catcher samples of Cores 129-801A-17R to 129-801B-5R are barren of foraminifers. Sample 129-801B-5R-CC contains a single specimen of *Ticinella bejaouensis*, indicating a middle Albian age (Caron 1985). Core-catcher samples from Cores 129-801B-6R and -7R contain the species *Hedbergella infracretacea*, *H. globigerinelloides*, *H. planispira*, *H. simplex*, and *Globigerinelloides bentonensis*, all of which are common in the middle Albian. The first occurrence of *Globigerinelloides bentonensis* in the *Ticinella primula* Zone (middle Albian) of Caron (1985) excludes an early Albian or older age for the sample. No more foraminifers were encountered in the remainder of the cores in Hole 801B.

### Radiolarians

Twenty core-catcher samples and 32 additional samples within the cores were examined in Hole 801A. Thirty-seven core-catcher samples and 76 additional samples within the cores were investigated in Hole 801B. No Cenozoic radiolarians were obtained from this site.

Samples 129-801A-1R-CC to 129-801A-6R-CC are barren of radiolarians. Cores 129-801A-7R to -20R yielded abundant but poorly preserved radiolarians. Samples 129-801A-7R-CC, 129-801A-8R-1, 31–33 cm, and 129-801A-8R-CC contain *Dictyomitra koslovae*, a species restricted to the upper *Amphipyndax pseudoconulus* Zone and lower *Amphipyndax tylotus* Zone. *Theocampe urna* was obtained from Samples 129-801A-8R-1, 31–33 cm, 129-801A-8R-CC, 129-801A-9R-1, 13–15 cm, and 129-801A-9R-CC. The occurrence of *T. urna* is confined to the *T. urna* Zone and the next younger *A. pseudocolunus* Zone. The co-occurrence of *T. urna* and *D. koslovae*, which was recognized in Samples 129-801A-8R-1, 31–33 cm, and 129-801A-8R-CC indicates the upper part of the *A. pseudocolunus* Zone, assignable to the middle Campanian. The first occurrence of *T. urna* defines the boundary between the *T. urna* Zone and the next older *Obesacapsula somphedia* Zone, situated within the Coniacian. The interval between Samples 129-801A-12R-CC and 129-801A-20R-CC contains few to common *Pseudodictyomitra pseudomacrocephala* associated with rare *Thanarla elegantissima*. The co-occurrence of *P. pseudomacrocephala* and *T. elegantissima* characterizes the upper *Acaeniotyle umbilicata* to lower *Obesacapsula somphedia* Zones (upper Albian to Cenomanian). The boundary between the *A. umbilicata* and *O. somphedia* Zones is regarded to correspond to the Albian/Cenomanian boundary (Sanfilippo and Riedel, 1985). Although no diagnostic radiolarians were found that enabled definition of the boundary between these two zones, the boundary may be inferred as lying above Sample 129-801A-16R-CC, dated by planktonic foraminifers as late Albian.

In Samples 129-801B-1R-CC to 129-801-13R-CC, radiolarian abundance appears to depend on lithology. Coarse volcaniclastic sediments contain sparse radiolarian tests, if any, whereas fine-grained pelagic sediments are generally rich in radiolarians. The poor preservation does not permit zonal assignment of this interval.

The brown radiolarites and cherts of Cores 129-801B-14R to -32R yielded common to abundant and poorly to moderately preserved radiolarians. This interval is divided into four radiolarian zones on the basis of the first occurrence of marker species: *Cecropus septemporatus*, *Pseudodictyomitra carpat-*

*ica*, *Pseudodictyomitra primitiva*, and *Cinguloturris carpatica* Zones in descending order. The bases of the *C. septemporatus* and *P. carpatica* Zones are situated within the Valanginian and upper Tithonian, respectively. The zonal boundary between the *P. primitiva* and *C. carpatica* Zones is drawn near the Oxfordian/Kimmeridgian boundary. This interval is therefore tentatively assigned to the Oxfordian to Valanginian.

Samples 129-801B-14R-1, 14–15 cm, and 129-801B-14R-1, 47–49 cm, contain only a few poorly preserved radiolarians. Sample 129-801B-14R-CC contains species found in both the *C. septemporatus* and the younger *D. thytthopora* Zones, including *C. septemporatus*, *Acanthocircus dicranacanthos*, and *P. carpatica*. However, the faunal composition itself appears to be more typical of the *C. septemporatus* Zone, supported by the absence of *C. septemporatus* from samples below Sample 129-801B-14R-CC. Although the interval between Cores 129-801B-9R and -13R could not be dated by microfossils, we speculate that a hiatus may be present between Cores 129-801B-13R and -14R, corresponding to the boundary between the lithologic Units III and IV.

The red and brown radiolarites between Samples 129-801B-33R-1, 8–10 cm, and 129-801B-39R-CC contain abundant but poorly to moderately preserved radiolarians assignable to the *Stylocapsa(?) spiralis* and *Tricolocapsa conexa* Zones. Samples 129-801B-33R-1, 131–133 cm, 129-801B-33R-2, 14–17 cm, and 129-801B-33R-CC include abundant specimens of *S.(?) spiralis*, *T. conexa*, and *Stichocapsa robusta*. The dominance of the latter three species in this assemblage, combined with the absence of *Stichocapsa naradaniensis*, typical of the upper part of the *S.(?) spiralis* Zone, suggests that only the lower half of the zone is present. The implication of this is that a hiatus may be present between Cores 129-801B-32R and -33R, corresponding to the boundary between lithologic Units IV and V. This hiatus may correspond to the lower Oxfordian. The interval below the hiatus (129-801B-33R-1, 131 cm, to 129-801B-33R-CC) is therefore tentatively assigned to the Callovian.

Samples 129-801B-34R-CC to 129-801B-35R-CC yield *T. conexa*, *Stylocapsa tecta*, and *Stylocapsa oblongula*, which in the absence of *S.(?) spiralis* is characteristic of the upper part of the *T. conexa* Zone. In Sample 129-801B-37R-1, 16–20 cm, *T. conexa* and *Guexella nudata* occur, whereas *S. tecta* does not, indicating the middle part of the *T. conexa* Zone. From Core 129-801B-39R, five samples (129-801B-39R-1, 7–9 cm, 16–18 cm, 20–21 cm, 26–28 cm, and -CC) were examined. All samples yielded common to abundant, poorly preserved radiolarian assemblages, although those from Sample 129-801B-39R-1, 16–18 cm, are better preserved and of similar composition to the assemblage in Sample 129-801B-37R-1, 16–20 cm, indicating a Callovian-Bathonian age.

Sample 129-801B-44R-1, 127–128 cm, is red claystone intercalated with the basalt. It contains a small number of radiolarians, but these are of extremely poor preservation and cannot be assigned an age.

### Palynomorphs

Fifty-seven core-catcher samples and 51 additional samples were investigated from Site 801. All samples of Site 801 are barren of palynomorphs. Cores 129-801B-16R through -32R contain rare to abundant amorphous organic matter, but no palynomorphs.

### Sedimentation Rates

Figure 24 shows the sedimentation rates for Site 801, as determined on the basis of nannofossil, radiolarian, and foraminiferal biostratigraphy. A hiatus was depicted at the top of the Valanginian corresponding to the boundary between lithologic Units III and IV. Another hiatus was determined at the base of the Oxfordian and it coincides with the boundary between lithologic Units IV and V.

### Discussion

The paleoenvironment of Site 801 is interpreted as abyssal with deposition below the CCD during the late Cenomanian through the Tertiary, based principally on the presence of abundant radiolarians and *in-situ* deep-water agglutinated foraminifers. The allochthonous calcareous nannofossils seen in the Paleocene samples support deposition below the CCD. Rare planktonic foraminifers and abundant, apparently autochthonous nannofossils in the Albian to Cenomanian volcaniclastic intervals (lithologic Unit III, see "Lithostratigraphy and Sedimentology" section, this chapter) may suggest deposition above the CCD, but we lack benthic foraminiferal evidence to support this. Paleobathymetry for the Jurassic interval cannot be determined from radiolarians and nannofossils alone.

Preliminary data regarding the abundance of calcareous nannofossils and radiolarians are plotted in Figure 23 against ages, lithostratigraphy, and paleolatitude. The distribution of each group appears somewhat mutually exclusive, and possibly relates to paleolatitude. Highest nannofloral abundance and diversity corresponds to a decrease in abundance of radiolarians in the interval correlated to the southernmost paleolatitude.

Nannofossil assemblages in the Tithonian sediments of Site 801, while scarce and found in only two samples, may be suggestive of high-fertility conditions. In fact, they contain similar numbers of *Watznaueria* and *Biscutum*. The occurrence of a significant number of *Biscutum* relative to the number of *Watznaueria* is considered to indicate high-fertility conditions in Cretaceous sediments (e.g., Roth and Krumbach, 1986; Erba, 1987; Premoli-Silva et al., 1989). However, the reliability of this relative abundance indicator for Jurassic and for Pacific fertility conditions is not yet known.

## PALEOMAGNETISM

### Methods

All sediment cores from Holes 801A and 801B (except for most of the brown pelagic clay interval, lithologic Unit I) were measured and alternating field (AF) demagnetized with the shipboard automated cryogenic magnetometer. Much of the recovery from this hole was in the form of discrete fragments of sedimentary rock rather than continuous core. Of the 55 cores recovered, only 14 were composed of continuous or semicontinuous sedimentary material. Therefore, most of the Site 801 remanent magnetization shipboard measurements were accomplished by individually taping these fragments into the magnetometer tray at spaced intervals. All pieces that had well-defined bedding planes and were larger than 20 cm$^3$ were measured. The pieces were oriented in the magnetometer so that the bedding planes were perpendicular to the horizontal (z) axis of the magnetometer, spaced about 10 cm apart (the width of the magnetometer sensor regions). The core volume parameter in the magnetometer program was adjusted each time to the average volume of the collection of fragments being measured. In sections of good core recovery, whole cores were measured.

### Magnetic Behavior

After measurement of the natural remanent magnetization (NRM), samples were stepwise AF-demagnetized generally

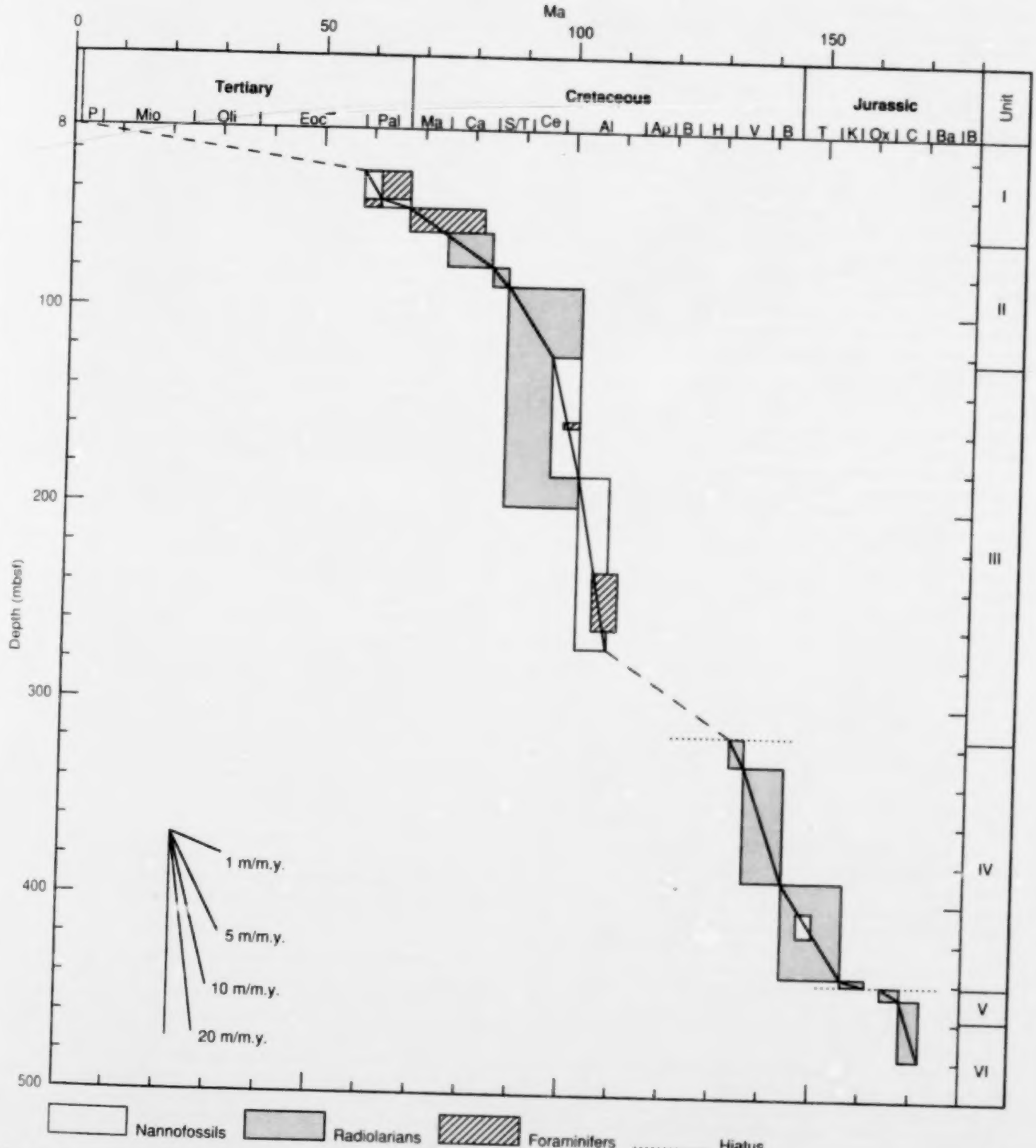

Figure 24. Sedimentation rates for Holes 801A and 801B. (Note: No recovery between 0 and 8 mbsf.)

using field strengths of 5, 10, and 15 mT, chosen on the basis of our experience with Site 800 sediments. Susceptibility was measured on all cores prior to splitting. Susceptibility and AF demagnetization response varied with the lithologic variations. Therefore, properties will be discussed on the basis of lithologic units.

The brown pelagic clay interval from Cores 129-801A-1R through -7R (lithologic Unit I) shows evidence of both homogenization due to mixing and viscous plastic flow in the nonhomogenized material within the core liner. Consequently, these cores have mixed lithologies and partially or wholly obscured bedding. The red-brown color of the cores indicates the probable presence of hematite or iron hydroxides which are not susceptible to AF demagnetization. For these reasons, this interval could not provide much data. Susceptibility measurements from Cores 129-801A-5R and -7R show a range from 65 to 126 SI units and average approximately 85 SI units. AF demagnetization of two of the least disturbed cores yielded no coherent data.

The properties of the brown chert and porcellanite interval from the base of Section 129-801A-7R-4 through Core 129-801A-13R (lithologic Unit II) have susceptibilities ranging from 13 to 46 SI units, averaging approximately 33 units. NRM intensities average about 6 mA/m and AF demagnetization in fields of about 11 mT results in the loss of approximately half of the remanence. Demagnetization vectors do not decay directly to the origin when viewed on orthogonal axis plots; this in conjunction with the large remanence remaining after 15 mT demagnetization suggests the presence of two vectors that cannot be separated by low field AF demagnetization.

The volcaniclastic turbidites from Cores 129-801A-14R through 129-801B-13R (lithologic Unit III) are distinct in magnetic character from the overlying cherty interval. NRM intensity ranges from 2.6 to greater than 200 mA/m; susceptibility also showed great variability, ranging from less than 50 SI units to greater than 300. The variation may be due, at least in part, to the large range in grain size within the turbidites; larger values for susceptibility seem to be associated with the coarser grained fractions. The response to AF demagnetization was generally poorer in the coarser materials than in the fine-grained sediments. Most of the coarse sediments show considerable overlap in coercivity spectra and, in both fine- and coarse-grained materials, mean demagnetizing fields are quite high and generally not revealed with the low level of alternating fields available in the shipboard magnetometer system.

The underlying sedimentary unit, the brown radiolarite of Cores 129-801B-14R through -32R (lithologic Unit IV), showed a markedly lower NRM intensity, approximately 8 mA/m, and a susceptibility of only 16 SI units. In the upper portion of this interval (Subunit IVA; see "Lithostratigraphy and Sedimentology" section, this chapter), more than 90% of the magnetization of this lithology was removed by the first or second AF step (by 10 mT). The demagnetization behavior is difficult to interpret, possibly because of the weak sample intensities and/or the overlap of coercivity spectra. On orthogonal axes plots, trends move beyond the origin, possibly due to the presence of reversed polarity. The lower, more clay-rich portion of the unit (lithologic Subunit IVB) contains samples exhibiting clearer demagnetization behavior, indicative of both normal and reversed polarities. However, large overlaps in coercivity spectra of the lower portion make inclination values somewhat unreliable.

The lowest unit, the alternating claystone-radiolarite interval from Cores 129-801B-33R through -35R (lithologic Unit V), is not represented by much material. Susceptibilities and NRM intensities are similar to the previous unit, but AF demagnetization causes little change in directions or decay of intensities. One or more magnetizations of high coercive force are indicated by the lack of response to AF, consistent with the bright red color that suggests the presence of hematite, goethite, or other iron hydroxides.

## Magnetostratigraphy

Despite the poor recovery of much of the sediment of Holes 801A and 801B, key biostratigraphic markers made possible the recognition of certain polarity intervals. The methods used to define polarity intervals were similar to those discussed for Site 800. The youngest or stratigraphically highest reversals were encountered in Core 129-801A-7R. The reversals in Sections 129-801A-7R-4 and 129-801A-7R-CC appear to be two different intervals separated by a distinct normal polarity zone. The biostratigraphic evidence suggests that the reversed Sample 129-801A-7R-4, 30 cm, is probably of Maestrichtian age and may represent interval 31R or 32R, whereas the lowermost reversed sample, 129-801A-7R-CC, 7 cm, is probably Campanian in age and therefore representative of interval 33R. Interval 33R was also observed at Site 800 (see "Site 800" chapter, this volume).

The next reversed interval was not observed until well down in Hole 801B, in Core 129-801B-14R. The normal polarity interval between this core and Core 129-801A-7R most likely represents the Cretaceous long normal polarity interval (Helsley and Steiner, 1969; Irving and Pullaiah, 1976; Kent and Gradstein, 1986). Beginning at Core 129-801B-14R, reversals become more common. Although in most cases reversed intervals are based on single discrete samples, these are nonetheless thought to reliably indicate geomagnetic field polarity because of the large declination changes in their AF demagnetization responses. The polarity interpretation of Cores 129-801B-13R through -28R is shown in Figure 25.

Cores 129-801B-21R through -30R are biostratigraphically constrained by the radiolarian zone *P. primitiva* as Tithonian to Kimmeridgian in age. The presence of diagnostic nannofossils allows further narrowing of the time of deposition for the majority of these cores (see "Biostratigraphy" section, this chapter). The first and last occurrences of the nannofossil *P. beckmannii* place Cores 129-801B-25R and -26R within an interval including Chrons M19–M21 (Bralower et al., 1989). Further, Core 129-801B-25R contains an assemblage of nannofossils of the *H. noelae* Subzone (see "Biostratigraphy" section, this chapter). As the base of this subzone is placed within Chron M20R, and in conjunction with the implications of the occurrence of *P. beckmannii*, the reversals of Cores 129-801B-25R and -26R likely represent either Chrons M19 or M20. These correlations and observations suggest the tentative chron assignments shown in Figure 25.

Reversals observed within the Kimmeridgian to Callovian part of Hole 801B (Cores 129-801B-29R through -36R) could not be identified with recognized polarity chrons because of the poor recovery and insufficiently detailed paleontologic data.

## Paleolatitude

Determination of the paleolatitudes of this site is hampered by both the low recovery and the relative ineffectiveness of AF demagnetization on much of the material recovered. Furthermore, except for the volcaniclastic interval (lithologic Unit III), the amount of material for which uphole orientation was known was small. In both the chert-porcellanite interval (lithologic Unit II) lying above the volcaniclastics and the radiolarites lying below (lithologic Units IV and V), recovery was of small pieces in which only about 50% had known up-directions. We adopted the approach of measuring and demagnetizing the unoriented pieces in addition to the oriented ones, in the hope of inferring polarity from their demagnetization behavior, as explained in the "Site 800" chapter (this volume). The polarity, in combination with the sign of the inclinations, should indicate the hemisphere of origin, thus allowing us to determine paleolatitudes for the site. Nevertheless, because the plate was near the equator, the shallowness of the inclinations combined with incomplete removal of secondary magnetization (which generally ap-

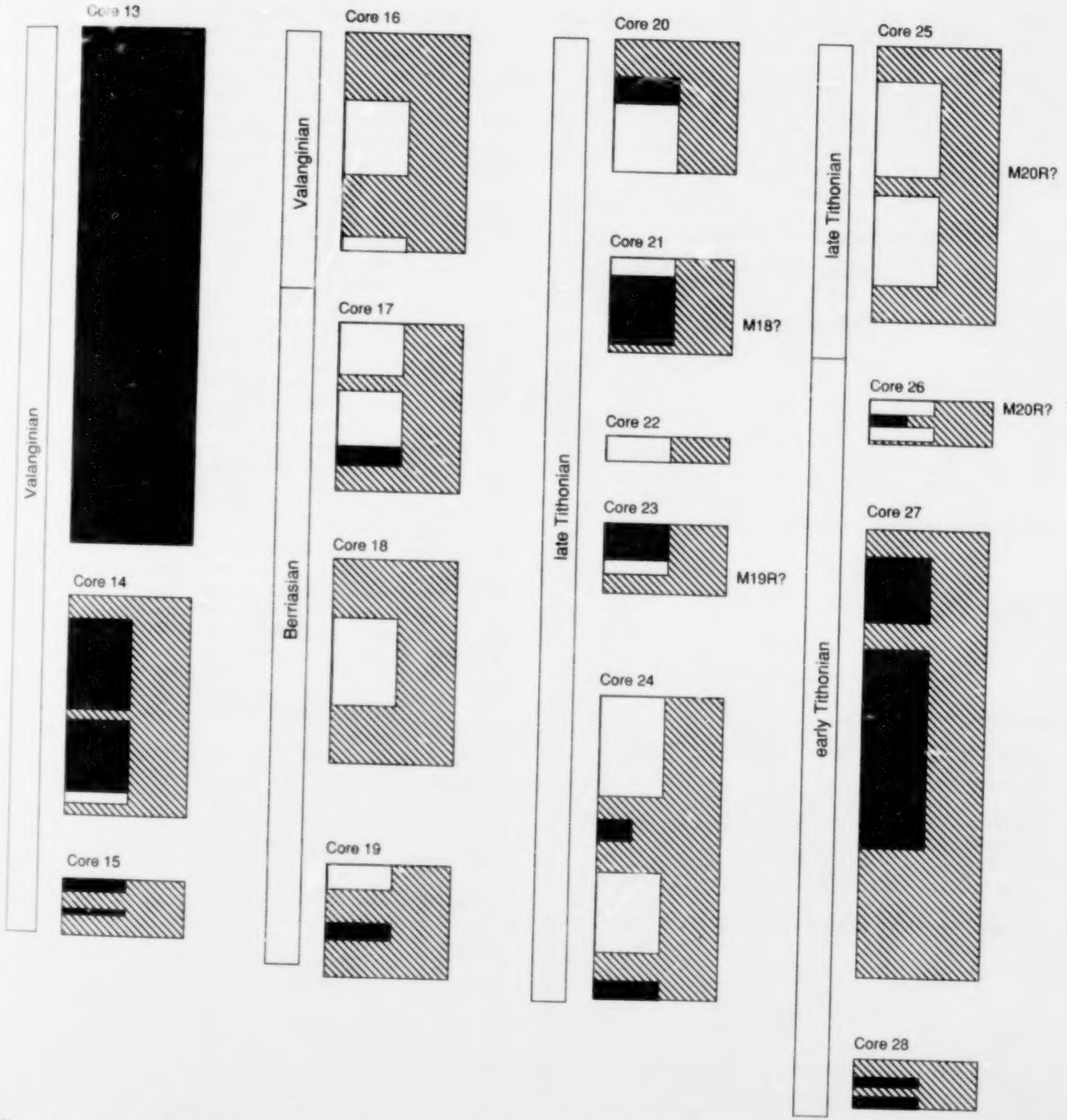

Figure 25. Interpretations of polarity and tentative identification of Tithonian polarity chrons. Each segment represents the recovered portion of individual, numbered cores from Hole 801B. Black bars indicate normal polarity, white is reversed polarity, half-filled columns reflect polarity interpretations made from discrete fragments rather than continuous recovery, one-quarter filling indicates fragments with uncertain polarity identifications, and hachured areas represent areas of no data.

peared to be a late Tertiary direction from the similarity of removed inclinations to that of the present direction of the Earth's field at this site), made distinguishing between the Northern and Southern hemispheres somewhat difficult. An additional uncertainty in paleolatitude determinations for this site was introduced by a significant dip to the beds in the lower part of both holes, but particularly in Hole 801B. More than half of the discrete pieces measured were too large to allow correction for the dip of the beds by simple positioning in the magnetometer tray; for these pieces, careful measurement of the dip and orientation were made and used to correct the magnetization directions.

The resulting data set displays a large amount of dispersion, which may be attributed to a combination of incomplete demagnetization, uncertainty in the up-direction, and possibly some uncertainties in the correction for the tilt of the strata. Nevertheless, despite the scatter, a pattern is apparent in the data. To view this pattern, all inclinations initially were converted to their corresponding latitudes and plotted against depth (Fig. 26A).

A concave band of data points south of the equator is observed. The data are generally concentrated in southern latitudes with dispersion toward and into northern latitudes. The relatively well-grouped data between 180 and 260 mbsf are from the volcaniclastic sequence of lithologic Unit III. The scattered data on either side represent the porcellanites and radiolarites. In an attempt to determine the source of the scatter, all samples for which stratigraphic up was unknown were removed. The result is a much-reduced data base (Fig. 26B) that retains the same general pattern, with only slightly less dispersion. The pattern is somewhat more evident, but the persistence of the dispersion suggests that incomplete demagnetization is probably a significant factor in this data.

Most of the samples of Figure 26B are of normal polarity and overprinting of normal directions in the Southern Hemisphere with the direction of the present field would bias the data toward apparently shallower, southerly paleolatitudes and to apparent northern paleolatitudes, up to the latitude of the site (18.6°N). The characteristic magnetization of many of the chert/porcellanite and radiolarite samples could not be completely separated from the secondary magnetization by AF demagnetization. These particularly give results dispersed to the north, supporting this as the probable origin of the dispersion. Therefore, the true paleolatitudes are probably approximated by the southern edge of the data band of Figure 26B.

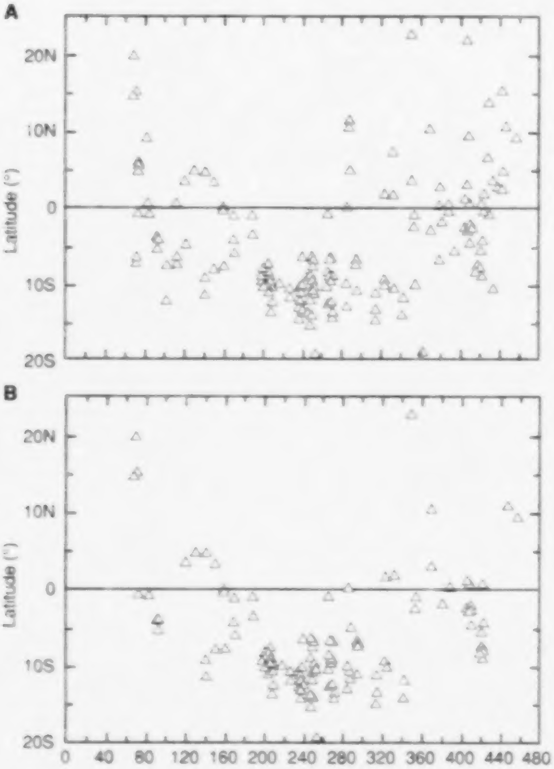

Figure 26. Paleolatitude values for individual samples, plotted against their depth (mbsf). **A.** All data plotted. **B.** Plot displaying only those samples in which stratigraphic "up" is known.

We were reluctant to average data containing so many obviously contaminated data points, but the true mean paleolatitudes cannot be determined by picking the midpoint of the lower part of the data band of Figure 26B. This is because paleomagnetic inclinations are distributed in a manner analogous to a circular Gaussian distribution. When declination is not known, as is the case in rotary cores in which azimuth is unknown, simple numerical averaging of the inclinations gives undue weight to the higher values, and paleolatitudes thus generated are a few degrees steeper than the true paleolatitude. Kono (1980) developed a statistical method to average such data to obtain true mean inclinations. Mean values were calculated with the Kono method from inclination groupings apparent within the data. Paleolatitudes computed from the mean inclinations are shown in Figure 27, along with their associated standard deviations.

The youngest data obtained suggest that Site 801 was probably still in the Southern Hemisphere during Campanian time. Cores 129-801A-7R to -10R, 60–97 mbsf (Fig. 26), yielded southern paleolatitude values. The northern paleolatitudes in this same interval (responsible for the "7-10" point in Fig. 27) are most probably an expression of strongly overprinted data, as the 15°N to 20°N values in Figure 26B bracket the present 18°N latitude of the site. Figures 26 and 27 indicate that the maximum southern latitude of the site occurred between middle Albian and Valanginian time (about Cores 129-801B-5R through -16R). The site appears to have been in the Southern Hemisphere through the Late Jurassic. The incomplete demagnetization make the data inconclusive re-

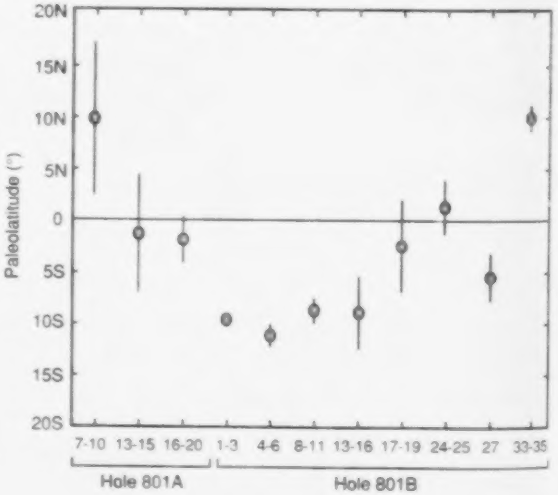

Figure 27. Paleolatitudes of Site 801 plotted for groups of cores. Error bars are one standard deviation of the mean.

garding whether (and when) the site may have crossed the equator in the Jurassic. Because significant secondary magnetization remains, particularly in the Berriasian through Tithonian samples (points 17-19 and 24-25 in Fig. 27) and in the red Callovian-Bathonian samples (point 33-35), the most probable interpretation of this data is that the site was in the Southern Hemisphere from Callovian-Bathonian time onward. However, it cannot be ruled out that those northern paleolatitudes in the Callovian-Bathonian samples (point 33-35, Fig. 27) have some validity and thus that the site may have been in the Northern Hemisphere during the Middle Jurassic. Shore-based analysis of thermally demagnetized samples will resolve this ambiguity.

### Basalt Magnetism

Segments of basaltic basement from Site 801 were analyzed with the cryogenic magnetometer. NRM measurements of core segments were followed by AF demagnetization using a variety of field steps. The highest field used was 20 mT but treatment to 15 mT was more common. Volume susceptibility was routinely measured on all cores.

The cryogenic magnetometer appeared to be able to measure most of the basalt in Hole 801B, but in Hole 801C the basalts generally exceeded the range of the magnetometer. In addition, measurements at Hole 801C were complicated by an apparent electronic chip failure in the magnetometer. NRM intensities of the basalts in Hole 801B were low for submarine basalt, about 0.1 mA/m. Response to AF demagnetization was quite varied and thus the data are difficult to interpret. Both normal and reversed polarity appear to be present, although it not possible at this time to determine whether both are characteristic. Normal polarity with shallow, near-zero inclinations was often observed in the finer-grained materials; reversed polarity with steeper (positive) inclinations was observed in the coarser grained units. However, while these were general observations, other coarse- and fine-grained units gave results inconsistent with these.

Only a few of the basalts from Hole 801C could be successfully measured with the cryogenic magnetometer, both because of the high intensities and malfunction of the magnetometer. Time did not permit discrete sampling and measurement with the spinner magnetometer. Samples of these basalts will be investigated onshore.

Susceptibility measurements of the basalts lead to some interesting results. Although preliminary, values of susceptibility seem to correlate with the alteration state of the basalts. Four major susceptibility horizons are recognized. The first of these horizons is composed of Cores 129-801B-37R through -44R and Cores 129-801C-1R through -2R. Susceptibilities in this interval are generally low, averaging approximately 100 SI, but range widely from 30 to 1600 SI. Although the range in values is high, the variation seems confined to specific zones that, at present, appear to correlate with lithologic boundaries or alteration phenomena (described in the "Igneous Petrology" section, this chapter).

The second and most obvious horizon occurs immediately above, into, and below the hydrothermal deposit from Core 129-801C-3R through -7R. Here the susceptibility not only outlines the hydrothermal deposit itself, but perhaps the entire event. The zone is characterized by extremely low susceptibility with the lowest values, approximately 2 to 16 SI, registered by the hydrothermal deposit. Immediately above and below the unit (Cores 129-801C-3R and Section 129-801C-5R-3) values for susceptibility rise to only a range of 15 to 87 SI. Beneath Section 129-801C-5R-3, values begin to rise to greater than 100 SI in Section 129-801C-5R-4. This marks the beginnings of the third or transition horizon beginning in Section 129-801C-5R-4 and continuing to Section 129-801C-7R-2. This horizon has much the same properties as the first interval described.

The final horizon begins at Section 129-801C-7R-3 and continues to the base of the hole, Section 129-801C-12R-3. Susceptibilities in this horizon, with minor exceptions (e.g., Core 129-801C-8R) have values consistently above 1000 SI and reaching as high as 3500 SI. These high susceptibility values may reflect the visibly relatively fresh, unaltered state of the basalt in this interval.

## INORGANIC GEOCHEMISTRY

Interstitial water samples were squeezed from sediment cores from seven depths in Holes 801A and 801B. The samples came only from the brown pelagic clay of lithologic Unit I, the volcaniclastic turbidites of Unit II, and the red radiolarite and claystone of Unit V. Because the chert and porcellanite of Unit II and the brown radiolarite of Unit IV have very low water content and were poorly recovered, no samples came from these units. Chemical analyses are summarized in Table 4 and presented in Figures 28 and 29. Yields from squeezing, in mL/cm of whole-round core, varied between lithologies: nearly 8 mL/cm in Unit I, nearly 1.5 mL/cm in Unit III, and 2 mL/cm in Unit V. Pollution by drilling fluids (see Table 3, "Inorganic Geochemistry" section, "Site 800," this chapter) is difficult to rule out for the samples at 23 and 44 mbsf, as these waters have chemical composition close to seawater. For the deeper samples, the very low potassium content of the samples suggests that fluid contamination is unlikely.

### Results

Interstitial waters are very similar to seawater at 23 and 44 mbsf in the brown clays of Unit I. Only silicon and sulfate significantly increase at 44 mbsf. Below Unit II (brown chert and porcellanite), interstitial waters extracted from the volcaniclastic turbidites at 175, 233, and 265 mbsf display a general depletion in magnesium, potassium, sodium, and an enrichment in calcium. The overall depletion in cations is balanced by alkalinity, and sulfate decreases while chlorine remains constant. Magnesium is reduced to 28%–35% of seawater content, potassium to 21%–34%, sodium (Na$^{*}$) to about 95%, and calcium increases to 450%–538% of seawater content. From 175 to 265 mbsf, manganese content increases gradually from 51 to 123 μmol/L, silicon sinks rapidly from 427 to 233 mmol/L and strontium is variable between 280 and 543 mmol/L. Between 444 and 454 mbsf (below Unit IV), magnesium is less depleted than between 175 and 233 mbsf and calcium is less enriched (respectively, 68% and 390%, relative to seawater). Potassium decreases to about 2 mmol/L, whereas sodium increases to near its initial value. Silicon remains constant and manganese is highly depleted compared to concentrations between 444 and 454 mbsf.

Concentration profiles of magnesium, calcium, and potassium display a clear variation from samples from Unit I to samples from Unit III. As in Hole 800A, it is the presence of a lithological barrier for diffusion over sediments undergoing diagenetic reactions (cherts over volcaniclastic turbidites) that generates these breaks. This effect is caused by to the low water content and low porosity of Unit II (3%–10% and 8%–21%, respectively (see "Physical Properties" section, this chapter). A similar barrier to diffusion probably operates in the radiolarites of Unit IV in the interval where water content remains between 1% and 3.8%, between 365 and 396 mbsf. Despite the absence of large concentration gradients between Units III and V, the fact that magnesium and sodium are higher and calcium is lower in Unit V than in Unit III is

Table 4. Chemical composition of interstitial water extracted from sediments in Holes 801A and 801B.

| Core, section, interval (cm) | Depth (mbsf)[a] | Alkalinity (meq/L) | Cl (mmol/L) | $SO_4$ (mmol/L) | pH | Salinity (‰) | Ca (mmol/L) | Mg (mmol/L) | K (mmol/L) | Na* (mmol/L) | Mn (μmol/L) |
|---|---|---|---|---|---|---|---|---|---|---|---|
| 129-801A- | | | | | | | | | | | |
| 3R-2, 145–150 | 23 | 2.8 | 562.0 | 29.3 | 7.5 | 35.5 | 10.9 | 52.0 | 11.2 | 483 | l.d. |
| 5R-3, 145–150 | 44 | 2.9 | 564.0 | 37.2 | 7.6 | 36.0 | 12.0 | 53.2 | 11.6 | 496 | 3.7 |
| 19R-1, 65–73 | 175 | 0.7 | 560.0 | 19.3 | 8.0 | 34.0 | 53.2 | 15.1 | 3.8 | 457 | 51.4 |
| 129-801B- | | | | | | | | | | | |
| 5R-2, 0–10 | 233 | 0.5 | 569.0 | 16.1 | 7.7 | 35.5 | 56.1 | 14.9 | 2.7 | 455 | 87.1 |
| 8R-3, 115–125 | 265 | 0.6 | 543.0 | 16.8 | 8.1 | 34.5 | 46.6 | 18.6 | 2.4 | 442 | 123.0 |
| 33R-1, 143–150 | 444 | 1.4 | 586.0 | 17.5 | 7.5 | 36.2 | 40.9 | 35.3 | 1.9 | 465 | 27.8 |
| 35R-2, 0–10 | 454 | 1.3 | 572.0 | 21.0 | 8.0 | 35.2 | 40.4 | 36.0 | 2.0 | 458 | 25.2 |

[a] Depth rounded to the nearest meter.

Note: Na* is calculated by charge balance. l.d. = less than detection level.

likely to be related to the presence of the low water content level.

The changes in calcium and magnesium are typical of gradients in sediment pore waters controlled by alteration reactions in underlying basalts (e.g., Gieskes and Johnson, 1981). In Unit III the presence of altered volcanic glass, plagioclase, and green magnesian smectite (see "Lithology and Sedimentology" section, this chapter) suggest that *in-situ* alteration and diagenetic reactions uptake magnesium and release calcium. In contrast, no mineral subject to calcium release has been identified in Unit V. Calcium and magnesium concentrations in Unit V are therefore more likely to be related to alteration of the underlying basement than by *in-situ* reactions.

The potassium concentration profile shows depletion below 175 mbsf in Unit III. Formation of clinoptilolite, observed in Unit II as well as in Unit III, certainly represents the major sink for potassium. In Unit V no zeolites have been recognized, and potassium, as for calcium and magnesium, may be controlled by reactions in the basement.

Sodium is depleted only in the samples of Unit III and, as in Hole 800A, it is probably the *in-situ* formation of zeolite which uptakes sodium.

A silica increase in Unit I is probably due to diffusion from the chert and porcelanite of Unit II. In Unit III, the silica decrease between 175 and 233 mbsf is certainly due to silicon uptake during the formation of authigenic clays and zeolites. The high concentration at 175 mbsf is likely to be linked to the presence of silicified radiolarian claystones at about 183 mbsf in Core 129-801A-20R. Hence, it should be only a local high concentration due to a particular change in lithology.

Manganese reaches significant concentrations only in Unit III, which reflects (1) the general reducing conditions in the volcaniclastic turbidites and (2) the oxidizing conditions in the red claystones of Unit V. Manganese oxides related to fractures are frequent in Unit V.

### Conclusions

In sediments of Site 801, the presence of cherts and radiolarites with very low porosity (10%–20%) in Units II and IV appears to isolate the three sampled lithologic units. In Unit I, interstitial water composition is very close to that of seawater and only the silica diffusing from the underlying radiolarite increases significantly. In the volcaniclastics of Unit III, *in-situ* diagenetic and alteration reactions deplete the waters in magnesium, potassium, silicon, and sodium, and release calcium. In Unit V, the magnesium-calcium exchange is more likely to be related to alteration in basement than to *in-situ* reactions. In contrast to Hole 800A, chloride concentration remains constant at all depths.

## PHYSICAL PROPERTIES

Physical properties measurements were collected on discrete sediment and rock samples recovered at Site 801. These measurements are presented in Tables 5, 6, and 7 for Holes 801A, 801B, and 801C, respectively, and include index properties (wet-bulk density, porosity, water content, and grain density), compressional-wave velocity, and thermal conductivity. Continuous GRAPE density and *P*-wave velocity measurements, on the multisensor track, were not collected due to coring disturbance and incomplete filling of core liners. However, GRAPE density measurements were made on discrete sediment and rock samples. The above measurements were obtained on average once every other section. Methodologies and equipment used in collecting these data are described in the "Explanatory Notes" chapter (this volume).

### Index Properties

Porosity measurements were determined from gravimetric measurements, except where only GRAPE analysis was employed. Wet-bulk density measurements were determined by gravimetric and 2-min GRAPE methods. Grain densities were determined mostly from solid pieces, but for 18 samples, measurements were determined using powdered samples (Tables 5, 6, and 7).

The pelagic brown clays of Unit I (8.0–63.8 mbsf), recovered in Cores 129-801-1R to -7R and sampled for physical properties in Cores 129-801-1R, -3R, -4R, -5R, and -7R, were highly disturbed as a result of rotary coring. The porosity, wet-bulk density, and grain density of these sediments average 75.6%, 1.41 g/cm$^3$, and 2.56 g/cm$^3$, respectively. Porosity and wet-bulk density values should be viewed with caution because of the drilling disturbance. Overall, porosity decreases downsection, ranging from 84.0% to 60.1%, whereas wet-bulk density increases with depth and ranges from 1.27 to 1.69 g/cm$^3$ (Fig. 30).

Brown chert and porcellanite are the dominant lithologies recovered in Unit II (63.8–126.5 mbsf) and show downsection trends of increasing porosity (8.3%–36.1%) and grain density (2.15–2.44 g/cm$^3$), with wet-bulk density values averaging 2.05 g/cm$^3$ (Fig. 30, Tables 5 and 6). The increase in porosity and grain density with depth may be related to a downward increase in abundance of calcareous beds (see "Lithostratigraphy and Sedimentology" section, this chapter).

The volcaniclastic turbidite sequences of lithologic Unit III (126.5–318.3 mbsf) are characterized by highly variable physical properties (Fig. 30). Porosity and grain density range from

Table 4 (continued).

| Si (µmol/L) | Sr (µmol/L) | Lithology |
|---|---|---|
| 200 | 84 | Pelagic brown clay |
| 323 | 8 | Pelagic brown clay |
| 427 | 289 | Volcanogenic silty claystone |
| | | |
| 249 | 280 | Volcanogenic silty claystone |
| 233 | 543 | Volcanogenic silty claystone |
| 212 | 274 | Red clay |
| 218 | 280 | Red clay |

21.7% to 71.9% and 2.44 to 2.98 g/cm³, respectively, with wet-bulk density ranging from 1.50 to 2.17 g/cm³. Textural variations, ranging from claystone to sandstone, account for the high variation within these volcaniclastic sediments. Fine-grained pelagic interbeds are common in the upper part of this unit (126–208 mbsf) and also account for the greater variability in porosity, grain density, and wet-bulk density. Porosity, grain density, and wet-bulk density range from 21.7% to 71.9%, 2.29 to 2.98 g/cm³, and 1.50 to 2.05 g/cm³, respectively, in this part of Unit III (Tables 5 and 6).

Pelagic interbeds and volcaniclastic sandstones are less common in the central part of the volcaniclastic unit (208–278 mbsf). The index properties of volcaniclastic siltstones and claystones, which dominate this part of Unit III, are more closely grouped (Fig. 30). Porosity and grain density range from 56.9% to 68.4% and 2.68 to 2.86 g/cm³, respectively. Wet-bulk density values range from 1.59 to 1.81 g/cm³ (Tables 5 and 6).

The lower part of Unit III (278–318 mbsf) is a transition zone between overlying volcaniclastic sediments and underlying brown radiolarites of Unit IV. It consists of volcaniclastic turbidites interbedded with radiolarian claystones (see "Lithostratigraphy and Sedimentology" section, this chapter). Such an assemblage produces a wide range of values for porosity (25.9%–61.5%), grain density (2.57–2.74 g/cm³), and wet-bulk density (1.69–2.03 g/cm³). A sharp decrease in porosity and grain density and an increase in wet-bulk density characterize the base of this transition zone, with respective values of 37.6%, 2.64 g/cm³, and 2.03 g/cm³ at 280.27 mbsf (Fig. 30, Table 6).

The radiolarites and cherts of Unit IV yielded wide-ranging values for porosity (2.5%–49.6%), and wet-bulk density (1.91–2.61 g/cm³). Grain density is more nearly constant, averaging 2.68 g/cm³, and ranging from 2.60 to 2.85 g/cm³ throughout this unit (Table 6). The radiolarites have a high porosity, ranging from 35.3% to 49.6%, relative to the cherts, which have a range of 2.5% to 8.9%. The wet-bulk density of the cherts ranges between 2.46 and 2.61 g/cm³ and is distinctly higher than that of the radiolarites which ranges from 1.91 to 2.21 g/cm³ (Fig. 30).

The lowermost sedimentary unit at Site 801, Unit V (442.9–461.6 mbsf), consists of interbedded red radiolarite and claystone. Claystone, sampled at 443.35 mbsf, displays values of 46.2%, 2.76 g/cm³, and 1.96 g/cm³ for porosity, grain density, and wet-bulk density, whereas radiolarite, sampled at 453.61 mbsf, is characterized by values of 46.8%, 2.73 g/cm³, and 1.93 g/cm³ (Table 5).

The interbedded basalts and silicified claystones of the upper part (above 563 mbsf) of lithologic Unit VI (461.6–90.9 mbsf) show more variation in physical properties (Table 6) than the basalts of the lower part (below 563 mbsf). Index

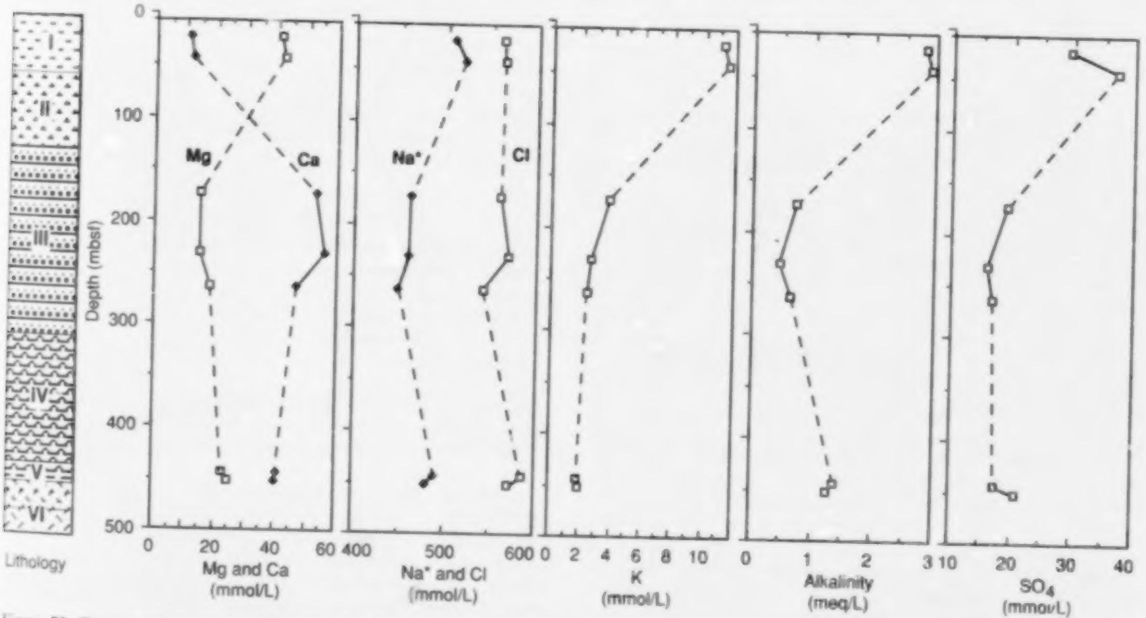

Figure 28. Concentration vs. depth profiles for Mg, Ca, Na*, Cl, K, alkalinity, and $SO_4$ in interstitial water extracted from sediments in Holes 801A and 801B. Connection lines are dashed for the intervals 44–175 mbsf and 265–444 mbsf because of low porosities in Units II and IV. The lithostratigraphic column refers to the lithologic units defined in the "Lithostratigraphic and Sedimentology" section (this chapter). Unit I, brown pelagic clay; Unit II, brown chert and porcelanite; Unit III, volcaniclastic turbidites; Unit IV, brown radiolarite; Unit V, red radiolarite and claystone; and Unit VI, aphyric basalts.

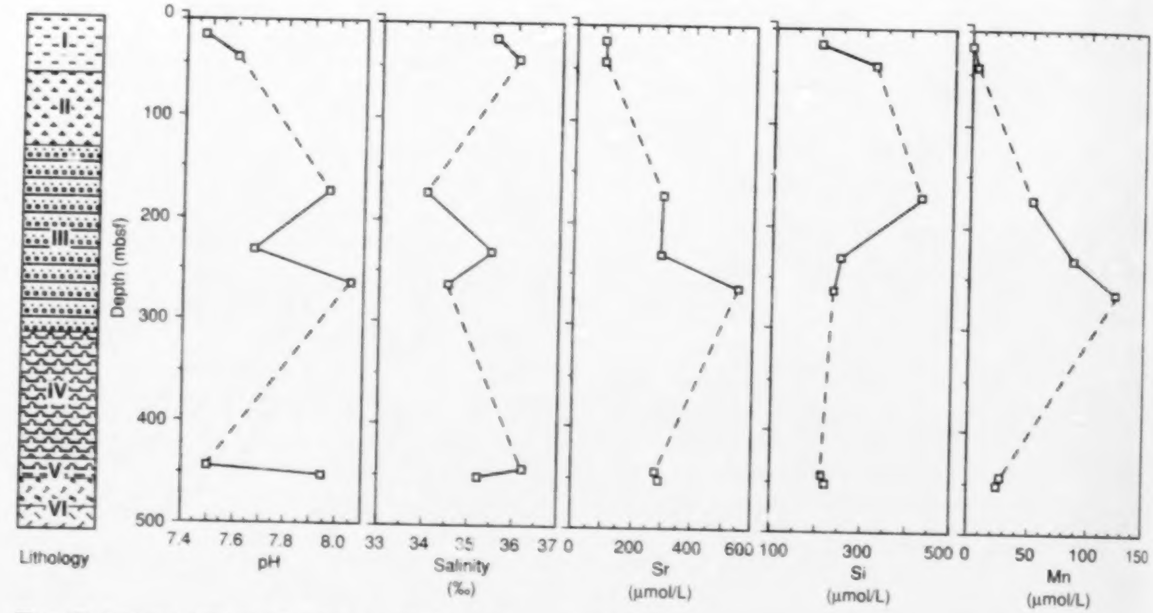

Figure 29. Profiles of depth vs. pH, salinity, and Sr, Si, and Mn concentrations in interstitial water extracted from sediments in Holes 801A and 801B. See Figure 28 for legend.

Table 5. Physical properties summary for Hole 801A.

| Core, section, interval (cm) | Depth (mbsf) | Wet-bulk density Gravimetric (g/cm³) | Wet-bulk density GRAPE (g/cm³) | Grain density[a] (g/cm³) | Porosity (%) | Water content (%) | Vertical velocity (m/s) | Horizontal velocity (m/s) | Velocity anisotropy (%) | Thermal conductivity (W/m · K) | Remarks |
|---|---|---|---|---|---|---|---|---|---|---|---|
| 129-801A- | | | | | | | | | | | |
| 1R-1, 60–61 | 8.60 | 1.28 | | 2.58 | 83.8 | 66.7 | | | | 0.90 | Pelagic clay |
| 3R-1, 76–79 | 21.16 | 1.27 | | 2.38 | 81.5 | 65.3 | 1517 | | | 1.02 | Pelagic clay |
| 3R-3, 94–97 | 24.34 | 1.32 | | 2.34 | 77.4 | 59.5 | 1494 | | | 0.96 | Pelagic clay |
| 4R-1, 77–79 | 30.77 | 1.27 | | 2.54 | 84.0 | 67.4 | 1508 | | | 0.89 | Pelagic clay |
| 4R-2, 50–50 | 32.00 | | | | | | | | | 0.94 | Pelagic clay |
| 5R-1, 74–76 | 40.34 | 1.69 | | 2.70 | 60.1 | 36.2 | 1556 | | | 1.04 | Nannofossil ooze |
| 5R-3, 74–76 | 43.34 | 1.44 | | 2.60 | 73.5 | 51.8 | 1527 | | | 0.95 | Pelagic clay |
| 5R-5, 74–76 | 46.34 | 1.45 | | 2.62 | 73.3 | 51.4 | 1550 | | | 1.04 | Pelagic clay |
| 7R-1, 75–77 | 59.75 | 1.47 | | 2.61 | 72.3 | 50.3 | | | | 0.94 | Pelagic clay |
| 7R-3, 76–78 | 62.76 | 1.46 | | 2.67 | 73.9 | 51.7 | | | | 0.97 | Pelagic clay |
| 7R-CC, 11–13 | 64.06 | 2.33 | 2.22 | 2.29(2.45) | 8.3 | 3.6 | 4116 | 4638 | 3.0 | 1.69 | Radiolarian chert |
| 9R-1, 17–19 | 78.37 | 1.93 | 2.01 | 2.15 | 19.2 | 10.0 | 3468 | 3605 | 1.0 | 1.91 | Radiolarian chert |
| 10R-1, 22–24 | 87.72 | 1.97 | 2.01 | 2.23 | 21.7 | 11.2 | 3577 | 3356 | -1.6 | 1.82 | Radiolarian porcellanite |
| 12R-1, 1–3 | 106.81 | 1.98 | | 2.32 | 26.3 | 13.5 | | | | | Chert/porcellanite |
| 13R-1, 13–15 | 116.63 | 2.13 | 1.94 | 2.19(2.44) | 21.7 | 10.4 | 3391 | 3619 | 1.6 | 1.86 | Radiolarian porcellanite |
| 14R-1, 51–53 | 126.71 | 1.93 | 1.90 | 2.44 | 36.1 | 19.0 | 2569 | 2648 | 0.8 | 1.54 | Radiolarian porcellanite |
| 15R-1, 11–13 | 136.01 | 1.99 | 1.95 | 2.91 | 49.1 | 25.2 | 2463 | 2492 | 0.3 | 1.43 | Volcaniclastic sandstone |
| 16R-1, 39–41 | 145.49 | 1.80 | 1.76 | 2.97 | 60.6 | 34.4 | 2135 | 2167 | 0.4 | 1.20 | Volcaniclastic sandstone |
| 17R-1, 64–66 | 155.84 | 1.98 | 1.94 | 2.29(2.44) | 32.4 | 16.6 | 2997 | 3156 | 1.3 | 1.70 | Chert/porcellanite |
| 18R-1, 49–51 | 165.49 | 1.70 | 1.68 | 2.80 | 62.0 | 37.2 | 2038 | 2025 | -0.2 | 1.14 | Volcaniclastic sandstone |
| 19R-1, 33–35 | 175.63 | 1.50 | 1.48 | 2.72 | 71.9 | 48.7 | 1642 | 1667 | 0.4 | | Volcaniclastic silty claystone |
| 20R-1, 15–17 | 184.55 | 2.09 | 2.12 | 2.38 | 21.7 | 10.6 | 3488 | 3636 | 1.0 | 1.79 | Radiolarian claystone |

[a] Values in parentheses were determined using powdered samples.

properties were measured using gravimetric techniques and 2-min GRAPE for all samples except three, for which only the 2-min GRAPE was used. Porosities were estimated for these three samples, using the relationship between porosity, wet-bulk density, and fluid density (see "Explanatory Notes" chapter, this volume). Porosities, ranging from 1.0% to 23.0%, characterize the basalts and dolerites of the upper part of Unit VI. The highest porosity (23.0%) occurs in a heavily altered flow unit sampled at 541.65 mbsf. The grain density of the basalts and dolerites ranges from 2.67 to 2.99 g/cm³ and wet-bulk density varies between 2.37 and 2.97 g/cm³. Chert, interbedded with basalt at 470.79 mbsf, is characterized by porosity, wet-bulk density, and grain density values of 3.3%, 2.66 g/cm³, and 2.71 g/cm³, respectively. A sedimentary hydrothermal deposit, sampled at 530.14 mbsf, has a wet-bulk density of 2.52 g/cm³, grain density of 2.65 g/cm³, and porosity of 8.0%. Between 563 and 594 mbsf, index properties are characterized by low variability (Fig. 30). Excluding a

Table 6. Physical properties summary for Hole 801B.

| Core, section, interval (cm) | Depth (mbsf) | Wet-bulk density: Gravimetric ($g/cm^3$) | Wet-bulk density: GRAPE ($g/cm^3$) | Grain density[a] ($g/cm^3$) | Porosity (%) | Water content (%) | Vertical velocity (m/s) | Horizontal velocity (m/s) | Velocity anisotropy (%) | Thermal conductivity (W/m · K) | Remarks |
|---|---|---|---|---|---|---|---|---|---|---|---|
| 129-801B- | | | | | | | | | | | |
| 1R-1, 55–57 | 194.55 | 1.83 | 1.81 | 2.71 | 52.3 | 29.1 | 1929 | 1959 | 0.4 | 1.34 | Radiolarian claystone |
| 1R-3, 81–83 | 197.81 | 2.01 | 1.99 | 2.98 | 49.7 | 25.2 | 2421 | 2481 | 0.6 | 1.33 | Volcaniclastic sandstone |
| 2R-1, 92–94 | 204.42 | 2.05 | 2.03 | 2.82 | 43.1 | 21.4 | 2625 | 2618 | −0.1 | 1.38 | Volcaniclastic sandstone |
| 3R-CC, 0–2 | 214.06 | 1.59 | 1.56 | 2.78(2.82) | 68.4 | 43.9 | 1802 | 1881 | 1.1 | | Clayey siltstone |
| 4R-1, 17–19 | 222.47 | 1.70 | 1.70 | 3.20(2.83) | 62.7 | 37.8 | 1894 | 1919 | 0.3 | 1.22 | Volcaniclastic sandy claystone |
| 5R-1, 64–66 | 232.34 | 1.80 | 1.80 | 2.91(2.84) | 57.0 | 32.3 | 1739 | 2021 | 3.8 | 1.43 | Volcaniclastic claystone |
| 5R-2, 145–147 | 234.65 | 1.69 | 1.68 | 3.02(2.75) | 61.2 | 36.9 | 1820 | 1860 | 0.5 | 1.29 | Volcaniclastic sandstone |
| 6R-1, 12–14 | 241.42 | 1.68 | 1.68 | 2.86 | 64.6 | 39.3 | 1711 | 1836 | 1.8 | 1.25 | Volcaniclastic silty sandstone |
| 6R-3, 6–8 | 244.36 | 1.81 | 1.80 | 2.84 | 56.9 | 32.0 | 1736 | 1960 | 3.0 | 1.38 | Volcaniclastic sandy siltstone |
| 6R-4, 10–12 | 245.90 | 1.7 | 1.69 | 2.73 | 60.2 | 36.0 | 1887 | 2046 | 2.0 | 1.23 | Volcaniclastic clayey siltstone |
| 7R-1, 3–5 | 251.03 | 1.81 | 1.82 | 2.84 | 57.1 | 32.2 | 1728 | 1904 | 2.4 | 1.43 | Volcaniclastic claystone |
| 8R-2, 24–26 | 262.44 | 1.76 | 1.68 | 2.77 | 57.7 | 33.4 | 1808 | 2027 | 2.9 | 1.35 | Volcaniclastic silty claystone |
| 8R-4, 126–128 | 266.46 | 1.59 | 1.58 | 2.69(2.68) | 65.7 | 42.2 | 1763 | 1864 | 1.4 | 1.14 | Volcaniclastic silty claystone |
| 10R-1, 27–29 | 280.27 | 2.03 | 2.03 | 2.64 | 37.6 | 18.8 | 2454 | 2779 | 3.1 | | Calcareous siltstone |
| 11R-1, 22–24 | 289.92 | 2.17 | 2.00 | 2.57 | 25.9 | 12.2 | 3076 | 3914 | 6.0 | | Clayey radiolarite |
| 12R-1, 15–17 | 299.45 | 1.92 | 1.91 | 2.82 | 50.2 | 26.6 | 2362 | 2303 | −0.6 | 1.31 | Volcaniclastic siltstone |
| 13R-1, 47–49 | 309.47 | 1.69 | 1.68 | 3.24(2.74) | 61.5 | 37.3 | 1899 | 1977 | 1.0 | 1.22 | Volcaniclastic claystone |
| 14R-1, 19–21 | 318.49 | 1.91 | 1.74 | 2.78 | 49.6 | 26.5 | 1927 | 2028 | 1.3 | 1.39 | Clayey radiolarite |
| 16R-1, 30–32 | 337.50 | 2.54 | 2.48 | 2.54(2.60) | 3.7 | 1.5 | 5072 | 5078 | 0.0 | 2.31 | Radiolarian chert |
| 17R-1, 346.60 | 346.60 | 1.96 | 1.93 | 2.63 | 42.1 | 21.9 | 2355 | 2153 | −2.2 | 1.61 | Radiolarite |
| 18R-1, 17–19 | 355.97 | 1.99 | 1.95 | 2.66 | 41.3 | 21.2 | 2198 | 2304 | 1.2 | 1.55 | Radiolarite |
| 19R-1, 26–28 | 365.56 | 2.61 | 2.73 | 2.60(2.65) | 2.5 | 1.0 | 5280 | 4987 | −1.4 | | Chert |
| 20R-1, 21–23 | 374.71 | 2.61 | 2.51 | 2.58(2.65) | 2.5 | 1.0 | 5173 | 5305 | 0.6 | | Chert |
| 21R-1, 10–12 | 383.80 | 2.46 | 2.42 | 2.47(2.60) | 8.9 | 3.7 | 4568 | 4250 | −1.8 | 2.16 | Chert |
| 23R-CC, 13–15 | 396.03 | 2.58 | 2.47 | 2.54(2.65) | 4.5 | 1.8 | 5035 | 4904 | −0.7 | | Chert |
| 25R-1, 41–43 | 405.61 | 1.95 | 1.89 | 2.73 | 45.7 | 23.9 | 1965 | 2016 | 0.6 | 1.50 | Clayey radiolarite |
| 27R-1, 37–39 | 415.07 | 1.95 | 1.93 | 2.68 | 44.3 | 23.1 | 2059 | 2155 | 1.1 | 1.72 | Clayey radiolarite |
| 31R-1, 25–27 | 433.85 | 2.21 | 2.07 | 2.85 | 35.3 | 16.3 | 2389 | 2562 | 1.7 | 1.68 | Clayey radiolarite |
| 33R-1, 55–57 | 443.35 | 1.96 | 1.93 | 2.76 | 46.2 | 24.0 | 1840 | 1945 | 1.4 | 1.39 | Claystone with radiolarians |
| 35R-1, 131–133 | 453.61 | 1.93 | 1.94 | 2.73 | 46.8 | 24.6 | 1761 | 1861 | 1.4 | 1.66 | Radiolarite |
| 37R-1, 56–58 | 462.04 | 2.38 | 2.34 | 2.75(2.70) | 19.3 | 8.3 | 3461 | 3622 | 1.1 | 1.50 | Aphyric basalt |
| 39R-1, 9–11 | 470.79 | 2.66 | 2.52 | 2.60(2.71) | 3.3 | 1.3 | 5035 | 5138 | 0.5 | | Chert |
| 40R-1, 38–40 | 477.28 | | 2.42 | | 19.1[b] | | 3805 | 3565 | −1.6 | 1.65 | Aphyric basalt |
| 41R-2, 95–97 | 485.45 | | 2.63 | | 11.6[b] | | 4843 | 4451 | −2.1 | 1.76 | Aphyric basalt |
| 42R-2, 95–97 | 490.00 | 2.71 | 2.65 | 2.85(2.89) | 9.6 | 3.6 | 4838 | 4694 | −0.8 | 1.75 | Aphyric dolerite |
| 43R-1, 42–44 | 492.62 | | 2.61 | | 12.7[b] | | 4945 | 4889 | −0.3 | 1.80 | Phyric basalt |
| 43R-3, 121–123 | 496.19 | 2.63 | 2.54 | 2.69(2.81) | 9.8 | 3.8 | 5105 | 4902 | −1.0 | 1.80 | Phyric basalt |
| 44R-1, 54–56 | 502.24 | 2.65 | 2.57 | 2.77(2.83) | 10.2 | 3.9 | 4766 | 4515 | −1.4 | 1.67 | Aphyric basalt |

[a] Values in parentheses were determined using powdered samples.

[b] Porosity determined from GRAPE wet-bulk density.

moderately high-porosity (9.4%), low-density sample at 588.00 mbsf, ranges for porosity, wet-bulk density, and grain density are 2.1% to 3.3%, 2.85 to 2.92 $g/cm^3$, and 2.91 to 2.97 $g/cm^3$, respectively (Table 7).

### Compressional-Wave Velocity

Compressional-wave velocities, measured perpendicular and horizontal to bedding on discrete samples in the Hamilton Frame Velocimeter, show considerable variation downsection. These changes in velocity correspond with variations in index properties and lithologies. Unless otherwise noted the velocities cited are for the vertical propagation direction.

Throughout lithologic Unit I (soft brown pelagic clay), the compressional-wave velocities are closely grouped (Fig. 31). Velocity averages 1525 m/s and ranges from 1494 to 1556 m/s (Table 5).

Compressional-wave velocities in Unit II decrease downsection from a maximum of 4116 m/s at 64.06 mbsf to a low of 3391 m/s at the base of the unit (116.63 mbsf), with an overall unit average of 3638 m/s. The highest velocity and velocity anisotropy in Unit II occur in chert near the top of the unit (Fig. 31). Values for both parameters decrease downsection in Unit II.

In Unit III, sonic velocity is highly variable in the upper part of the unit (126–208 mbsf), low and less variable in the central part of the unit (208–278 mbsf), and high with a distinct trend decreasing downsection in the lower part of the unit (278–318 mbsf) (Fig. 31). The scatter in the data from the upper part of Unit III can be attributed to a variety of textural and physical changes in lithologies (Tables 5 and 6, Fig. 31). Compressional-wave velocities range from 1642 m/s in volcaniclastic silty claystone, at 175.03 mbsf, to 3488 m/s in radiolarian claystone, at 184.55 mbsf. Consistently low velocities occur within the volcaniclastic siltstones and claystones of the central part of Unit III. These velocities range from 1711 to 1894 m/s and average 1789 m/s. These velocity values are associated with high porosities (ranging from 56.9%–68.4%) and low wet-bulk densities (ranging from 1.59–1.81 $g/cm^3$). Velocity anisotropy for these sediments ranges from 0.5% to 3.8% and maintains a higher overall average (1.92%) than the upper and lower parts of this unit (Fig. 31). The lower part of Unit III is characterized by higher velocities, associated with the occurrence of clayey radiolarite. Velocity decreases downsection, in this part of Unit III, from 3076 m/s in clayey radiolarite at 289.92 mbsf to 1899 m/s in the volcaniclastic claystone, at 309.47 mbsf (Fig. 31).

Distinct differences in velocity values between chert and radiolarite characterize lithologic Unit IV. Velocities in chert range from 4568 m/s to 5280 m/s and average 5026 m/s. Velocities in radiolarite range from 1927 to 2389 m/s and average 2149 m/s. Variations in velocity with depth are not well defined (Fig. 31). Anisotropy for the cherts ranges from 1.8% to 0.6% and from 2.2% to 1.7% for the radiolarites. The cherts are characterized by negative anisotropy, and the

**Table 7. Physical summary for Hole 801C.**

| Core, section, interval (cm) | Depth (mbsf) | Wet-bulk density Gravimetric (g/cm³) | Wet-bulk density GRAPE (g/cm³) | Grain density (g/cm³) | Porosity (%) | Water content (%) | Vertical velocity (m/s) | Horizontal velocity (m/s) | Velocity anisotropy (%) | Thermal conductivity (W/m · K) | Remarks |
|---|---|---|---|---|---|---|---|---|---|---|---|
| 129-801C- | | | | | | | | | | | |
| 1R-1, 90–92 | 494.60 | 2.67 | 2.62 | 2.84 | 9.5 | 3.6 | 4589 | 4652 | 0.2 | 1.82 | Aphyric microdolerite |
| 1R-3, 82–84 | 497.13 | 2.59 | 2.6 | 2.77 | 10.4 | 4.1 | 4436 | 4374 | −0.4 | 1.62 | Sparcely plagioclase phyric basalt |
| 1R-5, 29–31 | 498.84 | 2.59 | 2.61 | 2.71 | 7.1 | 2.8 | 5154 | 5087 | −0.3 | 1.91 | Aphyric basalt |
| 2R-1, 14–16 | 503.14 | 2.47 | 2.48 | 2.69 | 13.2 | 5.4 | 4267 | 4266 | 0.0 | | Sparsely plagioclase phyric basalt |
| 2R-2, 81–83 | 505.19 | 2.63 | 2.65 | 2.8 | 9.6 | 3.7 | 4866 | 4866 | 0.0 | | Aphyric basalt |
| 2R-4, 76–78 | 507.86 | 2.66 | 2.63 | 2.94 | 10.1 | 3.9 | 4757 | 4808 | 0.3 | 1.82 | Sparsely plagioclase microphyric basalt |
| 3R-1, 32–34 | 512.52 | 2.38 | 2.39 | 2.69 | 18.7 | 8.0 | 3746 | 3755 | 0.1 | 1.60 | Aphyric basalt |
| 4R-1, 44–46 | 522.14 | 2.52 | 2.49 | 2.65 | 8.0 | 3.2 | 5141 | 5112 | −0.1 | 4.98 | Yellow hydrothermal deposit |
| 5R-1, 103–105 | 532.23 | 2.41 | 2.35 | 2.67 | 16.0 | 6.8 | 3982 | 3879 | −0.7 | 1.65 | Highly plagioclase megaphyric basalt |
| 5R-2, 87–89 | 533.33 | 2.53 | 2.52 | 2.77 | 14.0 | 5.6 | 4510 | 4592 | 0.5 | 1.65 | Moderately plagioclase megaphyric basalt |
| 5R-3, 43–45 | 534.20 | 2.64 | 2.62 | 2.84 | 10.8 | 4.2 | 4990 | 4966 | −0.1 | 1.73 | Moderately plagioclase megaphyric basalt |
| 6R-1, 115–117 | 541.65 | 2.37 | 2.36 | 2.78 | 23.0 | 9.8 | 3690 | 3479 | −1.5 | 1.69 | Sparsely plagioclase phyric basalt |
| 6R-2, 35–37 | 542.14 | 2.80 | 2.70 | 2.85 | 2.4 | 0.9 | 5994 | 5975 | −0.1 | 1.74 | Aphyric basalt |
| 6R-4, 111–113 | 545.76 | 2.36 | 2.36 | 2.70 | 20.3 | 8.7 | 3773 | 3879 | 0.7 | 1.49 | Moderately olivine plagioclase phyric basalt |
| 6R-5, 68–70 | 546.71 | 2.94 | 2.92 | 2.98 | 1.7 | 0.6 | 6313 | 6323 | 0.0 | 1.94 | Sparsely olivine-plagioclase microphyric basalt |
| 7R-1, 35–37 | 550.45 | 2.96 | 2.92 | 2.99 | 1.3 | 0.5 | 6333 | 6414 | 0.3 | 2.02 | Aphyric basalt |
| 7R-2, 37–39 | 551.92 | 2.67 | 2.71 | 2.81 | 7.9 | 3.0 | 5281 | 5248 | −0.2 | 1.80 | Aphyric basalt |
| 8R-1, 65–67 | 560.15 | 2.47 | 2.48 | 2.81 | 18.8 | 7.7 | 4108 | 4088 | −0.1 | 1.60 | Aphyric basalt |
| 8R-2, 78–80 | 561.35 | 2.97 | 2.94 | 2.99 | 1.0 | 0.3 | 6588 | 6593 | 0.0 | 1.95 | Aphyric basalt |
| 9R-1, 49–51 | 563.69 | 2.86 | 2.85 | 2.92 | 3.3 | 1.2 | 6367 | 6442 | 0.3 | 2.10 | Aphyric basalt |
| 9R-3, 121–123 | 567.15 | 2.88 | 2.88 | 2.93 | 2.5 | 0.9 | 6077 | 6364 | 1.2 | 1.95 | Aphyric basalt |
| 9R-4, 137–139 | 568.58 | 2.91 | 2.91 | 2.96 | 2.7 | 0.9 | 6325 | 6114 | −0.8 | 1.97 | Aphyric basalt |
| 10R-2, 55–57 | 571.05 | 2.92 | 2.90 | 2.97 | 2.6 | 0.9 | 6218 | 6224 | 0.1 | 2.16 | Aphyric basalt |
| 10R-5, 3–5 | 574.84 | 2.92 | 2.91 | 2.96 | 2.1 | 0.7 | 6234 | 6275 | 0.2 | 1.99 | Sparsely olivine microphyric basalt |
| 10R-6, 65–67 | 576.81 | 2.86 | 2.86 | 2.91 | 2.7 | 1.0 | 6040 | 5981 | −0.2 | 2.11 | Sparsely olivine microphyric basalt |
| 11R-2, 119–121 | 580.49 | 2.85 | 2.84 | 2.91 | 2.9 | 1.0 | 6102 | 6050 | −0.2 | 2.24 | Sparsely plagioclase-olivine microphyric basalt |
| 11R-3, 40–42 | 581.20 | 2.87 | 2.87 | 2.91 | 2.3 | 0.8 | 6304 | 6204 | −0.4 | 2.43 | Aphyric basalt |
| 12R-1, 70–72 | 588.00 | 2.59 | 2.66 | 2.75 | 9.4 | 3.6 | 5011 | 5027 | 0.3 | 1.75 | Aphyric basalt |
| 12R-2, 109–111 | 589.89 | 2.92 | 2.91 | 2.96 | 2.1 | 0.7 | 6178 | 6245 | 1.1 | 1.79 | Aphyric basalt |

radiolarites, other than one anomalous negative value (2.2%), display positive anisotropy.

Only two velocity measurements were obtained for rocks from Unit V (Fig. 31), 1761 m/s for red radiolarite at 453.61 mbsf and 1840 m/s for claystone at 443.35 mbsf. Both rocks display a velocity anisotropy of 1.4%.

The basalts and dolerites of the upper part of Unit VI (above 563 mbsf) have velocities ranging from 3461 to 6588 m/s with an average velocity of 4765 m/s. Low velocities occur in altered basalt flows with high porosities. Sonic velocities are highest in the vertical propagation direction at the top of Unit VI, with a trend of negative velocity anisotropy changing to positive anisotropy downsection (Tables 6 and 7, Fig. 31). Microfractures or large crystals oriented vertically could explain the high vertical velocities within this part of Unit VI. Below 563 mbsf, velocity anisotropy is nearly constant downsection, averaging 0.2%. The interbedded chert (470.79 mbsf) has a compressional-wave velocity of 5035 m/s. The hydrothermal deposit (522.14 mbsf) has a sonic velocity of 5141 m/s. The velocities of basalts in the lower part of Unit VI range from 5011 to 6367 m/s (Table 7, Fig. 31). Excluding the sample at 588 mbsf, velocities of basalt from this part of Unit IV show little variability (Table 7) and are tightly clustered about an average of 6205 m/s (Fig. 31).

The various lithologies recovered at Site 801 show a direct relationship of increasing compressional-wave velocity with increasing wet-bulk density. The soft pelagic muds have the lowest velocity/density gradient and occupy the lowest field in the velocity/density crossplot (Fig. 32). The volcaniclastic sandstones and volcaniclastic siltstones and claystones plot in similarly tight fields. However, the volcaniclastic sandstones are characterized by a higher gradient and slightly higher velocities than the volcaniclastic siltstones (Fig. 32). Radiolarites are generally tightly clustered and have a higher gradient than the volcaniclastics. The cherts and porcellanites have a moderate to high velocity/density gradient and occupy a wide field on the velocity/density crossplot. The range of velocities for the cherts overlaps that of the basalts and dolerites; however, at equivalent wet-bulk densities, chert velocities are typically higher than those of the igneous rocks. Basalts and dolerites are characterized by high velocity and density values and a very steep velocity/density gradient. These basalts are clustered into two distinct groups (see Fig. 32), one having markedly higher overall velocity values than the other.

## Thermal Conductivity

Thermal conductivity was measured in soft sediments and lithified rock recovered at Site 801. Procedures for thermal conductivity measurements are described in the "Explanatory Notes" chapter (this volume). Thermal conductivity measurements are listed in Tables 5, 6, and 7, and are plotted against depth in Figure 33 and against porosity in Figure 34.

Thermal conductivity of the pelagic clays of Unit I ranges from 0.89 to 1.04 W/m · K and averages 0.97 W/m · K. A sharp increase in conductivity characterizes the boundary between Unit I and Unit II. The siliceous sediments of Unit II have an average thermal conductivity of 1.76 W/m · K with a range of 1.54 to 1.91 W/m · K. The thermal conductivity values of the

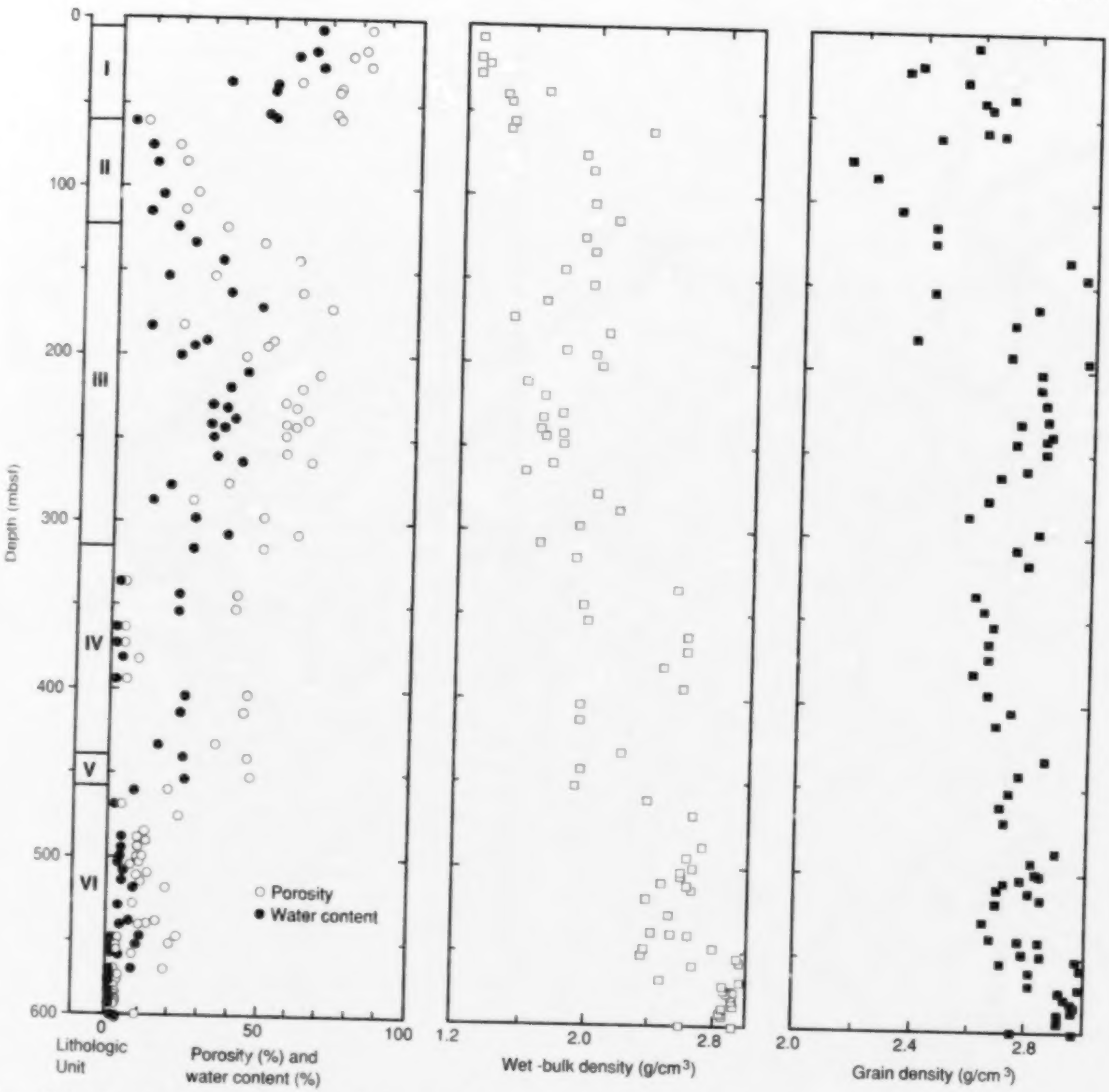

Figure 30. Index properties (porosity, wet-bulk density, and grain density) vs. depth for Holes 801A, 801B, and 801C.

upper part of the volcaniclastic Unit III (126–208 mbsf) are variable, ranging from 1.14 to 1.79 W/m · K. Thermal conductivity in the remaining parts of Unit III is less variable, ranging from 1.14 to 1.43 W/m · K. Conductivity in this interval remains nearly constant downsection. Wide-ranging thermal conductivity values characterize the biogenic silica-rich sediments of Unit IV with minimum and maximum values of 1.39 and 2.31 W/m · K, respectively. The highest conductivity values (2.16 and 2.31 W/m · K) occur in cherts at 337.50 and 383.80 mbsf in Unit IV. The thermal conductivity of Unit V is 1.39 for claystone and 1.66 for radiolarite. The thermal conductivity of the basalts of Unit VI ranges from 1.50 to 2.39 W/m · K and averages 1.73 W/m · K. The lowest conductivity (1.49 W/m · K) was measured in altered basalt sampled at 545.76 mbsf (Table 7). The hydrothermal deposit within Unit VI has an extremely high thermal conductivity (4.98 W/m · K) because of its probable high iron content. This value is highly uncertain because it is considerably above our highest calibration standard (macor 1.61 W/m · K).

A strong inverse relationship between porosity and thermal conductivity characterizes sediments and sedimentary rocks at Site 801 (Fig. 34). Basalts and dolerites with less than 5% porosity display a wide variation in thermal conductivity (1.70–2.45 W/m · K). A general inverse relationship between porosity and thermal conductivity characterizes the entire igneous rock data set. The trend of this relationship lies approximately 0.2 W/m · K below the trend for siliceous sedimentary rocks with comparable porosities (Fig. 34).

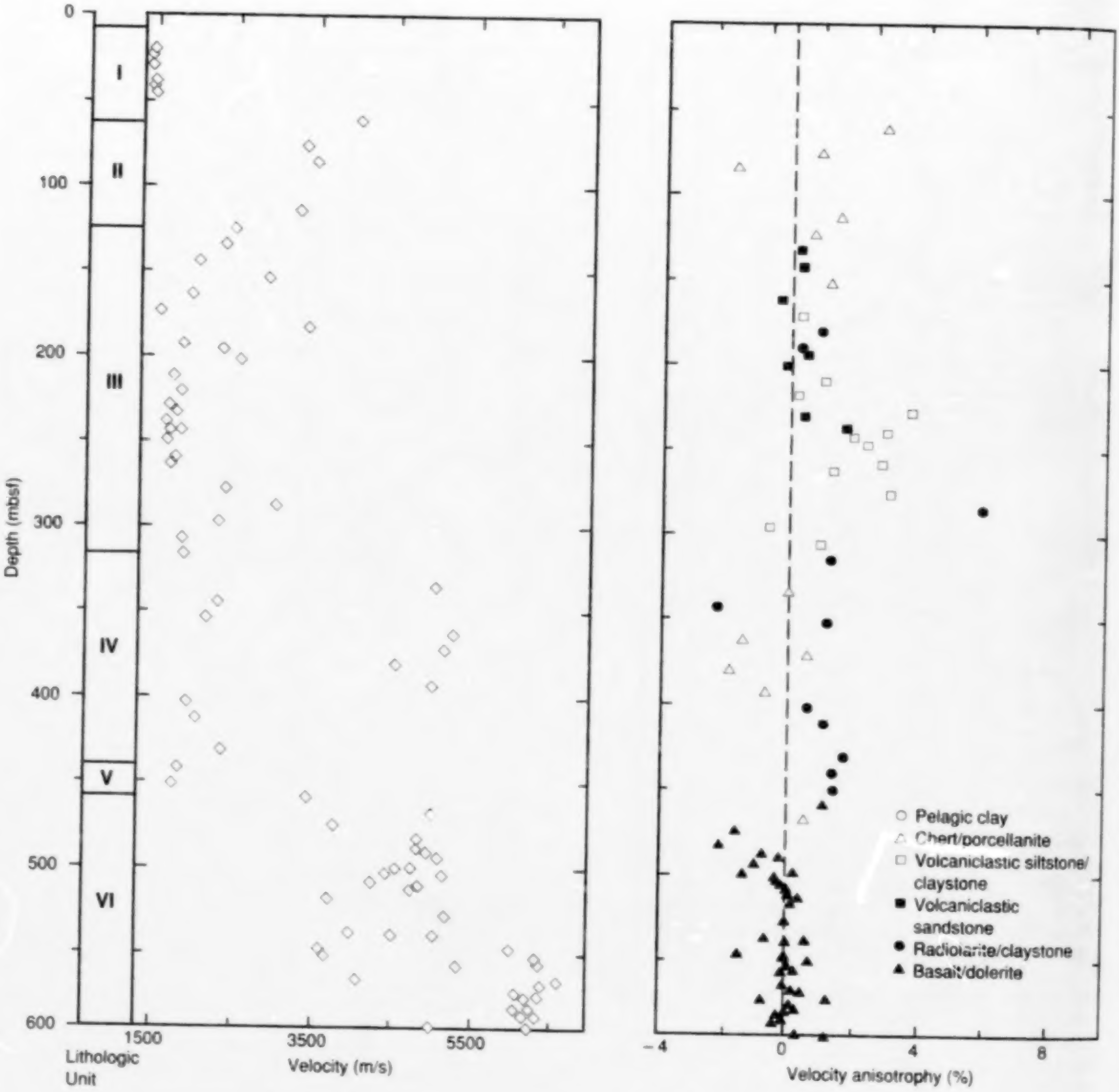

Figure 31. Compressional-wave velocity ($V_P$) and velocity anisotropy vs. depth for Holes 801A, 801B, and 801C.

## IGNEOUS PETROLOGY

Igneous rocks overlain by sediments that are at least late Middle Jurassic in age (~165 Ma) were recovered at Site 801 in the southern Pigafetta Basin. These igneous rocks are different from those drilled at Site 800 in the northern part of the basin, which occur below Lower Cretaceous (~140 Ma) sediments, because rock units that were recognized at Site 801 are mostly fine-grained basalts and microdolerites emplaced as lava flows (a few, possibly, as thin intrusions) whereas those at Site 800 are mainly medium-grained dolerite intruded as sills. Site 801 igneous rocks are also different from the extrusive basalts recovered at Site 802 in the East Mariana Basin because Site 802 rock units were emplaced generally as thin (<1 m) pillow lavas and occur just below middle Cretaceous (~110 Ma) sediments. Although there are no absolute age or chemical data yet available, we propose that the igneous rocks at Site 801 in the southern Pigafetta Basin represent the first Jurassic oceanic crust ever sampled *in-situ* in the Pacific Ocean because (1) the presence of extrusive lava flows indicates that the Jurassic sediments were deposited on top of a pre-existing oceanic crust and (2) even if some of Site 801 rock units were intrusives, at least a part of the intrusive event was penecontemporaneous with Jurassic sedimentation in the Pigafetta Basin.

### Hole 801B

#### *Lithology and Mode of Emplacement*

A total of 15.42 m of igneous and sedimentary rocks were recovered from 462.3 mbsf to 511.2 mbsf at Hole 801B, representing an average recovery of 31.3%. Using similar

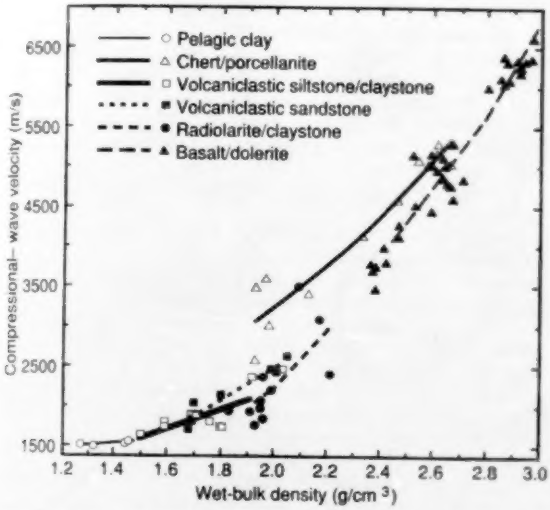

Figure 32. Wet-bulk density vs. compressional-wave velocity ($V_P$) for Holes 801A, 801B, and 801C, coded according to sediment and rock type.

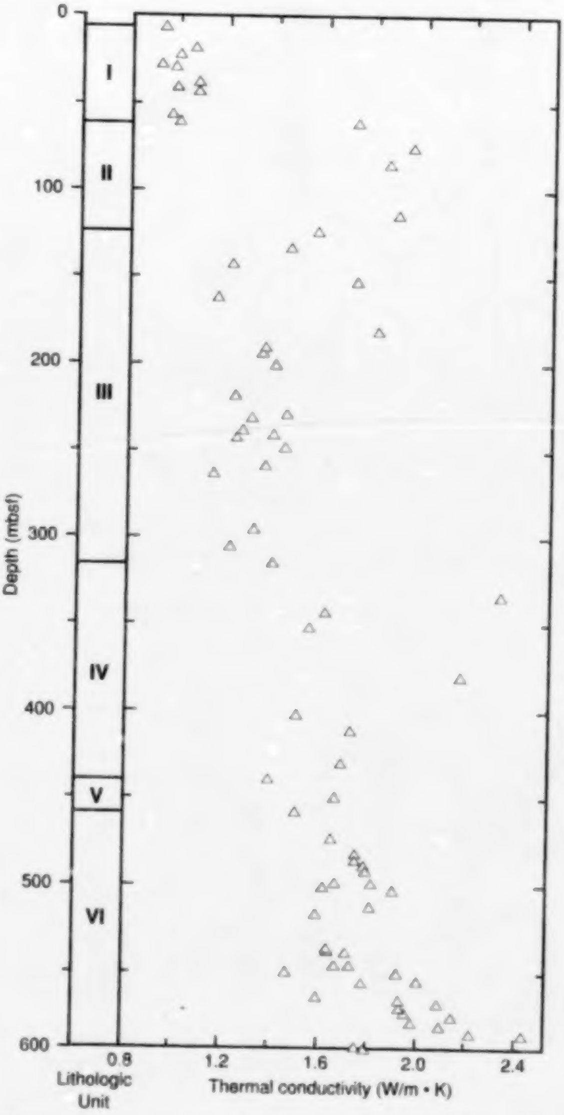

Figure 33. Thermal conductivity vs. depth for Holes 801A, 801B, and 801C.

criteria employed in Hole 800A (see also, "Explanatory Notes" chapter, this volume), 14 cooling units were observed starting from interval 129-801B-37R-1, 18 cm, down to 129-801B-44R-3, 47 cm. A summary of the features of these units is presented in Table 8 and Figure 35.

It is very important to point out, however, that whereas all the units were identified based on actual observations, critical contacts bearing on the mode of emplacement of some of the units (i.e., Units 1, 2, 3, 4, 5, 6, 10, and 11) were not recovered. Available data suggest that Unit 9 consists of pillow lavas, Units 8 and 14 are intrusive bodies, and Units 7 and 12 are lava flows. For simplicity of presentation, however, we consider the remainder of the units as thin (~1 m but <4 m) lava flows although some of these can not be completely ruled out as parts of thin intrusive sills. A more detailed discussion of the most important features of some of the units is presented below.

Units 1 to 4 are aphyric basalts interlayered with cherts and silicified claystones. None of the actual contacts was observed, but the top portions of these units and the whole of Unit 1, which is composed of centimeter-sized basaltic fragments, are finer grained and more oxidized than the lower, recovered portions. Based on these limited data, these units could be interpreted as either thin lava flows (Anderson, Honnorez, Becker et al., 1985) or thin sills (Larson, Schlanger, et al., 1981). Some of the interlayered, silicified sediments are poorly laminated and have preserved bioturbations, whereas others have desiccation cracks that are now filled, sometimes only partially, with drusy quartz. The combined features of these interlayered sedimentary and volcanic rocks suggest that if the basalts were extruded as thin flows, then these units are undoubtedly Jurassic in age because the overlying sediments in Core 129-801B-36R were dated as late Middle Jurassic (see "Biostratigraphy" section, this chapter). On the other hand, if these were intruded as sills, then the intrusion event most probably occurred penecontemporaneously with sedimentation in the southern Pigafetta Basin.

The grain size of Unit 7 systematically increases from top to interior and then decreases again to a subrounded bottom with a chilled glassy margin. These data suggest that Unit 7 is a thin lava flow. Furthermore, the quenched bottom margin of Unit 7 is most probably a pre-existing feature that formed prior to intrusion of Unit 8, which is an irregularly shaped, thin (~8 cm at its widest), sparsely plagioclase phyric, feldspar-rich, basaltic andesite. Only a thin (~1 mm) chilled zone was observed at the margin of Unit 8 but it contains isolated fragments of Unit 7 that show the thermal effect of assimilation. Some of the xenoliths can be easily fitted back to their original positions in Unit 7. Because of its unique intrusive features and more differentiated composition, Unit 8 has been interpreted as a late-stage differentiation magma that intruded the interstices between flow units.

As noted above, Unit 8 is also in contact with Unit 9, which consists of fragments of sparsely plagioclase phyric basalts

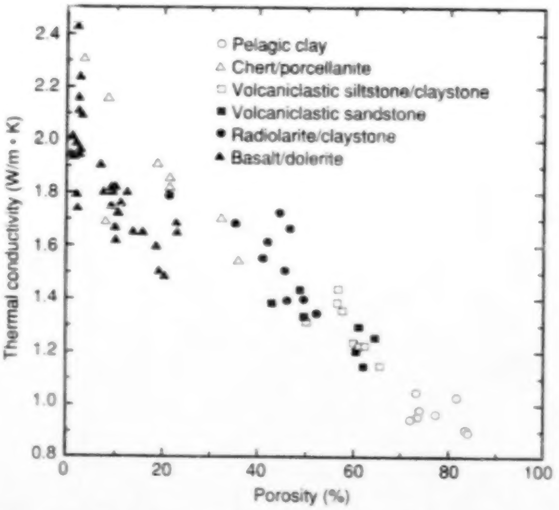

Figure 34. Porosity vs. thermal conductivity for Holes 801A, 801B, and 801C, coded according to sediment and rock type.

Table 8. Extent of igneous units actually observed in Hole 801B.

| Unit | Top | Bottom | Thickness (cm) |
|---|---|---|---|
| | 129-801B- | 129-801B- | |
| 1 | 37R-1, 18 cm | 37R-1, 22 cm | 4 |
| 2 | 37R-1, 27 cm | 37R-1, 80 cm | 53 |
| 3 | 38R-1, 14 cm | 39R-1, 3 cm | 14 |
| 4 | 40R-1, 14 cm | 40R-1, 102 cm | 88 |
| 5 | 41R-1, 6 cm | 41R-2, 120 cm | 264 |
| 6 | 42R-1, 0 cm | 42R-2, 145 cm | 245 |
| 7 | 43R-1, 0 cm | 43R-3, 36 cm | 327 |
| 8 | 43R-3, 36 cm | 43R-4, 44 cm | 8 |
| 9 | 43R-3, 44 cm | 43R-4, 4 cm | 109 |
| 10 | 43R-4, 4 cm | 43R-4, 14 cm | 10 |
| 11 | 43R-4, 14 cm | 43R-4, 101 cm | 87 |
| 12 | 44R-1, 0 cm | 44R-1, 124 cm | 124 |
| 13 | 44R-2, 23 cm | 44R-3, 13 cm | 140 |
| 14 | 44R-3, 13 cm | 44R-3, 47 cm | 3 |

Note: Total thickness of igneous rocks recovered is 15.07 m. Total core recovered from Cores 129-801B-37R to 129-801B-44R, including sediments, is 15.42 m, representing 31.3% recovery for this portion of Hole 801B.

and silica-calcite (± green clays) veinlets. The basalt fragments were interpreted as parts of pillow lavas. For example, one of the fragments (piece 14) is a pillow margin with a well-developed, subvertical holohyaline rim that grades into a curved spherulitic zone, and finally to a crystalline interior (Fig. 36). Another fragment (piece 17) contains a boundary between two pillows which is now filled with a calcite-silica veinlet. The rest of the veinlets are also probably pillow lava infill and a couple of these contain millimeter-sized claystone with very sparse, ill-preserved nannofossils of *Watznaueria manivitae* that range from Middle Jurassic to Cretaceous. Thus, Unit 9 was interpreted as a pillow lava unit based on the following observations: (1) the presence of Unit 8 filling the interstices between lava flows, (2) the presence of fragments of secondary silica-calcite veinlets carrying millimeter-sized fragments of claystone, which, similar to Unit 8, may have preferred the interstices between flows as the easiest avenues of intrusion, and (3) the presence of chilled pillow margins that are generally vertical in orientation.

Unit 12 is an aphyric basalt conformably overlying sediments and has moderately preserved, fine-grained top and bottom margins. Thus, it is probably a thin lava flow (Anderson, Honnorez, Becker et al., 1985). If this is the case, Hole 801B must have been drilled through a sequence of lava flows starting from the top of Unit 7 (Section 129-801B-42R-1, 29 cm) down to the bottom of Unit 12 (Section 129-801B-44R-1, 124 cm).

Finally, Unit 14 is a quenched, semirounded margin of a moderately plagioclase, microphyric glassy basalt. It resembles a half cross-section of a pillow lava from its shape and its hypohyaline texture with a chilled, holohyaline rim (Fig. 37). However, the overlying Unit 13, a moderately altered, aphyric basalt, apparently wraps around the relatively less altered Unit 14 and does not have a systematic grain-size coarsening away from the contact (see thin-section description below). This is somewhat surprising because Unit 13 is a massive, continuously cored, hypocrystalline to holocrystalline, aphyric basalt unit and its top contact with sediments at 129-801B-44R-2, 23 cm, does have a wide (~30 cm), well-developed, systematic fining margin. These observations suggest that Unit 14 could be intrusive (Anderson, Honnorez, Becker et al. 1985). Moreover, fragments very similar to Unit 13 are present underneath and as a xenolith within Unit 14. Finally, two clearly intrusive units, which are very similar and most probably correlative with Unit 14, were recovered at Hole 801C (see below). Thus, Unit 14 has the shape and internal texture typical of a pillow lava but other evidence suggests that it is an apophysis of an intrusive unit that penetrated the previously emplaced and crystallized Unit 13.

### *Petrography*

#### *Texture*

Thin-section examination showed that the igneous rocks recovered in Hole 801B range in texture from glassy basalt (Sample 129-801B-44R-3, 26–27 cm, piece 3A) to predominantly medium-grained, hypidiomorphic-granular dolerite (Sample 129-801B-43R-2, 103–104 cm, piece 5C) (see also Fig. 35). A majority of the samples, however, are fine- to medium-grained, hypidiomorphic-granular microdolerites (Samples 129-801B-41R-1, 25–26 cm, piece 3; 129-801B-42R-1, 86–87 cm, piece 5C; 129-801B-43R-1, 20–21 cm, piece 4A; and 129-801B-44R-3, 25–26 cm, piece 3A). There is no systematic textural variation among the igneous units despite the general fining of grain size from interior to margins within most units. Only two of the thin sections studied are phyric: (1) the glassy basalt of Unit 14 (Sample 129-801B-44R-3, 26–27 cm, piece 3A), which originally contained as much as ~13% phenocrysts of plagioclase, olivine, and a trace of clinopyroxene, and (2) the basal margin of Unit 7 (Sample 129-801B-43R-3, 35–37 cm, piece 2B), which contains 1% plagioclase and traces of clinopyroxene and olivine. The remainder of the samples are aphyric. Almost all crystalline samples have interstitial glass or mesostasis that had been completely altered to clay and invariably contains quenched microlites of plagioclase with or without relict pyroxene.

A brief discussion of the most interesting petrographic features of a few specific units follows. The top of Unit 7 (Sample 129-801B-43R-1, 20–21 cm, piece 4A) contains euhedral to subhedral crystal outlines of olivine that are now completely filled with corrugated plates of talc(?) and brownish smectite. The pseudomorphs range in size from 0.5 to 1.5 mm and constitute as much as ~20% of the thin section, thus making this the most mafic igneous rock sampled so far from the Pigafetta Basin. Equally interesting is the basal margin of

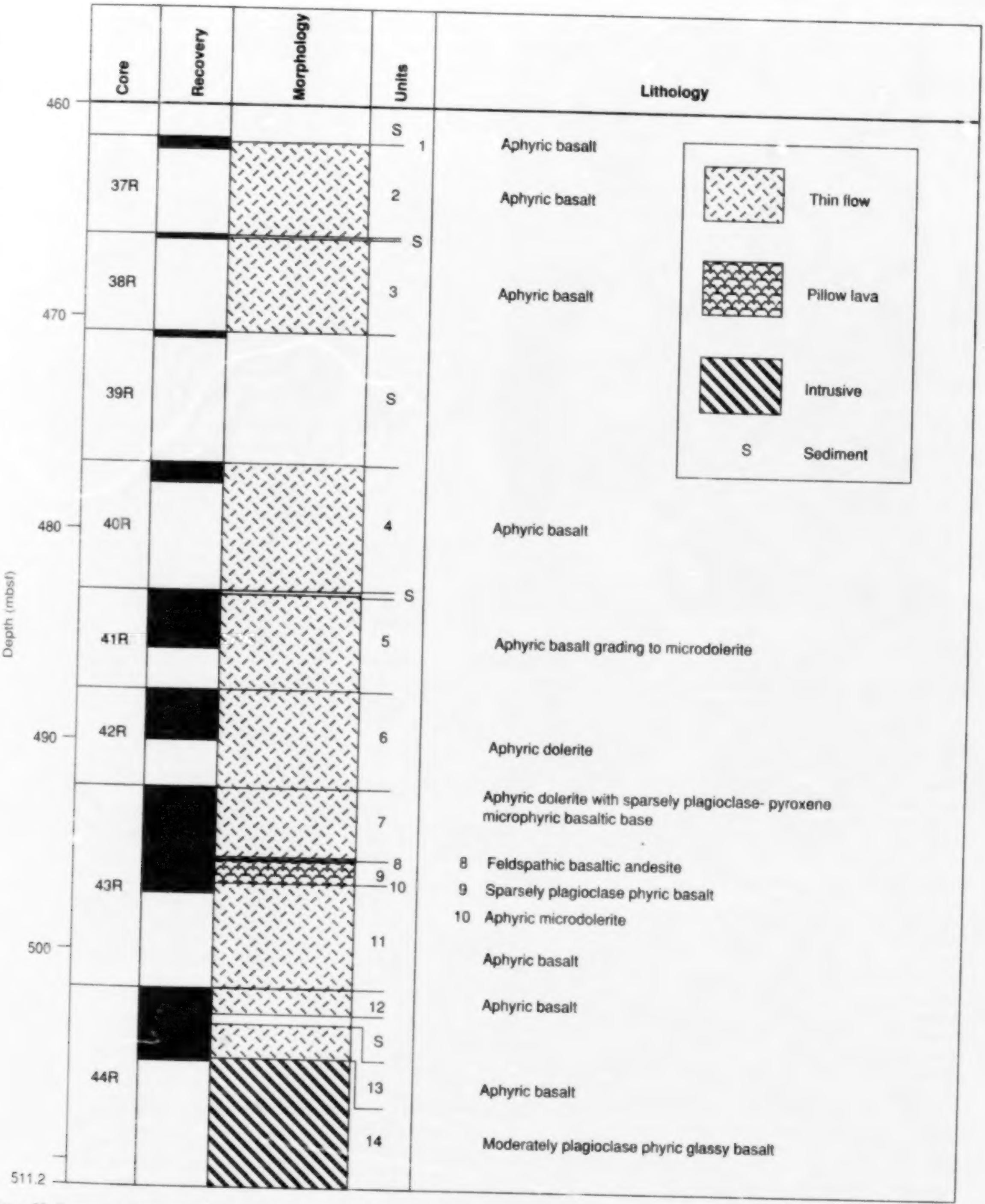
Core
Recovery
Morphology
Units
Lithology
Depth (mbsf)
460
470
480
490
500
511.2
37R
38R
39R
40R
41R
42R
43R
44R
S
1
2
S
3
S
4
S
5
6
7
8
9
10
11
12
S
13
14
Aphyric basalt
Aphyric basalt
Aphyric basalt
Aphyric basalt
Aphyric basalt grading to microdolerite
Aphyric dolerite
Aphyric dolerite with sparsely plagioclase- pyroxene microphyric basaltic base
8 Feldspathic basaltic andesite
9 Sparsely plagioclase phyric basalt
10 Aphyric microdolerite
Aphyric basalt
Aphyric basalt
Aphyric basalt
Moderately plagioclase phyric glassy basalt
Thin flow
Pillow lava
Intrusive
S Sediment

Figure 35. Summary of lithostratigraphy of igneous rocks in Hole 801B.

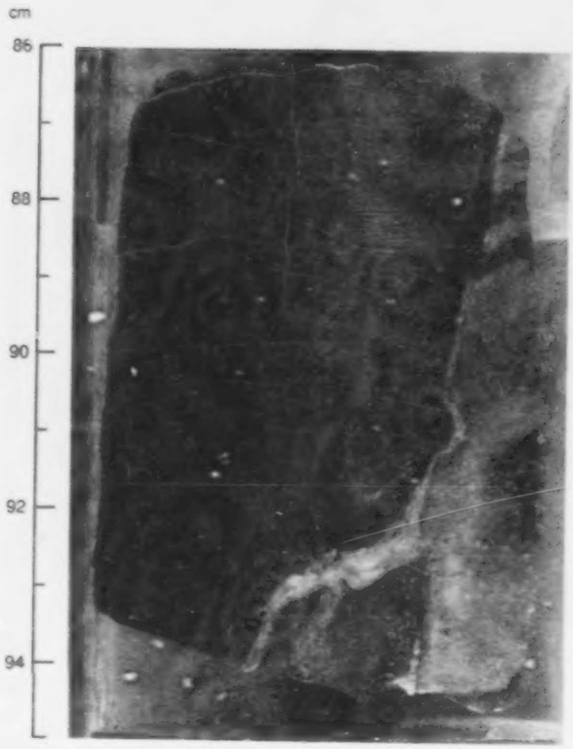

Figure 36. Photograph of a fragment of a pillow lava margin (piece 14) in interval 129-801B-43R-3, 86–95 cm. From right to left of the photograph: (1) a portion of a light gray, upright silica-calcite vein, (2) a thin (~1 mm), white calcite veinlet between the vein and the pillow fragment (this veinlet is connected to the wider (~5 mm) but irregular, diagonal, white veinlet in the lower part of the fragment), (3) a dark gray, glassy rim of the pillow fragment with a few white amygdales, (4) spherulitic zone (~1 mm) containing radiating fibers of quenched plagioclase and pyroxene, and (5) a black, hypocrystalline basalt. A moderate amount (~5%) of feathery plagioclase microlites is randomly distributed throughout the pillow fragment but especially along the glassy rim. Note that the spherulitic zone is concaved towards the hypocrystalline basalt.

this unit (Sample 129-801B-43R-3, 35–37 cm, piece 2B) because it appears to have been metamorphosed during the intrusion of Unit 8 (Sample 129-801B-43R-3, 37–39 cm, piece 2B) as discussed in the previous section. The margin starts from a convex glassy rim, which is now replaced by brown smectite and contains skeletal plagioclase microlites, and then passes to a crystallite-rich interior zone devoid of the microlites. Superimposed on the two zones are randomly oriented grains and plates of secondary biotite. The intrusive Unit 8, on the other hand, is a fine-grained, hypocrystalline basaltic andesite that contains small (a few millimeters in length), glassy xenoliths derived from Unit 7.

Petrographic examination confirmed that Unit 14 (Sample 129-801B-44R-3, 26–27 cm, piece 3A) is relatively younger than Unit 13 (Sample 129-801B-44R-3, 25–26 cm, piece 3A) as previously discussed. The contact is very sharp but cuspate because the palagonitized glassy rim of Unit 14 penetrates the moderately altered, hypocrystalline Unit 13, causing some of its plagioclase and clinopyroxene crystals to terminate

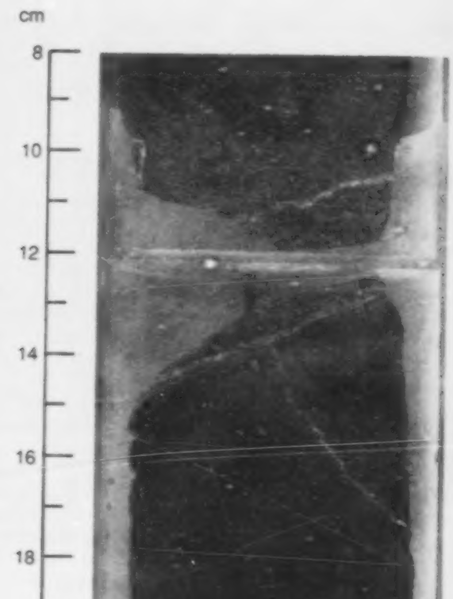

Figure 37. Photograph of pieces 1 (lower part), 2, and 3A (upper part) in interval 129-801B-44R-3, 8–30 cm. In piece 2, a subrounded portion of a moderately plagioclase, phyric, glassy basalt is partially wrapped by hypocrystalline aphyric basalt, a typical specimen of which is clearly shown in piece 1. The glassy basalt has a light grayish-brown glassy rim that grades into a dark gray, holohyaline interior. The white specks throughout the glassy basalt are quenched microlites of feathery plagioclase. The outline of the subrounded margin continues in piece 3A and cuts another fragment of glassy basalt. Note that in piece 3A, the contact between the glassy and the hypocrystalline basalt is sharp and a small fragment of hypocrystalline basalt is enclosed in the glassy basalt. The nature of the intrusive contact between the two igneous units is discussed in more detail in the text.

abruptly against the contact. There is no apparent change in texture of Unit 13 with increasing distance from the contact, whereas Unit 14 clearly changes from yellow to brown, palagonitized glass to opaque, smectite-replaced glass, and then finally to a hypohyaline interior containing variolitic plagioclase and clinopyroxene. Phenocrysts of quenched, swallow-tailed plagioclase, skeletal to euhedral relicts of olivine, and traces of clinopyroxene are randomly distributed throughout Unit 14.

### *Mineralogy*

The approximate proportions of primary and secondary minerals actually present in thin sections of Hole 801B igneous rocks are summarized in Table 9. As expected, plagioclase is ubiquitous in all samples ranging in abundance from 25% to 60% in crystalline samples and from 1% to 35% in glassy samples. Its crystal morphology ranges from quenched spherulites in the spherulitic zone, to feathery microlites in mesostasis, and finally to well-developed, subhedral laths that are sometimes as long as 5 mm. Plagioclase laths form phenocrysts in the two phyric samples previously mentioned and groundmass phases in all the rock units. These laths range in composition from $An_{38}$ to $An_{74}$ but it must be noted that plagioclase is almost always oscillatory zoned to variable extent.

Pyroxene is also ubiquitous in all samples save for the most altered one (Sample 129-801B-37R-1, 36–38 cm, piece 2) but, although its variability is partly due to replacement, its abundance generally is less than that of the plagioclase (<1% to 22%). Pyroxene morphology ranges from quenched microlites in mesostasis to elongate or stubby, millimeter-sized prisms. Some pyroxene crystals are relatively long (up to 3 mm in length) and are mostly represented by optically continuous relicts separated by alteration products. Optical properties indicate that the pyroxene is mainly titanaugite.

Titanomagnetite is also present in all samples ranging from ~2% to a maximum of 8% in abundance (Table 9). A majority of titanomagnetite occurs as fine (<0.5 mm), subhedral grains but some occur as long (up to 1.5 mm in length), skeletal needles.

As noted previously, a few samples contain subhedral to euhedral pseudomorphs of olivine (Table 9). The pseudomorphs range in size from ~0.1 to 1.5 mm and occur as a major phase in a microdolerite (Sample 129-801B-43R-1, 20–21 cm, piece 4A) and as phenocrysts in glassy rims (Samples 129-801B-43R-3, 35–37 cm, piece 2B, and 129-801B-44R-3, 26–27 cm, piece 3A). Small, euhedral grains of spinel are included in these olivine pseudomorphs as well as in phenocrystic plagioclase in the same glassy rims.

The presence of groundmass olivine, titanaugite, and titanomagnetite suggests that many of the microdolerites are alkaline in character.

### *Alteration*

All 801B igneous rocks are variably altered, from at least 10% to as high as 75%. Surprisingly, the least altered one observed in thin section was Unit 14. It still has a thin (~1 cm) palagonitized glassy rim and, despite complete alteration of its few olivine and pyroxene phenocrysts, its plagioclase phenocrysts with delicate swallow-tailed crystal morphology are moderately well preserved. The most obvious sign of alteration in this unit is the presence of almost opaque, smectite-replaced glass behind the palagonitized rim. Unit 2 (Sample 129-801B-37R-1, 36–38 cm, piece 2) is the most altered sample studied under the microscope. Except for ~25% plagioclase, the unit is essentially made up of clays (Table 9). About 2% opaques are still visible but these are also rimmed or totally replaced with iron-hydroxide (limonite?). The style of alteration of other Hole 801B samples is generally within the range of these two extremes, except perhaps for the previously described bottom margin of Unit 7, which also had been clearly contact-metamorphosed, probably during the intrusion of Unit 8.

The most common type and also the probable first stage of alteration that occurred in these rocks was the transformation of glassy rim, as well as mesostasis, into yellow-brown palagonite and then, together with pyroxene and plagioclase, into pale to opaque brown and slightly greenish smectitic clays. Olivine, whenever present, is also altered to smectite and corrugated plates of talc(?) that are always spatially

**Table 9. Approximate proportions (visual estimate) of primary and secondary phases in some representative igneous samples from Hole 801B.**

| Core, section<br>Sample interval (cm)<br>Piece number | 129-801B-37R-1<br>36–38 | 41R-1<br>25–26<br>3 | 42R-1<br>86–89<br>5C | 43R-1<br>20–21<br>4A | 43R-2<br>103–104<br>5C | 43R-3<br>35–37<br>2B | 43R-3<br>37–39<br>2B | 44R-3<br>25–26<br>3A | 44R-3<br>26–27<br>3A |
|---|---|---|---|---|---|---|---|---|---|
| Primary minerals | | | | | | | | | |
| Olivine | — | — | — | o.p. | — | o.p. | — | — | o.p. |
| Plagioclase | 25 | 45 | 45 | 38 | 50 | 1 | 59 | 30 | 35 |
| Clinopyroxene | — | 20 | 20 | 22 | 8 | o.p. | tr | 5 | 10 |
| Titanomagnetite | 2 | 4 | 3 | 5 | 7 | 2 | 2 | 8 | 5 |
| Spinel | — | — | tr | — | — | — | — | — | tr |
| Mesostatis[a] | — | o.p. | o.p. | o.p. | o.p. | 35 | tr | o.p. | tr |
| Secondary minerals | | | | | | | | | |
| Palagonite | — | — | — | — | — | — | 10 | — | 2 |
| Smectitic clays | 70 | 20 | 27 | 20 | 31 | 38 | 16 | 53 | 44 |
| Carbonate | tr | 5 | 1 | tr | tr | tr | tr | 2 | 4 |
| Zeolites | — | 2 | 1 | 3 | 1 | — | 3 | 1 | tr |
| Chlorite | — | 1 | 1 | tr | tr | — | 5 | tr | — |
| Biotite | — | 3 | 2 | 8 | 3 | 25 | 2 | 1 | tr |
| Pyrite | — | tr | tr | — | — | — | — | — | — |
| Talc | — | — | — | 4 | — | — | — | — | — |
| Limonite | 3 | — | — | — | — | — | 3 | — | — |

[a] Interstitial glass generally, except in Sample 129-801B-43R-3, 37–39 cm, piece 2B, in which it is composed of crystallites.

Notes: Dashes = not observed; o.p. = originally present but now almost entirely altered to clay; and tr = trace. Some of the olivine, plagioclase, and clinopyroxene in Sample 129-801B-43R-3, 35–37 cm, piece 2B, and Sample 129-801B-44R-3, 26–27 cm, piece 3A, occur as phenocrysts. The remainder of the primary minerals occur as groundmass phases.

restricted inside olivine pseudomorphs. Zeolites are also very common alteration products. These commonly occur as subparallel, clear, acicular prisms (phillipsite?) throughout the thin section. Less commonly, a variety of zeolites (natrolite?) occurs as irregular patches of radially arranged fibers inside plagioclase laths. Opaque grains, which are most probably titanomagnetites, are often rimmed with amorphous, dirty-white leucoxene(?) and pinkish iron-hydroxides, possibly limonite. Zeolite formation and titanomagnetite alteration were probably contemporaneous with smectite formation.

Chlorite is invariably present and probably also formed during the first stage of alteration because of its common occurrence with the clays. It must be noted, however, that some chlorite may have replaced some of the clays, which makes it suspect as a slightly later-stage alteration product. In any case, the formation of the bulk of the above-mentioned secondary minerals in the igneous rocks of the southern Pigafetta Basin probably occurred during a low-grade submarine alteration event in the zeolite facies.

Carbonate (invariably calcite) is also always present but occurs in variable amounts (Table 9). It is most commonly found replacing plagioclase but it also can be traced, together with clays, in altered olivine, pyroxene, and mesostasis. It is possible that calcite was formed together with the other secondary minerals during the low-grade submarine alteration stage, but because a majority of the several generations of veinlets are also infilled with carbonate (see below), some secondary calcite was formed or introduced into these rocks in several stages.

The brown, pleochroic biotite is quite different from the above secondary minerals because it commonly occurs as tiny grains or flakes (generally <1 mm) that commonly nucleate on the opaques or replace pyroxene and secondary minerals. A few isolated subhedral crystals of biotite were also observed in some thin sections. The formation of biotite is therefore considered to be the last stage of secondary alteration of the major phases in Hole 801B igneous rocks.

Trace amounts of pyrite were observed in a couple of thin sections (Table 9) and although they were put under secondary minerals, it is also possible that these are of magmatic origin (Deer et al., 1966).

Finally, it was mentioned previously that Units 1 to 4 are the most oxidized among the units. As in Hole 800A, these are the topmost units and may imply that the oxidation was due to the downwards percolation of oxygenated seawater probably soon after their emplacement. The fact that oxidation is most intense at the top of Unit 2 and slightly decreases towards its interior is consistent with this interpretation.

### *Fractures and Veins*

All units are cut by veinlets to varying degrees (1% to 5%), with the top three units having the fewest veins. Veinlets range in width from ~0.1 mm to as much as ~1.5 cm, and as mentioned earlier, decimeter-sized pieces of veinlets or infill materials (as much as 15%) were recovered within Unit 9. A majority of the veinlets are subhorizontal but oblique (~45° dip) to vertical ones are not uncommon. In general, these veinlets have very irregular shapes; some are braided and branching, and cross-cutting is very common, suggesting that there are several stages of vein formation.

Calcite, quartz, green clays, and a combination of these are the vein materials that were commonly observed. There is no unequivocal evidence that would suggest the paragenesis of these minerals. Black, shiny veinlets infilled with dark, submetallic materials (manganese?) are limited to the oxidized Units 2 and 3 and perhaps represent the earliest generation of veinlets, as one of these is cut by a calcite veinlet. Moreover, a thin section of Unit 2 (Sample 129-801B-37R-1, 36–38 cm, piece 2) shows a manganese veinlet almost eradicated by clay alteration, suggesting that its formation was at least contemporaneous with, if not earlier than, the pervasive submarine alteration.

### *Geochemistry*

Table 10 shows calcium carbonate, organic carbon, and sulfur contents of representative samples from the base of Hole 801B. Sulfur content is relatively low and quite normal for these igneous rocks. Calcium carbonate content, however, is generally high, which is consistent with the persistence of secondary calcite in all thin sections (Table 9). With the exception of one sample (129-801B-38R-1, 22–25 cm), carbonate concentration is generally higher in the lower part, starting from slightly below the top of Section 129-801B-44R-1. This could be due to the higher degree of oxidation and alteration of the upper units, but probably reflects the presence of more veinlets in the lower part of the hole (see previous discussion).

## Hole 801C

### *Lithology and Mode of Emplacement*

About 61 m of mostly igneous and a few sedimentary rocks were cored from 493.7 mbsf to 594.3 mbsf in Hole 801C. This represents an average recovery of 60.2%, the highest among the holes drilled during Leg 129. Thirty-two lithologic units were identified from the cored samples but only 29 of these are volcanic cooling units (Table 11, Fig. 38). Available data suggest that Unit 17 is a sheet flow, Unit 25 is a thick (>5 m) flow, Units 4 and 6 are intrusive bodies, and Units 9, 10, 11, 20, 29, 30, and 31 are pillow lavas. Data also suggest that Units 13, 16, 21, 22, and 24 are probably thin (~1 to 4 m thick) lava flows but, as in Hole 801B, the remainder of the cooling units without well-preserved boundaries were interpreted as thin lava flows. Actual observation of a few thin lava flows with preserved boundaries in cores in which recovery is good (i.e., ~50% recovery and higher as in Cores 129-801C-5R, -6R, -7R, and -9R) lends support to this interpretation. This is in sharp contrast with Hole 802A, in which the number of cooling units (mostly glassy pillow lavas) is relatively large where core recovery is good (see "Igneous Petrology" section, "Site 802" chapter, this volume). The most important features of some the Hole 801C petrologic units are presented below.

**Table 10. Carbonate, organic carbon, and sulfur analyses for igneous rocks at the base of Hole 801B.**

| Core, section, interval (cm) | $CaCO_3$ (wt%) | $C_{org}$ (wt%) | S (wt%) |
|---|---|---|---|
| 129-801B- | | | |
| 37R-1, 54–56 | 0.4 | 0.00 | 0.05 |
| 37R-1, 66–71 | 0.5 | | |
| 38R-1, 22–25 | 1.9 | | |
| 39R-1, 9–11 | 0.4 | | |
| 40R-1, 20–23 | 0.2 | | |
| 40R-1, 38–40 | 1.7 | 0.00 | 0.05 |
| 40R-1, 85–91 | 9.1 | | |
| 41R-1, 26–31 | 6.8 | | |
| 41R-2, 95–97 | 8.2 | 0.03 | 0.03 |
| 42R-2, 93–95 | 1.2 | 0.01 | 0.05 |
| 43R-1, 42–44 | 2.0 | 0.00 | 0.04 |
| 43R-3, 119–121[a] | 23.0 | 0.06 | 0.00 |
| 44R-1, 52–54 | 8.8 | 0.03 | 0.04 |

[a] Contains veinlet.

Table 11. Extent of lithologic units actually observed in Hole 801C.

| Unit | Top | Bottom | Thickness (cm) |
|---|---|---|---|
| | 129-801C- | 129-801C- | |
| 1 | 1R-1, 0 cm | 1R-3, 103 cm | 363 |
| 2 | 1R-3, 103 cm | 1R-6, 131 cm | 395 |
| 3 | 2R-1, 0 cm | 2R-3, 63 cm | 347 |
| 4 | 2R-3, 63 cm | 2R-3, 110 cm | 47 |
| 5 | 2R-3, 110 cm | 2R-3, 115 cm | 5 |
| 6 | 2R-3, 115 cm | 2R-5, 118 cm | 248 |
| 7 | 3R-1, 0 cm | 3R-1, 100 cm | 100 |
| 8[a] | 4R-1, 0 cm | 4R-2, 128 cm | 264 |
| 9 | 5R-1, 0 cm | 5R-3, 69 cm | 324 |
| 10 | 5R-3, 69 cm | 5R-3, 104 cm | 35 |
| 11 | 5R-3, 104 cm | 5R-3, 150 cm | 46 |
| 12[a] | 5R-4, 0 cm | 5R-4, 31 cm | 31 |
| 13 | 5R-4, 31 cm | 5R-5, 130 cm | 241 |
| 14 | 5R-5, 130 cm | 5R-5, 142 cm | 12 |
| 15[a] | 6R-1, 0 cm | 6R-1, 96 cm | 96 |
| 16 | 6R-1, 96 cm | 6R-2, 137 cm | 170 |
| 17 | 6R-2, 137 cm | 5R-2, 150 cm | 13 |
| 18 | 6R-3, 0 cm | 6R-3, 14 cm | 14 |
| 19 | 6R-3, 14 cm | 6R-3, 34 cm | 20 |
| 20 | 6R-3, 34 cm | 6R-5, 44 cm | 294 |
| 21 | 6R-5, 44 cm | 7R-1, 129 cm | 195 |
| 22 | 7R-1, 129 cm | 74-2, 143 cm | 159 |
| 23 | 7R-3, 0 cm | 8R-1, 32 cm | 389 |
| 24 | 8R-1, 32 cm | 8R-2, 142 cm | 216 |
| 25 | 9R-1, 31 cm | 10R-6, 75 cm | 1345 |
| 26 | 10R-6, 81 cm | 11R-1, 17 cm | 70 |
| 27 | 11R-1, 17 cm | 11R-2, 126 cm | 248 |
| 28 | 11R-2, 126 cm | 11R-3, 60 cm | 84 |
| 29 | 11R-3, 60 cm | 12R-1, 5 cm | 102 |
| 30 | 12R-1, 19 cm | 12R-1, 49 cm | 30 |
| 31 | 12R-1, 49 cm | 12R-1, 150 cm | 101 |
| 32 | 12R-2, 0 cm | 12R-3, 91 cm | 234 |

[a] Not cooling unit. Unit 8 is a hydrothermal deposit, Unit 12 is an interpillow deposit, and Unit 15 is composed of basaltic fragments of questionable order and orientations.

Unit 3 in Core 129-801C-2R is an aphyric basalt and, although the actual top contact was not recovered, it had a glassy top rim with sparse plagioclase phenocrysts. It contains a few, randomly distributed, subrounded, millimeter-sized carbonate grains and is diagonally (40° inclination) intruded by 47-cm-thick Unit 4, which has dense, brownish, moderately plagioclase, microphyric glassy top and bottom margins (Fig. 39). It is interesting to note that Unit 13 in Hole 801B has textural features very similar to Unit 3 of Hole 801C and, although at a higher level, is intruded by a 34-cm-thick subrounded apophysis of Unit 14, which is a dense, brownish, moderately plagioclase phyric glassy basalt (see previous discussion and Fig. 37). Moreover, Unit 13 of Hole 801B and Unit 3 of Hole 801C are at about the same level below seafloor and are only several meters apart (see "Operations" section, this chapter). Based on these observations, these four units were used as the basis for correlating the few overlapping cooling units of Hole 801B and 801C (Fig. 39).

Unit 6 is separated from Unit 4 by 5-cm-thick Unit 5, which is an aphyric basalt probably separated from Unit 3 during the intrusion of Unit 4 (Fig. 40). Unit 6 also intruded Unit 5 and has an inclined, dense, brownish, sparsely plagioclase phyric glassy rim quite similar to the glassy margin of Unit 4. Thus, both Units 4 and 6 may have come from the same body although the latter grades to an aphyric microdolerite because it is relatively thick (248 cm; Table 11).

A highly silicified, yellow hydrothermal deposit (Unit 8) was the only sample recovered in Core 129-801C-8R. It is important to note that, although not a cooling unit, the formation of this deposit may have affected the style of alteration of the underlying units, and surprisingly, the overlying Unit 7 as well (see below). If this is the case, then the hydrothermal activity that deposited Unit 8 must have continued for some period of time even if the deposit had been covered by later lava flows.

Subrounded margins of pillow lavas rimmed with devitrified glass were recovered in Units 9, 10, and 11 (Fig. 41). These are in contact with reddish and white carbonate ± greenish clay (e.g., Unit 12), which are probably previous interpillow sediments but are now almost totally replaced. The pillow lavas are interbedded with thin lava flows. A devitrified sheet flow (Unit 17) occurs below the sequence of pillows and flows in Core 129-801C-5R.

Unit 25 is an unusually thick (~13.5 m) lava flow that was fully recovered in Cores 129-801C-9R and -10R (Fig. 38). This unit contains several interesting features, interpreted as the result of flow differentiation, that also characterize some of the thin flows directly above and below this unit. It is a fine-grained, aphyric basalt but it contains variable patches or layers with sparse plagioclase and/or olivine microphenocrysts. It also contains subrounded to rounded vesicles that range in size from 0.1–0.6 mm and in amount from 0%–5%, generally distributed at random at different levels within the unit. The vesicles are always infilled with green, smectitic(?) clays or white calcite ± fine pyrite. Although it is not uncommon to find smectite and calcite (and even pyrite, but in a much lesser amount) to be concentrically interlayered within a single vesicle, it is important to note that calcite- and smectite-infilled vesicles usually occur at separate levels within the unit. This usually gives the flow units alternating, conspicuous, white and very dark green spotted zones. The only characteristic feature of the vesicles that was not observed in the flows, other than in Unit 25, is that these attain sizes up to 5 mm in diameter. These large vesicles are almost exclusively infilled with white calcite and occur in a ~2-m section just 1 m above the base of Unit 25.

### *Petrography*

A majority of the cooling units are fine-grained, aphyric basalts, particularly those in the lower portion of Hole 801C (Fig. 38). Samples from the lower portion of the hole are slightly finer in grain size, less variable in texture, and as previously mentioned, more vesicular than those in the upper portion. The overall texture of the upper cooling units (i.e., Units 1 to 6) in Hole 801C are similar to those of the lower units in Hole 801B. For example, Units 3 and 4 of Hole 801C are texturally very similar to Units 13 and 14 of Hole 801B, as already mentioned. Moreover, the coarsest unit recovered in Hole 801C is the aphyric microdolerite Unit 1, which has a very similar texture and degree of alteration (e.g., presence of secondary biotite in Sample 129-801C-1R-1, 119–120 cm, piece 2G) to some of the aphyric basalts and microdolerite units in Cores 129-801B-41R to -44R (Table 9).

Except for Unit 9, which contains 6% to 10% plagioclase phenocrysts that are up to 4 mm in size, the rest of the units generally range from sparsely to moderately microphyric (1% to 4% phenocrysts), and contain fine-grained (~1 mm on the average) crystals of plagioclase and olivine or only plagioclase. These are typically set in a hypocrystalline groundmass consisting of plagioclase, pyroxene, olivine, titanomagnetite, and mesostasis. The estimated proportions of glass, mesostasis, crystallites, and primary minerals in thin sections are shown in Table 12.

Another important feature shown by the thin-section data is that a majority of Hole 801C basalts have olivine, at least in the groundmass (Table 11). Moreover, one of the samples

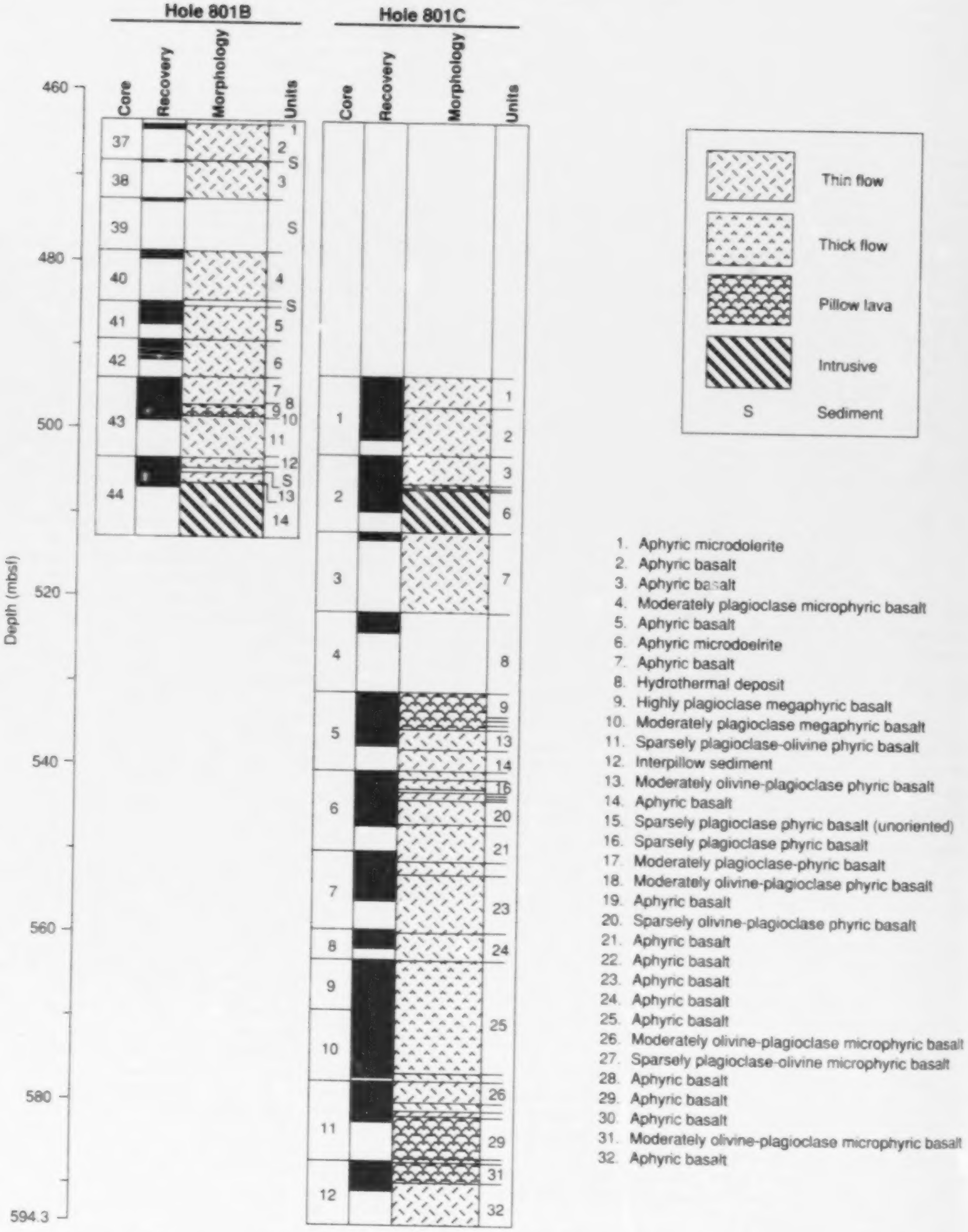
Hole 801B
Hole 801C
Core
Recovery
Morphology
Units
Depth (mbsf)
460
480
500
520
540
560
580
594.3
37
38
39
40
41
42
43
44
1
2
3
4
5
6
7
8
9
10
11
12
S
13
14
16
20
21
23
24
25
26
29
31
32
Thin flow
Thick flow
Pillow lava
Intrusive
S Sediment
1. Aphyric microdolerite
2. Aphyric basalt
3. Aphyric basalt
4. Moderately plagioclase microphyric basalt
5. Aphyric basalt
6. Aphyric microdoelrite
7. Aphyric basalt
8. Hydrothermal deposit
9. Highly plagioclase megaphyric basalt
10. Moderately plagioclase megaphyric basalt
11. Sparsely plagioclase-olivine phyric basalt
12. Interpillow sediment
13. Moderately olivine-plagioclase phyric basalt
14. Aphyric basalt
15. Sparsely plagioclase phyric basalt (unoriented)
16. Sparsely plagioclase phyric basalt
17. Moderately plagioclase-phyric basalt
18. Moderately olivine-plagioclase phyric basalt
19. Aphyric basalt
20. Sparsely olivine-plagioclase phyric basalt
21. Aphyric basalt
22. Aphyric basalt
23. Aphyric basalt
24. Aphyric basalt
25. Aphyric basalt
26. Moderately olivine-plagioclase microphyric basalt
27. Sparsely plagioclase-olivine microphyric basalt
28. Aphyric basalt
29. Aphyric basalt
30. Aphyric basalt
31. Moderately olivine-plagioclase microphyric basalt
32. Aphyric basalt

Figure 38. Summary of lithostratigraphy of igneous rocks in Holes 801B and 801C.

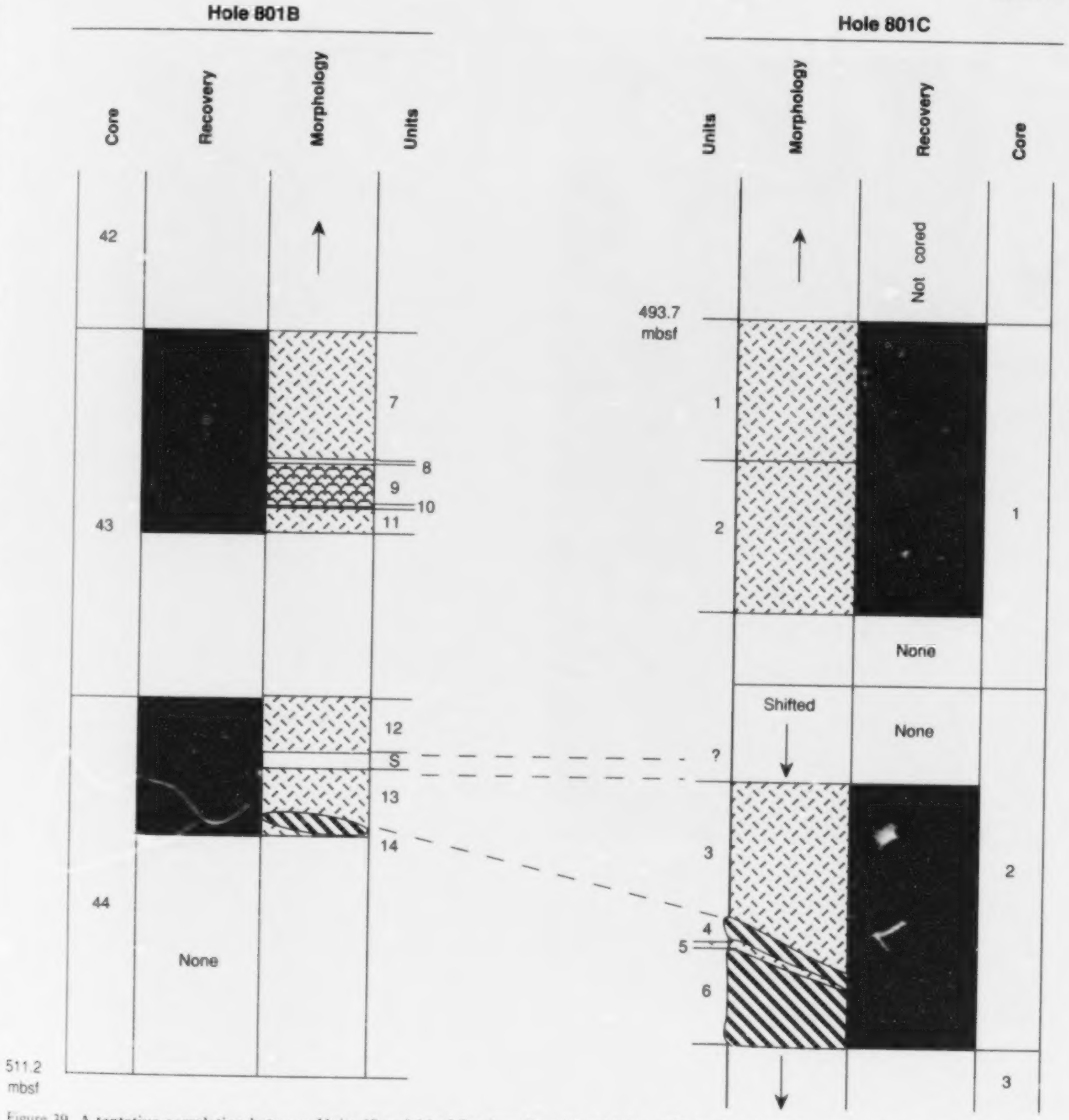
Hole 801B
Core
Recovery
Morphology
Units
42
43
44
7
8
9
10
11
12
S
13
14
None
511.2 mbsf
Hole 801C
Units
Morphology
Recovery
Core
Not cored
493.7 mbsf
1
2
None
Shifted
None
?
3
4
5
6
2
3

Figure 39. A tentative correlation between Units 13 and 14 of Section 129-801B-44R-3 and Units 3 and 4 of Sections 129-801C-2R-1 to -2R-3. See text for explanation. Stratigraphic correlation above these units is difficult to make because of a lack of close similarities among the other recovered units. See Figure 38 for explanation of symbols. Recovered samples were shifted into the lower portion of Core 129-801C-2R in order to match the top of the presumably flat-lying lava flows in Sections 129-801B-44R-3 (Unit 13) and 129-801C-2R-1 (Unit 3).

studied (129-801C-5R-5, 70–71 cm, piece 3D) has brown, spinel microphenocrysts (up to ~0.4 mm in size), which are either free-floating or enclosed in phenocrystic olivine. These data suggest that olivine (± spinel) is a liquidus phase in a majority of Hole 801 basalts and that their crystallization sequence is olivine (± spinel)-clinopyroxene-plagioclase, which is typical of primitive mid-ocean ridge basalts. Groundmass olivine is typically granular whereas phenocrystic olivine ranges from hopper-shaped to subhedral- and even euhedral-shaped crystals.

The margins of pillow lavas (Fig. 41) and thin lava flows (Fig. 42) appear to have well-preserved glassy rims. However, thin-section examination also showed that all of these had been completely devitrified and altered to brown, almost opaque smectitic clays. These glassy rims generally grade to a variolitic to spherulitic zone and finally to a hypocrystal-

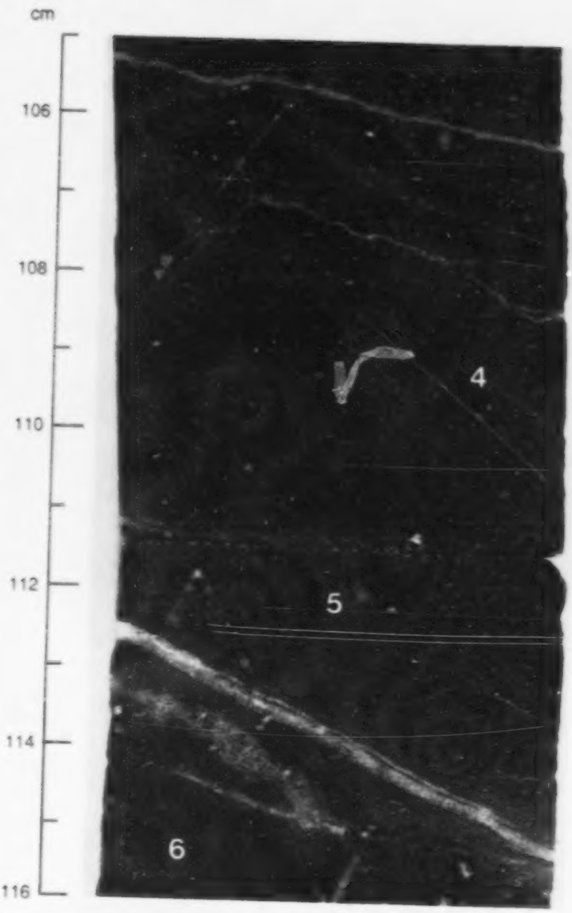

Figure 40. Photograph illustrating the contacts between Units 4 and 5, and between Units 5 and 6. Interval 129-801C-2R-3, 105–116 cm. (Numbers in the photograph correspond to respective units.) The contact of Unit 4 with Unit 5 is relatively sharp and originally glassy, whereas that of Unit 6 with Unit 5 is cuspate although originally glassy. The texture of Unit 5 is generally constant; except in thin section, its crystals are clearly cut or abruptly terminated by the opaque brown, smectitic rims of Units 4 and 6.

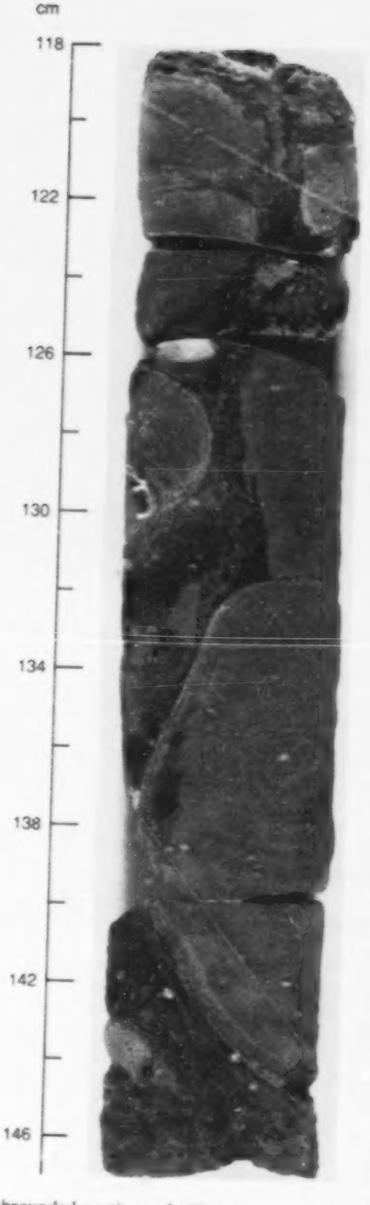

Figure 41. Subrounded portions of pillow lavas separated by interpillow material that has altered to smectite and carbonate. Note the light gray-colored, relatively sharp, originally glassy margins of the pillows. Interval 129-801C-5R-3, 118–147.

line interior, which is typical of submarine extrusive lavas. The typical texture of the interior of Hole 801C pillow and flow basalts range from intergranular to intersertal.

### *Alteration*

The thin flows and pillow lavas of Hole 801C are moderately to highly altered and exhibit a higher degree and a wider range of alteration features than seen previously in samples from the other holes. Apart from typical, low-grade submarine alteration of the matrix and ubiquitous carbonate-smectite veinlets, there are hydrothermal breccia zones and vesicles infilled with secondary minerals. In general, however, the degree of alteration is often highly variable from core to core, and shows no clear relationship to depth or cooling unit type. For example, although the most highly altered basalts occur immediately below the hydrothermal deposit (see below) in the pillow lavas and thin flows of Units 9 to 13 (Core 129-801C-5R), units above (including those in Hole 801B) and below this zone are slightly to moderately altered. The intensity and type of alteration can also vary considerably within any cooling unit, such that the upper segment may show a high proportion of smectitic clays, whereas the central and lower part is dominated by relatively minor carbonate replacement (e.g., Units 9 and 24).

A late, oxidative type of alteration, which is typically absent from the other sites, is particularly well developed at

Table 12. Visual estimate (in vol%) of proportion of primary and secondary minerals from thin-section studies, Hole 801C.

| Core, section<br>Sample interval (cm)<br>Piece number | 129-801B-1R-1<br>119–120<br>2G | 2R-2<br>2–3<br>1A | 2R-3<br>64–68<br>2A | 5R-1<br>12–13<br>2A | 5R-1<br>124–125<br>4 | 5R-5<br>70–71<br>3B | 7R-3<br>64–66<br>3A |
|---|---|---|---|---|---|---|---|
| Phenocrysts | | | | | | | |
| Olivine | — | — | o.p. | o.p. | o.p. | o.p. | — |
| Plagioclase | — | — | o.p. | o.p. | o.p. | — | — |
| Spinel | — | — | — | — | — | tr | — |
| Primary minerals | | | | | | | |
| Olivine | o.p. | o.p. | — | o.p. | o.p. | o.p. | o.p. |
| Plagioclase | 50 | 60 | — | 10 | 20 | 35 | 30 |
| Clinopyroxene | 12 | 7 | — | tr | 0 | 35 | 15 |
| Opaques | 8 | 4 | 1 | 1 | tr | 1 | 3 |
| Glass + spherulites[a] | o.p. | o.p. | 40 | o.p. | o.p. | — | o.p. |
| Spinel | — | — | — | — | — | tr | — |
| Apatite | tr | — | — | — | — | — | — |
| Secondary minerals | | | | | | | |
| Clays | 25 | 18 | 50 | 66 | 60 | 27 | 51 |
| Carbonate | — | 10 | 5 | 3 | 5 | — | 1 |
| Zeolites | 4 | 1 | — | — | — | — | — |
| Chlorite | tr | — | — | — | 10 | — | — |
| Limonite | — | — | 4 | 20 | 5 | — | — |
| "Iddingsite" | — | — | — | tr | tr | tr | — |
| Talc | — | — | — | tr | tr | — | — |
| Quartz | — | — | — | tr | tr | — | — |
| Prehnite | tr | tr | — | — | — | — | — |
| Biotite | 1 | tr | — | — | — | — | — |
| Hematite | — | — | — | — | — | 2 | — |

[a] Includes mesostasis glass.

Notes: Dashes = not observed; o.p. = originally present but totally altered; and tr = trace.

the top of Unit 9 (interval 129-801C-5R-1, 0–35 cm). In Unit 9, there exists a sharp boundary between the upper brownish oxidized zone (with limonite and hematite) and the lower, adjacent light gray colored zone (with carbonate and smectite) (Fig. 43). The oxidative alteration is post-clay production as the green smectites are colored red, and being related to the top of the unit, indicates the oxidizing fluid was downward percolating seawater. This oxidized flow top may represent either a pause in a fairly rapid and continuous extrusion of lavas to allow time for alteration by seawater or, alternatively, may be directly related to the hydrothermal activity that formed the deposit just directly above Unit 9. Either case is consistent with the general lack of interflow oxidized zones throughout the lava pile except that the presence of a similar, but definitely smaller, type of oxidative alteration in the reverse order (i.e., brownish oxidized zone below and light gray-colored zone above) in Unit 7 directly above the hydrothermal deposit tends to favor the latter scenario. The presence of scattered pristine pyrite in most cooling units of Hole 801C indicates a predominantly reducing environment was (and has been) maintained throughout the lavas.

In general, alteration affected a number of different domains and environments within the Hole 801C lava sequence: matrix (including phenocrysts and mesostasis), vesicles, interpillow material, veins, and brecciated zones. Some of the typical features exhibited are described below.

### *Matrix*

Matrix color often provided a visible means to the presence and domination of secondary minerals, such that strong green indicates smectite replacement, whereas pale gray indicates carbonate replacement. Color zonation is characteristic of some of the units directly below the hydrothermal deposit of Unit 8. Both groundmass and microphenocrystic olivine was always totally replaced, either by dirty green smectite with iddingsitic (or limonitic) veinlets or irregular carbonate patches within smectite. Depending on the degree of alteration, plagioclase was variably replaced by pale green and brown to opaque smectites, minor limonite, carbonate, zeolite, and prehnite. Clinopyroxene is often fresh, but under extreme conditions can be totally replaced by clays and limonite. Other secondary matrix minerals include two types of zeolite, one forming hemispheres of radiating fibers replacing mesostasis glass (natrolite?) and the other, acicular clear prisms (phillipsite?) piercing plagioclase laths. The devitrified glass along the rims of cooling units and spherulite zones directly below these are always replaced by brown smectites. In medium-grained hypocrystalline basalts in the upper units of Hole 801C, biotite may be developed from elongate titanomagnetite needles (e.g., Sample 129-801C-1R-1, 119–120 cm, piece 2G), but is relatively rare. Mesostasis glass is totally replaced by brown smectite or sometimes a radiate zeolite.

### *Vesicles*

Thin-section examination confirmed the presence of small, subrounded to rounded vesicles, infilled with either smectite or carbonate. Some of the infilling materials are zoned with a thin, pale green, granular smectite rim and an interior of either dark green radiating fibers of smectite or carbonate plates or more rarely, pyrite. A few rare examples were observed of vesicle walls decorated with scattered pyrite granules and an interior of smectite. Based on observation, the general order of development and replacement within vesicles appears to be (1) pale smectite, (2) dark green smectite, (3) pyrite, and, finally, (4) carbonate.

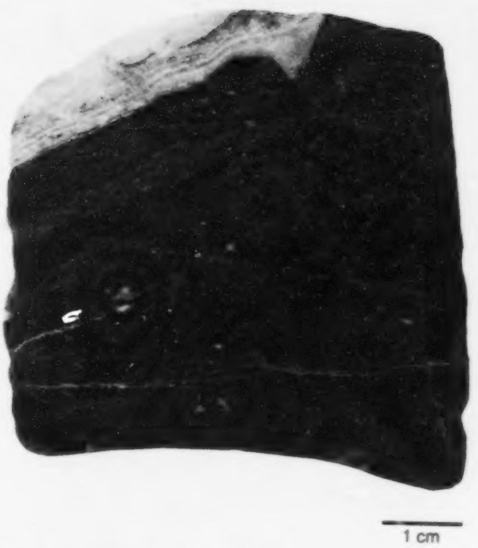

Figure 42. A typical recovered margin of a volcanic cooling unit in Hole 801C. Interval 129-801C-1R-3, 103–109. From top to bottom, a thin glassy rim, a spherulitic zone, and a hypocrystalline interior. The glass is totally replaced by brown smectitic clays and the spherulitic zone and the hypocrystalline interior are also in various degrees of alteration.

Because of the hydrostatic pressure of seawater at normal depths of mid-ocean ridges (3–4 km), vesiculation caused by the exsolution of water vapor from basaltic lava is generally inhibited; thus, the presence of a small volume of vesicles in some Hole 801C lavas implies either a "shallow" active axis or possibly the presence of gases (e.g., carbon dioxide) other than water vapor.

*Interpillow Material*

Altered material fills the spaces between the pillows of Unit 11 (Section 129-801C-5R-3) and is composed of greenish, smectite-replaced, glassy, spherulitic fragments derived from the pillow margins during rapid quenching (Fig. 44). Unit 12 (interval 129-801C-5R-4, 0–31 cm) is entirely composed of interpillow sediments and, in this case, consists of a reddish, highly calcareous material with relicts of small fragments of brown claystone hydrothermal deposit similar to that in Unit 8, and basalt.

*Veins*

Small, ramifying, cross-cutting veinlets of widely varying widths (0.1–80.0 mm) are very common throughout the lava sequence. These are generally randomly oriented and are commonly infilled with either carbonate or smectite. If there is a mixture of both phases, the carbonate generally is later and occupies the central portion of the larger veins. Pyrite may also occur as minute veinlets or lines the walls of the fractures infilled with smectite or carbonate. Some veinlet halos (e.g., in Units 27, 28, and 29) consisting of more clay-rich groundmass also contain very finely disseminated pyrite. In more oxidized sections, limonite and hematite, which the likely result of oxidation of pyrite, are present, forming a yellowish or brownish margin to the veinlets. Larger veins (up to 30 mm) may have multiple or zoned deposits of carbonate, smectite, pyrite, and quartz, suggesting a number of stages of fracturing and infilling.

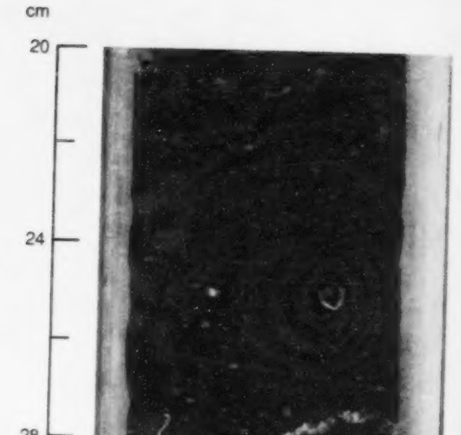

Figure 43. Sharp demarcation of the lower margin of the oxidized zone at the top of Unit 9. The white crystals in the lower part of the photograph are carbonate-replaced plagioclase megaphenocrysts. Interval 129-801C-5R-1, 20–40 cm.

*Brecciated Zones*

Units 9, 13, and 24 contain highly irregular (10–35 mm wide), subvertical breccia zones filled with angular basaltic material derived from the adjacent lavas and cemented by late green smectite and carbonate. Brecciation in Unit 9 extends over 1 m of core, with large, angular, displaced blocks at the base, ending in a close-fitting mosaic of smectite netveined fragments, and may be related to the hydrothermal activity that formed Unit 8 directly above it. However, the presence of brecciated zones in other zones away from Unit 8 may also be

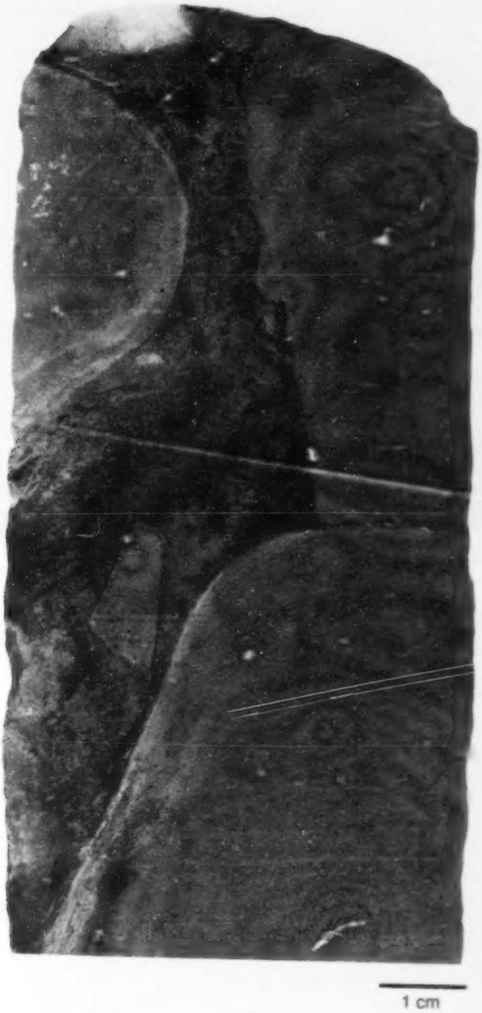

Figure 44. A close-up photograph of the interpillow material shown in Figure 41. The material is altered to smectite and carbonate, with glassy pillow fragments showing spherulitic texture (white dots).

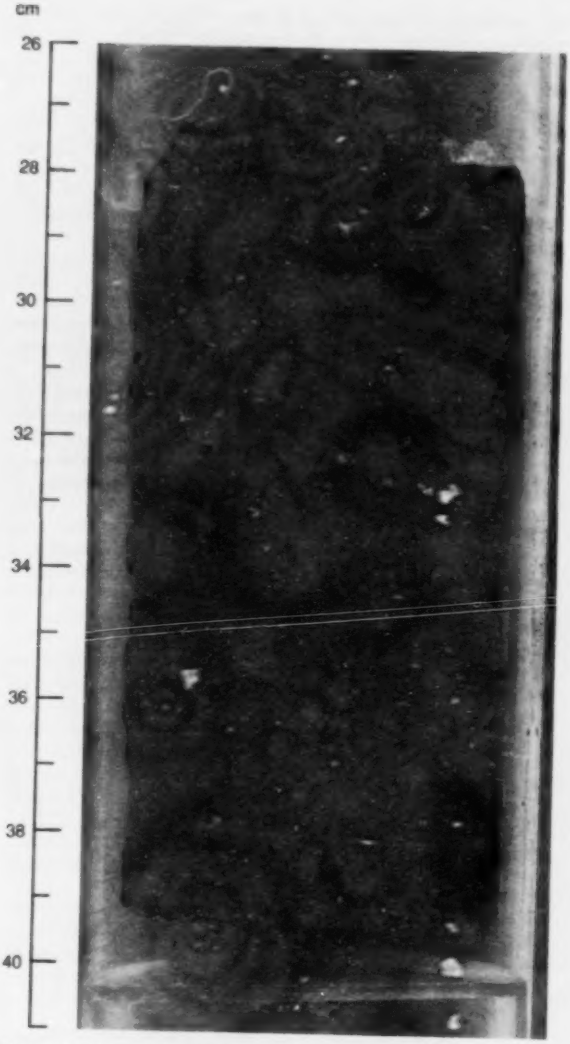

Figure 45. Disrupted, color-zoned, irregular laminations within the yellow hydrothermal deposit. Interval 129-801C-4R-2, 26–40 cm.

interpreted as small, hydrothermally brecciated pipes produced by the sudden release of water-rich volatiles possibly trapped within pillows or flows.

### *Hydrothermal Deposit*

Unit 8 (Sections 129-801C-4R-1 and 129-801C-4R-2) within the basalt lavas is a bright yellow, ochrous material cemented by silica and interpreted as a hydrothermal, iron-rich precipitate. It is composed of somewhat irregular, yellow bands which may show botryoidal hemispheres or radiate coalesced spheres on the upper surface of the bands that merge together downward. Much of the banding is disrupted, however, with broken and disorientated fragments apparently suspended in a silica matrix (Fig. 45). Some fragments are color zoned with paler yellow margins and exhibit minute, internal shrinkage cracks. Without X-ray-diffraction analysis confirmation, it was considered that the yellow material was probably some form of Fe oxyhydroxide.

Thin-section examination revealed growth patterns and a number of development stages for the hydrothermal deposit. Much of the yellow, iron-rich material is composed of small interlocking platelets with a dark red granular core, and occasional star-shaped shrinkage cracks. Other morphologies show hemispherical or small columnar forms with circular and asymmetric growth rings, respectively, nucleated on an opaque growth point. Many of the better-developed hemispheres and almost spherical bodies exhibit a radial fibrous structure. This preliminary examination suggests a possible sequence of events as follows: The forms exhibiting growth rings appear to be the original material, deposited layer by layer, possibly from a colloid that subsequently devitrified with the development of radially disposed fibers. Further development is represented by the formation of fine shrinkage cracks that define the edges of the yellow platelets subsequently formed by recrystallization of the original growth-ring bodies. Relicts of hemispheres and their growth point may sometimes be seen within a group of adjacent platelets. After this stage, the crudely layered deposit was partly replaced by silica, which contains relicts of the platelets within patches of small equant quartz crystals. The apparently forceful invasion by silica-rich solutions also disrupted the layering, enclosing angular yellow fragments within a silica "matrix." Finally, the iron-silica deposit was fractured and further siliceous solutions formed the coarser grained quartz veins that traverse the whole deposit. Some veins have a vuggy interior lined with the inward pointing terminations of quartz crystals.

It seems likely that this approximately 3-m-thick (after recovery) iron-silica-rich deposit was formed by precipitation from seawater enriched by hydrothermal solutions ultimately derived from Jurassic "black smokers" situated in an active ridge system. However, the apparent lack of associated metalliferous sediments or sulfides in the deposit could imply that it was formed some distance away from the active axial zone. Alternatively, it is possible that this deposit was formed near silica-rich "white smokers" on the ridge flanks.

#### *Geochemistry*

Table 13 shows calcium carbonate contents of representative samples from Hole 801C. Similar to the samples from the bottom portion of Hole 801B, calcium carbonate contents of Hole 801C samples are generally high except for that from the hydrothermal deposit (Sample 129-801C-4R-1, 44–46 cm). Some of the higher values may be due to the nearness of the sample analyzed to a carbonate veinlet, but even if these were excluded, Hole 801C and Hole 801B samples, on the average, have the highest carbonate contents among the basaltic rocks from all sites. This is confirmed by the presence of moderate amounts of secondary carbonate (up to 10 vol%) in a majority of thin sections examined (Table 11).

### Summary and Conclusion

1. Site 801 igneous rocks were recovered from below Middle Jurassic (~165 Ma) sediments.

2. Fourteen cooling units were observed in Hole 801B and 29 in Hole 801C. A vast majority of these units are basalts and the rest are dolerites, microdolerites, and a basaltic andesite.

3. Cooling unites in Holes 801B and 801C are morphologically and petrographically similar to typical ocean ridge lavas. These were emplaced as lava flows and pillow lavas with variably altered glass along their rims and all the textures typical of basalts erupted in a marine environment. The units contain predominantly plagioclase, varying proportions of clinopyroxene and titanomagnetite. Olivine (± spinel) occur only in a few samples from Hole 801B but are more common in samples from Hole 801C.

4. Site 801 igneous rocks are moderately to highly altered. The stratigraphically higher Hole 801B units were variably affected by low-grade alteration in the zeolite facies. The main alteration products are clays (mostly smectite), carbonate, zeolites, chlorite, iron-hydroxides, and talc(?). Biotite is also present but its formation probably occurred later and possibly at a slightly higher grade of alteration. The stratigraphically lower Hole 801C units exhibit a wider range and generally higher degree of alteration features. In addition to the type of alteration observed in Hole 801B, Hole 801C units are generally more vesicular and contain secondary features, which are probably related to hydrothermal activities.

5. Calcium carbonate contents of Site 801 igneous rocks generally increase downward in Hole 801B and remain generally high throughout Hole 801C, except in the hydrothermal deposit. Calcium carbonate contents of Site 801 basaltic rocks are the highest among the sites drilled in Leg 129.

6. Based on these observations, we propose that Site 801 basaltic rocks represent a piece of Pacific oceanic crust that was formed in the Jurassic.

## DOWNHOLE MEASUREMENTS

### Operations

On 14 December 1989, after reaching a total depth (TD) of 511.2 mbsf in Hole 801B, a complete wiper trip was made and salt water was circulated in preparation for logging. The bit was dropped at the bottom of the hole and pipe was raised to 77.6 mbsf. The last circulation into Hole 801B was at 0200 hr UTC on 15 December. Logging operations began at 0515 hr on 15 December 1989 and were completed at 0430 hr on 16 December, corresponding to a total logging time of 23.25 hr (Table 14). The pipe was pulled to 78 mbsf for the beginning of

**Table 13. Carbonate content of basaltic samples from Hole 801C.**

| Core, section, interval (cm) | $CaCO_3$ (wt%) |
|---|---|
| 129-801C- | |
| 1R-1, 90–92 | 3.5 |
| 1R-3, 82–84 | 8.0 |
| 1R-5, 29–31 | 3.4 |
| 2R-1, 14–16 | 6.0 |
| 2R-2, 81–83 | 8.6 |
| 2R-4, 76–78 | 11.4 |
| 3R-1, 32–34 | 3.4 |
| 4R-1, 44–46 | 0.1 |
| 5R-1, 103–105 | 7.2 |
| 5R-2, 87–89 | 13.3 |
| 5R-3, 43–45 | 7.2 |
| 6R-1, 115–117 | 17.7 |
| 6R-2, 35–37 | 5.9 |
| 6R-4, 111–113 | 3.4 |
| 6R-5, 68–70 | 5.7 |
| 7R-1, 35–37 | 3.0 |
| 7R-2, 37–39 | 7.7 |
| 8R-1, 65–67 | 11.9 |
| 8R-2, 78–80 | 6.7 |

**Table 14. Actual time schedule (UTC) for logging operations at Hole 801B, including a list of tools used during each logging run.**

| Tool String | Time | Procedure |
|---|---|---|
| Quad Combination (TCCB-LSS-HLDT-NGT-DIL-TLT) | RIH 0515 hr UTC<br>15 December 1989<br>POOH 1145 hr | Log down to 470 mbsf, log up to 64.4 mbsf. Log down to 167 mbsf, log up to 64.4 mbsf. |
| Formation Microscanner (FMS-TCCB-NGT-TLT) | RIH 1330 hr<br>POOH 1950 hr | Run down to 470 mbsf, log up to 64.4 mbsf. Run down again to 470 mbsf, log up to 64.4 mbsf. |
| Geochemical Combination (TCCB-NGT-ACT-GST) | RIH 2100 hr<br>POOH 0430 hr<br>16 December 1989 | Run down to 452 mbsf, log up to 54.1 mbsf. Run down to 166 mbsf, log up to 54.1 mbsf. |

Notes: Total logging time is 23.25 hr, including initial rig-up and final rig-down of tool strings. Abbreviations are as follows: TCCB = telemetry tool; FMS = formation microscanner; LSS = long-spaced sonic tool; ACT = aluminum clay tool; HLDT = lithodensity tool; GST = induced gamma-ray spectrometry tool; NGT = natural gamma-ray spectrometry tool; RIH = run in to hole; DIL = dual induction tool; POOH = pull out of hole; TLT = Lamont temperature tool.

each logging run and raised to approximately 64 mbsf while logging uphole.

The quad combination tool string included, from top to bottom, telemetry, long-spaced sonic, lithodensity, natural gamma-ray spectrometry, dual-induction resistivity tools, and the Lamont temperature tool (TLT). These tools were rigged at 0515 hr on 14 December, creating a tool string 30.72 m long. At 0655 hr this string was run down to 6.5 m below the mud line and held stationary for 3 min to obtain a bottom-water calibration point for the TLT. The depth to the end of pipe recorded on this logging run was within 2.1 m of that calculated by the driller. As logging continued downhole it was reported that the wireline heave compensator (WHC) was not operating. The WHC again had checked out without any additional load applied and failed under full tensional load. Down-going data were recorded while the tool string was lowered downhole until a bridge was encountered at 470 mbsf. Logging data were recorded successfully as the tool string moved uphole at 300 m/hr from 470 to 64.4 mbsf (Fig. 46) with a repeat section taken from 167 to 64.4 mbsf. The bottom of the pipe was encountered at approximately 64.4 mbsf and another bottom-water temperature calibration point for the TLT was obtained inside the pipe at 14.5 m below the mud line. The quad combination tool string was returned to the rig floor at 1145 hr on 15 December. The TLT was then taken from the rig floor to the downhole measurements lab, opened, and hard-wired to the Masscomp computer to download the recorded temperature/time measurements.

The formation microscanner (FMS) string included telemetry, natural gamma-ray spectrometry, general-purpose inclinometer, the FMS, and the TLT. This tool string was rigged and in the hole at 1330 hr on 15 December. This tool combination was lowered down the pipe and held stationary for 3 min at 14.5 m below the mud line to obtain a bottom-water calibration point for the TLT. Two full passes of FMS data were recorded uphole at 260 m/hr from 470 to 64.4 mbsf with no problems. The FMS tool string was run twice with the hope that the tool would be rotated on the second run relative to the first in order to obtain greater coverage of the borehole wall, and indeed this was the case. Another bottom-water temperature calibration point for the TLT was obtained inside the pipe at 14.5 m below the mud line. The WHC was also successfully operating during both of the FMS runs but failed to operate during the subsequent geochemical logging run. The FMS tool string was returned to the drill floor at 1950 hr on 15 December.

The final run at Site 801 was with the geochemical combination tool string, which included telemetry, natural gamma-ray spectrometry, aluminum clay, and induced gamma-ray spectrometry tools. The string was rigged at 2100 hr on 15 December, creating a tool string 18.13 m long. The tool string encountered the bridge at 470 mbsf and logging data were recorded from 452 mbsf up into pipe at 64.1 mbsf as the tool string moved uphole at 200 m/hr (Figs. 47 and 48). A repeat logging run beginning at 166 mbsf was also completed.

This final logging run ended at 0430 hr on 16 December with all tools off of the wireline and secured on deck. All logging runs were shifted by the Schlumberger engineer relative to the quad combination logging run using the natural gamma-ray log response. The geochemical and FMS runs were shifted to shallower depths by 4.27 m and 7.9 m, respectively. All logs were then tied into the drill-string depth.

## Log Quality

The logs are generally of good quality (Figs. 46, 47, and 48). The raw sonic data, however, required significant shipboard processing and editing in an attempt to create a useful sonic log (Figs. 46 and 49). The data recorded from the induced gamma-ray spectrometry tool require post-cruise processing; references made to silicon, calcium, and iron are therefore only broadly qualitative. In contrast, the natural gamma-ray spectrometry tool produces reliable values for the concentration of potassium, thorium, and uranium, and the aluminum clay log is generally little improved through post-cruise processing. The quad combination and geochemical logs are not obviously affected by the ship's heave; the small degree of elasticity within the wireline summed over its extreme length (6000 m) may have acted to slightly decouple these logging tools from the heave of the ship. The WHC was operational only during the FMS logging run and effectively decoupled the FMS tool string from the heave of the ship. No adverse effects from the ship's motion are apparent on the raw FMS records; however, the FMS data will still require significant shore-based image-processing to achieve an interpretable record.

Summary log figures appear at the end of this chapter. The FMS images are presented on microfiche in the back of this volume.

## Logging Units

Five logging units were identified in Hole 801B (Figs. 46 to 50), based on log response and analyses of recovered cores, but are not to be confused with the lithologic units defined previously (see "Lithostratigraphy and Sedimentology" section, this chapter). The boundaries between adjacent logging units were placed at significant inflection points resulting from simultaneous variations on at least several of the logs illustrated in Figures 46 to 50. These units display consistent log responses or distinct overall trends. In general, the logging unit boundaries in Hole 801B are characterized by a single shift in the log values rather than the sinusoidal log responses observed at Site 800. The potassium values displayed much greater variability at this site than at Site 800 and were used effectively to choose logging boundaries, whereas the calcium values were more uniform at this site and less useful for defining logging units.

Core recovery was poor throughout most of the logged interval (less than 10%) and only fragments of the most indurated portions of the formation were usually recovered. The lithologies for unrecovered intervals have been inferred from the logs based on the broad assumption that the logging tools responded to varying proportions of the primary constituents in samples actually recovered (e.g., biogenic silica, carbonate, pelagic clay, and volcanogenic clay) and to their relative porosity.

### *Logging Unit 1 (64.4–126 mbsf)*

Logging Unit 1 is characterized by generally high sonic velocity (2.1–2.6 km/s), resistivity (2–6 ohm-m), density (1.8–2.0 g/cm$^3$), silicon content, and variable but relatively high sulfur content along with relatively low values of aluminum (.5 wt%), iron, and total gamma-ray counts (22–30 API). Logging Unit 1 is also uniquely distinguished by relatively low thorium (1.2–1.8 ppm) and potassium (.4–.8 wt%) concentrations and relatively high uranium values (.5–1.25 ppm). This kind of log response is indicative of a diagenetic interval in which pore spaces are filled with recrystallized silica where the mobile uranium ion was concentrated. The overall log responses suggest that the porcellanite and chert fragments recovered in this section accurately reflect the most indurated portion of this formation. The variability in the above-mentioned logs indicates the presence of unrecovered clay-rich intervals (e.g., pelagic clay, 98–103 mbsf, and volcanogenic clay, 111–116 mbsf). The boundary between logging Unit 1 and Unit 2 is marked by a sharp unidirectional shift to lower velocity, resistivity, density, sulfur, and silicon content along with increasing aluminum content and total gamma-ray counts.

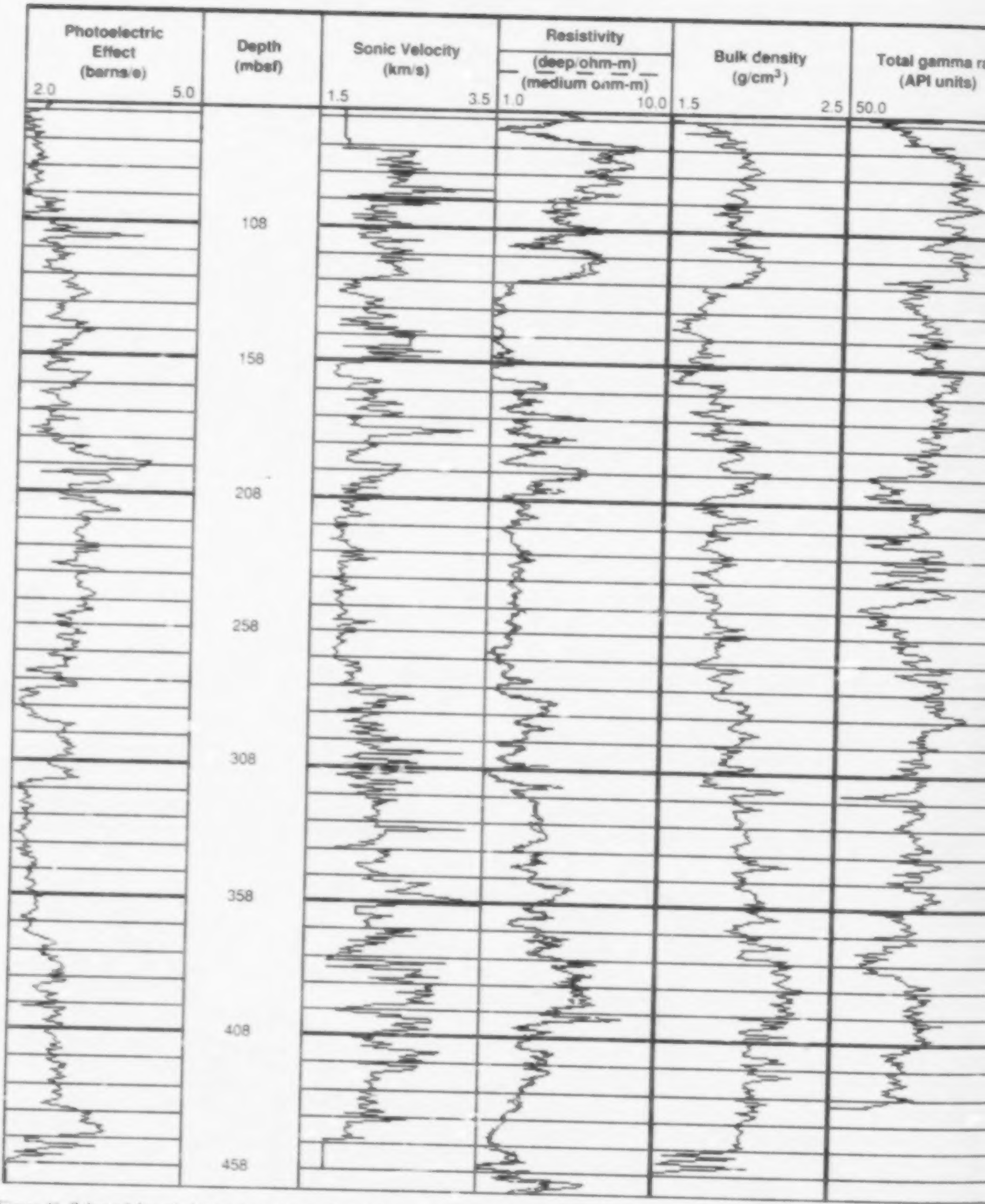

Figure 46. Selected downhole logs from the quad combination tool string for the interval 64.4 to 466 mbsf in Hole 801B: Photoelectric effect, son velocity, resistivity, bulk density, and total gamma ray. Stratigraphic units defined by logging data (logging units) are shown in Figure 50. Son velocity, resistivity, and density reflect the porosity of the formation and therefore the degree of lithification or cementation (e.g., chert v radiolarite).

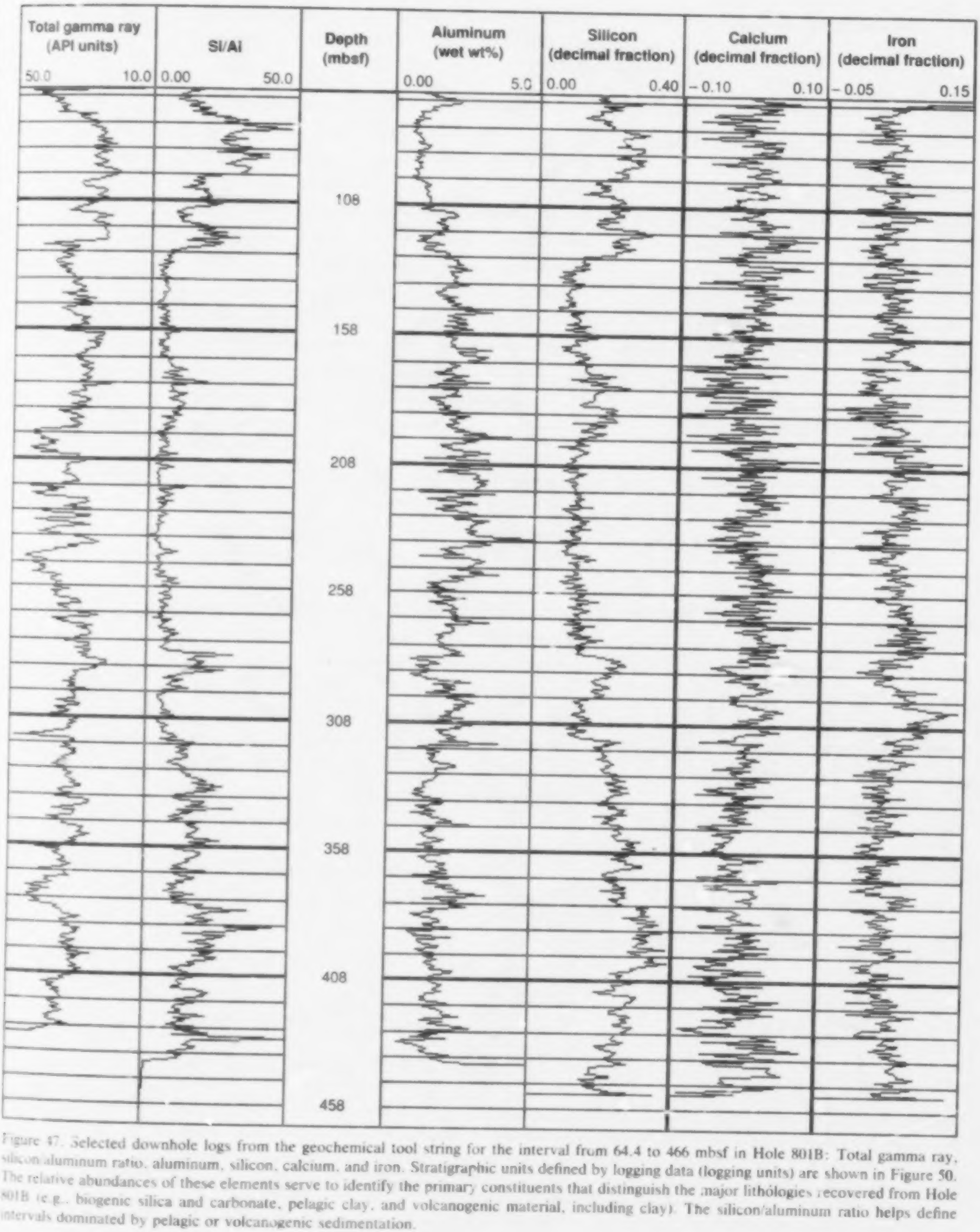

Figure 47. Selected downhole logs from the geochemical tool string for the interval from 64.4 to 466 mbsf in Hole 801B: Total gamma ray, silicon/aluminum ratio, aluminum, silicon, calcium, and iron. Stratigraphic units defined by logging data (logging units) are shown in Figure 50. The relative abundances of these elements serve to identify the primary constituents that distinguish the major lithologies recovered from Hole 801B (e.g., biogenic silica and carbonate, pelagic clay, and volcanogenic material, including clay). The silicon/aluminum ratio helps define intervals dominated by pelagic or volcanogenic sedimentation.

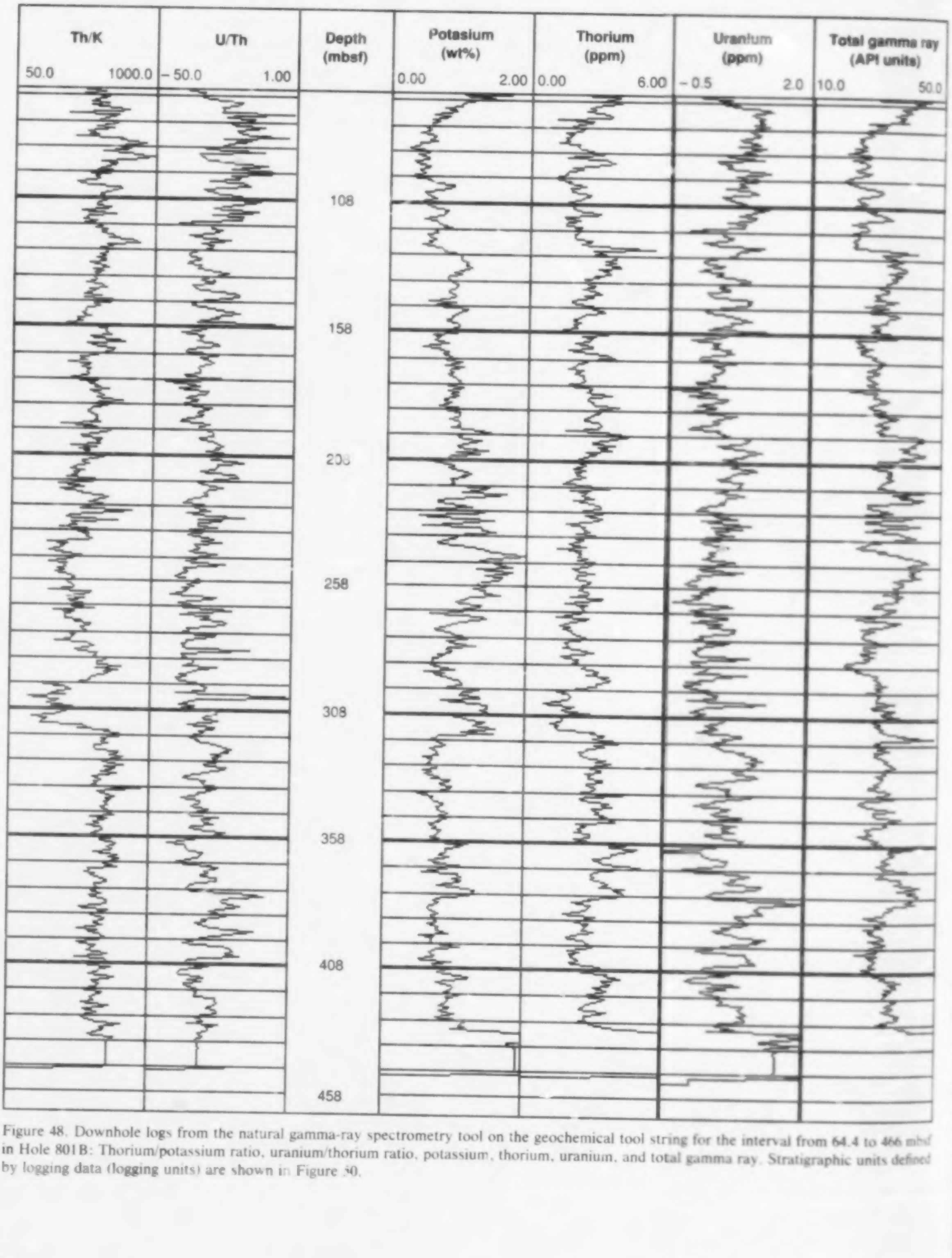

Figure 48. Downhole logs from the natural gamma-ray spectrometry tool on the geochemical tool string for the interval from 64.4 to 466 mbsf in Hole 801B: Thorium/potassium ratio, uranium/thorium ratio, potassium, thorium, uranium, and total gamma ray. Stratigraphic units defined by logging data (logging units) are shown in Figure 50.

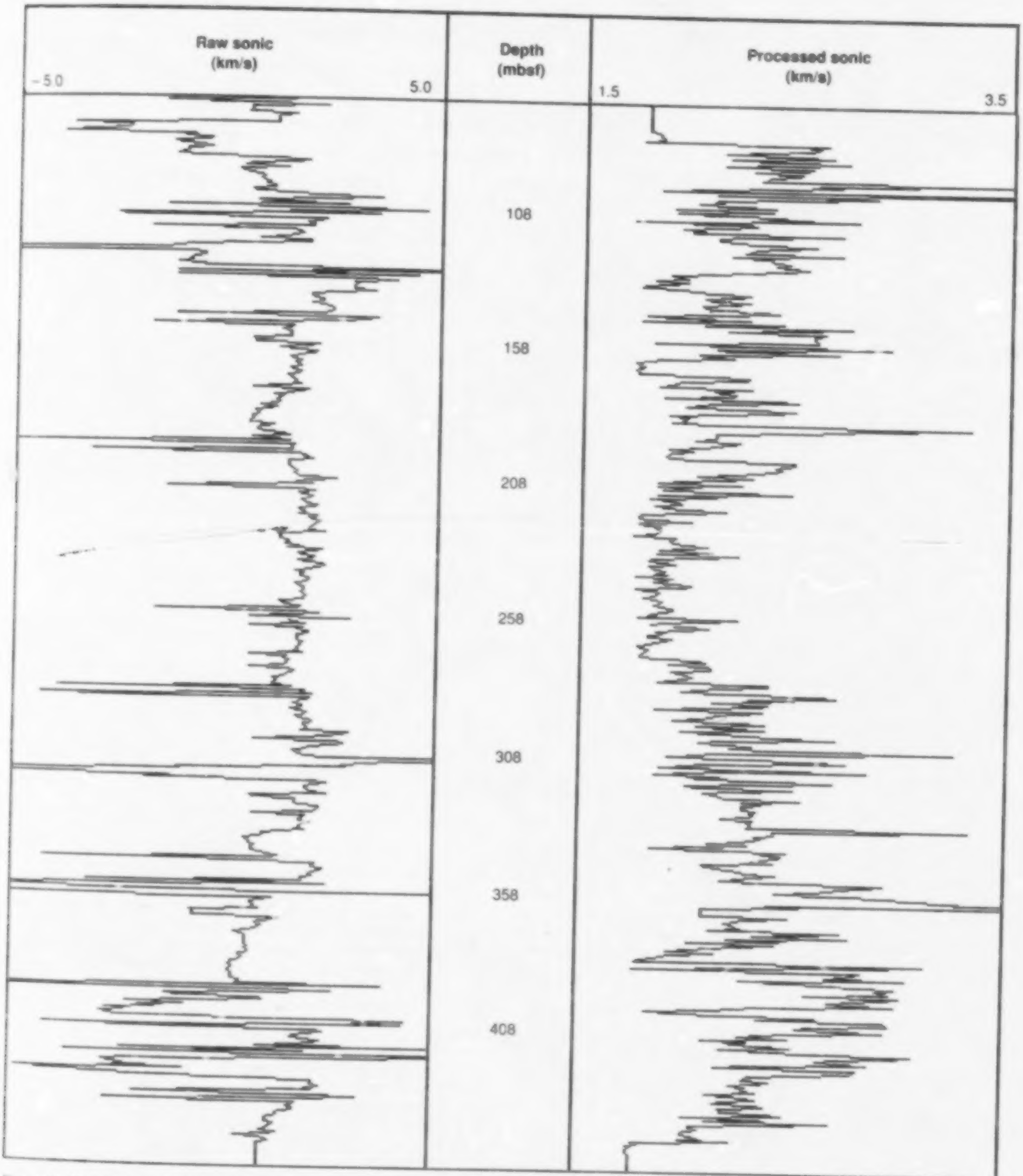

Figure 49. Comparison of observed "raw" (left column) and processed (right column) velocity logs for Hole 801B. Covariation of the processed sonic log with resistivity, gamma ray, and bulk density logs occurs where logging unit boundaries were chosen (Figs. 46 and 50), indicating that a useful velocity log was produced. There are still several intervals where significant velocity variations occur with no covarying response from other logs, making it difficult to confidently interpret a synthetic seismogram made from this sonic log.

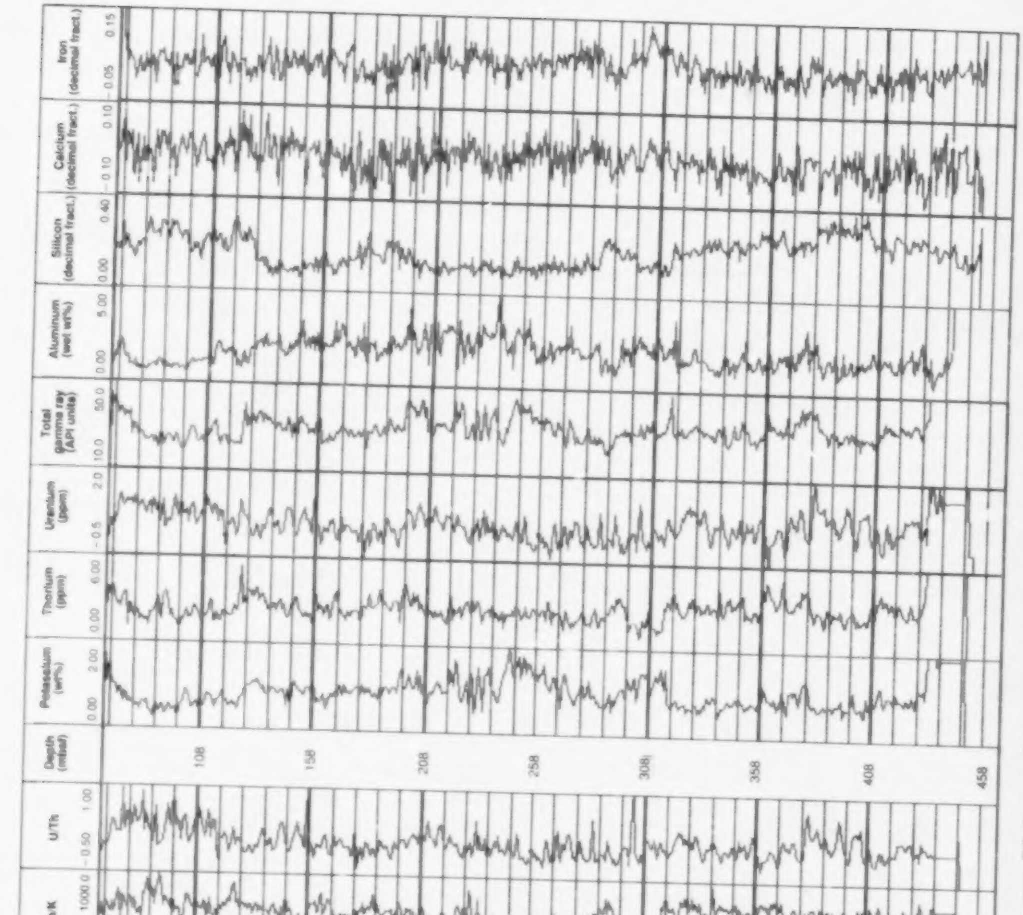

Figure 50. Summary compilation of downhole logs, intervals of core recovery, lithology, and downhole logging units at Hole 801B. Lithologic units are based on coring results (see "Lithostratigraphy and Sedimentology" section, this chapter).

This boundary is also characterized by abrupt shifts toward higher potassium and thorium and lower uranium content. The log responses at this boundary argue for an abrupt contact at 126 mbsf between the diagenetic pelagic sediments (64–126 mbsf) and an underlying volcanic clay-rich, chert-poor sequence. The logging data correlate well with lithofacies Unit II (see "Lithostratigraphy and Sedimentology" section, this chapter), with the base of logging Unit I and lithofacies Unit II coinciding exactly.

### *Logging Unit 2A (126–193 mbsf)*

Logging Unit 2A is characterized initially by the lowest resistivities (1 ohm-m), densities (<1.8 g/cm$^3$), and silicon content observed at Hole 801B, and by relatively high total gamma ray (42 API) decreasing to 30 API at 158 mbsf. There is also a local minima in velocity, density, silicon, aluminum, potassium, and thorium values from 158 to 166 mbsf with calcium and iron displaying no change in trend. Sulfur content is variable but steadily decreases through Unit 2A, reaching an absolute minimum value at the base of this logging unit (193 mbsf). The remaining portion of Unit 2A from 166 to 193 mbsf is distinguished by variable but generally increasing resistivity (1.5 to 3.0 ohm-m), density (1.8–2.1 g/cm$^3$), and silicon content with generally lower calcium values of higher frequency variability. The lower boundary of logging Unit 2A at 193–198 mbsf is marked by an abrupt, sinusoidal variation on several logs at 193 mbsf with local minima in velocity (1.9 km/s), resistivity (1.2 ohm-m), and density (1.8 g/cm$^3$) juxtaposed against local maxima in these logs along with maximum values for potassium, thorium, uranium, and aluminum at 198 mbsf.

The logging responses defining logging Unit 2A from 126 to 158 mbsf are interpreted to result from poorly cemented, clay-rich volcanogenic material. Nannofossils become abundant in this interval but the relative concentration of calcium remains essentially the same as in logging Unit 1, which is barren of nannofossils. Radiolarians are abundant in both Unit 1 and Unit 2A but the relative concentration of silicon reaches a minimum in Unit 2A where no recrystalization of silica is evident. The logging response at 158 to 166 mbsf strongly indicates a clay-poor (both volcanic and pelagic) as well as poorly cemented interval that corresponds with the coarser-grained volcanic sandstone (probably high porosity) recovered at this level (e.g., Core 129-801A-18R). The log response over the interval from 166 to 193 mbsf indicates a trend toward greater siliceous and lower calcareous pelagic input within the still dominant volcanics, resulting in a somewhat less porous, better cemented interval that is punctuated by chert/porcellanite lenses (e.g., 178 mbsf). This lowermost interval is also observed to contain greater abundances of radiolarians and is barren of nannofossils (see "Biostratigraphy" section, this chapter). Finally, the simultaneous variation on nearly all the logs, which distinguishes the lower boundary of logging Unit 2A at 193–198 mbsf, is interpreted to indicate a well-indurated sequence of altered volcanics possibly including high-potassium zeolites with recrystallized calcium carbonate rather than silica as the dominant cementing agent. Logging Unit 2A is considered a transition zone between logging Unit 1 and underlying Unit 2B and, as such, corresponds quite well with the lithologies and trends reported in the upper portion of lithologic Unit III (i.e., Cores 129-801A-14R to 129-801B-1R; see "Lithostratigraphy and Sedimentology" section, this chapter).

### *Logging Unit 2B (193–280 mbsf)*

Logging Unit 2B is distinguished by a relatively uniform and extended zone of low velocity (<1.9 km/s), resistivity (1.5 ohm-m), density (1.7–1.9 g/cm$^3$.) and silicon content. This unit is also characterized by variable but generally the most elevated concentrations of potassium (>.8%), aluminum, and iron.

This type of logging response is interpreted to result from a sequence dominated by volcaniclastics and various alteration products such as clays and high potassium zeolites. This interval appears to have the least amount of pelagic input (especially silica) over the entire interval logged at Site 801, and corresponds to the interval where radiolarians are least abundant (see "Biostratigraphy" section, this chapter).

### *Logging Unit 2C (280–313 mbsf)*

The boundary between logging Units 2B and 2C is marked by a unidirectional shift to higher velocities (2.1–2.5 km/s), resistivities (1.9 ohm-m), densities (1.9–2.0 g/cm$^3$), and silicon values along with local minima in calcium, iron, aluminum, and total gamma-ray counts. The remainder of logging Unit 2C is characterized by steadily decreasing silicon content matched by increasing iron, aluminum, and potassium. The interval from 298 to 313 mbsf is uniquely characterized by the highest relative concentration of iron along with elevated potassium content, relative minima in silicon, and an absolute minima in thorium. The lower boundary of Unit 2C is marked at 313 mbsf by relative minima in resistivity, density, silicon, iron, and calcium.

The log response defining Unit 2C from 280 to 298 mbsf is representative of a restricted interval of low porosity resulting from silicification within a unit where pelagic sedimentation temporarily dominates redeposited volcanics. The logging reaction from 313 to 298 mbsf is indicative of altered, poorly cemented volcanogenic material. The relatively extreme values observed for potassium, thorium, and iron suggest that some unusual rock type may be present. This depth interval corresponds to Cores 129-801B-12R and -13R, which contain the only recovered occurrence of closely spaced bands of white crystalline material within green volcaniclastics (see "Lithostratigraphy and Sedimentology" section, this chapter). The white crystalline bands are interpreted to be zeolites and anhydrite, and their unusual abundance may create the distinctive logging response that marks the lower boundary of Unit 2C. Logging Unit 2C corresponds to the base of lithologic Unit III and illustrates the transition from nonvolcanogenic lithologies to a sequence dominated by volcanogenic turbidites.

### *Logging Unit 3 (313–448 mbsf)*

Logging Unit 3 begins at 313 mbsf and terminates at 448 mbsf approximately 20 m above the TD for logging operations at Site 801. This unit is distinguished by variable but relatively high velocities, resistivities (1.9–4.6 ohm-m), densities (1.9–2.3 g/cm$^3$), and silicon concentrations along with reduced aluminum (<0.2%) and iron concentrations and generally low total gamma-ray counts. This type of log response is interpreted to result from variations in porosity because of varying degrees of silicification within the sediments. Intervals of lower silica, resistivity, velocity, and density are considered to be dominated by poorly cemented radiolarite sand rather than chert, and in the instances where an increase in aluminum and total gamma-ray counts are observed (e.g., 373–378 mbsf), volcanic clays are expected to be present. In general, logging Unit 3 is quite similar to Unit 1. However, Unit 1 appears to be nearly free of any volcanic influence (e.g., lowest aluminum values), whereas Unit 3 exhibits evidence for some volcanogenic components.

A distinctive interval occurs within Unit 3 from 378 to 403 mbsf which is marked by the highest relative concentrations of silicon and uranium (2 ppm) and the highest densities (2.3 g/cm$^3$) recorded by logging tools at Site 801. This interval also displays uniformly high velocities (2.9 km/s) and resistivities (3.7 ohm-m) along with low potassium (0.8%) and thorium (<3 ppm) concentrations. This interval, which is interpreted to contain the greatest percentage of chert at Site 801, is sandwiched between a radiolarite, pelagic clay-rich layer at 403 mbsf and an interval of radiolarite with volcanic clay at 378 mbsf. Paleomagnetic studies on cores from this interval indicate that these diagenetically altered sediments were deposited during an equatorial crossing (see "Paleomagnetism" section, this chapter). The Jurassic/Cretaceous boundary coincides with the clay and radiolarite layer at 370 mbsf, and directly overlies the chert-rich interval that marks the equatorial crossing (see "Biostratigraphy" section, this chapter).

### Synthetic Seismogram

The raw sonic log at this site is of considerably poorer quality than the sonic log recorded at Site 800, and the results of our initial processing of this raw sonic log are considered unsatisfactory for production of a useful synthetic seismogram (Fig. 49). A synthetic seismogram will be produced for Site 801 after further shore-based processing that will incorporate physical properties data and a repicking of traveltimes using the full sonic waveform (Borehole Research Group, 1988).

### Summary

A suite of eight different downhole logs was successfully recorded at Site 801, resulting in the identification of five distinct logging units. Compositional trends and boundaries were inferred from these logs through intervals of poor recovery by assuming that unrecovered intervals are composed of varying proportions of recovered materials. The logs were most useful in defining boundaries and in characterizing the unrecovered majority of the formation.

## SITE GEOPHYSICS AND SEISMIC STRATIGRAPHY

### Site Geophysics

Site selection for Leg 129 was based on the multichannel seismic (MCS) surveys described in the "Site Geophysics and Seismic Stratigraphy" section, "Explanatory Notes" chapter (this volume). Underway geophysical data were collected as we approached all sites and provided the correlations with principal MCS sections needed to position the ship at preferred locations.

Site 801 (proposed site PIG-3A) in the central Pigafetta Basin is located within the Jurassic magnetic quiet zone (JQZ) near the intersection of lines 6 and 10 of an MCS survey obtained during the MESOPAC II expedition aboard the *Le Suroit* in August-September 1989. Because Leg 129 began less than three months after the *Le Suroit* cruise, only single-channel, real-time records of both water-gun and air-gun data, as well as sonobuoy refraction data obtained during MESOPAC II, were used to locate proposed site PIG-3A (Figs. 51 and 52). The location of these MESOPAC II MCS profiles was dictated by an earlier MCS expedition aboard the *Fred H. Moore* (FM35-12, November-December 1987). Although the proposed site is not located on an FM35-12 profile, the MCS basement images and velocity structure derived from sonobuoy data (specifically, SB-22) obtained during the FM35-12 expedition provided the regional seismic framework for locating Site 801. Proposed site PIG-3A was specifically located at 0600 hr UTC on 26 August 1989 along MESOPAC II line 10 approximately 3 km southeast of its intersection with MESOPAC II line 6. MESOPAC II sonobuoys 6m (45 km south of Site 801), 4m (93 km east of Site 801), and FM35-12 sonobuoy 22 (located 55 km northeast of Site 801) were used to constrain basement depth and velocity structure (Fig. 56). The only other seismic data in the area are a few widely spaced single-channel air-gun analog profiles (e.g., C1005).

Single-channel seismic (SCS) reflection and 3.5-kHz and 12-kHz profiling were conducted both during the approach of the *JOIDES Resolution* to Site 801 and upon departure for Site 802 (see "Operations" section, this chapter, for detailed approach plan). The actual site is located on the approaching SCS water-gun profile at 1600 hr on 7 December 1989 and on the departing SCS profile at 0110 hr on 23 December 1989 (Figs. 51 and 54) within 0.4 km of the proposed site location on MESOPAC II line 10. Unfortunately, only 0.5 s (7.5–8.0 s two-way traveltime, or twt) of SCS data were recorded digitally during the approach because of a mistake in setting the deep-water delay, but a full 5 s of SCS data were recorded across the site upon departure.

The water-gun data collected during Leg 129 (two 80-in.$^3$) and MESOPAC II (six 80-in.$^3$), and the FM35-12 air-gun data (2819 in.$^3$) are corroborative, and together with 3.5-kHz and sonobuoy data, provided the following seismic criteria for locating Site 801:

1. The relatively thick (53–79 ms) transparent layer over acoustic basement imaged with an excellent 3.5-kHz record (Fig. 55) indicated that enough soft sediment is present over the first cherts to provide lateral support for the drill string during spud-in.
2. A high-amplitude reflection imaged regionally at 0.41 to 0.48 s below the seafloor (bsf) corresponds to the onset of velocities characteristic of oceanic crust as recorded on sonobuoys 4m and 6m (MESOPAC II) and 22 (FM35-12), indicating that approximately 410 to 480 m of sediment overlies oceanic crust in this area.
3. This high-amplitude reflection appears rough, undulating, and diffractive, resulting in an image characteristic of the top of oceanic crust.

### Seismic Stratigraphy

The acoustic stratigraphy of large portions of the western Pacific consists of four units originally defined by Ewing et al. (1968): (1) an upper transparent layer, (2) an upper opaque layer, (3) a lower transparent layer, and (4) acoustic basement. These seismic facies descriptions were made from observations of SCS analog air-gun profiles. Acoustic basement has been characterized by the presence of a prominent zone of flat-lying ("smooth"), high amplitude, and closely spaced reflections referred to as "horizon B" by Ewing et al., (1968), the "deep opaque layer" (Heezen, MacGregor, et al., 1973) and as the "reverberant layer" by Houtz et al., (1970) and Houtz and Ludwig (1979). It is now recognized that the reverberant nature of acoustic basement in such profiles is usually the result of a trailing bubble pulse oscillation reflecting from a single high-impedance boundary (Shipley et al., 1983). This characteristic of the air-gun source is now routinely compensated for through the use of tuned air-gun arrays and deconvolution techniques. The use of water-guns in these surveys provides a much more implosive and bubble pulse-free source signature that provides a high-resolution record with little processing effort (Hutchinson and Detrick, 1984).

Although modern acquisition and processing techniques have allowed a more detailed and quantitative assessment of the stratigraphic units originally proposed by Ewing et al. (1968) (especially acoustic basement), these units can still serve to describe the general seismic character of the Pigafetta Basin. It is understood that the following qualitative seismic facies descriptions are largely controlled by the type of seismic source (air gun vs. water gun), processing, and display

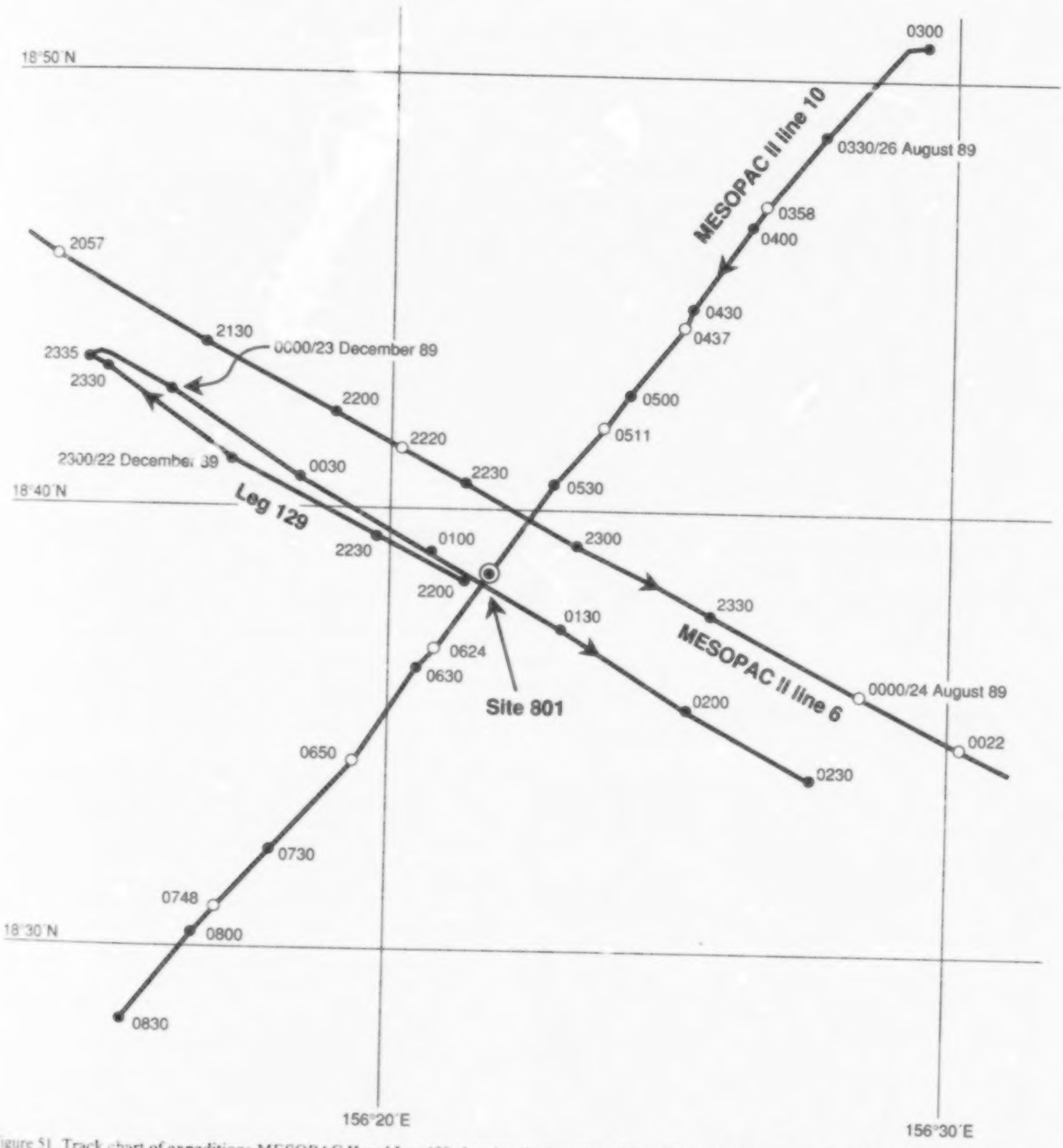
18°50'N
18°40'N
18°30'N
156°20'E
156°30'E
MESOPAC II line 10
MESOPAC II line 6
Leg 129
Site 801
0300
0330/26 August 89
0358
0400
0430
0437
0500
0511
0530
0624
0630
0650
0730
0748
0800
0830
2057
2130
2200
2220
2230
2300
2330
0000/24 August 89
0022
2335
2330
0000/23 December 89
2300/22 December 89
0030
2230
0100
2200
0130
0200
0230

Figure 51. Track chart of expeditions MESOPAC II and Leg 129 showing the location of Site 801 at the intersection of MESOPAC II line 10 (0600 hr UTC, 26 August 1989) and Leg 129 SCS line (0110 hr, 23 December 1989) within 400 m of the location of originally proposed site PIG-3A.

parameters. The final seismic facies identification and interpretation will be made after the MESOPAC II MCS data have been stacked and properly displayed and a synthetic seismogram has been generated.

The lowermost sequence, the reverberant layer, is composed of closely spaced, high-amplitude, continuous reflections that directly overlie a less continuous, more diffractive surface. This most prominent horizon is continuous, flat-lying, and shallow (250–300 ms bsf) in the southeastern Pigafetta Basin and is observed to monotonically deepen (400–480 ms bsf), becoming fragmented or absent altogether, revealing rougher, undulating reflections beginning approximately 130 km south of and including Site 801. To the northeast (but still within the JQZ) this horizon appears tectonized, often exhibiting smooth, block-faulted slabs that have an apparent dip to the northeast. This distinctive lowermost horizon is associated with the onset of velocities characteristic of oceanic crust as determined from sonobuoy data collected during FM35-12

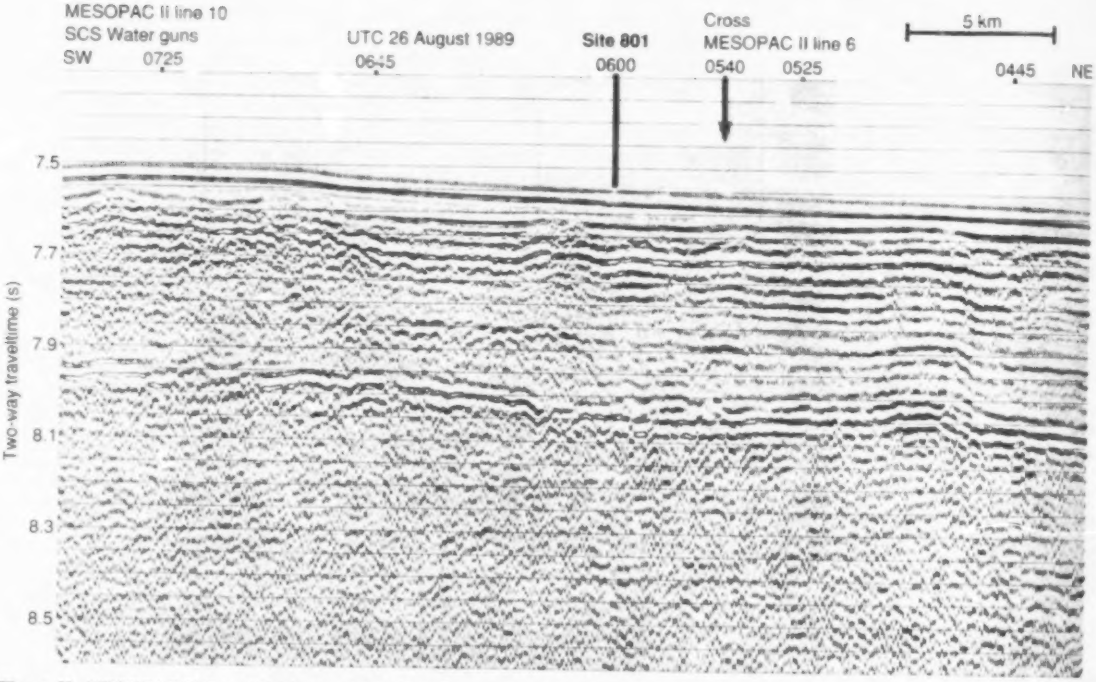

Figure 52. MESOPAC II line 10 SCS record (six 80-in.$^3$ water guns) showing location of Site 801 (0600 hr UTC, 26 August 1989) at the intersection with Leg 129 SCS (0110 hr, Fig. 54), and the intersection with MESOPAC II line 6 (Fig. 53). The top of oceanic crust and total depth at Site 801 lie at approximately 8.0 and 8.064 s twt, respectively. This near-channel record was processed and displayed with the following parameters: water velocity F/k migration, mute, 2-trace mix, band-pass filter 25–100 Hz, 500 ms AGC, and vertical exaggeration ~22× at 1.5 km/s.

and MESOPAC II (Abrams et al., 1988). At Site 801, the reverberant sequence ranges from 50 to 100 ms in thickness beginning at 8.0 s twt or 460 ms bsf (Figs. 52, 53, and 54). This lowermost sequence of reflections does not appear as the typical, flat-lying, smooth horizon that is one of the primary characteristics of the reverberant layer and may be better termed "the basement reflector." However, this surface does appear to be contiguous with such a flat-lying horizon that extends for hundreds of kilometers to the southeast. Immediately overlying this interval is the lower transparent layer which is characterized by lower amplitude, widely spaced, and less continuous reflections that range from 250 to 460 ms bsf (7.79–8.00 s twt) and may extend as high as 140 ms bsf. This relatively transparent layer appears to thin to the southeast as the underlying reverberant layer rises in the section and changes to its more typical, flat-lying, smooth appearance. The lower transparent layer includes a distinct high-amplitude, quite continuous reflection that mimics the underlying relief and appears to be draping deposit. In the immediate vicinity of Site 801 this high-amplitude reflection at 310 ms bsf (7.85 s twt) appears to divide the lower transparent layer in two (e.g., Fig. 53) and in other instances it seems to mark the base of an overlying opaque layer or becomes part of an opaque layer that extends all the way to basement (e.g., left side of Fig. 52). The lower transparent layer is bounded on top by a distinctly higher amplitude, more continuous sequence of reflections that also appear to drape over underlying relief. This unit appears to maintain a fairly uniform thickness throughout extended portions of the Pigafetta Basin.

The upper transparent zone as envisioned by Ewing et al. (1968) is very much attenuated in the Pigafetta Basin and extends from 0 to approximately 79 ms bsf (7.54–7.619 s twt) at Site 801. This interval is best displayed on the 3.5-kHz records obtained during Leg 129 (Fig. 55) and MESOPAC II, but is also apparent on SCS records. These four seismic facies are essentially identical on the SCS monitor records of both Leg 129 and MESOPAC II.

## Correlation between Seismic Stratigraphy and Lithology at Site 801

DSDP Legs 6, 17, 61, and 89 had instances during which a flat-lying, high-amplitude "acoustic basement" or "reverberant layer" was correlated to middle Cretaceous volcanic material (sills, flows, and volcanogenic turbidites) which, according to magnetic lineations, significantly post-date the formation of oceanic crust. However, the physical nature of a similar seismic facies observed throughout the East Mariana and Pigafetta basins had not been determined before Leg 129.

The reverberant layer at Site 800, located on a correlatable magnetic anomaly (M33) in the northern Pigafetta Basin is created by a massive chert overlying a series of dolerite sills and appears as a flat-lying sequence of reflections approximately 100 ms thick (see "Site Geophysics and Seismic Stratigraphy" section, "Site 800" chapter, this volume). This type of smooth, flat-lying, high-velocity horizon is characteristic of much of the Pigafetta Basin and the majority of the East Mariana Basin (Abrams et al., 1988). In contrast, the

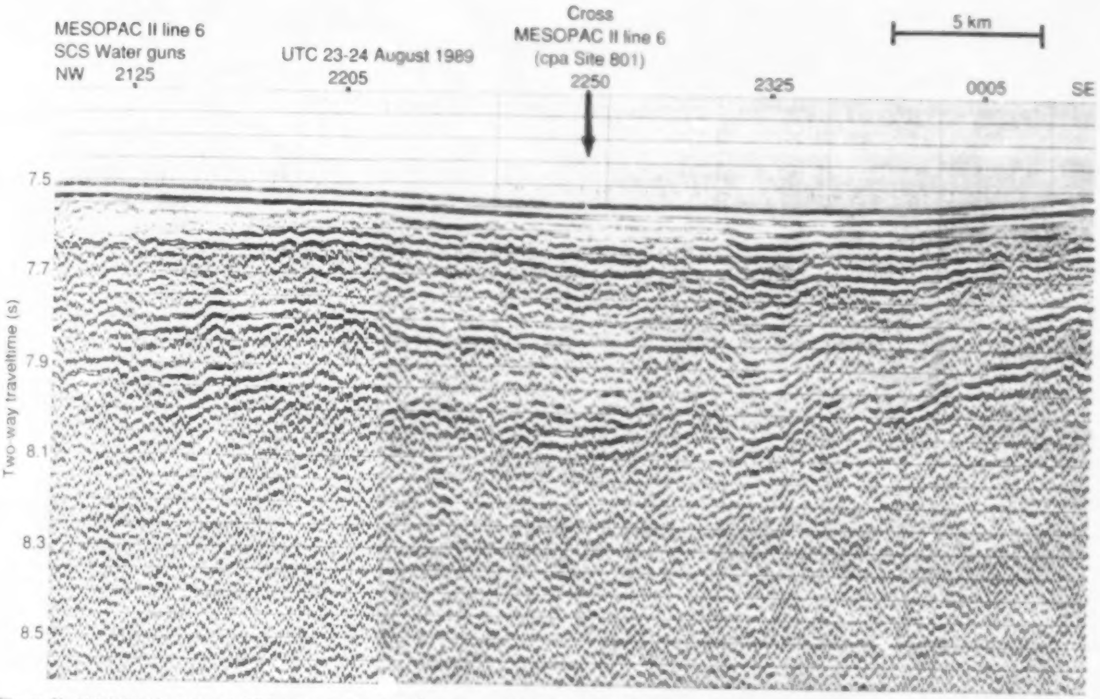

Figure 53. MESOPAC II line 6 SCS record (six 80-in.$^3$ water guns) showing intersection with MESOPAC II line 10 (Fig. 52) approximately 3 km northeast of Site 801. The basement reflection along this inferred flow-line profile varies from 7.85 to 8.0 s twt, displaying the relief that characterizes buried abyssal hill bathymetry. This "rough" basement reflection is coincident with the onset of velocities and velocity gradients characteristic of oceanic crust (Fig. 56). Processing and display parameters are identical to those given for Figure 52.

reverberant layer at Site 801, located well within the JQZ, appears as a rough, undulating horizon that is created by interbedded basalt and chert overlying a series of contiguous basalt flow units (see "Igneous Petrology" section, this chapter). This seismic facies is interpreted to result primarily from a single impedance contrast between the radiolarite clays and the top of chert overlying basalt at 461 mbsf.

The velocity structure of this area of the Pigafetta Basin is well constrained by refraction data from three long-range sonobuoys that produce nearly identical velocity vs. depth solutions (Fig. 56). These solutions show velocities and velocity gradients characteristic of "normal" oceanic crust beginning from 410 to 440 ms bsf, which correlates to the reverberant layer imaged regionally at 410 to 480 ms bsf. The high-relief horizon penetrated in Holes 801B and 801C is interpreted to be the top of oceanic crust. In the areas where the reverberant horizon becomes flat-lying and shallow, cherts overlying sills and/or flows which are significantly younger than those recovered at Site 801 are expected to overlie oceanic crust. This observation has significant implications for the lateral extent of middle Cretaceous deep-sea volcanism within the "Jurassic" western Pacific, considering that most of the Pigafetta and East Mariana basins is characterized by such a flat-lying, high-amplitude, high-velocity basement reflection.

This distinctive change in the seismic character of the reverberant layer from smooth to rough can also be correlated to a change in magnetic anomaly amplitudes and field strength that was first observed in the aeromagnetics data of Handschumacher et al. (1988) and also displayed on the shipboard magnetics of FM35-12 and MESOPAC II. The "rough-smooth" reverberant horizon boundary corresponds to a change in magnetic anomalies from higher field/low amplitude anomalies to lower field/high amplitude anomalies. A comparable boundary within the East Mariana Basin, which is characterized by the nearly ubiquitous presence of the high-amplitude, flat-lying reverberant layer, is not apparent (see "Site Geophysics and Seismic Stratigraphy" section, "Site 802" chapter, this volume).

The lower transparent layer correlates with the thin (18 m) sequence of red radiolarite and claystone and brown radiolarite between 318.3 and 461.6 mbsf (lithologic Units IV and V), as well as the lower portion of the volcaniclastic turbidites (about 193 to 318 mbsf). The high-amplitude reflection dividing the transparent layer in half at 310 ms bsf is believed to correspond to an unrecovered massive chert layer (abrupt decrease in drilling rate and apparent on logs), which marks the beginning of a transition from nonvolcanogenic lithologies below 318 mbsf to an overlying sequence dominated by volcanogenic turbidites. The low-amplitude reflections are created by small impedance contrasts within two different but internally homogenous intervals. The lower pelagic interval shows uniformly low porosity (inferred from logs) punctuated by variations in porosity because of radiolarite-rich or chert-rich intervals. The overlying turbidites display uniformly high porosity with well-developed graded bedding structures and variations in calcite cementation that may create relatively low-amplitude reflections (see "Downhole Measurements" and "Lithostratigraphy and Sedimentology" sections, this chapter).

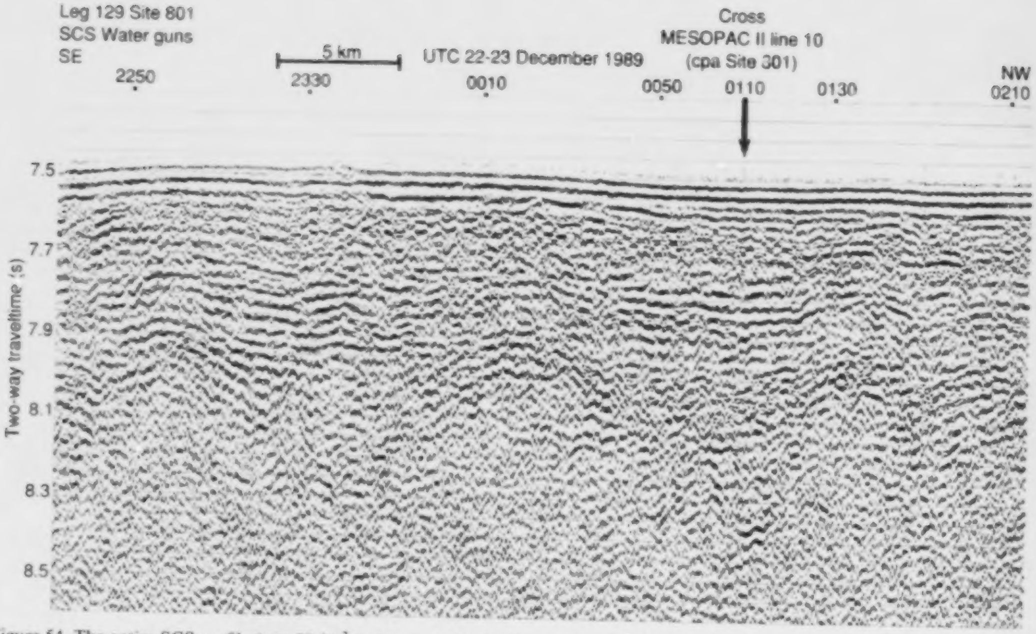

Figure 54. The entire SCS profile (two 80-in.$^3$ water guns) obtained upon departure from Site 801 (0110 hr UTC, 23 December 1989) during Leg 129. This SCS profile crosses MESOPAC II line 10 (Fig. 52) at 0110 hr at its closest approach to Site 801. This seismic record is obviously of poorer quality than that obtained at Sites 800 and 802 during Leg 129 because of problems during digital acquisition (for details, see "Site Geophysics and Seismic Stratigraphy" section, "Explanatory Notes" chapter, this volume). This record is displayed with the following parameters: mute, 2-trace mix, band-pass filter 30–100 Hz, 500 ms AGC, vertical exaggeration ~22× at 1.5 km/s.

A transition zone (logging Unit 2A), which consists of both volcanogenic and pelagic material at approximately 193 mbsf, correlates to the relative increase in reflection amplitude that marks the change from lower transparent to upper opaque seismic facies. The distinctive high-amplitude reflection at 160 ms bsf correlates to a chert-rich interval at 178 mbsf interbedded with volcaniclastic claystone. This chert-rich interval lies beneath a poorly cemented volcaniclastic sandstone (see "Lithostratigraphy and Sedimentology" section, this chapter). These high-amplitude reflections also encompass the overlying pelagic interval where impedance contrasts occur between interbedded chert/porcellanite and pelagic clay.

The transparent nature of the uppermost 79 ms bsf (upper transparent layer) is indicative of a relatively homogenous interval containing no significant impedance contrasts. This interval correlates to pelagic brown clay (8–61 mbsf) underlain by the uppermost cherts.

The depths of specific horizons mentioned in the above correlation of seismic facies with lithofacies within the sedimentary section were assigned without the guidance and constraints provided by a log-generated synthetic seismogram and should be considered only as general estimates (see Fig. 57). A synthetic seismogram will be used to accurately tie the drilled sequence in the hole to seismic reflection data over the site.

## SUMMARY AND CONCLUSIONS

### Jurassic in the Pacific (At Last)

Site 801 is the first site to have reached the Jurassic in the Pacific, and it might remain the only one for a long time. This simple statement does not really do justice to the importance of the discovery considering the years of hope, effort, and frustration spent in the search for the oldest record of the world's Jurassic "superocean." Site 801 represents a milestone in our quest for the earliest evolution of the part of the world's oceanic record that is still accessible. Given the relatively small size of the Pacific plate in the Middle to Late Jurassic, compared to the enormous size of the ocean at that time, we admittedly have only a very partial view of Jurassic oceanic paleoenvironments. Nevertheless, we have broken entirely new ground at this site, which will certainly represent a reference for the Mesozoic history of the Pacific and of the world ocean. The site has been continuously cored to the basement. Unfortunately, core recovery was rather poor in most of the pelagic sediments, because of the abundance of chert interlayered in relatively soft claystones. On the other hand, despite technical mishaps that made operations quite acrobatic toward the end of the leg, we achieved substantial penetration (131 m) into the oldest *in-situ* oceanic crust of the world and were blessed with good basement recovery and particularly interesting discoveries.

Site 801 lies in the Jurassic quiet zone, almost 150 nmi southeast of the oldest magnetic anomaly ever recognized in an ocean basin (M37). The age of the crust falls almost exactly on the predictive plot derived from a simple linear extrapolation of the ages of the M-series (See Fig. 3). This finding provides indisputable proof that the quiet zone is indeed of Jurassic age, and that it is not the result of subsequent erasure of magnetic anomalies by middle Cretaceous volcanic events. Despite the fact that this site was not located on a magnetic lineation, this finding also indirectly confirms the Late Jurassic age of the sequence of magnetic anomalies from M17 through M37. This confirmation is of extreme importance because the "type locality" of the M-series magnetic reversal stratigraphy is the western Pacific, although the oldest well-

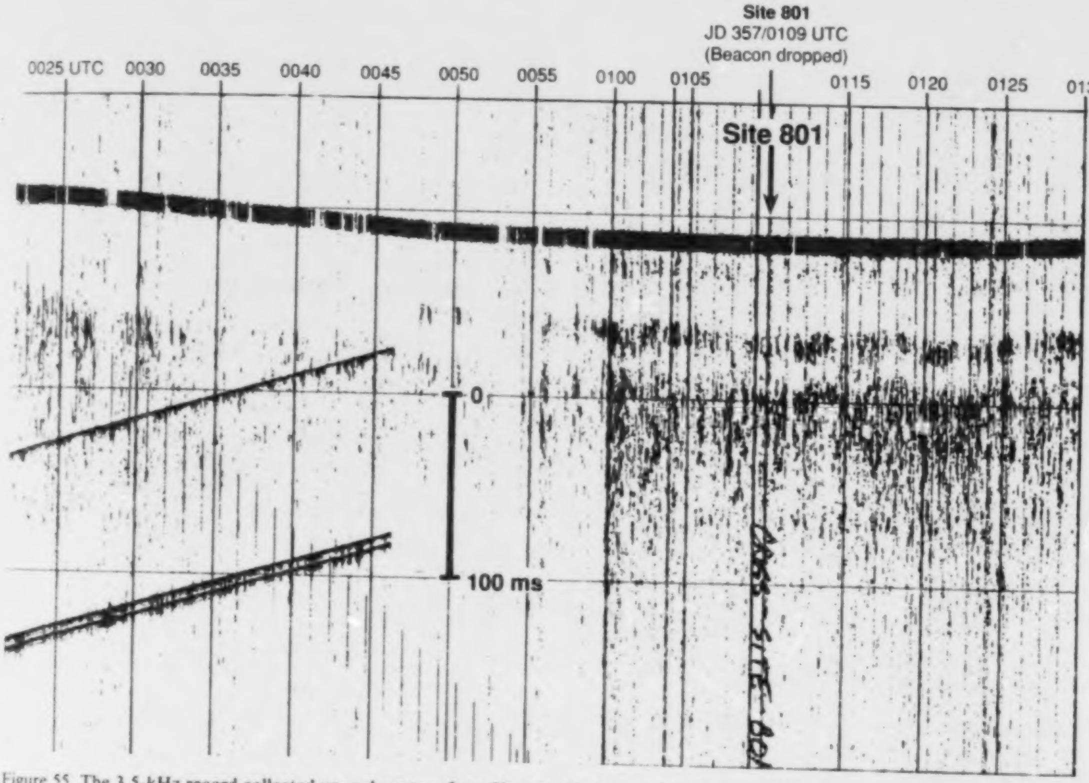

Figure 55. The 3.5-kHz record collected upon departure from Site 801. Horizontal lines represent 100-ms intervals. Acoustic basement on this record marks the top of the first chert and indicates 79 ms of pelagic clay. A weak intermittent reflection is also visible at 53 mbsf. The 53-m thickness for the pelagic interval overlying the first chert is derived from the drillers' determination of the mud line to the depth of the first impenetrable interval encountered during jet-in tests. A thickness of 53 m over 79 ms results in an unreasonable interval velocity of 1.34 km/s. During camera-guided re-entry operations at Site 801, depth to mud line was observed to be 8 m shallower, making the actual thickness of pelagic clay 61 m, which results in a more reasonable interval velocity of 1.544 km/s. The thickness of the pelagic clay layer measured from jet-in tests at Site 800 was probably also underestimated by 10 m (see "Site Geophysics and Seismic Stratigraphy" section, "Site 800" chapter, this volume).

dated magnetic lineation in this area is M9 on the Japanese sequence, dated as Hauterivian at DSDP Site 304. The seismic profiles from the recent MCS surveys provided excellent continuity between Sites 800 and 801, and we anticipated a sediment section roughly similar at both sites except for the lowermost levels. The acoustic basement in particular was inviting as a target when compared to that of Site 800. It presented all the characteristics of oceanic crust and certainly appeared to be the best possible prospect, together with Site 802 farther to the southwest in the Mariana Basin.

### The Jurassic Crust

A total of 131 m of igneous basement section was penetrated at Holes 801B and 801C, and a 20-m overlap is included at the bottom of Hole 801B and top of Hole 801C. Most of this section consists of interlayering lava flows of varying thicknesses and pillow basalts. The pillow basalts exhibit chilled margins, variolitic textures, and microcrystalline interiors. There is a minor amount of baked and silicified claystone near the top of the section, and a 3-m-thick sill is present at 510 mbsf. There is little doubt on the basis of its physical appearance that this igneous section consists of basalts extruded under submarine conditions. Because it underlies sediments dated as Callovian-Bathonian in age, it is at least Middle Jurassic in age.

A total of 40 physical units were recovered from the complete crustal section, including the overlap. Most of this material is extrusive flow units varying from 0.2 to 7 m in thickness. These flows are mainly composed of aphyric basalts, although a significant fraction of moderately olivine/plagioclase, microphyric/phyric basalt is present. A few of the flows have an aphyric, microdoleritic texture.

There is a remarkable hydrothermal deposit included in the basement section at 520 to 530 mbsf. It is chrome yellow and consists of iron oxides/hydroxides that are well cemented, and largely replaced, by silica. It is directly underlain by highly altered pillow basalts, apparently the result of hydrothermal solutions percolating up through the basement section that deposited the hydrothermal concretion. Obvious cracks and fissures are present which acted as conduits for part of this circulation system.

It is likely that this entire hydrothermal system was buried beneath the uppermost basalt flows soon after its deposition, which allowed its preservation. Beneath these altered basalts, the flows become markedly fresher and are often characterized by vesicles up to 1.5 cm in diameter. Although such

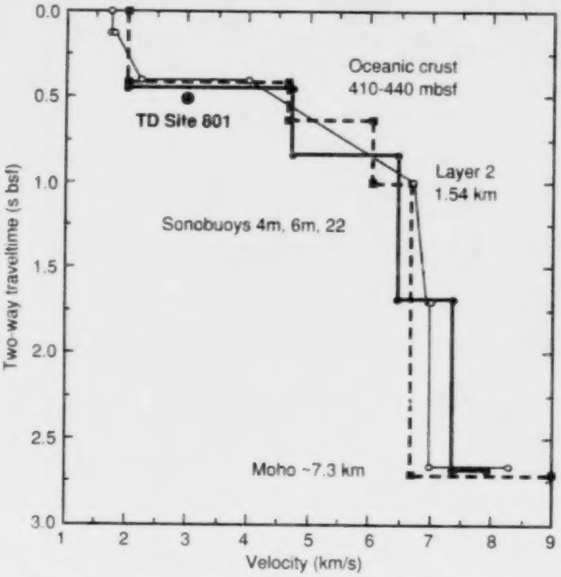

Figure 56. Velocity vs. two-way traveltime below seafloor (bsf) from sonobuoy data collected during FM35-12 and MESOPAC II. The onset of velocities and velocity gradients characteristic of oceanic crust at approximately 410 to 440 mbsf corresponds to the reflection imaged at approximately 8.0 s twt in Figures 52, 53, and 54.

vesicles are not unknown from modern ridge crests, they are less common than at Hole 801C, possibly indicating an anomalously shallow ridge-crest depth.

Radiometric dating of this basement sequence will be of great interest from two independent points of view. First, there is the question of a possible age progression that could be recognized from bottom to top which would yield insight into the history of the hydrothermal system and its subsequent burial. Second, the youngest radiometrically dated rocks with an extrusive character can be considered as contemporaneous with the overlying Callovian-Bathonian sediments, and thus will provide valuable, absolute calibration for that part of geological time, as well as for the magnetic reversal time scale. This calibration is especially critical because (1) it provides the oldest point that can be dated on a marine magnetic anomaly reversal sequence and (2) the Middle Jurassic is heretofore the most poorly calibrated part of the last 200 m.y. of geologic time.

We also note that Hole 801C is cased through the entire sediment section and cemented into basement. Through a combination of luck and persistence, it is free of any drilling junk in the hole. Thus, a golden opportunity exists for future expeditions to deepen this hole into the oldest crustal section in the world's ocean basins and subsequently to conduct logging and downhole measurements that were not accomplished during this expedition.

### Early History of the Pacific

Data from Site 801 pertain only to a rather small, low-latitude area of the Mesozoic Pacific, at least with respect to the Jurassic. Cores from Holes 801A and 801B sampled only deep-water facies, so that our view of the early evolution of the Pacific plate remains limited.

The earliest sediments found just on top of the Jurassic crust are reddish brown radiolarites interbedded with claystones in a more or less rhythmic fashion. This facies is reminiscent of the radiolarites of the Tethys and circum-Pacific regions, even if actual "ribbon radiolarites" are not present. These sediments indicate relatively high productivity that may be associated with the proximity of the site to the equatorial zone. Rates of accumulation, however, remained rather low until the latest Jurassic-earliest Cretaceous, when a peak in biogenic silica is well documented both in the cores and in the geochemical logs. It is too early to determine with confidence whether the variations in the abundance of radiolarians or chert in the sediments directly reflect the transit of the site across the equatorial zone or whether they correspond with fluctuations in the productivity of the surface waters. In any case the conditions of sedimentation for the Late Jurassic and early Neocomian times reflect a deep-water environment characterized by a relatively elevated CCD and a moderate style of bottom-water circulation, nevertheless sufficient to maintain permanent oxidizing conditions. The absence of carbonates in the sediments found directly above the ridge crest basalts, presumed to have erupted in water depths averaging 2800 m, seems to be better explained by reduced production of calcareous plankton in the surface waters than by accelerated dissolution on the seafloor.

### Paleolatitudes and Plate Motion

Paleomagnetic measurements performed on the sediments aboard the ship provide a preliminary estimate of the successive paleolatitudes occupied by Site 801 that confirms the trends already observed at Site 800. The distribution of various sediment facies in time shows a relatively good agreement with the paleomagnetic determination. The combination of the two data sets helps to explain the relative variations in the abundance of biogenic silica in the sediments. In particular, results from this site document again the latitudinal reversal in plate motion that seems to have occurred sometime between the Valanginian and the Aptian. Prior to the Valanginian, Site 801 may have been close to the equator for most of its early history, although paleomagnetic data are too preliminary to determine if the site actually formed in the Northern Hemisphere during the Middle Jurassic. The youngest equatorial crossing seems to have occurred during the Campanian according to the paleomagnetic data, although they show some dispersion for that interval. The sediment record, which shows a predominance of chert from the Turonian through at least the Campanian, appears to agree well with this estimate.

### Middle Cretaceous Volcanic Events

A pulse of volcanic activity was recorded at Site 801. This pulse was characterized by massive redeposition of volcanogenic material shed from the slopes of seamounts when they nearly reached the surface of the sea. These active volcanos were probably the major seamounts lying less than 100 nmi north and south of Site 801. The beginning of the volcanic pulse is not accurately dated because the lowermost redeposited beds are barren of age-diagnostic microfossils. These beds may be of Aptian age because they lack magnetic reversals, but a more precise determination will require more shore-based work. Variations in the volume of the redeposited volcaniclastics suggest that there were several pulses of volcanic activity. The major one seems to have occurred during the Albian and is recorded by a turbidite sequence over 4 m thick and by possible debris flows that confer a proximal character to most of this interval. Fragments of shallow-water fossils (red algae and echinoderms) confirm that the nearby seamounts had reached very near the surface by the late Albian.

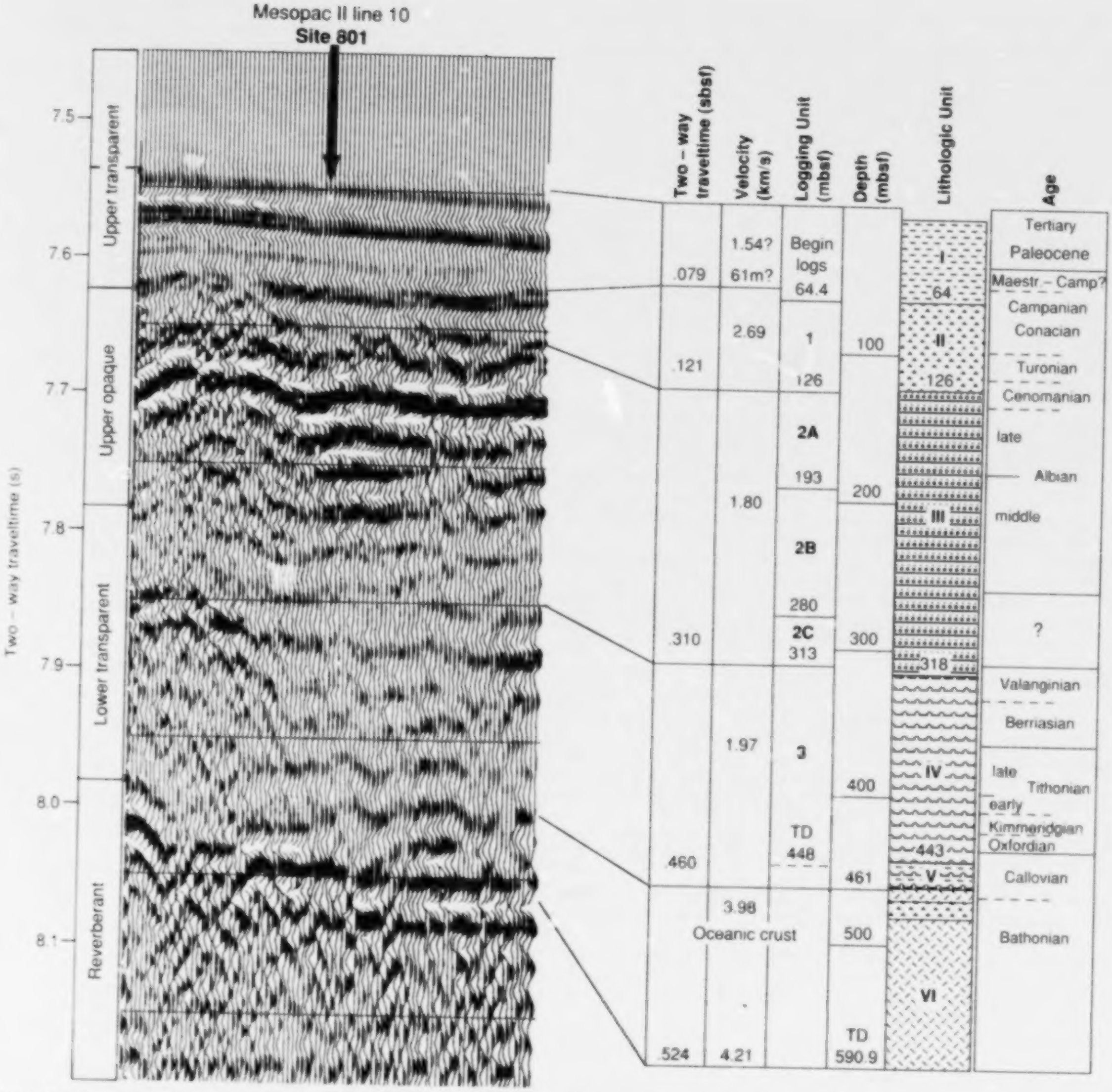

Figure 57. Summary of seismic stratigraphy at Site 801 showing correlations with logging units, lithologic units, ages, and depths. These correlations were made without the constraints provided by a log-generated seismogram, and should be considered only as a best estimate. The crustal velocities given are based on traveltime modeling of sonobuoy data. The 2.69 km/s velocity is based on the interval between 56.4 and 118 mbsf. See Figure 55 for an explanation of 1.54-km/s pelagic-clay velocity. This SCS water-gun record is displayed with a vertical exaggeration of ~33× at 1.5 km/s with the same parameters as described in the caption for Figure 52.

Volcanic activity lasted throughout the Albian and apparently ended sometime during the Cenomanian. Thus, the record from Sites 800 and 801 indicates that most of the seamounts surrounding the Pigafetta Basin may have been built during the middle Cretaceous. The relation between edifice-building and deep-basin sill-intrusion processes remains a mystery, however, and the original Jurassic crust may be generally covered with Cretaceous intrusives. In retrospect, we may have found at Site 801 one of the very rare "windows" allowing us a peek into the well-defended Jurassic.

## REFERENCES

Abrams, L. J., Larson, R. L., Shipley, T., and Lancelot, Y., 1988. Cretaceous volcanic sequences and Jurassic(?) crust in the western Pacific. *Trans. Am. Geophys. Union*, 69:1442.

Adachi, M., Koshi, Y., and Ryuichi, S., 1986. Hydrothermal chert and associated siliceous rocks from the northern Pacific: their geological significance as an indication of ocean ridge activity. *Sediment. Geol.*, 47:125–148.

Anderson, R. N., Honnorez, J., Becker, K., et al., 1985. *Init. Repts. DSDP*, 83: Washington (U.S. Govt. Printing Office).

Baumgartner, P. O., 1987. Age and genesis of Tethyan radiolarites. *Eclogae Geol. Helv.*, 80:831–879.

Bernoulli, D., 1972. North Atlantic and Mediterranean Mesozoic facies: a comparison. *In* Hollister, C. D., Ewing, J. I., et al., *Init. Repts. DSDP*, 11: Washington (U.S. Govt. Printing Office), 801–871.

Bonatti, E., 1981. Metal deposits in the oceanic lithosphere. *In* Emiliani, C. (Ed.), *The Sea* (Vol. 7): New York (Wiley), 639–686.

Borehole Research Group, 1988. *Ocean Drilling Program Wireline Logging Manual:* New York (Lamont-Doherty Geological Observatory, Columbia Univ.).

Boström, K., and Peterson, M.N.A., 1965. Precipitates from hydrothermal exhalations on the East Pacific Rise. *Econ. Geol.*, 61:1258–1265.

Bralower, T. J., Monechi, S., and Thierstein, H. R., 1989. Calcareous nannofossil zonation of the Jurassic-Cretaceous boundary interval and correlation with the geomagnetic polarity timescale. *Mar. Micropaleontol.*, 14:153–235.

Caron, M., 1985. Cretaceous planktonic foraminifera. *In* Bolli, H. M., Saunders, J. B., and Perch-Nielsen, K. (Eds.), *Plankton Stratigraphy:* Cambridge (Cambridge Univ. Press), 17–86.

Cotillon, P., 1984. Tentative world-wide correlation of Early Cretaceous strata by limestone-marl cyclicities in pelagic deposits. *Bull. Geol. Soc. Den.*, 33:91–102

Cotillon, P., 1985. Les variations à différentes échelles du taux d'accumulation sédimentaire dans les séries pélagiques alternantes du Crétacé inférieur, conséquences de phénomènes globaux. Essai d'évaluation. *Bull. Soc. Géol. Fr.*, Ser. 8, 1:59–68.

Deer, W. A., Howie, R. A., and Zussman, J., 1978. *An Introduction to the Rock Forming Minerals:* New York (Longman Group).

Erba, E., 1987. I Nannofossili calcarei nell'Aptiano-Albiano (Cretacico inferiore): biostratigrafia, paleoceanografia e diagenesi degli Scisti a Fucoidi del pozzo Piobbico (Marche) [Ph.D. dissert.], Univ. of Milan.

Ewing, J., Ewing, M., Aitken, T., and Ludwig, W. J., 1968. North Pacific sediment layers measured by seismic profiling. *In* Drake, C. L., and Hart, P. J. (Eds.), *The Crust and Upper Mantle of the Pacific Area*. Am. Geophys. Union. Monogr., 12:147–173.

Garrison, E. D., 1974. Radiolarian cherts, pelagic limestones and igneous rocks in eugeosynclinal assemblages. *In* Hsü, K. J., and Jenkyns, H. C. (Eds.), *Pelagic Sediments on Land and Under the Sea*. Spec. Publ. Int. Assoc. Sedimentol., 1:367–399.

Gieskes, J. M., and Johnson, J., 1981. Interstitial water studies, Leg 58. *In* Larson, R. L., and Schlanger, S. O., *Init. Repts. DSDP*, 61: Washington (U.S. Govt. Printing Office), 607–611.

Gradstein, F. M., Kaminski, M. A., and Berggren, W. A., 1988. Cenozoic foraminiferal biostratigraphy of the Central North Sea. *Abh. Geol. Bundensanst. Austria.*, 41:97–108.

Gradstein, F. M., and Sheridan, R. E., 1983. On the Jurassic Atlantic Ocean and a synthesis of results of DSDP Leg 76. *In* Gradstein, F. M., and Sheridan, R. E., *Init. Repts. DSDP*, 76: Washington (U.S. Govt. Printing Office), 913–943.

Handschumacher, D. W., and Gettrust, J. F., 1985. Mixed polarity model for the Jurassic "Quiet Zones": new oceanic evidence of frequent pre-M25 reversals. *Eos*, 66:867.

Handschumacher, D. W., Sager, W. W., Hilde, T.W.C., and Bracey, D. R., 1988. Pre-Cretaceous tectonic evolution of the Pacific Plate and extension of the geomagnetic polarity reversal time scale with implications for the origin of the Jurassic "Quiet Zone." *Tectonophysics*, 155:365–380.

Harland, W. B., Cox, A. V., Llewellyn, P. G., Pickton, C.A.G., Smith, D. G., and Walters, R., 1982. *A Geologic Time Scale:* Cambridge (Cambridge Univ. Press).

Heezen, B. C., MacGregor, I. D., and DSDP Leg 20 Scientific Party, 1973. Mesozoic chalks beneath the Caroline abyssal plain: DSDP Site 199. *In* Heezen, B. C., MacGregor, I. D., et al., *Init. Repts. DSDP*, 20: Washington (U.S. Govt Printing Office), 65–85.

Helsley, C. E., and Steiner, M. D., 1969. Evidence for long intervals of normal polarity during the Cretaceous period. *Earth Planet. Sci. Lett.*, 5:325–332.

Hemleben, C., and Troester, J., 1984. Campanian-Maestrichtian deep-water foraminifers from Hole 534A, Deep Sea Drilling Project. *In* Biju-Duval, B., Moore, J. C., et al., *Init. Repts. DSDP*, 78A: Washington (U.S. Govt. Printing Office), 509–532.

Houtz, R. E., J. Ewing, and P. Buhl, 1970. Seismic data from sonobuoy stations in the northern and equatorial Pacific, *J. Geophys. Res.*, 75:5093–5111.

Houtz, R. E., and Ludwig, W. J., 1979. Distribution of reverberant subbottom layers in the southwest Pacific basin. *J. Geophys. Res.*, 84:3497–3505.

Hutchinson, D. R., and Detrick, R. S., 1984. Water gun vs. air gun: a comparison. *Mar. Geophys. Res.*, 6:295–310.

Irving, E., and Pullaiah, G., 1976. Reversal of the geomagnetic field, magnetostratigraphy and relative magnitude of palaeosecular variation in the Phanerozoic. *Earth-Sci. Rev.*, 12:35–64.

Karpoff, A. M., 1989. Les faciès pélagiques condensés cénozoiques des océans Pacifique et Atlantique. témoins des grandes crises géodynamiques [Thèse Doc. ès Sci.], Univ. Louis Pasteur, Strasbourg.

Karpoff, A. M., Walter, A. V., and Pflumio, C., 1988. Mettaliferous sediments within lava sequences of the Sumail ophiolite (Oman): mineralogical and geochemical characterization, origin and evolution. *Tectonophysics*, 151:223–245.

Kent, D. V., and Gradstein, F. M., 1985. A Cretaceous and Jurassic geochronology. *Geol. Soc. Am. Bull.*, 96:1419–1427.

________, 1986. A Jurassic to Recent chronology. *In* Tucholke, B. E., and Vogt, P. R. (Eds.), *The Geology of North America: The Western Atlantic Region*. Geol. Soc. Am. DNAG Ser., 1:45–50.

Kono, M., 1980. Statistics of paleomagnetic inclination data. *J. Geophys. Res.*, 85:3878–3882.

Lancelot, Y., 1973. Chert and silica diagenesis in sediments from the central Pacific. *In* Winterer, E. L., Ewing, J. I., et al. *Init. Repts. DSDP*, 17: Washington (U.S. Govt. Printing Office), 377–405.

________, 1978. Relation entre évolutions sédimentaire et tectonique de la plaque Pacifique depuis le Crétacé inférieur. *Mem. Soc. Geol. Fr.*, Nelle Ser., 134.

Lancelot, Y., Hathaway, J. C., and Hollister, C. D., 1972. Lithology of sediments from the western from the western North Atlantic. *In* Hollister, C. D., Ewing, J. I., et al., *Init. Repts. DSDP*, 11: Washington (U.S. Govt. Printing Office): 901–949.

Lancelot, Y., and Larson, R. L., 1975. Sedimentary and tectonic evolution of the northwestern Pacific. *In* Larson, R. L., Moberly, R., et al., *Init. Repts. DSDP*, 32: Washington (U.S. Govt. Printing Office), 925–939.

Larson, R. L., and Hilde, T.W.C., 1975. A revised time scale of magnetic reversals for the Early Cretaceous and Late Jurassic. *J. Geophys. Res.*, 80:2586–2594.

Larson, R. L., and Lowrie, W., 1975. Paleomagnetic evidence for motion of the Pacific plate from Leg 32 basalts and magnetic anomalies. *In* Larson, R. L., Moberly, R., et al., *Init. Repts. DSDP*, 32: Washington (U.S. Govt. Printing Office), 571–577.

Larson, R. L., Schlanger, S. O., et al., 1981. *Init. Repts. DSDP*, 61: Washington (U.S. Govt. Printing Office).

Lynn, D. C., and Bonatti, E., 1965. Mobility of manganese in diagenesis of deep-sea sediments. *Mar. Geol.* 3:457–474.

Martini, E., 1971. Standard Tertiary and Quaternary calcareous nannoplankton zonation. *In* Farinacci, A. (Ed.), *Proc. 2nd Planktonic Conf. Roma:* Rome (Ed. Technosci.), 2:739–785.

Matsuoka, A., and Yao, S., 1986. A newly proposed radiolarian zonation for the Jurassic of Japan. *Mar. Micropaleontol.*, 11:91–105.

McCave, I. N., 1979. Depositional features of organic-carbon-rich black and green mudstones at DSDP Sites 386 and 387, western North Atlantic. *In* Tucholke, B. E., Vogt, P. R., et al., *Init. Repts. DSDP*, 43: Washington (U.S. Govt. Printing Office): 411–416.

Morkhoven, F.P.C.M. van, Berggren, W. A., and Edwards, A. S., 1986. Cenozoic cosmopolitan deep-water benthic foraminifera. *Mem. Cent. Rech. Explor. Prod. Elf Aquitaine*, 11:1–421.

Moullade, M., Kuhnt, W., and Thurow, J., 1988. Agglutinated benthic foraminfers from Upper Cretaceous vareigated clays of the North Atlantic Ocean (DSDP Leg 93 and ODP Leg 103). *In* Boillot, G., Winterer, E. L., et al., *Proc. ODP, Sci. Results*, 103: College Station, TX (Ocean Drilling Program), 349–377.

Ogg, J. G., Robertson, A.H.F., and Jansa, L. F., 1983. Jurassic sedimentation history of Site 534 (western North Atlantic) and the Atlantic-Tethys seaway. *In* Sheridan, R. E., Gradstein, F. M., et al., *Init. Repts. DSDP*, 76: Washington (U.S. Govt. Printing Office), 829–884.

Perch-Nielsen, K., 1985. Mesozoic calcareous nannofossils. *In* Bolli, H., Saunders, J. B., and Perch-Nielsen, K. (Eds.), *Plankton Stratigraphy:* Cambridge (Cambridge Univ. Press), 329–426.

Premoli-Silva, I., Erba, E., and Tornaghi, M. E., 1989. Paleoenvironmental signals and changes in surface fertility in mid-Cretaceous $C_{org}$-rich pelagic facies of the Fucoid Marls (central Italy). *Geobios,* 11:225–236.

Roth, P. H., 1978. Cretaceous nannoplankton biostratigraphy and oceanography of the northwestern Atlantic Ocean. *In* Benson, W. E., Sheridan, R. E., et al., *Init. Repts. DSDP,* 44: Washington (U.S. Govt. Printing Office), 731–759.

Roth, P. H., and Krumbach, K. R., 1986. Middle Cretaceous calcareous nannofossil biogeography and preservation in the Atlantic and Indian Oceans: implications for paleoceanography. *Mar. Micropaleont.* 10:235–266.

Sanfilippo, A., and Riedel, W. R., 1985. Cretaceous radiolaria. *In* Bolli, H. M., Saunders, J. B., and Perch-Nielsen, K. (Eds.), *Plankton Stratigraphy:* Cambridge (Cambridge Univ. Press), 573–630.

Shipboard Scientific Party, 1973. Site 167. *In* Winterer, E. L., Ewing, J. I., et al., *Init. Repts. DSDP,* 17: Washington (U.S. Govt. Printing Office), 145–234.

Shipboard Scientific Party, 1976. Site 319. *In* Yeats, R. S., Hart, S. R., et al., *Init. Repts. DSDP,* 34: Washington (U.S. Govt. Printing Office), 19–80.

Shipley, T. H., Whitman, J. M., Dunnebier, F. K., and Peterson, L. D., 1983. Seismic strtigraphy and sedimentation history of the East Mariana Basin, Western Pacific. *Earth Planet. Sci. Lett.,* 64:257–275.

Sissingh, W., 1977. Biostratigraphy of Cretaceous calcareous nannoplankton. *Geol. Mijnbouw,* 56:37–65.

Tamaki K., Nakanishi, M., Sayanagi, K., and Kobayashi, K., 1987. Jurassic magnatic anomaly lineations of the western Pacific Ocean and the origin of the Pacific plate. *Eos,* 68:1493.

Thierstein, H. R., 1971. Tentative Lower Cretaceous nannoplankton zonation. *Eclogae Geol. Helv.,* 64:459–488.

———, 1973. Lower Cretaceous calcareous nannoplankton biostratigraphy. *Abh. Geol. Bundesanst. Austria,* 29:1–52.

———, 1976. Mesozoic calcareous nannoplankton biostratigraphy of marine sediments. *Mar. Micropaleontol.,* 1:325–362.

Tsunogai, S., and Kusakabe, M., 1982. Migration of manganese in the deep-sea sediments. *In* Fanning, K. A., and Manheim, F. T. (Eds.), *The Dynamic Environment of the Ocean Floor:* Lexington, MA (Lexington Books), 257–273.

Wise, S. W., and Wind, F. H., 1977. Mesozoic and Cenozoic calcareous nannofossils recovered by Deep Sea Drilling Project Leg 36 drilling on the Falkland Plateau, Southwest Atlantic sector of the Southern Ocean. *In* Barker, P., Dalziel, I.W.D., et al., *Init. Repts. DSDP,* 36: Washington (U.S. Govt. Printing Office), 269–491.

Zotto, M., Drugg, W. S., and Habib, D., 1987. Kimmeridgian dinoflagellate stratigraphy in the Southwestern North Atlantic. *Micropaleontology,* 33:193–213.

**Ms 129A-103**

**NOTE: All core description forms (''barrel sheets'') and core photographs have been printed on coated paper and bound as Section 3, near the back of the book, beginning on page 247.**

## Hole 801B: Density-Caliper-Gamma Ray Log Summary

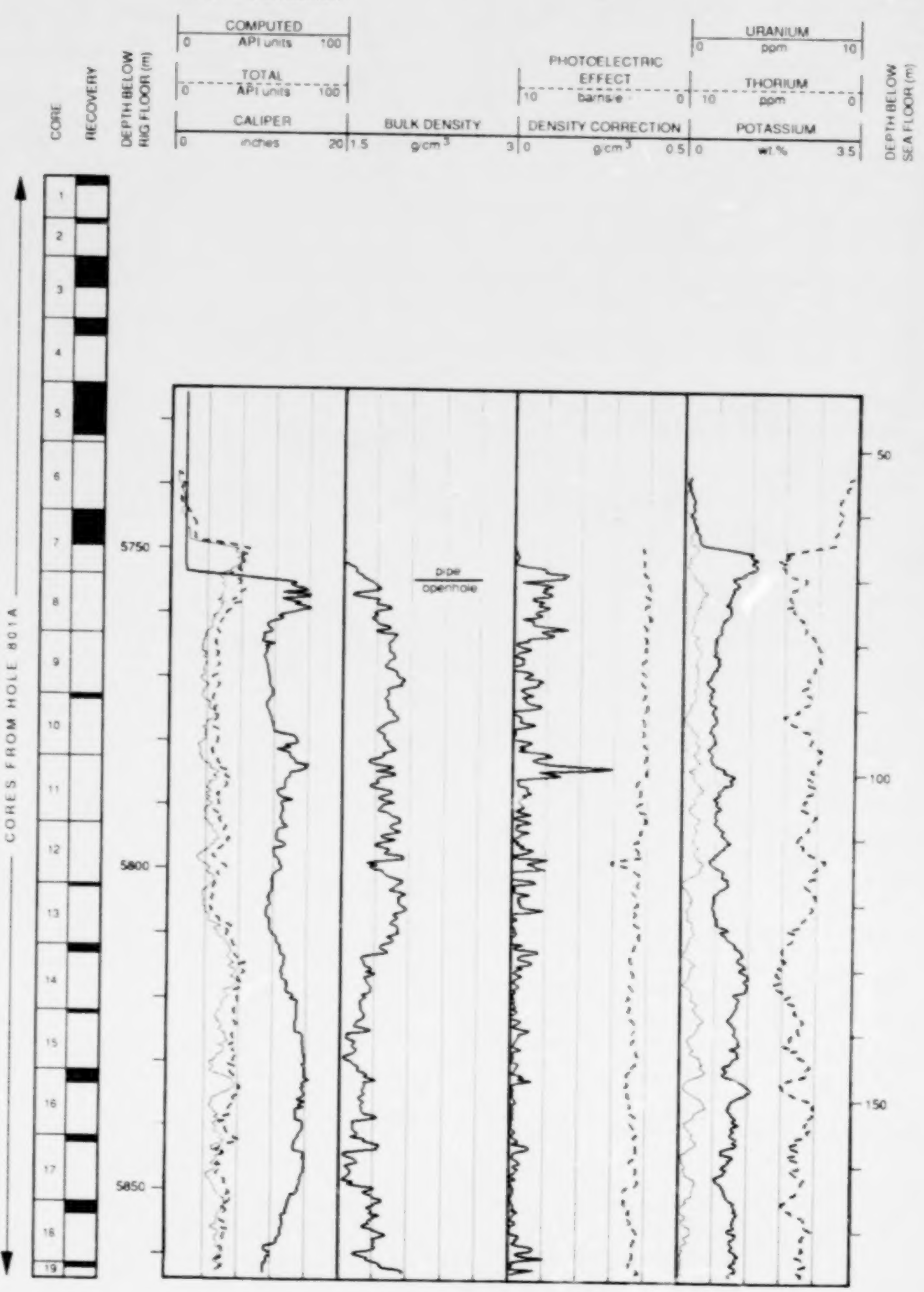

## Hole 801B: Density-Caliper-Gamma Ray Log Summary (continued)

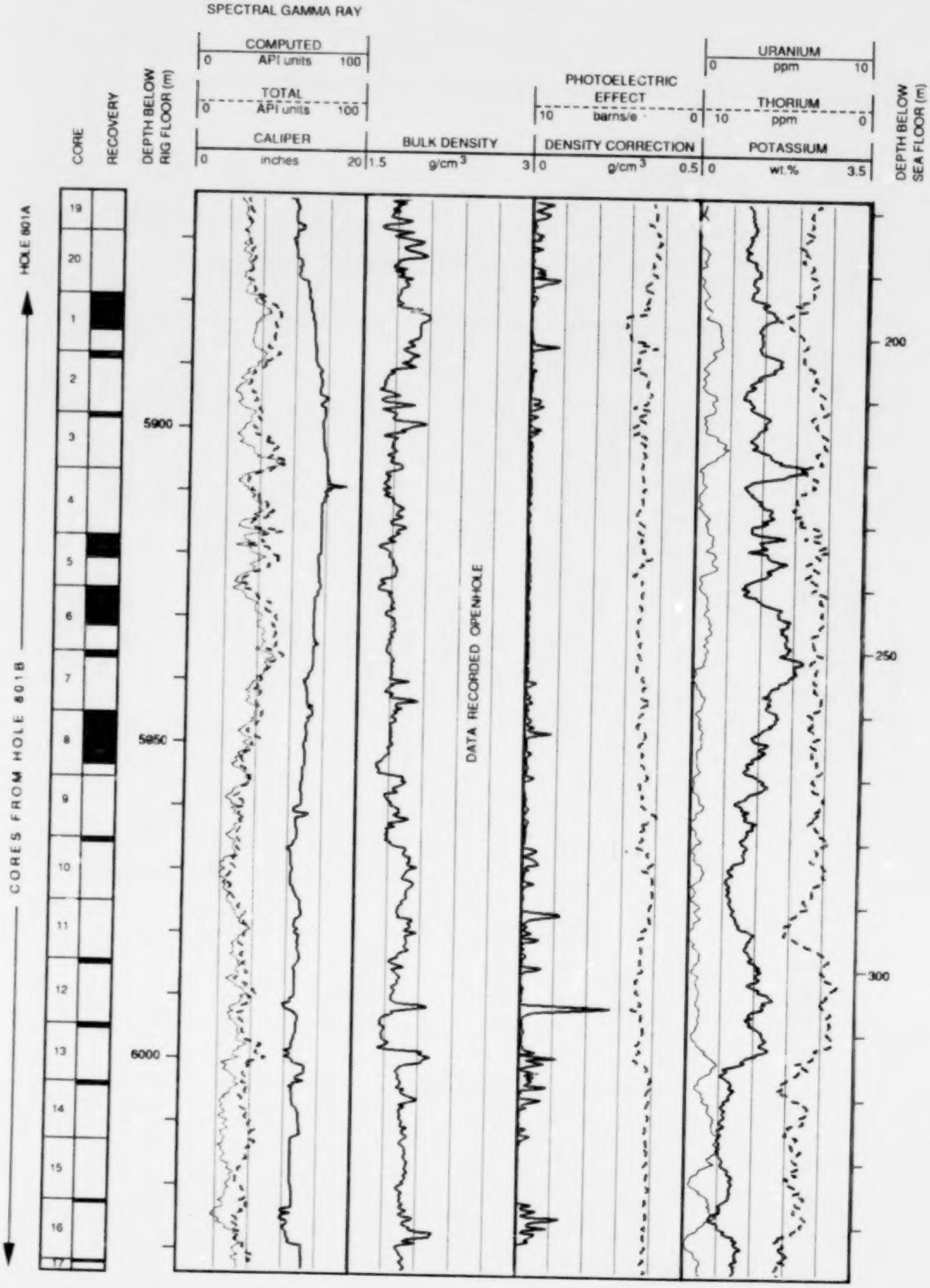

Hole 801B: Density-Caliper-Gamma Ray Log Summary (continued)

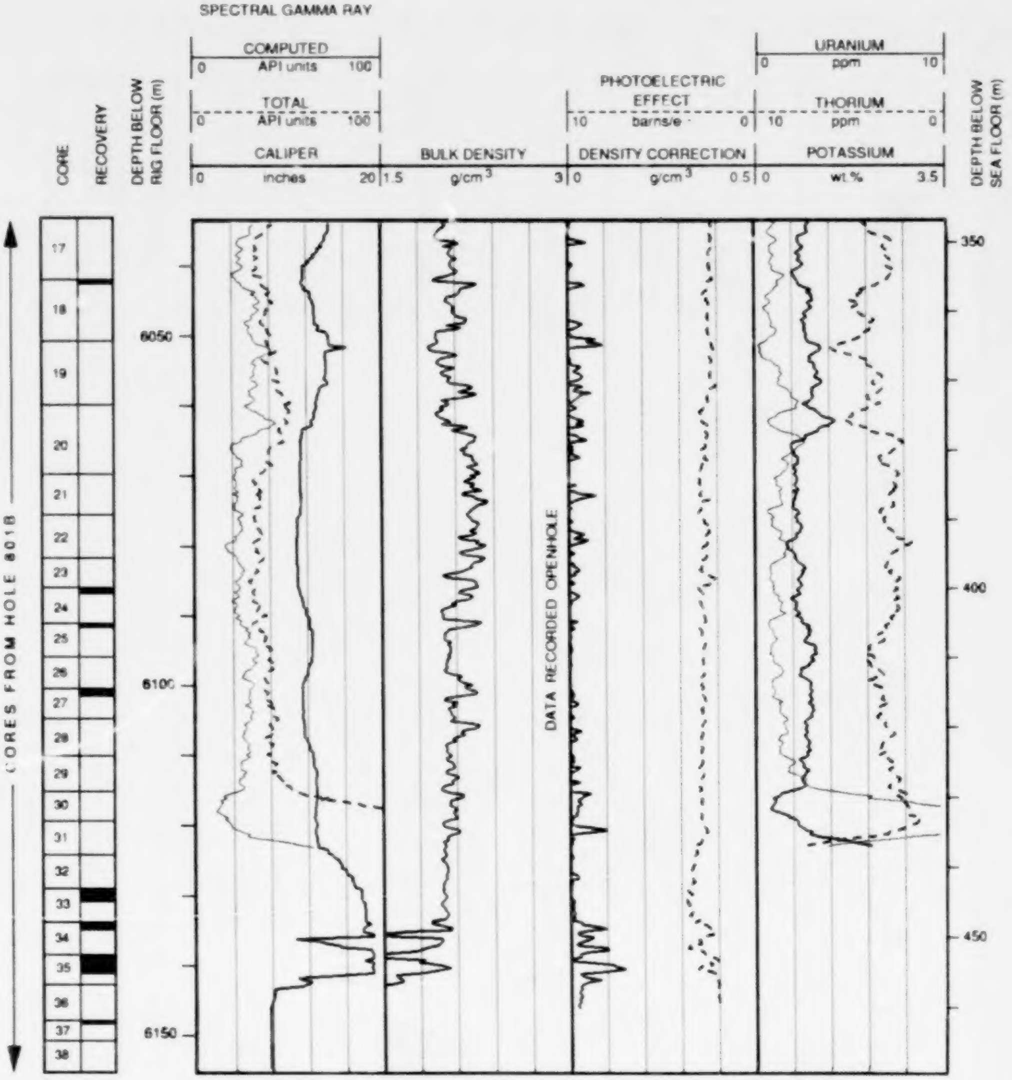

# Hole 801B: Geochemical Log Summary

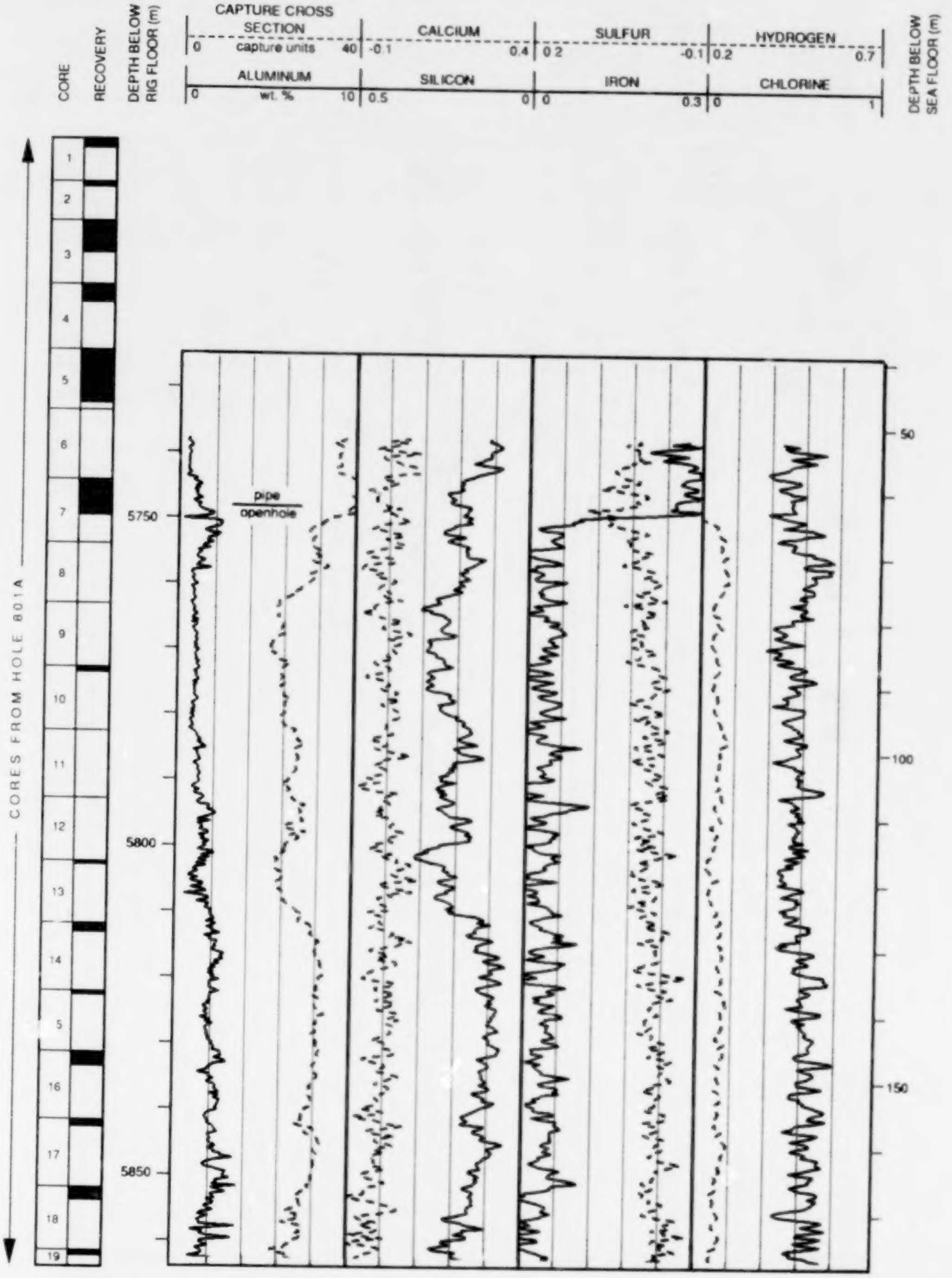

## Hole 801B: Geochemical Log Summary (continued)

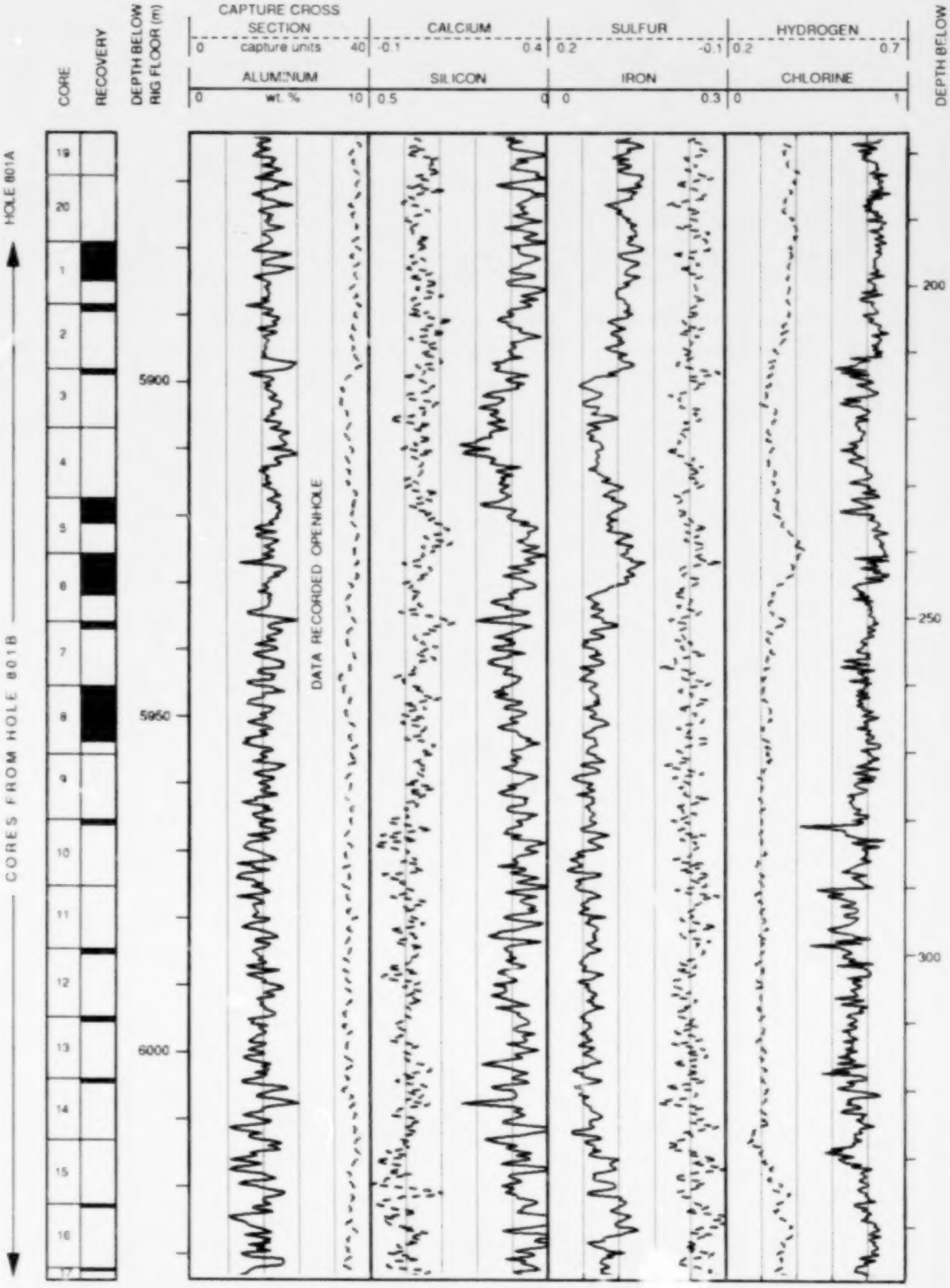

Hole 801B: Geochemical Log Summary (continued)

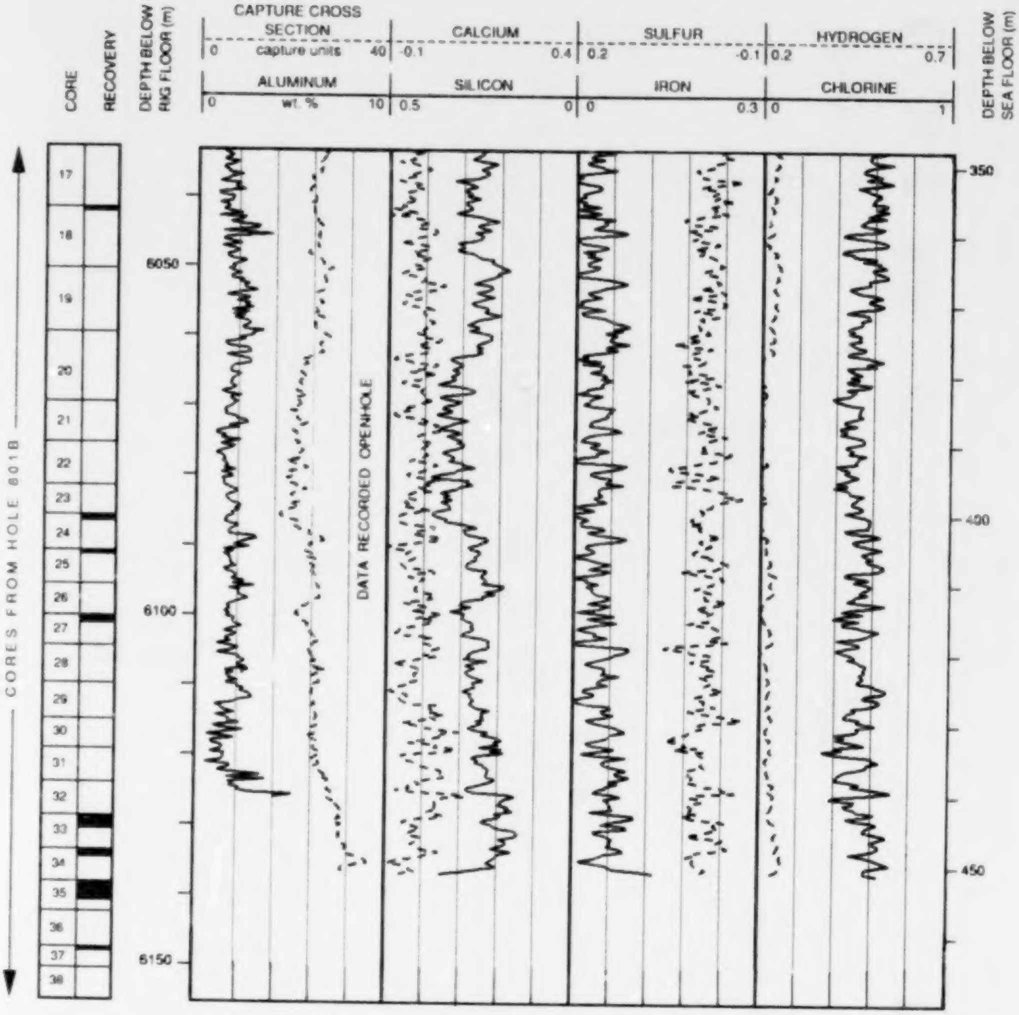

## Hole 801B: Resistivity-Sonic-Gamma Ray Log Summary

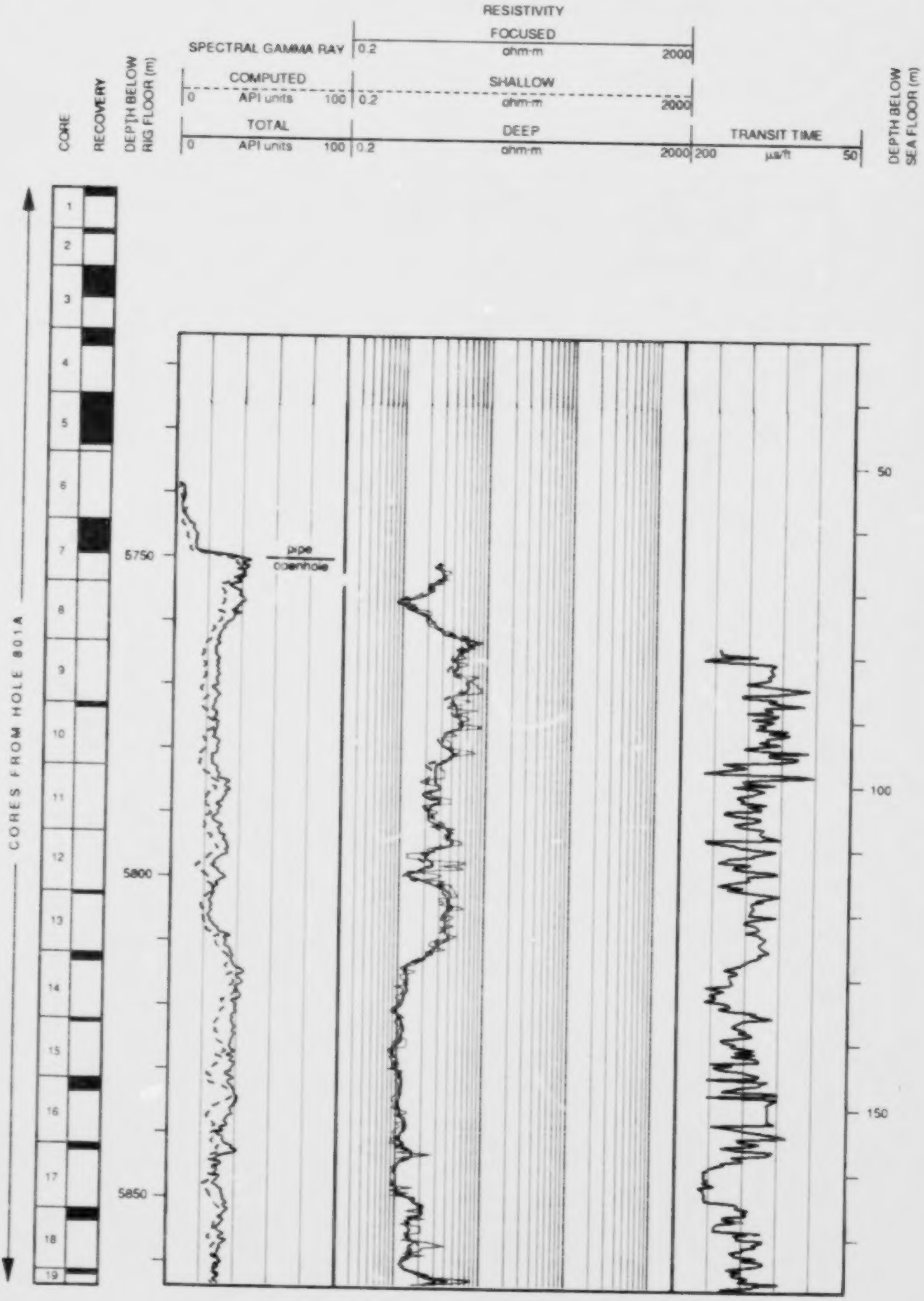

Hole 801B: Resistivity-Sonic-Gamma Ray Log Summary (continued)

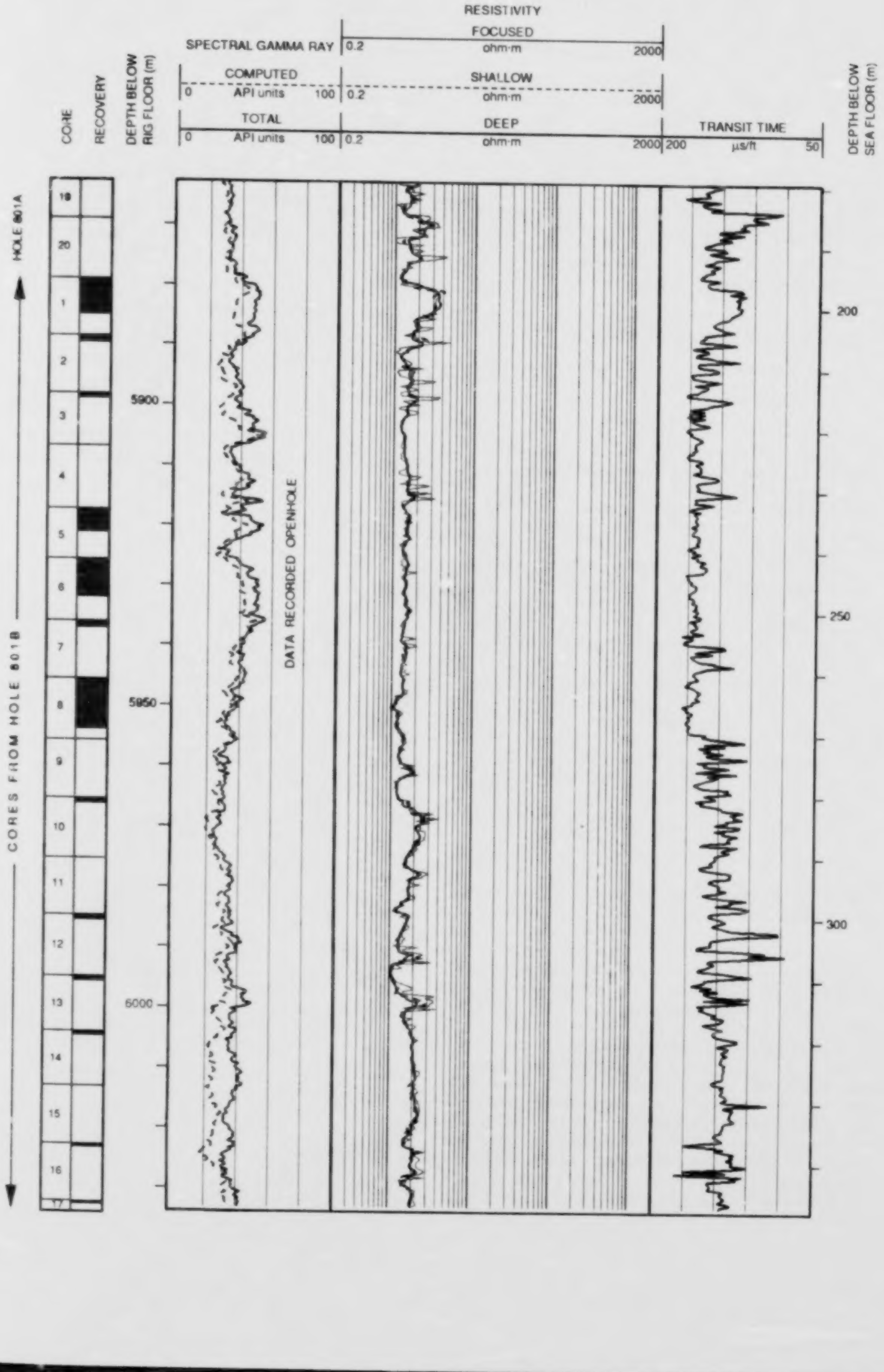

Hole 801B: Resistivity-Sonic-Gamma Ray Log Summary (continued)

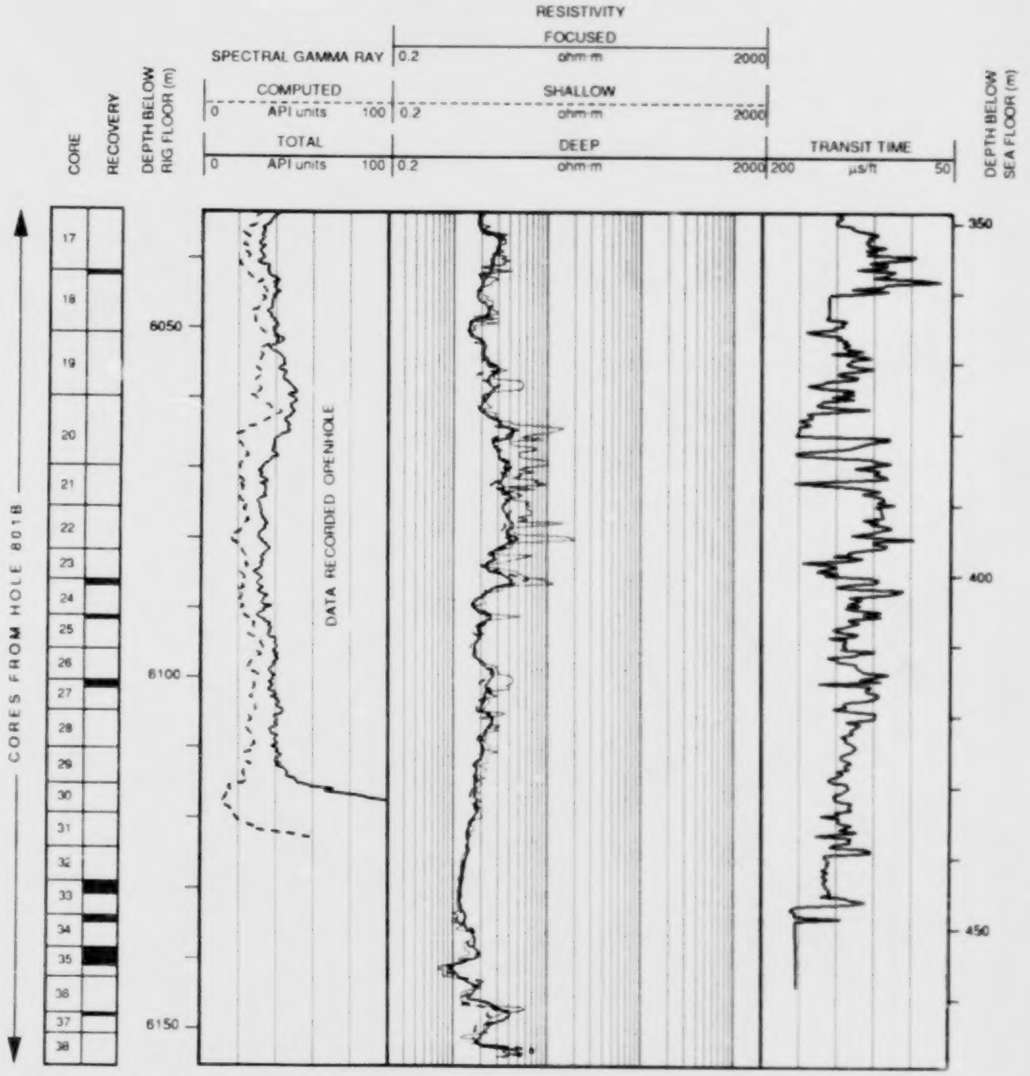

Lancelot, Y., Larson, R. L., et al., 1990
*Proceedings of the Ocean Drilling Program, Initial Reports*, Vol. 129

# 4. SITE 802[1]

Shipboard Scientific Party[2]

## HOLE 802A

**Date occupied:** 25 December 1989

**Date departed:** 4 January 1990

**Time on hole:** 10 days, 13 hr, 45 min

**Position:** 12°5.778′N, 153°,12.6258′E

**Bottom felt (rig floor; m; drill-pipe measurement):** 5980.0

**Distance between rig floor and sea level (m):** 11.40

**Water depth (drill-pipe measurement from sea level; m):** 5968.6

**Total depth (rig floor; m):** 6539.80

**Penetration (m):** 559.80

**Number of cores (including cores with no recovery):** 62

**Total length of cored section (m):** 559.80

**Total core recovered (m):** 165.01

**Core recovery (%):** 29

**Oldest sediment cored:**
  Depth (mbsf): 499.70
  Nature: claystone
  Earliest age: Albian-late Aptian
**Basement:**
  Depth (mbsf): 509.20
  Nature: basalt

**Principal Results:** Site 802 is located in the central Mariana Basin at the southeastern end of a magnetic lineation sequence partially identified to the northwest as M22 to M31, which suggests a Late Jurassic basement age. Extrusive basalt underlies late Aptian-Albian (Lower Cretaceous) claystones, suggesting that the basement age should be revised as younger by 60 m.y. at this location, or that original Jurassic basement, and perhaps a significant sedimentary section, has been covered by subsequent Cretaceous lava flows. The overlying sediment section consists mainly of redeposited material, suggesting massive lateral transport over long distances (>300 km) or unmapped large elevations in the more immediate vicinity. Hole 802A consists of the following stratigraphic sequence.

0–15 mbsf: Neogene brown pelagic clay.

15–159 mbsf: Miocene tuff consisting of well-indurated and well-preserved hyaloclastites and volcaniclastic turbidites, presumably derived from the Caroline Island volcanic chain.

159–254 mbsf: Miocene to Eocene tuff, chalk, claystone, volcaniclastic turbidites, and debris flows, apparently all redeposited.

254–330 mbsf: Upper Paleocene nannofossil chalk.

330–348 mbsf: Maestrichtian zeolitic pelagic claystone.

348–460 mbsf: Campanian volcaniclastic turbidites with clay, claystone, silty claystone, porcellanite, and debris flow, mainly redeposited.

460–509 mbsf: Cenomanian to late Aptian-Albian brown claystone, calcareous claystone, radiolarian limestone, and volcaniclastic turbidites with wood fragments in lowest two cores.

509–560 mbsf: Extrusive basalt, uniformly fine-grained, with multiple cooling units and no included sediment. Sheet flow volcanism with some evidence for pillow basalts is suggested. The chilled zone immediately below the sediment contact suggests that the uppermost basalts were recovered.

Standard logging was conducted on the interval from 110 to 320 mbsf after eliminating a bridge above this level and encountering another at its base. A vertical seismic experiment was attempted to test for seismic horizons deeper than the sampled Cretaceous basalts that might indicate underlying Jurassic strata. The experiment was unsuccessful because the tool became stuck in the hole, requiring the logging cable to be severed and terminating operations at this site. A summary of coring statistics for this site appears in Table 1.

## BACKGROUND AND OBJECTIVES

After reaching Jurassic sediments and oceanic crust in the single-bit pilot Hole 801B, our plan called for setting a reentry cone at Site 801, drilling a new hole, and casing it all the way into the basement in order to achieve substantial penetration into the oceanic crust. The accidental loss of the reentry camera, however, forced us to delay these operations until a replacement camera could be delivered. Thus, we proceeded to Site 802, proposed site EMB-2A, in the central part of the East Mariana Basin (Fig. 1). We had essentially the same general objectives at Site 802 as at the previous two sites; that is, to sample Jurassic sediments and oceanic crust in order to study the early evolution of the Pacific Ocean.

The East Mariana Basin had already been the location of several attempts to reach Jurassic crust. The earliest was DSDP Leg 20, during which Site 199 was drilled in the northwestern part of the basin near the base of the Ita Mai Tai guyot. Penetration at Site 199 was limited to 565 mbsf and only calcareous turbidites of Campanian age were recovered. The second attempt was at Site 585 (DSDP Leg 89), located approximately 50 nautical miles (nmi) east of Site 199. At Site 585, extremely thick middle Cretaceous volcaniclastic turbidites prevented reaching Jurassic material. These were attributed to a major phase of volcanic edifice-building of Aptian through Cenomanian age, and the likely source for the redeposited material has been recognized as the Ita Mai Tai guyot and other seamounts in the immediate vicinity. Recent multichannel seismic surveys showed that Site 585 is actually located in a basement depression, probably associated with a thinned, crustal section in a fracture zone, and that the sediment at the site is abnormally thick.

The same series of magnetic anomalies as in the Pigafetta Basin has been recognized in the northwestern part of the East Mariana Basin (Handschumacher and Gettrust, 1985; Tamaki et al., 1987; Handschumacher et al., 1988) (Fig. 2), although this basin is separated from the former by the Magellan seamounts, possibly associated with a fracture zone. Near the northern extension of the Mariana trench the youngest, well-identified magnetic anomalies on the Pacific plate are M23–M25. Toward the center of the basin, older anomalies are clearly visible and might extend to M37. Beyond M33, however, their precise identification is less certain than in the Pigafetta Basin.

---

[1] Lancelot, Y., Larson, R. L., et al., 1990. *Proc. ODP, Init. Repts.*, 129: College Station, TX (Ocean Drilling Program).

[2] Shipboard Scientific Party is as given in the list of participants preceding the contents.

Table 1. Coring summary for Hole 802A.

| Core no. | Date | Time (UTC) | Depth (mbsf) | Length cored (m) | Length recovered (m) | Recovery (%) |
|---|---|---|---|---|---|---|
| 1R | 25 Dec. 1989 | 1345 | 0.0–5.0 | 5.0 | 0.01 | 0.2 |
| 2R | 25 Dec. 1989 | 1730 | 5.0–14.6 | 9.6 | 0.00 | 0.0 |
| 3R | 25 Dec. 1989 | 1935 | 14.6–24.3 | 9.7 | 1.43 | 14.7 |
| 4R | 25 Dec. 1989 | 2250 | 24.3–33.7 | 9.4 | 3.00 | 31.9 |
| 5R | 26 Dec. 1989 | 0135 | 33.7–42.9 | 9.2 | 1.93 | 21.0 |
| 6R | 26 Dec. 1989 | 0350 | 42.9–52.4 | 9.5 | 2.58 | 27.1 |
| 7R | 26 Dec. 1989 | 0745 | 52.4–61.9 | 9.5 | 1.46 | 15.3 |
| 8R | 26 Dec. 1989 | 1110 | 61.9–71.1 | 9.2 | 3.29 | 35.7 |
| 9R | 26 Dec. 1989 | 1410 | 71.1–80.4 | 9.3 | 0.00 | 0.0 |
| 10R | 26 Dec. 1989 | 1620 | 80.4–89.6 | 9.2 | 3.42 | 37.2 |
| 11R | 26 Dec. 1989 | 1830 | 89.6–98.9 | 9.3 | 1.91 | 20.5 |
| 12R | 26 Dec. 1989 | 2020 | 98.9–108.3 | 9.4 | 0.13 | 1.4 |
| 13R | 26 Dec. 1989 | 2230 | 108.3–114.4 | 6.1 | 1.67 | 27.4 |
| 14R | 27 Dec. 1989 | 0100 | 114.4–122.1 | 7.7 | 3.37 | 43.7 |
| 15R | 27 Dec. 1989 | 0445 | 122.1–131.1 | 9.0 | 2.87 | 31.9 |
| 16R | 27 Dec. 1989 | 0655 | 131.1–140.4 | 9.3 | 2.00 | 21.5 |
| 17R | 27 Dec. 1989 | 0845 | 140.4–149.7 | 9.3 | 2.13 | 22.9 |
| 18R | 27 Dec. 1989 | 1055 | 149.7–159.1 | 9.4 | 0.39 | 4.2 |
| 19R | 27 Dec. 1989 | 1330 | 159.1–168.3 | 9.2 | 3.55 | 38.6 |
| 20R | 27 Dec. 1989 | 1530 | 168.3–177.6 | 9.3 | 0.30 | 3.2 |
| 21R | 27 Dec. 1989 | 1740 | 177.6–187.0 | 9.4 | 1.75 | 18.6 |
| 22R | 27 Dec. 1989 | 1940 | 187.0–196.4 | 9.4 | 0.45 | 4.8 |
| 23R | 27 Dec. 1989 | 2230 | 196.4–206.1 | 9.7 | 2.68 | 27.6 |
| 24R | 28 Dec. 1989 | 0010 | 206.1–215.7 | 9.6 | 0.17 | 1.8 |
| 25R | 28 Dec. 1989 | 0450 | 215.7–225.4 | 9.7 | 1.07 | 11.0 |
| 26R | 28 Dec. 1989 | 0640 | 225.4–235.1 | 9.7 | 3.63 | 37.4 |
| 27R | 28 Dec. 1989 | 0805 | 235.1–244.7 | 9.6 | 8.15 | 84.9 |
| 28R | 28 Dec. 1989 | 0935 | 244.7–254.5 | 9.8 | 4.38 | 44.7 |
| 29R | 28 Dec. 1989 | 1105 | 254.5–264.2 | 9.7 | 3.65 | 37.6 |
| 30R | 28 Dec. 1989 | 1400 | 264.2–273.8 | 9.6 | 1.63 | 17.0 |
| 31R | 28 Dec. 1989 | 1630 | 273.8–283.5 | 9.7 | 1.95 | 20.1 |
| 32R | 28 Dec. 1989 | 1900 | 283.5–292.8 | 9.3 | 3.37 | 36.2 |
| 33R | 28 Dec. 1989 | 2125 | 292.8–302.3 | 9.5 | 1.64 | 17.2 |
| 34R | 28 Dec. 1989 | 2355 | 302.3–311.5 | 9.2 | 1.40 | 15.2 |
| 35R | 29 Dec. 1989 | 0220 | 311.5–320.7 | 9.2 | 1.04 | 11.3 |
| 36R | 29 Dec. 1989 | 0445 | 320.7–329.9 | 9.2 | 1.12 | 12.2 |
| 37R | 29 Dec. 1989 | 0650 | 329.9–339.2 | 9.3 | 0.19 | 2.0 |
| 38R | 29 Dec. 1989 | 0900 | 339.2–348.7 | 9.5 | 7.89 | 83.0 |
| 39R | 29 Dec. 1989 | 1120 | 348.7–358.1 | 9.4 | 0.90 | 9.6 |
| 40R | 29 Dec. 1989 | 1325 | 358.1–365.5 | 7.4 | 4.58 | 61.9 |
| 41R | 29 Dec. 1989 | 1540 | 365.5–372.8 | 7.3 | 5.85 | 80.1 |
| 42R | 29 Dec. 1989 | 2000 | 372.8–382.1 | 9.3 | 2.69 | 28.9 |
| 43R | 29 Dec. 1989 | 2210 | 382.1–391.3 | 9.2 | 3.90 | 42.4 |
| 44R | 30 Dec. 1989 | 0015 | 391.3–400.5 | 9.2 | 1.24 | 13.5 |
| 45R | 30 Dec. 1989 | 0215 | 400.5–410.0 | 9.5 | 3.53 | 37.1 |
| 46R | 30 Dec. 1989 | 0405 | 410.0–419.2 | 9.2 | 1.34 | 14.5 |
| 47R | 30 Dec. 1989 | 0600 | 419.2–428.7 | 9.5 | 6.16 | 64.8 |
| 48R | 30 Dec. 1989 | 0750 | 428.7–438.1 | 9.4 | 0.99 | 10.5 |
| 49R | 30 Dec. 1989 | 1000 | 438.1–447.4 | 9.3 | 6.85 | 73.6 |
| 50R | 30 Dec. 1989 | 1200 | 447.4–453.5 | 6.1 | 3.15 | 51.6 |
| 51R | 30 Dec. 1989 | 1420 | 453.5–459.8 | 6.3 | 4.71 | 74.7 |
| 52R | 30 Dec. 1989 | 1800 | 459.8–469.4 | 9.6 | 4.03 | 42.0 |
| 53R | 30 Dec. 1989 | 2045 | 469.4–478.6 | 9.2 | 2.59 | 28.1 |
| 54R | 30 Dec. 1989 | 2335 | 478.6–487.9 | 9.3 | 6.50 | 69.9 |
| 55R | 31 Dec. 1989 | 0220 | 487.9–497.1 | 9.2 | 1.48 | 16.1 |
| 56R | 31 Dec. 1989 | 0445 | 497.1–506.6 | 9.5 | 5.11 | 53.8 |
| 57R | 31 Dec. 1989 | 0820 | 506.6–516.0 | 9.4 | 3.34 | 35.5 |
| 58R | 31 Dec. 1989 | 1440 | 516.0–525.4 | 9.4 | 5.02 | 53.4 |
| 59R | 31 Dec. 1989 | 2130 | 525.4–534.7 | 9.3 | 3.89 | 41.8 |
| 60R | 1 Jan. 1990 | 0140 | 534.7–544.2 | 9.5 | 0.96 | 10.1 |
| 61R | 1 Jan. 1990 | 0620 | 544.2–550.6 | 6.4 | 1.50 | 23.4 |
| 62R | 1 Jan. 1990 | 1910 | 550.6–559.8 | 9.2 | 3.10 | 33.7 |
|  | Coring totals |  |  | 559.8 | 165.01 | 29.5 |

Two drill sites were proposed in this area. They present very similar characteristics on seismic profiles. Proposed site EMB-1 is located near anomaly M33, whereas proposed site EMB-2A was selected farther to the southeast, within the Jurassic quiet zone. Our choice of proposed site EMB-2A as a preferred target was mainly dictated by its distance from major seamounts. Indeed, we tried to locate this site as far from any large seamount as we could (approximately 160 nmi), although still on what we believed to be Jurassic crust.

Seismic reflection profiles from both of the survey cruises, *Fred H. Moore* 35-12 and MESOPAC II, show the acoustic basement to be alternatively smooth and rough. Site 802 is located in an area characterized by a rough acoustic basement that lies slightly deeper than its adjacent smooth counterpart (see "Site Geophysics and Seismic Stratigraphy" section, this chapter). The total depth of approximately 8.4 seconds two-way traveltime (s twt) below sea level to this reflector, together with its relatively rough or "hummocky" aspect led us to believe that it could very well correspond to the top of the extrusive Jurassic oceanic crust, whereas the smooth and slightly shallower acoustic basement of adjacent areas could indicate the presence of sills covering the old crust. As true oceanic crust had just been found at Site 801 at 8.0 s twt, we had reason to believe that this lowermost reflector would indeed again correspond to Jurassic basaltic extrusives.

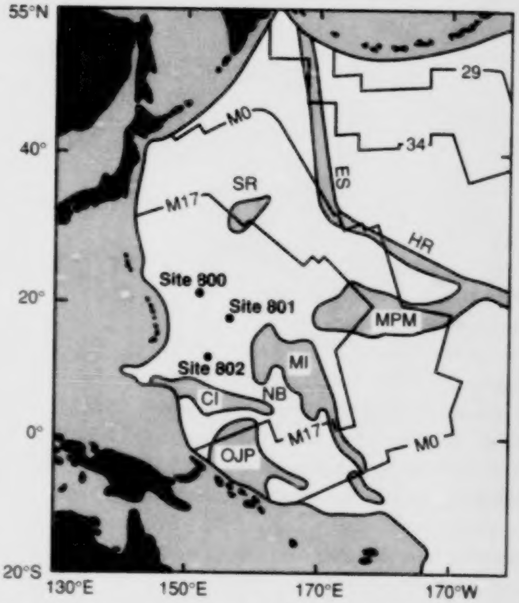

Figure 1. Map showing location of Pigafetta, Mariana, and Nauru basins, and location of Sites 800, 801, and 802. (Feature abbreviations are as follows: Caroline Islands (CI), Ontong Java Plateau (OJP), Marshall Islands (MI), Nauru Basin (NB), Mid-Pacific Mountains (MPM), Shatsky Rise (SR), Hawaiian Ridge (HR), and Emperor Seamounts (ES). Jagged contours represent magnetic lineations and unshaded areas represent normal Pacific oceanic crust. Shaded areas represent volcanic edifices with thickened crustal sections, as well as the younger areas beyond the Pacific subduction zones.

The age of the crust was tentatively inferred from a simple extrapolation of the nearby magnetic anomalies to be Callovian or Oxfordian (165 to 168 m.y.) (Fig. 3). The total thickness of the section between the seafloor reflector and the acoustic basement is about 500 ms twt. Based on an average sound velocity of 2 km/s for this acoustic interval, we expected the total sediment section to be about 500 m thick. That section on seismic profiles can be roughly divided in two intervals. The uppermost of these, from 0 to 375 ms below the seafloor, appears well layered and shows evidence of ponding. It is tentatively correlated with a series of turbiditic deposits recovered at Site 199 located approximately 170 nmi to the northeast (Heezen, MacGregor, et al., 1973). Below that interval the section is more transparent, and we anticipated that it consisted mostly of pelagic sediments ranging in age from Late Cretaceous at the top to Callovian-Oxfordian at the bottom. The youngest of the two successive equatorial cross-

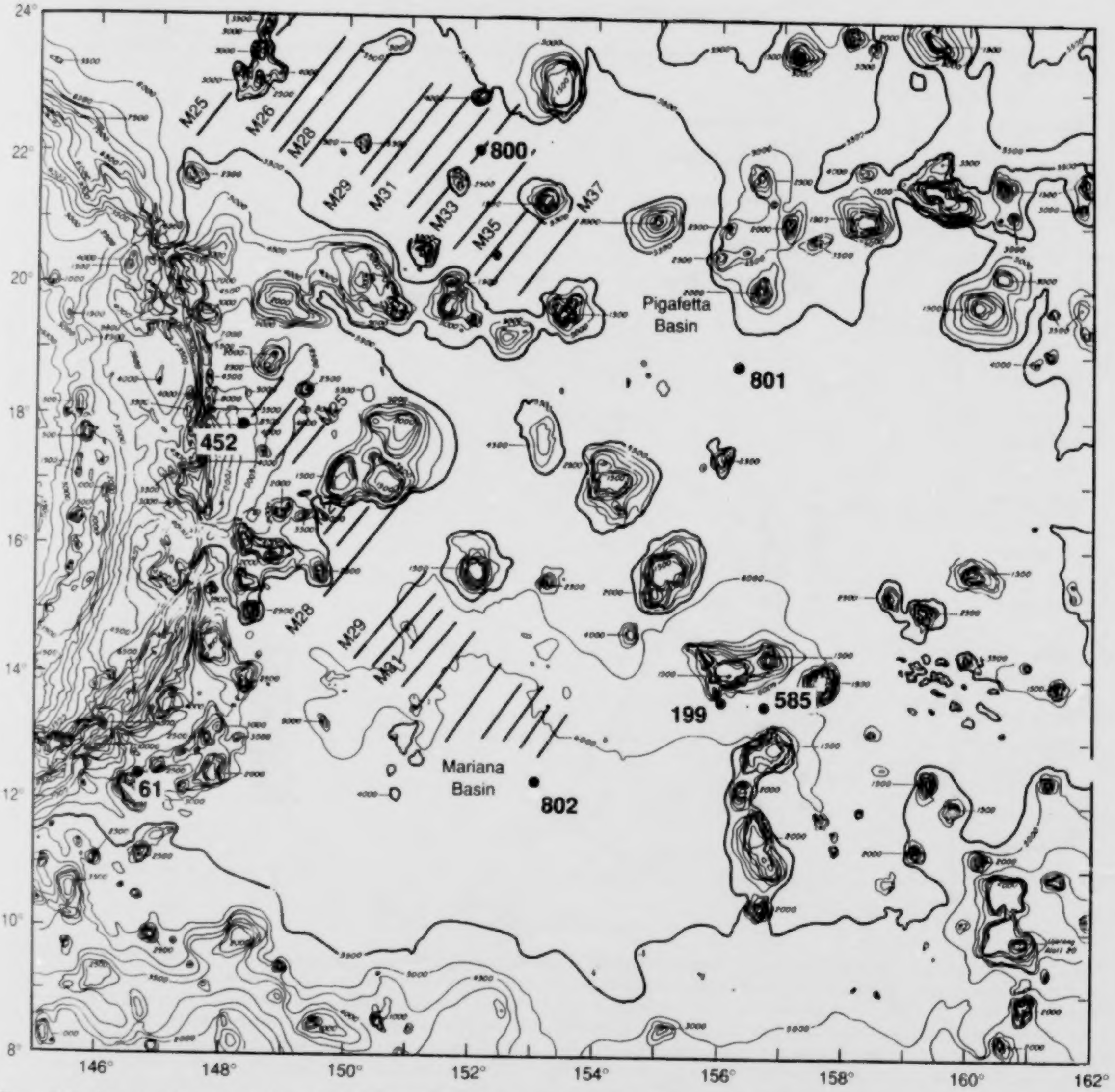

Figure 2. Bathymetry (in meters) of the central western Pacific (from M. Angell and C. Brenner, pers. comm., 1990) showing location of the Pigafetta and Mariana basins, ODP Sites 800, 801, and 802, DSDP Sites 199 and 585, and magnetic lineations, with seafloor topography. Magnetic anomalies modified from Handschumacher and Gettrust (1985), Tamaki et al. (1987), and Handschumacher et al. (1988).

ings predicted for this site was estimated to have occurred during the earliest Tertiary (Lancelot and Larson, 1975; Lancelot, 1978) and, therefore, siliceous pelagic deposits were anticipated to have been incorporated and somewhat diluted within the turbiditic sediments. As a consequence, we expect chert in that interval to be less concentrated than it is to the north. The oldest equatorial crossing, based on experience gained from the two previous sites that documented the geophysical predictions of Larson and Lowrie (1975), was expected to have occurred sometime during the Late Jurassic. We expected chert and possibly some limestone in the lowermost levels of the sediment column just above the basement.

Our strategy for this site was to drill a single-bit hole all the way to basement in order to achieve as much penetration as possible into the oceanic crust, and then to run a full suite of logs, while leaving enough time to sail back to Site 801 in order to fish the lost camera out of the reentry cone if necessary and drill approximately 100 m into the upper layers of the Jurassic crust.

## OPERATIONS

### Approach to the Site

We approached Site 802 from the north-northeast on course 203°, subparallel to MESOPAC II line 18, at 6 knots, shooting a seismic line with two 80-in.$^3$ water guns (Fig. 4). Our target was a point at 0030 hr (Universal Time Coordinated, or UTC), 18 November 1987, on FM35-12 line 7, 5 km

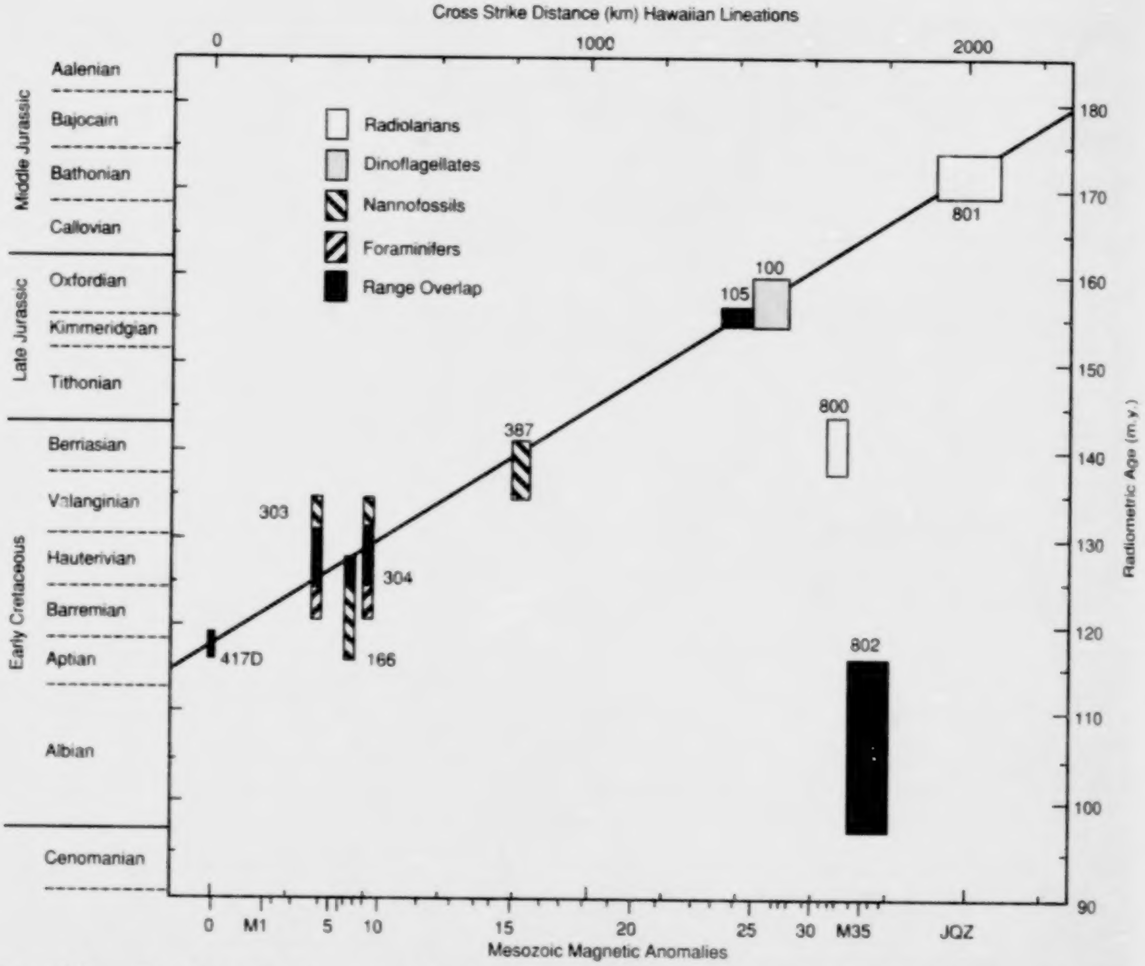

Figure 3. Time calibration plot of the Mesozoic anomalies M0 to M37 and the preceding Jurassic magnetic quiet zone (JQZ). Magnetic anomalies are plotted as cross-strike distance across the Hawaiian lineations for M0 to M25. Anomalies M25 to M37 are normalized to that parameter afte Handschumacher et al. (1988). Geologic time scale and radiometric ages are from Harland et al. (1982), as modified by Kent and Gradstein (1985) at the Tithonian/Kimmeridgian boundary. Age ranges from Leg 129 Sites 800, 801, and 802 are also shown. Oldest paleontologic ages in various DSDP holes (numbered) shown as rectangles. Vertical lengths of rectangles show paleontological age ranges from DSDP *Initial Reports* except for Site 100 (Zotto et al., 1987) and Site 105 (Gradstein and Sheridan, 1983). Horizontal lengths show magnetic age ranges from Larson and Hilde (1975) for Sites 303, 304, 166, 100, and 105 and from DSDP *Initial Reports* for Sites 387 and 417D.

west of its intersection with MESOPAC II line 18. At 2035 hr, 24 December 1989, we crossed FM35-12 line 7 at the target location and continued on course for another 10 km, where we reversed course with a Williamson turn and returned toward the target location. At 2303 hr, 24 December 1989, we launched a beacon at 12°5.79′N, 153°12.59′E over a very clear seismic section on the system of the *JOIDES Resolution* (see Fig. 56, "Site Geophysics and Seismic Stratigraphy" section, this chapter) about 2 km south of the original target location.

### Hole 802A

The bottom-hole assembly (BHA) for Hole 802A consisted of 120 m of 8¼-in. drill collars with a 3-m-long set of Hydrolex jars at 98 m, providing 40,000 lb drilling weight available below the jars. A Rock Bit International C4 coring bit was chosen as the coring tool. The corrected depth obtained by the precision depth recorder at Hole 802A is 5988 m to the rig floor. The first core taken with the pipe lowered to 5985 m was coated with mud up a length of 5 m, so the mud line was established at 5980 m. We then cored ahead, recovering almost none of the first 21 m of soft pelagic ooze. At 21 mbsf the bit met a hard surface that proved to be very well-indurated, brown clay turbidites. The hard drilling continued, making the next 50 m of penetration a precarious operation. A combination of very light bit weight and slow rotation was used to ease the BHA down into the formation. The lithology quickly graded down into very fresh, coal-black volcaniclastics or reworked hyaloclastites with a high ash content below 40 mbsf. Hard drilling continued until about 100 mbsf, where a soft interval about

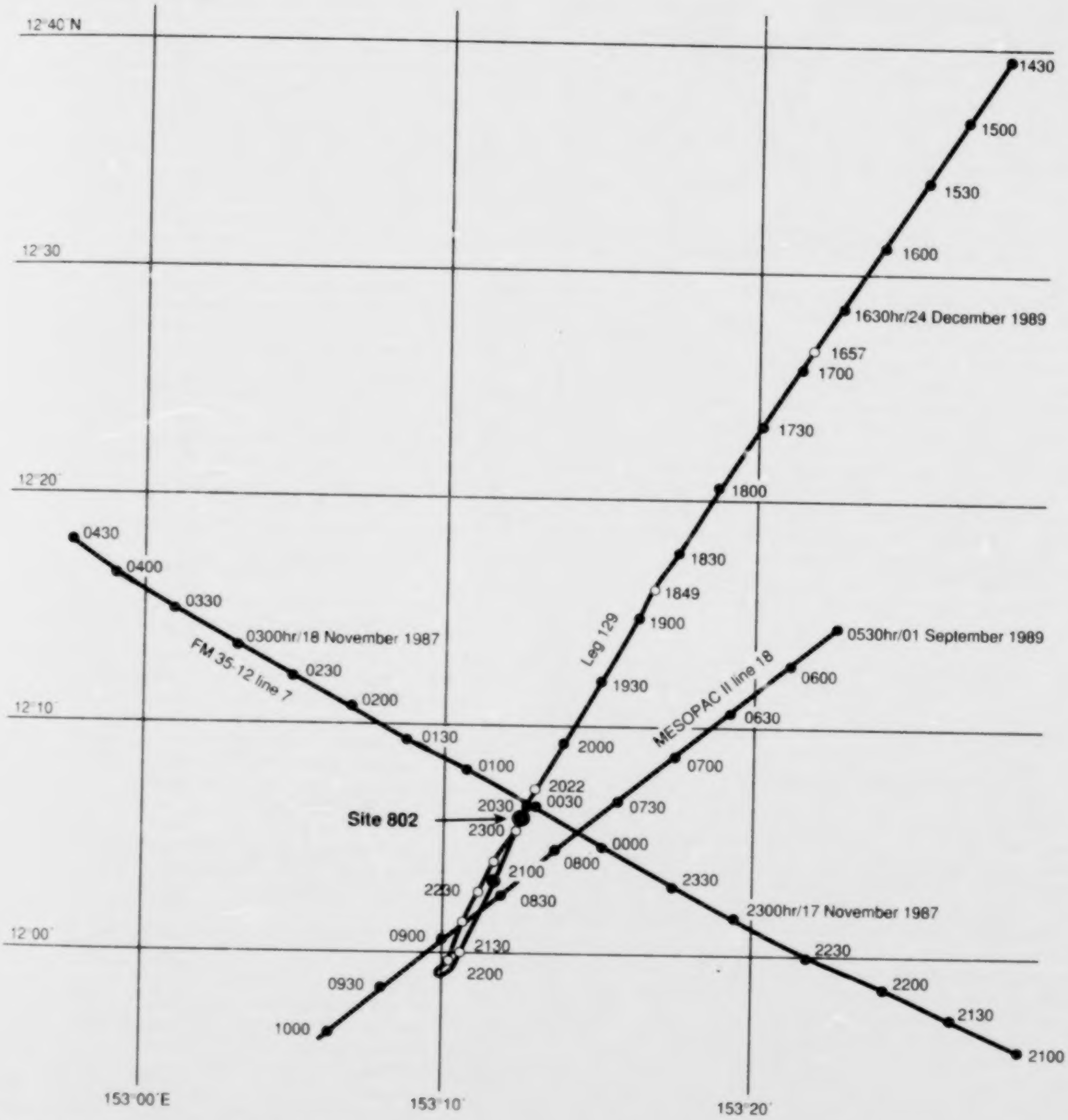
12°40'N
12°30'
12°20'
12°10'
12°00'
153°00'E
153°10'
153°20'
1430
1500
1530
1600
1630hr/24 December 1989
1657
1700
1730
1800
1830
1849
1900
1930
2000
2022
2030
2300
2100
2230
2130
2200
Leg 129
0430
0400
0330
0300hr/18 November 1987
0230
0200
0130
0100
0030
0000
2330
2300hr/17 November 1987
2230
2200
2130
2100
FM 35-12 line 7
0530hr/01 September 1989
0600
0630
0700
0730
0800
0830
0900
0930
1000
MESOPAC II line 18
Site 802

Figure 4. Track chart of expeditions FM35-12, MESOPAC II, and Leg 129. Site 802 is located on Leg 129 SCS line (2040 hr UTC, 24 December 1989) at approximately 2 km south of its intersection with FM35-12 line 7 and 4 km east of the intersection of FM35-12 line 7 (0010 hr, 18 November 1987) and MESOPAC II line 6 (0750 hr, 1 September 1989). Portions of each of these lines are displayed in Figures 53, 54, and 56.

20 m thick was cored, but mostly not recovered. Below that level, drilling alternated between hard and soft layers, although the recovery was dominated by the coal-black volcaniclastics or hyaloclastites. Inclination surveys were run at 71 mbsf and at subsequent 100-m intervals that showed 1° or less of hole inclination. At about 150 mbsf the drilling rate of penetration increased dramatically, indicating that we were now coring essentially soft sediment. Recovery was generally very poor in this section. It improved considerably below about 225 mbsf where the formation consists of moderately well-lithified, Miocene turbidites with a high carbonate content. From 300 to 330 mbsf we cored through Paleocene chalks and minor chert with moderate recovery. Recovery generally improved below 340 mbsf in Campanian volcaniclastics. Below 460 mbsf the volcaniclastics/turbidites graded down into alternating brown claystone, calcareous claystone, and radiolarite, with some black, volcaniclastic turbidites at the base of the sedimentary section. The recovery in the interval from 340 to 516 mbsf at the top of basalt was moderate, ranging from about 15% to 60%.

Solid basalt was encountered at 509 mbsf and it was the only lithology recovered from 509 mbsf to the bottom of the hole at 560 mbsf. Drilling records indicate that little, if any, sediment was encountered but not recovered in this interval. The basalt was entirely extrusive in nature and presented no problems for drilling other than a slow rate of penetration. The hole stood up well until just before the last core, when 43 m of fill was encountered in returning to the bottom of the hole after a short wiper trip. That fill, the slow rate of penetration, the uniform nature of the recovered basalts, and the arrival of the replacement television camera by supply boat led us to terminate coring at this point and rig for logging.

The bit was dropped without problem at the bottom of the hole, and the bottom of the pipe was raised to about 60 mbsf. No wiper run was made because of the previously mentioned hole instability. Standard logging was planned for this site using the same three tool strings as at the previous holes. On the first quad combination logging run-in, the tool encountered a bridge at 103 mbsf. We decided this section was too short to log, pulled the logging tool out of the pipe, and lowered the drill pipe to 127 mbsf, below the base of the clay zone that created the bridge. We then ran the quad combination tool string down the pipe a second time and encountered a second bridge at 323 mbsf. We decided to conduct logging in this clear section of hole and collected a quad combination log from 323 to 108 mbsf. We then ran the geochemical and formation microscanner tool strings, but encountered the same bridge and logged essentially the same interval.

Because the age of the oldest sediment above basalt at this site is about 60 m.y. younger than its predicted Jurassic age, the possibility exists that we drilled into a lava flow sequence that covers the original basement surface and perhaps the predicted older sediments. In order to test this possibility, we attempted to run a vertical seismic profile to look for seismic reflectors deeper than the basalt surface that we had sampled, which forms the most obvious, acoustic basement return on the multichannel seismic records across the site. The 400-in.$^3$ water-gun source was set up and hung off the port-side crane using two large flotation balls. The well seismic tool (WST) was then run into the hole, apparently about 60 m deeper than was reached by the previous tool strings. Although the water gun functioned normally when fired from the logging unit, the WST produced a low signal-to-noise level record despite repeated adjustments. We suspected that the caliper arms had been sheared off the tool while passing out of the bottom of the pipe. When we attempted to raise the tool we discovered that it was also stuck in the hole. Repeated pulls of about 9500 lb (4000 lb overpulls) failed to dislodge the tool. In order to recover as much cable as possible for potential logging runs at the last site, we attempted to sever the cable at the splice 500 m above the WST. The severing tool cut the cable, but on retrieval, we discovered that the cut had been made 3164 m above the WST. We then retrieved the remainder of the logging cable (including the severed section and the WST that were snagged in the BHA) and the drill string, and got underway for our return to Site 801.

## LITHOSTRATIGRAPHY AND SEDIMENTOLOGY

### Lithostratigraphy

Site 802 was continuously cored from the mud line at 5969.6 meters below sea level (mbsl) to a total depth of 559.8 mbsf. The stratigraphic section recovered from Hole 802A is divided into 10 lithologic units (I through X) based on composition and color (Fig. 5, Table 2). Unit I, very poorly recovered, is inferred to be 14.6 m of brown pelagic clay. Subunit IIA is 146.0 m thick and consists dominantly of tuff deposited as mass flows, grain flows, and turbidites. Subunit IIB is 76.8 m thick and consists of tuff intercalated with a significant proportion of redeposited calcareous claystone and chalk. Unit III is a 92.5-m interval of nannofossil chalk with minor amounts of interbedded claystone and nodular chert. Unit IV is composed of 19.3 m of zeolitic pelagic claystone and calcareous nannofossil claystone with minor porcellanite, chert, and calcareous siltstone or sandstone. Unit V is 110.8 m thick and consists of volcaniclastic grain flows and turbidites that grade up into pelagic claystones containing both radiolarians and nannofossils. Unit VI is a 9.9-m interval of interbedded claystone and radiolarite. Unit VII is a 27.2-m-thick interval of predominantly calcareous lithologies, chiefly radiolarian limestone, nannofossil chalk, and calcareous claystone, with minor clayey sandstone, radiolarite, porcellanite, and chert. Unit VIII is contained entirely in Core 129-802A-56R and consists of 2.4 m of claystone with thin interbeds of radiolarite. Unit IX is 9.6 m thick and consists of volcaniclastic turbidites and tuffaceous claystone, with minor radiolarite. Unit X is a 50.6-m-thick series of basaltic pillow lava units and one thin flow unit. Because sediment accumulation rates for all units are calculated without including known hiatuses, the values are minimum sedimentation rates only. These calculations are for compacted sediments, as recovered.

### Lithologic Units

#### ***Unit I. Cores 129-802A-1R through 129-802A-2R (0.0–14.6 mbsf): Pelagic Brown Clay; Quaternary to upper Pliocene***

Unit I is composed of homogeneous dark brown pelagic clay. Smear slides show that the main constituents are clay and aggregates of metal-oxyhydroxides, with minor zeolites, micronodules, quartz silt, and radiolarian spines. Although Unit I is considered to extend from the mud line to 14.6 mbsf, recovery was less than 1 m, all from Core 129-802A-1R. The base of this unit is placed above the highest occurrence of tuff (Section 129-802A-3R-1, 0 cm).

#### ***Unit II. Core 129-802A-3R to Section 129-802A-27R-2, 81 cm (14.6–237.4 mbsf): Tuff (Volcaniclastic Turbidites); middle Pliocene(?) to lower Miocene***

*Subunit IIA. Tuff with pelagic clay, middle Pliocene to lower Miocene (Core 129-802A-3R to Section 129-802A-19R-2, 0 cm; 14.6–160.6 mbsf)*

Subunit IIA is 146 m thick and consists dominantly of tuff deposited as mass flows, grain flows, and turbidites. Between the tuff beds are pelagic claystone layers representing background sedimentation. Lack of recovery in Core 129-802A-2R precludes speculation about the termination of the influx of volcaniclastic material. The base of Subunit IIA is gradational to Subunit IIB.

Tuff beds are massive and meter-scale in thickness. Overall, Subunit IIA is a sequence that is coarsening and thickening upward, from thin, 5- to 10-cm-thick turbidite beds at the base to mass flows several meters thick at the top. Locally, some beds have planar or cross-laminations, dish or pipe fluid-escape structures, and basal scours or flame structures. In general, beds are normally graded but very poorly sorted, with common lapilli isolated in the tuff matrix or concentrated in indistinct bands. Minor amounts of lapilli tuff (Fig. 6) are intercalated with the tuff; lapilli are subrounded and consist dominantly of volcanic ash (Fig. 7). Rarely are they calcareous, clayey, or palagonitic.

The tuff is very dark, ranging from black to greenish black, and consists of 60%–80% angular, fresh glass shards and

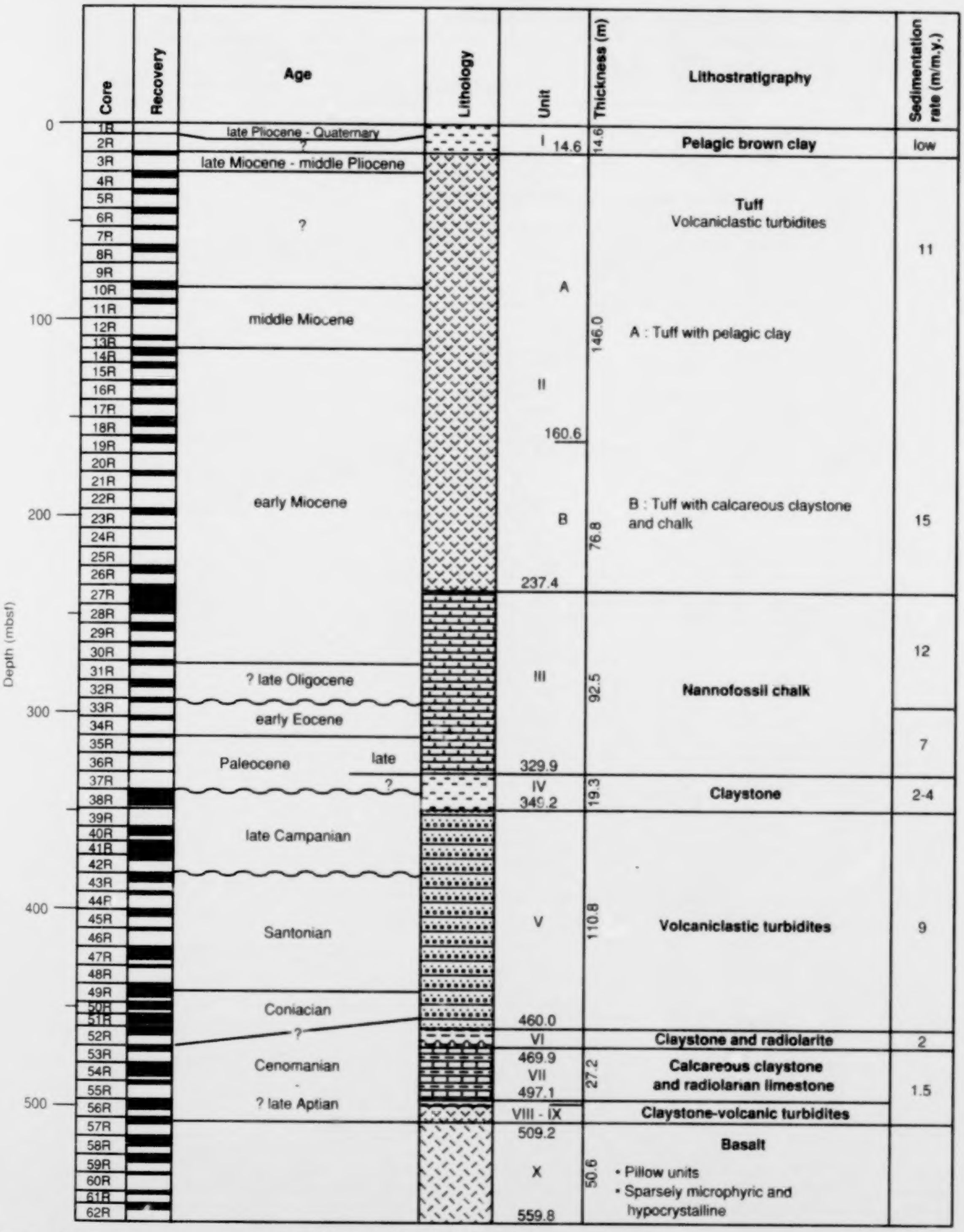
Core
Recovery
Age
Lithology
Unit
Thickness (m)
Lithostratigraphy
Sedimentation rate (m/m.y.)
Depth (mbsf)
0
100
200
300
400
500
1R
2R
3R
4R
5R
6R
7R
8R
9R
10R
11R
12R
13R
14R
15R
16R
17R
18R
19R
20R
21R
22R
23R
24R
25R
26R
27R
28R
29R
30R
31R
32R
33R
34R
35R
36R
37R
38R
39R
40R
41R
42R
43R
44R
45R
46R
47R
48R
49R
50R
51R
52R
53R
54R
55R
56R
57R
58R
59R
60R
61R
62R
late Pliocene - Quaternary
?
late Miocene - middle Pliocene
?
middle Miocene
early Miocene
? late Oligocene
early Eocene
Paleocene
late
?
late Campanian
Santonian
Coniacian
?
Cenomanian
-
? late Aptian
I
14.6
A
II
160.6
B
237.4
III
329.9
IV
349.2
V
460.0
VI
469.9
VII
497.1
VIII - IX
509.2
X
559.8
14.6
146.0
76.8
92.5
19.3
110.8
27.2
50.6
Pelagic brown clay
Tuff
Volcaniclastic turbidites
A : Tuff with pelagic clay
B : Tuff with calcareous claystone and chalk
Nannofossil chalk
Claystone
Volcaniclastic turbidites
Claystone and radiolarite
Calcareous claystone and radiolarian limestone
Claystone-volcanic turbidites
Basalt
• Pillow units
• Sparsely microphyric and hypocrystalline
low
11
15
12
7
2-4
9
2
1.5

Figure 5. Stratigraphic summary of Hole 802A. (Note: Total depth is 5969 mbsl.)

**Table 2. Lithology and ages of cores recovered from Hole 802A.**

| Core | Depth (mbsf) | Length cored (m) | Length recovered (m) | Major lithology | Age (downcore) |
|---|---|---|---|---|---|
| Unit I– Pelagic clay; Cores 129A-802A-1R and -2R (0–14.6 mbsf) | | | | | |
| 1R | 0.0–5.0 | 5.0 | 0.01 | Pelagic clay | Quaternary to upper Pliocene |
| 2R | 5.0–14.6 | 9.6 | 0.00 | Pelagic clay (no recovery) | ? |
| Unit II – Tuff (volcaniclastic turbidites); Core 129A-802A-3R to Section 129A-802A-27R-2, 81 cm (14.6–237.41 mbsf) | | | | | |
| Subunit IIA – Tuff with pelagic clay; Core 129-802A-3R through Section 129-802A-9R-2, 0 cm (14.6–160.6 mbsf) | | | | | |
| 3R | 14.6–24.3 | 9.7 | 1.43 | Tuff and pelagic clay | middle Pliocene to lower Miocene |
| 4R | 24.3–33.7 | 9.4 | 3.00 | Tuff and lapilli tuff | |
| 5R | 33.7–42.9 | 9.2 | 1.93 | Tuff (volcaniclastic sandstone) | |
| 6R | 42.9–52.4 | 9.5 | 2.58 | Tuff (volcaniclastic sandstone) and lapilli tuff | |
| 7R | 52.4–61.9 | 9.5 | 1.46 | Tuff to lapilli tuff (volcaniclastic sandstone/conglomerate) | ? |
| 8R | 61.9–71.1 | 9.2 | 3.29 | Tuff (volcaniclastic sandstone/siltstone) | |
| 9R | 71.1–80.4 | 9.3 | 0.00 | Tuff (?, no recovery) | |
| 10R | 80.4–89.6 | 9.2 | 3.42 | Tuff (volcaniclastic sandstone) | |
| 11R | 89.6–98.9 | 9.3 | 1.91 | Tuff (volcaniclastic sandstone/siltstone) | |
| 12R | 98.9–108.3 | 9.4 | 0.13 | Tuff (volcaniclastic sandstone) | middle Miocene |
| 13R | 108.3–114.4 | 6.1 | 1.67 | Pelagic clay and tuff | |
| 14R | 114.4–122.1 | 7.7 | 3.37 | Tuff (volcaniclastic sandstone turbidites) | |
| 15R | 122.1–131.1 | 9.0 | 2.87 | Tuff (volcaniclastic sandstone turbidites) | |
| 16R | 131.1–140.4 | 9.3 | 2.00 | Tuff (volcaniclastic turbidites) | |
| 17R | 140.4–149.7 | 9.3 | 2.13 | Tuff (volcaniclastic turbidites) | |
| 18R | 149.7–159.1 | 0.4 | 4.20 | Tuff (volcaniclastic sandstone) | |
| Subunit IIB – Tuff (volcaniclastic turbidites) with calcareous claystone and chalk Sections 129-802A-19R-2, 0 cm, to 129-802A-27R-2, 81 cm (160.6–237.41 mbsf) | | | | | |
| 18R | (continued) | | | Tuff (volcaniclastic sandstone) | |
| 19R | 159.1–168.3 | 9.2 | 3.55 | Tuff (volcaniclastic turbidites, clay); chalk | |
| 20R | 168.3–177.6 | 9.3 | 0.30 | Tuff (volcaniclastic sandstone) | |
| 21R | 177.6–187.0 | 9.4 | 1.75 | Tuff (volcaniclastic sandstone), claystone-siltstone | |
| 22R | 187.0–196.4 | 9.4 | 0.45 | Tuff (volcaniclastic silty sandstone) | lower Miocene |
| 23R | 196.4–206.1 | 9.7 | 2.68 | Tuff (volcaniclastic turbidites) nannofossil clay | |
| 24R | 206.1–215.7 | 9.6 | 0.17 | Chalk; nannofossil clayey siltstone | |
| 25R | 215.7–225.4 | 9.7 | 1.07 | Claystone with nannofossils | |
| 26R | 225.4–235.1 | 9.7 | 3.63 | Clayey chalk; chalk; minor tuff-clay | |
| 27R | 235.1–237.4 | 9.6 | 8.15 | Tuff (volcaniclastic sandstone) | |
| Unit III – Nannofossil chalk; Section 129-802A-27-2, 81 cm, to Core 129-802A-36R (237.41–329.9 mbsf) | | | | | |
| 27R | (continued) | | | Chalk – debris flow | |
| 28R | 44.7–254.5 | 9.8 | 4.38 | Graded bed – chalk to packstone | |
| 29R | 254.5–264.2 | 9.7 | 3.65 | Claystone; calcareous claystone | |
| 30R | 264.2–273.8 | 9.6 | 1.63 | Nannofossil chalk | |
| 31R | 273.8–283.5 | 9.7 | 1.95 | Nannofossil chalk | |
| 32R | 283.5–292.8 | 9.3 | 3.37 | Nannofossil chalk | ?upper Oligocene |
| 33R | 292.8–302.3 | 9.5 | 1.64 | Nannofossil chalk | |
| 34R | 302.3–311.5 | 9.2 | 1.40 | Nannofossil chalk | lower Eocene |
| 35R | 311.5–320.7 | 9.2 | 1.04 | Nannofossil chalk; chert | |
| 36R | 320.7–329.9 | 9.2 | 1.12 | Nannofossil chalk with foraminifers | upper Paleocene |

palagonite (Fig. 7). The glass is typically vesicular, sometimes spherulitic, and locally palagonitized. In thin section, the tuff contains up to 10% subhedral feldspar crystals, up to 15% clinopyroxene (augite), and rare olivine crystals, and ranges from crystal vitric tuff to vitric crystal lithic tuff. The tuff also contains a few percent to traces of igneous rock fragments, tachylite, iron oxides, and opaques. Varying proportions of secondary smectites, zeolites, and calcite may constitute as much as 20% of the tuff. Coarser-grained beds contain planktonic and neritic benthic foraminifers (Fig. 7). The high percentage of glass shards and crystals and the freshness of the glass shards distinguish this tuff from Cretaceous volcani-

Table 2 (continued).

| Core | Depth (mbsf) | Length cored (m) | Length recovered (m) | Major lithology | Age (downcore) |
|---|---|---|---|---|---|
| Unit IV – Claystone; Core 129-802A-37R to Section 192-802A-39R-1, 45 cm (329.9–349.2 mbsf) | | | | | |
| 37R | 329.9–339.2 | 9.3 | 0.19 | Zeolitic pelagic claystone | Paleocene |
| 38R | 339.2–348.7 | 9.5 | 7.89 | Zeolitic pelagic claystone; calcareous silty claystone | upper Campanian |
| 39R | 348.7–358.1 | 9.4 | 0.90 | Porcellanite; claystone | |
| Unit V – Volcaniclastic turbidites; Sections 129-802A-39R-1, 45 cm, to 129-802A-52R-1, 15 cm (349.2–460.0 mbsf) | | | | | |
| 39R | (continued) | | | Clayey chalk | Santonian |
| 40R | 358.1–365.5 | 7.4 | 4.58 | Volcaniclastic turbidites, clay; porcellanite | |
| 41R | 365.5–372.8 | 7.3 | 5.85 | Volcaniclastic claystone, siltstone | |
| 42R | 372.8–382.1 | 9.3 | 2.69 | Volcaniclastic turbidites, claystone | |
| 43R | 382.1–391.3 | 9.2 | 3.90 | Volcaniclastic turbidites, calcareous claystone | |
| 44R | 391.3–400.5 | 9.2 | 1.24 | Silty claystone, claystone (volcaniclastic?) | |
| 45R | 400.5–410.0 | 9.5 | 3.53 | Turbidites of silty claystone (volcaniclastic?) | |
| 46R | 410.0–419.2 | 9.2 | 1.34 | Turbidites of silty claystone (volcaniclastic?) | |
| 47R | 419.2–428.7 | 9.5 | 6.16 | Turbidites of silty claystone with radiolarians | |
| 48R | 428.7–438.1 | 9.4 | 0.99 | Turbidites of volcaniclastic sandstone to nannofossil clay | |
| 49R | 438.1–447.4 | 9.3 | 6.85 | Silty claystone; siltstone | |
| 50R | 447.4–453.5 | 6.1 | 3.15 | Volcaniclastic silty claystone (debris flow) | Coniacian |
| 51R | 453.5–459.8 | 6.3 | 4.71 | Claystone, debris flow | |
| 52R | 459.8–469.4 | 9.6 | 4.03 | Claystone | |
| Unit VI – Brown claystone and radiolarite; Sections 129-802A-52R-1, 15 cm, to 129-802A-53R-1, 45 cm (460.0–469.9 mbsf) | | | | | |
| 52R | (continued) | | | Claystone; clayey radiolarite | Coniacian-Cenomanian |
| 53R | 469.4–478.6 | 9.2 | 2.59 | Claystone | |
| Unit VII – Calcareous claystone and radiolarian limestone; Sections 129-802A-53R-1, 45 cm, to 129-802A-56R-1, 0 cm (469.9–497.1 mbsf) | | | | | |
| 53R | (continued) | | | Nannofossil chalk; clayey radiolarite | Cenomanian |
| 54R | 478.6–487.9 | 9.3 | 6.50 | Limestone; calcareous claystone | |
| 55R | 487.9–497.1 | 9.2 | 1.48 | Radiolarian limestone | Cenomanian to Albian |
| 56R | 497.1–506.6 | 9.5 | 5.11 | Calcareous claystone | Albian to ?upper Aptian |
| Unit VIII – Claystone and radiolarite; Sections 129-802A-56R-1, 0 cm, to 129-802A-56R-2, 93 cm (497.1–499.6 mbsf) | | | | | |
| 56R | (continued) | | | Claystone; radiolarite | upper Aptian |
| Unit IX – Volcaniclastic turbidites and claystone; Sections 129-802A-56R-2, 93 cm, to 129-802A-57R-2, 112 cm (499.6–509.2 mbsf) | | | | | |
| 57R | 506.6–516.0 | 9.4 | 3.34 | Tuffaceous claystone; volcaniclastic turbidites | ? |
| Unit X – Basalt; Section 129-802A-57R-2, 112 cm, to Core 129-802A-62R (509.2–559.8 mbsf) | | | | | |
| 57R | (continued) | | | Basalt | |
| 58R | 516.0–525.4 | 9.4 | 5.02 | Basalt | |
| 59R | 525.4–534.7 | 9.3 | 3.89 | Basalt | |
| 60R | 534.7–544.2 | 9.5 | 0.96 | Basalt | |
| 61R | 544.2–550.6 | 6.4 | 1.50 | Basalt | |
| 62R | 550.6–559.8 | 9.2 | 3.10 | Basalt | |

clastic sediments at Sites 800 and 801, and from those lower at Site 802.

Lithologic trends in the tuff of Subunit IIA include a decrease in bed thickness downsection, and a less-pronounced decrease in grain size. Lapilli tuff is ubiquitous as a minor lithology. Microfossils were observed only in the tuff of Cores 129-802A-10R to -19R. Miocene foraminifers and nannofossils are abundant in Core 129-802A-10R.

Fractures and voids in Cores 129-802A-7R and -8R, and Coares 129-802A-14R through -18R, are filled with a combination of white zeolites and anhydrite. X-ray-diffraction (XRD) analysis of one fracture filling indicates these zeolites

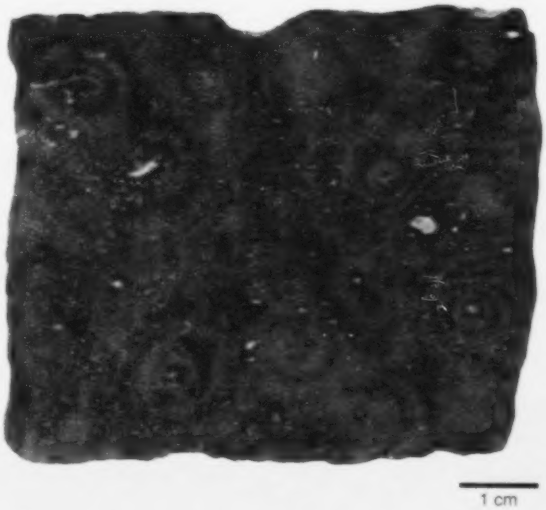

Figure 6. Photograph of lapillistone from tuff Subunit IIA, interval 129-802A-4R-1, 134–141 cm. (Note the subrounded clasts and poor sorting.)

include laumontite, analcime, and some members of the solid solution series between analcime and wairakite, which are calcium-rich varieties. Petrographic inspection shows the intergrowth and successive growth of zeolites and anhydrite (Fig. 8). XRD analysis also indicates the presence of phillipsite in tuff of Sample 129-802A-15R-1, 149 cm.

The tuff, redeposited as grain flows or turbidites, is sharply interbedded in Cores 129-802A-3R, -13R, and -19R with dark brown to greenish gray pelagic claystone. The claystone is massive to very finely laminated where it is not disturbed by drilling, and in Core 129-802A-3R contains up to 35% iron oxides and opaques, up to 15% zeolites, up to 10% volcanic glass, and, in one smear slide, 65% micrite. An agglutinated foraminifer and a trace of nannofossils were noted in single slides. Smear slides from Core 129-802A-13R contain up to 20% nannofossils, 10% volcanic glass, 5% zeolites, 5% iron oxides and opaques, and a few percent radiolarian spines. The claystone in Core 129-802A-19R contains 30% nannofossils, 20% volcanic glass, and only traces of metal oxides. Therefore, a general downhole decrease in the metal component and an increase in nannofossil content are observed. The nannofossil claystone in Core 129-802A-19R also indicates a transition to the nannofossil chalk that characterizes Subunit IIB and Unit III. XRD analyses indicate that the claystone contains various zeolites, clinoptilolite or phillipsite, and accessory minerals, possibly barite and celestite.

The calculated minimum sedimentation rate for Subunit IIA is 11 m/m.y.

*Subunit IIB. Tuff with calcareous claystone and chalk; lower Miocene (Sections 129-802A-19R-2, 0 cm, to 129-802A-27R-2, 81 cm; 160.6–237.41 mbsf)*

Subunit IIB is 76.8 m thick and consists of tuff intercalated with a significant proportion of redeposited calcareous claystone and chalk. The upper and lower boundaries of this subunit are gradational. Tuff is not present in every core, but its presence defines Unit II. The base of Subunit IIB is placed at the lowest occurrence of volcaniclastic sandstone, and the top is placed at the highest occurrence of chalk.

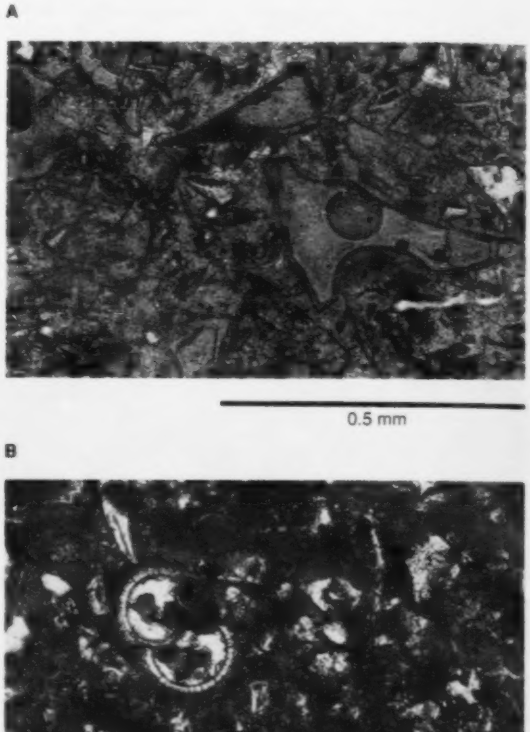

Figure 7. Photomicrographs of thin sections from tuff Subunit IIA. **A.** Sample 129-802A-5R-1, 21–22 cm, plane light, showing cuspate glass shards. **B.** Sample 129-802A-11R-1, 64–66 cm, plane light, showing Miocene foraminifers and volcanic glass. **C.** Sample 129-802A-11R-1, 64–66 cm, plane light, showing rounded lapilli composed of ash in vitric tuff matrix.

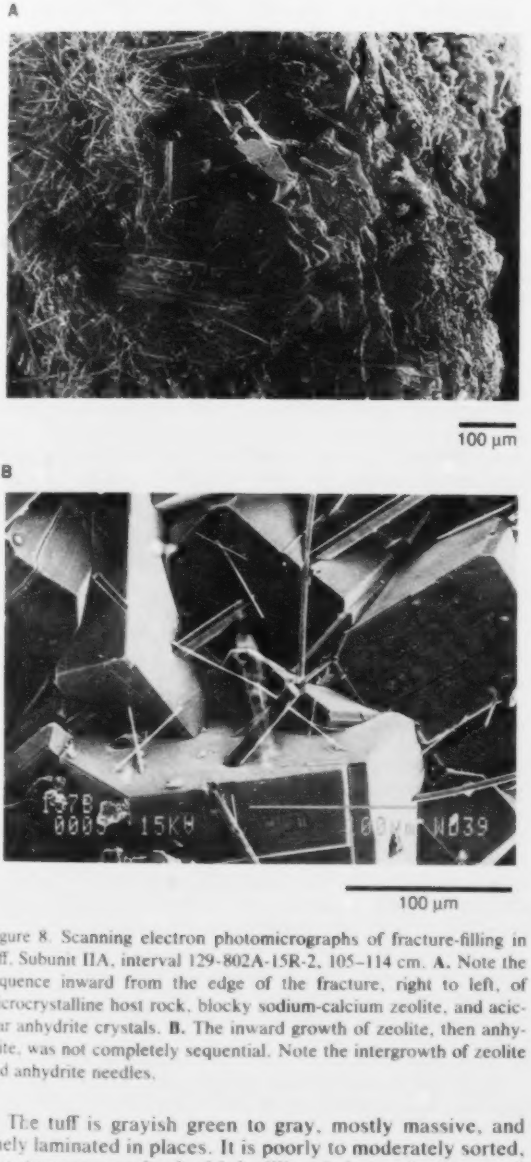

Figure 8. Scanning electron photomicrographs of fracture-filling in tuff, Subunit IIA, interval 129-802A-15R-2, 105–114 cm. **A.** Note the sequence inward from the edge of the fracture, right to left, of microcrystalline host rock, blocky sodium-calcium zeolite, and acicular anhydrite crystals. **B.** The inward growth of zeolite, then anhydrite, was not completely sequential. Note the intergrowth of zeolite and anhydrite needles.

The tuff is grayish green to gray, mostly massive, and finely laminated in places. It is poorly to moderately sorted, fine- to coarse-grained with lapilli and rip-up clasts up to 3 cm in diameter. Massive beds with sharp contacts are mass flows and grain flows (Fig. 9); beds that grade to glass-rich claystone or chalk are turbidites (Fig. 10). Thin sections of the volcaniclastic deposits indicate that Core 129-802A-19R contains crystal vitric tuff consisting of approximately 70% volcanic glass and 5% clinopyroxene, with 20% igneous rock fragments, and a few percent of smectites, secondary calcite, and trace foraminifers. The base of Subunit IIB, in Core 129-802A-27R, is a tuffaceous sandstone that contains about 55% volcanic glass, 10% igneous rock fragments, a trace of clinopyroxene, and about 30% benthic and planktonic foraminifers, bryozoans, red and green algae, nannofossils, and microspar calcite (Fig. 11). There are wood fragments in the core catcher of Core 129-802A-25R.

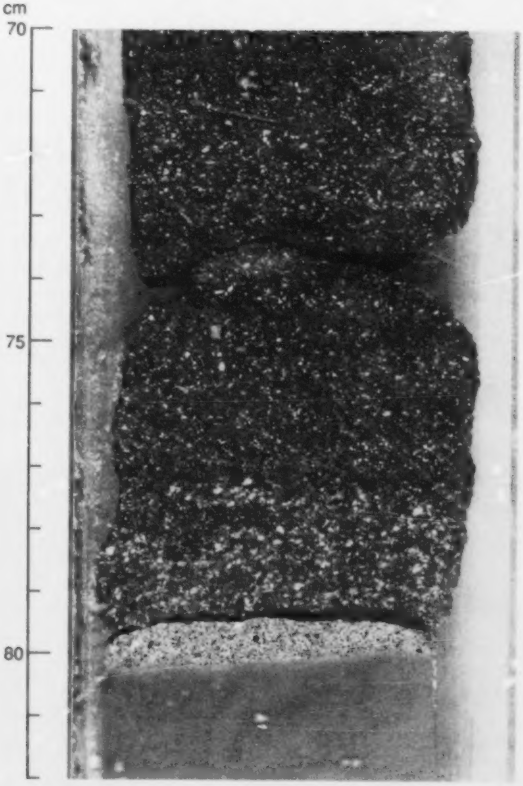

Figure 9. Photograph of contact at base of Subunit IIB, interval 129-802A-27R-2, 70–82 cm. Note 1 cm of alteration to white zeolites at contact, grading, and indistinct laminations in tuff. Below contact is nannofossil chalk of Unit III.

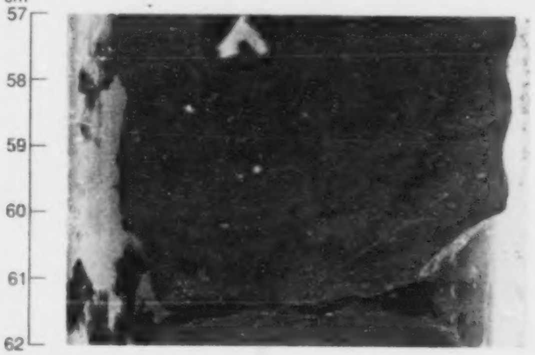

Figure 10. Photograph of tuffaceous turbidites from Subunit IIB, interval 129-802A-19R-2, 57–62 cm, showing flame structures and deformed (convoluted) laminations.

Tuffaceous claystone in Subunit IIB is dark gray to dark greenish gray, consisting of roughly 40% clay, 30% volcanic glass, 15% igneous rock fragments, and 5% nannofossils and calcite. It grades to claystone composed of about 80% clay, 10% volcanic glass, and 10% oxides, opaques, crystals, and igneous rock fragments, or to olive gray clayey chalk composed of 35% clay, 30% nannofossils, 20% secondary calcite, 10% volcanic glass, and 5% igneous rock fragments.

The chalk grades locally to clayey chalk with up to 25% clay and 5% volcanic glass. It is olive gray to pale brown, and contains up to 50% nannofossils, 20% secondary calcite, and 15% clay, with a few percent volcanic glass, radiolarians, foraminifers, fish remains, and zeolites. The chalk is found in Core 129-802A-19R and from Core 129-802A-24R to -27R in Subunit IIB, and is thus more prevalent near the basal contact with the underlying chalk (Unit III). The chalk is massive, moderately bioturbated, and contains up to 10% angular to subrounded rip-up clasts up to 1 cm long of moderate yellowish brown calcareous claystone, indicating that it consists predominantly of redeposited pelagic sediments.

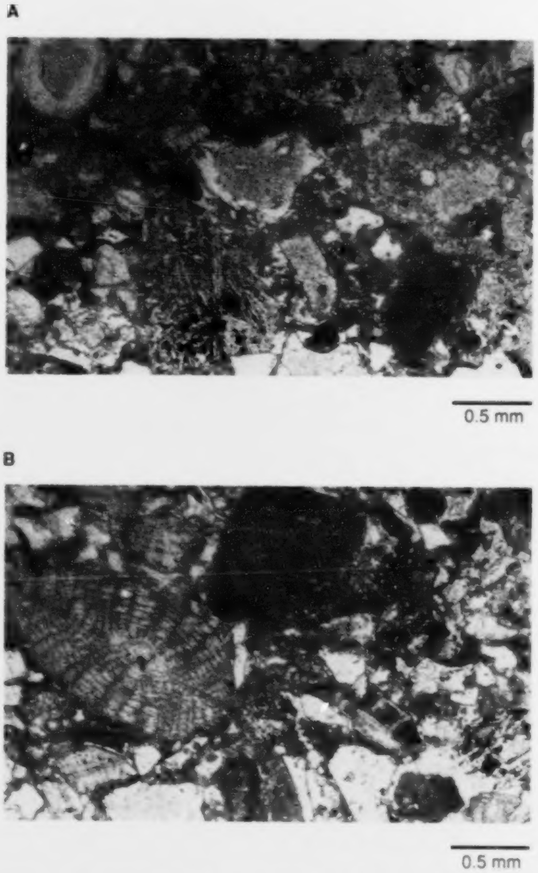

Figure 11. Photomicrographs of thin section from base of Subunit IIB. **A.** Sample 129-802A-27R-2, 73–78 cm, plane light, showing igneous rock fragment and shallow-water carbonate debris, including red algae, echinoderm fragments, and coated grain. **B.** Photomicrograph in plane light showing bryozoans, foraminifers, and other shallow-water carbonate debris, tachylite, and igneous rock fragments.

The calculated minimum sedimentation rate for this unit is 15 m/m.y.

### *Unit III. Section 129-802A-27R-2, 81 cm, to Core 129-802A-36R (237.4–329.9 mbsf): Nannofossil Chalk; lower Miocene to upper Paleocene*

Unit III is a 92.5-m-interval of nannofossil chalk with foraminifers and minor amounts of interbedded foraminiferal chalk, claystone, porcellanite, and nodular chert. As tuff and chalk are intercalated throughout much of Subunit IIB, the top of Unit III is placed at the base of the lowest tuffaceous turbidite. The base of this unit is set between the lowest chalk and the top of the nearly continuous claystone of Unit IV. Unit III is thickly bedded, with beds ranging from 10 cm to 5.5 m, most of which are between 50 and 80 cm thick. Many strata are graded, with thinly laminated or cross-laminated bases defined by foraminiferal fragments. Bioturbation is common throughout, with burrows especially numerous near the top of beds. The chalk contains many small flakes or clasts of claystone or mudstone. Bedding characteristics and mixed assemblages of Late Cretaceous through Oligocene nannofossils suggest that these chalks are redeposited and reworked nannofossil oozes, not *in-situ* pelagic deposits.

The nannofossil chalk trends from light brown to light grayish brown in Cores 129-802A-27R to -33R, to light gray to pinkish white in Cores 129-802A-34R to -36R. The change in color at Core 129-802A-33R corresponds with a downhole increase in silica and a change in associated minor lithologies from zeolitic claystone (upper half) to nodular chert (lower half). An Oligocene through Eocene hiatus was recognized between Sections 129-802A-32R-CC and 129-802A-33R-CC on the basis of nannofossils and foraminifers (see "Biostratigraphy" section, this chapter). Foraminifers are common in the chalk, usually comprising 5%–20%, and locally up to 35% of the sediments, in which case it is designated foraminiferal chalk (Fig. 12A, -B). Thinly laminated (millimeter- to centimeter-scale) chalk turbidites toward the base of the unit are composed of foraminifer-rich layers overlying micrite-rich layers with exceedingly small (1 mm high) flame structures (Fig. 13). Hard silicified chalks with subconchoidal fractures that are present in Cores 129-802A-35R and -36R contain 10%–25% replacement microquartz.

Thinner beds, 5 to 50 cm thick, of dark brown zeolitic claystone are interbedded with the nannofossil chalk in the upper half of this unit (237.4–284.3 mbsf). The claystone is extensively bioturbated, and claystone fills burrows in the tops of underlying, lighter-colored chalk beds (Fig. 14). Smear slides show that the claystone contains 50%–80% clay, 10%–30% zeolites, up to 10% volcanic glass and oxides, and a few percent radiolarians or nannofossils. The complete bioturbation of chalk and zeolitic claystone in Core 129-802A-29R produced some nearly homogeneous beds of light yellowish brown nannofossil claystone.

Chert comprises less than 3% of the total recovery of Unit III, and occurs as scattered nodules only in the lower portion of the unit, from 293 to 321.7 mbsf. The chert is dark brown to dark red to olive gray, with a vitreous luster and conchoidal fracture. Chert nodules have sharp, irregular contacts with the nannofossil chalk. They contain abundant calcareous inclusions and usually reflect the locally massive or laminated structure of the host chalk. Only a few pieces of porcellanite were recovered in Core 129-802A-32R, immediately above the hiatus in the upper part of the unit.

Cores 129-802A-27R and -28R are distinguished by the thickest single bed recovered in the unit: a 5.5-m graded bed that fines upward from a grain-supported algal foraminiferal packstone to a matrix-supported nannofossil chalk (base of

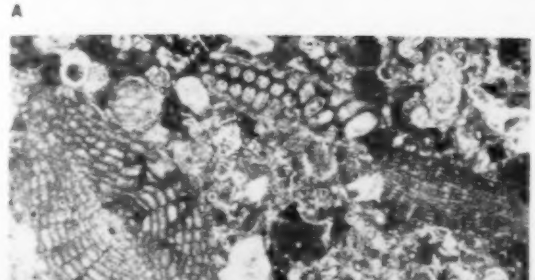

Figure 12. **A.** Photomicrograph of thin section from Unit III, Sample 129-802A-28R-3, 117–122 cm, plane light, showing algal foraminiferal packstone with foraminifers, bryozoans, and other shallow-water carbonate debris. **B.** Photomicrograph of thin section from the base of Unit III, Sample 129-802A-36R-1, 61–63 cm, plane light, showing a lamination of densely packed, broken foraminifers in chalk turbidite.

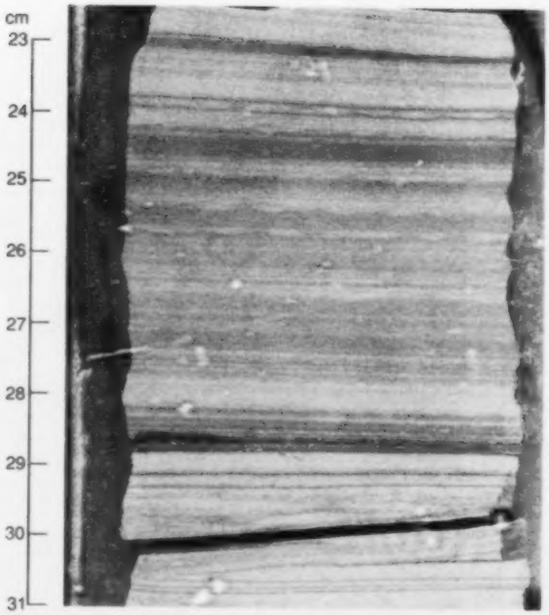

Figure 13. Photograph of thinly laminated chalk turbidites from the base of Unit III, interval 129-802A-36R-1, 23–31 cm. Light laminations are foraminifer-rich; darker laminations are dominantly micrite.

Core 129-802A-28R to Section 129-802A-27R-5, 100 cm). The very coarse-grained lower half is composed chiefly of neritic benthic foraminifers and red algae, along with planktonic foraminifers (see "Biostratigraphy" section, this chapter), bryozoans, echinoid fragments, and volcanic rock fragments in a nannofossil and micrite matrix (Fig. 12A). The upper part of the bed is a deformed, horizontally sheared nannofossil chalk with abundant fine-grained rip-up clasts and incorporated coarse-grained carbonate material similar to that found at the base of the bed (Fig. 15). This very thick gravity-flow deposit directly underlies the mixed tuffaceous/bioclastic turbidites at the base of Subunit IIB.

The calculated minimum sedimentation rate is about 12 m/m.y. above the Oligocene through Eocene hiatus, and about 7 m/m.y. below.

#### *Unit IV. Core 129-802A-37R through Section 129-802A-39R-1, 45 cm (329.9–349.2 mbsf) Claystone; Paleocene to upper Campanian*

Unit IV consists of 19.3-m beds of zeolitic pelagic claystone and calcareous nannofossil silty claystone with minor porcellanite, chert, and calcareous siltstone or sandstone. The top of this unit is placed below the lowermost chalk bed; the lower boundary is set at the top of the highest occurrence of Cretaceous volcaniclastics. The upper part of this unit (329.9–345.8 mbsf) contains interbedded zeolitic pelagic claystone and calcareous siltstone or sandstone. The pelagic claystone is very similar to that of Unit I, containing 15%–40% zeolites and 3%–10% radiolarian spines and tests, with the remainder made up of aggregates of clay and iron-manganese oxyhydroxides; it is mottled light brown to gray. This entire section is thinly laminated and burrowed. Layers of thinly laminated, gray and black calcareous siltstone or sandstone, 2 to 5 cm thick, or millimeter-scale interlaminated sandstone and claystone, make up the graded bases of pelagic claystone beds. Flame structures, basal cross-lamination, and convolute layering indicate that the coarser-grained material was redeposited. Silt and sand grains are composed of foraminifers, volcanic material, and some radiolarians. One piece of pale yellowish brown chert (silicified claystone) was recovered in Core 129-802A-37R.

The lower section of Unit IV (345.8–349.2 mbsf) is composed of calcareous nannofossil silty claystone and porcellanite. The brown to olive gray silty claystone is massive to thinly laminated with some small flame structures, distinctly lacking in burrows, and composed of 10%–25% nannofossils and 5%–10% micrite. The porcellanite is reddish brown, thinly laminated, and contains scattered dark grains of metal oxides.

The calculated minimum sedimentation rate of 2 to 4 m/m.y. for this unit probably reflects a Paleocene through upper Campanian hiatus.

#### *Unit V. Sections 129-802A-39R-1, 45 cm, to 129-802A-52R-1, 15 cm (349.2–460.0 mbsf): Volcaniclastic Turbidites; upper Campanian to Coniacian-Cenomanian*

Unit V is 110.8 m thick and consists of volcaniclastic grain flows and turbidites that grade up into pelagic claystones

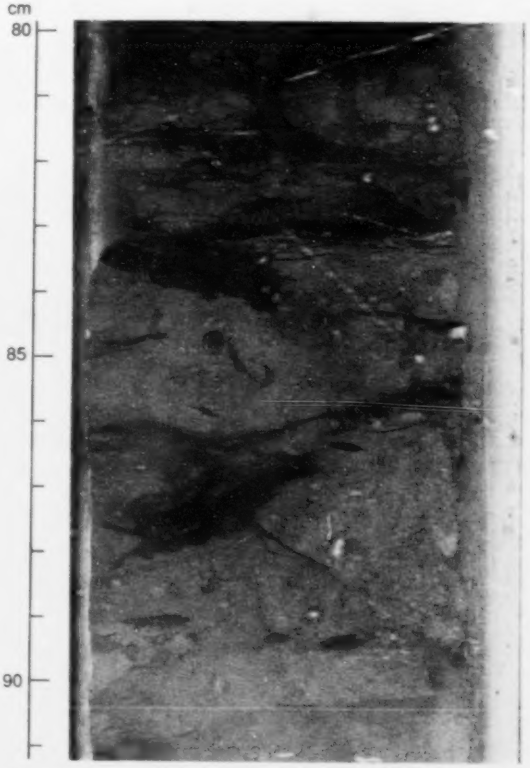

Figure 14. Photograph of burrows at the top of chalk turbidite filled with pelagic clay from Unit III, interval 129-802A-32R-1, 80–91 cm.

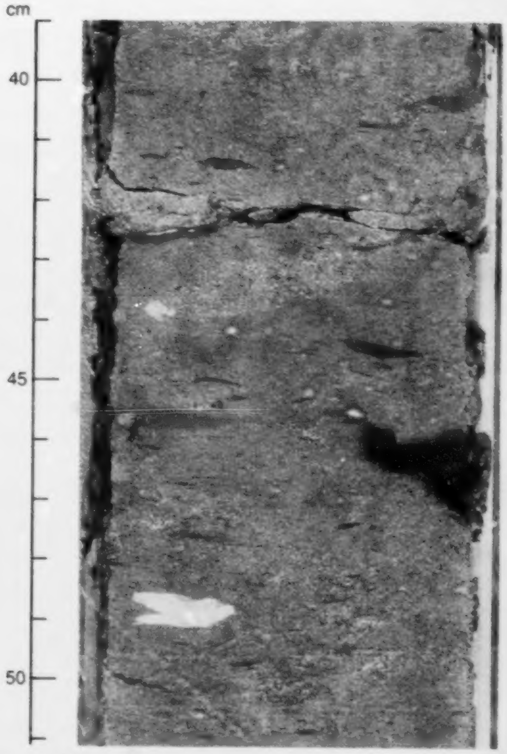

Figure 15. Photograph of chalk debris flow deposit from top of Unit III, interval 129-802A-27R-5, 39–51 cm, showing matrix-supported fragments of claystone and coarser-grained carbonate material.

containing both radiolarians and nannofossils. The top of the unit is placed at the level of the highest tuffaceous sandstone bed in Core 129-802A-39R, which also corresponds to a downward color change from green to brown and gray. The base of the unit is placed at the lowermost claystone that still contains significant amounts of volcanic glass. It corresponds to a downhole color change from green (Unit V) to brown (Unit VI). Both unit boundaries are gradational.

The volcaniclastic sandstones, siltstones, and claystones in Unit V are generally dark blue-gray to greenish gray. The lowest beds in the unit are debris flow deposits composed of pebbly claystone up to several meters thick. These give way upsection to coarser-grained (silty and sandy) but thinner-bedded turbidites (Fig. 16). The turbidites vary from 10 cm to 1 m thick; there are no overall stratigraphic trends of thinning or fining upward in this unit. The turbidites are characterized by sedimentary structures such as graded beds with basal scour, flame structures or load casts, planar- and cross-laminations, convolute layers (Fig. 17), and rip-up clasts. Some beds are bioturbated. The pelagic claystones between turbidite beds are finely laminated to massive.

The volcaniclastic sandstones include some tuff, but are mostly tuffaceous sandstones with abundant, rounded igneous rock fragments of unknown derivation. A thin section of tuffaceous sandstone in Sample 129-802A-39R-1, 52–55 cm (Fig. 18A), contains roughly 60% volcanic glass and palagonite, 15% igneous rock fragments, 10% iron oxides and opaques, 5% clinopyroxene, 5% feldspar, and a few percent each of secondary calcite, smectites, radiolarians, and red algae. Tuffaceous claystones in the unit contain up to 35% volcanic glass and 15% igneous rock fragments, a few percent radiolarians and/or nannofossils, and as much as 25% secondary calcite. These tuffaceous claystones grade to pelagic claystones containing up to 20% radiolarians or nannofossils (Fig. 18B). A clayey radiolarite in Sample 129-802A-51R-3, 14 cm, marks a transition to the underlying claystone and radiolarite unit. A rip-up clast of radiolarite in the debris flow in Sample 129-802A-49R-3, 25 cm, is probably derived from the underlying unit. At the top of the unit, in Sample 129-802A-39R-1, 64–89 cm, is the only clayey chalk in Unit V, consisting of 60% nannofossils, 25% clay, 5% volcanic glass, and a few zeolites. This chalk is overlain by 10 cm of tuffaceous claystone with 15% radiolarians, in turn overlain by the uppermost tuffaceous sandstone in the unit. The chalk marks a transition to the overlying claystone and nannofossil chalk units.

Diagenetic minerals in Unit V include various zeolites which are present in both the sandstones and claystones. The claystone also contains rather remarkable blades of celestite(?), up to 6 mm long, in interval 129-802A-49R-4, 59–72 cm, and green spherules composed of celadonite or glauconite in Sections 129-802A-41R-2 and 129-802A-41R-3. The volcanic glass in the sandstones is 30% to 50% palagonitized; volcanic glass in the claystones is almost entirely palagonitized.

The calculated minimum sedimentation rate is 9 m/m.y., with a probable brief hiatus in the lower Campanian.

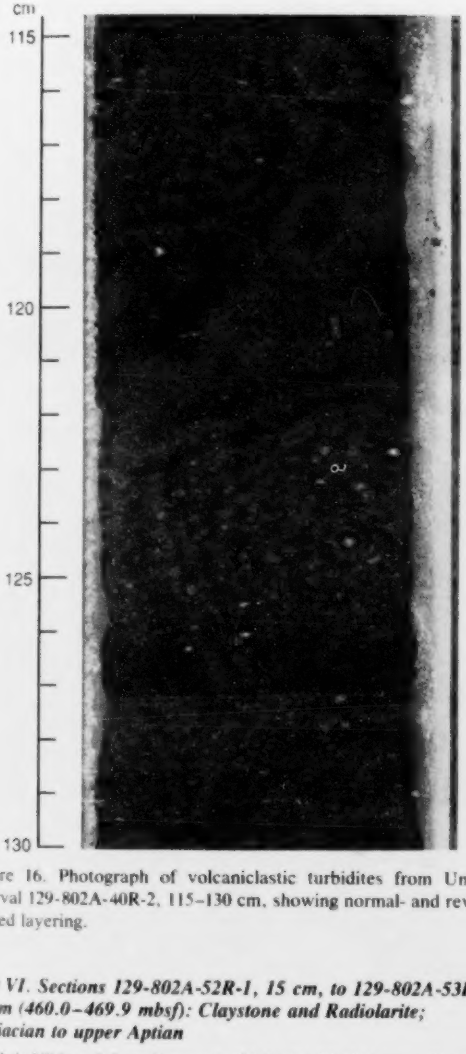

Figure 16. Photograph of volcaniclastic turbidites from Unit V, interval 129-802A-40R-2, 115–130 cm, showing normal- and reverse-graded layering.

### *Unit VI. Sections 129-802A-52R-1, 15 cm, to 129-802A-53R-1, 45 cm (460.0–469.9 mbsf): Claystone and Radiolarite; Coniacian to upper Aptian*

Unit VI is a 9.9-m-interval of interbedded brown claystone and radiolarite. The top of the unit is placed between the lowermost bluish gray volcaniclastic deposits and the uppermost reddish brown claystone; the base of the unit is set at the top of the underlying nannofossil chalk. Both lower and upper boundaries are gradational.

The reddish brown to dark brown claystone occurs in thick, mostly massive beds (40 to 125 cm thick; 65 cm is average), and is thinly interlayered with radiolarite. The claystone has a composition similar to pelagic clay, containing approximately 70% clay, 30% iron-manganese oxides, minor zeolites, and minor radiolarians concentrated in some layers, which provide a locally slightly sandy texture. Thin (<1 mm), discontinuous black layers, producing a distinct horizontal fabric in the interval 129-802A-52R-1, 80–140 cm, are composed of up to 50% iron-manganese oxides. Centimeter-scale, light green reduction halos surround a few dark green, pyritic concretions, 1-2 mm in diameter.

Radiolarite occurs as laminations to thin beds that are 0.3–4.0 cm thick, light grayish green to light brown, and interlayered with claystone. The radiolarite contains trace to abundant (50%) clay, with the radiolarians providing a friable, sandy texture (Fig. 19). Contacts with the claystone are mostly sharp, but some are gradational (Fig. 20). The inferred, relatively high permeability of the radiolarite layers may control the location of greenish bands of reduction that occasionally blossom discordantly outward into the neighboring claystone.

The calculated minimum accumulation rate for Unit VI is 2 m/m.y.

### *Unit VII. Sections 129-802A-53R-1, 45 cm, to 129-802A-56R-1, 0 cm (469.9–497.1 mbsf): Calcareous Claystone and Radiolarian Limestone; Cenomanian to upper Aptian*

Unit VII is a 27.2-m-thick interval of predominantly calcareous lithologies, chiefly radiolarian limestone, nannofossil chalk, and calcareous claystone, with minor clayey sandstone, radiolarite, porcellanite, and chert. This unit contains fine-grained calcareous turbidites and radiolarian silty sand layers. Bedding is quite variable, ranging from 2 to 135 cm thick, averaging 35 cm thick. Beds range from laminated to massive; many are gently graded with burrowed tops. Turbiditic deposition is chiefly indicated only by a color change to darker clay-rich tops and by sharp bedding contacts (Fig. 21). The boundaries of this unit are placed at the highest and lowest occurrences of carbonate rocks.

The limestone is dark brown to light gray to bluish gray, and contains 10%–35% clay, 10%–30% nannofossils, and 5%–25% calcitized radiolarians. Some of the limestone is silicified, especially where it is adjacent to brown chert and pinkish gray porcellanite in Cores 129-802A-54R and -55R, respectively.

The nannofossil chalk varies widely in composition, with 40%–70% nannofossils, 5%–25% clay, 7%–15% volcanic glass, and up to 5% foraminifers. The chalk is light brown to pinkish brown, mostly massive to thinly laminated, in graded beds with sharp, sometimes scoured bases. The calcareous claystone occurs in numerous shades of grayish blue and green; it is thinly laminated and displays few burrows. The claystone contains 20% nannofossils, 15% micite and calcite, and a few percent foraminifers and radiolarians.

Brown to light reddish brown radiolarite, and bluish gray to greenish gray clayey siltstone and sandstone, make up thin, 2-cm-thick layers between limestone or claystone beds. The coarser texture of the clayey siltstone and sandstone is derived from the presence of foraminifers, radiolarians, volcanic glass, and zeolites. All lithologies are thinly laminated, but the siltstone and sandstone often have sharp, scoured bases, and the radiolarite layers commonly have gradational clay-rich upper and lower boundaries.

A minimum accumulation rate is calculated for Units VII, VIII, and IX together because the resolution of the biostratigraphy is inadequate for discrete calculations for individual units. The average accumulation rate for this lowest part of the stratigraphic section is low, approximately 1.5 m/m.y.

### *Unit VIII. Sections 129-802A-56R-1, 0 cm, to 129-802A-56R-2, 93 cm (497.1–499.6 mbsf): Claystone and Radiolarite; Cenomanian to upper Aptian*

Unit VIII is contained entirely in Core 129-802A-56R and is composed of 2.4 m of claystone with thin interbeds of radiolarite. The unit is bounded by carbonates above and volcaniclastic turbidites below.

The claystone is light brown to dusky yellowish brown, pervasively thinly laminated, with common burrows. It is hematitic, containing 10%–25% iron oxides, up to 10% zeolites, as well as abundant dark metalliferous nodules (sometimes with pyrite), 1–2 mm in diameter. The occurrence of these nodules shows some association with bioturbation.

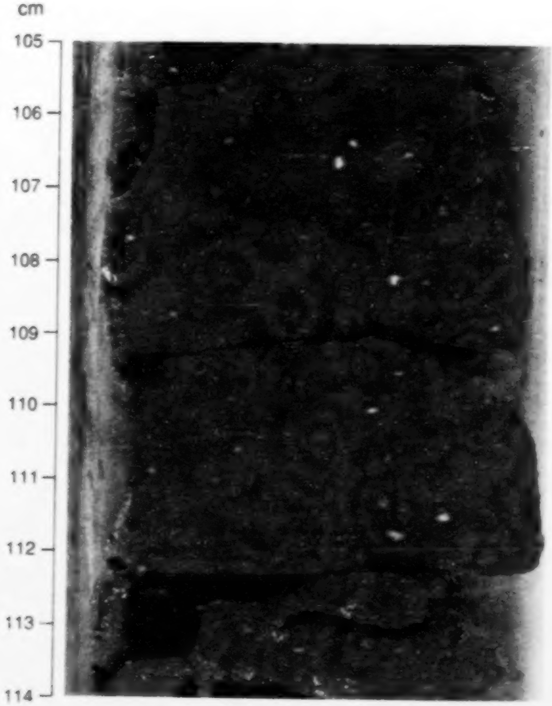

Figure 17. Photograph of deformed (convolute) layers in fine-grained volcaniclastic turbidites from Unit V, interval 129-802A-15R-2, 105–114.

Radiolarite beds, 1 to 4 cm thick, are scattered through the claystone (Fig. 22), making up about 10% of the recovered interval. The radiolarite is light to moderate brown and friable, with a medium-grained sandy texture. Layers are sometimes graded, with sharp tops and bottoms, but not with scoured bases. Interval 129-802A-56R-2, 80–83 cm, is reduced and bleached to olive green.

### *Unit IX. Sections 129-802A-56R-2, 93 cm, to 129-802A-57R-2, 112 cm (499.6–509.2 mbsf): Volcaniclastic Turbidites and Claystone; Cenomanian to upper Aptian*

Unit IX is 9.6 m thick and consists of volcaniclastic turbidites and tuffaceous claystone, with minor radiolarite. The top of the unit is placed at the highest occurrence of green, volcaniclastic material; the base of the unit is placed at a sharp depositional contact on pillow basalt. Both unit boundaries are sharp, but the presence of radiolarite in Sections 129-802A-56R-3 and 129-802A-56R-4 links Unit IX environmentally with Unit VIII (claystone and radiolarite).

The volcaniclastic turbidites consist of 2- to 25-cm-thick beds of tuffaceous sandstone grading to radiolarian claystone. The turbidites have sharp, scoured bases and are pervasively bioturbated. The tuffaceous claystone is finely laminated to massive, and commonly burrowed (Fig. 23). The turbidites are greenish gray to dusky green and composed of igneous rock fragments, volcanic glass, smectites, opaques, a trace of nannofossils, and up to 20% radiolarians. The tuffaceous claystone is brownish black to black, and contains approximately 50% volcanic glass, abundant smectites, and minor amounts of igneous rock fragments and metal oxides or opaques.

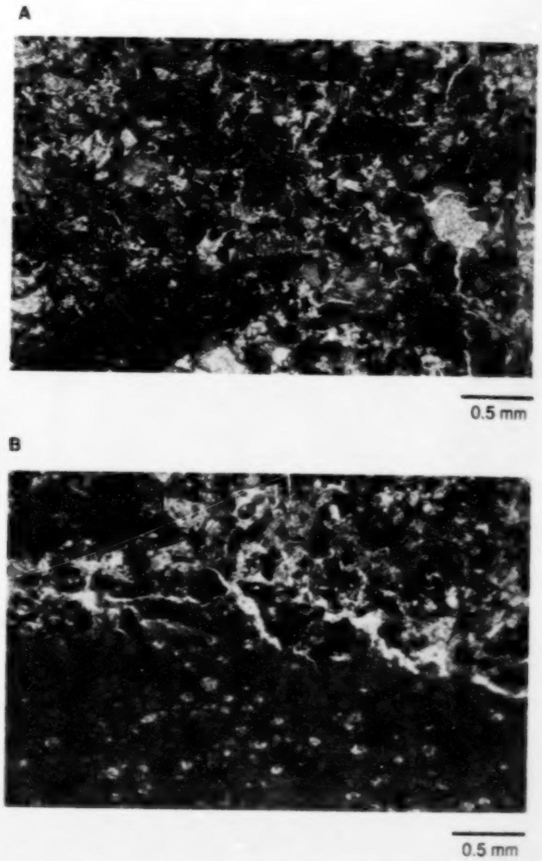

Figure 18. **A.** Photomicrograph of volcaniclastic sandstone thin section from Unit V, Sample 129-802A-39R-1, 52–55 cm, plane light, showing poorly sorted volcanic rock fragments and palagonite. **B.** Photomicrograph of same thin section showing contact of volcaniclastic sandstone above radiolarian claystone, with zeolitic alteration at contact.

Radiolarite intercalated with the tuffaceous claystone is light to moderate brown, and locally reduced to olive green. The beds are planar, laminated, with sharp (but not scoured) contacts, and subtly graded. The laminations, together with the low clay content, suggest deposition by currents and possible winnowing of fines.

Diagenetic features in Unit IX include prolific crystallization of dark green clay minerals in burrows within the turbidites, silicification of the radiolarian-rich tops of the turbidite beds, and convoluted and faulted calcite veins in the tuffaceous claystone.

### *Unit X. Section 129-802A-57R-2, 112 cm, to Core 129-802A-62R (509.2–559.8 mbsf): Basalt; upper Aptian(?)*

Unit X is a 50.6-m-thick series of thin (<1–2 m thick) basaltic pillow lava units and one thin (4 m thick) basaltic flow unit. Seventeen units are described in the "Igneous Petrology" section (this chapter). Alteration is slight and dominated by smectites, carbonate, and pyrite, characteristic of low-

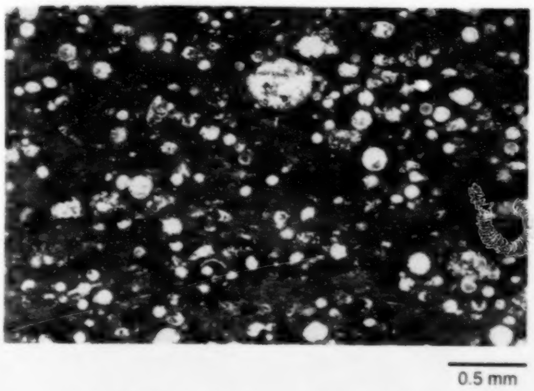

Figure 19. Photomicrograph of siliceous clayey radiolarite from Unit VI, Sample 129-802-53R-1, 4–6 cm, showing matrix-supported texture.

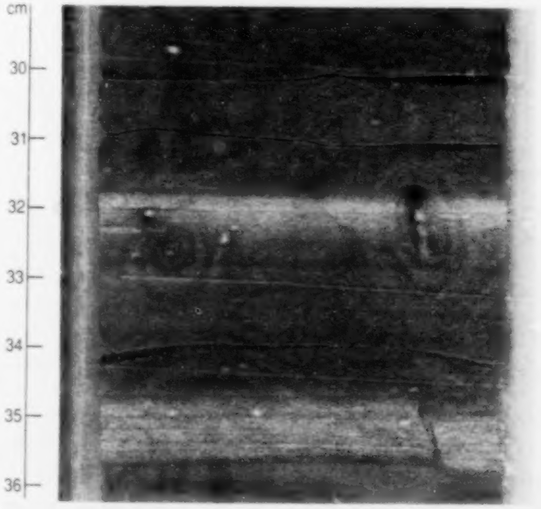

Figure 20. Photograph of alternating radiolarite and claystone layers in Unit VI, interval 129-802A-52R-2, 30–36 cm, showing sharp contacts and laminations in radiolarite.

grade, submarine "weathering" under mildly alkaline, reducing conditions.

### Sedimentology

Sedimentological observations and their implications are presented below in chronological order, or from the base of Hole 802A to the top, and followed by a brief sedimentation history of this site. The Cretaceous basaltic flows at the base of the hole may overlie older sedimentary deposits, so the history presented here could represent only the later history of the eastern Mariana Basin.

The main implications of sedimentary features observed at Site 802 include the following:

1. The stratigraphic section at Site 802 is dominated by redeposited material.

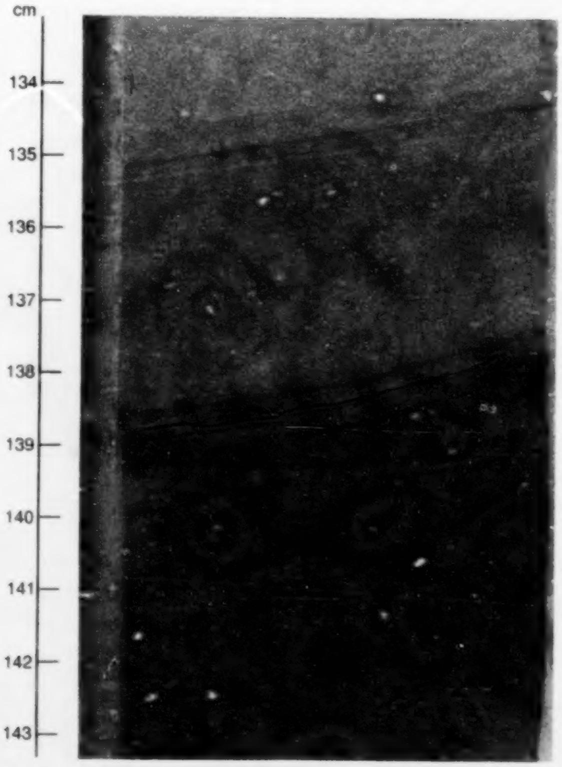

Figure 21. Photograph of calcareous claystone and radiolarian limestone turbidites of Unit VII, interval 129-802A-54R-1, 134–143 cm.

2. Since middle Cretaceous time the background sedimentation of the Mariana Basin (Fig. 1) has been pelagic, frequently interrupted by redeposited volcaniclastic material derived from sporadic volcanic activity in the general vicinity, and by intermittent calcareous or siliceous turbidites made up of redeposited pelagic biogeneous material.

3. Comparison of thicknesses of correlative lithologies from other DSDP holes drilled in this area indicate that chalk deposits in the eastern part of the Mariana Basin may have been transported from the northeast during the Late Cretaceous through the Eocene, and volcaniclastics from the south to southeast during the Miocene.

4. Volcaniclastic sediments from both the Cretaceous and Miocene contain shallow-water carbonate debris and wood fragments, indicating that the source seamounts were at least temporarily above sea level.

5. Site 802 was located in very deep water, well below the carbonate compensation depth (CCD), from the middle Cretaceous to the present. The only preserved calcareous- or radiolarian-rich sediments were redeposited from higher elevations as turbidites, and preserved by rapid burial.

6. From the middle Cretaceous to the present, while Site 802 drifted northward from approximately 15°S to 12°N latitude (see "Paleomagnetism" section, this chapter), the background (nonturbiditic) sedimentation changed from pure clay to clay with radiolarians, to clay with few radiolarians and nannofossils (nearest the equator), to clay with radiolarians, and finally to clay rich in metal oxides and opaques.

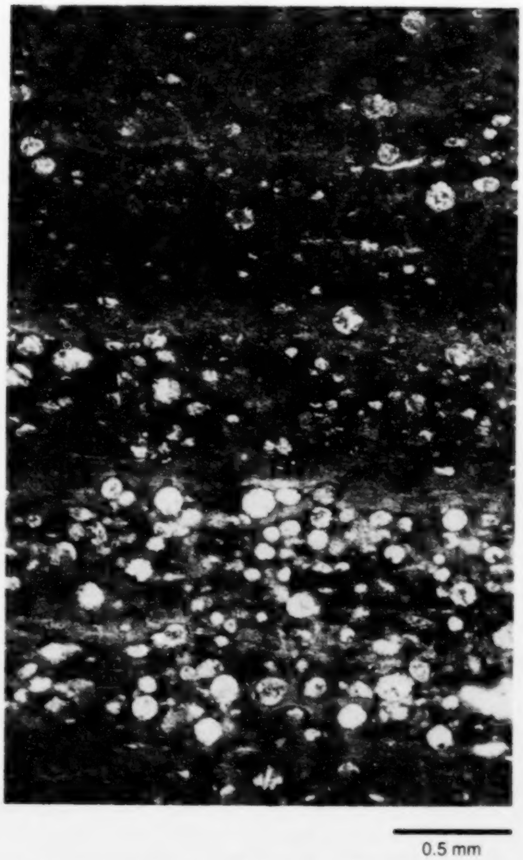

Figure 22. Photomicrograph of laminated claystone and radiolarite from Unit VIII, Sample 129-802-56-1, 55–56 cm.

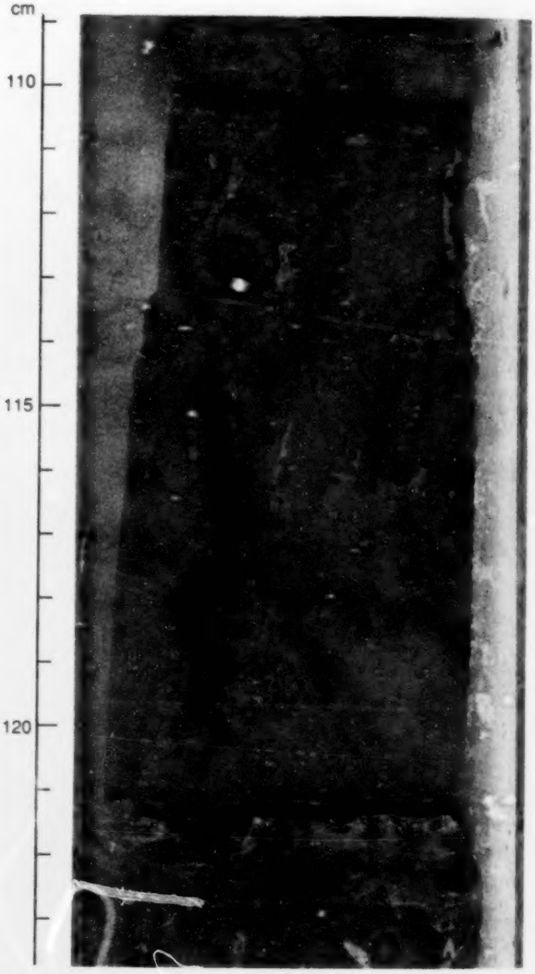

Figure 23. Photograph of volcaniclastic turbidite from Unit IX, interval 129-802A-56R-2, 109–123 cm. Note graded beds and smectite(?)-filled burrows. Bed tops grade to silicified radiolarian claystone.

7. The most abundant redeposited chalks correspond to the time of equator crossing, and these chalks contain chert nodules, signifying the presence of siliceous as well as calcareous plankton.

8. Bottom waters were mildly oxidizing after the middle Cretaceous.

### *Implications of Sedimentary Features Observed in Each Lithostratigraphic Unit*

#### *Upper Aptian(?) to Cenomanian Volcaniclastic Turbidites and Claystone (Unit IX)*

The base of Unit IX is marked by a depositional contact of tuffaceous turbidites 3–8 cm thick on pillow basalt. Grain size and bed thickness suggest that these deposits are probably distal to their source. Their age relation to the underlying basalt flows is unknown. Volcanic activity that produced seamounts and volcaniclastic turbidites of similar age was noted at Site 585 (Moberly, Schlanger, et al., 1986), located to the northeast of Site 802 (Figs. 23 and 24). Volcaniclastic turbidites at Site 801 are pre-Albian to mid-Cenomanian (see "Site 801" chapter, this volume), and thus overlap in age with Unit IX of Site 802 (Figs. 2 and 25).

The tuffaceous turbidites grade upward into a tuffaceous claystone that dominates the unit. The claystone is extremely dark brown to black in color, suggesting low oxygen conditions. The claystone contains a few obvious burrows, and its massive character may be due to homogenization by bioturbation; the underlying turbidites contain burrows as well. Chemical analyses (Table 3) of the dark claystones indicate extremely low organic carbon content, whereas yellow sulfur blooms suggest that the dark, reduced color may be derived from finely disseminated iron sulfides. The presence of pollen and wood fragments in the claystone suggests that some of the seamounts in the vicinity had formed islands.

During the middle Albian, Site 802 may have been at approximately 15°S latitude, which would be an area of low surface productivity. Few microfossils were observed in the tops of the tuffaceous turbidites, although this site was well below the CCD at this time (with a depth calculated according to the thermal subsidence curve of Parsons and Sclater (1977) and Marty and Cazenave (1989), assuming a basement

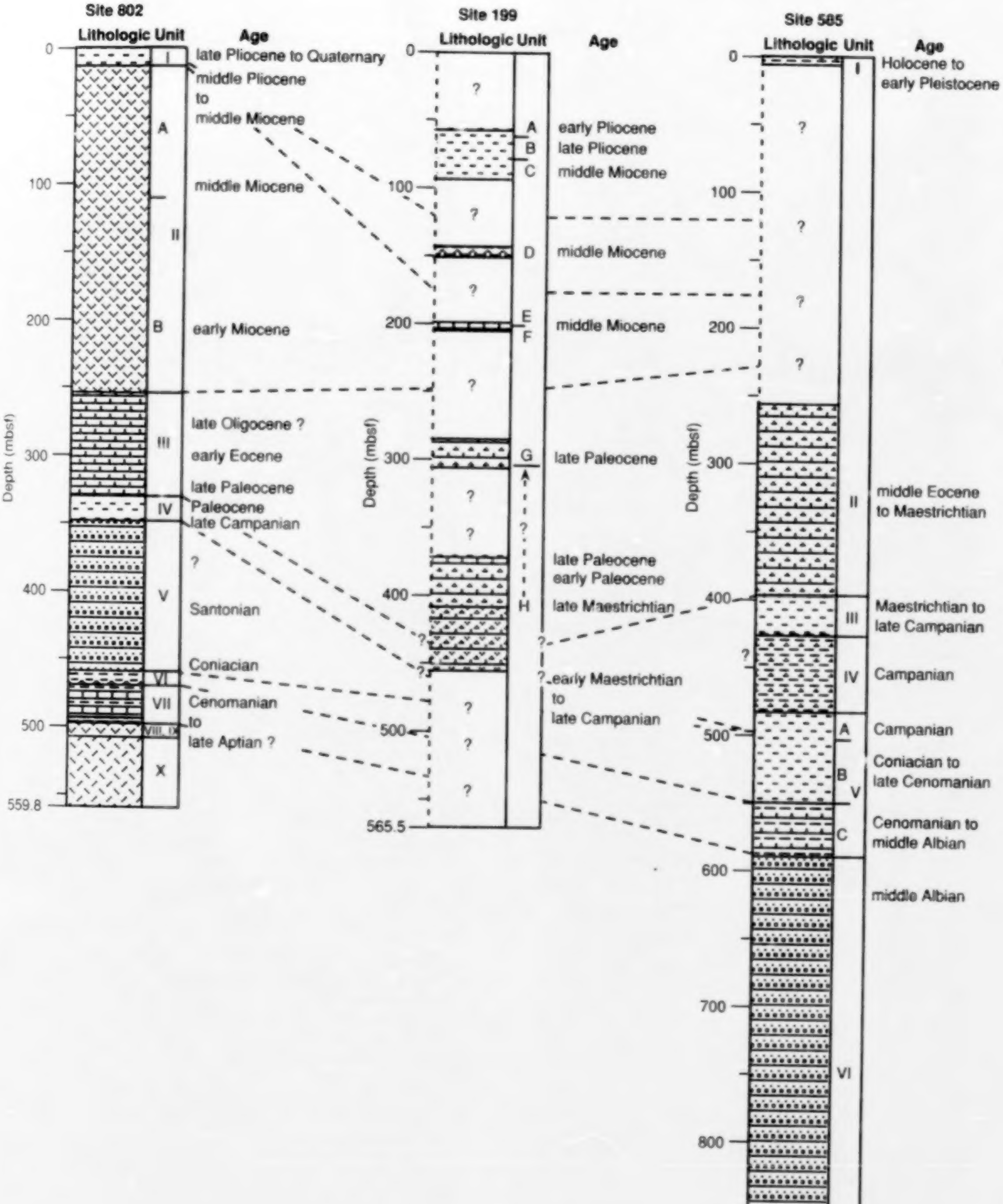
Site 802
Lithologic Unit
Age
0
100
200
300
400
500
559.8
Depth (mbsf)
I
A
II
B
III
IV
V
VI
VII
VIII, IX
X
late Pliocene to Quaternary
middle Pliocene
to
middle Miocene
middle Miocene
early Miocene
late Oligocene ?
early Eocene
late Paleocene
Paleocene
late Campanian
?
Santonian
Coniacian
Cenomanian
to
late Aptian ?
Site 199
Lithologic Unit
Age
0
100
200
300
400
500
565.5
Depth (mbsf)
?
A
B
C
D
E
F
G
H
early Pliocene
late Pliocene
middle Miocene
middle Miocene
middle Miocene
late Paleocene
late Paleocene
early Paleocene
late Maestrichtian
early Maestrichtian
to
late Campanian
Site 585
Lithologic Unit
Age
0
100
200
300
400
500
600
700
800
892.8
Depth (mbsf)
I
II
III
IV
A
B
C
V
VI
?
Holocene to
early Pleistocene
middle Eocene
to Maestrichtian
Maestrichtian to
late Campanian
Campanian
Campanian
Coniacian to
late Cenomanian
Cenomanian to
middle Albian
middle Albian
late Aptian

Figure 24. Lithologic correlation diagram for Site 802, and for DSDP Sites 199 and 585. Lithologic symbols are explained in Figure 5.

Table 3. Calcium carbonate and organic carbon of samples from Hole 802A.

| Core, section, interval (cm) | Depth (mbsf) | $CaCO_3$ (wt%) | Organic carbon (wt%) | Lithology |
|---|---|---|---|---|
| 129-802A- | | | | |
| 3R-1, 21–23 | 14.81 | 0.2 | | Tuff (sand) |
| 3R-1, 110–113 | 15.70 | 0.3 | | Pelagic brown clay |
| 4R-1, 140–150 | 25.70 | 10.0 | | Tuff (silty sand) |
| 4R-2, 6–8 | 25.86 | 33.1 | | Volcaniclastic breccia |
| 4R-2, 86–88 | 26.66 | 0.2 | | Volcaniclastic sandy |
| 5R-1, 126–128 | 34.96 | 0.3 | | Tuff (sand) |
| 6R-2, 0–10 | 44.40 | 0.7 | | Tuff (silty sand) |
| 6R-2, 60–62 | 45.00 | 0.6 | | Volcaniclastic sandstone |
| 7R-1, 101–103 | 53.41 | 0.8 | | Volcaniclastic sandstone |
| 8R-2, 41–43 | 63.81 | 0.8 | | Tuffaceous silty sandstone |
| 10R-1, 69–71 | 81.09 | 1.5 | | Tuff (sand) |
| 10R-2, 140–150 | 83.30 | 1.8 | | Tuff (sand), foraminifers |
| 11R-2, 10–12 | 91.20 | 2.5 | | Tuff (sand) |
| 12R-1, 7–9 | 98.97 | 1.0 | | Volcaniclastic sandstone |
| 13R-1, 47–49 | 108.77 | 0.3 | | Pelagic brown clay |
| 13R-1, 53–58 | 108.83 | 0.5 | | Pelagic brown clay |
| 14R-2, 73–75 | 116.63 | 0.5 | | Volcaniclastic sandstone |
| 15R-2, 37–39 | 123.97 | 1.0 | | Volcaniclastic sandstone |
| 16R-1, 108–110 | 132.18 | 0.9 | 0.01 | Volcaniclastic sandstone |
| 17R-1, 36–38 | 140.76 | 1.1 | | Tuff (sand) |
| 18R-1, 3–5 | 149.73 | 1.0 | | Tuff (sand) |
| 19R-1, 112–114 | 160.22 | 1.1 | | Siltstone |
| 19R-2, 79–81 | 161.39 | 2.1 | | Volcaniclastic sandstone |
| 19R-2, 107–117 | 161.67 | 3.0 | | Calcareous silty clay |
| 20R-1, 10–12 | 168.40 | 1.1 | | Volcaniclastic sandstone |
| 21R-1, 103–110 | 178.63 | 2.7 | | Claystone |
| 21R-2, 9–11 | 178.79 | 2.2 | | Volcaniclastic silty |
| 21R-2, 50–52 | 179.20 | 1.2 | | Volcaniclastic silty sandstone |
| 22R-1, 10–12 | 187.10 | 1.2 | | Volcaniclastic sandstone |
| 23R-1, 10–12 | 196.50 | 14.1 | | Calcareous nannofossil clay |
| 23R-1, 66–68 | 197.06 | 1.1 | | Volcaniclastic sandstone |
| 24R-1, 3–5 | 206.13 | 29.7 | | Calcareous mudstone |
| 25R-1, 12–14 | 215.82 | 5.2 | | Claystone with nannofossils |
| 25R-CC, 5–8 | 216.67 | 4.2 | 1.16 | Tuffaceous claystone |
| 26R-1, 0–10 | 225.40 | 21.8 | | Calcareous nannofossil claystone |
| 26R-1, 42–44 | 225.82 | 25.5 | | Calcareous claystone |
| 27R-1, 103–105 | 236.13 | 40.2 | | Volcaniclastic sandstone |
| 27R-3, 112–114 | 239.22 | 60.9 | | Nannofossil chalk |
| 27R-5, 26–28 | 241.36 | 43.3 | | Nannofossil chalk |
| 28R-1, 36–38 | 245.06 | 53.6 | | Nannofossil chalk |
| 28R-3, 54–56 | 248.24 | 78.3 | | Tuffaceous packstone with nannofossil foraminifers |
| 29R-1, 15–17 | 254.65 | 78.8 | | Calcareous claystone |
| 29R-2, 68–70 | 256.68 | 46.1 | | Calcareous claystone |
| 29R-3, 29–34 | 257.79 | 0.4 | | Pelagic clay |
| 30R-1, 71–73 | 264.91 | 75.5 | | Nannofossil chalk |
| 31R-1, 20–22 | 274.00 | 52.2 | | Nannofossil chalk |
| 32R-1, 13–15 | 283.63 | 83.5 | | Nannofossil chalk |
| 32R-2, 96–98 | 285.96 | 40.4 | | Nannofossil chalk |
| 32R-2, 140–150 | 286.40 | 53.5 | | Nannofossil chalk |
| 33R-1, 53–55 | 293.33 | 81.8 | | Nannofossil chalk |
| 34R-1, 60–62 | 302.90 | 90.3 | | Nannofossil chalk |
| 35R-1, 6–8 | 311.56 | 42.6 | | Nannofossil chalk |
| 35R-CC, 5–7 | 312.42 | 0.2 | | Chert |
| 36R-1, 31–33 | 321.01 | 91.0 | | Nannofossil chalk |
| 36R-1, 80–88 | 321.50 | 85.4 | | Nannofossil chalk |
| 38R-2, 63–65 | 341.33 | 0.2 | | Pelagic clay |
| 38R-4, 91–93 | 344.61 | 39.7 | | Pelagic clay |
| 39R-1, 58–60 | 349.28 | 3.0 | | Tuff (fine-grained) |
| 40R-2, 103–105 | 360.63 | 4.8 | | Volcaniclastic sandstone |
| 40R-2, 140–150 | 361.00 | 0.5 | | Volcaniclastic claystone |
| 40R-3, 11–13 | 361.21 | 4.5 | | Volcaniclastic claystone |
| 41R-1, 10–12 | 365.60 | 0.2 | | Volcaniclastic claystone |
| 41R-4, 121–123 | 371.21 | 9.3 | | Volcaniclastic sandy/silty claystone |
| 42R-1, 96–98 | 373.76 | 7.0 | | Volcaniclastic sandy siltstone |
| 42R-2, 111–113 | 375.29 | 6.4 | | Volcaniclastic claystone |
| 43R-1, 114–116 | 383.24 | 9.1 | | Volcaniclastic claystone |
| 43R-1, 140–150 | 383.50 | 13.0 | | Volcaniclastic sandstone |
| 43R-2, 15–17 | 383.75 | 8.8 | | Volcaniclastic sandstone |
| 44R-1, 50–52 | 391.80 | 2.2 | | Silty claystone |
| 45R-2, 41–43 | 402.41 | 2.1 | | Silty claystone |
| 46R-1, 60–62 | 410.60 | 7.6 | | Silty claystone |
| 47R-1, 45–47 | 419.65 | 3.7 | | Silty claystone |
| 47R-2, 140–150 | 422.10 | 2.2 | | Volcaniclastic silty claystone |
| 47R-3, 74–76 | 422.94 | 3.6 | | Silty claystone |
| 47R-4, 30–32 | 424.00 | 1.7 | | Volcaniclastic sandstone |
| 48R-1, 66–68 | 429.36 | 2.0 | | Silty claystone |
| 49R-1, 17–19 | 438.27 | 0.3 | | Silty claystone |
| 49R-3, 128–130 | 442.38 | 6.1 | | Silty claystone |
| 50R-1, 92–94 | 448.32 | 0.4 | | Volcaniclastic silty claystone |
| 50R-2, 66–68 | 449.56 | 1.3 | | Claystone breccia |
| 50R-2, 140–150 | 450.30 | 1.7 | | Volcaniclastic silty claystone |
| 51R-1, 66–68 | 454.16 | 5.2 | | Claystone breccia |
| 51R-3, 98–100 | 457.48 | 0.4 | | Claystone |
| 52R-2, 114–116 | 462.44 | 0.2 | | Claystone |
| 52R-3, 34–36 | 463.14 | 0.2 | | Radiolarite |
| 53R-1, 75–77 | 470.15 | 22.7 | | Clayey nannofossil chalk |
| 53R-1, 120–130 | 470.60 | 23.2 | | Volcaniclastic claystone with nannofossils |
| 53R-2, 23–25 | 470.93 | 37.3 | 0.19 | Nannofossil chalk |
| 54R-1, 15–17 | 478.75 | 59.9 | | Clayey limestone |
| 54R-3, 15–17 | 481.75 | 31.8 | | Clayey siltstone |
| 54R-3, 50–52 | 482.10 | 28.7 | 0.11 | Claystone |
| 55R-1, 114–116 | 489.04 | 35.9 | | Siliceous limestone |
| 56R-1, 101–103 | 498.11 | 0.2 | 0.09 | Claystone |
| 56R-2, 140–150 | 500.00 | 0.6 | 0.02 | Tuffaceous silty claystone |
| 56R-3, 33–35 | 500.43 | 0.9 | 0.06 | Volcaniclastic sandstone |
| 56R-4, 7–8 | 501.67 | 0.2 | 0.02 | Claystone with radiolarians |
| 56R-4, 34–35 | 501.94 | 0.4 | 0.12 | Claystone with radiolarians |
| 57R-1, 37–39 | 506.97 | 0.5 | 0.06 | Claystone |
| 57R-1, 72–74 | 507.32 | 1.4 | 0.22 | Claystone |
| 57R-1, 127–129 | 507.87 | 1.0 | 0.26 | Claystone |
| 57R-2, 87–89 | 508.97 | 0.4 | 0.02 | Tuffaceous turbidite |
| 57R-2, 104–106 | 509.14 | 0.6 | 0.04 | Tuffaceous turbidite |

age of 165 Ma). Thin layers of laminated radiolarite with sharp tops and bases occur in a few intervals in the claystone; these are interpreted as redeposited sediments. Thus the dominant background sedimentation at Site 802 at this time was of tuffaceous pelagic clay, at very low rates of deposition.

### *Upper Aptian(?) to Cenomanian Claystone and Radiolarite*

The brown, thinly laminated claystone that comprises most of Unit VIII is probably representative of background pelagic sedimentation below the CCD. It accumulated at a very slow rate. The claystone is iron oxide-rich and zeolitic. It includes scattered micronodules and few radiolarians; thus, it closely resembles the Cenozoic pelagic clay recovered at all sites on Leg 129 (Fig. 2 and 25). The small metalliferous nodules are most commonly associated with burrowed intervals and may be related to periods of unusually slow deposition and associated early diagenesis.

Thin beds of radiolarite, intercalated within the dominant claystone, are for the most part graded, with sharp tops and bottoms, but do not display scoured bases or load casts. These layers are most likely the results of redeposition. They are either downslope turbidites or condensed deposits transported and winnowed by bottom currents.

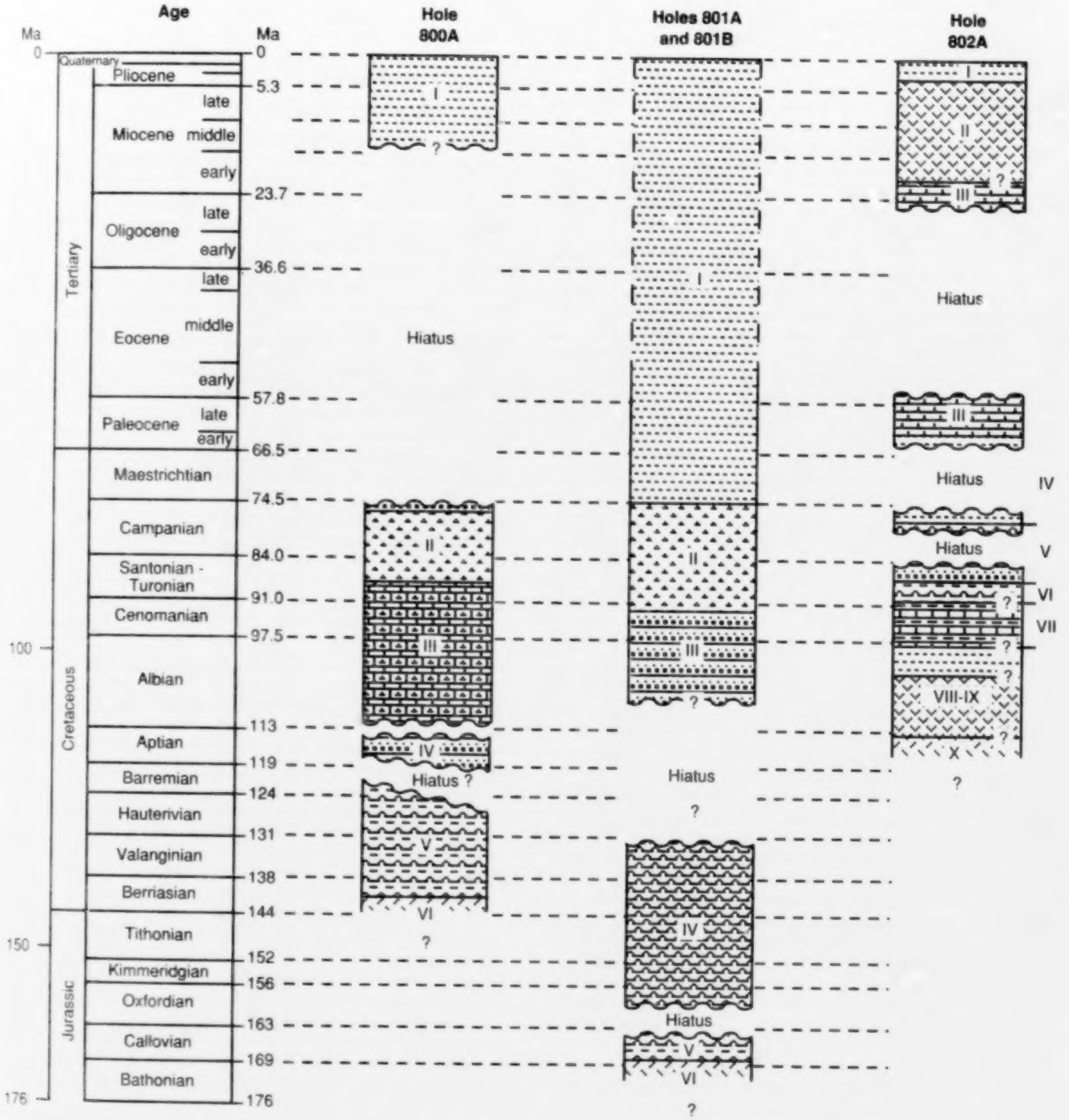
Age
Ma
Ma
Hole 800A
Holes 801A and 801B
Hole 802A
0
100
150
176
Quaternary
Pliocene
Miocene
late
middle
early
Oligocene
late
early
Eocene
late
middle
early
Paleocene
late
early
Tertiary
Maestrichtian
Campanian
Santonian - Turonian
Cenomanian
Albian
Aptian
Barremian
Hauterivian
Valanginian
Berriasian
Cretaceous
Tithonian
Kimmeridgian
Oxfordian
Callovian
Bathonian
Jurassic
0
5.3
23.7
36.6
57.8
66.5
74.5
84.0
91.0
97.5
113
119
124
131
138
144
152
156
163
169
176
I
?
Hiatus
II
III
IV
Hiatus ?
V
VI
?
I
II
III
?
Hiatus
?
IV
Hiatus
V
VI
?
I
II
?
III
Hiatus
III
Hiatus
IV
Hiatus
V
VI
?
VII
?
?
VIII-IX
?
X
?

Figure 25. Age correlation diagram for Sites 800, 801, and 802. Lithologic symbols are explained in Figure 5.

### *Upper Aptian(?) to Cenomanian Calcareous Claystone and Radiolarian Limestone*

Unit VII consists mainly of fine-grained radiolarian limestone, nannofossil chalk, and calcareous claystone turbidites. Turbiditic deposition is indicated by laminated to massive, gently graded beds with scoured bases that darken and become more clay-rich upward. The tops of the beds are commonly bioturbated. Although most of Unit VII was probably redeposited from above the CCD, much of the radiolarian limestone is poorly sorted and probably represents minimally reworked (unsorted) pelagic sedimentation.

Intercalated with the limestone, chalk, and claystone are thin beds of massive to planar- and cross-laminated radiolarite and clayey bio-volcaniclastic siltstone or sandstone. The radiolarite layers have sharp boundaries, but some beds are graded. These coarse-grained deposits may have several different modes of origin, including (1) turbiditic deposition, (2) transportation and reworking by bottom currents, (3) winnowing, and (4) pelagic deposition (radiolarian blooms).

Most of the radiolarians in the carbonate rocks are replaced and filled by calcite, probably during or subsequent to the formation of beds and nodules of chert and porcellanite, and the silicification of limestone in Cores 129-802A-54R and -55R (see the following discussion of Unit III, this section).

The Cenomanian to Coniacian claystone and radiolarite (Unit VI) is very similar to Unit VIII in terms of composition, bedding, and sedimentary structures. Compositionally, the claystone is comparable to pelagic clay and apparently represents normal background sedimentation below the CCD. Overall, the sedimentary rocks of Unit VI accumulated at the moderately slow rate of about 2 m/m.y. Black, iron-manganese oxide-rich discontinuous laminations in Section 129-802A-52R-1 may record extremely slow rates of deposition or perhaps more oxygenated bottom water. These primary depositional conditions are contrasted by later diagenesis in which small pyritic concretions were surrounded by light green, reduction halos. The originally oxide-rich bands of the claystone are sharply truncated at the circumferences of the halos; the metals have evidently been remobilized within the reducing diagenetic microenvironment.

Thin deposits of structureless to laminated radiolarite are probably reworked. Most bedding contacts with the claystone are sharp. The beds are not clearly graded, but deposits of well-sorted radiolarians allow little grain-size differentiation. These sediments may have been deposited by turbidity or grain-flow mechanisms. Zones of diagenetic reduction are mostly restricted to the granular radiolarite beds inferred to have relatively high permeability.

### *Cenomanian(?) to upper Campanian Volcaniclastic Turbidites*

The base of Unit V is a debris flow of volcaniclastic material that overlies a larger debris flow of pebbly claystone with a minor component of volcanic glass. These debris flows are as much as several meters thick but cannot be truly "proximal" facies because the nearest possible sediment sources are seamounts at least 100 km to the northeast (Fig. 2). Unit V has no correlative volcaniclastic deposit at Site 585 (Moberly, Schlanger, et al., 1986; Fig. 24), indicating that the source of these sediments was to the south or west. Upsection in Unit V the redeposited volcaniclastic sediments become coarser-grained and thinner-bedded. The lack of any consistent fining- or thinning-upward stratigraphic trends implies that they are the product of intermittent depositional events, and are thus "distal" to their source rather than the product of an evolving sedimentary apron to a seamount. The thick beds must therefore represent fairly intense seismo-volcanic events. The presence of shallow-water carbonate debris, including red algae, is evidence that the source was near or above sea level.

The volcaniclastic deposits of Unit V are coeval with long-lived edifice-building Cretaceous volcanic activity (late Albian to Maestrichtian) that followed the major Hauterivian-Aptian phase at Site 462 in the Nauru Basin (Larson, Schlanger, et al., 1981). The deposits overlap only slightly with the last phase of volcanic activity recorded at Site 801 (see "Site 801" chapter, this volume), which is pre-Albian to mid-Cenomanian (Fig. 26). The data from Sites 801, 802, 585, and 462 indicate that volcanism in this part of the Pacific Ocean was diachronous in the Mesozoic (Figs. 24 and 26).

The background sedimentation in Unit V is pelagic clay, richer in radiolarians near the base of the unit, when the site was located at approximately 10°S latitude, and richer in nannofossils near the top of the unit, when the site had moved to within a few degrees of the equator (see "Paleomagnetism" section, this chapter). During this time, the site was always well below the CCD, but because of high rates of turbidite accumulation, nannofossils were buried and preserved together with the radiolarians. The dark bluish and greenish gray colors of these deposits indicate relatively low oxygen depositional and/or diagenetic conditions.

### *Upper Campanian to Paleocene Claystone*

The laminated and burrowed zeolitic claystone of Unit IV records normal, slow pelagic sedimentation below the CCD (as in Units VIII and VI), occasionally punctuated by redepositional events that left thin beds of calcareous siltstone and sandstone. The upper part of this unit is virtually identical to the claystone and radiolarite of Units VIII and VI, except for the better development of graded beds, cross-lamination, and flame structures that clearly identify the coarse-grained deposits as turbidites.

### *Paleocene to lower Miocene Nannofossil Chalk (Unit III)*

Unit III is defined by the predominance of foraminiferal-nannofossil-chalk turbidites, indicated by graded beds with laminated and cross-laminated bases, rip-up clasts, and increased bioturbation toward the tops of beds. Mixed Mesozoic and Cenozoic fossil assemblages (see "Biostratigraphy" section, this chapter) also indicate redeposition and reworking of nannofossil oozes. The unit can be subdivided into an upper and a lower part on the basis of minor lithologies, color, and biostratigraphy at an Eocene through Oligocene hiatus (Fig. 25), during which time Site 802 crossed the equator (see "Paleomagnetism" section, this chapter). Unit III sediments accumulated at the relatively fast rate of 7 m/m.y., closer to the accumulation rates of the volcaniclastic turbidites than to the those rates of the principally pelagic intervals. The much greater thickness of correlative Upper Cretaceous through Paleogene chalk and chert at Sites 199 and 585 (Heezen, MacGregor, et al., 1973; Moberly, Schlanger, et al., 1986) indicate that their principal source was to the northwest (Fig. 24).

The upper Paleocene to lower Eocene part of this unit contains light gray to pale pink, thinly laminated chalk turbidites with scattered chert nodules. Radiolarians in the chalk are replaced and filled by calcite, whereas foraminiferal casts are quartz-filled. A thin bed of pelagic claystone may be the only indicator of the background sedimentation during this period, which was dominated by carbonate redeposition.

In lower Unit III (below the hiatus), the biogenic components had sufficient time or the proper environment to undergo the following observed diagenetic sequence: (1) beginning of radiolarian dissolution, (2) infilling of foraminifers with quartz, (3) beginning of chert nodule formation during ongoing radiolarian and sponge spicule dissolution, (4) completion of radiolarian dissolution, leaving hollow molds, and (5) calcite precipitation in molds. This diagenetic sequence finally resulted in the peculiar association of radiolarian molds filled with calcite and foraminiferal molds filled with quartz.

The upper half of this unit contains upper Oligocene to lower Miocene, dark brown zeolitic claystone interbedded with light grayish brown carbonate turbidites. The zeolitic claystone is representative of normal pelagic sedimentation at that time. Redeposition from above the CCD was less common than in the lower part of this unit, and a much larger proportion of pelagic claystone was able to accumulate between carbonate redeposition events. In the upper part of Unit III (above the hiatus), siliceous microfossils are well-preserved and abundant in the chalk and coarser beds. Porcellanite is very rare.

Our observations support the thesis of Keene (1975), who suggested that in areas of normal geothermal gradient, the

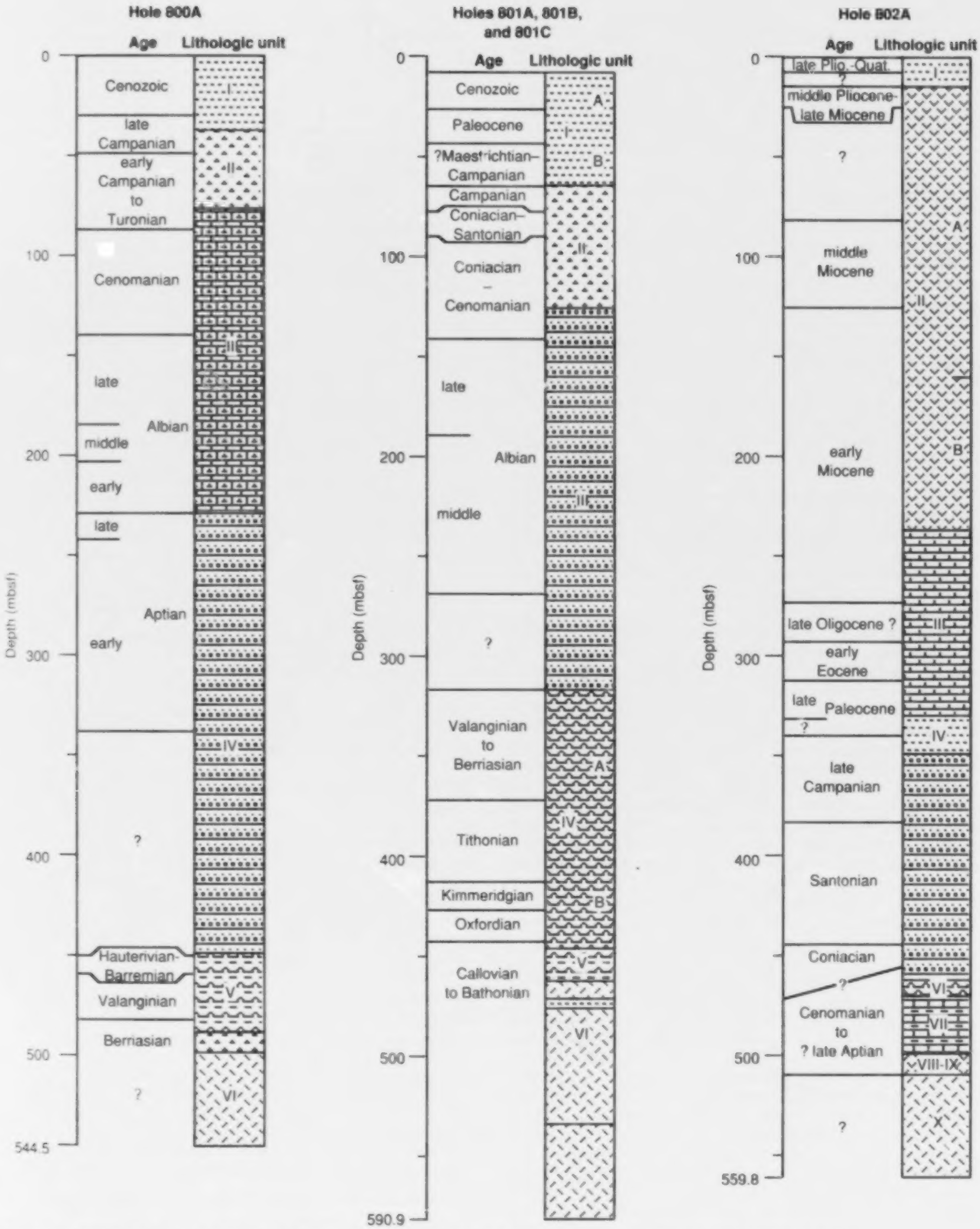
Hole 800A
Age
Lithologic unit
Depth (mbsf)
0
100
200
300
400
500
544.5
Cenozoic
late Campanian
early Campanian to Turonian
Cenomanian
late
middle
early
Albian
late
early
Aptian
?
Hauterivian-Barremian
Valanginian
Berriasian
?
I
II
III
IV
V
VI
Holes 801A, 801B, and 801C
Age
Lithologic unit
Depth (mbsf)
0
100
200
300
400
500
590.9
Cenozoic
Paleocene
?Maestrichtian–Campanian
Campanian
Coniacian–Santonian
Coniacian – Cenomanian
late
middle
Albian
?
Valanginian to Berriasian
Tithonian
Kimmeridgian
Oxfordian
Callovian to Bathonian
A
I
B
II
III
A
IV
B
V
VI
Hole 802A
Age
Lithologic unit
Depth (mbsf)
0
100
200
300
400
500
559.8
late Plio.-Quat.
?
middle Pliocene-late Miocene
?
middle Miocene
early Miocene
late Oligocene ?
early Eocene
late
Paleocene
?
late Campanian
Santonian
Coniacian
?
Cenomanian to ? late Aptian
?
I
A
II
B
III
IV
VI
VII
VIII-IX
X

Figure 26. Stratigraphic depth correlation diagram for Sites 800, 801, and 802. Lithologic symbols are explained in Figure 5.

formation of deep-sea chert and porcellanite may require 40–50 m.y. to occur. In Unit III above the hiatus, radiolarians are undissolved and only rare porcellanite has formed in the carbonates, which are less than 30 m.y. old. Below the hiatus, in the lower part of Unit III, which is greater than 52 m.y. old, radiolarians have completely dissolved, and significant quantities of chert and porcellanite have formed. These two distinct diagenetic states occur in physically adjacent, originally similar rocks, deposited on either side of a 20-m.y. hiatus.

*Lower Miocene Tuff with Calcareous Claystone and Chalk*

Lower Miocene tuffs overlie and are intercalated with redeposited chalks and clayey nannofossil chalks. Subunit IIB is characterized by a decrease in calcium carbonate content upsection (Fig. 27); the transition to Subunit IIA corresponds to the upward transition from tuff interbedded with chalk to tuff interbedded with pelagic clay.

The tuffs were deposited mainly as mass flows and grain flows with meter-scale thicknesses toward the base of the unit. These beds thin and fine upward to turbidite beds 10–30 cm thick. Near the base of the unit, shallow-water carbonate debris and wood fragments indicate that the sources of some of the turbidites were above sea level. The nearest volcanos dated as Miocene are the islands of Truk and Pohnpei along the Caroline Ridge, 350 km south of Site 802 (Fig. 1). Thus, although some of the beds are quite thick, the sediments have traveled a considerable distance. The upward-thinning stratigraphic trend is probably the result of a large initial build-up of volcaniclastic material in the Caroline Islands associated with the construction of the Miocene islands, followed by gradual sloughing of slope accumulations of tuffaceous debris.

The interbedded chalks and calcareous claystones are redeposited pelagic material, as indicated by matrix-supported debris-flow textures and mixtures of Miocene to Cretaceous microfossils. The source of the pelagic calcareous material is not established, but could be various seamounts in the vicinity of the Mariana Basin or the Caroline Ridge. Site 802 was probably moving northward across 5°N latitude during the early Miocene (see "Paleomagnetism" section, this chapter), at depths exceeding 5000 m. At these depths, background sediment accumulation would be expected to be dominantly pelagic clay, although south of 5°N the surface waters would be expected to be highly productive. The dark blue, gray, reduced colors of the deposits may be the result of post-burial diagenetic reduction of the normal pelagic components by interaction with the volcanic material. Bioturbation is ubiquitous in the unit, especially at the tops of turbidite beds and in clay intervals.

*Lower Miocene to middle Pliocene(?) Tuff with Pelagic Clay*

The tuffs of Subunit IIA are turbidite and mass flow deposits interbedded with brown to green pelagic claystones. The unit displays an overall thickening- and coarsening-upward of bedding and grain size, from thin (5–10 cm) turbidites to meter-scale, massive beds at the top. The very thick beds at the top of the unit are remarkable, like those at the base of Subunit IIB, because they are at least 350 km from their inferred source in the Caroline Islands (Fig. 1). The coarsening- and thickening-upward trend may reflect an increase in volcanic or tectonic activity toward the end of the Miocene and early Pliocene for at least one source seamount on the Caroline hotspot chain. Benthic, neritic foraminifers included in the unit indicate that the summits of the edifices were near sea level.

The pelagic claystone with abundant zeolites, iron oxyhydroxides, and opaques is more metalliferous than the older pelagic deposits at Site 802. The higher metal content is typical of sediments that very slowly accumulated below the CCD (Karpoff, 1989). The uphole decrease in nannofossils and increase in metal content are consistent with passage of the site away from the highly fertile environment of the equatorial divergence zone to about 10°N (see "Paleomagnetism" section, this chapter), and with water depths approaching 6000 m. The slow sedimentation rates for the claystone in this subunit are masked by the thick tuff deposits in the general accumulation rate calculated for this subunit.

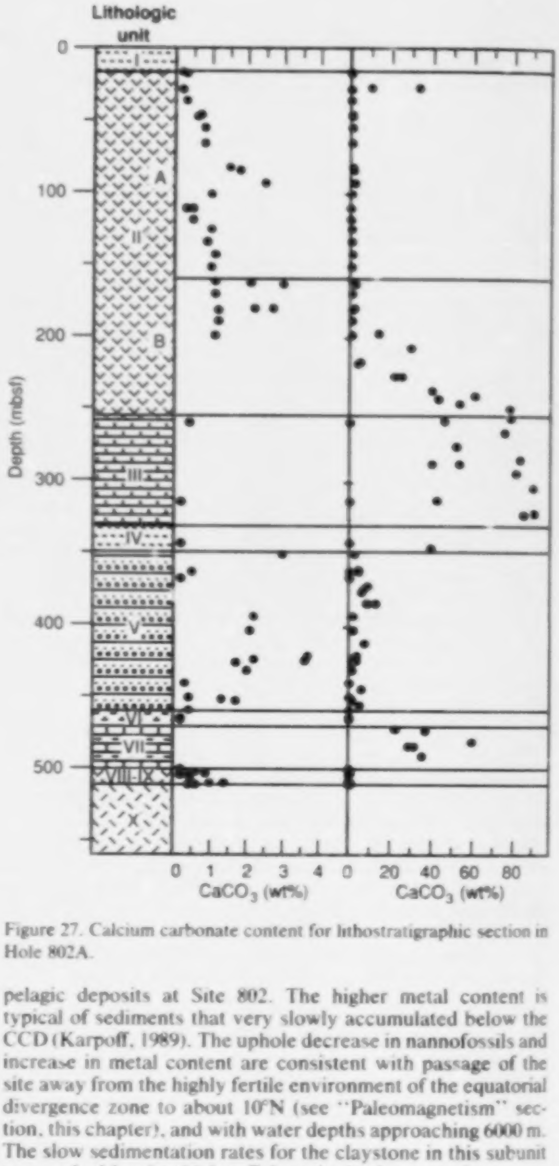

Figure 27. Calcium carbonate content for lithostratigraphic section in Hole 802A.

*Upper Pliocene to Quaternary Pelagic Clay*

The zeolitic, iron-manganese oxyhydroxide-rich clay of Unit I is representative of slow pelagic deposition and authigenesis below the CCD, undiluted by volcaniclasts and carbonate. This clay is the unlithified equivalent of much of the claystone of Units VIII, VI, and IV, and is comparable to that found in the upper parts of the sedimentary sections at Sites 800 and 801.

## Summary of Sedimentation History at Site 802

Pillow basalts, remote from any seamounts or mid-ocean ridge, were extruded at the seafloor no later than the Cenomanian. The oldest sediments above this basalt are tuffaceous clays that accumulated slowly, interrupted by rare, distal, volcaniclastic turbidites. From the Albian-Cenomanian to the Coniacian, pelagic clay accumulated slowly, punctuated by occasional events of radiolarian redeposition. Within this interval, during the late Albian to Cenomanian, the background sedimentation was overwhelmed by a more rapid accumulation of radiolarian-rich calcareous turbidites from sources above the CCD. The Coniacian to the late Campanian was dominated by volcaniclastic turbidites, with radiolarian clay deposited in between turbidite events. Sediments from the Maestrichtian through the earliest Paleocene are missing. Slow deposition of pelagic clay from the Paleocene was overwhelmed by pelagic chalk turbidites during the late Paleocene through the early Miocene. Most of the Eocene through Oligocene section is missing. The Miocene was characterized by the accumulation of abundant tuff, at first alternating with chalk turbidites, and later with slowly deposited pelagic clays. Slow pelagic clay sedimentation continued on into the late Pliocene to the present.

## BIOSTRATIGRAPHY

The sediment sequence recovered at Site 802 consists of 57 cores dated Pliocene-Quaternary to late Aptian-Albian in age. Core-catcher samples and, when necessary, additional samples from within the cores were investigated for nannofossils, foraminifers, radiolarians, and palynomorphs.

The biostratigraphy is based mainly on nannofossils and planktonic foraminifers. In Cenozoic sediments radiolarians occur sporadically and are rare; in Mesozoic sediments they are few to abundant. Palynomorphs are absent through most of the sequence, except for one sample from the lower Miocene and some samples dated as late Aptian to Albian at the bottom of the hole.

The nannofossils provided useful datums for the middle to early Miocene, late Paleocene, and middle to Late Cretaceous. The foraminifers were useful for age determination in the Miocene, Eocene, and Cretaceous. Radiolarian biozones were recognized as Albian to Cenomanian, and palynomorphs were used to date the last two cores above the basalt as upper Aptian to Albian. A summary of the biostratigraphy of Site 802A is provided in Figure 28.

A hiatus is suspected at the base of Core 129-802A-32R, from which core-catcher samples are tentatively dated as upper Oligocene. Another hiatus is suspected at the base of Core 129-802A-37R, between Paleocene and upper Campanian samples. The position of the Cretaceous/Tertiary boundary could not be determined at Site 802. An additional hiatus may be present between the upper Campanian and Santonian sediments at the base of Core 129-802A-42R.

The microfossil assemblages in the Tertiary sediments were frequently reworked, making precise zonation and dating difficult.

Sporomorphs, wood fragments, and cuticles indicate sources from emergent seamounts during the late Aptian-Albian. Dominance of spores in this interval indicates a humid climate. Further emergence of seamounts is suggested by abundant terrestrial palynomorphs in early Miocene sediments. Abundant larger foraminifers typical of shallow-water reefal habitats support this interpretation.

### Calcareous Nannofossils

One-hundred twenty-four samples were examined for nannofossils from Hole 802A. Thirty-five were barren, whereas the remaining 89 contained rare to very abundant nannoflora. Preservation of the nannofossils from this site was generally poor to moderate. Figure 29 shows the distribution of nannofossils compared to the abundance of radiolarians and to the paleolatitudes recorded from Site 802.

Three distinct intervals were discernible and dated using nannofossils: (1) middle to early Miocene (possibly latest Oligocene), (2) late Paleocene, and (3) Late to middle Cretaceous. Most of the Tertiary samples contain a considerable amount of reworked nannofossils from significantly older sediments. Figure 28 summarizes nannofossil zonal assignments compared to those of other fossil groups at Site 802. In the description below we use zonal schemes of Martini (1971) and Okada and Bukry (1980) for the Cenozoic section. For the Cretaceous we used the zonal scheme of Sissingh (1977).

#### *Cenozoic Sediments*

Core 129-802A-1R is barren of nannofossils and Core 129-802A-2R had no recovery. The core-catcher sample from Core 129-802A-3R, however, contains rare specimens of *Discoaster pentaradiatus*, *D. variabilis*, and *Coccolithus* sp. These discoasters range roughly from the middle Pliocene to upper Miocene.

Subsequent cores are barren down to Core 129-802A-10R, in which rare specimens of *Reticulofenestra pseudoumbilica* (middle Pliocene to middle Miocene) and *Sphenolithus moriformis* (late Miocene to early Eocene) were encountered within the core catcher.

An increase in nannofossil abundance was observed near the top of Section 129-802A-11R-1, along with the first paleontologic evidence of reworked sediments recovered from this site. The assemblage is characterized by *Cyclicargolithus floridanus*, *Discoaster deflandrei*, *Sphenolithus moriformis*, *S. conicus*, *S. heteromorphus*, and *Cyclicargolithus abisectus*. The two latter species are not known to co-exist, so we deduce that at least the older fossils are reworked. The first occurrence of *S. heteromorphus* defines the base of the lower Miocene CN3 Zone, and we assign samples recovered down to Core 129-802A-23R to that zone.

Despite the significant problem of reworking, two reliable nannofossil markers were encountered in their proper sequence within the ensuing cores. Rare specimens of *Sphenolithus belemnos* were observed only in Sample 129-802A-24R-CC. The total range of this species defines the upper and lower limits of the lower Miocene NN3 Zone. The last occurrence of *Triquetrorhabdulus carinatus* coincides with the first occurrence of *S. belemnos* on the range chart of Perch-Nielsen (1985a, p. 442). We observed the last occurrence of the former only two cores below in Sample 129-802A-26R-CC, and encountered that species fairly consistently down to Sample 129-802A-32R-CC. Although the *T. carinatus* Zone (CN1) is actually defined on other markers, the nominal species is reported to generally range throughout that zone (Perch-Nielsen, 1985a). Perch-Nielsen (1985a) also reports that *T. carinatus* is sometimes found in the uppermost Oligocene NP25 Zone, so it is possible that the aforementioned interval extends into the Oligocene.

A significant change in the nannofossil assemblage was observed in Samples 129-802A-33R-CC to 129-802A-36R-CC. The Miocene assemblage with reworked Oligocene and Eocene nannofossils described above is replaced by a predominantly late Paleocene assemblage occurring with abundant reworked Late Cretaceous nannofossils. The youngest fossil identified thus far is *Discoaster multiradiatus*, which ranges through the uppermost Paleocene and up into the lowermost Eocene. We therefore assign this sequence of cores to the NP9/CP8 Zone to possibly the NP10/CP9A Zone. Cores 129-802A-33R and -34R are assigned to the lowermost

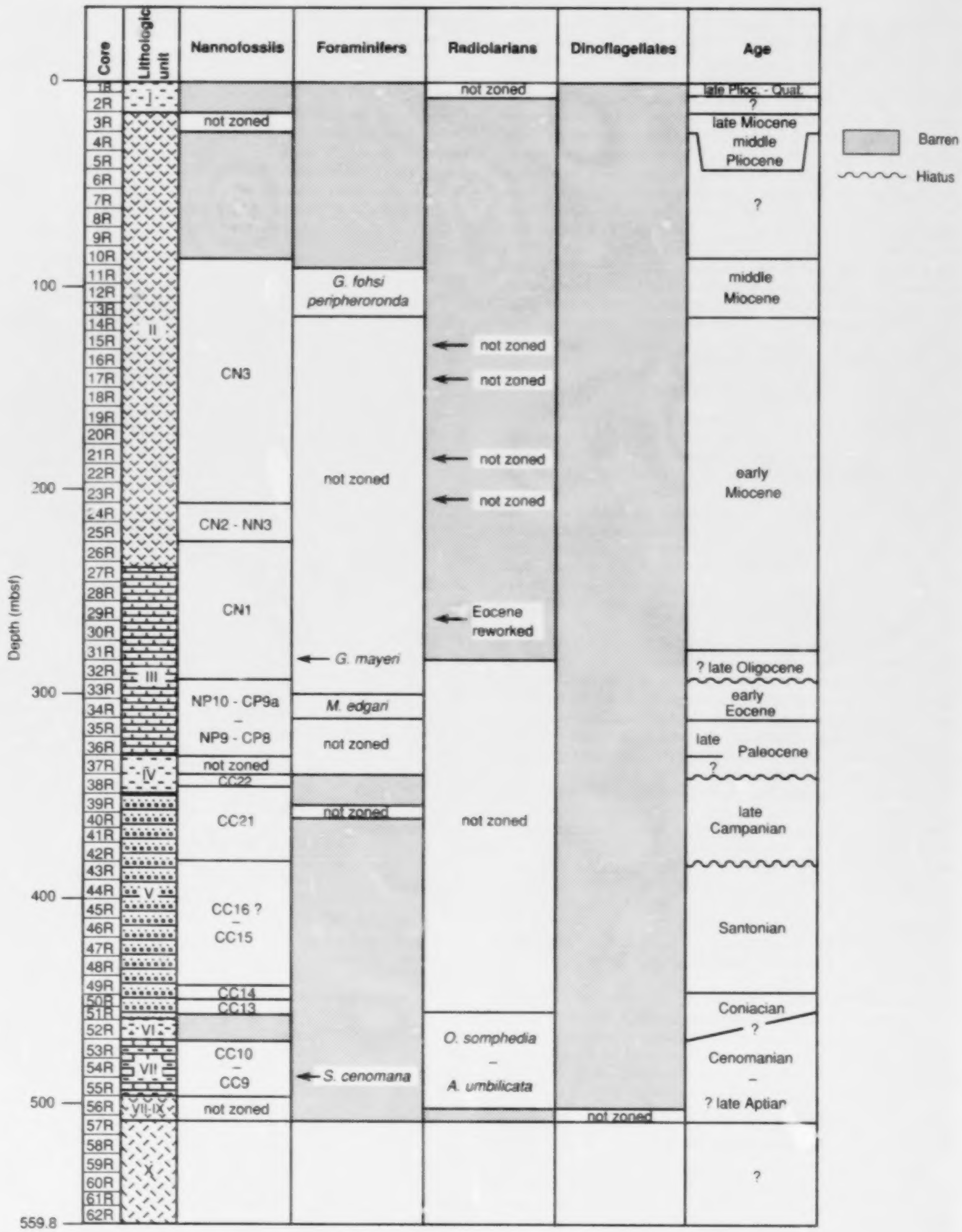

Figure 28. Summary of the biostratigraphy for Hole 802A.

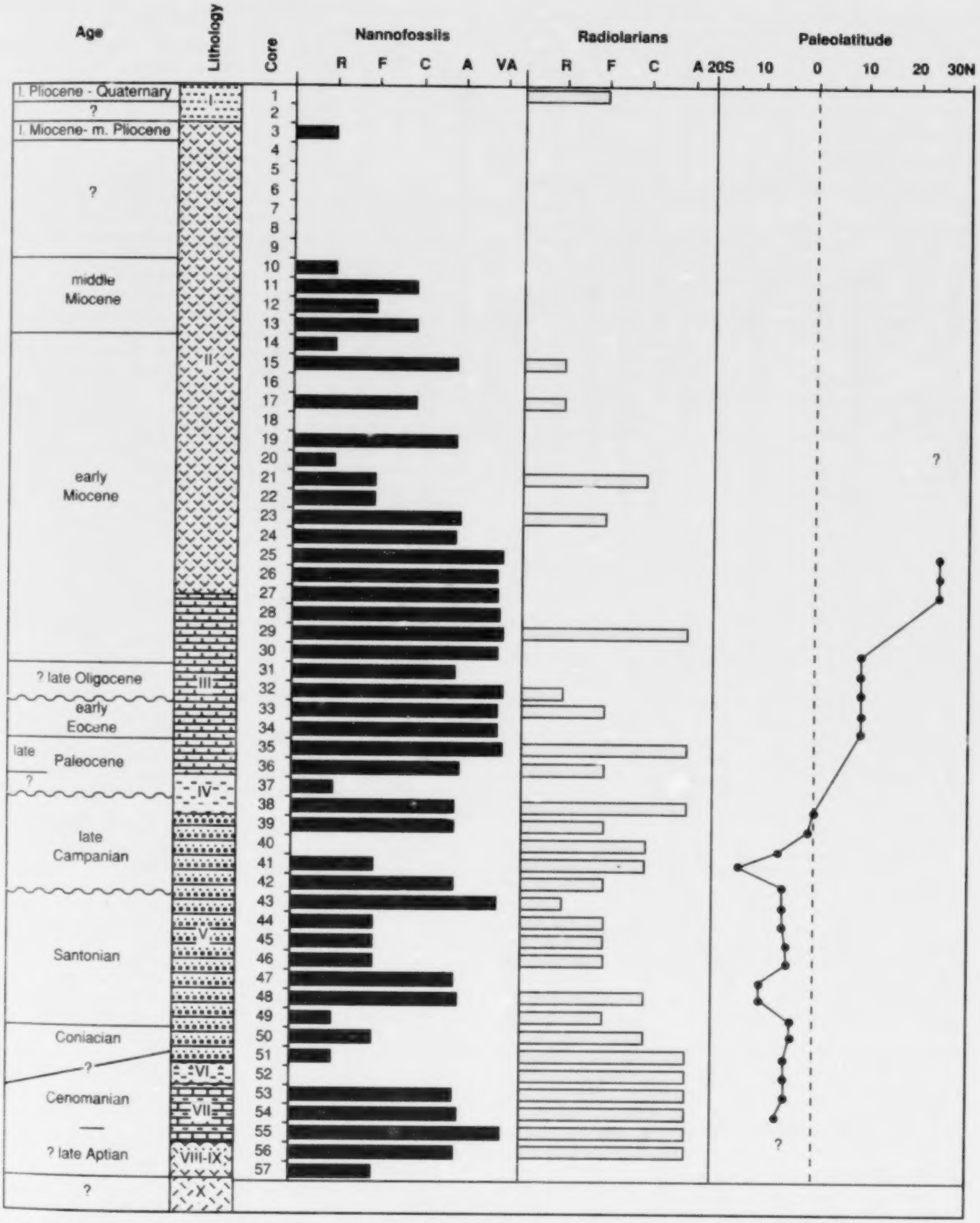

Figure 29. Abundance of calcareous nannofossils and radiolarians in Hole 802A plotted against age, lithostratigraphy, and paleolatitude. Relative abundance is denoted as rare (R), few (F), common (C), abundant (A), and very abundant (VA). (See "Explanatory Notes" chapter, this volume, for further discussion of abundance parameters.)

Eocene *Morozovella edgari* Zone by the Leg 129 foraminiferal paleontologists. Other Paleocene nannofossils noted include *Chiasmolithus* sp., *Fasciculithus* sp., *Cruciplacolithus tenuis*, *Toweius eminens*, and *Heliolithus kleinpelii*. Core 129-802A-37R consists only of a core-catcher sample that contained only very rare Paleocene nannofossils in calcareous claystone adjacent to chert.

### *Cretaceous Sediments*

The first Cretaceous sediments encountered were from Sample 129-802A-38R-1, 1 cm, and included rare specimens of *Watznaueria*, *Micula*, and *Cretarhabdus*. Total abundance fluctuates from very abundant to barren throughout the remainder of Hole 802A. Reworking of sediments was not obvious, as is the case in the Tertiary sediments described previously.

Whereas several reliable nannofossil markers occurred in their expected stratigraphic sequence, other diagnostic species were conspicuously absent or very rare. These include *Lithastrinus floralis*, *L. septenarius*, *Calculites obscurus*, *Reinhardtites anthophorus*, *Aspidolithus parcus*, *A. parcus constrictus*, *Lucianorhabdus cayeuxii*, and *L. maleformis*.

Nannofossils provided several reliable and useful age determinations constituting the basic biostratigraphic framework for the Cretaceous interval of Hole 802A. Figure 30 illustrates the ranges of important species used in age determination from the Cretaceous sequence.

Sections 129-802A-38R-1, 1 cm, through 129-802A-38R-2, 29 cm, were assigned to the upper Campanian CC22 Zone, based on the first occurrence of *Quadrum trifidum* and the extinction of *Lithastrinus grillii* within this interval. The last occurrence of *Ceratolithoides verbeekii* also coincides with the lower boundary of this zone.

Samples 129-802A-38R-3, 105–106 cm, through 129-802A-42R-CC were assigned to the CC21 Zone of early late Campanian age. A hiatus may be present between Samples 129-802A-42-CC and 129-802A-43-1, 112–113 cm. *Ceratolithoides aculeus*, *C. verbeekii*, *Calculites obscurus*, *Quadrum gothicum*, and *Q. sissinghii* have their last downhole occurrence in the former sample, while *Marthasterites furcatus* was first observed in the latter sample. The Cretaceous range chart of Perch-Nielsen (1985b) shows considerable overlap of these species. The remaining Campanian Zones CC21b down through CC17, and the Santonian Zone CC16, are not represented in this sequence.

Subsequent samples down through Sample 129-802A-49R-3, 107–109 cm, were assigned to the Santonian Zone CC15 (and part of Zone CC16), based on the first occurrence of *Lithastrinus grillii*. A very short Zone CC14 spans only the interval from Samples 129-802A-49R-CC through 129-802A-50R-2, 45–46 cm, where the first occurrence of *Micula decussata* was observed. The Santonian/Coniacian boundary falls within the Zone CC14.

Only the next four samples examined, from 129-802A-50R-2, 83–85 cm, to 129-802A-51R-1, 89-90 cm, can be assigned to Zone CC13 with any certainty, as they contain the lowermost occurrence of *Marthasterites furcatus*. Sections 129-802A-51R-CC through 129-802A-52R-CC are barren or contain very rare nannofossils, which does not allow further zonal or boundary assignment to be made.

Nannofossils are abundant in Samples 129-802A-53R-1, 66–67 cm, down to 129-802A-55R-CC. Markers observed in this interval include *Eiffellithus turriseiffelii* and *Cruciellipsis chiastia*. The first occurrence of the former marks the lower boundary of Zone CC9 (beginning of the late Albian) while the last occurrence of *C. chiastia* marks the upper boundary of Zone CC10 (late Cenomanian). In Section 129-802A-55R-1, 16 cm, poorly preserved specimens resembling *Lithraphidites acutus*, a species restricted to the Cenomanian Zone CC10, were observed. We assign this interval to Zones CC9 and CC10.

All samples from Sections 129-802A-56R-1, 69 cm, through 129-802A-57R-2, 100 cm, are barren or contain rare, poorly preserved nannofossils. The occurrence of *Lithastrinus floralis* and *Parhabdolithus angustus* indicates an age younger than late Aptian.

## Foraminifers

A total of 51 core-catcher samples and two additional samples from within the cores were examined for foraminifers in Hole 802A. Twenty-four of the samples yielded foraminifer assemblages that were common to abundant and of moderate to good preservation. Although the assemblages provided a biostratigraphic framework for the Neogene, Paleogene, and Cretaceous, the precision normally offered by evolutionary lineages of planktonic foraminifers cannot be realized in material from Hole 802A because of a high degree of reworking. Despite this problem, two planktonic foraminiferal biozones are recognized in the lower Miocene and the lower Eocene.

Foraminifers are absent from Samples 129-802A-1R-CC to 129-802A-10R-CC. Sample 129-802A-11R-1, 116-120 cm, yielded an abundant, well-preserved assemblage of planktonic foraminifers assignable to the *Globorotalia fohsi peripheroronda* Zone (early middle Miocene; Bolli and Saunders, 1985). The relatively diverse assemblage found in this zone contains *G. fohsi peripheroronda*, *Orbulina universa*, *O. suturalis*, *Globorotalia scitula*, *G. obesa*, *G. continuosa*, *G. mayeri*, *Globigerina venezuelana*, *G. praebulloides*, *Globigerinoides obliquus*, *G. ruber*, *G. trilobus*, and *Globoquadrina dehiscens*. Rare specimens of *Globigerinoides altiaperturus*, *G. bisphericus*, and *Catapsydrax dissimilis* in this interval appear to be reworked from the lower Miocene sediments.

The oldest find of *Orbulina universa* in Sample 129-802A-13R-CC was used to place the boundary with the underlying lower Miocene. Subsequent assemblages of planktonic foraminifers recovered down to Sample 129-802-23R-CC are very similar to those mentioned previously; however, the presence of *Globigerinoides bispericus* indicates that this interval is not older than the *Praeorbulina glomerosa* and/or *Globigerinatella insueta* Zone (upper part of the lower Miocene; Bolli and Saunders, 1985).

Samples 129-802A-24R-CC through 129-802A-31R-CC lack representatives of the *G. bisphericus-Praeorbulina-Orbulina* evolutionary lineage, and are therefore considered to be early early Miocene in age. The absence of other age-diagnostic foraminifers precludes more detailed subdivision of these cores. Reworking of the assemblages in samples from Cores 129-802A-25R to -28R makes biostratigraphic zonation difficult. Most species typical of the early Miocene, such as *Catapsydrax dissimilis*, *Globorotalia mayeri*, *G. continuosa*, *G. dehiscens* and *G. obesa* are found in comparatively low abundance in contrast to the abundant Cretaceous and Paleogene species. Sample 129-802A-27R-CC in particular contains typical Eocene species such as *Turborotalia cerroazulensis*, *Morozovella aragonensis*, *Acarinina* div. spec., *Hantkenina* sp., and *Globigerina* div. spec., in addition to representatives of the Cretaceous genera *Globigerinelloides*, *Rugoglobigerina*, *Hedbergella*, and *Globotruncana* that indicate reworking.

Diverse foraminifer assemblages recovered from Sample 129-802A-28R-CC include shallow-water larger foraminifers belonging to the *Nummulitidae* and *Lepidocyclinidae*, which are typical of reef paleoenvironments. Neritic to bathyal benthic genera were also found including *Pararotalia*, *Rotalia*, *Amphistegina*, *Asterigerina*, *Stichocibicides*, *Vaginuli-*

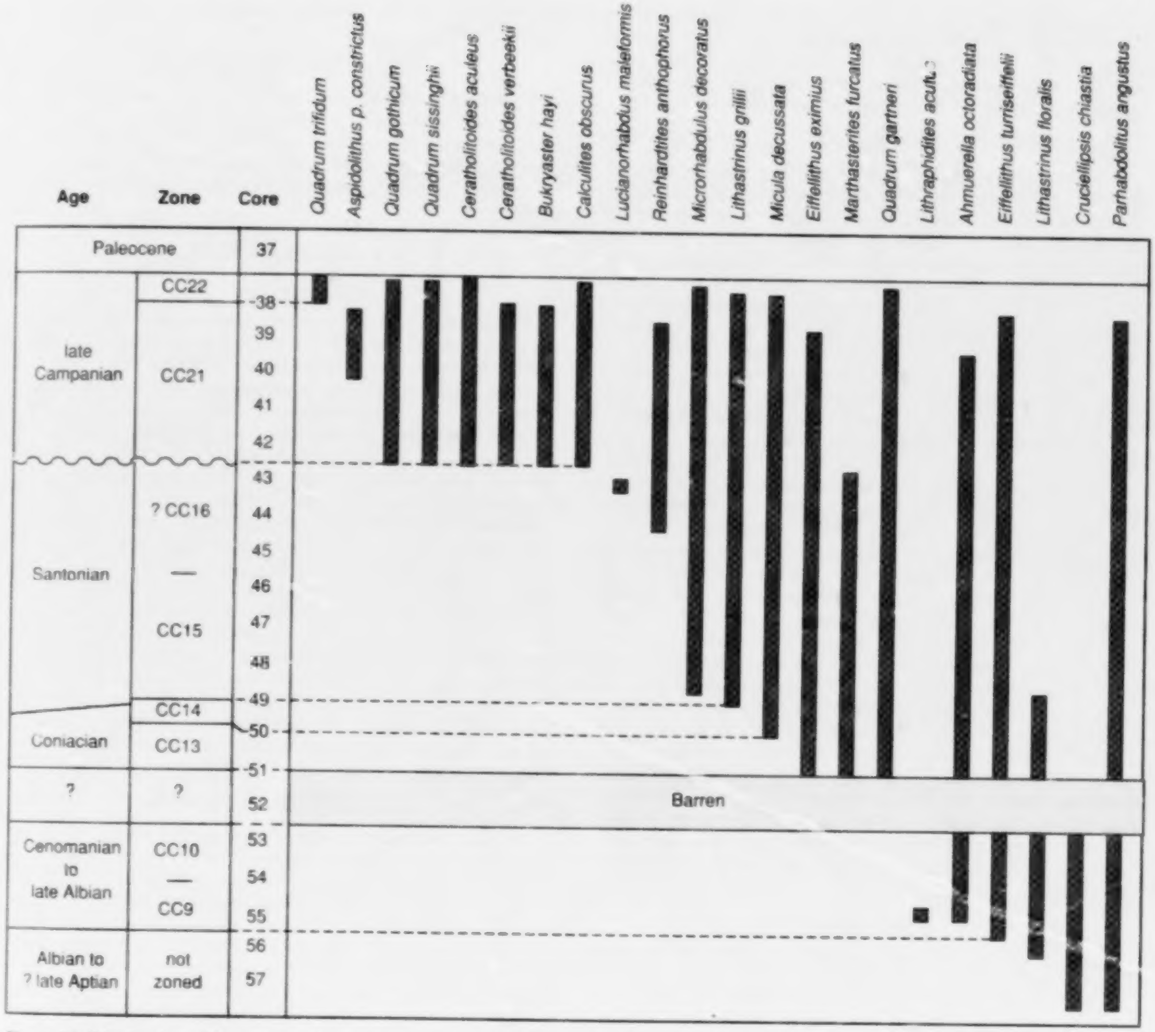

Figure 30. Distribution of important calcareous nannofossils in Cretaceous sediments of Hole 802A.

*nopsis*, *Stilostomella*, *Chrysalogonium*, and *Bolivina*, in addition to several reworked planktonic species.

Core-catcher samples from Cores 129-802A-29R to -31R contained few planktonic foraminifers of only moderate preservation. However, the presence of *Globorotalia mayeri* in Sample 129-802-31R-CC indicates a late Oligocene or younger age according to the range chart of Bolli and Saunders (1985).

Sample 129-802A-32R-CC is barren. Samples 129-802A-33R-CC and 129-802A-34R-CC contain diverse planktonic foraminifer assemblages including *Morozovella edgari*, *M. subbotinae*, *M. formosa gracilis*, *M. acuta*, *Planorotalites chapmani*, *Acarinina primitiva*, *A. nitida*, *A. soldadoensis*, and *Globigerina triloculinoides*. These assemblages are attributed to the *M. edgari* Zone, dated as earliest early Eocene (Toumarkine and Luterbacher, 1985). Also present are *Globotruncanella citae*, *Hedbergella holmdelensis*, *Heterohelix striata*, *H. navarroensis*, *Globigerinoides ultramicra*, *Morozovella pseudobulloides*, and *Acarinina mckannai*, which are regarded as reworked Campanian to Paleocene species. In subsequent core-catcher samples from Cores 129-802A-35R to -37R, Tertiary planktonic foraminifers were still observed but were of very poor preservation and did not allow precise age determination.

Sample 129-802A-38R-CC and an additional Sample 129-802A-38R-3, 101–105 cm, were barren of foraminifers.

The first evidence of Cretaceous age sediments is in Sample 129-802A-39R-CC, where we observed a diverse and moderately preserved assemblage dominated by very small specimens of *Brizalina* sp., *Heterohelix globulosa*, *Globigerinelloides praehillensis*, *Globigerinoides ultramicra*, *Hedbergella holmdellensis*, *Rugoglobigerina* sp., and *Archaeoglobigerina* sp. The planktonic species indicate a Campanian age according to the range chart of Caron (1985), but do not permit a more exact zonation.

Very small specimens of *Schackoina cenomana* in Sample 129-802A-54R-CC indicate a Cenomanian age. Small undetermined species of *Hedbergella* sp. and *Globigerinelloides* sp. were also found in this interval. The remaining core-catcher samples from Hole 802A are barren of foraminifers.

### Radiolarians

Fifty-three core-catcher samples and 97 additional samples within the cores were examined for radiolarians in Hole 802A.

Sample 129-802A-1R-CC contains few but well-preserved radiolarians, together with a few diatoms. Species observed include *Spongaster tetras* and *Euchitonia* sp., indicating a late Pliocene to Quaternary age. Cenozoic sediments from Cores 129-802A-3R to -37R are almost barren of radiolarians. Of 73 samples examined from this interval, 10 contain poorly preserved radiolarians in low abundances ("rare" to "few"). Sample 129-802A-29R-CC, however, yielded an abundant, well-preserved assemblage of reworked Eocene radiolarians, including *Podocyrtis mitra, P. chalara, P. trachodes, Dictyopora mongolofieri, D. amphora, Phormocyrtis trachodes*, and *Lithochytris vespertilio*.

Cores 129-802A-38R to -50R contain rare to few (rarely common) but poorly preserved radiolarians of Cretaceous age. The scarcity of radiolarian-rich horizons and the poor preservation do not permit zonal assignment of this interval. The interval from Samples 129-802A-51R-3, 11–13 cm, to 129-802A-56R-2, 57–61 cm, yielded abundant, poorly to moderately preserved radiolarians. Samples 129-802A-51R-3, 11–13 cm, to 129-802A-55R-1, 59–62 cm, contained *Thanarla veneta* and/or *Pseudodictyomitra pseudomacrocephala*. The possible co-occurrence of these species indicates that the upper *Acaeniotyle umbilicata* to lower *Obesacapsula somphedia* Zone (upper Albian to Cenomanian) may be present. The interval between Samples 129-802A-55R-CC and 129-802A-56R-2, 57–61 cm, does not contain the above-mentioned diagnostic species but is otherwise similar to the radiolarian faunal association seen in the overlying sediments, indicating that the interval is still within the same zones. The dark gray claystone of Cores 129-802A-56R and -57R is barren of radiolarians.

### Palynomorphs

Fifty-six core-catcher samples and 15 additional samples from within the cores were investigated for palynomorphs. Samples 129-802A-1R-CC through 129-802A-24R-CC and Samples 129-802A-26R-CC through 129-802A-55R-CC are barren of palynomorphs. Sample 129-802A-25R-CC contains abundant wood fragments, cuticles, and a few spores and pollen grains. The palynologic evidence indicates that some of the seamounts were above sea level during the early Miocene.

Samples 129-802A-56R-CC and 129-802A-57R-2, 57–61 cm, yielded a rich palynoflora including common dinoflagellate cysts. The dinoflagellate assemblage is characterized by the *Oligosphaeridium* group (*O. pulcherrimum* and *O. complex*), *Cassiculosphaeridia* sp., *Canninginopsis collivieri*, and *Dingodinium cerviculum*. *Dingodinium cerviculum* ranges from the Valanginian to the late Aptian/early Albian and *Canninginopsis collivieri* ranges from the Aptian to the Turonian, indicating an Aptian to Albian age for these samples. Sporomorphs in this interval are dominated by spores; pollen grains are rare. The spore assemblage is dominated by *Cyathidites* spp., and rare specimens of *Cicatricosisporites* spp. Bisaccate pollen are rare, although the monosaccate pollen *Callialasporites dampieri* and *C. trilobatus* are relatively common. The abundance of sporomorphs, wood fragments, and cuticles indicates emergent seamounts during the late Aptian to Albian, and the dominance of spores implies a humid climate.

### Sedimentation Rates

Figure 31 shows the sedimentation rates for Site 802, as determined on the basis of nannofossil, radiolarian, foraminiferal, and dinoflagellate biostratigraphy. Three hiatuses were depicted at the base of the late(?) Oligocene, at the base of the Paleocene, and at the base of the late Campanian, respectively.

## PALEOMAGNETISM

### Methods

Measurements of natural remanent magnetization (NRM) were made on all cores in the interval from Cores 129-802A-30R to -56R and on a few selected cores higher in the hole. As most cores of this hole represented semicontinuous recovery, nearly all were measured as continuous cores rather than discrete fragments. Alternating field (AF) demagnetization was generally performed using steps of 5, 10, and 15 mT. More detailed demagnetization was done in certain intervals, for example in the Upper Cretaceous cores where, in order to investigate small intervals of apparent reversed polarity, a larger number of more closely spaced steps were used. The measurement interval chosen for this site was 3 cm, and the near-continuous recovery for most of the hole allowed the use of this interval in most of the magnetic measurements. Magnetic behavior was analyzed by the systematic evaluation of equal area and orthogonal-axis vector plots, intensity-decay patterns ($J/J_0$), and raw volume-susceptibility ($K_a$) data for the different lithologic groups. Inclinations and relative declinations were calculated for selected core levels using least squares regression along linear segments of the magnetization decay trajectories.

### Sediment Magnetic Behavior

AF demagnetization response and susceptibility values are characteristically different for the various lithologic units encountered at Site 802, and the properties will be discussed on the basis of the major lithologic groups (as defined in "Lithostratigraphy and Sedimentology" section, this chapter).

The Miocene tuff unit (Cores 129-802A-3R through -26R) was investigated by an examination of Cores 129-802A-3R, -6R, -10R, -19R, -25R, and -27R. Intensity of NRM magnetization for the more tuffaceous upper part of the unit averages approximately 22 mA/m; median destructive fields (MDF) range widely from as low as 3 mT to greater than 200 mT. Analysis of the magnetization decay on orthogonal axes plots indicated a general ineffectiveness of AF demagnetization to separate the magnetic components in these samples. Susceptibilities were notably uniform in this upper portion of the tuff unit, ranging from core averages of 103 to 207 SI units.

The lower portion of the tuff unit contains chalks and calcareous claystones, which yielded higher NRM intensities (approximately 103 mA/m). Consistently higher values for susceptibility were also observed. Unlike the upper part of this unit, response to AF demagnetization showed a tendency to decay in the general direction of origin, although not yet directly toward it.

The nannofossil chalks, Cores 129-802A-27R through -36R, have low NRM intensities, and generally quite low values of MDF (about 5 mT). These cores also show greatly reduced susceptibility, especially in the base of the unit. Core-averaged susceptibility ranges from 223 SI units at the uppermost portion of the unit (chalk debris flow) to 14 SI units in the lowermost core of this lithology.

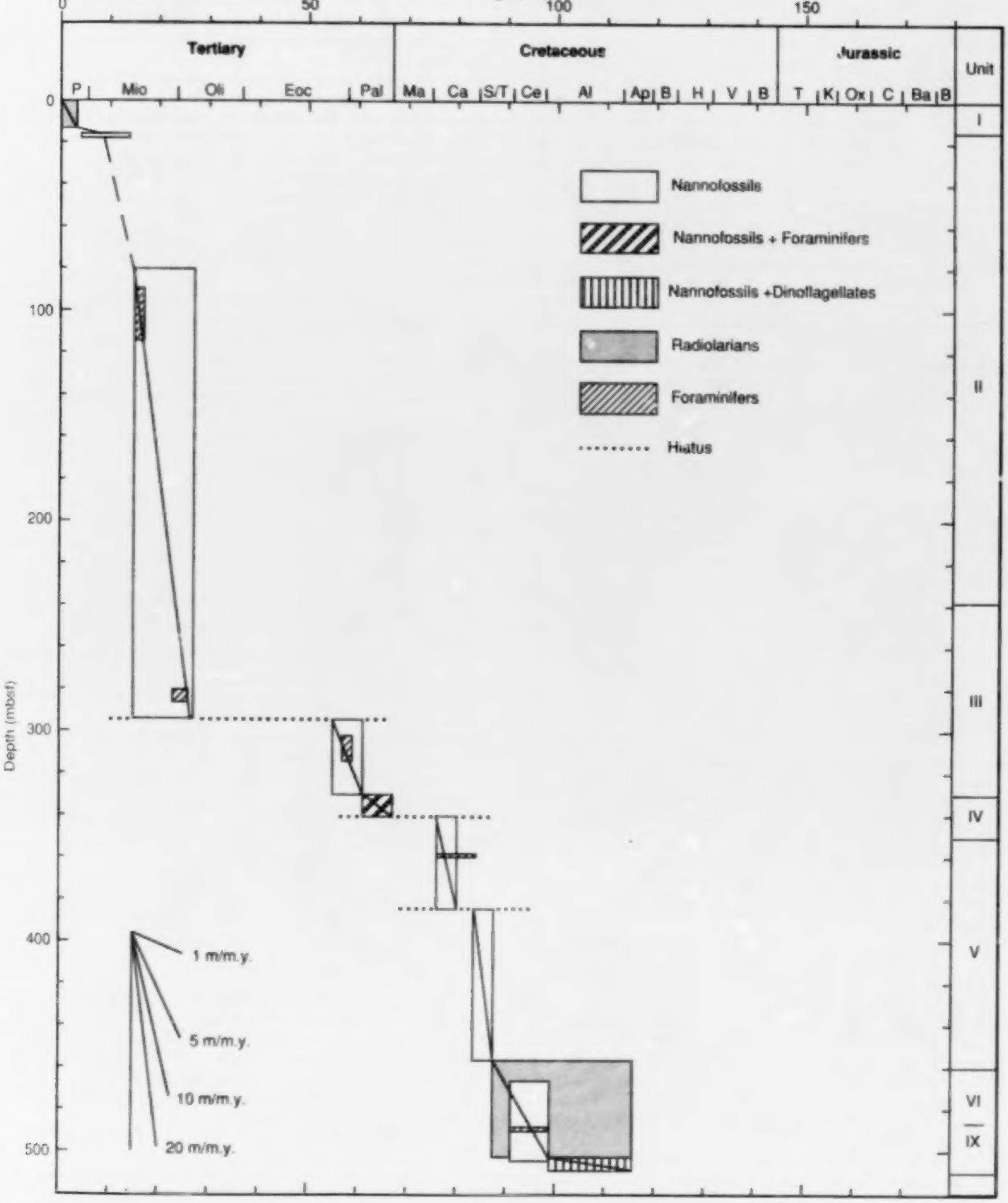

Figure 31. Sedimentation rates for Hole 802A.

The claystone unit consisted of only a single core, 129-802A-38R. Susceptibility values ranged widely from approximately 90 to nearly 700 SI units. Such high susceptibilities had not been encountered in sedimentary units previously on this leg. NRM intensities are also high, averaging approximately 205 mA/m. In addition, MDF values were consistently high, around 15 mT. Overall, the response to AF demagnetization was good. Decay of magnetization as indicated on orthogonal-axis plots showed movement in the direction of, although not yet directly toward, the origin, indicating that a significant portion of the overprinting magnetization was removed by demagnetization to 15 mT. However, the fact that appreciable magnetization intensity remains and that spectra still overlap indicate the presence of higher coercivities in this lithology.

The volcaniclastic turbidites (Cores 129-802A-39R through -51R) show variability in susceptibility ranging from approximately 200 to 500 SI units. The variability, in this case, can be accounted for by changes in grain size. NRM, MDF values, and general magnetic behavior are quite similar to those the overlying claystone unit.

The lowest sediment cores, 129-802A-52R through -56R, showed basically the same characteristics as the volcaniclastic turbidites and claystones located above, except that the variability in susceptibility is much reduced in magnitude, by a factor of approximately 10.

### Magnetostratigraphy

Reversals of magnetic polarity were observed in many of the cores from this site. A large number of reversed polarity intervals are observed in the lower Miocene through Santonian sequence (Cores 129-802A-30R through -46R). Exclusively normal polarity is observed in all cores below Core 129-802A-46R. The polarity interpretations are diagrammed in Figure 32, along with the biostratigraphic age determinations from the "Biostratigraphy" section (this chapter).

For the sequence encompassing the early Miocene through Paleocene (Cores 129-802A-30R through -37R), there are no serious discrepancies between the biostratigraphic and the magnetostratigraphic age determinations. The early Miocene and late Oligocene ages of Cores 129-802A-30R through -32R are compatible with the magnetostratigraphy, but the abundance of reversals of polarity in this time interval precludes assignment of the observed reversals to recognized polarity chrons. The lower Eocene Cores 129-802A-33R and -34R are suggested by the magnetostratigraphy to be of middle to early Eocene age because of the predominance of reversed polarity in the recovered portions of these cores and the large interval of reversed polarity in the geomagnetic polarity time scale for that time. The biostratigraphic late Paleocene age of Cores 129-802A-35R through -37R is in good agreement with the magnetostratigraphic evidence of dominantly reversed polarity.

Disagreement between magneto- and biostratigraphy begins with upper Campanian Cores 129-802A-38R through -42R. The biostratigraphic age would predict that these cores should have exclusively normal polarity magnetizations. While they are predominantly normally magnetized, there are four to five relatively short intervals which are either of clearly reversed magnetization or display demagnetization behavior suggestive of reversed magnetization. In Core 129-802A-38R two intervals show behavior suggesting, but not clearly indicating, reversed magnetization. The observed high coercivities, in conjunction with the red-brown color, indicate that demagnetization is incomplete. Therefore, the reality of these apparent reversed intervals, and hence their significance, must await more extensive demagnetization. However, Core 129-802A-39R, a mixture of chert/porcellanite and volcaniclastics, contains true reversed polarity, although the length of the interval cannot be determined because of the fragmentary recovery. Core 129-802A-40R also has two intervals of definite reversed polarity; these are represented only by small blocks, as the material above and below the reversed portions has been crushed into very small pieces or ground into a mush, so again the length of the reversed polarity intervals cannot be determined. In the case of Core 129-802A-40R it is possible that core disturbance, coupled with the width of the sense region of the magnetometer, has caused the apparent reversed characteristics. Overall, however, the reason for the discrepancy of numerous small indications of reversed polarity in the late Campanian, within an interval that should be entirely normal, is presently unclear, but the problem is compounded by further conflicts between the magneto- and biostratigraphy in the Santonian-age cores immediately below this interval.

Cores 129-802A-43R through -46R are biostratigraphically determined to be of Santonian age, but again, their magnetization displays reversed polarity intervals. The Santonian is well known as a time of exclusively normal polarity, as it is the youngest part of the 34 m.y. of extended normal polarity during the Cretaceous long normal polarity interval (Helsley and Steiner, 1969; Irving and Pullaiah, 1976; Kent and Gradstein, 1986). However, two or three intervals of definite reversed polarity are observed in Cores 129-802A-43R and -44R (Fig. 32). In addition, we observed a relatively small interval of probable reversed polarity in Core 129-802A-45R, as well as another interval in Core 129-802A-46R with clear and less clear reversed polarity characteristics in the demagnetization response (Fig. 32). The intervals in the latter two cores are suggestive of reversed polarity, but the evidence is not entirely certain; the former two or three are clearly intervals of reversed polarity.

The definite reversed polarity in Cores 129-802A-43R and -44R precludes them from being Santonian in age unless some peculiarity resulting from redeposition or remagnetization is somehow responsible for the reversed polarity. It might be, for example, that the reversed remanent magnetization remaining after demagnetization is not the primary magnetization, but a drilling remanence or the result of some other secondary magnetization. There is no evidence for this at present, but such possibilities cannot be entirely ruled out. More extensive demagnetization studies in shore-based investigations will address these ambiguities.

Below Core 129-802A-46R no further reversals of polarity are observed and it would appear that Cores 129-802A-47R through -56R are within the Cretaceous long normal polarity interval.

### Paleolatitude

An important objective of Leg 129 was the determination of paleolatitudes from the measured paleomagnetic inclinations. The improved recovery at Site 802 permitted calculation of paleolatitude data from a large portion of the recovery, although these results are nevertheless preliminary because the AF demagnetization was insufficient to completely reveal the characteristic magnetization.

As at previous sites, selected core levels were chosen for least squares regression analysis on the basis of a uniformity of declination and inclination over a given portion of a core segment. While all samples showed progressive decay of magnetic vectors in the general direction of the origin on orthogonal-axis plots, decay directly to the origin was rare.

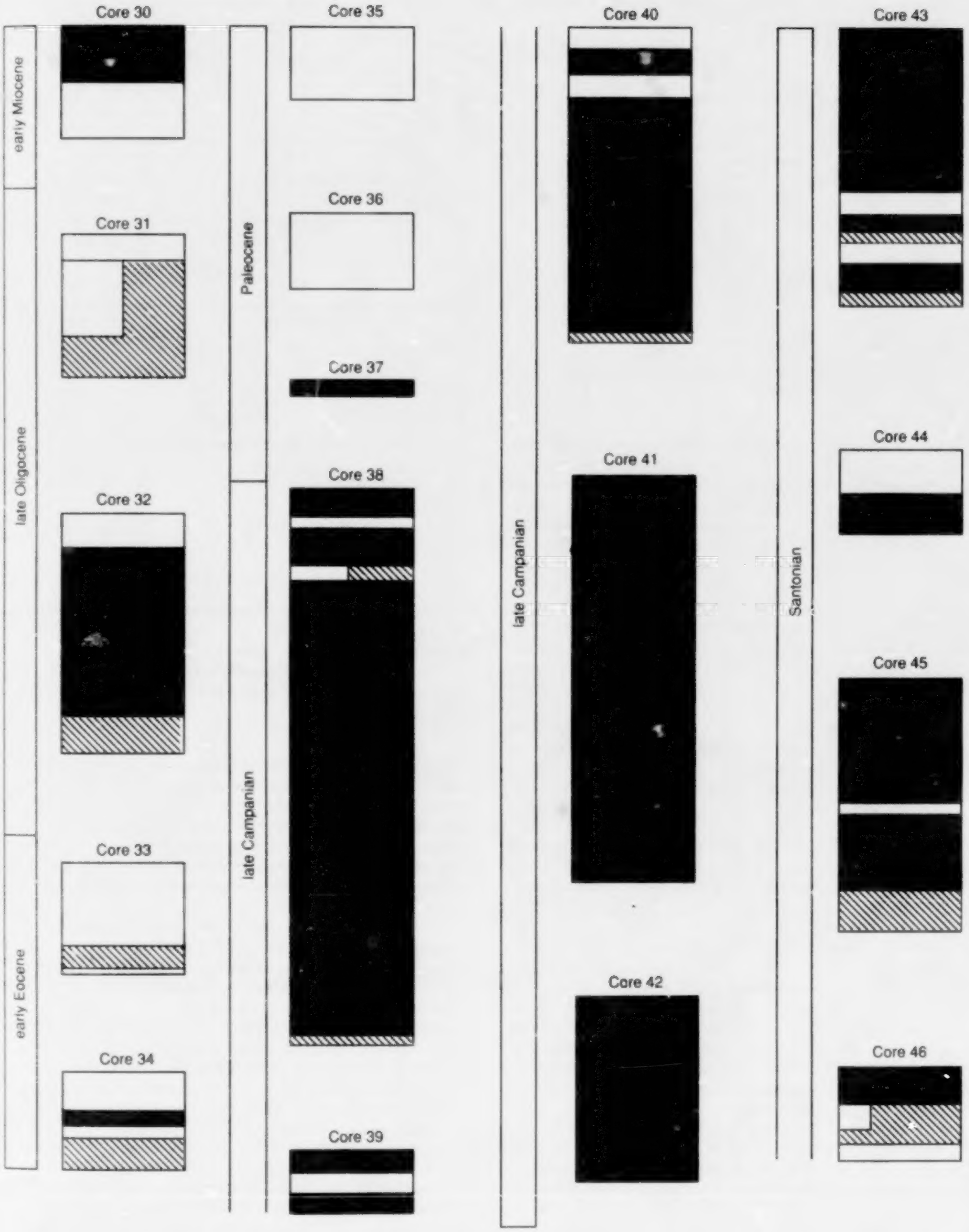

Figure 32. Polarity interpretation of lower Tertiary through Upper Cretaceous cores from Hole 802A in which intervals of reversed polarity were observed. Individual segments represent the core recovery, hachured areas indicate the absence of data, black areas are normal polarity, and white areas are reversed polarity. Half-column width indicates uncertainty in the polarity interpretation. Ages of each column are to the left of the respective columns.

**Table 4. Inclination and paleolatitude values from selected segments of the sedimentary cores.**

| Core(s) | N | INC | K | Paleolatitude (°) | $\alpha_{95}$ | SD |
|---|---|---|---|---|---|---|
| 129-802A- | | | | | | |
| 25R–27R | 8 | 40.1 | 8.3 | 22.9N | 18.0 | 10.4 |
| 30R–34R | 7 | 15.5 | 43.1 | 7.9N | 5.1 | 3.0 |
| 38R | 15 | −2.4 | 198.4 | 1.2S | 1.6 | 0.9 |
| 39R | 6 | −4.7 | 83.8 | 2.3S | 5.8 | 3.3 |
| 40R | 13 | 15.8 | 30.9 | 8.0N | 5.6 | 3.2 |
| 41R | 11 | 29.5 | 31.1 | 15.8N | 5.9 | 3.4 |
| 42R–44R | 14 | 14.0 | 35.8 | 7.1N | 4.2 | 2.4 |
| 45R–46R | 10 | −12.8 | 40.8 | 6.5S | 5.2 | 3.0 |
| 47R–48R | 9 | −23.7 | 47.4 | 12.4S | 5.6 | 3.2 |
| 49R–50R | 9 | −11.5 | 102.4 | 5.9S | 2.8 | 1.6 |
| 51R–53R | 11 | −13.8 | 42.3 | 7.0S | 4.3 | 2.5 |
| 54R | 12 | −16.6 | 170.7 | 8.5S | 1.8 | 1.0 |

Note: N is the number of regions used to calculate each point; INC is the mean inclination; K is the precision parameter; $\alpha_{95}$ is the half-radius of the 95% circle of confidence; and SD is the standard deviation.

This indicates the presence of secondary magnetization that was not removed by the low-level demagnetization. The secondary magnetization appears to be similar to the present-day magnetic inclination at the site, and thus will bias Southern Hemisphere normal polarity samples toward shallower inclinations, and reversed polarity ones toward steeper ones. Statistical analysis was performed on the inclinations generated by regression analysis, using the method of Kono (1980), and the results are listed in Table 4.

Figure 33A illustrates the inferred latitudinal component of Pacific plate motion as recorded at Site 802. Although preliminary, the results suggest that this part of the Pacific plate crossed the paleoequator in the period of time spanning the earliest Paleocene to late Campanian. Again the data used in the calculation of the paleolatitudes were predominantly of normal polarity. If the data are preferentially shallow because of incomplete demagnetization, as previously suggested, a Campanian age for the equator crossing is the least plausible, and a crossing in the Paleocene (or possibly Eocene) is more likely.

Data from Cores 129-802-40R through -44R show an anomalous equator crossing, unexpected both in terms of the results from Sites 800 and 801, and from previous paleomagnetic and magnetic anomaly studies (see "Site 800" and "Site 801" chapters, this volume). Samples within these cores display significant intensity increases during demagnetization and a subsequent decay pattern on orthogonal-axis plots that could be associated with reversed polarity, although they lack the characteristic large-scale shift in declination. If these are reversed and have a secondary magnetization that is sufficiently resistant to the low-level AF demagnetization employed, the demagnetization may well have been be inadequate to reveal the declination shift and the reversed nature of the magnetization. If the samples are of reversed polarity and are not representative of Northern Hemisphere paleolatitudes, then the paleolatitude plot for Site 802 should look like that shown in Figure 33B. More extensive demagnetization studies onshore will ascertain the true polarity and paleolatitude in this interval.

## Basalt Magnetism

Core segments from three of the six basalt cores were analyzed using the cryogenic magnetometer. Most of the remainder of the recovered basalts could not be measured with the cryogenic magnetometer because the intensities were too strong to be able to keep accurate count of the scale over-ranging. AF demagnetization was carried out on the three segments that could be measured with the cryogenic magnetometer; AF increments from 2 to 20 mT were used. Volume magnetic susceptibility was measured for all basalt cores.

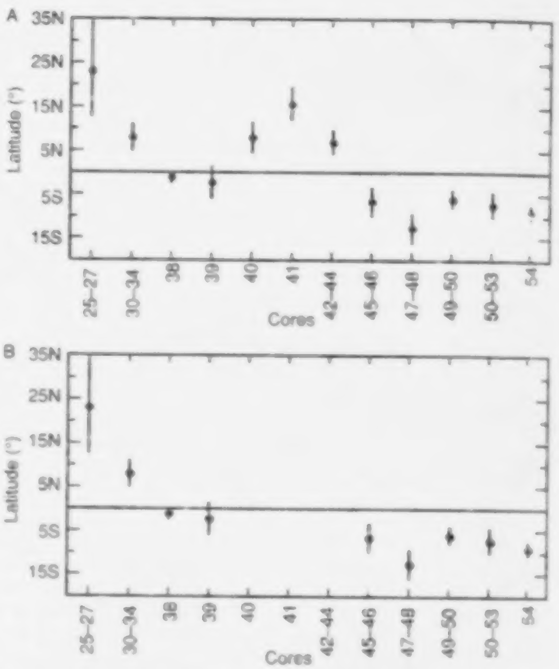

Figure 33. **A.** Paleolatitude values plotted against their corresponding Cores 129-802A-25R through -54R. Error bars represent one standard deviation on either side of the mean value. **B.** The same data as in as (A), but with Cores 129-802A-40R through -44R removed because of the possibility of reversed polarity and significantly incomplete demagnetization.

NRM intensity varies between 1.1 and 3.2 mA/m, but most samples have values below 2.0 mA/m (Fig. 34A). NRM intensities that exceed this value seem to be related to microphyric textures, although the number of data available does not allow positive correlation.

In response to AF demagnetization, all samples displayed large rises in intensity, most probably associated with the overprinting of a normal Northern Hemisphere polarity magnetization (Brunhes Chron) onto a normal Southern Hemisphere characteristic remanence. The majority of samples are not sufficiently demagnetized by the AF treatment to reveal the median destructive fields. Inclinations were calculated by linear regression of segments of the decay path; these are plotted in Figure 34B. The negative inclinations indicate normal polarity in the Southern Hemisphere. The dispersion displayed by the data probably results from incomplete demagnetization. Higher AF demagnetization in shore-based studies will be necessary to define the true inclinations of these basalts. Despite the dispersion, the few data, and the

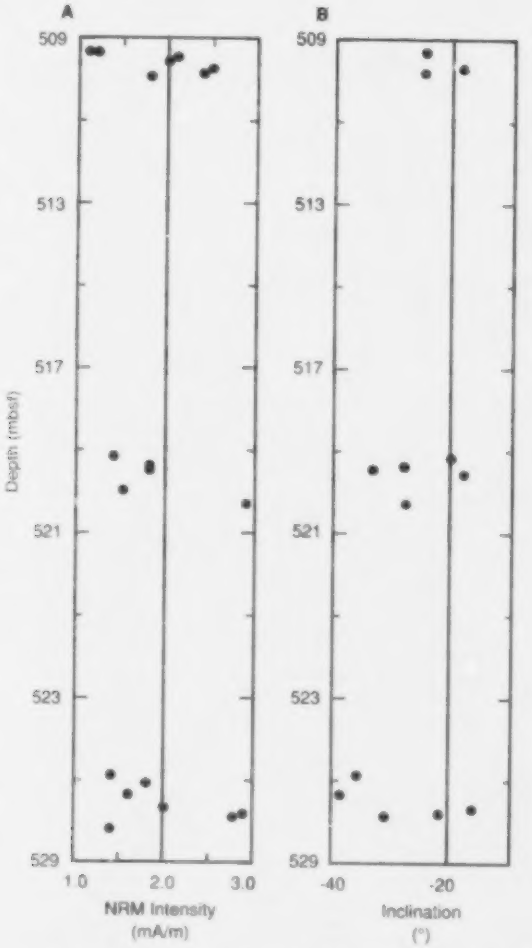

Figure 34. Basalt NRM intensity (A) and inclinations (B) plotted against depth (mbsf) for sections within Cores 129-802A-57R through -59R.

probable lack of averaging of secular variation, the inclinations imply a paleolatitude consistent with the 12° to 15° paleolatitudes for Aptian/Albian sediments of Sites 800 and 801.

Susceptibility values are shown Figure 35. Correlations with the observed petrographic units (as defined in the "Igneous Petrology" section, this chapter) are not obvious except for the unit located between 545 and 552 mbsf (Fig. 35). Susceptibility values are notably higher here than in the basalts above, averaging about 2.0 SI units, approximately twice that of the rest of the basalt. These high values seem to correspond to a sparsely microphyric flow unit in Cores 129-802A-61R and -62R. Other high values of susceptibility in the cores recovered above seem to be associated with well-defined pillow lavas.

## INORGANIC GEOCHEMISTRY

Interstitial water samples were squeezed from sediment cores at sixteen levels in Hole 802A. The samples are distributed between 26 and 500 mbsf in the tuff of lithologic Unit II, the nannofossil chalk of Unit III, the volcaniclastics turbidites

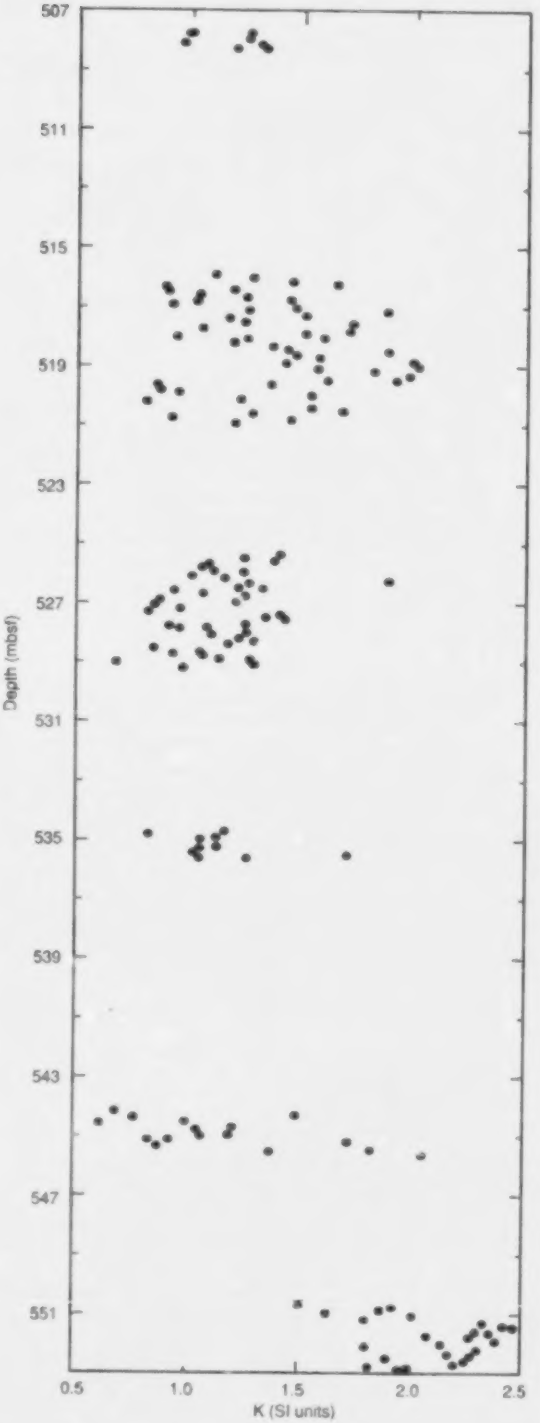

Figure 35. Volume magnetic susceptibility plotted against depth (mbsf) for all basalts from Site 802 (Cores 129-802A-57R through -62R). Every third value of susceptibility from the shipboard measurements is plotted in the diagram.

**Table 5. Chemical composition of interstitial water extracted from sediments in Hole 802A.**

| Core, section, interval (cm) | Depth (mbsf)[a] | Alkalinity (meq/L) | Cl (mmol/L) | $SO_4$ (mmol/L) | pH | Salinity (‰) | Ca (mmol/L) | Mg (mmol/L) | K (mmol/L) | $Na^+$ (mmol/L) | Mn (µmol/L) | Si (µmol/L) | Sr (µmol/L) | Lithology |
|---|---|---|---|---|---|---|---|---|---|---|---|---|---|---|
| 129-802A | | | | | | | | | | | | | | |
| 4R-1, 140–150 | 26 | 1.4 | 554.1 | 26.8 | 7.8 | 34.8 | 16.2 | 50.9 | 12.2 | 464 | 7 | 162 | 99 | Tuff (silty sand) |
| 6R-2, 0–10 | 44 | 0.8 | 547.2 | 36.5 | 8.3 | 36.1 | 42.3 | 15.7 | 11.0 | 466 | 15 | 76 | 167 | Tuff (silty sand) |
| 10R-2, 140–150 | 83 | 0.6 | 631.1 | 0.4 | 9.0 | 39.0 | 125.2 | 0.2 | 2.7 | 378 | 19 | 194 | 381 | Tuff (silty sand) |
| 13R-1, 53–58 | 109 | 0.5 | 627.2 | 3.7 | 7.8 | 39.0 | 130.2 | 4.0 | 2.1 | 364 | 22 | 197 | 380 | Pelagic brown clay |
| 19R-2, 107–117 | 162 | 0.6 | 610.4 | 9.9 | 8.5 | 37.7 | 108.3 | 5.8 | 2.1 | 404 | 17 | 157 | 447 | Calcareous silty clay |
| 21R-1, 103–110 | 179 | 0.6 | 613.3 | 11.9 | 8.5 | 38.5 | 114.3 | 3.6 | 1.7 | 400 | 11 | 124 | 459 | Claystone |
| 26R-1, 0–10 | 225 | 0.4 | 612.3 | 12.2 | 8.1 | 38.3 | 118.4 | 2.7 | 1.6 | 392 | 20 | 151 | 400 | Calcareous claystone |
| 29R-3, 29–34 | 258 | 0.6 | 583.7 | 12.0 | 7.2 | 37.5 | 115.5 | 4.4 | 1.9 | 363 | 41 | 913 | 473 | Pelagic clay |
| 32R-2, 140–150 | 286 | 0.2 | 575.8 | 12.5 | 6.5 | 37.5 | 96.1 | 12.9 | 4.6 | 376 | 46 | 637 | 395 | Nannofossil chalk |
| 40R-2, 140–150 | 361 | 0.6 | 587.6 | 15.0 | 8.0 | 36.5 | 80.5 | 10.2 | 2.6 | 432 | 35 | 399 | 230 | Volcaniclastic turbidite |
| 43R-1, 140–150 | 384 | 0.6 | 578.8 | 15.1 | 7.9 | 36.0 | 77.3 | 11.7 | 2.5 | 427 | 43 | 556 | 295 | Volcaniclastic sandstone |
| 47R-2, 140–150 | 422 | 0.6 | 530.4 | 13.2 | 7.9 | 33.8 | 66.8 | 11.5 | 2.2 | 398 | 53 | 203 | 255 | Volcaniclastic sandstone |
| 50R-2, 140–150 | 450 | 0.8 | 553.1 | 13.6 | 7.9 | 34.7 | 74.0 | 10.5 | 2.2 | 405 | 54 | 179 | 274 | Volcaniclastic sandstone |
| 56R-2, 140–150 | 500 | 0.8 | 585.7 | 15.7 | 8.2 | 36.5 | 81.5 | 2.8 | 1.2 | 447 | 22 | 216 | 167 | Tuffaceous claystone |

Note: $Na^+$ calculated by charge balance.

[a] Depth rounded to nearest meter.

of Unit V, and the claystone of Units VIII–IX. Squeezing yielded between 0.9 ml/cm and 5.5 ml/cm in whole-round samples. Highest yields (3.3–5.5 ml/cm) were obtained between 109 and 226 mbsf. At 321 and 471 mbsf the amount of water recovered was so low that analysis will be required onshore. Chemical analyses are summarized in Table 5 and presented in Figures 36 and 37. Except at 26 mbsf, pollution by drilling fluids can be ruled out, as potassium, calcium, and magnesium have concentrations very different from those of seawater or drilling mud (see Table 4, "Inorganic Geochemistry" section, "Site 800" chapter).

### Results

From 22 to 83 mbsf, concentration profiles show very intense enrichments in calcium and chloride and depletions in magnesium, potassium, sodium, strontium, sulfate, and alkalinity. Within only 60 m, salinity increases from 34.8‰ to 39‰, calcium increases to 770% of seawater content, strontium to 400%, and chloride to 114%. In the same interval, magnesium is reduced to 0.5% of seawater content, potassium to about 22%, and sodium to about 78%. Below 83 mbsf compositions are roughly similar until 225 mbsf. At 258 mbsf, within a level of pelagic clay in the chalk of Unit III concentrations remain similar except for silica, which increases to 913 µmol/L. Below this level, from 258 to 500 mbsf, the general trend is a progressive decrease of salinity (about 39‰ to 34‰) as a result of decreases in calcium and chloride contents. In this interval, sodium and magnesium increase slightly.

Manganese gradually increases from seawater concentration at 26 mbsf to 54 µmol/L at 450 mbsf and drops down to 22 µmol/L at 500 mbsf.

### Discussion

The most important feature of concentration profiles in Hole 802A is the very large increase in calcium and chloride concentrations between 26 and 83 mbsf. This very high gradient is not related to any kind of porosity or water content change in the first hundred meters of the hole (see "Physical Properties" section, this chapter). Therefore, it implies that the tuffs of Unit II are presently undergoing very intense reactions; otherwise, diffusion would have reduced the gradients. These reactions are likely to be limited to Unit II because the calcium and chloride contents begin to decrease below 258 mbsf (top of the chalk of Unit III). In Unit II, the calcium release can be due either to alteration of the volcanic glass and the plagioclase, which are abundant in this unit, or to dissolution of carbonates, which represent 0.5% to 1% of the rock at the top of Unit II (see "Lithostratigraphy and Sedimentology" section, this chapter). Dissolution of carbonate should be accompanied by an increase in alkalinity and is therefore unlikely. The alteration of volcanic material is probably responsible for the strontium release which correlates with the calcium release.

In Unit II the calcium change is balanced by the uptake of sodium, magnesium, and potassium and also by a chloride increase. Chloride concentration in pore water can be enhanced by dissolution of evaporites, gas hydrate formation, clay membrane filtration, or uptake of water by early diagenetic reactions. As evaporites are not present in the sediment and organic matter content is very low, the first two processes can be ruled out. Membrane filtration is also unlikely because the clay content is typically below 20% and the compaction of this unit is not very important. Formation of authigenic phases such as smectite and zeolite is therefore the most probable process and it is consistent with the reactions that deplete the pore water in magnesium, sodium, and potassium. This is supported by the presence of fractures filled by mixtures of zeolites such as analcime, analcime-wairakite, and/or laumontite at 63, 81, 115, and 168 mbsf (XRD determination). At the limit between Unit II and III, the silica content changes abruptly from 151 µmol/L at 225 mbsf to 913 µmol/L at 258 mbsf. This very rapid change suggests that silica is intensively taken up in diagenetic reactions in Unit II.

Below 258 mbsf the calcium and chloride contents decrease and the depletions in magnesium and sodium are less extreme. Concentrations in the underlying units are probably influenced by those of Unit II because of diffusion. It is therefore difficult to determine if reactions occur in these units or not. Unit V and VIII through X are likely to undergo reactions, as suggested by a decrease in silica content below Unit III.

### Conclusion

Pore-water chemistry in Hole 802A is dominated by intense alteration and diagenetic reactions in the tuff of Unit II. These reactions are responsible for a extremely high gradients in calcium and chloride contents in the first 100 m of the hole. Similar gradients in calcium and chloride have been reported in ODP Hole 793 due to reactions within volcanic material (Leg 126, Shipboard Scientific Party, 1990). However, in that case the high gradients were enhanced by a slow diffusion barrier at the top of the formation. There is no such barrier in Hole 802A, suggesting that the rate of alteration of volcanic material and of zeolite and smectite formation is sufficiently high to overprint the influence of diffusion from seawater.

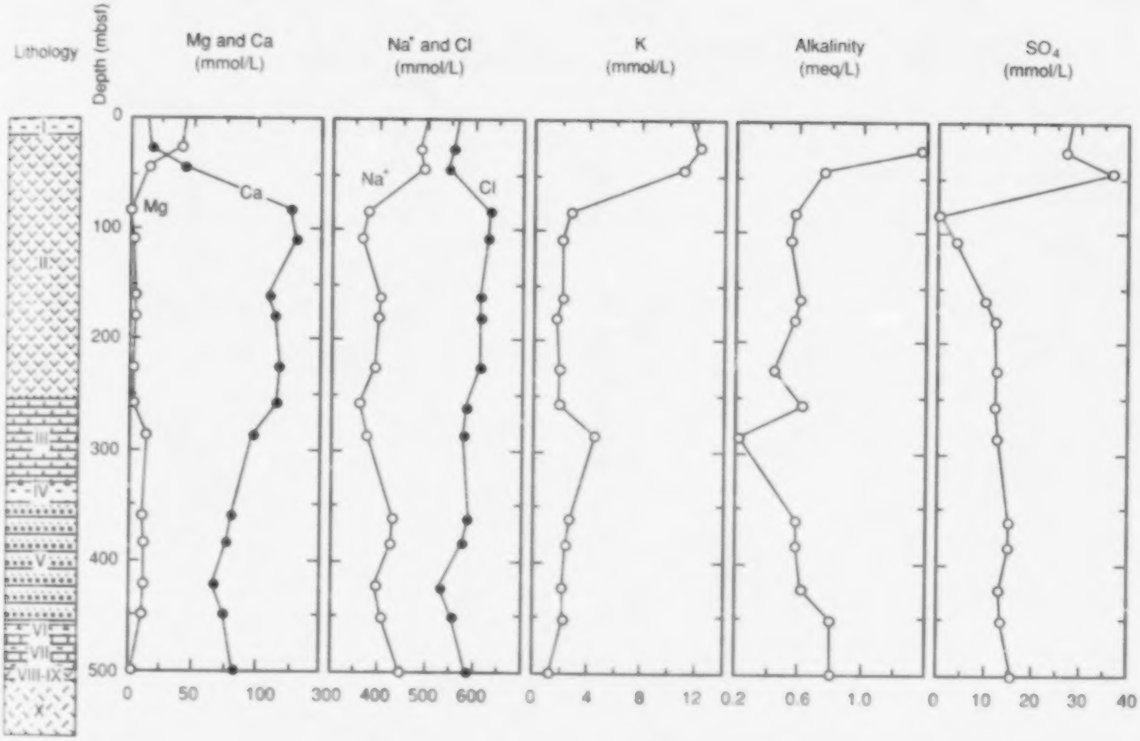

Figure 36. Concentration vs. depth profiles for Mg, Ca, Na*, Cl, K, alkalinity, and $SO_4$ in interstitial water extracted from sediments in Hole 802A. The lithostratigraphic column refers to the lithologic units defined in the "Lithostratigraphy and Sedimentology" section (this chapter). Unit I, brown pelagic clay; Unit II, tuff; Unit III, nannofossil chalk; Unit IV, claystone; Unit V, volcaniclastic turbidites; Unit VI, claystone and radiolarite; Unit VII, calcareous claystone and radiolarian limestone; Units VIII and IX, claystone and volcaniclastic turbidites; and Unit X, basalt.

## PHYSICAL PROPERTIES

Determination of physical properties of sediments and rocks recovered at Site 802 was based only on measurements using discrete samples. Continuous measurements provided by the GRAPE and *P*-wave logger were not obtained because sediments and rocks did not completely fill core liners. Physical properties measured on discrete samples are listed in Table 6 and include index properties (wet-bulk density, porosity, water content, and grain density), compressional-wave velocity, and thermal conductivity. All techniques and equipment used in making the measurements are described in the "Explanatory Notes" chapter (this volume). Physical properties were determined for samples from lithologic Units II through X. Sediment recovery from Unit I (1 cm) was insufficient for physical properties measurements.

### Index Properties

Variations in index properties among the lithologic units identified at Site 802 are described in the following section in terms of porosity, wet-bulk density, and grain density. Water content varies directly with porosity, and values for water content are listed in Table 6 and plotted in Figure 38. Wet-bulk density was determined by gravimetric and 2-min GRAPE techniques. Values cited for bulk density are those of gravimetric analyses, unless otherwise specified. Grain density was determined using "solid" chunks for all samples and powdered specimens for four samples (Table 6). The use of pycnometer-chamber inserts designed and fabricated for cube samples reduced previous volume measurement errors and yielded grain density measurements comparable to those obtained using powdered samples.

Index properties of lithologic Unit II (14.6–237.4 mbsf) reflect the division of this unit into two subunits. Subunit IIA (14.6–160.6 mbsf) consists predominantly of sand-sized tuffs (volcaniclastic turbidites), which typically contain 60% to 80% angular, fresh glass shards and tachylite (see "Lithostratigraphy and Sedimentology" section, this chapter). Index properties of the tuffs are moderately variable and display no downsection trends in variation (Fig. 38). Porosity of these rocks ranges from 31.3% to 60.4% and averages 49.3% (Table 6). Wet-bulk density of the tuffs ranges from 1.62 to 2.14 g/cm³ and averages 1.85 g/cm³. Pelagic brown clays, sampled at 15.70 and 108.77 mbsf, are a minor component of Subunit IIA and possess index properties distinctly different than those of the tuffs. At 15.70 and 108.77 mbsf the pelagic clays display porosities of 86% and 78% and wet-bulk densities of 1.25 and 1.35 g/cm³, respectively. Grain density in lithologic Subunit IIA ranges from 2.52 to 2.78 g/cm³ and averages 2.65 g/cm³.

Subunit IIB (160.6–237.4 mbsf) is distinguished from Subunit IIA by an increase in the proportion of redeposited

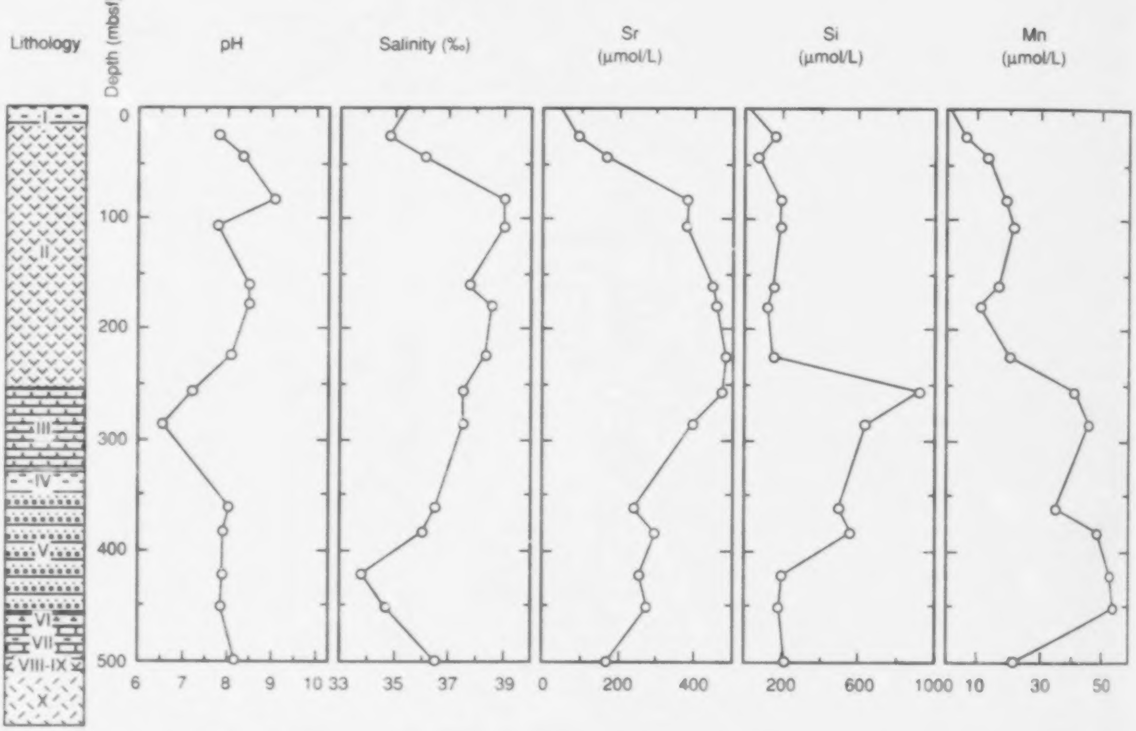

Figure 37. Profiles of depth vs. pH, salinity, and Sr, Si, and Mn concentrations in interstitial water extracted from sediments in Hole 802A. See Figure 36 for legend.

calcareous claystone and chalk and a change in composition of volcaniclastic sandstones, represented by decreased abundance of volcanic glass and increased abundance of igneous rock fragments, secondary calcite, and in some instances, microfossils. The increased abundance of fine-grained sedimentary rocks and the change in composition of volcaniclastic sandstones are reflected in the variation of index properties (Fig. 38). Properties of the sandstones, claystones, and siltstones in Subunit IIB are distinct. The volcaniclastic sandstones are characterized by porosities that range from 44.6% to 54.9% and average 51.1%. The wet-bulk density of these rocks ranges from 1.79 to 2.02 g/cm$^3$ and averages 1.87 g/cm$^3$. The ranges of porosity and wet-bulk density for fine-grained rocks in Subunit IIB are 58.7% to 72.3% and 1.48 to 1.73 g/cm$^3$, respectively. From the top of Subunit IIB to 215.82 mbsf, porosity of the fine-grained rocks increases and their wet-bulk density decreases with depth. At 215.82 mbsf a porosity of 72.3% and wet-bulk density of 1.48 g/cm$^3$ coincide with a local calcium carbonate concentration minimum of 5.2% (see "Lithostratigraphy and Sedimentology" section, this chapter). Below 215.82 mbsf, porosity decreases steadily and wet-bulk density increases in association with increasing carbonate concentration in the claystones. These trends culminate in Unit III at 254.65 mbsf where porosity is 30.9%, wet-bulk density is 2.18 g/cm$^3$, and calcium carbonate content is 78.8%. Grain density in Subunit IIB is slightly higher than that in Subunit IIA, reflecting the decreased abundance of glass and increased concentrations of igneous rock fragments and calcareous constituents. Grain density ranges from 2.63 to 2.86 g/cm$^3$ and averages 2.73 g/cm$^3$ in Subunit IIB.

The chalks and calcareous claystones of lithologic Unit III (237.4–329.9 mbsf) are characterized by highly variable porosity and wet-bulk density (Fig. 38). Grain density, however, is extremely uniform in Unit III with most sediments displaying values between 2.65 and 2.72 g/cm$^3$ (Fig. 38). Sediments sampled at 285.96, 311.56, and 312.42 mbsf exhibit grain densities between 2.49 and 2.59 g/cm$^3$ (Table 6) and occur in an interval marked by a significant increase in silica concentration on wireline geochemical logs (see "Downhole Measurements" section, this chapter) and an increase in the degree of silicification in the cores. As a consequence of the uniformity in grain density, there is a strong inverse relationship between porosity and wet-bulk density. The inverse relationship between porosity and calcium carbonate concentration, which is present in the transition between Subunit IIB and Unit III, is also well developed in the chalks and claystones of Unit III. In these sedimentary rocks porosity ranges from 18.5% to 53.8%, and wet-bulk density ranges from 1.76 to 2.39 g/cm$^3$. One chert nodule was sampled at 312.42 mbsf, and it displays a porosity of 1.5% and wet-bulk density of 2.53 g/cm$^3$.

Only two samples were obtained in the zeolitic pelagic claystones of lithologic Unit IV (329.9–349.2 mbsf). Averages for porosity, wet-bulk density, and grain density for this interval are 49.8%, 1.84 g/cm$^3$, and 2.64 g/cm$^3$, respectively.

The volcaniclastic turbidites of lithologic Unit V (349.2–460.0 mbsf) are similar to those of Unit II in that the properties of sand-sized and fine-grained sediments are distinct and display little evidence of downsection change. The silty claystones of Unit V differ from those of Unit II in that they display a slightly greater degree of compaction. Volcaniclastic sandstones of Unit V are characterized by porosity and wet-bulk density ranges of 43.2% to 51.7% and 1.86 to 2.04 g/cm$^3$ and averages of 48.5% and 1.94 g/cm$^3$, respectively. Excluding a sample with anomalously low porosity (38.4%) at 457.48 mbsf, porosity of the silty claystones ranges from 49.7% to 61.8% and averages 56.7%. Wet-bulk density of these rocks ranges from 1.60 to 1.89 g/cm$^3$ and averages 1.74 g/cm$^3$. Grain density is moderately variable in Unit V, with sandstones exhibiting slightly higher grain densities than those of the finer-grained sediments. Grain density ranges from 2.76 to 2.85 g/cm$^3$ for the volcaniclastic sandstones and from 2.44 to 2.82 g/cm$^3$ for the silty claystones. Low grain density at 438.27 mbsf (2.44 g/cm$^3$) is associated with increases in radiolarian abundance and degree of silicification of the sediments (see "Lithostratigraphy and Sedimentology" section, this chapter).

The lowermost 45 m of the sedimentary section at Site 802, which encompass lithologic Units VI (460.0–469.9 mbsf), VII (469.9–497.1 mbsf), VIII (497.1–499.6 mbsf), and IX (499.6–509.2 mbsf), contain a variety of rock types, including claystone, radiolarite, nannofossil chalk, siliceous limestone, and volcaniclastic sandstone (Table 6). From Unit VI through Unit VIII, claystones are characterized by decreasing porosity and increasing wet-bulk density, trends initiated in the basal part of Unit V. In this interval porosity decreases from 45.7% to 42.9%, and wet-bulk density increases from 1.90 to 1.93 g/cm$^3$. The volcaniclastic claystone of Unit IX differs from claystones in Units VI through VIII, and at 507.32 mbsf displays a porosity of 48.1%, a wet-bulk density of 1.87 g/cm$^3$, and grain density of 2.77 g/cm$^3$. Radiolarite was sampled at 463.14 mbsf and is characterized by a porosity of 42.0% and wet-bulk density of 1.90 g/cm$^3$. The relatively low grain density (2.53 g/cm$^3$) at this depth reflects the greater abundance of biogenic silica in this sediment. Chalks and limestones of Unit VII are characterized by lower porosities and higher wet-bulk densities than other rock types in Units VI through IX. Porosity of the carbonate rocks decreases downsection, from 43.8% at 470.15 mbsf to 26.1% at 489.04 mbsf, the latter value representing the porosity of a siliceous limestone. Coinciding with the porosity reduction is an increase in wet-bulk density from 1.95 to 2.22 g/cm$^3$. One volcaniclastic sandstone interval was sampled in Unit IX, at 500.43 mbsf, and its index properties are similar to those of sandstones in Unit V. The sandstone in Unit IX is characterized by a porosity of 48.1%, wet-bulk density of 1.93 g/cm$^3$, and grain density of 2.75 g/cm$^3$. With the exception of the low grain density of the radiolarite and the slightly higher density of the volcaniclastic sandstone and claystone, the grain density of rocks from the lowermost 45 m of the sedimentary section at Site 802 is relatively uniform and closely grouped about a mean of 2.66 g/cm$^3$.

Index properties of the basalts of lithologic Unit X (509.2–559.8 mbsf) are representative of fine-grained extrusive basalts. Porosity of five of the seven basalt samples analyzed ranges from 1.2% to 2.6% (Table 6). Rocks from 519.86 and 535.60 mbsf display porosities of 6.3% and 8.2%, respectively. Grain density of the basalts varies in a narrow range between 2.92 and 2.97 g/cm$^3$. The low porosity and narrow range in grain density reflect the relative lack of alteration of basalts recovered at Site 802. At Sites 800 and 801 significant basalt alteration is accompanied by high porosity, between 10% and 20%, and grain densities as low as 2.70 g/cm$^3$. Wet-bulk density of the basalt ranges from 2.77 to 2.94 g/cm$^3$.

### Compressional-Wave Velocity

At Site 802 compressional-wave velocities were measured in both vertical and horizontal propagation directions. Velocity anisotropy was calculated as the ratio of the velocity difference and the mean velocity, expressed as a percentage (see "Explanatory Notes" chapter, this volume). Variations in the velocity data generally conform with changes in lithology and physical properties. Unless otherwise noted, the velocity values cited are for measurements made in the vertical propagation direction.

The coarse-grained volcaniclastic turbidites of Subunit IIA are characterized by high and highly variable sonic velocity. Velocity of the sand-sized tuffs ranges from 2221 to 4080 m/s with no apparent downsection trend (Fig. 39). The average velocity for these rocks is 3024 m/s. The tuffs of Subunit IIA are nearly elastically isotropic, with values of velocity anisotropy ranging from 3.6% to 2.6% and averaging 0.4%. The uniformity of composition of the tuffs and abundance of volcanic glass in the rocks is most likely responsible for the low velocity anisotropy. In Subunit IIB, ranges for compressional-wave velocity of the tuffs and silty claystones are distinct (Table 6). The velocity of the tuffs varies narrowly between 2230 and 2562 m/s. The average velocity of these rocks, 2351 m/s, is substantially lower than that of tuffs in Subunit IIA. Higher velocity anisotropy of tuffs of Subunit IIB also distinguishes them from the rocks of Subunit IIA. Velocity anisotropy of the tuffs of the lower subunit range from 1.1% to 2.6% and average 2.2%. Claystones and siltstones of Subunit IIB exhibit sonic velocities that range from 1632 to 1962 m/s and average 1719 m/s. The velocity anisotropy of the fine-grained rocks varies from 0.5% to 3.5% and displays a general downsection increase.

The rocks of Unit III are characterized by highly variable sonic velocity (Fig. 39). Chert sampled at 312.42 mbsf displays the highest velocity measured for sedimentary rocks at Site 802 (5301 m/s). The compressional-wave velocity of the chalks and calcareous claystones that comprise the bulk of Unit III ranges from 1669 to 3181 m/s. The velocity of the chalks varies directly with the calcium carbonate concentration and increases slightly downsection, from approximately 1900 m/s at the top of Unit III to 2500 m/s at the base of the unit (Fig. 39). The most striking feature of sonic velocity variation in Unit III is high anisotropy displayed by chalks and claystones between 254 mbsf and the base of Unit III. Excluding a calcareous claystone sample at 256.68 mbsf, which is approximately isotropic, the range in velocity anisotropy is 5.9% to 13.2%. Anisotropy in this interval averages 8.7%. The range of velocity anisotropy for carbonate rocks of Unit III is comparable to that reported for similar rocks from the Rio Grande Rise (Carlson et al., 1983). Carlson et al. (1983) determined that a negative correlation ($r = 0.74$) exists between velocity anisotropy and carbonate content for the rocks of the Rio Grande Rise and concluded that the anisotropy was primarily controlled by bedding. A positive correlation ($r = 0.70$) between calcium carbonate concentration and velocity anisotropy characterizes the chalks and calcareous claystones of Unit III and may be the result of preferred orientation of calcite, as suggested by Carlson et al. (1983).

The lithologic change from nannofossil chalk in Unit III to pelagic claystone in Unit IV is marked by a sharp decrease in compressional-wave velocity from approximately 3100 m/s in the chalk to 1700 m/s in the claystone. Velocity variation in the volcaniclastic turbidites of Unit V, which underlie the pelagic claystones, is similar to the pattern of velocity variation in Subunit IIB. Sonic velocity of the sandstones in Unit V ranges from 2190 to 2613 m/s and averages 2377 m/s. Velocity anisotropy of these rocks is slightly higher than that of volcaniclastic sandstones and tuffs in overlying units, ranging from 1.2% to 3.9% and averaging 2.9%. Sonic velocity of the claystones in Unit V varies between 1713 and 2234 m/s;

**Table 6. Summary of physical properties for Hole 802A.**

| Core, section, interval (cm) | Depth (mbsf) | Wet-bulk density Gravimetric (g/cm³) | Wet-bulk density GRAPE (g/cm³) | Grain density[a] (g/cm³) | Porosity (%) | Water content (%) | Vertical velocity (m/s) | Horizontal velocity (m/s) | Velocity anisotropy (%) | Thermal conductivity (W/m · K) | Remarks |
|---|---|---|---|---|---|---|---|---|---|---|---|
| 129-802A | | | | | | | | | | | |
| 3R-1, 21–23 | 14.81 | 1.88 | 1.94 | 2.58 | 45.0 | 24.4 | 3325 | 3379 | 1.6 | 1.07 | Tuff (sand-size) |
| 3R-1, 110–113 | 15.70 | 1.25 | | 2.62 | 86.0 | 70.1 | | | | | Pelagic clay |
| 4R-2, 6–8 | 25.86 | 2.05 | 2.05 | 2.78 | 41.3 | 20.5 | 2881 | 2779 | −3.6 | 1.31 | Volcaniclastic breccia |
| 4R-2, 86–88 | 26.66 | 1.71 | 1.74 | 2.65 | 57.6 | 34.2 | 2393 | 2426 | 1.4 | 0.99 | Volcaniclastic sandy siltstone |
| 5R-1, 126–128 | 34.96 | 1.94 | 1.99 | 2.64 | 43.3 | 22.7 | 3259 | 3214 | −1.4 | 1.10 | Tuff (sand-size) |
| 6R-2, 70–72 | 45.10 | 1.62 | 1.67 | 2.54 | 60.4 | 37.9 | 2223 | 2212 | −0.5 | 1.06 | Tuff (sand-size) |
| 7R-1, 101–103 | 53.41 | 1.79 | 1.77 | 2.68 | 54.0 | 30.8 | 2507 | 2548 | 1.6 | 1.05 | Tuff (sand-size) |
| 8R-2, 41–43 | 63.81 | 1.93 | 2.00 | 2.60 | 42.5 | 22.4 | 3377 | 3352 | −0.7 | 1.17 | Tuffaceous silty sandstone |
| 10R-1, 69–71 | 81.09 | 1.71 | 1.74 | 2.67 | 58.3 | 34.7 | 2428 | 2472 | 1.8 | 1.09 | Tuff (sand-size) |
| 11R-1, 10–12 | 91.20 | 1.75 | 1.77 | 2.72 | 57.4 | 33.4 | 2654 | 2674 | 0.8 | 1.12 | Tuff (sand-size) |
| 12R-1, 7–9 | 98.97 | 1.83 | 1.88 | 2.62 | 49.4 | 27.5 | 3309 | 3396 | 2.6 | 1.12 | Tuff (sand-size) |
| 13R-1, 47–49 | 108.77 | 1.35 | | 2.56 | 78.4 | 58.9 | | | | 0.86 | Pelagic clay |
| 13R-2, 61–61 | 109.50 | | | | | | | | | 0.95 | Pelagic clay |
| 14R-2, 73–75 | 116.63 | 2.14 | 2.22 | 2.65 | 31.3 | 14.9 | 4082 | 4163 | 2.0 | 1.48 | Tuff (sand-size) |
| 15R-2, 37–39 | 123.97 | 1.71 | 1.74 | 2.68 | 58.5 | 34.8 | 2393 | 2376 | −0.7 | 1.11 | Tuff (sand-size) |
| 16R-1, 108–110 | 132.18 | 2.01 | 2.06 | 2.52 | 34.4 | 17.4 | 3841 | 3856 | 0.4 | 1.17 | Tuff (sand size) |
| 17R-1, 36–38 | 140.76 | 1.74 | 1.77 | 2.66 | 56.0 | 32.7 | 2393 | 2376 | −0.7 | 1.08 | Tuff (sand-size) |
| 18R-1, 3–5 | 149.73 | 1.88 | 1.91 | 2.72 | 49.5 | 26.8 | 2896 | 2958 | 2.1 | | Tuff (sand-size) |
| 19R-1, 112–114 | 160.22 | 1.71 | 1.70 | 2.75 | 60.5 | 36.0 | 1632 | 1652 | 1.2 | | Silty claystone |
| 19R-2, 79–81 | 161.39 | 1.73 | 1.76 | 2.74 | 58.7 | 34.4 | 1962 | 1992 | 1.5 | 1.15 | Siltstone |
| 20R-1, 10–12 | 168.40 | 2.02 | 2.04 | 2.82 | 44.6 | 22.4 | 2562 | 2627 | 2.5 | | Tuff (sand-size) |
| 21R-2, 9–11 | 178.79 | 1.54 | 1.56 | 2.63 | 68.1 | 45.1 | 1773 | 1782 | 0.5 | | Volcaniclastic silty claystone |
| 21R-2, 50–52 | 179.20 | 1.80 | 1.84 | 2.72 | 53.9 | 30.4 | 2294 | 2319 | 1.1 | 1.12 | Tuff (sand-size) |
| 22R-1, 10–12 | 187.10 | 1.79 | 1.79 | 2.72 | 54.9 | 31.2 | 2254 | 2310 | 2.5 | 1.14 | Tuff (sand-size) |
| 23R-1, 10–12 | 196.50 | 1.63 | 1.61 | 2.86 | 67.2 | 42.0 | 1632 | 1677 | 2.7 | | Calcareous nannofossil clay |
| 23R-1, 66–68 | 197.06 | 1.93 | 1.98 | 2.76 | 47.7 | 25.1 | 2413 | 2472 | 2.4 | 1.21 | Tuff (sand-size) |
| 24R-1, 3–5 | 206.13 | 1.57 | | 2.68 | 66.7 | 43.0 | 1662 | 1722 | 3.5 | 1.13 | Calcareous mudstone |
| 25R-1, 12–14 | 215.82 | 1.48 | 1.40 | 2.68 | 72.3 | 49.5 | 1635 | 1649 | 0.9 | | Claystone with nannofossils |
| 26R-1, 42–44 | 225.82 | 1.64 | 1.64 | 2.73 | 63.6 | 39.3 | 1652 | 1690 | 2.3 | 1.11 | Calcareous claystone |
| 27R-1, 103–105 | 236.13 | 1.79 | 1.78 | 2.70 | 54.4 | 30.9 | 2230 | 2289 | 2.6 | 1.27 | Tuff (sand-size) |
| 27R-3, 112–114 | 239.22 | 1.89 | 1.89 | 2.72 | 48.9 | 26.3 | 1880 | 1953 | 3.8 | 1.54 | Nannofossil chalk |
| 27R-5, 26–28 | 241.36 | 1.89 | 1.89 | 2.65 | 46.5 | 25.0 | 1889 | 1901 | 0.6 | 1.48 | Nannofossil chalk |
| 28R-1, 36–38 | 245.06 | 1.93 | 1.90 | 2.68 | 45.3 | 23.9 | 1983 | 2039 | 2.8 | 1.78 | Nannofossil chalk |
| 28R-3, 54–56 | 248.24 | 2.08 | 2.06 | 2.70 | 37.2 | 18.2 | 2496 | 2411 | −3.5 | 1.57 | Tuffaceous nannofossil foraminiferal packstone |
| 29R-1, 15–17 | 254.65 | 2.18 | 2.18 | 2.70 | 30.9 | 14.4 | 2205 | 2517 | 13.2 | 2.13 | Calcareous claystone |
| 29R-2, 68–70 | 256.68 | 1.79 | 1.91 | 2.68 | 53.7 | 30.5 | 1669 | 1673 | 0.2 | 1.44 | Calcareous claystone |
| 30R-1, 71–73 | 264.91 | 1.78 | 1.78 | 2.65 | 53.8 | 30.8 | 1808 | 1960 | 8.1 | 1.46 | Nannofossil chalk |
| 31R-1, 20–22 | 274.00 | 2.00 | 2.02 | 2.65 | 40.2 | 20.4 | 1911 | 2027 | 5.9 | 1.59 | Nannofossil chalk |
| 32R-1, 13–15 | 283.63 | 2.38 | 2.21 | 2.70 | 19.2 | 8.2 | 2394 | 2652 | 10.2 | 2.03 | Nannofossil chalk |
| 32R-2, 96–98 | 285.96 | 1.77 | 1.84 | 2.49 | 48.9 | 28.0 | 2243 | 2417 | 7.5 | 1.59 | Nannofossil chalk |
| 33R-1, 54–56 | 293.34 | 2.12 | 2.08 | 2.71 | 34.8 | 16.7 | 2023 | 2164 | 6.7 | 1.95 | Nannofossil chalk |
| 34R-1, 60–62 | 302.90 | 2.39 | 2.36 | 2.70 | 18.5 | 7.8 | 3181 | 3476 | 8.9 | 2.48 | Nannofossil chalk |
| 35R-1, 6–8 | 311.56 | 1.76 | 1.75 | 2.49 | 49.7 | 28.7 | 1975 | 2114 | 6.8 | 1.33 | Nannofossil chalk |
| 35R-CC, 5–7 | 312.42 | 2.53 | 2.50 | 2.55(2.59) | 1.5 | 0.6 | 5301 | 4993 | −6.0 | | Chert |
| 36R-1, 31–33 | 321.01 | 2.33 | 2.29 | 2.70 | 22.0 | 9.6 | 3093 | 3439 | 10.6 | 2.36 | Nannofossil chalk |
| 38R-2, 63–65 | 341.33 | 1.78 | 1.82 | 2.62 | 52.7 | 30.1 | 1699 | 1729 | 1.8 | 1.24 | Pelagic claystone |
| 38R-4, 91–93 | 344.61 | 1.90 | 1.93 | 2.67 | 46.9 | 25.1 | 1728 | 1774 | 2.6 | 1.15 | Pelagic claystone |
| 39R-1, 58–60 | 349.28 | 1.86 | 1.84 | 2.76 | 51.7 | 28.2 | 2304 | 2396 | 3.9 | 1.22 | Tuff (sand-size) |
| 40R-2, 103–105 | 360.63 | 1.94 | 1.96 | 2.82 | 48.8 | 25.6 | 2399 | 2474 | 3.1 | 1.27 | Volcaniclastic sandstone |
| 40R-3, 11–13 | 361.21 | 1.80 | 1.83 | 2.77 | 55.2 | 31.1 | 1713 | 1770 | 3.3 | 1.23 | Volcaniclastic claystone |
| 41R-1, 10–12 | 365.60 | 1.76 | 1.78 | 2.69 | 55.7 | 32.2 | 1728 | 1809 | 4.6 | 1.21 | Volcaniclastic claystone |
| 41R-4, 121–123 | 371.21 | 1.78 | 1.80 | 2.82 | 57.9 | 33.0 | 2034 | 2081 | 2.3 | 1.25 | Volcaniclastic sandy, silty claystone |
| 42R-1, 96–98 | 373.76 | 1.74 | 1.73 | 2.77 | 59.3 | 34.7 | 1809 | 1856 | 2.6 | 1.19 | Volcaniclastic sandy siltstone |
| 42R-2, 111–113 | 375.29 | 1.78 | 1.81 | 2.67 | 54.1 | 30.9 | 1755 | 1811 | 3.1 | 1.30 | Volcaniclastic claystone |
| 43R-1, 114–116 | 383.24 | 1.83 | 1.85 | 2.78 | 54.2 | 30.1 | 1771 | 1879 | 5.9 | 1.33 | Volcaniclastic claystone |
| 43R-2, 15–17 | 383.75 | 2.06 | 2.05 | 2.85 | 43.2 | 21.3 | 2613 | 2697 | 3.2 | 1.43 | Volcaniclastic sandstone |
| 44R-1, 50–52 | 391.80 | 1.67 | 1.68 | 2.50 | 56.2 | 34.2 | 1892 | 2004 | 5.7 | 1.29 | Silty claystone |
| 45R-2, 41–43 | 402.41 | 1.76 | 1.76 | 2.78 | 58.4 | 33.8 | 1957 | 2023 | 3.3 | 1.17 | Silty claystone |
| 46R-1, 60–62 | 410.60 | 1.69 | 1.71 | 2.76 | 61.8 | 37.2 | 1759 | 1850 | 5.0 | 1.24 | Silty claystone |
| 47R-1, 45–47 | 419.65 | 1.74 | 1.74 | 2.73 | 58.0 | 33.9 | 1781 | 1885 | 5.7 | 1.25 | Silty claystone |
| 47R-3, 74–76 | 422.94 | 1.71 | 1.73 | 2.72 | 59.6 | 35.4 | 1760 | 1887 | 7.0 | 1.22 | Silty claystone |
| 47R-4, 30–32 | 424.00 | 1.91 | 1.89 | 2.80 | 50.3 | 26.8 | 2190 | 2216 | 1.2 | 1.26 | Volcaniclastic sandstone |
| 48R-1, 66–68 | 429.36 | 1.84 | 1.83 | 2.78 | 53.6 | 29.7 | 2125 | 2149 | 1.1 | 1.20 | Silty claystone |
| 49R-1, 17–19 | 438.27 | 1.60 | 1.60 | 2.44 | 59.3 | 37.7 | 1753 | 1775 | 1.2 | 1.27 | Silty claystone |
| 49R-3, 128–130 | 442.38 | 1.71 | 1.74 | 2.72 | 59.3 | 35.2 | 1761 | 1857 | 5.3 | 1.24 | Silty claystone |

Table 6. Summary of physical properties for Hole 802A.

| Core, section, interval (cm) | Depth (mbsf) | Wet-bulk density Gravimetric (g/cm$^3$) | Wet-bulk density GRAPE (g/cm$^3$) | Grain density[a] (g/cm$^3$) | Porosity (%) | Water content (%) | Vertical velocity (m/s) | Horizontal velocity (m/s) | Velocity anisotropy (%) | Thermal conductivity (W/m · K) | Remarks |
|---|---|---|---|---|---|---|---|---|---|---|---|
| 50R-1, 92–94 | 448.32 | 1.89 | 1.90 | 2.74 | 49.7 | 26.8 | 1761 | 1895 | 7.3 | 1.40 | Volcaniclastic silty claystone |
| 50R-2, 66–68 | 449.56 | 1.79 | 1.82 | 2.62 | 52.2 | 29.7 | 1867 | 1973 | 5.5 | 1.27 | Claystone breccia |
| 51R-1, 66–68 | 454.16 | 1.71 | 1.73 | 2.75 | 60.1 | 35.7 | 1761 | 1904 | 7.8 | 1.24 | Claystone breccia |
| 51R-3, 98–100 | 457.48 | 2.03 | 2.04 | 2.66 | 38.4 | 19.2 | 2234 | 2514 | 11.8 | 1.55 | Claystone |
| 52R-2, 114–116 | 462.44 | 1.90 | 1.92 | 2.63 | 45.7 | 24.5 | 1889 | 1984 | 4.9 | 1.40 | Claystone |
| 52R-3, 34–36 | 463.14 | 1.90 | 1.90 | 2.53 | 42.0 | 22.5 | 2132 | 2451 | 13.9 | 1.45 | Radiolarite |
| 53R-1, 75–77 | 470.15 | 1.95 | 1.88 | 2.67 | 43.8 | 22.8 | 1872 | 1968 | 5.0 | 1.46 | Clayey nannofossil chalk |
| 53R-2, 23–25 | 470.93 | 2.10 | 2.12 | 2.64 | 33.7 | 16.3 | 2274 | 2372 | 4.2 | 1.56 | Nannofossil chalk |
| 54R-1, 15–17 | 478.75 | 2.14 | 2.15 | 2.71 | 33.5 | 15.9 | 2111 | 2302 | 8.7 | 1.98 | Clayey limestone |
| 54R-3, 15–17 | 481.75 | 1.98 | 1.98 | 2.70 | 42.8 | 22.0 | 2034 | 2145 | 5.3 | 1.71 | Clayey siltstone |
| 54R-3, 50–52 | 482.10 | 2.00 | 2.00 | 2.68 | 41.3 | 21.1 | 2089 | 2260 | 7.9 | 1.64 | Claystone |
| 55R-1, 114–116 | 489.04 | 2.22 | 2.18 | 2.64 | 26.1 | 12.0 | 3070 | 3344 | 8.5 | 1.78 | Siliceous limestone |
| 56R-1, 101–103 | 498.11 | 1.95 | 1.99 | 2.64 | 42.9 | 22.4 | 2088 | 2244 | 7.2 | 1.44 | Claystone |
| 56R-3, 33–35 | 500.43 | 1.87 | 1.87 | 2.75 | 50.8 | 27.6 | 2124 | 2108 | −0.8 | 1.39 | Volcaniclastic sandstone |
| 57R-1, 72–74 | 507.32 | 1.93 | 1.97 | 2.77 | 48.1 | 25.3 | 1925 | 2114 | 9.4 | 1.51 | Claystone |
| 58R-1, 38–40 | 516.38 | 2.93 | 2.89 | 2.97(2.99) | 1.9 | 0.5 | 6217 | 6167 | −0.8 | 2.01 | Aphyric basalt |
| 58R-2, 53–55 | 518.03 | 2.88 | 2.87 | 2.92 | 2.5 | 0.7 | 5966 | 5992 | 0.4 | 2.00 | Aphyric basalt |
| 58R-2, 105–107 | 518.55 | 2.92 | 2.92 | 2.97 | 2.6 | 0.8 | 5944 | 5939 | −0.1 | 1.86 | Moderately olivine-plagioclase microphyric basalt |
| 58R-3, 86–88 | 519.86 | 2.82 | 2.83 | 2.94 | 6.3 | 2.1 | 5344 | 5274 | −1.3 | 1.85 | Sparsely olivine microphyric basalt |
| 59R-1, 83–85 | 526.23 | 2.92 | 2.91 | 2.96(3.04) | 2.3 | 0.7 | 6182 | 6311 | 2.1 | 1.94 | Sparsely olivine-plagioclase microphyric basalt |
| 60R-1, 90–92 | 535.60 | 2.77 | 2.78 | 2.92 | 8.2 | 2.8 | 5072 | 5074 | 0.0 | 1.82 | Sparsely plagioclase microphyric to aphyric basalt |
| 62R-1, 129–131 | 551.89 | 2.94 | 2.97 | 2.97(3.03) | 1.2 | 0.40 | 6200 | 6197 | 0.0 | 2.09 | Moderately olivine-plagioclase microphyric basalt |

[a] Values in parentheses were determined using powdered samples.

however, most of the values lie in a relatively narrow range between 1700 and 1900 m/s. A consistent downsection trend in velocity variation is lacking for the claystones, and the rocks are characterized by an average velocity of 1846 m/s. The fine-grained rocks of Unit V, combined with the pelagic claystones of Unit IV, exhibit a general increase in velocity anisotropy with depth, from approximately 2% at 341 mbsf to 8% at 454 mbsf. Over this interval anisotropy of the claystones ranges from 1.1% to 11.8%.

Velocity variation in lithologic Units VI through IX reflects the mixture of lithologies present in this interval. Compressional-wave velocity of the claystones increases from 1889 m/s at 462.44 mbsf to 2088 m/s at 498.11 mbsf (Table 6). Velocity decreases to 1925 m/s in the claystone at 507.32 mbsf in Unit IX. The carbonate sediments of Unit VII display a range in velocities from 1872 m/s in chalk at 470.15 mbsf to 3070 m/s in siliceous limestone at 489.04 mbsf. Other values for compressional-wave velocity measured for rocks in the lowermost 45 m of the sedimentary section include 2132 m/s for radiolarite at 463.14 mbsf and 2124 m/s for volcaniclastic sandstone at 500.43 mbsf. The downsection increase in velocity anisotropy displayed by fine-grained rocks of Units IV and V continues for fine-grained rocks of Units VI through IX, culminating with at a value of 9.4% in the claystone of Unit IX. The radiolarite, which was sampled at 463.14 mbsf, is characterized by thin, parallel laminae and possesses the highest anisotropy (13.9%) in the lower part of the sedimentary section. Velocity anisotropy of the volcaniclastic sandstone of Unit IX is 0.8%.

A sharp increase in compressional-wave velocity marks the boundary between the sedimentary section at Site 802 and the underlying basalt. Sonic velocity in the basalt is high, varying between 5072 and 6217 m/s and averaging 5846 m/s, which attests to the high density and minimal alteration of these rocks. The basalts are essentially elastically isotropic, with velocity anisotropy ranging from 0.13% to 2.1% and averaging zero.

Variation of compressional-wave velocity at Site 802 displays consistent relationships with wet-bulk density that vary with lithology (Fig. 40). The lithologic grouping that includes clays, claystones, and siltstones displays the lowest velocities and the lowest velocity/density gradient (Fig. 40). The field represented by the variety of chalks and limestones sampled at Site 802 overlaps the field for fine-grained sediments and rocks and extends to higher wet-bulk density and velocity values. The velocity/density gradient for the chalks and limestones is greater than that of the claystones and siltstones; however, the carbonate rocks are also characterized by the greatest scatter on the density-velocity crossplot. Variations in composition and degree of silicification possibly influence the variability in the behavior of the carbonate rocks. Based on differences in the relationship between wet-bulk density and compressional-wave velocity, the coarse-grained volcaniclastic rocks at Site 802 can be divided into two groups: (1) tuffs of Subunit IIA and (2) tuffs and volcaniclastic sandstones of the other lithologic units. At equivalent wet-bulk densities, the tuffs and volcaniclastic sandstones of Subunit IIB and underlying lithologic units are characterized by higher velocities than are the chalks, limestones, fine-grained sediments, and rocks. The velocity/density gradient of these sandstones is intermediate between that of the claystone/siltstone group and that of the carbonate rocks. Tuffs of Subunit IIA are characterized by velocities distinctly higher than those of other volcaniclastic rocks at Site 802. These rocks are also

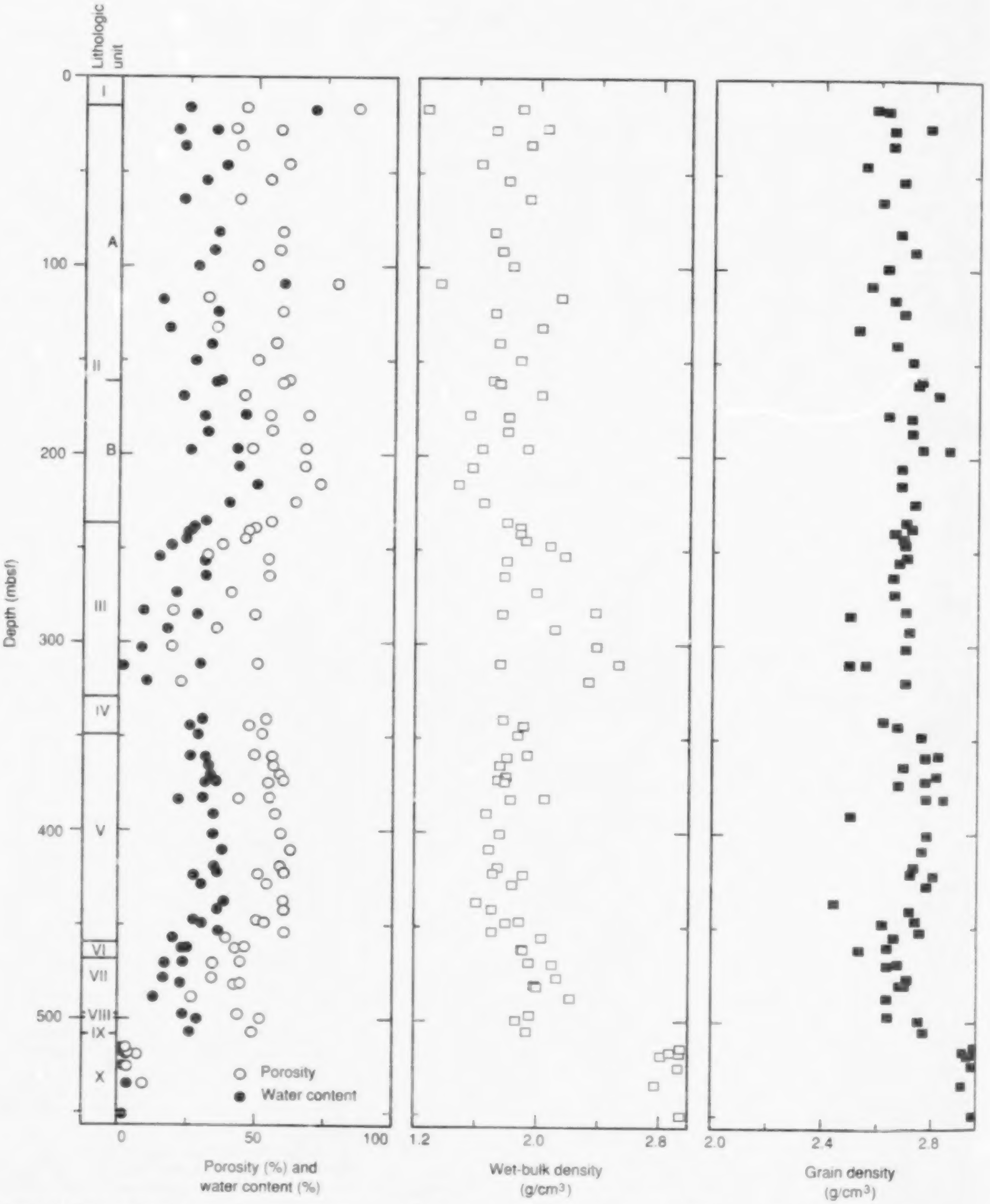

Figure 38. Index properties (porosity, water content, wet-bulk density, and grain density) for Hole 802A.

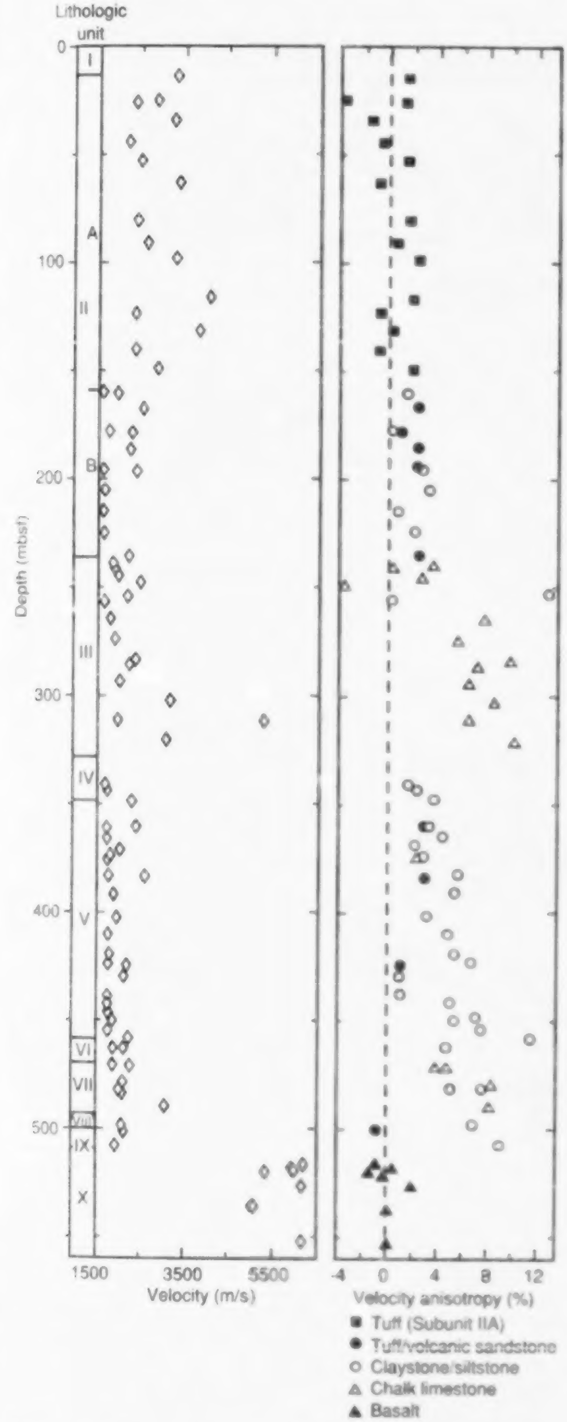

Figure 39. Compressional-wave velocity measured perpendicular to bedding and velocity anisotropy vs. depth for Hole 802A. Velocity anisotropy profile is coded according to sediment and rock type.

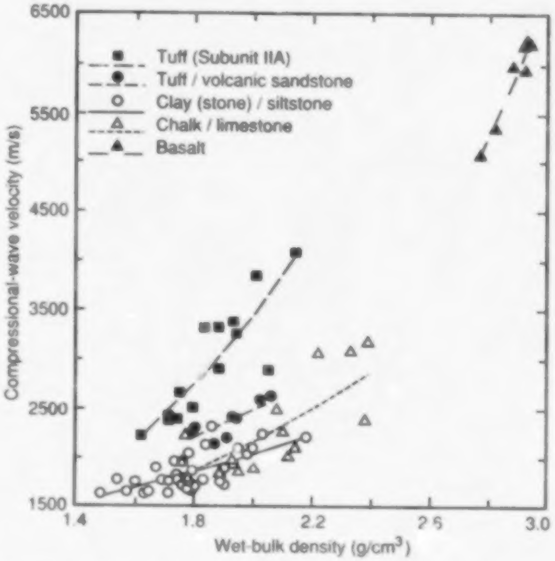

Figure 40. Wet-bulk density vs. compressional-wave velocity (measured perpendicular to bedding) for Hole 802A, coded according to sediment and rock type. Lines are best-fit exponential lines for the data.

characterized by the steepest velocity/density gradient for sedimentary rocks at Site 802.

The basalts sampled at Site 802 are characterized by a very steep velocity/density gradient (Fig. 39), 7700 ms$^{1}$/g cm$^{3}$. This gradient is twice the gradient of 3850 ms$^{1}$/g cm$^{3}$ that Christensen and Salisbury (1975) determined in their summary of DSDP basalt velocity data. However, the gradient for the basalts at Site 802 is comparable to that of basalts of the Gulf of California, which display a velocity/density gradient of approximately 7600 ms$^{1}$/g cm$^{3}$ (Christensen and Lewis, 1983). The basalts sampled in the Gulf of California are similar to those at Site 802 in that they are characterized by a low degree of alteration.

## Thermal Conductivity

At Site 802 thermal conductivity measurements were primarily made on sedimentary and igneous rocks. Only two samples of unlithified sediments were analyzed. The conductivity of soft sediments was measured by a heated needle probe inserted in the sediment. Conductivity of lithified sediments and basement rocks was measured by a heated needle probe sandwiched between the sample and a slab of low conducting material. Details for both procedures for measuring thermal conductivity are described in the "Explanatory Notes" chapter (this volume).

Variation of thermal conductivity at Site 802 is characterized by relatively uniform, consistent trends (Fig. 41). In Subunit IIA thermal conductivity of the tuffs and volcaniclastic sandstones ranges from 0.99 to 1.48 W/m · K; however, excluding the two measurements greater than 1.3 W/m · K (from 25.86 and 116.63 mbsf), the conductivities of the coarse-grained volcaniclastic sediments are centered about a mean of 1.09 W/m · K. The thermal conductivity of the coarse- and fine-grained volcaniclastic rocks of Subunit IIB is slightly higher than that of rocks in Subunit IIA. The conductivity of rocks of Subunit IIB ranges from 1.11 to 1.27 W/m · K and averages 1.16 W/m · K. In contrast to patterns of index prop-

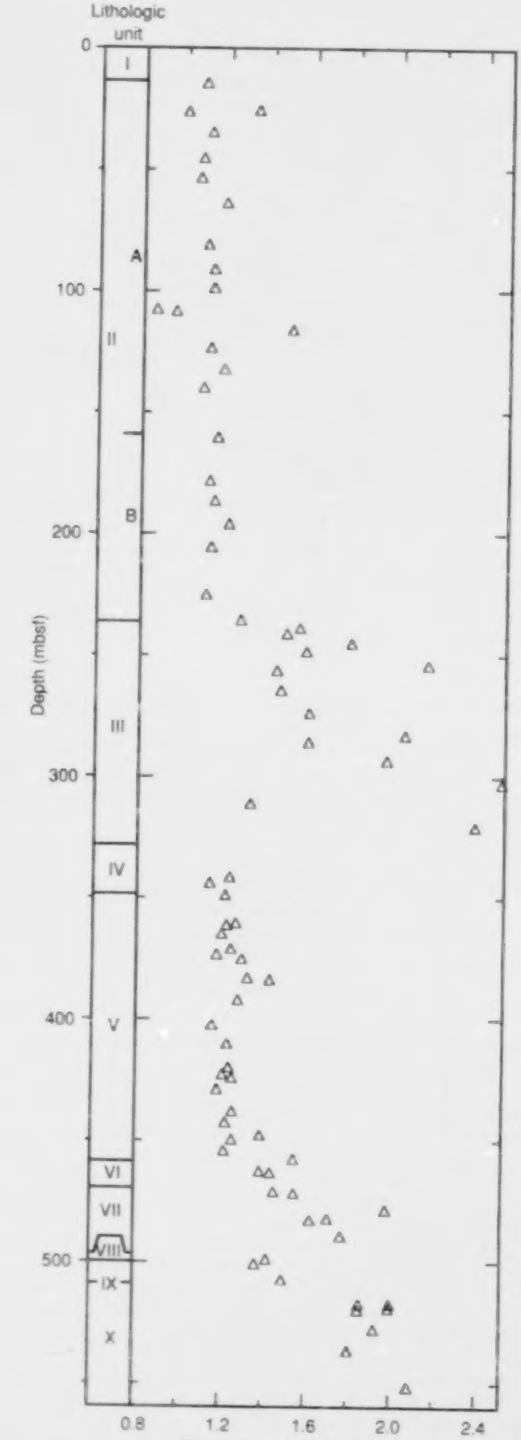

Figure 41. Thermal conductivity vs. depth for Hole 802A.

erty and compressional-wave velocity variation in Subunit IIB, there is not a distinction in thermal conductivity values between volcaniclastic sandstones and volcaniclastic claystones/siltstones. A distinct increase in conductivity is present at the base of Subunit IIB (Fig. 41) and corresponds with an increase in carbonate content.

The chalks and limestones of lithologic Unit III are characterized by high and highly variable thermal conductivity (Fig. 41). Conductivity ranges from 1.33 to 2.48 W/m · K (Table 6). The carbonate rocks of Unit III display a strong inverse relationship between thermal conductivity and porosity, which itself varies inversely with calcium carbonate concentration.

Thermal conductivity is relatively uniform in the pelagic claystones of Unit IV and the volcaniclastic claystones and sandstones of Unit V. In these two units conductivity ranges from 1.15 to 1.43 W/m · K and averages 1.27 W/m · K. As in Subunit IIB, ranges for the conductivities of the claystones and siltstones and sandstones overlap. In Units IV and V there is little change in conductivity with increasing burial depth. In contrast to this pattern a distinct downsection increase in thermal conductivity is present in Units VI and VII (Fig. 41). In these two units conductivity increases from 1.40 W/m · K at 462.44 mbsf to 1.78 W/m · K at 489.04 mbsf. The increase in conductivity in this part of the sedimentary section coincides with an increase in calcium carbonate concentration. A sharp decrease in thermal conductivity marks the boundary between Units VII and VIII. In Units VIII and IX thermal conductivity ranges from 1.39 to 1.51 W/m · K and averages 1.45 W/m · K.

Thermal conductivity of the aphyric to microphyric basalts of Unit X ranges from 1.82 to 2.09 W/m · K. Conductivity variation in the basalts displays a moderately strong inverse relationship with porosity. Average thermal conductivity of the basalts is 1.94 W/m · K.

The combined sediment, sedimentary rock, and igneous rock data sets display a strong inverse relationship between porosity and thermal conductivity that in part varies with lithology (Fig. 42). The grouping of rock types, including tuffs and volcaniclastic sandstones (excluding those of Subunit IIA), claystone and siltstone, and chalk and limestone, exhibits a well-defined trend of increasing conductivity with decreasing porosity. In this grouping the fields that encompass the different lithologies overlap extensively, suggesting that porosity exerts a greater control over thermal conductivity than does variation in grain size or sediment composition. The tuffs and volcaniclastic sandstones of Subunit IIA are represented in a field on the crossplot of porosity vs. thermal conductivity that is, for the most part, separate from the field encompassing the rest of the sedimentary rocks. Lower conductivity of the rocks of Subunit IIA is consistent with the abundant volcanic glass in these rocks and the lower thermal conductivity of silica glass relative to the mineral constituents of the other sedimentary rocks (Clark, 1966). The field represented by basalt in the porosity vs. conductivity crossplot is separate from the trend of the sedimentary rocks. The inverse relationship between porosity and thermal conductivity for these rocks is relatively strong ($r = 0.80$). Glass is abundant in the basalts at Site 802 (see "Igneous Petrology" section, this chapter), which may be responsible for the extent to which the trend of the basalts on the porosity vs. conductivity crossplot falls off the trend of the sedimentary rocks. The compositional similarity of the glass-rich tuffs of Subunit IIA and the basalts is suggested by the appearance of the basalt data falling along the trend defined by the Subunit IIA tuffs on the porosity-conductivity crossplot (Fig. 42).

## IGNEOUS PETROLOGY

One of the objectives of Hole 802A in the East Mariana Basin was to recover, on the basis of magnetic lineation data, Jurassic oceanic basement situated beyond magnetic anomaly M37 (~165 Ma). To minimize the input of middle Cretaceous volcanic material (either as volcaniclastics or intrusives), Hole 802A was drilled in an area apparently well removed from mapped seamounts and where "basement" was indicated by seismic stratigraphy at about 500 mbsf. However, a thick sequence of reworked, distal, Cretaceous volcaniclastics was recovered from Hole 802A, as well as a series of extrusive basalt lavas below Cenomanian-late Aptian volcanogenic sediments at about the predicted depth. The sediment data implies an age at least as old as middle Cretaceous for the extrusive rocks directly below. A widespread edifice-building event occurred during the Aptian-Albian in the western Pacific (e.g., Winterer, Riedel, et al., 1971; Larson, Schlanger, et al., 1981) and, hence, the presence of middle Cretaceous volcanics was perhaps not entirely unexpected. Also, extrusive lavas (together with an upper sequence of sills) are a feature of the Nauru Basin igneous complex (Hole 462A), again of a similar or possibly slightly older age (Moberly, Schlanger, et al., 1986). Based on the nature of the extrusive rocks recovered from Hole 802A, however, another possibility is that they could represent local basement, as suggested by the seismic stratigraphy. Unfortunately, shipboard X-ray-fluorescence analytical data were not available during Leg 129, so a chemical signature for the basalts could not be used to constrain their composition and possible eruptive environment.

### Lithology

A total of about 16.6 m of basalts were sampled from Cores 129-802A-57R to -62R (32.8% recovery) and divided into 17 volcanic cooling units. The actual recovered portion of each unit and its top and bottom position are shown in Table 7 and Figure 43. The criteria for subdivision are similar to those use in previous holes, although in this case the preservation of glassy margins, as well as macroscopic textural and grain-size variations, were particularly useful.

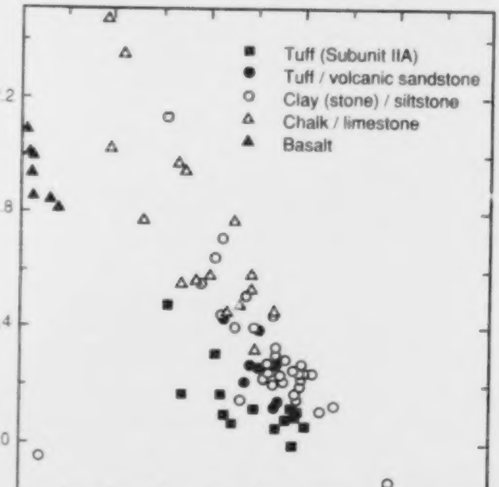

Figure 42. Porosity vs. thermal conductivity for Hole 802A, coded according to sediment and rock type.

One characteristic feature of this hole is the relatively large number of small cooling units recognized, especially where the recovery was good (e.g., Cores 129-802A-58R and -59R; Fig. 43). The curved, glassy selvages that terminate Units 3 and 4 indicate that these are sections of small basaltic pillow lavas, probably no more than about 40–50 cm in diameter (Fig. 44). The glassy rims show all the features that indicate rapid quenching of lavas by seawater, with the preservation of different textural zones (grading inward from glass with coalesced spherulites to quenched crystal morphologies) typical of pillow lavas (Bryan, 1972; Natland, 1980). Many of the other units show similar features and are often quenched throughout, with either preserved subhorizontal margins or very fine-grained contact zones. Hence, these units are also considered to be part of a pillowed sequence. Moreover, the slow rate of drilling coupled with the nature of the recovery (as numerous small, short core lengths) suggest that a number of very thin flow units are present. All these features differ considerably from the thin flows sampled at Hole 801B and from the thick sills at Hole 800A. Only Unit 17 is different from the rest and is interpreted as a thin (<5 m) lava flow, as it is an almost continuously cored segment with a relatively coarser grain size, although it still exhibits a quench texture throughout.

The following discussion illustrates some of the important features displayed by various units. Dark brown and black featureless claystones are separated from the glassy top of Unit 1 by drilling rubble (Fig. 45) composed of similar claystones containing small green glassy fragments and brown smectite. The green clasts match the altered glass in the basalt just below and probably represent spalled pillow rinds subsequently incorporated in the sediment. The reddish brown sediment fragment at the top of Unit 2 (Fig. 43) does not look like interpillow material and probably represents the cave-in of material higher in the hole. As previously noted, the best-preserved pillow sections are exhibited by Units 3 and 4, although other units (e.g., Units 7, 8, and 9) invariably have margins that exhibit coalesced spherulites or fan and plume variolites together with interstitial glass (now altered to smectite). This outer zone is rapidly replaced by larger crystals, although often with quench-texture morphologies that coarsen toward the center of the unit. The top of Unit 11 (Section 129-802A-59R-2, 122 cm) is one of the few rim zones that retains unaltered black glass within a

**Table 7. Extent of igneous units actually observed in Hole 802A.**

| Unit | Top | Bottom | Thickness (cm) |
|---|---|---|---|
| | 129-802A- | 129-802A- | |
| 1 | 57R-2, 110 cm | 57R-3, 43 cm | 79 |
| 2 | 58R-1, 2 cm | 58R-2, 98 cm | 243 |
| 3 | 58R-2, 98 cm | 58R-2, 117 cm | 19 |
| 4 | 58R-2, 117 cm | 58R-2, 149 cm | 32 |
| 5 | 58R-3, 0 cm | 58R-4, 101 cm | 249 |
| 6 | 59R-1, 0 cm | 59R-1, 7 cm | 7 |
| 7 | 59R-1, 7 cm | 59R-1, 51 cm | 44 |
| 8 | 59R-1, 51 cm | 59R-1, 129 cm | 78 |
| 9 | 59R-1, 129 cm | 59R-2, 57 cm | 78 |
| 10 | 59R-2, 57 cm | 59R-2, 122 cm | 65 |
| 11 | 59R-2, 122 cm | 59R-3, 9 cm | 30 |
| 12 | 59R-3, 9 cm | 59R-3, 40 cm | 31 |
| 13 | 59R-3, 0 cm | 59R-3, 142 cm | 102 |
| 14 | 60R-1, 0 cm | 61R-1, 31 cm | 136 |
| 15 | 61R-1, 31 cm | 61R-1, 110 cm | 79 |
| 16 | 61R-1, 110 cm | 61R-2, 22 cm | 62 |
| 17 | 62R-1, 0 cm | 62R-3, 40 cm | 328 |

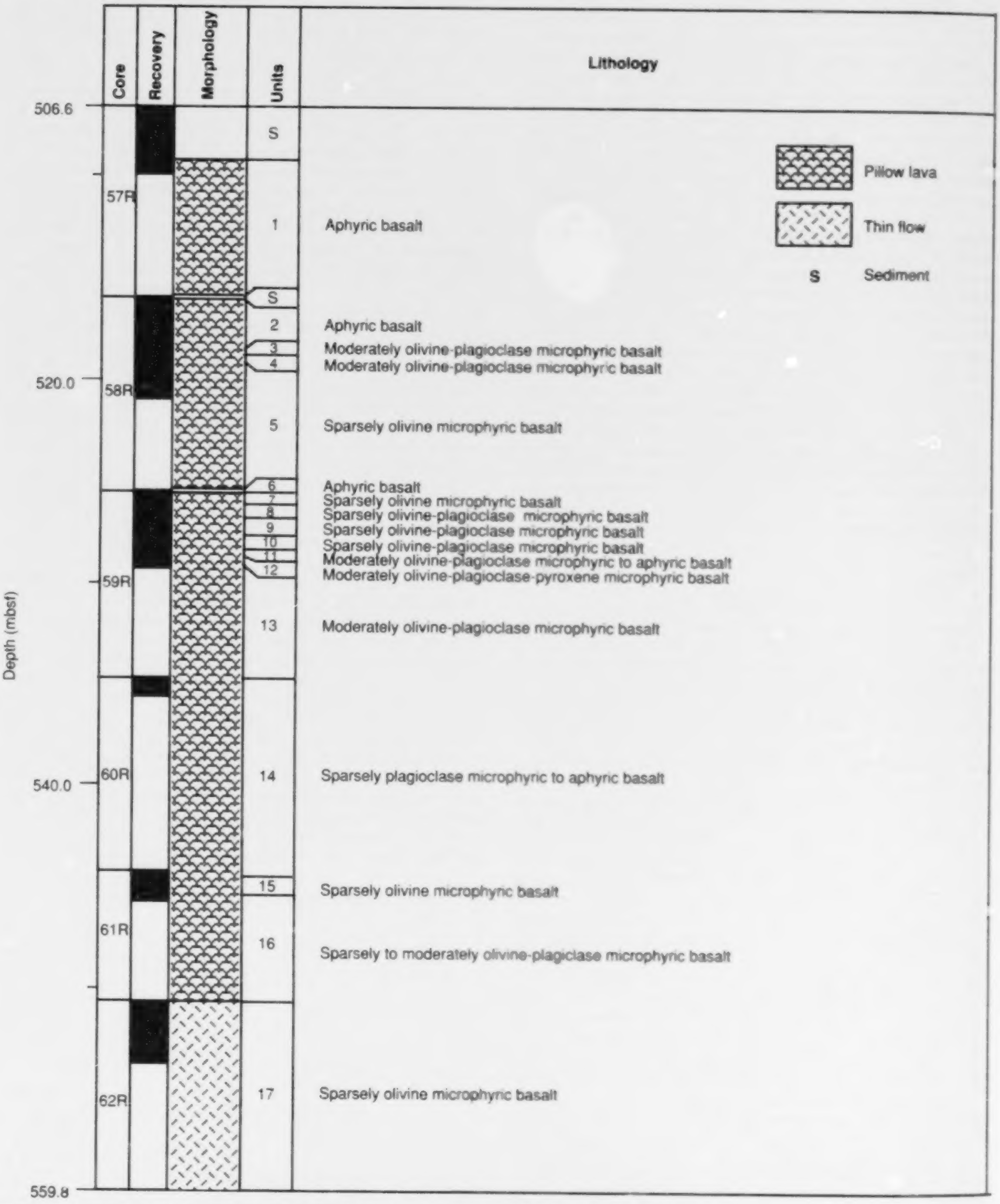
Core
Recovery
Morphology
Units
Lithology
506.6
520.0
540.0
559.8
Depth (mbsf)
57R
58R
59R
60R
61R
62R
S
1
S
2
3
4
5
6
7
8
9
10
11
12
13
14
15
16
17
Aphyric basalt
Aphyric basalt
Moderately olivine-plagioclase microphyric basalt
Moderately olivine-plagioclase microphyric basalt
Sparsely olivine microphyric basalt
Aphyric basalt
Sparsely olivine microphyric basalt
Sparsely olivine-plagioclase microphyric basalt
Sparsely olivine-plagioclase microphyric basalt
Sparsely olivine-plagioclase microphyric basalt
Moderately olivine-plagioclase microphyric to aphyric basalt
Moderately olivine-plagioclase-pyroxene microphyric basalt
Moderately olivine-plagioclase microphyric basalt
Sparsely plagioclase microphyric to aphyric basalt
Sparsely olivine microphyric basalt
Sparsely to moderately olivine-plagioclase microphyric basalt
Sparsely olivine microphyric basalt
Pillow lava
Thin flow
S Sediment

Figure 43. Log of basaltic extrusives at Hole 802A showing distribution of different volcanic units.

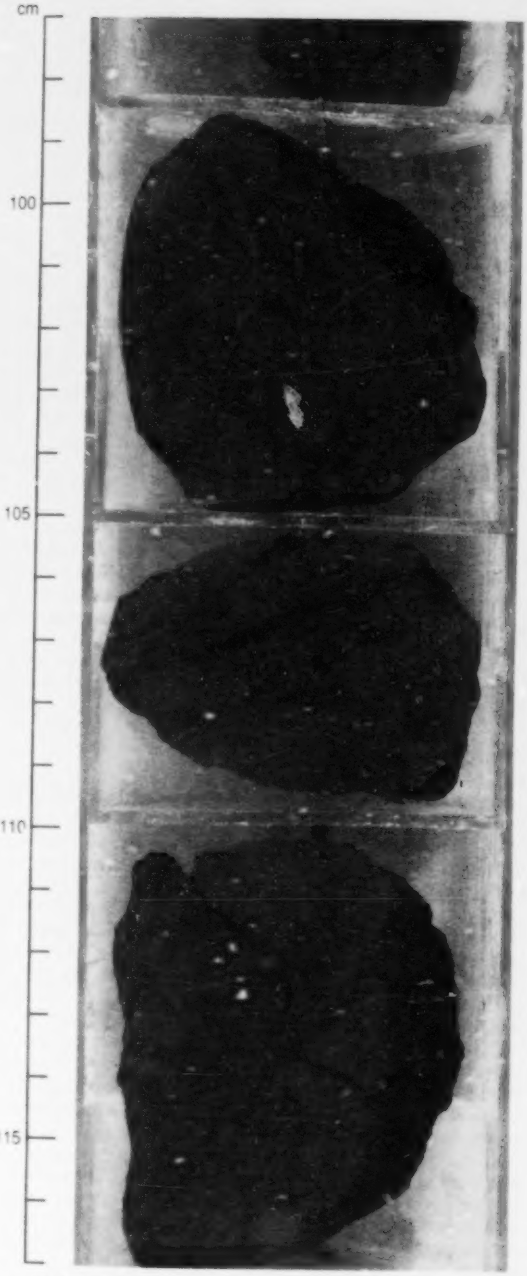

Figure 44. Unit 3 pillow lava (interval 129-802A-58R-2, 98–117 cm). Photograph shows curved glassy rims and speckled spherulitic zone of a small pillow segment.

2-mm-thick spherulitic zone. Unit 17 is a fine-grained hypocrystalline basalt and is distinct from the units above it in being more massive and displaying little internal variation in grain size over its full length. However, Unit 17 has a quench texture throughout and is considered to represent a thin lava flow.

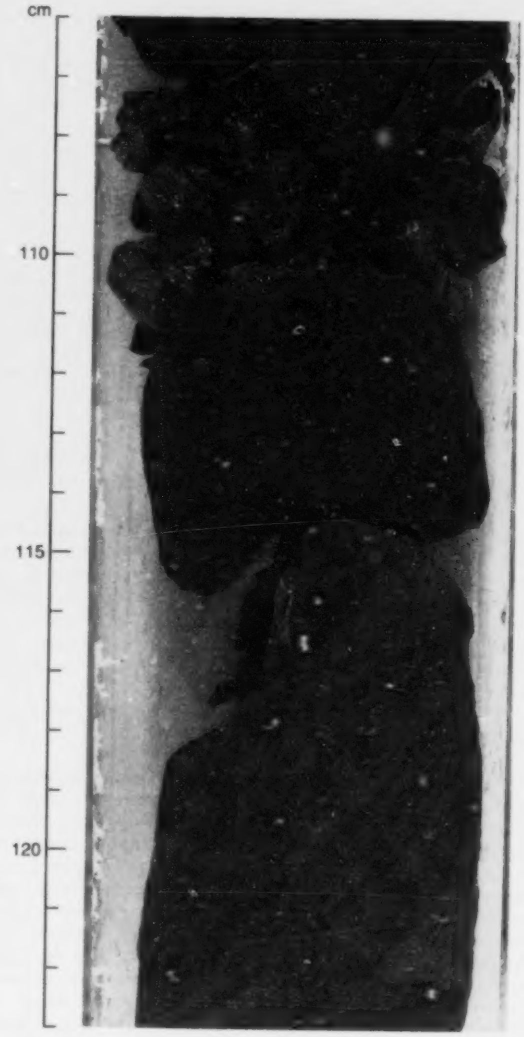

Figure 45. Contact zone between Cenomanian claystones (above) and basalt extrusives at Hole 802A (Section 129-802A-57R-2, 110 cm). The basalt has a thin curved glassy rim largely replaced by smectite.

### Petrography

The extrusive sequence is dominated by fine-grained, pale gray, largely nonvesicular, aphyric olivine basalts and sparsely plagioclase-clinopyroxene-olivine microphyric hypocrystalline basalts. Predominantly glassy and spherulitic-textured porphyritic basalts are confined to the rapidly chilled zones at the margins of cooling units. Green smectite-replaced glassy mesostasis is a common feature in all units, although its distribution is variable.

In hand specimen and under the binocular microscope, the proportions of phenocrysts estimated within any cooling unit were generally very low (rarely exceeding about 3%–4%). Their apparent concentration in the glassy and spherulitic contact zones is a consequence of their small size (0.2–0.5 mm), which is more readily recognized within a crypocrystalline matrix

Table 8. Proportions of primary and secondary minerals visually estimated from thin-section studies.

| Core, section<br>Sample interval (cm)<br>Piece number | 129-802A-57R-2<br>126–128<br>1B | 58R-2<br>145–149<br>15 | 58R-4<br>55–57<br>7 | 59R-1<br>126–128<br>11 | 61R-1<br>50–52<br>8 | 62R-2<br>50–51<br>3 |
|---|---|---|---|---|---|---|
| Primary minerals | | | | | | |
| (1) Phenocrysts | | | | | | |
| Olivine | 0 | 0 | 0 | 0 | 0 | – |
| Plagioclase | 1 | 3 | 2 | 6 | 1 | – |
| Clinopyroxene | <1 | 1 | 1 | 3 | tr | – |
| (2) Matrix | | | | | | |
| Olivine | 0 | 0 | 0 | – | 0 | 0 |
| Plagioclase | 50 | 5 | 5 | tr | 53 | 40 |
| Clinopyroxene | 37 | 5 | 3 | – | 40 | 50 |
| Opaques | 2 | 3 | 3 | 5 | 4 | 4 |
| Glass | – | 3 | – | – | – | – |
| Crystallites | – | 76 | 82 | 85 | – | – |
| Mesostatis | tr | – | 0 | – | 0 | 0 |
| Secondary minerals | | | | | | |
| Clays[a] | 9 | 4 | 4 | 1 | 2 | 6 |
| Carbonate | tr | – | – | – | – | – |

Notes: 0 = present but totally replaced; dash = not observed; tr = trace.

[a] Mostly smectite but include some "iddingsite."

relative to the fine-grained matrix of the central portion of the unit. Porphyritic basalts are characterized by plagioclase and, more commonly, by plagioclase-clinopyroxene-olivine microphenocryst assemblages. Plagioclase and clinopyroxene may form small glomerophyric groups (0.5–1.25 mm in diameter) or more dispersed clumps of crystals. Single microphenocrysts or glomerocrysts often provide nucleation sites for spherulites within the chilled rims of some pillows.

The estimated proportions of primary and secondary minerals, together with crystallite material (in spherulites), are shown in Table 8.

The following brief descriptions, based on thin-section studies, illustrate and contrast the typical textures and features of basalts from the spherulitic rim zone (e.g., Sample 129-802A-59R-1, 126-128 cm) and the central hypocrystalline segment (e.g., Sample 129-802A-62R-2, 50-51 cm) of a cooling unit. The outer completely holohyaline rinds of some pillows are missing, although a thin sliver of yellowish sideromelane with small, individual, reddish brown, poorly birefringent spherulites may be preserved. Away from this outer glassy zone, the spherulites are much larger and begin to coalesce, trapping dark brown glass between their round and ovoid-shaped cross sections. Microphenocrysts and glomerocrysts of plagioclase, clinopyroxene, and, to a lesser extent, olivine may form up to 10% of the matrix and provide nucleation sites for the larger spherulites. Plagioclase microlites, sometimes with tuning-fork terminations, are also common in this zone. The red-brown spherulites continue to increase in size, although they begin to lose their round cross section and become more plumose, with several plumes growing from a central nucleation point. No glass remains and opaque ore forms larger granules that are concentrated around the margins of the spherulitic plumes. At about 20–25 mm from the preserved glassy rim the grain size continues to increase, and separate groups of plume-shaped variolites composed of clinopyroxene and/or plagioclase are clearly visible. In contrast, the central portion of large pillows (or thin flows, as in Unit 17) are fine-grained and hypidiomorphic-granular, although many crystals exhibit quench-textured morphologies. Clinopyroxene forms large fan- and plume-shaped variolites, sometimes coaxial with skeletal plagioclase laths. Commonly, plagioclase is present as elongate crystals with serrated edges that may form "bow-tie" pairs that grow out of a central anhedral clinopyroxene crystal. Apart from these morphologies, olivine, plagioclase, and clinopyroxene are also present as small clumps of subhedral to anhedral grains, which appear to have grown earlier than the quenched crystals. They sometimes act as nucleation sites for the variolites and may range up to the size of any microphenocrysts. These crystals (and the microphenocrysts) are probably pre-eruptive in origin and crystallized during transportation of the lava to the seafloor. After initial quenching and variolite growth, any remaining melt produced a glassy mesostasis often crowded with dendritic and skeletal opaque ore.

### Alteration and Geochemistry

In general terms, all the basalts show only slight or occasionally moderate alteration (up to about 15%). Apart from the low degree of post-consolidation alteration, secondary processes are dominated by the development of smectitic clays, carbonate, and pyrite; no zeolites were observed. The preservation of pyrite, both within veins and the matrix of the basalts, indicates a reducing environment. Late oxidative alteration, often typical of the oceanic crust with the development of iron oxyhydroxide-reddened zones (e.g., Robinson et al., 1977; Humphris et al, 1979), is not evident here. This may be a consequence of the mass flow deposition of the featureless volcanogenic claystones that rapidly covered the young extrusive rocks and provided a blanket to downward-seeping oxygenated seawater. The high organic content of the claystones may also have deoxygenated the seawater prior to penetration of the extrusive pile.

Glassy rims and mesostasis are commonly replaced by dark brown and sometimes green smectite and, more rarely, by late carbonate. Rare, irregularly shaped miaroles (<0.5 mm) may be partly lined with smectite or open and showing protruding crystal terminations. Carbonate occurs in random patches throughout the matrix, lining and partly replacing plagioclase laths and sometimes olivine grains. Olivine microphenocrysts are always replaced by brown or green smectite and sometimes by "iddingsite," but generally retain their euhedral or subhedral form.

Much of the macroscopic alteration is related to fractures, although their proportion of the bulk rock is generally only 1%–2%. Veins are normally thin (<0.1–0.2 mm), irregular, branching, and sometimes cross-cutting. No regular pattern or orientation was discerned, with the majority of veins being infilled with light or dark green smectites, with or without carbonate and pyrite. A few larger veins (1–3 mm) may exhibit a zonation of infilling materials (e.g., Section 129-802A-57R-3, piece 3) with the walls lined with botryoidal masses of radiate smectite fibers and a carbonate center. Associated with some veins was the development of dark gray or greenish alteration halos (e.g., Sections 129-802A-58R-1, piece 12, and 129-802A-60R-1, piece 6) that represented zones of more extensive clay development (Fig. 46). Carbonate analyses for the basalts are presented in Table 9.

### Summary and Conclusions

1. The basaltic extrusive rocks from Hole 802A are a series of pillow lavas with a thin lava flow at the base. They are mainly aphyric and sparsely plagioclase-clinopyroxene-olivine microphyric basalts that exhibit glassy spherulitic rims and quench-textured flow interiors.

2. Alteration is generally slight and dominated by smectitic clays, carbonate, and pyrite. The secondary assemblages are typical of the early stages of low-grade submarine weathering, formed under mildly alkaline, reducing conditions. A later, extensive oxidative phase was not developed, possibly because of subsequent rapid sedimentation and burial by impervious, reducing claystones.

3. The development of middle Cretaceous basalts at Site 802 either (1) may be tentatively correlated with or have a lithological analog within the Nauru Basin igneous complex that exhibits a series of pillow lavas in the upper extrusive sequence, or (2) may represent local basement of middle Cretaceous age.

## DOWNHOLE MEASUREMENTS

### Operations

On 1 January 1990, after reaching a total depth (TD) of 559.8 mbsf, the hole was swept with freshwater bentonite mud, which was subsequently displaced by seawater circulation during bit-release operations at 2230 hr UTC. The bit was dropped at the bottom of the hole and the drill pipe was raised to 50.1 mbsf in preparation for logging. The pipe was eventually placed at 127 mbsf for the beginning of each logging run and raised to approximately 108 mbsf while logging uphole. The three standard logging runs began at Site 802 at 0205 hr on 2 January 1990 and were completed at 0630 hr on 3 January, corresponding to a total logging time of 28 hr (Table 10). An additional 30 hr were spent during an attempted vertical seismic profiling (VSP) experiment and subsequent retrieval of the well seismic tool (WST) that had been stuck. The WST and wireline were successfully recovered and brought on deck at 1209 hr on 4 January. However, no VSP data were recorded.

The quad combination tool string included, from top to bottom, telemetry, long-spaced sonic, lithodensity, natural gamma-ray spectrometry, and dual induction resistivity tools in addition to the Lamont temperature tool (TLT). These tools were rigged at 0205 hr on 2 January, creating a tool string 30.72 m long. At 0400 hr the quad combination tools were run down to the level of the mud line and held stationary for 3 min to obtain a bottom-water calibration point for the TLT. The depth to the end of pipe as recorded on this logging run was within 3 m of that calculated by the driller. As logging continued downhole it was reported that the wireline heave compensator (WHC) was not operating. The tool string continued downhole until a bridge was encountered at 104 mbsf (0410 hr). The tool string was unable to penetrate below this depth and at 0433 hr it was decided to trip the tool out of the hole without recording any data, and to run the pipe through this bridge. The quad combination tool string was returned to the rig floor at 0615 hr. At 1027 hr the pipe was able to break the bridge with 5000–8000 lb of bit weight. The quad combination tool string was rigged again at 1050 hr and the tool was lowered down the pipe and held stationary for 3 min at the mud line at 1310 hr. Again it was reported that the WHC was not operating. Downgoing logging data were acquired to 325 mbsf, where the tool string hit another bridge. The tool string

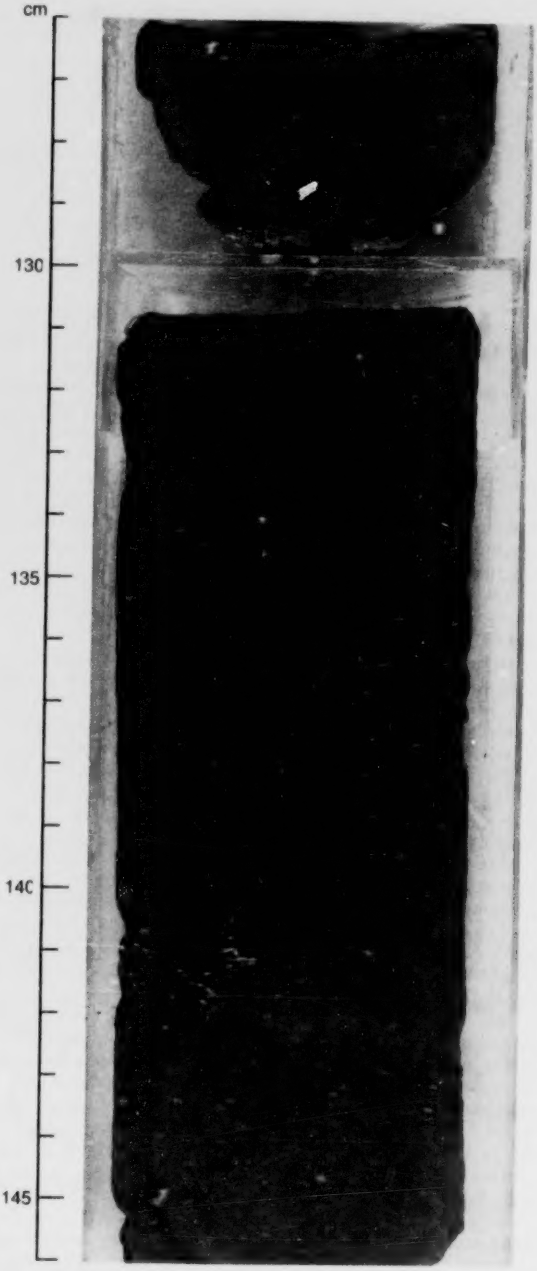

Figure 46. Dark alteration halos associated with smectite-carbonate veins in Hole 802A (interval 129-802A-58R-1, 126–146 cm).

**Table 9. Carbonate analyses of basalts from Hole 802A.**

| Core, section, interval (cm) | Depth (mbsf) | $CaCO_3$ (wt%) |
|---|---|---|
| 129-802A- | | |
| 58R-1, 38–40 | 516.38 | 0.8 |
| 58R-2, 53–55 | 518.03 | 0.3 |
| 58R-2, 105–107 | 518.55 | 0.3 |
| 58R-3, 86–88 | 519.86 | 0.2 |
| 59R-1, 83–85 | 526.23 | 0.4 |
| 60R-1, 90–92 | 535.60 | 0.4 |
| 62R-1, 129–131 | 551.89 | 0.4 |

was unable to go through this bridge and at 1354 hr it was decided to record what was left of the hole. Logging data were recorded successfully as the tool string moved uphole at 300 m/hr from 323 to 108 mbsf (Figs. 47, 48, and 49), with a repeat section taken from 207 to 108 mbsf. The bottom of pipe was encountered at 127 mbsf and another bottom-water temperature calibration point for the TLT was obtained at the mud line. The quad combination tool string was returned to the rig floor at 1735 hr on 2 January. The TLT was then taken to the downhole measurements lab, opened, and hard-wired to the Masscomp computer to download the recorded temperature/time measurements.

The geochemical combination tool string, which included telemetry, natural gamma-ray spectrometry, aluminum clay, and induced gamma-ray spectrometry tools and the TLT, was rigged at 1830 hr on 2 January, creating a tool string 18.13 m long. The string was lowered down the pipe and held stationary for 3 min at the mud line to obtain a bottom-water calibration point for the TLT. Logging data were recorded from 323 mbsf up into the pipe as the tool string moved uphole at 200 m/hr (Figs. 48 and 49), with a repeat section taken from 207 to 108 mbsf. During this run the WHC was operating. The geochemical logging run was completed at 0100 hr on 3 January.

The next tool combination run at Site 802 was the formation microscanner (FMS), which included telemetry, natural gamma-ray spectrometry, and FMS tools and the TLT. This tool string was rigged and in the hole at 0115 hr on 3 January. FMS data were recorded uphole at 260 m/hr from 323 to 108 mbsf without problems. The FMS tool string was returned to the drill floor at 0620 hr on 3 January.

The final tool run at Site 802 was the WST, which was rigged and in the hole at 0711 hr on 3 January. The 400-in.$^3$ water gun was operating at 2000 psi, but no signal was apparent on the real-time WST display. Test shots were taken in pipe down to the TD of the previous logging runs, during which time it appeared as if the caliper arms of the WST were not locking the instrument securely against the borehole wall, resulting in an extremely poor signal-to-noise ratio. At 1244 hr on 3 January we finally received a good signal at 248 and 253 mbsf and we lowered the tool back to the TD. The WST apparently broke through the bridge at 325 mbsf and reached a depth of 370 mbsf, where test shots were again poorly received, and at 1327 hr it was decided to trip out of the hole in order to replace the WST. At 1345 hr the tool became stuck at 245 mbsf by a bridge not previously encountered, and from this time to 1500 hr we attempted to pull free with up to 9500 lb of tension on the wireline (hanging weight was 5500 lb). At this time it was decided to crimp and cut the wireline at the base of pipe (500 m above the WST), reel in the remaining cable, and pull up pipe, with little hope of recovering anything but the majority of the wireline. This would at least assure us of enough wireline to log Hole 801C. The severing tool cut the cable, but on retrieval, we discovered that the cut had been made 3164 m above the WST. The remaining wireline (including 100 m of knots) was recovered along with an apparently undamaged WST at 1209 hr on 4 January.

The quad combination logging run was tied into the depth given from the drill string (i.e., log depth tied to core depth). All logging runs were then shifted by the Schlumberger engineer relative to the quad combination logging run using the natural gamma-ray log response. The geochemical combination run was shifted to shallower depths by 1.78 m and the FMS was shifted to greater depths by 1.14 m.

Summary log figures appear at the end of this chapter. The FMS images are presented on microfiche in the back of this volume.

### Log Quality

These are the highest quality logs recorded during Leg 129 (Figs. 47, 48, and 49). The raw sonic data required only minor shipboard processing and editing to create a useful sonic log (Figs. 47 and 50). The data recorded from the induced gamma-ray spectrometry tool will require post-cruise processing; references made to silicon, calcium, and iron are therefore only broadly qualitative. In contrast, the natural gamma-ray spectrometry tool produces reliable values for the concentration of potassium, thorium, and uranium, and the aluminum clay log is generally little improved through post-cruise processing. The quad combination was not obviously affected by the ship's heave; the small degree of elasticity within the wireline summed over its extreme length (6000 m) may have acted to slightly decouple these logging tools from the heave of the ship. The WHC was operational during the geochemical and FMS logging runs and effectively decoupled these tool strings from the heave of the ship. No adverse effects from ship's motion are apparent on the raw FMS records; however, the FMS data will still require significant shore-based image processing to achieve an interpretable record. The FMS images are presented on microfiche in the back of this volume.

### Logging Units

Four logging units were identified in Hole 802A (Fig. 51) based on log response and analyses of recovered cores. These logging units should not be confused with the lithologic units defined earlier (see "Lithostratigraphy and Sedimentology" section, this chapter). The boundaries between adjacent logging units were placed at significant inflection points resulting from simultaneous variations on at least several of the logs illustrated in Figures 47 through 51. These units display consistent log responses or distinct overall trends.

Core recovery was much higher throughout the logged interval (average recovery 26%) than at either Sites 800 or 801, as both well-indurated and softer interbedded portions of Hole 802A were actually recovered. The lithologies for unrecovered intervals have been inferred from the logs based on the broad assumption that the logging tools respond to varying proportions of the primary constituents in samples actually recovered (e.g., biogenic silica, carbonate, pelagic clay, volcanogenic clay) and to their relative porosity.

#### *Logging Unit 1 (108–167 mbsf)*

Logging Unit 1 is distinguished by extreme variability in covarying velocity (1.7–4.1 km/s), resistivity (1–11 ohm-m), density (1.5–2.4 g/cm$^3$), aluminum (1.2–6 wt%), and silica (0.026–0.156) contents. The topmost (108–118 mbsf) portion of Unit 1 contains local maxima in potassium and thorium and an absolute minimum in uranium concentration along with minima in resistivity, density, and aluminum values. The abrupt change from highly variable logging responses to uniformly low values for velocity, resistivity, and density at 167 mbsf was chosen as the lower boundary of logging Unit 1.

Table 10. Actual time schedule (UTC) for logging operations at Hole 802A and tools used during each logging run.

| Tool String | Time | Procedure |
|---|---|---|
| Quad combination (TCCB-LSS-HLDT-NGT-DIL-TLT) | RIH 0205 hr<br>2 January 1990<br>POOH 1735 hr | Log down to 104 mbsf. Hit a bridge. Run pipe through bridge. Log down to 325 mbsf. Log up to 108 mbsf with repeat section from 207 to 108 mbsf. |
| Geochemical combination (TCCB-NGT-ACT-GST-TLT) | RIH 1830 hr<br>POOH 0100 hr<br>3 January 1990 | Run down to 323 mbsf, log up to 108 mbsf. Run down to 207 mbsf, log up to 108 mbsf. |
| Formation microscanner (FMS-TCCB-NGT) | RIH 0115 hr<br>POOH 0620 hr | Run down to 323 mbsf, log up to 108 mbsf. |
| Vertical seismic profile (WST) | RIH 0711 hr<br>POOH 1209 hr<br>4 January 1990 | Run down to 323 mbsf, log up with poor results. Run down and break through bridge. Test at 370 mbsf. Run up. Tool stuck at 245 mbsf; decide to crimp and cut wireline. |

Notes: Total logging time is 58 hr, including initial rig-up and final rig-down of tool strings. Abbreviations used above are as follows: TCCB = telemetry tool, LSS = long-spaced sonic tool, HLDT = lithodensity tool, NGT = natural gamma-ray spectrometry tool, DIL = dual induction tool, TLT = Lamont temperature tool, FMS = formation microscanner, ACT = aluminum clay tool, GST = induced gamma-ray spectrometry tool, WST = well seismic tool, RIH = run in to hole, and POOH = pull out of hole.

The extreme logging responses appear to correlate to changes in grain size and an inferred variation in the amount of silica cementation. The highest values of velocity, resistivity, density, aluminum, and silica correlate to relatively coarse-grained intervals (volcaniclastic sandstone), inferred to be relatively well cemented by recrystallized silica (e.g., Cores 129-802A-14R and -15R). The coarse-grained interval is juxtaposed against a less-indurated, finer-grained (silty sandstone) interval that is also apparent on the logs. The distinct logging response observed from 108 to 117 mbsf is indicative of a poorly cemented, nonvolcaniclastic, clay-rich interval and suggests that the 1.67 m of pelagic clay recovered in Core 129-802A-13R is representative of the entire cored interval. The uniformly low total gamma-ray values which do not covary with velocity, resistivity, and density indicate that volcaniclastic clay-rich intervals observed within volcaniclastic deposits at Sites 800 and 801 are not abundant within logging Unit 1 in Hole 802A.

### *Logging Unit 2A (167–210 mbsf)*

Logging Unit 2A is characterized by uniformly low velocities (1.75–1.9 km/s), resistivities (1 ohm-m), densities (1.55–1.9 g/cm$^3$), and relatively low total gamma-ray (10–21 API) and silicon values. Aluminum concentration remains elevated. These general logging responses also characterize the upper portion of logging Unit 2B (210–233 mbsf). However, a logging boundary was chosen at 210 mbsf based on a distinct shift toward higher potassium concentration along with restricted local maxima in thorium and uranium and local minima in density, aluminum, calcium, and iron values. The logging responses defining this unit appear to be an extended version of those responses observed in logging Unit 1 that characterized the poorly cemented, finer-grained portion of lithologic Unit IIA. The lack of interbedded, well-cemented volcaniclastic sandstone results in the more uniform and lower log values.

The logging responses that define the boundary between logging Units 2A and 2B at 210 mbsf provide evidence of an unidentified unconformity (a contact between two turbidite events) within the lower Miocene sediments. This boundary is inferred to result from juxtaposition of a clay-rich layer below 210 mbsf with a relatively coarser-grained (siltstone), clay-poor interval above. This boundary also roughly correlates to a reported increase in nannofossil clay and chalk lithologies below Core 129-802A-23R, although there is no corresponding increase in relative calcium concentration at this depth (see "Lithostratigraphy and Sedimentology" section, this chapter).

### *Logging Unit 2B (210–260 mbsf)*

Logging Unit 2B is characterized by initially high values of potassium, thorium (total gamma ray), and aluminum, which steadily decline to relative minima at approximately 232 mbsf. Restricted local minima in silicon, calcium, and iron also occur at this depth.

The logging responses at the top of Unit 2B (210–232 mbsf) provide evidence of a volcanic clay-rich interval that gradually becomes more carbonate-rich with depth. The logging responses at 232 mbsf may indicate an unconformity corresponding to a contact between coarse-grained debris flow deposits below 232 mbsf (e.g., base of lithologic Unit IIB) to more uniformly fine-grained deposits above this level.

From 232 to 250 mbsf, logging Unit 2B displays gradually increasing density and calcium values, along with covarying maxima/minima in velocity, resistivity, density, aluminum, and, to a lesser extent, calcium. This type of logging response appears to correspond to interbedded, coarse-grained, well-cemented debris flows with less-indurated, fine-grained, nannofossil clay- or chalk-dominated intervals where calcium carbonate is the primary cementing agent rather than silica (as in logging Unit 1).

A distinct sinusoidal variation on nearly all the logs was observed at 250 mbsf. This boundary is characterized by relative minima in potassium, total gamma-ray, aluminum, silicon, iron, and sulfur values along with maxima in velocity, resistivity, density, uranium, and calcium. These variations

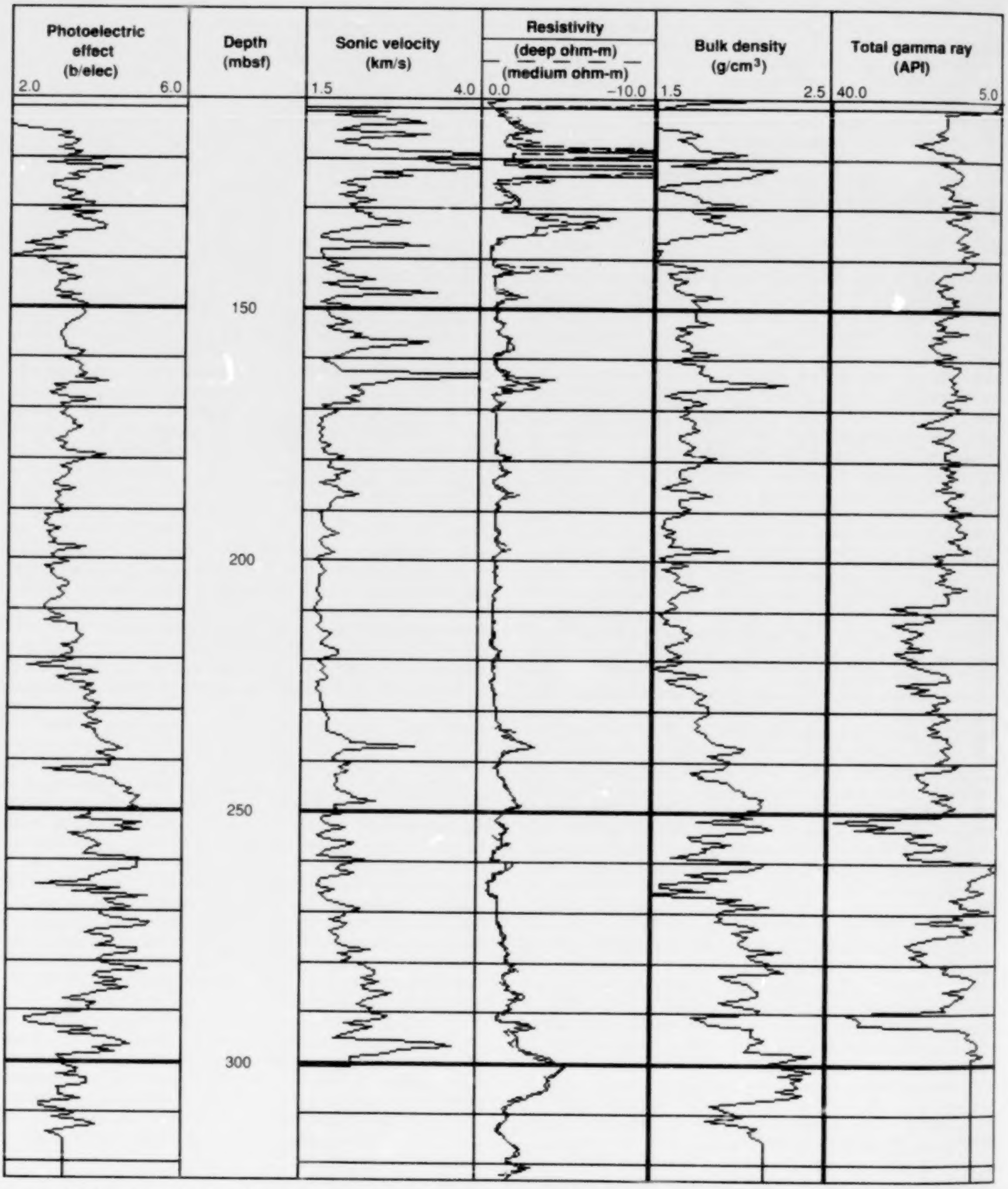

Figure 47. Selected downhole logs from the quad combination tool string for the interval from 108 to 323 mbsf in Hole 802A: Photoelectric effect, sonic velocity, resistivity, bulk density, and total gamma ray. Stratigraphic units defined by logging data (logging units) are shown in Figure 51. Sonic velocity, resistivity, and density reflect the porosity of the formation and thus the degree of lithification or cementation.

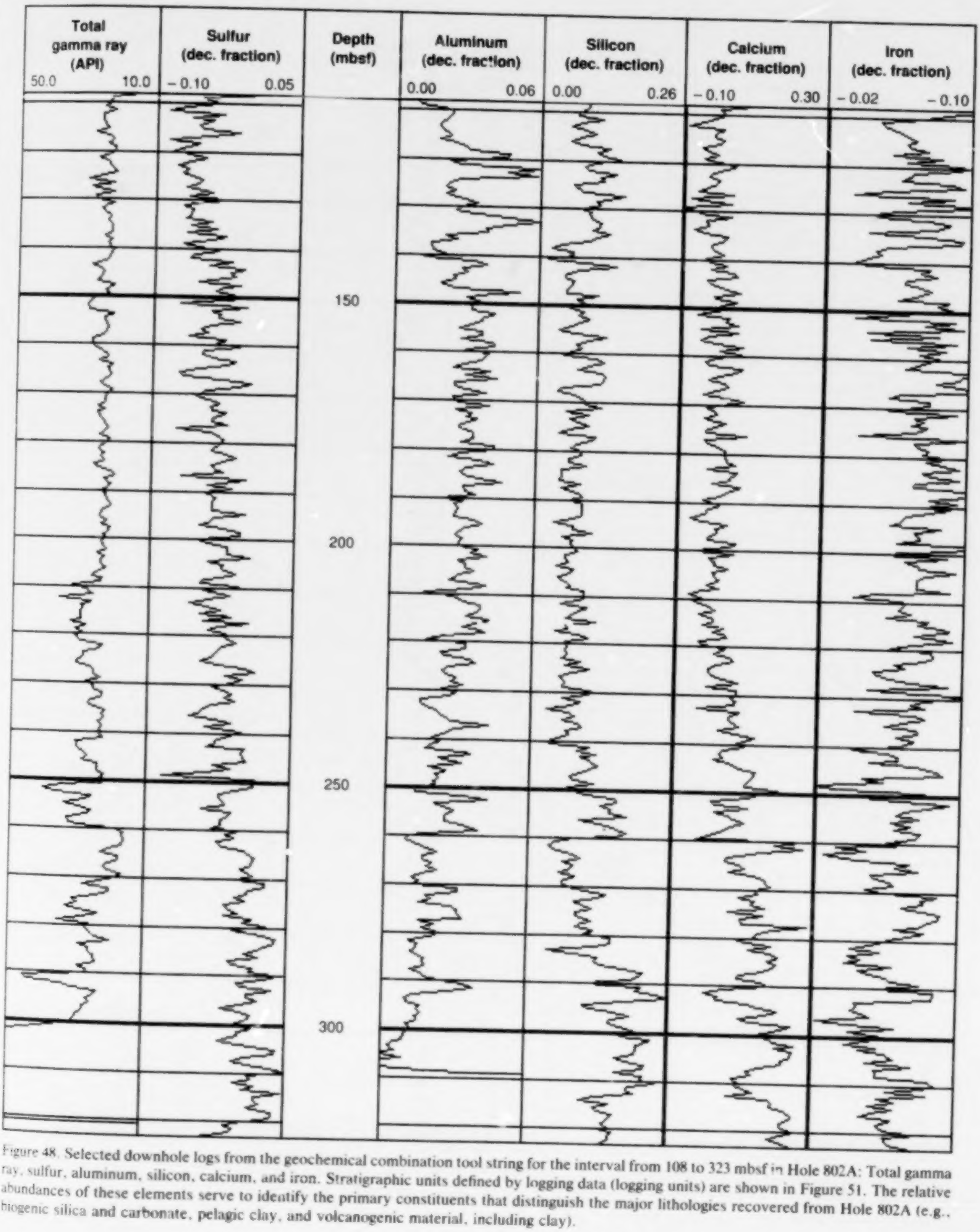

Figure 48. Selected downhole logs from the geochemical combination tool string for the interval from 108 to 323 mbsf in Hole 802A: Total gamma ray, sulfur, aluminum, silicon, calcium, and iron. Stratigraphic units defined by logging data (logging units) are shown in Figure 51. The relative abundances of these elements serve to identify the primary constituents that distinguish the major lithologies recovered from Hole 802A (e.g., biogenic silica and carbonate, pelagic clay, and volcanogenic material, including clay).

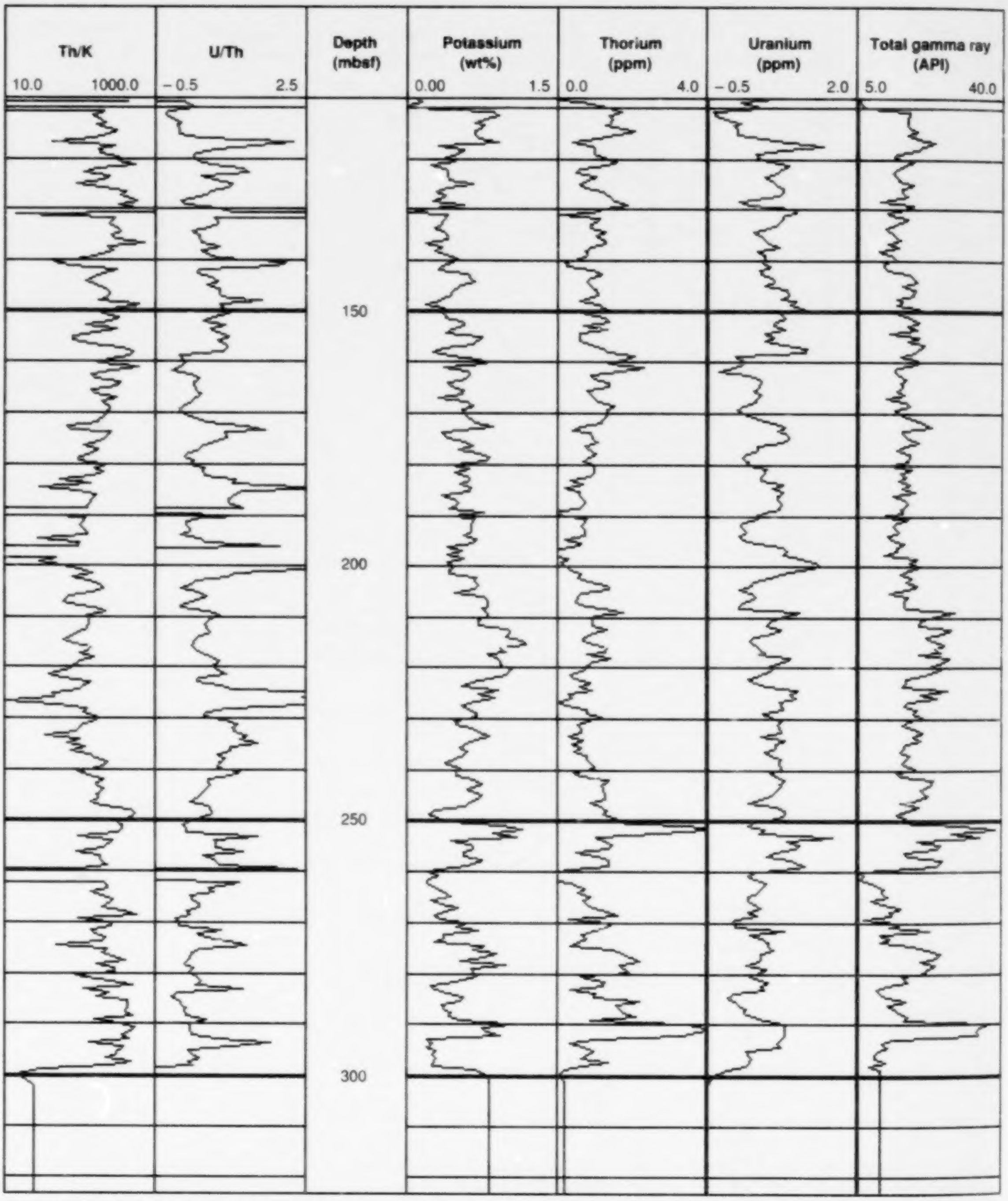

Figure 49. Downhole logs from the natural gamma-ray spectrometry tool on the quad combination tool string for the interval from 108 to 323 mbsf in Hole 802A: thorium/potassium ratio, uranium/thorium ratio, potassium, thorium, uranium, and total gamma ray. Stratigraphic units defined by logging data (logging units) are shown in Figure 51.

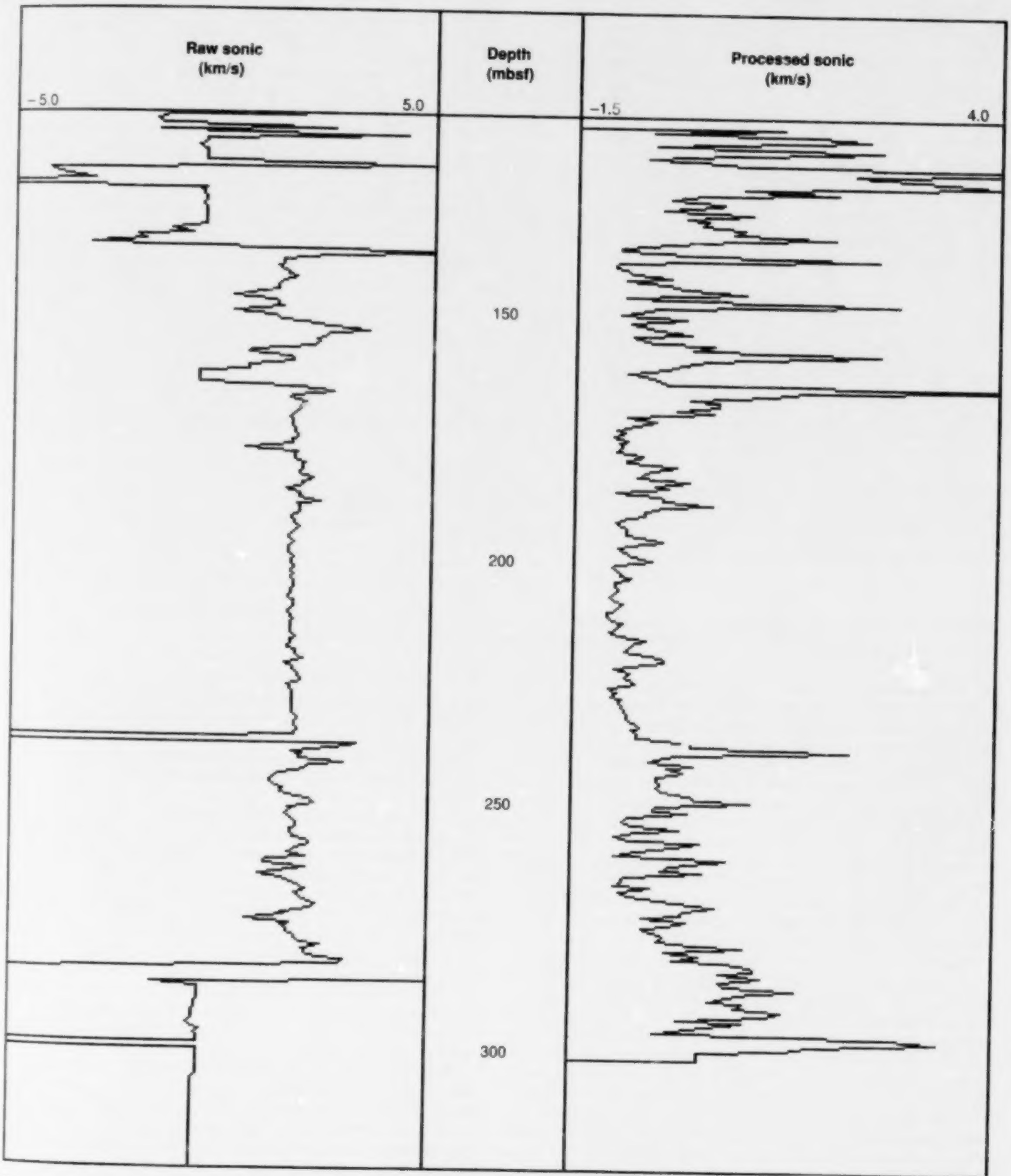

Figure 50. Comparison of observed "raw" (left column) and processed (right column) velocity logs for Hole 802A. Covariation of the processed sonic log with resistivity, gamma ray, and bulk density logs (Figs. 47 and 51) indicates that a useful velocity log was produced. One notable exception occurs at about 108 mbsf, where high velocities are matched by low resistivities and densities.

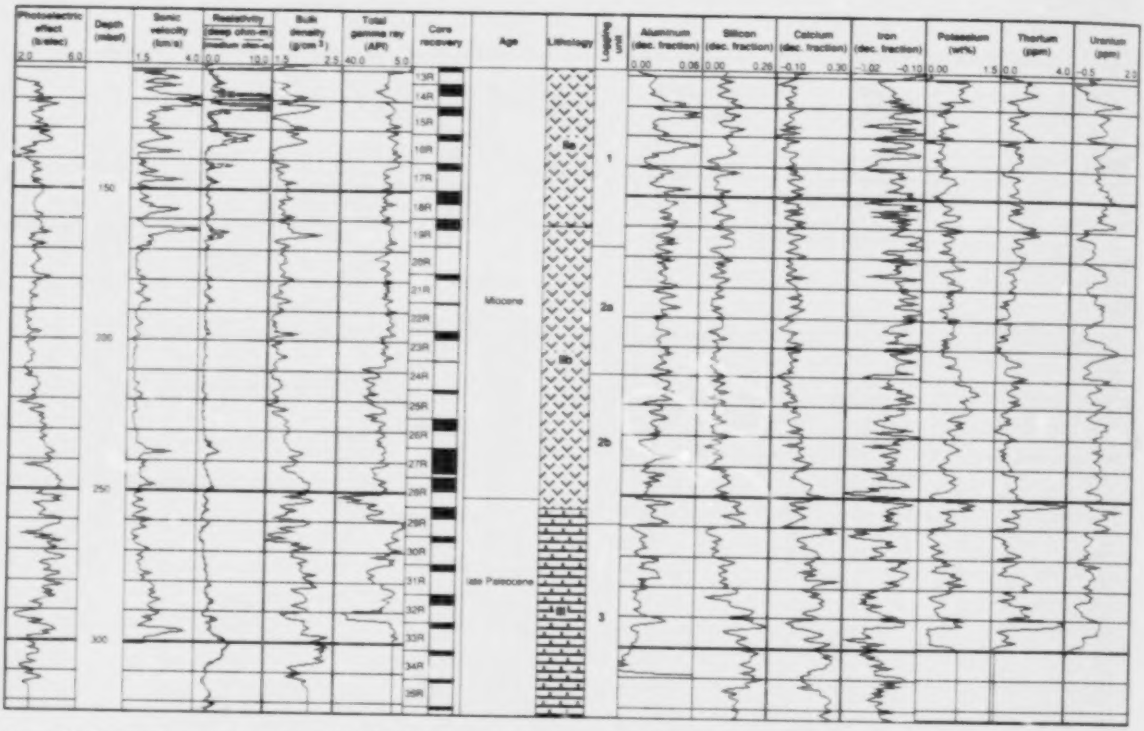

Figure 51. Summary compilation of downhole logs, intervals of core recovery, lithology, and downhole logging units at Hole 802A. Lithologic units are based on coring results (see "Lithostratigraphy and Sedimentology" section, this chapter).

are juxtaposed against underlying local minima/maxima in the opposite sense for all the above-mentioned logs, including an absolute maximum in thorium concentration (>4.0 ppm). This logging response indicates a well-cemented, clay-poor interval overlying poorly cemented volcanic clay and silica-rich sediments with carbonate cement. This boundary corresponds to a sharp contact between coarse-grained volcanic debris flows (Core 129-802A-28R) and the underlying fine-grained claystone/siltstone, which is poorly cemented despite evidence for high silicon content. This interval from 250 to 260 mbsf corresponds to Core 129-802A-28R and -29R, which are reported to contain abundant, redeposited radiolarians, perhaps accounting for the high silicon concentration (see "Biostratigraphy" section, this chapter).

The base of logging Unit 2B at 260–262 mbsf is marked by a dramatic minima in potassium, thorium, uranium, aluminum, silicon, and iron concentrations coinciding with an abrupt unidirectional shift to high calcium concentrations coupled with small maxima in velocity, resistivity, and density values. The logging response at this boundary marks a sharp contact between a clay-rich, poorly cemented interval overlying a clay-poor, well-cemented (calcareous cement) unit. This boundary correlates to a major lithologic change from claystone to nannofossil chalk at 260 mbsf (see "Lithostratigraphy and Sedimentology" section, this chapter).

### *Logging Unit 3 (260–323 mbsf)*

Logging Unit 3 extends from 260 mbsf to the TD for logging operations at Site 802. This unit is defined by generally high calcium values along with consistently increasing potassium, thorium, velocity, resistivity, density, and silicon values. This unit also contains the highest sulfur concentrations observed at Site 802. This logging response strongly suggests the declining phase of an interval of high primary productivity which reaches a maximum no shallower than 290 mbsf. This evidence suggests that Site 802 was within a region of high productivity, presumably associated with an equatorial crossing no later than the late Paleocene, which by the early Eocene had moved beyond this high productivity zone (see "Paleomagnetism" and "Biostratigraphy" sections, this chapter). At 270–280 mbsf there is a maximum in iron concentration which possibly reflects the iron-manganese oxides recovered in Core 129-802A-31R (see "Lithostratigraphy and Sedimentology" section, this chapter).

Logging Unit 3 is punctuated at 292 mbsf by local maxima in potassium, thorium, uranium, aluminum, silicon, and iron, coupled with local minima in resistivity, density, and calcium. Calcium, resistivity, and density return to elevated levels below this depth and reach maximum values, including high silicon, at approximately 300 mbsf.

The logging responses observed at 292 mbsf again indicate an unconformity, in this case marked by a clay-rich interval (the base of Core 129-802A-32R) overlying an extended interval high in silica and calcium. This logging response illustrates the abrupt change from nannofossil chalk to nannofossil chalk with chert nodules below 292 mbsf, which can be interpreted to represent hard ground development resulting from a hiatus. This boundary corresponds exactly to a hiatus between upper Oligocene and lower Eocene ages determined from micropaleontology studies (see "Biostratigraphy" section, this chapter).

## Synthetic Seismogram

A synthetic seismogram was computed for Hole 802A to accurately tie the drilled sequence in the hole to seismic reflection data over the site (Fig. 52). The seismogram covers the interval from 110 to 300 mbsf, approximately 7.576 to 8.185 seconds two-way traveltime (s twt).

The unprocessed sonic velocity log from Hole 802A (Fig. 50) contains very high and/or low values corresponding to cycle skipping ("Downhole Measurements" section, "Explanatory Notes" chapter, this volume), almost exclusively from 108 to 140 mbsf. The sonic log-processing software aboard the ***JOIDES Resolution*** allowed us to set a window of possible velocity values and then recalculate a new log using only the traveltime data that result in velocities within the chosen window. A minimum-maximum window of 1.69 to 5.1 km/s was chosen, resulting in the processed sonic log displayed in Figure 50. This processed sonic log was used in combination with the raw bulk density log to calculate reflection coefficients which were convolved with a source wavelet to produce a synthetic seismogram. The synthetic seismogram shown in Figure 52 incorporated the source wavelet from the air-gun array used during FM35-12. The synthetic seismogram was shifted to the proper two-way traveltime on the seismic profile by matching the reflection created by the first chert encountered at this site. This method of matching synthetic to seismic profile works well if both the depth and the two-way traveltime to a given horizon are known (as was the case with first chert at Site 800). In the case of Site 802 we assumed that the relatively high amplitude reflection at 8.185 s twt corresponded to 300 mbsf, just below the first chert horizon. This correlation does not result in the best possible match between synthetic and multichannel seismic (MCS) reflections. It does, however, result in more reasonable interval velocities and velocity trends (i.e., high velocities over low velocities). The synthetic seismogram (Fig. 51) is compared with the MCS line shot during FM35-12 at its closest approach to Site 802 (within 2 km). The major reflectors apparent on the derived synthetic seismogram are correlated with the seismic 10-trace mix and seismic reflection profile. Improved synthetic seismograms will be produced for Site 802 after shore-based processing, which will include incorporation of physical properties data, repicking of sonic traveltimes, and the use of improved source wavelets.

A few general interpretations of the rocks comprising a portion of the sedimentary section at Site 802 have been made by extrapolating the downhole logging results onto the seismic profile. A further description of the correlation between seismic stratigraphy and lithostratigraphy is given in the "Site Geophysics and Seismic Stratigraphy" section (this chapter).

### Seismic Intervals

*1. 7.88 to 7.985 s twt (average velocity 2.06 km/s).* This zone encompasses a thin layer of pelagic clay (lithologic Unit I). The thickness of this unit is most accurately determined with the 3.5-kHz profiler at 30 ms, where the first lithified volcanic tuff was encountered (Fig. 53; see "Site Geophysics and Seismic Stratigraphy" section, this chapter). The velocity (porosity) contrasts between alternating zones of coarse-grained and fine-grained, variably cemented tuff with pelagic clay create these high-amplitude reflections (also observed within logging Unit 1). Measurements made on individual samples show both high and highly variable velocities within lithologic Unit IIA (see "Physical Properties" section, this chapter).

*2. 7.985 to 8.041 s twt, logging Unit 1 (average velocity 2.11 km/s).* The velocity (porosity) contrasts between alternating zones of coarse-grained and fine-grained, variably cemented tuff create these high-amplitude, flat-lying reflections (lithologic Subunit IIA).

*3. 8.041 to 8.144 s twt, logging Unit 2A and 2B (average velocity 1.81 km/s).* This interval contains less-continuous, moderate-to-low-amplitude reflections that are the result of small velocity-density contrasts within an interval of more uniform, generally fine-grained material with fewer interbedded, well-cemented volcaniclastic sandstones. A single low-amplitude reflector observed on the synthetic seismogram and MCS profile at 8.088 s twt corresponds to the inferred unconformity at the base of logging Unit 2A (210 mbsf). A high-amplitude reflection observed on the synthetic seismogram at 8.11 s twt, matched by a lower amplitude event on the MCS profile, is correlated to another apparent unconformity at 232 mbsf.

*4. 8.144 to 8.210 s twt, logging Unit 3 (average velocity 1.91 km/s).* This interval contains the transition from low-amplitude, discontinuous reflections to slightly higher amplitude and more continuous flat-lying reflections. This transition occurs at 8.185 s twt or approximately 300 mbsf, just below the first occurrence of chert within a chalk-dominated sequence (lithologic Unit III). The high carbonate content inferred for this interval from both logs and cores apparently creates a low-porosity matrix that results in a high-interval velocity.

The synthetic seismogram coupled with the geochemical logs indicate that the moderate-amplitude reflections at approximately 8.2 stwt are created by velocity/density (porosity) contrasts associated with sharp changes in silicon and calcium content.

## Summary

A suite of eight downhole logs were successfully recorded at Site 802, resulting in the identification of four distinct logging units. Compositional trends and boundaries were inferred from these logs through intervals of poor recovery by assuming that unrecovered intervals are composed of varying proportions of recovered materials. The logs were most useful in defining boundaries (unconformities) and in characterizing the unrecovered majority of the formation.

A synthetic seismogram correlates moderately well with the observed seismic profile and indicates (along with geochemical logs, physical properties, and lithostratigraphy) that the largest impedance contrasts are associated with significant changes in grain size within the volcaniclastic section, often corresponding to variations in silica concentration. These correlations also indicate that the moderate-amplitude reflections at approximately 8.2 s twt are created by impedance (porosity) contrasts associated with variations in silicon and calcium content.

# SITE GEOPHYSICS AND SEISMIC STRATIGRAPHY

Site 802 (proposed site EMB-2A) in the East Mariana Basin is located within the Jurassic magnetic quiet zone (JQZ) near the intersection of MCS line 18 (six 80-in.$^3$ water guns) obtained during the MESOPAC II expedition aboard *Le Suroit* in August-September 1989 and MCS line 7 (2576-in.$^3$ air-gun array) collected during the FM35-12 expedition aboard the *Fred H. Moore* in November-December 1987. Because Leg 129 began only three months after the *Le Suroit* cruise, only single-channel, real-time records of the water-gun data obtained during MESOPAC II were used to locate proposed site EMB-2A. The location of this MESOPAC II MCS profile was dictated by the preceding MCS expedition aboard the

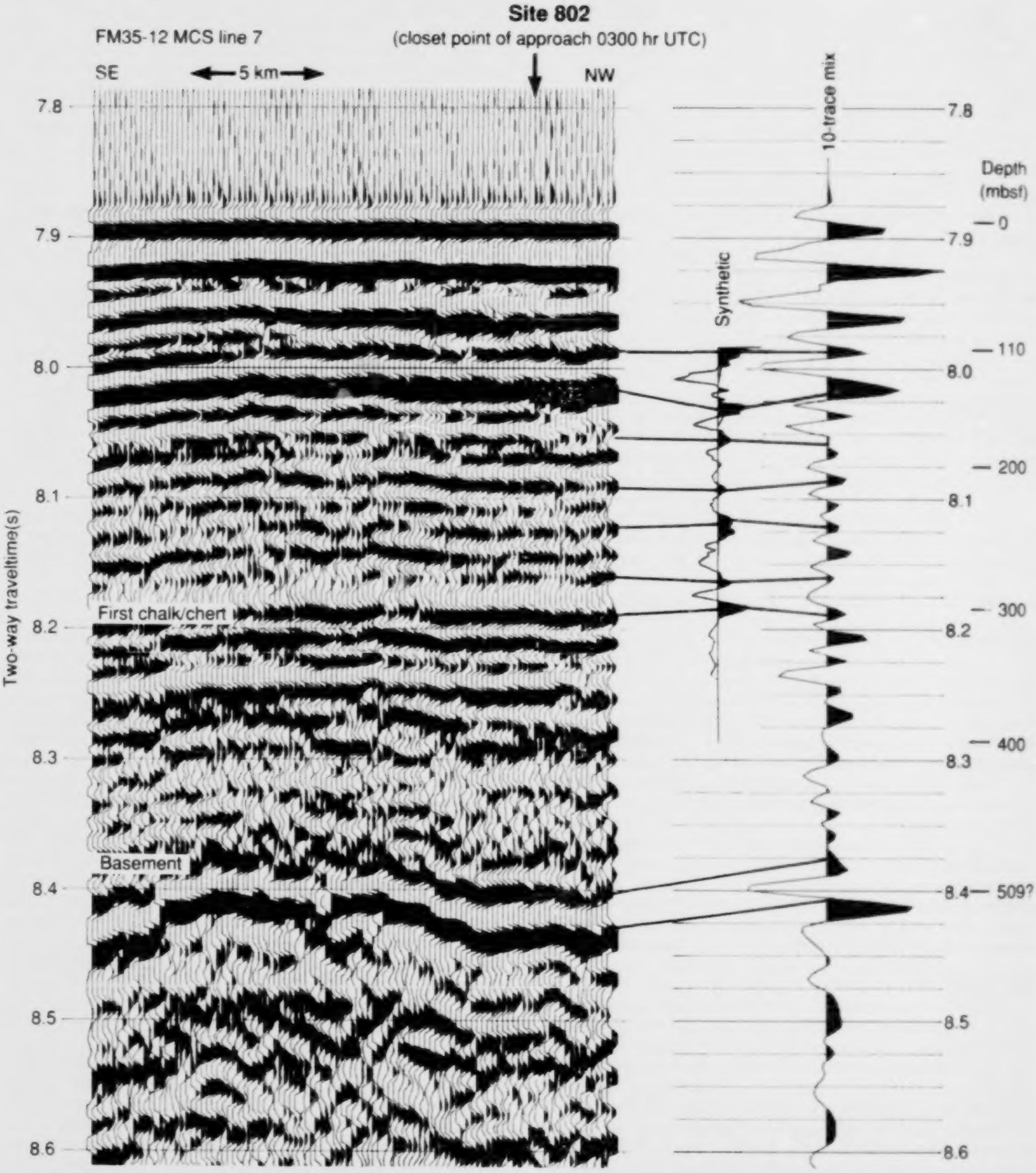

Figure 52. Comparison of vertical incident MCS data recorded during the FM35-12 expedition, with a 10-trace mix of this data and a synthetic seismic reflection trace computed from logged velocity and density measurements and the far-field source signature of the air-gun array used during FM35-12. Basement at this location along FM35-12 line 7 (within 2 km of Site 802) is imaged at 8.4 s twt, whereas at Site 802 basement deepens to 8.425 s twt (see Figs. 54 and 56). The seismic processing and display parameters are as follows: 120-fold stack, post-stack predictive decon, band-pass filter 20–60 Hz, and 500 ms AGC.

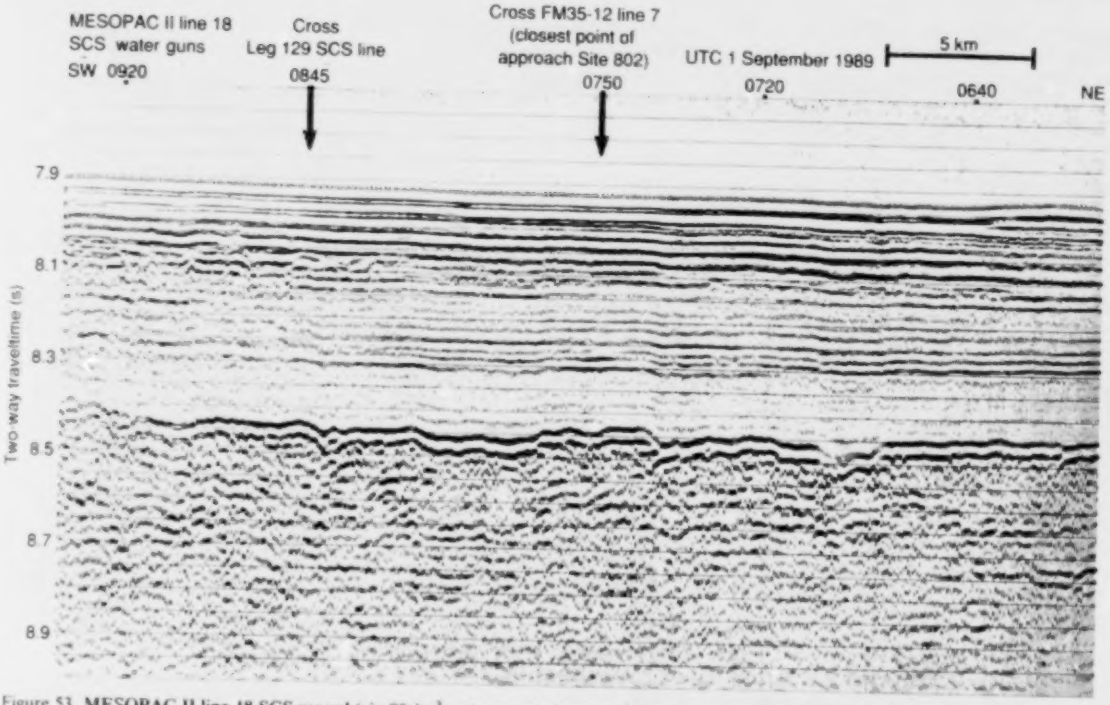

Figure 53. MESOPAC II line 18 SCS record (six 80-in.$^3$ water guns) showing closest approach to Site 802 at its intersection with FM35-12 line 7 (0750 hr UTC, 1 September 1989). High-velocity basement lies at approximately 8.4 s twt, 0.4 s deeper than Jurassic oceanic crust penetrated at Site 801. This near-channel record was processed and displayed with the following parameters: water-velocity F/K migration, mute, 2-trace mix, band-pass filter 25–100 Hz, 500 ms AGC, and vertical exaggeration ~22× at 1.5 km/s.

*Fred H. Moore* (FM35-12). The proposed site was located approximately 2 km southwest of FM35-12 profile 7 at its closest approach and about 4 km west of the intersection of FM35-12 line 7 and MESOPAC II line 18 (see Figs. 4, 53, and 54). The MCS basement images and velocity structure derived from sonobuoy data (specifically, sonobuoys 7, 8, 18, and 20) obtained during the FM35-12 expedition provided the regional seismic framework for locating Site 802 (Fig. 55). Site EMB-2A was specifically located at 0030 hr UTC on 17 November 1987 along FM35-12 line 7, approximately 5 km northwest of its intersection with MESOPAC II line 18. FM35-12 sonobuoy 7 (167 km northwest of Site 802), sonobuoy 8 (120 km northwest of Site 802), sonobuoy 18 (130 km northeast of Site 802), and sonobuoy 20 (370 km northeast of Site 802) were used to constrain basement depth and velocity structure (Fig. 55). The only other seismic data in the area are single-channel air-gun analog profiles (e.g., V3506) and a digitally recorded, two 80-in.$^3$ water-gun, single-channel survey collected aboard the *Kana Keoki* (KK 810626 Leg 4; Shipley et al., 1983).

Single-channel seismic (SCS) reflection and 3.5-kHz and 12-kHz profiling were conducted during the approach of the *JOIDES Resolution* to Site 802 (see "Operations" section, this chapter, for detailed approach plan). The actual site is located on the approach SCS water-gun profile at 2040 hr on 24 December 1989 (Figs. 4 and 56) within 2 km of the proposed site location on FM35-12 line 7.

The water-gun data collected during Leg 129 (two 80-in.$^3$) and from MESOPAC II (six 80-in.$^3$), and the FM35-12 air-gun data (2576-in.$^3$) are corroborative, and together with 3.5-kHz and sonobuoy data, provided the following seismic criteria for locating Site 802:

1. The relatively thin (30 ms) transparent layer over acoustic basement imaged with an excellent 3.5-kHz record (Fig. 57) was interpreted as pelagic clay overlying distal turbidites. We believed these turbidites could be penetrated with a minimum thickness of pelagic clay, providing lateral support for the drill string during spud-in.
2. A high-amplitude reflection imaged regionally at 0.30 to 0.55 s below the seafloor (bsf) corresponds to the onset of velocities characteristic of oceanic crust as recorded on FM35-12 sonobuoys 7, 8, and 18, indicating that approximately 300 to 550 m of sediment overlie volcanic basement in this area.
3. In the majority of the East Mariana Basin, this horizon is flat-lying and smooth. However, in restricted areas (e.g., Site 802), this high-amplitude reflection appears relatively rough, undulating, and slightly deeper, resulting in an image interpreted to be the top of oceanic crust, although not as clear as example of buried abyssal hills as found in the vicinity of Site 801.

### Seismic Stratigraphy

The acoustic stratigraphy of large portions of the western Pacific consists of four units originally defined by Ewing et al. (1968); (1) an upper transparent layer, (2) an upper opaque layer, (3) a lower transparent layer, and (4) acoustic basement. These seismic facies descriptions were made from observations of SCS analog air-gun profiles. Acoustic basement has been characterized by the presence of a prominent zone of

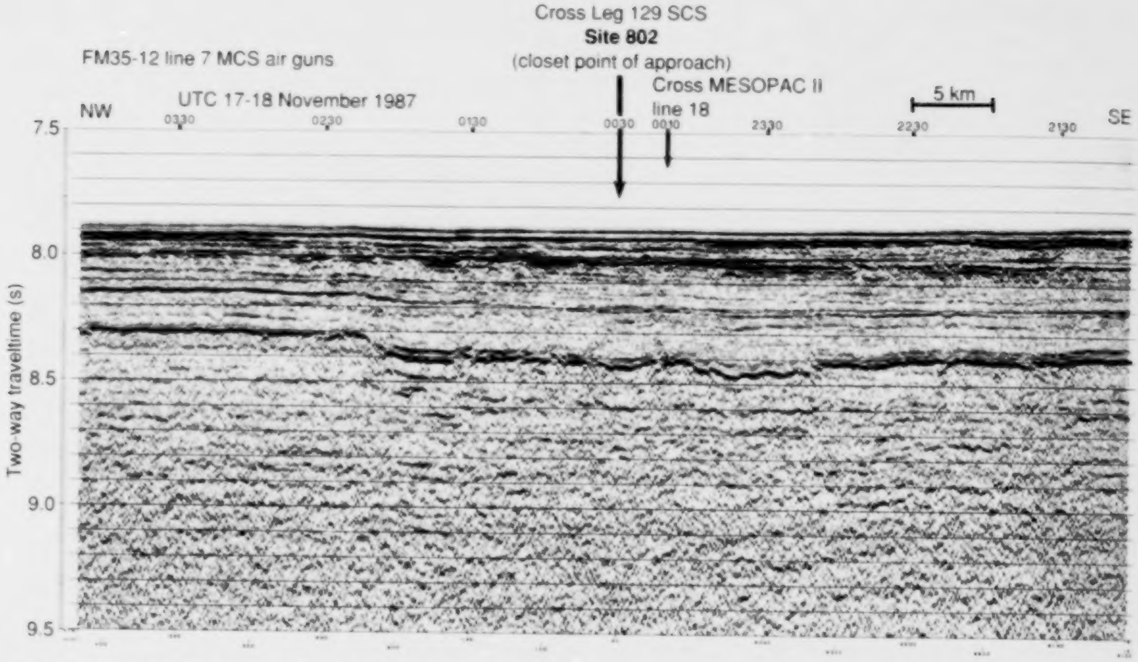

Figure 54. FM35-12 MCS air-gun profile showing the intersection with Leg 129 SCS (Fig. 56) at its closest approach (0030 hr UTC) to Site 802 and the intersection with MESOPAC II line 18 (Fig. 53) approximately 4 km east of Site 802. The depth and character of the basement reflector changes from a flat-lying, smooth reflection at 8.3 s twt to a rolling, higher-relief reflection at 8.4 s twt between 2300 and 0200 hr. These reflection characteristics were interpreted as a change from flat-lying sills to extrusive igneous material. This rough basement surface was correctly interpreted as extrusive basalt. However, it is not as obvious an example of buried abyssal hills as is found in the vicinity of Site 801. The seismic processing and display parameters are as follows: pre-stack spike decon, 120-fold stack, time-varying band-pass filter (20–60 Hz), 500 ms AGC, drop every other trace, and vertical exaggeration ~22× at 1.5 km/s.

flat-lying (''smooth''), high-amplitude, closely spaced reflections referred to as ''horizon B'' by Ewing et al. (1968), as the ''deep opaque layer'' by Heezen et al. (1973), and as the ''reverberant layer'' by Houtz et al. (1970) and Houtz and Ludwig (1979). It is now recognized that the reverberant nature of acoustic basement in such profiles is usually the result of a trailing bubble pulse oscillation reflecting from a single high-impedance boundary (Shipley et al., 1983). This characteristic of the air-gun source is now routinely compensated for through the use of tuned air-gun arrays and deconvolution techniques. The use of water guns in these surveys provides a much more implosive and bubble pulse-free source signature that provides a high-resolution record with little processing effort (Hutchinson and Detrick, 1984).

Although modern acquisition and processing techniques have allowed a more detailed and quantitative assessment of the stratigraphic units originally proposed by Ewing et al. (1968) (especially acoustic basement), these units can still serve to describe the general seismic character of the Pigafetta Basin. It is understood that the following qualitative seismic facies descriptions are largely controlled by the type of seismic source (air gun vs. water gun), processing, and display parameters. The final seismic facies identification and interpretation will be made after the MESOPAC II MCS data have been stacked and properly displayed and a final synthetic seismogram has been generated.

The East Mariana Basin is bounded to the south by the Caroline Ridge and is separated from the Pigafetta Basin tectonically and physically by the northwest-trending Ogasawara fracture zone and Magellan seamounts (Tamaki et al., 1987; Handschumacher et al., 1988). These features isolated the Pigafetta Basin from the sources that supplied extensive Tertiary volcaniclastic turbidites to the East Mariana Basin. These Tertiary deposits represented the greatest anticipated difference in the stratigraphy between the East Mariana and Pigafetta basins.

The stratigraphy of the East Mariana Basin can be divided into three sequences (Fig. 58) that are comparable to the lowest three units of Ewing et al. (1968) and essentially to those described by Shipley et al. (1983). The lowermost sequence known as ''horizon B'' or the ''reverberant layer'' can be better characterized as a single, very high-amplitude, smooth reflector at approximately .30 to .55 s twt bsf. This most prominent horizon is continuous and flat-lying in the majority of the East Mariana Basin and identical in appearance to the reverberant layer in the southeastern Pigafetta Basin (see ''Site Geophysics and Seismic Stratigraphy'' section, ''Site 801'' chapter). There is no clear relationship between this horizon and the seamounts surrounding the East Mariana Basin. In restricted areas of this basin the reverberant layer deepens and becomes noticeably more rugged and undulating, for example, between 2330 and 0200 hr on FM35-12 line 7 (Fig. 54). The relief displayed by the reverberant layer in the East Mariana Basin, however, is never as great as observed in portions of the central Pigafetta Basin within the JQZ (e.g., Site 801). Site 802 was specifically

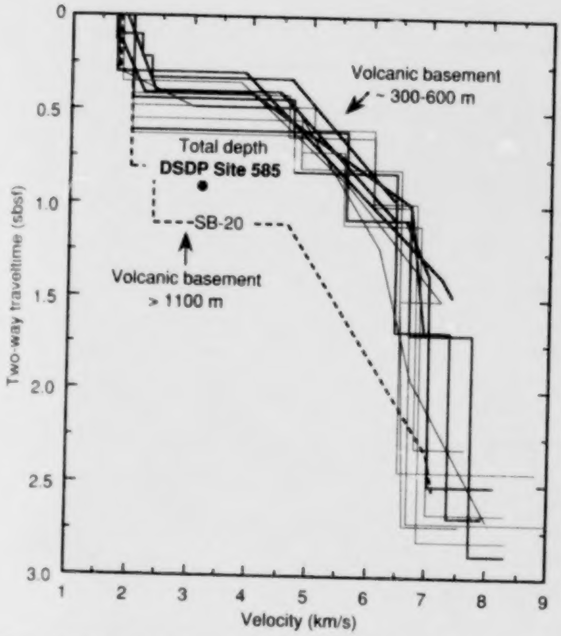

Figure 55. Velocity vs. two-way traveltime below seafloor (bsf) from sonobuoy data collected during FM35-12 and MESOPAC II in the East Mariana and Pigafetta basins. Crustal velocities begin from 300 to 600 ms bsf (approximately 300 to 600 mbsf), with the exception of sonobuoy 20. Sonobuoy 20 (dashed line) was shot over DSDP Site 585 and indicates that approximately 1150 m of sediment overlie the anomalously deep basement of the Ogasawara Fracture Zone trough (see total depth of DSDP Site 585). The onset of velocities and velocity gradients characteristic of oceanic crust corresponds to the reflection imaged at approximately 8.4 s twt in Figures 53, 54, and 56. (Note total depth of Hole 802A at about 560 ms bsf.)

located where the reverberant layer is deepest and relatively rough (8.4 to 8.425 s twt or 520 to 545 ms bsf).

There is a third, somewhat questionable type of basement reflection event observed in the East Mariana Basin. The suppression of any bubble pulse multiples from the flat-lying reverberant horizon on the processed FM35-12 MCS data has revealed much weaker discontinuous reflections approximately 100 ms below the reverberant horizon. The identification of these weak reflections, which are often identical in shape to the overlying dominant reflection (multiples?), as "real" primary reflection interfaces rather than bubble pulse or interbedded multiples is strengthened by the appearance of a similar sequence imaged with a water-gun source (Shipley et al., 1983). There are isolated instances where these weak reflections display significant relief independent of the flat, overlying reverberant layer, further indicating that they may be real events, possibly representing extrusive basement beneath basaltic sills and/or flows.

Sonobuoy velocity solutions indicate that velocities and velocity gradients characteristic of oceanic crust begin at or just below the dominant flat-lying reverberant horizon imaged regionally at 300 to 550 ms bsf (Fig. 55). Sonobuoy 7, for instance, displays crustal arrivals that begin .491 s bsf, just below the deepest high-amplitude reverberant-layer reflection, and may correlate to a weaker, high-relief basement reflector (Abrams et al., 1988). Sonobuoy 20, located on the eastern border of the East Mariana Basin over DSDP Site 585, is the one exception to this trend and indicates that approximately 1150 m of sediment overlie the anomalously deep basement of the Ogasawara fracture zone trough. The reverberant layer at this location lies at approximately 9.0 s twt and is apparently created by well-cemented volcaniclastic debris flows that lie about 260 m above basement.

Immediately overlying the reverberant layer (Fig. 58) is the "lower transparent" layer (8.041–8.425 s twt), which is characterized by low-amplitude, more widely separated, discontinuous reflectors, making this sequence distinctly transparent on both air-gun and water-gun seismic records (Figs. 53, 54, and 56). This sequence is flat-lying, mirroring the dominant reverberant horizon and does not appear to pond (onlap) against any of the large guyots traversed during FM35-12. However, it does thin in areas where the underlying reverberant horizon rises (300 ms), suggesting that this sequence is not pelagic drape. At Site 802 the lower transparent layer is bounded on top by another sequence of high-amplitude, flat-lying, continuous reflectors that are visible at 161 ms twt bsf (8.041 s twt). The transparent layer is divided in two by a sequence of distinct, moderate-amplitude, continuous reflections from approximately 8.185 to 8.275 s twt. The top of this sequence can be traced for hundreds of kilometers across the majority of the East Mariana Basin, including the area surrounding DSDP Sites 199 and 585.

The sequence from the seafloor down to approximately 8.04 s twt (Fig. 58) is comparable to that described by Ewing et al. (1968) as the "upper opaque layer." This interval contains closely spaced, moderate- to high-amplitude reflections that are traceable for 30 to 50 km. This uppermost sequence is distinct in that reflections onlap basement highs including a large, unnamed Magellan seamount to the north and Ita Mai Tai guyot to the south, and tends to thicken in minor lows and thin over minor highs.

The upper transparent zone as envisioned by Ewing et al. (1968) is very much attenuated in the East Mariana Basin and extends from 0 to approximately 30 ms bsf (7.88–7.91 s twt) at Site 802. This interval is best displayed on the 3.5-kHz records obtained during Leg 129 (Fig. 52) and MESOPAC II, and is not apparent on SCS records. These four seismic facies are essentially identical on the SCS monitor records of both Leg 129 and MESOPAC II, and are comparable to the processed FM35-12 air-gun data.

## Correlation between Seismic Stratigraphy and Lithology at Site 802

During DSDP Legs 6, 17, 61, and 89, there were instances when a flat-lying, high-amplitude "acoustic basement" or "reverberant layer" was correlated to middle Cretaceous volcanic material (sills, flows, and volcanogenic turbidites) which, according to magnetic lineations, significantly postdate the formation of oceanic crust. However, the physical nature of a similar seismic facies observed throughout the majority of the East Mariana Basin and all of the Pigafetta Basin had not been determined before Leg 129.

The reverberant layer at Site 800, located on a correlatable magnetic anomaly (M33) in the northern Pigafetta Basin, is created by a massive chert overlying a series of dolerite sills and appears as a flat-lying sequence of reflections approximately 100 ms thick (see "Site Geophysics and Seismic Stratigraphy" section, "Site 800" chapter, this volume). This type of smooth, flat-lying, high-velocity horizon is characteristic of much of the Pigafetta Basin and the majority of the East Mariana Basin (Abrams et al., 1988). In contrast, the reverberant layer at Site 801, located well within the JQZ, appears as a rough, undulating horizon that is created by

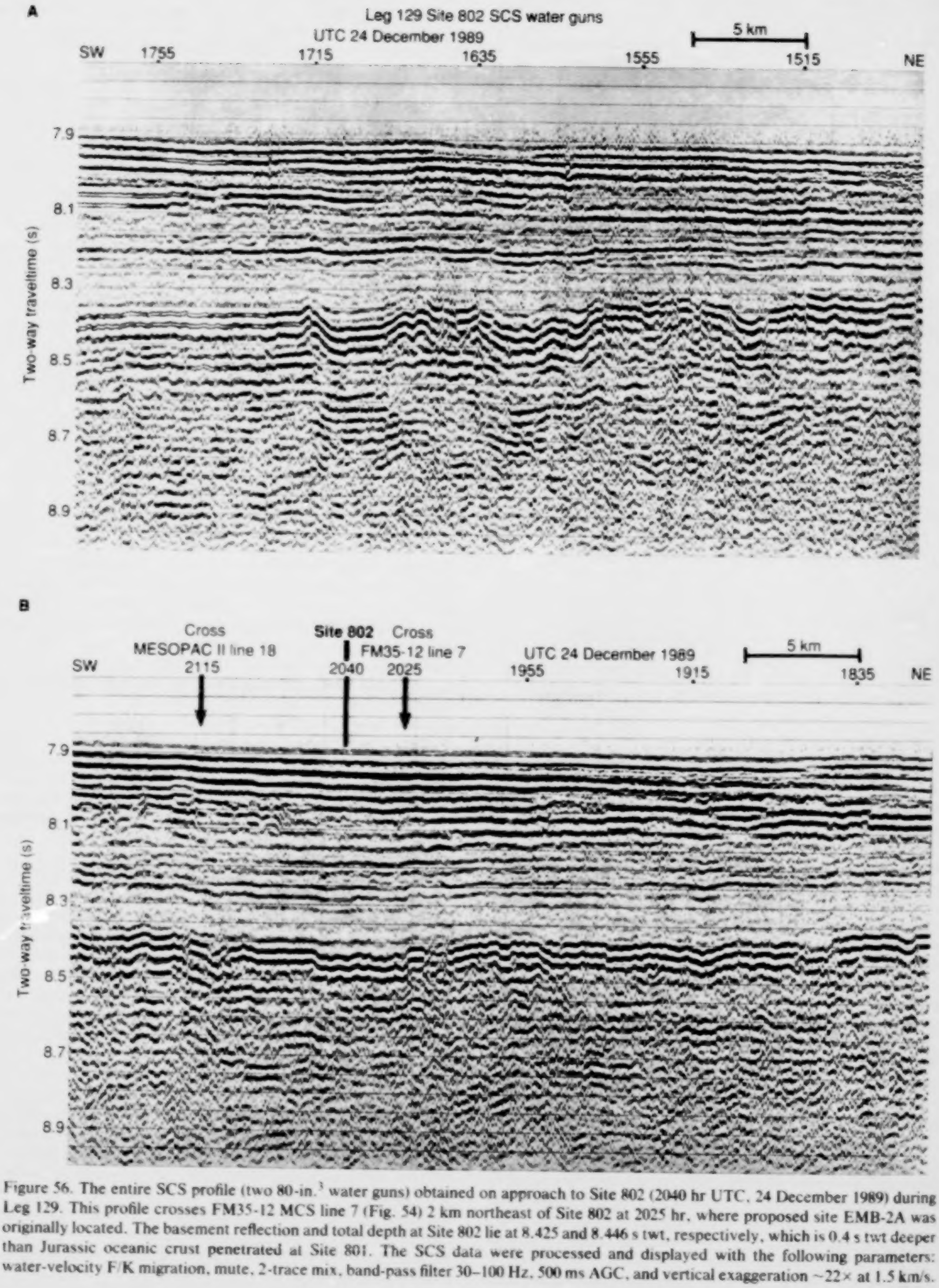

Figure 56. The entire SCS profile (two 80-in.$^3$ water guns) obtained on approach to Site 802 (2040 hr UTC, 24 December 1989) during Leg 129. This profile crosses FM35-12 MCS line 7 (Fig. 54) 2 km northeast of Site 802 at 2025 hr, where proposed site EMB-2A was originally located. The basement reflection and total depth at Site 802 lie at 8.425 and 8.446 s twt, respectively, which is 0.4 s twt deeper than Jurassic oceanic crust penetrated at Site 801. The SCS data were processed and displayed with the following parameters: water-velocity F/K migration, mute, 2-trace mix, band-pass filter 30–100 Hz, 500 ms AGC, and vertical exaggeration ~22× at 1.5 km/s.

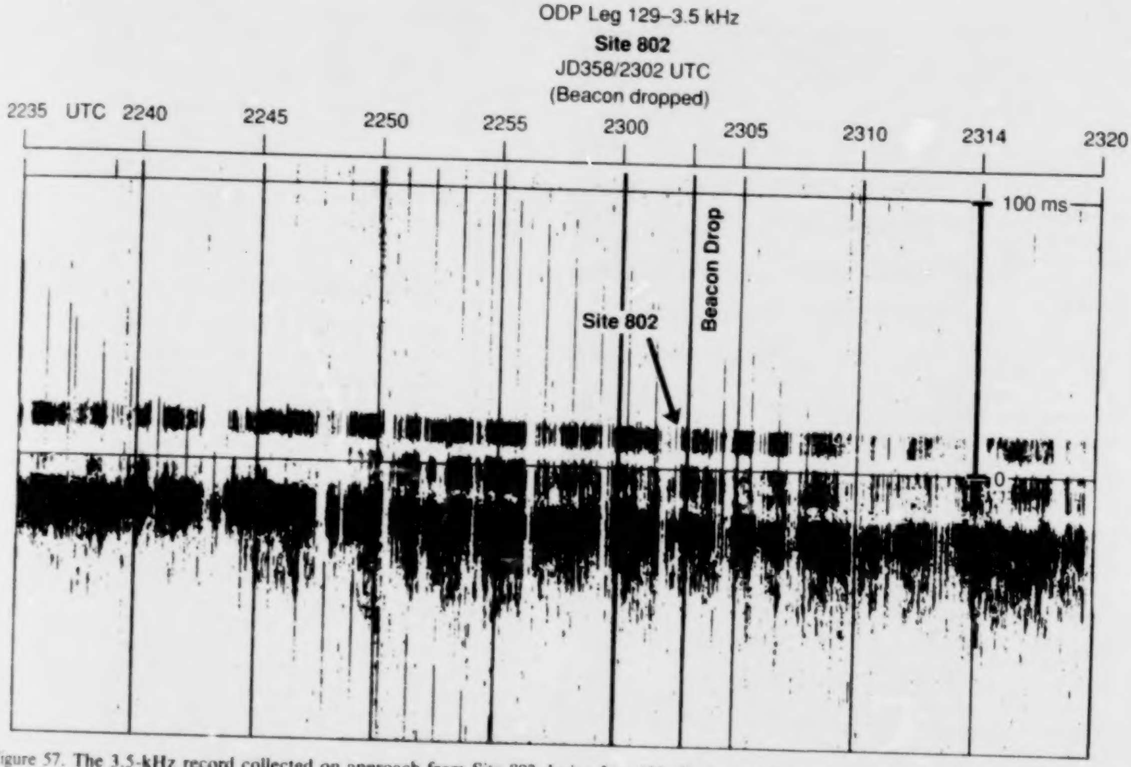

Figure 57. The 3.5-kHz record collected on approach from Site 802 during Leg 129. Horizontal lines represent 100-ms intervals. Acoustic basement on this record marks the top of the first volcaniclastics and indicates 30 ms of pelagic clay. A weak, intermittent reflection is also visible at 13 ms bsf.

interbedded basalt and chert overlying a series of contiguous basalt flow units (see "Igneous Petrology" section, "Site 801" chapter, this volume). The reverberant layer at Site 802, located within the JQZ of the East Mariana Basin appears as a restricted (30-km-wide) window of relatively rough, high-amplitude reflections lying slightly deeper than the surrounding, more typical, flat-lying reverberant horizon. This seismic facies is interpreted to result primarily from a single impedance contrast between the claystone/radiolarite and the top of extrusive basalt at 509 mbsf.

Sonobuoy solutions show velocities and velocity gradients characteristic of "normal" oceanic crust beginning from 300 to 490 ms bsf, which correlates to the reverberant layer imaged at 520 to 540 ms over Site 802. The relatively high relief horizon penetrated by Hole 802A appears to be the top of oceanic crust. This interpretation is questionable, however, because the basement age is at least 50 m.y. less than predicted (see "Summary and Conclusions" section, this chapter), while lying at a depth of nearly 6500 mbsf. In the areas where the reverberant horizon becomes flat-lying and shallow and the overlying transparent layer thins, intrusive volcanics are expected to overly extrusive basement (oceanic crust?).

In the East Mariana Basin there is no comparable distinctive change in the seismic character of the reverberant layer from smooth to rough that can also be correlated to a change in magnetic anomaly amplitudes and field strength as observed in the JQZ of the Pigafetta Basin (Handschumacher et al., 1988) (see "Site Geophysics and Seismic Stratigraphy" section, "Site 801" chapter, this volume).

The lower transparent layer at Site 802 (Fig. 58) correlates with the sequence of calcareous claystone and radiolarite between 460 and 509 mbsf (lithologic Units VI through IX), as well as the lower portion of the volcaniclastic turbidites (388 to 460 mbsf within lithologic Unit V). The moderate-amplitude reflections dividing the transparent layer in half at 305 to 395 ms bsf (8.185–8.275 s twt) are believed to correspond to the occurrence of chert within a chalk-dominated sequence overlying a transition zone containing volcaniclastic turbidites, calcareous claystone, and porcellanite (lithologic Units III, IV, and V). Downhole logging results indicate that these moderate-amplitude reflections are created by velocity-density contrasts associated with variations in the extent and concentration of recrystallized silica and/or calcium carbonate (see "Downhole Measurements" section, this chapter). The reflector at approximately 305 ms bsf that marks the top of this unit has been assigned an age of late Paleocene to early Eocene (see "Biostratigraphy" section, this chapter). This distinctive horizon can be traced eastward for over 360 km along the FM35-12 MCS track past a point 40 km south of DSDP Site 199 and directly over DSDP Site 585. This horizon can be correlated to the first cherts of similar age encountered at 285 mbsf at DSDP Site 199 and at 256 mbsf at DSDP Site 585 and is believed to mark the passage of the Pacific plate beneath the equatorial zone of high productivity (Lancelot and Larson, 1975; see "Paleomagnetism" section, this chapter).

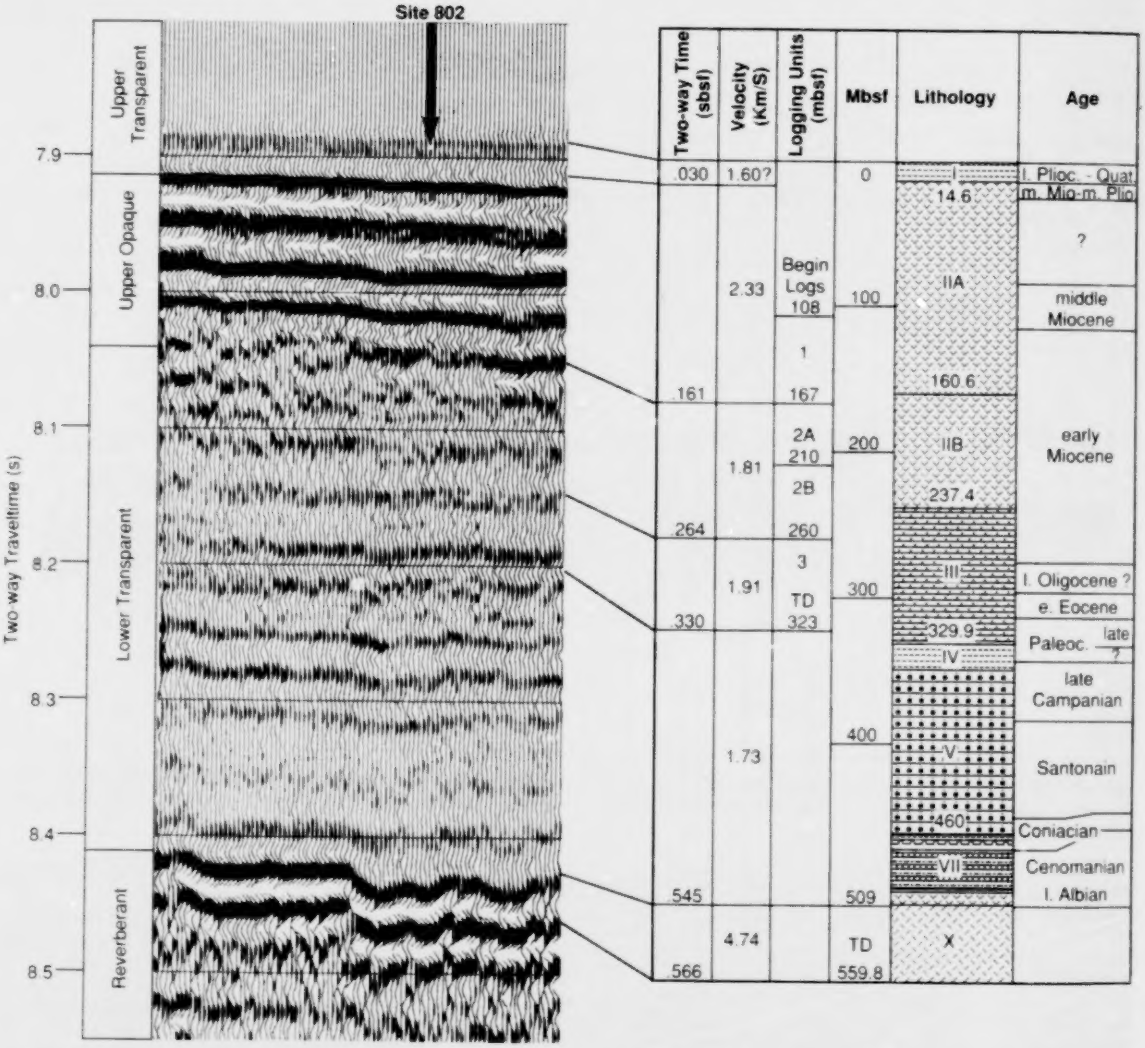

Figure 58. Summary of seismic stratigraphy at Site 802 showing correlations with logging units, lithologic units, ages, and depths. These correlations should be considered only as best estimates until further constraints are provided by improved synthetic seismograms. The velocity of volcanic basement (Unit X) is based on traveltime modeling of sonobuoy data. The 1.6-km/s(?) velocity given for the pelagic clay interval assumes 24 m thickness over .03 s twt, which is 10 m more than indicated from the drill-string mud line (see text and Fig. 56 in "Site Geophysics and Seismic Stratigraphy" section, "Site 801" chapter, this volume). The 2.33-km/s velocity corresponds to the interval from 14.6 to 167 mbsf. This SCS water-gun record is displayed with a vertical exaggeration of 33× at 1.5 km/s and with the same parameters given for Figure 56.

The relatively transparent interval above the first chert at 8.185 s twt and below the onset of high-amplitude reflections at 8.041 s twt corresponds to lithologic Unit IIB and the upper portion of Unit III between approximately 167 to 300 mbsf. This interval is characterized by lower and less variable compressional-wave velocities relative to Unit IIA (see "Physical Properties" and "Downhole Measurements" sections, this chapter). In this interval, moderate- to low-amplitude reflections are the result of small velocity-density contrasts within relatively uniform, fine-grained claystone/siltstone, with few interbedded, well-cemented, coarser-grained volcaniclastic sandstone intervals (see "Lithostratigraphy and Sedimentology" and "Downhole Measurements" sections, this chapter).

The upper opaque zone corresponds to lithologic Unit IIA and extends essentially from 30 to approximately 161 ms bsf. This interval is characterized by high and highly variable compressional-wave velocities relative to the transparent layer below (see "Physical Properties" and "Downhole Measurements" sections, this chapter). The high-amplitude, continuous reflections that characterize this interval are interpreted to arise from impedance contrasts between alternating zones of variably cemented, coarse-grained volcanic sandstone, fine-grained volcanic siltstone/claystone, and pelagic clay. The topmost 30 ms correspond to the pelagic brown clay of lithologic Unit I. The thickness of this interval derived from the drill string length is 14.6 m. We believe that, as at Site 801, this layer is actually 5 to 10 m thicker (see Fig. 56, "Site 801" chapter, this volume). These correlations are based on preliminary, log-generated synthetic seismograms (108–323 mbsf), and are consistent with the trends in velocities given by physical properties measurements. The two-way traveltime and depth to the seafloor reflector, the reflections at approximately 0.330 s bsf that can be correlated to DSDP Site 199, and the volcanic basement reflector also provided a framework for correlations. The seismic stratigraphic correlations, summarized in Figure 58, should be considered only as best estimates until further constraints are provided by a improved synthetic seismogram.

## SUMMARY AND CONCLUSIONS

### Introduction (Nauru Basin Revisited?)

Although Site 801 provided the most immediately spectacular result of Leg 129 in the form of Jurassic sediments and oceanic crust, Site 802 provided the greatest justification for future exploration work in the deep western Pacific, as it poses more basic questions than it answers. Because this site was chosen as a typical deep-water site in the East Mariana Basin, these questions apply to the geology and geophysics of an area that encompasses at least this deep basin and, as we shall see, extends considerably beyond its margins for adequate explanations of certain problems.

Site 802 was positioned at the southeastern edge of a set of low-amplitude magnetic lineations that are not positively identified at Site 802. However, M22 to M31 have been identified to the northwest as part of this same lineation sequence, and the simplest explanation is that the lineations near Site 802 are an older continuation of this sequence, probably extending to about M35. The site is located in the middle of the East Mariana Basin, more than 300 km from any known seamounts, guyots, island chains, or plateaus, and beneath nearly 6000 m of water. This was done in order to minimize the possibility that the site would be "contaminated" with volcaniclastic or carbonate turbidites in the sedimentary section, and/or with off-ridge volcanism in the igneous section. These precautions failed on both counts, and yielded instead what will eventually prove to be the most intriguing results recovered on Leg 129.

### Acoustic Basement: "The Real Thing" or a "Pepsi Generation" Volcanic Event?

Igneous volcanic rocks were recovered from Hole 802A below 509 mbsf to the bottom of the hole at 560 mbsf. These equate to total depths of 6478 to 6529 mbsl. Multiple cooling units were identified that consist mainly of thin sequences of pillow basalts. They are olivine basalts with aphyric to microphyric textures that are remarkably fresh. They have about 10% matrix alteration, which is consistent with low-grade alteration under mildly alkaline, *reducing* conditions. Based on their crystal textures and pillow basalt structures, there is almost no doubt that they cooled under extrusive, submarine conditions.

This conclusion is consistent with the interpretation of the seismic reflection data that show a "rough" acoustic basement surface interpreted as extrusive basement, in contrast to adjacent areas that have a "smooth" or "flat" surface interpreted as intrusive sills. The rough basement at Site 802 is not as obviously a case of buried abyssal hills, as were found at Site 801. It is better described as "rolling" than "hyperbolic echoing" and its lineation, parallel to the magnetic anomaly lineations, is suppressed. Nevertheless, our prediction that it is an extrusive, igneous, volcanic surface proved to be correct.

The only problem with equating these extrusive basalts with original basement formed by seafloor spreading at a Mesozoic ridge crest is the age of the oldest sediments. They are dated by both nannofossils and dinoflagellates to range from Albian to late Aptian in age, whereas the magnetic anomalies, supported by the depth to basement, predict an Oxfordian/Callovian age. Thus, the oldest sediments are *at least* 50 m.y. younger than the age suggested by the magnetic anomalies/basement depth. Either the magnetic anomaly identifications are incorrect, and the basement is anomalously deep, or the basalts represent an off-ridge volcanic event that extruded igneous volcanic rocks over Jurassic-aged crust and possibly sediments that were already 50 m.y. old at the time. Because these rocks are extrusive, and there is no adjacent volcanic edifice to act as a point source, it is more difficult to be convinced that these basalts represent off-ridge volcanism than was the case for the dolerites recovered at Site 800. However, Site 802 is reminiscent of DSDP Site 462 in the Nauru Basin located about 1200 km to the southeast on magnetic anomaly M26 of Oxfordian age (160 m.y.). At DSDP 462, Cenomanian/Upper Albian sediments overlie a sequence of basalts that consist of 200 m of intrusive sills at the top, underlain by at least 450 m of extrusive flows. The upper sills have been radiometrically dated at 110 m.y., and the lower flows at 130 m.y., both ages being intermediate between the overlying sediments and the magnetic anomaly sequence.

Because the magnetic anomalies are well preserved at DSDP Site 462, it is difficult to argue that any of these basalts represent the original basement of the Nauru Basin. Put another way, the results from DSDP Site 462 and ODP Site 802 suggest that Jurassic magnetic anomalies are a necessary but insufficient condition for the recovery of Jurassic basement rocks just below the base of their sediment sections. It is likely that the basalts of Site 802 also resulted from an off-ridge volcanic eruption in the Cretaceous. Radiometric dating of this material and its geochemistry will lend considerable insight on this problem. Of special interest will be their rare earth element chemistry that may demonstrate a clear relationship, or lack thereof, with the basalts of Sites 800 and 462.

### Cretaceous and Tertiary Volcanic Events

The majority of the sediment section is dominated by tuffs and volcaniclastic turbidites of Miocene and Late Cretaceous age. In addition, volcaniclastic turbidites occur in the thin, basal sedimentary sequence of late Aptian to Albian age. These latter turbidites are notable because they contain the only dinoflagellates recovered on Leg 129. The dinoflagellates are associated with wood fragments and spores that indicate a warm, humid climate at their source. As with the much thicker, Upper Cretaceous volcaniclastics, this source is unknown.

The lower portion of the sediment section is dominated by 110 m of volcaniclastic turbidites ranging in age from Coniacian to Late Campanian. Much of the sequence is coarse-grained, indicating debris flows from a relatively proximal source. No edifices are known to exist within 300 km of Site 802. The most likely sources of known or probable Late Cretaceous age are the seamounts and guyot platforms that fringe the East Mariana Basin on its north and east sides. However, the mystery is heightened because the Upper Cretaceous volcaniclastics do not thicken to the east at DSDP Sites 199 and 585, which is the most likely source direction. Instead, the dominant volcaniclastics found there are of Albian to Aptian age.

The upper portion of the sediment section is dominated by 146 m of tuff, regarded as volcaniclastic turbidites or redeposited hyaloclastites. They range in age from early to middle Miocene, with a small amount of Pliocene material at the top of the sequence. They are notably well-lithified, coal-black sedimentary rocks. Pelagic clay and calcareous claystone are included in the lower and upper parts, respectively. They are most likely derived from the Caroline Islands and their associated volcanic platform 350 km south of Site 802.

In summary, the majority of the sediment section at Site 802 is dominated by unexpected thicknesses of turbidite deposits. Most of this material appears either to have been derived from proximal sources that are unknown on the most recent bathymetric charts of the area, or to have been transported over several hundred kilometers by exceptionally high-energy turbidity currents.

## Paleolatitudes Recorded at Site 802

Paleolatitude information to be gained from Site 802 is more limited than at our two previous sites because the hole terminated in younger (Aptian) material. In addition, most of the "background sedimentation" is limited to brown pelagic clays, whereas the main sedimentary component is turbiditic material of dubious value for biogenic accumulation studies.

Remanent magnetic inclination values for the sedimentary section yield a reasonable story. Low northern paleolatitudes are recorded down to Campanian/upper Paleocene sediments, and appear to coincide with the equator crossing of Site 802. Remanent inclination values then increase, indicating higher southern paleolatitudes, leveling off at about 10°S latitude for Santonian to Cenomanian time. These results are consistent with previous models for Pacific plate motion for the last 100 m.y. Because drilling at this site terminated in middle Cretaceous material, the results do not add a large body of new information to this subject.

## REFERENCES

Abrams, L. J., Larson, R. L., Shipley, T., and Lancelot, Y., 1988. Cretaceous volcanic sequences and Jurassic(?) crust in the western Pacific. *Trans. Am. Geophys. Union*, 69:1442.

Bolli, H. M., and Saunders, J. B., 1985. Oligocene to Holocene low latitude planktonic foraminifera. *In* Bolli, H. M., Saunders, J. B., and Perch-Nielsen, K. (Eds.), *Plankton Stratigraphy:* Cambridge (Cambridge Univ. Press), 155–262.

Bryan, W. B., 1972. Morphology of quench crystals in submarine basalts. *J. Geophys. Res.*, 77:5281–5289.

Carlson, R. L., Schaftenaar, C. H., and Moore, R. P., 1979. Causes of compressional-wave anisotropy in calcareous sediments from the Rio Grand Rise. *In* Barker, P. F., Carlson, R. L., et al., *Init. Repts. DSDP*, 72: Washington (U.S. Govt. Printing Office), 565–576.

Caron, M., 1985. Cretaceous planktonic foraminifera. *In* Bolli, H. M., Saunders, J. B., and Perch-Nielsen, K. (Eds.), *Plankton Stratigraphy:* Cambridge (Cambridge Univ. Press), 17–86.

Christensen, N. L., and Lewis, B.T.R., 1983. Physical properties of Leg 65 basalts. *In* Lewis, B.T.R., Robinson, P., et al., *Init. Repts. DSDP*, 65: Washington (U.S. Govt. Printing Office), 693–696.

Christensen, N. L., and Salisbury, M. H., 1975. Structure and constitution of the lower oceanic crust. *Rev. Geophys. Space Phys.*, 13:57–86.

Clark, S. P. (Ed.), 1966. *Handbook of Physical Constants*. Mem. Geol. Soc. Am., 97:1–587.

Ewing, J., Ewing, M., Aitken, T., and Ludwig, W. J., 1968. North Pacific sediment layers measured by seismic profiling. *In* Drake, C. L., and Hart, P. J. (Eds.), *The Crust and Upper Mantle of the Pacific Area*. Am. Geophys. Union. Monogr., 12:147–173.

Gradstein, F. M., and Sheridan, R. E., 1983. On the Jurassic Atlantic Ocean and a synthesis of results of DSDP Leg 76. *In* Sheridan, R. E., Gradstein, F. M., et al., *Init. Repts. DSDP*, 76: Washington (U.S. Govt. Printing Office), 913–943.

Handschumacher, D. W., and Gettrust, J. F., 1985. Mixed polarity model for the Jurassic "Quiet Zones": new oceanic evidence of frequent pre-M25 reversals. *Eos*, 66:867.

Handschumacher, D. W., Sager, W. W., Hilde, T.W.C., and Bracey, D. R., 1988. Pre Cretaceous tectonic evolution of the Pacific Plate and extension of the geomagnetic polarity reversal time scale with implications for the origin of the Jurassic "Quiet Zone." *Tectonophysics*, 155:365–380.

Harland, W. B., Cox, A. V., Llewellyn, P. G., Pickton, C.A.G., Smith, D. G., and Walters, R., 1982. *A Geologic Time Scale:* Cambridge (Cambridge Univ. Press).

Heezen, B. C., MacGregor, I. D., et al., 1973. *Init. Repts. DSDP*, 20: Washington (U.S. Govt. Printing Office).

________, 1973. Mesozoic chalks beneath the Caroline abyssal plain: DSDP Site 199. *In* Heezen, B. C., MacGregor, I. D., et al., *Init. Repts. DSDP*, 20: Washington (U.S. Govt. Printing Office), 65–85.

Helsley, C. E., and Steiner, M. D., 1969. Evidence for long intervals of normal polarity during the Cretaceous period. *Earth Planet. Sci. Lett.*, 5:325–332.

Houtz, R. E., Ewing, J., and Buhl, P., 1970. Seismic data from sonobuoy stations in the northern and equatorial Pacific. *J. Geophys. Res.*, 75:5093–5111.

Houtz, R. E., and Ludwig, W. J., 1979. Distribution of reverberant subbottom layers in the southwest Pacific Basin. *J. Geophys. Res.*, 84:3497–3504.

Humphris, S. E., Thompson, R. N., and Marriner, G. F., 1979. The mineralogy and geochemistry of basalt weathering, Holes 417A and 418A. *In* Donnelly, T., Francheteau, J., Bryan, W., Robinson, P., Flower, M., Salisbury, M., et al., *Init. Repts. DSDP*, 51, 52, 53: Washington (U.S. Govt. Printing Office), 1201–1217.

Hutchinson, D. R., and Detrick, R. S., 1984. Water gun vs. air gun: a comparison. *Mar. Geophys. Res.*, 6:295–310.

Irving, E., and Pullaiah, G., 1976. Reversal of the geomagnetic field, magnetostratigraphy and relative magnitude of palaeosecular variation in the Phanerozoic. *Earth-Sci. Rev.*, 12:35–64.

Karpoff, A. M., 1989. Les faciès pélagiques condensés cénozoiques des océans Pacifique et Atlantique: témoins des grandes crises géodynamiques [Thèse Doc. ès Sci.]. Univ. Louis Pasteur, Strasbourg.

Keene, J. B., 1975. Cherts and porcellanites from the North Pacific DSDP, Leg 32. *In* Larson, R. L., Moberly, R., et al. *Init. Repts. DSDP*, 32: Washington (U.S. Govt. Printing Office), 429–507.

Kent, D. V., and Gradstein, F. M., 1985. A Cretaceous and Jurassic geochronology. *Geol. Soc. Am. Bull.*, 96:1419–1427.

________, 1986. A Jurassic to Recent chronology. *In* Tucholke, B. E., and Vogt, P. R. (Eds.), *The Geology of North America: The Western Atlantic Region*. Geol. Soc. Am. DNAG Ser., 1:45–50.

Kono, M., 1980. Statistics of paleomagnetic inclination data. *J. Geophys. Res.*, 85:3878–3882.

Lancelot, Y., 1978. Evolution sedimentaire et tectonique de la plaque Pacifique. *Mem. Soc. Geol. France*, Nelle Ser., 134.

Lancelot, Y., and Larson, R. L., 1975. Sedimentary and tectonic evolution of the northwestern Pacific. *In* Larson, R. L., Moberly, R., et al., *Init. Repts. DSDP*, 32: Washington (U.S. Govt. Printing Office), 945–957.

Larson, R. L., and Hilde, T.W.C., 1975. A revised time scale of magnetic reversals for the Early Cretaceous and Late Jurassic. *J. Geophys. Res.*, 80:2586–2594.

Larson, R. L., and Lowrie, W., 1975. Paleomagnetic evidence for motion of the Pacific plate from Leg 32 basalts and magnetic anomalies. *In* Larson, R. L., and Moberly, R., et al., *Init. Repts. DSDP*, 32: Washington (U.S. Govt. Printing Office), 571–577.

Larson, R. L., Schlanger, S. O., et al., 1981. *Init. Repts. DSDP*, 61: Washington (U.S. Govt. Printing Office).

Martini, E., 1971. Standard Tertiary and Quaternary calcareous nannoplankton zonation. *In* Farinacci, A. (Ed.), *Proc. 2nd Planktonic Conf. Roma:* Rome (Ed. Technosci.), 2:739–785.

Marty, J. C., and Cazenave, A., 1989. Regional variations in subsidence rate of oceanic plates: a global analysis. *Earth Planet. Sci. Lett.*, 94:301–315.

Moberly, R., Schlanger, S. O., et al., 1986. *Init. Repts. DSDP*, 89: Washington (US Govt. Printing Office).

________, 1986. Site 585. *In* Moberly, R., Schlanger, S. O., et al., *Init. Repts. DSDP*, 89: Washington (U.S. Govt. Printing Office): 29–99.

Natland, J. H., 1980. Crystal morphologies in basalts dredged and drilled from the East Pacific Rise near 9°N and the Sequeiros fracture zone. *In* Rosendahl, B. R., Hekinian, R., et al., *Init. Repts. DSDP*, 54: Washington (U.S. Govt. Printing Office), 605–634.

Okada, H., and Bukry, D., 1980. Supplementary modification and introduction of code numbers to the low-latitude coccolith biostratigraphic zonation (Bukry, 1973; 1975). *Mar. Micropaleontol.*, 5:321–325.

Palmer, A. R., 1983. The decade of North American geology, 1983 geological time scale. *Geology*, 11:503–504.

Parsons, B. and Sclater, J. G., 1977. An analysis of the variation of ocean floor bathymetry and heat flow with age. *J. Geophys. Res.*, 82:803–827.

Perch-Nielsen, K., 1985a. Cenozoic calcareous nannofossils. *In* Bolli, H. M., Saunders, J. B., and Perch-Nielsen, K. (Eds.), *Plankton Stratigraphy:* Cambridge (Cambridge Univ. Press), 427–554.

________, 1985b. Mesozoic calcareous nannofossils. *In* Bolli, H., Saunders, J. B., and Perch-Nielsen, K. (Eds.), *Plankton Stratigraphy:* Cambridge (Cambridge Univ. Press), 329–426.

Robinson, P. R., Flower, M.F.J., Schmincke, H.-U., and Ohnmacht, W., 1977. Low temperature alteration of oceanic basalts, DSDP Leg 37. *In* Aumento, F., Melson, W. G., et al., *Init. Repts. DSDP*, 37: Washington (U.S. Govt. Printing Office), 775–793.

Sager, W. W., and Pringle, M. S., 1989. Mid-Cretaceous to Early Tertiary apparent polar wander path of the Pacific Plate. *J. Geophys. Res.*, 93:11753–11771.

Shipboard Scientific Party, 1981. Site 462: Nauru Basin, Western Pacific Ocean, DSDP Leg 61. *In* Larson, R. L., Schlanger, S. O., et al., *Init. Repts. DSDP*, 61: Washington (U.S. Govt. Printing Office), 19–395.

Shipboard Scientific Party, 1990. Site 793. *In* Taylor, B., Fujioka, K., et al., *Proc. ODP, Init. Repts.*, 126: College Station, TX (Ocean Drilling Program).

Shipley, T. H., Whitman, J. M., Dunnebier, F. K., and Peterson, L. D., 1983. Seismic stratigraphy and sedimentation history of the East Mariana Basin, Western Pacific. *Earth Planet. Sci. Lett.*, 64:257–275.

Sissingh, W., 1977. Biostratigraphy of Cretaceous calcareous nannoplankton. *Geol. Mijnbouw*, 56:37–65.

Tamaki, K., Nakanishi, M., Sayanagi, K., and Kobayashi, K., 1987. Jurassic magnetic lineations of the western Pacific Ocean and the origin of the Pacific plate. *Eos*, 68:1493.

Toumarkine, M., and Luterbacher, H., 1985. Paleocene and Eocene planktic foraminifera. *In* Bolli, H. M., Saunders, J. B., and Perch-Nielsen, K. (Eds.), *Plankton Stratigraphy:* Cambridge (Cambridge Univ. Press), 87–154.

Tucholke, B. E., and Vogt, P. R., 1979. Western North Atlantic: sedimentation evolution and aspects of tectonic history. *In* Tucholke, B. E., Vogt, P. R., et al., *Init. Repts. DSDP*, 43: Washington (U.S. Govt. Printing Office), 791–825.

Winterer, E. L., Riedel, W. R., et al., 1971. *Init. Repts. DSDP*, 7: Washington (U.S. Govt. Printing Office).

Zotto, M., Drugg, W. S., and Habib, D., 1987. Kimmeridgian dinoflagellate stratigraphy in the Southwestern North Atlantic. *Micropaleontology*, 33:193–213.

**Ms 129A-104**

**NOTE: All core description forms ("barrel sheets") and core photographs have been printed on coated paper and bound as Section 3, near the back of the book, beginning on page 247.**

## Hole 802A: Resistivity-Sonic-Gamma Ray Log Summary

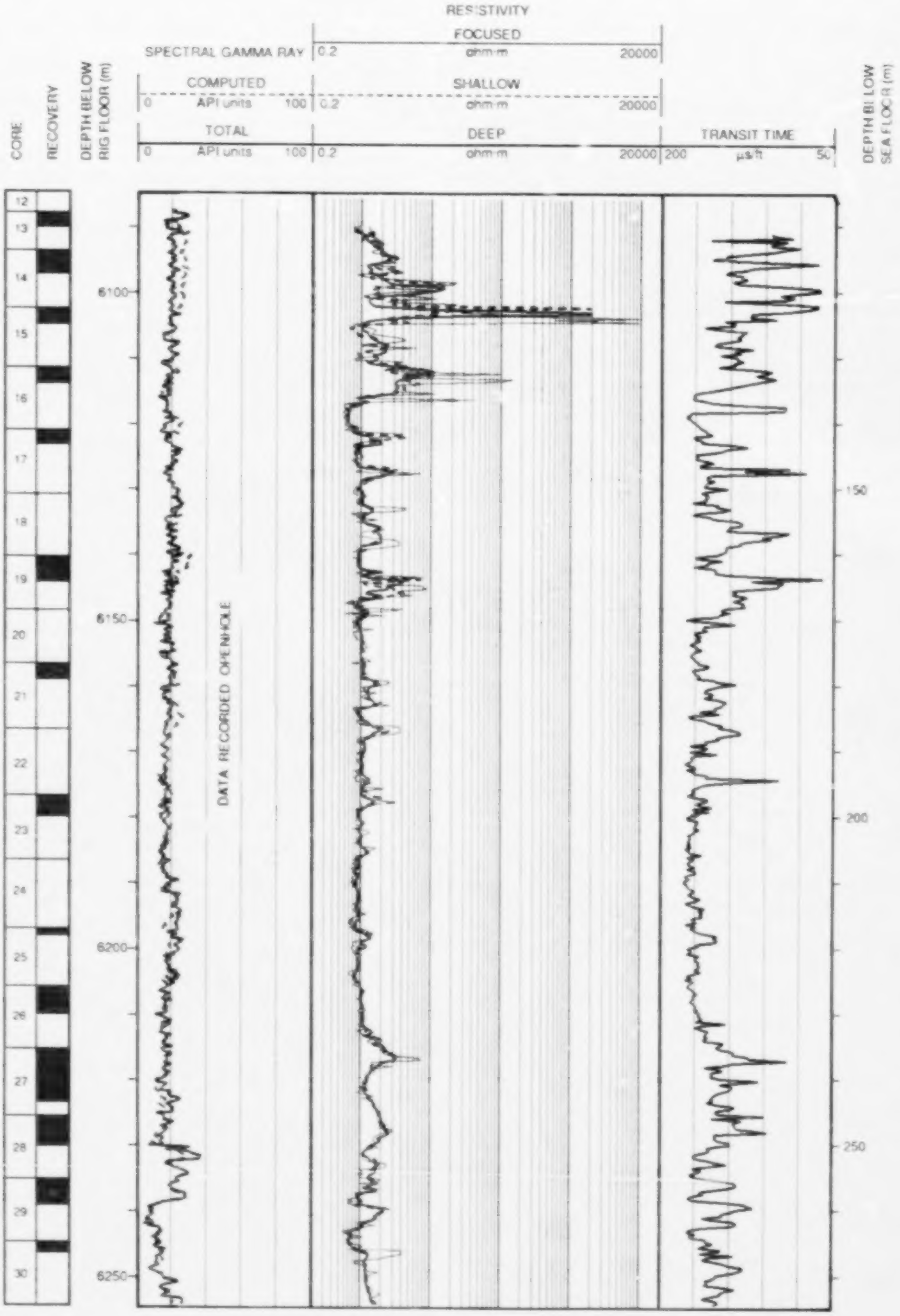

Hole 802A: Resistivity-Sonic-Gamma Ray Log Summary (continued)

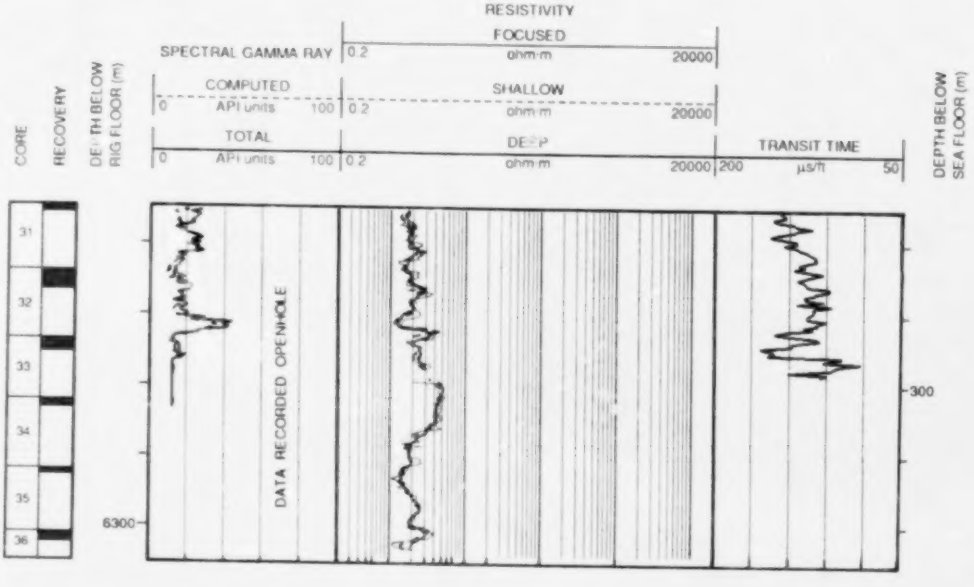

## Hole 802A: Density-Caliper-Gamma Ray Log Summary

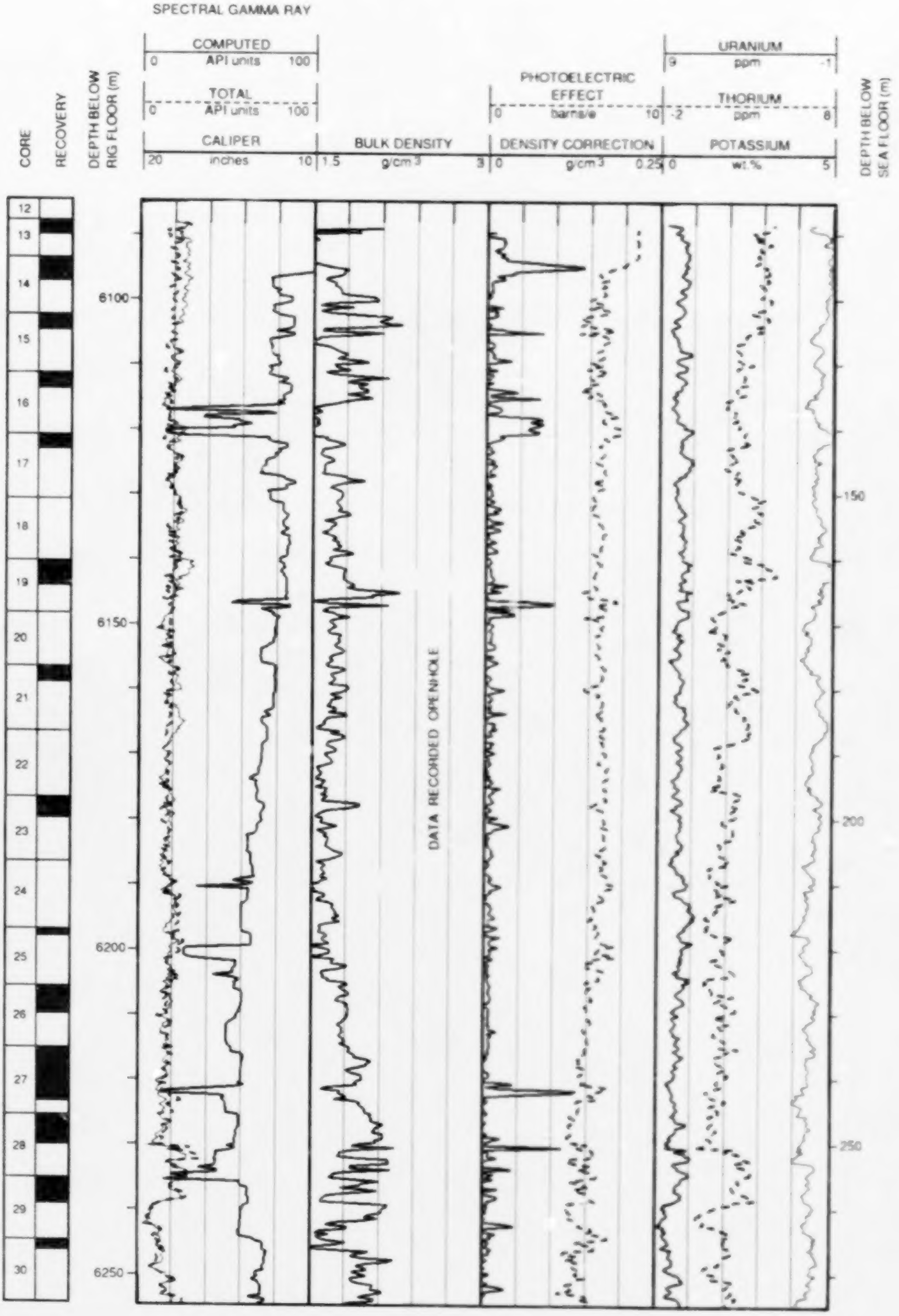

Hole 802A: Density-Caliper-Gamma Ray Log Summary (continued)

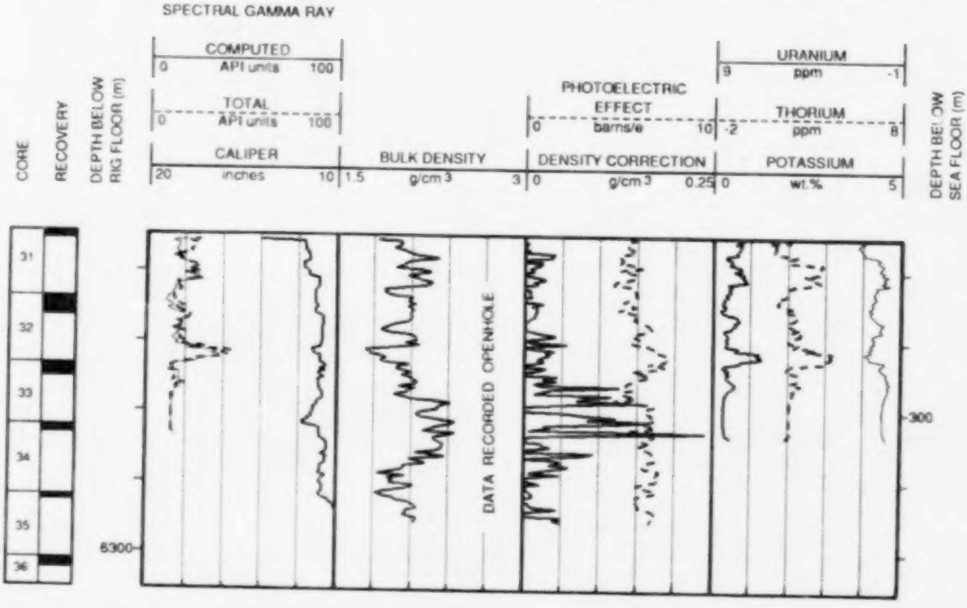

## Hole 802A: Geochemical Log Summary

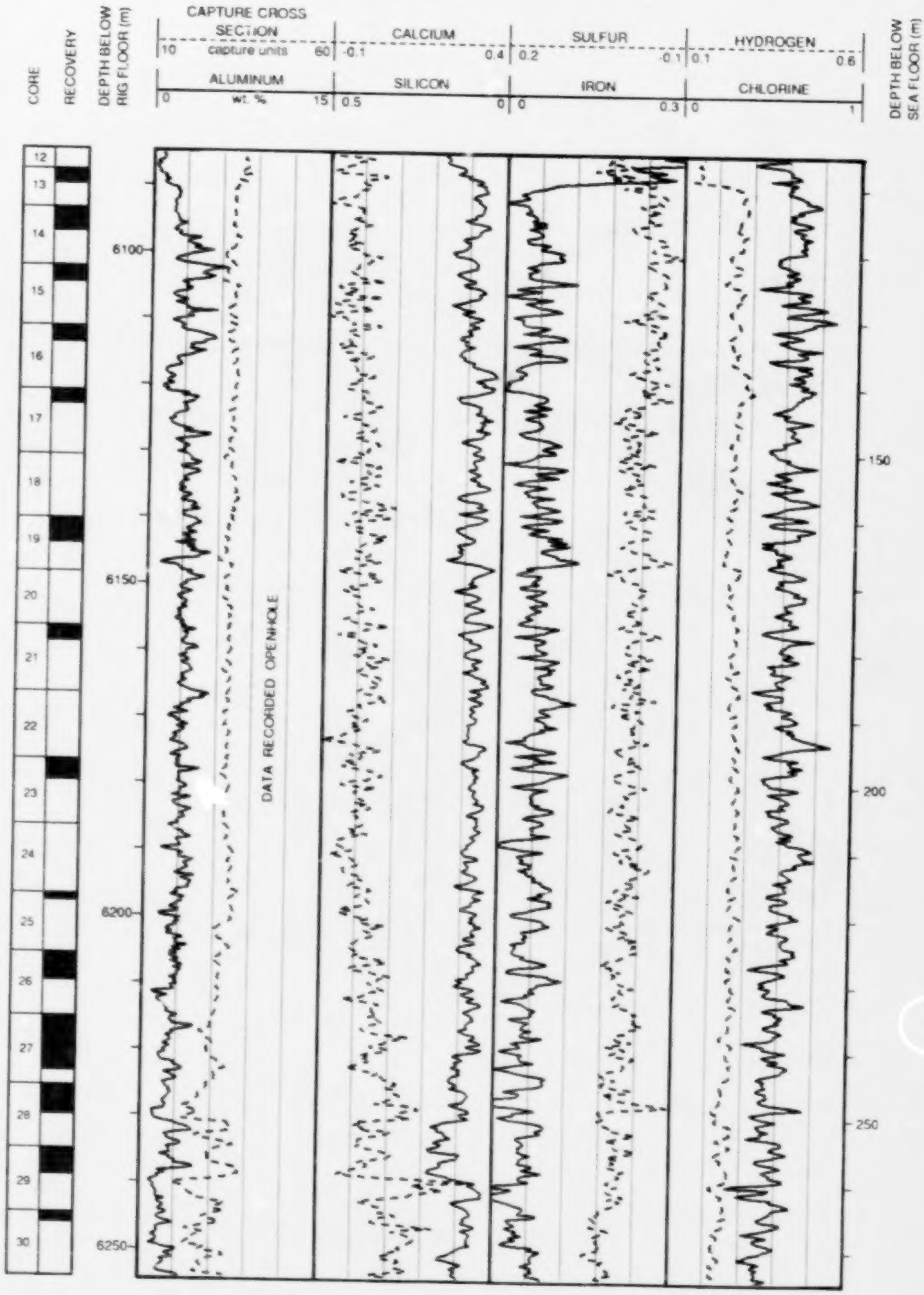

## Hole 802A: Geochemical Log Summary (continued)

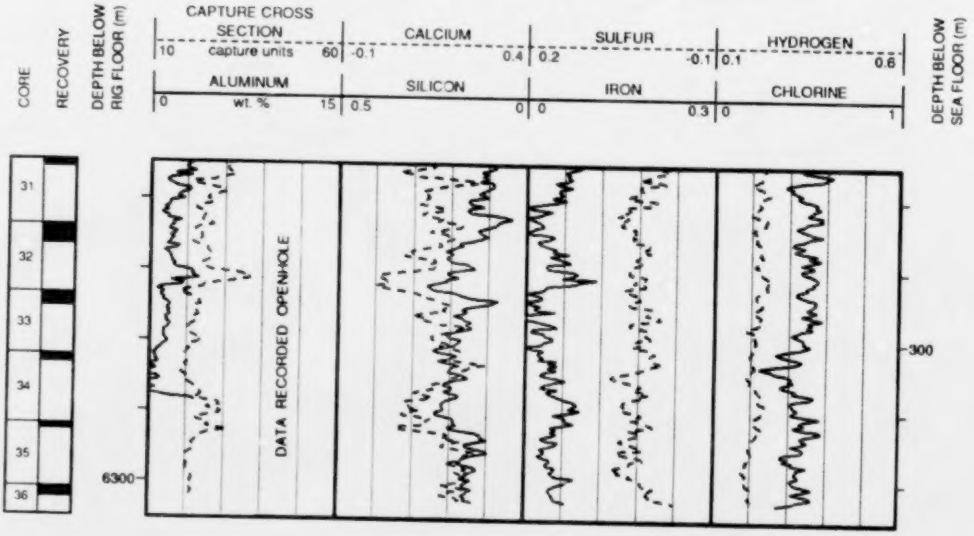

# SECTION 3: CORES

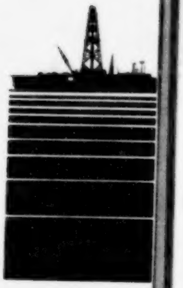

SITE 800 HOLE A CORE 1R CORED INTERVAL 5686.0-5687.0 mbsl; 0.0-1.0 mbsf

| TIME-ROCK UNIT | BIOSTRAT. ZONE/ FOSSIL CHARACTER | | | | | PALEOMAGNETICS | PHYS. PROPERTIES | CHEMISTRY | SECTION | METERS | GRAPHIC LITHOLOGY | DRILLING DISTURB. | SED. STRUCTURES | SAMPLES | LITHOLOGIC DESCRIPTION |
|---|---|---|---|---|---|---|---|---|---|---|---|---|---|---|---|
| | FORAMINIFERS | NANNOFOSSILS | RADIOLARIANS | DIATOMS | PALYNOMORPHS | | | | | | | | | | |
| | B | B | B | | B | | | | 1 | | | ~ | | ●<br>● | PELAGIC CLAY |

Major lithology: PELAGIC CLAY, soft, fine-grained, homogeneous. The color is dark reddish brown (5YR 3/2). Sediment is highly disturbed, even soupy. Clay contains micronodules of metal oxides. XRD from Section 1, 4 cm indicates illite, kaolinite and smectite clays. XRD from Section 1, 69 cm contains phillipsite, smectite and goethite.

SLIDE SUMMARY (%):

| | 1, 10<br>D | CC<br>D |
|---|---|---|
| TEXTURE | | |
| Sand | 1 | 5 |
| Silt | 20 | 30 |
| Clay | 79 | 65 |
| COMPOSITION | | |
| Clay | 35 | 30 |
| Micronodule | 5 | 10 |
| Oxide | 30 | 35 |
| Quartz | 20 | 25 |
| Zeolite | 05 | Tr |

SITE 800 HOLE A CORE 2R CORED INTERVAL 5687.0-5696.6 mbsl; 1.0-10.6 mbsf

| TIME-ROCK UNIT | BIOSTRAT. ZONE/ FOSSIL CHARACTER | | | | | PALEOMAGNETICS | PHYS. PROPERTIES | CHEMISTRY | SECTION | METERS | GRAPHIC LITHOLOGY | DRILLING DISTURB. | SED. STRUCTURES | SAMPLES | LITHOLOGIC DESCRIPTION |
|---|---|---|---|---|---|---|---|---|---|---|---|---|---|---|---|
| | FORAMINIFERS | NANNOFOSSILS | RADIOLARIANS | DIATOMS | PALYNOMORPHS | | | | | | | | | | |
| | B | B | B | | B | | | | CC | | | | | ● | PELAGIC CLAY |

Major lithology: PELAGIC CLAY, soft, fine-grained, homogeneous. Color is dark brown (7.5YR 3/4), due to presence of metal oxides and micronodules.

SLIDE SUMMARY (%):

| | CC<br>D |
|---|---|
| TEXTURE | |
| Sand | Tr |
| Silt | 30 |
| Clay | 70 |
| COMPOSITION | |
| Clay | 35 |
| Micronodule | 10 |
| Oxide | 30 |
| Quartz | 20 |
| Zeolite | 5 |

Information on Core Description Forms, for ALL sites, represents field notes taken aboard ship. Some of this information has been refined in accord with post-cruise findings, but production schedules prohibit definitive correlation of these forms with subsequent findings. Thus, the reader should be alerted to the occasional ambiguity or discrepancy.

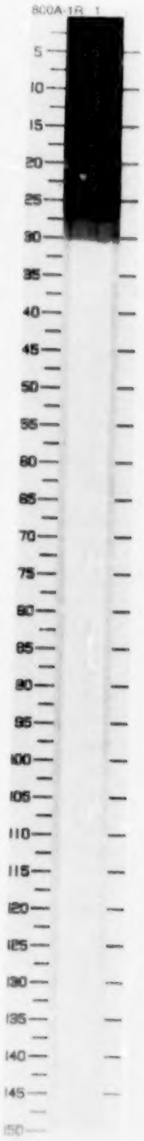

SITE 800 HOLE A CORE 3R CORED INTERVAL 5696.6-5706.2 mbsl; 10.6-20.2 mbsf

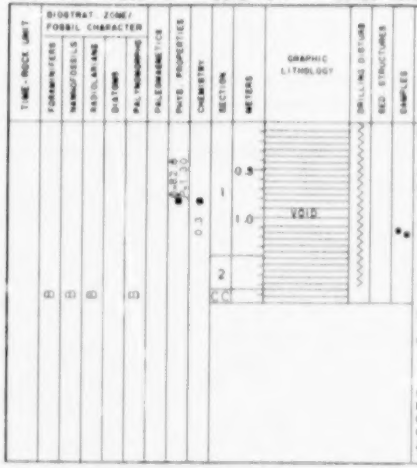
TIME-ROCK UNIT
BIOSTRAT. ZONE/ FOSSIL CHARACTER
FORAMINIFERS
NANNOFOSSILS
RADIOLARIANS
DIATOMS
PALYNOMORPHS
PALEOMAGNETICS
PHYS. PROPERTIES
CHEMISTRY
SECTION
METERS
GRAPHIC LITHOLOGY
DRILLING DISTURB.
SED. STRUCTURES
SAMPLES
B
B
B
B
ø-82.8
γ-1.30
0.3
1
2
CC
0.5
1.0
VOID

LITHOLOGIC DESCRIPTION

PELAGIC CLAY

Major lithology: PELAGIC CLAY, soft, fine-grained, highly disturbed, even soupy, dark reddish brown (5YR 3/2, slight change to 5YR 3/3). Difference between darker and lighter clays is due to variable concentration of iron oxides and metallic micro-nodules. XRD from Section 3, 80 cm contains hematite, smectite, illite and possible barite.

SLIDE SUMMARY (%)

| | 1, 115<br>D | 1, 120<br>D |
|---|---|---|
| TEXTURE | | |
| Sand | Tr | Tr |
| Silt | 20 | 20 |
| Clay | 80 | 80 |
| COMPOSITION | | |
| Clay | 50 | 45 |
| Micronodule | 5 | 5 |
| Oxide | 15 | 30 |
| Quartz | 20 | 15 |
| Zeolite | 10 | 5 |

SITE 800 HOLE A CORE 4R CORED INTERVAL 5706.2-5715.9 mbsl; 20.2-29.9 mbsf

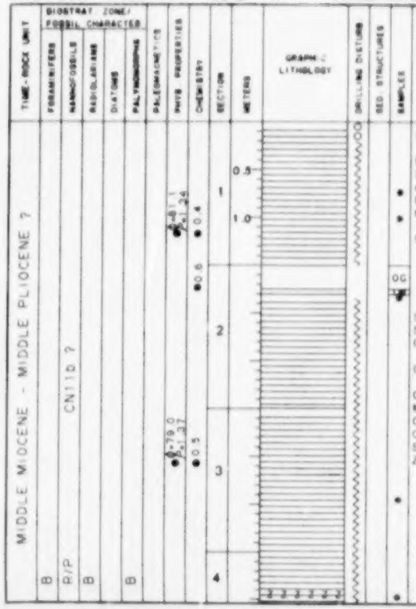
TIME-ROCK UNIT
BIOSTRAT. ZONE/ FOSSIL CHARACTER
FORAMINIFERS
NANNOFOSSILS
RADIOLARIANS
DIATOMS
PALYNOMORPHS
PALEOMAGNETICS
PHYS. PROPERTIES
CHEMISTRY
SECTION
METERS
GRAPHIC LITHOLOGY
DRILLING DISTURB.
SED. STRUCTURES
SAMPLES
MIDDLE MIOCENE - MIDDLE PLIOCENE ?
CN11b ?
B
R/P
B
B
ø-81.1
γ-1.24
ø-79.0
γ-1.37
0.4
0.6
0.5
1
2
3
4
0.5
1.0
OG

LITHOLOGIC DESCRIPTION

PELAGIC CLAY

Major lithology: PELAGIC CLAY, abundant metal oxides, with minor zeolitic component. Stiff, fine grained, very disturbed, sedimentary structures obliterated. Dominant color is very dark brown (10YR 2/2). Yellow (10YR 7/7) to reddish yellow (7.5YR 6/6) spots or wispy layers, especially in Section 1, 70-75 cm and Section 3, 94-115 cm, have a lower concentration of iron oxide aggregates. Radiolarian spines are common.

SLIDE SUMMARY (%)

| | 1, 72<br>M | 1, 100<br>D | 2, 33<br>D | 3, 94<br>M | 4, 48<br>D |
|---|---|---|---|---|---|
| TEXTURE | | | | | |
| Sand | Tr | — | 15 | 5 | Tr |
| Silt | 35 | 20 | 25 | 30 | 15 |
| Clay | 65 | 80 | 60 | 65 | 85 |
| COMPOSITION | | | | | |
| Clay | 43 | 37 | 65 | 55 | 45 |
| Micronodule | 5 | 10 | 2 | 10 | 5 |
| Oxide | 2 | 15 | 10 | 10 | 20 |
| Quartz | 35 | 20 | 15 | 5 | 10 |
| Spines | 10 | 15 | 3 | 15 | 20 |
| Zeolite | 5 | 3 | 5 | Tr | Tr |

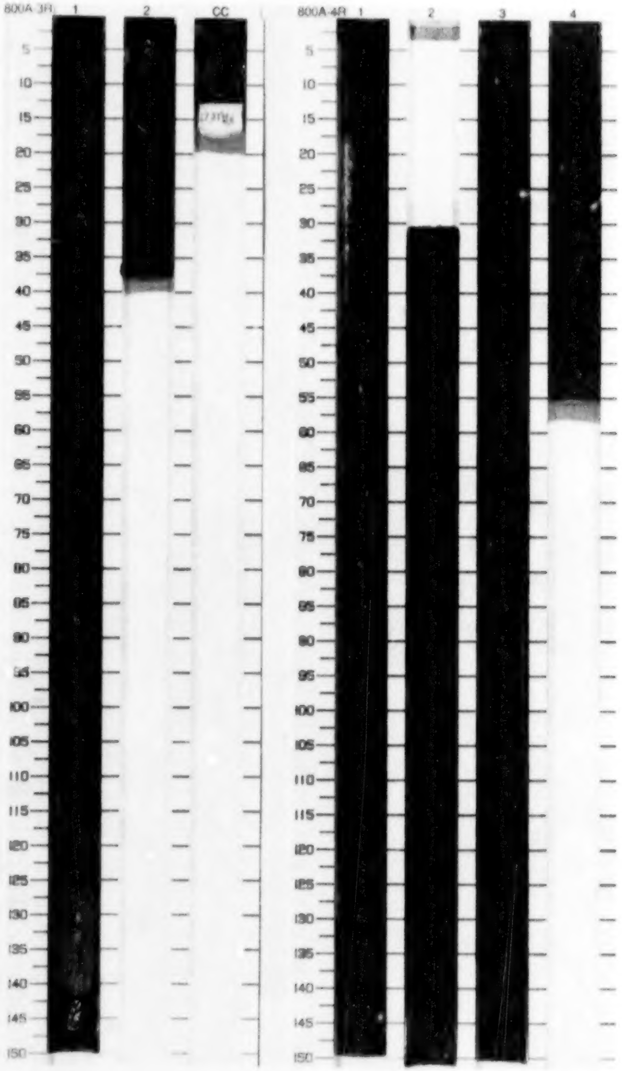
800A-3R
1
2
CC
800A-4R
1
2
3
4
5
10
15
20
25
30
35
40
45
50
55
60
65
70
75
80
85
90
95
100
105
110
115
120
125
130
135
140
145
150

SITE 800 HOLE A CORE 5R CORED INTERVAL 5715.9-5725.6 mbsl; 29.9-39.6 mbsf

| TIME-ROCK UNIT | BIOSTRAT. ZONE/ FOSSIL CHARACTER: FORAMINIFERS | NANNOFOSSILS | RADIOLARIANS | DIATOMS | PALYNOMORPHS | PALEOMAGNETICS | PHYS. PROPERTIES | CHEMISTRY | SECTION | METERS | GRAPHIC LITHOLOGY | DRILLING DISTURB. | SED. STRUCTURES | SAMPLES | LITHOLOGIC DESCRIPTION |
|---|---|---|---|---|---|---|---|---|---|---|---|---|---|---|---|
| CAMPANIAN | C/P | B | C/P *Amphipyndax tylotus* | B | | | | | 1<br>CC | | | | | *<br>*<br>* | PELAGIC CLAY |

Major lithology: PELAGIC CLAY, stiff, fine-grained, mottled with light orange clay, very disturbed, sedimentary structures obliterated. Dominant color is dark yellowish brown (10YR 4/4); lightest color is reddish yellow (7.5YR 7/6); rare streaks of very dark gray (10YR 3/1) metalliferous clay. Clay composition locally quite variable, for example with 15% zeolites in Section 5, 4-5 cm, 1% volcanic glass in Section 5, 16-17 cm, and 20% iron oxides in Section CC, 6-7 cm. In other smear slides from this core, these components may appear only in trace amounts or not at all.

SLIDE SUMMARY (%):

| | 1, 4<br>M | 1, 15<br>D | CC, 6<br>D |
|---|---|---|---|
| TEXTURE: | | | |
| Sand | Tr | — | Tr |
| Silt | 10 | 15 | 10 |
| Clay | 90 | 85 | 90 |
| COMPOSITION: | | | |
| Clay | 80 | 82 | 55 |
| Glass | — | 1 | Tr |
| Micronodule | — | — | 10 |
| Oxide | 2 | 4 | 20 |
| Quartz | 1 | 1 | 5 |
| Spines | 2 | 2 | 8 |
| Zeolite | 15 | 10 | 2 |

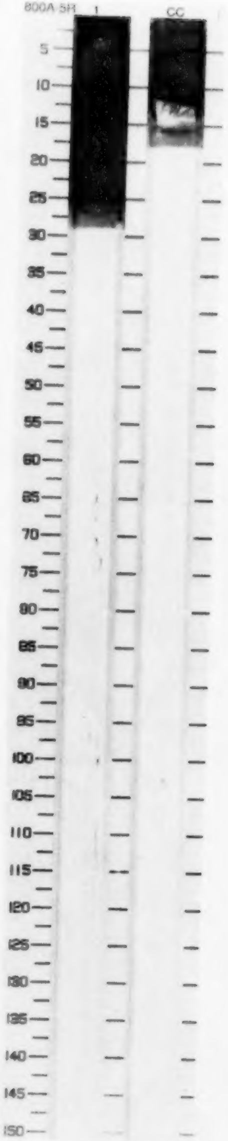

SITE 800 HOLE A CORE 6R CORED INTERVAL 5725.6-5735.2 mbsl; 39.6-49.2 mbsf

| TIME-ROCK UNIT | BIOSTRAT. ZONE/ FOSSIL CHARACTER |  |  |  |  | PALEOMAGNETICS | PHYS. PROPERTIES | CHEMISTRY | SECTION | METERS | GRAPHIC LITHOLOGY | DRILLING DISTURB. | SED. STRUCTURES | SAMPLES |
|---|---|---|---|---|---|---|---|---|---|---|---|---|---|---|
|  | FORAMINIFERS | NANNOFOSSILS | RADIOLARIANS | DIATOMS | DINO-FLAGELLATES |  |  |  |  |  |  |  |  |  |
| CAMPANIAN | B | R/P unzoned | A/P *Amphipyndax tylotus* |  | B | N | ● | ● 0.10 | 1 |  |  | ×<br>×<br>×<br>× |  | ●<br>●<br>● |

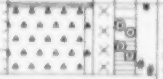

LITHOLOGIC DESCRIPTION

RADIOLARIAN PORCELLANITE with CHERT

Major lithology: RADIOLARIAN PORCELLANITE, silty, laminated on a millimeter scale. Some brown porcellanite is in gradational transition to CHERT. Laminations range in color from very dark brown to brown (10YR 2/2 to 10YR 4/3) and are due to abundance changes in silica filled radiolarians. Porcellanite contains up to 10% clay.

Minor lithologies:
a. Light brown (7.4YR 6/4), patchy CHERT cuts across porcellanite laminations. Maximum size of chert patches is 1 X 2 cm.
b. Pink (7.5YR 7/4) PELAGIC CLAY at top of core contains volcanic glass, iron oxide aggregates, metallic micronodules and abundant zeolites.

SLIDE SUMMARY (%):

|  | 1, 1<br>M | 1, 63<br>D | 1, 70<br>D |
|---|---|---|---|
| TEXTURE: |  |  |  |
| Sand | 5 | 10 | 15 |
| Silt | 15 | 20 | 15 |
| Clay | 80 | 70 | 70 |
| COMPOSITION: |  |  |  |
| Clay | 60 | 10 | 5 |
| Fish | Tr | — | — |
| Glass | 10 | — | — |
| Micronodule | 5 | — | — |
| Nannofossils | Tr | — | — |
| Opaques | — | — | 1 |
| Oxide | 5 | — | 1 |
| Quartz | Tr | — | — |
| Radiolarians | — | 25 | 30 |
| Silica | — | 65 | 63 |
| Spines | Tr | — | — |
| Zeolite | 20 | — | — |

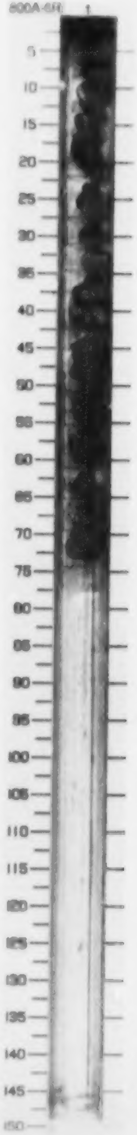

SITE 800 HOLE A CORE 7R CORED INTERVAL 5735.2-5744.9 mbsl; 49.2-58.9 mbsf

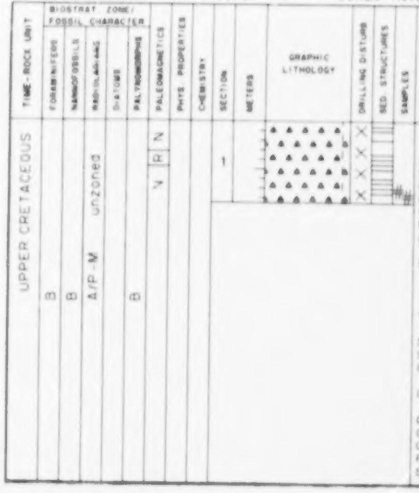
TIME-ROCK UNIT
BIOSTRAT. ZONE/ FOSSIL CHARACTER
FORAMINIFERS
NANNOFOSSILS
RADIOLARIANS
DIATOMS
PALYNOMORPHS
PALEOMAGNETICS
PHYS. PROPERTIES
CHEMISTRY
SECTION
METERS
GRAPHIC LITHOLOGY
DRILLING DISTURB.
SED. STRUCTURES
SAMPLES
UPPER CRETACEOUS
B
B
A/P-M unzoned
B
N R N
1

LITHOLOGIC DESCRIPTION

RADIOLARIAN CHERT with PORCELLANITE

Major lithology: RADIOLARIAN CHERT with millimeter scale laminations, locally gradational to dark brown radiolarian PORCELLANITE, very dark brown (10YR 2/2). Chert ranges from dark brown (10YR 2/2) through dusky red (2.5YR 2.5/2) to reddish yellow (7.5YR 6/6). Light colored replacement chert layers and patches increase down core. Dark chert and light replacement chert are cut by fractures filled with clear silica. At 65 cm silica fills numerous fractures at 30° to 60° to bedding. Laminations are due to relative abundance of radiolarians and iron oxides.

SLIDE SUMMARY (%):

| | 1, 64<br>D | 1, 70<br>D |
|---|---|---|
| TEXTURE | | |
| Sand | 5 | 10 |
| Silt | 5 | 10 |
| Clay | 90 | 80 |
| COMPOSITION | | |
| Calcite | Tr | — |
| Clay | 20 | 5 |
| Opaques | 2 | — |
| Radiolarians | 10 | 20 |
| Silica | 68 | 75 |

SITE 800 HOLE A CORE 8R CORED INTERVAL 5744.9-5754.5 mbsl; 58.9-68.5 mbsf

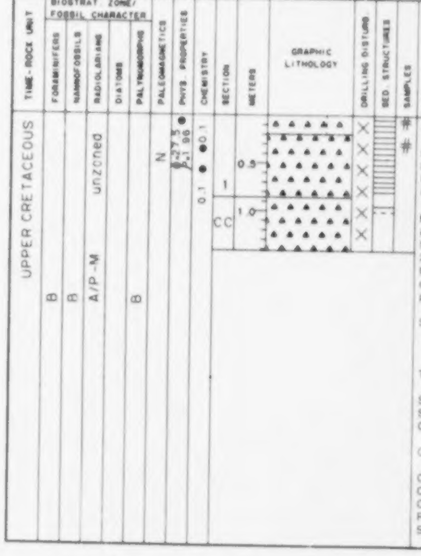
TIME-ROCK UNIT
BIOSTRAT. ZONE/ FOSSIL CHARACTER
FORAMINIFERS
NANNOFOSSILS
RADIOLARIANS
DIATOMS
PALYNOMORPHS
PALEOMAGNETICS
PHYS. PROPERTIES
CHEMISTRY
SECTION
METERS
GRAPHIC LITHOLOGY
DRILLING DISTURB.
SED. STRUCTURES
SAMPLES
UPPER CRETACEOUS
B
B
A/P-M unzoned
B
N
φ=27.5
ρ=1.96
0.1
0.1
1
CC
0.5
1.0

LITHOLOGIC DESCRIPTION

RADIOLARIAN CHERT

Major lithology: RADIOLARIAN CHERT mainly very dark brown (10YR 2/2) with irregular bands and lenses of yellowish red (5YR 4.5/6) to dark reddish brown (5YR 3/2). The yellowish features are from 1 mm to cm in thickness, 1 to 4 cm in width and generally lack internal structure. The main chert facies is thinly laminated.

Minor lithologies:
a. RADIOLARIAN PORCELLANITE, very dark brown (10YR 2/2), matte texture, less hard than chert. This porcellanite can form alternating bands with chert (thin section at Section 1, 29 to 33 cm).
b. Dark brown (10YR 3/3) ZEOLITIC CLAYSTONE at Section 1, 35-40 and 63-64 cm, displays a transition to chert. XRD of this claystone at Section 1, 63 cm has smectite and possibly barite.

SLIDE SUMMARY (%):

| | 1, 8<br>D | 1, 29<br>D |
|---|---|---|
| TEXTURE | | |
| Sand | 5 | 15 |
| Silt | 10 | 5 |
| Clay | 85 | 80 |
| COMPOSITION | | |
| Clay | 2 | 3 |
| Opaques | 1 | 1 |
| Oxide | 2 | 1 |
| Radiolarians | 15 | 20 |
| Silica | 80 | 75 |

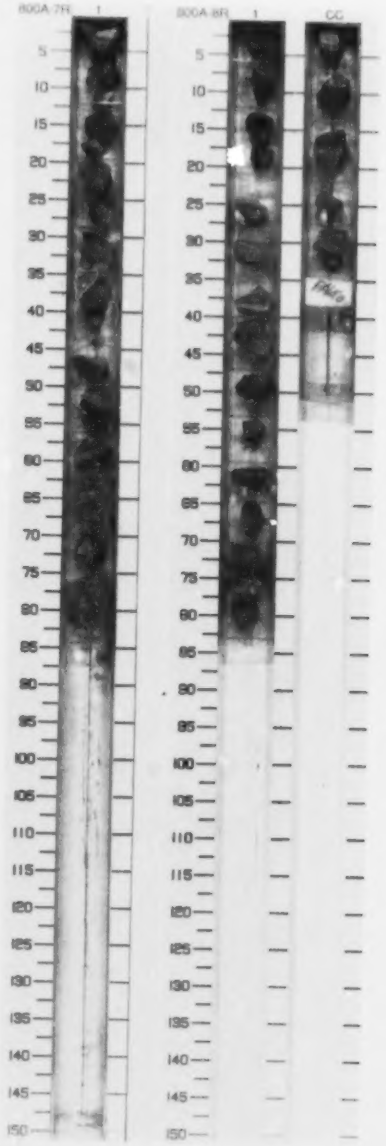
800A-7R 1
800A-8R 1
CC
5
10
15
20
25
30
35
40
45
50
55
60
65
70
75
80
85
90
95
100
105
110
115
120
125
130
135
140
145
150

SITE 800 HOLE A CORE 9R CORED INTERVAL 5754.2-5764.2 mbsl; 68.5-78.2 mbsf

| TIME-ROCK UNIT | BIOSTRAT. ZONE/ FOSSIL CHARACTER FORAMINIFERS | NANNOFOSSILS | RADIOLARIANS | DIATOMS | PALYNOMORPHS | PALEOMAGNETICS | PHYS. PROPERTIES | CHEMISTRY | SECTION | METERS | GRAPHIC LITHOLOGY | DRILLING DISTURB. | SED. STRUCTURES | SAMPLES |
|---|---|---|---|---|---|---|---|---|---|---|---|---|---|---|
| UPPER CRETACEOUS | B | B | A/P-B unzonec | | B | N | ● [illegible] | ● 0.1 | 1 | | | X<br>X | | #<br>#<br># |

LITHOLOGIC DESCRIPTION

CHERT and PORCELLANITE with RADIOLARIANS

Major lithologies:
a. CHERT: yellowish red (5YR 4/6) to very dark brown (10YR 2/2). Fractures have megaquartz filling.
b. PORCELLANITE with RADIOLARIANS is hard with thin, wavy, planar lenticular bedding. Porcellanite is light red brown (5YR 6/4) to very dark brown (10YR 2/2). Rare graded laminae of radiolarians in both lithologies. Chert locally replaces porcellanite discordantly to bedding.

SLIDE SUMMARY (%):

| | 1, 3<br>D | 1, 20<br>D | 1, 35<br>D |
|---|---|---|---|
| TEXTURE | | | |
| Sand | Tr | 5 | 15 |
| Silt | 5 | 10 | 8 |
| Clay | 95 | 85 | 77 |
| COMPOSITION | | | |
| Clay | 5 | — | — |
| Opaques | — | — | 4 |
| Oxide | Tr | 5 | — |
| Radiolarians | 5 | 15 | 20 |
| Silicia | 90 | 80 | 75 |

SITE 800 HOLE A CORE 10R CORED INTERVAL 5764.2-5773.8 mbsl; 78.2-87.8 mbsf

| TIME-ROCK UNIT | BIOSTRAT. ZONE/ FOSSIL CHARACTER FORAMINIFERS | NANNOFOSSILS | RADIOLARIANS | DIATOMS | PALYNOMORPHS | PALEOMAGNETICS | PHYS. PROPERTIES | CHEMISTRY | SECTION | METERS | GRAPHIC LITHOLOGY | DRILLING DISTURB. | SED. STRUCTURES | SAMPLES |
|---|---|---|---|---|---|---|---|---|---|---|---|---|---|---|
| UPPER CRETACEOUS | B | B | A/P unzoned | | B | N | ● [illegible] | ● 0.1 | 1 | | | X<br>X<br>X | | # |

LITHOLOGIC DESCRIPTION

RADIOLARIAN CHERT and PORCELLANITE

Major lithologies:
a. RADIOLARIAN CHERT: gray to olive gray, even black (5BG 4.5/1, 5G 5-6/1, 5Y 6-7/1). Lamination is often deformed and lenticular. Chert is calcareous below 58 cm.
b. PORCELLANITE: gray to olive gray (5G 6/1 to 5Y 6/1), rich in quartz replaced radiolarians.

Minor lithology: LIMESTONE at 63 to 71 cm, gray (5Y 7/1).

Note: Marked change in color at top of core; lithology changes from reddish and yellowish browns (YR- and R- hues) to olive gray and grays (G- and Y- hues).

SLIDE SUMMARY (%):

| | 1, 1<br>D | 1, 20<br>D |
|---|---|---|
| TEXTURE | | |
| Sand | 3 | 5 |
| Silt | 2 | Tr |
| Clay | 95 | 95 |
| COMPOSITION | | |
| Clay | 10 | 10 |
| Glass | — | Tr |
| Opaques | 2 | 2 |
| Radiolarians | 3 | 5 |
| Silicia | 75 | 83 |
| Spines | 10 | — |

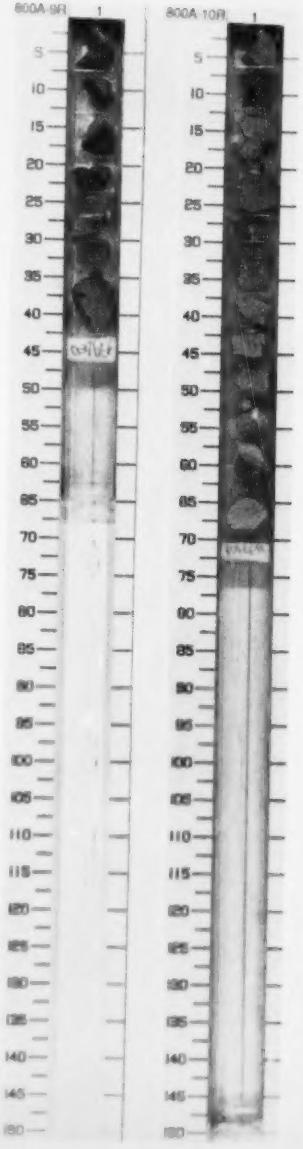

SITE 800 HOLE A CORE 11R CORED INTERVAL 5773.8-5483.3 mbsl; 87.8-97.3 mbsf

| TIME-ROCK UNIT | BIOSTRAT. ZONE/ FOSSIL CHARACTER: FORAMINIFERS | NANNOFOSSILS | RADIOLARIANS | DIATOMS | PALYNOMORPHS | PALEOMAGNETICS | PHYS. PROPERTIES | CHEMISTRY | SECTION | METERS | DRILLING DISTURB. | SED. STRUCTURES | SAMPLES |
|---|---|---|---|---|---|---|---|---|---|---|---|---|---|
| CENOMANIAN | B | C-M *E. turriseiffeli* (CC9) (NC10) | A/P-M unzoned | | B | N | $\phi$=40.0 $\rho$=2.30 | | 1 | 0.5<br>1.0 | ×<br>×<br>×<br>×<br>× | | # |

**LITHOLOGIC DESCRIPTION**

SILICEOUS LIMESTONE and RADIOLARIAN CHERT

Major lithologies:
a. SILICEOUS LIMESTONE, light to dark gray (5Y 7/1), hard matte to granular texture from abundant radiolarians.
b. RADIOLARIAN CHERT is olive gray (5Y 4/2, 5/2), hard, with fine texture, smooth surfaces, waxy luster; variable abundance of radiolarians produce laminae; contains up to 5% calcite, locally replaces limestone discordantly, wispy, discontinuous dark laminations.

Minor lithology: PORCELLANITE, light olive gray (5GY 4/1).

SLIDE SUMMARY (%):

| | 1, 1<br>D |
|---|---|
| TEXTURE: | |
| Sand | 25 |
| Silt | 20 |
| Clay | 55 |
| COMPOSITION: | |
| Calcite | 4 |
| Clay | Tr |
| Opaques | Tr |
| Oxide | 1 |
| Radiolarians | 25 |
| Silica | 50 |
| Spines | 20 |

SITE 800 HOLE A CORE 12R CORED INTERVAL 5783.3-5792.8 mbsl; 97.3-106.8 mbsf

| TIME-ROCK UNIT | BIOSTRAT. ZONE/ FOSSIL CHARACTER: FORAMINIFERS | NANNOFOSSILS | RADIOLARIANS | DIATOMS | PALYNOMORPHS | PALEOMAGNETICS | PHYS. PROPERTIES | CHEMISTRY | SECTION | METERS | DRILLING DISTURB. | SED. STRUCTURES | SAMPLES |
|---|---|---|---|---|---|---|---|---|---|---|---|---|---|
| CENOMANIAN | B | B | A/P-M unzoned | | B | | $\phi$=14.3 $\rho$=2.26 ● | 18.2 ● | 1 | | ×<br>× | | #<br>#<br># |

**LITHOLOGIC DESCRIPTION**

SILICEOUS LIMESTONE and RADIOLARIAN CHERT

Major lithologies:
a. SILICEOUS LIMESTONE grading to CALCAREOUS PORCELLANITE with RADIOLARIANS, ranging in color from dark gray to olive gray (5Y 4-5/1), green to greenish gray (5G 5/1, 5BG 5/1) and light greenish gray (5BG 5/1), matte to sandy texture due to 10 to 25% radiolarians.
b. RADIOLARIAN CHERT, dark gray to light greenish gray (5Y 4/1 to 5G 7/1) is typically contains fine, lenticular laminations, contains up to 45% radiolarians, some of which have barite crystals in the silica filling.

SLIDE SUMMARY (%):

| | 1, 1<br>D | 1, 29<br>D | 1, 41<br>D |
|---|---|---|---|
| TEXTURE: | | | |
| Sand | 40 | 7 | 10 |
| Silt | 15 | 3 | 5 |
| Clay | 45 | 90 | 85 |
| COMPOSITION: | | | |
| Barite | Tr | — | — |
| Calcite | — | — | 25 |
| Clay | 3 | Tr | — |
| Opaques | 1 | 1 | Tr |
| Oxide | — | 1 | — |
| Radiolarians | 45 | 10 | 10 |
| Silica | 41 | 80 | 65 |
| Spines | 10 | 5 | — |
| Unknown | — | 2 | — |

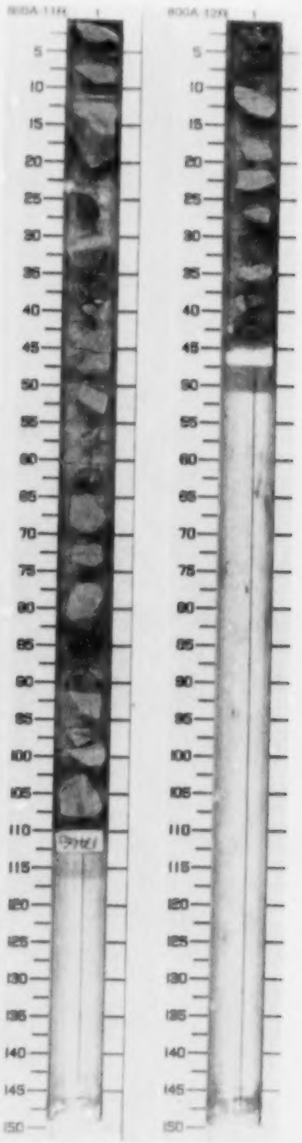

SITE 800 HOLE A CORE 13R CORED INTERVAL 5792.8-5812.2 mbsl; 106.8-116.2 mbsf

| TIME-ROCK UNIT | FORAMINIFERS | NANNOFOSSILS | RADIOLARIANS | DIATOMS | PALYNOMORPHS | PALEOMAGNETICS | PHYS. PROPERTIES | CHEMISTRY | SECTION | METERS | DRILLING DISTURB. | SED. STRUCTURES | SAMPLES |
|---|---|---|---|---|---|---|---|---|---|---|---|---|---|
| CENOMANIAN | B | R/P unzoned | A/P unzoned |  | B | N | ● $\phi$ 27.1 $\gamma$ 2.22 | ● 21.7 | 1 | 0.5 | × × × |  | # # |

**LITHOLOGIC DESCRIPTION**

SILICEOUS LIMESTONE

Major lithology: SILICEOUS LIMESTONE, micritic, with abundant radiolarians; color is light gray (5Y 7/1), featureless. Rare "rinds" of chalky LIMESTONE suggests that some of the non-recovered sediment may be soft chalk.

Minor lithologies:
Several intervals of silicification resulting in formation of PORCELLANITE and CHERT nodules or bands; both are dark gray (5Y 4.5/1) to gray (5Y 5.6/1). Porcellanite bands display wavy to flaser lamination, partial bioturbation and small light colored nodules.

SLIDE SUMMARY (%):

|  | 1, 6<br>D | 1, 29<br>D |
|---|---|---|
| TEXTURE |  |  |
| Sand | 20 | 30 |
| Silt | 10 | 5 |
| Clay | 70 | 65 |
| COMPOSITION |  |  |
| Calcite | 10 | — |
| Fish | — | Tr |
| Micrite | — | 55 |
| Oxide | — | Tr |
| Radiolarians | 30 | 35 |
| Silica | 60 | 10 |

SITE 800 HOLE A CORE 14R CORED INTERVAL 5812.2-5811.4 mbsl; 116.2-125.4 mbsf

| TIME-ROCK UNIT | FORAMINIFERS | NANNOFOSSILS | RADIOLARIANS | DIATOMS | PALYNOMORPHS | PALEOMAGNETICS | PHYS. PROPERTIES | CHEMISTRY | SECTION | METERS | DRILLING DISTURB. | SED. STRUCTURES | SAMPLES |
|---|---|---|---|---|---|---|---|---|---|---|---|---|---|
| CENOMANIAN | B | F/M *Eiffellithus turriseiffeli* (CC9)(NC10) | A/P unzoned |  | B | N | ● $\phi$ 27.0 $\gamma$ 2.02 | ● 0.2<br>● 0.2 | 1 | 0.5<br>1.0 | × × × × × × |  | # # |

**LITHOLOGIC DESCRIPTION**

SILICEOUS LIMESTONE

Major lithology: SILICEOUS LIMESTONE, light gray (5Y 7.6/1), mostly fine grained (micrite to microsparite), with some radiolarians. Small lenses, wedge laminations, flaser laminations, planar laminations and possible bioturbation are locally present.

Minor lithology: CHERT, dark gray (5Y 4.5/1), very hard, conchoidal fracture; occurs as thin beds and nodules in the siliceous limestone. Glassy chert pieces at 76-85 cm have pockets of chalk on their outside surfaces, suggesting that these are nodules within softer CHALK beds which were not recovered.

SLIDE SUMMARY (%):

|  | 1, 45<br>D | 1, 114<br>D |
|---|---|---|
| TEXTURE |  |  |
| Sand | 25 | 10 |
| Silt | 15 | 5 |
| Clay | 60 | 85 |
| COMPOSITION |  |  |
| Fish | Tr | — |
| Micrite | 58 | — |
| Microsparite | — | 45 |
| Opaques | 2 | 3 |
| Plant | Tr | — |
| Radiolarians | 35 | 10 |
| Silica | 5 | 42 |

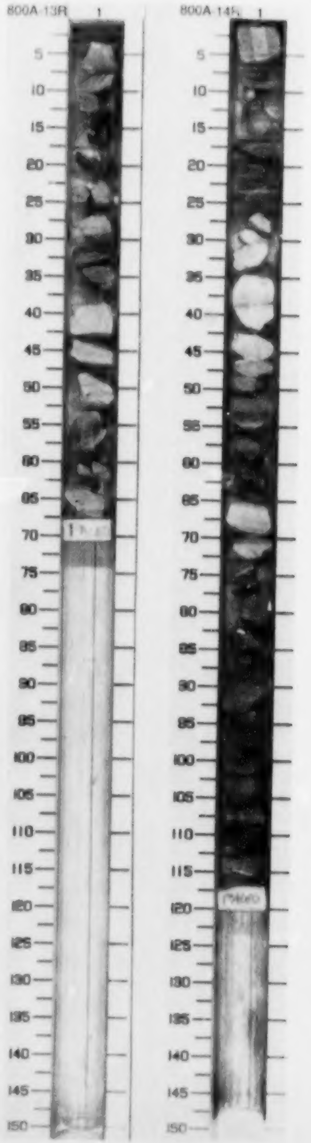

SITE 800 HOLE A CORE 15R CORED INTERVAL 5811.4-5820.2 mbsl; 125.4-134.9 mbsf

| TIME-ROCK UNIT | BIOSTRAT. ZONE/ FOSSIL CHARACTER | | | | | PALEOMAGNETICS | PHYS. PROPERTIES | CHEMISTRY | SECTION | METERS | GRAPHIC LITHOLOGY | DRILLING DISTURB. | SED. STRUCTURES | SAMPLES |
|---|---|---|---|---|---|---|---|---|---|---|---|---|---|---|
| | FORAMINIFERS | NANNOFOSSILS | RADIOLARIANS | DIATOMS | PALYNOMORPHS | | | | | | | | | |
| UPPER ALBIAN - CENOMANIAN | B | F/M *Eiffellithus turriseiffelii* (CC9) (NC10) | A/P unzoned | | B | N | $\phi$=7.00 ●<br>$\rho$=2.41 | 27.3 ● | 1 | | | ×<br>×<br>× | | # |

LITHOLOGIC DESCRIPTION

SILICEOUS LIMESTONE

Major lithology: SILICEOUS LIMESTONE, light gray (10YR 8/1 to N8), with nodules of chert. Siliceous limestone contains abundant radiolarians and within minor intervals displays thin laminae and small lenses.

Minor lithology: CHERT, dark gray (N3) to very dark grayish brown (10YR 3/2), nodules in limestone; displays conchoidal fracturing, and sharp contact or diagenetic boundary of chertification with the otherwise uniform host limestone.

SLIDE SUMMARY (%):

| | 1, 38 |
|---|---|
| | D |
| TEXTURE: | |
| Sand | 10 |
| Silt | 10 |
| Clay | 80 |
| COMPOSITION: | |
| Calcite | 3 |
| Clay | Tr |
| Foraminifers | 2 |
| Micrite | 22 |
| Nannofossils | Tr |
| Opaques | Tr |
| Radiolarians | 14 |
| Silica | 55 |
| Spicules | 4 |

SITE 800 HOLE A CORE 16R CORED INTERVAL 5820.9-5830.2 mbsl; 134.9-144.2 mbsf

| TIME-ROCK UNIT | BIOSTRAT. ZONE/ FOSSIL CHARACTER | | | | | PALEOMAGNETICS | PHYS. PROPERTIES | CHEMISTRY | SECTION | METERS | GRAPHIC LITHOLOGY | DRILLING DISTURB. | SED. STRUCTURES | SAMPLES |
|---|---|---|---|---|---|---|---|---|---|---|---|---|---|---|
| | FORAMINIFERS | NANNOFOSSILS | RADIOLARIANS | DIATOMS | PALYNOMORPHS | | | | | | | | | |
| UPPER ALBIAN | B | F/M *Eiffellithus turriseiffelii* (CC9) (NC10) | A/P *A. umbilicata* | | B | N | $\phi$=18.4 ●<br>$\rho$=2.17 | 21.2 ● | 1 | | | ×<br>×<br>× | ⓖ | #<br># |

LITHOLOGIC DESCRIPTION

SILICEOUS LIMESTONE to LIMESTONE

Major lithology: SILICEOUS LIMESTONE, light gray (5Y 7/1), gradational to LIMESTONE, gray (5Y 5/1), micritic with calcareous bioclasts and abundant silica-filled radiolarians. Variable degrees of silicification, but no significant chertification; lower pieces are mainly limestone.

Minor lithologies:
a. CHERT, dark gray (N4) at 3-8 cm, and
b. CALCAREOUS OOZE, gray (5Y 7/1), (created by drilling), which yielded a mid-Cretaceous nannofossil assemblage.

SLIDE SUMMARY (%):

| | 1, 26 | 1, 53 |
|---|---|---|
| | D | D |
| TEXTURE: | | |
| Sand | 20 | 15 |
| Silt | 10 | 10 |
| Clay | 70 | 75 |
| COMPOSITION: | | |
| Bioclast | 10 | — |
| Micrite | 54 | 35 |
| Opaques | 1 | 3 |
| Radiolarians | 20 | 25 |
| Silica | 15 | 37 |

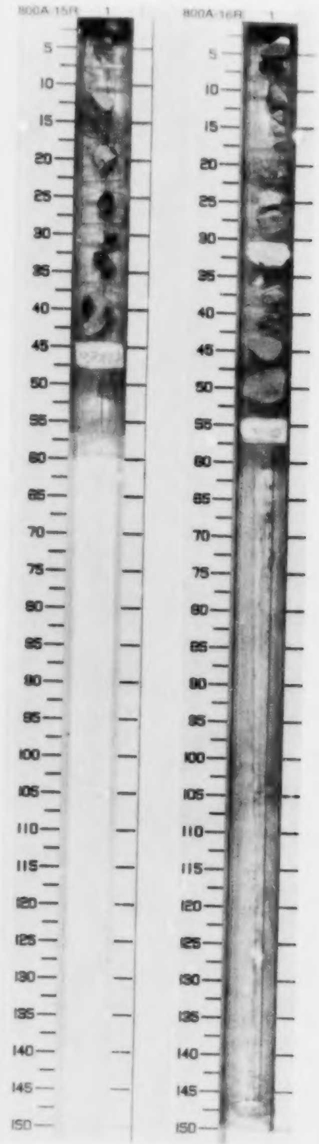

SITE 800 HOLE A CORE 17R CORED INTERVAL 5830.2-5839.7 mbsl; 144.2-153.6 mbsf

| TIME-ROCK UNIT | BIOSTRAT. ZONE/ FOSSIL CHARACTER: FORAMINIFERS | NANNOFOSSILS | RADIOLARIANS | DIATOMS | PALYNOMORPHS | PALEOMAGNETICS | PHYS. PROPERTIES | CHEMISTRY | SECTION | METERS | GRAPHIC LITHOLOGY | DRILLING DISTURB. | SED. STRUCTURES | SAMPLES | LITHOLOGIC DESCRIPTION |
|---|---|---|---|---|---|---|---|---|---|---|---|---|---|---|---|
| UPPER ALBIAN | B | F/M *Eiffellithus turriseiffeli* (CC9) (NC10) | A/M unzoned | | B | N | ● ϕ=16.5 ρ=2.36 | ●37.2 23.3● | 1 | 0.5 | | | | | |

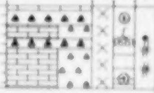

SILICEOUS LIMESTONE

Major lithology: SILICEOUS LIMESTONE, light gray (5Y 7/1) to greenish gray (5BG 7/1), with 10% chert nodules, dark reddish brown (5YR 3/2). Siliceous limestone contains flaser structures and indistinct color laminations; rare 1 cm thick layers of soft micritic NANNOFOSSIL LIMESTONE. Siliceous limestone contains abundant, silica filled radiolarians and up to 5% foraminifers. XRD from Section 1, 31 cm indicates calcite, opal CT and smectite.

Minor lithology: CHERT, dark reddish brown (5YR 3/2) and light gray (7.5YR 7/0); nodules have sharp irregular contacts, and sometimes include lighter colored rims; contacts cut layering in SILICEOUS LIMESTONE.

SLIDE SUMMARY (%):

| | 1, 37<br>M | 1, 44<br>D | 1, 68<br>D |
|---|---|---|---|
| TEXTURE: | | | |
| Sand | — | 20 | 15 |
| Silt | 15 | 15 | 15 |
| Clay | 85 | 65 | 70 |
| COMPOSITION: | | | |
| Bioclast | — | 5 | — |
| Calcite | 60 | — | — |
| Fish | — | 1 | — |
| Foraminifers | — | 5 | — |
| Micrite | — | 65 | 15 |
| Nannofossils | 40 | — | — |
| Opaques | — | 2 | 2 |
| Radiolarians | — | 20 | 30 |
| Silica | — | — | 53 |
| Spicules | — | 2 | — |

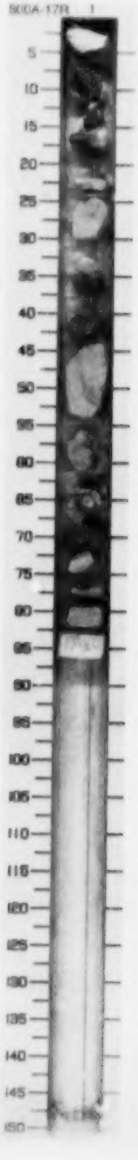

SITE 800 HOLE A CORE 18R CORED INTERVAL 5839.7-5848.9 mbsl; 153.7-162.9 mbsf

| TIME-ROCK UNIT | BIOSTRAT. ZONE/ FOSSIL CHARACTER: FORAMINIFERS | NANNOFOSSILS | RADIOLARIANS | DIATOMS | PALYNOMORPHS | PALEOMAGNETICS |
|---|---|---|---|---|---|---|
| UPPER ALBIAN | B | A/M *Eiffellithus turriseiffelii* (CC9) (NC10) | C/P unzoned | | B | N |

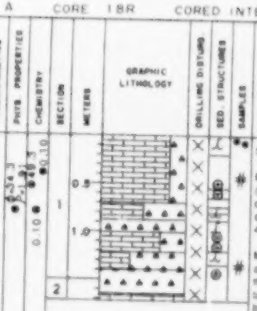
PHYS. PROPERTIES
CHEMISTRY
0.10
0.10
SECTION
1
2
METERS
0.5
1.0
GRAPHIC LITHOLOGY
DRILLING DISTURB.
SED. STRUCTURES
SAMPLES

LITHOLOGIC DESCRIPTION

SILICEOUS RADIOLARIAN LIMESTONE

Major lithology: SILICEOUS RADIOLARIAN LIMESTONE, light gray (5Y 7/1) to greenish gray (5BG 6/1), generally micritic, with 15% chert nodules; contains flasers and subtle laminations defined by changes in color and the concentration of radiolarians. Some limestone has a sandy texture; some is micritic to clayey and rich in nannofossils; [illegible] Section 1, 41-43 cm has 2% small foraminifers and 12% bioclasts.

Minor lithologies:

a. CHERT, dark greenish gray (10Y 3/1) to reddish brown (10YR 4/1), nodules, up to 15 cm thick in Section 2. Chert contacts are sharp and smooth to irregular, and truncate sedimentary structures.

b. CLAYSTONE with zeolites and radiolarians, greenish gray (5Y 4/1), at top of core may be uphole contamination.

SLIDE SUMMARY (%):

| | 1, 2<br>M | 1, 8<br>M | 1, 41<br>D | 1, 125<br>D |
|---|---|---|---|---|
| TEXTURE: | | | | |
| Sand | 10 | 5 | 20 | 15 |
| Silt | 15 | 25 | 20 | 20 |
| Clay | 75 | 70 | 60 | 65 |
| COMPOSITION: | | | | |
| Accessory minerals | Tr | — | — | — |
| Bioclast | — | — | 12 | 5 |
| Calcite | Tr | 30 | — | — |
| Clay | 67 | 40 | — | — |
| Foraminifers | — | — | 2 | — |
| Glass | 1 | — | — | — |
| Micrite | — | — | 60 | 40 |
| Nannofossils | Tr | 20 | — | — |
| Opaques | 3 | 2 | 1 | 2 |
| Oxide | 2 | 1 | — | — |
| Quartz | 2 | — | — | — |
| Radiolarians | 10 | 5 | 25 | 25 |
| Siliceous sponge spicules | — | 1 | — | — |
| Silica | — | — | — | 28 |
| Zeolite | 15 | 1 | — | — |

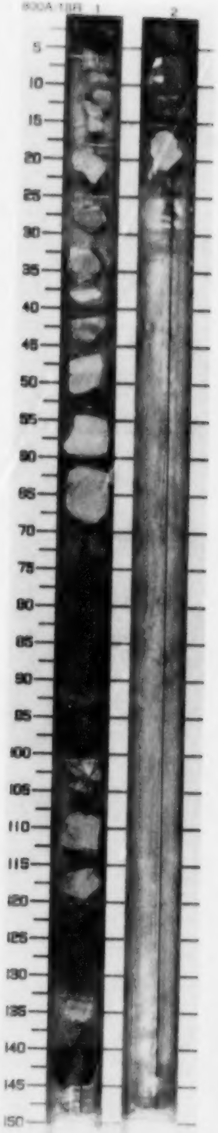
800A 18R
1
2
5
10
15
20
25
30
35
40
45
50
55
60
65
70
75
80
85
90
95
100
105
110
115
120
125
130
135
140
145
150

SITE 800 HOLE A CORE 19R CORED INTERVAL 5848.9-5858.4 mbsl; 162.9-172.4 mbsf

| TIME-ROCK UNIT | BIOSTRAT. ZONE/ FOSSIL CHARACTER: FORAMINIFERS | NANNOFOSSILS | RADIOLARIANS | DIATOMS | PALYNOMORPHS | PALEOMAGNETICS | PHYS. PROPERTIES | CHEMISTRY | SECTION | METERS | GRAPHIC LITHOLOGY | DRILLING DISTURB. | SED. STRUCTURES | SAMPLES |
|---|---|---|---|---|---|---|---|---|---|---|---|---|---|---|
| UPPER ALBIAN | B | C/P *Eiffellithus turriseiffeli* (CC9) (NC10) | F/P unzoned | | B | N | ● φ=33.5<br>● γ=1.99 | ● 29.4<br>● 88 | 1 | 0.5 | | X X X X X | | |

SILICEOUS LIMESTONE

Major lithology: SILICEOUS LIMESTONE, white (5Y 8/1) to light gray (5Y 7/1), firm to hard, micritic to sandy (from abundant radiolarians), mostly structureless, bioturbation evident within 2 to 4 cm of overlying argillaceous lithologies.

Minor lithologies:
a. CHERT to PORCELLANITE, dark to light gray (N4 to 5Y 4/1), with cuspate, convex outward replacement contacts with LIMESTONE, occurring as nodules and thin layers (lenses truncated by core?).
b. SILICEOUS CLAYSTONE, greenish gray to dark olive gray (5G 5/1 to 5Y 4/1.5), with sandy layers composed of radiolarians.

SLIDE SUMMARY (%):

| | 1, 1<br>D | 1, 8<br>D |
|---|---|---|
| TEXTURE: | | |
| Sand | 10 | 10 |
| Silt | 5 | 25 |
| Clay | 85 | 65 |
| COMPOSITION: | | |
| Bioclast | 3 | — |
| Micrite | 13 | 50 |
| Opaques | 2 | 5 |
| Radiolarians | 12 | 15 |
| Silica | 70 | 30 |

SITE 800 HOLE A CORE 20R CORED INTERVAL 5858.4-5867.3 mbsl; 172.4-181.3 mbsf

| TIME-ROCK UNIT | BIOSTRAT. ZONE/ FOSSIL CHARACTER: FORAMINIFERS | NANNOFOSSILS | RADIOLARIANS | DIATOMS | PALYNOMORPHS | PALEOMAGNETICS | PHYS. PROPERTIES | CHEMISTRY | SECTION | METERS | GRAPHIC LITHOLOGY | DRILLING DISTURB. | SED. STRUCTURES | SAMPLES |
|---|---|---|---|---|---|---|---|---|---|---|---|---|---|---|
| UPPER ALBIAN | B | C/M *Eiffellithus turriseiffeli* (CC9) (NC10) | A/P unzoned | | B | N | | | 1 | | | X X | | ● |

CHERT and RADIOLARIAN LIMESTONE

Major lithologies:
CHERT, light to very dark gray (10YR 6/1 to 7.5YR 3/0), mostly bedding parallel reaction fronts are very irregular at a subcentimeter scale. RADIOLARIAN LIMESTONE, very light to medium gray (N8 to N5), locally siliceous, friable with a silty/sandy texture.

Minor lithology: Crushed NANNOFOSSIL CHALK mud coats some of the drilling brecciated fragments.

SLIDE SUMMARY (%):

| | 1, 28<br>M |
|---|---|
| TEXTURE: | |
| Silt | 35 |
| Clay | 65 |
| COMPOSITION: | |
| Calcite | 55 |
| Clay | Tr |
| Nannofossils | 45 |

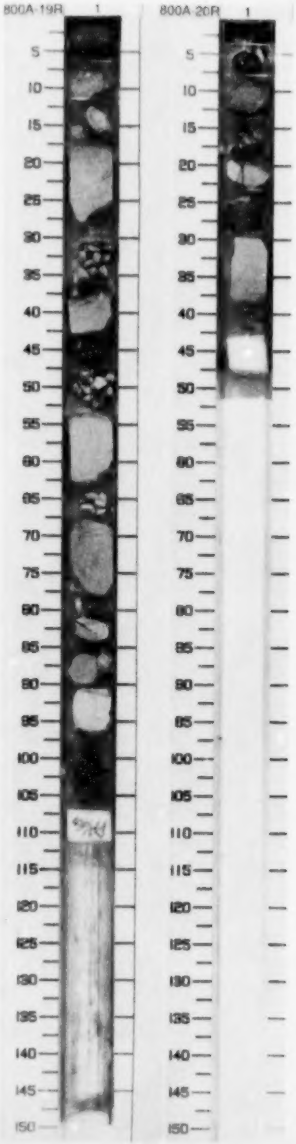

SITE 800 HOLE A CORE 21R CORED INTERVAL 5867.3-5869.0 mbsl; 181.3-191.0 mbsf

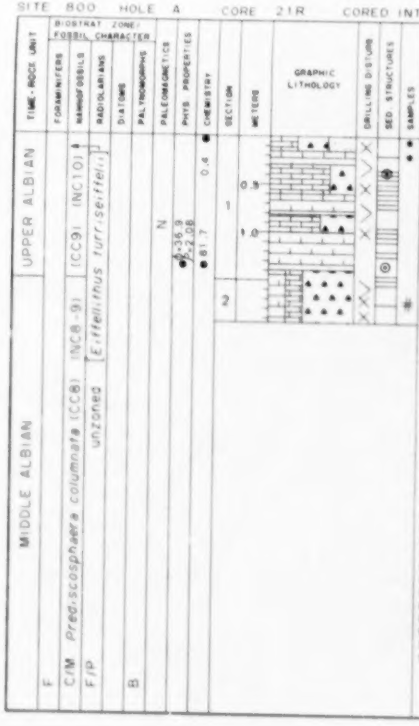
TIME-ROCK UNIT
BIOSTRAT. ZONE/ FOSSIL CHARACTER
FORAMINIFERS
NANNOFOSSILS
RADIOLARIANS
DIATOMS
PALYNOMORPHS
PALEOMAGNETICS
PHYS. PROPERTIES
CHEMISTRY
SECTION
METERS
GRAPHIC LITHOLOGY
DRILLING DISTURB.
SED. STRUCTURES
SAMPLES
UPPER ALBIAN
MIDDLE ALBIAN
F
C/M Prediscosphaera columnata (CC8) (NC8-9) (CC9) (NC10)
F/P unzoned
Eiffellithus turriseiffeli
B
N
φ=36.9
ρ=2.08
0.4
81.7
1
2
0.5
1.0

**LITHOLOGIC DESCRIPTION**

NANNOFOSSIL CHALK LIMESTONE with CHERT

Major lithologies:
a. NANNOFOSSIL CHALK, gradational to
b. LIMESTONE, white to light gray (N8 to 5Y 7/1), soft to hard, micritic, granular to matte texture with increased silica cementation, faintly microlaminated, with replacement CHERT, dark to very dark gray (2.5YR 4/1 to 10YR 3/1); discordant replacement surfaces are usually separated from CHALK by 3-5 cm of gray SILICIFIED LIMESTONE.

Minor lithology: CLAYEY RADIOLARITE, dark greenish gray (5GY 4/1) to very dark gray (5Y 3/1). XRD from Section 1, 53 cm, contains smectite, goethite and opal-CT.

Note: Highest significant recovery of NANNOFOSSIL CHALK is at 17 cm.

SLIDE SUMMARY (%):

|  | 1, 1<br>M | 1, 20<br>D | 2, 23<br>D |
|---|---|---|---|
| TEXTURE: |  |  |  |
| Sand | 30 | 5 | 15 |
| Silt | 40 | 40 | 10 |
| Clay | 30 | 55 | 75 |
| COMPOSITION: |  |  |  |
| Bioclast | — | — | 5 |
| Calcite | — | 45 | — |
| Clay | 35 | 5 | — |
| Foraminifers | — | — | 5 |
| Glass | Tr | — | — |
| Inorganic calcite | — | — | 5 |
| Micronodule | — | — | 1 |
| Micrite | — | — | 44 |
| Nannofossils | — | 50 | 10 |
| Oxide | 5 | — | — |
| Quartz | Tr | — | — |
| Radiolarians | 60 | — | 10 |
| Siliceous sponge spicules | Tr | — | — |
| Silica | — | — | 20 |

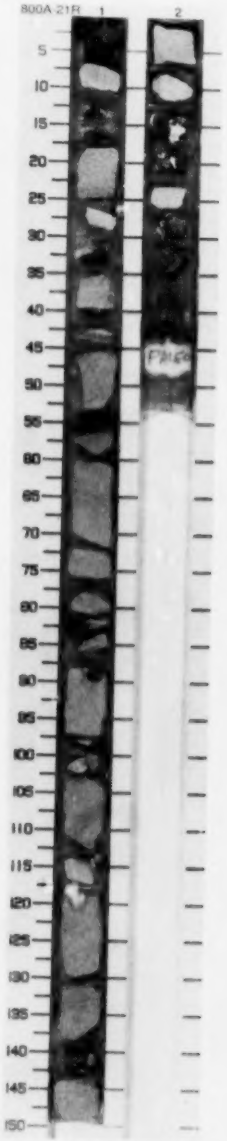
800A 21R
1
2
5
10
15
20
25
30
35
40
45
50
55
60
65
70
75
80
85
90
95
100
105
110
115
120
125
130
135
140
145
150

SITE 800 HOLE A CORE 22R CORED INTERVAL 5869.0-5886.5 mbsl; 191.0-200.5 mbsf

| TIME-ROCK UNIT | FORAMINIFERS | NANNOFOSSILS | RADIOLARIANS | DIATOMS | PALYNOMORPHS | PALEOMAGNETICS | PHYS. PROPERTIES | CHEMISTRY | SECTION | METERS | GRAPHIC LITHOLOGY | DRILLING DISTURB. | SED. STRUCTURES | SAMPLES |
|---|---|---|---|---|---|---|---|---|---|---|---|---|---|---|
| MIDDLE ALBIAN | B | F/P *Prediscosphaera columnata* (CC8) (NC8-9) | A/P unzoned | | B | N | [illegible] | [illegible] | 1 | 0.5 | 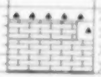 | X X X X | | ● ● |

LITHOLOGIC DESCRIPTION

SILICEOUS LIMESTONE and CHERT

Major lithologies:

a. SILICEOUS LIMESTONE, light gray (5Y 7/1) to white (5Y 8/1), micritic, hard and matte to firm and rough/sandy (radiolarians). Variation in texture is apparently chiefly due to degree of radiolarian dissolution and cementation of diagenetic silica.

b. CHERT, dark gray (5Y 4/1) to very dark gray (5Y 3/1), bedding parallel laminations and lenses, and bedding discordant cuspate, convex outward silicification fronts.

Minor lithology: CLAYEY NANNOFOSSIL CHALK at 19-22 cm, gray (N6), homogeneous, dull luster with fine sparkles. Hydrochloric acid cleaned residue contains abundant volcanic glass and zeolites. XRD from Section 1, 22 cm, contains opal-CT, calcite and smectite.

SLIDE SUMMARY (%):

| | 1, 21<br>D | 1, 50<br>D |
|---|---|---|
| TEXTURE | | |
| Sand | 5 | 10 |
| Silt | 30 | 50 |
| Clay | 65 | 40 |
| COMPOSITION | | |
| Calcite | 5 | 60 |
| Clay | 35 | 5 |
| Glass | Tr | — |
| Nannofossils | 55 | 20 |
| Opaques | 5 | Tr |
| Radiolarians | — | 15 |

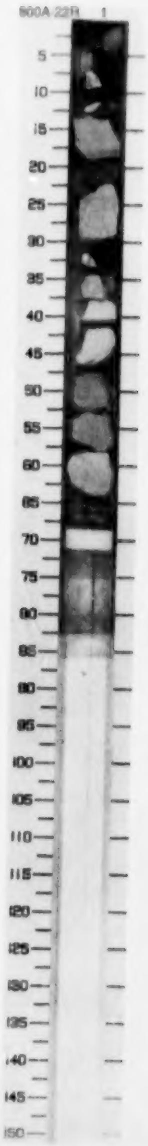

SITE 800 HOLE A CORE 23R CORED INTERVAL 5886.5-5889.9 mbsl, 200.5-209.9 mbsf

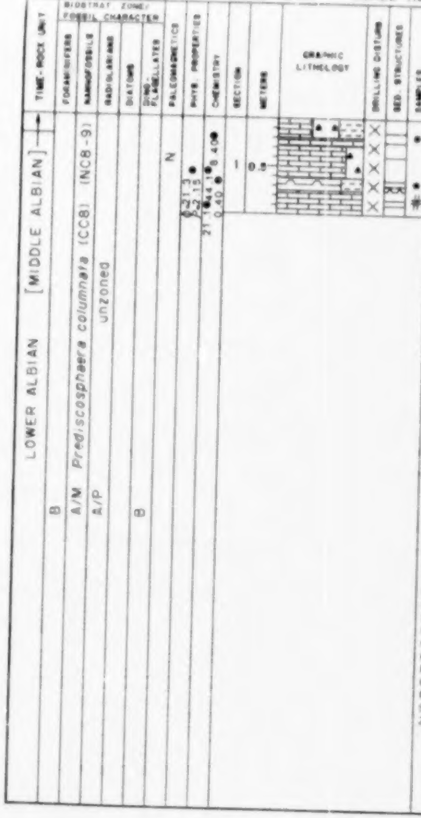
TIME-ROCK UNIT
BIOSTRAT. ZONE/ FOSSIL CHARACTER
FORAMINIFERS
NANNOFOSSILS
RADIOLARIANS
DIATOMS
DINO-FLAGELLATES
PALEOMAGNETICS
PHYS. PROPERTIES
CHEMISTRY
SECTION
METERS
GRAPHIC LITHOLOGY
DRILLING DISTURB.
SED. STRUCTURES
SAMPLES
[MIDDLE ALBIAN]
LOWER ALBIAN
B
A/M Prediscosphaera columnata (CC8) (NC8-9)
A/P unzoned
B
N
1
0.5
21
44.1
0.40
6.40

## LITHOLOGIC DESCRIPTION

SILICEOUS LIMESTONE to LIMESTONE

Major lithology: SILICEOUS LIMESTONE to LIMESTONE, white (5Y 8/1) to gray (5Y 6/1), biomicrite with foraminifers, calcareous bioclasts and silica-filled radiolarians, minor bioturbation to lamination formed by variable bioclast content, with some intervals containing possible volcanic clasts. XRD from Section 1, 90 cm, indicates opal-CT, calcite and smectite.

Minor lithologies:
a. CLAYEY RADIOLARITE (63-76 cm), dark olive gray with reddish tints (5Y 3.5/2), laminated, with possible scour contact with underlying LIMESTONE;
b. CLAYSTONE with radiolarians and volcanic material (16-20 cm), dark gray (7.5Y 4/1) and massive;
c. thin bands of CHERT (0-12 cm) with SILICIFIED LIMESTONE (at 30-33 cm), dark brown (7.5YR 4/2), laminated to featureless.
d. RADIOLARIAN CLAYSTONE at Section 1, 18 cm, contains opal-CT, calcite, clinoptilolite and smectite. XRD from clayey radiolarite at Section 1, 68 cm, indicates clinoptilolite, smectite and barite.

SLIDE SUMMARY (%):

| | 1, 18<br>M | 1, 69<br>M | 1, 83<br>D |
|---|---|---|---|
| TEXTURE | | | |
| Sand | 15 | 40 | 15 |
| Silt | 15 | 50 | 15 |
| Clay | 70 | 10 | 70 |
| COMPOSITION | | | |
| Accessory minerals | 1 | — | — |
| Bioclast | — | — | 10 |
| Calcite | 3 | — | — |
| Clay | 60 | 5 | — |
| Feldspar | 1 | — | — |
| Foraminifers | — | — | 5 |
| Glass | 6 | — | — |
| Micrite | — | — | 70 |
| Nannofossils | 2 | — | — |
| Opaques | 3 | — | — |
| Oxide | — | 10 | Tr |
| Plant | 1 | — | — |
| Quartz | 2 | 80 | — |
| Radiolarians | 20 | 5 | 15 |
| Silica | — | — | Tr |
| Zeolite | 1 | — | — |

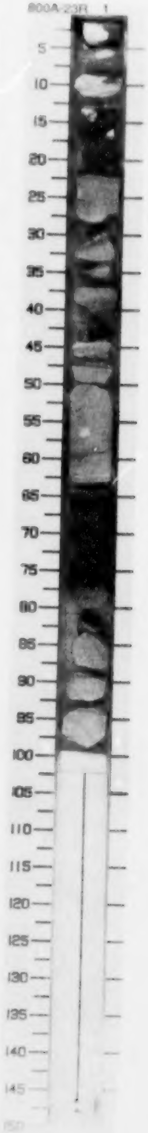
800A-23R 1
5
10
15
20
25
30
35
40
45
50
55
60
65
70
75
80
85
90
95
100
105
110
115
120
125
130
135
140
145
150

SITE 800 HOLE A CORE 24R CORED INTERVAL 5595.9-5905.3 mbsl; 209.9-219.3 mbsf

| TIME-ROCK UNIT | FORAMINIFERS | NANNOFOSSILS | RADIOLARIANS | DIATOMS | PALYNOMORPHS | PALEOMAGNETICS | PHYS. PROPERTIES | CHEMISTRY | SECTION | METERS |
|---|---|---|---|---|---|---|---|---|---|---|
| LOWER ALBIAN | B | C/M *Prediscosphaera columnata* (CC8) (NC8-9) | A/P unzoned | | B | N | [illegible] | [illegible] | 1 | 0.5<br>1.0 |

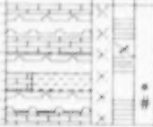
GRAPHIC LITHOLOGY
DRILLING DISTURB.
SED. STRUCTURES
SAMPLES

### LITHOLOGIC DESCRIPTION

RADIOLARITE and SILICEOUS LIMESTONE

Major lithologies:
a. Porcelaneous to calcareous RADIOLARITE, brownish gray (5Y 5/2, 10YR 4/1, 10YR 3/2) with laminations defined by radiolarian concentrations, locally clayey.
b. SILICEOUS LIMESTONE, gray (5Y 6/1 to 10YR 7/1), with abundant radiolarians and laminations of variable color or radiolarian content.

Minor lithology: CALCAREOUS CLAYSTONE, olive gray (5Y 4/1 to 5Y 6/1) with abundant nannofossils, subtle laminations, (pieces at 76-91 cm). XRD from Section 1, 86 cm, indicates opal-CT and calcite.

SLIDE SUMMARY (%):

| | 1, 87<br>M | 1, 101<br>D |
|---|---|---|
| TEXTURE: | | |
| Sand | 5 | 30 |
| Silt | 20 | 10 |
| Clay | 75 | 60 |
| COMPOSITION: | | |
| Accessory minerals | Tr | — |
| Calcite | 10 | — |
| Clay | 55 | — |
| Glass | 2 | — |
| Micrite | — | 29 |
| Nannofossils | 20 | — |
| Opaques | 2 | — |
| Oxide | — | 1 |
| Quartz | 3 | — |
| Radiolarians | 8 | 30 |
| Silica | — | 10 |
| Spicules | — | 10 |
| Spines | — | 20 |
| Unspecified minerals | 1 | — |

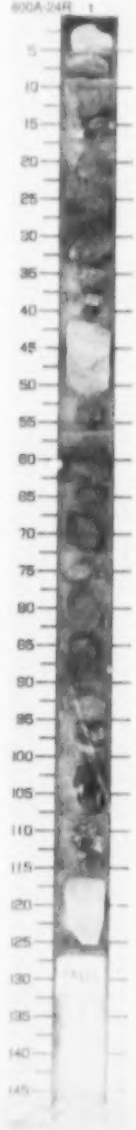
800A-24R 1
5
10
15
20
25
30
35
40
45
50
55
60
65
70
75
80
85
90
95
100
105
110
115
120
125
130
135
140
145

SITE 800 HOLE A CORE 25R CORED INTERVAL 5905.3-5914.6 mbsl; 219.3-228.6 mbsf

| TIME-ROCK UNIT | BIOSTRAT. ZONE/ FOSSIL CHARACTER: FORAMINIFERS | NANNOFOSSILS | RADIOLARIANS | DIATOMS | PALYNOMORPHS | PALEOMAGNETICS | PHYS. PROPERTIES | CHEMISTRY | SECTION | METERS | GRAPHIC LITHOLOGY | DRILLING DISTURB. | SED. STRUCTURES | SAMPLES |
|---|---|---|---|---|---|---|---|---|---|---|---|---|---|---|
| UPPER APTIAN | B | C/M *Parhabdolithus angustus* (NC7) | R/P unzoned |  | B |  | ● [illegible] | ● [illegible]<br>● [illegible] | 1 |  | 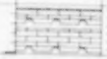 | X<br>X<br>X |  | ●<br>● |

**LITHOLOGIC DESCRIPTION**

RADIOLARITE and SILICEOUS LIMESTONE

Major lithologies:
a. RADIOLARITE to RADIOLARIAN CHERT, dark brown (7.5YR 4/2) with planar, flaser and wedge laminations, some with conchoidal fracturing.
b. SILICEOUS LIMESTONE, light gray to dark gray (10YR 7/1 to 10Y 4/2), massive.

Minor lithology: NANNOFOSSIL CLAYSTONE with radiolarians, dark gray (10Y 4/1), massive. XRD from Section 1, 49 cm, indicates opal-CT, calcite, smectite and barite.

SLIDE SUMMARY (%):

|  | 1, 31<br>D | 1, 50<br>M |
|---|---|---|
| TEXTURE: |  |  |
| Sand | 10 | — |
| Silt | 15 | — |
| Clay | 75 | 100 |
| COMPOSITION: |  |  |
| Clay | — | 53 |
| Nannofossils | — | 30 |
| Oxide | 1 | 2 |
| Quartz | — | 5 |
| Radiolarians | 25 | 10 |
| Silica | 74 | — |

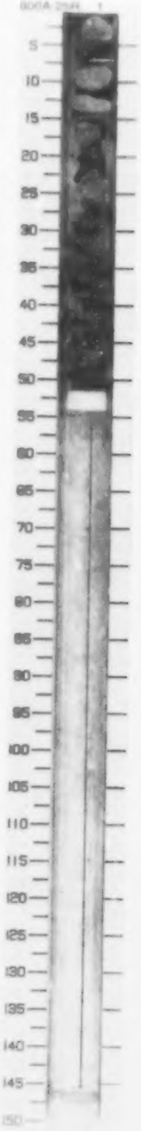

SITE 800 HOLE A CORE 26R CORED INTERVAL 5914.6-5924.0 mbsl; 228.6-238.0 mbsf

| TIME-ROCK UNIT | FORAMINIFERS | NANNOFOSSILS | RADIOLARIANS | DIATOMS | PALYNOMORPHS | PALEOMAGNETICS | PHYS. PROPERTIES | CHEMISTRY | SECTION | METERS |
|---|---|---|---|---|---|---|---|---|---|---|
| UPPER APTIAN | B | F/M *Parhabdolithus angustus* (NC7) | B | | P | N | •φ=42.9 γ=1.96<br>•φ=46.2 γ=2.0 | •5.80<br>•5.30<br>•1.4<br>•0.5 | 1<br>2<br>3<br>CC | 0.5<br>1.0 |

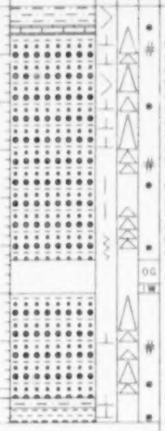

LITHOLOGIC DESCRIPTION

VOLCANICLASTIC TURBIDITES

Major lithology: VOLCANICLASTIC TURBIDITES (redeposited ash and tuff), consisting of silty sandstone fining upwards to clayey siltstone, in cycles up to 75 cm thick. VOLCANICLASTIC SANDSTONE fractions are dark gray (N4) with angular grains composed of feldspar, volcanic Rock fragments, volcanic glass, and sparse radiolarians. These grade upwards to greenish blue (5BG 5/1) VOLCANICLASTIC CLAYSTONE containing up to 10% radiolarians, trace nannofossils, 20% feldspar microlites, volcanic Rock fragments, volcanic glass, chloritic clay minerals, zeolites, opaque minerals, and microcrystalline silica. XRD from Section 1, 11 cm, indicates opal-CT, calcite, clinoptilolite and smectite; from CC, 1 cm, indicates calcite and smectite. Thin section (Section 3, 56-58 cm) has volcanic glass, igneous Rock fragments, pyroxene, zeolite and smectite.

Minor lithologies:
a. CALCAREOUS CLAYSTONE, olive gray (5GY 5/1), up to 10 cm thick, containing up to 25% radiolarians, 15% nannofossils, calcite, clay, and glauconite, representing pelagic intervals between turbidite events.
b. RADIOLARIAN LIMESTONE, light greenish gray (5GY 6.5/1), laminated, Section 1, 19-27 cm and 65-67 cm.

SLIDE SUMMARY (%):

| | 1, 22<br>M | 1, 45<br>D | 1, 107<br>D | 2, 16<br>D | 2, 38<br>D | 2, 102<br>D | 3, 56<br>D |
|---|---|---|---|---|---|---|---|
| TEXTURE: | | | | | | | |
| Sand | 20 | 40 | 80 | 60 | — | — | 90 |
| Silt | 40 | 30 | 18 | 20 | 25 | 30 | 10 |
| Clay | 40 | 30 | 2 | 20 | 75 | 70 | — |
| COMPOSITION: | | | | | | | |
| Accessory minerals | — | — | Tr | — | 1 | — | — |
| Aragonite | — | Tr | — | — | — | — | — |
| Augite | — | — | — | 10 | — | — | — |
| Biotite | — | — | — | Tr | — | — | — |
| Calcite | 50 | Tr | 2 | — | 20 | 20 | — |
| Clay | 10 | 5 | 2 | 20 | 55 | 50 | — |
| Feldspar | — | 2 | 20 | 3 | 5 | 5 | Tr |
| Foraminifers | — | 1 | — | — | — | — | — |
| Glass | — | 60 | 2 | 40 | 5 | — | 80 |
| Glauconite | Tr | — | — | — | — | — | — |
| Igneous rock fragments | — | 15 | — | 20 | — | — | 15 |
| Nannofossils | 15 | — | — | — | 5 | 15 | — |
| Opaques | — | — | 1 | — | 1 | Tr | — |
| Pyroxene | — | 5 | 1 | — | — | — | 5 |
| Quartz | Tr | — | Tr | — | — | — | — |
| Radiolarians | 25 | 10 | 10 | 5 | 8 | 5 | — |
| Rock fragment | — | — | 60 | — | Tr | — | — |
| Smectite | — | — | — | 2 | — | — | Tr |
| Zeolite | — | — | — | — | — | — | Tr |

SLIDE SUMMARY (%):

| | 3, 96<br>D | CC, 20<br>D |
|---|---|---|
| TEXTURE: | | |
| Sand | 10 | Tr |
| Silt | 50 | 5 |
| Clay | 40 | 95 |
| COMPOSITION: | | |
| Accessory minerals | 2 | 2 |
| Calcite | Tr | 10 |
| Chlorite | — | 5 |
| Clay | 40 | 55 |
| Feldspar | 20 | 10 |
| Glass | 8 | 10 |
| Nannofossils | — | 5 |
| Opaques | 2 | — |
| Quartz | Tr | — |
| Radiolarians | 10 | Tr |
| Rock fragment | 12 | — |
| Zeolite | 5 | — |

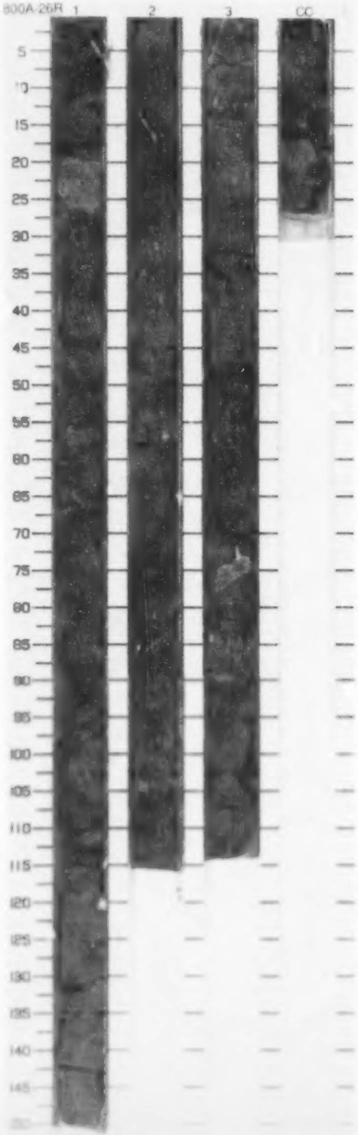

SITE 800 HOLE A CORE 27R CORED INTERVAL 5924.0-5933.2 mbsl; 238.0-247.2 mbsf

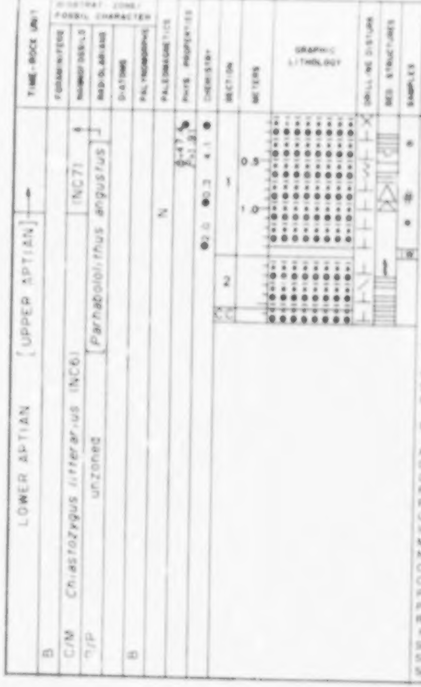
TIME-ROCK UNIT
BIOSTRAT. ZONE/ FOSSIL CHARACTER
FORAMINIFERS
NANNOFOSSILS
RADIOLARIANS
DIATOMS
PALYNOMORPHS
PALEOMAGNETICS
PHYS. PROPERTIES
CHEMISTRY
SECTION
METERS
GRAPHIC LITHOLOGY
DRILLING DISTURB.
SED. STRUCTURES
SAMPLES
LOWER APTIAN
[UPPER APTIAN]
B
C/M
Chiastozygus litterarius (NC6)
(NC7)
T/P
unzoned
Parhabdolithus angustus
B
N
4.1
0.3
2.0
1
2
CC
0.5
1.0

LITHOLOGIC DESCRIPTION

VOLCANICLASTIC TURBIDITES

Major lithology: VOLCANICLASTIC TURBIDITES, consisting of SILTSTONE and CLAYSTONE, dark blue gray (5B 4/1), composed of clay, volcanic glass, feldspar, volcanic rock fragments, opaque minerals, and calcite; massive to laminated; some layers are graded; approximately 75% of core. XRD's (Section 1, 10 cm and 97 cm) indicate opal-CT, plagioclase, smectite and pyroxene.

Minor lithology: SILICEOUS NANNOFOSSIL CLAYSTONE, olive gray (5Y 5/1), containing nannofossils, radiolarians, foraminifers, volcanic fragments and clay; silty texture in base of coarser graded beds. Claystone is laminated, with graded beds, lode casts, flasers, and convolute layers, and makes up approximately 25% of core.

SLIDE SUMMARY (%):

| | 1, 21<br>D | 1, 88<br>M | 1, 112<br>M |
|---|---|---|---|
| TEXTURE: | | | |
| Sand | — | 10 | — |
| Silt | 20 | 30 | 5 |
| Clay | 80 | 60 | 95 |
| COMPOSITION: | | | |
| Accessory minerals | Tr | — | — |
| Calcite | 5 | — | 20 |
| Clay | 75 | 11 | 70 |
| Feldspar | 5 | Tr | Tr |
| Foraminifers | — | 3 | — |
| Glass | 3 | 5 | — |
| Inorganic calcite | — | 5 | — |
| Micrite | — | 15 | — |
| Nannofossils | — | 30 | 10 |
| Opaques | 2 | — | Tr |
| Oxide | — | 2 | — |
| Pellets | — | 3 | — |
| Pyroxene | — | Tr | — |
| Radiolarians | 5 | 10 | — |
| Rock fragment | 5 | — | Tr |
| Silica | — | 10 | — |
| Smectite | — | 3 | — |
| Spicules | — | 2 | — |

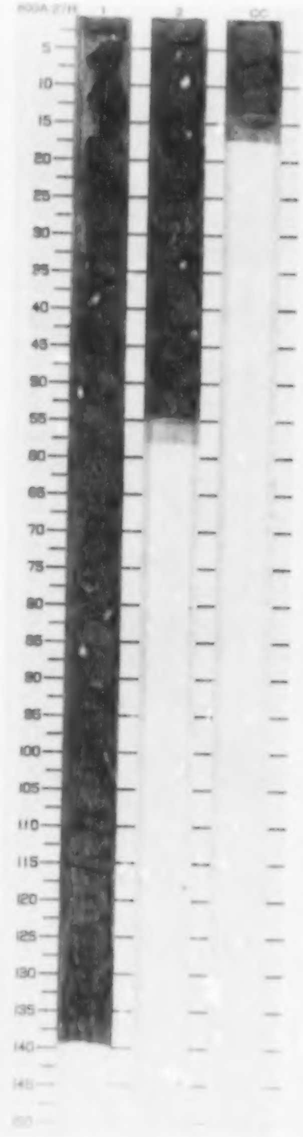
800A 27R
1
2
CC
5
10
15
20
25
30
35
40
45
50
55
60
65
70
75
80
85
90
95
100
105
110
115
120
125
130
135
140
145
150

SITE 800 HOLE A CORE 28R CORED INTERVAL 5933.2-5942.6 mbsl; 247.2-256.5 mbsf

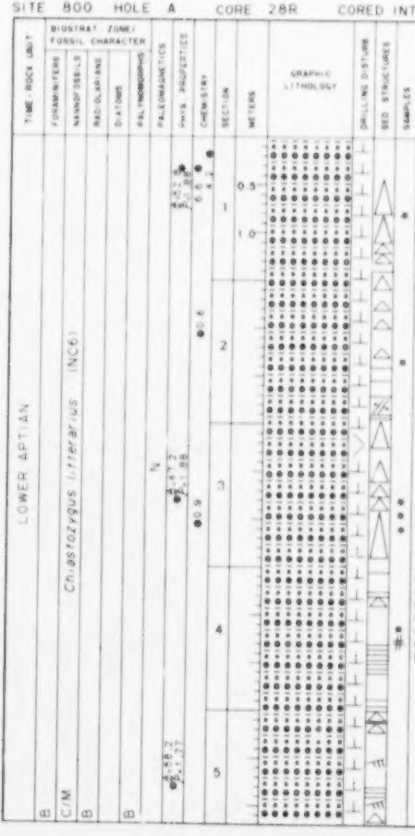
TIME-ROCK UNIT
BIOSTRAT. ZONE/ FOSSIL CHARACTER
FORAMINIFERS
NANNOFOSSILS
RADIOLARIANS
DIATOMS
PALYNOMORPHS
PALEOMAGNETICS
PHYS. PROPERTIES
CHEMISTRY
SECTION
METERS
GRAPHIC LITHOLOGY
DRILLING DISTURB.
SED. STRUCTURES
SAMPLES
LOWER APTIAN
Chiastozygus litterarius (NC6)
B
C/M
B
B
N
1
2
3
4
5
0.5
1.0
6.6
4.2
6.8
6.9

LITHOLOGIC DESCRIPTION

VOLCANICLASTIC TURBIDITES

Major lithology: VOLCANICLASTIC TURBIDITES consisting of SANDSTONE, SILTSTONE and CLAYSTONE, thinly interlaminated in 10- to 70-cm thick beds. Bedding cycles start with greenish gray (5Y 5/1) to dark gray (N4) sandstone, poorly sorted, fine to medium grained, principally volcanic rock fragments, palagonized glass and sericitized or chloritized feldspars. Sandstone grades upwards into dark blue gray (5B 4/1) to dark gray (N4) thinly laminated, or massive, and fissile, siltstone and claystone of similar composition. Sand/shale ratio is approximately 10/90. Sedimentary structures include scoured bases, cross-lamination, climbing ripples, deformed beds, and bioturbation. Sandstones contain about 55% volcanic rock fragments and 20% feldspar.

Minor lithology: CALCAREOUS TURBIDITE in Section 3, 43-91 cm, yellowish gray (5Y 8/1) to light greenish gray (5GY 7/1) has sand, FORAMINIFER and NANNOFOSSIL RICH LIMESTONE with feldspar at base.

SLIDE SUMMARY (%):

| | 1, 76<br>D | 2, 83<br>D | 3, 77<br>D | 3, 89<br>M | 3, 107<br>D | 4, 68<br>D | 4, 75<br>D |
|---|---|---|---|---|---|---|---|
| TEXTURE: | | | | | | | |
| Sand | 50 | 20 | 20 | 20 | 5 | Tr | — |
| Silt | 45 | 45 | 40 | 35 | 55 | 30 | 30 |
| Clay | 5 | 35 | 40 | 45 | 40 | 70 | 70 |
| COMPOSITION: | | | | | | | |
| Accessory minerals | 12 | 5 | — | Tr | 5 | 5 | — |
| Calcite | — | 5 | 40 | 35 | Tr | 5 | 15 |
| Clay | 5 | 10 | 10 | 5 | 15 | 10 | 70 |
| Feldspar | 30 | 25 | 15 | 10 | 30 | 20 | Tr |
| Foraminifers | — | — | 10 | 25 | — | — | — |
| Glass | — | — | — | — | — | — | 5 |
| Igneous rock fragments | 50 | 55 | — | Tr | 50 | 60 | 5 |
| Nannofossils | — | — | 25 | 25 | — | — | — |
| Oxide | — | — | — | — | — | — | 3 |
| Pyroxene | — | — | — | — | Tr | — | 1 |
| Quartz | Tr | Tr | — | — | — | — | 1 |
| Radiolarians | Tr | — | — | — | — | — | Tr |

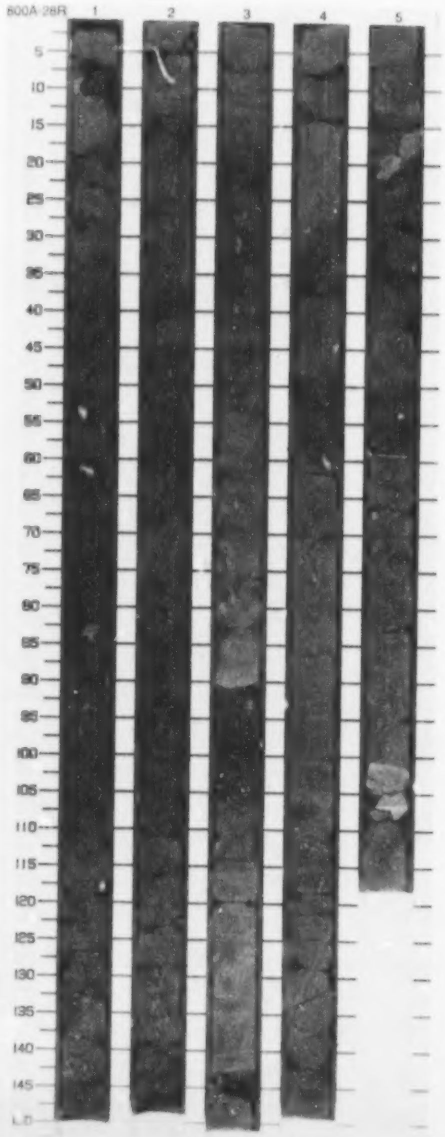
800A-28R
1
2
3
4
5
5
10
15
20
25
30
35
40
45
50
55
60
65
70
75
80
85
90
95
100
105
110
115
120
125
130
135
140
145
LD

SITE 800 HOLE A CORE 29R CORED INTERVAL 5942.5-5951.9 mbsl; 256.6-265.9 mbsf

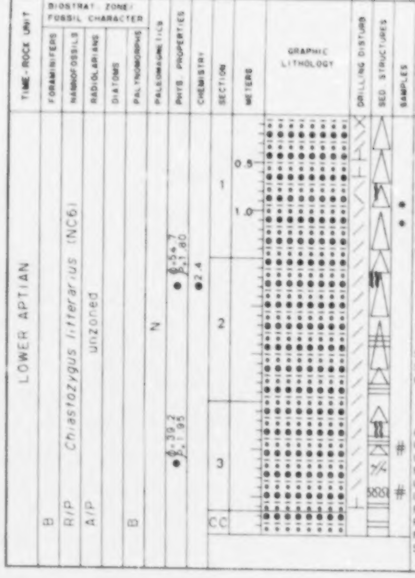

LITHOLOGIC DESCRIPTION

VOLCANICLASTIC TURBIDITES

Major lithologies: VOLCANICLASTIC TURBIDITES, consisting mostly of VOLCANICLASTIC SILTY CLAYSTONE to SANDY SILTSTONE, dark gray (N4-5) to dark blue gray (5B 4/1), dark greenish gray (5G 4/1) below Section 3, 26 cm, fissile, thinly laminated to massive, composition as in core 28R. Less abundant VOLCAN ICLASTIC SANDSTONE is greenish gray (5G 5/1-5BG 4/1), planar to cross laminated. Tops of some turbidites consist of SILICEOUS CLAYSTONE with up to 20% radiolarians. Change in color from dark grays and dark blue grays to yellowish and brownish grays, and more strongly green zones below Section 3, 26 cm. Sub-vertical fractures in Section 3, 70-77 cm and 92-95 cm, are cemented with quartz.

SLIDE SUMMARY (%):

| | 1, 93<br>D | 1, 112<br>D | 3, 46<br>D | 3, 92<br>D |
|---|---|---|---|---|
| TEXTURE: | | | | |
| Sand | 30 | 5 | 10 | 5 |
| Silt | 50 | 40 | 10 | 10 |
| Clay | 20 | 55 | 80 | 85 |
| COMPOSITION: | | | | |
| Accessory minerals | 5 | 5 | 1 | Tr |
| Calcite | — | Tr | — | — |
| Clay | 15 | — | 50 | 50 |
| Feldspar | 20 | 15 | — | 3 |
| Glass | — | 10 | — | — |
| Opaques | — | Tr | 2 | 1 |
| Pyroxene | 5 | — | 1 | — |
| Radiolarians | — | — | 20 | 10 |
| Rock fragment | 55 | 70 | — | 5 |
| Silica | — | — | 26 | 30 |

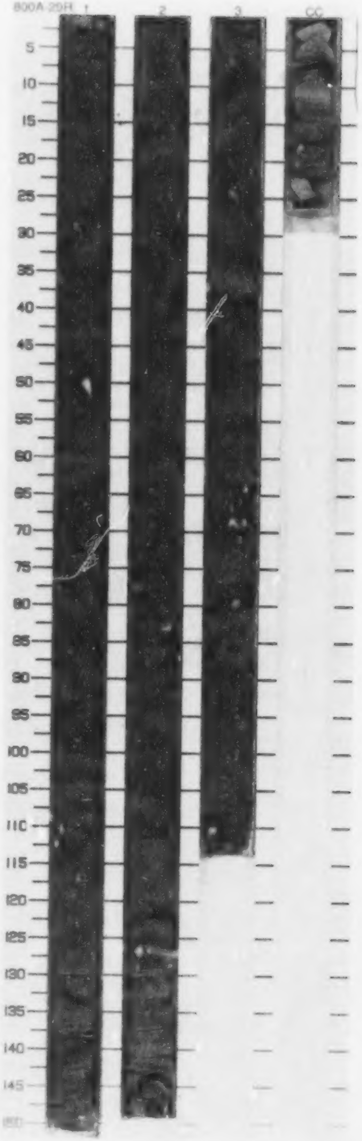

SITE 800 HOLE A CORE 30R CORED INTERVAL 5951.9-5958.0 mbsl; 265.9-272.0 mbsf

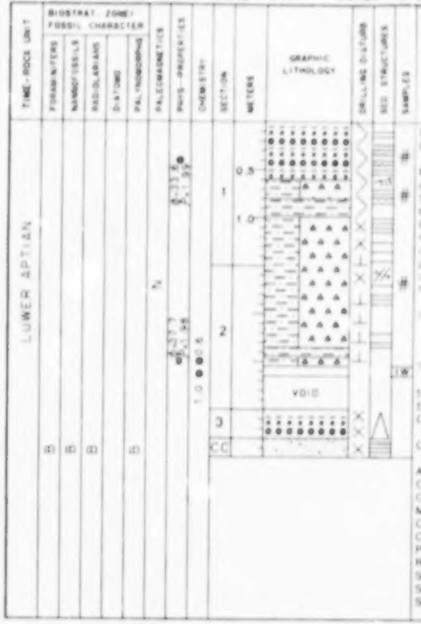
TIME-ROCK UNIT
BIOSTRAT. ZONE/ FOSSIL CHARACTER
FORAMINIFERS
NANNOFOSSILS
RADIOLARIANS
DIATOMS
PALYNOMORPHS
PALEOMAGNETICS
PHYS. PROPERTIES
CHEMISTRY
SECTION
METERS
GRAPHIC LITHOLOGY
DRILLING DISTURB.
SED. STRUCTURES
SAMPLES
LOWER APTIAN
B
B
B
B
N
1.0 ●●0.6
1
2
3
CC
0.5
1.0
VOID
#
#
#
IW

LITHOLOGIC DESCRIPTION

VOLCANICLASTIC TURBIDITES, RADIOLARIAN PORCELLANITE and VOLCANICLASTIC CLAYSTONE

Major lithologies:

a. VOLCANICLASTIC TURBIDITES, consisting of grayish green (5GY 4/1, 5G 4/2, 5B 5/1) SILTSTONE and CLAYSTONE.

b. RADIOLARIAN PORCELLANITE, gradational to CLAYEY RADIOLARITE or RADIOLARIAN SILICEOUS CLAYSTONE, dark grayish brown (10YR 2/2 to 2.5Y 4/2); abundant silica-replaced microfossils give an overall sandy texture; thinly interbedded with

c. grayish green (5G 4/2) VOLCANICLASTIC CLAYSTONE layers, possibly tuffaceous, with pinch and swell geometry. XRD's from claystones at Section 1, 95 cm and 96 cm indicate opal-CT, plagioclase, zeolites and smectite.

Note: Highest appearance of PORCELLANITE is at top of core in Section 1, 0 cm.

SLIDE SUMMARY (%):

| | 1, 34<br>D | 1, 75<br>D | 2, 19<br>D |
|---|---|---|---|
| TEXTURE: | | | |
| Sand | 20 | 25 | 15 |
| Silt | 5 | 25 | 10 |
| Clay | 75 | 50 | 75 |
| COMPOSITION: | | | |
| Accessory minerals | Tr | — | 1 |
| Clay | 42 | 11 | 40 |
| Glass | 1 | 15 | — |
| Micrite | — | 5 | — |
| Opaques | 2 | — | — |
| Oxide | — | 2 | 2 |
| Pyroxene | Tr | — | — |
| Radiolarians | 25 | 25 | 25 |
| Silica | 30 | 30 | 32 |
| Smectite | — | 2 | — |
| Spines | — | 10 | — |

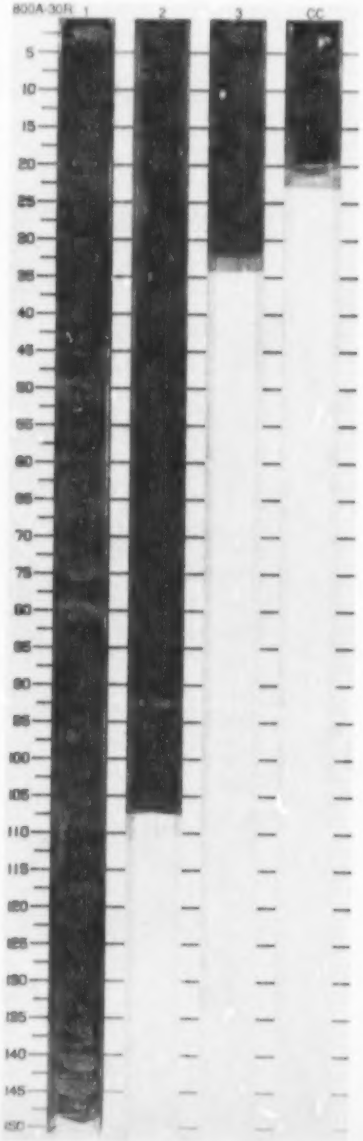
800A-30R
1
2
3
CC
5
10
15
20
25
30
35
40
45
50
55
60
65
70
75
80
85
90
95
100
105
110
115
120
125
130
135
140
145
150

SITE 800 HOLE A CORE 31R CORED INTERVAL 5958.0-5964.1 mbsl; 272.0-278.1 mbsf

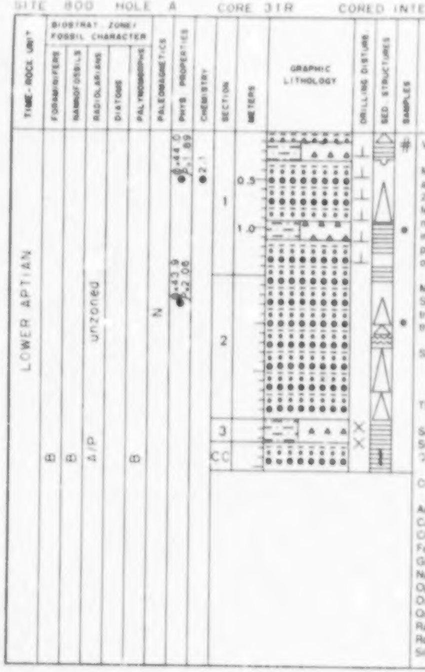
TIME-ROCK UNIT
BIOSTRAT. ZONE/ FOSSIL CHARACTER
FORAMINIFERS
NANNOFOSSILS
RADIOLARIANS
DIATOMS
PALYNOMORPHS
PALEOMAGNETICS
PHYS. PROPERTIES
CHEMISTRY
SECTION
METERS
GRAPHIC LITHOLOGY
DRILLING DISTURB.
SED. STRUCTURES
SAMPLES
LOWER APTIAN
B
B
unzoned
A/P
B
N
ϕ-44.0
γ-1.89
●2.1
ϕ-43.9
γ-2.06
1
2
3
CC
0.5
1.0
#

LITHOLOGIC DESCRIPTION

VOLCANICLASTIC TURBIDITES

Major lithology: VOLCANICLASTIC TURBIDITES, consisting of SANDSTONE, SILTSTONE and CLAYSTONE, bluish gray to dark gray (5B 4/1 to N4), in full sequences approximately 1-2 m thick. SANDSTONE composed of volcanic Rock fragments, fresh and palagonized glass, feldspar laths, olive green pyroxenes, zeolites, and mudstone chips up to 5 mm in diameter, moderately well sorted with subangular to subrounded grains. XRD from Section 2, 13 cm indicates opal-CT, plagioclase and smectite. Sedimentary structures include grading, ripple, planer and cross-laminations, disturbed laminations, lode casts and flame structures. Bases of beds scour into RADIOLARIAN PORCELLANITE.

Minor lithology: RADIOLARIAN PORCELLANITE gradational to RADIOLARIAN CLAYSTONE, olive gray (5Y 5/1), millimeter scale laminations, with abundant radiolarians and traces of authigenic calcite, volcanic glass, and feldspar. Pelagic intervals are 15 to 20 cm thick between turbidite events, roughly 25% of core.

SLIDE SUMMARY (%)

|  | 1, 12<br>M | 1, 113<br>D | 2, 50<br>M |
|---|---|---|---|
| TEXTURE: |  |  |  |
| Sand | — | 20 | 20 |
| Silt | 15 | 40 | 40 |
| Clay | 85 | 40 | 40 |
| COMPOSITION: |  |  |  |
| Accessory minerals | — | 1 | 1 |
| Calcite | — | — | 10 |
| Clay | 72 | 30 | 30 |
| Feldspar | 1 | 3 | 5 |
| Glass | — | 5 | 2 |
| Nannofossils | — | — | 2 |
| Opaques | — | 1 | 2 |
| Oxide | 2 | — | — |
| Quartz | — | — | 5 |
| Radiolarians | 15 | 5 | 35 |
| Rock fragment | — | 55 | — |
| Silica | 10 | — | — |

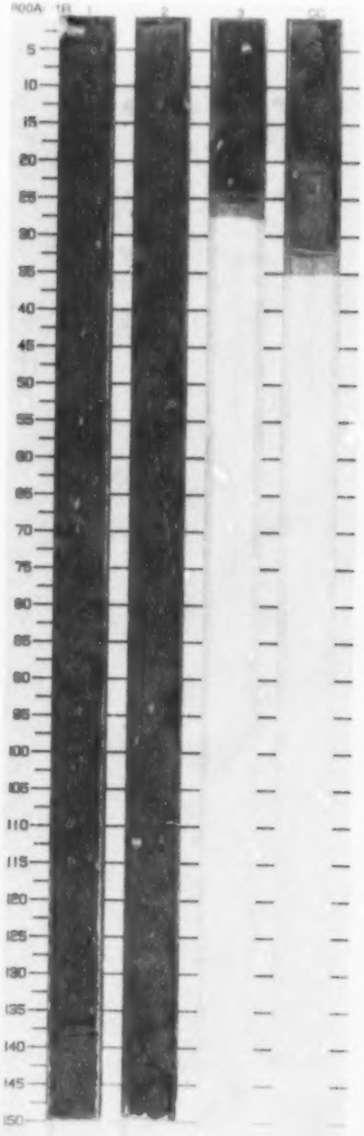
800A 1
2
3
CC
5
10
15
20
25
30
35
40
45
50
55
60
65
70
75
80
85
90
95
100
105
110
115
120
125
130
135
140
145
150

SITE 800 HOLE A CORE 32R CORED INTERVAL 5964.1-5973.5 mbsl; 278.1-287.5 mbsf

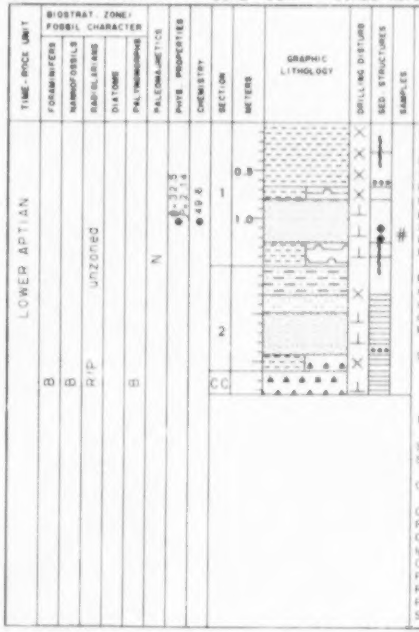
TIME-ROCK UNIT
BIOSTRAT. ZONE/ FOSSIL CHARACTER
FORAMINIFERS
NANNOFOSSILS
RADIOLARIANS
DIATOMS
PALYNOMORPHS
PALEOMAGNETICS
PHYS. PROPERTIES
CHEMISTRY
SECTION
METERS
GRAPHIC LITHOLOGY
DRILLING DISTURB.
SED. STRUCTURES
SAMPLES
LOWER APTIAN
B
B
unzoned
R/P
B
N
φ-32.5
γ-2.14
●49.6
1
2
CC
0.5
1.0
#

LITHOLOGIC DESCRIPTION

VOLCANICLASTIC SANDSTONE, SILTSTONE and CLAYSTONE

Major lithologies:
VOLCANICLASTIC SANDSTONE, SILTSTONE and CLAYSTONE in the form of turbidites, light green (5G 6/1), coarser grained than all overlying cores, with claystone rip-up clasts up to 1 cm long in sandstone, which consists of angular to subrounded clasts, moderately to poorly sorted: volcanic rock fragments, pyroxene, feldspar, volcanic glass, red algae, and zeolites. Two turbidite beds in this core, slightly greater than 1 m thick, representing about 80% of the core. The claystone at the top of the turbidite grades up into PORCELLANEOUS RADIOLARIAN CLAYSTONE.

Minor lithology: PORCELLANEOUS RADIOLARIAN CLAYSTONE, olive brown (7.5YR 3/2), massive to thinly laminated. A 5 mm bright green alteration zone at the base of the turbidite in Section 2 (at 90 cm) indicates some form of chemical diagenesis. XRD from Section CC, 1 cm indicates clinoptilolite and smectite.
Note: An overall fining-upward sequence dominates Cores 32 through 26.

SLIDE SUMMARY (%)

|  | 1, 117<br>D |
|---|---|
| TEXTURE: |  |
| Sand | 95 |
| Silt | 5 |
| COMPOSITION: |  |
| Calcite | 4 |
| Feldspar | 3 |
| Glass | 10 |
| Igneous rock fragments | 15 |
| Oxide | 3 |
| Pyroxene | 5 |
| Radiolarians | Tr |
| Red algae | 55 |
| Smectite | 5 |

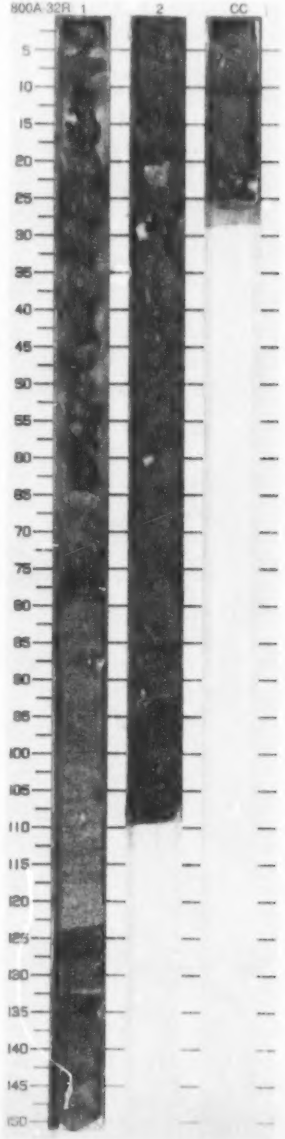
800A-32R 1
2
CC
5
10
15
20
25
30
35
40
45
50
55
60
65
70
75
80
85
90
95
100
105
110
115
120
125
130
135
140
145
150

SITE 800 HOLE A CORE 33R CORED INTERVAL 5973.5-5983.0 mbsl; 287.5-297.0 mbsf

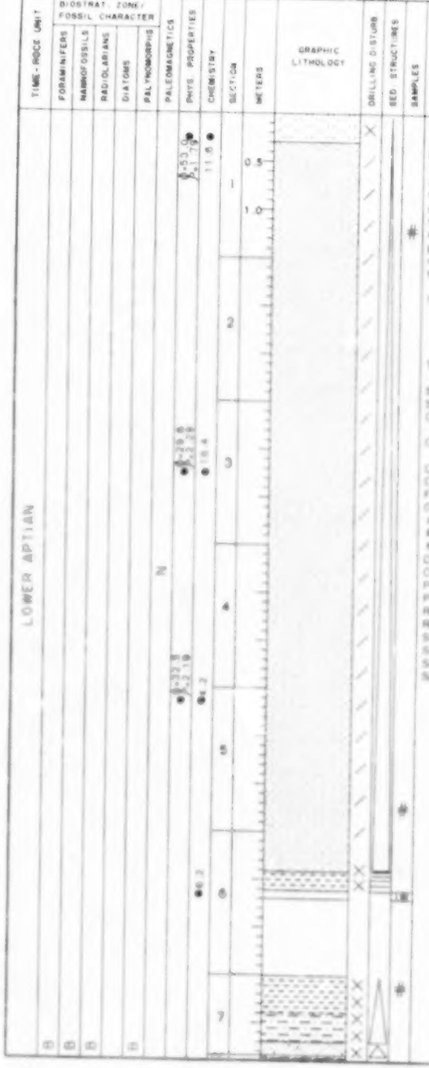
TIME-ROCK UNIT
BIOSTRAT. ZONE/ FOSSIL CHARACTER
FORAMINIFERS
NANNOFOSSILS
RADIOLARIANS
DIATOMS
PALYNOMORPHS
PALEOMAGNETICS
PHYS. PROPERTIES
CHEMISTRY
SECTION
METERS
GRAPHIC LITHOLOGY
DRILLING DISTURB.
SED. STRUCTURES
SAMPLES
LOWER APTIAN
B
B
B
B
N
53.0
1.79
29.6
2.28
32.8
2.19
11.6
10.4
4.2
0.2
1
2
3
4
5
6
7
0.5
1.0

LITHOLOGIC DESCRIPTION

VOLCANICLASTIC SANDSTONE, SILTSTONE and CLAYSTONE

Major lithologies:

VOLCANICLASTIC SANDSTONE, SILTSTONE and CLAYSTONE in the form of turbidites, up to 8 m thick, dark bluish green gray (5G 4/1, 5BG 4/2) to gray (N6, 10G 5/2), overall fining upward from gravel to fine-grained sandstone, but with several intervals of reverse grading. Component grains include dark volcanic rock fragments with light rims, gray altered volcanics, brownish gray claystone intraclasts, and light gray carbonate grains. Upper portion contains variety of ripple and cross- laminations. Calcite veins in lower portion. There is a portion of a second turbidite in the base of the core. Claystone to clays[illegible]stone is dark reddish brown (5YR 3/3), with laminae consisting of volcaniclastic silt or radiolarian concentrations. XRD from Section 7, 5 cm indicates calcite, plagioclase and smectite.

SLIDE SUMMARY (%):

| | 1, 127<br>D | 5, 127<br>D | 7, 8<br>D |
|---|---|---|---|
| TEXTURE: | | | |
| Sand | 5 | 95 | — |
| Silt | 45 | 5 | 15 |
| Clay | 50 | — | 85 |
| COMPOSITION: | | | |
| Calcite | 10 | 2 | 15 |
| Clay | — | — | 31 |
| Feldspar | — | 1 | 3 |
| Glass | 52 | 53 | — |
| Igneous rock fragments | 15 | 30 | — |
| Magnetite | — | Tr | — |
| Mica | — | — | 2 |
| Opaques | — | — | 10 |
| Oxide | 2 | — | 20 |
| Pellets | 10 | Tr | — |
| Pyroxene | 5 | 5 | — |
| Radiolarians | — | — | 5 |
| Red algae | 5 | 1 | 10 |
| Shell debris | Tr | — | — |
| Silica | — | — | 5 |
| Smectite | 1 | 3 | — |
| Spherulite | — | 5 | — |

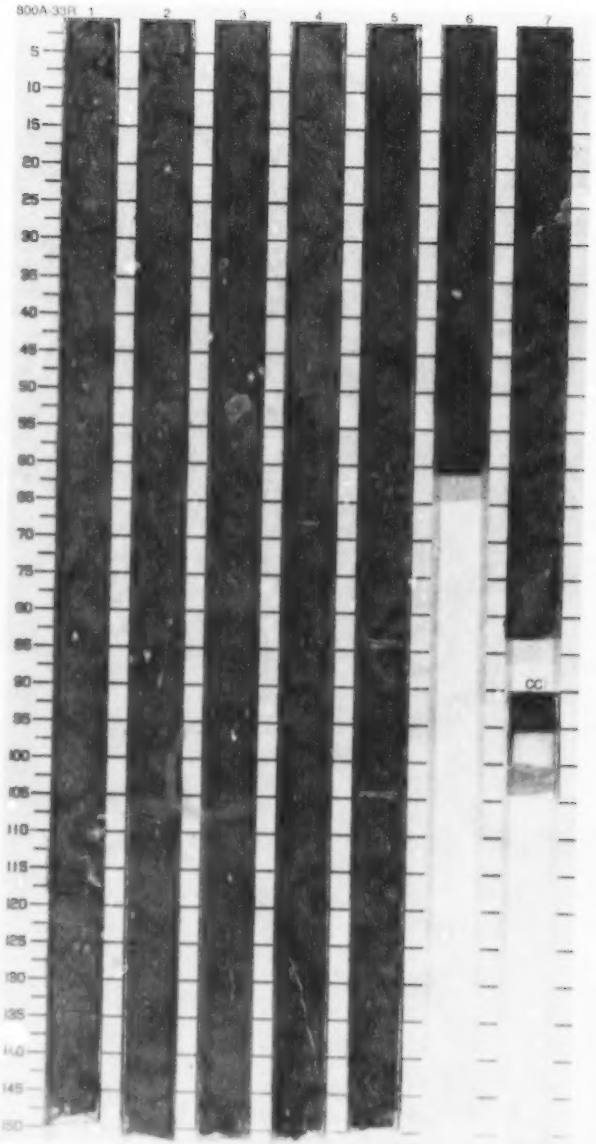
800A-33R
1
2
3
4
5
6
7
CC
5
10
15
20
25
30
35
40
45
50
55
60
65
70
75
80
85
90
95
100
105
110
115
120
125
130
135
140
145
150

SITE 800 HOLE A CORE 34R CORED INTERVAL 5983.0-5992.4 mbsl; 297.0-306.4 mbsf

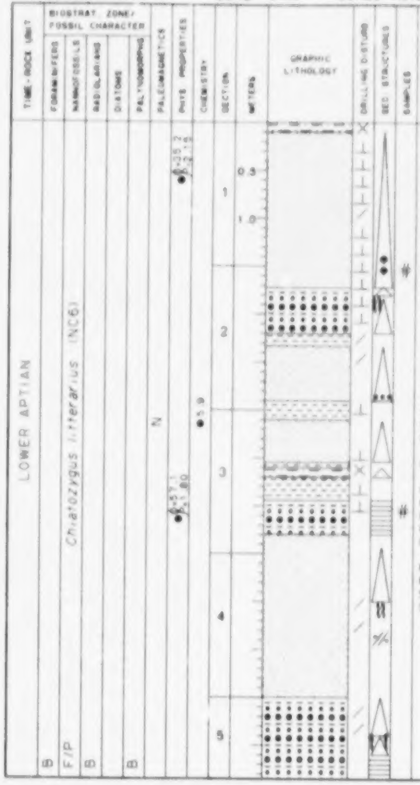
TIME-ROCK UNIT
BIOSTRAT. ZONE/ FOSSIL CHARACTER
FORAMINIFERS
NANNOFOSSILS
RADIOLARIANS
DIATOMS
PALYNOMORPHS
PALEOMAGNETICS
PHYS. PROPERTIES
CHEMISTRY
SECTION
METERS
GRAPHIC LITHOLOGY
DRILLING DISTURB.
SED. STRUCTURES
SAMPLES
LOWER APTIAN
Chiatozygus litterarius (NC6)
B
F/P
B
B
N
35.2
57.1
1.80
5.9
1
2
3
4
5
0.5
1.0

LITHOLOGIC DESCRIPTION

VOLCANICLASTIC TURBIDITES and SANDSTONE

Major lithologies:

VOLCANICLASTIC TURBIDITES, dark greenish gray (5BG 4/1), consisting of SANDSTONE in graded beds 1 to 3 m thick, coarse- to fine-grained, poorly sorted, angular to subrounded. Grains include volcanic rock fragments, glass, feldspar, zeolites and claystone intraclasts. Greenish gray (5G 5/1) reduction fronts extend downward from the sharp scoured bases of turbidites into underlying reddish brown CLAYSTONE. XRD from Section 5, 51 cm indicates calcite, phillipsite(?) and smectite.

Minor lithology: RADIOLARIAN CLAYSTONE, reddish brown (5YR 3/3), with laminae or thin flasers of concentrated volcaniclastic silt or radiolarians. XRD from Section 1, 1 cm indicates calcite, plagioclase and smectite.

SLIDE SUMMARY (%):

| | 2, 10<br>D | 3, 107<br>D |
|---|---|---|
| TEXTURE: | | |
| Sand | 80 | — |
| Silt | 20 | 60 |
| Clay | — | 40 |
| COMPOSITION: | | |
| Calcite/Dolomite | — | 1 |
| Calcite | 25 | 15 |
| Clay | — | 20 |
| Feldspar | 2 | 2 |
| Glass | 30 | 20 |
| Igneous rock fragments | 25 | 30 |
| Pyroxene | 3 | 10 |
| Red algae | 8 | — |
| Silica | 2 | — |
| Smectite | 5 | 2 |

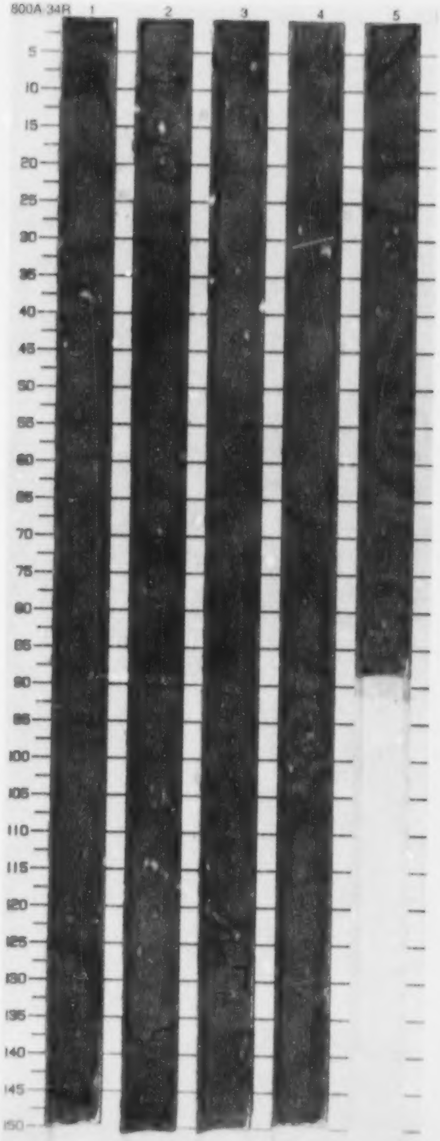
800A-34R
1
2
3
4
5
5
10
15
20
25
30
35
40
45
50
55
60
65
70
75
80
85
90
95
100
105
110
115
120
125
130
135
140
145
150

SITE 800 HOLE A CORE 35R CORED INTERVAL 5992.4-6001.9 mbsl; 306.4-315.9 mbsf

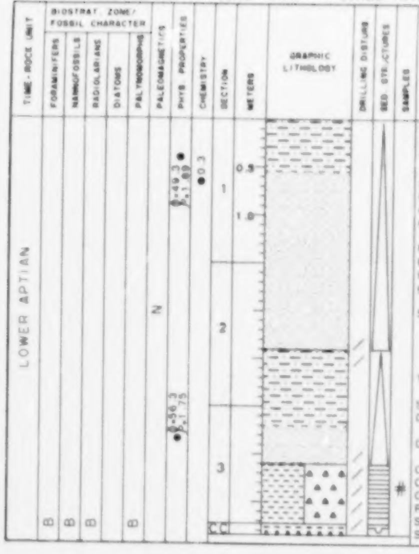
TIME-ROCK UNIT
BIOSTRAT. ZONE/ FOSSIL CHARACTER
FORAMINIFERS
NANNOFOSSILS
RADIOLARIANS
DIATOMS
PALYNOMORPHS
PALEOMAGNETICS
PHYS. PROPERTIES
CHEMISTRY
SECTION
METERS
GRAPHIC LITHOLOGY
DRILLING DISTURB.
SED. STRUCTURES
SAMPLES
LOWER APTIAN
B
B
B
B
N
φ-49.3
γ-1.89
φ-56.3
γ-1.75
0.3
1
2
3
CC
0.5
1.0
#

LITHOLOGIC DESCRIPTION

VOLCANICLASTIC TURBIDITES, SANDSTONE and CLAYSTONE

Major lithologies:

VOLCANICLASTIC TURBIDITES, SANDSTONE and CLAYSTONE, greenish gray (5GY 5/1, 5G 6/1, 5G 4/1, N4); graded beds 1.5 to 2 m thick, very coarse- to fine-grained sandstone, moderately to poorly sorted, with angular to subrounded clasts, grading to claystone. Grains include clay rip-ups up to 1 cm long, volcanic rock fragments, altered glass, feldspar, pyroxene, zeolites, clayey alteration zones on some clasts. Sedimentary structures include convolute, planar and cross laminations, amalgamated beds in Section 1, 55-150 cm.

Minor lithology: RADIOLARIAN PORCELLANITE grading to CLAYEY RADIOLARITE, brownish gray (5Y 4/1) with some laminations altered to light green (5GY 7/1). Contains fine laminations of volcaniclastic claystone. Porcellanite contains disseminated clasts of volcanic glass, feldspar and zeolites. XRD from Section 3, 78 cm indicates clinoptilolite and smectite.

SLIDE SUMMARY (%):

| | 3, 84 |
|---|---|
| | D |
| TEXTURE: | |
| Silt | 5 |
| Clay | 95 |
| COMPOSITION: | |
| Clay | 30 |
| Opaques | 1 |
| Oxide | 1 |
| Radiolarians | 5 |
| Silica | 60 |
| Smectite | 3 |

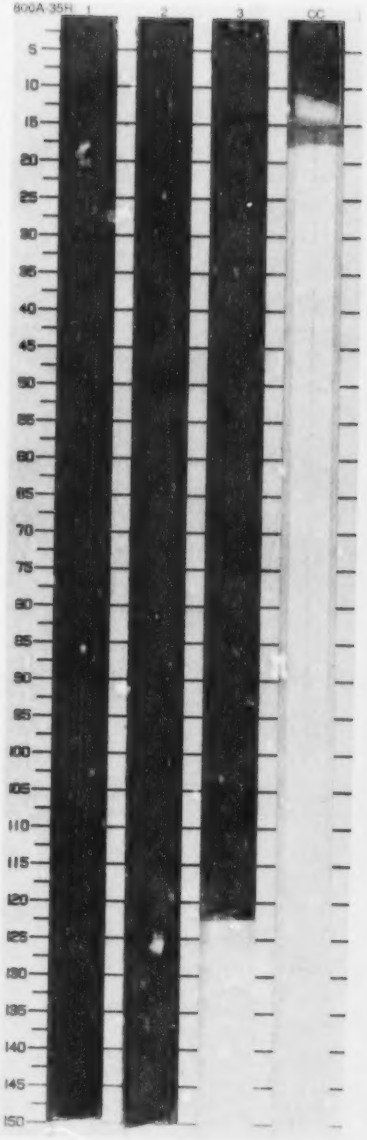
800A-35R 1
2
3
CC
5
10
15
20
25
30
35
40
45
50
55
60
65
70
75
80
85
90
95
100
105
110
115
120
125
130
135
140
145
150

SITE 800 HOLE A CORE 36R CORED INTERVAL 6001.9-6011.1 mbsl; 315.9-325.1 mbsf

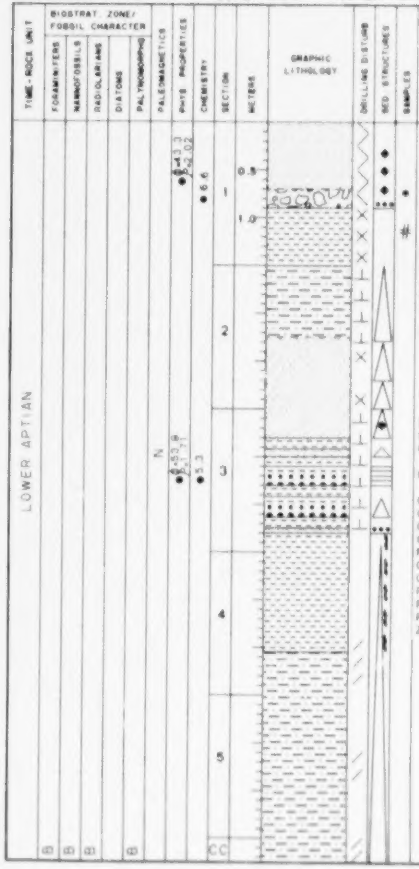
TIME-ROCK UNIT
BIOSTRAT. ZONE/ FOSSIL CHARACTER
FORAMINIFERS
NANNOFOSSILS
RADIOLARIANS
DIATOMS
PALYNOMORPHS
PALEOMAGNETICS
PHYS. PROPERTIES
CHEMISTRY
SECTION
METERS
GRAPHIC LITHOLOGY
DRILLING DISTURB.
SED. STRUCTURES
SAMPLES
LOWER APTIAN
B
B
B
B
N
φ=43.3
γ=2.02
φ=53.9
γ=2.17
6.6
5.3
1
2
3
4
5
CC
0.5
1.0
#

LITHOLOGIC DESCRIPTION

VOLCANICLASTIC TURBIDITES, SANDSTONE, and CLAYSTONE

Major lithology: VOLCANICLASTIC TURBIDITES, SANDSTONE and CLAYSTONE bluish gray (5BG 4/1), grading upward to pelagic CALCAREOUS CLAYSTONE, with the bases of beds cutting into the claystone. Turbidite beds up to 4 m thick, some are amalgamated flows; claystone rip-up clasts are common. Clasts are subrounded volcanic rock fragments and volcanic glass, with feldspar, pyroxene, and iron oxides. Matrix is locally altered to clay or zeolites. XRD from Section 4, 3 cm indicates calcite, plagioclase and smectite.

Minor lithology: CALCAREOUS CLAYSTONE, reddish brown (5YR 3/1), with variable proportions of calcite, iron oxides, volcanic glass, zeolites, nannofossils, and rare radiolarians. Generally massive and featureless. Usually altered green at fractures and basal contacts of turbidite beds (alteration a few millimeters thick). Rare bioturbation. XRD from Section 1, 97 cm indicates calcite and clays.

SLIDE SUMMARY (%):

|  | 1, 77<br>D | 1, 117<br>D |
|---|---|---|
| TEXTURE: |  |  |
| Sand | 50 | — |
| Silt | 20 | 2 |
| Clay | 30 | 98 |
| COMPOSITION: |  |  |
| Calcite | 10 | 15 |
| Clay | 2 | 25 |
| Glass | 45 | 30 |
| Igneous rock fragments | 30 | — |
| Nannofossils | — | 5 |
| Opaques | 5 | — |
| Oxide | 2 | 15 |
| Pyroxene | 3 | — |
| Radiolarians | — | 2 |
| Red algae | 3 | — |
| Zeolite | — | 5 |

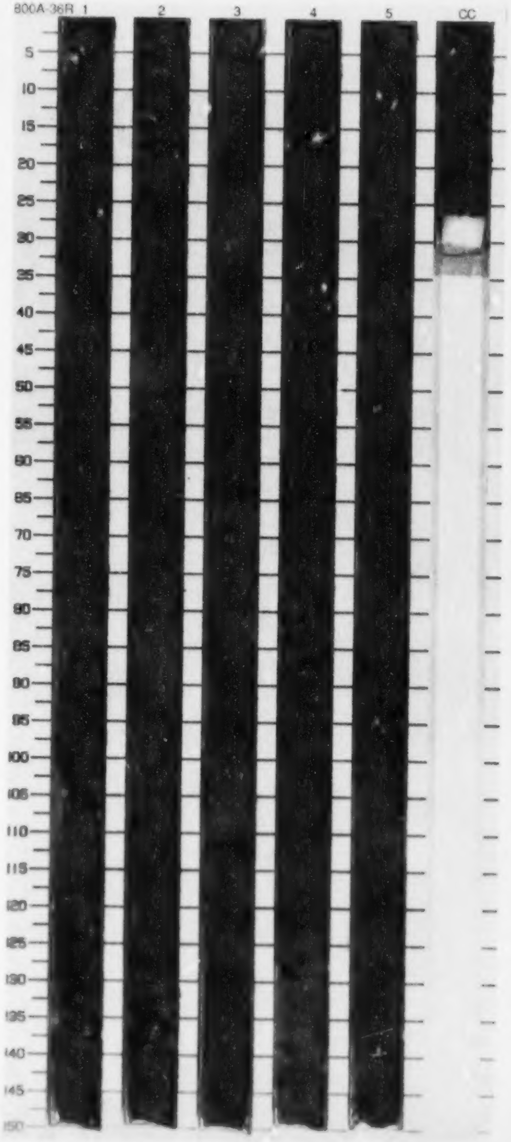
800A-36R 1
2
3
4
5
CC
5
10
15
20
25
30
35
40
45
50
55
60
65
70
75
80
85
90
95
100
105
110
115
120
125
130
135
140
145
150

SITE 800 HOLE A CORE 37R CORED INTERVAL 6011.1-3020.5 mbsl; 225.1-334.5 mbsf

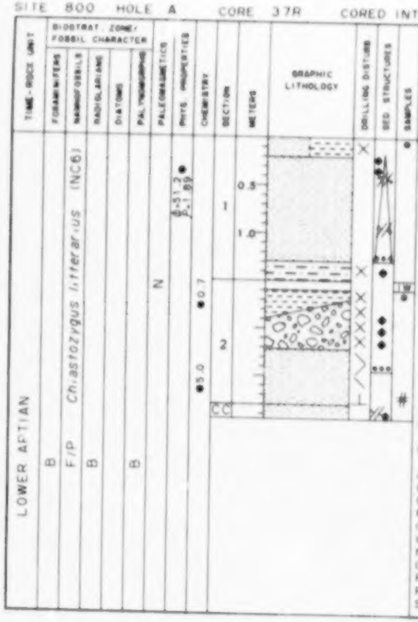
TIME-ROCK UNIT
BIOSTRAT. ZONE/ FOSSIL CHARACTER
FORAMINIFERS
NANNOFOSSILS
RADIOLARIANS
DIATOMS
PALYNOMORPHS
PALEOMAGNETICS
PHYS. PROPERTIES
CHEMISTRY
SECTION
METERS
GRAPHIC LITHOLOGY
DRILLING DISTURB.
SED. STRUCTURES
SAMPLES
LOWER APTIAN
B
F/P Chiastozygus litterarius (NC6)
B
B
N
ϕ=51.2
ρ=1.89
●0.7
●5.0
1
2
CC
0.5
1.0

LITHOLOGIC DESCRIPTION

VOLCANICLASTIC SANDSTONE

Major lithology: VOLCANICLASTIC SANDSTONE, dark greenish gray (5BG 4/1) overall, locally conglomeratic, with pale green, greenish black, and dark reddish brown grains, and bluish gray to greenish gray (5B 5/1 to 5BG 5/1) rip-up clasts. Grains are medium- to very coarse-grained, angular to subangular, altered, volcanic glass fragments, feldspars, volcanic rock fragments, and oxides; rip-up clasts are 5 to 60 mm in length, and composed of rounded, volcaniclastic to calcareous claystone, with nannofossils, sponge spicules, volcanic glass, metallic oxides, and rare foraminifers.

Minor lithology: TUFFACEOUS CLAYSTONE, olive gray to greenish gray (5GY 4/1 to 5Y 3/2), soft, plastic to scaly, noncalcareous, contains volcanic glass and clay.

SLIDE SUMMARY (%):

| | 1, 5<br>M | 2, 26<br>M | 2, 123<br>D |
|---|---|---|---|
| TEXTURE: | | | |
| Sand | 20 | Tr | 80 |
| Silt | 30 | 30 | 10 |
| Clay | 50 | 70 | 10 |
| COMPOSITION: | | | |
| Accessory minerals | 5 | Tr | — |
| Calcite | 15 | Tr | 5 |
| Clay | 50 | 50 | 5 |
| Feldspar | Tr | — | 1 |
| Glass | 10 | 45 | 66 |
| Igneous rock fragments | — | — | 20 |
| Nannofossils | 5 | — | — |
| Oxide | 10 | 5 | — |
| Pyroxene | — | — | 3 |
| Rock fragment | Tr | — | — |
| Spicules | 5 | — | — |

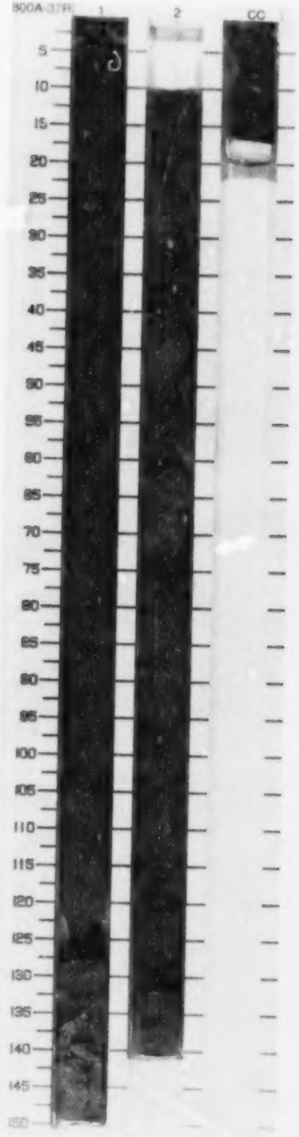
800A-37R
1
2
CC
5
10
15
20
25
30
35
40
45
50
55
60
65
70
75
80
85
90
95
100
105
110
115
120
125
130
135
140
145
150

SITE 800 HOLE A CORE 38R CORED INTERVAL 6020.5-6029.8 mbsl; 334.5-343.8 mbsf

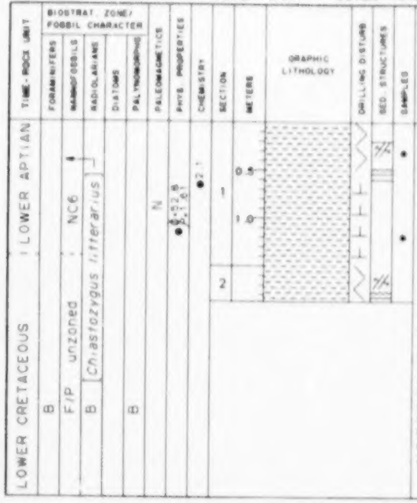
TIME-ROCK UNIT
BIOSTRAT. ZONE/ FOSSIL CHARACTER
FORAMINIFERS
NANNOFOSSILS
RADIOLARIANS
DIATOMS
PALYNOMORPHS
PALEOMAGNETICS
PHYS. PROPERTIES
CHEMISTRY
SECTION
METERS
GRAPHIC LITHOLOGY
DRILLING DISTURB.
SED. STRUCTURES
SAMPLES
LOWER CRETACEOUS
LOWER APTIAN
B
F/P
unzoned
NC6
B
Chiastozygus litterarius
B
N
52.8
1.61
2.1
1
2
0.5
1.0

LITHOLOGIC DESCRIPTION

CLAYSTONE

Major lithology: CLAYSTONE, with distinct layers and front oxidation/reduction, greenish gray to reddish brown (5GY 5/1 to 5YR 4/2), generally massive, locally laminated, locally bioturbated. Fractures between Section 1, 25-40 cm are filled with hard, dense manganite.

SLIDE SUMMARY (%):

| | 1, 36<br>M | 1, 122<br>D |
|---|---|---|
| TEXTURE: | | |
| Sand | — | Tr |
| Silt | — | 35 |
| Clay | 100 | 65 |
| COMPOSITION: | | |
| Accessory minerals | — | 5 |
| Calcite | — | 5 |
| Clay | 30 | 55 |
| Glass | — | 20 |
| Nannofossils | — | Tr |
| Oxide | 70 | 5 |
| Zeolite | — | 10 |

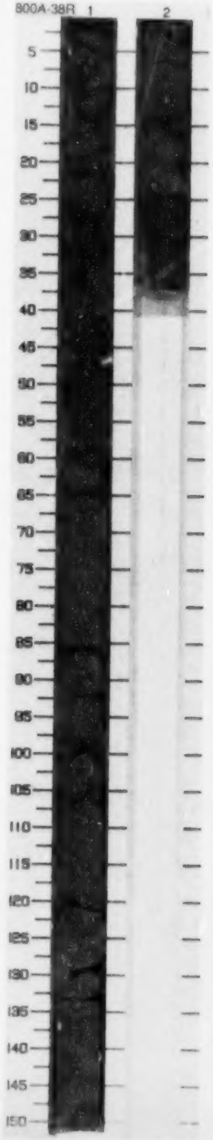
800A-38R
1
2
5
10
15
20
25
30
35
40
45
50
55
60
65
70
75
80
85
90
95
100
105
110
115
120
125
130
135
140
145
150

SITE 800 HOLE A CORE 39R CORED INTERVAL 6029.8-6039.1 mbsl; 343.8-353.1 mbsf

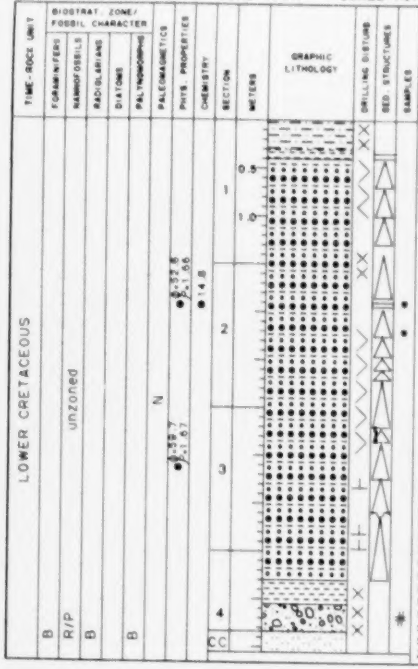
TIME-ROCK UNIT
BIOSTRAT. ZONE/ FOSSIL CHARACTER
FORAMINIFERS
NANNOFOSSILS
RADIOLARIANS
DIATOMS
PALYNOMORPHS
PALEOMAGNETICS
PHYS. PROPERTIES
CHEMISTRY
SECTION
METERS
GRAPHIC LITHOLOGY
DRILLING DISTURB.
SED. STRUCTURES
SAMPLES
LOWER CRETACEOUS
B
R/P
unzoned
B
B
N
φ-52.8
γ-1.66
φ-59.7
γ-1.67
14.8
1
2
3
4
CC
0.5
1.0

## LITHOLOGIC DESCRIPTION

VOLCANICLASTIC TURBIDITES

Major lithology: VOLCANICLASTIC TURBIDITES, consisting of SANDSTONE, dark greenish gray (5BG 4/1), fine to silty, moderately well sorted, angular to subrounded grains, planar to cross-laminated, contorted lamination probably representing wholesale disturbed bedding rather than Bouma C unit. Grades upward to SILTY CLAYSTONE, massive to finely laminated, slightly calcareous, containing volcanic glass and metal oxides, with minor calcite and nannofossils. Turbidite beds 20 to 50 cm thick display gradual color change from green (5G 5/1) (reduced) to reddish brown (5YR 4/3 to 10YR 4/3) (oxidized), and then abrupt transformation back to green (reduction) within 4 cm of overlying scoured base of volcaniclastic turbidite. Sandstone dikes in Section 2, 60-66 cm, and 123-130 cm.

Minor lithology: CLAYSTONE, grayish brown (5YR 3/3) grading to greenish gray (5BG 5/1), massive.

SLIDE SUMMARY (%):

| | 2, 44<br>D | 2, 70<br>D | 4, 70<br>D | 4, 70<br>M |
|---|---|---|---|---|
| TEXTURE | | | | |
| Sand | 10 | 20 | 2 | — |
| Silt | 30 | 50 | 25 | 30 |
| Clay | 60 | 30 | 73 | 70 |
| COMPOSITION | | | | |
| Accessory minerals | Tr | Tr | — | — |
| Calcite | Tr | 5 | — | 2 |
| Clay | 60 | 20 | 51 | — |
| Feldspar | — | — | 1 | — |
| Glass | 15 | 75 | 20 | 72 |
| Igneous rock fragments | — | — | 5 | 5 |
| Oxide | 15 | Tr | 2 | 3 |
| Pellets | — | — | Tr | — |
| Pyroxene | — | — | 5 | 3 |
| Radiolarians | — | — | Tr | 10 |
| Silica | — | — | 10 | — |
| Smectite | — | — | 3 | 2 |
| Spicules | — | — | 3 | — |
| Zeolite | 5 | — | — | — |

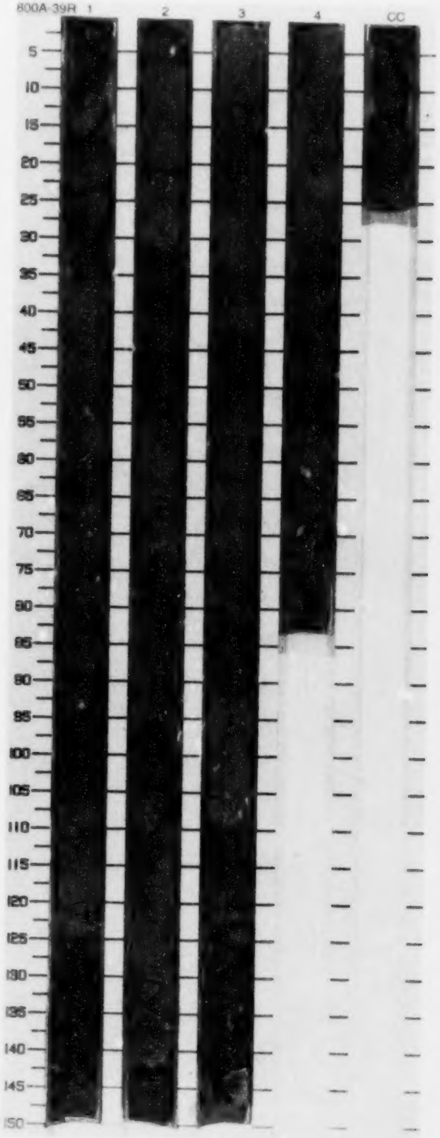
800A-39R 1
2
3
4
CC
5
10
15
20
25
30
35
40
45
50
55
60
65
70
75
80
85
90
95
100
105
110
115
120
125
130
135
140
145
150

SITE 800 HOLE A CORE 40R CORED INTERVAL 6039.1-6048.5 mbsl; 353.1-362.5 mbsf

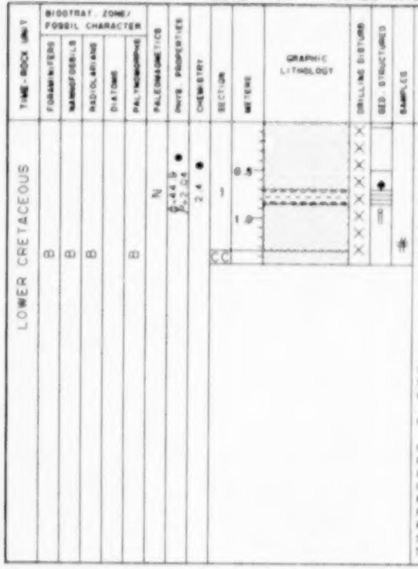
TIME-ROCK UNIT
BIOSTRAT. ZONE/ FOSSIL CHARACTER
FORAMINIFERS
NANNOFOSSILS
RADIOLARIANS
DIATOMS
PALYNOMORPHS
PALEOMAGNETICS
PHYS. PROPERTIES
CHEMISTRY
SECTION
METERS
GRAPHIC LITHOLOGY
DRILLING DISTURB.
SED. STRUCTURES
SAMPLES
LOWER CRETACEOUS
B
B
B
B
N
φ=44.5
γ=2.04
2.4
1
CC
0.5
1.0

LITHOLOGIC DESCRIPTION

VOLCANICLASTIC SANDSTONE

Major lithology: VOLCANICLASTIC SANDSTONE, greenish gray (5G 4/1, 5BG 4/1, 5Y 4/1), massive to laminated (laminations very thin and silty), fine-grained, moderately to poorly sorted. Clasts are mainly volcanic rock fragments in a clayey matrix. Larger, angular clasts of claystone are found in Section 1 at 30, 70 and 130 cm. Sandstone is 90% of core.

Minor lithology: CLAYSTONE, reddish brown (10YR 4/3, 10 YR 3/2), forms one 15 cm-thick layer between sandstone beds, finely laminated, and also is present as rip-up clasts in the sandstone. Claystone is 10% of core.

SLIDE SUMMARY (%):

| | 1, 120<br>D |
|---|---|
| TEXTURE: | |
| Sand | 60 |
| Silt | 20 |
| Clay | 20 |
| COMPOSITION: | |
| Calcite | 10 |
| Glass | 46 |
| Igneous rock fragments | 20 |
| Oxide | 3 |
| Pyroxene | 5 |
| Radiolarians | 2 |
| Red algae | 1 |
| Silica | 10 |
| Smectite | 3 |

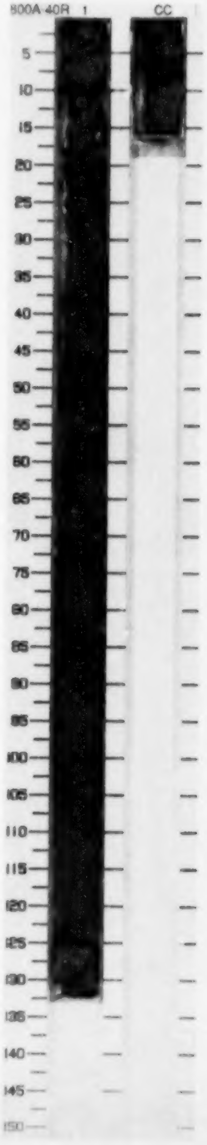
800A-40R 1
CC
5
10
15
20
25
30
35
40
45
50
55
60
65
70
75
80
85
90
95
100
105
110
115
120
125
130
135
140
145
150

SITE 800 HOLE A CORE 41R CORED INTERVAL 6048.5-6054.6 mbsl; 362.5-368.6 mbsf

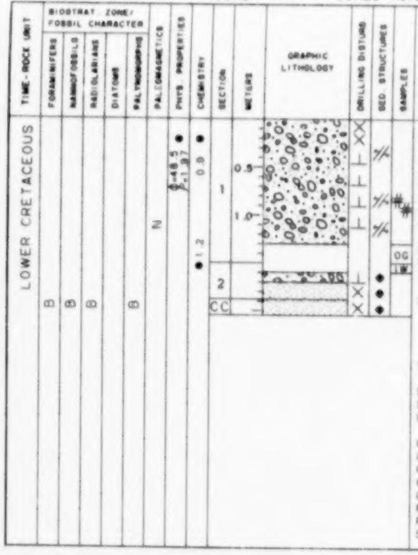
TIME-ROCK UNIT
BIOSTRAT. ZONE/ FOSSIL CHARACTER
FORAMINIFERS
NANNOFOSSILS
RADIOLARIANS
DIATOMS
PALYNOMORPHS
PALEOMAGNETICS
PHYS. PROPERTIES
CHEMISTRY
SECTION
METERS
GRAPHIC LITHOLOGY
DRILLING DISTURB.
SED. STRUCTURES
SAMPLES
LOWER CRETACEOUS
B
B
B
B
N
ϕ=48.5
ρ=1.97
0.9
1.2
1
2
CC
0.5
1.0
OG
IW

LITHOLOGIC DESCRIPTION

VOLCANICLASTIC SANDSTONE and BRECCIA

Major lithologies:
a. VOLCANICLASTIC SANDSTONE and
b. BRECCIA, dark greenish gray (5G 4/1, 5BG 4/1, 5BG 3/1, 5BG 6/1), massive, fine-grained to silty, poorly sorted, with clasts mainly volcanic rock fragments and claystone. Two generations of fractures noted in breccia: 1) early, filled with fine sandstone, 2) late network of crosscutting calcite and palygorskite-filled fractures.

Minor lithology: CLAYSTONE BRECCIA, greenish-gray (5GY 5/1, 5BG 4/1), with irregular fragments of different color; fractures filled with poorly sorted SANDSTONE and CLAYSTONE.

SLIDE SUMMARY (%):

| | 1, 87 D | 1, 90 D |
|---|---|---|
| TEXTURE: | | |
| Sand | 10 | 70 |
| Silt | 90 | 30 |
| COMPOSITION: | | |
| Calcite | 15 | 5 |
| Clay | — | 7 |
| Glass | 62 | 65 |
| Igneous rock fragments | 10 | 5 |
| Opaques | 3 | 10 |
| Pyroxene | — | 5 |
| Radiolarians | — | 3 |
| Smectite | 10 | — |

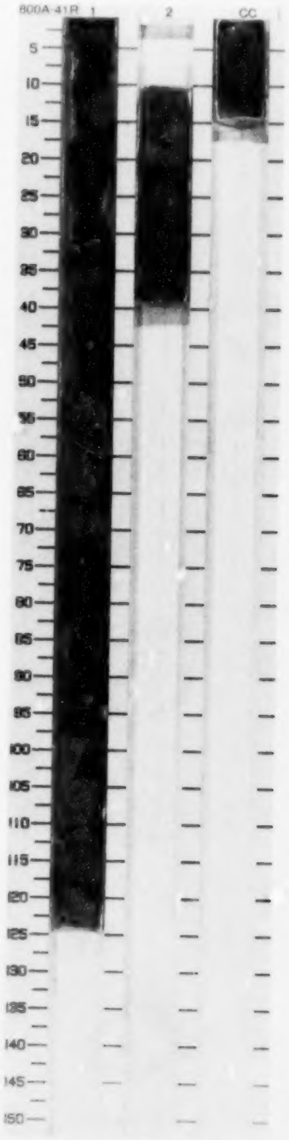
800A-41R 1
2
CC
5
10
15
20
25
30
35
40
45
50
55
60
65
70
75
80
85
90
95
100
105
110
115
120
125
130
135
140
145
150

SITE 800 HOLE A CORE 42R CORED INTERVAL 6054.6-6060.7 mbsl; 368.6-374.7 mbsf

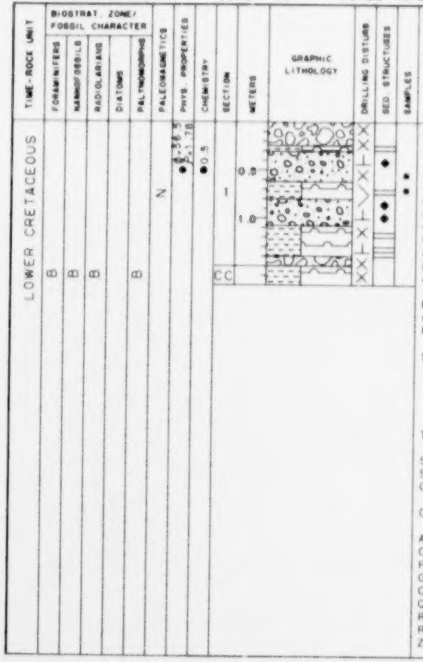
TIME-ROCK UNIT
BIOSTRAT. ZONE/ FOSSIL CHARACTER
FORAMINIFERS
NANNOFOSSILS
RADIOLARIANS
DIATOMS
PALYNOMORPHS
PALEOMAGNETICS
PHYS. PROPERTIES
CHEMISTRY
SECTION
METERS
GRAPHIC LITHOLOGY
DRILLING DISTURB.
SED. STRUCTURES
SAMPLES
LOWER CRETACEOUS
B
B
B
B
N
φ=56.5
γ=1.78
0.5
1
CC
0.5
1.0

LITHOLOGIC DESCRIPTION

CLAYSTONE BRECCIA and RADIOLARIAN CLAYSTONE to RADIOLARITE

Major lithologies:

a. CLAYSTONE BRECCIA with dark greenish gray (5G 4/1, 5GY 4/1, 5BG 4/1) clasts in a greenish gray 5GY 5/1, 5G 5/1) matrix, 45% of core, with angular, internally fractured clasts up to 5 cm long, in a poorly sorted SANDSTONE to CLAYEY SILTSTONE matrix. Claystone clasts contain radiolarians and volcanic glass.

b. RADIOLARIAN CLAYSTONE to RADIOLARITE, dark grayish brown (10YR 3/2, 7.5YR 4/2) with greenish gray (5G 6/1, 5GY 6/1) mottles, 50% of core, contains smectite. Radiolarians form millimeter scale laminations. At Section 1, 116-118 cm, a CHERT nodule formed in a radiolarian lamination.

Minor lithology: SANDSTONE, greenish gray (5BG 5/1, 5G 4/1), consisting mainly of volcanic rock fragments and glass and claystone chips, in beds with basal scour cutting RADIOLARIAN CLAYSTONE. Comprises 5% of core.

SLIDE SUMMARY (%):

| | 1, 56<br>D | 1, 76<br>D |
|---|---|---|
| **TEXTURE:** | | |
| Sand | — | 20 |
| Silt | 5 | 10 |
| Clay | 95 | 70 |
| **COMPOSITION:** | | |
| Accessory minerals | Tr | Tr |
| Clay | 90 | 68 |
| Feldspar | 1 | 2 |
| Glass | 3 | 1 |
| Opaques | 2 | 3 |
| Quartz | 1 | — |
| Radiolarians | 1 | 25 |
| Rock fragment | 2 | — |
| Zeolite | — | 1 |

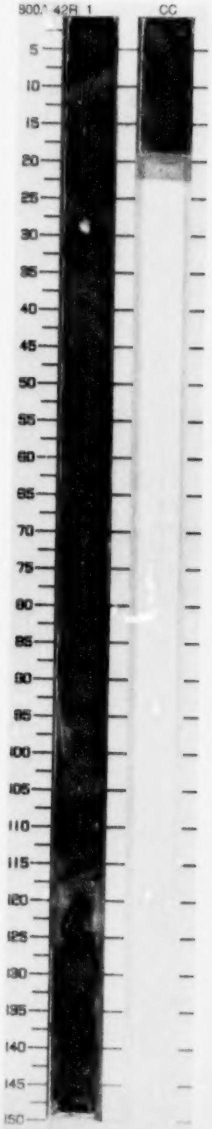
800A 42R 1
CC
5
10
15
20
25
30
35
40
45
50
55
60
65
70
75
80
85
90
95
100
105
110
115
120
125
130
135
140
145
150

SITE 800 HOLE A CORE 43R CORED INTERVAL 6060.7-6069.7 mbsl; 374.7-383.7 mbsf

| TIME-ROCK UNIT | BIOSTRAT. ZONE/ FOSSIL CHARACTER | | | | | PALEOMAGNETICS | PHYS. PROPERTIES | CHEMISTRY | SECTION | METERS | GRAPHIC LITHOLOGY | DRILLING DISTURB. | SED. STRUCTURES | SAMPLES |
|---|---|---|---|---|---|---|---|---|---|---|---|---|---|---|
| | FORAMINIFERS | NANNOFOSSILS | RADIOLARIANS | DIATOMS | PALYNOMORPHS | | | | | | | | | |
| LOWER CRETACEOUS | B | B | B | | B | N | φ=57.4<br>γ=1.74 | ●0.6 | 1 | 0.5<br>1.0 | | X X X X X X X | | * |

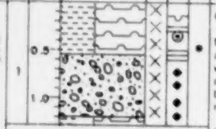

LITHOLOGIC DESCRIPTION

CLAYEY RADIOLARITE and CLAYSTONE BRECCIA

Major lithologies:
a. CLAYEY RADIOLARITE, gray (5Y 5/1), bluish gray (5B 5/1), and grayish brown (5YR3/2), with occasional laminations. 30% of core, contains up to 50% radiolarians and minor feldspar, oxides and zeolites, and
b. CLAYSTONE BRECCIA, bluish grey (5B 5/1), randomly oriented trains of clasts may represent a debris flow. 50% of core.

Minor lithology: CHERT with PORCELLANITE, grayish red (5R 4/2), the porcellanite forms lighter colored, softer, duller layers in the chert, millimeter-scale laminations. Together these make up 20% of the core.

SLIDE SUMMARY (%):

| | 1, 50<br>D |
|---|---|
| TEXTURE: | |
| Sand | 30 |
| Silt | 25 |
| Clay | 45 |
| COMPOSITION: | |
| Clay | 45 |
| Feldspar | 3 |
| Oxide | 1 |
| Quartz | 1 |
| Radiolarians | 50 |
| Zeolite | Tr |

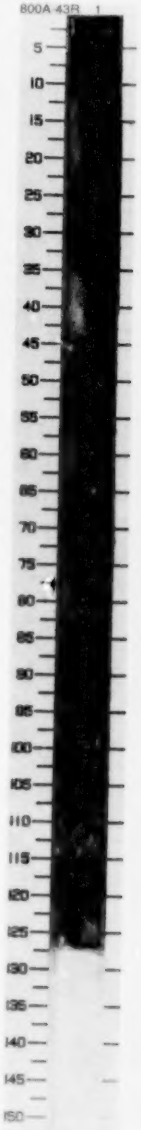

SITE 800 HOLE A CORE 44R CORED INTERVAL 6069.7-6079.1 mbsl; 383.7-393.1 mbsf

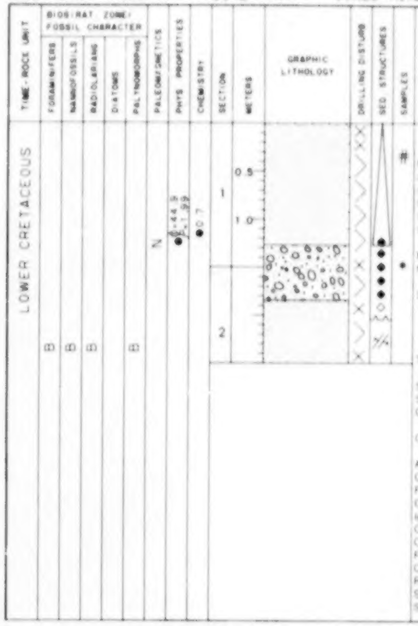
TIME-ROCK UNIT
BIOSTRAT. ZONE/ FOSSIL CHARACTER
FORAMINIFERS
NANNOFOSSILS
RADIOLARIANS
DIATOMS
PALYNOMORPHS
PALEOMAGNETICS
PHYS. PROPERTIES
CHEMISTRY
SECTION
METERS
GRAPHIC LITHOLOGY
DRILLING DISTURB.
SED. STRUCTURES
SAMPLES
LOWER CRETACEOUS
B
B
B
B
N
φ=44.9
ρ=1.99
●0.7
1
2
0.5
1.0
#

LITHOLOGIC DESCRIPTION

SANDSTONE and CLAYSTONE BRECCIA

Major lithologies:
a. SANDSTONE: dark greenish gray to dark gray (5GY 4/1 to 5Y 4/1); volcaniclastic; fine- to medium grained; massive; 74% of core; and
b. CLAYSTONE BRECCIA: with reddish brown (5YR 4/4, 5YR 3/3) claystone clasts containing traces of radiolarians, oxides and feldspar, in a greenish gray (5G 5/1) sandstone matrix with trains of clasts in different concentrations; 25% of core.

Minor lithology: CLAYSTONE: dark reddish brown (5YR 3/2); upper contact with breccia is flame structures; comprises 1% of core.

SLIDE SUMMARY (%):

| | 1, 31<br>D | 2, 2<br>M |
|---|---|---|
| TEXTURE: | | |
| Sand | 95 | — |
| Silt | 5 | 10 |
| Clay | — | 90 |
| COMPOSITION: | | |
| Accessory minerals | — | Tr |
| Clay | — | 85 |
| Feldspar | 2 | 2 |
| Glass | 60 | — |
| Igneous rock fragments | 25 | — |
| Opaques | 5 | — |
| Oxide | — | 5 |
| Pyroxene | 5 | — |
| Quartz | — | 1 |
| Radiolarians | — | 1 |
| Silica | — | 5 |
| Smectite | 3 | — |

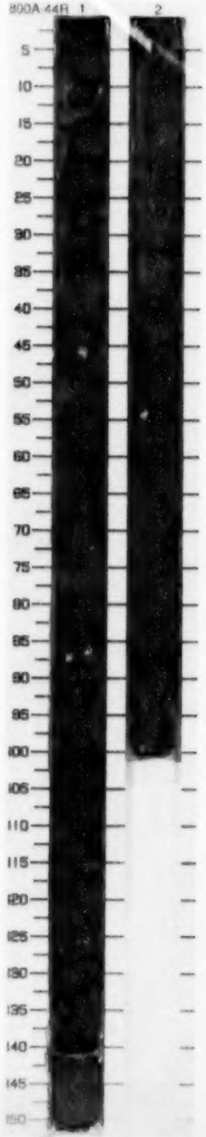
800A-44R 1
2
5
10
15
20
25
30
35
40
45
50
55
60
65
70
75
80
85
90
95
100
105
110
115
120
125
130
135
140
145
150

SITE 800 HOLE A CORE 45R CORED INTERVAL 6079.1-6088.5 mbsl; 393.1-402.5 mbsf

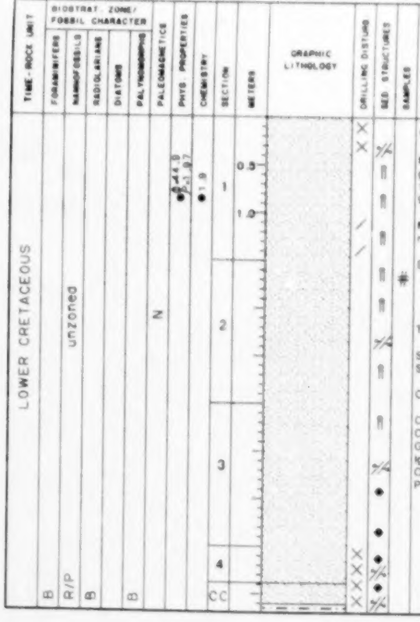
TIME-ROCK UNIT
BIOSTRAT. ZONE/ FOSSIL CHARACTER
FORAMINIFERS
NANNOFOSSILS
RADIOLARIANS
DIATOMS
PALYNOMORPHS
PALEOMAGNETICS
PHYS. PROPERTIES
CHEMISTRY
SECTION
METERS
GRAPHIC LITHOLOGY
DRILLING DISTURB.
SED. STRUCTURES
SAMPLES
LOWER CRETACEOUS
unzoned
B
R/P
B
B
N
φ=44.0
ρ=1.97
●1.9
1
2
3
4
CC
0.5
1.0
#

LITHOLOGIC DESCRIPTION

VOLCANICLASTIC SANDSTONE

Major lithology: VOLCANICLASTIC SANDSTONE, dusky green (5G 3/2) to dark greenish gray (5G 4/1, 5BG 4/1), massive, medium-grained, poorly sorted, with brownish gray (5YR 3/1) clay rip-up clasts, fluid escape structures, and calcite-filled fractures dipping 45° to 60°, 99% of core.

Minor lithology: SILTY CLAYSTONE, olive black (5Y 2/1) to brownish black (5YR 2/1), massive, 1% of core.

SLIDE SUMMARY (%):

| | 2, 24<br>D |
|---|---|
| TEXTURE: | |
| Sand | 95 |
| Silt | 5 |
| COMPOSITION: | |
| Calcite | 5 |
| Chlorite | Tr |
| Glass | 35 |
| Igneous rock fragments | 54 |
| Opaques | 4 |
| Pyroxene | 2 |

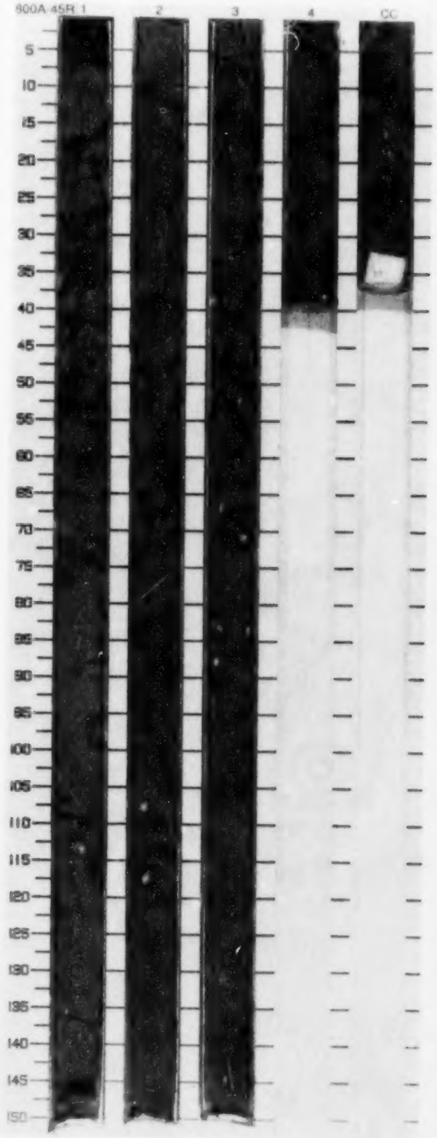
800A-45R 1
2
3
4
CC
5
10
15
20
25
30
35
40
45
50
55
60
65
70
75
80
85
90
95
100
105
110
115
120
125
130
135
140
145
150

SITE 800 HOLE A CORE 46R CORED INTERVAL 6088.5-6097.9 mbsl; 402.5-411.9 mbsf

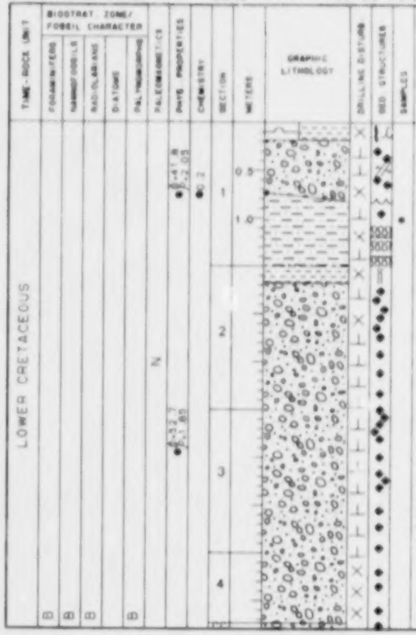
TIME-ROCK UNIT
BIOSTRAT. ZONE/ FOSSIL CHARACTER
FORAMINIFERS
NANNOFOSSILS
RADIOLARIANS
DIATOMS
PALYNOMORPHS
PALEOMAGNETICS
PHYS. PROPERTIES
CHEMISTRY
SECTION
METERS
GRAPHIC LITHOLOGY
DRILLING DISTURB.
SED. STRUCTURES
SAMPLES
LOWER CRETACEOUS
B
B
B
B
N
φ=41.8
γ=2.05
φ=32.7
γ=1.85
0.2
1
2
3
4
0.5
1.0

LITHOLOGIC DESCRIPTION

BRECCIA

Major Lithology: BRECCIA, bluish gray (5B 5/1, 5BG 5/1) to greenish gray (5GY 6/1), poorly sorted, matrix supported, massive, with clasts of volcanic rock fragments and PELAGIC CLAYSTONE. In Section 2 the breccia is oxidized to medium gray (N5) and grayish red (5R 4/2) from 18 to 150 cm. Matrix is greenish gray (5GY 6/1) sand; clasts are darker bluish gray (5BG 5/1) and reddish brown (10R 3/4). Breccia is 75% of core.

Minor lithologies:
a. SILTY CLAYSTONE, moderate brown (5YR 3/4) with flaser laminae.
b. RADIOLARIAN CLAYSTONE, dark reddish brown (10R 3/4) to grayish red (5R 4/2), interlaminated on a scale of millimeters to centimeters. XRD of radiolarian claystone at Section 1, 93 cm contains smectite and goethite(?).

SLIDE SUMMARY (%):

| | 1, 104 |
|---|---|
| | D |
| **TEXTURE:** | |
| Sand | 10 |
| Silt | 30 |
| Clay | 60 |
| **COMPOSITION:** | |
| Accessory minerals | Tr |
| Clay | 52 |
| Feldspar | 5 |
| Oxide | 3 |
| Radiolarians | 35 |

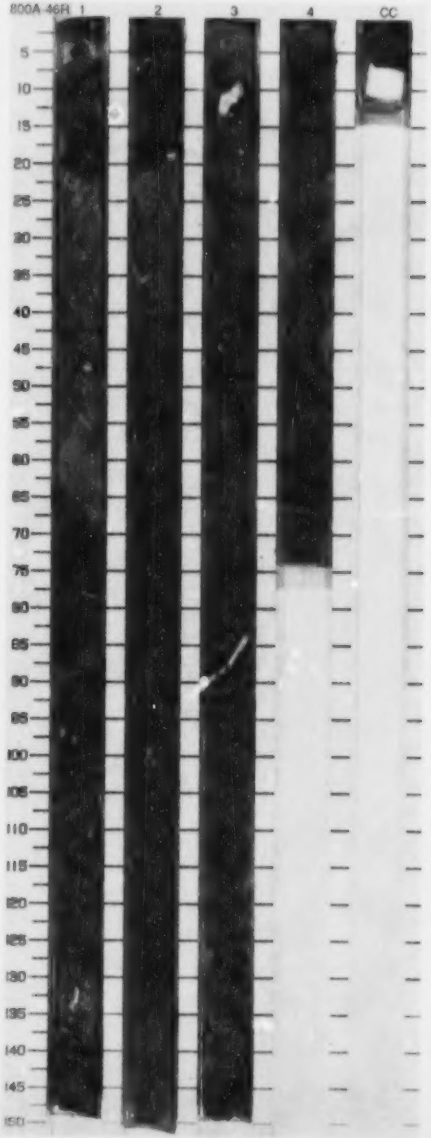
800A-46R
1
2
3
4
CC
5
10
15
20
25
30
35
40
45
50
55
60
65
70
75
80
85
90
95
100
105
110
115
120
125
130
135
140
145
150

SITE 800 HOLE A CORE 47R CORED INTERVAL 6097.9-6107.4 mbsl; 411.9-421.4 mbsf

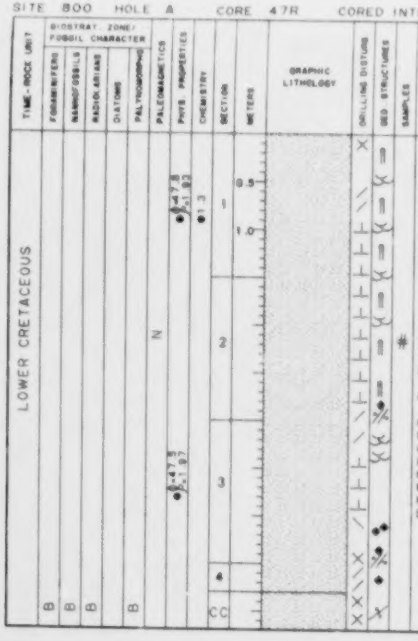
TIME-ROCK UNIT
BIOSTRAT. ZONE/ FOSSIL CHARACTER
FORAMINIFERS
NANNOFOSSILS
RADIOLARIANS
DIATOMS
PALYNOMORPHS
PALEOMAGNETICS
PHYS. PROPERTIES
CHEMISTRY
SECTION
METERS
GRAPHIC LITHOLOGY
DRILLING DISTURB.
SED. STRUCTURES
SAMPLES
LOWER CRETACEOUS
B
B
B
B
N
φ-47.8
ρ-1.93
φ-47.5
ρ-1.97
1.3
1
2
3
4
CC
0.5
1.0
#

LITHOLOGIC DESCRIPTION

VOLCANICLASTIC SANDSTONE

Major lithology: VOLCANICLASTIC SANDSTONE, dusky green to blue green (5G 3/2, 5G 4/1, 5BG4/1), partly oxidized to maroon (5R 2.5/6) in the core catcher. Clasts are matrix supported, angular to subrounded, dominantly volcanic rock fragments, with rare out-sized clasts of RADIOLARIAN CLAYSTONE. Sections 1 and 2 have abundant dish (fluid escape) structures. Millimeter-scale fractures are filled with calcite.

SLIDE SUMMARY (%):

| | |
|---|---|
| | 2, 64 |
| | D |
| TEXTURE | |
| Sand | 40 |
| Silt | 30 |
| Clay | 30 |
| COMPOSITION | |
| Calcite | 5 |
| Feldspar | 3 |
| Glass | 65 |
| Igneous rock fragments | 20 |
| Oxide | 3 |
| Pellets | 2 |
| Radiolarians | 1 |
| Smectite | 1 |

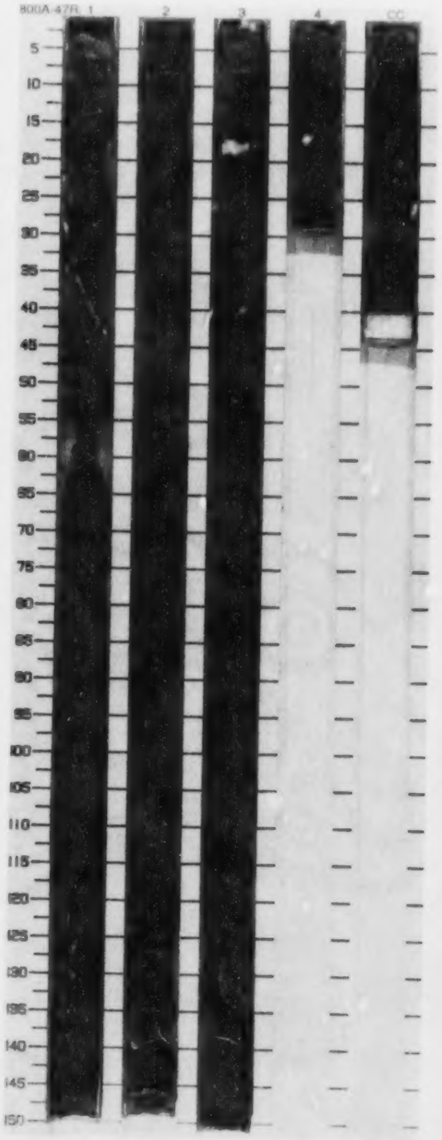
800A-47R, 1
2
3
4
CC
5
10
15
20
25
30
35
40
45
50
55
60
65
70
75
80
85
90
95
100
105
110
115
120
125
130
135
140
145
150

## SITE 800 HOLE A CORE 48R CORED INTERVAL 6107.4-6116.9 mbsl; 421.4-430.9 mbsf

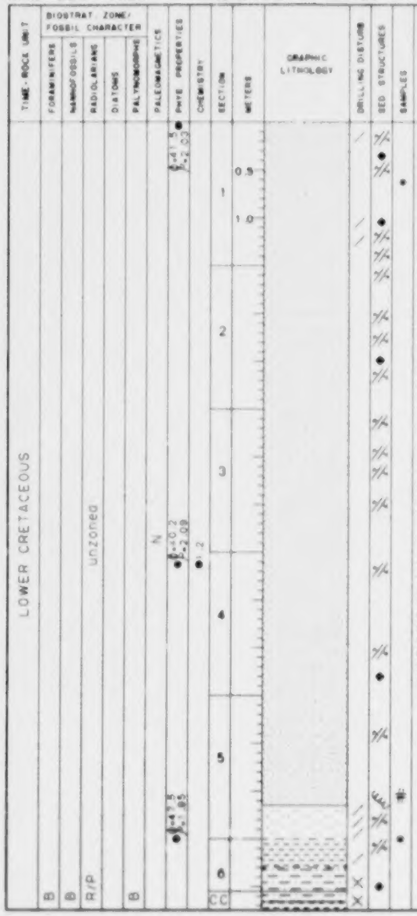
TIME-ROCK UNIT
BIOSTRAT. ZONE/ FOSSIL CHARACTER
FORAMINIFERS
NANNOFOSSILS
RADIOLARIANS
DIATOMS
PALYNOMORPHS
PALEOMAGNETICS
PHYS. PROPERTIES
CHEMISTRY
SECTION
METERS
GRAPHIC LITHOLOGY
DRILLING DISTURB.
SED. STRUCTURES
SAMPLES
LOWER CRETACEOUS
B
B
R/P
unzoned
B
N
φ=41.5
γ=2.03
φ=40.2
γ=2.09
φ=47.5
γ=1.85
1.2
1
2
3
4
5
6
CC
0.5
1.0

LITHOLOGIC DESCRIPTION

VOLCANICLASTIC SANDSTONE

Major lithology: VOLCANICLASTIC SANDSTONE, dark greenish gray (5BG 3/1 to 5BG 5/1), locally with dusky red (5R 3/2) matrix and granule-sized, fine-grained clasts; framework grains chiefly palagonized volcanic glass shards, massive structure. Horizontal calcite filled veins approximately every 10 to 30 cm. Gold/dark yellowish brown (10YR4/6) alteration of sandstone matrix and grains occurs at red/green (5R 3/2 - 5BG 4/1) redox boundaries and adjacent to calcite-filled veins.

Minor lithologies:

a. Gradational VOLCANICLASTIC SILTSTONE and SILTY CLAYSTONE below Section 5, 120 cm, dusky red (10R 3/2), mostly structureless with ill defined sandy zones. Sandstone in this section contains fresher volcanic glass than overlying sandstone. Silty claystone contains volcanic glass, oxides, clay and traces of calcite. XRD from a fracture fill at Section 5, 11 cm, contains calcite and a trace of clay.

b. SILICEOUS CLAYSTONE vein at Section 1, 73 cm, reddish brown (5YR 4/3), containing clay and silica with volcanic glass, feldspar, oxides and calcite.

c. DOLOMITIZED CLAYSTONE in Section 5, 107-118 cm, greenish gray (5GY 6/1 to 5GY 6/2) and weak red (10R 5/4); coarse grains of dolomite give interval a sandy texture; dolomitization follows silicification.

SLIDE SUMMARY (%):

| | 1, 73<br>M | 5, 111<br>M | 6, 5<br>D |
|---|---|---|---|
| TEXTURE: | | | |
| Sand | Tr | — | 15 |
| Silt | 5 | — | 35 |
| Clay | 95 | 95 | 50 |
| COMPOSITION: | | | |
| Calcite | 5 | — | 5 |
| Clay | 45 | 5 | 20 |
| Dolomite | — | 82 | — |
| Feldspar | 5 | — | — |
| Glass | 10 | 5 | 40 |
| Nannofossils | — | Tr | — |
| Oxide | 5 | 5 | 35 |
| Quartz | — | — | Tr |
| Silica | 30 | 2 | — |
| Smectite | — | 1 | — |

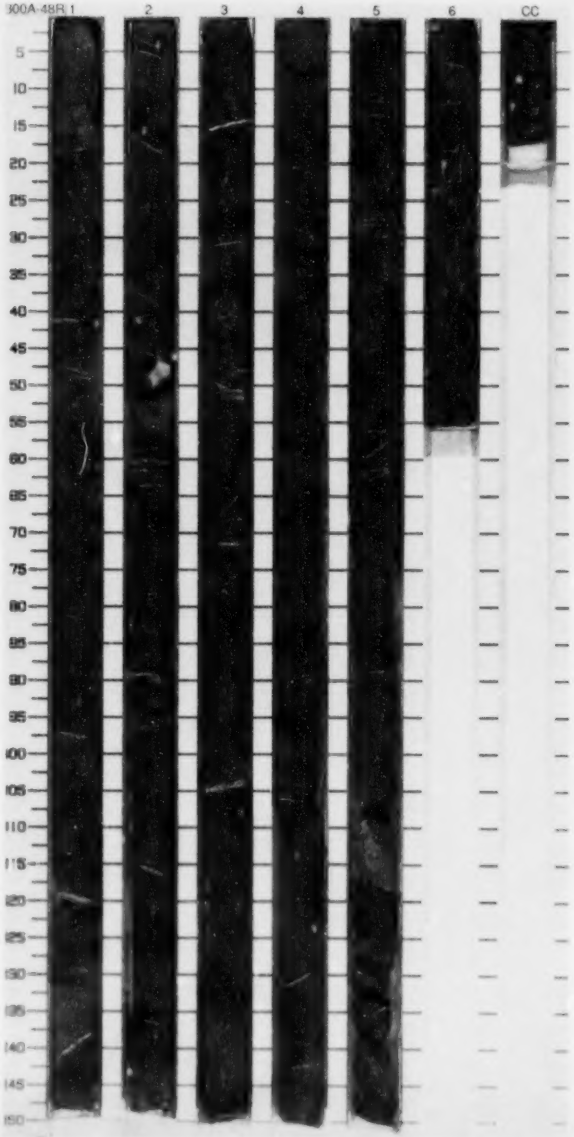
800A-48R 1
2
3
4
5
6
CC
5
10
15
20
25
30
35
40
45
50
55
60
65
70
75
80
85
90
95
100
105
110
115
120
125
130
135
140
145
150

SITE 800 HOLE A CORE 49R CORED INTERVAL 6116.9-6126.2 mbsl; 430.9-440.2 mbsf

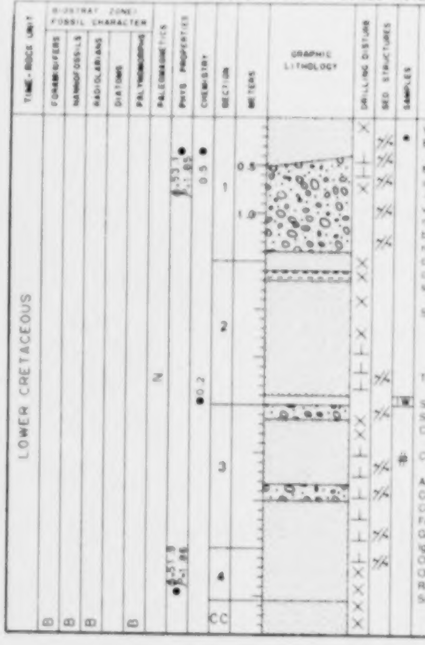
TIME-ROCK UNIT
BIOSTRAT. ZONE/ FOSSIL CHARACTER
FORAMINIFERS
NANNOFOSSILS
RADIOLARIANS
DIATOMS
PALYNOMORPHS
PALEOMAGNETICS
PHYS. PROPERTIES
CHEMISTRY
SECTION
METERS
GRAPHIC LITHOLOGY
DRILLING DISTURB.
SED. STRUCTURES
SAMPLES
LOWER CRETACEOUS
B
B
B
B
N
φ=53.1
γ=1.85
φ=51.8
γ=1.86
0.5
0.2
1
2
3
4
CC
0.5
1.0

LITHOLOGIC DESCRIPTION

VOLCANICLASTIC SANDSTONE, VOLCANICLASTIC SILTSTONE and VOLCANICLASTIC BRECCIA

Major lithologies:

a. VOLCANICLASTIC SANDSTONE, very dusky red (10R 2/2) to dark greenish gray (5GY 4/1), very fine to silty, with subrounded to subangular clasts consisting chiefly of devitrified volcanic glass grains and igneous rock fragments with oxides and minor feldspar, generally massive, with some hints of planar lamination. Sandstone grades to

b. VOLCANICLASTIC SILTSTONE with similar composition and color. Color changes define redox boundaries near veins and compositional changes in sandstone.

c. VOLCANICLASTIC BRECCIA, clasts of above lithologies are principally separated by calcite or greenish black (5G 2/1) authigenic clay veins, sedimentary matrix (sandstone or siltstone) is rare. Calcite-filled fractures.

SLIDE SUMMARY (%):

| | 1, 18<br>D | 3, 55<br>D |
|---|---|---|
| TEXTURE: | | |
| Sand | 60 | 60 |
| Silt | 30 | 40 |
| Clay | 10 | — |
| COMPOSITION: | | |
| Accessory minerals | 5 | — |
| Calcite | — | 2 |
| Clay | 10 | — |
| Feldspar | 5 | — |
| Glass | 15 | 62 |
| Igneous rock fragments | 50 | 3 |
| Opaques | — | 10 |
| Oxide | 15 | 5 |
| Radiolarians | — | 8 |
| Smectite | — | 10 |

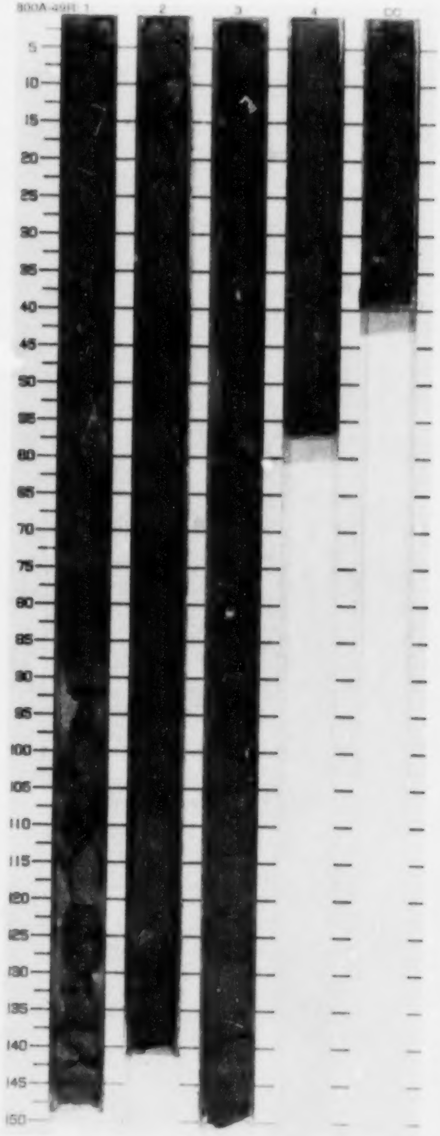
800A-49R 1
2
3
4
CC
5
10
15
20
25
30
35
40
45
50
55
60
65
70
75
80
85
90
95
100
105
110
115
120
125
130
135
140
145
150

SITE 800 HOLE A CORE 50R CORED INTERVAL 6126.2-6135.6 mbsl; 440.2-449.6 mbsf

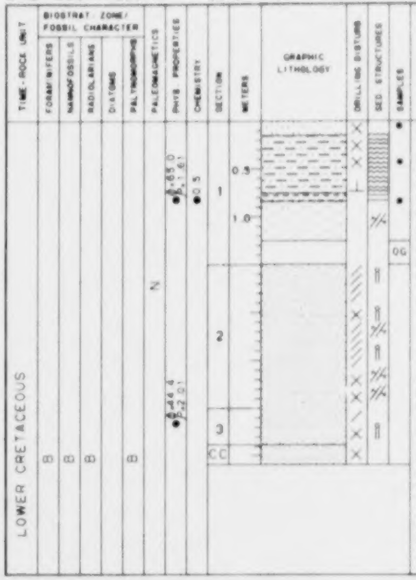
TIME-ROCK UNIT
BIOSTRAT. ZONE/ FOSSIL CHARACTER
FORAMINIFERS
NANNOFOSSILS
RADIOLARIANS
DIATOMS
PALYNOMORPHS
PALEOMAGNETICS
PHYS. PROPERTIES
CHEMISTRY
SECTION
METERS
GRAPHIC LITHOLOGY
DRILLING DISTURB.
SED. STRUCTURES
SAMPLES
LOWER CRETACEOUS
B
B
B
B
N
φ-65.0
ρ-1.61
φ-44.4
ρ-2.01
0.5
1
2
3
CC
0.5
1.0
OG

LITHOLOGIC DESCRIPTION

VOLCANICLASTIC SANDSTONE, SILTSTONE and CLAYSTONE

Major lithologies

a. Interlaminated SILTSTONE and CLAYSTONE, chiefly very dusky red and dark reddish brown (2.5YR 2.5/2, 2.5YR 2.5/4), grades to grayish green (5G 5/2). Very disturbed, irregular flame structures between claystone and overlying siltstone laminations, possible burrows evident in claystone layers. Claystone contains minor radiolarians, oxides and possible zeolites.

b. VOLCANICLASTIC SANDSTONE, grades to siltstone, dark greenish gray (5G 4/1-5BG 4/2), altered glass, abundant oxides and locally, fine grained subrounded very coarse sedimentary clasts. Numerous white (N9) calcite, and dark green (5G 2/1 to 5G 4/1) clay-filled fractures.

SLIDE SUMMARY (%):

|  | 1, 8<br>D | 1, 51<br>D | 1, 84<br>M |
|---|---|---|---|
| TEXTURE: |  |  |  |
| Sand | — | 20 | Tr |
| Silt | 30 | 30 | 5 |
| Clay | 70 | 50 | 95 |
| COMPOSITION: |  |  |  |
| Accessory minerals | — | — | Tr |
| Calcite | — | — | Tr |
| Clay | — | 40 | 90 |
| Glass | — | 10 | — |
| Oxide | 20 | 35 | 4 |
| Quartz | — | Tr | — |
| Radiolarians | 30 | 15 | 3 |
| Silica | 50 | — | — |
| Zeolite | — | — | 3 |

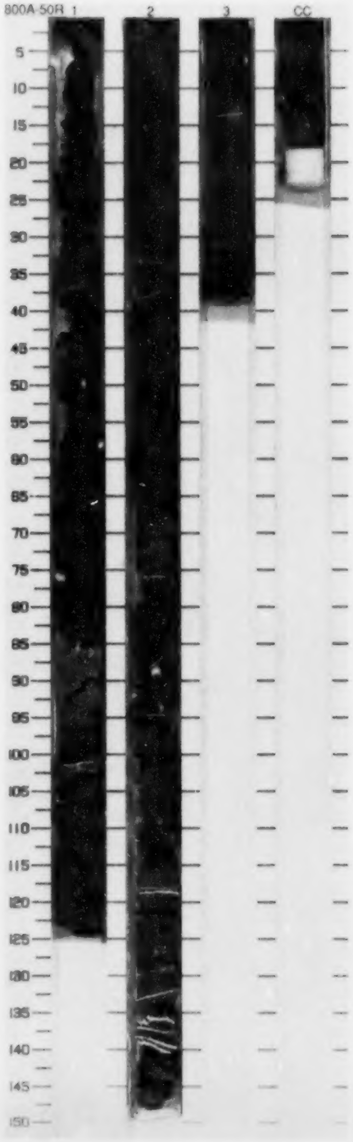
800A-50R 1
2
3
CC
5
10
15
20
25
30
35
40
45
50
55
60
65
70
75
80
85
90
95
100
105
110
115
120
125
130
135
140
145
150

SITE 800 HOLE A CORE 51R CORED INTERVAL 6135.6-6144.8 mbsl; 449.6-458.8 mbsf

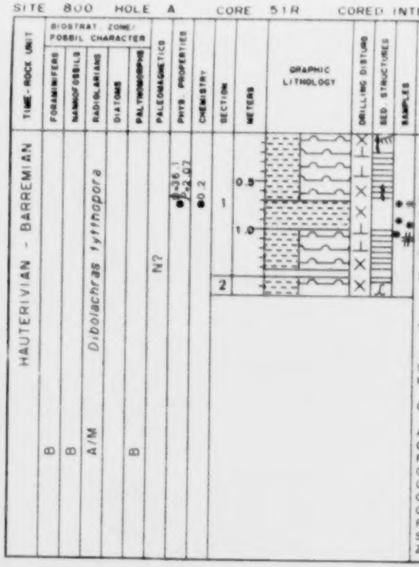
TIME-ROCK UNIT
BIOSTRAT. ZONE/ FOSSIL CHARACTER
FORAMINIFERS
NANNOFOSSILS
RADIOLARIANS
DIATOMS
PALYNOMORPHS
PALEOMAGNETICS
PHYS. PROPERTIES
CHEMISTRY
SECTION
METERS
GRAPHIC LITHOLOGY
DRILLING DISTURB.
SED. STRUCTURES
SAMPLES
HAUTERIVIAN - BARREMIAN
B
B
A/M
Dibolachras tytthopora
B
N?
φ=36.1
γ=2.07
0.2
1
2
0.5
1.0

LITHOLOGIC DESCRIPTION

CLAYEY RADIOLARITE

Major lithology: CLAYEY RADIOLARITE, dark red to light red (2.5YR 3/2, 5YR 3/4, 5YR 6/4), millimeter-scale laminations defined by color and concentration of radiolarians; contains up to 50% radiolarians with clay (smectite) and minor metallic oxides. Red color is due to iron oxides; locally centimeter-scale zones are reduced to light green (5GY 7/1). 80% of core.

Minor lithology: SILICEOUS CLAYSTONE, red to reddish brown (2.5YR 4/6 to 5YR 5/4), massive, contains clay and minor oxides with zeolite and traces of feldspar. 20% of core.

SLIDE SUMMARY (%):

| | 1, 72<br>D | 1, 72<br>M | 1, 90<br>M | 1, 94<br>M | 1, 105<br>M | 1, 106<br>D |
|---|---|---|---|---|---|---|
| TEXTURE: | | | | | | |
| Sand | 30 | 5 | — | 3 | — | — |
| Silt | 30 | 30 | 2 | 25 | 5 | 15 |
| Clay | 40 | 65 | 98 | 72 | 95 | 85 |
| COMPOSITION: | | | | | | |
| Accessory minerals | — | — | 1 | Tr | Tr | — |
| Clay | 30 | 75 | 87 | 84 | 90 | 80 |
| Feldspar | — | — | 2 | 3 | 1 | — |
| Glass | Tr | Tr | — | Tr | — | — |
| Opaques | — | — | 1 | 1 | 1 | — |
| Oxide | 20 | 20 | 3 | 1 | 5 | — |
| Quartz | Tr | Tr | — | — | — | — |
| Radiolarians | 50 | 5 | — | 3 | — | 15 |
| Silica | — | — | — | — | — | 5 |
| Zeolite | — | — | 5 | 4 | 2 | — |

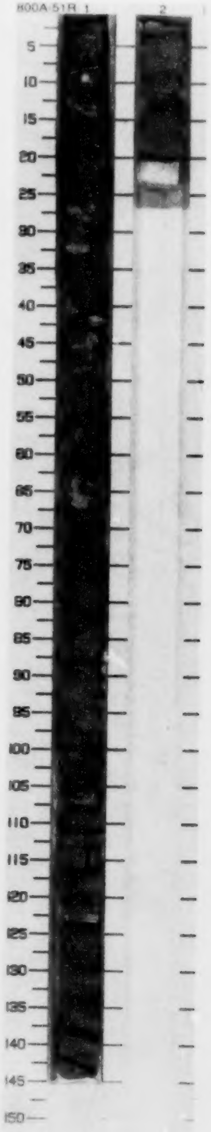
800A-51R 1
2
5
10
15
20
25
30
35
40
45
50
55
60
65
70
75
80
85
90
95
100
105
110
115
120
125
130
135
140
145
150

SITE 800 HOLE A CORE 52R CORED INTERVAL 6144.8-6150.9 mbsl; 458.8-464.9 mbsf

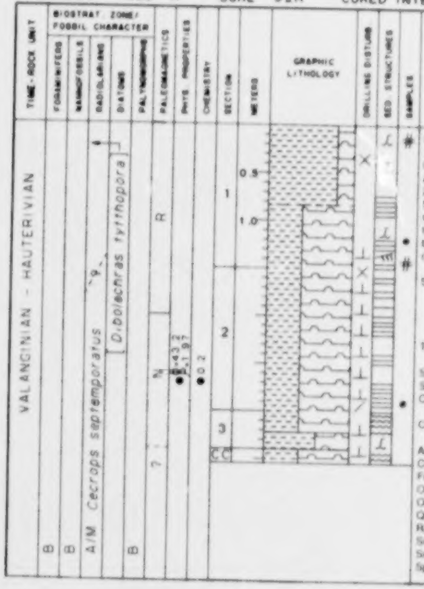
TIME-ROCK UNIT
BIOSTRAT. ZONE/ FOSSIL CHARACTER
FORAMINIFERS
NANNOFOSSILS
RADIOLARIANS
DIATOMS
PALYNOMORPHS
PALEOMAGNETICS
PHYS. PROPERTIES
CHEMISTRY
SECTION
METERS
GRAPHIC LITHOLOGY
DRILLING DISTURB.
SED. STRUCTURES
SAMPLES
VALANGINIAN - HAUTERIVIAN
B
B
A/M Cecrops septemporatus
Dibolachras tytthopora
?
B
R
N
?
-43.2
-1.97
0.2
1
2
3
CC
0.5
1.0
#
#

LITHOLOGIC DESCRIPTION

CLAYEY RADIOLARITE and RADIOLARIAN CLAYSTONE

Major lithologies:

a. CLAYEY RADIOLARITE: reddish brown (5YR 4/4) and very dark grayish brown (10YR 3/2) with irregular zones of light olive brown (7.5YR 5/4) that cut across laminations. XRD from Section 1, 44 cm indicates smectite. Laminations are subtle and often contain discontinuous streaks of black (N2) MnO2, which also forms dendrites on fracture surfaces. Some fractures are filled with white silica.

b. RADIOLARIAN CLAYSTONE: dark brown (7.5YR 4/4), thinly laminated, with lighter colored alteration zones, similar to the radiolarite.

SLIDE SUMMARY (%):

| | 1, 17<br>D | 1, 115<br>D | 1, 145<br>D | 2, 138<br>D |
|---|---|---|---|---|
| TEXTURE: | | | | |
| Sand | — | 50 | — | 5 |
| Silt | 5 | 40 | 40 | 10 |
| Clay | 95 | 10 | 60 | 85 |
| COMPOSITION: | | | | |
| Accessory minerals | — | Tr | — | 1 |
| Clay | 66 | 14 | 23 | 80 |
| Feldspar | 1 | — | — | — |
| Opaques | 5 | — | 10 | — |
| Oxide | 10 | 1 | 10 | 5 |
| Quartz | — | — | — | 1 |
| Radiolarians | 5 | 85 | 40 | 10 |
| Silica | 10 | — | 10 | — |
| Smectite | — | — | 5 | — |
| Spines | 3 | — | 2 | — |

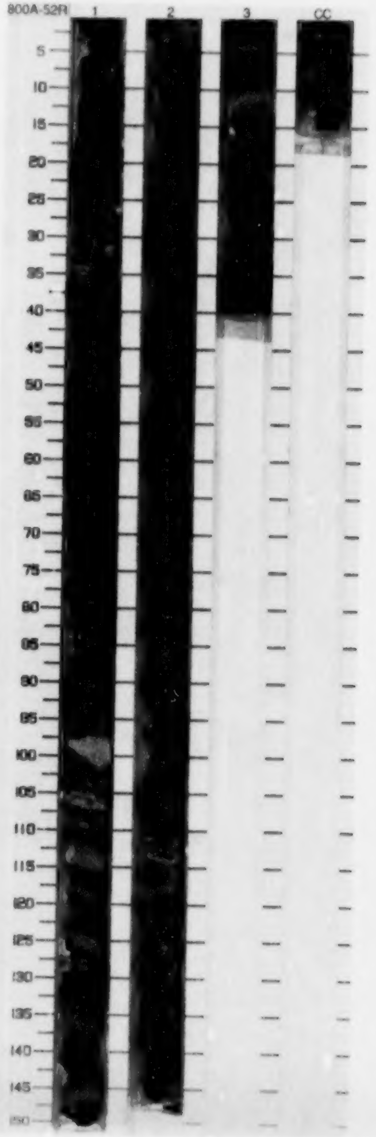
800A-52R
1
2
3
CC
5
10
15
20
25
30
35
40
45
50
55
60
65
70
75
80
85
90
95
100
105
110
115
120
125
130
135
140
145
150

SITE 800 HOLE A CORE 53R CORED INTERVAL 6150.9-6157.0 mbsl; 464.9-471.0 mbsf

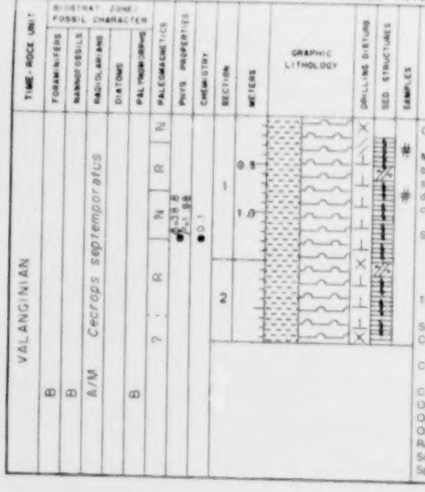
TIME-ROCK UNIT
BIOSTRAT. ZONE/ FOSSIL CHARACTER
FORAMINIFERS
NANNOFOSSILS
RADIOLARIANS
DIATOMS
PALYNOMORPHS
PALEOMAGNETICS
PHYS. PROPERTIES
CHEMISTRY
SECTION
METERS
GRAPHIC LITHOLOGY
DRILLING DISTURB.
SED. STRUCTURES
SAMPLES
VALANGINIAN
B
B
A/M
Cecrops septemporatus
B
N
R
N
R
?
1.98
0.1
1
2
0.5
1.0

LITHOLOGIC DESCRIPTION

CLAYEY RADIOLARITE

Major lithology: CLAYEY RADIOLARITE, with alternating color laminations from very dark brown (7.5YR 3/2 to 7.5YR 2/1) to brown (7.5YR 5/4 to 7.5YR 4/2) with black (5YR 2/1) streaks of MnO2, and MnO2 dendrites on fractures, moderate bioturbation mottles (chondrites) throughout the core, laminations dip 2°, silica-filled fractures. XRD from Section 1, 12 cm, indicates smectite.

SLIDE SUMMARY (%):

| | 1, 31<br>D | 1, 79<br>D |
|---|---|---|
| TEXTURE: | | |
| Silt | 25 | 35 |
| Clay | 75 | 65 |
| COMPOSITION: | | |
| Clay | 50 | 30 |
| Opal | 5 | — |
| Opaques | 3 | 5 |
| Oxide | 15 | 15 |
| Radiolarians | 25 | 35 |
| Silica | — | 10 |
| Spines | 2 | 5 |

SITE 800 HOLE A CORE 54R CORED INTERVAL 6157.0-6165.1 mbsl; 471.0-479.1 mbsf

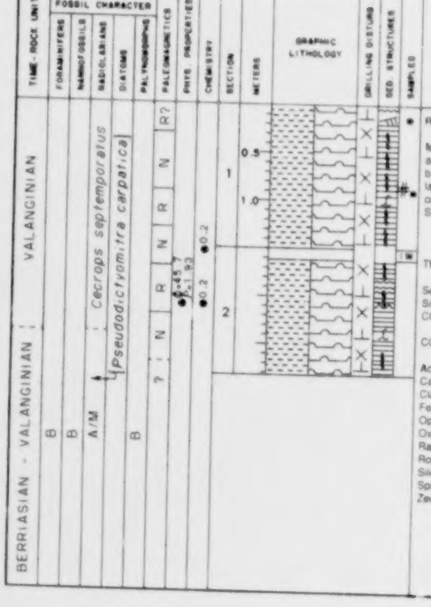
TIME-ROCK UNIT
BIOSTRAT. ZONE/ FOSSIL CHARACTER
FORAMINIFERS
NANNOFOSSILS
RADIOLARIANS
DIATOMS
PALYNOMORPHS
PALEOMAGNETICS
PHYS. PROPERTIES
CHEMISTRY
SECTION
METERS
GRAPHIC LITHOLOGY
DRILLING DISTURB.
SED. STRUCTURES
SAMPLES
VALANGINIAN
BERRIASIAN - VALANGINIAN
B
B
A/M
Cecrops septemporatus
Pseudodictyomitra carpatica
B
R?
N
R
N
R
N
?
45.7
1.93
0.2
0.2
1
2
0.5
1.0

LITHOLOGIC DESCRIPTION

RADIOLARIAN CLAYSTONE and CLAYEY RADIOLARITE

Major lithologies:

a. RADIOLARIAN CLAYSTONE and

b. CLAYEY RADIOLARITE, grayish brown (5YR 3/2) and moderate brown (5YR 4/2), finely laminated, containing minor oxides and traces of feldspar and zeolite; silty texture varies with concentration of radiolarians (up to 85%). MnO2 flasers.

SLIDE SUMMARY (%):

| | 1, 13<br>D | 1, 86<br>D | 1, 88<br>D |
|---|---|---|---|
| TEXTURE: | | | |
| Sand | 50 | Tr | — |
| Silt | 35 | 10 | 20 |
| Clay | 15 | 90 | 80 |
| COMPOSITION: | | | |
| Accessory minerals | Tr | Tr | — |
| Calcite | — | Tr | — |
| Clay | 13 | 80 | 60 |
| Feldspar | — | 3 | — |
| Opaques | — | — | 5 |
| Oxide | 1 | 5 | — |
| Radiolarians | 85 | 10 | 20 |
| Rock fragment | — | 1 | — |
| Silica | — | — | 10 |
| Spines | — | — | 5 |
| Zeolite | 1 | — | — |

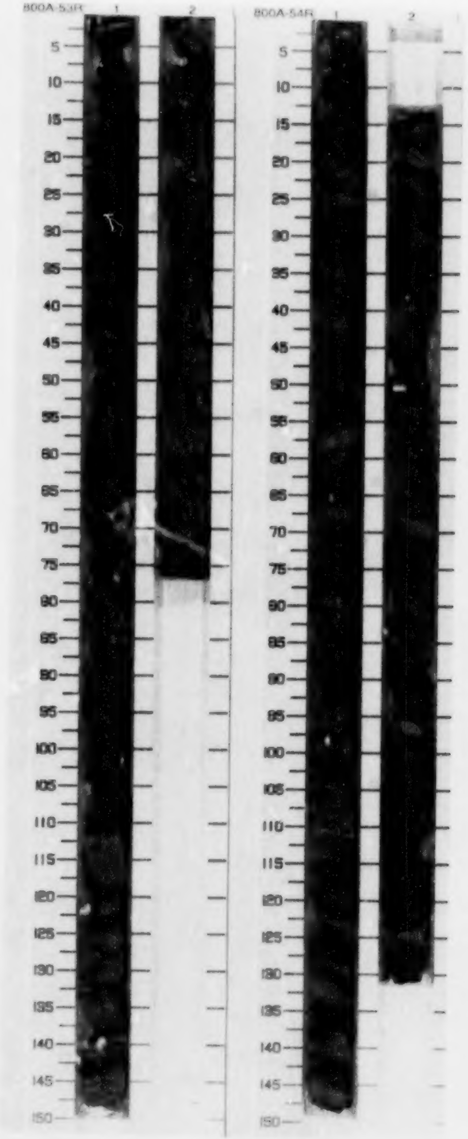
800A-53R
1
2
800A-54R
1
2
5
10
15
20
25
30
35
40
45
50
55
60
65
70
75
80
85
90
95
100
105
110
115
120
125
130
135
140
145
150

SITE 800 HOLE A CORE 55R CORED INTERVAL 6165.0-6174.5 mbsl; 479.1-488.5 mbsf

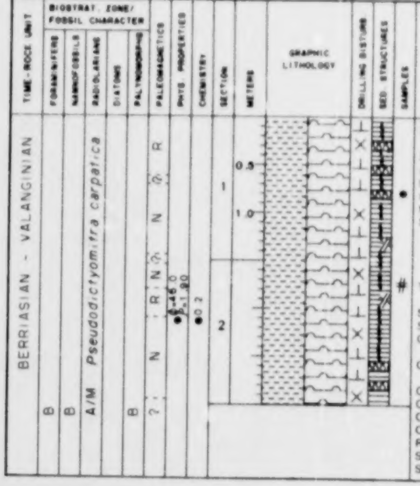
TIME-ROCK UNIT
BIOSTRAT. ZONE/ FOSSIL CHARACTER
FORAMINIFERS
NANNOFOSSILS
RADIOLARIANS
DIATOMS
PALYNOMORPHS
PALEOMAGNETICS
PHYS. PROPERTIES
CHEMISTRY
SECTION
METERS
GRAPHIC LITHOLOGY
DRILLING DISTURB.
SED. STRUCTURES
SAMPLES
BERRIASIAN - VALANGINIAN
B
B
A/M Pseudodictyomitra carpatica
B
R
N
N
R
N
?
φ-46.0
ρ-1.90
0.2
1
2
0.5
1.0

LITHOLOGIC DESCRIPTION

RADIOLARITE and RADIOLARIAN CLAYSTONE

Major lithologies
a. RADIOLARITE, brown (7.5YR 4.5/2), and
b. RADIOLARIAN CLAYSTONE, dark brown (7.5YR 3/1), finely laminated with centimeter-scale color alternations, with black (N2) MnO2 streaks, flasers, bioturbation common throughout, layering dips 30° to 35°, common silica-filled fractures.
SLIDE SUMMARY (%):

| | 1, 76<br>D | 2, 25<br>D |
|---|---|---|
| TEXTURE: | | |
| Sand | 10 | 50 |
| Silt | 50 | — |
| Clay | 40 | 50 |
| COMPOSITION: | | |
| Clay | 28 | 10 |
| Opal | — | 1 |
| Opaques | 10 | 10 |
| Oxide | 20 | 10 |
| Radiolarians | 40 | 50 |
| Silica | — | 19 |
| Spines | Tr | — |

SITE 800 HOLE A CORE 56R CORED INTERVAL 6174.5-6184.0 mbsl; 488.5-498.0 mbsf

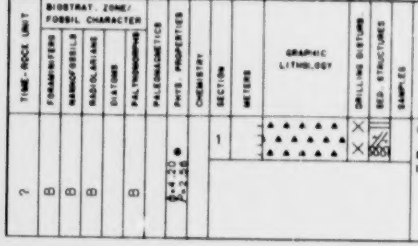
TIME-ROCK UNIT
BIOSTRAT. ZONE/ FOSSIL CHARACTER
FORAMINIFERS
NANNOFOSSILS
RADIOLARIANS
DIATOMS
PALYNOMORPHS
PALEOMAGNETICS
PHYS. PROPERTIES
CHEMISTRY
SECTION
METERS
GRAPHIC LITHOLOGY
DRILLING DISTURB.
SED. STRUCTURES
SAMPLES
?
B
B
B
B
φ-4.20
ρ-2.38
1

LITHOLOGIC DESCRIPTION

CHERT

Major lithology: CHERT, grayish brown (5YR 3/2), grayish orange (5YR 7/2), dark yellowish brown (10YR 4/2), and moderate brown (5YR 3/4), subtle laminations in some pieces.

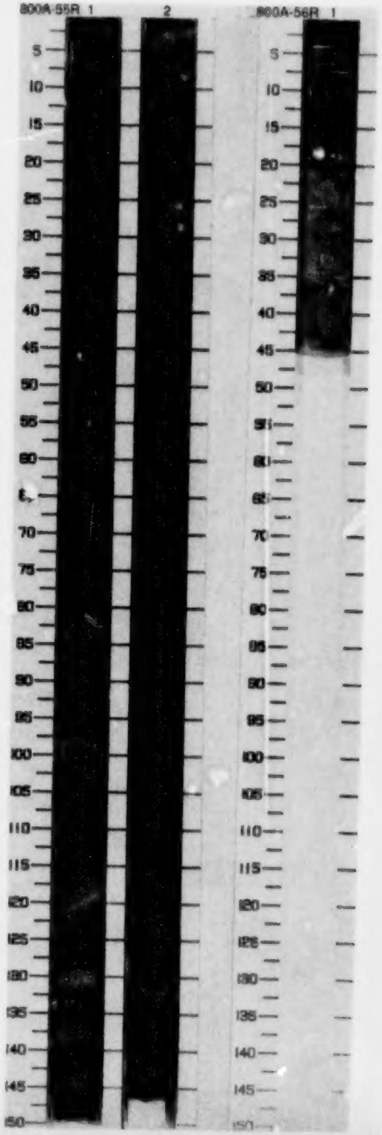
800A-55R 1
2
800A-56R 1
5
10
15
20
25
30
35
40
45
50
55
60
65
70
75
80
85
90
95
100
105
110
115
120
125
130
135
140
145
150

## SITE 800 HOLE A CORE 57R CORED INTERVAL 6184.0-6193.2 mbsl; 49[illegible]0-507.2 mbsf

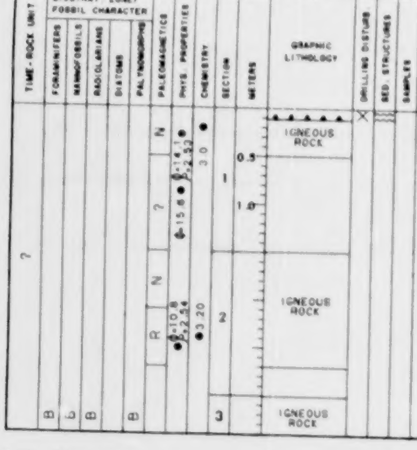

LITHOLOGIC DESCRIPTION

CHERT

Major lithology: CHERT. Section 1, 0 to 13 cm only; pieces at 0 to 7 cm are dusky red (2.5YR 3/2) to dark reddish brown (2.5YR 3/4), showing patchy recrystallization of radiolarite; piece at 7 to 13 cm is dark brown (7.5YR 3/3) and displays an anastomozing pattern of cherty and clay-rich laminations.

## SITE 800 HOLE A CORE 58R CORED INTERVAL 6193.2-6202.6 mbsl; 507.2-516.6 mbsf

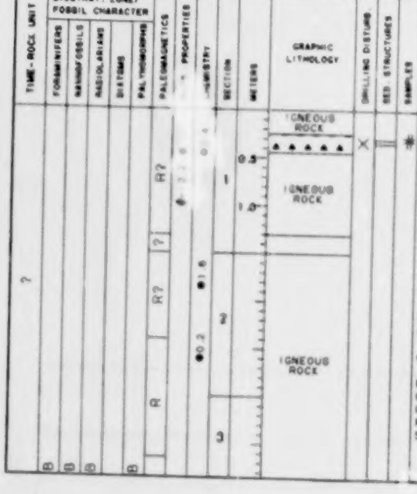

LITHOLOGIC DESCRIPTION

CHERT and RADIOLARITE

Major lithologies:
a. CHERT: Section 1, 27 to 33 cm and 37 to 43 cm, dark reddish brown (5YR 4/2), mottled.
b. RADIOLARITE: Section 1, 33 to 37 cm, weak red (7.5YR 5/2), with bleached color laminations.

SLIDE SUMMARY (%):

| | 30<br>M |
|---|---|
| TEXTURE: | |
| Silt | 1 |
| Clay | 99 |
| COMPOSITION: | |
| Barite | 1 |
| Opaques | Tr |
| Oxide | 10 |
| Radiolarians | 5 |
| Silica | 84 |

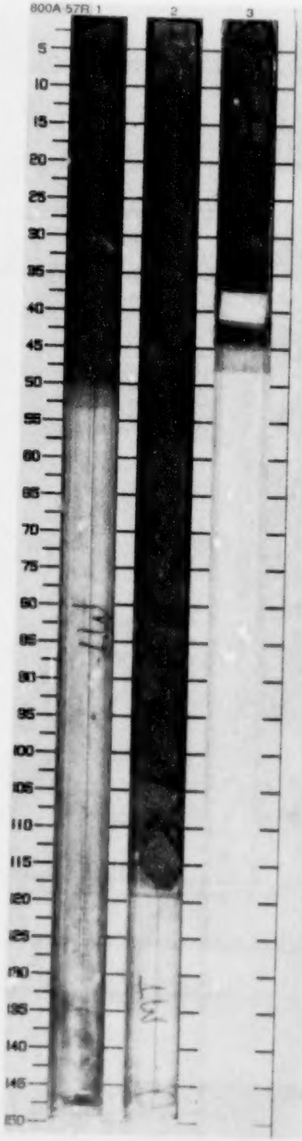
800A-57R 1
2
3
5
10
15
20
25
30
35
40
45
50
55
60
65
70
75
80
85
90
95
100
105
110
115
120
125
130
135
140
145
150
MT
MT

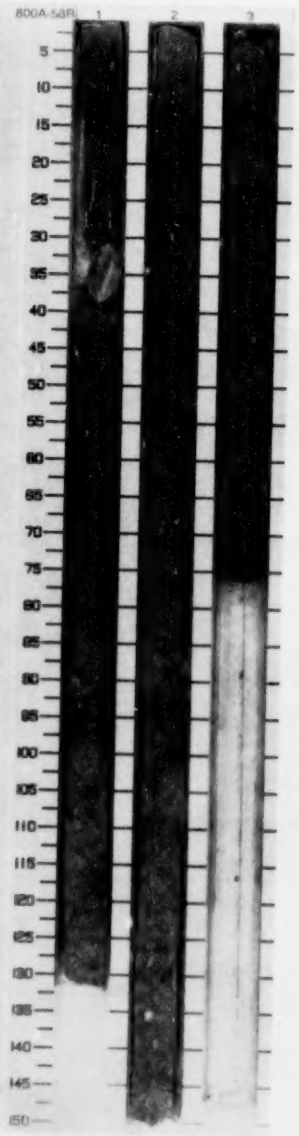
800A-58R 1
2
3
5
10
15
20
25
30
35
40
45
50
55
60
65
70
75
80
85
90
95
100
105
110
115
120
125
130
135
140
145
150

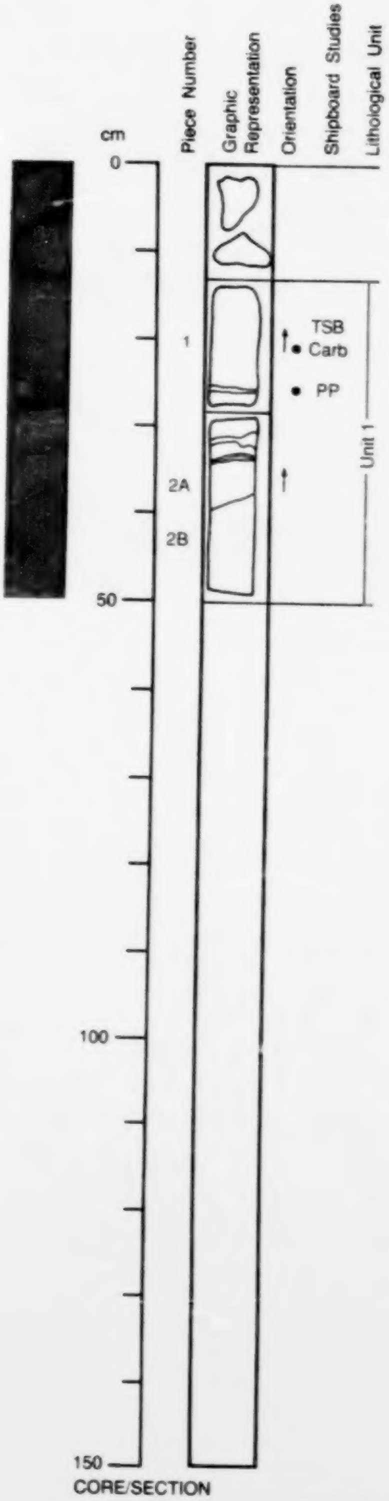
cm
0
50
100
150
Piece Number
Graphic Representation
Orientation
Shipboard Studies
Lithological Unit
1
2A
2B
TSB
Carb
PP
Unit 1
CORE/SECTION

## 129-800A-57R-1

### UNIT 1: APHYRIC DOLERITE

### Pieces 1-2

**CONTACTS:** Not observed, but finer grained directly below cherts.
**PHENOCRYSTS:** No phenocrysts.
**GROUNDMASS:** Medium-grained, hypidiomorphic-granular; slight coarsening of grain-size from Piece 1 to 2.
**VESICLES:** No vesicles (or <1% in total section).
Miaroles: None.
**COLOR:** Mottled pale brown (5YR 6/3) to greenish gray (5GY 5/1).
**STRUCTURE:** Massive.
**ALTERATION:** Moderate alteration from oxidized top (14-24 cm) to clay and oxidized base.
**VEINS/FRACTURES:** 2%; 1 mm; horizontal; calcite infillings, sometimes associated with oxidized zones.
**ADDITIONAL COMMENTS:** Possibly intrusive sill.

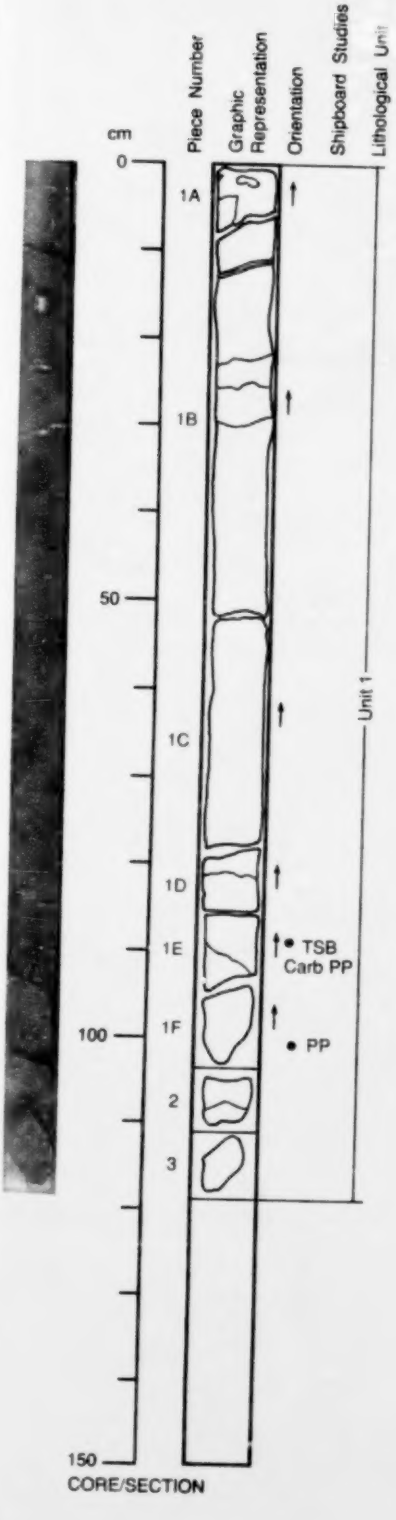
cm
0
50
100
150
CORE/SECTION
Piece Number
Graphic Representation
Orientation
Shipboard Studies
Lithological Unit
1A
1B
1C
1D
1E
1F
2
3
TSB
Carb PP
PP
Unit 1

## 129-800A-57R-2

### UNIT 1: APHYRIC DOLERITE

### Pieces 1A-1F, 2, 3

**CONTACTS:** None observed.
**PHENOCRYSTS:** No phenocrysts.
**GROUNDMASS:** Medium-grained, holocrystalline.
**VESICLES:** No vesicles.
Miaroles: 0.5-1.0 mm, lensoid, irregular distribution, plagioclase growths.
**COLOR:** Greenish gray (5G 5/1 to 5GY 5/1).
**STRUCTURE:** Massive.
**ALTERATION:** Moderate, mainly green clays/chlorite in plagioclase; oxidized in patches especially pieces 1A-1C.
**VEINS/FRACTURES:** 2%; <1 mm; horizontal & 40; infilling calcite and calcite+pyrite
**ADDITIONAL COMMENTS:** Possibly intrusive sill continued from 57-1.

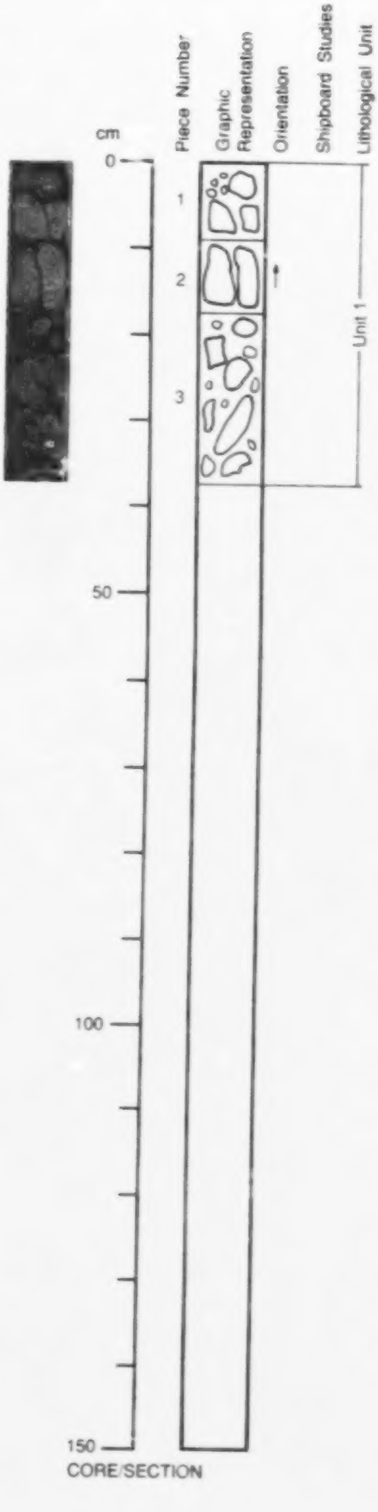
cm
0
50
100
150
Piece Number
Graphic Representation
Orientation
Shipboard Studies
Lithological Unit
1
2
3
Unit 1
CORE/SECTION

## 129-800A-57R-3

## UNIT 1: APHYRIC DOLERITE

### Pieces 1-3

**CONTACTS:** None observed.
**PHENOCRYSTS:** No phenocrysts.
**GROUNDMASS:** Medium-grained, holocrystalline.
**VESICLES:** Non-vesicular.
**COLOR:** Gray-green (5B 5/1).
**STRUCTURE:** Massive.
**ALTERATION:** Slightly altered throughout all pieces; green clay/chlorite replacing plagioclase.
**VEINS/FRACTURES:** Multiple fractures due to drilling.
**ADDITIONAL COMMENTS:** Probably intrusive sill, continued from 57-2.

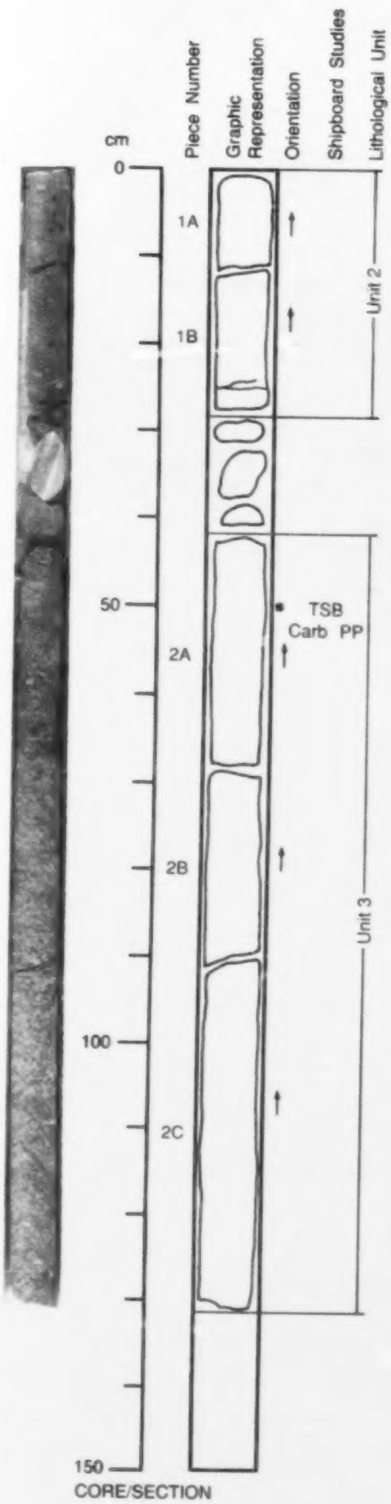
cm
Piece Number
Graphic Representation
Orientation
Shipboard Studies
Lithological Unit
0
50
100
150
1A
1B
2A
2B
2C
TSB
Carb PP
Unit 2
Unit 3
CORE/SECTION

## 129-800A-58R-1

## UNIT 2: APHYRIC DOLERITE

### Pieces 1A & 1B

**CONTACTS:** Neither upper or lower contacts visible.
**PHENOCRYSTS:** Aphyric.
**GROUNDMASS:** Medium-grained, holocrystalline.
**VESICLES:** Non-vesicular.
**COLOR:** Mottled light gray (5B 6/1).
**STRUCTURE:** Massive.
**ALTERATION:** Slight alteration, green clays replacing plagioclase.
**VEINS/FRACTURES:** 1%; 1 mm; horizontal; calcite veinlets at base of Piece 1B.
**ADDITIONAL COMMENTS:** Unit 2 recognized on basis of different texture with prominent altered plagioclase.

## UNIT 3: APHYRIC DOLERITE

### Pieces 2A - 2C

**CONTACTS:** Actual upper contact not visible, but separated from Unit 2 by cherty sediment horizon.
**PHENOCRYSTS:** Aphyric.
**GROUNDMASS:** Medium-grained, holocrystalline.
**VESICLES:** Non-vesicular.
**COLOR:** Mottled light gray (5B 6/1).
**STRUCTURE:** Massive.
**ALTERATION:** Slight alteration, green clays and calcite replacing plagioclase and mesostasis.
**VEINS/FRACTURES:** <1%; 0.5 mm; almost horizontal; carbonate veinlets.
**ADDITIONAL COMMENTS:** (a) Unit 3 distinguished from previous units by characteristic long (5-15 mm) black clinopyroxene skeletal crystals.
(b) Units 2 & 3 probably represent sills as interlayered sediments appear indurated and bleached by intrusive contact.

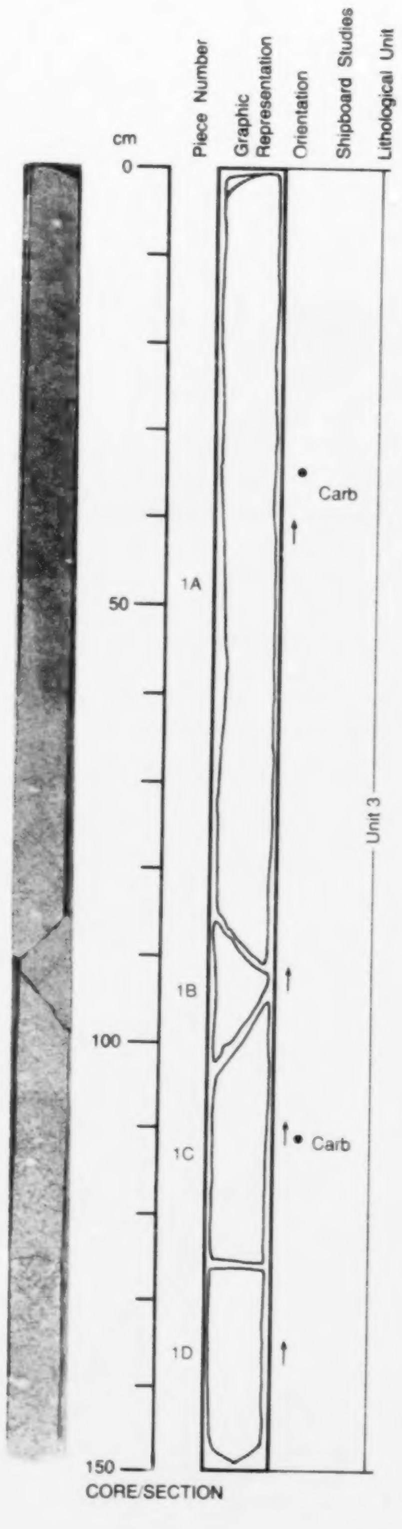
cm
Piece Number
Graphic Representation
Orientation
Shipboard Studies
Lithological Unit
0
50
100
150
1A
1B
1C
1D
Carb
Carb
Unit 3
CORE/SECTION

## 129-800A-58R-2

## UNIT 3: APHYRIC DOLERITE

### Pieces 1A - 1D

**CONTACTS:** Not observed.
**PHENOCRYSTS:** Aphyric.
**GROUNDMASS:** Medium-grained, holocrystalline.
**VESICLES:** Non-vesicular.
**COLOR**: Mottled light gray (5B 6/1).
**STRUCTURE:** Massive.
**ALTERATION:** Slight alteration, green clays and calcite replacing plagioclase and mesostasis.
**VEINS/FRACTURES:** <1%; 1 mm but irregular; horizontal to 45 degrees.
**ADDITIONAL COMMENTS:** Overall, distribution of long, black clinopyroxene crystals is patchy.

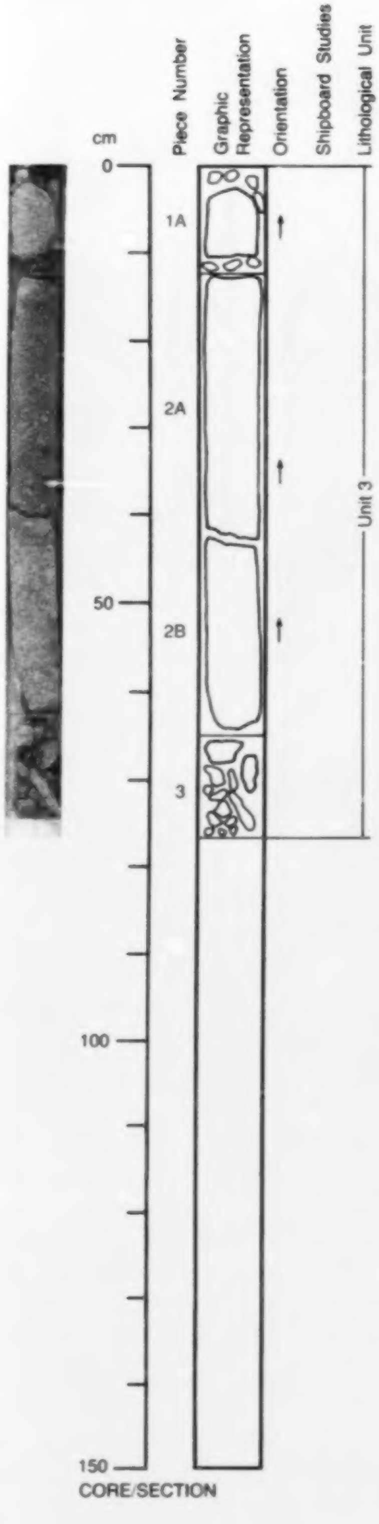
cm
0
50
100
150
Piece Number
Graphic Representation
Orientation
Shipboard Studies
Lithological Unit
1A
2A
2B
3
Unit 3
CORE/SECTION

## 129-800A-58R-3

## UNIT 3: APHYRIC DOLERITE

### Pieces 1A - 3

**CONTACTS:** Not observed.
**PHENOCRYSTS:** Aphyric.
**GROUNDMASS:** Medium-grained, holocrystalline.
**VESICLES:** Non-vesicular.
**COLOR:** Mottled light gray (5B 6/1).
**STRUCTURE:** Massive.
**ALTERATION:** Slight alteration, green clays and calcite replacing plagioclase and mesostasis.
**VEINS/FRACTURES:** <1%; 0.5 mm; almost horizontal; carbonate fillings.

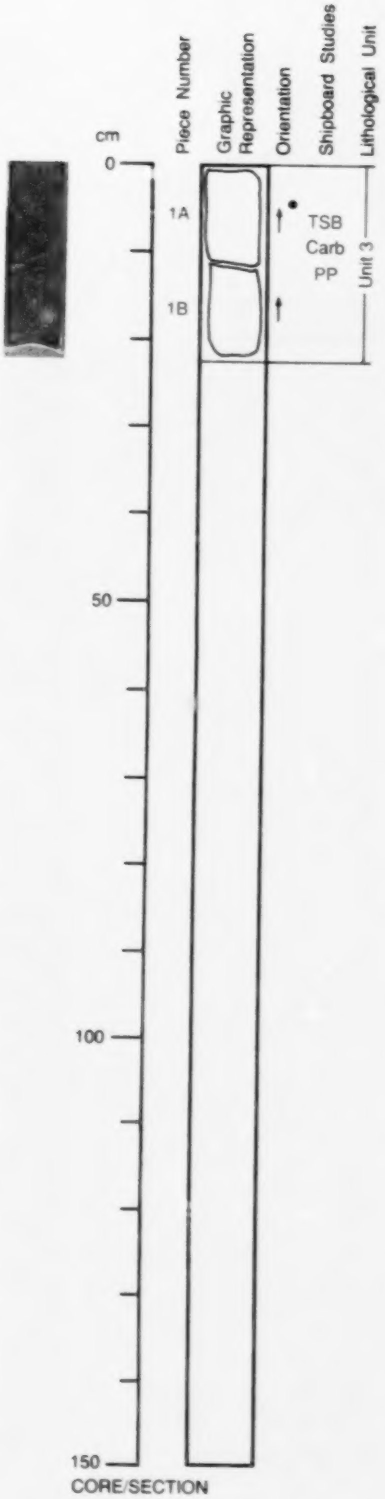
cm
Piece Number
Graphic Representation
Orientation
Shipboard Studies
Lithological Unit
0
1A
1B
TSB
Carb
PP
Unit 3
50
100
150
CORE/SECTION

## 129-800A-59R-1

### UNIT 3: APHYRIC DOLERITE

### Pieces 1A and 1B

**CONTACTS:** Not observed.
**PHENOCRYSTS:** Aphyric.
**GROUNDMASS:** Medium-grained, holocrystalline.
**VESICLES:** Non-vesicular.
**COLOR:** Mottled light gray (5B 6/1).
**STRUCTURE:** Massive.
**ALTERATION:** Slight alteration, green clays and calcite replacing plagioclase and mesostasis.
**VEINS/FRACTURES:** <1%; 0.5 mm; almost horizontal; no fillings observed.

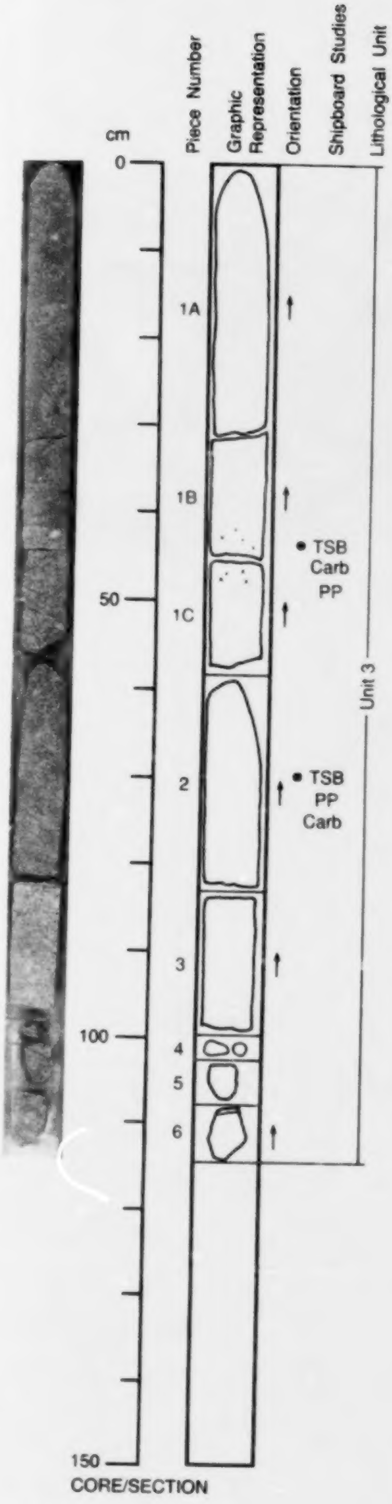
cm
Piece Number
Graphic Representation
Orientation
Shipboard Studies
Lithological Unit
0
50
100
150
1A
1B
1C
2
3
4
5
6
• TSB
Carb
PP
• TSB
PP
Carb
Unit 3
CORE/SECTION

## 129-800A-60R-1

## UNIT 3: APHYRIC DOLERITE

### Pieces 1A - 6

**CONTACTS:** Not observed.
**PHENOCRYSTS:** Aphyric.
**GROUNDMASS:** Medium-grained, holocrystalline.
**VESICLES:** Miaroles are present at the bottom of Piece 1B and top of 1C.
Miaroles: <1%; <1 mm; irregular; no fillings observed.
**COLOR:** Mottled light gray (5B 6/1).
**STRUCTURE:** Massive.
**ALTERATION:** Slight alteration, green clays and calcite replacing plagioclase and mesostasis.
**VEINS/FRACTURES:** 1%; 1 mm but irregular; almost horizontal; no fillings observed.

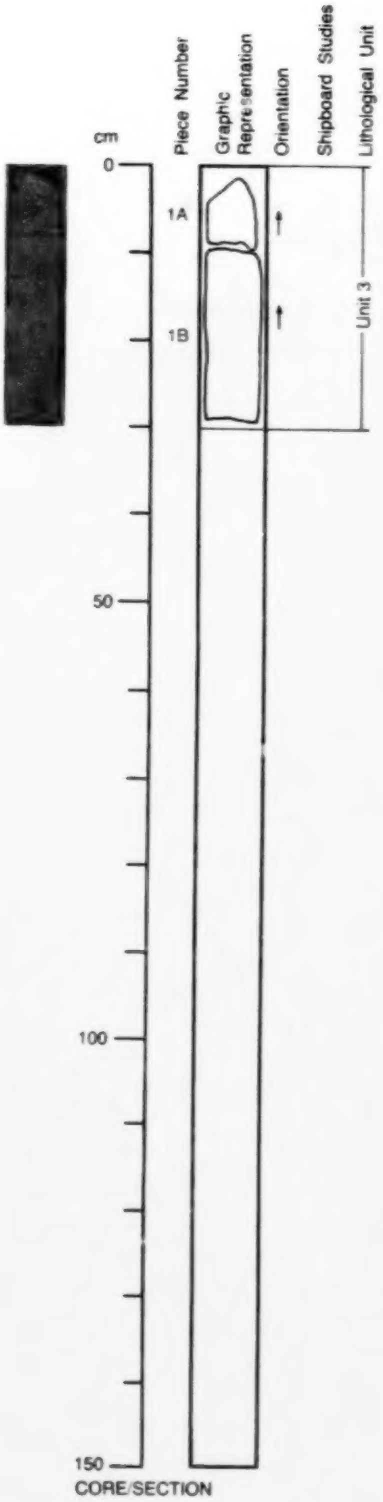
cm
Piece Number
Graphic Representation
Orientation
Shipboard Studies
Lithological Unit
0
50
100
150
1A
1B
Unit 3
CORE/SECTION

## 129-800A-61R-1

## UNIT 3: APHYRIC DOLERITE

### Pieces 1A & 1B

**CONTACTS:** None observed.
**PHENOCRYSTS:** No phenocrysts.
**GROUNDMASS:** Medium-grained, holocrystalline.
**VESICLES:** Non-vesicular.
Miaroles: 1-2%, 1 mm, random distribution.
**COLOR:** Mottled pale gray (5B 6/1).
**STRUCTURE:** Massive.
**ALTERATION:** Slight; green clays replacing long plagioclase laths and possibly glassy mesostasis; uniform distribution.
**VEINS/FRACTURES:** No veins or fractures.
**ADDITIONAL COMMENTS:** Continuation of Unit 3. Some variation, grain-size of plagioclase laths - longer and more acicular here relative to Core 60.

SITE 801 HOLE A CORE 1R CORED INTERVAL 5681.8-5688.3 mbsl; 8.0-14.5 mbsf

| TIME-ROCK UNIT | BIOSTRAT. ZONE/ FOSSIL CHARACTER | | | | | PALEOMAGNETICS | PHYS. PROPERTIES | CHEMISTRY | SECTION | METERS | GRAPHIC LITHOLOGY | DRILLING DISTURB. | SED. STRUCTURES | SAMPLES |
|---|---|---|---|---|---|---|---|---|---|---|---|---|---|---|
| | FORAMINIFERS | NANNOFOSSILS | RADIOLARIANS | DIATOMS | PALYNOMORPHS | | | | | | | | | |
| ? | B | B | B | | B | | ● φ-83.8<br>● γ-1.28 | | 1<br>CC | 0.5<br>1.0 | | | | ●<br>● |

### LITHOLOGIC DESCRIPTION

PELAGIC CLAY with ZEOLITES

Major lithology: PELAGIC CLAY with ZEOLITES, dark brown (7.5YR 3/2 -3/3), soft, homogeneous, very disturbed by drilling, composed of clay, iron-oxide/hydroxide aggregates and elongate zeolite crystals (philipsite, commonly twinned) with minor opaque micronodules and quartz silt.

SLIDE SUMMARY (%):

| | 1, 57<br>D | CC, 1<br>D |
|---|---|---|
| TEXTURE: | | |
| Silt | 10 | 10 |
| Clay | 90 | 90 |
| COMPOSITION: | | |
| Accessory minerals | — | 1 |
| Clay | 62 | 64 |
| Fish | — | 1 |
| Micronodule | 3 | 1 |
| Nannofossils | Tr | — |
| Oxide | 20 | 20 |
| Quartz | Tr | 2 |
| Radiolarians | — | 3 |
| Zeolite | 15 | 8 |

SITE 801 HOLE A CORE 2R CORED INTERVAL 5688.3-5694.2 mbsl; 14.5-20.4 mbsf

| TIME-ROCK UNIT | BIOSTRAT. ZONE/ FOSSIL CHARACTER | | | | | PALEOMAGNETICS | PHYS. PROPERTIES | CHEMISTRY | SECTION | METERS | GRAPHIC LITHOLOGY | DRILLING DISTURB. | SED. STRUCTURES | SAMPLES |
|---|---|---|---|---|---|---|---|---|---|---|---|---|---|---|
| | FORAMINIFERS | NANNOFOSSILS | RADIOLARIANS | DIATOMS | PALYNOMORPHS | | | | | | | | | |
| ? | B | B | B | | B | | | | 1<br>CC | | | | | ● |

### LITHOLOGIC DESCRIPTION

PELAGIC CLAY with ZEOLITES

Major lithology: PELAGIC CLAY with ZEOLITES, dark brown to dark reddish brown (7.5YR 3/2-7.5YR 3/3.5), soft, homogeneous, very disturbed by drilling, composed of clay, iron-oxide/hydroxide aggregates and zeolite crystals (philipsite) with traces of opaque micronodules and quartz silt. Transition downward from lighter to darker color at Section 1, 16-19 cm.

SLIDE SUMMARY (%):

| | 1, 28<br>D |
|---|---|
| TEXTURE: | |
| Sand | 1 |
| Silt | 15 |
| Clay | 84 |
| COMPOSITION: | |
| Clay | 55 |
| Micronodule | 1 |
| Oxide | 22 |
| Quartz | Tr |
| Spicules | 2 |
| Zeolite | 20 |

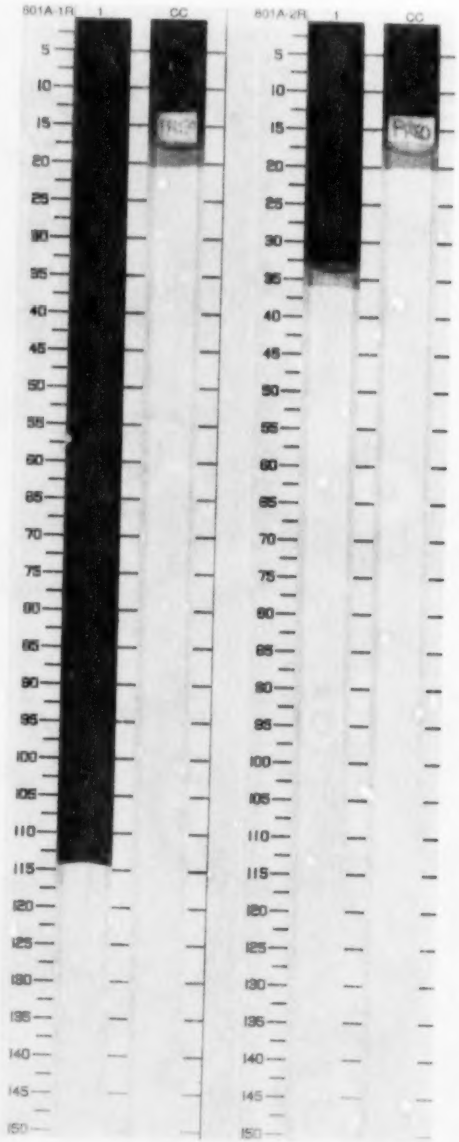

SITE 801 HOLE A CORE 3R CORED INTERVAL 5894.2-5703.8 mbsl; 20.4-30.0 mbsf

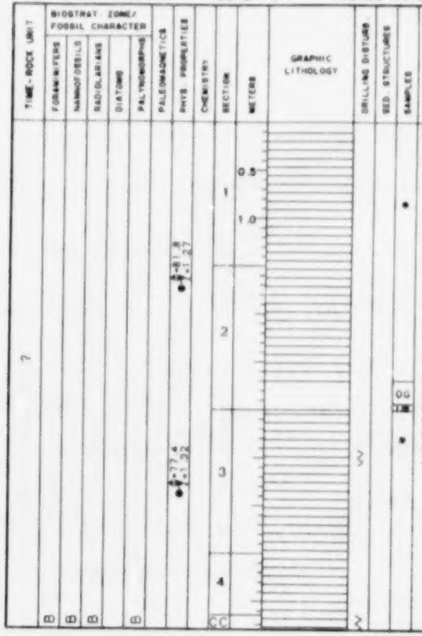
TIME-ROCK UNIT
BIOSTRAT. ZONE/ FOSSIL CHARACTER
FORAMINIFERS
NANNOFOSSILS
RADIOLARIANS
DIATOMS
PALYNOMORPHS
PALEOMAGNETICS
PHYS. PROPERTIES
CHEMISTRY
SECTION
METERS
GRAPHIC LITHOLOGY
DRILLING DISTURB.
SED. STRUCTURES
SAMPLES
?
B
B
B
B
-81.8
-1.27
-77.4
-1.32
1
2
3
4
CC
0.5
1.0
OG

LITHOLOGIC DESCRIPTION

PELAGIC CLAY with ZEOLITES

Major lithology: PELAGIC CLAY with ZEOLITES, dark reddish brown (7.5YR 2.5/2), soft, homogeneous, very disturbed by drilling, composed of iron-oxide/hydroxide aggregates, clay and zeolite crystals with traces of opaque micronodules, benthic foraminifers and quartz silt.

SLIDE SUMMARY (%):

| | 1, 85 | 3, 30 |
|---|---|---|
| | D | D |
| TEXTURE | | |
| Sand | Tr | 2 |
| Silt | 30 | 45 |
| Clay | 70 | 53 |
| COMPOSITION | | |
| Clay | 39 | 38 |
| Foraminifers | Tr | Tr |
| Micronodule | 1 | 1 |
| Oxide | 50 | 45 |
| Quartz | Tr | Tr |
| Spicules | — | 1 |
| Zeolite | 10 | 15 |

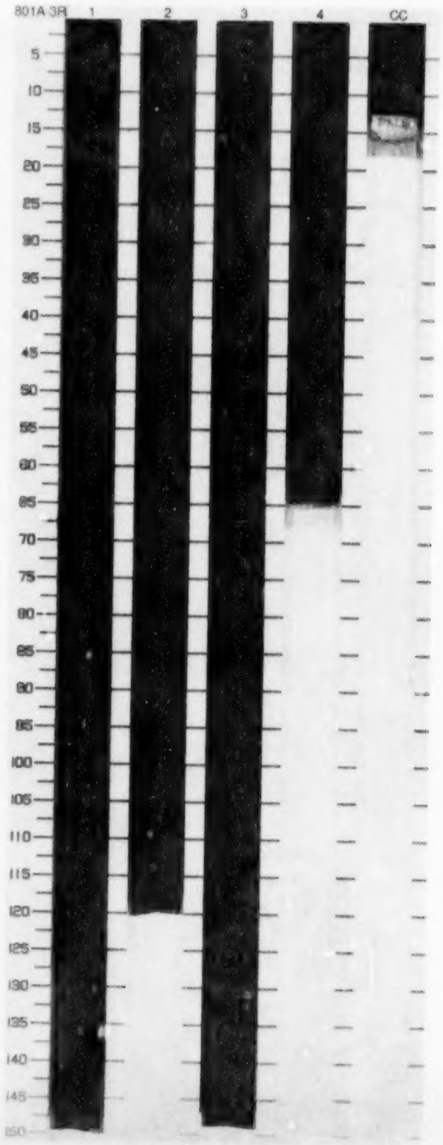
801A-3R
1
2
3
4
CC
5
10
15
20
25
30
35
40
45
50
55
60
65
70
75
80
85
90
95
100
105
110
115
120
125
130
135
140
145
150

SITE 801 HOLE A CORE 4R CORED INTERVAL 5703.8-5713.4 mbsl; 30.0-39.6 mbsf

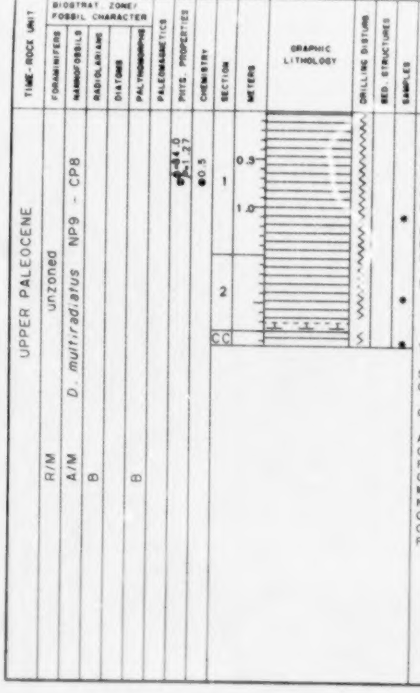
TIME-ROCK UNIT
BIOSTRAT. ZONE/ FOSSIL CHARACTER
FORAMINIFERS
NANNOFOSSILS
RADIOLARIANS
DIATOMS
PALYNOMORPHS
PALEOMAGNETICS
PHYS. PROPERTIES
CHEMISTRY
SECTION
METERS
GRAPHIC LITHOLOGY
DRILLING DISTURB.
SED. STRUCTURES
SAMPLES
UPPER PALEOCENE
unzoned
D. multiradiatus NP9 - CP8
R/M
A/M
B
B
φ-84.0
γ-1.27
●0.5
1
2
CC
0.5
1.0

LITHOLOGIC DESCRIPTION

PELAGIC CLAY

Major lithology: PELAGIC CLAY, dark reddish brown to dark brown (5YR 2.5/2- 7.5YR 3.5/2), soft, homogeneous, very disturbed by drilling, composed of clay and iron-oxide/hydroxide aggregates with minor opaque micronodules and volcanic glass with traces of palagonite and benthic foraminifers. XRD data from Section 1, 110 cm and 139 cm, indicate the presence of phillipsite and celestite.

Minor lithology: NANNOFOSSIL OOZE, light yellowish brown (10YR 6/4) mottled with dark brown (7.5YR 3.5/2), composed of nannofossils with traces of metallic oxides, lower part of Section 2 and CC.

SLIDE SUMMARY (%):

| | 1, 110<br>D | 2, 46<br>D | CC, 13<br>M |
|---|---|---|---|
| TEXTURE: | | | |
| Silt | 10 | 10 | 25 |
| Clay | 90 | 90 | 75 |
| COMPOSITION: | | | |
| Accessory minerals | — | Tr | — |
| Clay | 50 | 50 | Tr |
| Foraminifers | Tr | — | — |
| Glass | 10 | 5 | — |
| Micronodule | 5 | 10 | — |
| Nannofossils | — | — | 99 |
| Opaques | — | — | Tr |
| Oxide | 35 | 35 | 1 |
| Palagonite | Tr | Tr | — |

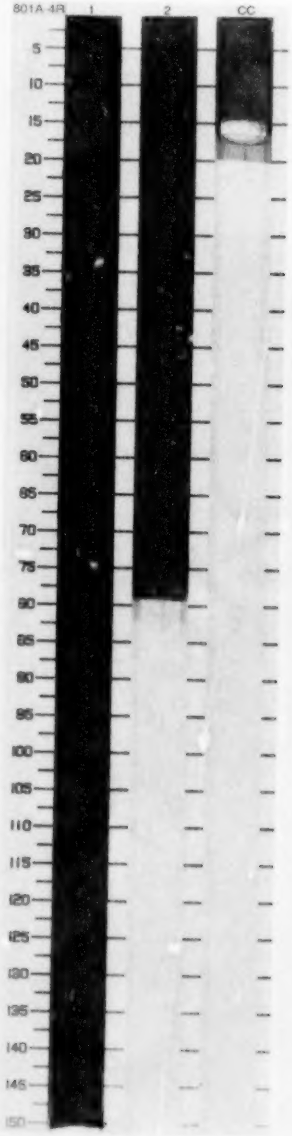
801A-4R
1
2
CC
5
10
15
20
25
30
35
40
45
50
55
60
65
70
75
80
85
90
95
100
105
110
115
120
125
130
135
140
145
150

SITE 801 HOLE A CORE 5R CORED INTERVAL 5713.4-5723.1 mbsl; 39.6-49.3 mbsf

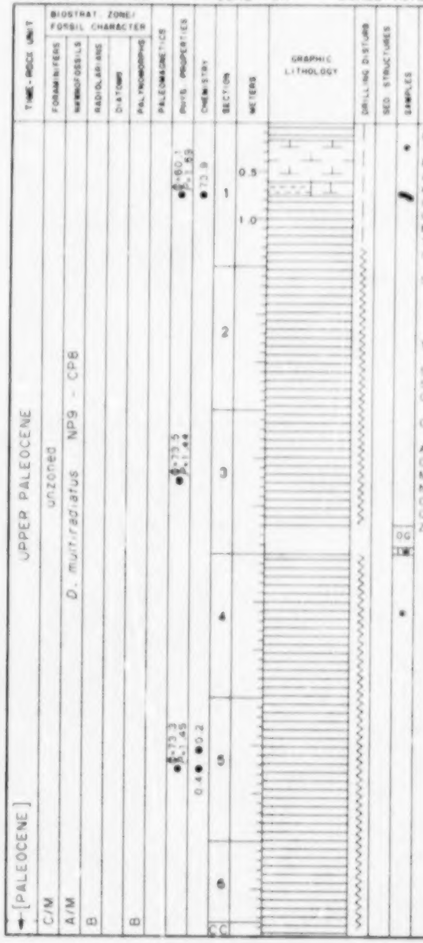
TIME-ROCK UNIT
BIOSTRAT. ZONE/ FOSSIL CHARACTER
FORAMINIFERS
NANNOFOSSILS
RADIOLARIANS
DIATOMS
PALYNOMORPHS
PALEOMAGNETICS
PHYS. PROPERTIES
CHEMISTRY
SECTION
METERS
GRAPHIC LITHOLOGY
DRILLING DISTURB.
SED. STRUCTURES
SAMPLES
UPPER PALEOCENE
[PALEOCENE]
unzoned
D. multiradiatus NP9 - CP8
C/M
A/M
B
B
φ-60.1
γ-1.59
●73.9
φ-73.5
γ-1.44
φ-73.3
γ-1.45
0.4● ●0.2
1
2
3
4
5
6
CC
0.5
1.0
OG

LITHOLOGIC DESCRIPTION

PELAGIC CLAY with ZEOLITES and NANNOFOSSIL OOZE

Major lithologies:
a. PELAGIC CLAY with ZEOLITES, dark reddish brown (5YR 3/4) changing downward to dark brown (10YR 3/3) with small patches of light yellow (10YR 5/4) in Section 2 and below; soft; possible vague laminations but features mainly obliterated by drilling disturbance; consisting of clay, zeolites and iron oxide/ hydroxide aggregates with traces of nannofossils.
b. NANNOFOSSIL OOZE, pale yellow (2.5Y 7/4) to light olive brown (2.5Y 5/4), in Section 1, 18-63 cm and 68-76 cm; featureless; sharp contacts to adjacent pelagic clay intervals (redeposited?).

SLIDE SUMMARY (%):

|  | 1, 26<br>D | 1, 74<br>M | 1, 75<br>M | 4, 60<br>D |
|---|---|---|---|---|
| TEXTURE: |  |  |  |  |
| Sand | Tr | Tr | Tr | — |
| Silt | 20 | 17 | 25 | 15 |
| Clay | 80 | 83 | 75 | 85 |
| COMPOSITION: |  |  |  |  |
| Accessory minerals | — | — | — | Tr |
| Clay | 10 | 18 | 15 | 70 |
| Micrite | 15 | 20 | 20 | — |
| Nannofossils | 73 | 60 | 63 | Tr |
| Oxide | 2 | 2 | 2 | 5 |
| Quartz | — | — | — | 1 |
| Zeolite | — | — | — | 15 |

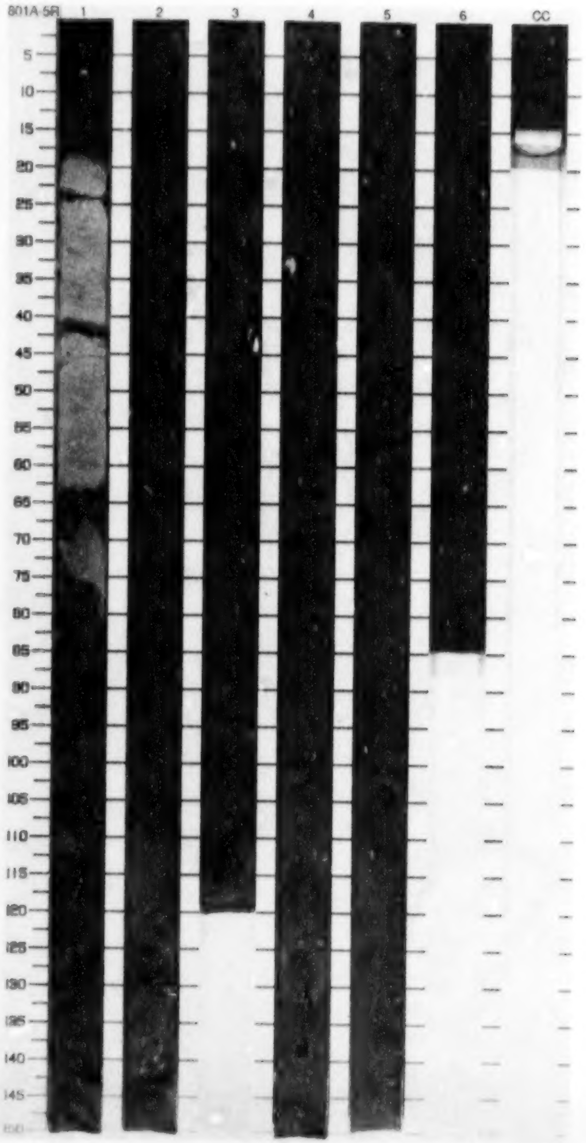
801A-5R
1
2
3
4
5
6
CC
5
10
15
20
25
30
35
40
45
50
55
60
65
70
75
80
85
90
95
100
105
110
115
120
125
130
135
140
145
150

SITE 801 HOLE A CORE 6R CORED INTERVAL 5723.1-5732.8 mbsl; 49.3-59.0 mbsf

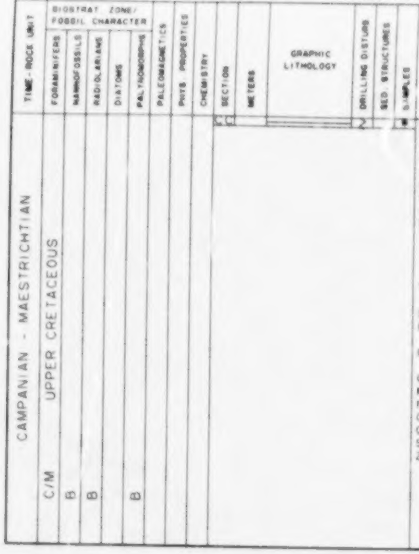
TIME-ROCK UNIT
BIOSTRAT. ZONE/ FOSSIL CHARACTER
FORAMINIFERS
NANNOFOSSILS
RADIOLARIANS
DIATOMS
PALYNOMORPHS
PALEOMAGNETICS
PHYS. PROPERTIES
CHEMISTRY
SECTION
METERS
GRAPHIC LITHOLOGY
DRILLING DISTURB.
SED. STRUCTURES
SAMPLES
CAMPANIAN - MAESTRICHTIAN
UPPER CRETACEOUS
C/M
B
B
B
CC
2

LITHOLOGIC DESCRIPTION

PELAGIC CLAY

Major lithology: PELAGIC CLAY, brown (10YR 4/3) with millimeter-scale mottles of reddish yellow (7.5YR 7/6), soft, homogenized by drilling, composed of clay with minor radiolarian spines, nannofossils, iron oxide/hydroxide aggregates, quartz silt and opaque micronodules with traces of zeolites. Entire sample went to paleontology.

SLIDE SUMMARY (%):

| | CC<br>D |
|---|---|
| TEXTURE | |
| Silt | 5 |
| Clay | 95 |
| COMPOSITION | |
| Clay | 70 |
| Micronodule | 3 |
| Nannofossils | 7 |
| Oxide | 5 |
| Quartz | 5 |
| Spines | 10 |
| Zeolite | Tr |

SITE 801 HOLE A CORE 7R CORED INTERVAL 5732.8-5742.4 mbsl; 59.0-68.6 mbsf

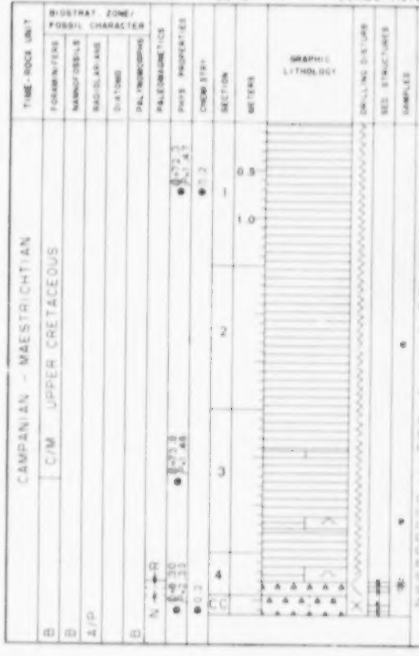
TIME-ROCK UNIT
BIOSTRAT. ZONE/ FOSSIL CHARACTER
FORAMINIFERS
NANNOFOSSILS
RADIOLARIANS
DIATOMS
PALYNOMORPHS
PALEOMAGNETICS
PHYS. PROPERTIES
CHEMISTRY
SECTION
METERS
GRAPHIC LITHOLOGY
DRILLING DISTURB.
SED. STRUCTURES
SAMPLES
CAMPANIAN - MAESTRICHTIAN
C/M
UPPER CRETACEOUS
B
B
A/P
B
N
R
0.2
0.2
1
2
3
4
CC
0.9
1.0

LITHOLOGIC DESCRIPTION

PELAGIC CLAY with ZEOLITES

Major lithology: PELAGIC CLAY with ZEOLITES, overall dark reddish gray (5YR 4/2.5) with intermixed streaks and mottles ranging from light brown (7.5YR 6/4) to grayish brown (5YR 3/2), probably originally banded but has been highly distorted by drilling; composed of clay and zeolites with minor iron oxide/hydroxide aggregates and opaques.

Minor lithologies:
a. RADIOLARIAN CLAY, brown (7.5YR 5/4), occurring in distorted bands in Section 3 (49-51, 63-65, 96-100, and 113-122 cm) and Section 4 (14-29 cm); contains up to 50% radiolarians.
b. CLAYEY RADIOLARIAN PORCELLANITE to CHERT, grayish brown (5YR 3/2 - 7.5YR 3/3) mottled with grayish orange pink or light reddish pink (5YR 7/2 - 5YR 6/4); planar or faser laminated with bioturbation; variable silicification from CLAYEY PORCELLANITE to conchoidal fracturing CHERT; occurring from Section 4, 29 cm to base of core.

SLIDE SUMMARY (%):

| | 2, 80<br>D | 3, 117<br>M | 4, 12<br>D |
|---|---|---|---|
| TEXTURE: | | | |
| Sand | — | 30 | 10 |
| Silt | 20 | 15 | 10 |
| Clay | 80 | 55 | 80 |
| COMPOSITION: | | | |
| Clay | 74 | 50 | 19 |
| Glass | Tr | — | — |
| Opaques | 1 | — | 1 |
| Oxide | 3 | 5 | Tr |
| Quartz | 1 | Tr | — |
| Radiolarians | 1 | 45 | 15 |
| Silica | — | — | 60 |
| Spicules | — | — | 5 |
| Zeolite | 20 | Tr | — |

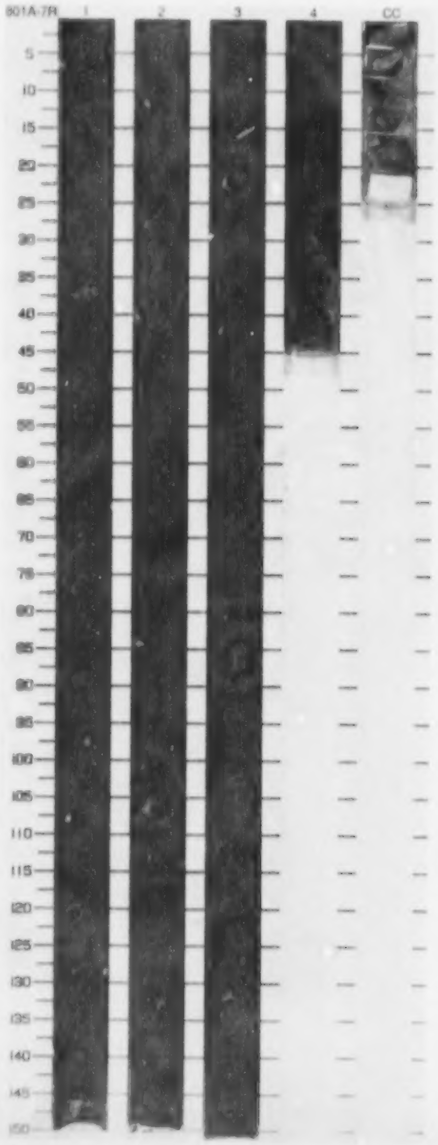
801A-7R
1
2
3
4
CC
5
10
15
20
25
30
35
40
45
50
55
60
65
70
75
80
85
90
95
100
105
110
115
120
125
130
135
140
145
150

SITE 801 HOLE A CORE 8R CORED INTERVAL 5742.4-5752.0 mbsl; 68.6-78.2 mbsf

| TIME-ROCK UNIT | BIOSTRAT. ZONE/ FOSSIL CHARACTER FORAMINIFERS | NANNOFOSSILS | RADIOLARIANS | DIATOMS | PALYNOMORPHS | PALEOMAGNETICS | PHYS. PROPERTIES | CHEMISTRY | SECTION | METERS | GRAPHIC LITHOLOGY | DRILLING DISTURB. | SED. STRUCTURES | SAMPLES |
|---|---|---|---|---|---|---|---|---|---|---|---|---|---|---|
| CONIACIAN - COMPANIAN | *Amphipyndax pseudoconulus - Amphipyndax tylotus* | B | A/P | B | N N<br>B | R?<br>R? | R? | | 1 | | | X<br>X | | |

## LITHOLOGIC DESCRIPTION

RADIOLARIAN CHERT with PORCELLANITE

Major lithology: RADIOLARIAN CHERT with PORCELLANITE, moderate brown (5YR 4/4 - 5YR 3/4), thin bedded with distinct planar and flaser laminations (laminations are a function of relative concentrations of radiolarians and clay), cross lamination (at Section 1, 21-23 cm) and minor bioturbation; manganese oxide dendrites on some fracture surfaces.

Minor lithology: CLAYSTONE (16-20 cm), dark yellowish brown (10YR 4/2), mottled and totally disrupted by drilling, and light brown (7.5YR 6/4), on basal bedding plane of banded chert piece at Section 1, 34 cm, contains clay with minor zeolites, iron oxides and radiolarians, possibly represents interbeds between cherty horizons.

SLIDE SUMMARY (%)

| | 1, 1<br>D | 1, 34<br>M |
|---|---|---|
| TEXTURE | | |
| Sand | 10 | — |
| Silt | 15 | 2 |
| Clay | 75 | 98 |
| COMPOSITION | | |
| Clay | 25 | 90 |
| Fish | Tr | — |
| Glass | — | Tr |
| Opaques | 3 | — |
| Oxide | 2 | 6 |
| Radiolarians | 20 | 2 |
| Silica | 50 | — |
| Zeolite | — | 2 |

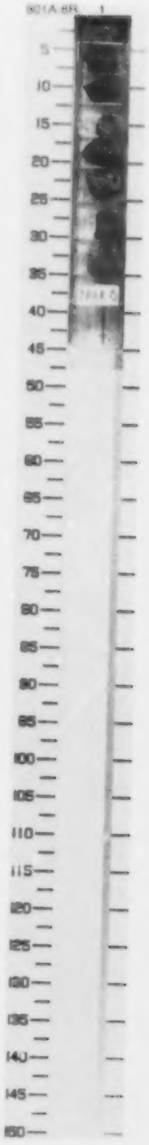

SITE 801 HOLE A CORE 9R CORED INTERVAL 5752.0-5767.3 mbsl; 78.2-87.5 mbsf

| TIME-ROCK UNIT | BIOSTRAT. ZONE/ FOSSIL CHARACTER | | | | | PALEOMAGNETICS | PHYS. PROPERTIES | CHEMISTRY | SECTION | METERS | GRAPHIC LITHOLOGY | DRILLING DISTURB. | SED. STRUCTURES | SAMPLES | LITHOLOGIC DESCRIPTION |
|---|---|---|---|---|---|---|---|---|---|---|---|---|---|---|---|
| | FORAMINIFERS | NANNOFOSSILS | RADIOLARIANS | DIATOMS | PALYNOMORPHS | | | | | | | | | | |
| CONIACIAN - CAMPANIAN | B | B | A/P *Theocampe urna* - *Amphipyndax pseudoconulus* | | B | N | ● $\phi=21.7$<br>● $\gamma=1.97$ | ● 0.1 | 1 | | ▲ ▲ ▲ ▲ ▲ | > | | # | RADIOLARIAN CHERT<br>Major lithology: RADIOLARIAN CHERT, moderate brown (5YR 4/4) to grayish brown (5YR 3/2), mottled to planar laminated to massive, minor bioturbation, manganese oxide dendrites on some fracture surfaces, lowest piece has vertical fracture filled with grayish orange pink (5YR 7/2) material.<br>SLIDE SUMMARY (%):<br>1, 0<br>D<br>TEXTURE:<br>Sand 5<br>Silt 15<br>Clay 80<br>COMPOSITION:<br>Clay 40<br>Oxide 5<br>Radiolarians 20<br>Silica 20<br>Spines 15 |

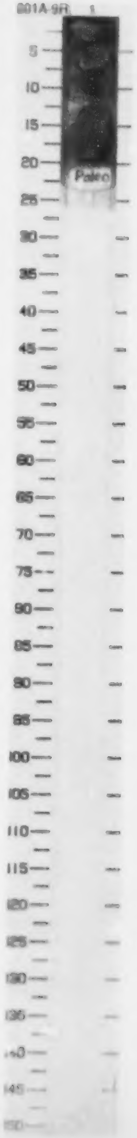
801A-9R
1
Paleo
5
10
15
20
25
30
35
40
45
50
55
60
65
70
75
80
85
90
95
100
105
110
115
120
125
130
135
140
145
150

SITE 801 HOLE A CORE 10R CORED INTERVAL 5761.3-5770.9 mbsl; 87.5-97.1 mbsf

| TIME-ROCK UNIT | FORAMINIFERS | NANNOFOSSILS | RADIOLARIANS | DIATOMS | PALYNOMORPHS | PALEOMAGNETICS | PHYS. PROPERTIES | CHEMISTRY | SECTION | METERS | GRAPHIC LITHOLOGY | DRILLING DISTURB. | SED. STRUCTURES | SAMPLES | LITHOLOGIC DESCRIPTION |
|---|---|---|---|---|---|---|---|---|---|---|---|---|---|---|---|
| CENOMANIAN - CONIACIAN | B | B | R/M unzoned | | B | N | [illegible] | | 1 | 0.5 | | | | ✱ | RADIOLARIAN PORCELLANITE with CHERT |

BIOSTRAT. ZONE/ FOSSIL CHARACTER

Major lithology: RADIOLARIAN PORCELLANITE with CHERT, grayish brown (5YR 3/2) to moderate brown (5YR 4/4), porcellanite and chert are interlaminated in variable proportions with chert being generally lighter in color than porcellanite.

Minor lithology: CLAYEY RADIOLARIAN PORCELLANITE to RADIOLARIAN SILICEOUS CLAYSTONE, dusky brown (5YR 2/2), moderate brown (5YR 3/4) and dark yellowish brown (10YR 4/2), easily scratched (pieces at 15-20, 30-45 and 49-58 cm).

SLIDE SUMMARY (%):

| | 1, 0<br>D |
|---|---|
| TEXTURE: | |
| Sand | 15 |
| Silt | 8 |
| Clay | 77 |
| COMPOSITION: | |
| Clay | 12 |
| Opaques | 1 |
| Organic matter | Tr |
| Radiolarians | 23 |
| Silica | 64 |

SITE 801 HOLE A CORE 11R CORED INTERVAL 5770.9-5780.6 mbsl; 97.1-106.8 mbsf

| TIME-ROCK UNIT | FORAMINIFERS | NANNOFOSSILS | RADIOLARIANS | DIATOMS | PALYNOMORPHS | PALEOMAGNETICS | PHYS. PROPERTIES | CHEMISTRY | SECTION | METERS | GRAPHIC LITHOLOGY | DRILLING DISTURB. | SED. STRUCTURES | SAMPLES | LITHOLOGIC DESCRIPTION |
|---|---|---|---|---|---|---|---|---|---|---|---|---|---|---|---|
| CENOMANIAN - CONIACIAN | B | B | A/M *Obesacapsula somphed-a* | | B | N | | | 1 | | | | | ✱ | RADIOLARIAN CHERT with PORCELLANITE |

BIOSTRAT. ZONE/ FOSSIL CHARACTER

Major lithology: RADIOLARIAN CHERT with PORCELLANITE, moderate brown (5YR 3/4 - 5YR 4/4) and light brown (5YR 5/6), banded to laminated with minor bioturbation, top piece has black (N2) laminations.

Minor lithology: (Section 1, 14-20 cm)
a. RADIOLARIAN PORCELLANITE, grayish brown (5YR 3/2) with dark laminations.
b. CLAYSTONE, light brown (5YR 5/6), as a thin "rind" to chert in piece at Section 1, 22 cm.

SLIDE SUMMARY (%):

| | 1, 25<br>M |
|---|---|
| TEXTURE: | |
| Sand | 2 |
| Silt | 10 |
| Clay | 88 |
| COMPOSITION: | |
| Clay | 53 |
| Mica | 2 |
| Oxide | 5 |
| Radiolarians | 15 |
| Silica | 15 |
| Spines | 10 |
| Zeolite | Tr |

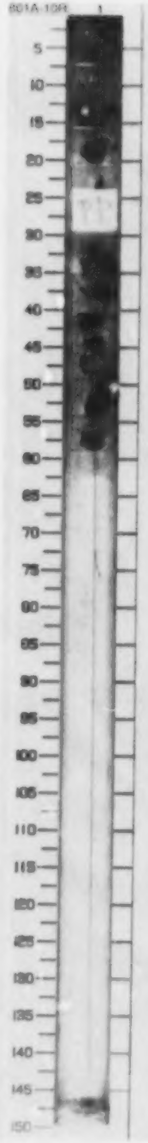

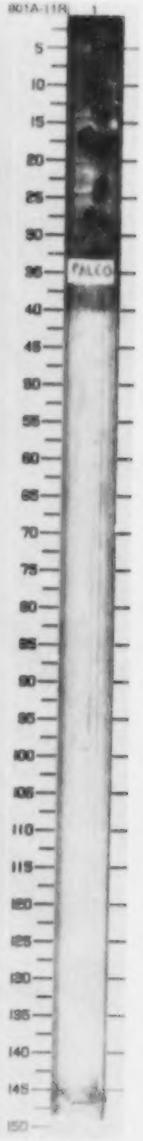

SITE 801 HOLE A CORE 12R CORED INTERVAL 5780.6-5790.3 mbsl; 106.8-116.5 mbsf

| TIME-ROCK UNIT | BIOSTRAT. ZONE/ FOSSIL CHARACTER: FORAMINIFERS | NANNOFOSSILS | RADIOLARIANS | DIATOMS | PALYNOMORPHS | PALEOMAGNETICS | PHYS. PROPERTIES | CHEMISTRY | SECTION | METERS | GRAPHIC LITHOLOGY | DRILLING DISTURB. | SED. STRUCTURES | SAMPLES |
|---|---|---|---|---|---|---|---|---|---|---|---|---|---|---|
| CENOMANIAN - CONIACIAN | B | B | A/P *Acaeniotyle umbilicata - Obesacapsula somphedia* | | B | N | ● $\phi=26.3$ <br> $\rho_b=1.98$ | ● 0.1 | 1 | | ▲ ▲ ▲ ▲ ▲ | | | # |

### LITHOLOGIC DESCRIPTION

RADIOLARIAN CHERT with PORCELLANITE

Major lithology: RADIOLARIAN CHERT with PORCELLANITE, moderate brown (5YR 4/4) grading to light brown (5YR 5/6); some pieces display thin bedding to planar lamination; rare fractures filled with black manganese oxide. Chert is dark yellowish orange (10YR 6/6) in a thin band at Section 1, 28-30 cm. Thin section at Section 1, 6-8 cm, contains radiolarians filled with silica and radiolarians filled with clay.

SLIDE SUMMARY (%):

| | 1, 6 <br> D |
|---|---|
| TEXTURE: | |
| Sand | Tr |
| Silt | 20 |
| Clay | 80 |
| COMPOSITION: | |
| Clay | 46 |
| Glass | 1 |
| Oxide | 3 |
| Radiolarians | 20 |
| Silica | 20 |
| Spines | 10 |

801A-12R 1

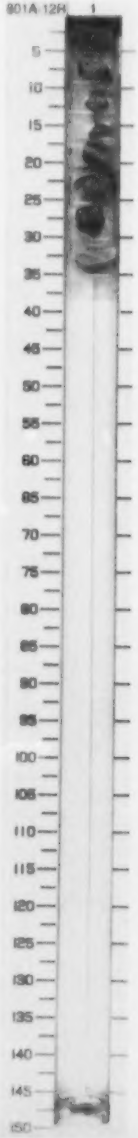

---

SITE 801 HOLE A CORE 13R CORED INTERVAL 5790.3-5800.0 mbsl; 116.5-126.2 mbsf

801A-13R 1

SITE 801 HOLE A CORE 13R CORED INTERVAL 5790.3-5800.0 mbsl; 116.5-126.2 mbsf

| TIME-ROCK UNIT | BIOSTRAT. ZONE/ FOSSIL CHARACTER | | | | | PALEOMAGNETICS | PHYS. PROPERTIES | CHEMISTRY | SECTION | METERS | GRAPHIC LITHOLOGY | DRILLING DISTURB. | SED. STRUCTURES | SAMPLES | LITHOLOGIC DESCRIPTION |
|---|---|---|---|---|---|---|---|---|---|---|---|---|---|---|---|
| | FORAMINIFERS | NANNOFOSSILS | RADIOLARIANS | DIATOMS | PALYNOMORPHS | | | | | | | | | | |
| CENOMANIAN - CONIACIAN | B | B | A/M *Acaeniotyle umbilicata - Obesacapsula somphedia* | | B | N | ●<br>ϕ=21.7<br>γ=2.13 | ●<br>5.4 | 1 | | | ×<br>× | | ●<br># | RADIOLARIAN PORCELLANITE with CALCAREOUS RADIOLARIAN PORCELLANITE |

Major lithology: RADIOLARIAN PORCELLANITE, grayish brown (10YR 5/2) interlaminated with CALCAREOUS RADIOLARIAN PORCELLANITE, light brownish gray (10YR 6/2), small lenses, truncated laminations, and minor bioturbation. Very dark green (10GY 3/2) clay filling and pale green (5G 7/2) zones of alteration or staining at microfractures.

Minor lithology: RADIOLARIAN CHERT, thinly laminated light to dark brown (7.5YR 6/4-7.5YR 4/2), minor bioturbation.
Note: Abrupt color change from browns and reddish browns (5YR-) downward to grays (10YR 5/2-10YR 6/2) at Section 1, 2.5 cm.

SLIDE SUMMARY (%)

| | 1, 1<br>D | 1, 18<br>D |
|---|---|---|
| TEXTURE | | |
| Sand | — | 15 |
| Silt | 15 | 10 |
| Clay | 85 | 75 |
| COMPOSITION | | |
| Barite | — | 1 |
| Clay | 20 | 20 |
| Micrite | — | 40 |
| Opaques | 1 | — |
| Oxide | 2 | 2 |
| Radiolarians | 15 | 15 |
| Silica | 62 | 15 |
| Spines | — | 4 |
| Zeolite | Tr | — |

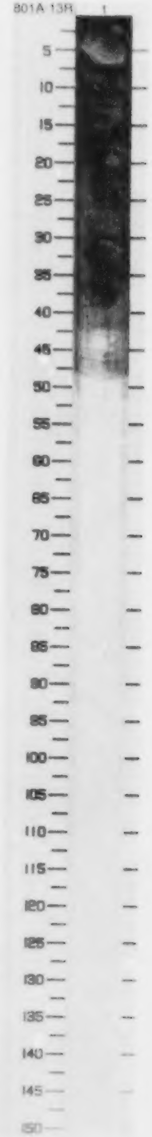

SITE 801 HOLE A CORE 14R CORED INTERVAL 5800.0-5809.7 mbsl; 126.2-135.9 mbsf

| TIME-ROCK UNIT | BIOSTRAT. ZONE/ FOSSIL CHARACTER |  |  |  |  | PALEOMAGNETICS | PHYS. PROPERTIES | CHEMISTRY | SECTION | METERS | GRAPHIC LITHOLOGY | DRILLING DISTURB. | SED. STRUCTURES | SAMPLES |
|---|---|---|---|---|---|---|---|---|---|---|---|---|---|---|
|  | FORAMINIFERS | NANNOFOSSILS | RADIOLARIANS | DIATOMS | PALYNOMORPHS |  |  |  |  |  |  |  |  |  |
| CENOMANIAN | B | A/M | A/M *Eiffellithus turriseiffeli* (CC9) (NC10) | unzoned | B | N | ● [illegible] | ● 0.2 | 1 | 0.5 | 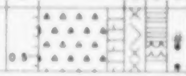 |  |  |  |

## LITHOLOGIC DESCRIPTION

RADIOLARIAN PORCELLANITE

Major lithology: RADIOLARIAN PORCELLANITE, dark gray (5Y 4/1 - 5Y 3/1), locally m-cl laminated, scattered bioturbation, dull luster and rougher fracture indicates increased clay content.

Minor lithologies:
a. TUFFACEOUS NANNOFOSSIL CLAYSTONE grading to NANNOFOSSIL CHALK, gray to dark gray (N5 -N4).
b. FELDSPATHIC RADIOLARIAN VOLCANICLASTIC SANDSTONE TURBIDITE (Section 1, 35-37 cm), dark gray (N4), scoured base, micro load casts, contains volcanic glass, plagioclase, oxides, and radiolarians.

SLIDE SUMMARY (%):

|  | 1, 32 D | 1, 40 M | 1, 61 M |
|---|---|---|---|
| TEXTURE: |  |  |  |
| Sand | 5 | Tr | 3 |
| Silt | 30 | 40 | 35 |
| Clay | 65 | 60 | 62 |
| COMPOSITION: |  |  |  |
| Accessory minerals | — | Tr | — |
| Calcite | — | — | 6 |
| Clay | 42 | 35 | 10 |
| Feldspar | — | 15 | — |
| Glass | — | 20 | 5 |
| Nannofossils | — | 15 | 65 |
| Opaques | — | 3 | 3 |
| Oxide | 5 | 2 | 1 |
| Radiolarians | 30 | 10 | 10 |
| Silica | 10 | — | — |
| Smectite | 3 | — | — |
| Spines | 10 | — | — |

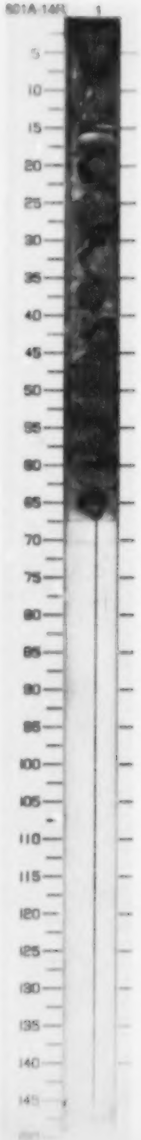

SITE 801 HOLE A CORE 15R CORED INTERVAL 5809.7-5819.4 mbsl; 135.9-145.6 mbsf

| TIME-ROCK UNIT | BIOSTRAT. ZONE/ FOSSIL CHARACTER: FORAMINIFERS | NANNOFOSSILS | RADIOLARIANS | DIATOMS | PALYNOMORPHS | PALEOMAGNETICS | PHYS. PROPERTIES | CHEMISTRY | SECTION | METERS | GRAPHIC LITHOLOGY | DRILLING DISTURB. | SED. STRUCTURES | SAMPLES |
|---|---|---|---|---|---|---|---|---|---|---|---|---|---|---|
| CENOMANIAN | B | A/M *Eiffellithus turriseiffelii* (CC9) (NC10) | A/P unzoned | | B | N | ●<br>49.1<br>1.99 | ●<br>1.2 | 1 | | | | | ●<br>✱ |

LITHOLOGIC DESCRIPTION

VOLCANICLASTIC SANDSTONE and RADIOLARIAN PORCELLANITE

Major lithologies:
a. VOLCANICLASTIC SANDSTONE, dark blue gray to greenish gray (5B 4/1 - 5BG 5/1), chiefly fresh glass with thin altered rims, oxides, plagioclase, and olivine(?). Grades to VOLCANICLASTIC CLAYEY RADIOLARITE.
b. RADIOLARIAN PORCELLANITE, dark gray (5Y 3/1 - 5Y 4/1), is interbedded with the volcaniclastic sandstone, locally with calcareous laminations and scoured contacts.

Minor lithology: TUFFACEOUS NANNOFOSSIL CHALK, gray (5Y 5/1), mostly homogeneous, rare microlaminations.

SLIDE SUMMARY (%):

| | 1, 16<br>M | 1, 36<br>D |
|---|---|---|
| TEXTURE: | | |
| Sand | 35 | 10 |
| Silt | 35 | 10 |
| Clay | 30 | 80 |
| COMPOSITION: | | |
| Accessory minerals | 1 | — |
| Clay | 34 | 30 |
| Feldspar | 5 | — |
| Glass | 5 | — |
| Opaques | — | 2 |
| Oxide | — | 1 |
| Radiolarians | 55 | 15 |
| Silica | — | 52 |

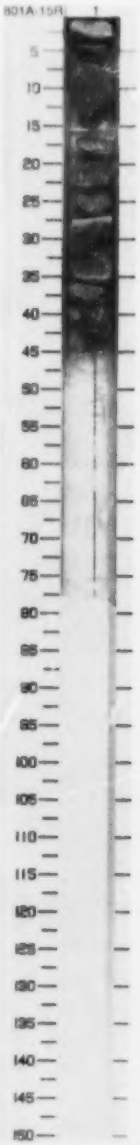

SITE 801 HOLE A CORE 16R CORED INTERVAL 5819.4-5829.0 mbsl; 145.6-155.2 mbsf

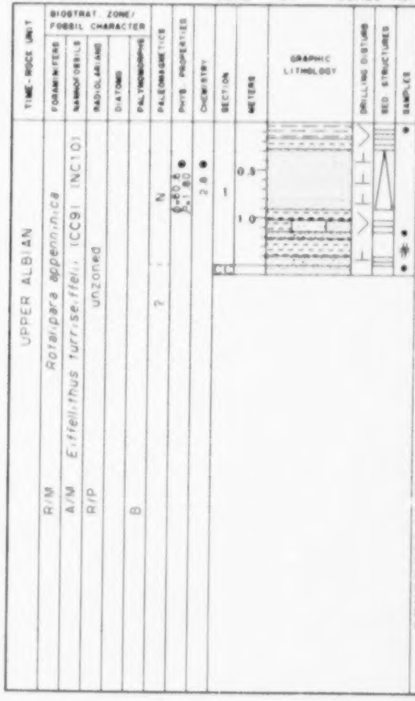
TIME-ROCK UNIT
BIOSTRAT. ZONE/ FOSSIL CHARACTER
FORAMINIFERS
NANNOFOSSILS
RADIOLARIANS
DIATOMS
PALYNOMORPHS
PALEOMAGNETICS
PHYS. PROPERTIES
CHEMISTRY
SECTION
METERS
GRAPHIC LITHOLOGY
DRILLING DISTURB.
SED. STRUCTURES
SAMPLES
UPPER ALBIAN
R/M Rotalipora appenninica
A/M Eiffellithus turriseiffeli (CC9) (NC10)
R/P unzoned
B
N
?
2.8
1
0.5
1.0
CC

LITHOLOGIC DESCRIPTION

VOLCANICLASTIC SANDSTONE to CLAYSTONE

Major lithology: VOLCANICLASTIC SANDSTONE to CLAYSTONE, dark greenish gray, greenish gray and bluish gray (5G 4/1, 5BG 4/1, 5GY 4/1, 5G 5/1, 5B 4/1). Finer-grained intervals are fine- to micro-laminated. The sandstone intervals are mostly well sorted; thick bed at Section 1, 25-91 cm, has various intraclasts including a laminated 3 cm wide mud clast near the base (turbiditic origin?). Claystone contains radiolarians and micrite.

Minor lithology: TUFFACEOUS SANDSTONE, dark gray to black (N4-N2), well sorted, in Section 1, 115-120 and 128-150 cm. May represent a coarse ash tuff deposit.

SLIDE SUMMARY (%):

| | 1, 8<br>D | 1, 117<br>D | 1, 133<br>M | CC, 1<br>M |
|---|---|---|---|---|
| TEXTURE: | | | | |
| Sand | 30 | 15 | 15 | — |
| Silt | 30 | 70 | 5 | 10 |
| Clay | 40 | 15 | 80 | 90 |
| COMPOSITION: | | | | |
| Calcite | 5 | Tr | — | 1 |
| Clay | 10 | 15 | 40 | 72 |
| Feldspar | Tr | — | — | Tr |
| Glass | 45 | 60 | — | — |
| Igneous rock fragments | — | 10 | — | — |
| Mica | — | — | — | 5 |
| Micrite | — | — | 20 | — |
| Nannofossils | 10 | — | — | 20 |
| Opaques | 10 | 10 | — | — |
| Oxide | — | — | 3 | — |
| Palagonite | — | 5 | — | — |
| Pyroxene | — | — | — | 2 |
| Radiolarians | Tr | — | 15 | — |
| Silica | — | — | 15 | — |
| Smectite | — | — | 5 | — |
| Spines | — | — | 2 | — |

801A-16R
1
CC
5
10
15
20
25
30
35
40
45
50
55
60
65
70
75
80
85
90
95
100
105
110
115
120
125
130
135
140
145
150

SITE 801 HOLE A CORE 17R CORED INTERVAL 5829.0-5838.8 mbsl; 155.2-165.0 mbsf

| TIME-ROCK UNIT | BIOSTRAT. ZONE/ FOSSIL CHARACTER | | | | | PALEOMAGNETICS | PHYS. PROPERTIES | CHEMISTRY | SECTION | METERS | GRAPHIC LITHOLOGY | DRILLING DISTURB. | SED. STRUCTURES | SAMPLES |
|---|---|---|---|---|---|---|---|---|---|---|---|---|---|---|
| | FORAMINIFERS | NANNOFOSSILS | RADIOLARIANS | DIATOMS | PALYNOMORPHS | | | | | | | | | |
| UPPER ALBIAN | B | A/M *Eiffellithus turriseiffeli* (CC9) (NC10) | C/P unzoned | | B | ? | ●φ32.4 γ1.98 | ●0.2 | 1 | 0.5 | | | | ● # |

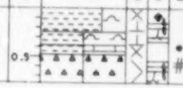

## LITHOLOGIC DESCRIPTION

CLAYEY RADIOLARITE interbedded with CALCAREOUS CLAYSTONE, and RADIOLARIAN CHERT with PORCELLANITE

Major lithologies:
a. CLAYEY RADIOLARITE, grayish olive green (5GY 3/2), laminated to vaguely flaser laminated, interbedded with CALCAREOUS CLAYSTONE, dusky green (5G 3/2), minor bioturbation.
b. RADIOLARIAN CHERT with PORCELLANITE, olive gray, grayish olive green and grayish olive (5Y 3/2, 5GY 3/2 and 10Y 4/2), piece at Section 1, 75 cm, has a band of vitreous, smoky-transparent quartz as fracture-fill. Thin section of porcellanite at Section 1, 59-60 cm contains 25% volcanic glass.

Minor lithologies:
a. (Section 1, 1-6 cm) CALCAREOUS SILTY SANDSTONE, light gray (N7), contains nannofossils and coarse-sand-size mud clasts.
b. (Section 1, 38-48 cm) NANNOFOSSIL CLAYSTONE, dusky green (5G 3/2), contains minor amounts of volcanic glass, mica and zeolites.
SLIDE SUMMARY (%):

| | 1, 40<br>D | 1, 59<br>D |
|---|---|---|
| TEXTURE: | | |
| Silt | 10 | 35 |
| Clay | 90 | 65 |
| COMPOSITION: | | |
| Clay | 49 | 10 |
| Feldspar | — | 5 |
| Glass | 3 | 22 |
| Mica | 3 | — |
| Nannofossils | 40 | — |
| Opaques | — | 3 |
| Oxide | 3 | 1 |
| Radiolarians | — | 2 |
| Silica | — | 56 |
| Zeolite | 2 | — |

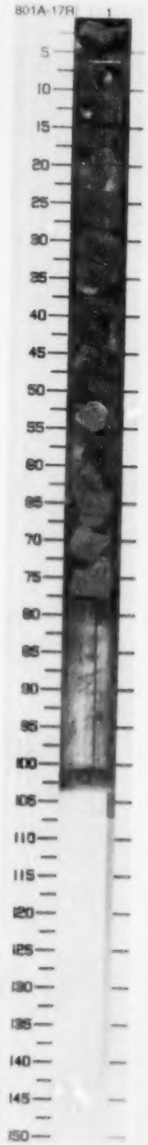

SITE 801 HOLE A CORE 18R CORED INTERVAL 5838.8-5848.5 mbsl; 165.0-174.7 mbsf

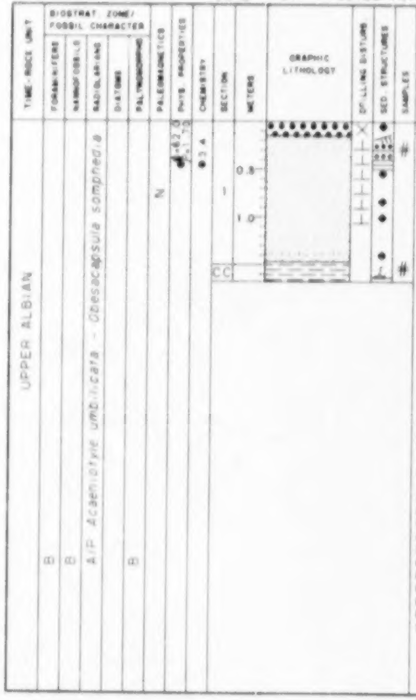
TIME-ROCK UNIT
BIOSTRAT. ZONE/ FOSSIL CHARACTER
FORAMINIFERS
NANNOFOSSILS
RADIOLARIANS
DIATOMS
PALYNOMORPHS
PALEOMAGNETICS
PHYS. PROPERTIES
CHEMISTRY
SECTION
METERS
GRAPHIC LITHOLOGY
DRILLING DISTURB.
SED. STRUCTURES
SAMPLES
UPPER ALBIAN
B
B
A/P Acaeniotyle umbilicata - Obesacapsula somphedia
B
N
1
CC
0.5
1.0
#
#

LITHOLOGIC DESCRIPTION

VOLCANICLASTIC SANDSTONE

Major lithology: VOLCANICLASTIC SANDSTONE, dark greenish gray (5G 4/1), poorly sorted with abundant claystone clasts in a calcareous sandy matrix; amalgamation of grain and debris flows is suggested; maximum clast size is >2 cm (at Section 1, 93 cm); laminated and cross laminated near top of core.

Minor lithologies:

a. VOLCANICLASTIC GRITSTONE, dark greenish gray (5G 4/1), with angular to subrounded clasts of claystone, chert and igneous rock fragments up to 1 cm long; some possible algal clasts. Section 1, 0-14 cm.

b. VOLCANICLASTIC SILTSTONE and CLAYSTONE, finely laminated with brownish gray (5YR 4/1), olive gray (5Y 4/1) and dark greenish gray (5G 4/1); some millimeter-scale lenses of light greenish gray (5G 8/1). Section 2, 0-18 cm. Claystone contains radiolarians.

SLIDE SUMMARY (%):

| | 1, 29<br>D | 2, 4<br>M |
|---|---|---|
| TEXTURE: | | |
| Sand | 40 | 10 |
| Silt | 30 | 5 |
| Clay | 30 | 85 |
| COMPOSITION: | | |
| Calcite | 20 | — |
| Clay | 10 | 48 |
| Feldspar | 10 | — |
| Glass | 32 | 5 |
| Igneous rock fragments | 20 | — |
| Opaques | — | 5 |
| Oxide | 2 | Tr |
| Pyroxene | 5 | — |
| Radiolarians | — | 12 |
| Red algae | 1 | — |
| Silica | — | 30 |

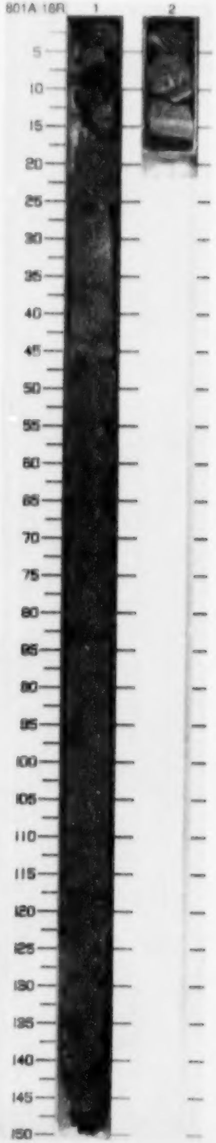
801A 18R
1
2
5
10
15
20
25
30
35
40
45
50
55
60
65
70
75
80
85
90
95
100
105
110
115
120
125
130
135
140
145
150

SITE 801 HOLE A CORE 19R CORED INTERVAL 5848.5-5858.2 mbsl; 174.7-184.4 mbsf

| TIME-ROCK UNIT | FORAMINIFERS | NANNOFOSSILS | RADIOLARIANS | DIATOMS | PALYNOMORPHS | PALEOMAGNETICS | PHYS. PROPERTIES | CHEMISTRY | SECTION | METERS | GRAPHIC LITHOLOGY | DRILLING DISTURB. | SED. STRUCTURES | SAMPLES |
|---|---|---|---|---|---|---|---|---|---|---|---|---|---|---|
| UPPER ALBIAN | B | C/M *Eiffellithus turriseiffelii* (CC9) (NC10) | A/P *Acaeniotyle umbilicata* - *Obesacapsula somphedia* | | B | N? | ● $\phi$ = 71.9<br>$\gamma$ = 1.50 | ● 7.7 | 1<br>CC | 0.5 | 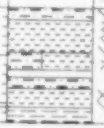 | / / / / <br>X | | ●<br>●<br>IW |

LITHOLOGIC DESCRIPTION

VOLCANICLASTIC SILTY CLAYSTONE and VOLCANICLASTIC SANDY SILTSTONE

Major lithologies:
a. VOLCANICLASTIC SILTY CLAYSTONE, dark greenish gray (5G 4/1), contains clay, volcanic glass and calcite with minor nannofossils and quartz, poorly consolidated and commonly reduced to drilling slurry.
b. VOLCANICLASTIC SANDY SILTSTONE, brownish black to greenish black (5YR 2/1, 5Y 2/1, 5GY 2/1), laminated to massive. XRD data from Section 1, 3 cm, indicates the presence of clinoptilolite.

Minor lithology: CLAYEY SILTSTONE, dark greenish gray (5GY 4/1) and massive, or olive gray (5Y 4/1) and laminated with minor mud clasts; comprises CC, 0-18 cm.

SLIDE SUMMARY (%):

| | 1, 1<br>D | 1, 43<br>D |
|---|---|---|
| TEXTURE: | | |
| Sand | 90 | 5 |
| Silt | 10 | 30 |
| Clay | Tr | 65 |
| COMPOSITION: | | |
| Accessory minerals | — | 2 |
| Calcite | 2 | 10 |
| Clay | — | 60 |
| Feldspar | 5 | 1 |
| Glass | 72 | 20 |
| Igneous rock fragments | 10 | — |
| Nannofossils | — | 4 |
| Opaques | 5 | — |
| Oxide | 3 | — |
| Pyroxene | 3 | — |
| Quartz | — | 3 |

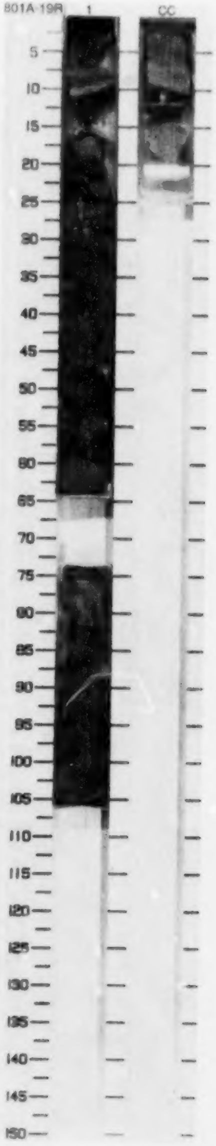

SITE 801 HOLE A CORE 20R CORED INTERVAL 5858.2-5867.8 mbsl; 184.4-194.0 mbsf

| TIME-ROCK UNIT | BIOSTRAT. ZONE/ FOSSIL CHARACTER: FORAMINIFERS | NANNOFOSSILS | RADIOLARIANS | DIATOMS | PALYNOMORPHS | PALEOMAGNETICS | PHYS. PROPERTIES | CHEMISTRY | SECTION | METERS | GRAPHIC LITHOLOGY | DRILLING DISTURB. | SED. STRUCTURES | SAMPLES | LITHOLOGIC DESCRIPTION |
|---|---|---|---|---|---|---|---|---|---|---|---|---|---|---|---|
| MIDDLE ALBIAN | B | R/P *Prediscosphaera columnata* (CC8) (NC8-9) | A/P *Acaeniotyle umbilicata* - *Dibolachras* (?) sp. | | B | N | ● [illegible] | ● 0.2 | 1 | | | | | ⊠ | RADIOLARIAN CLAYSTONE |

Major lithology: RADIOLARIAN CLAYSTONE, greenish gray (5BG 5/1) from 0-4 cm then dark olive gray (5Y 3/1 and 5Y 3/2) from 4-33 cm, rich in radiolarians, laminated with rare dark (N2) streaks 1-2 cm long. Siliceous recrystallization is in homogenous with some zones of 1.5 mm thick being almost porcellaneous.

SLIDE SUMMARY (%):

| | 1, 8 |
|---|---|
| | D |
| TEXTURE: | |
| Silt | 20 |
| Clay | 80 |
| COMPOSITION: | |
| Clay | 62 |
| Foraminifers | 1 |
| Oxide | 2 |
| Radiolarians | 20 |
| Silica | 10 |
| Spines | 5 |

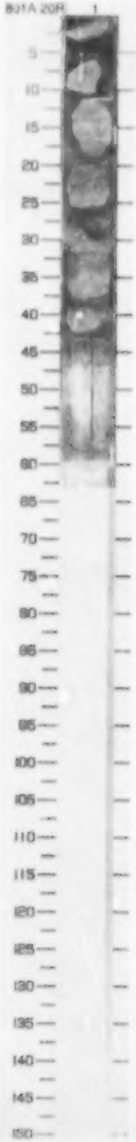

SITE 801 HOLE B CORE 1R CORED INTERVAL 5867.8-5877.3 mbsl; 194.0-203.5 mbsf

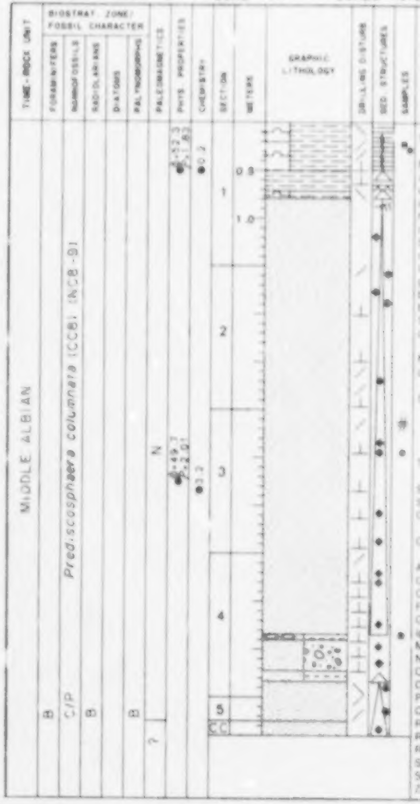
TIME-ROCK UNIT
BIOSTRAT. ZONE/ FOSSIL CHARACTER
FORAMINIFERS
NANNOFOSSILS
RADIOLARIANS
DIATOMS
PALYNOMORPHS
PALEOMAGNETICS
PHYS. PROPERTIES
CHEMISTRY
SECTION
METERS
GRAPHIC LITHOLOGY
DRILLING DISTURB.
SED. STRUCTURES
SAMPLES
MIDDLE ALBIAN
Prediscosphaera columnata (CC8) (NC8-9)
B
C/P
B
B
N
?
52.3
1.83
0.2
49.7
2.01
3.2
1
2
3
4
5
CC
0.5
1.0

LITHOLOGIC DESCRIPTION

VOLCANICLASTIC SANDSTONE and SILTY CLAYSTONE

Major lithologies:

a. VOLCANICLASTIC SANDSTONE (redeposited by debris flow or turbiditic processes), dark greenish gray (5G 4/1), grading to a very dark greenish gray (5BG 3/1) cross-laminated interval at Section 1, 78-82 cm; general fining upward trend, from coarse to medium grained, homogeneous, contains mainly grains of altered volcanic rock fragments and glass and is midly calcareous, with rare red algae grains and radiolarians; beds at Section 1, 78 cm, Section 4, 122 cm, Section 4, 00-126 cm (with high abundance of clasts) and Section 4, 134 cm to base of core. Several types of rip-up clasts up to 1 cm in length are present, including laminated to cross-laminated volcaniclastic siltstone-fine-grained sandstone (black, N2, to greenish gray, 5G 6/1) and clayey limestone (gray, 5Y 6/1).

b. VOLCANICLASTIC SILTY CLAYSTONE, dark gray (5Y 4/1), laminated with minor bioturbation, contains clay, radiolarians, feldspar, quartz and zeolites; with bands of CLAYSTONE (dark gray (N4 to 5Y 4/1), some of which are fine grained turbidites, Section 1, 0-16 cm and Section 4, 126-134 cm, and some of which contain up to 50% radiolarians.

Minor lithology: CALCAREOUS CLAYSTONE, bluish green gray (5BG 5/2), homogenous, contains traces of nannofossils.

SLIDE SUMMARY (%):

| | 1, 22<br>D | 1, 27<br>D | 3, 17<br>D | 3, 45<br>M | 4, 88<br>M |
|---|---|---|---|---|---|
| TEXTURE: | | | | | |
| Sand | 5 | 5 | 50 | 5 | — |
| Silt | 20 | 25 | 30 | 25 | 25 |
| Clay | 75 | 70 | 20 | 70 | 75 |
| COMPOSITION: | | | | | |
| Accessory minerals | — | Tr | — | — | — |
| Calcite | — | — | 3 | — | — |
| Clay | 63 | 67 | 25 | 40 | 68 |
| Feldspar | — | 12 | — | Tr | 1 |
| Glass | — | 3 | 35 | 3 | 1 |
| Igneous rock fragments | — | — | 20 | — | — |
| Microsparite | — | — | — | 50 | 25 |
| Nannofossils | — | — | — | — | 2 |
| Opaques | 5 | 3 | 3 | 1 | 3 |
| Oxide | 2 | — | 5 | — | — |
| Pyroxene | — | — | 5 | — | — |
| Quartz | — | 1 | — | — | — |
| Radiolarians | 20 | 10 | 1 | 5 | — |
| Red algae | — | — | 3 | — | — |
| Rock fragment | — | — | Tr | — | — |
| Smectite | Tr | — | — | — | — |
| Spines | 10 | — | — | — | — |
| Zeolite | — | 3 | — | — | — |

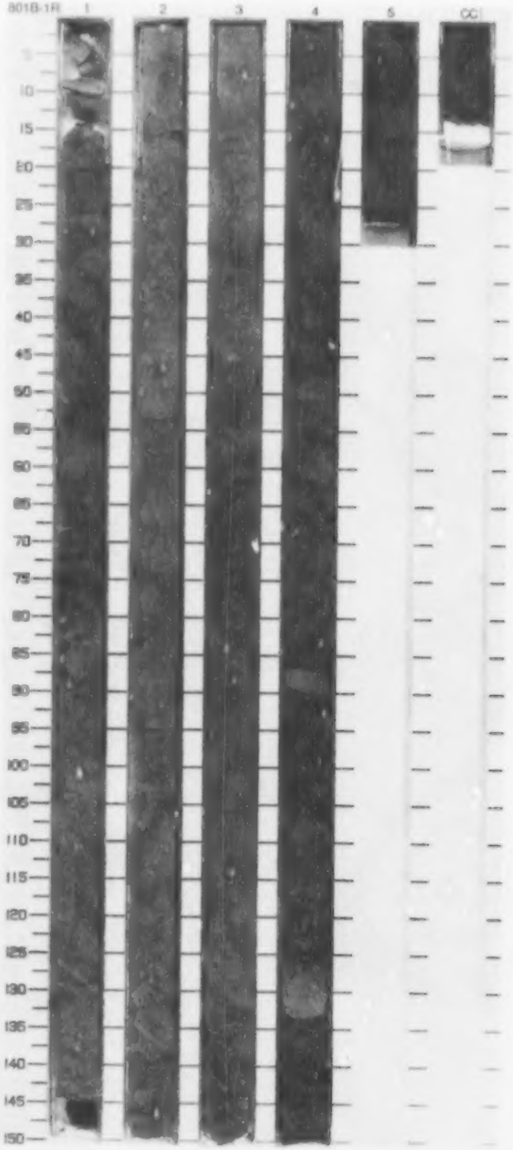
801B-1R
1
2
3
4
5
CC
5
10
15
20
25
30
35
40
45
50
55
60
65
70
75
80
85
90
95
100
105
110
115
120
125
130
135
140
145
150

SITE 801 HOLE B CORE 2R CORED INTERVAL 5877.3-5886.7 mbsl; 203.5-212.9 mbsf

| TIME-ROCK UNIT | BIOSTRAT. ZONE/ FOSSIL CHARACTER: FORAMINIFERS | NANNOFOSSILS | RADIOLARIANS | DIATOMS | PALYNOMORPHS | PALEOMAGNETICS | PHYS. PROPERTIES | CHEMISTRY | SECTION | METERS | GRAPHIC LITHOLOGY | DRILLING DISTURB. | SED. STRUCTURES | SAMPLES |
|---|---|---|---|---|---|---|---|---|---|---|---|---|---|---|
| MIDDLE ALBIAN | B | B | B |  | B | N | ● ϕ=43.1<br>γ=2.05 | ● 1.2 | 1 | 0.5<br>1.0 |  |  |  | *<br>IW |

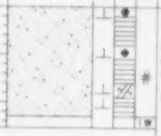

## LITHOLOGIC DESCRIPTION

VOLCANICLASTIC SILTY SANDSTONE

Major lithology: VOLCANICLASTIC SILTY SANDSTONE: olive black (5Y 2/1) to dark greenish gray (5Y 4/1), laminated with variable texture from fine-grained sand to silt; contains abundant glass, igneous rock fragments, and rare radiolarians.

SLIDE SUMMARY (%):

|  | 1, 73<br>D |
|---|---|
| TEXTURE: |  |
| Sand | 40 |
| Silt | 30 |
| Clay | 30 |
| COMPOSITION: |  |
| Calcite | 3 |
| Feldspar | 4 |
| Glass | 60 |
| Igneous rock fragments | 16 |
| Opaques | 3 |
| Oxide | 5 |
| Pyroxene | 5 |
| Radiolarians | 2 |
| Smectite | 2 |

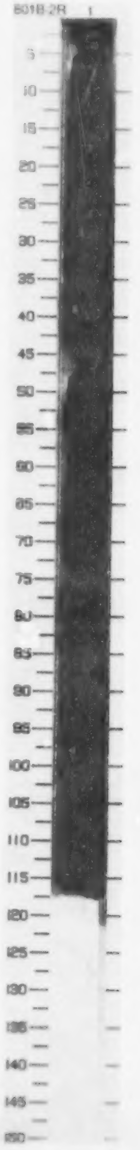
801B-2R
1
5
10
15
20
25
30
35
40
45
50
55
60
65
70
75
80
85
90
95
100
105
110
115
120
125
130
135
140
145
150

SITE 801 HOLE B CORE 3R CORED INTERVAL 5886.7-5896.1 mbsl; 212.9-222.3 mbsf

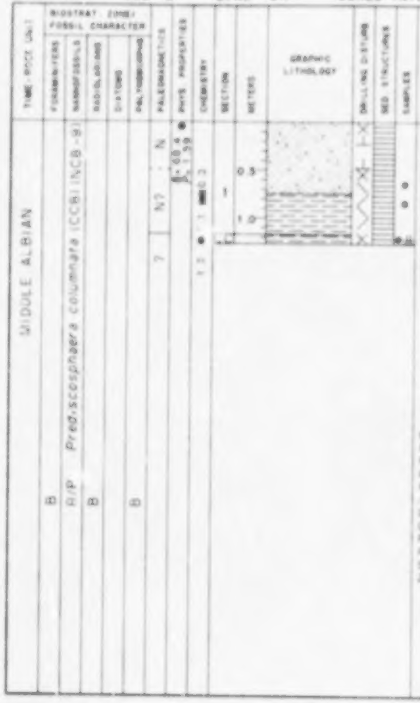
TIME-ROCK UNIT
BIOSTRAT. ZONE/ FOSSIL CHARACTER
FORAMINIFERS
NANNOFOSSILS
RADIOLARIANS
DIATOMS
PALYNOMORPHS
PALEOMAGNETICS
PHYS. PROPERTIES
CHEMISTRY
SECTION
METERS
GRAPHIC LITHOLOGY
DRILLING DISTURB.
SED. STRUCTURES
SAMPLES
MIDDLE ALBIAN
B
R/P Prediscosphaera columnata (CC8) (NC8-9)
B
B
N
N?
?
0.5
1
1.0

LITHOLOGIC DESCRIPTION

VOLCANICLASTIC SILTY SANDSTONE and CLAYEY SILTSTONE

Major lithologies:
a. VOLCANICLASTIC SILTY SANDSTONE, dark greenish gray (5GY 4/1), laminated; contains darker colored clayey siltstone laminations; Section 1, 3-75 cm.
b. VOLCANICLASTIC CLAYEY SILTSTONE, medium gray (N5, 5B 5/1) to medium light gray (N6), thin bedded; contains clay, volcanic glass, smectite, feldspar, pyroxene, igneous rock fragments, radiolarians, nannofossils and traces of zeolites; finely laminated to homogenous with some beds displaying fining upward grading.

SLIDE SUMMARY (%):

| | 1, 61<br>D | 1, 84<br>D | CC, 4<br>D | CC, 6<br>D |
|---|---|---|---|---|
| TEXTURE: | | | | |
| Sand | 60 | — | — | — |
| Silt | 40 | 70 | 40 | 20 |
| Clay | — | 30 | 60 | 80 |
| COMPOSITION: | | | | |
| Calcite | 1 | — | — | 1 |
| Clay | — | 30 | 60 | 54 |
| Feldspar | 1 | 1 | 1 | 5 |
| Glass | 75 | 30 | 15 | 5 |
| Igneous rock fragments | 10 | 20 | 5 | — |
| Nannofossils | — | 5 | 5 | — |
| Opaques | 6 | — | — | 5 |
| Oxide | 3 | 2 | 2 | 10 |
| Pyroxene | 3 | — | — | 5 |
| Radiolarians | 1 | — | — | 10 |
| Smectite | 1 | 12 | 10 | 5 |
| Zeolite | — | Tr | 2 | — |

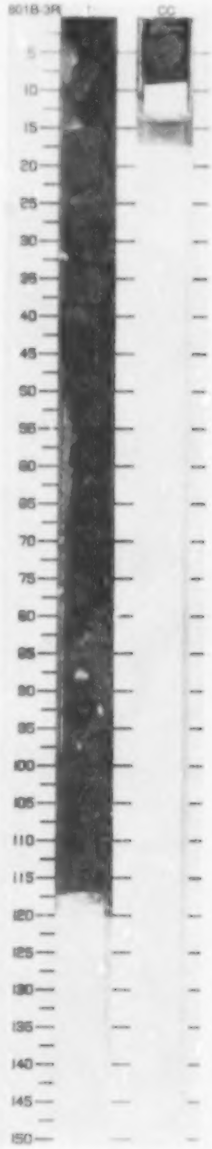
801B-3R
1
CC
5
10
15
20
25
30
35
40
45
50
55
60
65
70
75
80
85
90
95
100
105
110
115
120
125
130
135
140
145
150

SITE 801 HOLE B CORE 4R CORED INTERVAL 5896.1-5905.5 mbsl; 222.3-231.7 mbsf

| TIME-ROCK UNIT | FORAMINIFERS | NANNOFOSSILS | RADIOLARIANS | DIATOMS | PALYNOMORPHS | PALEOMAGNETICS | PHYS. PROPERTIES | CHEMISTRY | SECTION | METERS | GRAPHIC LITHOLOGY | DRILLING DISTURB. | SED. STRUCTURES | SAMPLES |
|---|---|---|---|---|---|---|---|---|---|---|---|---|---|---|
| MIDDLE ALBIAN | S | B | R/P unzoned | | B | N? | ● φ62.7 γ1.70 | ● 3.7 | 1 | | | | | ● |

LITHOLOGIC DESCRIPTION

VOLCANICLASTIC SANDY CLAYSTONE and SANDSTONE

Major lithologies:
a. VOLCANICLASTIC SANDY CLAYSTONE, gray (N5), structureless, very poorly sorted grains from clay to 4 mm. Grains include: mudstone clasts, glass, radiolarians, volcanic rock fragments, pyroxene and inorganic calcite. Probably a debris flow deposit.
b. VOLCANICLASTIC SANDSTONE, very dark green to dark greenish gray (5G 3/1-5G 4/1), moderately well sorted, very fine-grained angular grains, chiefly composed of volcanic glass shards, with rare red algae and radiolarians, well developed bedding parallel fabric of elongate glass grains enhances thin planar laminations.

SLIDE SUMMARY (%):

| | 1, 15<br>D | 1, 31<br>D |
|---|---|---|
| TEXTURE: | | |
| Sand | 25 | 80 |
| Silt | 35 | 10 |
| Clay | 40 | 10 |
| COMPOSITION: | | |
| Accessory minerals | 2 | — |
| Calcite | 5 | 1 |
| Clay | 40 | 10 |
| Feldspar | 15 | — |
| Glass | 15 | 50 |
| Igneous rock fragments | 5 | — |
| Mica | — | 1 |
| Opaques | 2 | 3 |
| Oxide | Tr | 1 |
| Pyroxene | 8 | 5 |
| Radiolarians | 5 | 5 |
| Red algae | — | 2 |
| Silica | — | 20 |
| Zeolite | Tr | — |

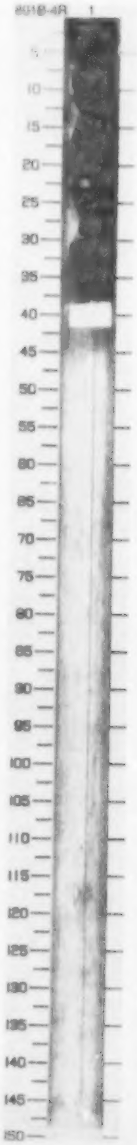

SITE 801 HOLE B CORE 5R CORED INTERVAL 5905.5-5915.1 mbsl; 231.7-241.3 mbsf

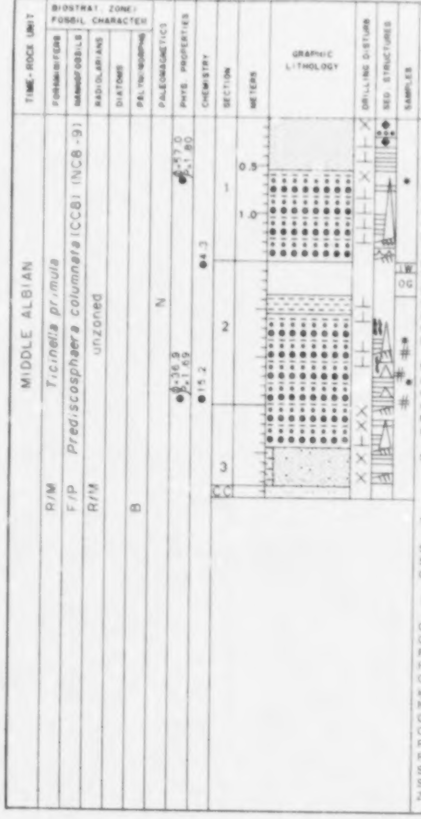
TIME-ROCK UNIT
BIOSTRAT. ZONE/FOSSIL CHARACTER
FORAMINIFERS
NANNOFOSSILS
RADIOLARIANS
DIATOMS
PALYNOMORPHS
PALEOMAGNETICS
PHYS. PROPERTIES
CHEMISTRY
SECTION
METERS
GRAPHIC LITHOLOGY
DRILLING DISTURB.
SED. STRUCTURES
SAMPLES
MIDDLE ALBIAN
R/M Ticinella primula
F/P Prediscosphaera columnata (CC8) (NC8-9)
R/M unzoned
B
N
φ=57.0
ρ=1.80
φ=36.9
ρ=1.69
●4.3
●15.2
1
2
3
CC
0.5
1.0
IW
OG

LITHOLOGIC DESCRIPTION

VOLCANICLASTIC CLAYSTONE, SILTSTONE and SANDSTONE, and VOLCANICLASTIC TURBIDITES

Major lithologies:

a. VOLCANICLASTIC CLAYSTONE, greenish gray to bluish gray (5BG 5/1 - 5B 5/1); contains volcanic glass, pyroxene, igneous rock fragments, smectite, feldspar, nannofossils and inorganic calcite. Common burrowing often accentuated by white (N9) calcitic burrows/nodules.

b. VOLCANICLASTIC SILTSTONE, greenish gray to bluish gray to dark gray (5BG 5/1, 5B 5/1, N4); typically thinly laminated, mottled or cross-laminated.

c. VOLCANICLASTIC SANDSTONE, greenish gray to greenish black to dark gray (5BG 5/1, 5G 2/1, N4); very fine to fine, locally silty, moderately well sorted, tightly packed angular glass fragments; also feldspar, pyroxene, oxides.

d. VOLCANICLASTIC TURBIDITES, greenish gray to gray (5BG 5/1 - N4); do not show scoured bases (probably due to incomplete recovery), but are identified by several fining upward beds that progress from cross and planar laminated siltstone and sandstone to bioturbated claystone.

Minor lithologies:

a. CALCAREOUS SANDSTONE, white to very light gray (N9 - N7); as laminations within volcaniclastic sandstone; composed of inorganic calcite and either calcite-replaced radiolarians or possibly ooids.

b. CALCAREOUS VOLCANICLASTIC CLAYSTONE with NANNOFOSSILS, gray (N6); an inorganic calcite and microfossil-rich end member of the volcaniclastic claystone.

SLIDE SUMMARY (%):

| | 1, 67<br>D | 2, 81<br>M | 2, 93<br>D | 2, 118<br>D | 2, 126<br>D | 2, 147<br>D |
|---|---|---|---|---|---|---|
| TEXTURE: | | | | | | |
| Sand | 1 | 40 | 50 | — | Tr | 25 |
| Silt | 20 | 30 | 30 | 30 | 40 | 30 |
| Clay | 79 | 30 | 20 | 70 | 60 | 45 |
| COMPOSITION: | | | | | | |
| Calcite | 3 | 80 | 5 | — | 20 | 15 |
| Clay | 65 | 20 | 20 | 30 | 45 | 44 |
| Feldspar | 8 | — | — | 3 | 5 | Tr |
| Foraminifers | — | — | 1 | — | — | — |
| Glass | 15 | — | 40 | 10 | 13 | — |
| Igneous rock fragments | — | — | 10 | 5 | — | 30 |
| Nannofossils | 5 | — | — | — | 10 | — |
| Opaques | 2 | — | — | 4 | 5 | 3 |
| Oxide | 1 | — | 3 | 4 | 2 | 4 |
| Pyroxene | — | — | 5 | 10 | — | 4 |
| Rock fragment | — | — | 1 | — | — | — |
| Silica | — | — | 15 | 20 | — | — |
| Smectite | — | — | — | 5 | — | — |
| Zeolite | Tr | — | — | — | Tr | — |

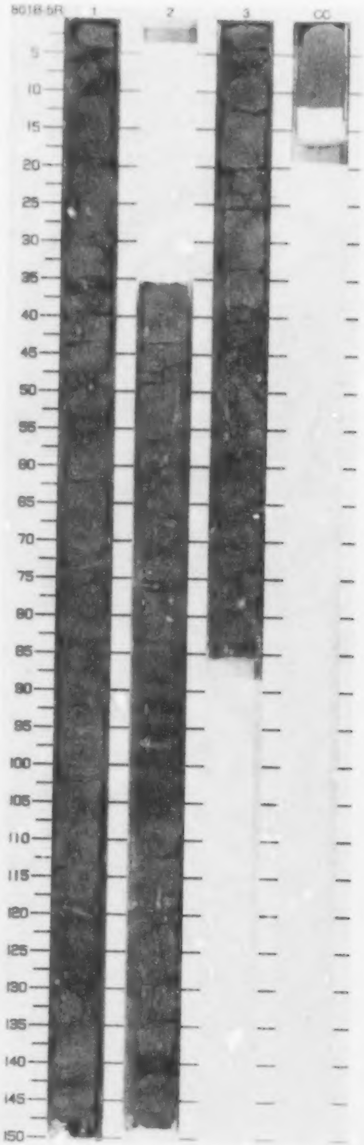
801B-5R
1
2
3
CC
5
10
15
20
25
30
35
40
45
50
55
60
65
70
75
80
85
90
95
100
105
110
115
120
125
130
135
140
145
150

SITE 801 HOLE D CORE 6R CORED INTERVAL 5915.1-5924.8 mbsl; 241.3-251.0 mbsf

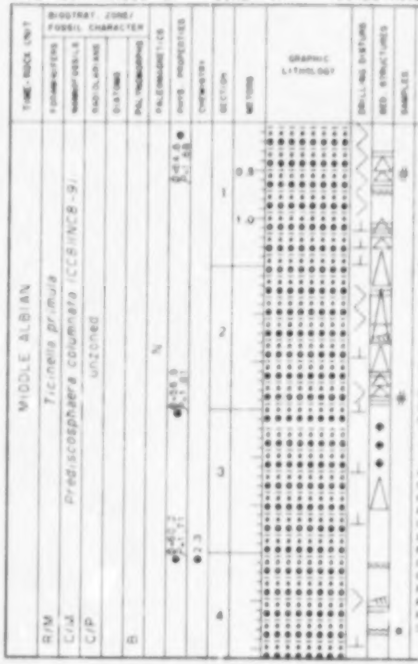

LITHOLOGIC DESCRIPTION

VOLCANICLASTIC TURBIDITES

Major lithology: VOLCANICLASTIC TURBIDITES, composed of CLAYSTONE, SILTSTONE and SANDSTONE, various shades of greenish gray (5G 5/1, 5BG 4/1), with greenish black (5GY 2/1) silty laminations locally accenting sedimentary structure. SILTY SANDSTONE or siltstone, planar to cross laminated, grades upward to claystone, which is mostly lighter in color, massive, and includes nannofossils. Some igneous rock fragments are rounded. Claystone contains volcanic glass and rare radiolarians. Burrows are sometimes filled by recrystallized calcite. Fining upward beds range from 20 to over 50 cm in size.

Minor lithology: CHERT, in Section 4, 80-82 cm, dark gray to black (5Y 4/1 - N1), apparently formed by silicification a claystone precursor.

SLIDE SUMMARY (%):

| | 1, 52<br>D | 2, 139<br>D | 4, 80<br>M |
|---|---|---|---|
| TEXTURE: | | | |
| Sand | 5 | 15 | 10 |
| Silt | 10 | 30 | 40 |
| Clay | 85 | 55 | 50 |
| COMPOSITION: | | | |
| Accessory minerals | — | — | 5 |
| Calcite | 1 | — | 5 |
| Clay | 72 | 57 | 40 |
| Feldspar | 5 | 2 | — |
| Glass | — | 30 | 50 |
| Igneous rock fragments | 7 | — | — |
| Nannofossils | — | — | Tr |
| Opaques | 2 | 3 | — |
| Oxide | 3 | 5 | — |
| Palagonite | — | — | Tr |
| Pyroxene | — | 1 | — |
| Radiolarians | — | 2 | Tr |
| Silica | 10 | — | — |

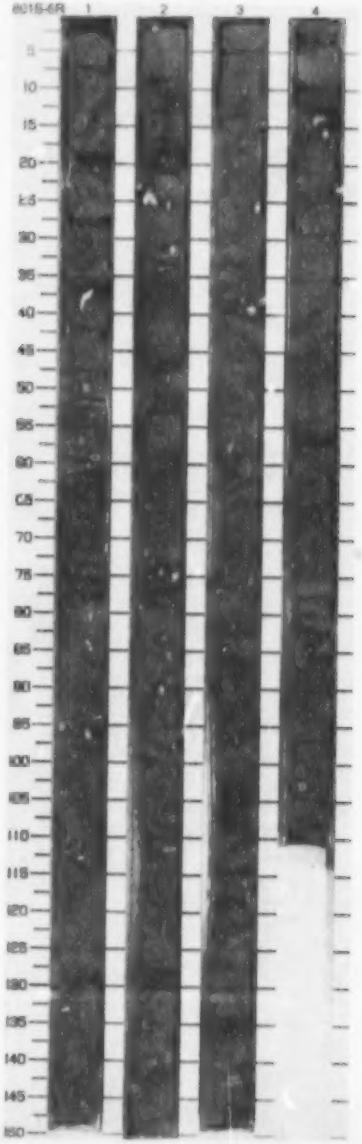

SITE 801 HOLE B CORE 7R CORED INTERVAL 5924.8-5934.5 mbsl; 251.0-260.7 mbsf

| TIME-ROCK UNIT | FORAMINIFERS | NANNOFOSSILS | RADIOLARIANS | DIATOMS | PALYNOMORPHS | PALEOMAGNETICS | PHYS. PROPERTIES | CHEMISTRY | SECTION | METERS |
|---|---|---|---|---|---|---|---|---|---|---|
| MIDDLE ALBIAN | R/M *Ticinella primula* | A/M *Prediscosphaera columnata* (CC8)(NC8-9) | R/P unzoned | | B | N? | ● ϕ=57.1<br>γ=1.81 | ● 15.5 | 1 | 0.5<br>1.0 |

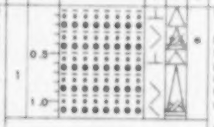
GRAPHIC LITHOLOGY
DRILLING DISTURB.
SED. STRUCTURES
SAMPLES
●

LITHOLOGIC DESCRIPTION

VOLCANICLASTIC TURBIDITES

Major lithology: VOLCANICLASTIC TURBIDITES, composed of CLAYEY and/or SANDY SILTSTONES which grade upward into CLAYSTONE. Siltstone is greenish gray to dark greenish gray (5G 5/1 - 5G4/1), massive to thinly laminated, and contains abundant radiolarians in the coarsest intervals. Volcaniclastic claystone is greenish gray (5G 5/1), largely homogeneous, with small, light greenish gray (5GY 7/1) patches of burrowing; contains volcanic glass, calcite, zeolites, smectite, radiolarians.

SLIDE SUMMARY (%):

| | 1, 36<br>D |
|---|---|
| TEXTURE: | |
| Silt | 15 |
| Clay | 85 |
| COMPOSITION: | |
| Calcite | 3 |
| Clay | 39 |
| Feldspar | 2 |
| Glass | 10 |
| Mica | 3 |
| Opaques | 10 |
| Oxide | 3 |
| Pyroxene | Tr |
| Quartz | Tr |
| Radiolarians | 5 |
| Silica | 20 |
| Zeolite | 5 |

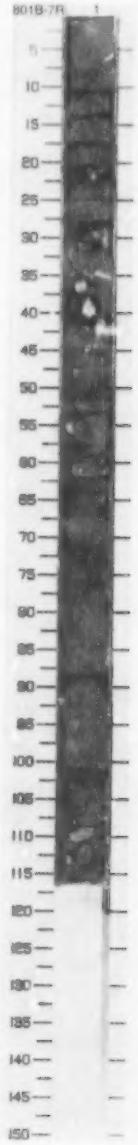
801B-7R
1
5
10
15
20
25
30
35
40
45
50
55
60
65
70
75
80
85
90
95
100
105
110
115
120
125
130
135
140
145
150

SITE 801 HOLE B CORE 8R CORED INTERVAL 5934.5-5944.1 mbsl; 260.7-270.3 mbsf

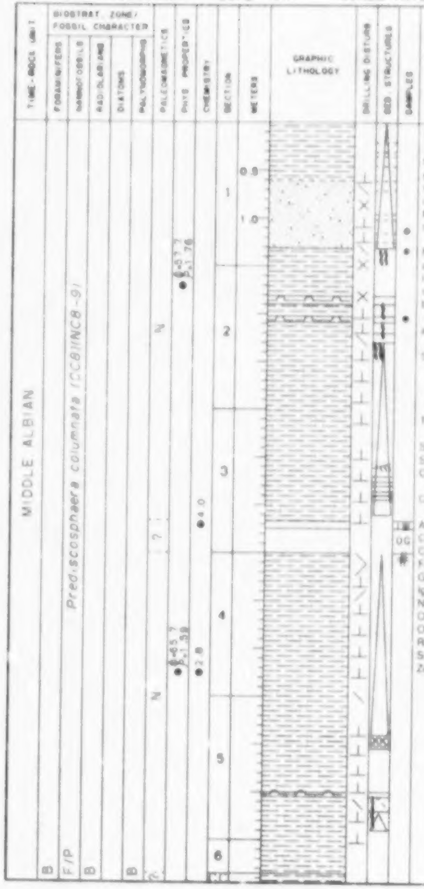
TIME-ROCK UNIT
BIOSTRAT. ZONE/ FOSSIL CHARACTER
FORAMINIFERS
NANNOFOSSILS
RADIOLARIANS
DIATOMS
PALYNOMORPHS
PALEOMAGNETICS
PHYS. PROPERTIES
CHEMISTRY
SECTION
METERS
GRAPHIC LITHOLOGY
DRILLING DISTURB.
SED. STRUCTURES
SAMPLES
MIDDLE ALBIAN
Prediscosphaera columnata (CC8/NC8-9)
B
F/P
B
B
N
?
N
?
φ-57.7
ρ-1.76
φ-65.7
ρ-1.59
●4.0
●2.8
1
2
3
4
5
6
0.5
1.0
OG

LITHOLOGIC DESCRIPTION

VOLCANICLASTIC SILTY CLAYSTONE

Major lithology: VOLCANICLASTIC SILTY CLAYSTONE forming turbidites; medium bluish gray to dark greenish gray (5B 5/1 5G 4/1); contain clay, volcanic glass, rock fragments and minor amounts of radiolarians, feldspar, opaques and calcareous grains. XRD data indicate clinoptilolite at Section 1, 118 cm, and Section 4, 8 cm; vague fining upward beds with bioturbation and darker coloration in upper portion; lower portions of beds commonly display some lamination to cross lamination; average turbidite thickness is about 1 m.

Minor lithologies:
a. VOLCANICLASTIC SILTY SANDSTONE: Section 1, 0-131 cm; greenish gray (5G 6/1) to light greenish gray (5G 8/1); laminated especially in lower portion; general fining upward sequence.
b. CLAYEY RADIOLARITE with SILT, to RADIOLARITE: olive gray to light olive gray (5Y 4/1 - 5Y 6/1); laminated to flaser laminated; six layers of 1-3 cm thickness occur in Sections 2 and 5 between turbidites.

SLIDE SUMMARY (%):

|  | 1, 111<br>TI | 1, 133<br>D | 2, 57<br>M | 4, 7<br>D |
|---|---|---|---|---|
| TEXTURE: |  |  |  |  |
| Sand | 5 | 1 | 35 | Tr |
| Silt | 35 | 12 | 35 | 20 |
| Clay | 60 | 87 | 30 | 80 |
| COMPOSITION: |  |  |  |  |
| Accessory minerals | 3 | Tr | Tr | — |
| Calcite | 1 | 1 | — | 2 |
| Clay | 58 | 84 | 25 | 65 |
| Feldspar | 2 | 3 | 1 | — |
| Glass | 15 | 3 | 5 | 2 |
| Igneous rock fragments | 15 | 2 | 6 | — |
| Nannofossils | — | 1 | — | — |
| Opaques | 5 | 3 | 3 | 10 |
| Oxide | — | — | — | 1 |
| Radiolarians | — | 2 | 60 | 10 |
| Silica | — | — | — | 10 |
| Zeolite | — | 1 | — | — |

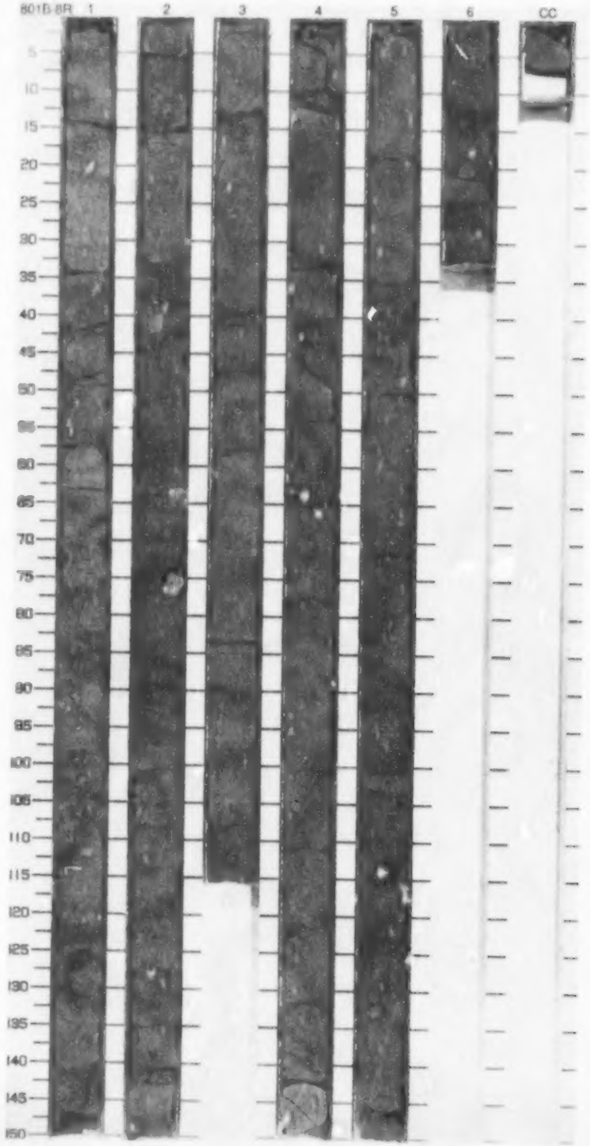
801B-8R
1
2
3
4
5
6
CC
5
10
15
20
25
30
35
40
45
50
55
60
65
70
75
80
85
90
95
100
105
110
115
120
125
130
135
140
145
150

SITE 801 HOLE B CORE 9R CORED INTERVAL 5944.1-5953.8 mbsl; 270.3-280.0 mbsf

| TIME-ROCK UNIT | BIOSTRAT. ZONE/ FOSSIL CHARACTER | | | | | PALEOMAGNETICS | PHYS. PROPERTIES | CHEMISTRY | SECTION | METERS | GRAPHIC LITHOLOGY | DRILLING DISTURB. | SED. STRUCTURES | SAMPLES | LITHOLOGIC DESCRIPTION |
|---|---|---|---|---|---|---|---|---|---|---|---|---|---|---|---|
| | FORAMINIFERS | NANNOFOSSILS | RADIOLARIANS | DIATOMS | PALYNOMORPHS | | | | | | | | | | |
| LOWER CRETACEOUS | B | B | C/P unzoned | | B | | | | 1 | 0.5<br>1.0 | | | | | VOLCANICLASTIC SILTSTONE (SLURRY)<br>Major lithology: VOLCANICLASTIC SILTSTONE (SLURRY), greenish gray (5GY 5/1); entire sample went to paleontology. |

SITE 801 HOLE B CORE 10R CORED INTERVAL 5953.8-5963.5 mbsl; 280.0-289.7 mbsf

| TIME-ROCK UNIT | BIOSTRAT. ZONE/ FOSSIL CHARACTER | | | | | PALEOMAGNETICS | PHYS. PROPERTIES | CHEMISTRY | SECTION | METERS | GRAPHIC LITHOLOGY | DRILLING DISTURB. | SED. STRUCTURES | SAMPLES | LITHOLOGIC DESCRIPTION |
|---|---|---|---|---|---|---|---|---|---|---|---|---|---|---|---|
| | FORAMINIFERS | NANNOFOSSILS | RADIOLARIANS | DIATOMS | PALYNOMORPHS | | | | | | | | | | |
| LOWER CRETACEOUS | B | B | R/P unzoned | | B | N | ●<br>•37.6<br>•2.03 | ●<br>5.7<br>●<br>0.1 | 1 | 0.5 | 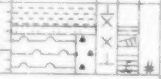 | ⊥<br>×<br>×<br>⊥ | | # | CALCAREOUS CLAYSTONE and RADIOLARITE<br>Major lithologies:<br>a. CALCAREOUS CLAYSTONE, dark greenish gray (5BG 4/1), massive with irregular calcite-filled fractures, Section 1, 0-23 cm.<br>b. RADIOLARITE, light olive gray (5Y 6/2), laminated and ripple-laminated, Section 1, 35-51, 55-68 cm.<br>Minor lithologies:<br>a. CALCAREOUS SILTSTONE, greenish gray (5G 5/1), laminated, Section 1, 23-35 cm.<br>b. CHERT, olive black (5Y 2.5/1), laminated, contains traces of volcanic glass and calcite secondary replacement of silty textured radiolarite; gradational contacts, Section 1, 51-55 and 68-73 cm. |

SLIDE SUMMARY (%):

| | 1, 58<br>M |
|---|---|
| TEXTURE: | |
| Sand | 10 |
| Silt | 5 |
| Clay | 85 |
| COMPOSITION: | |
| Calcite | Tr |
| Clay | 10 |
| Feldspar | 1 |
| Glass | 2 |
| Igneous rock fragments | 3 |
| Opaques | 3 |
| Oxide | 1 |
| Radiolarians | 15 |
| Silica | 57 |

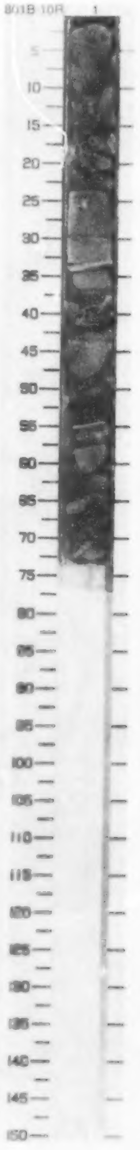

SITE 801 HOLE B CORE 11R CORED INTERVAL 5963.5-5973.1 mbls; 289.7-299.3 mbsf

| TIME-ROCK UNIT | BIOSTRAT. ZONE/ FOSSIL CHARACTER: FORAMINIFERS | NANNOFOSSILS | RADIOLARIANS | DIATOMS | PALYNOMORPHS | PALEOMAGNETICS | PHYS. PROPERTIES | CHEMISTRY | SECTION | METERS | GRAPHIC LITHOLOGY | DRILLING DISTURB. | SED. STRUCTURES | SAMPLES |
|---|---|---|---|---|---|---|---|---|---|---|---|---|---|---|
| LOWER CRETACEOUS | B | B | B |  | B | N | ● ϕ=25.9 γ=2.17 | ● 0.3 | 1 |  |  | X X |  | ● # |

LITHOLOGIC DESCRIPTION

RADIOLARITE with PORCELLANITE

Major lithology: RADIOLARITE with PORCELLANITE, light brown to pink (7.5YR 6/4 to 7.5YR 7/4) radiolarite with 0.5-1.0 cm thick bands of dark brown (7.5YR 3/4) porcellanite; some pieces are CLAYEY RADIOLARITE; sometimes laminated to flaser laminated with bioturbation; barite crystals in the center of some radiolarians.

Minor lithology: CLAYSTONE with RADIOLARIANS, very dark gray (5Y 3/1); bioturbated piece at Section 1, 37-40 cm.

SLIDE SUMMARY (%):

|  | 1, 2<br>D | 1, 28<br>D |
|---|---|---|
| TEXTURE: |  |  |
| Sand | 30 | 10 |
| Silt | 45 | 10 |
| Clay | 25 | 80 |
| COMPOSITION: |  |  |
| Accessory minerals | Tr | — |
| Barite | — | Tr |
| Calcite | Tr | — |
| Clay | 25 | 22 |
| Glass | Tr | — |
| Opaques | — | 3 |
| Oxide | 3 | 25 |
| Radiolarians | 70 | 15 |
| Silica | — | 35 |
| Zeolite | 2 | — |

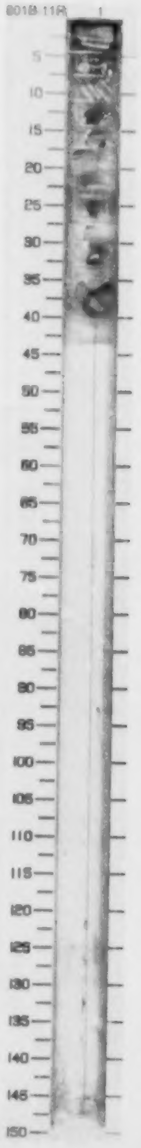

SITE 801 HOLE B CORE 12R CORED INTERVAL 5973.1-5982.8 mbsl; 299.3-309.0 mbsf

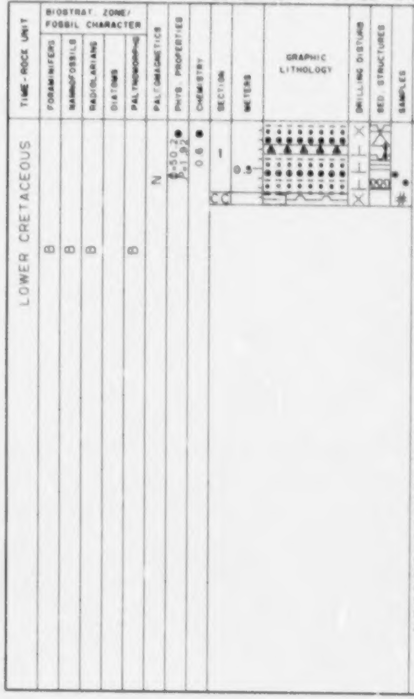
TIME-ROCK UNIT
BIOSTRAT. ZONE/ FOSSIL CHARACTER
FORAMINIFERS
NANNOFOSSILS
RADIOLARIANS
DIATOMS
PALYNOMORPHS
PALEOMAGNETICS
PHYS. PROPERTIES
CHEMISTRY
SECTION
METERS
GRAPHIC LITHOLOGY
DRILLING DISTURB.
SED. STRUCTURES
SAMPLES
LOWER CRETACEOUS
B
B
B
B
N
ϕ=50.2
ρ=1.92
0.6
1
0.5
CC

LITHOLOGIC DESCRIPTION

VOLCANICLASTIC TURBIDITES

Major lithology: VOLCANICLASTIC TURBIDITES of fine grained SANDSTONE to CLAYSTONE, grayish blue green (5BG 5/2), olive gray (5Y 4/1), dark greenish gray (5G 4/1), light greenish gray (5G 8/1) and brownish gray (5YR 4/1); sedimentary features include load casts, convolute and flame structures, laminated intervals and graded beds with bioturbated upper portions.

Minor lithologies:
a. CHERT with PORCELLANITE, grayish black (N2) to very dusky red (10R 2/2), laminated, Section 1, 26-34 cm and CC, 9-12 cm.
b. CLAYEY RADIOLARITE, mottled dark yellowish brown (10YR 4/6) and reddish brown (2.5YR 4/4), finely laminated, slightly calcareous, Section CC, 0-9 cm.
c. CLAYEY SILTSTONE, gray (N4), laminated, Section CC, 12-15 cm.

SLIDE SUMMARY (%):

| | 1, 55<br>D | 1, 63<br>M | CC, 6<br>D |
|---|---|---|---|
| TEXTURE: | | | |
| Silt | 60 | 2 | 25 |
| Clay | 40 | 98 | 75 |
| COMPOSITION: | | | |
| Accessory minerals | 2 | — | — |
| Calcite | — | — | 10 |
| Clay | 35 | 75 | 45 |
| Feldspar | 2 | — | — |
| Glass | 40 | — | — |
| Igneous rock fragments | 10 | — | — |
| Mica | — | 2 | — |
| Opaques | 5 | — | — |
| Oxide | — | — | 30 |
| Radiolarians | — | 3 | 15 |
| Silica | — | 20 | — |
| Zeolite | 6 | — | — |

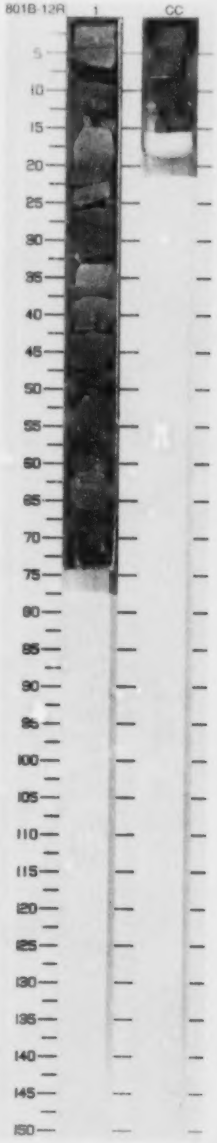
801B-12R
1
CC
5
10
15
20
25
30
35
40
45
50
55
60
65
70
75
80
85
90
95
100
105
110
115
120
125
130
135
140
145
150

SITE 801 HOLE B CORE 13R CORED INTERVAL 5982.8-5992.1 mbsl; 309.0-318.3 mbsf

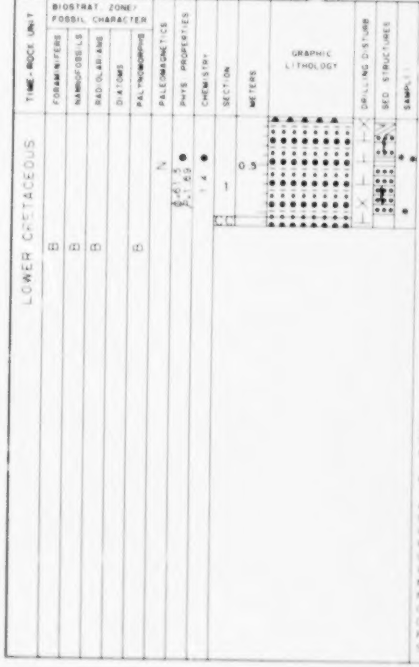
TIME-ROCK UNIT
BIOSTRAT. ZONE/ FOSSIL CHARACTER
FORAMINIFERS
NANNOFOSSILS
RADIOLARIANS
DIATOMS
PALYNOMORPHS
PALEOMAGNETICS
PHYS. PROPERTIES
CHEMISTRY
SECTION
METERS
GRAPHIC LITHOLOGY
DRILLING DISTURB.
SED. STRUCTURES
SAMPLES
LOWER CRETACEOUS
B
B
B
B
N
1.4
1
0.5
CC

### LITHOLOGIC DESCRIPTION

VOLCANICLASTIC TURBIDITES

Major lithologies:

a. VOLCANICLASTIC TURBIDITES composed of SILTSTONE grading to CLAYSTONE, grayish green (5BG 5/1) to green (10G 5/4), containing mainly altered volcanic glass and igneous rock fragments; layers are generally less than 2 cm thick, fining upward with some bioturbation in upper portions. Claystone portions of volcaniclastic turbidites are grayish green (5BG 5/1) to pinkish gray (7.5YR 6/2) contain abundant radiolarians and rare traces of nannofossils; <1 cm thick beds probably represent pelagic intervals between turbidites.

Minor lithologies: Clasts at top of Section 1 which may be downhole contamination:
a. CHERT, yellow, red and brown striped (10YR 2/2 to 10YR 4/4), laminated, at 0-4 cm.
b. SANDY SILTSTONE, gray (N5) with subtle laminations. Interval in Section 1, 7-12 cm, has post depositional fractures and microfaults filled with clear to white calcite with a zone of angular fragments in a calcite matrix.

SLIDE SUMMARY (%):

| | 1, 40<br>D | 1, 41<br>D | 1, 100<br>D |
|---|---|---|---|
| TEXTURE: | | | |
| Sand | 10 | — | — |
| Silt | 75 | 15 | 45 |
| Clay | 15 | 85 | 55 |
| COMPOSITION: | | | |
| Accessory minerals | — | Tr | — |
| Calcite | — | — | 13 |
| Clay | 10 | 80 | 51 |
| Feldspar | 5 | 2 | — |
| Glass | 50 | 2 | — |
| Igneous rock fragments | 30 | — | — |
| Mica | — | — | 1 |
| Nannofossils | — | 1 | — |
| Opaques | 5 | 2 | 5 |
| Oxide | — | — | 20 |
| Radiolarians | — | 12 | — |
| Silica | — | — | 10 |

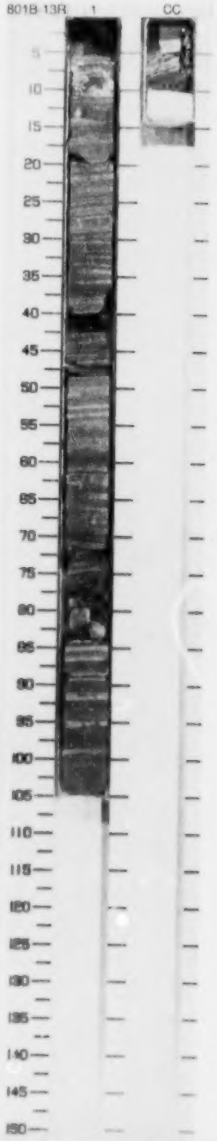
801B-13R
1
CC
5
10
15
20
25
30
35
40
45
50
55
60
65
70
75
80
85
90
95
100
105
110
115
120
125
130
135
140
145
150

SITE 801 HOLE B CORE 14R CORED INTERVAL 5992.1-6001.5 mbsl; 318.3-327.7 mbsf

| TIME-ROCK UNIT | BIOSTRAT. ZONE/ FOSSIL CHARACTER | | | | | PALEOMAGNETICS | PHYS. PROPERTIES | CHEMISTRY | SECTION | METERS | GRAPHIC LITHOLOGY | DRILLING DISTURB. | SED. STRUCTURES | SAMPLES |
|---|---|---|---|---|---|---|---|---|---|---|---|---|---|---|
| | FORAMINIFERS | NANNOFOSSILS | RADIOLARIANS | DIATOMS | PALYNOMORPHS | | | | | | | | | |
| VALANGINIAN | B | B | C/P *Cecrops septemporatus* | | B | N<br>R | ●<br>$\phi$=49.6<br>$\gamma$=1.91 | ●<br>0.2 | 1 | 0.5 | | ⊥<br>⊥ | | ● |

LITHOLOGIC DESCRIPTION

CLAYEY RADIOLARITE with PORCELLANITE

Major lithology: CLAYEY RADIOLARITE with PORCELLANITE, dark yellowish brown, dusky brown to moderate brown (10YR 4/2, 5YR 2/2, 5YR 4/4); color variation may partially reflect manganese mobilization; varying degrees of silicification; laminated to flaser-laminated; fractures have black specks of possible Mn oxide.

SLIDE SUMMARY (%):

| | 1, 5<br>D |
|---|---|
| TEXTURE: | |
| Silt | 10 |
| Clay | 90 |
| COMPOSITION: | |
| Clay | 43 |
| Opaques | 40 |
| Radiolarians | 15 |
| Spines | 2 |

SITE 801 HOLE B CORE 15R CORED INTERVAL 6001.5-6011.0 mbsl; 327.7-337.2 mbsf

| TIME-ROCK UNIT | BIOSTRAT. ZONE/ FOSSIL CHARACTER | | | | | PALEOMAGNETICS | PHYS. PROPERTIES | CHEMISTRY | SECTION | METERS | GRAPHIC LITHOLOGY | DRILLING DISTURB. | SED. STRUCTURES | SAMPLES |
|---|---|---|---|---|---|---|---|---|---|---|---|---|---|---|
| | FORAMINIFERS | NANNOFOSSILS | RADIOLARIANS | DIATOMS | PALYNOMORPHS | | | | | | | | | |
| BERRIASIAN - VALANGINIAN | B | B | R/P *Pseudodictyomitra carpatica* | | B | N | | | 1 | | | ⊥ | | ● |

LITHOLOGIC DESCRIPTION

RADIOLARITE to CHERT

Major lithology: RADIOLARITE, tan to dusky yellowish brown (5YR 7/4 - 10YR 2/2), laminated with some minor bioturbation; streaky Mn(?) oxide fracture coatings; varying degrees of silicification to PORCELLANITE (Section 1, 15-18 cm) or CHERT (Section 1, 18-22 cm) of laminated yellowish red (5YR 4/6) and massive dusky brown (5YR 2/2) respectively.

SLIDE SUMMARY (%):

| | 1, 1<br>D |
|---|---|
| TEXTURE: | |
| Silt | 30 |
| Clay | 70 |
| COMPOSITION: | |
| Clay | 35 |
| Opaques | 20 |
| Radiolarians | 30 |
| Silica | 10 |
| Spines | 5 |

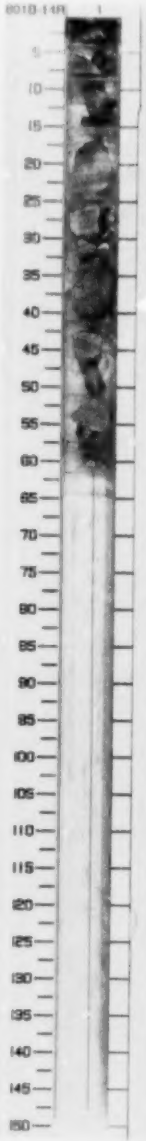

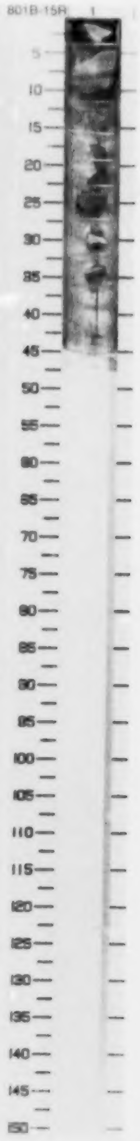

SITE 801 HOLE B CORE 16R CORED INTERVAL 6011.0-6020.4 mbsl; 337.2-346.6 mbsf

| TIME-ROCK UNIT | BIOSTRAT. ZONE/ FOSSIL CHARACTER: FORAMINIFERS | NANNOFOSSILS | RADIOLARIANS | DIATOMS | PALYNOMORPHS | PALEOMAGNETICS | PHYS. PROPERTIES | CHEMISTRY | SECTION |
|---|---|---|---|---|---|---|---|---|---|
| BERRIASIAN - VALANGINIAN | B | B | A/P *Pseudodictyomitra carpatica* | | B | R<br>R? | ● $\phi$3.70<br>$\rho$2.54 | ● 0.4 | 1 |

LITHOLOGIC DESCRIPTION

RADIOLARIAN CHERT and RADIOLARITE

Major lithologies:
a. RADIOLARIAN CHERT, chiefly dark brown to dusky yellowish brown (7.5YR 4/2 - 10YR 2/2); infrequent laminations are yellowish red to light brown (5YR 5/8 - 5YR 6/4), with scattered light-colored lenses and burrows. Fractures are filled with quartz or a silvery metallic mineral.
b. RADIOLARITE, reddish yellow to dark grayish brown (7.5YR 6/4 - 10YR 4/2), arenaceous texture and friable (from detached radiolarians); variable clay content; becomes porcellaneous with decreased clay and increased silica cementation.

SLIDE SUMMARY (%):

| | 1, 27<br>D | 1, 36<br>D |
|---|---|---|
| TEXTURE | | |
| Sand | — | 35 |
| Silt | 35 | 15 |
| Clay | 65 | 50 |
| COMPOSITION | | |
| Clay | 33 | 27 |
| Glass | — | 5 |
| Opaques | 2 | 1 |
| Oxide | 20 | — |
| Radiolarians | 35 | 45 |
| Silica | 10 | 20 |
| Zeolite | — | 2 |

SITE 801 HOLE B CORE 17R CORED INTERVAL 6020.4-6029.6 mbsl; 346.6-355.8 mbsf

| TIME-ROCK UNIT | BIOSTRAT. ZONE/ FOSSIL CHARACTER: FORAMINIFERS | NANNOFOSSILS | RADIOLARIANS | DIATOMS | PALYNOMORPHS | PALEOMAGNETICS | PHYS. PROPERTIES | CHEMISTRY | SECTION |
|---|---|---|---|---|---|---|---|---|---|
| BERRIASIAN - VALANGINIAN | B | B | C/P *Pseudodictyomitra carpatica* | | B | R? | ● $\phi$42<br>$\rho$1.96 | ● 0.2 | 1 |

LITHOLOGIC DESCRIPTION

RADIOLARITE and RADIOLARIAN CHERT

Major lithologies:
a. RADIOLARITE, brown to very dark grayish brown (10YR 3/2-10YR 4/3), with minor lenses and patches of pink (5YR 7/4); texture ranges from medium to fine silty sand, with radiolarians making up all of the sand-sized fraction; increased clay (up to 30%) relative to overlying Core 16. Pervasive, very thin (<0.1 mm), discontinuous dark microlaminations. Black (N1) 0.1 to 1.0 mm circular deposits of Mn(?) oxide on most natural fractures.
b. RADIOLARIAN CHERT, dusky yellowish brown (10 YR 2/2), hematite on grain boundaries of microcrystalline quartz in matrix, typically massive. Generally bedding parallel contacts with radiolarite, but one cross-cutting diagenetic nodule boundary is displayed in piece from Section 1, 29 - 33 cm.

SLIDE SUMMARY (%):

| | 1, 34<br>D |
|---|---|
| TEXTURE | |
| Silt | 5 |
| Clay | 95 |
| COMPOSITION | |
| Clay | 23 |
| Opaques | 2 |
| Oxide | 20 |
| Radiolarians | 15 |
| Silica | 40 |
| Zeolite | Tr |

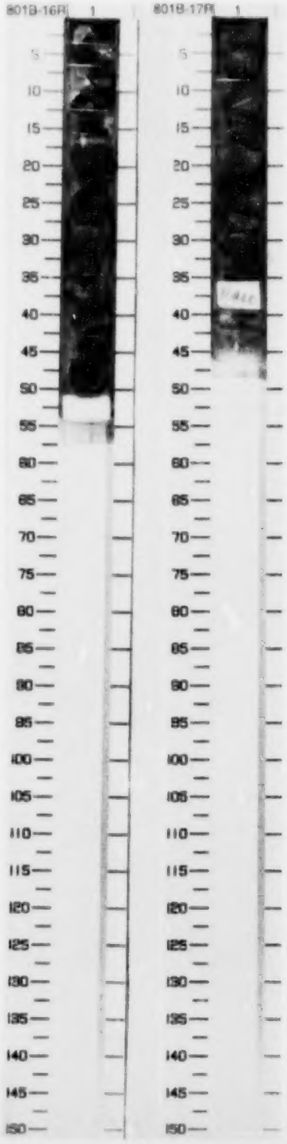

SITE 801 HOLE B CORE 18R CORED INTERVAL 6029.6-6039.1 mbsl; 355.8-365.3 mbsf

| TIME-ROCK UNIT | BIOSTRAT. ZONE/ FOSSIL CHARACTER: FORAMINIFERS | NANNOFOSSILS | RADIOLARIANS | DIATOMS | PALYNOMORPHS | PALEOMAGNETICS | PHYS. PROPERTIES | CHEMISTRY | SECTION | METERS | GRAPHIC LITHOLOGY | DRILLING DISTURB. | SED. STRUCTURES | SAMPLES |
|---|---|---|---|---|---|---|---|---|---|---|---|---|---|---|
| BERRIASIAN - VALANGINIAN | B | B | A/M *Pseudodictyomitra carpatica* | | B | N? | ●<br>φ=41.3<br>ρ=1.99 | ●<br>0.3 | 1 | | | ×<br>> | | #<br>\# |

LITHOLOGIC DESCRIPTION

RADIOLARITE and RADIOLARIAN CHERT

Major lithologies:
a. RADIOLARITE: dark grayish brown to very dark gray (10YR 4/3–10YR 3/1), very thinly laminated, very small (3 X 0.4 mm) light and dark patches may be microbioturbation. Cemented fractures are filled with quartz, Mn oxide white, elongate zeolite (?) crystals. Less clayey, more siliceous than uphole.
b. RADIOLARIAN CHERT: dusky yellowish brown (10YR 2/2) with sparse thin lenses of reddish brown (5YR 5/4), fractured, mostly cemented as above. Some light colored layers in chert show many radiolarian molds (hollow), as opposed to chalcedony-filled radiolarians elsewhere.

SLIDE SUMMARY (%):

| | 1, 9<br>D | 37<br>D |
|---|---|---|
| TEXTURE: | | |
| Silt | 15 | 2 |
| Clay | 85 | 98 |
| COMPOSITION: | | |
| Clay | 10 | 14 |
| Opaques | 8 | 1 |
| Oxide | 3 | 30 |
| Radiolarians | 15 | 30 |
| Silica | 60 | 20 |
| Spines | 3 | 5 |
| Zeolite | 1 | — |

SITE 801 HOLE B CORE 19R CORED INTERVAL 6039.1-6048.3 mbsl; 365.3-374.5 mbsf

| TIME-ROCK UNIT | BIOSTRAT. ZONE/ FOSSIL CHARACTER: FORAMINIFERS | NANNOFOSSILS | RADIOLARIANS | DIATOMS | PALYNOMORPHS | PALEOMAGNETICS | PHYS. PROPERTIES | CHEMISTRY | SECTION | METERS | GRAPHIC LITHOLOGY | DRILLING DISTURB. | SED. STRUCTURES | SAMPLES |
|---|---|---|---|---|---|---|---|---|---|---|---|---|---|---|
| BERRIASIAN - VALANGINIAN | B | B | A/P *Pseudodictyomitra carpatica* | | R?<br>B | N<br>N? | ●<br>2.50<br>2.61 | ●<br>0.2 | 1 | | | × | | # |

LITHOLOGIC DESCRIPTION

RADIOLARITE and CHERT

Major lithologies:
a. RADIOLARITE: light brown to brown (7.5YR 6/4–7.5YR 5/2), very thinly laminated, siliceous matrix-not clayey in texture. Mn oxide on fracture surfaces and along a thin horizon with vugs. Brecciated in part, becomes cherty near fractures.
b. CHERT: dark brown (7.5YR 3/3), decreased radiolarians evident. Chert is commonly brecciated with quartz cemented fractures. Quartz filled fractures act as permeability barriers that separate "compartments" of rock inferred to be originally identical, now siliceous radiolarite and glassy chert.

SLIDE SUMMARY (%):

| | 1, 12<br>M |
|---|---|
| TEXTURE: | |
| Silt | 10 |
| Clay | 90 |
| COMPOSITION: | |
| Clay | Tr |
| Opaques | 15 |
| Radiolarians | 60 |
| Silica | 25 |

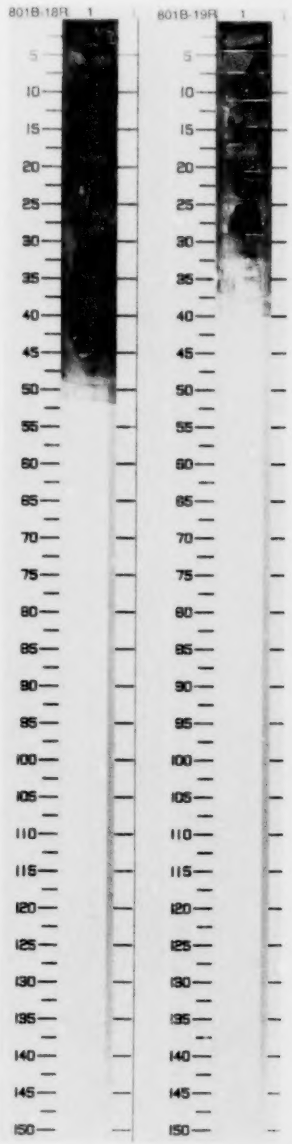

SITE 801 HOLE B CORE 20R CORED INTERVAL 6048.3-6057.5 mbsl; 374.5-383.7 mbsf

| TIME-ROCK UNIT | FORAMINIFERS | NANNOFOSSILS | RADIOLARIANS | DIATOMS | PALYNOMORPHS | PALEOMAGNETICS | PHYS. PROPERTIES | CHEMISTRY | SECTION | METERS | GRAPHIC LITHOLOGY | DRILLING DISTURB. | SED. STRUCTURES | SAMPLES |
|---|---|---|---|---|---|---|---|---|---|---|---|---|---|---|
| TITHONIAN - BERRIASIAN | B | B | C/M *Pseudodictyomitra carpatica* |  | B | NR<br>R | ●<br>[illegible] | ●<br>0.2 | 1 |  |  | × |  | ●● |

LITHOLOGIC DESCRIPTION

CHERT

Major lithology: CHERT, dark brown (7.5YR 3/2) with minor yellowish red (5YR 5/6) and red (5R 5/6) small streaks and patches associated with fractures (oxidation?). Increasingly fractured; most fractures are completely filled with quartz; one small (1 X 3 mm) open void lined by drusy quartz. Fewer radiolarians than above (10-35%). Trace components in chert include volcanic glass, clay, zeolites, opaques, iron oxides.

Minor lithology: RADIOLARITE, light brown (7.5YR 6/4), silty sandy texture, siliceous, approaching radiolarian porcellanite in texture and hardness.

SLIDE SUMMARY (%):

|  | 1, 6<br>D | 1, 8<br>D |
|---|---|---|
| TEXTURE: |  |  |
| Sand | — | 15 |
| Silt | 1 | 20 |
| Clay | 99 | 65 |
| COMPOSITION: |  |  |
| Clay | — | 15 |
| Glass | 2 | — |
| Opaques | 1 | Tr |
| Oxide | 10 | Tr |
| Radiolarians | 10 | 35 |
| Silica | 76 | 50 |
| Zeolite | 1 | — |

SITE 801 HOLE B CORE 21R CORED INTERVAL 6057.5-6063.6 mbsl; 383.7-389.8 mbsf

| TIME-ROCK UNIT | FORAMINIFERS | NANNOFOSSILS | RADIOLARIANS | DIATOMS | PALYNOMORPHS | PALEOMAGNETICS | PHYS. PROPERTIES | CHEMISTRY | SECTION | METERS | GRAPHIC LITHOLOGY | DRILLING DISTURB. | SED. STRUCTURES | SAMPLES |
|---|---|---|---|---|---|---|---|---|---|---|---|---|---|---|
| TITHONIAN | B | B | C/M *Pseudodictyomitra primitiva* |  | B | N | ●<br>[illegible] | ●<br>0.1 | 1 |  |  | × |  | ● |

LITHOLOGIC DESCRIPTION

CHERT

Major lithology: CHERT, very dark grayish brown to dark brown (10YR 3/2 - 10YR 3/3), with minor streaks and patches of yellowish red (5YR 5/6) or red (10R 5/6). Reddish areas are either thin zones adjacent to microfractures, or irregular amoeboid shapes, sometimes subtlety discordant to bedding. Fractures are more common than in overlying cores; several generations of silica deposition are evident in open voids up to 3 X 8 mm. Drusy quartz on the side of one piece suggests existence of much larger cavities in situ. "Compartmented" fragments of soft CLAYEY RADIOLARITE shows that some brecciation took place prior to full chertification.

SLIDE SUMMARY (%):

|  | 1, 17<br>D |
|---|---|
| TEXTURE: |  |
| Silt | 1 |
| Clay | 99 |
| COMPOSITION: |  |
| Clay | 30 |
| Opaques | 2 |
| Oxide | 20 |
| Radiolarians | 10 |
| Silica | 38 |
| Zeolite | 1 |

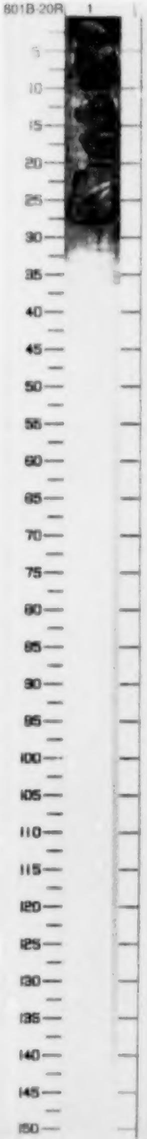

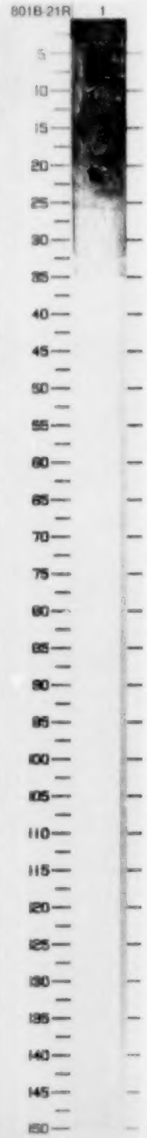

SITE 801 HOLE B CORE 22R CORED INTERVAL 6063.6-6069.7 mbsl; 381.8-387.9 mbsf

| TIME-ROCK UNIT | BIOSTRAT. ZONE/ FOSSIL CHARACTER | | | | | PALEOMAGNETICS | PHYS. PROPERTIES | CHEMISTRY | SECTION | METERS | GRAPHIC LITHOLOGY | DRILLING DISTURB. | SED. STRUCTURES | SAMPLES | LITHOLOGIC DESCRIPTION |
|---|---|---|---|---|---|---|---|---|---|---|---|---|---|---|---|
| | FORAMINIFERS | NANNOFOSSILS | RADIOLARIANS | DIATOMS | PALYNOMORPHS | | | | | | | | | | |
| TITHONIAN | B | B | A/P Pseudodictyomitra primitiva | | B | R? | | | CC | | ▲ ▲ ▲ ▲ ▲ | | | ■ | CHERT<br>Major lithology: CHERT, very dark grayish brown (10YR 3/2) with tan (10YR 6/3) mottling and slightly reddish oxidation (2.5YR 5/4) near unfilled fractures, subtle laminations. An r pat-filled fracture is parallel to laminations. Chert contains up to 10% clay.<br>SLIDE SUMMARY (%):<br>CC, 2 D<br>TEXTURE:<br>Silt 1<br>Clay 99<br>COMPOSITION:<br>Clay 10<br>Opaques 1<br>Oxide 5<br>Radiolarians 15<br>Silica 69 |

SITE 801 HOLE B CORE 23R CORED INTERVAL 6069.7-6074.4 mbsl; 395.9-400.6 mbsf

| TIME-ROCK UNIT | BIOSTRAT. ZONE/ FOSSIL CHARACTER | | | | | PALEOMAGNETICS | PHYS. PROPERTIES | CHEMISTRY | SECTION | METERS | GRAPHIC LITHOLOGY | DRILLING DISTURB. | SED. STRUCTURES | SAMPLES | LITHOLOGIC DESCRIPTION |
|---|---|---|---|---|---|---|---|---|---|---|---|---|---|---|---|
| | FORAMINIFERS | NANNOFOSSILS | RADIOLARIANS | DIATOMS | PALYNOMORPHS | | | | | | | | | | |
| TITHONIAN | B | B | C/P Pseudodictyomitra primitiva | | N<br>B | R | ●<br>[illegible]<br>2.58 | ● 0.1 | CC | | ▲ ▲ ▲ ▲ ▲ | X | | ✱ | CHERT and PORCELLANITE with CLAY<br>Major lithologies:<br>a. CHERT, dusky brown to grayish brown (5YR 2/2 to 5YR 3/2) with subtle flaser laminations or compacted bioturbation and tiny black flecks. Fractures are infilled by variously colored materials including grayish black (N2) Mn(?) oxide and medium brown (5YR 4/4) and dusky yellow (5Y 6/4) chert.<br>b. PORCELLANITE with CLAY. Section CC, 0-5 cm, dark yellowish brown to moderate brown (10YR 4/2 to 10YR 4/4) with tiny black flecks, variable degrees of silicification, flaser laminated to bioturbated.<br>SLIDE SUMMARY (%):<br>CC, 1 D<br>TEXTURE:<br>Silt 10<br>Clay 90<br>COMPOSITION:<br>Clay 20<br>Opaques 2<br>Oxide 20<br>Radiolarians 35<br>Silica 18<br>Spines 5 |

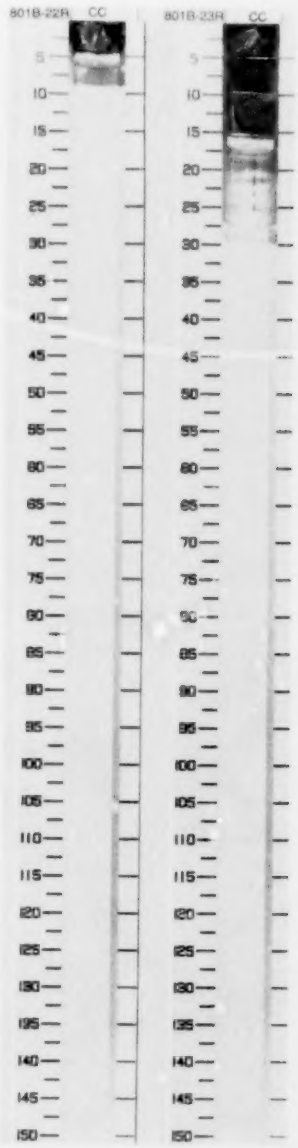

SITE 801 HOLE B CORE 24R CORED INTERVAL 6074.4-6079.0 mbsl; 400.6-405.2 mbsf

| TIME-ROCK UNIT | BIOSTRAT. ZONE/ FOSSIL CHARACTER: FORAMINIFERS | NANNOFOSSILS | RADIOLARIANS | DIATOMS | PALYNOMORPHS | PALEOMAGNETICS | PHYS. PROPERTIES | CHEMISTRY | SECTION | METERS | GRAPHIC LITHOLOGY | DRILLING DISTURB. | SED. STRUCTURES | SAMPLES |
|---|---|---|---|---|---|---|---|---|---|---|---|---|---|---|
| TITHONIAN | B | B | A/P unzoned | B |  | N : R? |  |  | 1 | 0.5 |  |  |  |  |

LITHOLOGIC DESCRIPTION

CLAYEY RADIOLARITE and CHERT

Major lithologies:
a. CLAYEY RADIOLARITE is dark brown (10YR 4/3) with light yellowish brown (10YR 6/4) bleached mottles and bands, finely laminated by black (N1) streaks or with moderate subhorizontal bioturbation. Thin section from Section 1, 28-31 cm, has a possible burrow structure which contains more abundant opaque micronodules than the host radiolarite. Micronodules of possible manganite are common secondary features which apparently predate silicification; a 1 cm-long string of micronodules is present at Section 1, 55 cm.
b. CHERT, very dark brown (10YR 2/2), occurs as lenses of secondary silicification within the radiolarite with fairly abrupt but gradational boundaries; can contain black micronodules.

SLIDE SUMMARY (%):

|  | 1, 28<br>D | 1, 50<br>D |
|---|---|---|
| TEXTURE: |  |  |
| Silt | 20 | 30 |
| Clay | 80 | 70 |
| COMPOSITION: |  |  |
| Clay | 20 | 10 |
| Glass | 1 | — |
| Opaques | 10 | 15 |
| Oxide | 2 | 3 |
| Radiolarians | 30 | 30 |
| Silica | 35 | 38 |
| Spines | 2 | 4 |

SITE 801 HOLE B CORE 25R CORED INTERVAL 6079.0-6083.8 mbsl; 405.2-410.0 mbsf

| TIME-ROCK UNIT | BIOSTRAT. ZONE/ FOSSIL CHARACTER: FORAMINIFERS | NANNOFOSSILS | RADIOLARIANS | DIATOMS | PALYNOMORPHS | PALEOMAGNETICS | PHYS. PROPERTIES | CHEMISTRY | SECTION | METERS | GRAPHIC LITHOLOGY | DRILLING DISTURB. | SED. STRUCTURES | SAMPLES |
|---|---|---|---|---|---|---|---|---|---|---|---|---|---|---|
| TITHONIAN | B | R/M *Hexalithus noelae* | A/P *Pseudodictyomitra primitiva* |  | B | R | ● ϕ=45.7<br>γ=1.95 | ● 0.2 | 1 | 0.5 |  |  |  |  |

LITHOLOGIC DESCRIPTION

CLAYEY RADIOLARITE with CHERT

Major lithology: CLAYEY RADIOLARITE, brown (10YR 5/3) grading to mottled to pink (7.5YR 7/4), moderately bioturbated to finely laminated; darker bands have more abundant volcanic glass, lighter bands are richer in radiolarians; contains black (N1) micronodules of probable manganite. Contains silicified zones ranging from 1 mm, round to ovoid, to chert nodules or lenses greater than 10 cm thick. CHERT is very dark brown (10YR 2/2), hematitic; pieces at Section 1, 69-74 cm have a 3-5 mm rim of reddish brown chert in transition to pink radiolarite.

SLIDE SUMMARY (%):

|  | 1, 7<br>D | 1, 9<br>D | 1, 12<br>D | 1, 35<br>D | 1, 50<br>D | 1, 59<br>D |
|---|---|---|---|---|---|---|
| TEXTURE: |  |  |  |  |  |  |
| Sand | — | 1 | 4 | 5 | — | — |
| Silt | 30 | 29 | 50 | 35 | 30 | 25 |
| Clay | 70 | 70 | 46 | 60 | 70 | 75 |
| COMPOSITION: |  |  |  |  |  |  |
| Accessory minerals | — | 1 | 1 | Tr | Tr | — |
| Clay | 2 | 65 | 40 | 63 | 67 | 5 |
| Feldspar | — | — | 1 | — | — | — |
| Glass | — | 6 | 3 | 1 | 5 | — |
| Opaques | 30 | — | — | 1 | 3 | 15 |
| Oxide | 10 | — | — | — | — | 2 |
| Quartz | — | 3 | 5 | — | — | — |
| Radiolarians | 35 | 25 | 50 | 30 | 25 | 20 |
| Silica | 20 | — | — | — | — | 57 |
| Spines | 3 | — | — | — | — | 1 |
| Zeolite | — | — | — | 5 | — | — |

801B-24R

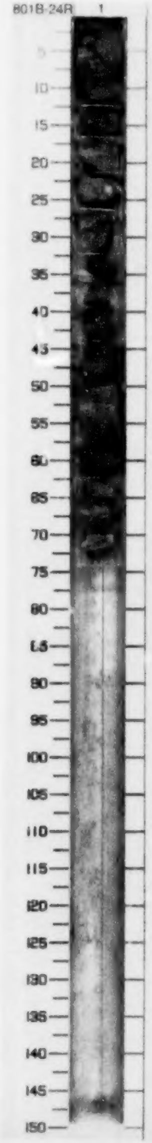

801B-25R

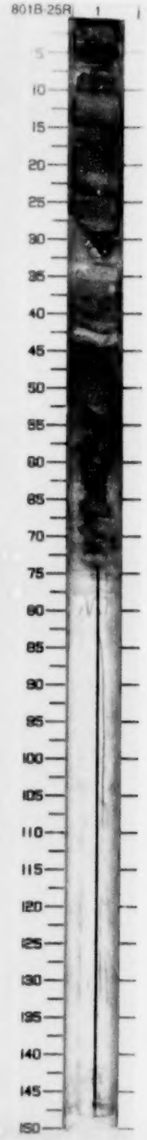

SITE 801 HOLE B CORE 26R CORED INTERVAL 6083.8-6088.5 mbsl; 410.0-414.7 mbsf

| TIME-ROCK UNIT | FORAMINIFERS | NANNOFOSSILS | RADIOLARIANS | DIATOMS | PALYNOMORPHS | PALEOMAGNETICS | PHYS. PROPERTIES | CHEMISTRY | SECTION | METERS | GRAPHIC LITHOLOGY | DRILLING DISTURB. | SED. STRUCTURES | SAMPLES |
|---|---|---|---|---|---|---|---|---|---|---|---|---|---|---|
| TITHONIAN | B | R/P unzoned | C/P unzoned | | N?<br>B | R | R | | CC | | | × | | # |

**LITHOLOGIC DESCRIPTION**

CLAYEY RADIOLARITE and CHERT

Major lithologies:
a. CLAYEY RADIOLARITE, dark grayish brown (10YR 4/2), with small dark patches as micronodules replacing radiolarian tests; deposits are thinly laminated.
b. CHERT, dark brown (7.5YR 3/2) with lighter reddish brown (5YR 5/4) layers and patches, small pieces.

SLIDE SUMMARY (%):

| | CC, 14<br>D |
|---|---|
| TEXTURE: | |
| Silt | 5 |
| Clay | 95 |
| COMPOSITION: | |
| Clay | 5 |
| Opaques | 2 |
| Oxide | 5 |
| Radiolarians | 30 |
| Silica | 58 |

SITE 801 HOLE B CORE 27R CORED INTERVAL 6088.5-6093.2 mbsl; 414.7-419.4 mbsf

| TIME-ROCK UNIT | FORAMINIFERS | NANNOFOSSILS | RADIOLARIANS | DIATOMS | PALYNOMORPHS | PALEOMAGNETICS | PHYS. PROPERTIES | CHEMISTRY | SECTION | METERS | GRAPHIC LITHOLOGY | DRILLING DISTURB. | SED. STRUCTURES | SAMPLES |
|---|---|---|---|---|---|---|---|---|---|---|---|---|---|---|
| KIMMERIDGIAN - TITHONIAN | B | B | C/P unzoned | | B | N | ●<br>44.3<br>1.95 | ●<br>0.2 | 1 | 0.5<br>1.0 | | ×××××× | | # |

**LITHOLOGIC DESCRIPTION**

RADIOLARIAN CLAYSTONE to CLAYEY RADIOLARITE, and CHERT

Major lithologies:
a. RADIOLARIAN CLAYSTONE gradational to CLAYEY RADIOLARITE, finely laminated dark grayish brown (10YR 4/2), with small dark patches as micronodules replacing and nucleating from radiolarian tests; some layers are dark brown (7.5YR 4/4).
b. CHERT, small varicolored pieces, dark browns (5YR 3/2) with lighter reddish brown and yellowish red (5YR 4/6-4/6) layers and lenses (burrows?) with mostly diffuse boundaries. Chert pieces have fractures filled by quartz.

Note: These beds have an apparent dip of 8-10 degrees.

SLIDE SUMMARY (%):

| | 1, 10<br>D | 1, 16<br>D |
|---|---|---|
| TEXTURE: | | |
| Sand | 10 | — |
| Silt | 40 | 5 |
| Clay | 50 | 95 |
| COMPOSITION: | | |
| Clay | 35 | 48 |
| Feldspar | — | Tr |
| Glass | — | Tr |
| Micronodule | 10 | — |
| Opaques | — | 5 |
| Oxide | — | 2 |
| Radiolarians | 55 | 15 |
| Silica | — | 30 |
| Zeolite | — | Tr |

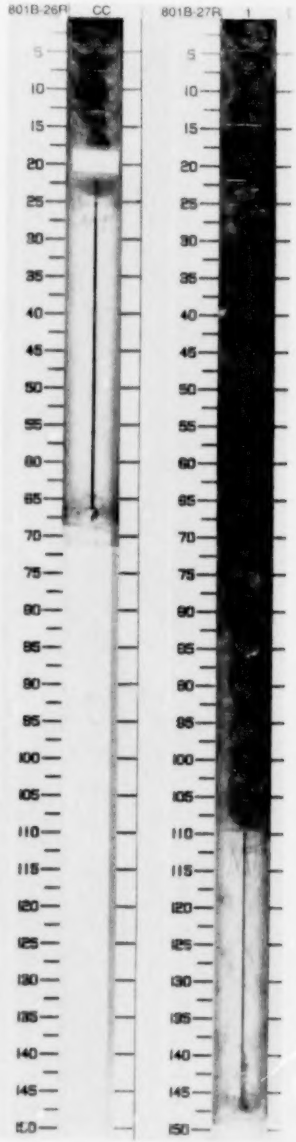

SITE 801 HOLE B CORE 28R CORED INTERVAL 6093.2-6098.0 mbsl; 419.4-424.2 mbsf

| TIME-ROCK UNIT | BIOSTRAT. ZONE/ FOSSIL CHARACTER | | | | | PALEOMAGNETICS | PHYS. PROPERTIES | CHEMISTRY | SECTION | METERS | GRAPHIC LITHOLOGY | DRILLING DISTURB. | SED. STRUCTURES | SAMPLES | LITHOLOGIC DESCRIPTION |
|---|---|---|---|---|---|---|---|---|---|---|---|---|---|---|---|
| | FORAMINIFERS | NANNOFOSSILS | RADIOLARIANS | DIATOMS | PALYNOMORPHS | | | | | | | | | | |
| KIMMERIDGIAN - TITHONIAN | B | B | A/M *Pseudodictyomitra primitiva* | | B | N | | | 1 | | | | | | CHERT, RADIOLARIAN PORCELLANITE, and CLAYEY RADIOLARITE<br>Major lithologies:<br>a. CHERT, dark brown (7.5YR 3/2) with reddish brown (2.5YR 5/4) patches that may be oxidized burrows. Other oxidized areas have diffuse boundaries and do not appear to reflect any primary features. Microquartz and chalcedony filled fractures in some pieces.<br>b. RADIOLARIAN PORCELLANITE, yellowish red to brown (5YR 5/6 - 7.5YR 4/4), smooth to slightly matte texture, angular and blocky fracture, grades to<br>c. CLAYEY RADIOLARITE. Planar fabric, not continuous lamination developed from horizontal alignment of very small (<1 mm X 1-8 mm) compositionally different areas (burrows or micronodules?). |

SITE 801 HOLE B CORE 29R CORED INTERVAL 6098.0-6102.7 mbsl; 424.2-428.9 mbsf

| TIME-ROCK UNIT | BIOSTRAT. ZONE/ FOSSIL CHARACTER | | | | | PALEOMAGNETICS | PHYS. PROPERTIES | CHEMISTRY | SECTION | METERS | GRAPHIC LITHOLOGY | DRILLING DISTURB. | SED. STRUCTURES | SAMPLES | LITHOLOGIC DESCRIPTION |
|---|---|---|---|---|---|---|---|---|---|---|---|---|---|---|---|
| | FORAMINIFERS | NANNOFOSSILS | RADIOLARIANS | DIATOMS | PALYNOMORPHS | | | | | | | | | | |
| KIMMERIDGIAN - TITHONIAN | B | B | A/M *Pseudodictyomitra primitiva* | | B | N | | | 1 | | | | | | CHERT and CLAYEY RADIOLARITE<br>Major lithologies:<br>a. CHERT, varicolored, dark reddish brown (5YR3/4) weak red (10Y 4/3), with scarce quartz filled fractures; the boundaries between the various colored zones are mostly diffuse.<br>b. CLAYEY RADIOLARITE, dark brown (7.5YR 4/4) with thin laminae overlaid by darker zones and patches.<br>SLIDE SUMMARY (%):<br>1, 0<br>D<br>TEXTURE:<br>Silt 2<br>Clay 98<br>COMPOSITION:<br>Calcite Tr<br>Clay 42<br>Glass Tr<br>Opaques 5<br>Oxide 2<br>Radiolarians 20<br>Silica 30<br>Zeolite Tr |

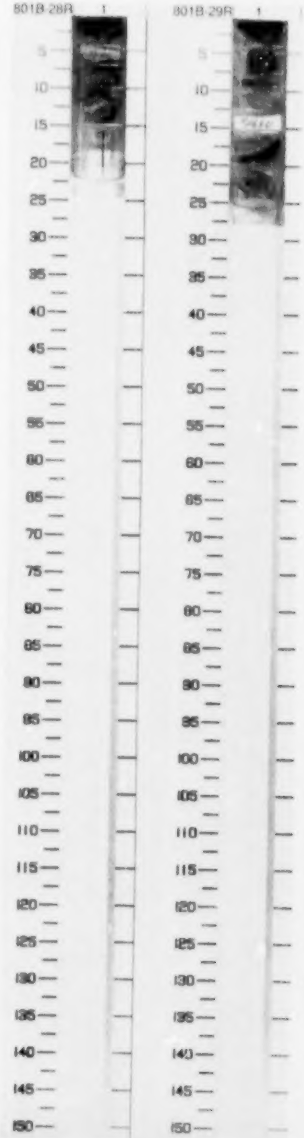

SITE 801 HOLE B CORE 30R CORED INTERVAL 6102.7-6107.4 mbsl; 428.9-433.6 mbsf

| TIME-ROCK UNIT | BIOSTRAT. ZONE/ FOSSIL CHARACTER |  |  |  |  | PALEOMAGNETICS | PHYS. PROPERTIES | CHEMISTRY | SECTION | METERS | GRAPHIC LITHOLOGY | DRILLING DISTURB. | SED. STRUCTURES | SAMPLES | LITHOLOGIC DESCRIPTION |
|---|---|---|---|---|---|---|---|---|---|---|---|---|---|---|---|
|  | FORAMINIFERS | NANNOFOSSILS | RADIOLARIANS | DIATOMS | PALYNOMORPHS |  |  |  |  |  |  |  |  |  |  |
| KIMMERIDGIAN - TITHONIAN | B | B | A/M *Pseudodictyomitra primitiva* |  | B | N |  |  | 1 |  | ▲ ▲ ▲ | X |  | ● | CHERT and CLAYEY RADIOLARIT.<br>Major lithologies<br>a. CHERT, dark reddish brown to dark brown (5YR 2.5/2 - 7.5YR 3/2), mottled with reddish brown (2.5YR 5/4). Most pieces show some fractures filled with up to three generations of clear, white (N9) or light gray (N7) botryoidal quartz/chalcedony. Relatively few radiolarians are evident.<br>b. CLAYEY RADIOLARITE, dark brown to pink (7.5YR 3/2 - 7.5YR 7/4), mostly firm and clayey to locally hard and siliceous, friable. Radiolarians are more abundant in lighter-colored areas.<br>SLIDE SUMMARY (%):<br>1, 7 D<br>TEXTURE:<br>Sand 30<br>Silt 40<br>Clay 30<br>COMPOSITION:<br>Clay 20<br>Micronodule 2<br>Radiolarians 45<br>Silica 33 |

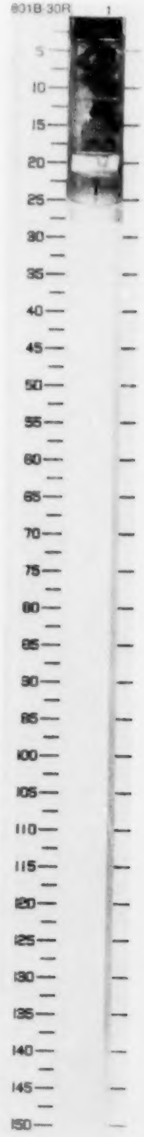

SITE 801 HOLE B CORE 31R CORED INTERVAL 6107.4-6112.0 mbsl; 433.6-438.2 mbsf

| TIME-ROCK UNIT | BIOSTRAT. ZONE/ FOSSIL CHARACTER |  |  |  |  | PALEOMAGNETICS | PHYS. PROPERTIES | CHEMISTRY | SECTION | METERS | GRAPHIC LITHOLOGY | DRILLING DISTURB. | SED. STRUCTURES | SAMPLES | LITHOLOGIC DESCRIPTION |
|---|---|---|---|---|---|---|---|---|---|---|---|---|---|---|---|
|  | FORAMINIFERS | NANNOFOSSILS | RADIOLARIANS | DIATOMS | PALYNOMORPHS |  |  |  |  |  |  |  |  |  |  |
| OXFORDIAN - KIMMERIDGIAN ? | B | unzoned<br>B/P | unzoned<br>A/P |  | B | N | ●<br>[illegible] | ●<br>0.2 | 1 |  | 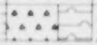 | ×<br>× |  |  | CHERT and CLAYEY RADIOLARITE to CLAYSTONE with RADIOLARIANS |

Major lithologies:

a. CHERT: dark brown (7.5YR 3/2) to yellowish red (5YR 4/4); very hard; conchoidal fracture; structureless except for vague planar fabric created by subparallel orientation of lighter colored, irregular lenticular areas, possibly small (2-1.0 mm X 3-10 mm) burrows. Same color oxidized zone surrounds open, unmineralized fractures.

b. CLAYEY RADIOLARITE gradational to CLAYSTONE with RADIOLARIANS: brown to reddish brown (7.5YR 4/4 - 2.5YR 4/4); sandy texture from radiolarians; rough, irregular fracture; firm, friable; 5-10 mm thick diffuse lamination, and vague planar, bedding parallel fabric. Areas of reddish oxidation. Thin section at Section 1, 11-12 cm, contains a radiolarian test which is wedged apart by opaque oxides and the halves were subsequently filled with opal surrounding central crystals of cristobalite. Same thin section also contains traces of zeolites, volcanic glass, and pieces of articulated fish(?) skeletal material.

SLIDE SUMMARY (%):

|  | 1, 11<br>D |
|---|---|
| TEXTURE: |  |
| Silt | 5 |
| Clay | 95 |
| COMPOSITION: |  |
| Clay | 47 |
| Feldspar | Tr |
| Fish | 2 |
| Glass | 1 |
| Opaques | 15 |
| Oxide | 5 |
| Quartz | Tr |
| Radiolarians | 10 |
| Silica | 20 |
| Zeolite | Tr |

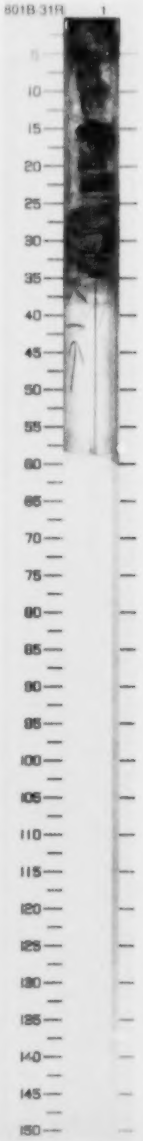

SITE 801 HOLE B CORE 32R CORED INTERVAL 6112.0-6116.6 mbsl; 438.2-442.8 mbsf

| TIME-ROCK UNIT | BIOSTRAT. ZONE/FOSSIL CHARACTER FORAMINIFERS | NANNOFOSSILS | RADIOLARIANS | DIATOMS | PALYNOMORPHS |
|---|---|---|---|---|---|
| OXFORDIAN | B | B | A/P *Cingulaturis carpatica* | | B |

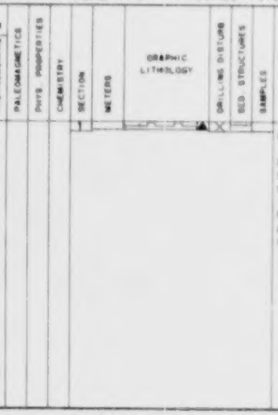
PALEOMAGNETICS
PHYS. PROPERTIES
CHEMISTRY
SECTION
METERS
GRAPHIC LITHOLOGY
DRILLING DISTURB.
SED. STRUCTURES
SAMPLES
1

LITHOLOGIC DESCRIPTION

CLAYEY RADIOLARITE

Major lithology: CLAYEY RADIOLARITE, dark brown to reddish yellow (7.5YR 3/2 - 5YR 6/5); light colored lenses and irregular patches appear less clayey and more radiolarian-rich than dark areas. Planar fabric, not distinct lamination.

Minor lithology: CHERT, dark brown to brown (7.5YR 3/4 - 7.5YR 4/4), more transparent than previous chert samples, also contains white microfossil molds (foraminifers?). Probably caving from overlying unit and not in place.

SITE 801 HOLE B CORE 33R CORED INTERVAL 6116.6-6121.4 mbsl; 442.8-447.6 mbsf

| TIME-ROCK UNIT | BIOSTRAT. ZONE/FOSSIL CHARACTER FORAMINIFERS | NANNOFOSSILS | RADIOLARIANS | DIATOMS | PALYNOMORPHS |
|---|---|---|---|---|---|
| CALLOVIAN | B | R/P unzoned | A/P *Stylocapsa (?) spiralis* | | B |

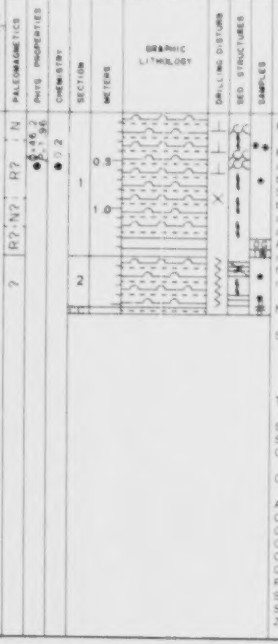
PALEOMAGNETICS
PHYS. PROPERTIES
CHEMISTRY
SECTION
METERS
GRAPHIC LITHOLOGY
DRILLING DISTURB.
SED. STRUCTURES
SAMPLES
N
R?
R?-N?
?
46.2
1.96
0.2
1
2
0.5
1.0

LITHOLOGIC DESCRIPTION

RADIOLARITE with CLAY, and CLAYSTONE with RADIOLARIANS

Major lithologies: Alternations of:
a. RADIOLARITE with CLAY, yellowish red (5YR 5/6), vaguely laminated to flaser mottled to bioturbated with some intervals displaying anastomosing flaser-type structures (especially Section 1, 40-50 cm); rare lenses of partial silicification; and
b. CLAYSTONE with RADIOLARIANS, red (2.5YR 4/6), moderately bioturbated. These alternations occur with approximately a 5 cm cyclicity; contacts between the two lithologies are fairly sharp, especially the tops of the radiolarite bands.
Alteration features: (1) opal-lined (<1 mm coating) fractures, white (N8), especially common in lower part of core, (2) brownish yellow (10YR 6/8 - 5/8) diffuse zones adjacent to some fractures, probably goethite-limonite staining, and (3) white (N8-N9) bleached zones occurring as reduction mottles, narrow bands parallel to bedding and adjacent to some fractures.

Note: These beds have an apparent dip of 27-30 degrees.

SLIDE SUMMARY (%):

| | 1, 33<br>D | 1, 37<br>D | 1, 70<br>M | 2, 20<br>D | 2, 42<br>D | CC<br>D |
|---|---|---|---|---|---|---|
| TEXTURE | | | | | | |
| Sand | 1 | 6 | 10 | 3 | — | 0 |
| Silt | 35 | 50 | 15 | 10 | 60 | 10 |
| Clay | 64 | 44 | 75 | 87 | 40 | 90 |
| COMPOSITION | | | | | | |
| Accessory minerals | — | 1 | — | — | — | — |
| Clay | 61 | 30 | 40 | 79 | 15 | 28 |
| Glass | 1 | — | — | — | — | — |
| Opaques | — | — | — | — | 5 | — |
| Oxide | 7 | 5 | 45 | 20 | 10 | 40 |
| Quartz | 15 | — | — | — | — | — |
| Radiolarians | 15 | 49 | 15 | 1 | 50 | 30 |
| Silica | — | 15 | — | — | 20 | — |
| Spines | — | — | — | — | — | 2 |
| Zeolite | — | — | — | Tr | — | — |

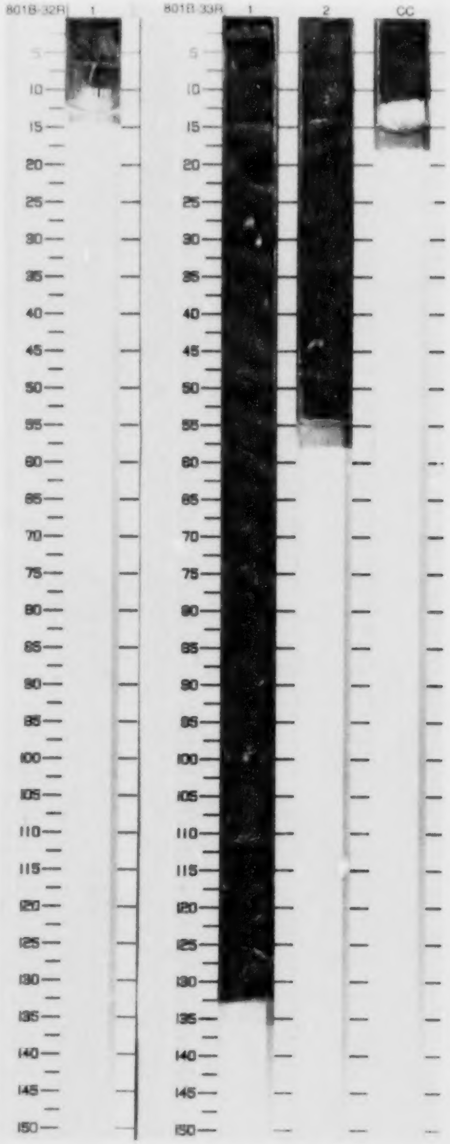
801B-32R
1
801B-33R
1
2
CC
5
10
15
20
25
30
35
40
45
50
55
60
65
70
75
80
85
90
95
100
105
110
115
120
125
130
135
140
145
150

SITE 801 HOLE B CORE 34R CORED INTERVAL 6121.4-6126.1 mbsl; 447.6-452.3 mbsf

| TIME-ROCK UNIT | BIOSTRAT. ZONE/ FOSSIL CHARACTER: FORAMINIFERS | NANNOFOSSILS | RADIOLARIANS | DIATOMS | PALYNOMORPHS | PALEOMAGNETICS | PHYS. PROPERTIES | CHEMISTRY | SECTION | METERS | GRAPHIC LITHOLOGY | DRILLING DISTURB. | SED. STRUCTURES | SAMPLES |
|---|---|---|---|---|---|---|---|---|---|---|---|---|---|---|
| CALLOVIAN | B | B | C/P *Tricolocapsa conexa* | | B | N?<br>R? | | | 1 | 0.5 | 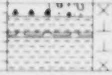 | X<br>⊥<br>⊥<br>X | | #<br>• |

LITHOLOGIC DESCRIPTION

CLAYSTONE and CLAYEY RADIOLARITE

Major lithologies:
a. CLAYSTONE, brownish red (2.5YR 4/6) grading upward to brick red (10YR 4/5) at Section 1, 15-30 cm, with light greenish gray (5GY 6.5/1) mottle (2 X 3 cm) at 25-28 cm; has moderate bioturbation; reddish yellow (7.5YR 6/8) mottles and streaks and rare opal-coated fractures (Section 1, 58-64 cm).
b. CLAYEY RADIOLARITE, in Section 1, 30-34 cm and in bands highly distorted by drilling; similar red (10YR 4/5) coloration as adjacent claystone beds.

Minor lithologies: 5 pieces of silicified sedimunt comprising top 15 cm of recovery, including CHERT PEBBLE CONGLOMERATE and CHERTIFIED BRECCIA, dark gray (N2) to dark reddish gray (5Y 4/4) angular to rounded 1-3 mm clasts in a light reddish brown (2.5YR 6/4) matrix, later chertified or partially silicified. CHERT varies considerably piece to piece from (1) olive yellow (2.5Y 6/6) and pale yellow (2.5Y 8/4), thin banded, with a 0.5 X 0.5 cm vug, to (2) light reddish brown (5YR 6/3) with yellowish mottles and black (Mn oxide?) surface stains, to (3) a silicified version of underlying claystone, red (10R 4/5) with black specks.

SLIDE SUMMARY (%):

| | 1, 8<br>M | 1, 44<br>D |
|---|---|---|
| TEXTURE: | | |
| Sand | 95 | — |
| Silt | — | 15 |
| Clay | 5 | 85 |
| COMPOSITION: | | |
| Accessory minerals | — | 1 |
| Clay | — | 83 |
| Feldspar | — | 1 |
| Opaques | 5 | — |
| Oxide | 10 | 6 |
| Quartz | — | 1 |
| Radiolarians | 25 | 6 |
| Silica | 60 | — |

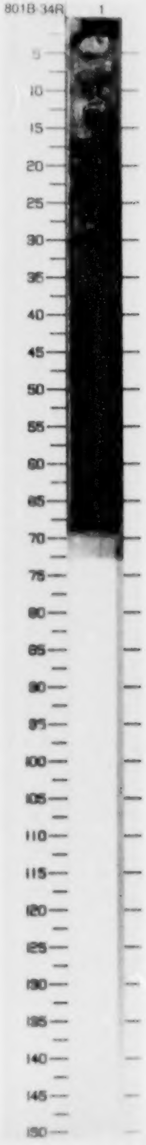

SITE 801 HOLE B CORE 35R CORED INTERVAL 6126.1-6130.7 mbsl; 452.3-456.9 mbsf

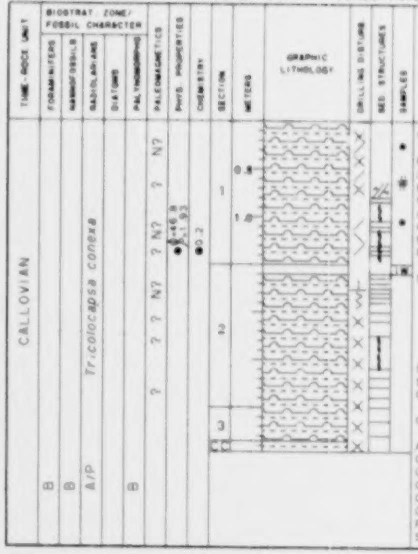
TIME-ROCK UNIT
BIOSTRAT. ZONE/ FOSSIL CHARACTER
FORAMINIFERS
NANNOFOSSILS
RADIOLARIANS
DIATOMS
PALYNOMORPHS
PALEOMAGNETICS
PHYS. PROPERTIES
CHEMISTRY
SECTION
METERS
GRAPHIC LITHOLOGY
DRILLING DISTURB.
SED. STRUCTURES
SAMPLES
CALLOVIAN
B
B
A/P
Tricolocapsa conexa
B
N?
?
? N?
? N?
? ?
?
46.8
1.93
0.2
1
2
3
CC
0.5
1.0

LITHOLOGIC DESCRIPTION

CLAYSTONE with RADIOLARIANS and RADIOLARITE

Major lithologies: Alternations of
a. CLAYSTONE with RADIOLARIANS, red (2.5YR 4/6 - 2.5YR 5/6); and
b. RADIOLARITE red (2.5YR 5/6), yellowish red (5YR 5/6) to brownish yellow (10YR 6/8), hematitic. These alternations have a 5 cm average spacing, but claystone layers are 0.5-2 cm thick and of radiolarites are 1-20 cm thick. White (10YR 8/1) bleach zones and patches cut across layering. Bioturbation abundant at Section 2, 95-100 cm, and locally present throughout. Thin coatings of silica (<1 mm thick) are found on some fractured pieces, and black (N1) manganese or iron-oxide coats a fracture in Section 3, 12-14 cm.

SLIDE SUMMARY (%):

| | 1, 28<br>D | 1, 62<br>D | 1, 103<br>D |
|---|---|---|---|
| TEXTURE: | | | |
| Sand | Tr | — | 10 |
| Silt | 35 | 5 | 48 |
| Clay | 65 | 95 | 42 |
| COMPOSITION: | | | |
| Accessory minerals | — | — | 1 |
| Clay | 60 | — | 36 |
| Opal | — | 5 | — |
| Opaques | — | 5 | — |
| Oxide | 10 | 3 | 8 |
| Quartz | 10 | — | 15 |
| Radiolarians | 20 | 50 | 40 |
| Silica | — | 37 | — |

SITE 801 HOLE B CORE 36R CORED INTERVAL 6130.7-6135.3 mbsl; 456.9-461.5 mbsf

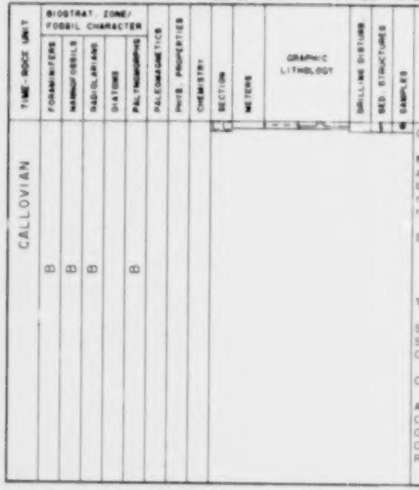
TIME-ROCK UNIT
BIOSTRAT. ZONE/ FOSSIL CHARACTER
FORAMINIFERS
NANNOFOSSILS
RADIOLARIANS
DIATOMS
PALYNOMORPHS
PALEOMAGNETICS
PHYS. PROPERTIES
CHEMISTRY
SECTION
METERS
GRAPHIC LITHOLOGY
DRILLING DISTURB.
SED. STRUCTURES
SAMPLES
CALLOVIAN
B
B
B
B
CC

LITHOLOGIC DESCRIPTION

CLAYEY RADIOLARITE and CLAYSTONE with RADIOLARIANS

Major lithologies: Adjacent layers of
a. CLAYEY RADIOLARITE and
b. CLAYSTONE with RADIOLARIANS, both are red (2.5YR 4/8) with lighter-colored silt-sized radiolarians; bioturbation vaguely present as compacted lenticular mottles. Only one piece recovered.

SLIDE SUMMARY (%):

| | CC, 1<br>D |
|---|---|
| TEXTURE: | |
| Sand | 10 |
| Silt | 45 |
| Clay | 45 |
| COMPOSITION: | |
| Accessory minerals | Tr |
| Clay | 39 |
| Glass | 1 |
| Oxide | 10 |
| Radiolarians | 50 |

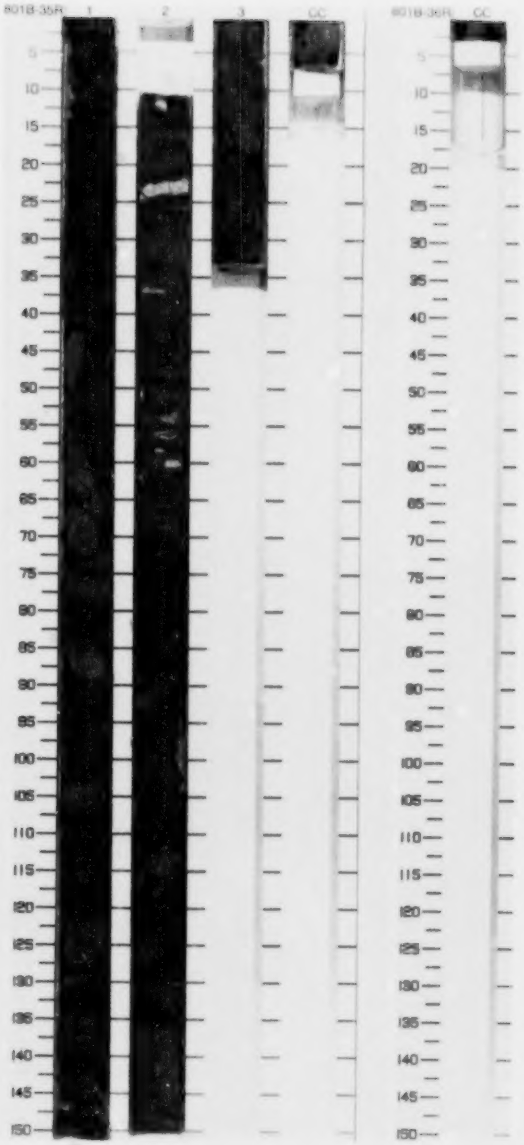
801B-35R
1
2
3
CC
801B-36R
CC
5
10
15
20
25
30
35
40
45
50
55
60
65
70
75
80
85
90
95
100
105
110
115
120
125
130
135
140
145
150

SITE 801 HOLE B CORE 37R CORED INTERVAL 6135.3-3139.9 mbsl; 461.5-466.1 mbsf

| TIME-ROCK UNIT | BIOSTRAT. ZONE/ FOSSIL CHARACTER | | | | | PALEOMAGNETICS | PHYS. PROPERTIES | CHEMISTRY | SECTION | METERS | GRAPHIC LITHOLOGY | DRILLING DISTURB. | SED. STRUCTURES | SAMPLES | LITHOLOGIC DESCRIPTION |
|---|---|---|---|---|---|---|---|---|---|---|---|---|---|---|---|
| | FORAMINIFERS | NANNOFOSSILS | RADIOLARIANS | DIATOMS | PALYNOMORPHS | | | | | | | | | | |
| BATHONIAN-CALLOVIAN | B | B | A/P *Tricolocapsa conexa* | | B | ? | ● | ● ● | 1 | 0.5 | BASALT | ×<br>×<br>⊥<br>⊥ | | | CHERT<br>Major sedimentary lithology: CHERT, light brown or reddish brown (5YR 5/4, 5YR 4/4, or 2.5YR 3/4); crackle breccia in which the pieces fit back together, with clear and white silica as matrix filler. Chert was brittly fractured, probably as softer sediment in some cases forming feathered sets of fractures penetrating into the host rock, then silica was introduced to form drusy quartz.<br>Minor lithology: Piece at of RADIOLARITE top of core: pink (5YR 6/4) and PORCELLANITE, brown (5YR 5/2), laminated with wispy bioturbation mottling. |

SITE 801 HOLE B CORE 38R CORED INTERVAL 6139.9-6144.5 mbsl; 466.1-470.7 mbsf

| TIME-ROCK UNIT | BIOSTRAT. ZONE/ FOSSIL CHARACTER | | | | | PALEOMAGNETICS | PHYS. PROPERTIES | CHEMISTRY | SECTION | METERS | GRAPHIC LITHOLOGY | DRILLING DISTURB. | SED. STRUCTURES | SAMPLES | LITHOLOGIC DESCRIPTION |
|---|---|---|---|---|---|---|---|---|---|---|---|---|---|---|---|
| | FORAMINIFERS | NANNOFOSSILS | RADIOLARIANS | DIATOMS | PALYNOMORPHS | | | | | | | | | | |
| BATHONIAN-CALLOVIAN | B | B | B | | B | ? | | | 1 | | BASALT | × | ⅹ⁄ᵪ | # | CHERT<br>Major lithology: CHERT, dark reddish brown (2.5YR 3/4 - 5YR 3/4), intensely brecciated; drusy quartz fills most fractures, but some open voids exist. No primary structures or visible radiolarians; completely recrystallized. Brecciation probably occurred while sediment was still somewhat soft, possibly by rapid dewatering or fluid injection; this is suggested by quartz filled fractures that have curved, nonparallel surfaces that taper into the host rock with a feathery or horsetail look. Some pieces can be reassembled into their original fit, i.e., a crackle breccia. Elsewhere, lenticular and sigmoidal gashes are present, whereas fractures in hard chert typically have matched and parallel sides.<br>SLIDE SUMMARY (%):<br>1, 4<br>M<br>TEXTURE:<br>Silt 1<br>Clay 99<br>COMPOSITION:<br>Clay 30<br>Opaques 1<br>Oxide 3<br>Quartz Tr<br>Silica 66 |

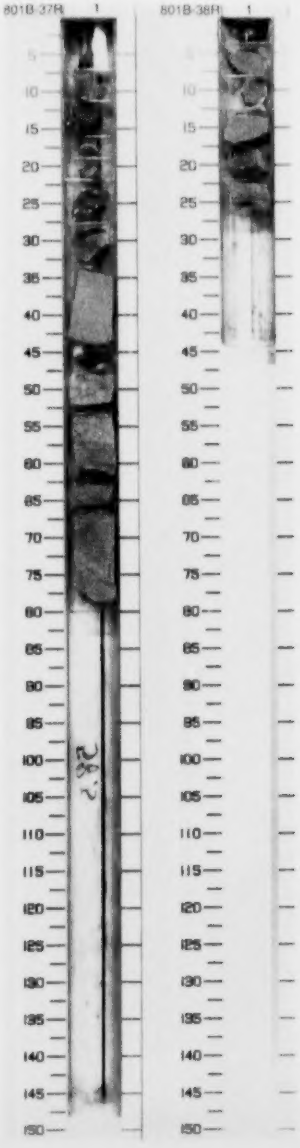

SITE 801 HOLE B CORE 39R CORED INTERVAL 6144.5-6150.7 mbsl; 470.7-476.9 mbsf

| TIME-ROCK UNIT | BIOSTRAT. ZONE/ FOSSIL CHARACTER: FORAMINIFERS | NANNOFOSSILS | RADIOLARIANS | DIATOMS | PALYNOMORPHS | PALEOMAGNETICS | PHYS. PROPERTIES | CHEMISTRY | SECTION | METERS | GRAPHIC LITHOLOGY | DRILLING DISTURB. | SED. STRUCTURES | SAMPLES |
|---|---|---|---|---|---|---|---|---|---|---|---|---|---|---|
| BATHONIAN-CALLOVIAN | B | B | C/P *Tricolocapsa conexa* | B | | ? | ● $\phi$=3.30<br>$\gamma$=2.66 | ● 0.4 | 1 | | | × | | ● # |

LITHOLOGIC DESCRIPTION

CHERT

Major lithology: CHERT, dark brown (7.5YR 3/2) with some dark reddish gray (5YR 4/2), hematitic, very hard, but dull with rougher, subconchoidal fracture probably chertified claystone and radiolarite. Superficially massive, faint burrow mottling is marked by concentrations of radiolarians, which are each infilled by clear, dark quartz.

Minor lithology: SILICIFIED RADIOLARITE (the bottom piece, Section 1, 26-32 cm), mostly dark reddish gray (5YR 4/2); radiolarians are replaced by opaque white (N9) silica, making burrowing much more clearly evident. In this piece, there is reaction front that makes a sharp contact between the slightly porous light colored radiolarite and a dark reddish brown, more silicified region where all radiolarians are filled with clear quartz, as in the chert.

SLIDE SUMMARY (%):

| | 1, 15<br>D | 1, 22<br>M |
|---|---|---|
| TEXTURE: | | |
| Silt | 1 | 5 |
| Clay | 99 | 95 |
| COMPOSITION: | | |
| Clay | 5 | 2 |
| Opaques | 2 | 3 |
| Oxide | 10 | — |
| Radiolarians | 40 | 60 |
| Silica | 28 | 35 |
| Spines | 15 | — |

SITE 801 HOLE B CORE 40R CORED INTERVAL 6150.7-6156.8 mbsl; 476.9-483.0 mbsf

| TIME-ROCK UNIT | BIOSTRAT. ZONE/ FOSSIL CHARACTER: FORAMINIFERS | NANNOFOSSILS | RADIOLARIANS | DIATOMS | PALYNOMORPHS | PALEOMAGNETICS | PHYS. PROPERTIES | CHEMISTRY | SECTION | METERS | GRAPHIC LITHOLOGY | DRILLING DISTURB. | SED. STRUCTURES | SAMPLES |
|---|---|---|---|---|---|---|---|---|---|---|---|---|---|---|
| MIDDLE JURASSIC | B | B | B | | B | ? | ● $\phi$=19.1<br>$\gamma$=2.42 | ● 0.2<br>● 1.7<br>● 9.1 | 1 | 0.5 | BASALT<br>BASALT | × | | ● |

LITHOLOGIC DESCRIPTION

CHERT

Major lithology: CHERT, red (2.5YR 4/6), intensely brecciated, fractures filled with drusy quartz. No primary sedimentary structures. One fragment is slightly lighter red (2.5YR 5/6), less hard, and less silicified. Fracture walls are generally not parallel, some fractures are lenticular, like tension gashes or mud cracks. Nearly identical with brecciated chert in core 37R, probably caving from above.

Minor lithology: METALLIFEROUS CLAY, red (2.5YR 4/8), 1 cm of clay recovered between basalt pieces in section 1, 66 cm. It is uncertain whether this clay was recovered in situ. Contains: 55% Fe oxides, 45% clay, traces of feldspar and pyroxene.

SLIDE SUMMARY (%):

| | 1, 66<br>M |
|---|---|
| TEXTURE: | |
| Silt | 20 |
| Clay | 80 |
| COMPOSITION: | |
| Clay | 45 |
| Feldspar | Tr |
| Oxide | 55 |
| Quartz | Tr |

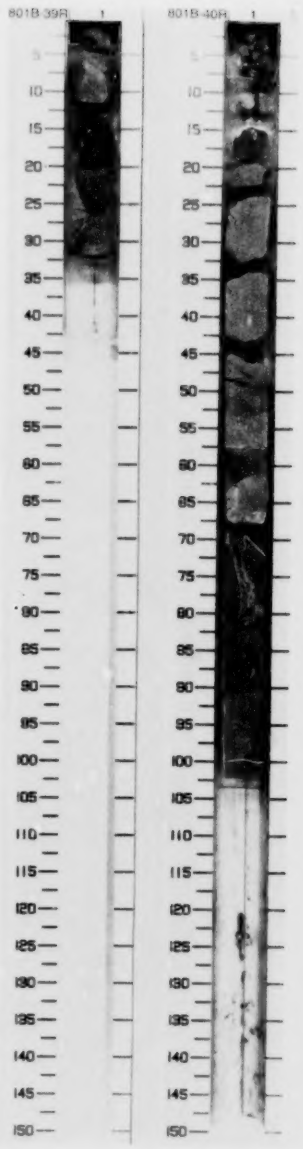

SITE 801 HOLE B CORE 41R CORED INTERVAL 6156.8-6161.4 mbsl; 483.0-487.6 mbsf

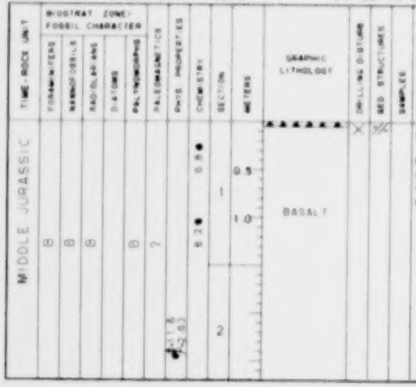

LITHOLOGIC DESCRIPTION

CHERT

Major lithology: CHERT, red (2.5YR 4/6), intensely brecciated, fractures filled with drusy quartz. Identical to samples in Cores 37R, 38R, and 40R. Chert breccia fragments were only recovered at the tops of Cores 38R, 40R, and 41R, thus suggesting that these pieces are probably cavings from the breccia zone first encountered in Core 37R.

## 801B 42R HARD ROCK

SITE 801 HOLE B CORE 43R CORED INTERVAL 6166.0-6175.5 mbsl; 492.2-501.7 mbsf

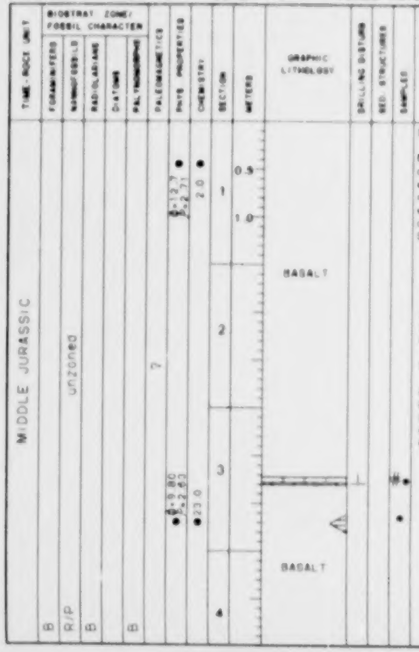

LITHOLOGIC DESCRIPTION

LIMESTONE

Major lithology: LIMESTONE between basalt pillows and sills, overall gray (N6), but actually composed of irregular pods of darker (N5) gray, densely crystalline calcite within a matrix of white (N9), more porous calcite. Very small (<0.3 mm) bean-shaped patches may be recrystallized foraminifers. Structure somewhat resembles a micro-"chicken-wire" fabric which may represent disruption or injection. Scraped smear slides reveal only inorganic calcite and one wide-ranging nannofossil.

SLIDE SUMMARY (%):

|  | 3, 76<br>M | 3, 77<br>M | 3, 116<br>M |
|---|---|---|---|
| TEXTURE: |  |  |  |
| Sand | — | 20 | — |
| Silt | 1 | 50 | 5 |
| Clay | 99 | 30 | 95 |
| COMPOSITION: |  |  |  |
| Calcite | 91 | — | 55 |
| Epidote | — | — | 45 |
| Foraminifers | 1 | — | — |
| Opaques | 5 | — | — |
| Radiolarians | 3 | — | — |

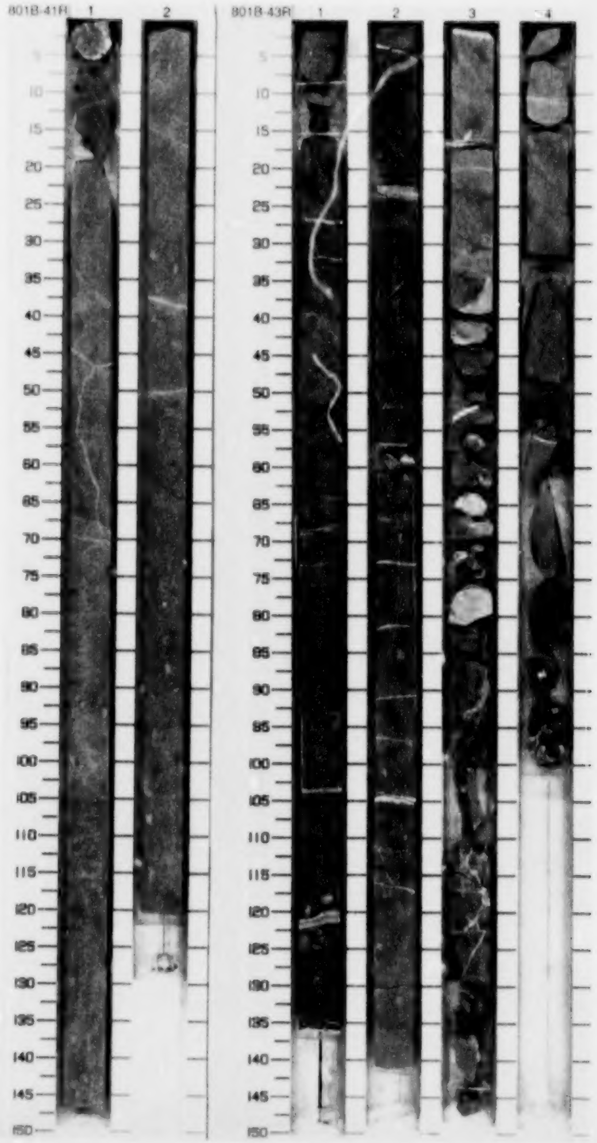

SITE 801 HOLE B CORE 44R CORED INTERVAL 6175.5-6185.0 mbsl; 501.7-511.2 mbsf

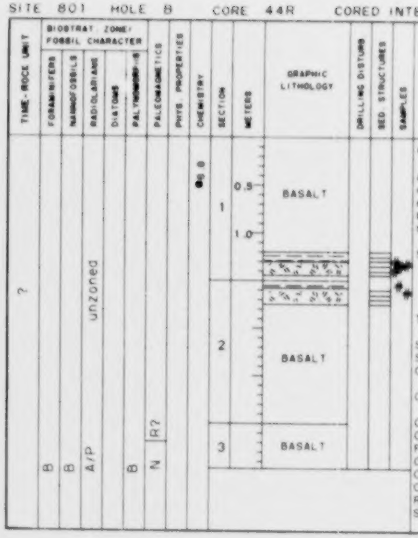
TIME-ROCK UNIT
BIOSTRAT. ZONE/ FOSSIL CHARACTER
FORAMINIFERS
NANNOFOSSILS
RADIOLARIANS
DIATOMS
PALYNOMORPHS
PALEOMAGNETICS
PHYS. PROPERTIES
CHEMISTRY
SECTION
METERS
GRAPHIC LITHOLOGY
DRILLING DISTURB.
SED. STRUCTURES
SAMPLES
?
B
B
unzoned
A/P
B
R?
N
1
2
3
0.5
1.0
BASALT
BASALT
BASALT

### LITHOLOGIC DESCRIPTION

CALCAREOUS SILICIFIED TUFF and RADIOLARIAN METASILTSTONE

Major lithology

a. CALCAREOUS SILICIFIED TUFF, reddish gray (5R 6/1 to N4), finely laminated, 1-3 mm calcareous ovoids with coarser crystalline calcite centers - possibly organic forms (foraminifers?). Aphanitic groundmass.

b. RADIOLARIAN METASILTSTONE, dark reddish brown (2.5YR 3/6), hematitic, cryptocrystalline to microcrystalline matrix, radiolarian ghosts. In depositional contact over the tuff.

SLIDE SUMMARY (%)

| | 1, 130<br>M | 1, 132<br>M | 1, 134<br>M | 1, 138<br>M | 2, 4<br>M | 2, 12<br>D |
|---|---|---|---|---|---|---|
| TEXTURE | | | | | | |
| Sand | — | 10 | — | — | — | — |
| Silt | 55 | — | 10 | 5 | 5 | 2 |
| Clay | 45 | 90 | 90 | 95 | 95 | 98 |
| COMPOSITION | | | | | | |
| Calcite | — | 20 | 10 | 65 | — | 70 |
| Clay | — | 5 | 5 | 2 | 2 | 5 |
| Feldspar | — | — | — | — | — | 2 |
| Glass | — | 10 | 20 | 5 | — | 10 |
| Opaques | 15 | 15 | 10 | 3 | 8 | 3 |
| Oxide | 30 | — | — | — | 5 | — |
| Radiolarians | 10 | — | Tr | 5 | 25 | — |
| Silica | 45 | 50 | 55 | 20 | 60 | 10 |

801C 1R HARD ROCK

801C 2R HARD ROCK

801C 3R HARD ROCK

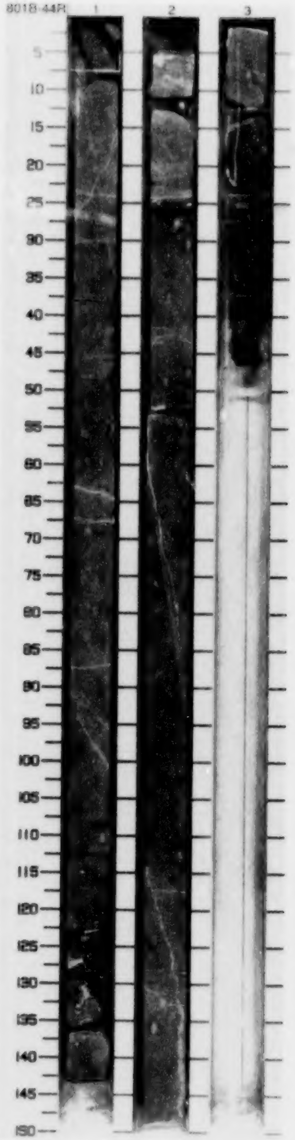
801B-44R
1
2
3
5
10
15
20
25
30
35
40
45
50
55
60
65
70
75
80
85
90
95
100
105
110
115
120
125
130
135
140
145
150

SITE 801 HOLE C CORE 4R CORED INTERVAL 6195.3-6204.8 mbsl; 521.7-531.2 mbsf

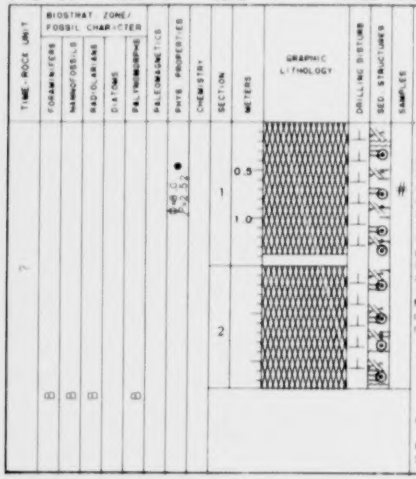
TIME-ROCK UNIT
BIOSTRAT. ZONE/ FOSSIL CHARACTER
FORAMINIFERS
NANNOFOSSILS
RADIOLARIANS
DIATOMS
PALYNOMORPHS
PALEOMAGNETICS
PHYS. PROPERTIES
CHEMISTRY
SECTION
METERS
GRAPHIC LITHOLOGY
DRILLING DISTURB.
SED. STRUCTURES
SAMPLES
?
B
B
B
B
1
2
0.5
1.0
#

LITHOLOGIC DESCRIPTION

HYDROTHERMAL DEPOSIT

Major lithology: HYDROTHERMAL DEPOSIT, mainly a siliceous to clay rich iron oxide hydroxide chemical precipitate (goethite), yellow (10Y 8/6 - 5Y 8/8), pseudo nodular texture of concentric laminated precipitate growths in a silica replaced matrix. Quartz filled veins and drusy cavities are common; rare intervals of chert formation. Some vein fillings of dark gray (N3 to N5) are calcareous (e.g., Section 1, 96-101 cm, Piece 10). Thin Section (Section 1, 70-71 cm, Piece 8) indicates that yellow iron oxyhydroxide deposits mainly grew outwards as radially fibrous coalescing botryoidal masses, commonly zoned, with later division into platelets, followed by partial replacement by small segment triple junctioned quartz grains; larger quartz grains fill secondary veins that traverse the whole laminated deposit. See accompanying igneous barrel sheet description.

Minor lithology: SILICEOUS BRECCIA, moderate reddish brown (10R 4/6) at Section 1, 0-4 cm (Piece 1) with white (N9) silica-filled fractures and dark gray (N4-N3) calcareous sediment mottled with yellow (5Y 8/6) material. No depositional features.

SLIDE SUMMARY (%):

| | 1, 70 |
|---|---|
| | D |
| COMPOSITION: | |
| Oxide | 75 |
| Silica | 25 |

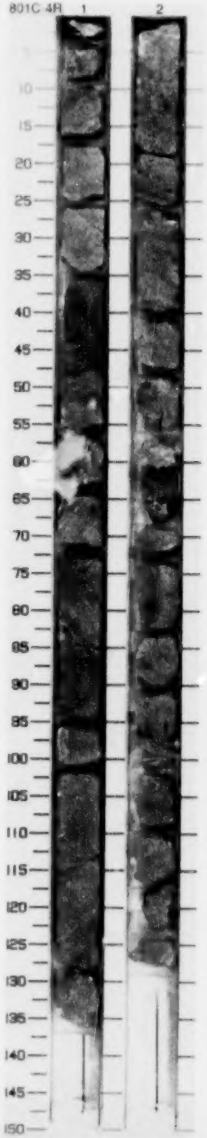
801C-4R
1
2
10
15
20
25
30
35
40
45
50
55
60
65
70
75
80
85
90
95
100
105
110
115
120
125
130
135
140
145
150

SITE 801 HOLE C CORE 5R CORED INTERVAL 6204.8-6214.1 mbsl; 531.2-540.5 mbsf

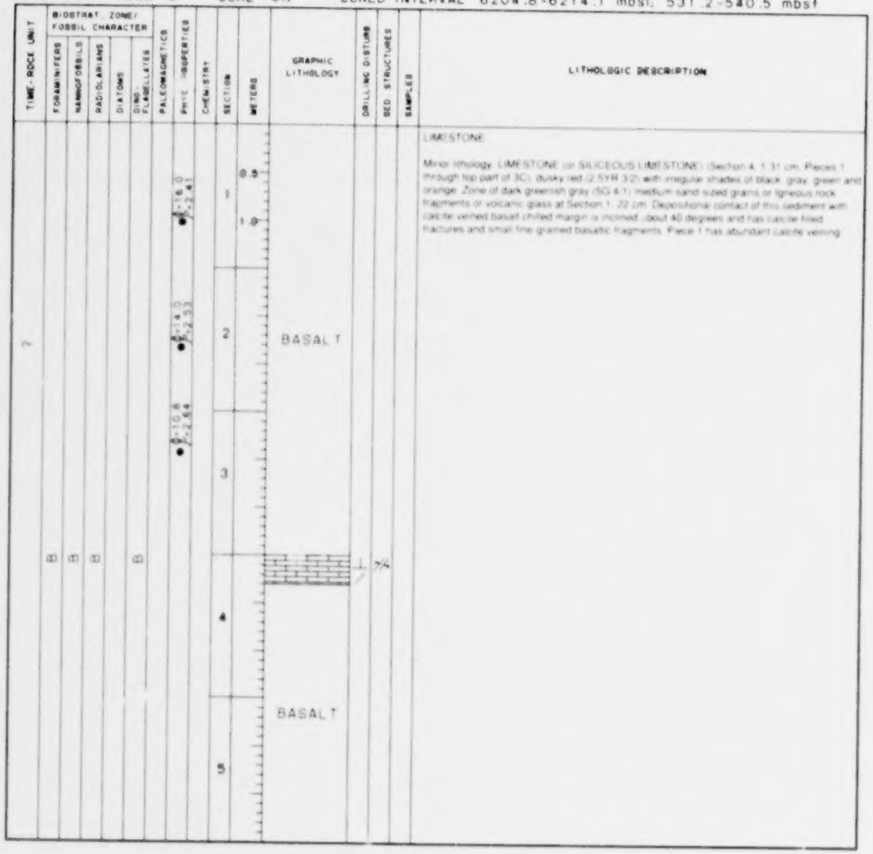
TIME-ROCK UNIT
BIOSTRAT. ZONE/ FOSSIL CHARACTER
FORAMINIFERS
NANNOFOSSILS
RADIOLARIANS
DIATOMS
DINO-FLAGELLATES
PALEOMAGNETICS
PHYS. PROPERTIES
CHEMISTRY
SECTION
METERS
GRAPHIC LITHOLOGY
DRILLING DISTURB.
SED. STRUCTURES
SAMPLES
LITHOLOGIC DESCRIPTION
?
B
B
B
B
$\phi$=16.0
$\gamma$=2.41
$\phi$=14.0
$\gamma$=2.53
$\phi$=10.8
$\gamma$=2.64
1
2
3
4
5
0.5
1.0
BASALT
BASALT
%

LIMESTONE

Minor lithology: LIMESTONE (or SILICEOUS LIMESTONE) (Section 4, 1-31 cm, Pieces 1 through top part of 3C): dusky red (2.5YR 3/2) with irregular shades of black, gray, green and orange. Zone of dark greenish gray (5G 4/1) medium sand-sized grains or igneous rock fragments or volcanic glass at Section 1, 22 cm. Depositional contact of this sediment with calcite veined basalt chilled margin is inclined about 40 degrees and has calcite filled fractures and small fine-grained basaltic fragments. Piece 1 has abundant calcite veining.

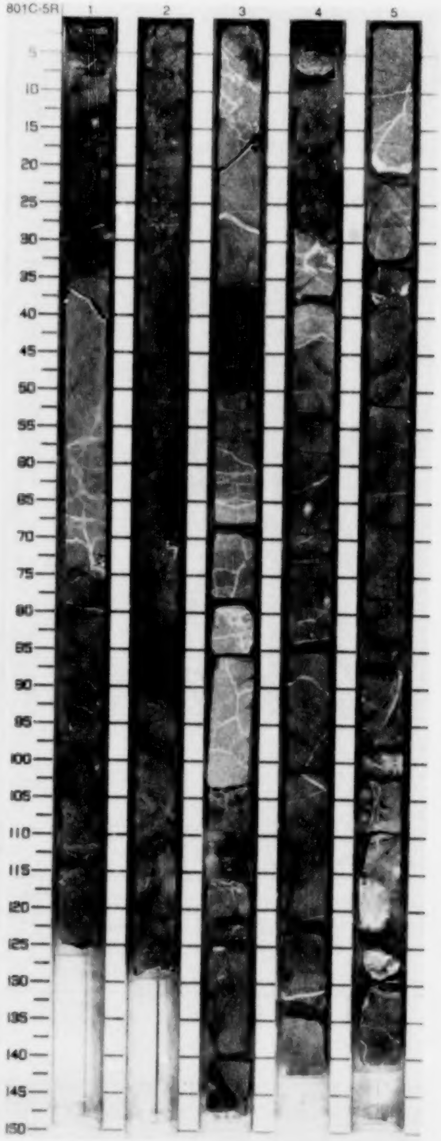
801C-5R
1
2
3
4
5
5
10
15
20
25
30
35
40
45
50
55
60
65
70
75
80
85
90
95
100
105
110
115
120
125
130
135
140
145
150

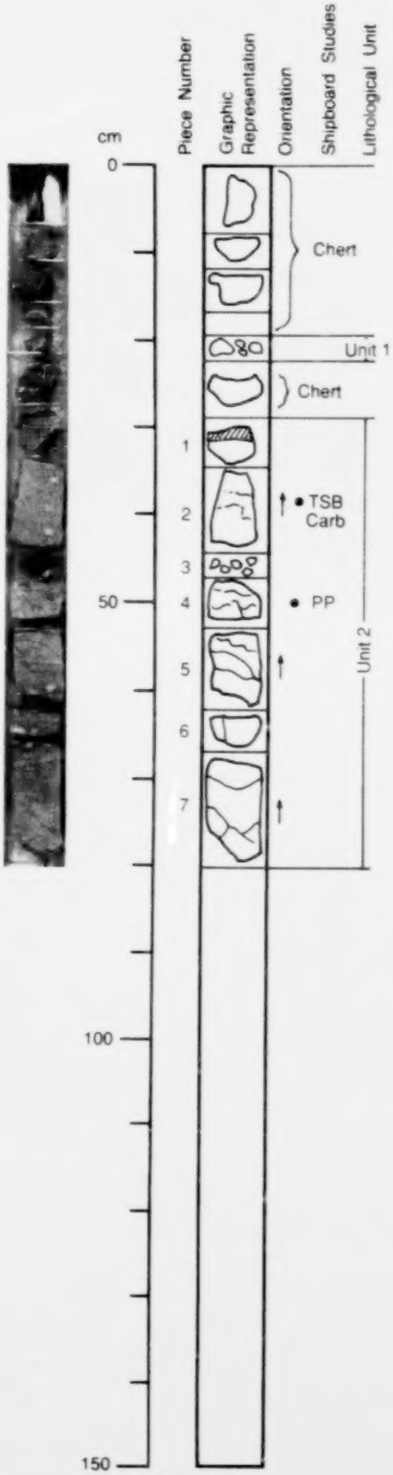
cm
Piece Number
Graphic Representation
Orientation
Shipboard Studies
Lithological Unit
0
50
100
150
Chert
Unit 1
Chert
1
2
3
4
5
6
7
• TSB
Carb
• PP
Unit 2
CORE/SECTION

## 129-801B-37R-1

## UNIT 1: APHYRIC BASALT

### Pieces Small fragments

**CONTACTS:** Not seen.
**PHENOCRYSTS:** No phenocrysts.
**GROUNDMASS:** Fine-grained, quenched textured.
**VESICLES:** No vesicles.
**COLOR:** Gray-green (5Y 5/1).
**STRUCTURE:** Possibly thin flow.
**ALTERATION:** Slight, yellowish patch of clay.
**VEINS/FRACTURES:** None.
**ADDITIONAL COMMENTS:** Although separated by chert from Unit 2 below, both units are very similar and could be the same; chert may be a cave-in fragment.

## UNIT 2: APHYRIC BASALT

### Pieces 1 to 7

**CONTACTS:** Not observed; oxidized and quenched texture of piece 1 suggests this is near top of unit.
**PHENOCRYSTS:** No phenocrysts.
**GROUNDMASS:** Fine-grained, hypocrystalline, quench textured. Grain-size increases from Pieces 1 & 2 to 3 through to 7.
**VESICLES:** No vesicles.
**COLOR:** Speckled gray-green (5GY 5/1).
**STRUCTURE:** Possibly a thin flow.
**ALTERATION:** Moderate. Oxidized 8 mm thick top to Piece 1; rest of pieces have irregular oxidized veinlets.
**VEINS/FRACTURES:** 2%; 0.5-1.0 mm; random; some with oxidized margins, coloring plagioclase yellow. Three types: metallic opaque ore; yellow oxidized clay; calcite (latest).
**ADDITIONAL COMMENTS:** Microphenocrysts of plagioclase, but <1%, random distribution.

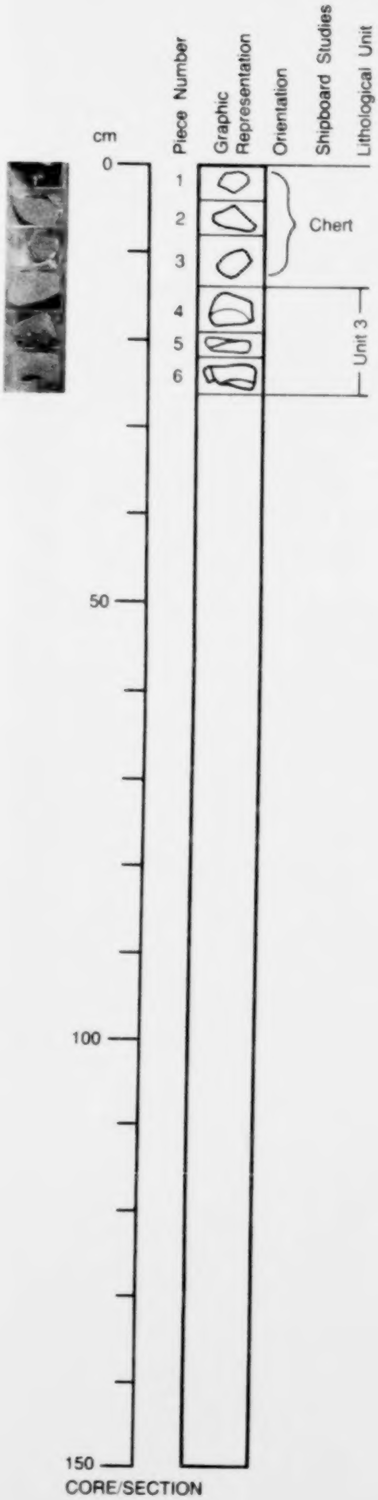
cm
Piece Number
Graphic Representation
Orientation
Shipboard Studies
Lithological Unit
0
50
100
150
1
2
3
4
5
6
Chert
Unit 3
CORE/SECTION

## 129-801B-38R-1

### UNIT 3: APHYRIC BASALT

### Pieces 4, 5, 6

**CONTACTS:** None observed.
**PHENOCRYSTS:** No phenocrysts.
**GROUNDMASS:** Fine-grained, hypocrystalline; similar to 37R-1, Piece 7.
**VESICLES:** No vesicles.
**COLOR:** Speckled grayish-green (5G 5/1).
**STRUCTURE:** Possibly a thin flow.
**ALTERATION:** High; green clays replacing glass in matrix, pervasive brown oxidized zones and veinlets, calcite veinlets.
**VEINS/FRACTURES:** 2%; 0.25-1.00 mm; random; pervasive oxidized zones and calcite veinlets with oxidized margins, also oxidized clay veinlets.
**ADDITIONAL COMMENTS:** Petrographically and texturally similar to 37R-1 pieces, however the presence of possible in situ chert fragments indicate this is probably another unit.

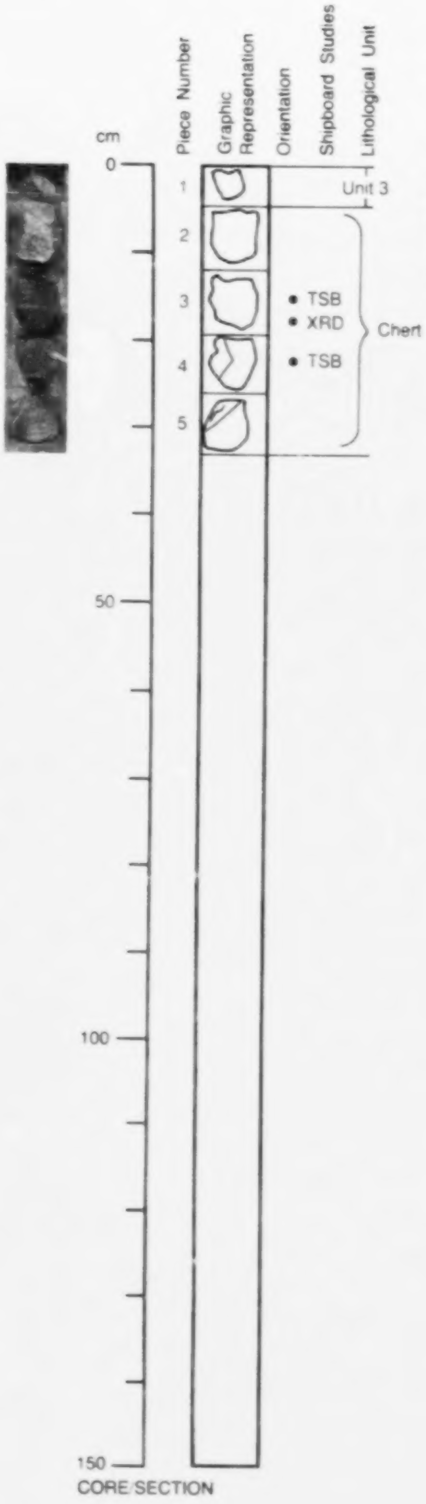
cm
Piece Number
Graphic Representation
Orientation
Shipboard Studies
Lithological Unit
0
50
100
150
1
2
3
4
5
Unit 3
TSB
XRD
TSB
Chert
CORE/SECTION

## 129-801B-39R-1

## UNIT 3: APHYRIC BASALT

### Piece 1

**CONTACTS:** None observed.
**PHENOCRYSTS:** Aphyric.
**GROUNDMASS:** Fine-grained; hypocrystalline.
**VESICLES:** None.
**COLOR:** Speckled gray-green (5GY 5/1).
**STRUCTURE:** Possibly a thin flow.
**ALTERATION:** Moderate to high; green clays replacing mesostasis; leucoxene and hematite/limonite replacing opaques; calcite along plagioclase margins.
**VEINS/FRACTURES:** None.
**ADDITIONAL COMMENTS:** Piece 1 is slightly darker green than the other parts of the same unit in lower portion of Core 38R-1, texture and mineralogy basically the same. The presence of cherts above, in between and at the bottom of the units suggests that the basalts are sills; these were intruded into soft sediments that later became cherts. Soft sediment structures prior to silicification and soft sediment deformational structures are preserved in the intercalated cherts.

## 129-801B-40R-1

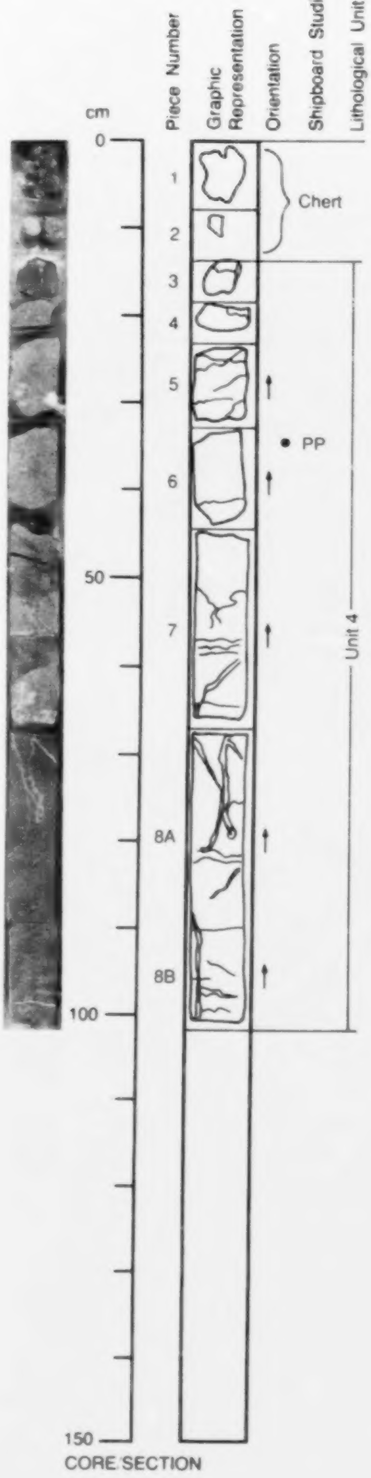
cm
Piece Number
Graphic Representation
Orientation
Shipboard Studies
Lithological Unit
0
50
100
150
1
2
3
4
5
6
7
8A
8B
Chert
PP
Unit 4
CORE SECTION

### UNIT 4: APHYRIC BASALT

### Pieces 3-8B

**CONTACTS:** Not observed although Piece 3 is finer-grained than the rest of the unit suggesting that it may be a piece of the chilled margin.
**PHENOCRYSTS:** None.
**GROUNDMASS:** Fine-grained; holocrystalline to hypocrystalline.
**VESICLES:** None.
**COLOR:** Gray (N5).
**STRUCTURE:** Possibly a thin flow.
**ALTERATION:** Slight to moderate; leucoxene (?) after opaques; green clay after mesostasis and some plagioclases; Fe-hydroxides after opaques; calcite along plagioclase margins.
**VEINS/FRACTURES:** 3%; 0.01 to 1.5 cm; 0-90 degrees; some are curved/irregular; ~90% are filled with carbonates with ocassional green clays whereas others are black, metallic ores and Fe-hydroxides. Metallic ores are older than the Fe-hydroxides but carbonates have a wide range resulting in several generations of carbonate veinlets.
**ADDITIONAL COMMENTS:** Unit 4 is relatively finer-grained, less green, and fresher than the other units above it.

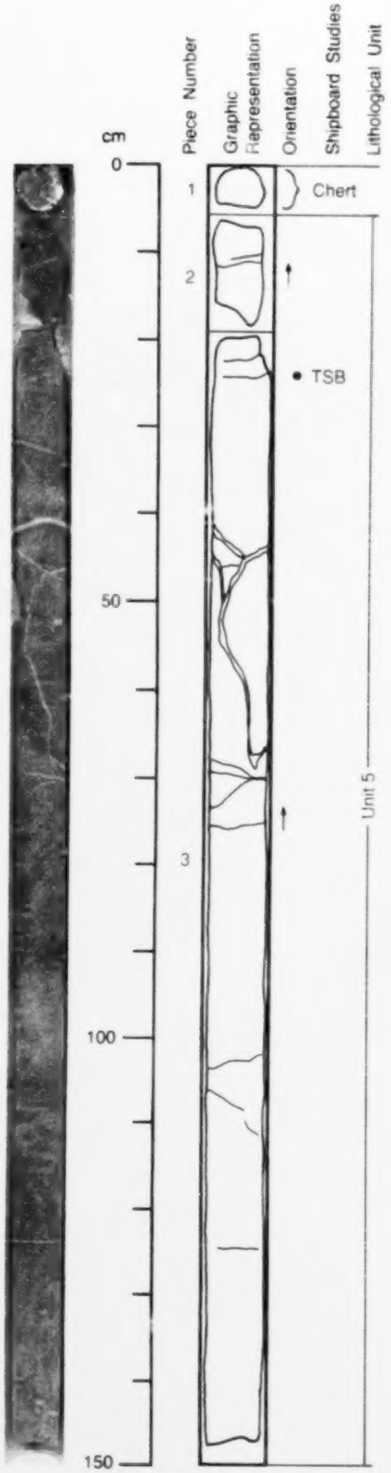
cm
Piece Number
Graphic Representation
Orientation
Shipboard Studies
Lithological Unit
0
50
100
150
1
2
3
Chert
TSB
Unit 5
CORE/SECTION

## 129-801B-41R-1

### UNIT 5: APHYRIC BASALT

### Pieces 2 and 3

**CONTACTS:** Not observed.
**PHENOCRYSTS:** Aphyric.
**GROUNDMASS:** Fine-grained to medium-grained towards the bottom of the unit; hypocrystalline with some quench-textured minerals (pyroxene).
**VESICLES:** None.
**COLOR:** Bluish-gray (5B 5/1).
**STRUCTURE:** Massive; either a flow or thin sill.
**ALTERATION:** Slightly to moderately altered; some plagioclase crystals are pseudomorphed by carbonate, a majority are altered to greenish clay; leucoxene (?) after opaques; some Fe stains around some opaques.
**VEINS/FRACTURES:** ~2%; 0.1 to 5.0 mm; 0-90 degrees, curved/irregular; veins composed of carbonate, with some green clays ocassionally.
**ADDITIONAL COMMENTS:** Unit 5 is relatively fresher than the other units above it. The top part of the unit has relatively stubby crystals whereas the bottom has lath-like, quench-textured pyroxenes that are coarser-grained.

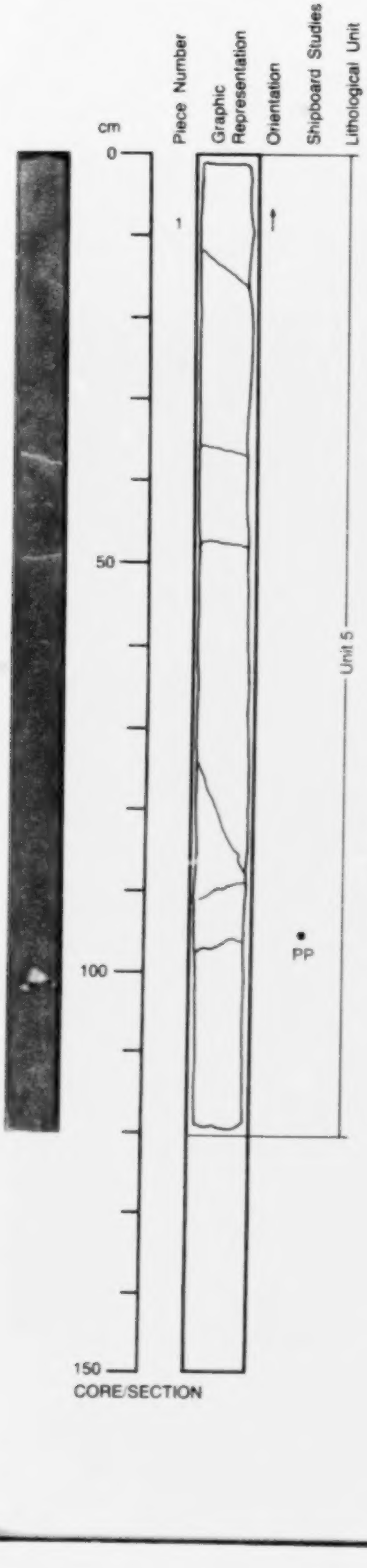
cm
Piece Number
Graphic Representation
Orientation
Shipboard Studies
Lithological Unit
0
50
100
150
1
PP
Unit 5
CORE/SECTION

## 129-801B-41R-2

## UNIT 5: APHYRIC MICRODOLERITE

### Piece 1

**CONTACTS:** None observed.
**PHENOCRYSTS:** No phenocrysts.
**GROUNDMASS:** Medium-grained, holocrystalline generally, minor glassy mesostasis. Overall coarser than same unit in 41R-1.
**VESICLES:** No vesicles.
**COLOR:** Mottled greenish-gray (5BG 5/1).
**STRUCTURE:** Massive; either the interior of a flow or thin sill.
**ALTERATION:** Moderate green clay replacement of matrix, especially plagioclase; uniform distribution down piece 1, but patchy. Random distribution of carbonate, with or without green clay, veinlets and disseminated pyrite.
**VEINS/FRACTURES:** 1%; 0.2-2.0 mm; 25-50 dip; random distribution of calcite, with or without green clay, veinlets. No marginal alteration zones.
**ADDITIONAL COMMENTS:** Continuation of Unit 5 with systematic increase in grain-size, especially growth of black elongate (4-5 mm) pyroxene prisms, towards base of Piece 1.

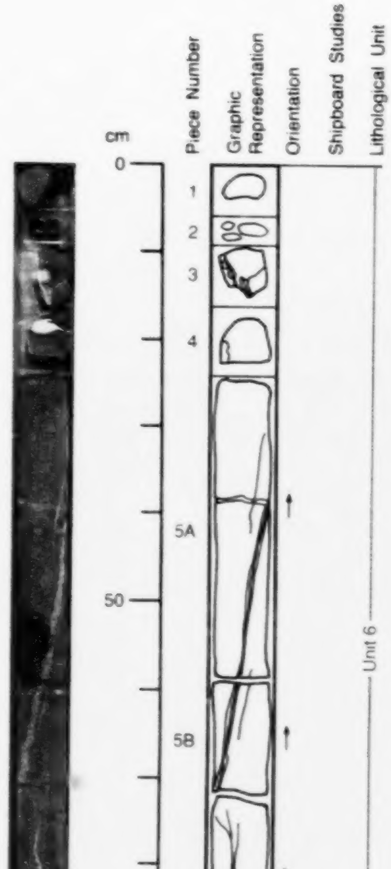
cm
Piece Number
Graphic Representation
Orientation
Shipboard Studies
Lithological Unit
0
50
100
150
1
2
3
4
5A
5B
5C
TSB
Unit 6
CORE/SECTION

## 129-801B-42R-1

## UNIT 6: APHYRIC MICRODOLERITE

### Pieces 1 to 5C

**CONTACTS:** None observed, but Pieces 1 and 2 are fine-grained with dark matrix and probably represent a chilled margin. Different texture to Unit 5 in 41R-2, Piece 1.
**PHENOCRYSTS:** None observed.
**GROUNDMASS:** Grading from fine (Pieces 1 and 2) to medium (Pieces 3 to 5) grained down unit. Generally holocrystalline; minor glassy mesostasis replaced by green clay.
**VESICLES:** None observed.
**COLOR:** Mottled gray (5B 5/1).
**STRUCTURE:** Massive; either a flow or thin sill.
**ALTERATION:** Slight/moderate (about 10-20%). Green clay in matrix and calcite-clay veins.
**VEINS/FRACTURES:** 4-5%; 0.2-6.0 mm; either near 0 or 80 dip; random distribution. Smaller veins of calcite tend to be subhorizontal, whereas larger greenish-yellow clay-calcite veins near vertical to 80 dip. Vein branching common with veinlet offshoots.
**ADDITIONAL COMMENTS:** Textural differences, pyroxene morphology and lack of patchy alteration distinguish this unit from Unit 5 above.

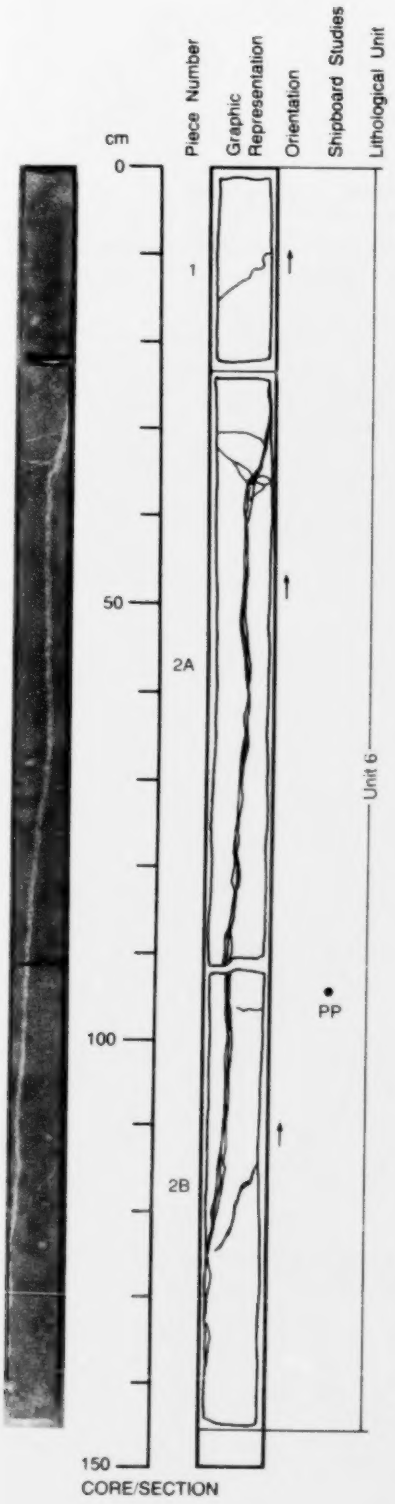
cm
Piece Number
Graphic Representation
Orientation
Shipboard Studies
Lithological Unit
0
50
100
150
1
2A
2B
PP
Unit 6
CORE/SECTION

## 129-801B-42R-2

## UNIT 6: APHYRIC DOLERITE

### Pieces 1, 2A & 2B

**CONTACTS:** None observed, continuation of Unit 6.
**PHENOCRYSTS:** None observed.
**GROUNDMASS:** Medium-grained, generally holocrystalline; minor green clay-replaced, glassy mesostasis. Marginally coarser than same unit in 42R-1.
**VESICLES:** None observed.
**COLOR:** Flecked medium gray (N5).
**STRUCTURE:** Massive; either a flow or a thin sill interior.
**ALTERATION:** Slight (about 10%). Mainly green clay and calcite replacing plagioclase and mesostasis. Minor disseminated pyrite. Green clay-calcite veins.
**VEINS/FRACTURES:** 5%; 0.2-5.0 mm; sub-vertical; veins almost totally represented by a single, sub-vertical, green clay-calcite complex vein with a microbrecciated interior and central calcite veinlet; cross-cuts earlier calcite-only veinlets.
**ADDITIONAL COMMENTS:** Slight increase in grain-size relative to 42R-1, especially in length of black pyroxene crystals and altered plagioclase laths. Additional feature is presence of bronzy colored plates replacing and/or associated with pyroxene throughout Pieces 1 and 2.

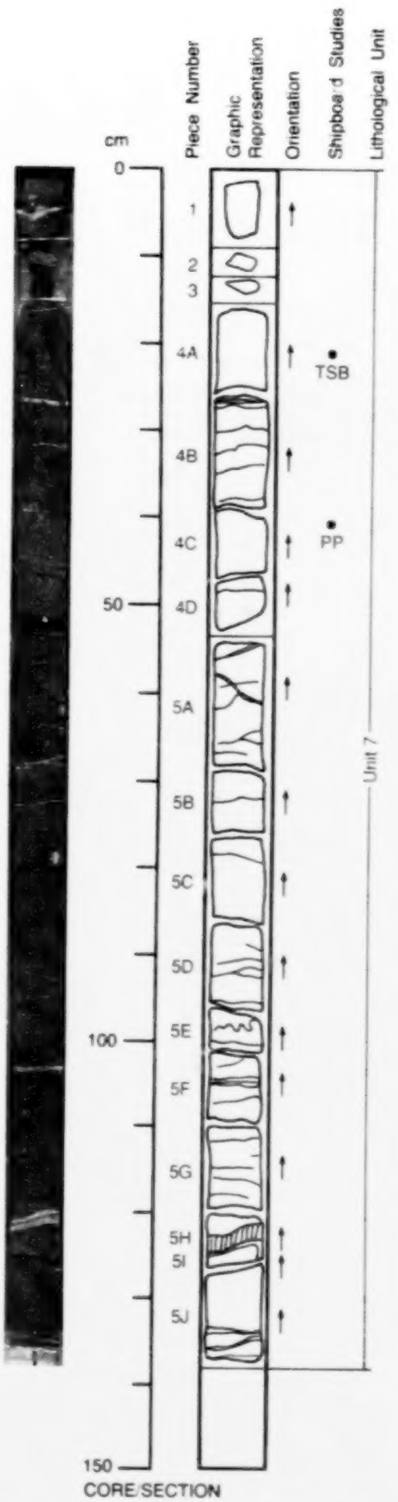
cm
0
50
100
150
Piece Number
Graphic Representation
Orientation
Shipboard Studies
Lithological Unit
1
2
3
4A
4B
4C
4D
5A
5B
5C
5D
5E
5F
5G
5H
5I
5J
TSB
PP
Unit 7
CORE/SECTION

## 129-801B-43R-1

### UNIT 7: APHYRIC DOLERITE

### Pieces 1 to 5J

**CONTACTS:** None observed, but Pieces 1 and 2 finer grained and exhibit different pyroxene morphology to rest of pieces; suggests part of chilled margin to this unit.
**PHENOCRYSTS:** None observed.
**GROUNDMASS:** Medium-grained; generally holocrystalline, but some green clay-replaced glassy mesostasis in piece 1.
**VESICLES:** None observed.
**COLOR:** Flecked medium gray (N5).
**STRUCTURE:** Massive; either a thin sill or flow with part of chilled upper contact.
**ALTERATION:** Slight, some green clays replacing non-pyroxene matrix. Calcite-greenish clay veins.
**VEINS/FRACTURES:** 5%; 0.5-15.0 mm; sub-horizontal; random distribution. Composed of calcite or dull green clay or admixture dominated by calcite; the finest calcite veinlets appear to be last filling event. Characteristic feature of large veins is the multiple infilling of open fractures by fibrous calcite normal to vein walls (up to 2 or 3 calcite zones).
**ADDITIONAL COMMENTS:** Pieces 1 and 2 different to Unit 6 in 42R-2. Due to the elongate pyroxenes being set in an altered matrix which makes them pronounced, they give the appearance of being microphenocrysts.

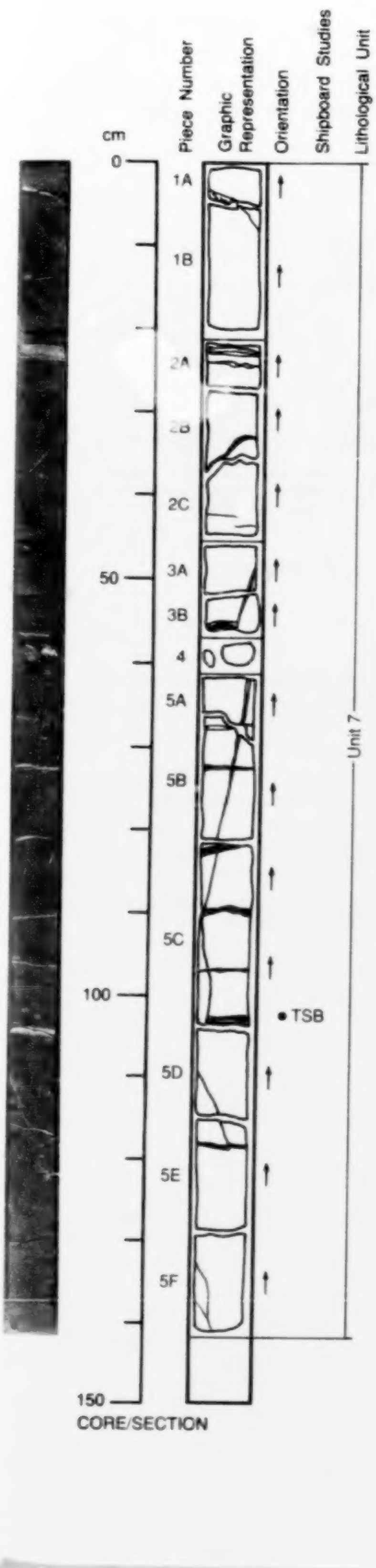
cm
Piece Number
Graphic Representation
Orientation
Shipboard Studies
Lithological Unit
0
50
100
150
1A
1B
2A
2B
2C
3A
3B
4
5A
5B
5C
5D
5E
5F
• TSB
Unit 7
CORE/SECTION

## 129-801B-43R-2

## UNIT 7: APHYRIC DOLERITE

### Pieces 1 to 5F

**CONTACTS:** None observed, continuation of Unit 7. Piece 5F finer grained (microdolerite) and may represent lower chilled margin of this unit.
**PHENOCRYSTS:** None observed.
**GROUNDMASS:** Medium-grained generally, but decreasing in grain-size down unit (much finer in piece 5F). Holocrystalline.
**VESICLES:** None observed.
**COLOR:** Speckled gray (from N5 to N6 down unit).
**STRUCTURE:** Massive; either a thin sill or flow with part of chilled lower contact.
**ALTERATION:** Slight. Some greenish clays replacing plagioclase. Calcite, silica and green clay veins.
**VEINS/FRACTURES:** 5%; 0.2-11.0 mm; 0-15 and 70-80; composed of calcite-green clay, calcite calcite-ribbon silica. Two main sets: an earlier teeply inclined minor group cut by later sub-horizontal, generally thicker group. Smaller of the two pieces numbered 4 is calcite with green and blue clays veneer.
**ADDITIONAL COMMENTS:** Decrease in grain-size of Piece 5F probably represents the start of the lower chilled margin to this unit.

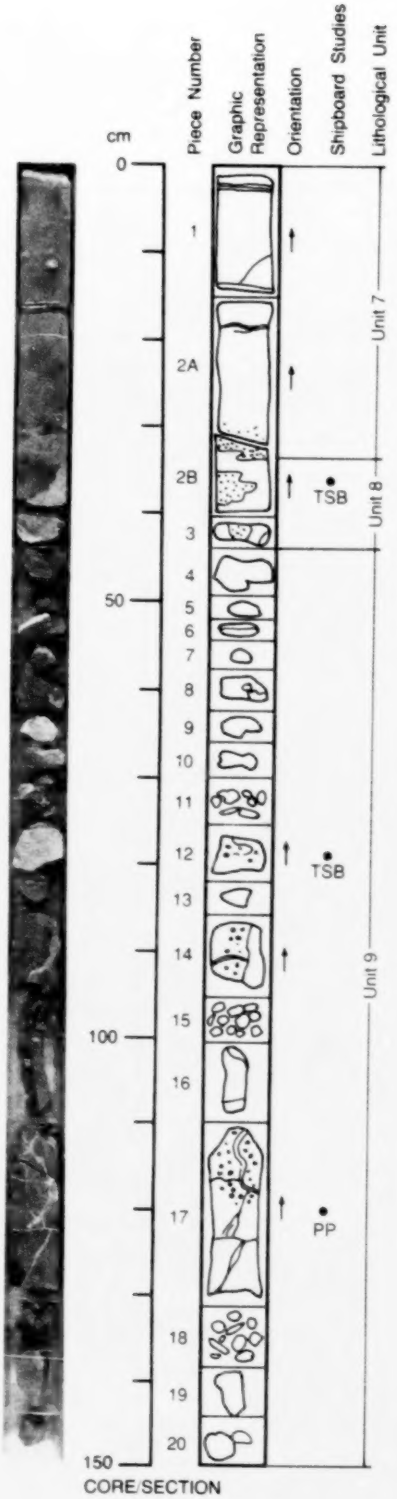

## 129-801B-43R-3

## UNIT 7: APHYRIC MICRODOLERITE GRADING TO SPARSELY PLAGIOCLASE-PYROXENE ICROPHYRIC BASALT

### Pieces 1 and 2A

**CONTACTS:** Lower contact seen between 29-43 cm interval. Irregular with bulbous protrusions with good glassy (replaced by greenish clay) chilled zone. Lithology now microphyric basalt.

**PHENOCRYSTS:** Only seen in the glassy lower chilled zone of this unit.
Plagioclase - 1%; 0.5-1.0; minute laths.
Pyroxene - 1%; 1.0-1.5; black prisms.

**GROUNDMASS:** Microcrystalline in Piece 2B. Rapid decrease in grain-size from fine/medium grained in Piece 1.

**VESICLES:** None observed.

**COLOR:** Gray (N5).

**STRUCTURE:** Massive; possibly a thin flow with curved and quenched base.

**ALTERATION:** Blue-green clays in fine matrix.

**VEINS/FRACTURES:** 4%; 1-5 mm; 50-60 dip; dominated by calcite or calcite-yellow clay infillings.

**ADDITIONAL COMMENTS:** Base of Unit 7 shows chilled glassy zone (2 mm) typified by acicular plagioclase microphenocrysts. This zone has been intruded and disrupted by Unit 8; partly digested, stoped inclusions of Unit 7 basalt seen within Unit 8 basalt.

## UNIT 8: SPARSELY PLAGIOCLASE PHYRIC FELDSPAR-RICH BASALT

### Pieces 2B and 3

**CONTACTS:** Sharp, bit irregular. Unit 8 intrudes Unit 7, showing cross-cutting relationship, disruption and inclusion stoping.

**PHENOCRYSTS:** Often packed close together in orientation stacks showing good fluidal or trachytic texture.
Plagioclase-2%; 0.5-1.0; elongate flow oriented laths

**GROUNDMASS:** Fine-grained overall, but medium-grained in trachytic regions. Hypocrystalline.

**VESICLES:** 0.5%; 0.5-1.0 mm; irregular; random; one example filled with sulfide.

**COLOR:** Speckled light greenish-gray (%G 7/1).

**STRUCTURE:** Intrusive.

**ALTERATION:** Slight to moderate (~15%). Plagioclase replaced by bluish-green clay.

**VEINS/FRACTURES:** <1%; 0.1-1.0 mm; 0-45; calcite infillings. Veins cut both Units 7 and 8.

**ADDITIONAL COMMENTS:** Unit 8 is plagioclase-rich and mafic mineral poor relative to other basic rocks to date-possibly a more differentiated, late-stage intrusion.

## 129-801B-43R-3 (continued)

## UNIT 9: SPARSELY PLAGIOCLASE PHYRIC BASALT

### Pieces 4 to 20

**CONTACTS:** Piece 3 has sharp, embayed boundary with Unit 8. Piece 14 shows typical curved, glassy pillow lava margin. Piece 17 and other pieces have sharp contact with veinlets.

**PHENOCRYSTS:** Random distribution, but some clumping into groups.

Plagioclase - 1-2%; 1-2; subhedral, elongate laths.

**GROUNDMASS:** Pieces with sharp contacts have devitrified, hypohyaline texture grading towards spherulitic and hypocrystalline texture away from the contact.

**VESICLES:** None observed.

**COLOR:** Different shades: Piece 14 ranges from gray (N5) to speckled pale red (5G 6/2) to gray again (N6) towards pillow interior; holocrystalline fragments range from dark gray (N4) to pale green (5G 6/2).

**STRUCTURE:** Pillow lavas. Other lava fragments and breccia.

**ALTERATION:** Moderate (pillows and other lava fragments) to high (greenish, breccia fragments). Most common alteration is greenish to bluish-green clays and carbonate; leucoxene (?) and Fe stains are present around opaques of the hypocrystalline fragments.

**VEINS/FRACTURES:** 15%; 1.0-15.0 mm; wide range 0-90; generally irregular, curved and braided. Some filled with calcite, with or without green clays; vein in Piece 17 has silicified clay inclusion.

**ADDITIONAL COMMENTS:** Unit 9 is an assemblage of pillow and other lava fragments, pieces of intrusive vein materials (i.e. Pieces 9, 12 and some of 11 and 15) and altered fragments (i.e. Pieces 7, 10 and some of 11 and 15). Some lava fragments are bounded by veins (Piece 6). Piece 8 has an infilling of bluish-green clay.

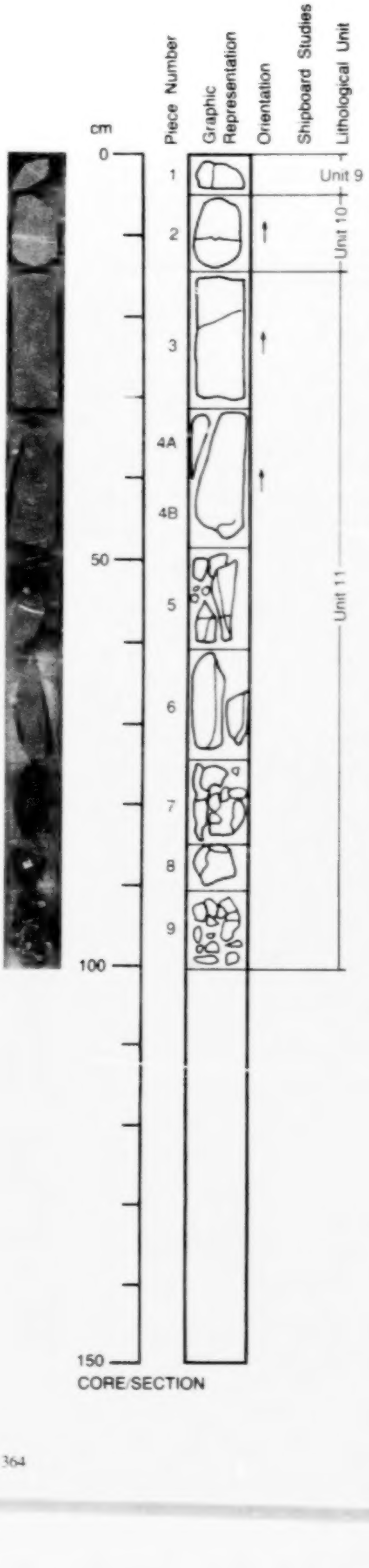

## 129-801B-43R-4

### UNIT 9: APHYRIC BASALT

#### Piece 1

**CONTACTS:** None observed.
**PHENOCRYSTS:** None observed.
**GROUNDMASS:** Fine-grained, hypocrystalline.
**VESICLES:** None observed.
**COLOR:** Gray (N6).
**STRUCTURE:** Lava fragment.
**ALTERATION:** Slight to moderate. Largely green clays after plagioclase, but leucoxene and Fe stains around opaques still preserved.
**VEINS/FRACTURES:** 1%; 0.1-1.0 mm; 0 with 45 veinlet; carbonate infilling.
**ADDITIONAL COMMENTS:** A lava fragment similar to other hypocrystalline fragments in 43R-3.

### UNIT 10: APHYRIC MICRODOLERITE

#### Piece 2

**CONTACTS:** None observed.
**PHENOCRYSTS:** None observed.
**GROUNDMASS:** Medium-grained, holocrystalline to hypocrystalline.
**VESICLES:** None observed.
**COLOR:** Speckled gray (N6).
**STRUCTURE:** Lava fragment.
**ALTERATION:** Slight to moderate. Plagioclase generally replaced by green to bluish-green clays; opaques by leucoxene and Fe hydroxides.
**VEINS/FRACTURES:** 5%; 0.1-4.0 mm; all 0, one at 80; carbonate filling, with or without green clay.
**ADDITIONAL COMMENTS:** Separated from Units 9 and 11 by its quench textured appearance.

### UNIT 11: APHYRIC BASALT

#### Pieces 3 to 9

**CONTACTS:** Not observed, but upper part (near Unit 10) is fine-grained.
PHENOCRYSTS: None observed.
**GROUNDMASS:** Fine-grained, a few patches containing >1 mm plagioclase laths. Holocrystalline to slightly hypocrystalline.
**VESICLES:** None observed.
**COLOR:** Speckled gray (N5).
**STRUCTURE:** Perhaps a lava flow.
**ALTERATION:** Moderate; plagioclase replaced by green and bluish-green clays and carbonate; opaques to Fe hydroxides, with rare leucoxene replacement.
**VEINS/FRACTURES:** 1%; 0.1-2.0 mm; horizontal, few 30-45; infilled with carbonate, with or without green clays.
**ADDITIONAL COMMENTS:** The top of Unit 11 is fine-grained, slightly increasing in grain-size towards bottom. Pieces 5, 7, 8 and 9 are a breccia of the same material. Unit 11 may be a lava flow with non-preserved top and bottom margins.

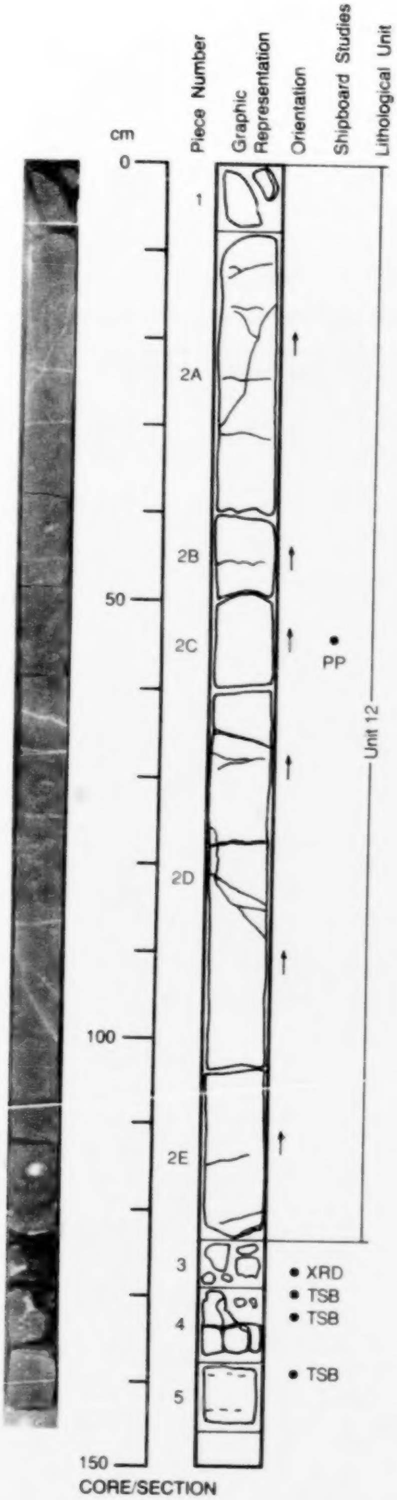
cm
Piece Number
Graphic Representation
Orientation
Shipboard Studies
Lithological Unit
0
50
100
150
1
2A
2B
2C
2D
2E
3
4
5
PP
Unit 12
XRD
TSB
TSB
TSB
CORE/SECTION

## 129-801B-44R-1

## UNIT 12: APHYRIC BASALT

### Pieces 1 to 2E

**CONTACTS:** Devitrified, hypocrystalline top and bottom observed. Base resting on a carbonate veinlet and adjacent brown silicified clays.

**PHENOCRYSTS:** None observed, except top and bottom margins have 1-2% stubby plagioclase crystals.

**GROUNDMASS:** Fine-grained, slightly coarsening towards Pieces 2B, C and D. Hypocrystalline to holocrystalline.

**VESICLES:** None observed.

**COLOR:** Speckled gray (N5).

**STRUCTURE:** Massive; perhaps a thin lava flow.

**ALTERATION:** Moderate. Plagioclase replaced by green clays and carbonate; opaques to leucoxene and Fe hydroxides.

**VEINS/FRACTURES:** 1%; 0.1-4.0 mm; horizotal some 50-60; most filled with carbonate, with or without green clays. More than one generation of veins.

**ADDITIONAL COMMENTS:** Unit has preserved slightly plagioclase phyric top and bottom margins that coarsen towards the center. Interpreted as a sheet flow over sediment surface.

## 129-801B-44R-2

## UNIT 13: APHYRIC BASALT

### Pieces 3 (lower part) to 4C

**CONTACTS:** Sharp contact with sediments; fine-grained coarsening towards the bottom.
**PHENOCRYSTS:** None observed.
**GROUNDMASS:** Fine-grained; holocrystalline to hypocrystalline.
**VESICLES:** None observed.
**COLOR:** Speckled gray (N6).
**STRUCTURE:** Massive, perhaps a thin flow or possibly a thin sill.
**ALTERATION:** Moderate. Plagioclase replaced by green clays and carbonate; opaques by leucoxene and Fe hydroxides.
**VEINS/FRACTURES:** 2%; 1-3 mm; sub-horizontal; infilled with carbonate, with or without green clays.
**ADDITIONAL COMMENTS:** Top contact is well-defined with glassy margin but bottom contact with Unit 14 appears to be sharp and lacks any apparent quenching effect.

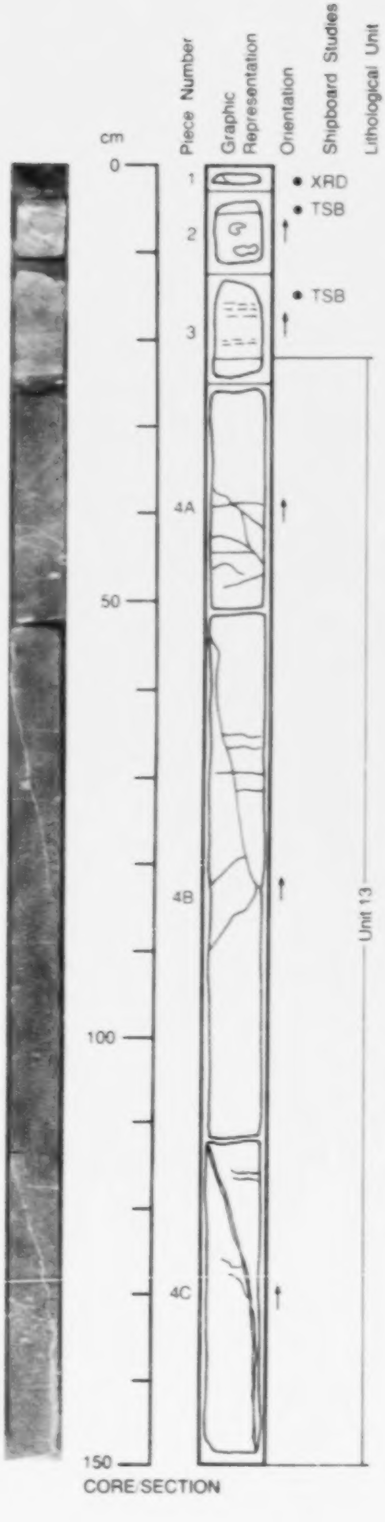
cm
Piece Number
Graphic Representation
Orientation
Shipboard Studies
Lithological Unit
0
50
100
150
1
2
3
4A
4B
4C
• XRD
• TSB
• TSB
Unit 13
CORE/SECTION

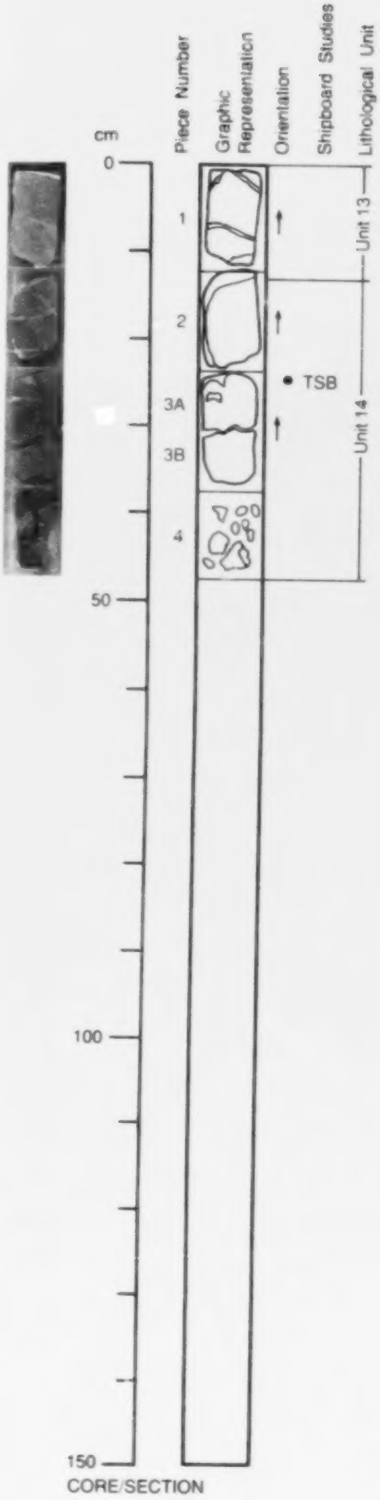
cm
Piece Number
Graphic Representation
Orientation
Shipboard Studies
Lithological Unit
0
50
100
150
1
2
3A
3B
4
TSB
Unit 13
Unit 14
CORE/SECTION

## 129-801B-44R-3

### UNIT 13: APHYRIC BASALT

### Pieces 1, 2 (top part) & 3 (top part)

**CONTACTS:** Sharp contact with Unit 14 but no change in grain size.
**PHENOCRYSTS:** None observed.
**GROUNDMASS:** Fine-grained; holocrystalline to hypocrystalline.
**VESICLES:** None observed.
**COLOR:** Speckled gray (N6).
**STRUCTURE:** Bottom part of thin flow or possibly thin sill.
**ALTERATION:** Moderate; plagioclase altered to green clays and carbonate: opaques to leucoxene and Fe-hydroxides.
**VEINS/FRACTURES:** 2%; 1-3 mm; sub-horizontal; infilled with carbonate with or without green clays.
**ADDITIONAL COMMENTS:** Curved contact with Unit 14.

### UNIT 14: MODERATE PLAGIOCLASE MICROPHYRIC BASALT

### Pieces 2 to 4

**CONTACTS:** Concentric, well-defined glassy margin; slight coarsening towards the interior.
**PHENOCRYSTS:**
Plagioclase - 8%, 2 mm; subhedral laths, slightly altered.
**GROUNDMASS:** Holohyaline.
**VESICLES:** None observed.
**COLOR:** Dark gray (N4).
**STRUCTURE:** Rounded outline.
**ALTERATION:** Slight, microphenocrysts slightly altered to green clays.
**VEINS/FRACTURES:** 1%, 0.1 to 1.0 mm; 30 to 45 degrees; infilled with carbonate and green clays.
**ADDITIONAL COMMENTS:** Either portion of a pillow lava or an apophysis of an intrusion.

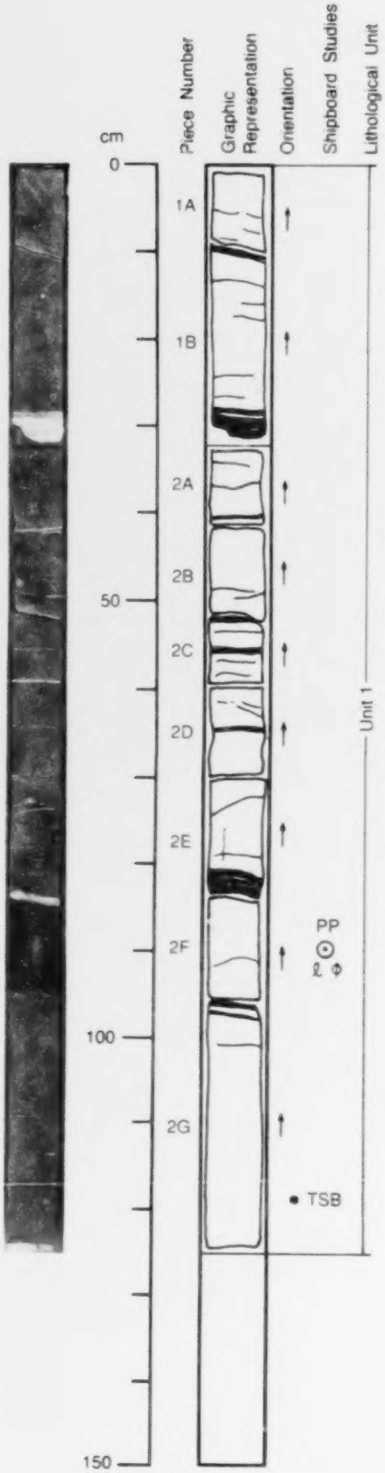
cm
Piece Number
Graphic Representation
Orientation
Shipboard Studies
Lithological Unit
0
1A
1B
2A
2B
50
2C
2D
2E
2F
PP
ℓ Φ
100
2G
TSB
Unit 1
150
CORE/SECTION

## 129-801C-1R-1

## UNIT 1: APHYRIC MICRODOLERITE

### Pieces 1A-2G

**CONTACTS:** None observed.
**PHENOCRYSTS:** None observed.
**GROUNDMASS:** Fine-to medium-grained, hypocrystalline. Possible very slight decrease down section (Piece 2G being finer than Piece 1A). Matrix plagioclase accentuated by white alteration.
**VESICLES:** None observed.
**COLOR:** White speckled gray (N5).
**STRUCTURE:** Massive, flow or sill interior.
**ALTERATION:** Moderate. Plagioclase partly replaced by white clay and general greenish tinge to matrix indicates replacement by smectite. Pyrite scattered throughout. Distribution of alteration relatively uniform.
**VEINS/FRACTURES:** 8%; 0.5-30 mm; subhorizontal; wide range in vein width, majority about 2 mm. Fine veins infilled with fibrous carbonate, larger veins have multiple infillings with carbonate, silica, smectite and pyrite, suggesting many opening and infilling events.
**ADDITIONAL COMMENTS:** None.

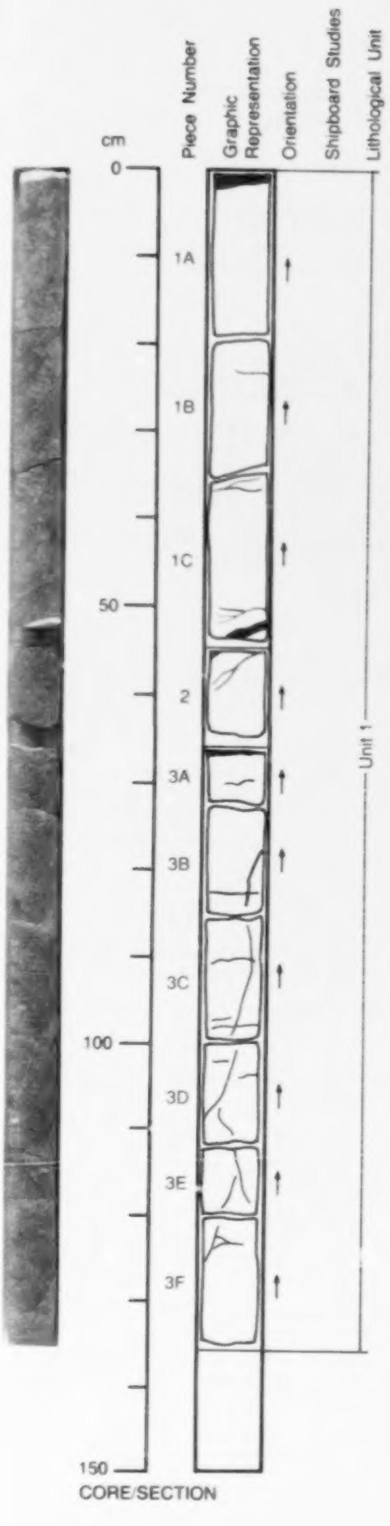
cm
0
50
100
150
Piece Number
Graphic Representation
Orientation
Shipboard Studies
Lithological Unit
1A
1B
1C
2
3A
3B
3C
3D
3E
3F
Unit 1
CORE/SECTION

## 129-801C-1R-2

## UNIT 1: APHYRIC MICRODOLERITE

### Pieces 1A-3F

**CONTACTS:** None observed.
**PHENOCRYSTS:** None observed.
**GROUNDMASS:** Holocrystalline to slightly hypocrystalline. Fine-to medium-grained, but patchy distribution; bottom Piece (3F) is slightly finer than top pieces. Occasional crystals larger than matrix present.
**VESICLES:** None observed.
**COLOR:** White speckled black (N2); white areas are plagioclase altered to white clay.
**STRUCTURE:** Massive; perhaps flow or sill interior.
**ALTERATION:** Moderate. Plagioclase altered to whitish and greenish clays, some with Fe-hydroxide stains. Dark green matrix generally. Relict clinopyroxene grains within original crystal morphology.
**VEINS/FRACTURES:** 5%; 1-12 mm; subhorizontal, vertical; wider veins are subhorizontal, narrower veins are vertical; both infilled with carbonate and green clays. Narrow veinlets are generally branching and cross-cutting. No alteration halos observed.
**ADDITIONAL COMMENTS:** Patchy texture with some portions slightly coarser than rest, but gradational boundaries. An autolith (3x4 cm oblong shape) is present in Piece 1C with pronounced outline relative to matrix.

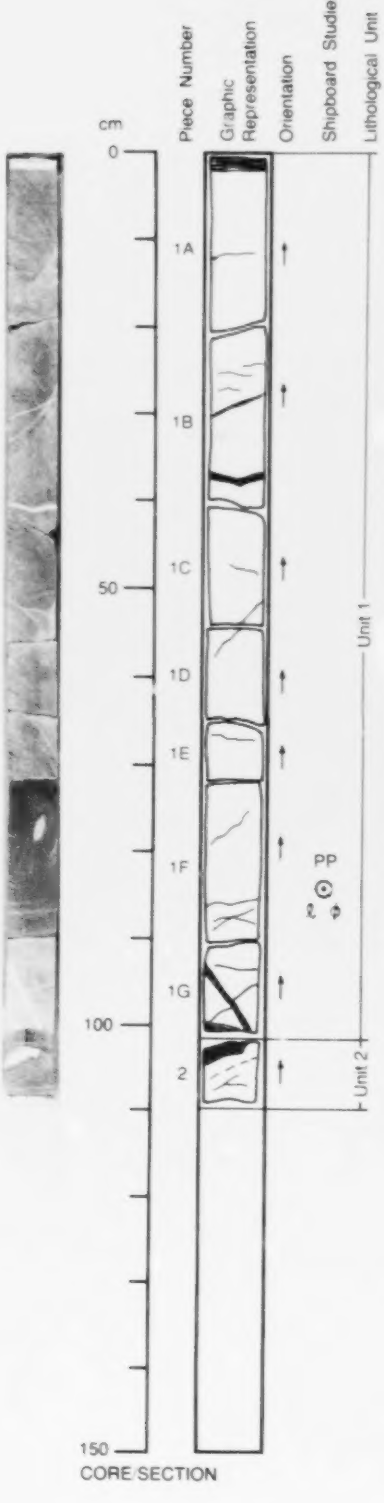

## 129-801C-1R-3

## UNIT 1: APHYRIC MICRODOLERITE GRADING TO SPARSELY PLAGIOCLASE PHYRIC BASALT

### Pieces 1A-1G

**CONTACTS:** Not actually observed, but grain-size fines towards the bottom (cut by veinlet).
**PHENOCRYSTS:**
Plagioclase - 1%, c 1.0, euhedral/subhedral laths, altered to white and green clays.
**GROUNDMASS:** Holocrystalline to hypocrystalline, particularly at bottom. Medium to fine grained, fining towards the bottom.
**VESICLES:** None observed.
**COLOR:** White fine-speckled black (N2).
**STRUCTURE:** Massive, perhaps base of sill or flow.
**ALTERATION:** Moderate. Plagioclase replaced by whitish and greenish clays, some with Fe-hydroxide staining. Generally greenish matrix. Whitish leucoxene associated with relict opaques. Carbonate present along grain boundaries. Short, whitish veinlets present in some areas.
**VEINS/FRACTURES:** 10%; 0.2-13 mm; 0-90 degrees; wide veins (0-45 orientation) and narrow veins (0-90 orinetation), both infilled with carbonate and greenish clays. Veinlets often branching and cross-cutting.
**ADDITIONAL COMMENTS:** Generally finer grained than Sections 1 and 2 and fining steadily towards the base.

## UNIT 2: SPARSELY PLAGIOCLASE-OLIVINE MICROPHYRIC BASALT

### Piece 2

**CONTACTS:** Not actually observed. Well preserved, devitrified glassy margin in contact with veinlet at margin. Glassy rim zone grades downwards to a cryptocrystalline bottom. 45 degree inclination.
**PHENOCRYSTS:**
Plagioclase - 1%, <1, Subhedral/euhedral; mostly altered to carbonate.
Olivine - trace; <1; Subhedral/euhedral (hopper crystal morphology).
**GROUNDMASS:** Ranges from (a) devitrified glassy rim, (b) transition zone consisting of glass mesostasis and spherulites, (c) spherulite zone, and (d) cryptocrystalline zone with plenty of feathery and plumose variolites. Plagioclase microlites present in transition zone downwards.
**VESICLES:** None observed.
**COLOR:** Brownish gray top (5Y 5/1) to dark gray bottom (N5).
**STRUCTURE:** Inclined; glassy margin of a pillow or thin flow.
**ALTERATION:** Moderate. Plagioclase phenocrysts and microlites mostly altered to carbonate; olivine phenocrysts pseudomorphed by whitish clay. Glass is devitrified, spherulites and glass interstices altered to brown clays.
**VEINS/FRACTURES:** 15%; 1-80 mm; irregular; most are subparallel to glassy rim, but rest are irregular; generally branching and cross-cutting. Infilled with carbonate +/- green clays. No halos observed.
**ADDITIONAL COMMENTS:** Typical quenched margin to a flow.

# 129-801C-1R-4

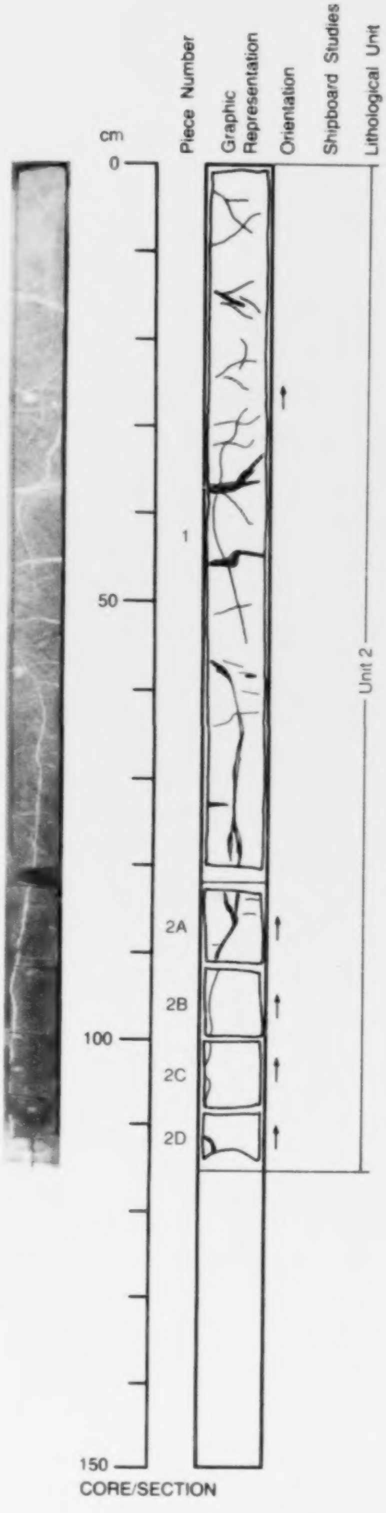
cm
0
50
100
150
Piece Number
Graphic Representation
Orientation
Shipboard Studies
Lithological Unit
1
2A
2B
2C
2D
Unit 2
CORE/SECTION

## UNIT 2: SPARSELY PLAGIOCLASE MICROPHYRIC BASALT GRADING TO APHYRIC BASALT

### Pieces 1-2D

**CONTACTS:** None observed.
**PHENOCRYSTS:** None.
Plagioclase - 1%; c.1.0; Subhedral laths altered to carbonate.
**GROUNDMASS:** Hypocrystalline, but with holocrystalline patches, particularly towards bottom part. Fine-grained/crypocrystalline; plenty of quenched, fan-shaped microlites. Minor mesostasis.
**VESICLES:** None observed.
**COLOR:** Bluish-gray top (5B 6/1) grading to gray bottom (N5).
**STRUCTURE:** Massive Piece 1, moderately fractured Pieces 2A-2D; perhaps top of an extrusive flow.
**ALTERATION:** Moderate. Plagioclase phenocrysts altered to carbonate; plagioclase in groundmass altered to white and green clays; green matrix throughout; carbonate also present along crystal margins.
**VEINS/FRACTURES:** 8%; 0.1-7.0 mm; very irregular; most infilled with carbonate +/- green clays, a few specks of pyrite. Subvertical veinlet in lower part of piece 1 and in Pieces 2A-2D has Fe-hydroxide grains and a 1-2 cm wide halo of more altered groundmass. Higher proportion of veinlets, branching and cross-cutting, in Piece 1 than rest.
**ADDITIONAL COMMENTS:** Continuation of same Unit (2) represented by glassy margin in base of 1R-3.

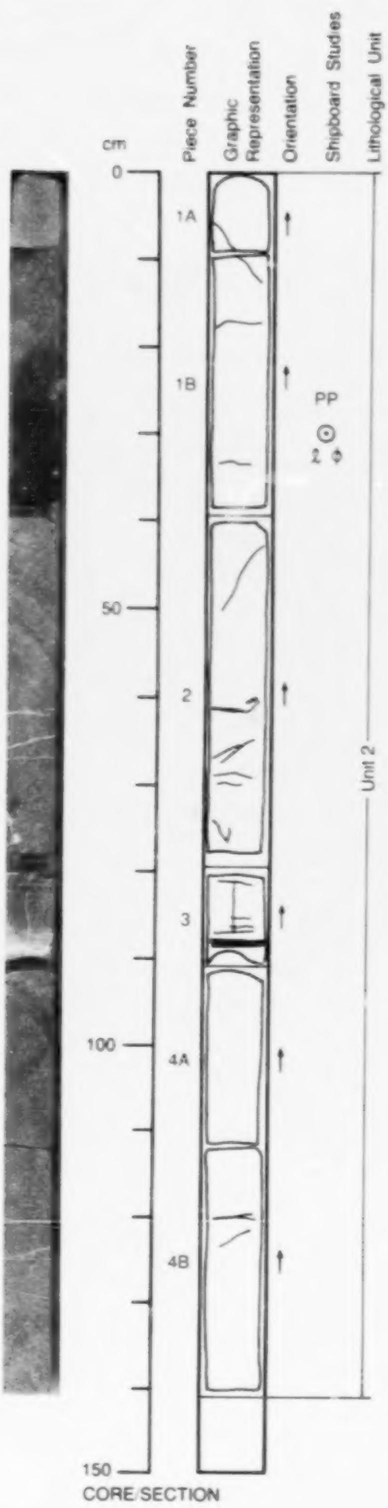
cm
0
50
100
150
CORE/SECTION
Piece Number
Graphic Representation
Orientation
Shipboard Studies
Lithological Unit
1A
1B
2
3
4A
4B
PP
Unit 2

## 129-801C-1R-5

## UNIT 2: APHYRIC BASALT

### Pieces 1A-4B

**CONTACTS:** None observed.
**PHENOCRYSTS:** None observed.
**GROUNDMASS:** Hypocrystalline to slightly holocrystalline in some parts. Fine-grained, but with patchy coarse-grained appearance due to differential alteration. Fan-shaped and glomerophyric microlites of plagioclase.
**VESICLES:** None observed.
**COLOR:** Fine-speckled gray (N5).
**STRUCTURE:** Almost massive; perhaps interior of flow or pillow lava.
**ALTERATION:** Moderate. Plagioclase altered to white and green clays, some of which have orange colored Fe-hydroxide stains. Greenish matrix throughout. Carbonate along some grain margins. Minor pyrite.
**VEINS/FRACTURES:** 3%; 0.1-7.0 mm (piece 3); highly irregular, most subhorizontal; infilled with carbonate +/- green clays, but one veinlet (Piece 4) entirely infilled with green clays. Widest veinlet near base of Piece 3.
**ADDITIONAL COMMENTS:** Overall basalt, although some groundmass crystals >1 mm in size.

## 129-801C-1R-6

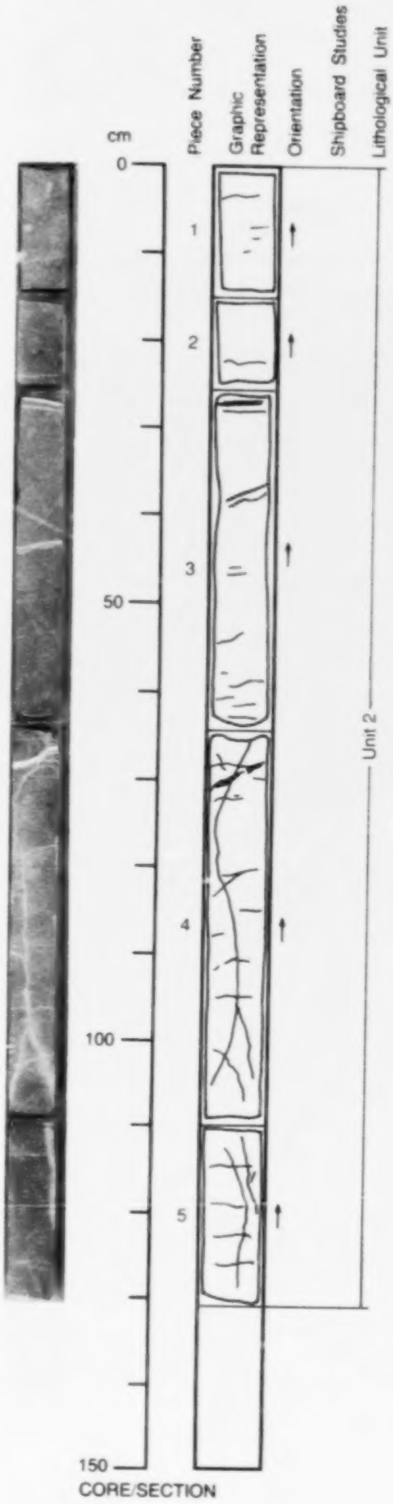
cm
0
50
100
150
Piece Number
Graphic Representation
Orientation
Shipboard Studies
Lithological Unit
1
2
3
4
5
Unit 2
CORE/SECTION

### UNIT 2: APHYRIC BASALT

### Pieces 1-5

**CONTACTS:** None observed, but fining towards bottom.
**PHENOCRYSTS:** None observed.
**GROUNDMASS:** Hypocrystalline grading to variolitic towards bottom. Fine-grained, quenched variolites with radiate plagioclase. Mesostasis common in basal part.
**VESICLES:** None observed.
**COLOR:** Fine speckled gray, top (N5) grading to lighter gray at bottom (N6).
**STRUCTURE:** Almost massive; perhaps bottom of extrusive unit, flow or pillow lava.
**ALTERATION:** Moderate. Plagioclase altered to white and green clays; orange colored Fe-hydroxide stained clays now make up 20% of top portion, but decreases in amount toward bottom. Matrix greenish. Yellowish-white fine-grained leucoxene very common in variolitic zone.
**VEINS/FRACTURES:** 2%; 0.1-6.0 mm (piece 4); subhorizontal, but irregular; top veins filled with carbonate +/- green clays, bottom veins narrower and mostly infilled by green clays +/- carbonate. An irregular sub-vertical green clay veinlet (Pieces 4 & 5) has 1 cm wide diffuse halo of more altered groundmass. Most veinlets are branching and cross-cutting.
**ADDITIONAL COMMENTS:** None.

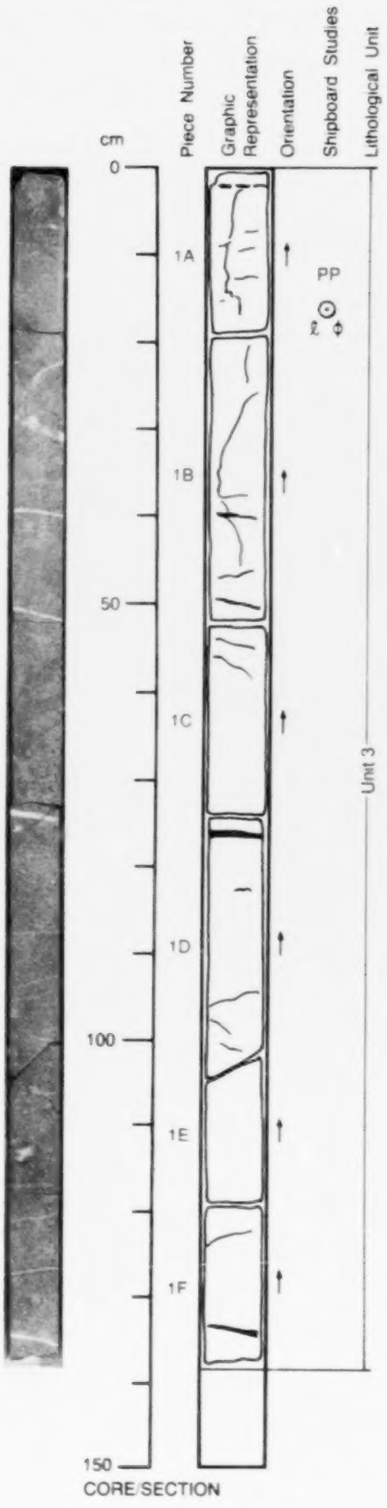
cm
Piece Number
Graphic Representation
Orientation
Shipboard Studies
Lithological Unit
0
50
100
150
1A
1B
1C
1D
1E
1F
PP
Unit 3
CORE/SECTION

## 129-801C-2R-1

## UNIT 3: SPARSELY PLAGIOCLASE PHYRIC BASALT GRADING TO APHYRIC BASALT

### Pieces 1A-1F

**CONTACTS:** Not observed, but top (Piece 1A) has devitrified glassy rim that coarsens downwards.

**PHENOCRYSTS:** None.

Plagioclase - 1%; 1-2; Subhedral/anhedral, altered to carbonate. A 10 mm megacryst with feathery edges present.

**GROUNDMASS:** Devitrified glassy rim followed by a wide (10-15 cm) variolitic zone and finally coarsening downwards to fine-grained hypocrystalline base.

**VESICLES:** None observed.

**COLOR:** Grayish-brown rim (5/2) grading to white-speckled gray (N5).

**STRUCTURE:** Almost massive; perhaps top of a flow.

**ALTERATION:** Moderate. Glass devitrified and together with variolitic zone altered to brown clays. Plagioclase phenocrysts altered to carbonate, matrix plagioclase either altered to green clays or milky-white in color. Leucoxene in variolitic and hypocrystalline portions. Occasional pyrite. Matrix generally greenish throughout hypocrystalline zone.

**VEINS/FRACTURES:** 2%; 0.1-3.0 mm; sub-horizontal, few vertical; carbonate and green clay infillings.

**ADDITIONAL COMMENTS:** None.

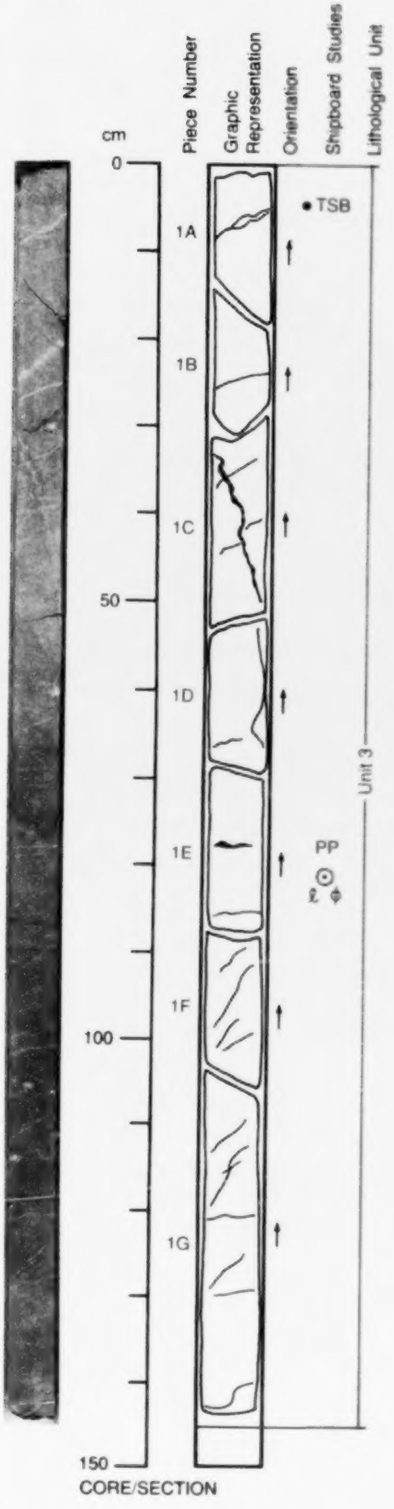
cm
0
50
100
150
CORE/SECTION
Piece Number
Graphic Representation
Orientation
Shipboard Studies
Lithological Unit
1A
1B
1C
1D
1E
1F
1G
TSB
PP
Unit 3

## 129-801C-2R-2

## UNIT 3: APHYRIC BASALT

### Pieces 1A-1G

**CONTACTS:** None observed.
**PHENOCRYSTS:** None observed.
**GROUNDMASS:** Hypocrystalline to slightly holocrystalline. Generally fine-grained, mesostasis and quenched crystals throughout section.
**VESICLES:** None observed.
**COLOR:** Speckled gray (N5).
**STRUCTURE:** Almost massive; interior of flow.
**ALTERATION:** Moderate. Plagioclase altered to white and green clays, pyroxene relicts, subhedral yellowish-white leucoxene around opaques common throughout. Clumps of pyrite grains. Mesostasis altered to greenish clays.
**VEINS/FRACTURES:** 2%; 0.1-6.0 mm; irregular, most inclined 20-45 degrees; often highly irregular. Infilled with carbonate or green clays or both. Branching and cross-cutting.
**ADDITIONAL COMMENTS:** Occasional, subrounded carbonate grains (after plagioclase?) present throughout, but preferentially concentrated at base of Piece 1C.

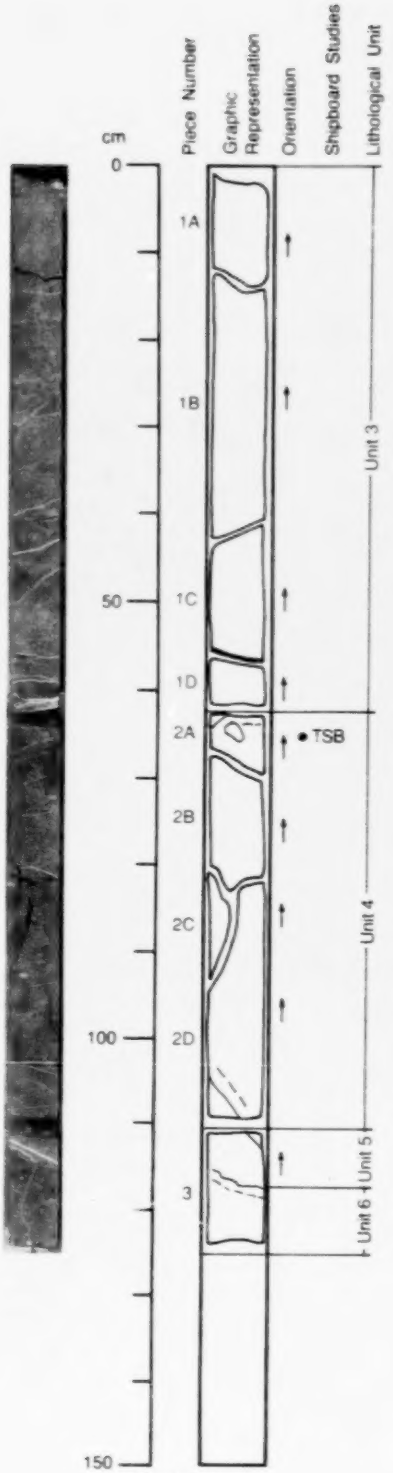

## 129-801C-2R-3

## UNIT 3: APHYRIC BASALT

### Pieces 1A-1D

**CONTACTS:** None observed, but fining towards Piece 1D.
**PHENOCRYSTS:** None observed.
**GROUNDMASS:** Holocrystalline top, but mostly hypocrystalline, particularly in lower portion (Piece 1D). Fine-grained.
**VESICLES:** None observed.
**COLOR:** Speckled gray (N5).
**STRUCTURE:** Almost massive, bottom portion of a flow.
**ALTERATION:** Moderate. Plagioclase altered to white and green clays, relict pyroxene, minor leucoxene, occasional pyrite clumps. Mesostasis altered to greenish clays.
**VEINS/FRACTURES:** 4%; 0.1-2.5 mm; mostly sub-horizontal, but irregular; infilled with carbonate or green clays or both. Branching and cross-cutting.
**ADDITIONAL COMMENTS:** None.

## UNIT 4: MODERATELY PLAGIOCLASE MICROPHYRIC BASALT GRADING TO APHYRIC BASALT

### Pieces 2A-2D

**CONTACTS:** Top contact with Unit 3 (above) and Unit 5 (below) are quenched, now devitrified glass. Contact with Unit 3 is irregular (carbonate veinlet present), contact with Unit 5 inclined at 40 degrees.
**PHENOCRYSTS:** None.
Plagioclase - 2%; 0.5; anhedral & euhedral laths, altered to milky white clay and trace of carbonate.
**GROUNDMASS:** Both top and bottom rims are glassy (now devitrified) that grade inwards to a variolitic zone, and finally to a hypocrystalline interior. Fine-grained.
**VESICLES:** None observed.
**COLOR:** Gray-brown rim (6/2) grading to fine speckled gray interior (N5).
**STRUCTURE:** Intrusive body with apparent thickness of 42 cm.
**ALTERATION:** Moderate. Glass now completely devitrified, and together with variolites, is replaced by brown clays. Plagioclase altered to milky white and green clays. Mesostasis altered to green clays.
**VEINS/FRACTURES:** 5%; 0.1-1.5 mm; mostly subpallel to glassy rim; green clay, some carbonate infilling. Branching and cross-cutting.
**ADDITIONAL COMMENTS:** Probably small apophysis derived from larger intrusive Unit 6 below which cuts and contains fragments of Units 3 & 5.

## UNIT 5: APHYRIC BASALT

### Pieces 2D (bottom part) & 3 (top part)

**CONTACTS:** Top contact (with Unit 4) defined by irregular, embayed boundary, whereas bottom contact (with Unit 6) is complicated by presence of veinlets, although margin appears inclined (60 degrees).
**PHENOCRYSTS:** None observed.
**GROUNDMASS:** Fine-grained, hypocrystalline.
**VESICLES:** None observed.
**COLOR:** Gray (N6).
**STRUCTURE:** Thin sliver of lava flow caught between intrusion of Units 4 & 6.
**ALTERATION:** Moderate, similar to Unit 2.
**VEINS/FRACTURES:** 10%; 0.1-3.0 mm; subparallel to intrusion margins; vein between Units 5 & 6 irregularly infilled with green clays; other veins contain carbonate +/- green clay and few pyrite specks.
**ADDITIONAL COMMENTS:** This Unit probably represents a lower portion of Unit 3 separated by the intrusion of Unit 4.

## 129-801C-2R-3 (continued)

## UNIT 6: SPARSELY PLAGIOCLASE PHYRIC BASALT

### Piece 3 (bottom part)

**CONTACTS:** Upper contact inclined (20 degrees), but partly obscurred by carbonate-smectite vein. Crypocrystalline at margin and grading to quenched textured zone in 5 cm. No fresh glass.

**PHENOCRYSTS:** Micro- and mega-phenocrysts present scattered throughout piece. Plagioclase - 1-2%; 0.3-1.0; Subhedral laths and tablets.

**GROUNDMASS:** Cryptocrystalline at margin grading to fine-grained quenched texture downwards.

**VESICLES:** None observed.

**COLOR:** Purplish-brown (5YR 4/1).

**STRUCTURE:** Possibly chilled margin of small intrusive.

**ALTERATION:** Moderate. Orginally glassy margin devitrified and much glass between variolites replaced by brownish clays. Mottled appearance of matrix due to variable alteration.

**VEINS/FRACTURES:** 5%; 0.2-3.0 mm; irregular; branching and cross-cutting common. Thickest vein runs along actual contact. Infilling of carbonate +/- green smectite.

**ADDITIONAL COMMENTS:** Similar features to Unit 4 above and part of same small intrusive.

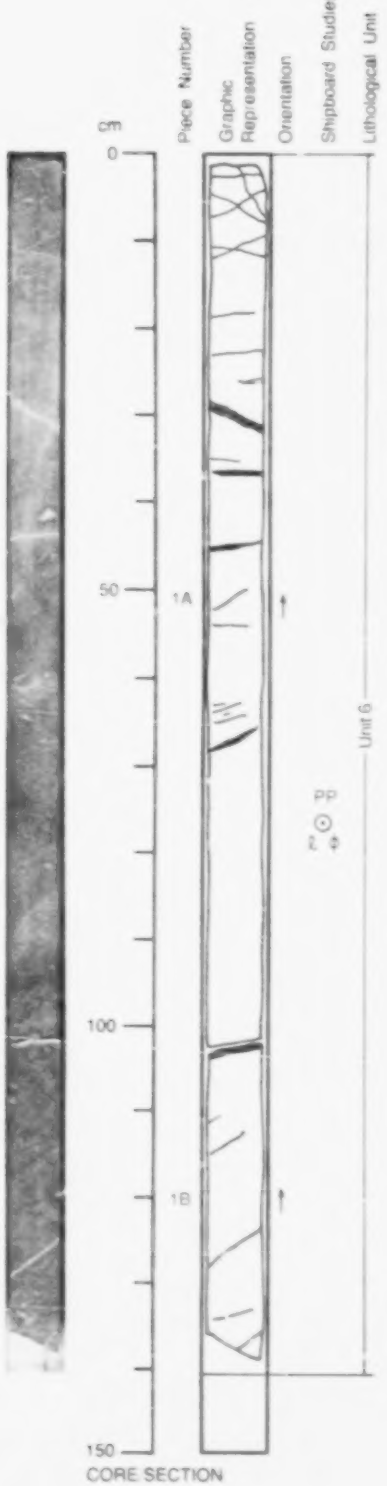

## 129-801C-2R-4

## UNIT 6: SPARSELY PLAGIOCLASE MICROPHYRIC BASALT GRADING TO APHYRIC BASALT

### Pieces 1A and 1B

**CONTACTS:** None observed, but top of Piece 1A very fine-grained and quench textured grading downwards to coarser-grained base.

**PHENOCRYSTS:**

Plagioclase - 1%; 2.5 average; fresh-looking, subhedral, random distribution in top 20 cm, then visible.

**GROUNDMASS:** Fine-grained, but coarsening rapidly downwards until approaching medium-grained. Holocrystalline, some minor mesostasis.

**VESICLES:** None observed.

**COLOR:** Speckled medium gray (5B 6/1).

**STRUCTURE:** Massive; top to central portion of a flow or more likely intrusive.

**ALTERATION:** Moderate. Patchy matrix replacement by carbonate, opaques replaced by white leucoxene, mesostasis by blue-green zoned smectites. Minor scattered pyrite and acicular crystals (zeolite) in Piece 1B. Veinlets throughout.

**VEINS/FRACTURES:** ~4%; <0.2 - 4 mm; majority are subhorizontal; branching and cross-cutting. Few larger green clay margined veins dip at steep angle (~70 degrees). Innumerable very fine carbonate and smectite veinlets are typical.

**ADDITIONAL COMMENTS:** As similar to Unit 4 and both 4 and 6 have inclined contacts, this unit is interpreted as a dyke-like intrusive.

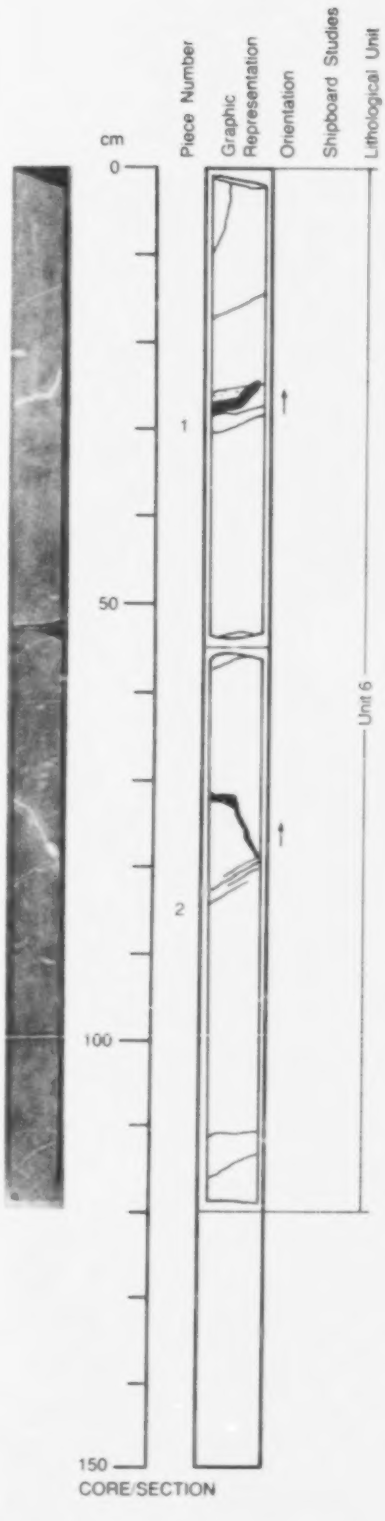

## 129-801C-2R-5

## UNIT 6: APHYRIC MICRODOLERITE

### Pieces 1 and 2

**CONTACTS:** None observed, except base of Piece 2 shows a slight decrease in grain-size relative to top portion of Piece 1. Contacts between small fine-grained a cm wide intrusive at ~27 cm and Unit 6.

**PHENOCRYSTS:** None observed (very occasional large plagioclase crystals).

**GROUNDMASS:** Fine to medium grained, hypocrystalline. Some textural variation with (1) spasmodic development of acicular black clinopyroxene prisms (up to 8 mm long) as well as as more stubby prisms, (2) base of Piece 2, texture finer, more granular and clinopyroxene prisms shorter.

**VESICLES:** None observed.

**COLOR:** Medium gray (N5).

**STRUCTURE:** Massive (central and lower part of the intrusive).

**ALTERATION:** Moderate. Mesostasis replaced by blue-green smectite, random carbonate patches, scattered pyrite. Acicular black clinopyroxene replaced by brown material adjacent to small intrusive (at 27 cm).

**VEINS/FRACTURES:** 3%; 0.5 - 4.0 mm; irregular; branching; 2 sets (i) thicker veins with irregular smectite margins and carbonate +/- pyrite concentrated in central region, and (ii) very fine carbonate only veins.

**ADDITIONAL COMMENTS:** Continuation of Unit 6, perhaps approaching base of intrusion.

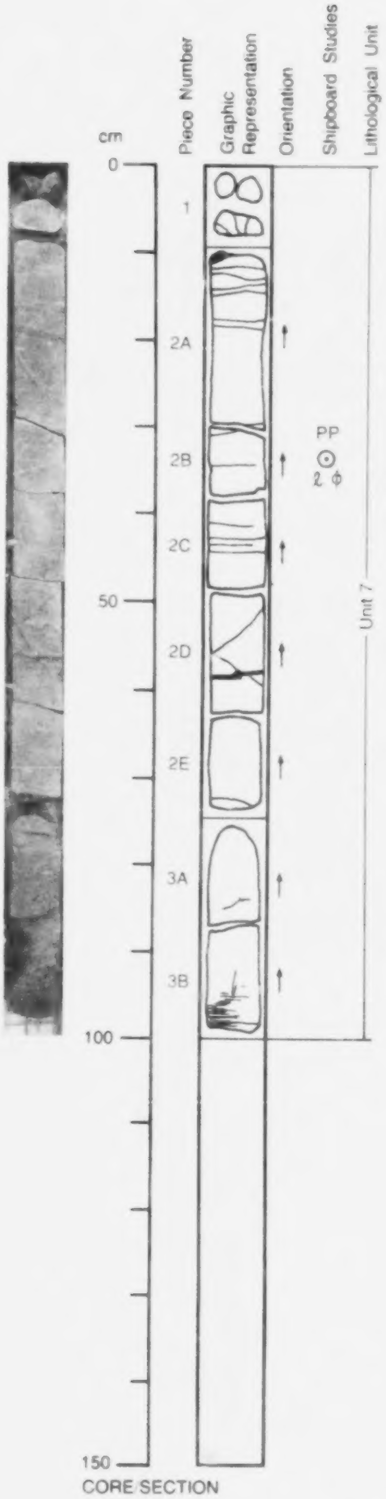
cm
Piece Number
Graphic Representation
Orientation
Shipboard Studies
Lithological Unit
0
1
2A
2B
PP
2C
50
2D
Unit 7
2E
3A
3B
100
150
CORE/SECTION

## 129-801C-3R-1

## UNIT 7: APHYRIC BASALT

### Pieces 1-3B

**CONTACTS:** None observed, except Pieces 1 are partially recrystallized, quench textured basalt and different to preceeding coarser Unit 6. Piece 3B with plume vanolites and few plagioclase microphenocrysts; possibly near base of unit.

**PHENOCRYSTS:** None observed.

**GROUNDMASS:** Fine-grained, hypocrystalline and quench textured throughout. Pieces 1 have a granular texture superimposed on normal quench texture due to recrystallization.

**VESICLES:** None observed.

**COLOR:** Purplish-gray (5YR 4/1) with brown at base of Piece 3 (5YR 4/4).

**STRUCTURE:** Thin flow.

**ALTERATION:** Highly altered. Mainly green (replacing mesostatsis), carbonate (plagioclase and around mineral grains) and Fe oxyhydroxides (throughout matrix) - later includes yellowish oxide material and red hematite. White leucoxene after opaques. Dominant alteration are oxidation products that are concentrated at base of Piece 3B and completely color the basalt brown with Fe oxyhydroxides coating vanolite plumes.

**VEINS/FRACTURES:** 1-2%; 0.1-1.0 mm; subhorizontal & steep (c.60 degrees); most are irregular and cross-cutting. Infilled with carbonate or green oxidized smectite with Fe oxyhydroxides, some hematite.

**ADDITIONAL COMMENTS:** Whole unit affected by dominant oxidative alteration.

## 129-801C-4R-1

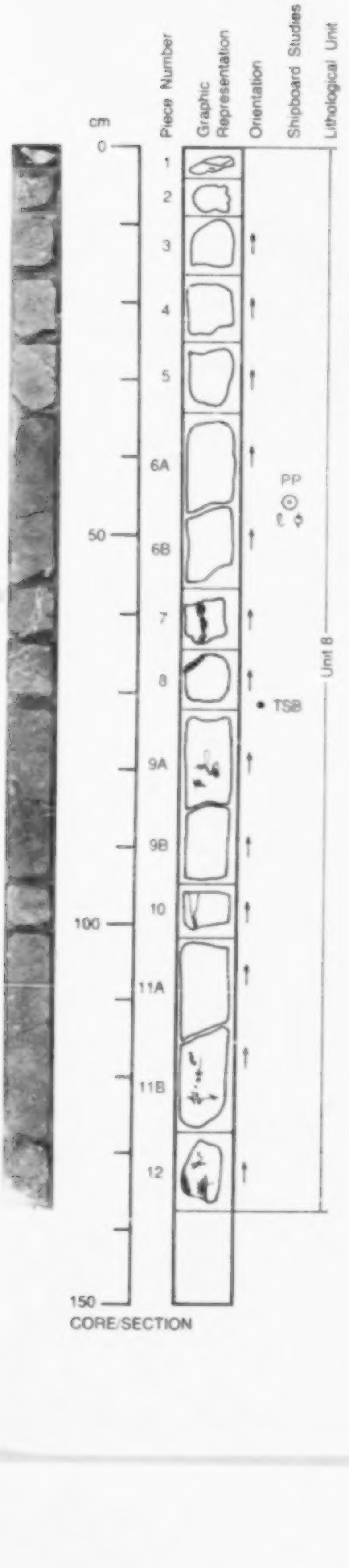

### UNIT 8: HYDROTHERMAL DEPOSIT

### Pieces 1-12

**CONTACTS:** None observed. Piece 1 is a highly silicified red breccia and clearly different to the oxidized base of basalt Unit 7. Rest of pieces are silicified yellow breccia.

**PHENOCRYSTS:** None observed.

**GROUNDMASS:** Generally fine-grained with various sized disrupted yellow fragments (1-50 mm) within a yellow highly siliceous "matrix". Some Pieces (9A & 9B) show an inclined crude wavy lamination partly disrupted by silica "veinlets". Small disorientated fragments have color zoned margins and shinkage cracks. Yellow matrix is sometimes crumbly, highly porous (c.5-10%), but very hard in small silica-rich areas.

**VESICLES:** None observed.

**COLOR:** Piece 1 red-brown (10R 4/6); Pieces 2-12 yellows (10YR 7/7, 10YR 6/8).

**STRUCTURE:** Probably an Fe-Si hydrothermal chemical deposit.

**ALTERATION:** Complete. Dominated by silica as "matrix" and veins and ochrous yellow Fe oxyhydroxides(?) fragments and "matrix".

**VEINS/FRACTURES:** 5%; 1-10 mm; random; silica infilling with larger veins exhibiting a central cavity with quartz crystal terminations growing inwards. Numerous small irregular silica ramifications throughout. Piece 1 has shinkage cracks filled with white opaline silica, also similar deposit around margins of red clast.

**ADDITIONAL COMMENTS:** As almost entirely composed of yellow oxyhydroxides and colorless silica interpretated as a hydrothermal deposit formed by precipitation from Fe-Si charged seawater. Some subsequent replacive silica veining. No evidence of any basaltic textures or relicts, so not directly derived from extensive oxidation of seafloor basalt. Good evidence for sedimentary lamination and their subsequent disruption.

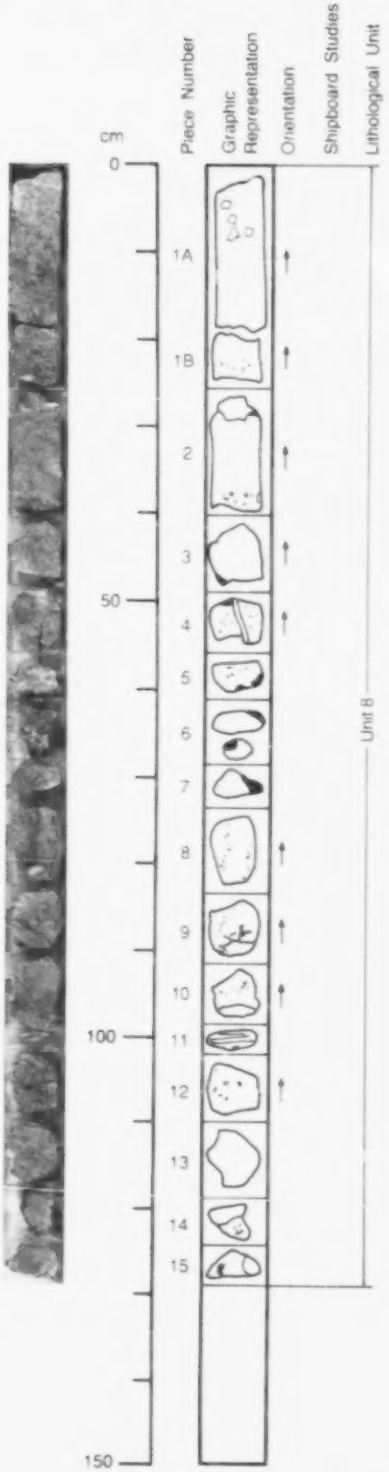
cm
Piece Number
Graphic Representation
Orientation
Shipboard Studies
Lithological Unit
0
50
100
150
1A
1B
2
3
4
5
6
7
8
9
10
11
12
13
14
15
Unit 8
CORE/SECTION

## 129-801C-4R-2

## UNIT 8: HYDROTHERMAL DEPOSIT

### Pieces 1A-15

**CONTACTS:** None observed. Slight differences in apparent fragmentary nature of yellow portions and also degree of regular lamination and disruption.

**PHENOCRYSTS:** None observed.

**GROUNDMASS:** Largely disrupted yellow laminations and fragments set in siliceous "matrix". Some areas are very porous (c.10%) due to dissolution and/or shrinkage, e.g. around fragments in Piece 1A and throughout Piece 8. Porous areas for a box-work with yellow coated silica walls. Laminated structure in Piece 11.

**VESICLES:** None observed.

**COLOR:** Yellows (10YR 7/8 & 10YR 6/8).

**STRUCTURE:** Probably an Fe-Si hydrothermal chemical deposit.

**ALTERATION:** Complete. Dominated by silica and yellowish Fe oxyhydroxides developed throughout. Hematite impregnated silica in Piece 2.

**VEINS/FRACTURES:** 5%; 1-5 mm; random; silica, with central cavity of larger veins lined with quartz crystals.

**ADDITIONAL COMMENTS:** Continuation of Fe-Si hydrothermal deposit from 4R-1. Again lack of basaltic relicts and partly preserved laminated nature suggests a chemical Fe-Si precipitate followed by silicification and attendant disruption.

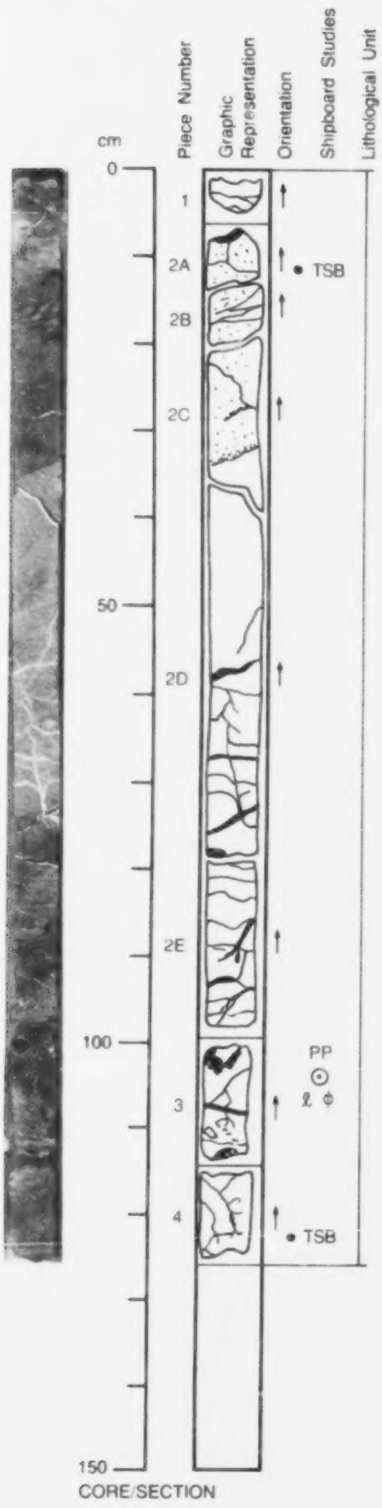

## 129-801C-5R-1

## UNIT 9: HIGHLY PLAGIOCLASE MEGAPHYRIC BASALT

### Pieces 1-4

**CONTACTS:** None observed. Piece 1 is spherulitic with numerous plagioclase microlites and could represent zone near top of a cooling unit.

**PHENOCRYSTS:** Two size populations for plagioclase phenocrysts: megacrysts (1-3 mm) sometimes in glomerocrystic groups and smaller laths (0.5 mm).
Plagioclase - 10%; 0.5-3; all extensively replaced by green smectite (Piece 1) or carbonate (Piece 2D) or combination of both with smectite on rims and carbonate in core.

**GROUNDMASS:** Microcrystalline and quench textured throughout with spherulites and attendant plagioclase microlites.

**VESICLES:** None observed.

**COLOR:** Variable from brownish green at top (Y 4/3 & 10YR 4/4) to light gray in center (5BG 6/1) and green at base (5G 5/2).

**STRUCTURE:** Thin flow.

**ALTERATION:** Highly altered. Development of yellow Fe oxyhydroxides and hematite in top section with sharp downward diffusion boundary at c. 35 cm. Carbonate replaces plagioclase phenocrysts. Lower portion generally greenish due to extensive smectite replacing microlites and phenocrysts. Highly altered zone at 107-114 cm showing patchy carbonate in smectite matrix with relict carbonate pseudomorphed plagioclase phenocrysts.

**VEINS/FRACTURES:** 15%; 0.5-3.0 mm; irregular; numerous irregular, branching and cross-cutting veins. One contains hematite and limonite replacing pyrite(?). Dark oxidized smectite net veining in Piece 4 gives fragmentary appearance.

**ADDITIONAL COMMENTS:** Highly altered thin flow with oxidized top.

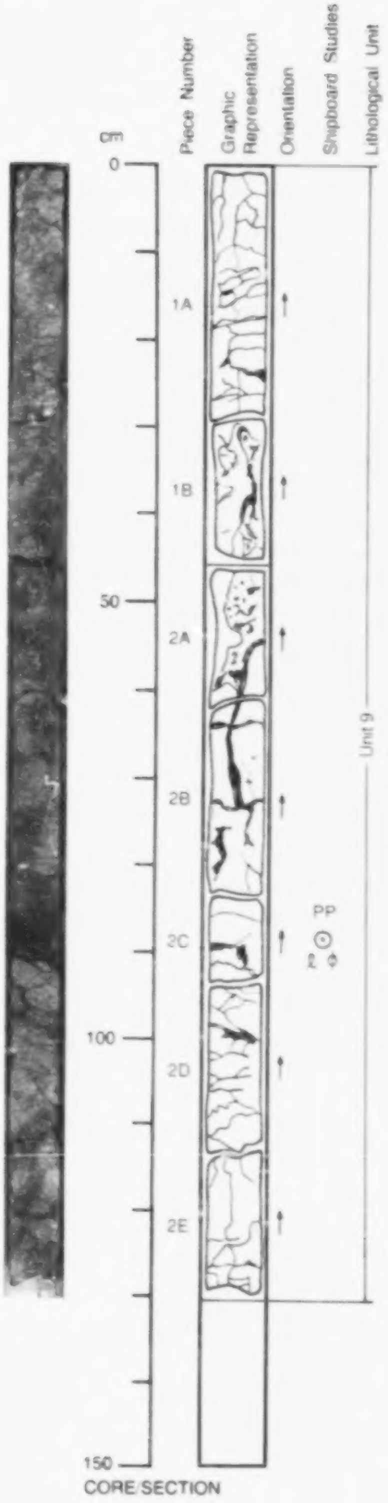

## 129-801C-5R-2

## UNIT 9: MODERATELY PLAGIOCLASE MEGAPHYRIC BASALT

### Pieces 1A-2E

**CONTACTS**: None observed, although Piece 2E is cryptocrystalline with much smaller spherulites and could represent basal part of unit.

**PHENOCRYSTS**: Possibly some small mafic phenocrysts in Piece 2E.
Plagioclase - 3%; 1-4, random distribution throughout.

**GROUNDMASS**: Spherulitic throughout, cryptocrystalline. General matrix disrupted in most pieces (especially 2A & 1B) by network of dark "veins" that enclose frgaments of basalt and phenocrysts, and finally end in a net vein breccia in Piece **1A**. Some of the vein material retain originally glassy material with minute spherulites, now seen as white spots.

**VESICLES**: None observed.

**COLOR**: Pale grayish green (5G 5/2 & 5BG 5/1).

**STRUCTURE**: Probably lower half of thin flow.

**ALTERATION**: Highly altered. Greenish tinge to matrix due to smectite; plagioclase phenocrysts totally replaced by carbonate.

**VEINS/FRACTURES**: 25%, 0.5-2.0 mm, irregular; numerous irregular carbonate veinlets. Main feature is series of dark smectite-bearing veins that form a network complex up the section and infill brecciated portions of flow. Pieces 2A and top of 2B show an infill of spherulitic basalt, variously altered fragments and broken phenocrysts, together with white devitrified spots in original glassy fragments.

**ADDITIONAL COMMENTS**: Thin flow unit invaded by forceful hydrothermal fluids that brecciated and altered basalt as they moved upwards.

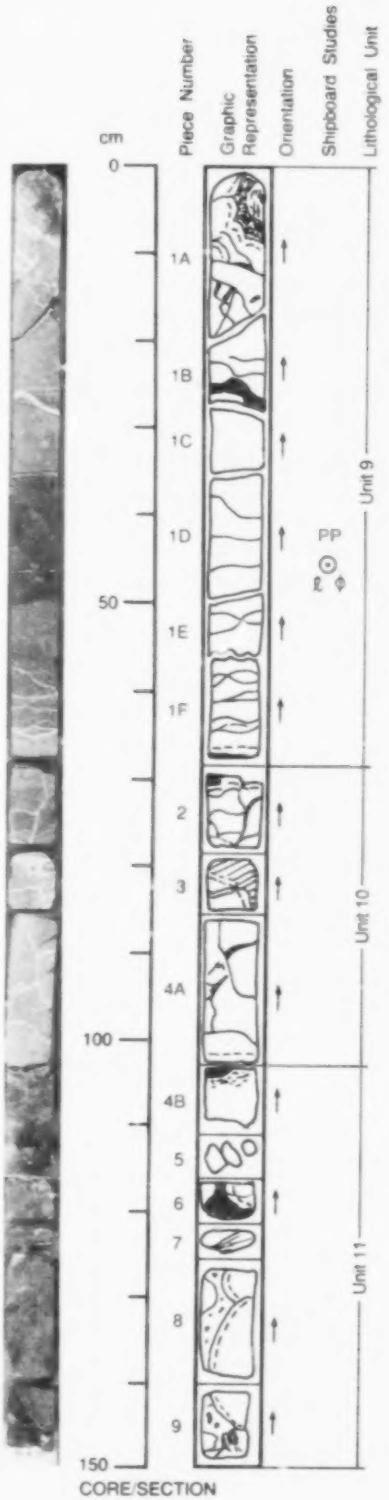

## 129-801C-5R-3

## UNIT 9: MODERATELY PLAGIOCLASE MEGAPHYRIC BASALT

### Pieces 1A - 1F

**CONTACTS:** Not observed, but the bottom Piece (1F) has a devitrified, almost black, glassy rim that could had been the margin of Unit 9.

**PHENOCRYSTS:**

Plagioclase - 10%; 2.5 on the average; anhedral to subhedral, glomerophyric, and slightly altered to white clays; trace of carbonate along grain margins.

**GROUNDMASS:** Variolitic; cryptocrystalline; perhaps variolites were in a glassy matrix that is now completely devitrified; devitrified glassy rims on top of pieces 1A and 1B; spalled glassy rims are enclosed in the dark green, interpillow sediments.

**VESICLES:** None observed.

**COLOR:** Light greenish gray (5GY 7/1) top, spotted gray (N6) mid-section, and darker gray (N5) bottom.

**STRUCTURE:** Most probably the lower portion of a pile of pillow lavas.

**ALTERATION:** Highly altered, particularly piece 1A; plagioclase are replaced partly with whitish clays and carbonate; groundmass had been completely devitrified and partly replaced by clays.

**VEINS/FRACTURES:** 20%; 0.1 to 7.0 mm; very irregular; Mostly infilled with carbonate and green clays; Piece 1A has dark green to almost black infillings.

**ADDITIONAL COMMENTS:** This lowermost portion of Unit 9 shows the transition from a highly altered top to a less altered bottom. The bottom pieces still show the texture and structure of the margin of a typical pillow. The higher portion of this Unit is most probabaly the highly fractured, altered, and clay-rich equivalent of the lower portion.

## UNIT 10: MODERATELY PLAGIOCLASE MEGAPHYRIC BASALT

### Pieces 2 - 4A

**CONTACTS:** Part of the glassy rim of Piece 2 is in contact with a secondary carbonate veinlet; the bottom glassy rim of Piece 4A is also in contact with a secondary smectite infilling.

**PHENOCRYSTS:**

Plagioclase - 6%; 2.0 on the average; Subhedral; some are partly altered to whitish clays and carbonate; the rest are fairly fresh; a few are glomerophyric.

**GROUNDMASS:** Devitrified, glassy rims to variolitic interior; cryptocrystalline; matrix is most probably originally holohyaline to hypohyaline but is now completely devitrified.

**VESICLES:** None observed.

**COLOR:** Spotted light greenish gray (5GY 7/1).

**STRUCTURE:** Most probably pillows.

**ALTERATION:** High; glassy rims and groundmass are highly altered to clays; phenocrystic plagioclase are partly altered to clays and carbonate; a few specks of pyrite present.

**VEINS/FRACTURES:** 15%; 0.1 - 4.0 mm; very irregular; infilled mostly with carbonate and less commonly with green clays; some veinlets assume stockwork networks.

**ADDITIONAL COMMENTS:** Consisting of two pieces of texturally and compositionally similar pillow lavas. The pillows are separated by interpillow sediments that are now completely replaced by carbonate, autogenic clays, and silica.

## 129-801C-5R-3 (continued)

## UNIT 11: SPARSELY PLAGIOCLASE-OLIVINE MICROPHYRIC BASALT

### Pieces 4B - 9

**CONTACTS:** Original contacts not actually observed because the surrounding materials consist of secondary minerals, but individual pieces have subrounded glassy rim that grades to holohyaline or hypohyaline interior.

**PHENOCRYSTS:**

Plagioclase - 1%; <1; Subhedral; some are glomerophyric and concentrated near the glassy rim.

Olivine - trace; <1; Subhedral to euhedral; completely pseudomorphed by clays and Fe-hydroxides.

**GROUNDMASS:** Devitrified glassy rims and holohyaline or hypohyaline interiors; variolitic texture common; cryptocrystalline.

**VESICLES:** Trace; 0.5 mm maximum; rounded; irregular but generally near the rim; infilled with green clays.

**COLOR:** Grayish green (5G 5/2) with blackish rim.

**STRUCTURE:** Fragments of pillow lavas.

**ALTERATION:** High; devitrified rims and interior groundmass now altered to green clays.

**VEINS/FRACTURES:** Trace; 0.1 mm; subhorizontal; boundaries of pillows are also generally lined with veinlets; infilled mostly with carbonate and less commonly with green clays.

**ADDITIONAL COMMENTS:** Pillow fragments are texturally and compositionally similar. The degree of alteration is the same throughout. Interpillow materials, which include spalled off pillow rims, are now altered to autogenic, dark green clays. Pieces 4B and 5 are actually pieces or rubbles of greenish and reddish (oxidized) interpillow materials.

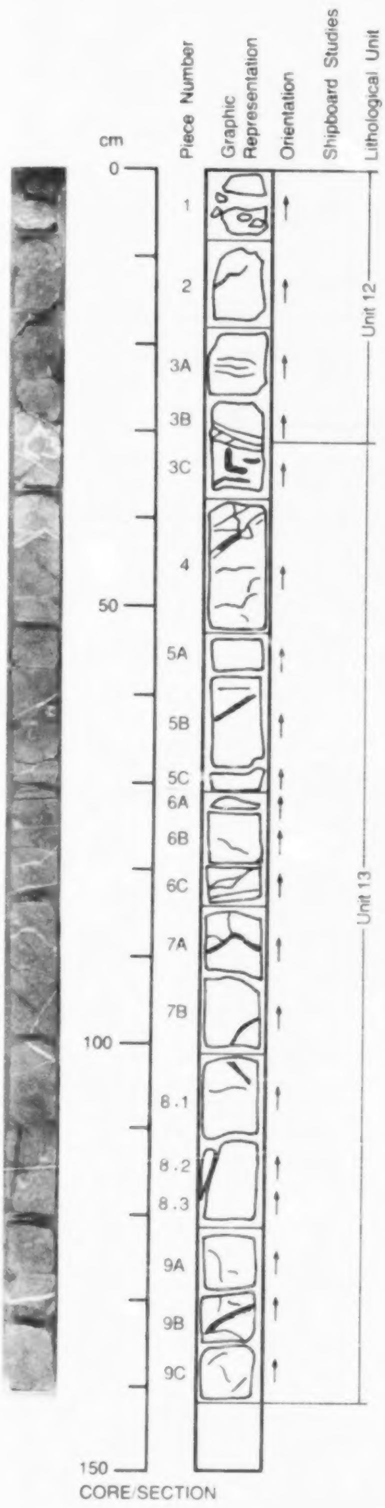

## 129-801C-5R-4

## UNIT 12: HIGHLY CALCIFIED INTERPILLOW MATERIALS

### Pieces 1 - 3C (top portion)

**CONTACTS:** Only bottom part observed - very irregular, inclined at 35 degrees, embayed, and seems to penetrate the underlying Unit 13.
**PHENOCRYSTS:** None observed.
**GROUNDMASS:** A mixture of cryptocrystalline carbonate.
**VESICLES:** None observed.
**COLOR:** Weak red (4/3) with irregular tinge of black, gray, green, and orange (Fe-hydroxides).
**STRUCTURE:** Fragmented, irregular pieces; Piece 3A shows some layering.
**ALTERATION:** Very high; almost completely altered to reddish carbonate and green clays.
**VEINS/FRACTURES:** 3%; 0.2 - 2.0 mm; irregular; Infilled with white carbonate and dark green clays.
**ADDITIONAL COMMENTS:** Most probably, this unit originally consisted of a mixture of broken basalt fragments, pieces of hydrothermal precipitates similar to Unit 8, pieces of claystone, pieces of veinlet materials, calcareous sediments, but are now completely altered to carbonate and green clays. Pseudomorphs of some of these pieces are present in the Unit. A similar, but smaller type of material is present between pillow Units 10 and 11.

## UNIT 13: APHYRIC BASALT GRADING TO MODERATELY PLAGIOCLASE-OLIVINE PHYRIC BASALT

### Pieces 3C (bottom part) - 9C

**CONTACTS:** Top contact with Unit 12 embayed; rim is devitrified glass followed by a spherulitic zone; 35 degrees inclination.
**PHENOCRYSTS:**
Plagioclase - 2%; 1.5 on the average; mostly anhedral due to alteration to carbonate.
Olivine - 1%; 1.5 on the average; mostly anhedral due to alteration to carbonate.
**GROUNDMASS:** Devitrified glassy rim grading to a spherulitic zone, then to a variolitic zone, and finally to a hypocrystalline bottom; generally quench textured.
**VESICLES:** None observed.
**COLOR:** Light gray (N7) grading to fine-speckled gray (N6).
**STRUCTURE:** Fractured; perhaps a moderate-sized pillow because of the inclined, glassy margin; can also be a thin flow.
**ALTERATION:** Moderate to high; devitrified glassy rim and mesostasis altered to light green clays; phenocrysts altered to carbonate; a few specks of pyrite present.
**VEINS/FRACTURES:** 5%; 0.2 - 6 mm; very irregular; infilled with carbonate +/- green clays; branching and cross-cutting, with some veinlets displaced by at least 4 mm; some have irregular, darker than normal groundmass halos.
**ADDITIONAL COMMENTS:** There seems to be differential alteration as the to portion is mostly altered to lighter green clays whereas the bottom part is mostly altered to darker green clays.

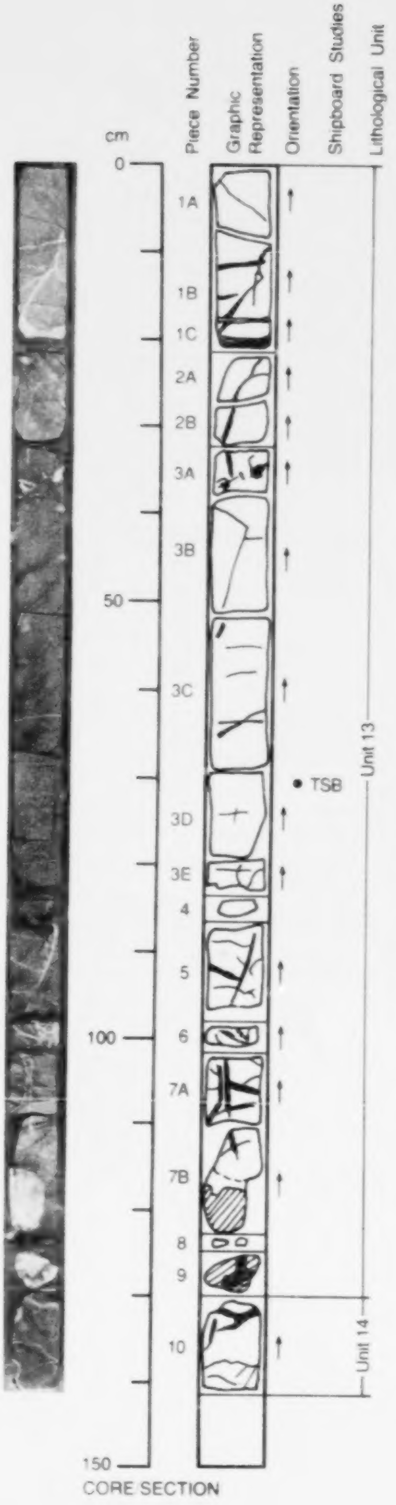

## 129-801C-5R-5

## UNIT 13: MODERATELY OLIVINE-PLAGIOCLASE PHYRIC BASALT WITH BAND OF APHYRIC BASALT

### Pieces 1A - 9

**CONTACTS:** Bottom contact is very irregular and highly shattered/replaced by bluish green clays; unit is directly in contact with secondary white carbonate, and thus, most probably not original.

**PHENOCRYSTS:**

Plagioclase - 1%; 1.5 on the average; Subhedral; completely replaced.

Olivine - 2%; 1.5 on the average; Subhedral to euhedral; completely pseudomorphed; can be recognized by the euhedral lantern and skeletal crystal morphologies typical of olivine.

**GROUNDMASS:** Hypocrystalline; fine-grained and quench textured throughout; overall texture is patchy, with some bands, particularly top and bottom are aphyric.

**VESICLES:** None observed.

**COLOR:** Fine-speckled gray (N5) grading to pale green (5G 6/2) at the bottom.

**STRUCTURE:** Possibly the bottom of a flow-differentiated thin lava flow; highly fractured bottom.

**ALTERATION:** High to very high; phenocrysts altered to clays and/or carbonate; mesostasis and groundmass microlites are greenish due to clay alteration; bottom margin is more altered than top.

**VEINS/FRACTURES:** 20%; 0.2 mm - 7 cm; very irregular; infilled with carbonate and green clays; cross-cutting and branching.

**ADDITIONAL COMMENTS:** Carbonate infillings (bottom of Piece 7B and Piece 9) are included in the Unit. Phenocryst alteration, similar to their distribution, is variable - those at the top bands are altered mostly to carbonate, those in mid-section to dark green clays, and those at the bottom are back to carbonate again.

## UNIT 14: APHYRIC BASALT

### Piece 10

**CONTACTS:** Not observed but topmost part is a devitrified, blackish glass grading to a spherulitic zone downwards.

**PHENOCRYSTS:** None observed.

**GROUNDMASS:** Devitrified glassy rim grading to a spherulitic zone, and finally to a variolitic bottom; cryptocrystalline overall.

**VESICLES:** None observed.

**COLOR:** Fine-speckled gray (N5).

**STRUCTURE:** Either a top of a pillow or a thin flow.

**ALTERATION:** Highly devitrified glassy rim altered to light brown clays; glass interstitial to spherulites altered to dark green clays; carbonate is present along grain boundaries. Ferromagnesian microlites are also altered to dark green clays.

**VEINS/FRACTURES:** 20%; 0.1 - 10 mm; very irregular; infilled mostly with reddish or white carbonate /- green clays; branching and cross cutting; the top glassy rim is separated from the rest of the Unit by a 10 mm wide, red and white carbonate veinlet.

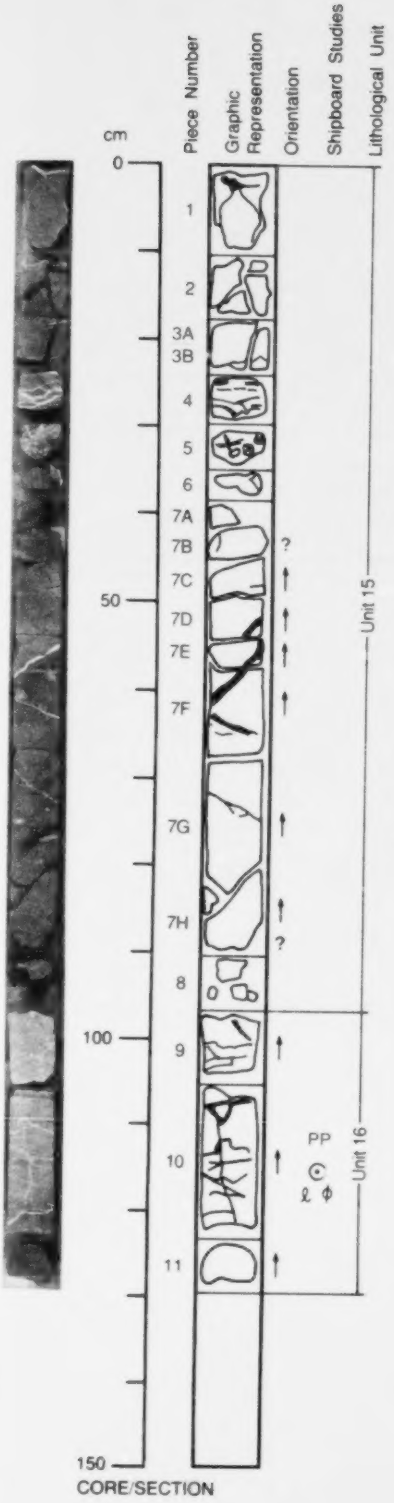

## 129-801C-6R-1

## UNIT 15: A COLLECTION OF BASALTIC FRAGMENTS WITH UNVERIFIED ORIENTATION AND ORDERING.

### Pieces 1 - 8

**CONTACTS:** None observed.
**PHENOCRYSTS:**
Plagioclase - 2%; 2 on average; Subhedral; only in Pieces 7A - 7H.
Pyroxene - 2%; 2 on average; Anhedral plates; also in Pieces 7A - 7H but hard to differentiate from plagioclase because of intense alteration; could be olivine.
**GROUNDMASS:** Pieces 4 and 5 have devitrified glassy rims; Pieces 1 - 3 are variolitic to hypocrystalline; Pieces 7A - 7H are hypocrystalline with abundant quenched microlites; overall, fragments are fine-grained.
**VESICLES:** None observed.
**COLOR:** Various shades of gray with greenish tinge.
**STRUCTURE:** Different fragments of basalts; Pieces 4 and 5 may represent a ~6 cm sheet flow with glassy top and bottom.
**ALTERATION:** Moderate to high; all pieces have greenish tinge indicating green clay alteration; devitrified glassy rims are most probabaly altered to brown clays; phenocrysts in Pieces 7A - 7H are altered to whitish clays.
**VEINS/FRACTURES:** 15%; 0.1 - 4.0 mm; irregular; some are infilled with whitish to greenish clays; others are infilled with carbonate.
**ADDITIONAL COMMENTS:** Pieces 1 - 8 fell from the drill pipe directly to the rig floor and so their orientations and ordering, except for Pieces 7C - 7H, perhaps, are uncertain.

## UNIT 16: SPARSELY PLAGIOCLASE PHYRIC BASALT GRADING TO APHYRIC BASALT

### Pieces 9 - 11

**CONTACTS:** Not observed but top margin has a devitrified glass rim.
**PHENOCRYSTS:**
Plagioclase - 1%; 1 on the average; Subhedral and concentrated near the top margin.
**GROUNDMASS:** Devitrified glassy rim grading to a spherulitic zone and then to a variolitic zone at the bottom; fine-grained throughout.
**VESICLES:** None observed.
**COLOR:** Light greenish gray (5GY 7/1) grading to greenish gray (5G 5/1).
**STRUCTURE:** Perhaps top of a thin lava flow.
**ALTERATION:** High; devitrified rim and mesostasis glass altered to light green clays; phenocrysts are altered to green clays and carbonate; carbonate grains and pyrite specks are occasionally present.
**VEINS/FRACTURES:** 20%; 0.2 - 4.0 mm; very irregular; Infilled with carbonate and whitish and greenish clays; stockwork orientation.

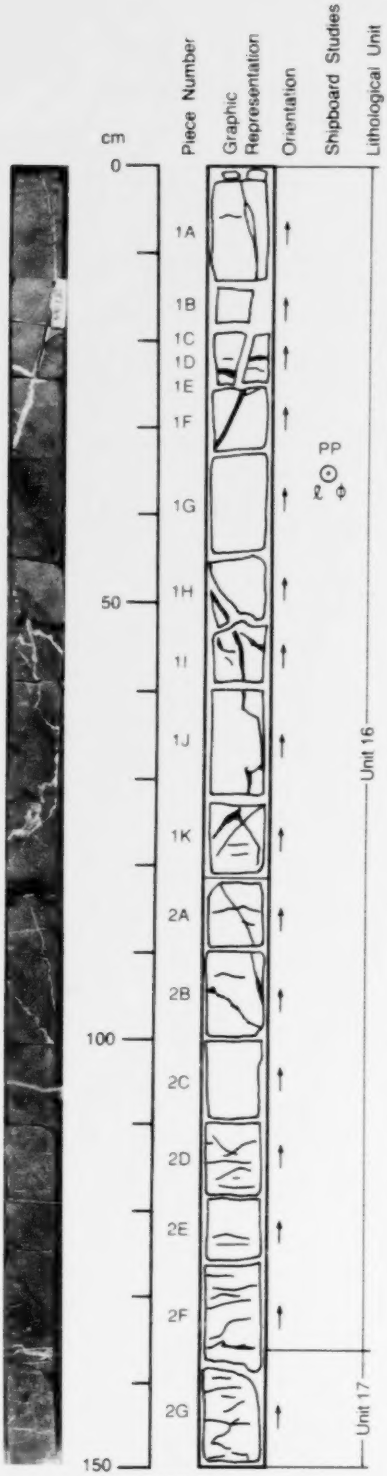

## 129-801C-6R-2

## UNIT 16: APHYRIC BASALT WITH BANDS OF MODERATELY OLIVINE-PLAGIOCLASE PHYRIC BASALT

### Pieces 1A - 2F

**CONTACTS:** None observed but bottom piece is variolitic with a devitrified glassy rim.
**PHENOCRYSTS:**
Plagioclase - 1%; 1 on the average; Subhedral; completely altered and so hard to differentiate from the olivine
Olivine - 3%; 1 on the average; Subhedral to skeletal; completely altered.
**GROUNDMASS:** Hypocrystalline with devitrified, glassy mesostasis; bottom part is variolitic although variolitic patches are common throughout; fine-grained; presence of subhorizontal veinlets with cryptocrystalline, very dark gray halos complicates the overall groundmass texture.
**VESICLES:** None observed.
**COLOR:** Fine-speckled gray (N5) grading to greenish gray (5G 5/1) at the bottom Piece (2G).
**STRUCTURE:** Perhaps a thin lava flow showing flow differentiation.
**ALTERATION:** Moderate-high; devitrified glassy mesostasis and rim are altered to green clays; phenocrysts are altered to clays; occasional carbonate grains and pyrite specks are present in the groundmass.
**VEINS/FRACTURES:** 4%; 0.1 - 10 mm; very irregular; infilled with carbonate and green clays; branching and cross-cutting; most of the fractures have very irregular, slightly darker gray or green halos.
**ADDITIONAL COMMENTS:** Very similar to Unit 13 in that it contains olivine-plagioclase phyric bands, which may indicate flow differentiation. Alteration of phenocrysts is also banded in that some layers are altered to whitish clays whereas others are altered to dark green clays. Fracture halos range from cryptocrystalline margins to more clay-altered groundmass.

## UNIT 17: MODERATELY OLIVINE-PLAGIOCLASE PHYRIC BASALT

### Pieces 2F (botttom part) and 2G

**CONTACTS:** Top and bottom contacts (obscurred by carbonate veinlets) are characterized by devitrified, glassy rims grading to variolitic interior.
**PHENOCRYSTS:**
Plagioclase - trace; 1 - 2; Subhedral; completely altered and difficult to differentiate from either pyroxene or olivine.
Olivine - 2%; 1 - 2; skeletal to subhedral; complete pseudomorphed.
**GROUNDMASS:** Devitrified, glassy rims grading to hypocrystalline, variolitic interior; quench textured minerals throughout.
**VESICLES:** None observed.
**COLOR:** Dark greenish gray (5GY 4/1 to 5G 4/1) with blackish patches.
**STRUCTURE:** A sheet flow with glassy top and bottom margins.
**ALTERATION:** High; phenocrysts altered to whitish clays; greenish throughout indicating that groundmass and devitrified glassy rims and mesostasis are altered to green clays.
**VEINS/FRACTURES:** 10%; 0.1 - 2.0 mm; mostly subhorizontal but irregular; infilled with carbonate and green clays; most with attendant black halos.

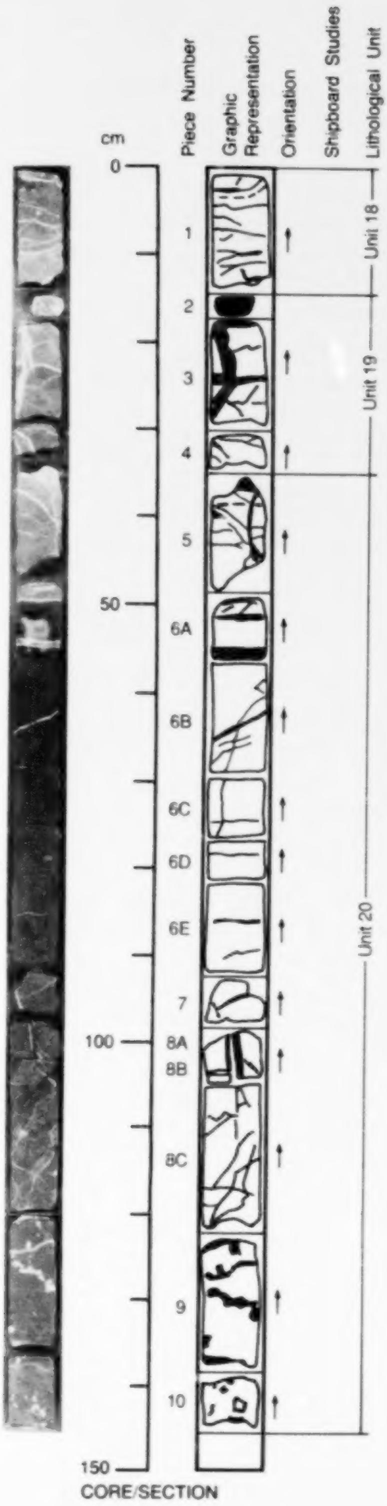

## 129-801C-6R-3

### UNIT 18: MODERATELY OLIVINE-PLAGIOCLASE PHYRIC BASALT

#### Piece 1

**CONTACTS:** Top rim is devitrified glass in contact with secondary carbonate veinlet; bottom margin not observed.

**PHENOCRYSTS:**

Plagioclase - trace; 1.0 on average; Subhedral; hard to differentiate from olivine due to high alteration.

Olivine - 2%; 1.5 on average; skeletal to subhedral; completely pseudomorphed.

**GROUNDMASS:** Glassy top rim grading to a variolitic zone, and then to a hypocrystalline bottom; fine-grained.

**VESICLES:** None observed.

**COLOR:** Greenish gray (5G 6/1) with grayish tinge (N6) on top.

**STRUCTURE:** Perhaps top of a sheet flow or thin lava flow.

**ALTERATION:** High; phenocrysts altered to whitish clays; greenish throughout suggesting that groundmass and devitrified glassy rim had been altered to green clays; carbonate grains occasionally present in the groundmass.

**VEINS/FRACTURES:** 20%; 0.1 - 4.0 mm; mostly subhorizontal but irregular; infilled with carbonate and green clays +/- pyrite; branching and cross-cutting.

### UNIT 19: APHYRIC BASALT

#### Pieces 2 - 4

**CONTACTS:** Top margin is devitrified glass grading to a spherulitic zone; in direct contact with a carbonate veinlet (including Piece 2); bottom contact not observed.

**PHENOCRYSTS:** None observed (<1% total).

**GROUNDMASS:** Devitrified glassy rim grades to a spherulitic zone, and then to a variolitic zone, and finally to a hypocrystalline bottom; cryptocrystalline overall.

**VESICLES:** None observed.

**COLOR:** Greenish gray (5G 6/1) with grayish tinge (N6) on the top margin.

**STRUCTURE:** Top of a sheet flow or a thin lava flow.

**ALTERATION:** High; few microlites present altered to carbonate; trace of carbonate also present along grain boundaries; mesostasis altered to green clays; greenish throughout.

**VEINS/FRACTURES:** 25%; 0.2 - 13 mm; orthogonal, generally; infilled with red and white carbonate and white clays +/- pyrite; the top of the Unit is a piece of red and white carbonate materials containing green clays which most probably are altered interpillow/inter-lava flow sediments.

### UNIT 20: APHYRIC BASALT WITH SPARSELY PLAGIOCLASE PHYRIC PATCHES

#### Pieces 5 - 10

**CONTACTS:** Top has double, devitrified glass rims, one on top of the other; second rim at the bottom is subrounded and inclined at 65 degrees; bottom contact not observed.

**PHENOCRYSTS:**

Plagioclase - 1%; 0.8 on average; Subhedral and stubby; widely dispersed.

**GROUNDMASS:** Devitrified glassy rims grading to spherulitic zone, then to a variolitic zone, and finally to a hypocrystalline interior; cryptocrystalline groundmass in general; very patchy groundmass texture with abundant variolites near top and bottom.

**VESICLES:** Some miarolitic cavities present in the carbonate veinlet in Piece 9; lined with calcite crystal terminations.

**COLOR:** Light greenish gray (5G 6/1) top with grayish tinge (N6) at the rim, grading to fine speckled gray (N5) towards the bottom.

**STRUCTURE:** Perhaps top of a pillow or a thin flow capped by another thin flow.

**ALTERATION:** High; most phenocrysts are altered to green clays and carbonate; greenish throughout suggesting groundmass and devitrified glassy rims had been altered to green clays.

**VEINS/FRACTURES:** 5%; 0.2 - 10 mm.; irregular; infilled with carbonarte and green clays; branching and cross-cutting; pieces 9 and 10 have very irregular, botryoidal carbonate veinlets with miaroles.

**ADDITIONAL COMMENTS:** Perhaps a pillow overran by another, thin, pillow or sheet flow.

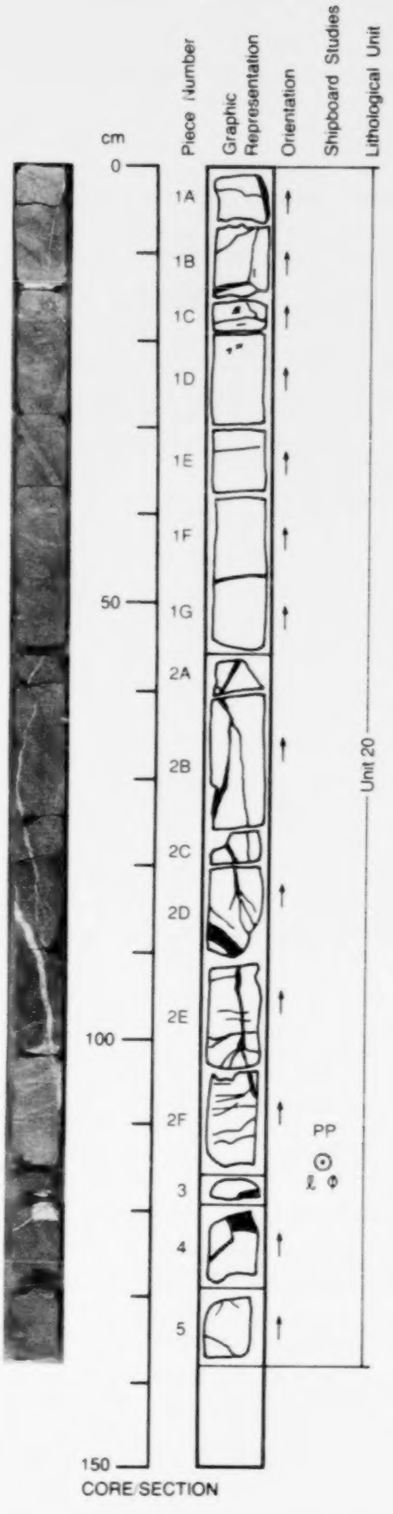
cm
Piece Number
Graphic Representation
Orientation
Shipboard Studies
Lithological Unit
0
50
100
150
1A
1B
1C
1D
1E
1F
1G
2A
2B
2C
2D
2E
2F
3
4
5
PP
Unit 20
CORE/SECTION

## 129-801C-6R-4

## UNIT 20: MODERATELY OLIVINE-PLAGIOCLASE PHYRIC BASALT

### Pieces 1A - 5

**CONTACTS:** None observed, although grain size decreases downwards and spherulitic texture developed in Piece 2F (at color change) and continued to base.

**PHENOCRYSTS:** Irregular distribution down section and in size developed - concentrated in 2A - 2E (large size) and lesser extent in 4 and 5 (small microphenocrysts).
Plagioclase - 1%; 0.5 - 1.0, Subhedral; sometimes corroded margins.
Olivine - 5%; 0.5 - 1.0; Subhedral; totally replaced by dark green smectite and laminated white clay.

**GROUNDMASS:** Fine-grained, hypocrystalline with spherulitic base.

**VESICLES:** None observed.

**COLOR:** Dominantly medium gray (N5) grading to pale green (5GY 7/1) in Pieces 2F, 3 and 4 (top).

**STRUCTURE:** Interior to basal portion of a flow.

**ALTERATION:** Moderate, but variable; olivine phenocrysts replaced by greenand white smectite clays, except in Pieces 4 and 5 where totally pseudomorphed by bright blue clay (celadonite?) and carbonate. Alteration of mesostasis to green clays in Pieces 2F and 3 produces paler color here. Some pyrite in lower section.

**VEINS/FRACTURES:** 5%; 0.2 - 6.0 mm; mostly subhorizontal; subhorizontal veinlets cut subvertical vein that traverses Pieces 2A to 2F. Alteration associated with carbonate concentration and vein in Piece 4 includes hematite replacing microlites and microphenocrysts marginal to veins.

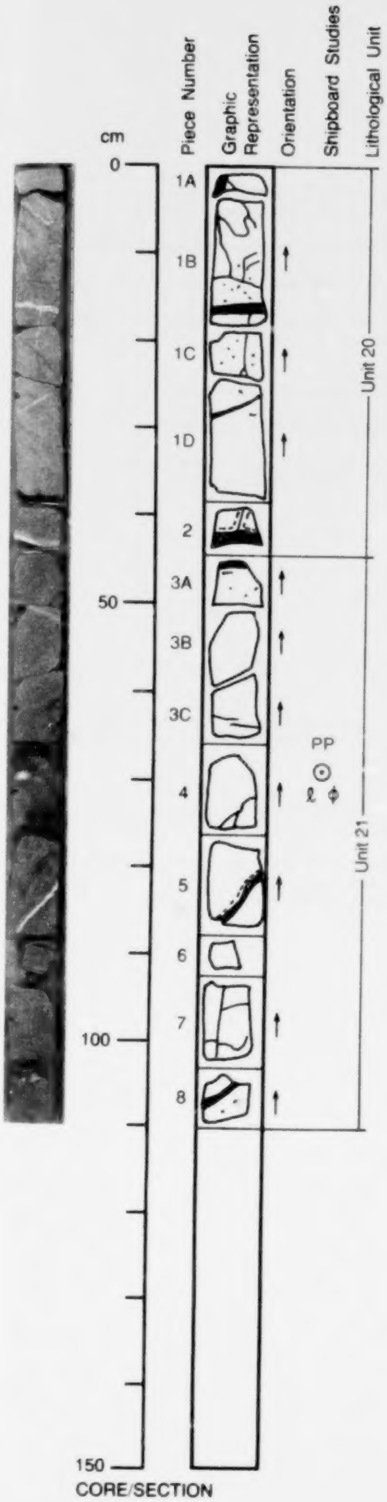

## 129-801C-6R-5

### UNIT 20: SPARSELY OLIVINE-PLAGIOCLASE MICROPHYRIC BASALT

#### Pieces 1A-2

**CONTACTS:** None observed, except Piece 2 has spherulitic texture and microlites, much finer grained than pieces above and represents basal part of Unit.
**PHENOCRYSTS:** Both types concentrated in basal portion (Piece 2).
Plagioclase - c.1%; 0.1-0.2; Subhedral to anhedral.
Olivine - c.1%; <0.1; replaced by green clays.
**GROUNDMASS:** Fine-grained, hypocrystalline. Quench textured throughout, with spherulitic zone and elongate microlites in Piece 2. Matrix and microphenocrysts affected by adjacent carbonate veins and altered to green clays.
**VESICLES:** 2%; 0.5-1.0 mm; circular; random; infilled with carbonate or green smectite with walls decorated with pyrite granules. Some vesicle centers all pyrite possibly replacing carbonate.
**COLOR:** Medium gray (N5).
**STRUCTURE:** Basal portion of thin flow.
**ALTERATION:** Moderate. Mesostasis and phenocrysts replaced by carbonate and green smectite, rarely pyrite. Carbonate and smectite infill vesicles. Green smectite alteration adjacent to carbonate vein in Piece 2.
**VEINS/FRACTURES:** 8%; 0.5-0.7 mm; random; most veins highly irregular, except for two major horizontal veins (Pieces 1B & 2) that cut all others. Carbonate infilling +/- minor green smectite.
**ADDITIONAL COMMENTS:** Continuation of Unit 20.

### UNIT 21: APHYRIC BASALT

#### Pieces 3A-8

**CONTACTS:** None observed, except top of Piece 3A is spherulitic with plagioclase microlites and grain-size increases downwards.
**PHENOCRYSTS:** Generally aphyric, but very minor plagioclase microphenocrysts and plagioclase-olivine glomerocrystic groups in contact zone (Piece 3A).
**GROUNDMASS:** Fine-grained, hypocrystalline. Quench textured throughout with elongate plagioclase microlites. Spherulitic contact zone.
**VESICLES:** <1%; 0.5-1.0 mm; circular; random; generally carbonate infilling, some zoned with pale green smectite and core of dark green clay (smectite or celadonite).
**COLOR:** Medium gray (N5).
**STRUCTURE:** Top and central portion of thin flow.
**ALTERATION:** Slight. Minor mesostasis replaced by smectite. Most alteration adjacent to large veins with development of smectite-rich 2-5 mm wide halos. Vesciles infilled with carbonate and variously colored smectites. Scattered pyrite, especially near veins.
**VEINS/FRACTURES:** 3%; 0.2-6.0 mm; Inclined 45-55 degrees; carbonate infilling, sometimes thin bright green smectite margins. Rarer pyrite-carbonate veinlets.

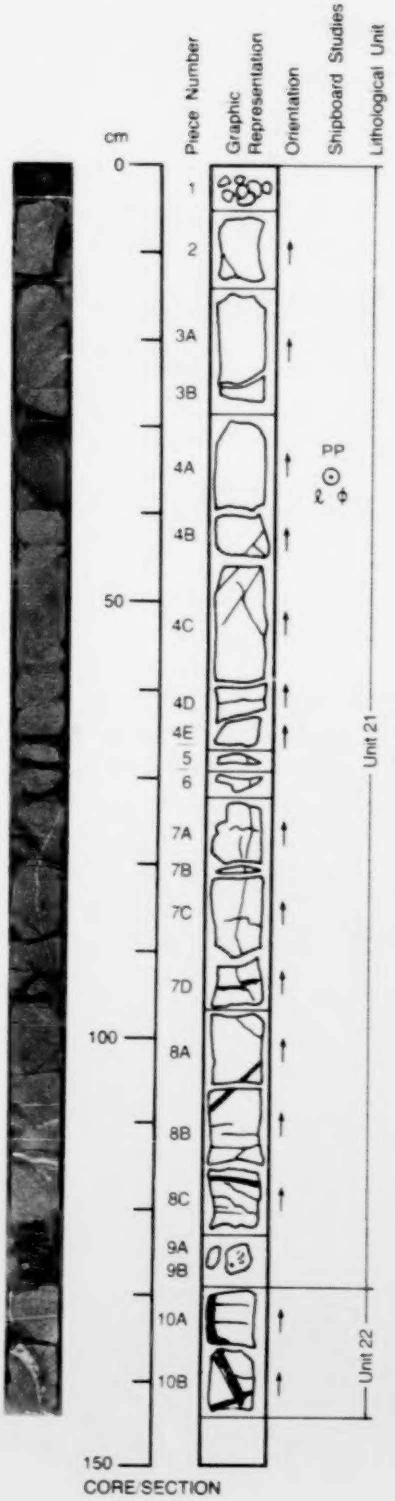

## 129-801C-7R-1

### UNIT 21: APHYRIC BASALT

### Pieces 1-9B

**CONTACTS:** None observed, but Piece 8C finer grained and more spherulitic relative to those above. Piece 9A contains fragmented spherulitic margins with plagioclase microlites and represents lower contact.
**PHENOCRYSTS:** None observed. Few plagioclase microphenocrysts in spherulitic lower contact.
**GROUNDMASS:** Fine-grained, hypocrystalline. Quench textured throughout with variolites; spherulitic in lower contact zone (Piece 8C).
**VESICLES:** <1%; 0.2-0.5 mm; circular; random; infilled with carbonate or zoned with narrow rim of white smectite and center of dark green smectite.
**COLOR:** Medium gray (N6).
**STRUCTURE:** Interior and lower portion of thin flow.
**ALTERATION:** Slight. Mesostasis replaced by pale yellow-green clays. Spherulitic zone has pale green tinge due to smectite replacement; some associated pyrite granules here also. Fragments in 9A totally replaced by bright green smectite with orange oxidized margins.
**VEINS/FRACTURES:** 3%; 0.1-4.0 mm; subhorizontal; mainly veinlets, but cut by later subvertical thicker long vein traversing pieces 5 to 7D. Infilling carbonate +/- green clays. Some oxidation adjacent to vein in Pieces 8B & 8C.
**ADDITIONAL COMMENTS:** None.

### UNIT 22: APHYRIC BASALT

### Pieces 10A & 10B

**CONTACTS:** None observed, but Piece 10A has spherulitic texture that coarsens in adjacent Piece 10B.
**PHENOCRYSTS:** None observed.
**GROUNDMASS:** Spherulitic grading to variolitic. Cryprocrystalline and fine-grained.
**VESICLES:** 2%; 0.2-0.5 mm; circular; random; Carbonate infilling, green smectite infilling near veins.
**COLOR:** Medium gray (N5).
**STRUCTURE:** Top of thin flow.
**ALTERATION:** Slight. Greenish tinge to matrix indicates replacement by smectite. Oxidation halos (2-4 mm wide) to major vein in Pieces 10A & 10B. Vesicles infilled with carbonate and smectite.
**VEINS/FRACTURES:** 10%; 0.5-12.0 mm; subhorizontal; early subhorizontal carbonate-clay veinlets cut by later, wide (12 mm) Fe-stained carbonate-smectite vein infilling fracture that offsets smaller vein at base of Piece 10B.
**ADDITIONAL COMMENTS:** None.

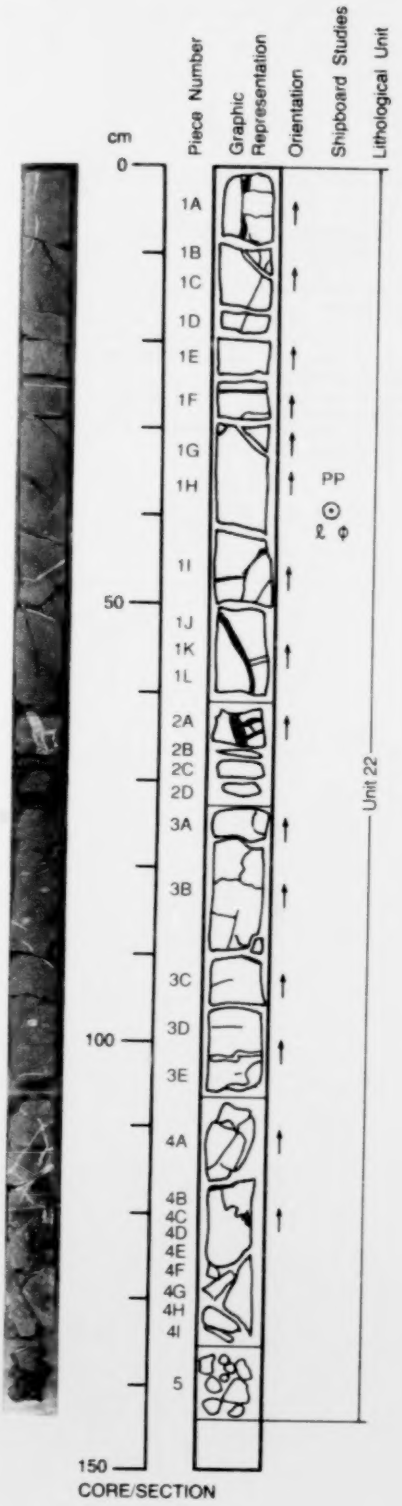
cm
Piece Number
Graphic Representation
Orientation
Shipboard Studies
Lithological Unit
0
50
100
150
1A
1B
1C
1D
1E
1F
1G
1H
1I
1J
1K
1L
2A
2B
2C
2D
3A
3B
3C
3D
3E
4A
4B
4C
4D
4E
4F
4G
4H
4I
5
PP
ℓ
Φ
Unit 22
CORE/SECTION

## 129-801C-7R-2

## UNIT 22: APHYRIC BASALT

### Pieces 1A-5

**CONTACTS:** None observed. Drilling rubble (Pieces 5) marginally finer grained than rest of Unit above in 7R-1.
**PHENOCRYSTS:** None observed.
**GROUNDMASS:** Fine-grained hypocrystalline. Quench textured throughout with fan variolites.
**VESICLES:** 2%; 0.1-0.4 mm; circular; random; infilled with either (mainly carbonate or zoned with green smectites and very occasionally a core of pyrite.
**COLOR:** Medium gray (N5).
**STRUCTURE:** Internal part of thin flow.
**ALTERATION:** Slight. Largely associated with vein material, then matrix adjacent replaced by smectite and/or pyrite.
**VEINS/FRACTURES:** 3%; 0.1-12.0 mm; random; irregular hair-like veinlets often cross-cut by large multiple carbonate-smectite +/- pyrite veins (Piece 2A); smectite may be oxidized and yellow stained.
**ADDITIONAL COMMENTS:** Continuation of Unit 22.

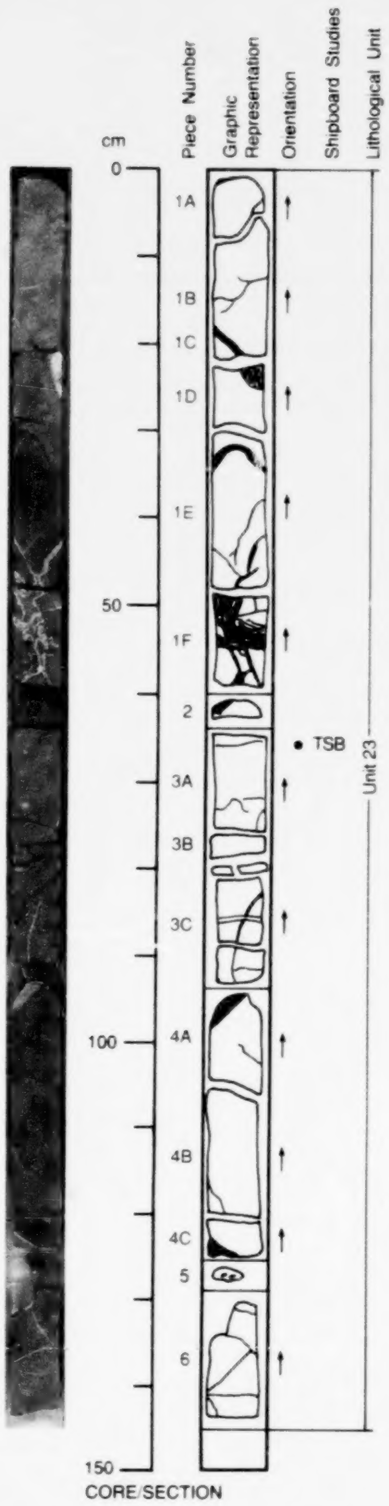
cm
Piece Number
Graphic Representation
Orientation
Shipboard Studies
Lithological Unit
0
50
100
150
1A
1B
1C
1D
1E
1F
2
3A
3B
3C
4A
4B
4C
5
6
TSB
Unit 23
CORE/SECTION

## 129-801C-7R-3

## UNIT 23: APHYRIC BASALT

### Pieces 1A-6

**CONTACTS:** None observed, but Piece 1A slightly finer in grain than rest of Unit below and may be near original flow top.

**PHENOCRYSTS:** None observed.

**GROUNDMASS:** Fine-grained, hypocrystalline. Quench textured throughout with fan variolites and skeletal plagioclase needles. Slight decrease in grain-size in Piece 3C and then increases again (no contacts seen).

**VESICLES:** 5%; 0.2-0.5 mm; circular; random; infilled with carbonate or green smectites; some with smectite rim and centre of coarse carbonate.

**COLOR:** Medium gray (N6).

**STRUCTURE:** Central portion of thin flow.

**ALTERATION:** Slight. Green smectites replace minor mesostasis. Carbonate and smectites infill vesicles. Smectite development in matrix adjacent to some veins.

**VEINS/FRACTURES:** 8%; 0.2-17.0 mm; variable; two sets (a) generally fine carbonate veins (<1 mm width) cut by (b) wide hydrothermal breccia zone (Pieces 1E, 1F, and 5); zone fragments coated with thin green smectite and then carbonate zones, with internal space filled with fine green smectite, sometimes oxidized, and carbonate.

**ADDITIONAL COMMENTS:** Hydrothermal breccia zone.

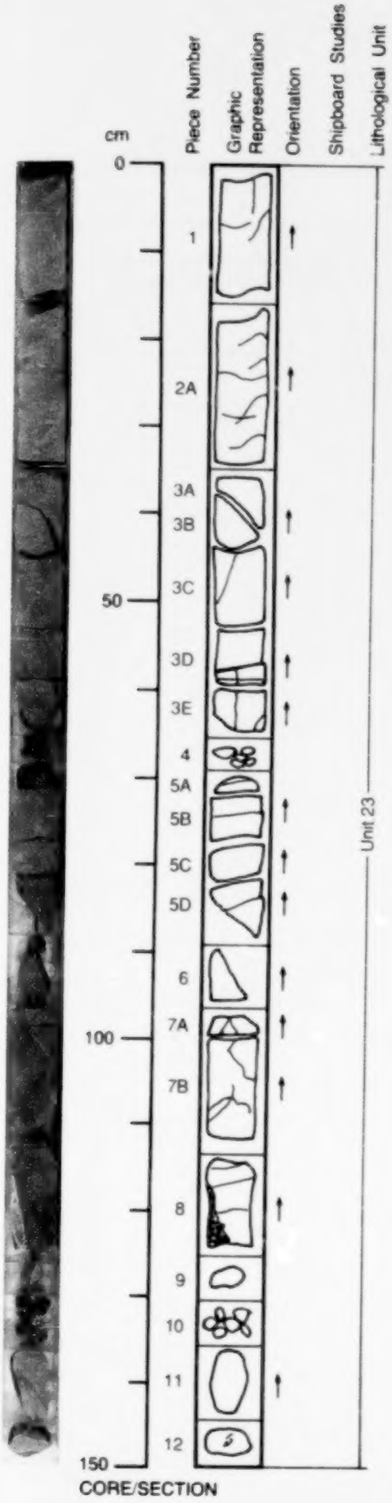
cm
Piece Number
Graphic Representation
Orientation
Shipboard Studies
Lithological Unit
0
50
100
150
1
2A
3A
3B
3C
3D
3E
4
5A
5B
5C
5D
6
7A
7B
8
9
10
11
12
Unit 23
CORE/SECTION

## 129-801C-7R-4

## UNIT 23: APHYRIC BASALT

### Pieces 1-12

**CONTACTS:** None observed. Piece 12 is marginally finer grained than rust of section and includes a few plagioclase microphenocrysts (possibly appraching Unit base?).
**PHENOCRYSTS:** None observed.
**GROUNDMASS:** Fine-grained, hypocrystalline. Quench textured throughout, but more granular appearance in some pieces.
**VESICLES:** 3%; 0.1-0.4 mm; circular; random; infilled with either carbonate or zoned smectites; rare pyrite granule-decorated vesicle walls with center of smectite or carbonate. Carbonate appears later and to replace smectite.
**COLOR:** Medium gray (N6).
**STRUCTURE:** Central portion of thin flow.
**ALTERATION:** Slight. Largely involving minor mesostasis, vesicles and matrix adjacent to the larger veins; smectite and carbonate replacements.
**VEINS/FRACTURES:** 2%; 0.1-16.0 mm; random; Often irregular, mainly small (0.1-1.0 mm) carbonate or smectite filled veinlets. Larger (16 mm wide) vein in Piece 8 composed of red & yellow oxidized green smectite and carbonate.
**ADDITIONAL COMMENTS:** None.

## 129-801C-7R-5

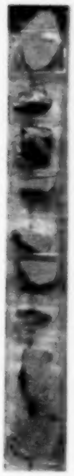

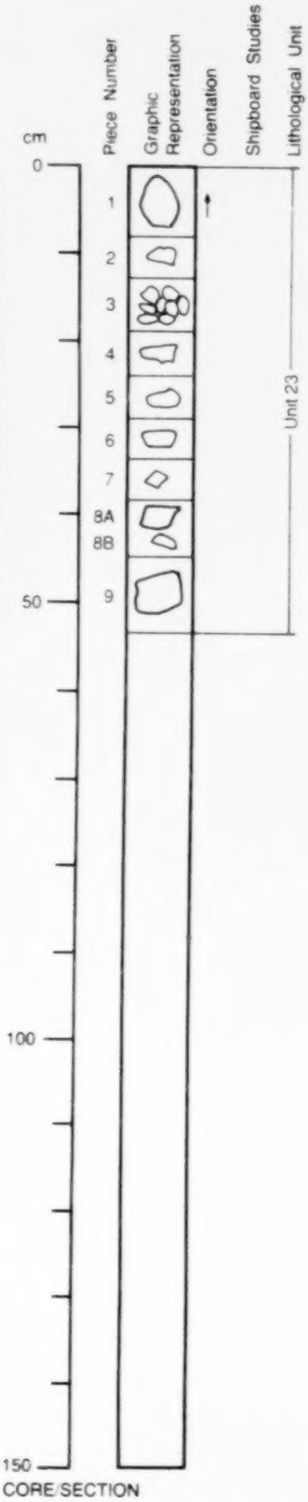
cm
Piece Number
Graphic Representation
Orientation
Shipboard Studies
Lithological Unit
0
1
2
3
4
5
6
7
8A
8B
9
50
100
150
Unit 23
CORE/SECTION

### UNIT 23: APHYRIC BASALT

### Pieces 1-9

**CONTACTS:** None observed. Piece 9 slightly finer grained than Piece 1 (and Section 7R-4 above.

**PHENOCRYSTS:** None observed.

**GROUNDMASS:** Fine-grained, hypocrystalline. Quench textured throughout, slight decrease in grain-size in Piece 9.

**VESICLES:** 1%; 0.2-0.4 mm; circular; spasmodic; carbonate or smectite infilling, some zoned with thin yellowish smectite rim, core of green smectite that may be replaced in the center by carbonate.

**COLOR:** Medium gray (N6).

**STRUCTURE:** Basal portion of a thin flow.

**ALTERATION:** Slight. Smectite and/or carbonate replacing mesostasis or infilling vesicles.

**VEINS/FRACTURES:** 1.0%; 0.2-1.0 mm; irregular; carbonate +/- smectite infilling.

**ADDITIONAL COMMENTS:** Continuation of Unit 23.

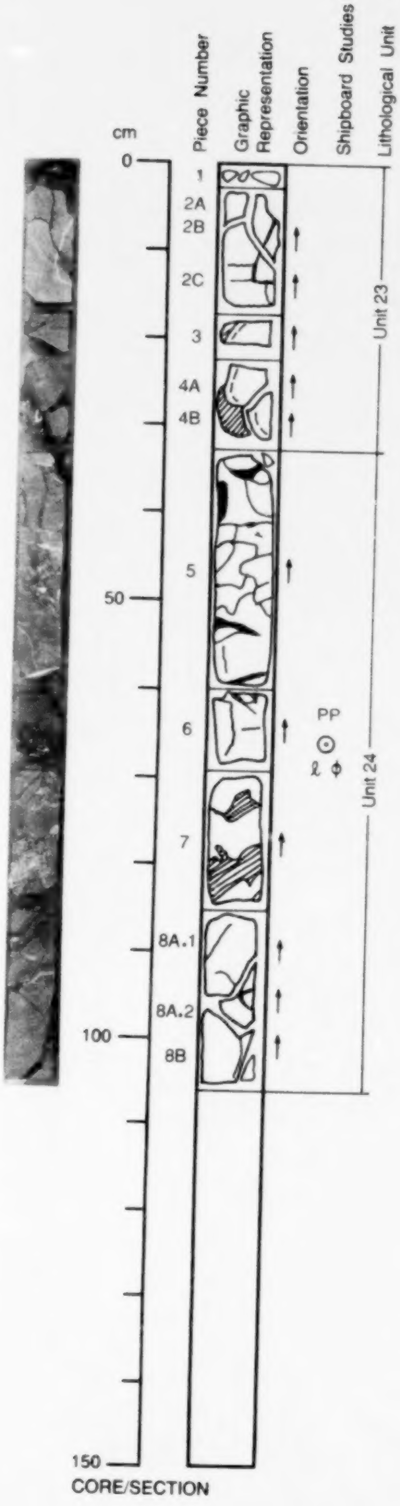

## 129-801C-8R-1

## UNIT 23: APHYRIC BASALT

### Pieces 1-4B

**CONTACTS:** Bottom margin is subrounded and adjacent to indurated, slightly calcareous, dark brown claystone.
**PHENOCRYSTS:** None observed.
**GROUNDMASS:** Glassy, devitrified rim grading to spherulitic zone, and finally to a hypocrystalline interior. Quench textured throughout; cryptocrystalline.
**VESICLES:** 1%; 0.2-0.5; subrounded; random; infilled with carbonate and smectite, sometimes zoned.
**COLOR:** Gray (N5-N6) with yellowish-brown tinge near the margin and grayish-green (5G 4/2) at the very rim.
**STRUCTURE:** Perhaps bottom part of a large pillow or thin flow.
**ALTERATION:** Moderate/high. Glassy rim shattered and replaced by white and green clays, spherulites and microlites turned to clays, vesicles all filled with carbonate and clays.
**VEINS/FRACTURES:** 5%; 0.1-2.0 mm; orthogonal; very irregular shapes and infilled with carbonate and green clays +/- pyrite.
**ADDITIONAL COMMENTS:** The upper Pieces (2A-2C) are texturally and compositionally similar to Unit 23 in 7R-5 and the above pieces probably represent the glassy margin to the whole Unit.

## UNIT 24: APHYRIC BASALT

### Pieces 5-8B

**CONTACTS:** None observed, but the top Pieces (5-7), which are cemented breccias, grade from glassy to variolitic from top to bottom.
**PHENOCRYSTS:** Few plagioclase, but <1%.
**GROUNDMASS:** Devitrified glassy fragments near the top, grading to spherulitic and variolitic fragments near the bottom of Piece 5. Pieces 6-8B are generally hypocrystalline. Fine-grained throughout.
**VESICLES:** 2%; 0.3-0.6 mm; round; random; infilled with dark green clays, or carbonate, or both.
**COLOR:** Greenish gray (5G 5/1) with brownish, Fe-hydroxoide stains grading to gray (N5) towards bottom Pieces (8A & 8B).
**STRUCTURE:** Top pieces are basically cemented breccias, but fragments of the breccia are texturally continuous and probably part of a pillow or lava flow top.
**ALTERATION:** Highly altered top to moderately altered bottom. Fragments in the cemented breccia on top are greenish throughout with Fe-hydroxide stained margins. Cementing the breccia are dark green clays and white carbonate; large cemented areas present in Piece 7; Pieces 8A & 8 are only moderately altered.
**VEINS/FRACTURES:** 45%; variable to 6 cm; irregular; infilled with green clays and carbonate. Narrow, regular veinlets are infilled with carbonate and pyrite +/- lighter green clays.
**ADDITIONAL COMMENTS:** Perhaps the top portion of this Unit was brecciated and then cemented in situ; consecutive fragments coarsen downwards.

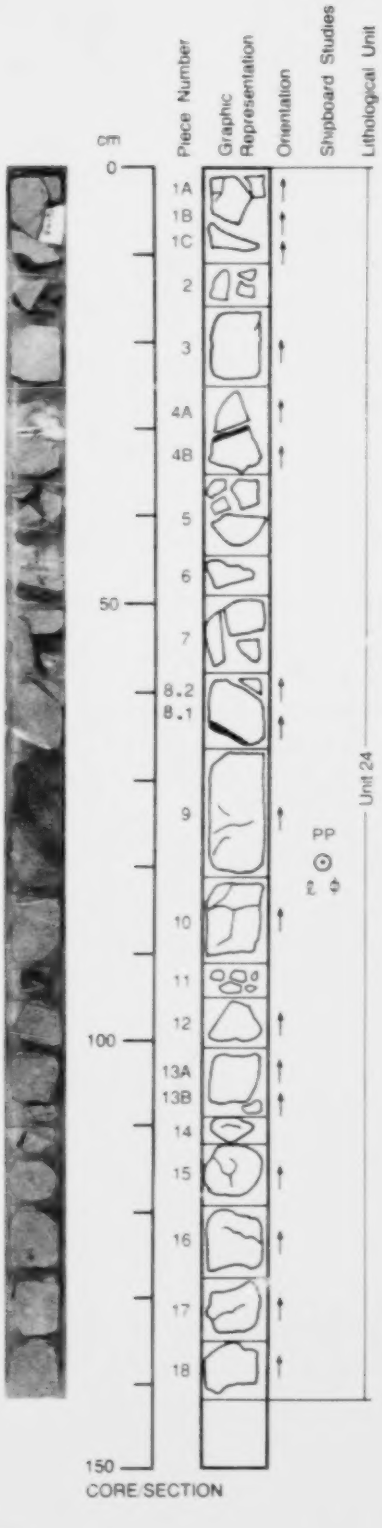
cm
Piece Number
Graphic Representation
Orientation
Shipboard Studies
Lithological Unit
0
50
100
150
1A
1B
1C
2
3
4A
4B
5
6
7
8.2
8.1
9
10
11
12
13A
13B
14
15
16
17
18
PP
Unit 24
CORE/SECTION

## 129-801C-8R-2

### UNIT 24: APHYRIC BASALT

### Pieces 1A-18

**CONTACTS:** Not observed.

**PHENOCRYSTS:** None observed.

**GROUNDMASS:** Fine-grained, hypocrystalline throughout, but slightly coarsening towards the bottom; more quench textured towards top portion.

**VESICLES:** 1%, 0.2-0.6 mm, rounded/subrounded; random; infilled with carbonate and clays that are sometimes interlayered together. A few vesicles near veinlets are infilled with dark green clays interlayered with fine pyrite grains.

**COLOR:** Gray (N5) with sparse, fine black and white dots.

**STRUCTURE:** Perhaps fragmented portion of pillow or thin flow.

**ALTERATION:** Slight/moderate. Glassy mesostasis turned into green clays; clays and carbonate vesicle infillings throughout. A few larger plagioclase microlites are altered to carbonate.

**VEINS/FRACTURES:** 10%, 0.1-6.0 mm, irregular; the pieces of 8R-2 are basically broken along fractures infilled with green clays or carbonate; some carbonate veinlets are lined with fine pyrite crystals.

**ADDITIONAL COMMENTS:** None.

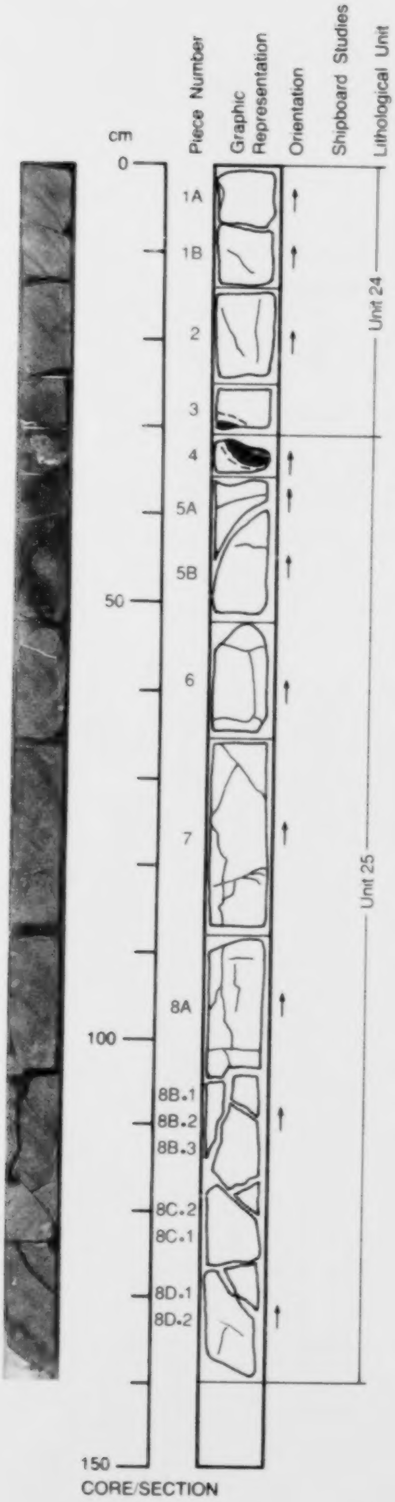

# 129-801C-9R-1

## UNIT 24: APHYRIC BASALT

### Pieces 1A-3

**CONTACTS:** Bottom contact with calcified reddish, interpillow sediment is a devitrified glassy rim with a few plagioclase and olivine microphenocrysts that grades upwards to a spherulitic zone.
**PHENOCRYSTS:** None observed, except for relatively few near bottom contact.
**GROUNDMASS:** Hypocrystalline, fine-grained. Devitrified glassy base coarsening upwards to a spherulitic zone. Abundant pyrite near rim zone.
**VESICLES:** 0.5%; 0.2-0.4 mm; Rounded/subrounded; random; infilled with translucent dark green clay, or more rarely carbonate +/- pyrite near base.
**COLOR:** Gray (N5).
**STRUCTURE:** Bottom of thin flow.
**ALTERATION:** Slight to moderate. Vesicles filled with clays and carbonate; original glassy mesostasis altered to greenish clays. Pyrite partly replaces crystals near base.
**VEINS/FRACTURES:** 2%; 0.2-1.5 mm; irregular; mostly infilled with carbonate; thicker veins (e.g. piece 2) have zones of greenish clays and a few specks of pyrite along the walls.
**ADDITIONAL COMMENTS:** Similar to upper part of Unit 24 in 8R-4, continuation of Unit. Pyrite replaces microlites and rim fractures at bottom margin.

## UNIT 25: APHYRIC BASALT (PATCHES OF SPARSELY PLAGIOCLASE MICROPHYRIC BASALT)

### Pieces 4-8D.2

**CONTACTS:** Top margin is in contact with green clay and red carbonate- altered interpillow material. Rim is devitrified glass tha grades downwards to a variolitic zone.
**PHENOCRYSTS:** Microphenocrysts very sparsely scattered throughout rest of section which is essentially aphyric.
Plagioclase <1%; 0.4 average; Subhedral small laths (one 2 mm long megacryst near glassy rim). Slight to moderate alteration to clays, carbonate and occasionally pyrite.
**GROUNDMASS:** Devitrified glassy rim grading to variolitic zone and then hypocrystalline interior. Generally fine-grained, but with patchy distribution of glassy mesostasis.
**VESICLES:** 2%; 0.15-0.60 mm; rounded/subrounded; random; infilled with carbonate, clays and occasional pyrite (zoning common). Patchy distribution. Piece 2 has >2%, other areas <1%.
**COLOR:** Gray (N5).
**STRUCTURE:** Thin flow top (drilling fractured, Piece 8).
**ALTERATION:** Slight to moderate. Vesicles infilled with green clays and carbonate; mesostasis and plagioclase variably replaced by green clays and carbonate. Specks of pyrite in groundmass and replacing microlites in rim zone near fractures.
**VEINS/FRACTURES:** 2%; 0.1-2.0 mm; irregular; mostly infilled with carbonate and some green clays. Green clays in fracture in Pieces 7& 8A. Pyrite fillings and attendant halos conspicous near top margin.
**ADDITIONAL COMMENTS:** Concentration of pyrite near top margin as vein infilling and replacement material.

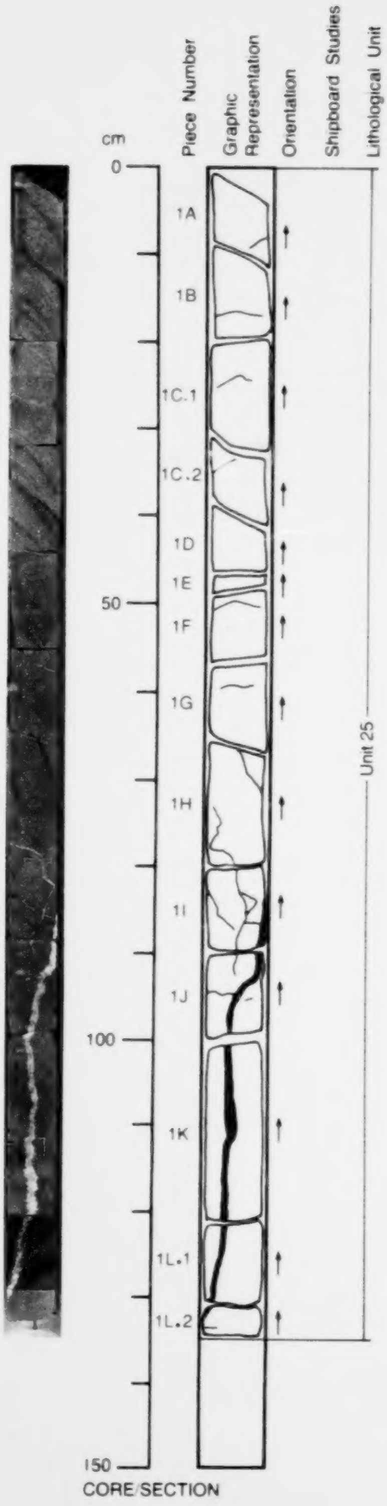
cm
Piece Number
Graphic Representation
Orientation
Shipboard Studies
Lithological Unit
0
50
100
150
1A
1B
1C.1
1C.2
1D
1E
1F
1G
1H
1I
1J
1K
1L.1
1L.2
Unit 25
CORE/SECTION

## 129-801C-9R-2

## UNIT 25: APHYRIC BASALT (PATCHES OF SPARSELY PLAGIOCLASE-OLIVINE MICROPHYRIC BASALT)

### Pieces 1A-1L.2

**CONTACTS:** Not observed.
**PHENOCRYSTS:** Highly variable and patchy distribution.
Plagioclase - 1%; 0.4; Subhedral laths. Partly altered to clays, carbonate and occasional pyrite when close to fracture.
Olivine - trace; 0.3; skeletal to subhedral. Altered to green clays.
**GROUNDMASS:** Hypocrystalline and fine-grained. Patchy distribution of glassy mesostasis and vesicles. Slight coarsening downwards.
**VESICLES:** 4-5%; 0.1-0.6 mm; subrounded; random; infilled with carbonate, pale and dark green clays, occasionally pyrite; zoning of infilling material not uncommon.
**COLOR:** Gray (N5).
**STRUCTURE:** Interior of a flow.
**ALTERATION:** Slight to moderate. Vesicles infilled, mesostasis, plagioclase and olivine replaced by green clays and carbonate. Replacement also by pyrite if near fracture. Occasional pyrite in groundmass.
**VEINS/FRACTURES:** 4%; 0.1-8.0 mm; random; irregular, branching and cross-cutting, infilled with white (or red stained) carbonate and less commonly green clay, sometimes pyrite; zoning common. Wide (c.8 mm), irregular carbonate infilled fracture in pieces 1I-1L.2 may be lined with zeolites.
**ADDITIONAL COMMENTS:** Patchy distribution of microphenocrysts and vesicles probably due to flow differentiation.

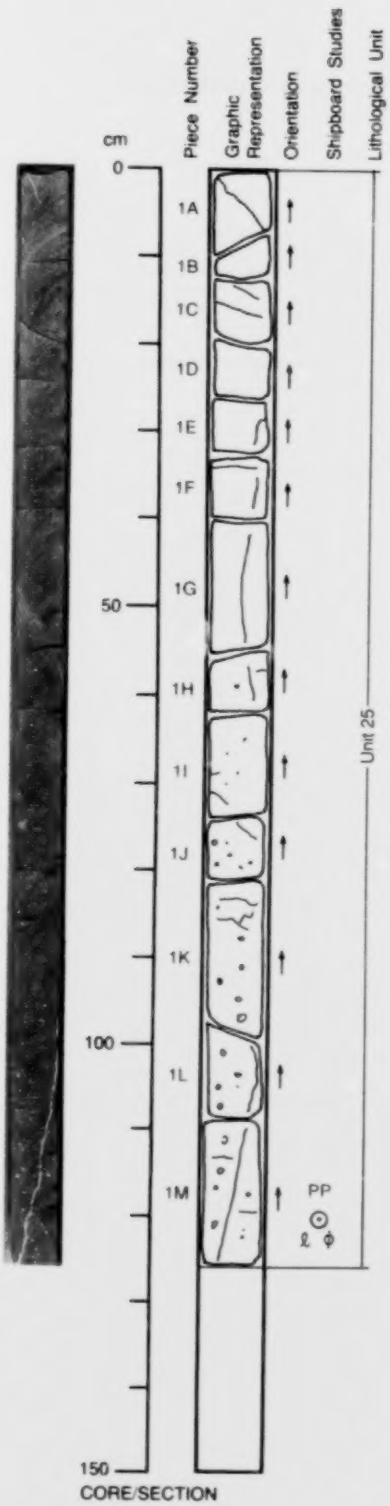
cm
Piece Number
Graphic Representation
Orientation
Shipboard Studies
Lithological Unit
0
50
100
150
1A
1B
1C
1D
1E
1F
1G
1H
1I
1J
1K
1L
1M
PP
ℓ ⊙ ϕ
Unit 25
CORE/SECTION

## 129-801C-9R-3

## UNIT 25: APHYRIC BASALT (PATCHS OF SPARSELY PLAGIOCLASE MICROPHYRIC BASALT)

### Pieces 1A-1M

**CONTACTS:** None observed.
**PHENOCRYSTS:** Patchy distribution.
Plagioclase - c.1%; 0.3; Subhedral laths. Altered to clays and carbonate.
**GROUNDMASS:** Hypocrystalline and fine-grained grading to slightly coarser, holocrystalline towards base. Patchy distribution of mesostasis, vesicles and microphenocrysts.
**VESICLES:** 10%; 0.2-5.0 mm; rounded/subrounded; random; infilled with carbonate, pale and dark green clays, occasionally pyrite; sometimes all three in concentric fashion. Vesicle size increases from top to bottom, with basal vesicles exclusively infilled with carbonate, often as large clear crystals in centre. Occasional pyrite specks on vesicle margins.
**COLOR:** Gray (N5) with dark green spots at the top and white spots at the base.
**STRUCTURE:** Massive, but fractured. Interior of thin flow.
**ALTERATION:** Slight to moderate, similar to 9R-2.
**VEINS/FRACTURES:** 3%; 0.1-3.0 mm; random; irregular, branching and cross-cutting infilled with mostly carbonate, less commonly green clays which are typical infill of narrower veinlets. Rarer pyrite infill.
**ADDITIONAL COMMENTS:** Unusually large, carbonate infilled vesicles at base. Flow distribution of microphenocrysts.

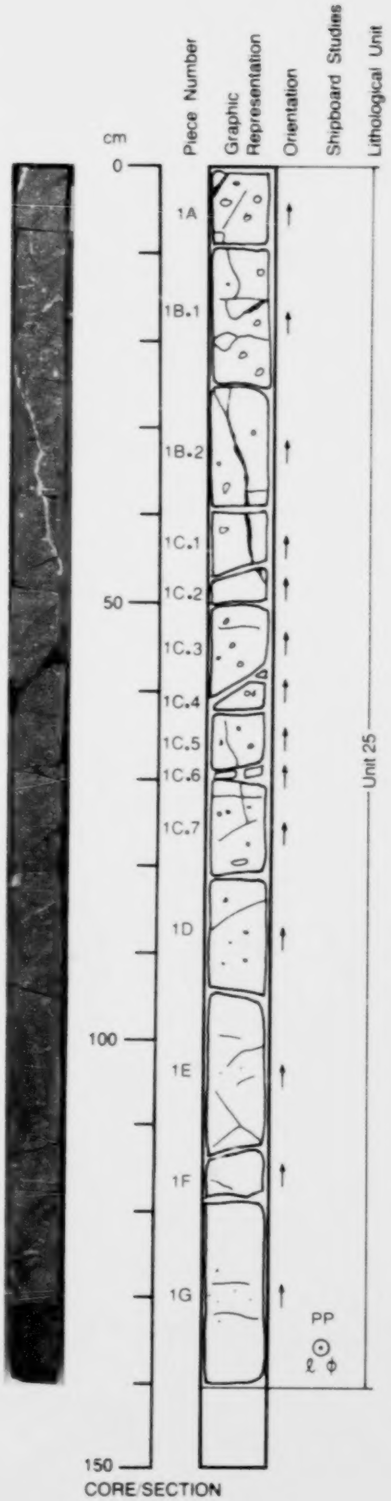
cm
Piece Number
Graphic Representation
Orientation
Shipboard Studies
Lithological Unit
0
50
100
150
1A
1B.1
1B.2
1C.1
1C.2
1C.3
1C.4
1C.5
1C.6
1C.7
1D
1E
1F
1G
PP
ℓ ϕ
Unit 25
CORE/SECTION

## 129-801C-9R-4

## UNIT 25: APHYRIC BASALT (PATCHES OF SPARSELY PLAGIOCLASE MICROPHYRIC BASALT)

### Pieces 1A-1G

**CONTACTS:** None observed.
**PHENOCRYSTS:** Very patchy distribution.
Plagioclase - c.1%; 0.4; Subhedral laths. Partly altered to clays and carbonate.
**GROUNDMASS:** Holocrystalline at top grading to slightly finer grained, hypocrystalline base. Random, patchy distribution of vesicles, microphenocrysts and mesostasis.
**VESICLES:** 8%; 0.6-7.0 mm; rounded to subangular; random; larger ones commonly infilled with carbonate +/- green clays and specks of pyrite on walls. Smaller ones infilled with pale and dark green clays with little pyrite. Larger vesicles may exhibit clear calcite crystals in center or a small cavity.
**COLOR:** Generally gray (N5) with white spots at the top grading to smaller dark green spots at base.
**STRUCTURE:** Massive, but fractured. Interior of a flow.
**ALTERATION:** Slight to moderate; similar to 9R-2.
**VEINS/FRACTURES:** 4%; 0.1-5.0 mm; irregular; infilled with carbonate +/- green clays and pyrite, with narrower veinlets preferentially infilled with green clays. Branching and cross-cutting. Traces of zeolites along the margin of wider veins.
**ADDITIONAL COMMENTS:** General tendency for grain-size and vesicle abundance to decrease towards base.

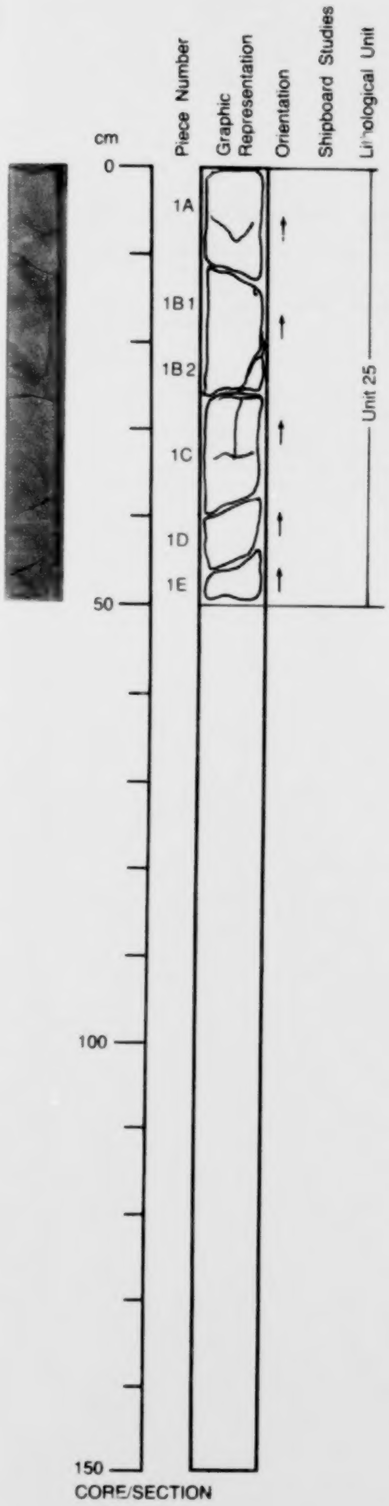
cm
Piece Number
Graphic Representation
Orientation
Shipboard Studies
Lithological Unit
0
50
100
150
1A
1B1
1B2
1C
1D
1E
Unit 25
CORE/SECTION

## 129-801C-9R-5

## UNIT 25: APHYRIC BASALT (PATCHES OF SPARSELY PLAGIOCLASE MICROPHYRIC BASALT)

### Pieces 1A-1E

**CONTACTS:** None observed, but fining towards bottom.
**PHENOCRYSTS:** Variable distribution.
Plagioclase - c.1%; 0.3; Subhedral laths. Partial replcement by carbonate and green clays.
**GROUNDMASS:** Hypocrystalline; fine-grained throughout but slight fining towards the bottom. Quench textured throughout with glassy mesostasis.
**VESICLES:** 1%; 0.8-1.9 mm; rounded/subrounded; random; infilled with pale and dark green clays; some pyrite lining walls. Vesicles in Pieces 1D & 1E show green clay infilling partly replaced by carbonate.
**COLOR:** Gray (N5) with some dark green spots.
**STRUCTURE:** Thin flow, but approaching base(?).
**ALTERATION:** Slight to moderate, similar to 9R-2.
**VEINS/FRACTURES:** 1%; 0.1-0.2 mm; mostly subhorizontal; infilled with carbonate, green clays and few specks of pyrite.
**ADDITIONAL COMMENTS:** Continuation of Unit 25 and still slightly fining downwards. Carbonate in vesicles replaces earlier green clays.

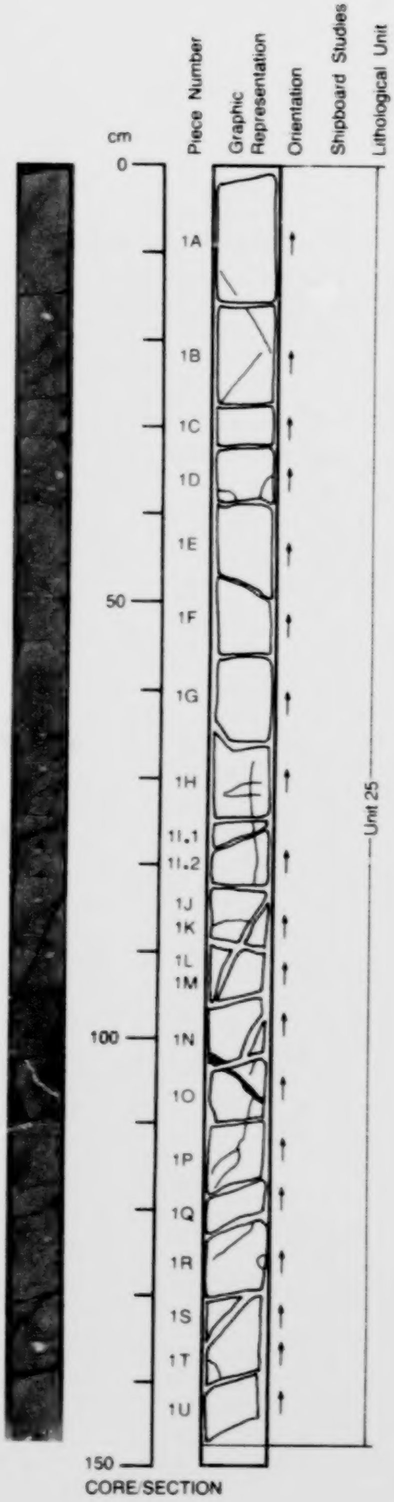
cm
Piece Number
Graphic Representation
Orientation
Shipboard Studies
Lithological Unit
0
50
100
150
1A
1B
1C
1D
1E
1F
1G
1H
1I.1
1I.2
1J
1K
1L
1M
1N
1O
1P
1Q
1R
1S
1T
1U
Unit 25
CORE/SECTION

## 129-801C-10R-1

## UNIT 25: APHYRIC BASALT (PATCHES OF SPARSELY PLAGIOCLASE MICROPHYRIC BASALT)

### Pieces 1A - 1U

**CONTACTS:** Not observed.
**PHENOCRYSTS:** Patchy distribution of microphenocrysts that have better morphologies than often quench textured matrix plagioclase.
Plagioclase - c.1%; 0.3; Subhedral laths. Slight alteration to greenish clays; some have specks of pyrite.
**GROUNDMASS:** Fine-grained and hypocrystalline throughout.
**VESICLES:** Trace; 0.5-1.0 mm; rounded/subrounded; random; mostly infilled with green clays and some carbonate; some zonation of clay and carbonate. Occasional pyrite infills.
**COLOR:** Grays (N5 & N6).
**STRUCTURE:** Interior of thick flow.
**ALTERATION:** Slight. Vesicles in filled with clays and carbonate; similar products replace microphenocrysts and mesostasis. Occasional specks of pyrite.
**VEINS/FRACTURES:** 3%; 0.1-5.0 mm; random; very irregular and infilled with mostly carbonate and, less commonly, green clays. Occasional specks of pyrite present in some veinlets. Radiate zeolite fibers present on margin of largest vein (Piece 1O).
**ADDITIONAL COMMENTS:** Texturally and compositionally the continuation of Unit 25.

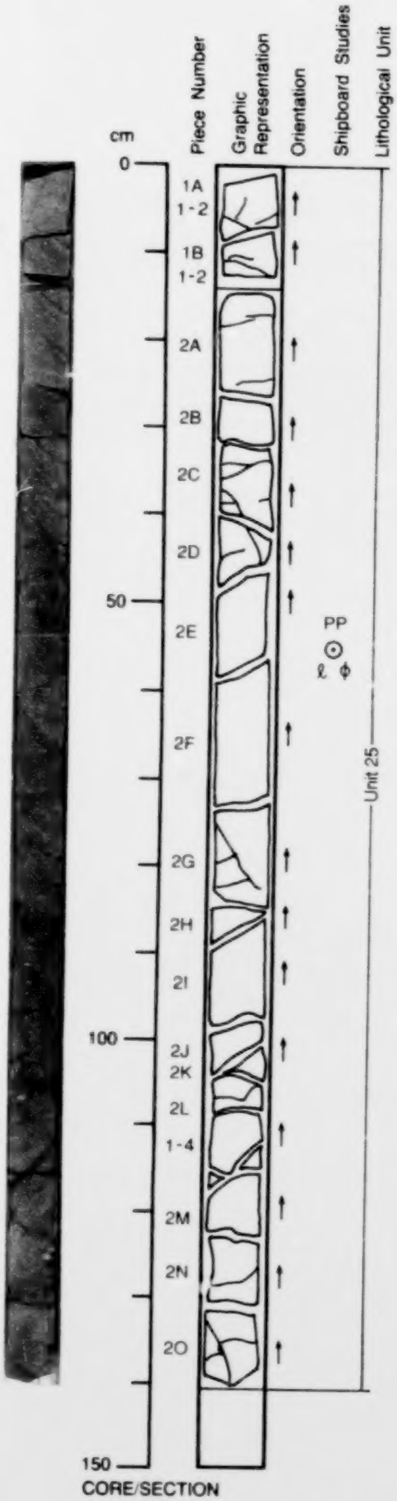
cm
Piece Number
Graphic Representation
Orientation
Shipboard Studies
Lithological Unit
0
50
100
150
1A
1-2
1B
1-2
2A
2B
2C
2D
2E
2F
2G
2H
2I
2J
2K
2L
1-4
2M
2N
2O
PP
ℓ ϕ
Unit 25
CORE/SECTION

## 129-801C-10R-2

## UNIT 25: APHYRIC BASALT

### Pieces (1A-2O)

**CONTACTS:** None observed.
**PHENOCRYSTS:** Very occasional olivine microphenocrysts and a lesser proportion of plagioclase (all <1%) randomly scattered throughout.
**GROUNDMASS:** Fine-grained, hypocrystalline. Often elongated quenched crystals; more intergranular texture elsewhere. Random mesostasis distribution.
**VESICLES:** <1%; 0.5-1.5 mm; circular; random; green smectite infilling.
**COLOR:** Gray (N5) with few dark green spots (Pieces 1A and 2C).
**STRUCTURE:** Massive, but fractured. Central portion of thick flow.
**ALTERATION:** Slight. Relatively uniform throughout. Largely pale and dark green smectite replacing original glassy mesostasis and infilling the few vesicles.
**VEINS/FRACTURES:** c.1%; 0.1-1.0 mm; random; no preferred orientation, irregular veinlets cross-cutting, infilled with either carbonate or green smectite.
**ADDITIONAL COMMENTS:** Continuation of Unit 25; decrease in proportion of vesicles relative to same unit in core 9R.

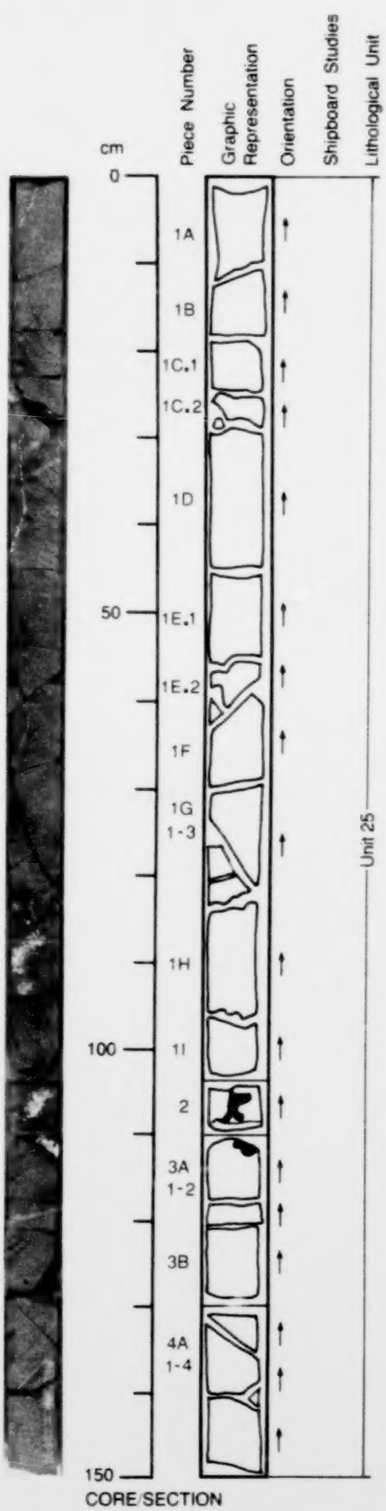
cm
Piece Number
Graphic Representation
Orientation
Shipboard Studies
Lithological Unit
0
50
100
150
1A
1B
1C.1
1C.2
1D
1E.1
1E.2
1F
1G
1-3
1H
1I
2
3A
1-2
3B
4A
1-4
Unit 25
CORE/SECTION

## 129-801C-10R-3

## UNIT 25: APHYRIC BASALT

### Pieces 1A-4A.4

**CONTACTS:** None seen.
**PHENOCRYSTS:** Few olivine (and possibly pyroxene) microphenocrysts scattered throughout section, but overall <1%.
**GROUNDMASS:** Fine-grained, with gradation downwards from holocrystalline, intergranular texture to well-defined quench texture with occasional mesostasis (now replaced).
**VESICLES:** None observed.
**COLOR:** Medium gray (N6).
**STRUCTURE:** Massive, but fractured. Interior of thick flow.
**ALTERATION:** Slight. Dark green smectite replaces olivine microphenocrysts and mesostasis.
**VEINS/FRACTURES:** 5%; 0.2-4.0 mm; mainly subvertical; infilled with mainly carbonate (larger veinlets) and dark green smectite (very fine veinlets). Also irregular carbonate-smectite replacement patches in matrix (e.g. Piece 2) with smectite halos (10 mm wide); three generations of carbonate replacement leaving smectite relicts, minor pyrite associated.
**ADDITIONAL COMMENTS:** Continuation of Unit 25.

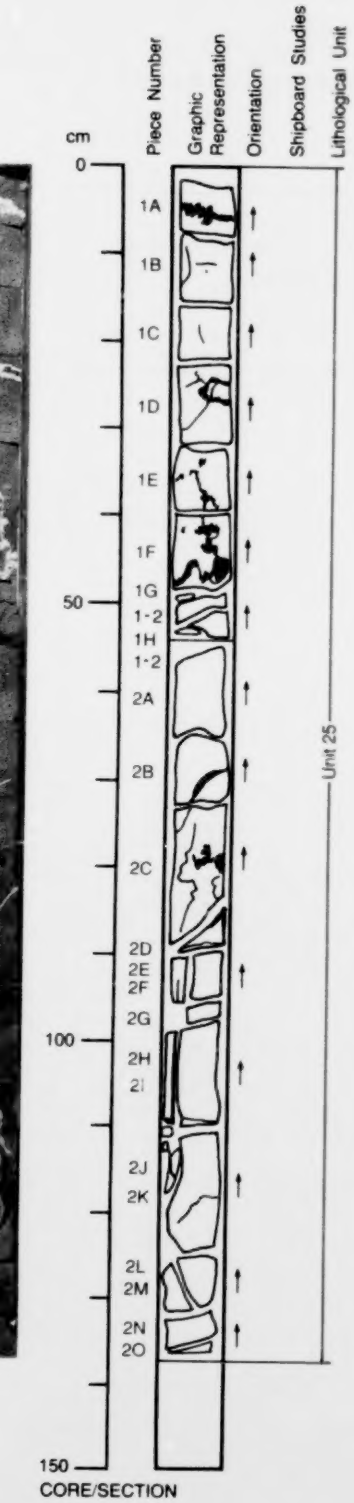
cm
Piece Number
Graphic Representation
Orientation
Shipboard Studies
Lithological Unit
0
50
100
150
1A
1B
1C
1D
1E
1F
1G
1-2
1H
1-2
2A
2B
2C
2D
2E
2F
2G
2H
2I
2J
2K
2L
2M
2N
2O
Unit 25
CORE/SECTION

## 129-801C-10R-4

## UNIT 25: APHYRIC BASALT

### Pieces 1A-2O

**CONTACTS:** None observed.
**PHENOCRYSTS:** None observed.
**GROUNDMASS:** Fine-grained, hypocrystalline; often intergranular texture, but still with some quenched crystals. Relative uniform throughout with little grain-size variation down section.
**VESICLES:** <0.5%; 0.5-1.0 mm; circular; random; carbonate infilling.
**COLOR:** Medium gray (N6) and finely speckled.
**STRUCTURE:** Massive, but fractured. Interior of thick flow.
**ALTERATION:** Slight. Green smectite replaces mesostasis; carbonate infills vesicles and veins; carbonate and smectite irregularly replace matrix adjacent to very irregular veins.
**VEINS/FRACTURES:** 8%; 0.2-3.0 mm; random; either green smectite or carbonate infillings. Larger very irregular, ramifying veins that also replace adjacent matrix - mainly carbonate with green smectite and pyrite (good crystal form).
**ADDITIONAL COMMENTS:** Continuation of Unit 25. Few occasional olivine microphenocrysts.

## 129-801C-10R-5

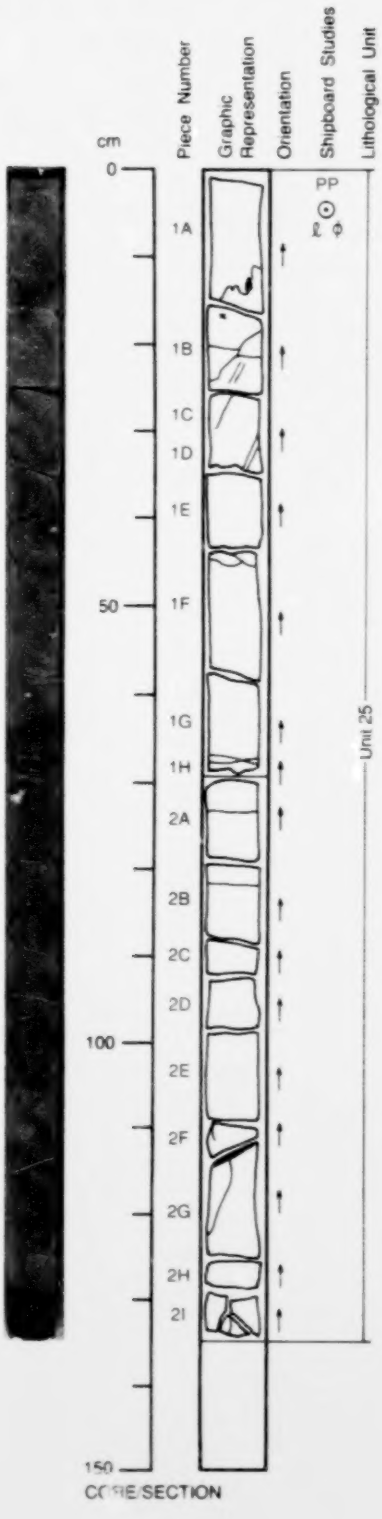
cm
Piece Number
Graphic Representation
Orientation
Shipboard Studies
Lithological Unit
0
PP
1A
1B
1C
1D
1E
50
1F
1G
1H
Unit 25
2A
2B
2C
2D
100
2E
2F
2G
2H
2I
150
CORE/SECTION

### UNIT 25: SPARSELY OLIVINE MICROPHYRIC BASALT

### Pieces 1A-2I

**CONTACTS:** None observed.

**PHENOCRYSTS:** Some of the smaller olivines may not be true microphenocrysts, but part of matrix.

Olivine - 1-2%; 0.1-0.2; Subhedral, replaced by green smectite.

**GROUNDMASS:** Fine-grained, largely holocrystalline, with very minor mesostasis. Intergranular with some long skeletal crystals.

**VESICLES:** <1%; 0.2 mm; circular; random; green smectite infilling.

**COLOR:** Medium gray (N5).

**STRUCTURE:** Massive, but fractured. Interior of thick flow.

**ALTERATION:** Slight few % only. Green smectite infilling vesicles, replacing olivine and mesostasis.

**VEINS/FRACTURES:** <1%; 0.2-0.8 mm; generally subhorizontal; carbonate and green smectite infillings.

**ADDITIONAL COMMENTS:** Continuation if Unit 25.

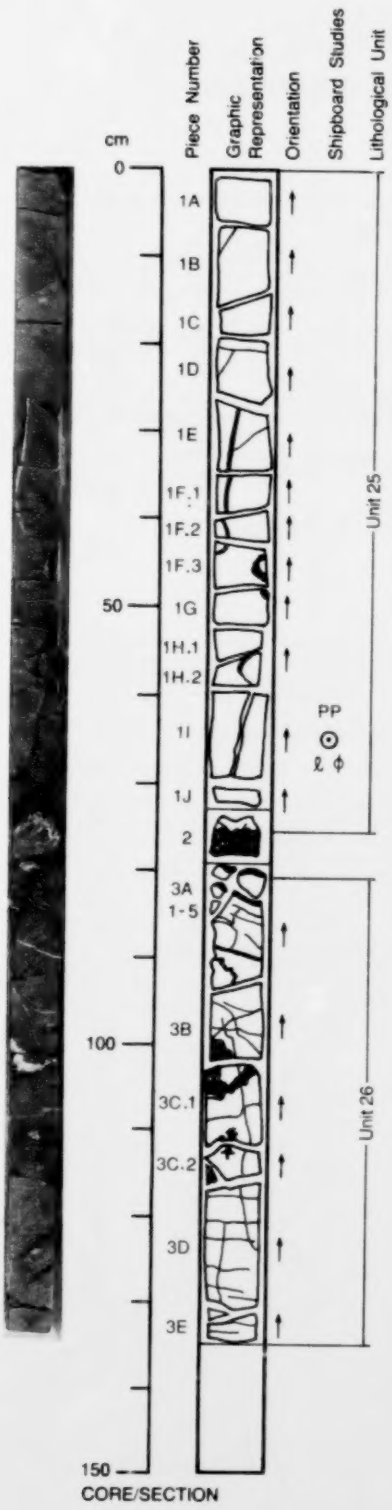

## 129-801C-10R-6

## UNIT 25: SPARSELY OLIVINE-PLAGIOCLASE MICROPHYRIC BASALT

### Pieces 1A-2 (top part)

**CONTACTS:** Base observed with interflow sediment in Piece 2. Also decrease downwards of grain-size and textural change from intergranular to fine quenched textured and spherultic margin at contact.

**PHENOCRYSTS:** Concentrated in upper part (generally absent in Pieces 1I & 1J) and basal contact zone.

Plagioclase - 1%; 0.3-0.5; two generations, larger crystals and small laths within margin spherulitic zone.

Olivine - 1%; 0.2; Subhedral. Replaced by green smectite.

**GROUNDMASS:** Fine-grained, holocrystalline in upper part, replaced by quenched textured matrix and spherulitic zone at contact.

**VESICLES:** <0.5%; 0.1-0.2 mm; circular; random; infilled with carbonate and green smectite.

**COLOR:** Medium/darkish gray (N5).

**STRUCTURE:** Fractured. Basal portion of thick flow.

**ALTERATION:** Slight (few % only). Olivine microphenocrysts replaced by green smectite. Vesicles and veins infilled with carbonate and/or clay.

**VEINS/FRACTURES:** 1%; 0.1-0.4 mm; random; finer veinlets infilled with dark green smectite, larger subvertical vein show coarse carbonate replacing dark green smectite. Intermittant pyrite veinlets, especially in contact zone.

**ADDITIONAL COMMENTS:** Base of thick flow Unit 25 adjacent to calcareous (replacement?) red claystone which represents interflow material.

## UNIT 26: MODERATELY OLIVINE-PLAGIOCLASE MICROPHYRIC BASALT

### Pieces 3A.1-3E

**CONTACTS:** Top margin indicated by interflow sediment adjacent to spherulitic zone that coarsens downwards with good quench texture developed.

**PHENOCRYSTS:** Glomerophyric groups of olivine in top margin zone.

Plagioclase - 1%; 0.1-0.2; Subhedral. Largely concentrated in top margin zone with few lower down Unit.

Olivine - 3%; 0.1; euhedral/subhedral. Partial replacement by green smectite and red "iddingsite" or hematite veinlets.

**GROUNDMASS:** Microcrystalline, fine-grained. Spherulitic in top margin zone, quenched crystals throughout.

**VESICLES:** None observed.

**COLOR:** Medium gray (N5/N6).

**STRUCTURE:** Top of thin flow.

**ALTERATION:** Slight. Largely green smectite replacing microphenocrysts with minor red "iddingsite" or hematite. Minor pyrite granules.

**VEINS/FRACTURES:** 10%; 0.2-2.0 mm; random, mainly subvertical or subhorizontal; infilling either carbonate or smectite with carbonate in centre. Patchy replacement of matrix adjacent to veins in Piece 3C.1 with smectite margins and dominant carbonate cores.

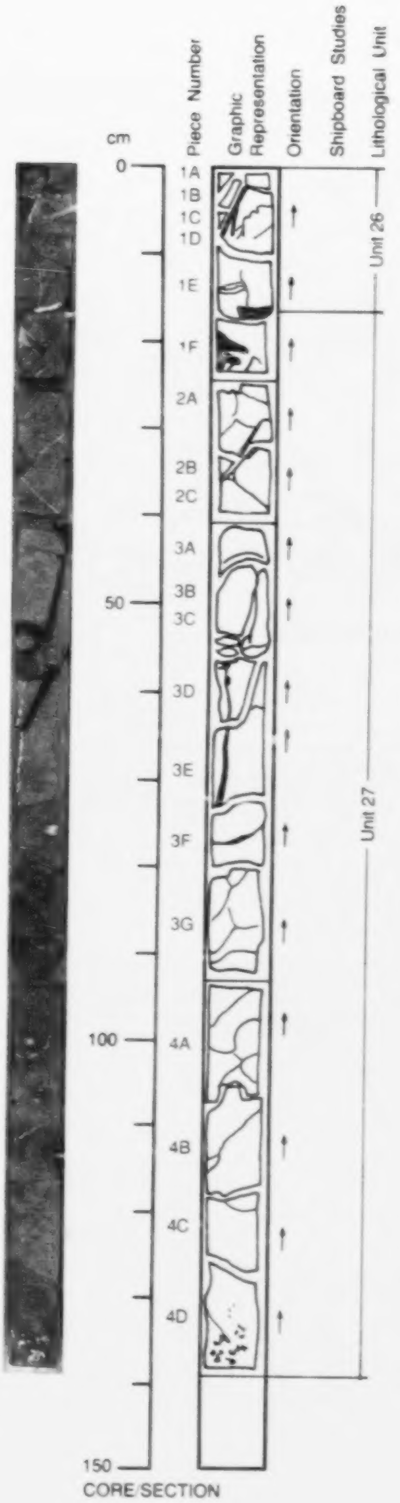

## 129-801C-11R-1

## UNIT 26: MODERATELY OLIVINE-PLAGIOCLASE MICROPHYRIC BASALT

### Pieces 1A - 1E

**CONTACTS:** Small 4 mm wide carbonated interflow material (?) at base of Piece 1E with an adjacent oxidized spherulitic zone that coarsens upwards.

**PHENOCRYSTS:**

Plagioclase - 2%; 0.7-1.2; Subhedral laths.

Olivine - 2%; 0.4; Euhedral/subhedral; minor smectite replacement.

**GROUNDMASS:** Fine-grained/microcrystalline with spherulites at contact. Grain-size coarsens upwards.

**VESICLES:** 3%; 0.2-0.4 mm; circular; random; infilled with carbonate, dark green smectite or late red hematite in oxidized zones of basal margin.

**COLOR:** Dark gray (N4).

**STRUCTURE:** Basal section of thin flow.

**ALTERATION:** Slight. Thin (2-4 mm) oxidation halos to veins in basal zone with development of hematite in matrix and vesicles. Scattered pyrite and yellow oxidized green smectite in veinlets.

**VEINS/FRACTURES:** 5%; 0.2-3.0 mm; random; irregular and branching with carbonate, smectite +/- pyrite infilling. Oxidized halos adjacent to veins in basal zone.

## UNIT 27: SPARSELY PLAGIOCLASE MICROPHYRIC BASALT

### Pieces 1F - 4D

**CONTACTS:** Not observed but top margin is cryptocrystalline and contains a xenolith of calcified interpillow sediments (?) rimmed with devitrified glass; coarsens slightly towards the bottom.

**PHENOCRYSTS:** A few olivine (+ pyroxene ?) microphenocrysts are present but the amount is <<1%; altered to dark green clays.

Plagioclase - ~1%; 0.3 - 1.5; Subhedral stubby to slender laths; a few are fairly fresh but others are moderately altered.

**GROUNDMASS:** Cryptocrystalline top grading to hypocrystalline bottom; a devitrified glassy rim around a reddish xenolith (?) near the top.

**VESICLES:** 5%; 0.2 - 0.8 mm; subrounded - rounded; random; infilled with carbonate and clays, or both, +/- pyrite; A few are completely infilled with pyrite, particularly those near the top or near veinlets; large, very irregular cavities in piece 4D are infilled with carbonate +/- green clays and occasionally rimmed with pyrite.

**COLOR:** Dark gray (N4) grading to gray (N5) towards the bottom; with fine, black or white dots.

**STRUCTURE:** Perhaps top of a thin flow.

**ALTERATION:** Slight to moderate; vesicles are infilled with secondary minerals; lots of pyrite near the top and along veinlets; mesostasis and olivine are altered to green clays.

**VEINS/FRACTURES:** 5%; 0.5 - 2.0 mm; very irregular; infilled with carbonate but rimmed with green clays +/- a few specks of pyrite; generally have well-defined and more altered than groundmass halos containing disseminated fine pyrite; branching and cross-cutting.

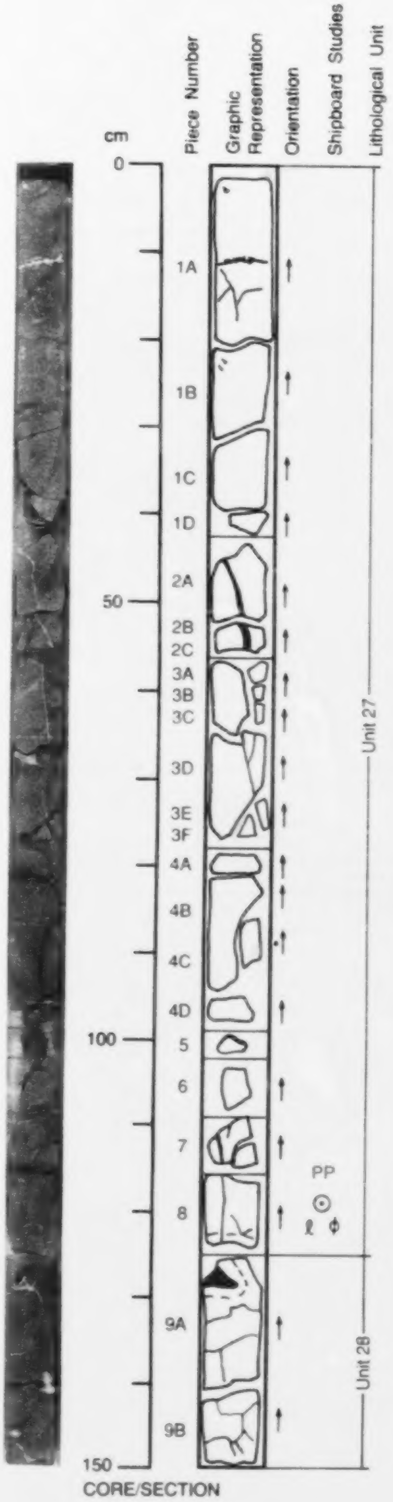

## 129-801C-11R-2

## UNIT 27: SPARSELY PLAGIOCLASE-OLIVINE MICROPHYRIC BASALT

### Pieces 1A - 8

**CONTACTS:** Not observed but the bottom margin has a portion of a devitrified glassy rim that coarsens towards the top.

**PHENOCRYSTS:**

Plagioclase - 1%; 0.4 - 1.2; Subhedral stubby and slender laths; slight to moderately altered; a couple of megaphyric ones (up to 1.2 cm) in piece 4B.

Olivine - trace; 0.2 - 1.0 mm; Subhedral plates and a few hopper shaped ones; altered to green clays veined with whitish clays; a couple of megacrysts (up to 3 mm) are attached to plagioclase megacrysts.

**GROUNDMASS:** Hypocrystalline with a devitrified, glass rims at the bottom; cryptocrystalline throughout.

**VESICLES:** ~2%; 0.3 - 0.6; subrounded - rounded; random; infilled with green clays, carbonate, and occasionally, pyrite.

**COLOR:** Dark gray (N4) with black (and a few white) fine spots.

**STRUCTURE:** Perhaps the bottom of a thin flow.

**ALTERATION:** Slight-moderate; vesicles are infilled with secondary minerals; mesostasis and microphenocrysts slight to moderately altered; a few specks of pyrite present in the groundmass.

**VEINS/FRACTURES:** 3%; 0.2 - 3.0 mm; very irregular; infilled with carbonate and lined by dark green clays and pyrite.

## UNIT 28: APHYRIC BASALT

### Pieces 9A and 9B

**CONTACTS:** Not observed but a piece of reddish, calcified, interpillow sediments included near the top margin is enclosed by a devitrified glass rim; top margin cryptocrystalline overall that coarsens slightly towards the bottom.

**PHENOCRYSTS:** Generally <1%; consisting of dark green clay-altered olivine (+ pyroxene ?) and slightly altered plagioclase.

**GROUNDMASS:** Devitrified glass along the contact with the included sediment grading to slightly variolitic zone, and then to a hypocrystalline bottom.

**VESICLES:** 1%; 0.3 - 0.5 mm; subrounded - rounded; random; infilled with dark green clays, pyrite, and less commonly, carbonate; these infillings sometimes occur together.

**COLOR:** Dark gray (N4).

**STRUCTURE:** Perhaps the top portion of a thin lava flow.

**ALTERATION:** Slight - moderate; vesicles are infilled with secondary minerals; mesostasis and the few microphenocrysts are altered, generally to green clays.

**VEINS/FRACTURES:** 6%; 0.2 - 3.0 mm; irregular but some are orthogonal; infilled with carbonate and green clays +/- pyrite; branching and cross-cutting.

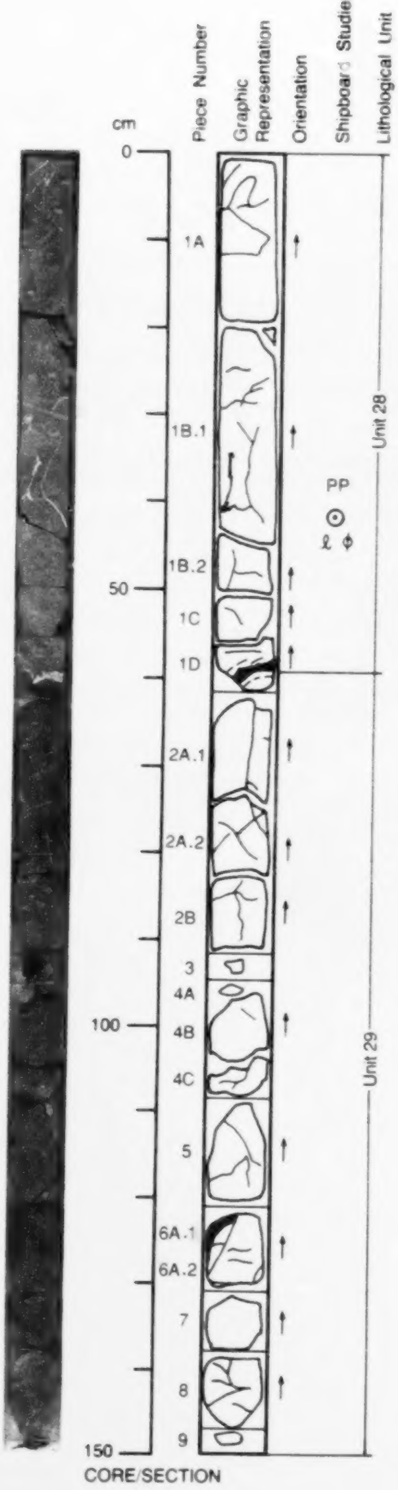

## 129-801C-11R-3

## UNIT 28: APHYRIC BASALT

### Pieces 1A - top portion of 1D

**CONTACTS**: Not observed although there is a general coarsening towards the middle; bottom contact is with a carbonate veinlet lined with green clays and pyrite.
**PHENOCRYSTS**: Generally aphyric but occasional olivine and plagioclase microphenocrysts (<1% total) are present.
**GROUNDMASS**: Hypocrystalline; cryptocrystalline but middle Piece (1.1B) is slightly coarser than other pieces.
**VESICLES**: ~1%; 0.3 - 0.6 mm; subrounded - rounded; random; infilled with green clays and carbonate, or both, and occasional pyrite.
**COLOR**: Dark gray (N4).
**STRUCTURE**: Perhaps the interior and bottom portions of a thin flow.
**ALTERATION**: Slight - moderate; vesicles are infilled with secondary minerals; the few olivine microphenocryts and mesostasis are altered to clays; a few specks of pyrite throughout the Unit.
**VEINS/FRACTURES**: 5%; 0.2 - 10 mm; very irregular; infilled with green clays and carbonate +/- clumps of pyrite; some have well-defined and more altered than groundmass halos containing fine particles of pyrite.

## UNIT 29: APHYRIC BASALT

### Pieces bottom of 1D - 9

**CONTACTS**: Not actually observed because the top glassy rim is in contact with a secondary carbonate veinlet; the devitrified glass rim grades downwards to a cryptocrystalline zone with plenty of variolites; subrounded top rim.
**PHENOCRYSTS**: Generally none but occasional microphenocrysts of olivine (+ pyroxene ?) and slightly altered plagioclase (<1% total) are present at random.
**GROUNDMASS**: Devitrified glass rim coarsening downwards to a hypocrystalline interior but fines again, to a variolitic, almost spherulitic bottom; groundmass texture is complicated by the presence of veinlet halos containing more clays than groundmass and disseminated fine pyrite.
**VESICLES**: ~1%, 0.3 - 0.4 mm; subrounded - rounded; random; infilled with green clays or carbonate, or both; a few are completely filled with pyrite.
**COLOR**: Dark gray (N4).
**STRUCTURE**: Perhaps a pillow with, a subrounded, originally glassy top rim.
**ALTERATION**: Slight - moderate; vesicles are infilled with secondary minerals; veinlets have altered halos with clays and pyrite; the few microphenocrysts, olivine in the groundmass, and mesostasis are altered to clays.
**VEINS/FRACTURES**: 7%; 0.2 - 1.5 mm; irregular; infilled with green clays and carbonate +/- pyrite; branching and cross-cutting; have well-developed halos containing more clays than groundmass and disseminated fine particles of pyrite.

## 129-801C-11R-4

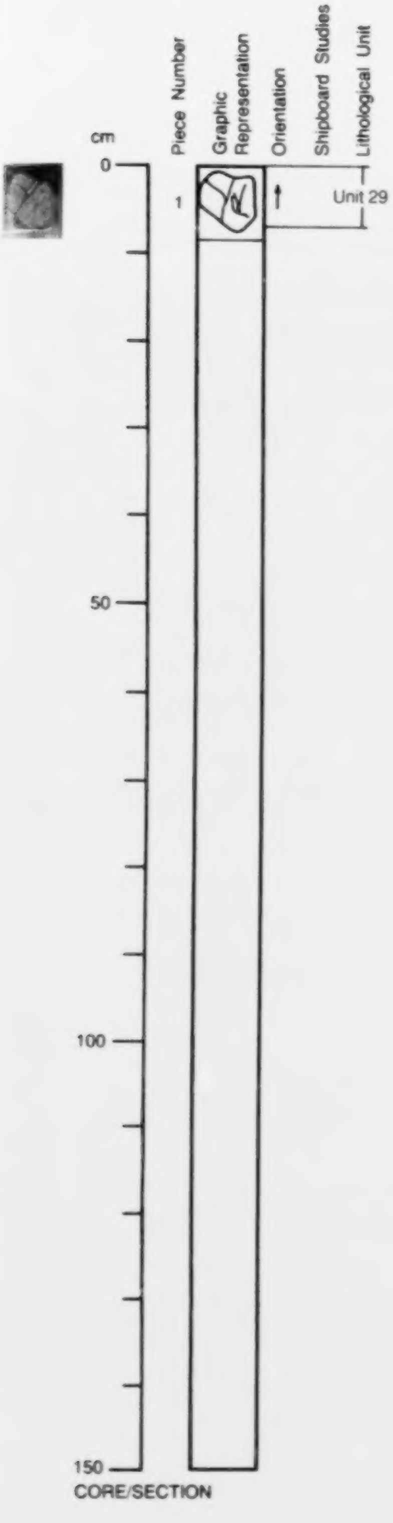
cm
Piece Number
Graphic Representation
Orientation
Shipboard Studies
Lithological Unit
0
1
Unit 29
50
100
150
CORE/SECTION

### UNIT 29: APHYRIC BASALT

### Piece 1

**CONTACTS:** None observed.
**PHENOCRYSTS:** Generally none; a few completely altered olivine and slightly altered plagioclase (<1% total) are randomly distributed.
**GROUNDMASS:** Variolitic to hypocrystalline fine-grained. Texture complicated by the presence of veinlets with conspicous halos.
**VESICLES:** ~1%; 0.2 - 0.6 mm; subrounded - rounded; random; filled with green clays, or carbonate, or both.
**COLOR:** Dark gray (N4) with a few white, fine spots.
**STRUCTURE:** A fragment of Unit 29 which is most probably a pillow lava.
**ALTERATION:** Slight - moderate; vesicles infilled with secondary minerals; halos along fractures heavily altered to clays and limonite (oxidized pyrite ?); glassy mesostasis and olivine altered to green clays.
**VEINS/FRACTURES:** 0%; 0.2 - 3.0 mm; irregular; infilled with carbonate or carbonate and green clays with limonite stains (oxidized pyrite ?); branching.

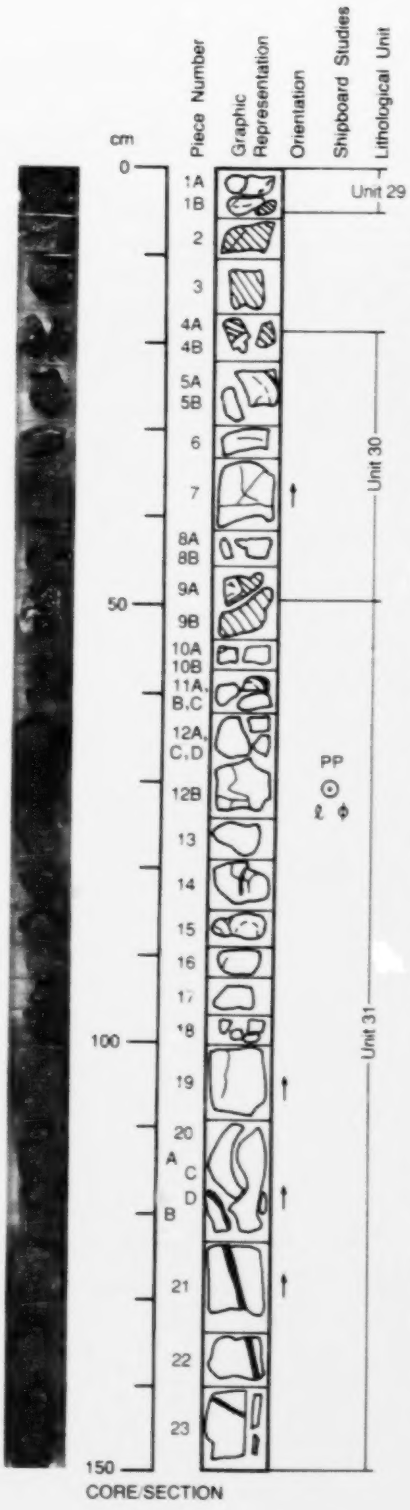

## 129-801C-12R-1

## UNIT 29: APHYRIC BASALT

### Pieces 1A and 1B

**CONTACTS:** Devitrified glass on the bottom rim that is contact with green clays and white carbonate, which most probably are altered interpillow sediments; glassy rim grades to a variolitic to spherulitic zone upwards; margin is subrounded.

**PHENOCRYSTS:** Generally <1%; the few microphenocrysts that are present are mostly altered olivine that rarely gets larger than 0.15 mm; a few plagioclase microphenocrysts are also present.

**GROUNDMASS:** Devitrified glass along the rim grades into a variolitic to spherulitic zone towards the top; cryptocrystalline with a few, subhedral olivine and plagioclase groundmass microlites.

**VESICLES:** <1%; 0.2 - 0.5; subrounded - rounded; random; infilled with green clays mostly and rarely with carbonate; green clays have limonitic stains and these are most probably due to the oxidation of pyrite.

**COLOR:** Dark gray (N5) with a blackish rim at the bottom.

**STRUCTURE:** Bottom of Unit 9 which is most probably a pillow because of subrounded top and bottom, and textural variations typical of pillow lavas.

**ALTERATION:** Slight - moderate; devitrified glass and most of the variolites and spherulites are altered to brown clays; vesicles are infilled with secondary minerals; olivine is altered to green clays.

**VEINS/FRACTURES:** 2%; 0.2 mm on the average; irregular; infilled with green clays stained with limonite (after pyrite ?).

## UNIT 30: APHYRIC BASALT

### Pieces 4A (bottom portion) - 9A

**CONTACTS:** Subrounded top and a lava toe-like bottom; both are rimmed by devitrified glass and are in contact with white carbonate and green clay, interpillow sediments; slightly coarsening towards the center.

**PHENOCRYSTS:** Generally <1%; microphenocrysts consist of a few clusters of plagioclase laths and dark green olivine pseudomorphs; some of the groundmass olivine and plagioclase microlites rarely exceed 0.1 mm.

**GROUNDMASS:** Devitrified glass along the rims grade toward a variolitic to almost spherulitic interior; cryptocrystalline with some groundmass microlites.

**VESICLES:** Trace; 0.2 - 0.3 mm; subrounded; random; infilled with green clays mostly and rarely with carbonate; limonitic stains are most probably due to oxidation of pyrite.

**COLOR:** Dark gray (N4).

**STRUCTURE:** A pillow as suggested by subrounded top and bottom margins and textural criteria.

**ALTERATION:** Slight - moderate; vesicles are infilled; microphenocrysts, groundmass phases, and mesostasis are altered to clays.

**VEINS/FRACTURES:** 3%; 0.2 - 2.0 mm; irregular; infilled with carbonate or clays, or both; limonitic stains are most probably due to oxidation of pyrite.

## UNIT 31: MODERATELY OLIVINE-PLAGIOCLASE MICROPHYRIC BASALT

### Pieces 9B - 23

**CONTACTS:** None observed, except Pieces 10A and B are directly below altered interlayered material and a number of Pieces (11B, 12A, 13, 15, and 19) have thin glassy and/or spherulitic margins retained that could represent the curved subvertical margin to a pillow.

**PHENOCRYSTS:**

Plagioclase - 1%; 0.2 - 0.4; Subhedral.

Olivine - 3%; 0.1 - 0.3; Subhedral, altered to dark green.

**GROUNDMASS:** Cryptocrystalline to fine-grained. Coalesced small spherulites in rim, larger and better crystallized plume variolites further away.

**VESICLES:** None observed.

**COLOR:** Dark gray (N4).

**STRUCTURE:** Pillow lava.

**ALTERATION:** Slight. Glassy rim zones replaced by bright green smectite and microlites outlined with white clay. Olivine microphenocrysts replaced by dark green smectite. Scattered carbonate-smectite and pyrite veinlets. Some green smectite oxidized with yellow coating which also stains adjacent matrix variolites.

**VEINS/FRACTURES:** 1%; 0.5-4.0 mm; subhorizontal & subvertical; infilled with yellow oxidized and stained green smectite with center of replacive carbonate.

**ADDITIONAL COMMENTS:** Presence of fragments of glassy curved margins throughout suggests the rim zone of a single pillow.

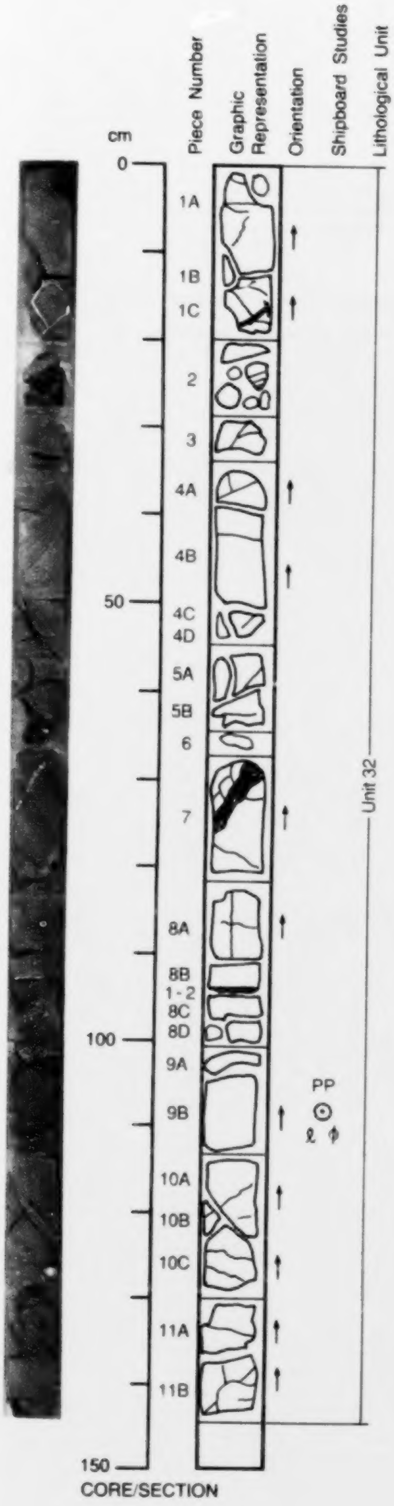
cm
Piece Number
Graphic Representation
Orientation
Shipboard Studies
Lithological Unit
0
50
100
150
1A
1B
1C
2
3
4A
4B
4C
4D
5A
5B
6
7
8A
8B
1-2
8C
8D
9A
9B
10A
10B
10C
11A
11B
PP
ℓ
Unit 32
CORE/SECTION

## 129-801C-12R-2

## UNIT 32: APHYRIC BASALT

### Pieces 1A-11B

**CONTACTS:** None observed, except Piece 1A is aphyric and vesicular relative to the phyric and non-vesicular Unit 31 in previous section (12R-1).
**PHENOCRYSTS:** Few, small, green smectite-replaced olivine microphenocrysts.
**GROUNDMASS:** Fine-grained and hypocrystalline throughout; variolitic with quench texture.
**VESICLES:** 3%; 0.2-0.5 mm; circular; random; infilled with either carbonate or dark green smectite.
**COLOR:** Medium grays (N5 & N6).
**STRUCTURE:** Thin flow.
**ALTERATION:** Slight. Largely veins and vesicle infillings. One larger vein has a dark 2-3 mm wide alteration halo in adjacent matrix composed of clays and pyrite granules.
**VEINS/FRACTURES:** 3%; 0.2-5.0 mm; random; irregular, often with corrugated margins. Smaller veins are either infilled with green smectite or carbonate; pyrite may sometimes be associated with smectite veins as plumose radiate crystals (Piece 4D). Larger veins (Piece 7) show carbonate replacing green smectite with pyrite granules along margins.

## 129-801C-12R-3

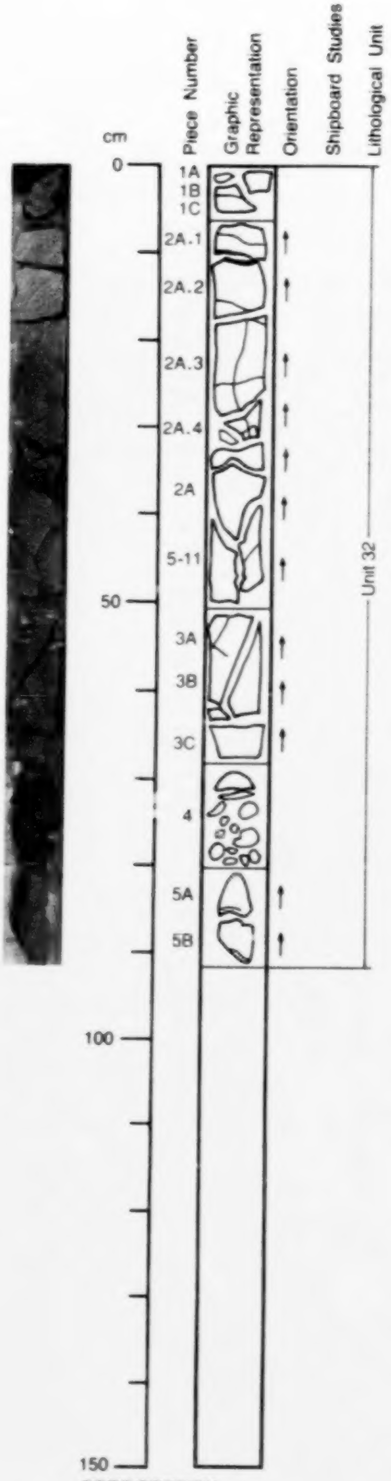
cm
Piece Number
Graphic Representation
Orientation
Shipboard Studies
Lithological Unit
0
50
100
150
1A
1B
1C
2A.1
2A.2
2A.3
2A.4
2A
5-11
3A
3B
3C
4
5A
5B
Unit 32
CORE/SECTION

## UNIT 32: APHYRIC BASALT

### Pieces 1A-5B

**CONTACTS:** None observed; uniform grain-size and texture throughout.
**PHENOCRYSTS:** Few olivine smectite-replaced microphenocrysts (<1%).
**GROUNDMASS:** Fine-grained and hypocrystalline; quenched textured with variolites.
**VESICLES:** 4%; 0.2-0.4 mm; circular, some more irregular shapes.; random; infilled with either smectite or carbonate.
**COLOR:** Medium gray (N5).
**STRUCTURE:** Interior of thin flow.
**ALTERATION:** Slight. Largely represented by veins and vesicle infillings; narrow halos to larger veins.
**VEINS/FRACTURES:** <1%; 0.2-1.5 mm; Subhorizontal & subvertical; infilled with green smectite and/or carbonate.

SITE 802 HOLE A CORE 1R CORED INTERVAL 5968.6-5973.6 mbsl; 0.0-5.0 mbsf

| TIME-ROCK UNIT | BIOSTRAT. ZONE/ FOSSIL CHARACTER | | | | | PALEOMAGNETICS | PHYS. PROPERTIES | CHEMISTRY | SECTION | METERS | GRAPHIC LITHOLOGY | DRILLING DISTURB. | SED. STRUCTURES | SAMPLES | LITHOLOGIC DESCRIPTION |
|---|---|---|---|---|---|---|---|---|---|---|---|---|---|---|---|
| | FORAMINIFERS | NANNOFOSSILS | RADIOLARIANS | DIATOMS | PALYNOMORPHS | | | | | | | | | | |
| UPPER PLIOCENE - QUATERNARY | B | B | F/G<br>unzoned | | B | | | | CC | | | | | * | PELAGIC CLAY<br>Major lithology: PELAGIC CLAY, dark brown (7.5YR 3/3), homogeneous, contains clay and metal-oxide/hydroxide aggregates with minor zeolites and traces of quartz silt and spines. Entire sample went to paleontologists. |

SLIDE SUMMARY (%):

| | CC<br>D |
|---|---|
| TEXTURE: | |
| Silt | 35 |
| Clay | 65 |
| COMPOSITION: | |
| Accessory minerals | 1 |
| Clay | 50 |
| Micronodule | 2 |
| Oxide | 38 |
| Quartz | 2 |
| Spines | 1 |
| Zeolite | 6 |

802 A 2R NO RECOVERY

SITE 802 HOLE A CORE 3R CORED INTERVAL 5983.2-5992.9 mbsl; 14.6-24.3 mbsf

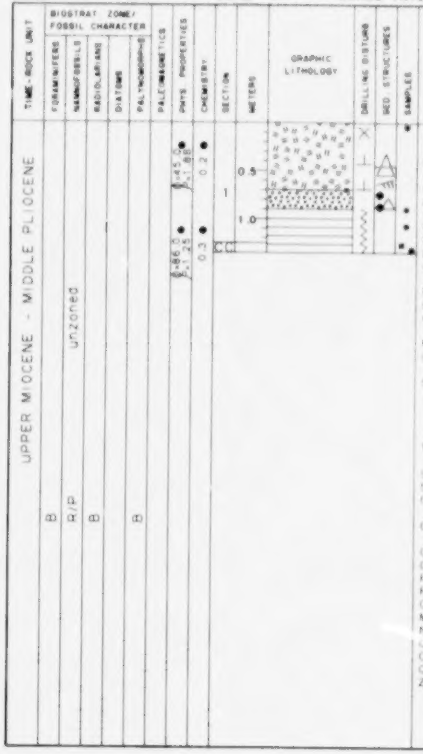
TIME-ROCK UNIT
BIOSTRAT. ZONE/FOSSIL CHARACTER
FORAMINIFERS
NANNOFOSSILS
RADIOLARIANS
DIATOMS
PALYNOMORPHS
PALEOMAGNETICS
PHYS. PROPERTIES
CHEMISTRY
SECTION
METERS
GRAPHIC LITHOLOGY
DRILLING DISTURB.
SED. STRUCTURES
SAMPLES
UPPER MIOCENE - MIDDLE PLIOCENE
B
R/P
unzoned
B
B
φ=45.0
γ=1.88
φ=86.0
γ=1.25
0.2
0.3
1
CC
0.5
1.0

LITHOLOGIC DESCRIPTION

TUFF and PELAGIC CLAY with ZEOLITES

Major lithologies:

a. TUFF, dark brown to dark yellowish brown (7.5YR 3/4 10YR 3/5), in Section 1, 0-72 cm: silty to sandy, speckled with manganese oxides (especially Section 1, 42-45 cm); minor palagonitization of volcanic glass; a few planar laminations of fine-grained ash and claystone fragments through cross laminations at Section 1, 64-72 cm; redeposited as grain flows or turbidites.

b. PELAGIC CLAY with ZEOLITES, dark brown to brown (7.5YR 4/2 10YR 5/3) to greenish gray (5GY 4/1): contains clay metal-oxide/hydroxide aggregate 10-15% zeolites, homogenized by drilling.

Minor lithology: LAPILLI TUFF, dark greenish gray (5GY 4/1), Section 1, 72-90 cm: clasts up to 7 mm in diameter consist of fine-grained tuff or volcaniclastic claystone are discrete in a matrix of very fine-grained volcaniclastic material and glass shards; normally graded.

Note: The recovered sediment displays a progressive downward color change from yellowish brown to dark greenish gray.

SLIDE SUMMARY (%):

| | 1, 1<br>M | 1, 90<br>M | 1, 108<br>D | CC, 2<br>D | CC, 11<br>D |
|---|---|---|---|---|---|
| TEXTURE: | | | | | |
| Sand | — | — | 2 | 2 | 1 |
| Silt | 15 | 30 | 20 | 35 | 25 |
| Clay | 85 | 70 | 78 | 63 | 74 |
| COMPOSITION: | | | | | |
| Calcite | — | 64 | — | Tr | — |
| Clay | 30 | 10 | 51 | 62 | 60 |
| Feldspar | 5 | 1 | — | — | — |
| Foraminifers | — | — | Tr | — | — |
| Glass | 62 | 20 | 5 | 10 | — |
| Micronodule | — | — | — | 2 | 5 |
| Nannofossils | — | Tr | — | — | — |
| Opaques | Tr | — | — | — | — |
| Oxide | 2 | 2 | 30 | 20 | 20 |
| Quartz | 1 | — | — | — | — |
| Zeolite | Tr | 3 | 10 | 6 | 15 |

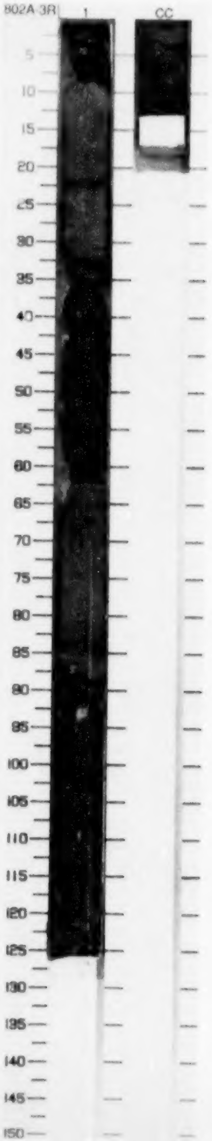
802A-3R
1
CC
5
10
15
20
25
30
35
40
45
50
55
60
65
70
75
80
85
90
95
100
105
110
115
120
125
130
135
140
145
150

SITE 802 HOLE A CORE 4R CORED INTERVAL 5992.9-6002.3 mbsl; 24.3-33.7 mbsf

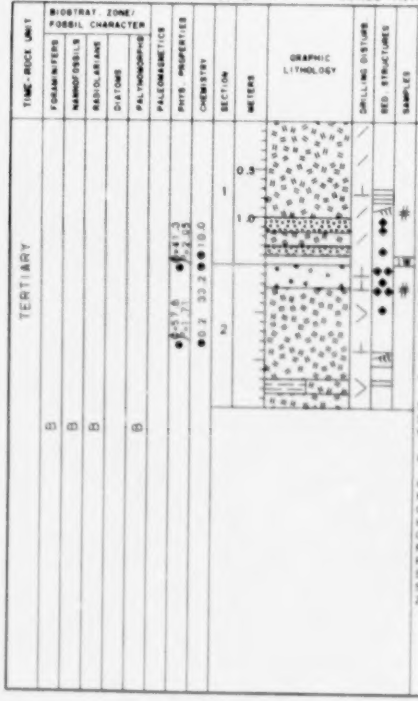
TIME-ROCK UNIT
BIOSTRAT. ZONE/ FOSSIL CHARACTER
FORAMINIFERS
NANNOFOSSILS
RADIOLARIANS
DIATOMS
PALYNOMORPHS
PALEOMAGNETICS
PHYS. PROPERTIES
CHEMISTRY
SECTION
METERS
GRAPHIC LITHOLOGY
DRILLING DISTURB.
SED. STRUCTURES
SAMPLES
TERTIARY
B
B
B
B
10.0
33.2
0.2
1
2
0.5
1.0

LITHOLOGIC DESCRIPTION

TUFF and LAPILLI TUFF

Major lithologies:

a. TUFF, dark brown to dark yellowish brown (7.5YR 3/4 10YR 3/5) in Section 1, 0-70 cm, and greenish black to olive gray (5GY 2/1 5Y 4/1) in Section 2, 24-150 cm, silty to sandy with silty CALCAREOUS CLAYSTONE in Section 2, 123-137 cm; consists mostly of fresh glass with feldspar and clinopyroxene (augite) crystals, and small lapilli of finer-grained ash; massive with intervals of cross-lamination.

b. LAPILLI TUFF, dark greenish gray to olive gray (5GY 4/1 5Y 4/1), composed of subangular to rounded lapilli of volcaniclastic claystone, tuff fragments or pumice from sand-size to 1.8 cm long; some lapilli are calcareous.

Note: Section 1, 0-118 cm is a duplication of Core 129-802A-3R, Section 1; interval was recored after adding a new joint of pipe. Section 1 displays a progressive downward color change from yellowish brown to dark greenish gray.

SLIDE SUMMARY (%):

| | 1, 95<br>D | 2, 25<br>D |
|---|---|---|
| TEXTURE: | | |
| Sand | 85 | 70 |
| Silt | 15 | 25 |
| Clay | — | 5 |
| COMPOSITION: | | |
| Calcite | 20 | 15 |
| Feldspar | 2 | 1 |
| Glass | 62 | 71 |
| Igneous rock fragments | Tr | 1 |
| Opaques | 5 | 1 |
| Pyroxene | 3 | 1 |
| Red algae | — | Tr |
| Silica | 1 | — |
| Smectite | 5 | 5 |
| Zeolite | — | 2 |

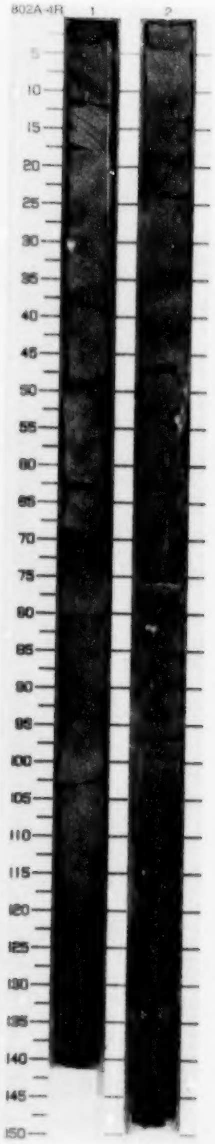
802A-4R
1
2
5
10
15
20
25
30
35
40
45
50
55
60
65
70
75
80
85
90
95
100
105
110
115
120
125
130
135
140
145
150

SITE 802 HOLE A CORE 5R CORED INTERVAL 6002.3-6011.5 mbsl; 33.7-42.9 mbsf

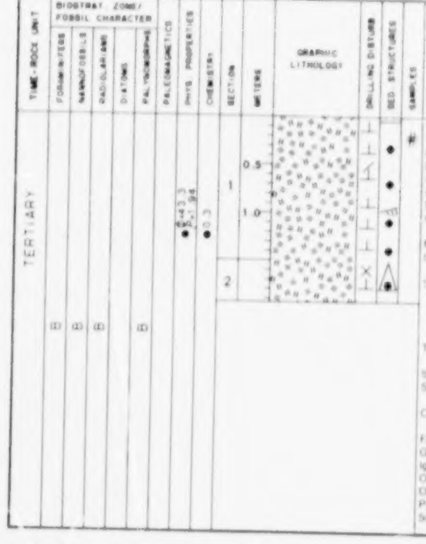
TIME-ROCK UNIT
BIOSTRAT. ZONE/ FOSSIL CHARACTER
FORAMINIFERS
NANNOFOSSILS
RADIOLARIANS
DIATOMS
PALYNOMORPHS
PALEOMAGNETICS
PHYS. PROPERTIES
CHEMISTRY
SECTION
METERS
GRAPHIC LITHOLOGY
DRILLING DISTURB.
SED. STRUCTURES
SAMPLES
TERTIARY
B
B
B
B
0.3
1
2
0.5
1.0
#

LITHOLOGIC DESCRIPTION

TUFF

Major lithology: TUFF, black (5B 2/1), medium grained, with variety of very light gray (N8) to black (N1) grains and angular to subrounded intraclasts of fine grained igneous rock or volcanic glass (2.5 mm size range); well cemented with abundant pore spaces (1 mm typical size). Lapilli occur concentrated in bands or dispersed in SANDSTONE. Normal grading in Section 2, 1-31 cm; otherwise turbidite beds not observed. Massive, with rare intervals of ripple cross lamination.

Note: TUFF fragment (Section 1, 0-6 cm), brown (7.5YR 4/4) with black specks, laminated band in center; probably displaced from uphole.

SLIDE SUMMARY (%)

| | 1, 21 |
|---|---|
| | D |
| TEXTURE | |
| Sand | 90 |
| Silt | 10 |
| COMPOSITION | |
| Feldspar | 8 |
| Glass | 78 |
| Igneous rock fragments | 5 |
| Olivine | 2 |
| Opaques | 2 |
| Pyroxene | 3 |
| Smectite | 2 |

SITE 802 HOLE A CORE 6R CORED INTERVAL 6011.5-6021.0 mbsl; 42.9-52.4 mbsf

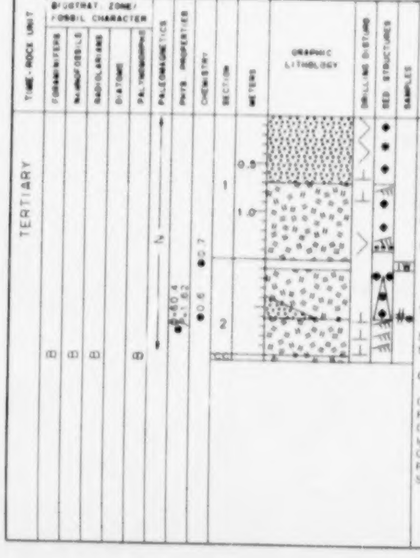
TIME-ROCK UNIT
BIOSTRAT. ZONE/ FOSSIL CHARACTER
FORAMINIFERS
NANNOFOSSILS
RADIOLARIANS
DIATOMS
PALYNOMORPHS
PALEOMAGNETICS
PHYS. PROPERTIES
CHEMISTRY
SECTION
METERS
GRAPHIC LITHOLOGY
DRILLING DISTURB.
SED. STRUCTURES
SAMPLES
TERTIARY
B
B
B
B
N
0.6
0.7
1
2
CC
0.5
1.0
IW
#

LITHOLOGIC DESCRIPTION

TUFF and LAPILLI TUFF

Major lithologies:

a. TUFF, grayish black to greenish black (N2 5G 2/1), sandy to silty, planar to through cross laminated to massive, but no complete turbidites were recovered; lapilli occur concentrated in bands.

b. LAPILLI TUFF, with 20% subrounded lapilli of finer grained volcanic material 2-10 mm long, in a matrix of sandy tuff, light olive gray to greenish gray (5Y 6/1-5GY 6/1).

SLIDE SUMMARY (%)

| | 2, 60 |
|---|---|
| | D |
| TEXTURE | |
| Sand | 90 |
| Silt | 10 |
| COMPOSITION | |
| Calcite | 5 |
| Feldspar | 10 |
| Glass | 63 |
| Igneous rock fragments | 10 |
| Opaques | 5 |
| Pyroxene | 3 |
| Smectite | 2 |

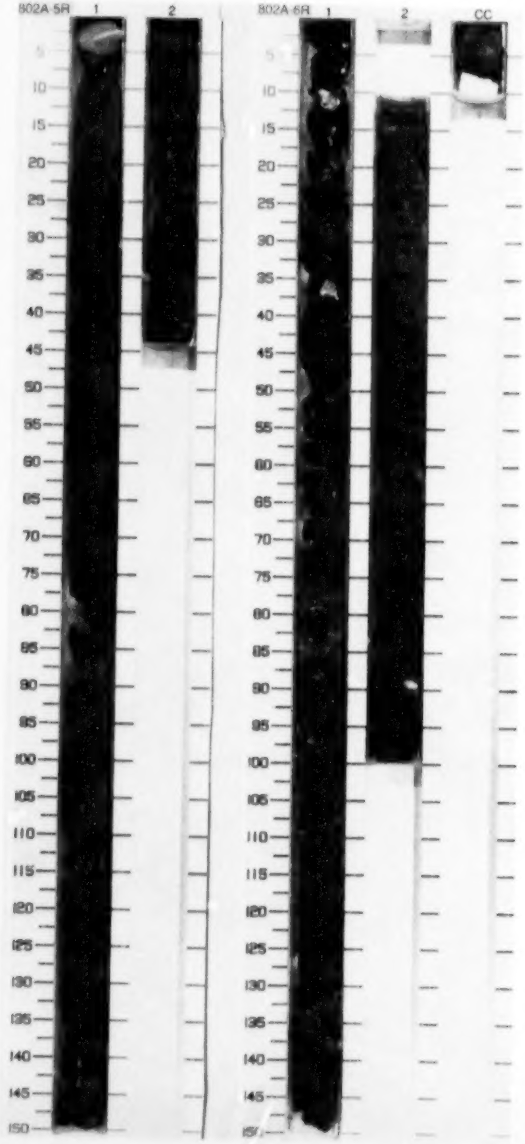
802A 5R
1
2
802A 6R
1
2
CC
5
10
15
20
25
30
35
40
45
50
55
60
65
70
75
80
85
90
95
100
105
110
115
120
125
130
135
140
145
150

## SITE 802 HOLE A CORE 7R CORED INTERVAL 6021.0-6030.5 mbsl; 52.4-61.9 mbsf

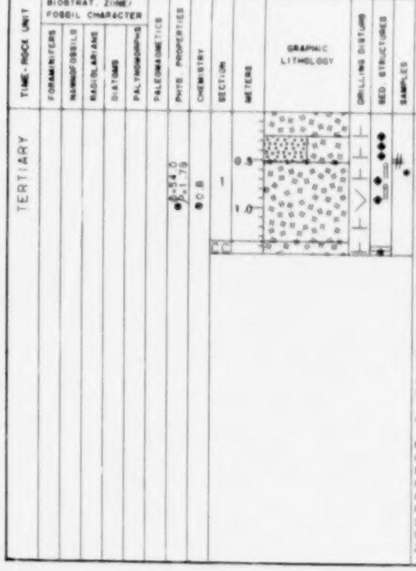
TIME-ROCK UNIT
BIOSTRAT. ZONE/ FOSSIL CHARACTER
FORAMINIFERS
NANNOFOSSILS
RADIOLARIANS
DIATOMS
PALYNOMORPHS
PALEOMAGNETICS
PHYS. PROPERTIES
CHEMISTRY
SECTION
METERS
GRAPHIC LITHOLOGY
DRILLING DISTURB.
SED. STRUCTURES
SAMPLES
TERTIARY
φ-54.0
ρ-1.79
●0.8
1
0.5
1.0
CC

LITHOLOGIC DESCRIPTION

TUFF to LAPILLI TUFF

Major lithology: TUFF to LAPILLI TUFF, grayish black to greenish black (N2 5G 2/1), fine-to medium-grained, consists of grains of volcanic rock fragments, glass and pyroxene in a clayey matrix; sedimentary structures include dish and pipe fluid-escape features, subtle normal and reverse grading, large, subrounded lapilli occurring dispersed in matrix or concentrated in bands. Lapilli are finer-grained volcanic material up to 1.6 cm long, commonly sub-parallel to bedding. Millimeter-size cavities and some fractures are filled with a micro-fibrous/platy white minerals, a combination of Ca-rich zeolite probably laumontite and some member(s) of the analcime-wairakite solid-solution series, according to preliminary XRD analysis.
laumontite and some member(s) of the analcime-wairakite solid solution series, according to preliminary XRD analysis.

SLIDE SUMMARY (%)

| | 1, 50<br>D | 1, 61<br>M |
|---|---|---|
| TEXTURE | | |
| Sand | 80 | — |
| Silt | 20 | 100 |
| COMPOSITION | | |
| Feldspar | 8 | — |
| Glass | 75 | — |
| Igneous rock fragments | 3 | — |
| Olivine | Tr | — |
| Opaques | 5 | — |
| Pyroxene | 2 | — |
| Silica | 2 | — |
| Smectite | 5 | — |
| Zeolite | — | 100 |

## SITE 802 HOLE A CORE 8R CORED INTERVAL 6030.5-6039.7 mbsl; 61.9-71.1 mbsf

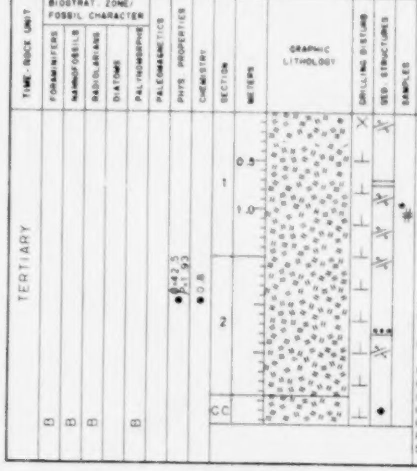
TIME-ROCK UNIT
BIOSTRAT. ZONE/ FOSSIL CHARACTER
FORAMINIFERS
NANNOFOSSILS
RADIOLARIANS
DIATOMS
PALYNOMORPHS
PALEOMAGNETICS
PHYS. PROPERTIES
CHEMISTRY
SECTION
METERS
GRAPHIC LITHOLOGY
DRILLING DISTURB.
SED. STRUCTURES
SAMPLES
TERTIARY
B
B
B
B
φ-42.5
ρ-1.93
●0.8
1
2
CC
0.5
1.0

LITHOLOGIC DESCRIPTION

TUFF

Major lithology: TUFF, grayish black (5BG 2/1), consists primarily of grains of volcanic glass, pyroxene and feldspar crystals, and volcanic rock fragments, moderately to poorly sorted with common lapilli of subrounded aphanitic volcanic material that are isolated in the sandy matrix or sometimes form indistinct layers. Horizontal fractures are filled with up to 3 mm of micro-fibrous/platy white Ca-zeolite minerals.

SLIDE SUMMARY (%)

| | 1, 96<br>D | 1, 108<br>D |
|---|---|---|
| TEXTURE | | |
| Sand | 70 | 70 |
| Silt | 30 | 30 |
| COMPOSITION | | |
| Feldspar | — | 7 |
| Glass | 75 | 77 |
| Igneous rock fragments | 20 | — |
| Olivine | — | 2 |
| Opaques | — | 3 |
| Pyroxene | 5 | 10 |
| Smectite | — | Tr |

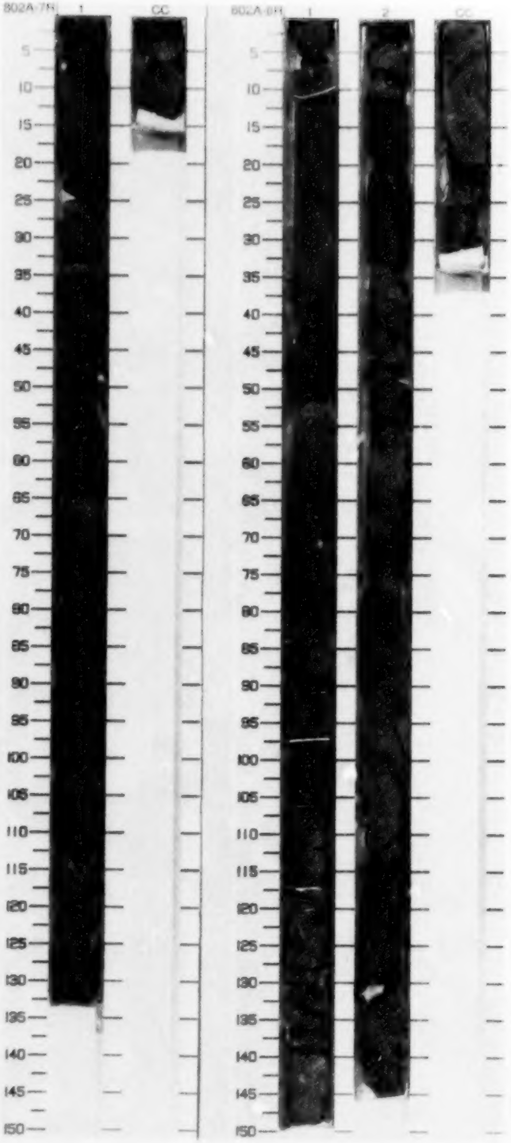
802A-7R
1
CC
802A-8R
1
2
CC
5
10
15
20
25
30
35
40
45
50
55
60
65
70
75
80
85
90
95
100
105
110
115
120
125
130
135
140
145
150

## 802A 9R NO RECOVERY

SITE 802 HOLE A CORE 10R CORED INTERVAL 6049.4-6058.2 mbsl; 80.4-89.6 mbsf

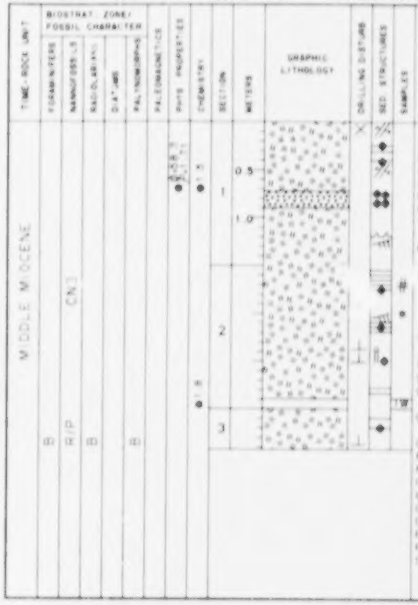
TIME-ROCK UNIT
BIOSTRAT. ZONE/ FOSSIL CHARACTER
FORAMINIFERS
NANNOFOSSILS
RADIOLARIANS
DIATOMS
PALYNOMORPHS
PALEOMAGNETICS
PHYS. PROPERTIES
CHEMISTRY
SECTION
METERS
GRAPHIC LITHOLOGY
DRILLING DISTURB.
SED. STRUCTURES
SAMPLES
MIDDLE MIOCENE
B
CN3
R/P
B
B
0.5
1.0
1
2
3
#
TW

LITHOLOGIC DESCRIPTION

TUFF

Major lithology: TUFF, black to greenish black (N1 5G 2/1), poorly to moderately sorted, angular grains of volcanic glass, crystals of pyroxene and feldspar, igneous rock fragments and oxides in an altered clayey matrix. Massive to planar laminated, with infrequent cross lamination. Rip up clasts are subrounded fragments of gray (N5) tuff (VOLCANICLASTIC CLAYSTONE). Large, spherical foraminifers middle Miocene Orbulina universa (Section 2, 12-32 cm). Possible fluid escape pipe at Section 2, 95-100 cm.

Minor lithology: LAPILLI TUFF, black (N1); lapilli are 2-8 mm long, gray (N5).

SMEAR SLIDE SUMMARY (%):

| | 2, 20<br>D | 2, 49<br>D |
|---|---|---|
| TEXTURE: | | |
| Sand | 80 | 10 |
| Silt | 15 | 50 |
| Clay | 5 | 20 |
| COMPOSITION: | | |
| Clay | 10 | 10 |
| Feldspar | Tr | 2 |
| Foraminifers | 2 | — |
| Glass | 75 | 75 |
| Igneous rock fragments | Tr | 5 |
| Opaques | 3 | — |
| Oxide | 2 | Tr |
| Pore space | 5 | — |
| Pyroxene | 3 | 8 |
| Smectite | Tr | — |

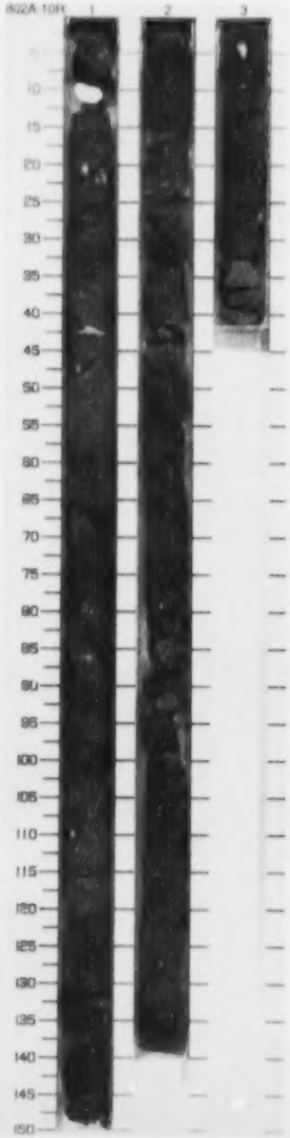
802A-10R
1
2
3
5
10
15
20
25
30
35
40
45
50
55
60
65
70
75
80
85
90
95
100
105
110
115
120
125
130
135
140
145
150

SITE 802 HOLE A CORE 11R CORED INTERVAL 6058.2-6067.5 mbsl; 89.6-98.9 mbsf

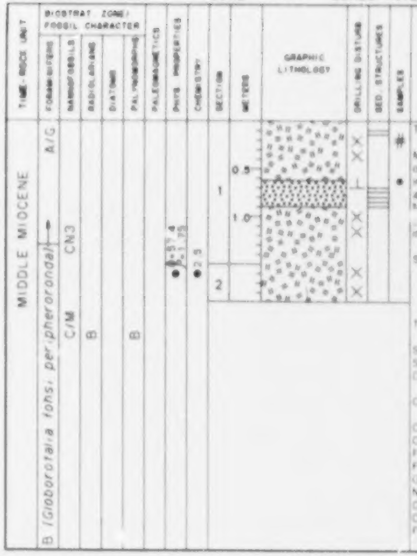
TIME-ROCK UNIT
BIOSTRAT. ZONE/ FOSSIL CHARACTER
FORAMINIFERS
NANNOFOSSILS
RADIOLARIANS
DIATOMS
PALYNOMORPHS
PALEOMAGNETICS
PHYS. PROPERTIES
CHEMISTRY
SECTION
METERS
GRAPHIC LITHOLOGY
DRILLING DISTURB.
SED. STRUCTURES
SAMPLES
MIDDLE MIOCENE
B (Globorotalia fohsi peripheroronda)
A/G
CN3
C/M
B
B
2.5
1
2
0.5
1.0

LITHOLOGIC DESCRIPTION

TUFF

Major lithology: TUFF, black to greenish black (N1 5G 2/1), angular glass fragments with oxides, pyroxene and some feldspar. Mostly massive, thinly laminated in some places; rare irregular scoured surfaces; fine, white cross laminations at Section 1, 112-120 cm, with abundant Miocene foraminifers and common nannofossils.

M[illegible] [illegible]ogy: LAPILLI TUFF, black to greenish black (N1 5G 2/1) with larger (2-8 mm) [illegible] ash lapilli that often define planar or cross lamination. Foraminifers present in [illegible] with 1-3 mm clasts.

SLIDE SUMMARY (%):

|  | 1, 20 | 1, 64 |
|---|---|---|
|  | M | D |
| TEXTURE: |  |  |
| Sand | 20 | 85 |
| Silt | 50 | 15 |
| Clay | 30 | Tr |
| COMPOSITION: |  |  |
| Calcite | 10 | — |
| Clay | 15 | 5 |
| Feldspar | — | Tr |
| Foraminifers | 10 | 3 |
| Glass | 60 | 80 |
| Nannofossils | 5 | — |
| Opaques | — | 8 |
| Oxide | — | 2 |
| Pyroxene | Tr | 2 |

SITE 802 HOLE A CORE 12R CORED INTERVAL 6067.5-6076.9 mbsl; 98.9-108.3 mbsf

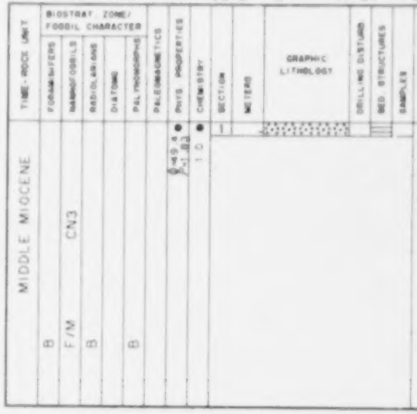
TIME-ROCK UNIT
BIOSTRAT. ZONE/ FOSSIL CHARACTER
FORAMINIFERS
NANNOFOSSILS
RADIOLARIANS
DIATOMS
PALYNOMORPHS
PALEOMAGNETICS
PHYS. PROPERTIES
CHEMISTRY
SECTION
METERS
GRAPHIC LITHOLOGY
DRILLING DISTURB.
SED. STRUCTURES
SAMPLES
MIDDLE MIOCENE
B
CN3
F/M
B
B
1.0
1

LITHOLOGIC DESCRIPTION

TUFF

Major lithology: TUFF, black (N1), sandy, moderately to poorly sorted, composed of angular glass and volcanic rock fragments with oxides, pyroxene and some feldspar. Massive to thinly laminated with 0.5-5.0 mm lighter colored clasts that are brownish gray (5YR 4/2), olive gray (5Y 4/1), and dark greenish gray (5GY 4/1).

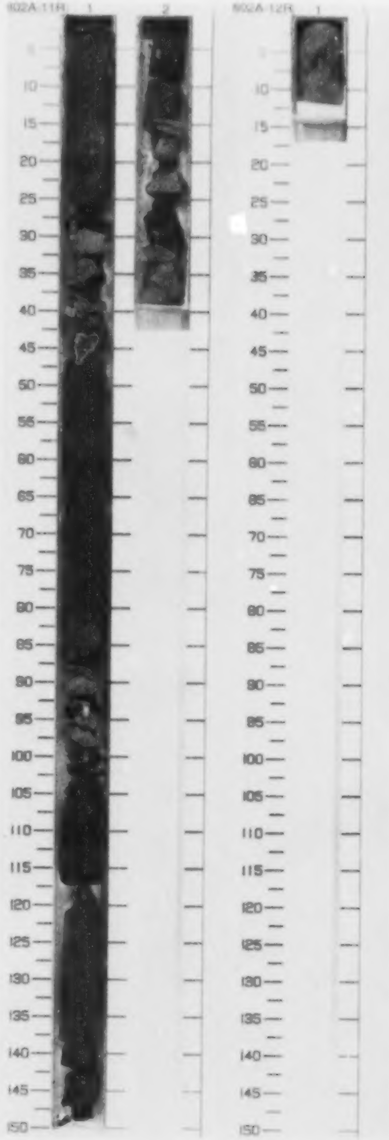
802A-11R
1
2
802A-12R
1
0
10
15
20
25
30
35
40
45
50
55
60
65
70
75
80
85
90
95
100
105
110
115
120
125
130
135
140
145
150

SITE 802 HOLE A CORE 13R CORED INTERVAL 6076.9-6083.0 mbsl; 108.3-114.4 mbsf

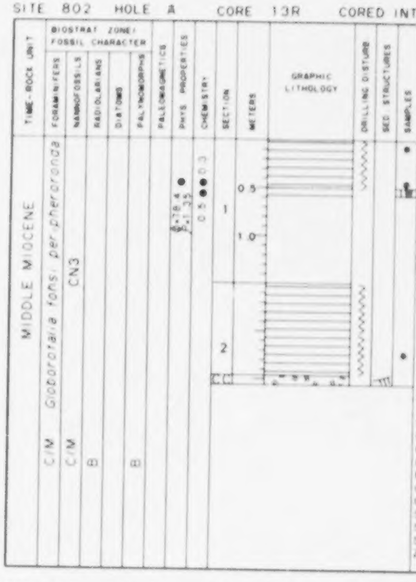
TIME-ROCK UNIT
BIOSTRAT. ZONE/ FOSSIL CHARACTER
FORAMINIFERS
NANNOFOSSILS
RADIOLARIANS
DIATOMS
PALYNOMORPHS
PALEOMAGNETICS
PHYS. PROPERTIES
CHEMISTRY
SECTION
METERS
GRAPHIC LITHOLOGY
DRILLING DISTURB.
SED. STRUCTURES
SAMPLES
MIDDLE MIOCENE
C/M Globorotalia fohsi peripheroronda
C/M CN3
B
B
Φ-78.4
γ-1.35
0.5
0.3
1
2
CC
0.5
1.0

LITHOLOGIC DESCRIPTION

PELAGIC CLAY and TUFF

Major lithologies:
a. PELAGIC CLAY, dark brown (10YR 3/2), with mottles of reddish yellow (7.5YR 7/6); thoroughly disrupted by drilling; contains rare volcanic glass, radiolarian spines, and zeolites; lighter colored clay contains fewer iron oxide aggregates.
b. TUFF, dark greenish gray (5BG 4/1); depositionally underlies pelagic clay but contact is disturbed by drilling; contains volcanic glass, feldspar, zeolites, and nannofossils.

SLIDE SUMMARY (%):

| | 1, 8<br>M | 1, 46<br>D | 2, 74<br>D |
|---|---|---|---|
| TEXTURE: | | | |
| Silt | 5 | 5 | 40 |
| Clay | 95 | 95 | 60 |
| COMPOSITION: | | | |
| Clay | 85 | 79 | 52 |
| Feldspar | — | — | 2 |
| Glass | Tr | — | 10 |
| Igneous rock fragments | — | — | 5 |
| Nannofossils | — | — | 20 |
| Opaques | 2 | Tr | 3 |
| Oxide | 2 | 10 | 2 |
| Silica | 3 | — | — |
| Smectite | — | — | 3 |
| Spines | 3 | 5 | Tr |
| Zeolite | 5 | 6 | 3 |

SITE 802 HOLE A CORE 14R CORED INTERVAL 6083.0-6090.7 mbsl; 114.4-122.1 mbsf

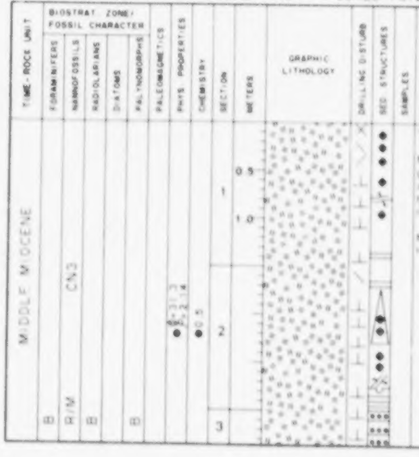
TIME-ROCK UNIT
BIOSTRAT. ZONE/ FOSSIL CHARACTER
FORAMINIFERS
NANNOFOSSILS
RADIOLARIANS
DIATOMS
PALYNOMORPHS
PALEOMAGNETICS
PHYS. PROPERTIES
CHEMISTRY
SECTION
METERS
GRAPHIC LITHOLOGY
DRILLING DISTURB.
SED. STRUCTURES
SAMPLES
MIDDLE MIOCENE
B
R/M CN3
B
B
Φ-31.3
γ-2.14
0.5
1
2
3
0.5
1.0

LITHOLOGIC DESCRIPTION

TUFF

Major lithology: TUFF, greenish black to grayish black (5BG 2/1 to N2), medium to coarse-grained sandy texture; some beds are turbidites and display basal scour or flame structures and fine upwards; subrounded lapilli of aphanitic to tuffaceous igneous rock are grayish black to very dark gray (N2 N3), and are abundant in portion of some beds. Some sub-horizontal fractures are filled with up to 1 cm of white (N9) slightly fibrous fill of Ca zeolites.

Minor lithology: (Section 1, 0-6 cm) CLAYSTONE, light yellowish brown (10YR 6/4); homogeneous. Probably displaced from up-hole.

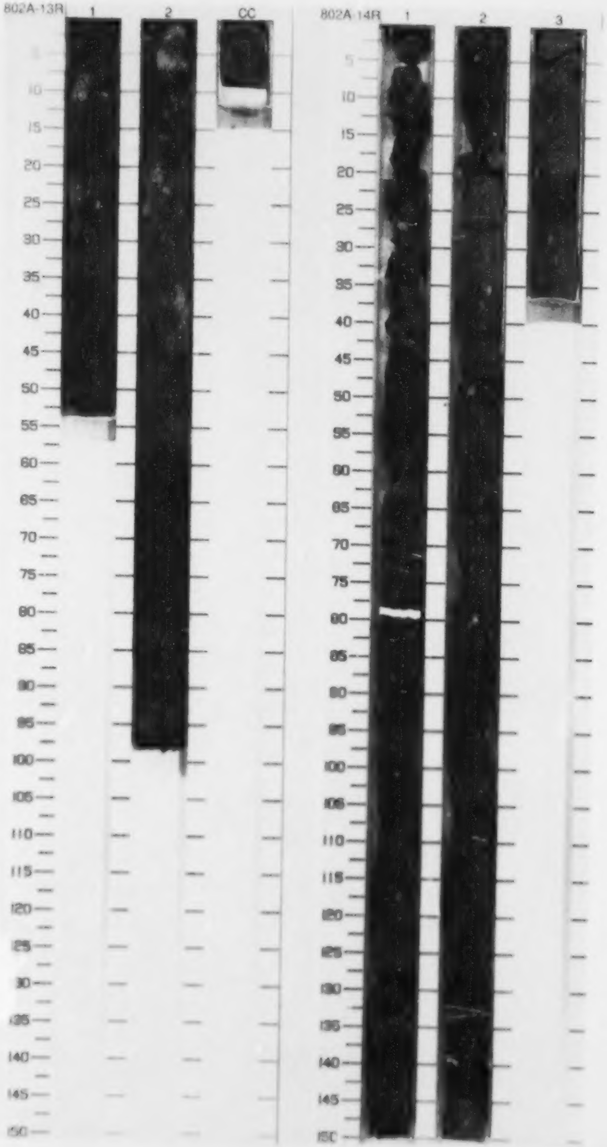
802A-13R
1
2
CC
802A-14R
1
2
3
5
10
15
20
25
30
35
40
45
50
55
60
65
70
75
80
85
90
95
100
105
110
115
120
125
130
135
140
145
150

SITE 802 HOLE A CORE 15R CORED INTERVAL 6090.7-6099.7 mbsl; 122.1-131.1 mbsf

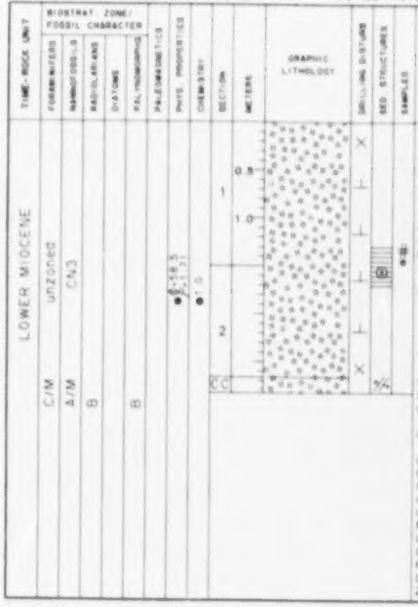
TIME-ROCK UNIT
BIOSTRAT. ZONE/ FOSSIL CHARACTER
FORAMINIFERS
NANNOFOSSILS
RADIOLARIANS
DIATOMS
PALYNOMORPHS
PALEOMAGNETICS
PHYS. PROPERTIES
CHEMISTRY
SECTION
METERS
GRAPHIC LITHOLOGY
DRILLING DISTURB.
SED. STRUCTURES
SAMPLES
LOWER MIOCENE
unzoned
CN3
C/M
A/M
B
B
φ=58.5
ρ=1.71
T 0
1
2
CC
0.5
1.0

LITHOLOGIC DESCRIPTION

TUFF

Major lithology: TUFF, greenish black to brownish black to greenish gray (5G 2/1 5YR 2/1 5G 4/1); silty to coarse sandy texture, massive, poorly sorted sandy tuff of Section 1, 0-141 cm, contains glass, igneous rock fragments, ash, foraminifers and pyroxene; laminated tuff of Section 1, 140-150 cm, contains clay (50%), volcanic glass (20%), zeolites (15%) and minor nannofossils, smectite and igneous rock fragments. Minor white patches, 1-3 mm, are probably zeolites. Sedimentary structures include isolate to concentrated subangular aphanitic lapilli up to 1 cm in diameter, cross lamination (in some finer grained intervals), planar lamination, normally graded beds, and concretions and vein fillings of white (N9) zeolites and acicular anhydrite.

SLIDE SUMMARY (%):

| | 1, 133<br>D | 1, 147<br>M |
|---|---|---|
| TEXTURE: | | |
| Sand | 40 | — |
| Silt | 30 | 1 |
| Clay | 30 | 99 |
| COMPOSITION: | | |
| Clay | — | 52 |
| Feldspar | 2 | 1 |
| Foraminifers | 1 | — |
| Glass | 74 | 20 |
| Igneous rock fragments | 3 | 2 |
| Nannofossils | — | 5 |
| Opaques | Tr | Tr |
| Oxide | Tr | Tr |
| Pyroxene | 15 | — |
| Smectite | 5 | 5 |
| Zeolite | — | 15 |

SITE 802 HOLE A CORE 16R CORED INTERVAL 6099.7-6109.0 mbsl; 131.1-140.4 mbsf

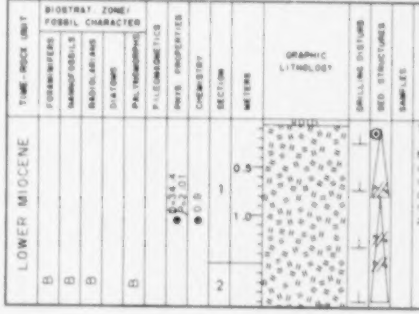
TIME-ROCK UNIT
BIOSTRAT. ZONE/ FOSSIL CHARACTER
FORAMINIFERS
NANNOFOSSILS
RADIOLARIANS
DIATOMS
PALYNOMORPHS
PALEOMAGNETICS
PHYS. PROPERTIES
CHEMISTRY
SECTION
METERS
GRAPHIC LITHOLOGY
DRILLING DISTURB.
SED. STRUCTURES
SAMPLES
LOWER MIOCENE
B
B
B
B
φ=34.4
ρ=2.01
0.9
1
2
0.5
1.0

LITHOLOGIC DESCRIPTION

TUFF

Major lithology: TUFF, greenish black to olive black (5G 2/1 to 5Y 2/1); fine sand to silty sandstone textures, composed mostly of glass and volcanic rock fragments. Sedimentary structures include normally graded beds, through cross lamination, planar lamination, and dispersed lapilli of finer grained volcanic material; beds are turbidites and grain flows with meter scale thicknesses. Concretions and horizontal fracture fillings of white (N9) Ca zeolites are diagenetic features.

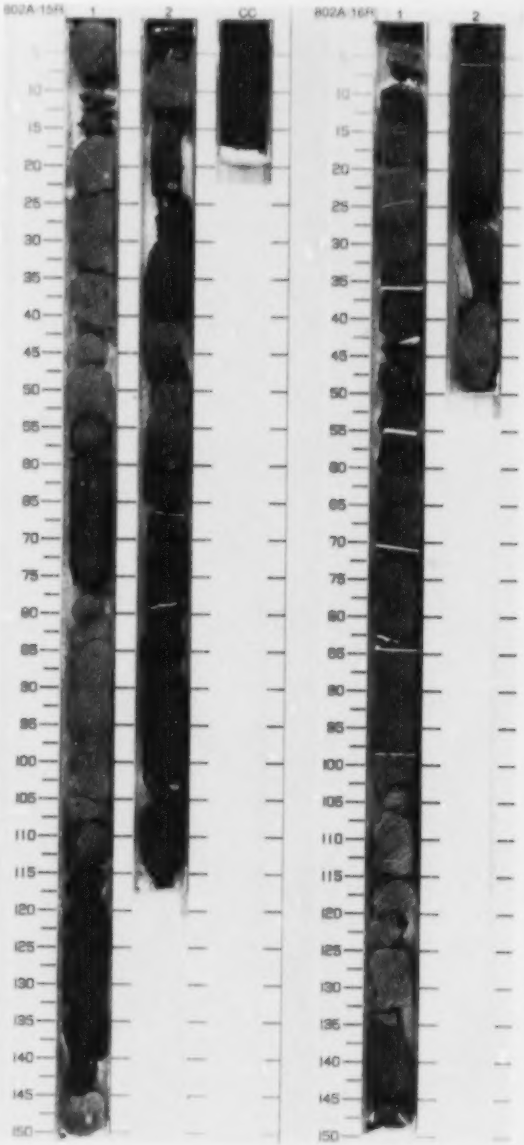
802A-15R
1
2
CC
802A-16R
1
2
10
15
20
25
30
35
40
45
50
55
60
65
70
75
80
85
90
95
100
105
110
115
120
125
130
135
140
145
150

SITE 802 HOLE A CORE 17R CORED INTERVAL 6109.0-6118.3 mbsl; 140.4-149.7 mbsf

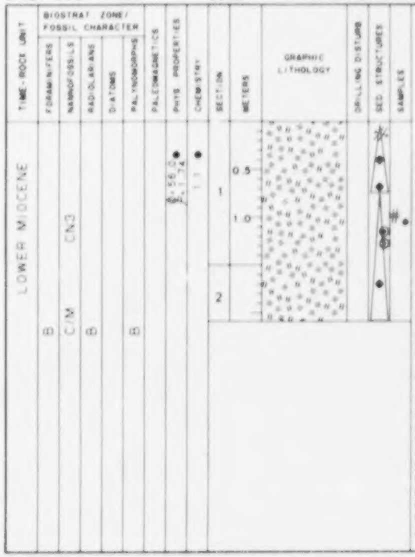
TIME-ROCK UNIT
BIOSTRAT. ZONE/ FOSSIL CHARACTER
FORAMINIFERS
NANNOFOSSILS
RADIOLARIANS
DIATOMS
PALYNOMORPHS
PALEOMAGNETICS
PHYS. PROPERTIES
CHEMISTRY
SECTION
METERS
GRAPHIC LITHOLOGY
DRILLING DISTURB.
SED. STRUCTURES
SAMPLES
LOWER MIOCENE
B
C/M
CN3
B
B
1.1
1
2
0.5
1.0

LITHOLOGIC DESCRIPTION

TUFF

Major lithology: TUFF, greenish black to brownish black (5G 2/1 5YR 2/1), medium- to coarse sandy texture; contains volcanic glass, clay, zeolites, smectite, feldspar and igneous rock fragments, with minor nannofossils in fine grained tops of turbidite beds. Sedimentary structures include meter scale normally graded beds with basal scour, isolated subrounded aphanitic lapilli up to 7 mm in diameter, planar laminations nodules (1-2 mm across) and small veins of white Ca zeolites.

SLIDE SUMMARY (%):

| | 1, 99 | 1, 107 |
|---|---|---|
| | D | M |
| TEXTURE: | | |
| Sand | 30 | — |
| Silt | 50 | 15 |
| Clay | 20 | 85 |
| COMPOSITION: | | |
| Clay | 10 | 25 |
| Feldspar | Tr | 3 |
| Foraminifers | 2 | — |
| Glass | 70 | 50 |
| Igneous rock fragments | — | 2 |
| Nannofossils | — | 5 |
| Opaques | 10 | Tr |
| Oxide | 3 | — |
| Pyroxene | 2 | — |
| Smectite | 3 | 5 |
| Zeolite | — | 10 |

SITE 802 HOLE A CORE 18R CORED INTERVAL 6118.3-6127.7 mbsl; 149.7-159.1 mbsf

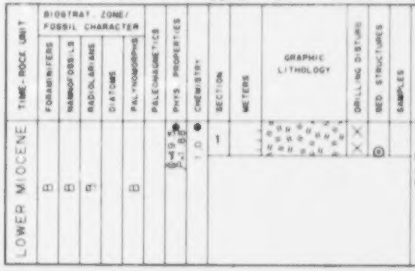
TIME-ROCK UNIT
BIOSTRAT. ZONE/ FOSSIL CHARACTER
FORAMINIFERS
NANNOFOSSILS
RADIOLARIANS
DIATOMS
PALYNOMORPHS
PALEOMAGNETICS
PHYS. PROPERTIES
CHEMISTRY
SECTION
METERS
GRAPHIC LITHOLOGY
DRILLING DISTURB.
SED. STRUCTURES
SAMPLES
LOWER MIOCENE
B
B
B
B
1.0
1

LITHOLOGIC DESCRIPTION

TUFF

Major lithology: TUFF, dark greenish gray (5G 2/1), sandy, massive; 1-cm thick vein of zeolites at Section 1, 35 cm. The disrupted pieces do not allow identification of any sedimentary structures.

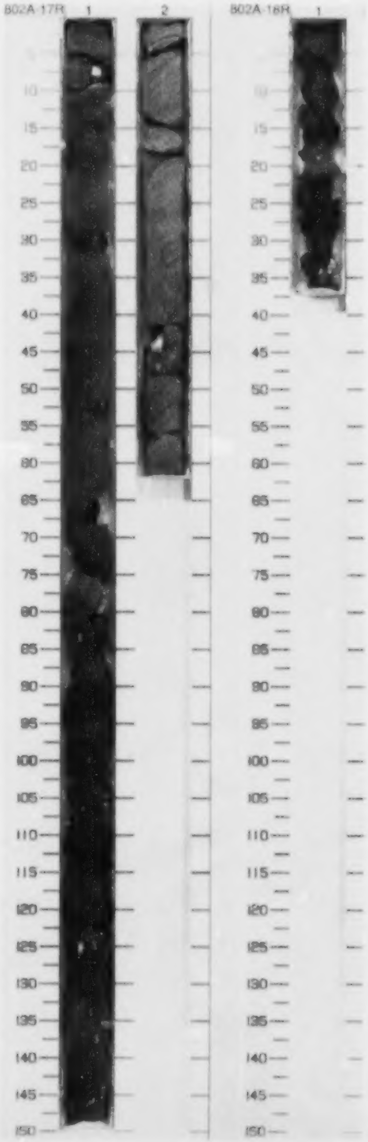
802A-17R
1
2
802A-18R
1
10
15
20
25
30
35
40
45
50
55
60
65
70
75
80
85
90
95
100
105
110
115
120
125
130
135
140
145
150

SITE 802 HOLE A CORE 19R CORED INTERVAL 6127.7-6136.9 mbsl; 159.1-168.3 mbst

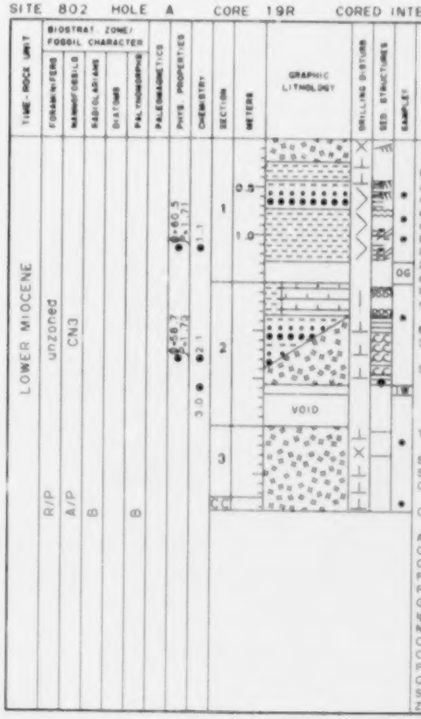
TIME-ROCK UNIT
BIOSTRAT. ZONE/ FOSSIL CHARACTER
FORAMINIFERS
NANNOFOSSILS
RADIOLARIANS
DIATOMS
PALYNOMORPHS
PALEOMAGNETICS
PHYS. PROPERTIES
CHEMISTRY
SECTION
METERS
GRAPHIC LITHOLOGY
DRILLING DISTURB.
SED. STRUCTURES
SAMPLES
LOWER MIOCENE
unzoned
CN3
R/P
A/P
B
B
ϕ-60.5
ρ-1.71
ϕ-58.7
ρ-1.73
1.1
2.1
3.0
1
2
3
CC
0.5
1.0
VOID
OG

LITHOLOGIC DESCRIPTION

TUFF, CLAYSTONE and TURBIDITES

Major lithologies:
a. TUFF, black to very dark gray (5Y 3/1), sand to clay size grains of volcanic rock fragments, glass, and pyroxene, typically planar or cross-laminated; abundant flame structures especially in Section 2, 50-90 cm, where tuffaceous turbidites grade upward to nonvolcaniclastic turbidites.
b. CLAYSTONE, gray to dark grayish brown (5Y 5/1 5YR 5/2), soft, massive locally thinly laminated, scattered microfaults and deformed beds, contains up to 30% nannofossils and 20% volcanic glass.
c. TURBIDITES, dark gray (5Y 4/1) and gray (N3), silty to clayey, thinly laminated with cross laminations, wavy laminations and flame structures. Minor volcaniclastic or biogenic components.

Minor lithology: CLAYEY NANNOFOSSIL CHALK, brown (10YR 5/3), massive, composed of 30% nannofossils, 30% inorganic calcite, 25% clay.

SLIDE SUMMARY (%)

| | 1, 58<br>D | 1, 82<br>D | 1, 103<br>D | 2, 33<br>D | 3, 17<br>D | CC, 6<br>D |
|---|---|---|---|---|---|---|
| TEXTURE | | | | | | |
| Sand | 1 | — | — | Tr | 50 | 25 |
| Silt | 60 | 35 | 20 | 15 | 45 | 45 |
| Clay | 39 | 65 | 80 | 85 | 5 | 30 |
| COMPOSITION | | | | | | |
| Accessory minerals | 3 | — | — | 10 | — | — |
| Calcite | 3 | 3 | — | 30 | — | 3 |
| Clay | 40 | 56 | 75 | 25 | 20 | Tr |
| Feldspar | Tr | — | — | — | 1 | — |
| Foraminifers | 1 | — | — | — | 1 | Tr |
| Glass | 20 | 10 | 10 | 5 | 30 | 60 |
| Igneous rock fragments | — | — | — | — | 36 | 20 |
| Nannofossils | 15 | 20 | — | 30 | — | — |
| Opaques | 2 | 5 | 10 | — | 3 | Tr |
| Oxide | 2 | 3 | 5 | Tr | 2 | Tr |
| Pyroxene | — | — | — | — | 5 | 1 |
| Quartz | Tr | Tr | — | — | — | — |
| Smectite | Tr | — | — | — | — | 3 |
| Zeolite | 5 | 3 | — | — | — | — |

SITE 802 HOLE A CORE 20R CORED INTERVAL 6136.9-6196.2 mbsl; 168.3-177.6 mbsf

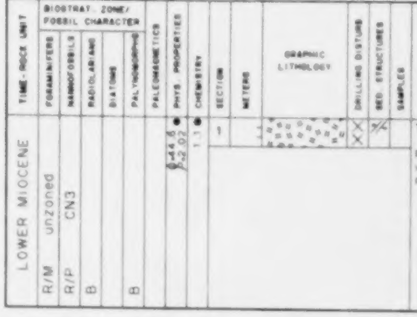
TIME-ROCK UNIT
BIOSTRAT. ZONE/ FOSSIL CHARACTER
FORAMINIFERS
NANNOFOSSILS
RADIOLARIANS
DIATOMS
PALYNOMORPHS
PALEOMAGNETICS
PHYS. PROPERTIES
CHEMISTRY
SECTION
METERS
GRAPHIC LITHOLOGY
DRILLING DISTURB.
SED. STRUCTURES
SAMPLES
LOWER MIOCENE
unzoned
CN3
R/M
R/P
B
B
ϕ-44.6
ρ-2.02
1.1
1

LITHOLOGIC DESCRIPTION

TUFF

Major lithology: TUFF, c[illegible] gray (N3), very fine- to fine-grained sandy texture mostly volcanic rock fragments and glass, no sedimentary structures. One large separate piece of dolomite is inferred to be a fracture filling.

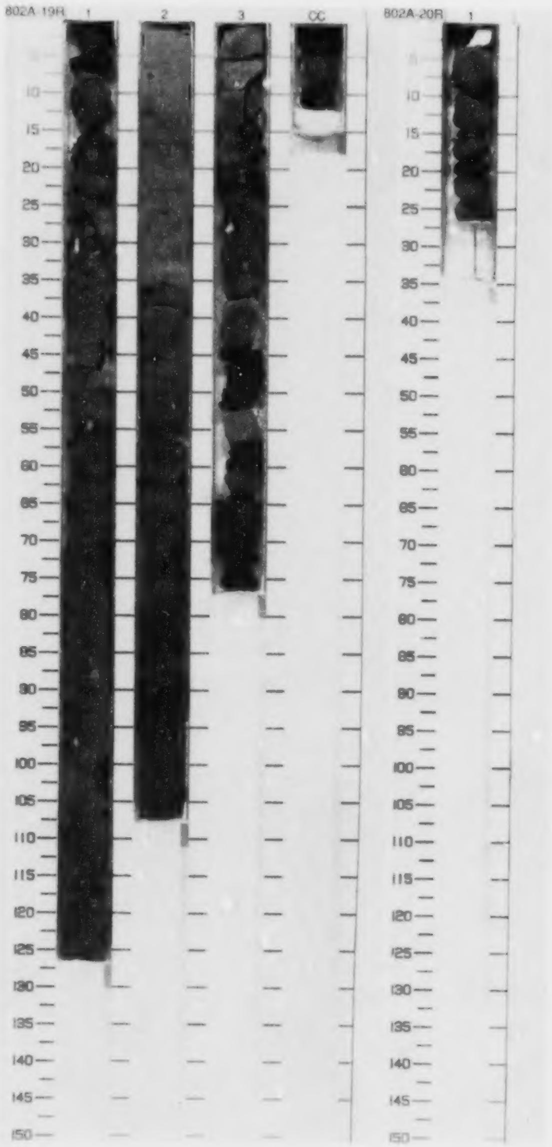
802A-19R
1
2
3
CC
802A-20R
1
5
10
15
20
25
30
35
40
45
50
55
60
65
70
75
80
85
90
95
100
105
110
115
120
125
130
135
140
145
150

SITE 802 HOLE A CORE 21R CORED INTERVAL 6146.2-6155.6 mbsl; 177.6-187.0 mbsf

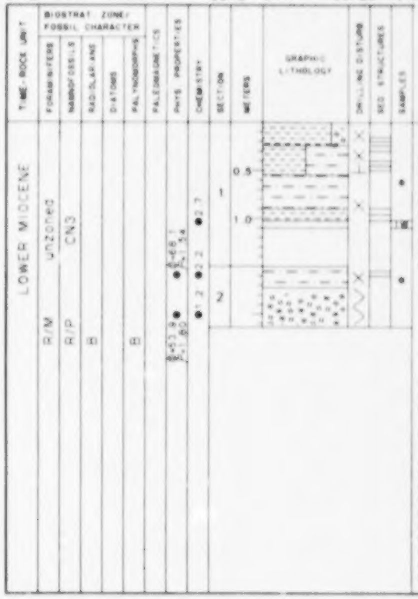
TIME-ROCK UNIT
BIOSTRAT. ZONE/ FOSSIL CHARACTER
FORAMINIFERS
NANNOFOSSILS
RADIOLARIANS
DIATOMS
PALYNOMORPHS
PALEOMAGNETICS
PHYS. PROPERTIES
CHEMISTRY
SECTION
METERS
GRAPHIC LITHOLOGY
DRILLING DISTURB.
SED. STRUCTURES
SAMPLES
LOWER MIOCENE
unzoned
CN3
R/M
R/P
B
B
0.5
1.0
1
2
●2.7
●2.2
●1.2
●φ=68.1 γ=1.54
●φ=53.9 γ=1.80

LITHOLOGIC DESCRIPTION

TUFF, CLAYSTONE and CLAYEY SILTSTONE

Major lithologies:

a. TUFF, grayish black to dark gray (N2 N3), silty to fine grained sandy texture, consisting of volcanic rock fragments and glass, massive.

b. CLAYSTONE, gray to olive gray (N5 5.5Y 4/2), massive to thinly laminated, firm and fissile to completely disrupted by drilling, <15% volcaniclastic in composition. Grades to, and interlaminated with:

c. CLAYEY SILTSTONE, dark gray to olive gray (N4 5Y 4/2), predominantly thinly laminated volcaniclastic content (glass, rock fragments, pyroxene, feldspar) 25-40%, up to 20% nannofossils.

SLIDE SUMMARY (%):

|  | 1, 82 D | 2, 16 D |
|---|---|---|
| TEXTURE: |  |  |
| Sand | — | 5 |
| Silt | 30 | 40 |
| Clay | 70 | 55 |
| COMPOSITION: |  |  |
| Accessory minerals | 5 | 15 |
| Calcite | — | 20 |
| Clay | 77 | 20 |
| Feldspar | 1 | — |
| Glass | 10 | 25 |
| Igneous rock fragments | 4 | — |
| Nannofossils | — | 20 |
| Opaques | 2 | — |
| Oxide | Tr | Tr |
| Pyroxene | 1 | — |

SITE 802 HOLE A CORE 22R CORED INTERVAL 6155.6-6165.0 mbsl; 187.0-196.4 mbsf

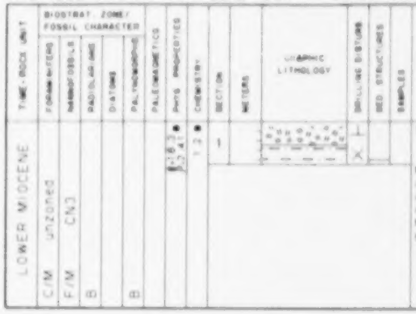
TIME-ROCK UNIT
BIOSTRAT. ZONE/ FOSSIL CHARACTER
FORAMINIFERS
NANNOFOSSILS
RADIOLARIANS
DIATOMS
PALYNOMORPHS
PALEOMAGNETICS
PHYS. PROPERTIES
CHEMISTRY
SECTION
METERS
GRAPHIC LITHOLOGY
DRILLING DISTURB.
SED. STRUCTURES
SAMPLES
LOWER MIOCENE
unzoned
CN3
C/M
F/M
B
B
1
●1.2
●φ=61.6 γ=2.41

LITHOLOGIC DESCRIPTION

TUFF and TUFFACEOUS CLAYSTONE

Major lithologies:

a. TUFF, black to dark gray (N1 N3), sandy to silty, massive, highly porous with abundant authigenic clays and zeolites as spherules and euhedral crystals in cavities. Cavities are of unknown origin possibly microfossil molds.

b. TUFFACEOUS CLAYSTONE, medium dark gray (N4), sharp change to dark greenish gray (5GY 4/1) at Section 1, 42 cm, homogeneous, massive.

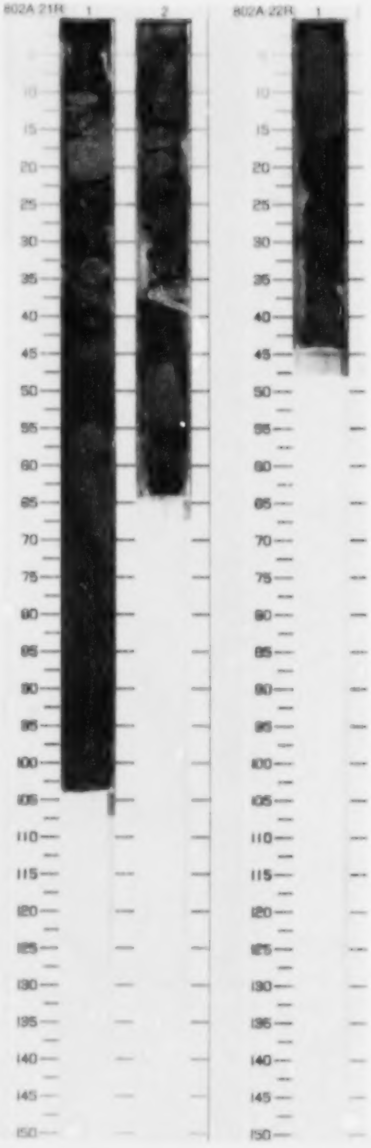
802A-21R
1
2
802A-22R
1
5
10
15
20
25
30
35
40
45
50
55
60
65
70
75
80
85
90
95
100
105
110
115
120
125
130
135
140
145
150

SITE 802 HOLE A CORE 23R CORED INTERVAL 6165.0-6175.1 mbsl; 196.4-206.1 mbsf

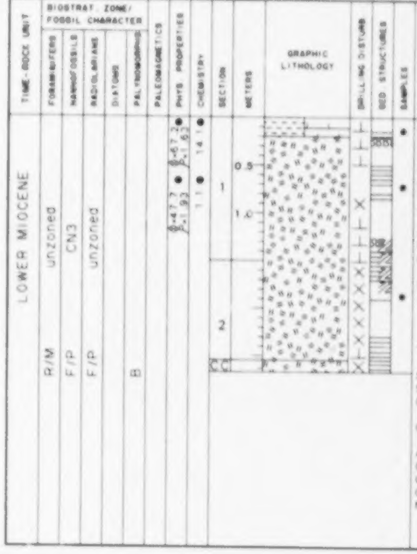
TIME-ROCK UNIT
BIOSTRAT. ZONE/ FOSSIL CHARACTER
FORAMINIFERS
NANNOFOSSILS
RADIOLARIANS
DIATOMS
PALYNOMORPHS
PALEOMAGNETICS
PHYS. PROPERTIES
CHEMISTRY
SECTION
METERS
GRAPHIC LITHOLOGY
DRILLING DISTURB.
SED. STRUCTURES
SAMPLES
LOWER MIOCENE
unzoned
CN3
unzoned
R/M
F/P
F/P
B
φ=67.2
γ=1.63
φ=47.7
γ=1.93
14.1
1.1
1
2
CC
0.5
1.0

**LITHOLOGIC DESCRIPTION**

TUFF and CALCAREOUS NANNOFOSSIL CLAY

Major lithologies:

a. TUFF, sandy to clayey; coarser lithologies are brownish black to black (5Y 2/1 N1), finer lithologies are mostly gray (5Y 4/1). Largely crushed to puree in this core; coherent pieces are massive to thinly laminated (<1 mm). The interval from Section 1, 130 cm, to Section 2, 16 cm, displays numerous microfaults and deformed laminations, probably synsedimentary slumping.

b. CALCAREOUS NANNOFOSSIL CLAY, gray (5Y 5/1 5Y 5/1), firm to soft, mostly massive, locally thinly laminated, rare burrows. Up to 30% nannofossils and 20% inorganic calcite.

SLIDE SUMMARY (%):

| | 1, 13<br>D | 1, 122<br>D | 2, 88<br>D |
|---|---|---|---|
| TEXTURE: | | | |
| Sand | Tr | Tr | 10 |
| Silt | 30 | 50 | 50 |
| Clay | 70 | 50 | 40 |
| COMPOSITION: | | | |
| Accessory minerals | 5 | 15 | 20 |
| Calcite | 20 | 5 | 10 |
| Clay | 35 | 40 | 40 |
| Glass | 10 | 30 | 30 |
| Nannofossils | 30 | 10 | Tr |

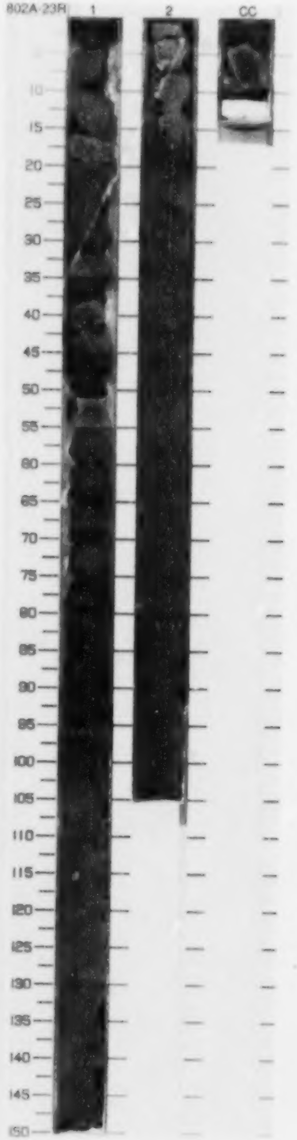
802A-23R
1
2
CC
10
15
20
25
30
35
40
45
50
55
60
65
70
75
80
85
90
95
100
105
110
115
120
125
130
135
140
145
150

SITE 802 HOLE A CORE 24R CORED INTERVAL 6174.7-6184.3 mbsl; 206.1-215.7 mbsf

| TIME-ROCK UNIT | BIOSTRAT. ZONE/ FOSSIL CHARACTER | | | | | PALEOMAGNETICS | PHYS. PROPERTIES | CHEMISTRY | SECTION | METERS | GRAPHIC LITHOLOGY | DRILLING DISTURB. | SED. STRUCTURES | SAMPLES | LITHOLOGIC DESCRIPTION |
|---|---|---|---|---|---|---|---|---|---|---|---|---|---|---|---|
| | FORAMINIFERS | NANNOFOSSILS | RADIOLARIANS | DIATOMS | PALYNOMORPHS | | | | | | | | | | |
| LOWER MIOCENE | unzoned<br>C/M | CN2 - NN3<br>A/P | B | | B | | ● φ=66.7<br>γ=1.57 | ● 29.7 | 1 | | | X | | ●<br>■ | CALCAREOUS NANNOFOSSIL CHALK and NANNOFOSSIL CLAYEY SILTSTONE |

Major lithologies:

a. CALCAREOUS NANNOFOSSIL CHALK, gray (5Y 5/1), firm, massive; composed of 50% nannofossils, 10% calcite, 20% clay, and 10% volcanic glass.

b. NANNOFOSSIL CLAYEY SILTSTONE, gray (5Y 5/1), firm, thinly laminated. Compositionally similar to a., except for increased volcaniclastic component (≈35%); also contains rare foraminifers.

SLIDE SUMMARY (%):

| | 1, 4<br>D | 1, 11<br>D |
|---|---|---|
| TEXTURE: | | |
| Sand | Tr | 5 |
| Silt | 30 | 45 |
| Clay | 70 | 50 |
| COMPOSITION: | | |
| Accessory minerals | 10 | 5 |
| Calcite | 10 | 10 |
| Clay | 20 | 25 |
| Foraminifers | — | Tr |
| Glass | 10 | 30 |
| Nannofossils | 50 | 30 |
| Oxide | Tr | — |

802A 24R
1
5
10
15
20
25
30
35
40
45
50
55
60
65
70
75
80
85
90
95
100
105
110
115
120
125
130
135
140
145
150

SITE 802 HOLE A CORE 25R CORED INTERVAL 6784.3-6194.0 mbsl; 215.7-225.4 mbsf

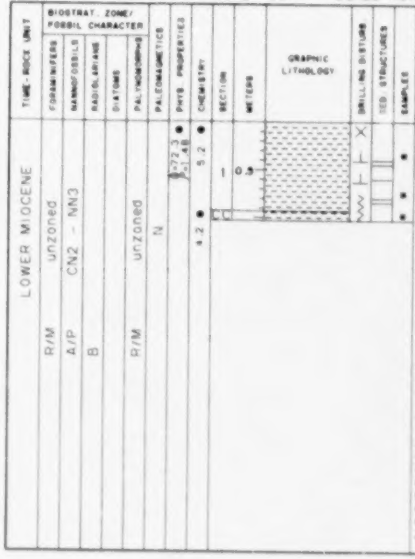
TIME-ROCK UNIT
BIOSTRAT. ZONE/ FOSSIL CHARACTER
FORAMINIFERS
NANNOFOSSILS
RADIOLARIANS
DIATOMS
PALYNOMORPHS
PALEOMAGNETICS
PHYS. PROPERTIES
CHEMISTRY
SECTION
METERS
GRAPHIC LITHOLOGY
DRILLING DISTURB.
SED. STRUCTURES
SAMPLES
LOWER MIOCENE
R/M unzoned
A/P CN2 - NN3
B
R/M unzoned
N
φ=72.3
γ=1.48
5.2
4.2
1
0.5
CC

**LITHOLOGIC DESCRIPTION**

CLAYSTONE with NANNOFOSSILS

Major lithology: CLAYSTONE with NANNOFOSSILS, olive brown (2.5YR 4/4) in Section 1, 0-50 cm, in sharp contact above gray (N5) claystone, with a layer (2-4 mm) of more indurated claystone of blue gray (5BG 4/1) at the contact; color change apparently due to a downward decrease in opaques and a lesser increase in nannofossil content. Reddish spots (1 mm in diameter) at Section 1, 20 cm and 32-37 cm. Rare subtle laminations.

Minor lithology: Core catcher contains pieces of TUFFACEOUS CLAYSTONE with NANNOFOSSILS, medium gray (N5), containing wood fragments.

SLIDE SUMMARY (%):

|  | 1, 35<br>D | 1, 75<br>D | CC, 6<br>D |
|---|---|---|---|
| TEXTURE: |  |  |  |
| Sand | — | — | 10 |
| Silt | 15 | 10 | 35 |
| Clay | 85 | 90 | 55 |
| COMPOSITION: |  |  |  |
| Accessory minerals | — | — | 1 |
| Calcite | — | — | 7 |
| Clay | 57 | 59 | 57 |
| Glass | 5 | 3 | 25 |
| Nannofossils | 20 | 30 | 10 |
| Opaques | 1 | 2 | — |
| Oxide | 15 | 1 | — |
| Zeolite | 2 | 5 | — |

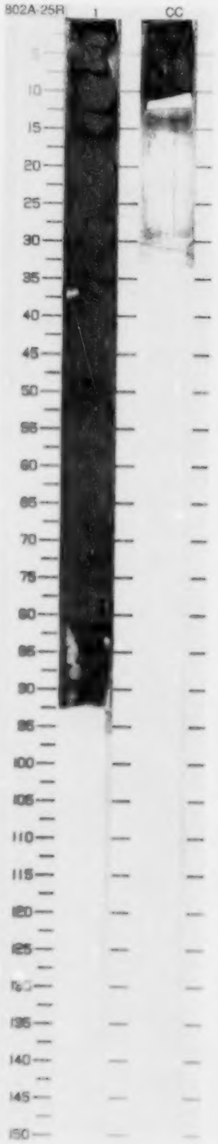
802A-25R
1
CC
5
10
15
20
25
30
35
40
45
50
55
60
65
70
75
80
85
90
95
100
105
110
115
120
125
130
135
140
145
150

SITE 802 HOLE A CORE 26R CORED INTERVAL 6194.0-6203.7 mbsl; 225.4-235.1 mbsf

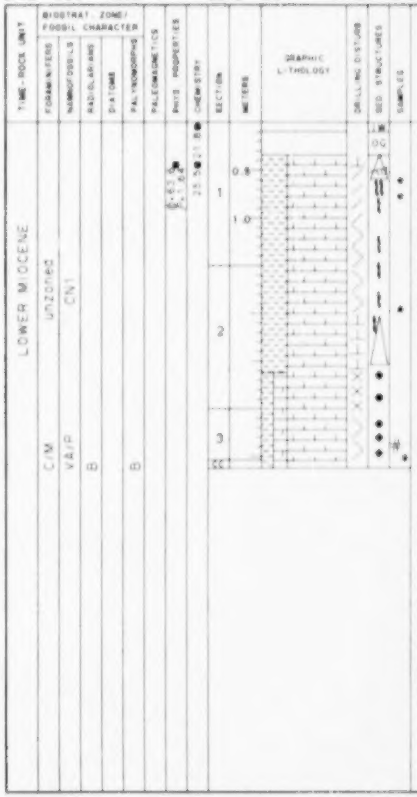
TIME-ROCK UNIT
BIOSTRAT. ZONE/ FOSSIL CHARACTER
FORAMINIFERS
NANNOFOSSILS
RADIOLARIANS
DIATOMS
PALYNOMORPHS
PALEOMAGNETICS
PHYS. PROPERTIES
CHEMISTRY
SECTION
METERS
GRAPHIC LITHOLOGY
DRILLING DISTURB.
SED. STRUCTURES
SAMPLES
LOWER MIOCENE
unzoned
C/M
CN1
VA/P
B
B
25.5
21.8
1
2
3
CC
0.5
1.0
OG

LITHOLOGIC DESCRIPTION

CLAYEY NANNOFOSSIL CHALK and NANNOFOSSIL CHALK with CLAY AND FORAMINIFERS

Major lithologies:
a. CLAYEY NANNOFOSSIL CHALK, light olive gray to light gray (5Y 6/1, N7), with dark streaks, moderately bioturbated, grading downward in the middle of Section 2 to:
b. NANNOFOSSIL CHALK with CLAY AND FORAMINIFERS, very pale brown (10YR 7/3), containing 5-10% of angular to subrounded calcareous claystone rip-up clasts, of moderate yellowish brown (10YR 5/4) and up to 1 cm in length.

Minor lithologies:
a. TUFFACEOUS CLAYSTONE (Section 1, 57-62 cm), medium light gray (N6), bioturbated upper portion of a bed of clayey nannofossil chalk.
b. SILTY CLAYSTONE (Section 1, 53-57 cm), through cross-laminated, base of a bed of clayey nannofossil chalk. These two minor lithologies suggest that some of the clayey nannofossil chalk beds are redeposited.

SLIDE SUMMARY (%):

| | 1, 61 | 1, 78 | 2, 96 | 3, 10 | 3, 54 |
|---|---|---|---|---|---|
| | M | D | D | M | D |
| TEXTURE: | | | | | |
| Sand | — | — | 5 | 20 | 15 |
| Silt | 30 | 40 | 35 | 30 | 10 |
| Clay | 70 | 60 | 60 | 50 | 75 |
| COMPOSITION: | | | | | |
| Accessory minerals | 1 | 1 | 1 | Tr | 1 |
| Bioclast | — | — | — | 3 | — |
| Calcite | 2 | 15 | 20 | — | 17 |
| Clay | 60 | 25 | 25 | 20 | 15 |
| Feldspar | — | — | 1 | 1 | Tr |
| Fish | — | — | Tr | — | 1 |
| Foraminifers | — | — | 6 | 6 | 10 |
| Glass | 25 | 3 | 5 | 16 | 2 |
| Mica | — | — | 2 | — | 1 |
| Micrite | — | — | — | 50 | — |
| Nannofossils | 2 | 50 | 35 | — | 40 |
| Opaques | 5 | 3 | 2 | — | 2 |
| Oxide | — | — | — | 2 | — |
| Quartz | 2 | 1 | — | — | 3 |
| Radiolarians | — | — | — | — | 6 |
| Smectite | — | — | — | 10 | — |
| Spines | — | — | — | — | Tr |
| Zeolite | 3 | 1 | 3 | — | 2 |

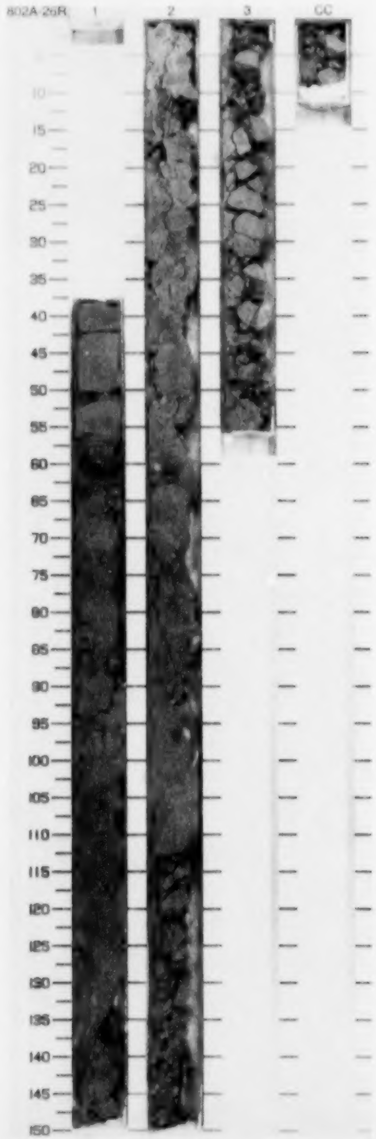
802A-26R
1
2
3
CC
10
15
20
25
30
35
40
45
50
55
60
65
70
75
80
85
90
95
100
105
110
115
120
125
130
135
140
145
150

SITE 802 HOLE A CORE 27R CORED INTERVAL 6203.7-6213.3 mbsl; 235.1-244.7 mbsf

| TIME-ROCK UNIT | BIOSTRAT. ZONE/ FOSSIL CHARACTER: FORAMINIFERS | NANNOFOSSILS | RADIOLARIANS | DIATOMS | PALYNOMORPHS | PALEOMAGNETICS | PHYS. PROPERTIES | CHEMISTRY | SECTION |
|---|---|---|---|---|---|---|---|---|---|
| LOWER MIOCENE | unzoned | CN1 | | | | | $\phi$=54.4 $\gamma$=1.79 | 40.2 | 1 |
| | | | | | | | | | 2 |
| | | | | | | | $\phi$=48.9 $\gamma$=1.89 | 60.8 | 3 |
| | | | | | | N | | | 4 |
| | | | | | | | $\phi$=46.5 $\gamma$=1.89 | 43.3 | 5 |
| | A/M | VA/P | B | | B | | | | 6 |

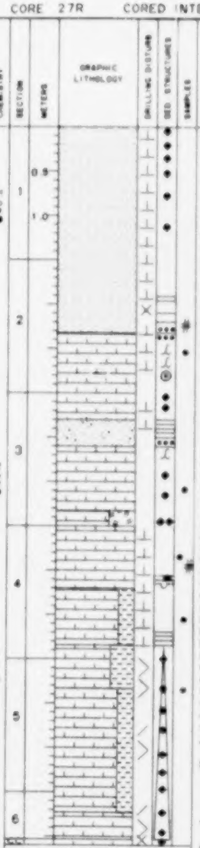

## LITHOLOGIC DESCRIPTION

TUFF, NANNOFOSSIL CHALK and TUFFACEOUS NANNOFOSSIL CHALK

Major lithologies:
a. TUFF, grayish green to gray (5G 5/1 N4), sandy, poorly to moderately sorted, fine- to coarse-grained, massive to laminated; contains clasts up to 3 cm in diameter of claystone, tuff and igneous rock. Bulk of rock consists of tuff, glass, feldspar and zeolites in a calcareous matrix/cement.
b. NANNOFOSSIL CHALK, greenish gray to light yellowish brown (5GY 6/1 10YR 6/4), massive with dark wispy structures and isolated claystone or tuff clasts. Grades to
c. TUFFACEOUS NANNOFOSSIL CHALK, light greenish gray (5GY 6/1); contains more dark, aphanitic tuff clasts.

Minor lithology: CLAYSTONE, brown to brownish black (7.5YR 5/4 5YR 2/1), zeolitic to tuffaceous, mostly as intraclasts in chalk, but also several layers too big to identify as clasts.

Note: Marked color change from grays to browns at Section 4, 145 cm, indicates the top of a large normally graded bed that extends to the base of Core 28R. Below this point, nannofossil chalk and claystone in Sections 5 and CC is disrupted, mixed and horizontally sheared as in a slump.

SLIDE SUMMARY (%):

| | 2, 73<br>D | 2, 103<br>D | 3, 109<br>D | 4, 35<br>D | 4, 46<br>M | 4, 106<br>D | 5, 33<br>M |
|---|---|---|---|---|---|---|---|
| TEXTURE: | | | | | | | |
| Sand | 70 | — | — | 5 | 10 | 4 | — |
| Silt | 25 | 20 | 20 | 50 | 30 | 38 | 20 |
| Clay | 5 | 80 | 80 | 45 | 60 | 58 | 80 |
| COMPOSITION: | | | | | | | |
| Accessory minerals | — | — | — | — | 1 | 1 | — |
| Algae | 15 | — | — | — | — | — | — |
| Bioclast | 8 | — | — | — | — | — | — |
| Calcite | 3 | 15 | 20 | 8 | — | 20 | Tr |
| Clay | — | — | — | 30 | 10 | 19 | 75 |
| Feldspar | — | — | — | — | 1 | — | — |
| Foraminifers | 5 | — | — | — | 15 | — | — |
| Glass | 55 | 10 | 5 | 5 | 5 | 5 | 20 |
| Glauconite | — | — | — | — | Tr | — | — |
| Igneous rock fragments | 10 | — | — | — | 5 | — | |
| Mica | — | 3 | 5 | — | — | — | — |
| Micrite | — | — | — | — | 60 | — | — |
| Nannofossils | 2 | 61 | 60 | 57 | — | 55 | — |
| Opaques | 1 | 4 | 5 | — | 2 | — | — |
| Oxide | Tr | 2 | 2 | — | — | — | — |
| Plant | — | — | — | — | 1 | — | — |
| Pyroxene | 1 | — | — | — | — | — | — |
| Quartz | — | — | — | — | Tr | — | — |
| Spines | — | — | — | — | — | — | 5 |
| Zeolite | — | 5 | 3 | — | — | — | Tr |

SLIDE SUMMARY (%):

| | 5, 65<br>D | 5, 121<br>M | 5, 143<br>D |
|---|---|---|---|
| TEXTURE: | | | |
| Sand | — | — | 12 |
| Silt | 20 | 15 | 33 |
| Clay | 80 | 85 | 55 |
| COMPOSITION: | | | |
| Accessory minerals | — | 1 | — |
| Algae | — | — | 5 |
| Bioclast | — | — | 10 |
| Calcite | 20 | — | — |
| Clay | — | 61 | 27 |
| Foraminifers | 15 | Tr | 15 |
| Glass | — | 16 | 4 |
| Micrite | — | — | 25 |
| Nannofossils | 65 | — | Tr |
| Opaques | — | 2 | 2 |
| Oxide | — | 2 | 2 |
| Pyroxene | — | — | Tr |
| Rock fragment | — | — | 10 |
| Zeolite | — | 15 | — |

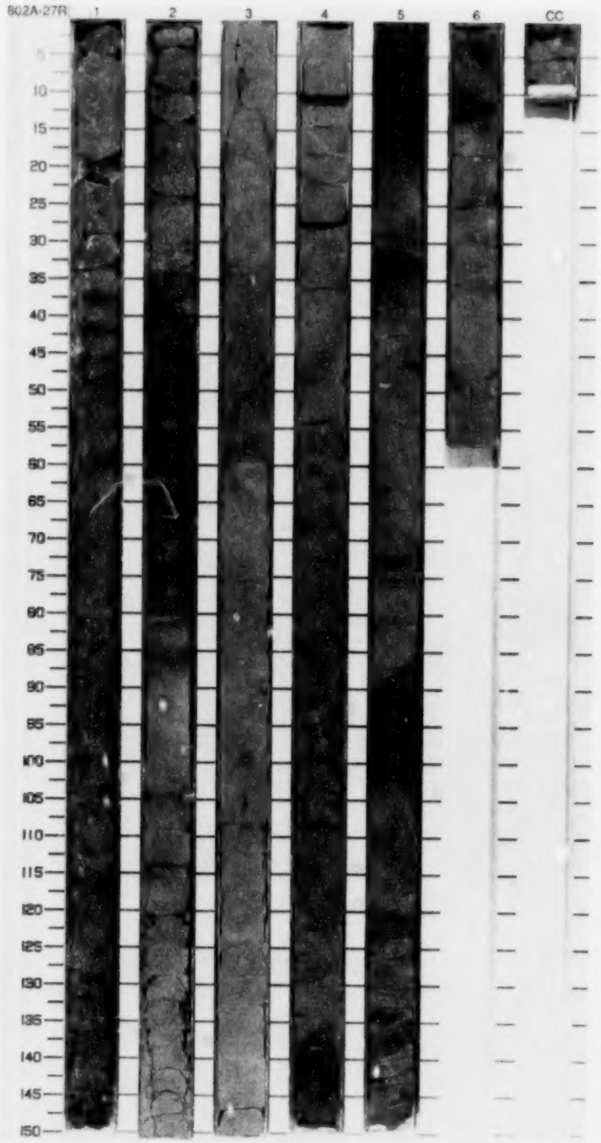

SITE 802 HOLE A CORE 28R CORED INTERVAL 6213.3-6 [illegible] mbsl; 244.7-254.5 mbsf

| TIME-ROCK UNIT | BIOSTRAT. ZONE/ FOSSIL CHARACTER: FORAMINIFERS | NANNOFOSSILS | RADIOLARIANS | DIATOMS | PALYNOMORPHS |
|---|---|---|---|---|---|
| LOWER MIOCENE | [illegible]<br>A/M | CN1<br>A/C | B | | B |

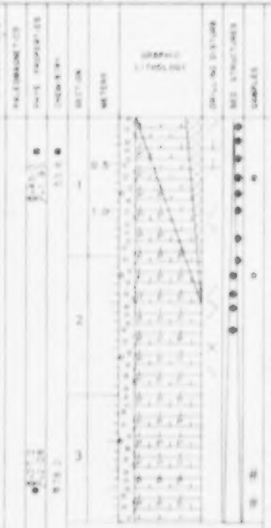
PALEOMAGNETICS
PHYS. PROPERTIES
CHEMISTRY
SECTION
METERS
GRAPHIC LITHOLOGY
DRILLING DISTURB.
SED. STRUCTURES
SAMPLES
1
2
3
0.5
1.0

LITHOLOGIC DESCRIPTION

CLAYEY NANNOFOSSIL CHALK with VOLCANICLASTICS and NANNOFOSSIL-RICH FORAMINIFERAL PACKSTONE with VOLCANICLASTICS

Major lithologies:

a. CLAYEY NANNOFOSSIL CHALK with VOLCANICLASTICS, light yellowish brown (10YR 6/4, 5/4). Mixed pelagic and volcanogenic sediments; contains rounded, subhorizontally oriented flakes of claystone, tuff and coarse-grained carbonates.

b. NANNOFOSSIL FORAMINIFERAL PACKSTONE with VOLCANICLASTICS, light gray to light greenish gray (N7, 7.5 5GY 7/1); continuous gradation from a above, with increased grain size and calcitic carbonate content. Silty to very coarse grained, poorly sorted, mostly [illegible]. Reef algae and other coarse carbonate clasts, including bryozoans, coated grains and shell fragments. Packstone also includes large clasts of claystone and tuff; minor amounts of [illegible] clasts. Moderately well cemented by calcite; still very porous and friable.

Note: This entire core consists of one thinly upward bed that starts with coarse packstone and grades through medium-grained packstone to chalk ultimately in Core 27R, Section 3. Mixed and disrupted sediments at top suggest a slump or mass flow deposit, whereas the lower part may be a coarse grained turbidite. All lithologies are tuffaceous (10-15% glass and lapilli) and volcanic clasts.

SMEAR SLIDE SUMMARY (%):

| | 1, 60<br>D | 2, 20<br>D | 3, 95<br>M | 3, 117<br>M |
|---|---|---|---|---|
| TEXTURE: | | | | |
| Sand | 20 | 10 | 70 | 70 |
| Silt | 20 | 30 | 15 | 15 |
| Clay | 60 | 60 | 15 | 15 |
| COMPOSITION: | | | | |
| Accessory minerals | 5 | 5 | 1 | — |
| Bioclasts | — | — | 30 | 58 |
| Calcite | 10 | 10 | — | — |
| Clay | 20 | 20 | — | — |
| Foraminifers | 5 | 15 | 20 | 10 |
| Glass | 10 | 10 | 2 | — |
| Igneous rock fragments | — | — | 5 | 15 |
| Intraclasts | — | — | 10 | 5 |
| Micrite | — | — | 20 | 10 |
| Nannofossils | 40 | 40 | — | — |
| Opaques | — | — | 2 | 1 |
| Plant | — | — | 1 | — |
| Quartz | — | — | 1 | — |
| Radiolarians | — | — | 2 | — |
| Smectite | — | — | 2 | 1 |
| Sponges | — | — | 1 | — |

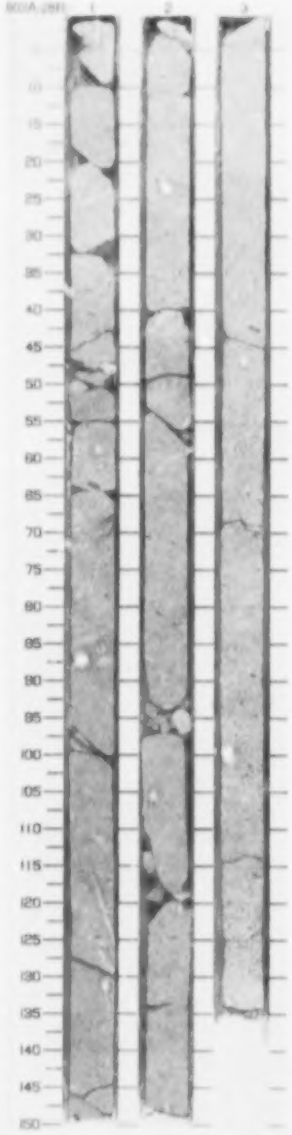
802A-28R
1
2
3
5
10
15
20
25
30
35
40
45
50
55
60
65
70
75
80
85
90
95
100
105
110
115
120
125
130
135
140
145
150

SITE 802 HOLE A CORL 29R CORED INTERVAL 6223.1-3232.8 mbsl; 254.5-264.2 mbsf

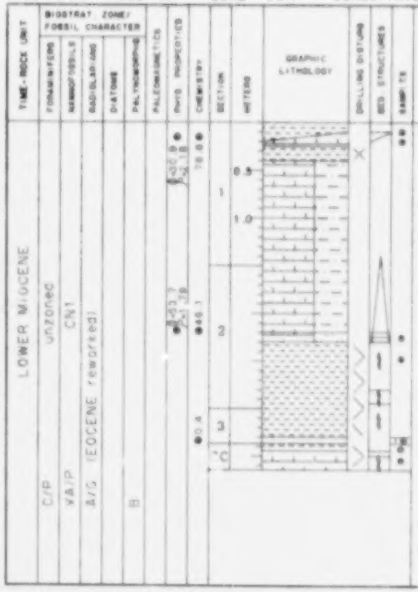
TIME-ROCK UNIT
BIOSTRAT. ZONE/ FOSSIL CHARACTER
FORAMINIFERS
NANNOFOSSILS
RADIOLARIANS
DIATOMS
PALYNOMORPHS
PALEOMAGNETICS
PHYS. PROPERTIES
CHEMISTRY
SECTION
METERS
GRAPHIC LITHOLOGY
DRILLING DISTURB.
SED. STRUCTURES
SAMPLES
LOWER MIOCENE
C/P unzoned
VA/P CN1
B/G (EOCENE reworked)
B
1
2
3
CC
0.5
1.0
78.0
46.1
0.4

### LITHOLOGIC DESCRIPTION

CLAYSTONE and NANNOFOSSIL CALCAREOUS SILTY CLAYSTONE to CLAYEY SILTSTONE

Major lithologies:

a. CLAYSTONE, very dark brown to light yellowish brown (10YR 2/2 10YR 6/4), firm, scattered patches of lighter and darker color, some bioturbation. Smear slides show abundant clay and iron oxide aggregates.

b. NANNOFOSSIL CALCAREOUS SILTY CLAYSTONE to CLAYEY SILTSTONE, silty to sandy texture, dark brown to light yellow brown (10YR 3/3 10YR 6/4) and one interval at Section 1, 0-10 cm that is greenish gray (5GY 6/1). Mostly massive to locally thinly laminated, contains small mud and sandy clasts.

SLIDE SUMMARY (%):

| | 1, 10<br>D | 1, 20<br>D | 2, 77<br>M | 2, 148<br>D | CC, 4<br>D | CC, 25<br>D |
|---|---|---|---|---|---|---|
| TEXTURE: | | | | | | |
| Sand | Tr | Tr | 20 | Tr | Tr | 15 |
| Silt | 20 | 15 | 40 | 20 | 15 | 15 |
| Clay | 80 | 85 | 40 | 80 | 85 | 70 |
| COMPOSITION: | | | | | | |
| Accessory minerals | — | — | 5 | 5 | — | — |
| Calcite | 5 | 5 | 50 | 5 | 5 | 5 |
| Clay | 75 | 10 | 5 | 80 | 80 | 5 |
| Foraminifers | — | 5 | 5 | Tr | — | 15 |
| Glass | 5 | 5 | 15 | — | 5 | Tr |
| Micronodule | 5 | — | 10 | 5 | — | — |
| Nannofossils | 5 | 75 | 10 | Tr | Tr | 65 |
| Radiolarians | — | Tr | Tr | — | — | 5 |
| Spines | — | — | — | — | — | 5 |
| Zeolite | 5 | — | — | Tr | 10 | — |

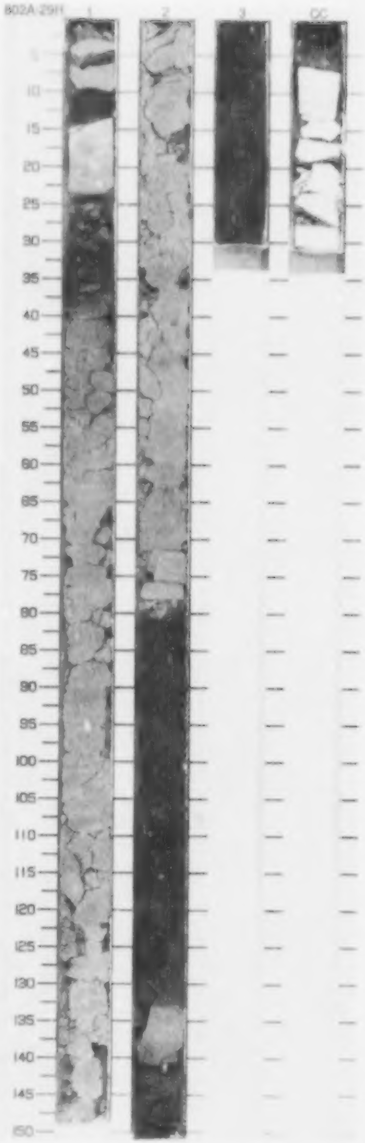
802A-29R
1
2
3
CC
5
10
15
20
25
30
35
40
45
50
55
60
65
70
75
80
85
90
95
100
105
110
115
120
125
130
135
140
145
150

SITE 802 HOLE A CORE 30R CORED INTERVAL 6232.8-6242.4 mbsl; 264.2-273.8 mbsf

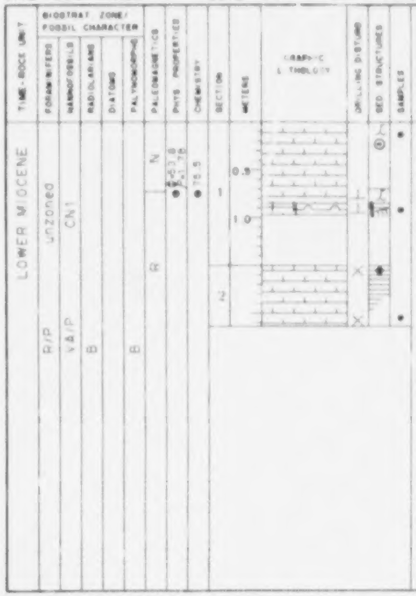
TIME-ROCK UNIT
BIOSTRAT. ZONE/ FOSSIL CHARACTER
FORAMINIFERS
NANNOFOSSILS
RADIOLARIANS
DIATOMS
PALYNOMORPHS
PALEOMAGNETICS
PHYS. PROPERTIES
CHEMISTRY
SECTION
METERS
GRAPHIC LITHOLOGY
DRILLING DISTURB.
SED. STRUCTURES
SAMPLES
LOWER MIOCENE
unzoned
R/P
CN1
VA/P
B
B
N
R
53.8
1.78
75.5
1
2
0.5
1.0

LITHOLOGIC DESCRIPTION

NANNOFOSSIL CHALK

Major lithology: NANNOFOSSIL CHALK, pale brown to yellowish brown to light gray (10YR 6/3 10YR 4/4 10YR 7/2), firm, laminated to massive with wispy lenticular patches of different hue (bioturbation?), small oxidation aureoles around some flaky claystone inclusions. Darkens with increased radiolarian and sponge spicule content.

Minor lithology: SPICULAR BIOGENIC SANDSTONE at Section 1, 87-94 cm; white and dark yellowish brown (10YR 8/1 & 10YR 4/4), thinly laminated and cross laminated, large cross cutting U-shaped burrow.

SLIDE SUMMARY (%):

| | 1, 12<br>D | 1, 91<br>M | 2, 55<br>D |
|---|---|---|---|
| TEXTURE: | | | |
| Sand | — | 40 | 2 |
| Silt | 35 | 30 | 10 |
| Clay | 65 | 30 | 88 |
| COMPOSITION: | | | |
| Calcite | 15 | 10 | 40 |
| Clay | 5 | — | 5 |
| Foraminifers | Tr | 10 | 5 |
| Glass | 5 | — | — |
| Nannofossils | 65 | 25 | 45 |
| Opaques | — | — | Tr |
| Oxide | — | — | Tr |
| Radiolarians | Tr | 40 | 5 |
| Spicules | 10 | 10 | — |
| Spines | — | 5 | — |
| Zeolite | — | — | Tr |

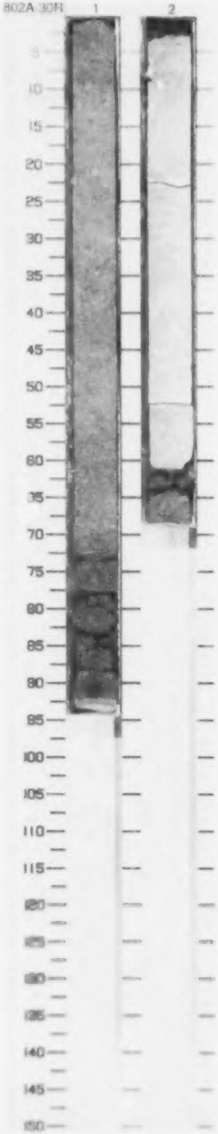
802A-30R
1
2
5
10
15
20
25
30
35
40
45
50
55
60
65
70
75
80
85
90
95
100
105
110
115
120
125
130
135
140
145
150

SITE 802 HOLE A CORE 31R CORED INTERVAL 6242.4-6252.1 mbsl; 273.8-283.5 mbsf

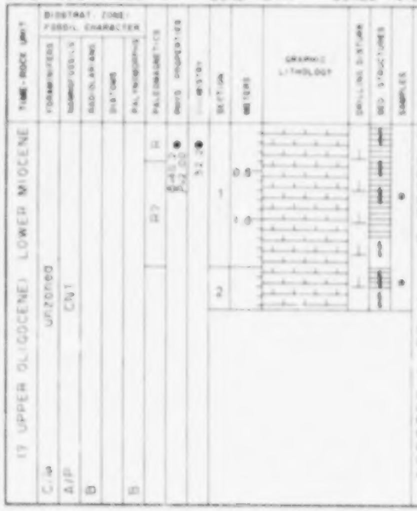
TIME-ROCK UNIT
BIOSTRAT. ZONE/ FOSSIL CHARACTER
FORAMINIFERS
NANNOFOSSILS
RADIOLARIANS
DIATOMS
PALYNOMORPHS
PALEOMAGNETICS
PHYS. PROPERTIES
CHEMISTRY
SECTION
METERS
GRAPHIC LITHOLOGY
DRILLING DISTURB.
SED. STRUCTURES
SAMPLES
(?) UPPER OLIGOCENE/ LOWER MIOCENE
unzoned
CN1
C/M
A/P
B
B
R
R?
52.2
1
2
0.5
1.0

LITHOLOGIC DESCRIPTION

NANNOFOSSIL CHALK

Main lithology: NANNOFOSSIL CHALK, light brown (10YR 6/3) grading to 7.5YR 6/2) with grayish brown (10YR 6/2) in Section 2, 30-45 cm; laminated with common bioturbation. Chalk consists mainly of nannofossils (mixed upper Cretaceous and Paleocene assemblages) and micrite with traces of FeMn oxides, clay, mica and zeolites. Dark grains in Section 1, 120-150 cm may be metal oxide concretions.

SLIDE SUMMARY (%):

| | 1, 75<br>D | 2, 17<br>D |
|---|---|---|
| TEXTURE: | | |
| Silt | 3 | 1 |
| Clay | 97 | 99 |
| COMPOSITION: | | |
| Clay | 1 | — |
| Glass | 1 | — |
| Mica | 2 | 1 |
| Nannofossils | 90 | 94 |
| Opaques | 2 | 3 |
| Oxide | 3 | 2 |
| Zeolite | 1 | — |

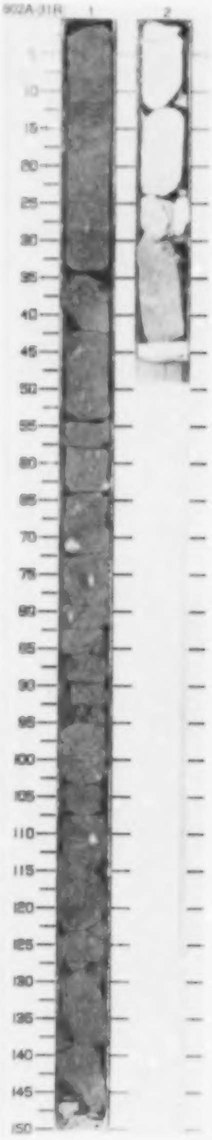
802A-31R
1
2
5
10
15
20
25
30
35
40
45
50
55
60
65
70
75
80
85
90
95
100
105
110
115
120
125
130
135
140
145
150

SITE 802 HOLE A CORE 32R CORED INTERVAL 6252.1-6261.4 mbsl; 283.5-292.8 mbsf

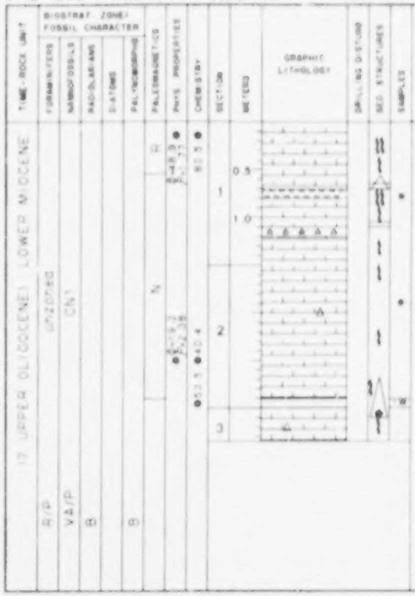
TIME-ROCK UNIT
BIOSTRAT. ZONE/ FOSSIL CHARACTER
FORAMINIFERS
NANNOFOSSILS
RADIOLARIANS
DIATOMS
PALYNOMORPHS
PALEOMAGNETICS
PHYS. PROPERTIES
CHEMISTRY
SECTION
METERS
GRAPHIC LITHOLOGY
DRILLING DISTURB.
SED. STRUCTURES
SAMPLES
?? UPPER OLIGOCENE/ LOWER MIOCENE
unzoned
R/P
CN1
VA/P
B
B
R
N
82.5
40.4
83.5
1
2
3
0.5
1.0

LITHOLOGIC DESCRIPTION

NANNOFOSSIL CHALK

Major lithology: NANNOFOSSIL CHALK, dark grayish brown to light brownish gray (10YR 4/2, 10YR 6/2) with upper portions of beds commonly having the lighter coloration; moderately bioturbated by 0.5 cm oval to irregular corkscrew burrows penetrating up to 15 cm. Some beds have a laminated basal coarse-grained interval that is foraminifer and radiolarian rich and white to light gray (10YR 8/2, 10YR 7/2). Black 1-4 mm flakes or streaks parallel to bedding may be FeMn oxide concentrations.

Minor lithologies: ZEOLITIC CLAYSTONE, very dark gray (10YR 3/1) with minor burrows infilled by nannofossil chalk, Section 1, 21-23 cm and 75-80 cm. Claystone is carried downward by bioturbation into upper portion of underlying nannofossil chalk beds. Nannofossil chalk is locally silified to CALCAREOUS PORCELLANITE (Section 1, 38-41 cm; Section 2, 56-60 cm; Section 3, 21-23 cm).

SMEAR SLIDE SUMMARY (%):

| | 1, 79 | 2, 46 |
|---|---|---|
| | M | D |
| TEXTURE: | | |
| Silt | 30 | 40 |
| Clay | 70 | 60 |
| COMPOSITION: | | |
| Clay | 54 | — |
| Foraminifers | — | 1 |
| Micrite | — | 60 |
| Nannofossils | — | 36 |
| Oxide | 10 | 1 |
| Quartz | — | 1 |
| Radiolarians | 6 | — |
| Zeolite | 30 | — |

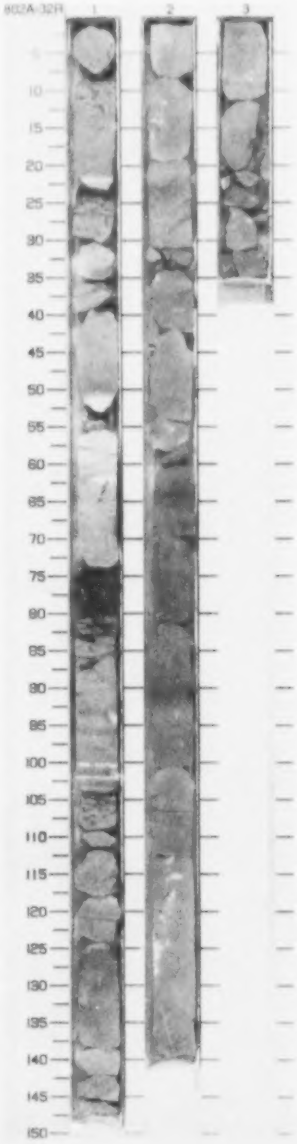
802A-32R
1
2
3
5
10
15
20
25
30
35
40
45
50
55
60
65
70
75
80
85
90
95
100
105
110
115
120
125
130
135
140
145
150

SITE 802 HOLE A CORE 33R CORED INTERVAL 6261.4-6270.9 mbsl; 292.8-302.3 mbsf

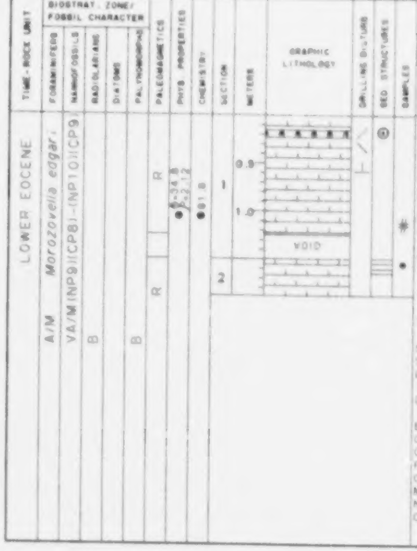
TIME-ROCK UNIT
BIOSTRAT. ZONE/ FOSSIL CHARACTER
FORAMINIFERS
NANNOFOSSILS
RADIOLARIANS
DIATOMS
PALYNOMORPHS
PALEOMAGNETICS
PHYS. PROPERTIES
CHEMISTRY
SECTION
METERS
GRAPHIC LITHOLOGY
DRILLING DISTURB.
SED. STRUCTURES
SAMPLES
LOWER EOCENE
A/M Morozovella edgari
VA/M (NP9)(CP8)-(NP10)(CP9)
B
B
R
R
φ-34.8
ρ-2.12
81.8
1
2
0.5
1.0
VOID

LITHOLOGIC DESCRIPTION

NANNOFOSSIL CHALK

Major lithology: NANNOFOSSIL CHALK, light grayish brown to yellowish gray (10YR 7/2, 10YR 6/2, 5Y 8/1), massive with rare bleached spots of 1-... mm diameter. Interval containing smeared grains (1 x 2-8 mm) of black (N2) metal oxide concentrations occur in lower Section 1 and upper Section 2.

Minor lithology: CHERT nodule, brown (10YR 2/2) with irregular contact with chalk, containing inclusions of chalk up to 1 cm in diameter. Section 1, 16-22 cm.

SLIDE SUMMARY (%):

|  | 1, 113 D | 2, 7 D |
|---|---|---|
| TEXTURE |  |  |
| Sand | 5 | 10 |
| Silt | 50 | 35 |
| Clay | 45 | 55 |
| COMPOSITION |  |  |
| Bioclast | 5 | — |
| Calcite | 10 | 11 |
| Clay | — | 5 |
| Foraminifers | 10 | 10 |
| Glass | 5 | 2 |
| Micrite | 65 | — |
| Nannofossils | — | 70 |
| Oxide | 5 | 2 |

SITE 802 HOLE A CORE 34R CORED INTERVAL 627.9-628.2 mbsl; 302.3-311.5 mbsf

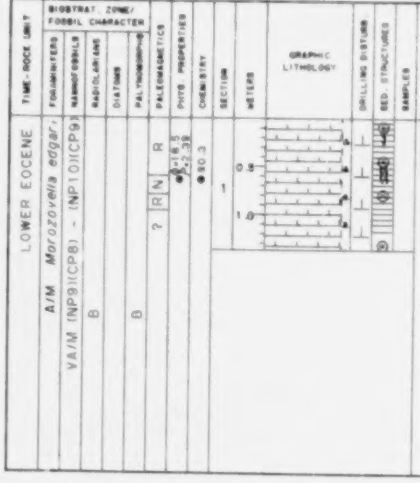
TIME-ROCK UNIT
BIOSTRAT. ZONE/ FOSSIL CHARACTER
FORAMINIFERS
NANNOFOSSILS
RADIOLARIANS
DIATOMS
PALYNOMORPHS
PALEOMAGNETICS
PHYS. PROPERTIES
CHEMISTRY
SECTION
METERS
GRAPHIC LITHOLOGY
DRILLING DISTURB.
SED. STRUCTURES
SAMPLES
LOWER EOCENE
A/M Morozovella edgari
VA/M (NP9)(CP8) - (NP10)(CP9)
B
B
R
N
R
?
φ-16.5
ρ-2.39
80.3
1
0.5
1.0

LITHOLOGIC DESCRIPTION

NANNOFOSSIL CHALK

Major lithology: NANNOFOSSIL CHALK, light gray to pinkish white (10YR 7/ to 10YR 8/1), with faint, fine laminations and rare light colored burrows; contains traces of metal oxide micronodules and radiolarians.

Minor lithology: CHERT, dark brown (10YR 2/1) and dark reddish brown (5YR 4/4), as nodules, with sharp, irregular contacts and chalk inclusions up to 8 mm in diameter. One nodule contains irregular rounded cavities lined with calcite crystals.

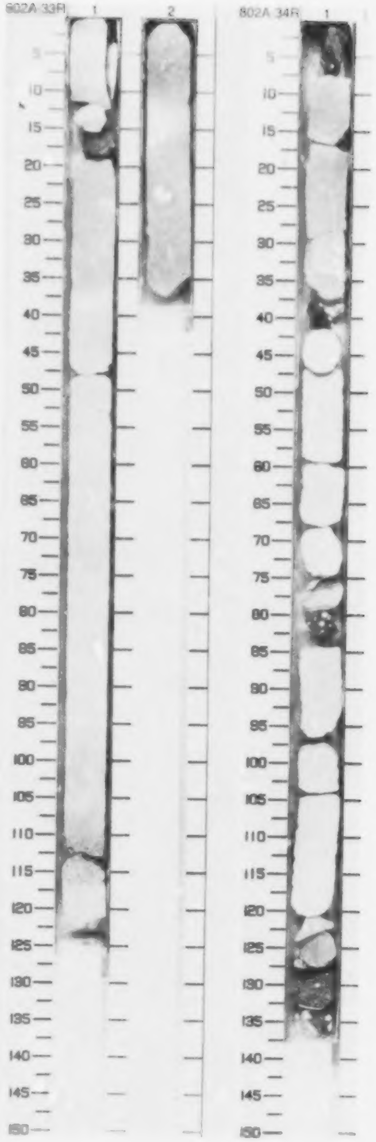
802A-33R
1
2
802A-34R
1
5
10
15
20
25
30
35
40
45
50
55
60
65
70
75
80
85
90
95
100
105
110
115
120
125
130
135
140
145
150

SITE 802 HOLE A CORE 35R CORED INTERVAL 6280.2-6289.3 mbsl; 311.5-320.7 mbsf

| TIME-ROCK UNIT | BIOSTRAT. ZONE/ FOSSIL CHARACTER: FORAMINIFERS | NANNOFOSSILS | RADIOLARIANS | DIATOMS | PALYNOMORPHS | PALEOMAGNETICS | PHYS. PROPERTIES | CHEMISTRY | SECTION | METERS | GRAPHIC LITHOLOGY / DRILLING DISTURB. / SED. STRUCTURES / SAMPLES | LITHOLOGIC DESCRIPTION |
|---|---|---|---|---|---|---|---|---|---|---|---|---|
| UPPER PALEOCENE | R/P unzoned | VA/G (NP9)(CP8) - (NP10)(CP9) | B | | B | R | ● φ=48.7<br>γ=1.76 | ● 42.8 | 1<br>CC | 0.5 | 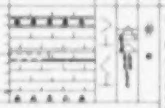 | see below |

NANNOFOSSIL CHALK and CHERT

Major lithologies:
a. NANNOFOSSIL CHALK, light olive gray (5Y 6/1) and pinkish gray (5YR 8/1) to pale yellowish brown (10YR 6/2); moderate bioturbation with laminations and fining upward grading in lower portions of some beds. Locally siliceous with up to 25% microquartz replacement. Contains nodules of:
b. CHERT, olive gray to olive black (5Y 4/1 - 5Y 2/1) with pinkish gray (5YR 8/1) calcareous spots of less silicified sediment.

Minor lithology: CLAYEY NANNOFOSSIL CHALK with ZEOLITES, dark yellowish brown (10YR 4/2), at the bioturbated top of a chalk bed; the zeolitic clay component may represent in situ sedimentation churned downward into the redeposited chalk.

SLIDE SUMMARY (%):

| | 1, 25<br>D | 1, 52<br>M |
|---|---|---|
| TEXTURE: | | |
| Sand | 5 | 5 |
| Silt | 45 | 30 |
| Clay | 50 | 65 |
| COMPOSITION: | | |
| Calcite | — | 11 |
| Chert | 25 | — |
| Clay | — | 30 |
| Foraminifers | 10 | — |
| Glass | — | 4 |
| Micrite | 63 | — |
| Nannofossils | — | 40 |
| Opaques | 1 | — |
| Radiolarians | 1 | — |
| Zeolite | — | 15 |

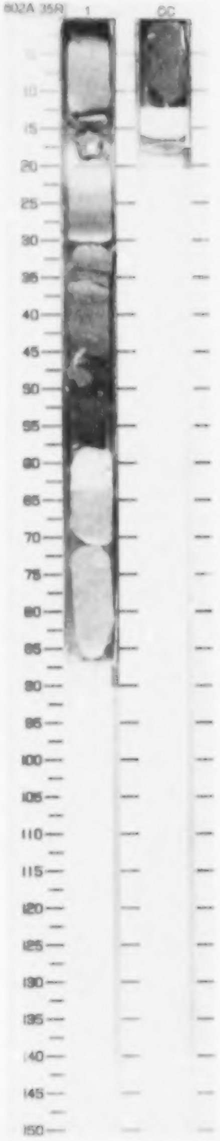

SITE 802 HOLE A CORE 36R CORED INTERVAL 6289.3-6298.5 mbsl; 320.7-329.9 mbsf

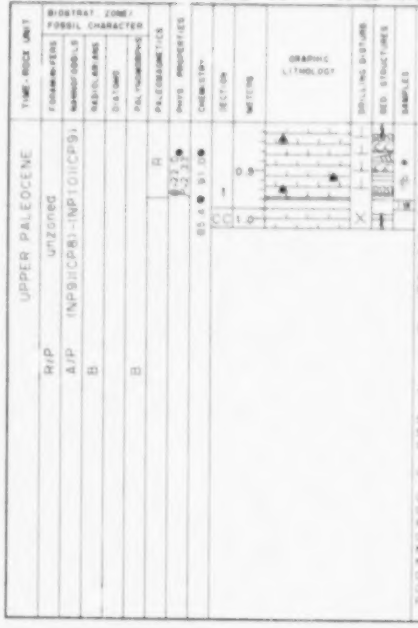
TIME-ROCK UNIT
BIOSTRAT. ZONE/ FOSSIL CHARACTER
FORAMINIFERS
NANNOFOSSILS
RADIOLARIANS
DIATOMS
PALYNOMORPHS
PALEOMAGNETICS
PHYS. PROPERTIES
CHEMISTRY
SECTION
METERS
GRAPHIC LITHOLOGY
DRILLING DISTURB.
SED. STRUCTURES
SAMPLES
UPPER PALEOCENE
R/P unzoned
A/P (NP9)(CP8)-(NP10)(CP9)
B
B
R
65.4 ● 91.0 ●
1
CC
0.9
1.0

LITHOLOGIC DESCRIPTION

NANNOFOSSIL CHALK with FORAMINIFERS

Major lithology: NANNOFOSSIL CHALK with FORAMINIFERS, generally pinkish gray (7.5YR 7/2), but composed of laminations of pinkish white (7.5YR 8/2) chalk, and light brown (7.5YR 6/4) chalk with clay; contains 15% foraminifers and 5% radiolarians; fine bedding displays wavy to planar laminations, through cross- laminations, flame structures, and contorted laminations.

Minor lithologies:
a. NANNOFOSSIL CHALK, light brownish gray (10YR 6.5/2) grading upward to pinkish gray (7.5YR 7/2) in Section 1, 0-15 cm, weakly bioturbated at top, and yellowish gray to light olive gray (5Y 8/1-5Y 6/1) in Section CC, with laminations, and minor bioturbation mottling.
b. CHERT, as nodules and layers in chalk, olive gray (5Y 4/1) to dark brown (7.5YR 4/4-7.5YR 3/4), with internal laminations and abundant calcareous inclusions of light brown.

SLIDE SUMMARY (%):

| | 1, 40<br>D | 1, 61<br>D |
|---|---|---|
| TEXTURE: | | |
| Sand | 2 | 20 |
| Silt | 35 | 50 |
| Clay | 63 | 30 |
| COMPOSITION: | | |
| Calcite | 40 | — |
| Clay | 5 | — |
| Foraminifers | 15 | 35 |
| Glass | — | 5 |
| Micrite | — | 55 |
| Nannofossils | 30 | — |
| Oxide | — | 2 |
| Quartz | 5 | 1 |
| Radiolarians | 5 | 1 |

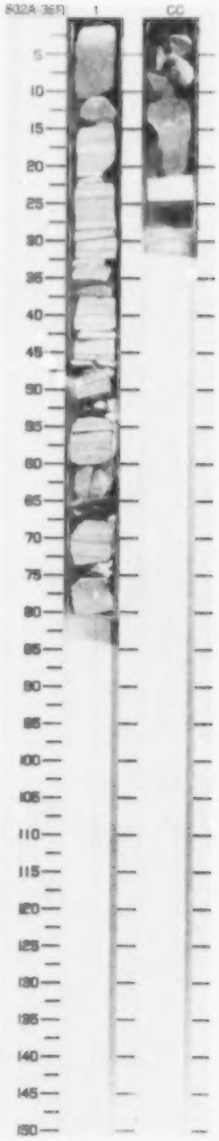
802A 36R
1
CC
5
10
15
20
25
30
35
40
45
50
55
60
65
70
75
80
85
90
95
100
105
110
115
120
125
130
135
140
145
150

SITE 802 HOLE A CORE 37R CORED INTERVAL 6298.5-6307.8 mbsl: 329.9-339.2 mbsf

| TIME-ROCK UNIT | BIOSTRAT. ZONE/ FOSSIL CHARACTER: FORAMINIFERS | NANNOFOSSILS | RADIOLARIANS | DIATOMS | PALYNOMORPHS | PALEOMAGNETICS | PHYS. PROPERTIES | CHEMISTRY | SECTION | METERS | GRAPHIC LITHOLOGY | DRILLING DISTURB. | SED. STRUCTURES | SAMPLES | LITHOLOGIC DESCRIPTION |
|---|---|---|---|---|---|---|---|---|---|---|---|---|---|---|---|
| PALEOCENE | R/P<br>unzoned | R/M<br>unzoned | B | | B | N | | | CC | | | ⊥ | | ● | PELAGIC CLAYSTONE |

Major lithology: PELAGIC CLAYSTONE (ZEOLITIC CLAYSTONE), brownish gray (5YR 4/1) with thin laminations and oval reduction mottles of light brown (5YR 6/4), weakly bioturbated and with wedge shaped and flaser laminations.

Minor lithology: CHERT, pale yellowish brown (10YR 6/2) and very pale orange (10YR 8/2), conchoidal fractures, laminated to weakly bioturbated, in Section CC, 10-15 cm.

SLIDE SUMMARY (%):

| | CC, 6<br>D |
|---|---|
| TEXTURE: | |
| Sand | 1 |
| Silt | 30 |
| Clay | 69 |
| COMPOSITION: | |
| Clay | 50 |
| Glass | 2 |
| Nannofossils | Tr |
| Oxide | 1 |
| Spines | 7 |
| Zeolite | 40 |

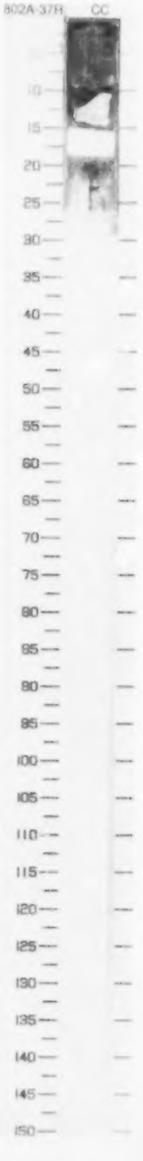

SITE 802 HOLE A CORE 38R CORED INTERVAL 6307.8-6317.3 mbsl; 339.2-348.7 mbsf

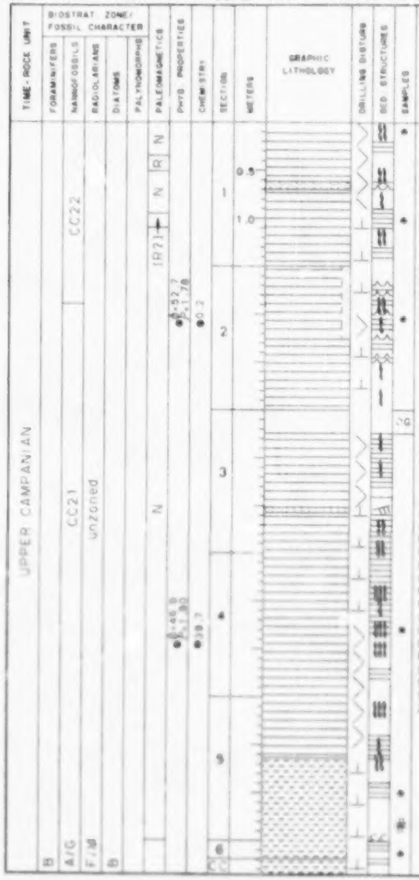
TIME-ROCK UNIT
BIOSTRAT. ZONE/ FOSSIL CHARACTER
FORAMINIFERS
NANNOFOSSILS
RADIOLARIANS
DIATOMS
PALYNOMORPHS
PALEOMAGNETICS
PHYS. PROPERTIES
CHEMISTRY
SECTION
METERS
GRAPHIC LITHOLOGY
DRILLING DISTURB.
SED. STRUCTURES
SAMPLES
UPPER CAMPANIAN
B
A/G
F/M
B
CC22
CC21
unzoned
N
R
N
(R?)
N
φ-52.7
P-1.78
●0.2
φ-46.0
P-1.80
●38.7
1
2
3
4
5
6
CC
0.5
1.0
OG

LITHOLOGIC DESCRIPTION

PELAGIC CLAYSTONE and CALCAREOUS CLAYSTONE

Major lithologies:

a. PELAGIC CLAYSTONE (ZEOLITIC CLAYSTONE), mottled light brown (5YR 6/4), light gray (10YR 8/1) and dark yellowish brown (10YR 2/2) with dark streaks; intensely bioturbated with few laminations preserved; contains abundant zeolites and common iron manganese oxides with rare radiolarians and siliceous spines.

b. CALCAREOUS CLAYSTONE, gradational from brown (7.5YR 4/4) to grayish brown (10YR 4/2) to light olive gray (5Y 6/1); some beds have basal CALCAREOUS SILTSTONE of alternating light gray clay-rich (10YR 8/1) and black silt-rich (7.5YR 2/0) laminations; claystone dominates Section 5 (64-150 cm) through CC with higher intervals containing more clay-rich bases; the calcareous siltstone layers also contain volcanic glass, radiolarians and rare foraminifers. In some places, these calcareous siltstone to claystone beds display fining-upward grading, basal cross-laminations or convoluted (disrupted) layering, scoured bases and flame structures.

SLIDE SUMMARY (%):

| | 1, 9<br>D | 1, 101<br>D | 2, 55<br>M | 4, 79<br>M | 5, 100<br>D | 5, 132<br>M | 6, 13<br>D |
|---|---|---|---|---|---|---|---|
| TEXTURE: | | | | | | | |
| Sand | — | — | 10 | 2 | 5 | — | 3 |
| Silt | 25 | 2 | 50 | 40 | 25 | 70 | 35 |
| Clay | 75 | 98 | 40 | 58 | 70 | 30 | 62 |
| COMPOSITION: | | | | | | | |
| Accessory minerals | — | — | 2 | Tr | 1 | 2 | 2 |
| Calcite | — | — | 20 | 3 | 10 | 3 | 5 |
| Clay | 60 | 75 | 20 | 40 | 60 | 9 | 60 |
| Feldspar | — | — | 2 | 1 | Tr | 5 | 1 |
| Foraminifers | — | — | 5 | — | — | 2 | — |
| Glass | 2 | — | 10 | 35 | 5 | 24 | 7 |
| Glauconite | — | — | — | — | Tr | — | — |
| Micrite | — | — | — | — | — | 15 | — |
| Nannofossils | — | — | 20 | 2 | 10 | — | 23 |
| Opaques | 3 | 2 | 10 | Tr | 5 | 8 | — |
| Oxide | — | 5 | — | — | — | — | — |
| Quartz | — | — | — | — | — | 2 | — |
| Radiolarians | 5 | — | 10 | 3 | 5 | — | 2 |
| Silica | — | — | — | — | — | 23 | — |
| Smectite | — | — | — | — | — | 2 | — |
| Spines | — | 3 | — | — | 1 | — | — |
| Zeolite | 30 | 15 | — | 15 | 2 | — | — |

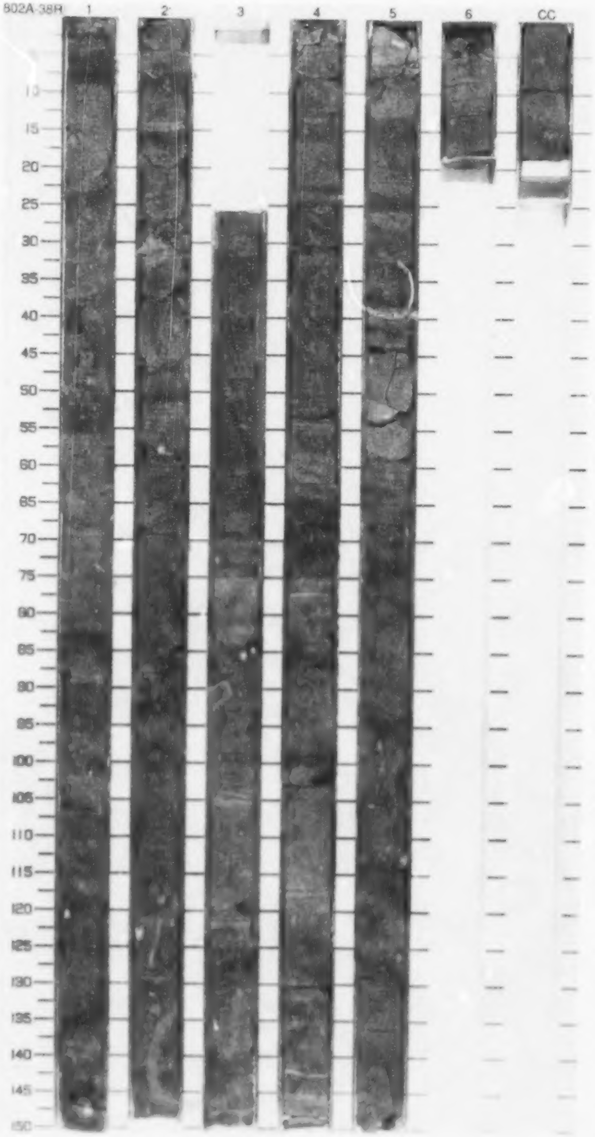
802A-38R
1
2
3
4
5
6
CC
10
15
20
25
30
35
40
45
50
55
60
65
70
75
80
85
90
95
100
105
110
115
120
125
130
135
140
145
150

SITE 802 HOLE A CORE 39R CORED INTERVAL 6317.3-6326.7 mbsl; 348.7-358.1 mbsf

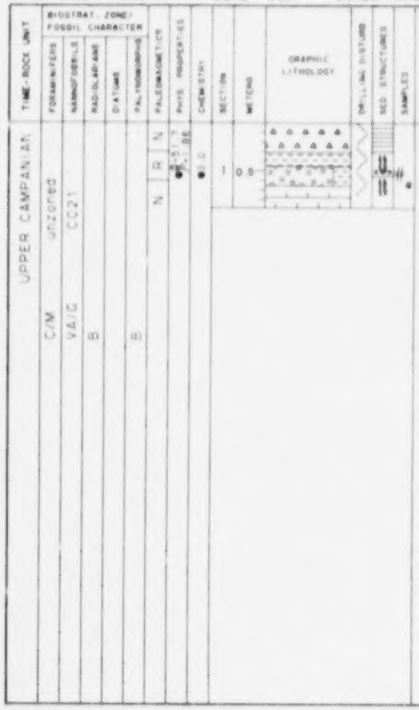
TIME-ROCK UNIT
BIOSTRAT. ZONE/ FOSSIL CHARACTER
FORAMINIFERS
NANNOFOSSILS
RADIOLARIANS
DIATOMS
PALYNOMORPHS
PALEOMAGNETICS
PHYS. PROPERTIES
CHEMISTRY
SECTION
METERS
GRAPHIC LITHOLOGY
DRILLING DISTURB.
SED. STRUCTURES
SAMPLES
UPPER CAMPANIAN
unzoned
C/M
CC21
VA/G
B
B
N
R
N
1
0.5

LITHOLOGIC DESCRIPTION

PORCELLANITE and CLAYEY NANNOFOSSIL CHALK

Major lithologies:
a. PORCELLANITE, reddish brown (5YR 4/4-5YR 5/4), finely laminated, contains grains of oxides.
b. CLAYEY NANNOFOSSIL CHALK, grayish blue (5BG 5/1) or olive gray (5Y 4/1), massive. Nannofossils plus clay, volcanic glass, iron oxides and zeolites.

Minor lithologies:
a. CLAYSTONE, moderate brown (5YR 5/2) to olive gray (5Y 4/1), burrowed, with diagenetically controlled color changes.
b. VOLCANICLASTIC SANDSTONE, greenish gray (5G 4/1), normally graded bed with basal scour, fine grained, moderately well sorted, contains glass, oxides, zeolites and igneous rock fragments.

SLIDE SUMMARY (%):

| | 1, 52<br>M | 1, 64<br>D |
|---|---|---|
| TEXTURE: | | |
| Sand | 90 | Tr |
| Silt | 10 | 5 |
| Clay | — | 95 |
| COMPOSITION: | | |
| Algae | 3 | — |
| Calcite | 2 | — |
| Clay | — | 25 |
| Feldspar | 3 | — |
| Glass | 29 | 5 |
| Igneous rock fragments | 15 | — |
| Nannofossils | — | 60 |
| Opaques | 5 | 3 |
| Oxide | 3 | 5 |
| Palagonite | 30 | — |
| Pyroxene | 6 | — |
| Radiolarians | 2 | — |
| Smectite | 2 | — |
| Zeolite | — | 2 |

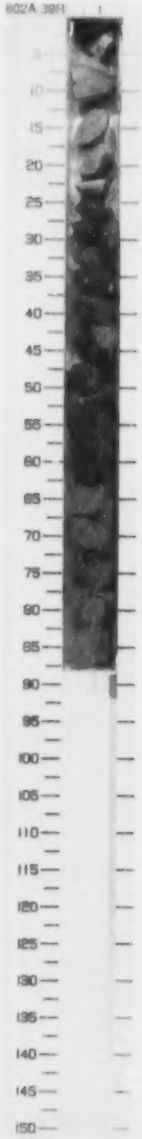
802A 39R
1
5
10
15
20
25
30
35
40
45
50
55
60
65
70
75
80
85
90
95
100
105
110
115
120
125
130
135
140
145
150

SITE 802 HOLE A CORE 40R CORED INTERVAL 6326.7-6334.1 mbsl; 358.1-372.8 mbsf

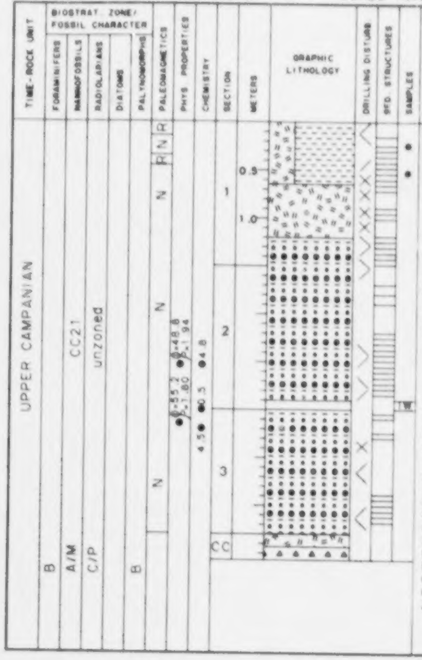
TIME-ROCK UNIT
BIOSTRAT. ZONE/ FOSSIL CHARACTER
FORAMINIFERS
NANNOFOSSILS
RADIOLARIANS
DIATOMS
PALYNOMORPHS
PALEOMAGNETICS
PHYS. PROPERTIES
CHEMISTRY
SECTION
METERS
GRAPHIC LITHOLOGY
DRILLING DISTURB.
SED. STRUCTURES
SAMPLES
UPPER CAMPANIAN
B
CC21
A/M
unzoned
C/P
B
R
N
R
N
N
N
φ-55.2
ρ-1.80
φ-48.8
ρ-1.94
4.5
0.5
4.8
1
2
3
CC
0.5
1.0
IW

LITHOLOGIC DESCRIPTION

VOLCANICLASTIC TURBIDITES: VOLCANICLASTIC SANDSTONE and VOLCANICLASTIC CLAYSTONE

Major lithologies:

a. VOLCANICLASTIC TURBIDITES, composed of normally graded sandy to clayey beds up to 1.5 m thick. Thinly laminated, locally with cross-laminations and flame structures.

b. VOLCANICLASTIC SANDSTONE, bluish gray to dark gray (5B 5/1 N4.5), moderately sorted, silty to fine grained, composed of glass, volcanic rock fragments, oxides, feldspar and olivine. Grades upward into, or interlaminated with:

c. VOLCANICLASTIC CLAYSTONE, dark gray (7.5YR 4/0 N4), laminated to massive, mostly overlying sandstone in thick beds, rarely burrowed.

Minor lithology: PORCELLANITE, gray (5Y 5/1) with slight greenish tint, smooth with blocky to conchoidal fracture, faint laminations, rare volcaniclastic silt lenses, quartz filled radiolarian casts. Probably the fine-grained top of an unrecovered turbidite.

SLIDE SUMMARY (%):

| | 1, 25<br>D | 1, 52<br>M |
|---|---|---|
| TEXTURE: | | |
| Silt | 20 | Tr |
| Clay | 80 | 100 |
| COMPOSITION: | | |
| Accessory minerals | — | Tr |
| Calcite | 2 | — |
| Clay | 63 | 75 |
| Feldspar | 1 | — |
| Glass | 30 | 25 |
| Nannofossils | Tr | — |
| Opaques | 3 | — |
| Oxide | 1 | Tr |
| Zeolite | Tr | — |

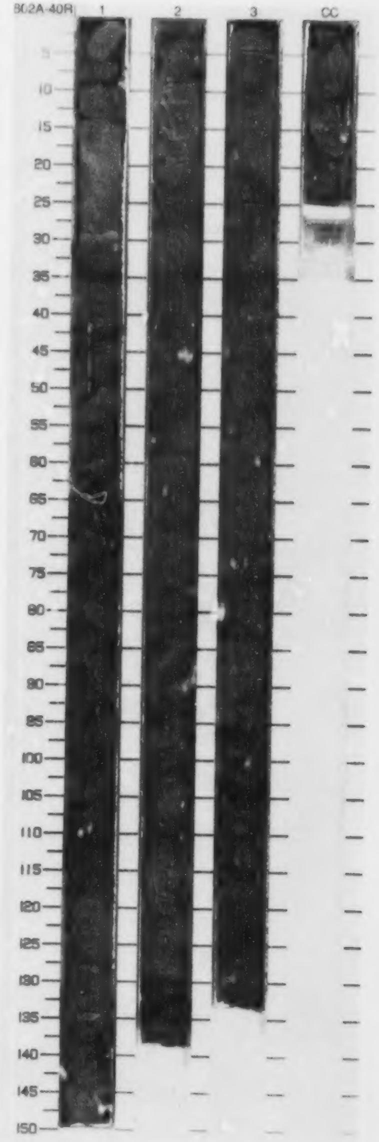
802A-40R
1
2
3
CC
5
10
15
20
25
30
35
40
45
50
55
60
65
70
75
80
85
90
95
100
105
110
115
120
125
130
135
140
145
150

SITE 802 HOLE A CORE 41R CORED INTERVAL 6334.1-6341.4 mbsl; 365.5-372.8 mbsf

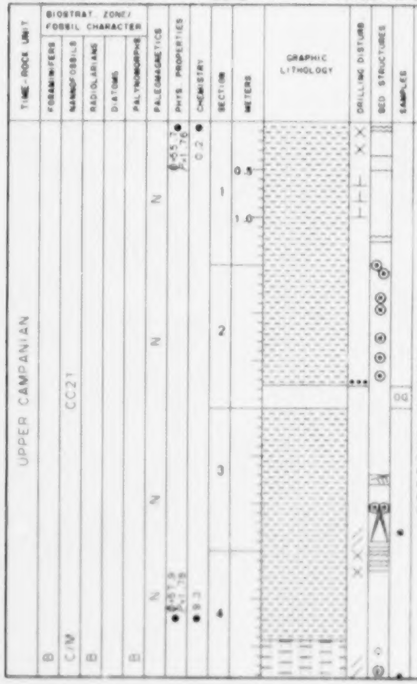

LITHOLOGIC DESCRIPTION

VOLCANICLASTIC CLAYSTONE

Major lithology: VOLCANICLASTIC CLAYSTONE, dark gray (N4 N5), massive to thinly laminated in greenish grays (5GY 4/1 5Y 5/1); in some intervals laminations are convolute, other massive beds are gently graded. Common spherules in Sections 2 and 3 have a glassy luster, but are composed of clay (glauconite/celadonite?).

Minor lithology: VOLCANICLASTIC SILTSTONE, dark greenish gray (5BG 4/1), very similar to volcaniclastic claystone, but silty sandy; contains scattered 0.5 mm claystone clasts.

SLIDE SUMMARY (%):

| | 3, 130<br>D | 4, 131<br>M |
|---|---|---|
| TEXTURE | | |
| Sand | 25 | 30 |
| Silt | 25 | 30 |
| Clay | 50 | 40 |
| COMPOSITION | | |
| Accessory minerals | 15 | — |
| Calcite | Tr | Tr |
| Clay | 45 | 80 |
| Glass | 35 | 20 |
| Opaques | 5 | — |
| Oxide | — | Tr |
| Radiolarians | Tr | — |

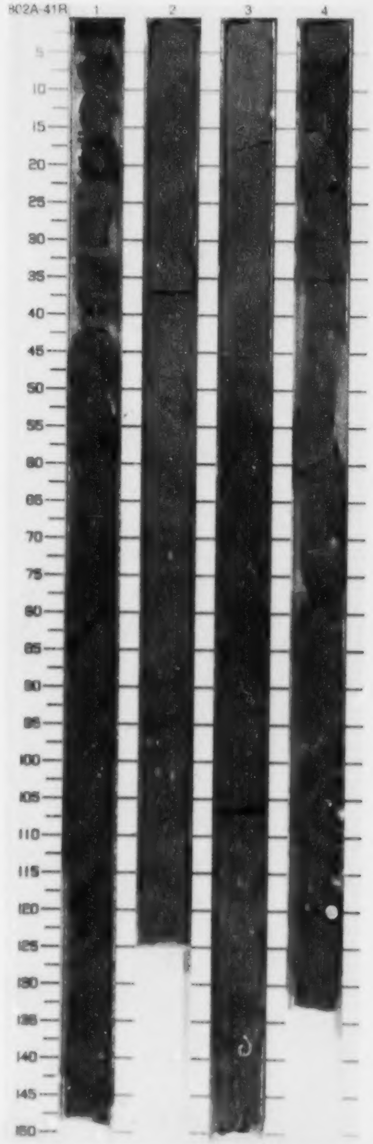
802A-41R
1
2
3
4
5
10
15
20
25
30
35
40
45
50
55
60
65
70
75
80
85
90
95
100
105
110
115
120
125
130
135
140
145
150

## SITE 802 HOLE A CORE 42R CORED INTERVAL 6341.4-6350.7 mbsl; 372.8-382.1 mbsf

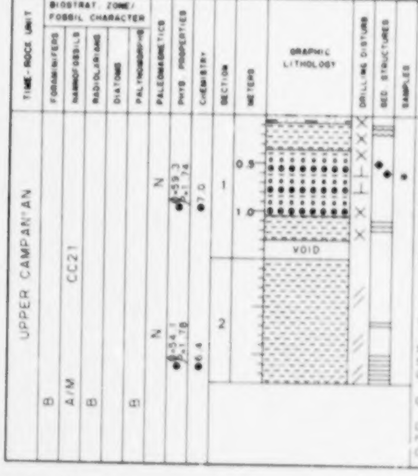
TIME-ROCK UNIT
BIOSTRAT. ZONE/ FOSSIL CHARACTER
FORAMINIFERS
NANNOFOSSILS
RADIOLARIANS
DIATOMS
PALYNOMORPHS
PALEOMAGNETICS
PHYS. PROPERTIES
CHEMISTRY
SECTION
METERS
GRAPHIC LITHOLOGY
DRILLING DISTURB.
SED. STRUCTURES
SAMPLES
UPPER CAMPANIAN
B
A/M
CC21
B
B
N
N
φ=59.3
ρ=1.74
7.0
φ=54.1
ρ=1.78
6.4
1
2
0.5
1.0
VOID

LITHOLOGIC DESCRIPTION

VOLCANICLASTIC CLAYSTONE and VOLCANICLASTIC SANDY SILTSTONE

Major lithologies:

a. VOLCANICLASTIC CLAYSTONE, dark gray (N4 N5), relatively homogeneous, massive to locally laminated, cherty brownish gray (5Y 4/1) horizon at bottom of Section 2.

b. VOLCANICLASTIC SANDY SILTSTONE, dark gray to dark bluish gray (N4 5B 4/1), fines upward to volcaniclastic claystone in a turbidite bed 1 m thick, sharp base, contains abundant claystone clasts of varied colors at Section 1, 50-75 cm; one light-colored clast is rich in cubic zeolite(?).

SLIDE SUMMARY (%):

| | 1, 62<br>M |
|---|---|
| TEXTURE: | |
| Sand | 3 |
| Silt | 74 |
| Clay | 23 |
| COMPOSITION: | |
| Clay | 20 |
| Feldspar | 1 |
| Glass | 79 |

## SITE 802 HOLE A CORE 43R CORED INTERVAL 6350.7-6359.9 mbsl; 382.1-391.3 mbsf

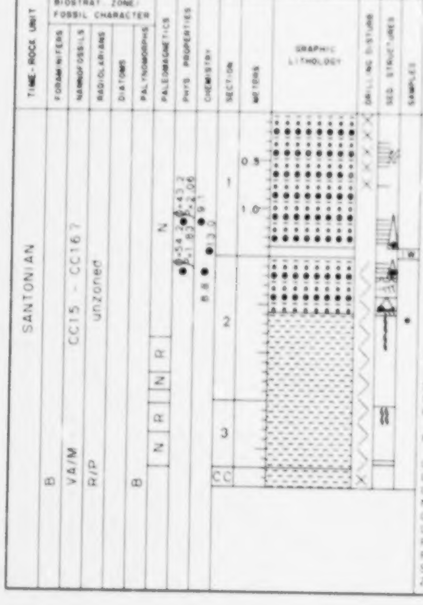
TIME-ROCK UNIT
BIOSTRAT. ZONE/ FOSSIL CHARACTER
FORAMINIFERS
NANNOFOSSILS
RADIOLARIANS
DIATOMS
PALYNOMORPHS
PALEOMAGNETICS
PHYS. PROPERTIES
CHEMISTRY
SECTION
METERS
GRAPHIC LITHOLOGY
DRILLING DISTURB.
SED. STRUCTURES
SAMPLES
SANTONIAN
B
VA/M
CC15 - CC16?
R/P
unzoned
B
N
R
N
R
N
φ=54.2
ρ=1.83
φ=43.2
ρ=2.06
9.1
13.0
8.8
1
2
3
CC
0.5
1.0

LITHOLOGIC DESCRIPTION

VOLCANICLASTIC TURBIDITES and CALCAREOUS VOLCANICLASTIC CLAYSTONE

Major lithologies:

a. VOLCANICLASTIC TURBIDITES, dark gray to dark bluish gray (N3 5B 4/1), sandy to clayey, normally graded beds, moderately well sorted, composed of volcanic rock fragments, glass, rip-up clasts of claystone, oxides and pyroxene, thinly laminated and locally cross-laminated. Sharp contacts with underlying.

b. CALCAREOUS VOLCANICLASTIC CLAYSTONE, bluish gray (5B 4/1 5BG 4/1), mostly massive; burrows in 3-10 cm below the contact with the overlying turbidites. Contains nannofossils and inorganic calcite; total calcite content increases upward within turbidite beds into the silt to clay grain size interval, then diminishes in the fine-grained claystone top. Present as part of turbidites, and as beds of uncertain depositional process.

SLIDE SUMMARY (%):

| | 2, 65<br>D |
|---|---|
| TEXTURE: | |
| Sand | 2 |
| Silt | 55 |
| Clay | 43 |
| COMPOSITION: | |
| Calcite | 25 |
| Clay | 39 |
| Glass | 20 |
| Nannofossils | 5 |
| Opaques | 2 |
| Oxide | 3 |
| Pyroxene | 1 |
| Radiolarians | 2 |
| Smectite | 1 |
| Zeolite | 2 |

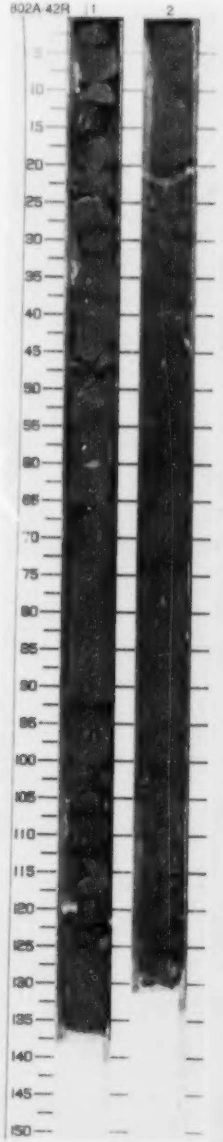
802A-42R
1
2
5
10
15
20
25
30
35
40
45
50
55
60
65
70
75
80
85
90
95
100
105
110
115
120
125
130
135
140
145
150

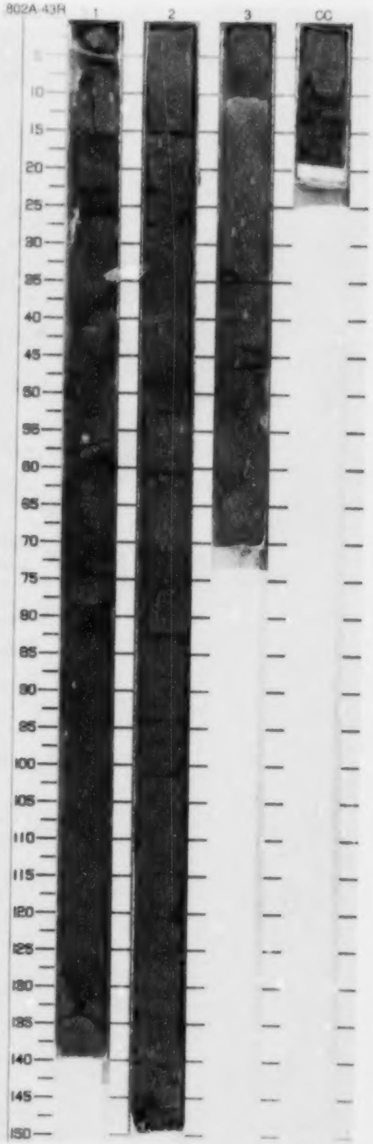
802A-43R
1
2
3
CC
5
10
15
20
25
30
35
40
45
50
55
60
65
70
75
80
85
90
95
100
105
110
115
120
125
130
135
140
145
150

SITE 802 HOLE A CORE 44R CORED INTERVAL 6359.9-6369.1 mbsl; 391.3-400.5 mbst

| TIME-ROCK UNIT | BIOSTRAT. ZONE/ FOSSIL CHARACTER: FORAMINIFERS | NANNOFOSSILS | RADIOLARIANS | DIATOMS | PALYNOMORPHS | PALEOMAGNETICS | PHYS. PROPERTIES | CHEMISTRY | SECTION | METERS | GRAPHIC LITHOLOGY | DRILLING DISTURB. | SED. STRUCTURES | SAMPLES |
|---|---|---|---|---|---|---|---|---|---|---|---|---|---|---|
| SANTONIAN | B | F/P CC15 - CC16 ? | F/P unzoned | | B | R<br>N | ●φ=56.2<br>●γ=1.67 | ●2.2 | 1 | 0.5<br>1.0 | | ⊥<br>⊥<br>⊥<br>×<br>× | | ● |

LITHOLOGIC DESCRIPTION

SILTY CLAYSTONE and CLAYSTONE

Major lithologies:
a. SILTY CLAYSTONE, dark bluish gray (5B 4/1), massive to faintly laminated; and
b. CLAYSTONE, also dark bluish gray (5B 4/1), massive, contains only traces of nannofossils, volcanic glass, feldspar, opaques, and zeolites.

Minor lithology: CLAYEY SANDSTONE, dark bluish gray (5B 4/1), fine grained; 3 cm layer contains volcanic glass, feldspar, zeolites, red oxidized grains; scoured base.

SLIDE SUMMARY (%):

| | 1, 86 D |
|---|---|
| TEXTURE: | |
| Silt | 1 |
| Clay | 99 |
| COMPOSITION: | |
| Clay | 84 |
| Feldspar | 1 |
| Glass | 3 |
| Nannofossils | 3 |
| Opaques | 5 |
| Oxide | 2 |
| Smectite | 1 |
| Zeolite | 1 |

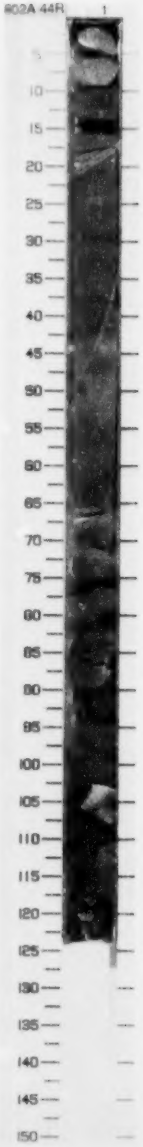

SITE 802 HOLE A CORE 45R CORED INTERVAL 6369.1-6378.6 mbsl; 400.5-410.0 mbsf

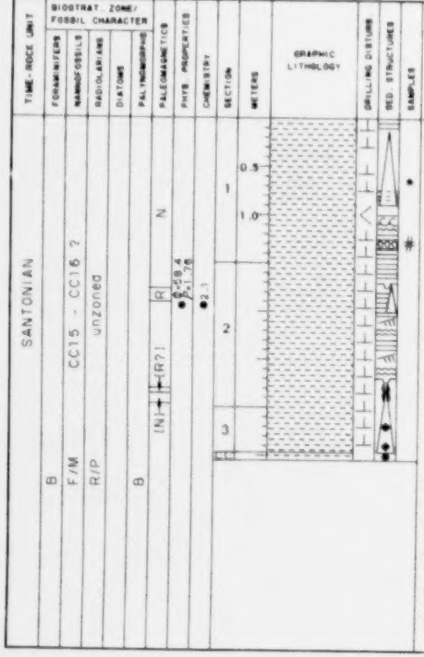
TIME-ROCK UNIT
BIOSTRAT. ZONE/ FOSSIL CHARACTER
FORAMINIFERS
NANNOFOSSILS
RADIOLARIANS
DIATOMS
PALYNOMORPHS
PALEOMAGNETICS
PHYS. PROPERTIES
CHEMISTRY
SECTION
METERS
GRAPHIC LITHOLOGY
DRILLING DISTURB.
SED. STRUCTURES
SAMPLES
SANTONIAN
B
CC15 - CC16 ?
F/M
unzoned
R/P
B
N
R
(N)
(R?)
φ-58.4
ρ-1.78
2.1
0.5
1.0
1
2
3
CC

**LITHOLOGIC DESCRIPTION**

SILTY CLAYSTONE to CALCAREOUS SILTY CLAYSTONE

Major lithology: SILTY CLAYSTONE to CALCAREOUS SILTY CLAYSTONE, dark bluish gray to gray (5B 4/1, N5, 5YR 4/1) with white grains of silicified radiolarians and rare foraminifers; smear slide indicates about 10% calcite grains and minor volcanic glass, opaques and nannofossils; redeposited as turbidite beds 30-80 cm thick. Sedimentary structures include 1-3 mm rip-up clasts of greenish gray to dark gray (5G 6/1, N4), normally graded beds with rip-up clast concentration and mean size also fining upward, planar to wavy to convolute laminations, cross-laminations, scour surfaces and rare bioturbated intervals.

SLIDE SUMMARY (%):

| | 1, 65<br>D | 1, 129<br>D |
|---|---|---|
| TEXTURE: | | |
| Sand | 3 | — |
| Silt | 22 | 10 |
| Clay | 75 | 90 |
| COMPOSITION: | | |
| Accessory minerals | 1 | — |
| Calcite | 8 | — |
| Clay | 68 | 32 |
| Feldspar | 1 | Tr |
| Foraminifers | Tr | — |
| Glass | 5 | — |
| Micrite | — | 10 |
| Nannofossils | 3 | — |
| Opaques | 3 | 15 |
| Radiolarians | 8 | — |
| Sericite | Tr | — |
| Silica | — | 30 |
| Spines | — | 10 |
| Zeolite | 2 | 3 |

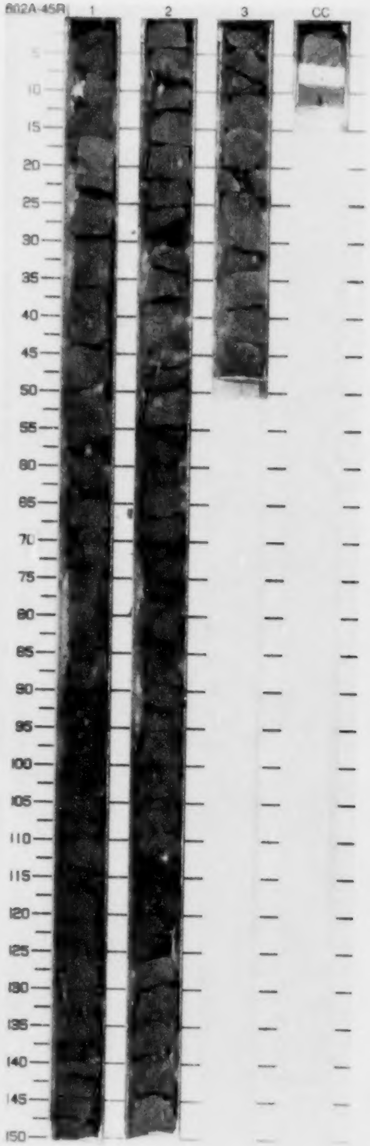
802A-45R
1
2
3
CC
5
10
15
20
25
30
35
40
45
50
55
60
65
70
75
80
85
90
95
100
105
110
115
120
125
130
135
140
145
150

SITE 802 HOLE A CORE 46R CORED INTERVAL 6378.6-6387.8 mbsl; 410.0-419.2 mbsf

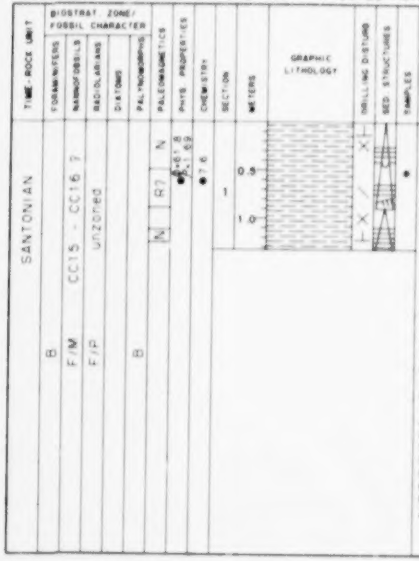
TIME-ROCK UNIT
BIOSTRAT. ZONE/ FOSSIL CHARACTER
FORAMINIFERS
NANNOFOSSILS
RADIOLARIANS
DIATOMS
PALYNOMORPHS
PALEOMAGNETICS
PHYS. PROPERTIES
CHEMISTRY
SECTION
METERS
GRAPHIC LITHOLOGY
DRILLING DISTURB.
SED. STRUCTURES
SAMPLES
SANTONIAN
B
F/M
CC15 - CC16 ?
F/P
unzoned
B
N
R?
N
61.8
1.69
7.6
1
0.5
1.0

LITHOLOGIC DESCRIPTION

CLAYEY SILTSTONE to SILTY CLAYSTONE

Major lithology: CLAYEY SILTSTONE to SILTY CLAYSTONE, dark bluish gray to brownish gray (5B 4/1 5YR 4/1); fining upward progression from clayey siltstone to silty claystone dominates Section 1 (89.0 cm); turbidite beds are 40-50 cm thick; a second underlying progression was incompletely recovered. Silt component of claystone includes volcanic glass, calcite and zeolites with rare nannofossils and foraminifers. Clayey siltstone has planar, cross and convolute laminations.

SLIDE SUMMARY (%):

| | 1, 51<br>D |
|---|---|
| TEXTURE: | |
| Sand | 5 |
| Silt | 30 |
| Clay | 65 |
| COMPOSITION: | |
| Accessory minerals | 1 |
| Calcite | 8 |
| Clay | 70 |
| Feldspar | 1 |
| Foraminifers | 1 |
| Glass | 10 |
| Nannofossils | 1 |
| Zeolite | 8 |

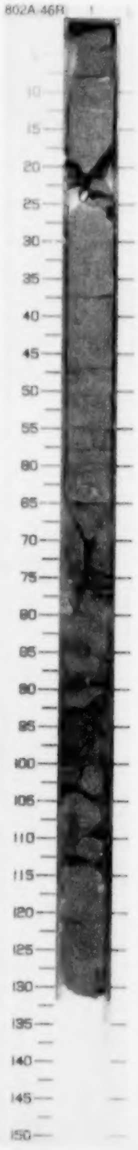
802A-46R
1
10
15
20
25
30
35
40
45
50
55
60
65
70
75
80
85
90
95
100
105
110
115
120
125
130
135
140
145
150

SITE 802 HOLE A CORE 47R CORED INTERVAL 6387.8-6397.3 mbsl; 419.2-428.7 mbsf

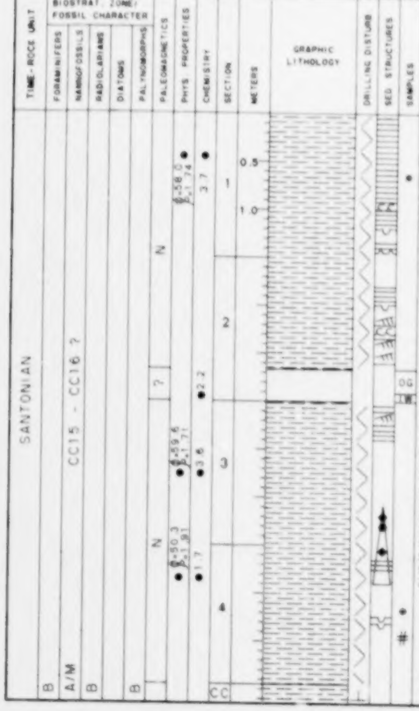
TIME-ROCK UNIT
BIOSTRAT. ZONE/ FOSSIL CHARACTER
FORAMINIFERS
NANNOFOSSILS
RADIOLARIANS
DIATOMS
PALYNOMORPHS
PALEOMAGNETICS
PHYS. PROPERTIES
CHEMISTRY
SECTION
METERS
GRAPHIC LITHOLOGY
DRILLING DISTURB.
SED. STRUCTURES
SAMPLES
SANTONIAN
B
A/M
CC15 - CC16 ?
B
B
N
?
N
φ=58.0
ρ=1.74
φ=59.6
ρ=1.71
φ=50.3
ρ=1.91
3.7
2.2
3.6
1.7
1
2
3
4
CC
0.5
1.0
OG
#

LITHOLOGIC DESCRIPTION

SILTY CLAYSTONE TURBIDITES

Major lithology: SILTY CLAYSTONE TURBIDITES, dark bluish gray to medium bluish gray (5B 4/1 5B 5/1), generally finely laminated; silt component includes radiolarians, opaques, zeolites, glass and calcite with rare foraminifers and nannofossils. Sedimentary features include normal grading, load casts, basal scour, flame structures, ripple and cross-lamination, convoluted layers and rare bioturbation, with rip-up clasts of darker claystone up to 3 mm in diameter (in Section 3, 99 cm; Section 4, 16 cm); beds are less than 50 cm thick.

SLIDE SUMMARY (%)

| | 1, 65<br>D | 4, 68<br>D | 4, 95<br>M |
|---|---|---|---|
| TEXTURE | | | |
| Sand | 5 | 4 | — |
| Silt | 25 | 30 | 20 |
| Clay | 70 | 66 | 80 |
| COMPOSITION | | | |
| Accessory minerals | 1 | 2 | — |
| Calcite | 3 | — | Tr |
| Clay | 64 | 68 | 38 |
| Feldspar | — | — | 1 |
| Foraminifers | 1 | 1 | — |
| Glass | 10 | 6 | 15 |
| Micrite | — | 4 | — |
| Nannofossils | 1 | 1 | — |
| Opaques | 5 | — | 8 |
| Radiolarians | 10 | 12 | 20 |
| Silica | — | 8 | 10 |
| Smectite | — | — | 3 |
| Spines | — | — | 5 |
| Zeolite | 5 | — | — |

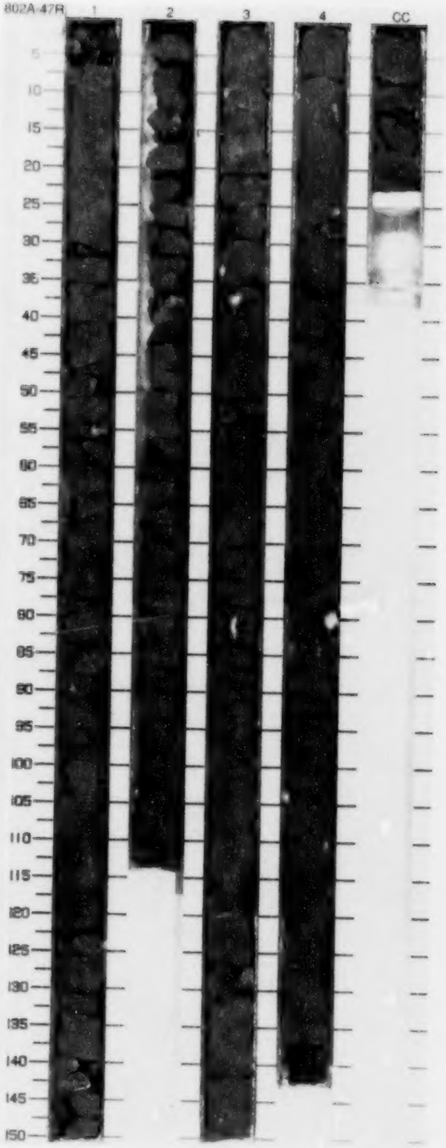
802A-47R
1
2
3
4
CC
5
10
15
20
25
30
35
40
45
50
55
60
65
70
75
80
85
90
95
100
105
110
115
120
125
130
135
140
145
150

SITE 802 HOLE A CORE 48R CORED INTERVAL 6397.3-6406.7 mbsl; 428.7-432.1 mbsf

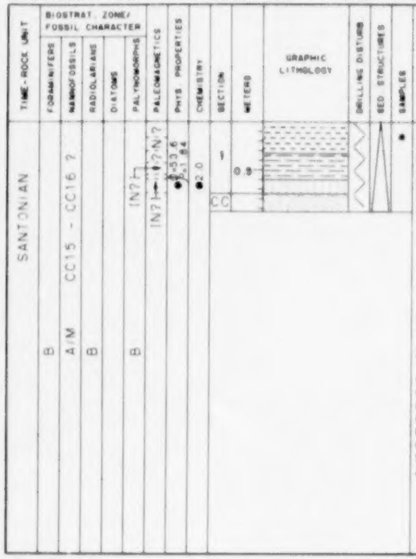

LITHOLOGIC DESCRIPTION

VOLCANICLASTIC TURBIDITES to NANNOFOSSIL CLAYSTONE

Major lithologies: VOLCANICLASTIC TURBIDITES grading upward to NANNOFOSSIL CLAYSTONE, dark bluish gray to dark gray (5B 4/1 N3). Volcaniclastic turbidites consist of VOLCANICLASTIC SANDSTONE, subtlely laminated with subangular clasts, grading to VOLCANICLASTIC SILTY CLAYSTONE, finely laminated to massive, and finally to massive nannofossil claystone.

SLIDE SUMMARY (%):

| | 1, 16<br>D |
|---|---|
| TEXTURE: | |
| Silt | 3 |
| Clay | 97 |
| COMPOSITION: | |
| Calcite | 5 |
| Clay | 63 |
| Feldspar | 1 |
| Glass | 5 |
| Nannofossils | 20 |
| Opaques | 3 |
| Smectite | 2 |
| Zeolite | 1 |

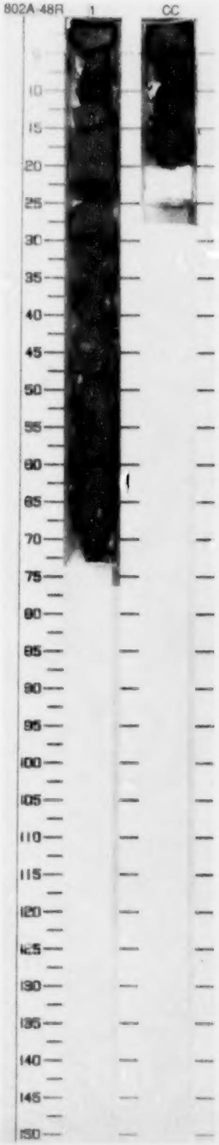
802A-48R
1
CC
5
10
15
20
25
30
35
40
45
50
55
60
65
70
75
80
85
90
95
100
105
110
115
120
125
130
135
140
145
150

SITE 802 HOLE A CORE 49R CORED INTERVAL 6406.7-6416.0 mbsl; 438.1-447.4 mbsf

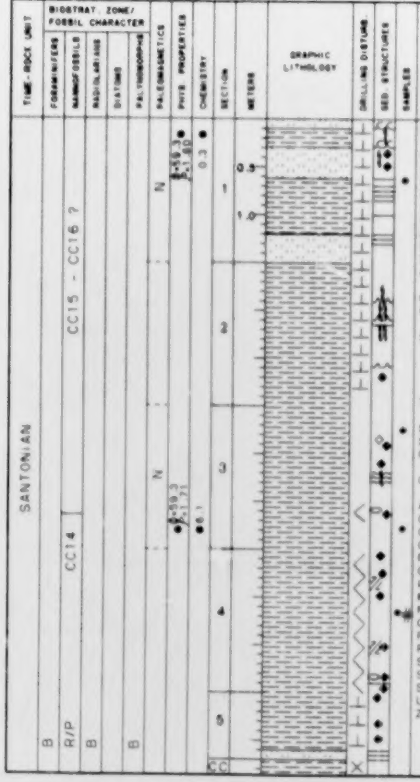
TIME-ROCK UNIT
BIOSTRAT. ZONE/ FOSSIL CHARACTER
FORAMINIFERS
NANNOFOSSILS
RADIOLARIANS
DIATOMS
PALYNOMORPHS
PALEOMAGNETICS
PHYS. PROPERTIES
CHEMISTRY
SECTION
METERS
GRAPHIC LITHOLOGY
DRILLING DISTURB.
SED. STRUCTURES
SAMPLES
SANTONIAN
B
R/P
B
B
CC15 - CC16 ?
CC14
N
N
φ=59.3 γ=1.80
φ=59.3 γ=1.71
0.3
6.1
1
2
3
4
5
CC
0.5
1.0

LITHOLOGIC DESCRIPTION

SILTY CLAYSTONE and SILTSTONE

Major lithologies:
a. SILTY CLAYSTONE, dark blue gray to dark green gray (5B 4/1 5BG 4/1), generally massive, but with weak horizontal fabric from aligned inclusions and small isolated clasts, locally laminated. Minor calcareous content and <20% volcaniclastic. Clasts are mostly 1-5 mm in diameter, one large (>7 cm) clast is a microcrystalline quartz radiolarite. Claystone at Section 4, 59-72 cm contains numerous authigenic acicular to bladed crystals (0.5 X 6 mm) possibly celestite.
b. SILTSTONE, blue green to dark greenish gray (5BG 4/1 5GY 4/1), massive to thinly laminated, locally graded, calcareous to clayey, flame structures at some preserved basal contacts; silty claystone and siltstone deposited as mass flows and turbidites.

Minor lithology: SILICIFIED CLAYSTONE, at Section 5, 58-60 cm, greenish gray (5GY 5/1), hard, blocky to subconchoidal fracture.

SLIDE SUMMARY (%):

| | 1, 64<br>M | 3, 25<br>M | 3, 128<br>D | 4, 68<br>M | 4, 68<br>M |
|---|---|---|---|---|---|
| TEXTURE: | | | | | |
| Sand | — | 50 | 5 | 50 | 5 |
| Silt | 25 | 30 | 20 | 30 | 10 |
| Clay | 75 | 20 | 70 | 20 | 85 |
| COMPOSITION: | | | | | |
| Accessory minerals | 1 | — | 1 | — | — |
| Calcite | 4 | Tr | 5 | — | — |
| Celestite | — | — | — | — | 5 |
| Clay | 65 | 15 | 68 | 20 | 40 |
| Feldspar | — | — | — | — | Tr |
| Glass | — | Tr | 8 | — | — |
| Igneous rock fragments | — | — | 7 | — | — |
| Micrite | — | — | — | — | 10 |
| Nannofossils | 2 | Tr | 1 | — | — |
| Opaques | 3 | — | 2 | — | 4 |
| Pyroxene | — | 1 | — | — | — |
| Radiolarians | 10 | 60 | 3 | — | 10 |
| Silica | — | 24 | — | — | 25 |
| Smectite | — | — | — | — | Tr |
| Spicules | — | — | 1 | — | — |
| Unknown | — | — | — | 80 | — |
| Zeolite | 15 | — | 4 | — | 6 |

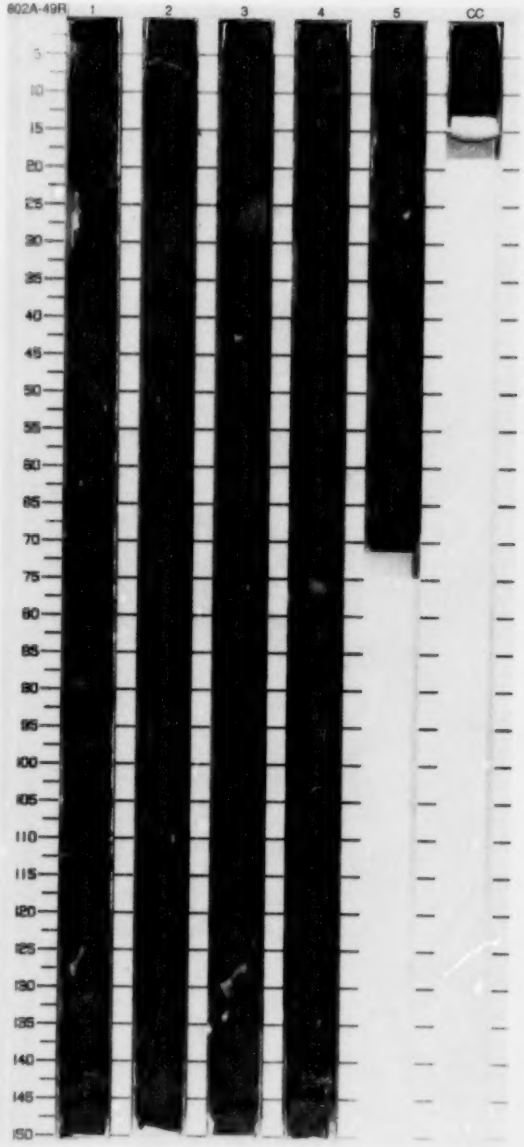
802A-49R
1
2
3
4
5
CC
5
10
15
20
25
30
35
40
45
50
55
60
65
70
75
80
85
90
95
100
105
110
115
120
125
130
135
140
145
150

SITE 802 HOLE A CORE 50R CORED INTERVAL 6416.0-6422.1 mbsl; 447.4-453.5 mbsf

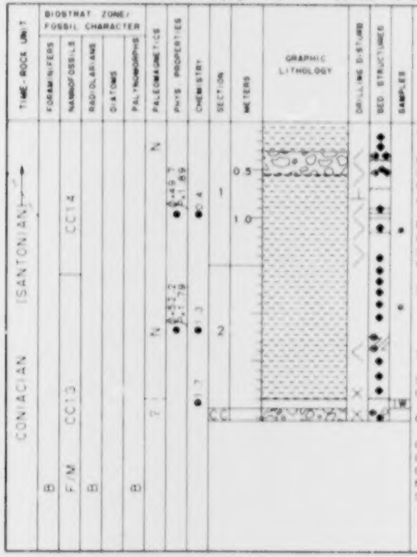
TIME-ROCK UNIT
BIOSTRAT. ZONE/ FOSSIL CHARACTER
FORAMINIFERS
NANNOFOSSILS
RADIOLARIANS
DIATOMS
PALYNOMORPHS
PALEOMAGNETICS
PHYS. PROPERTIES
CHEMISTRY
SECTION
METERS
GRAPHIC LITHOLOGY
DRILLING DISTURB.
SED. STRUCTURES
SAMPLES
CONIACIAN
SANTONIAN
CC14
CC13
F/M
B
B
B
N
N
?
49.7
1.89
52.2
1.79
0.4
1.3
1.7
1
2
CC
0.5
1.0
IW

LITHOLOGIC DESCRIPTION

VOLCANICLASTIC SILTY CLAYSTONE

Major lithology: VOLCANICLASTIC SILTY CLAYSTONE, dark blue gray to greenish gray (5B 4/1 5BG 5/1), firm, massive, rarely thinly laminated; contains 0-10% matrix supported fine-grained sedimentary clasts (as in a pebbly mudstone). Faint horizontal fabric from orientation of clasts. Probably deposited as a debris flow.

Minor lithology: PEBBLY SILTY CLAYSTONE, dark greenish gray (5g 4/1 5BG 4.5/1); matrix is identical to volcaniclastic silty claystone, matrix supported, fine-grained volcaniclastic sedimentary clasts are mostly dark blue gray to dark gray (5B4/1 5Y 4/1); 30:70 clast to matrix ratio; debris flow.

SLIDE SUMMARY (%):

| | 1, 112<br>D | 2, 44<br>D |
|---|---|---|
| TEXTURE: | | |
| Silt | 20 | 30 |
| Clay | 80 | 70 |
| COMPOSITION: | | |
| Calcite | — | 1 |
| Clay | 70 | 64 |
| Glass | 20 | 30 |
| Nannofossils | — | Tr |
| Smectite | 10 | 5 |

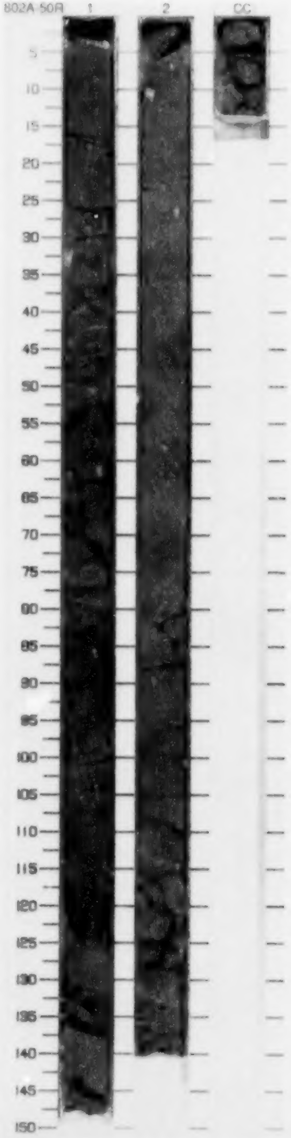
802A-50R
1
2
CC
5
10
15
20
25
30
35
40
45
50
55
60
65
70
75
80
85
90
95
100
105
110
115
120
125
130
135
140
145
150

SITE 802 HOLE A CORE 51R CORED INTERVAL 6422.1-6428.2 mbsl; 453.5-459.8 mbsf

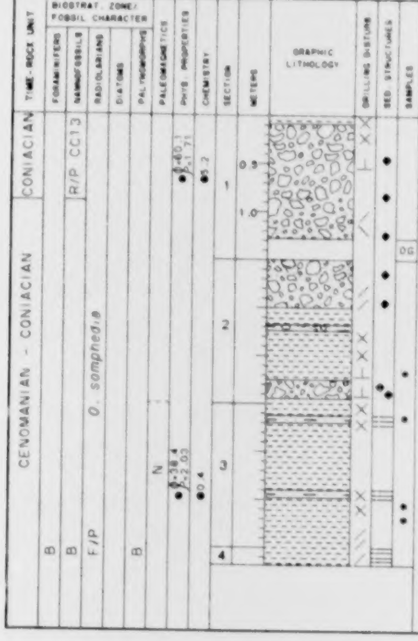
TIME-ROCK UNIT
BIOSTRAT. ZONE/ FOSSIL CHARACTER
FORAMINIFERS
NANNOFOSSILS
RADIOLARIANS
DIATOMS
PALYNOMORPHS
PALEOMAGNETICS
PHYS. PROPERTIES
CHEMISTRY
SECTION
METERS
GRAPHIC LITHOLOGY
DRILLING DISTURB.
SED. STRUCTURES
SAMPLES
CONIACIAN
CENOMANIAN - CONIACIAN
R/P CC13
B
B
F/P
O. somphedia
B
N
φ-60.1
γ-1.71
φ-38.4
γ-2.03
5.2
0.4
1
2
3
4
0.5
1.0
OG

LITHOLOGIC DESCRIPTION

CLAYSTONE and PEBBLY SILTY CLAYSTONE

Major lithologies:
a. CLAYSTONE: dark bluish gray (5B 4/1) to gray (N4) to greenish gray (5GY 5/1), firm, massive with scattered mudstone clasts, almost entirely clay mineralogy, trace only of volcanic glass.
b. PEBBLY SILTY CLAYSTONE: debris flow deposit, dark gray to dark bluish gray (N4 5B 4/1); matrix is the same as a., but supports 10-50% fine-grained sedimentary clasts (rip-ups). One extremely large clast (or folded bed) at Section 2, 48-65 cm is over 17 cm in diameter. Clasts are subangular to rounded, some are deformed as if they were still soft when deposited.

Minor lithology: SILTSTONE: dark greenish gray (5GY 4/1), thinly laminated and sandy.

Note: Marked change in color at Section 3, 91 cm from gray claystone downward to brown and green claystone (2.5YR 5/1 and 5G 6/2). The top of this interval is also silicified nearly to PORCELLANITE.

SLIDE SUMMARY (%):

| | 2, 118<br>D | 3, 14<br>M | 3, 106<br>D | 3, 120<br>D |
|---|---|---|---|---|
| TEXTURE: | | | | |
| Sand | — | 40 | — | — |
| Silt | 10 | 20 | 20 | 20 |
| Clay | 90 | 40 | 80 | 80 |
| COMPOSITION: | | | | |
| Clay | 95 | 45 | 100 | 100 |
| Glass | 5 | Tr | Tr | Tr |
| Micronodule | — | Tr | Tr | — |
| Radiolarians | — | 55 | — | — |

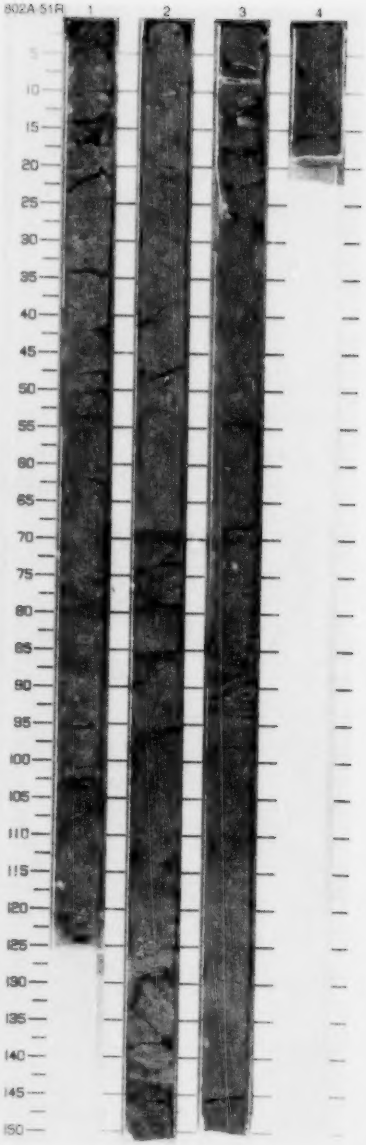
802A 51R
1
2
3
4
5
10
15
20
25
30
35
40
45
50
55
60
65
70
75
80
85
90
95
100
105
110
115
120
125
130
135
140
145
150

SITE 802 HOLE A CORE 52R CORED INTERVAL 6428.4-6438.0 mbsl; 459.8-469.4 mbsf

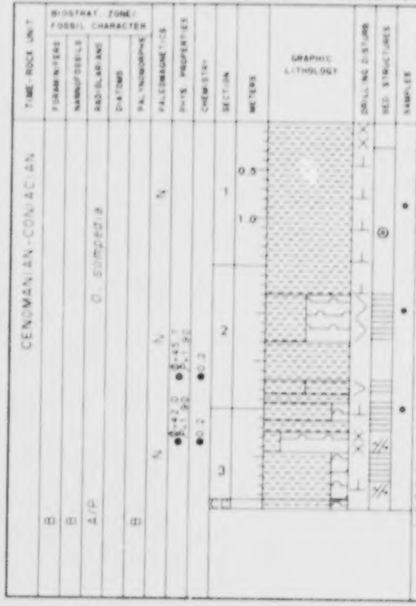
TIME-ROCK UNIT
BIOSTRAT. ZONE/ FOSSIL CHARACTER
FORAMINIFERS
NANNOFOSSILS
RADIOLARIANS
DIATOMS
PALYNOMORPHS
PALEOMAGNETICS
PHYS. PROPERTIES
CHEMISTRY
SECTION
METERS
GRAPHIC LITHOLOGY
DRILLING DISTURB.
SED. STRUCTURES
SAMPLES
CENOMANIAN-CONIACIAN
D. somphedia
B
B
A/P
B
N
N
N
ϕ=45.1
ϕ=42.0
0.2
0.2
1
2
3
CC
0.5
1.0

## LITHOLOGIC DESCRIPTION

CLAYSTONE and CLAYEY RADIOLARITE

Major lithologies:

a. CLAYSTONE: dark reddish brown to reddish brown (7.5YR 3/4-10YR 4/4); massive to subtly laminated; some intervals have discontinuous black streaks or greenish gray (5G 5/2) clasts (0.5-3.0 mm) or oval reduction mottle; dark bluish gray (5B 4/2) pieces at top of core may be contamination from uphole, similar to the claystone of upper Core 51; very dark brown (10YR 3/2-10YR 2/2), contains 30% iron manganese oxides, layers in Section 2, 136-137 and 148-150 cm.

b. CLAYEY RADIOLARITE: generally brown (7.5YR 4/4) with thin (2-3 mm) layers of strong brown (7.5YR 4/4 to 7.5YR 5/6) clay stone, but many intervals are grayish green to light grayish green (5G 5/2-5GY 7/1); generally finely laminated; occurs as bands within the claystone.

SLIDE SUMMARY (%):

| | 1, 86<br>M | 2, 47<br>D | 2, 149<br>M |
|---|---|---|---|
| TEXTURE: | | | |
| Sand | — | 40 | 5 |
| Silt | 10 | 30 | 25 |
| Clay | 90 | 30 | 70 |
| COMPOSITION: | | | |
| Clay | 50 | 50 | 70 |
| Glass | Tr | — | Tr |
| Oxide | 50 | — | 30 |
| Radiolarians | — | 50 | Tr |
| Zeolite | Tr | — | Tr |

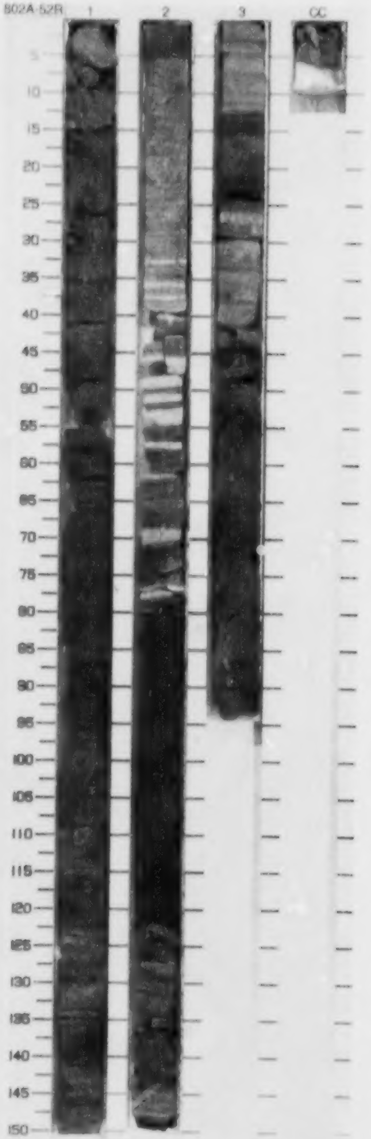
802A-52R
1
2
3
CC
5
10
15
20
25
30
35
40
45
50
55
60
65
70
75
80
85
90
95
100
105
110
115
120
125
130
135
140
145
150

## SITE 802 HOLE A CORE 53R CORED INTERVAL 6438.0-6447.2 mbsl; 469.4-478.6 mbsf

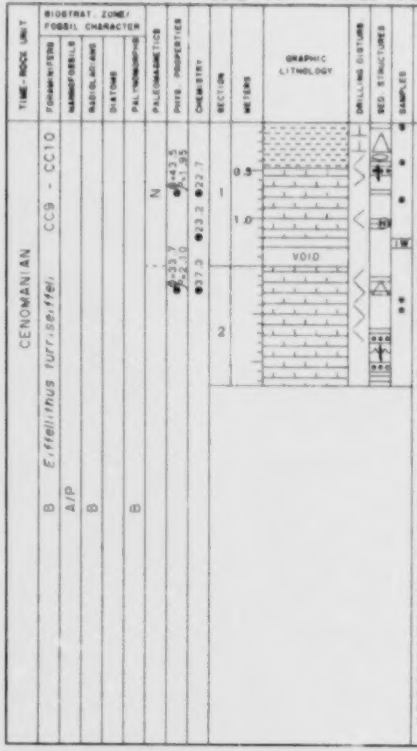
TIME-ROCK UNIT
BIOSTRAT. ZONE/ FOSSIL CHARACTER
FORAMINIFERS
NANNOFOSSILS
RADIOLARIANS
DIATOMS
PALYNOMORPHS
PALEOMAGNETICS
PHYS. PROPERTIES
CHEMISTRY
SECTION
METERS
GRAPHIC LITHOLOGY
DRILLING DISTURB.
SED. STRUCTURES
SAMPLES
CENOMANIAN
B
E. ffelli thus turriseiffeli
CC9 - CC10
A/P
B
B
N
φ=43.5
ρ=1.95
φ=33.7
ρ=2.10
●22.7
●23.2
●37.3
1
2
0.5
1.0
VOID

LITHOLOGIC DESCRIPTION

NANNOFOSSIL CHALK with VOLCANIC GLASS, CLAYEY NANNOFOSSIL CHALK with VOLCANIC GLASS, and VOLCANICLASTIC CLAYSTONE with NANNO- FOSSILS

Major lithologies:
a. NANNOFOSSIL CHALK with VOLCANIC GLASS, light to moderate pinkish brown (5YR 7/3 7.5YR 6/2), massive to finely laminated; sedimentary structures include basal scour, graded bedding and bioturbated tops of beds. Some fractures, parallel to bedding, have bleached halos. Rare dark layers contain concentrations of metal oxides; coarser layers contain radiolarians or volcanic glass. Gradational decrease in carbonate upward into Section 1 gives lithologies b. and (c).
b. CLAYEY NANNOFOSSIL CHALK with VOLCANIC GLASS, light brown to brown (7.5YR 6.4 7.5YR 5/4) massive, and
c. VOLCANICLASTIC CLAYSTONE with NANNOFOSSILS, reddish brown (5YR 5/4 5YR 4/3, 7.5YR 5/4), massive with slight fining upward grading and darkening of color in the 5-10 cm thick beds.

Minor lithology: CLAYEY RADIOLARITE to RADIOLARIAN CLAYSTONE, light reddish brown (5YR 6/4), occurs as 2-cm thick layers, commonly with clay-rich lower and uppermost portions and with vague laminations. Several layers occur within the major lithologies commonly between turbidite beds.

SLIDE SUMMARY (%):

| | 1, 4<br>D | 1, 40<br>D | 1, 80<br>D | 2, 36<br>M | 2, 44<br>D |
|---|---|---|---|---|---|
| TEXTURE: | | | | | |
| Sand | 5 | Tr | Tr | 5 | Tr |
| Silt | 10 | 25 | 20 | 50 | 3 |
| Clay | 85 | 75 | 80 | 45 | 97 |
| COMPOSITION: | | | | | |
| Accessory minerals | — | — | — | 1 | — |
| Calcite | — | 3 | 15 | 20 | 17 |
| Clay | 36 | 56 | 25 | 10 | 5 |
| Fish | 1 | — | — | — | — |
| Foraminifers | — | — | — | 5 | — |
| Glass | — | 25 | 10 | 15 | 7 |
| Nannofossils | — | 10 | 48 | 43 | 70 |
| Opaques | — | 4 | 2 | 3 | 1 |
| Oxide | 3 | 2 | Tr | 1 | |
| Palagonite | — | — | — | 2 | — |
| Radiolarians | 15 | — | Tr | Tr | — |
| Silica | 45 | — | — | — | — |

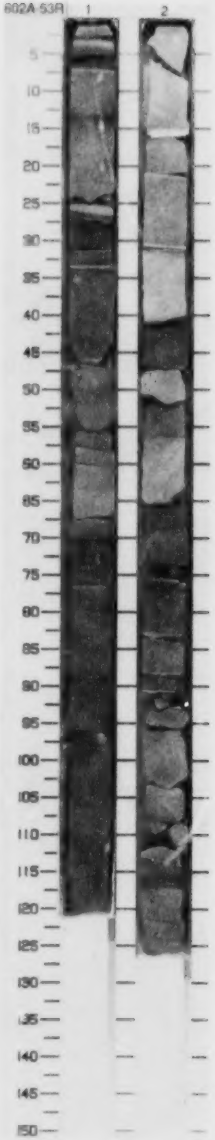
802A-53R
1
2
5
10
15
20
25
30
35
40
45
50
55
60
65
70
75
80
85
90
95
100
105
110
115
120
125
130
135
140
145
150

SITE 802 HOLE A CORE 54R CORED INTERVAL 6447.2-6456.5 mbsl; 478.6-487.9 mbsf

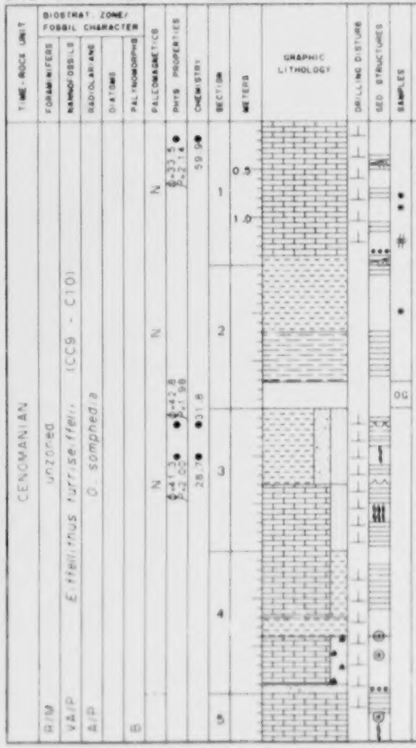
TIME-ROCK UNIT
BIOSTRAT. ZONE/ FOSSIL CHARACTER
FORAMINIFERS
NANNOFOSSILS
RADIOLARIANS
DIATOMS
PALYNOMORPHS
PALEOMAGNETICS
PHYS. PROPERTIES
CHEMISTRY
SECTION
METERS
GRAPHIC LITHOLOGY
DRILLING DISTURB.
SED. STRUCTURES
SAMPLES
CENOMANIAN
unzoned
Eiffellithus turriseiffelii (CC9 - C10)
D. somphedia
R/M
VA/P
A/P
B
N
N
N
ϕ-33.5
ρ-2.14
ϕ-42.8
ρ-1.98
ϕ-41.3
ρ-2.00
59.9
31.8
28.7
1
2
3
4
5
0.5
1.0
OG

LITHOLOGIC DESCRIPTION

LIMESTONE, CALCAREOUS CLAYSTONE, and CLAYEY SILTSTONE

Major lithologies:

a. LIMESTONE, light gray to blue gray (N7, N8, 5BG 5/1), massive, with rare burrows, rare laminations, clayey to sandy with calcified radiolarians, with CHERT nodules, brown (5YR 4/1).

b. CALCAREOUS CLAYSTONE, shades of grayish blue and green (5G 5/1, 5G 4/1, 5BG 5/2, 5Y 6/1, 5GY 5/1), mostly laminated, rare burrows.

c. CLAYEY SILTSTONE, bluish gray to gray (5BG 4/1 to N7), slightly calcareous massive or laminated.

Minor lithology: CLAYEY SANDSTONE, various shades of gray and green (5BG 5/1, 5G 5/1, 5GY 4/1, 5BG 4/2, 5Y 7/1) from diagenetic alteration, laminated or massive, some graded beds and scoured bases. Contains foraminifers, radiolarians, volcanic glass, zeolites.

SLIDE SUMMARY (%):

| | 1, 78<br>D | 1, 90<br>D | 1, 127<br>M | 2, 48<br>D |
|---|---|---|---|---|
| TEXTURE: | | | | |
| Sand | 3 | — | 15 | 5 |
| Silt | 17 | 30 | 15 | 20 |
| Clay | 80 | 70 | 70 | 70 |
| COMPOSITION: | | | | |
| Accessory minerals | 1 | — | — | — |
| Calcite | 15 | — | 10 | 5 |
| Clay | 35 | — | 10 | 57 |
| Feldspar | 1 | Tr | — | — |
| Foraminifers | — | 1 | — | 2 |
| Micrite | 45 | 94 | 29 | 10 |
| Nannofossils | 3 | — | 30 | 20 |
| Opaques | — | — | 1 | Tr |
| Quartz | — | Tr | — | — |
| Radiolarians | — | 5 | 20 | 5 |
| Smectite | — | — | — | 1 |
| Spicules | — | Tr | — | — |

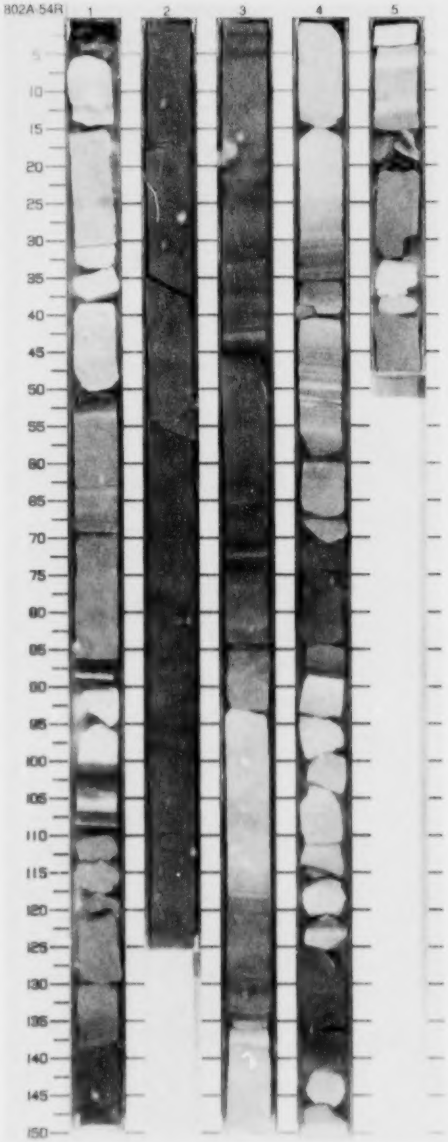
802A-54R
1
2
3
4
5
5
10
15
20
25
30
35
40
45
50
55
60
65
70
75
80
85
90
95
100
105
110
115
120
125
130
135
140
145
150

SITE 802 HOLE A CORE 55R CORED INTERVAL 6456.5-5465.7 mbsl; 487.9-497.1 mbsf

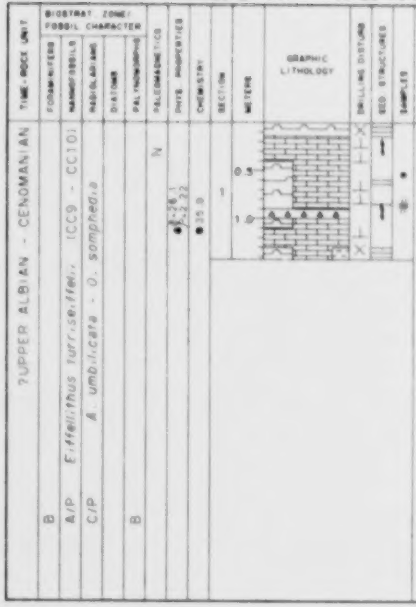
TIME-ROCK UNIT
BIOSTRAT. ZONE/ FOSSIL CHARACTER
FORAMINIFERS
NANNOFOSSILS
RADIOLARIANS
DIATOMS
PALYNOMORPHS
PALEOMAGNETICS
PHYS. PROPERTIES
CHEMISTRY
SECTION
METERS
GRAPHIC LITHOLOGY
DRILLING DISTURB.
SED. STRUCTURES
SAMPLES
?UPPER ALBIAN - CENOMANIAN
B
A/P Eiffellithus turriseiffeli, (CC9 - CC10)
C/P A. umbilicata - O. somphedia
B
N
φ-26.1
γ-2.22
●35.0
1
0.5
1.0

LITHOLOGIC DESCRIPTION

RADIOLARIAN LIMESTONE and LIMESTONE with RADIOLARIANS

Major lithologies:

a. RADIOLARIAN LIMESTONE, dark brown to gray (10YR 4/3 5Y 6/1), mostly massive with some laminations; locally burrowed; locally siliceous. Radiolarians are calcitized; grades to

b. LIMESTONE with RADIOLARIANS: identical except for reduced quantity of radiolarians.

Minor lithologies:

a. PORCELLANITE, pinkish gray (5YR 6/3 5YR 7/2), weakly bioturbated, and

b. CLAYEY CALCAREOUS RADIOLARITE, brown (10YR 5/3), laminated and fractured by drilling.

SLIDE SUMMARY (%):

| | 1, 53 | 1, 86 |
|---|---|---|
| | D | D |
| TEXTURE: | | |
| Sand | 5 | 10 |
| Silt | 35 | 40 |
| Clay | 60 | 50 |
| COMPOSITION: | | |
| Calcite | 15 | 10 |
| Clay | 10 | — |
| Fish | — | Tr |
| Foraminifers | — | 1 |
| Glass | — | 10 |
| Micrite | 54 | 62 |
| Nannofossils | 10 | — |
| Opaques | 1 | 4 |
| Radiolarians | 10 | 15 |

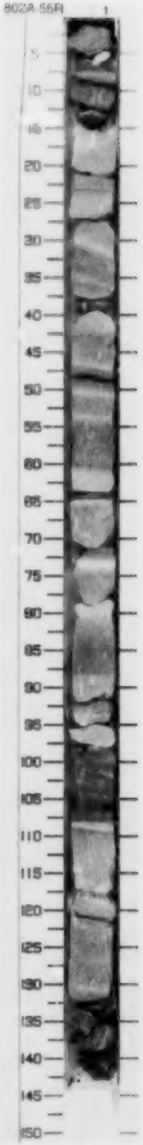
802A-55R
1
5
10
15
20
25
30
35
40
45
50
55
60
65
70
75
80
85
90
95
100
105
110
115
120
125
130
135
140
145
150

SITE 802 HOLE A CORE 56R CORED INTERVAL 6465.7-6475.2 mbsl; 497.1-506.6 mbsf

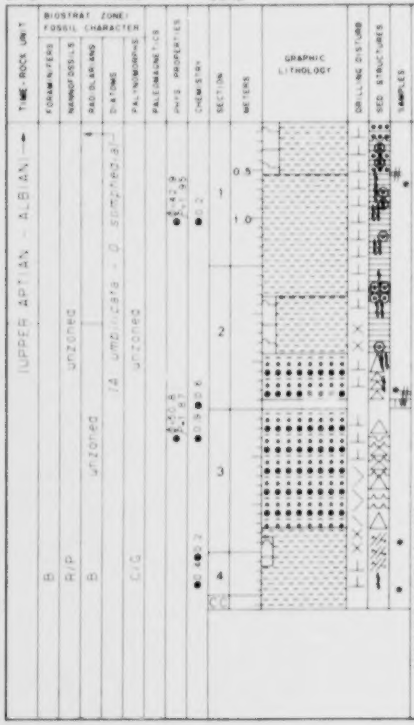
TIME-ROCK UNIT
BIOSTRAT. ZONE/ FOSSIL CHARACTER
FORAMINIFERS
NANNOFOSSILS
RADIOLARIANS
DIATOMS
PALYNOMORPHS
PALEOMAGNETICS
PHYS. PROPERTIES
CHEMISTRY
SECTION
METERS
GRAPHIC LITHOLOGY
DRILLING DISTURB.
SED. STRUCTURES
SAMPLES
UPPER APTIAN - ALBIAN
unzoned
(A. umbilicata - D. somphedia)
unzoned
unzoned
B
R/P
B
C/G
0.5
1.0
1
2
3
4
CC

LITHOLOGIC DESCRIPTION

CLAYSTONE and VOLCANICLASTIC TURBIDITES

Major lithologies:
a. CLAYSTONE, light brown to dusky yellowish brown to brownish black (5YR 6/4 10YR 2/2 5YR 2/1); mostly hematitic, zeolitic, locally radiolarian rich. Thinly laminated to massive, commonly burrowed. 1-2 mm metalliferous nodules of oxides or pyrite. Interval from Section 3, 127 cm to Section 4, 7 cm contains numerous folded and refractured calcareous veins.
b. VOLCANICLASTIC TURBIDITES, greenish gray to dusky green (5GY 6/1 5G 3/2); graded beds with load casts and sharp erosional bases. Typically fines upward from fine sand to clay size in beds 2-25 cm thick.

Minor lithology: RADIOLARITE, light to moderate brown (5YR 6/4 5YR 3/4), locally altered and mottled olive green (5GY 6/1), medium grained, sometimes graded, sharp top and bottom, but not scoured.

SLIDE SUMMARY (%):

| | 1, 55<br>D | 1, 67<br>D | 2, 130<br>D | 2, 133<br>D | 3, 140<br>M | 4, 40<br>M |
|---|---|---|---|---|---|---|
| TEXTURE: | | | | | | |
| Sand | 10 | — | Tr | 10 | Tr | Tr |
| Silt | 15 | 10 | 45 | 20 | 15 | 20 |
| Clay | 75 | 90 | 55 | 70 | 85 | 80 |
| COMPOSITION: | | | | | | |
| Calcite | — | — | — | — | 3 | — |
| Clay | 65 | 77 | 55 | 60 | 72 | 75 |
| Feldspar | — | — | — | — | — | 1 |
| Glass | — | — | 21 | 10 | 5 | 15 |
| Igneous rock fragments | — | — | — | 5 | — | — |
| Nannofossils | — | — | Tr | — | — | — |
| Opaques | — | 10 | 3 | — | 10 | 8 |
| Oxide | 10 | — | — | 5 | — | — |
| Quartz | — | — | — | Tr | — | — |
| Radiolarians | 20 | 10 | 20 | 5 | 10 | 1 |
| Silica | 5 | — | — | 5 | — | — |
| Smectite | — | — | 1 | 10 | — | — |
| Zeolite | — | 3 | — | — | — | — |

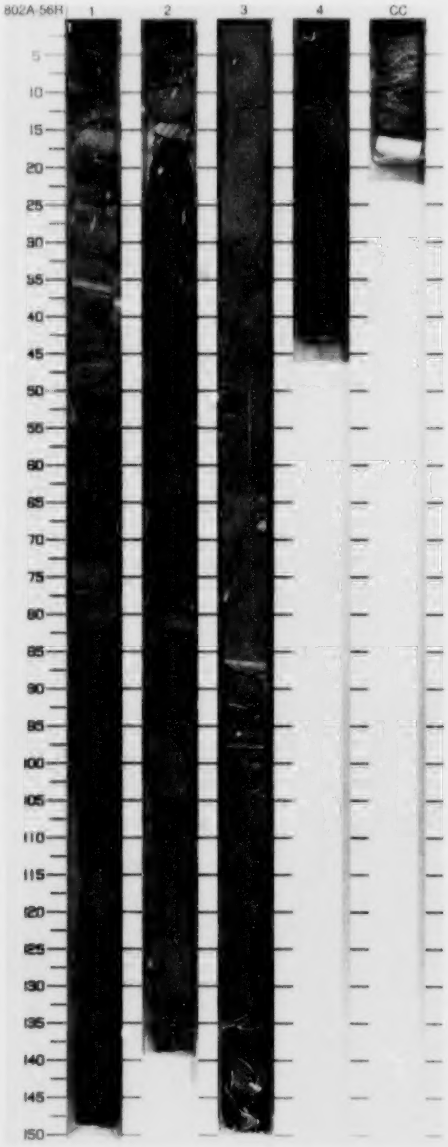
802A-56R
1
2
3
4
CC
5
10
15
20
25
30
35
40
45
50
55
60
65
70
75
80
85
90
95
100
105
110
115
120
125
130
135
140
145
150

SITE 802 HOLE A CORE 57R CORED INTERVAL 6475.2-6484.6 mbsl; 506.6-516.0 mbsf

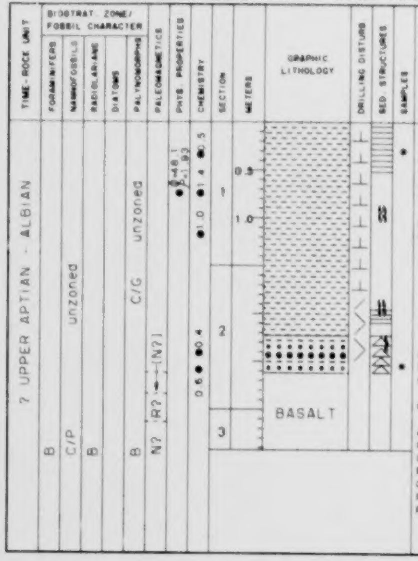
TIME-ROCK UNIT
BIOSTRAT. ZONE/ FOSSIL CHARACTER
FORAMINIFERS
NANNOFOSSILS
RADIOLARIANS
DIATOMS
PALYNOMORPHS
PALEOMAGNETICS
PHYS. PROPERTIES
CHEMISTRY
SECTION
METERS
GRAPHIC LITHOLOGY
DRILLING DISTURB.
SED. STRUCTURES
SAMPLES
? UPPER APTIAN - ALBIAN
B
C/P
unzoned
B
B
C/G
unzoned
N? (R?) (N?)
ϕ-48.1
γ-1.93
0.5
1.4
1.0
0.4
0.6
1
2
3
0.5
1.0
BASALT

LITHOLOGIC DESCRIPTION

TUFFACEOUS CLAYSTONE

Major lithology: TUFFACEOUS CLAYSTONE, black (N2), becomes darker downcore, tuffaceous, massive to discontinuously laminated, with rare burrows. Approximately 50% identifiable volcanic glass, rock fragments and accessory minerals. Chemical analysis indicates little or no organic carbon.

Minor lithology: TUFFACEOUS TURBIDITES, dark grayish green to black (5GY 4/1, N2), graded beds, burrowed, contains mostly volcanic glass and rock fragments, 20% clay.

SLIDE SUMMARY (%):

| | 1, 30<br>D | 2, 104<br>D |
|---|---|---|
| TEXTURE | | |
| Sand | Tr | Tr |
| Silt | 25 | 75 |
| Clay | 75 | 25 |
| COMPOSITION | | |
| Accessory minerals | — | Tr |
| Clay | 45 | 20 |
| Glass | 27 | 60 |
| Nannofossils | 1 | — |
| Opaques | 8 | 5 |
| Radiolarians | — | Tr |
| Rock fragment | 18 | 15 |

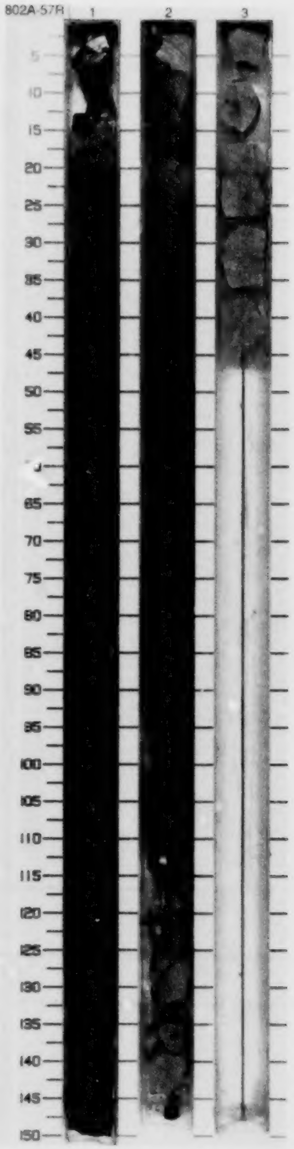
802A-57R
1
2
3
5
10
15
20
25
30
35
40
45
50
55
65
70
75
80
85
90
95
100
105
110
115
120
125
130
135
140
145
150

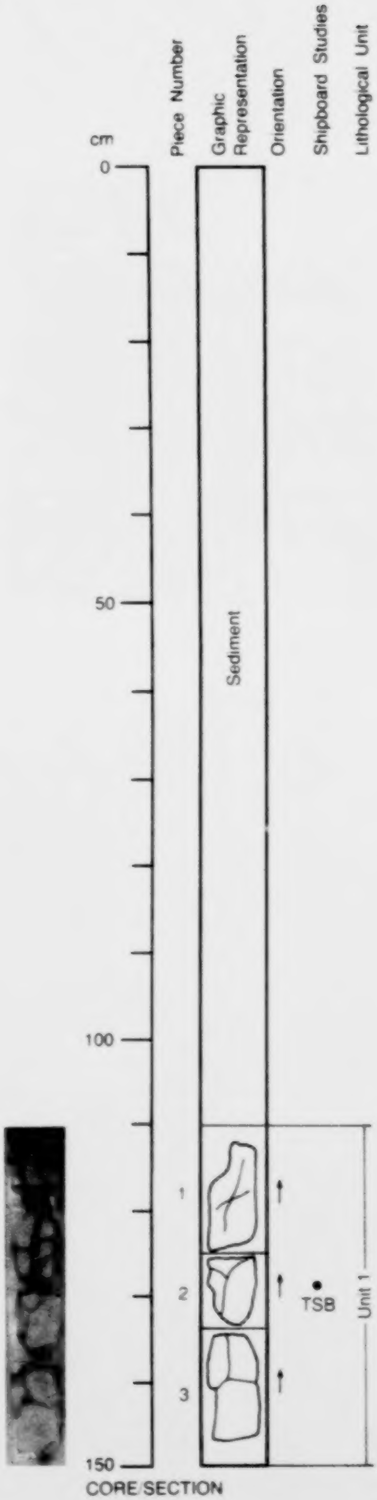

## 129-802A-57R-2

## UNIT 1: APHYRIC BASALT

### Pieces 1-3

**CONTACTS:** Not observed, but inferred from glassy zone to represent flow top. Directly above is drilling rubble of a vitric tuff; possibly c.4m of contact zone missing (basalt & sediment) from the record.

**PHENOCRYSTS:** One or two plagioclase and pyroxene microphenocrysts only in glassy spherulitic zone.

**GROUNDMASS:** Adjacent to contact (at 110 cm) is green smectite-replaced glass (2-3 mm preserved) that grades into a pale gray zone with spherulites that progressively coalesce away from contact. Rest of unit is fine-grained, quench textured with fan variolites and patches of green smectite-replaced glassy mesostasis.

**VESICLES:** 1%; <1 mm; irregular; concentrated at 114 cm; infilled with green smectite and sometimes calcite in central part.

**COLOR:** Dark to medium-gray (N4 at contact but generally N5).

**STRUCTURE:** Thin flow, possibly pillowed as curving "fracture" in Piece 2 appears to be a green smectite-replaced glassy selvage with variolitic fans further away from margin.

**ALTERATION:** Slight. Green smectite replacing glass margins and vesicles. Pyrite sometimes asssociated with glass. Minor carbonate.

**VEINS/FRACTURES:** 1%; 0.2 mm; sub-vertical & horizontal.

**ADDTIONAL COMMENTS:** Glassy sperulitic zone indicates top of lava flow, possibly pillowed, although curved selvages not well developed.

## 129-802A-57R-3

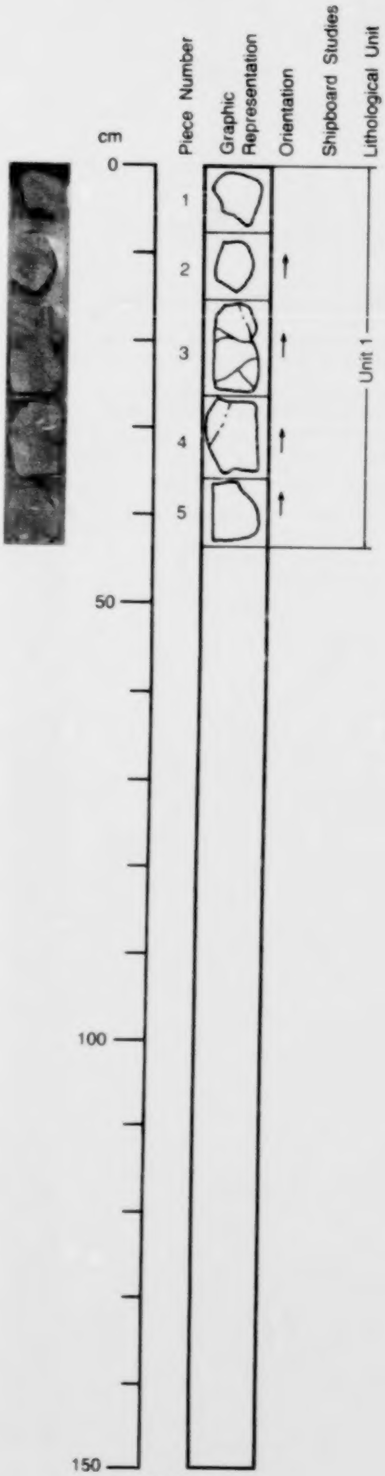
cm
Piece Number
Graphic Representation
Orientation
Shipboard Studies
Lithological Unit
0
50
100
150
1
2
3
4
5
Unit 1
CORE/SECTION

### UNIT 1: APHYRIC BASALT

### Pieces 1-5

**CONTACTS:** None observed, although all pieces have quench textures with smectite-replaced interstitial glass.

**PHENOCRYSTS:** None observed.

**GROUNDMASS:** Fine-grained, hypocrystalline. Uniform throughout all pieces with plagioclase-bearing fan and plume variolites.

**VESICLES:** None observed.

**COLOR:** Speckled pale gray (N6).

**STRUCTURE:** Part of a lava flow; no evidence for pillow surfaces.

**ALTERATION:** Slight. Largely replacement of mesostasis glass by green smectite and clay-pyrite veinlets.

**VEINS/FRACTURES:** 2%; <0.1 mm; 30-45 degrees; infilled with green smectite +/- pyrite and carbonate. Larger veins show zoned, semi-botryoidal growth of radiate smectite fibers with central zone infilled with carbonate, together with variable oxidized coating.

**ADDITIONAL COMMENTS:** All quenched texture suggests a thin flow.

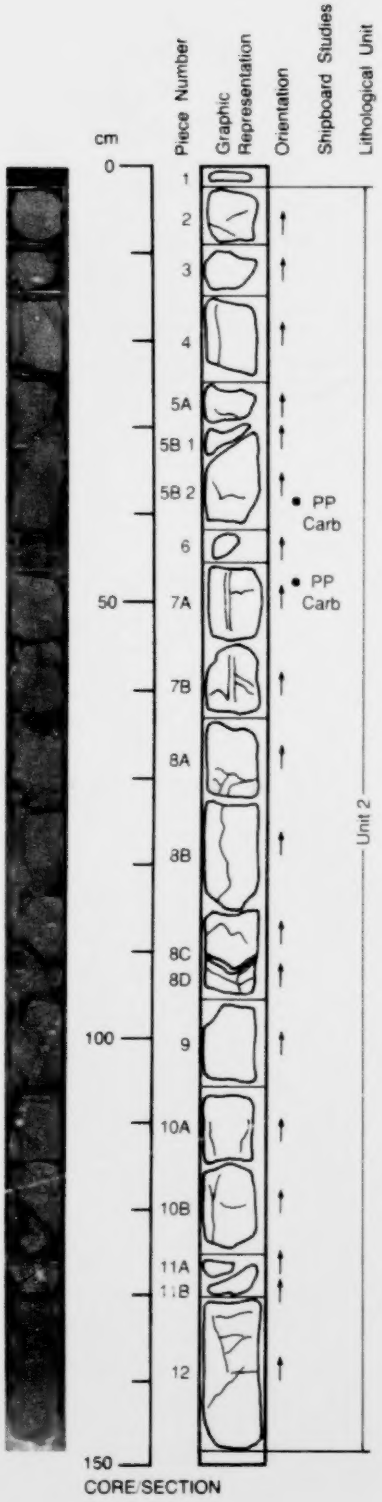
cm
Piece Number
Graphic Representation
Orientation
Shipboard Studies
Lithological Unit
0
50
100
150
1
2
3
4
5A
5B 1
5B 2
6
7A
7B
8A
8B
8C
8D
9
10A
10B
11A
11B
12
PP Carb
PP Carb
Unit 2
CORE/SECTION

## 129-802A-58R-1

## UNIT 2: APHYRIC BASALT

### Pieces 2-12

**CONTACTS:** None observed.
**PHENOCRYSTS:** None observed.
**GROUNDMASS:** Fine-grained, hypocrystalline; traces of quenched plagioclase microlites.
**VESICLES:** <<1%; <0.5 mm; irregular; irregular; a majority are infilled are completely infilled with green clays
**COLOR:** Speckled gray (N6).
**STRUCTURE:** Since no contacts recovered, possibly part of a lava flow.
**ALTERATION:** Slight to moderate. Glassy mesostasis altered to dark green clays; some plagioclase laths completely replaced by carbonate.
**VEINS/FRACTURES:** 2%; <0.1-3.0 mm; highly irregular; veins in Pieces 7A &7B infilled with green clays and carbonate, whereas rest filled with green clays. Dark green-gray halo, up to 3 cm wide in Piece 12.
**ADDITIONAL COMMENTS:** Could be a continuation of Unit 1 as (a) texturally very similar to lower purtion of Unit 1, (b) no actual contacts recovered and (c) sediment at top of section could be a cave-in from higher up the hole.

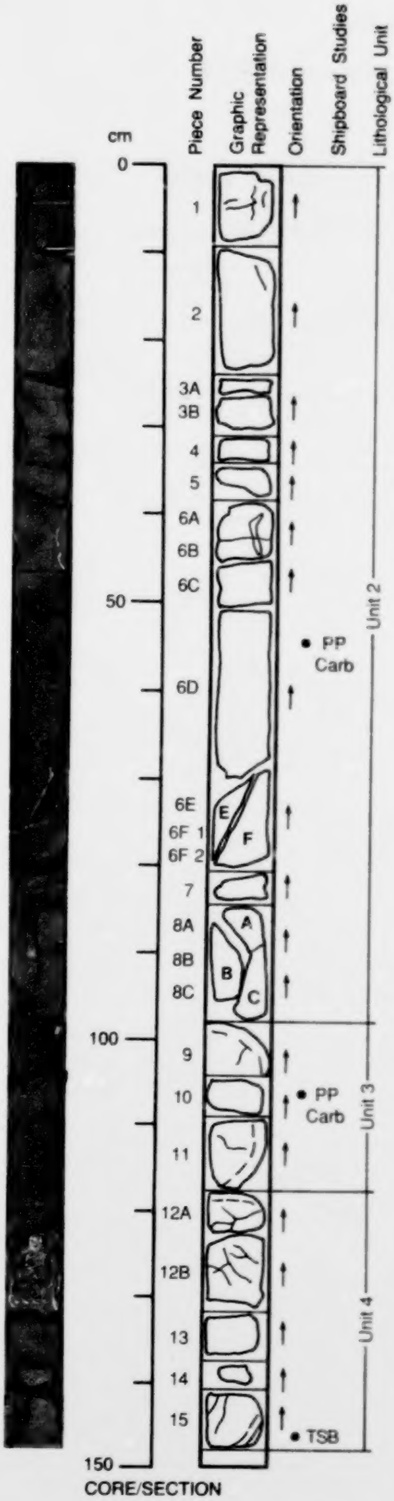

## 129-802A-58R-2

### UNIT 2: APHYRIC BASALT

#### Pieces 1-8C

**CONTACTS:** None observed, but grain-size fines downwards.
**PHENOCRYSTS:** None observed.
**GROUNDMASS:** Fine-grained, hypocrystalline. Glassy mesostasis and fan variolites of plagioclase. Quench texture more prevalent towards bottom part of Unit.
**VESICLES:** None observed.
**COLOR:** Speckled gray (N6).
**STRUCTURE:** Perhaps basal part of a lava flow.
**ALTERATION:** Slight to moderate. Glass altered to green clays; a few secondary calcite grains in matrix.
**VEINS/FRACTURES:** c.1%; <0.1-4.0 mm (P.4E); 0-90 degrees; irregular; often highly irregular and cross-cutting. Wider veins infilled with carbonate, narrower ones with green clay.
**ADDITIONAL COMMENTS:** Appears to be basal part of Unit 2 as suggested by the decreasing grain-size. Texturally the upper part is similar to Unit 2 in 58R-1.

### UNIT 3: MODERATELY OLIVINE-PLAGIOCLASE MICROPHYRIC BASALT

#### Pieces 9-11

**CONTACTS:** None observed, but rounded glassy margins are present in Piece 9 and 11.
**PHENOCRYSTS:**
Plagioclase - trace; <0.1; Subhedral, little alteration.
Olivine - ~3%; <0.1; Euhedral-subhedral, slightly altered.
**GROUNDMASS:** Glassy rim grading to a thin variolitic, hypohyaline zone, and then to a hypocrystalline interior. Quench textured throughout.
**VESICLES:** None observed.
**COLOR:** Gray (N5) with black glass rim (2/0).
**STRUCTURE:** Pillow lava.
**ALTERATION:** Slight. Most of glass rim is black and unaltered despite cracks filled with green clays. Some alteration to green smectite of phenocrysts.
**VEINS/FRACTURES:** <1%; <0.1 mm; parallel & radial to glassy rim; many fractures are also irregular and cross-cutting, infilled with green smectite (a few are open).
**ADDITIONAL COMMENTS:** Curved glassy margin and internal textural variations strongly suggest this is a pillow lava margin.

### UNIT 4: MODERATELY OLIVINE-PLAGIOCLASE MICROPHYRIC BASALT

#### Pieces 12A-15

**CONTACTS:** Not observed, but top is sub-horizontal and glassy and part of bottom margin is glassy and inclined.
**PHENOCRYSTS:** Slightly more abundant near Unit margins.
Plagioclase - trace; <0.1; Subhedral.
Olivine - ~2%; <0.1; Euhedral-subhedral; slightly altered.
**GROUNDMASS:** Glassy rims grading into thin, variolitic zones and then to a fine-grained, hypocrystalline interior. Quenched texture throughout.
**VESICLES:** Generally none, although a few are present in the glassy rim.
**COLOR:** Speckled gray (N6).
**STRUCTURE:** Pillow lava.
**ALTERATION:** Slight. Olivine microphenocrysts and mesostasis replaced by green clays.
**VEINS/FRACTURES:** 1-2%; <0.1 mm; irregular; a few are perpendicular to glassy rim, but generally irregular, infilled with green clays.
**ADDITIONAL COMMENTS:** Texturally similar to Unit 3 and probably represents another pillow section with an inclined bottom margin.

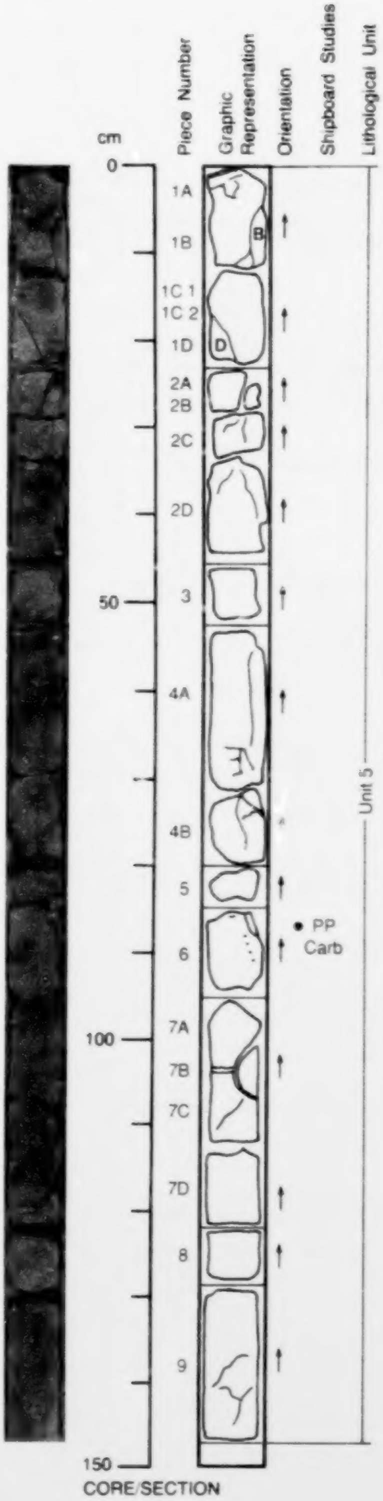
cm
Piece Number
Graphic Representation
Orientation
Shipboard Studies
Lithological Unit
0
50
100
150
1A
1B
B
1C 1
1C 2
1D
D
2A
2B
2C
2D
3
4A
4B
5
6
7A
7B
7C
7D
8
9
• PP
Carb
Unit 5
CORE/SECTION

## 129-802A-58R-3

## UNIT 5: SPARSELY OLIVINE MICROPHYRIC BASALT

### Pieces 1A-9

**CONTACTS:** None observed, but a part of the top margin is glassy and curved, and grain-size coarsens downwards.

**PHENOCRYSTS:** Slightly more abundant in top section.

Olivine - 1%; <0.1; Euhedral and subhedral; mostly altered to green smectite and/or yellowish-brown iddingsite(?).

**GROUNDMASS:** Glassy rim grading to a thin variolitic zone and then to a fine-grained, hypocrystalline zone (c.50 cm) which gradually gives way to an almost holocrystalline base. Quench texture dominant with patchy glassy mesostasis throughout.

**VESICLES:** <1%; up to 2 mm; irregular; in Piece 6; majority infilled with green clays but ~10% only partly filled.

**COLOR:** Speckled gray (N5).

**STRUCTURE:** Top of lava flow.

**ALTERATION:** Slight to moderate. Glassy rim is black and appears unaltered, although olivine microphenocrysts and mesostasis replaced by green smectite; minor granular carbonate in matrix.

**VEINS/FRACTURES:** c.1%; 0.05-0.1 mm; subhorizontal-vertical; infilled with green clays and carbonate; some with faint haloes. Cross-cutting relationship common.

**ADDITIONAL COMMENTS:** General increase in grain-size towards the base suggests a lava flow. Glassy mesostasis is generally larger and more irregular than olivine but both are altered to green clays so that these are hard to differentiate at times.

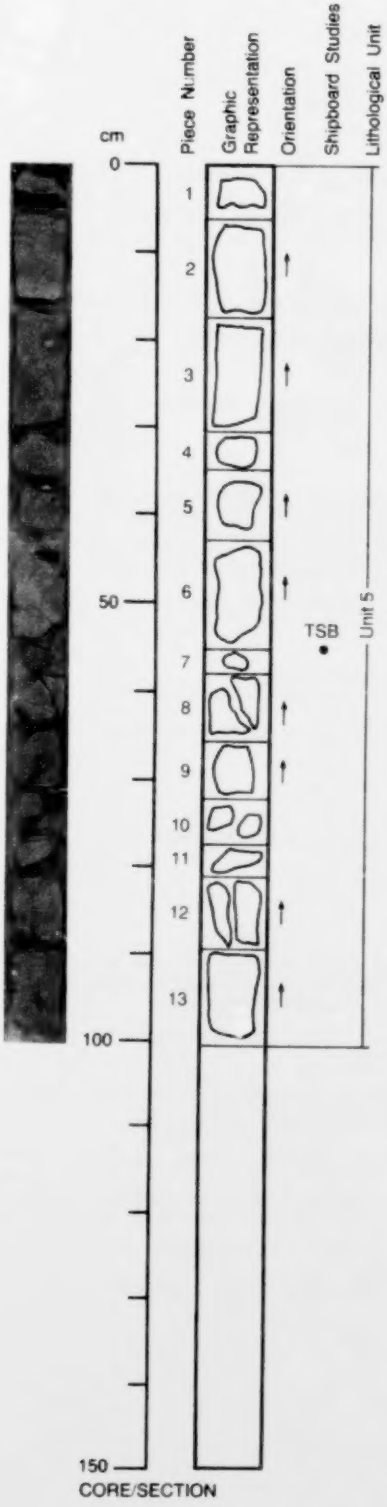
cm
Piece Number
Graphic Representation
Orientation
Shipboard Studies
Lithological Unit
0
50
100
150
1
2
3
4
5
6
7
8
9
10
11
12
13
TSB
Unit 5
CORE/SECTION

## 129-802A-58R-4

## UNIT 5: SPARSELY OLIVINE MICROPHYRIC BASALT

### Pieces 1-13

**CONTACTS:** None observed, but grain-size fines towards the bottom of Unit.

**PHENOCRYSTS:** Very limited distribution.

Olivine - c.1%; <0.1; Euhedral to subhedral; slightly altered.

**GROUNDMASS:** Top is fine-grained, hypocrystalline to hypohyaline, then grades towards a hypocrystalline quench-textured base. Glassy mesostasis throughout.

**VESICLES:** None observed.

**COLOR:** Speckled gray (N6).

**STRUCTURE:** Basal portion of a thin flow.

**ALTERATION:** Slight to moderate. Glassy mesostasis and olivine altered to green smectite; minor carbonate along some plagioclase margins.

**VEINS/FRACTURES:** <1%; <0.1 0.1 mm; sub-vertical and irregular; veinlets often very irregular, but most are sub-vertical; infilled with green smectite and carbonate.

**ADDITIONAL COMMENTS:** Grain-size fines towards mid-section (Pieces 7-10) and then slightly coarsens towards the bottom (Pieces 11-13). This could either represent internal flow differentiation or the presence of an additional unit. However, because the compositional make-up of all the pieces are similar, they have all been included within Unit 5.

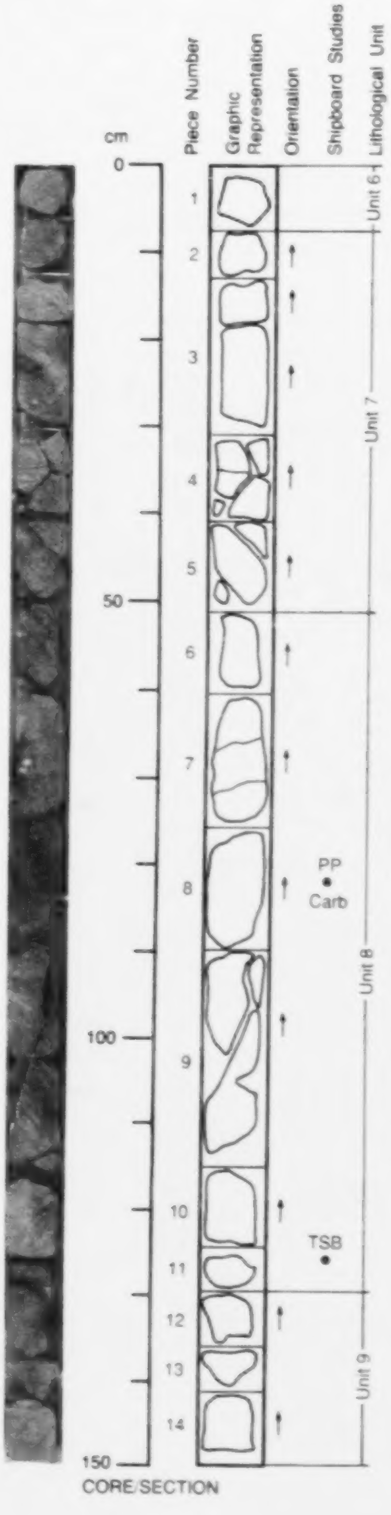

## 129-802A-59R-1

## UNIT 6: APHYRIC BASALT

### Piece 1

**CONTACTS:** None observed, but coarser grained and less glassy than base of Unit 5 (58R-4, Pieces 12 & 13).
**PHENOCRYSTS:** None observed, but possibly one or two olivine pseudomorphs.
**GROUNDMASS:** Fine-grained, hypocrystalline throughout.
**VESICLES:** None observed.
**COLOR:** Speckled pale gray (N6).
**STRUCTURE:** Possibly central part of thin flow.
**ALTERATION:** Slight. Glassy mesostasis replaced by green smectite.
**VEINS/FRACTURES:** None observed.
**ADDITIONAL COMMENTS:** Single piece, but sufficiently different to those above and below, to probably represent another small unit.

## UNIT 7: SPARSELY OLIVINE MICROPHYRIC BASALT

### Pieces 2-5

**CONTACTS:** None observed, except Piece 2 is finer-grained, contains high proportion of smectite-replaced glassy patches and has plagioclase bearing plume variolites (all different features relative to Piece 1).
**PHENOCRYSTS:** Random distribution, with some concentration towards top of Unit.
Olivine - 1-2%; 0.1; microphenocrysts replaced by green smectite and sometimes oxidized.
**GROUNDMASS:** Fine-grained, hypocrystalline throughout with plumose variolites at top, being replaced by more granular matrix lower in Unit.
**VESICLES:** None observed.
**COLOR:** Speckled pale gray (N6).
**STRUCTURE:** Thin flow, although glassy top and bottom missing.
**ALTERATION:** Slight. Glassy mesostasis replaced by zoned green smectite and a central core of carbonate.
**VEINS/FRACTURES:** <1%; 0.1-0.2 mm; 25 & 45 degrees; relatively minor occurrence, green smectite +/- pyrite infilling.
**ADDITIONAL COMMENTS:** None.

## UNIT 8: SPARSELY OLIVINE-PLAGIOCLASE PHYRIC BASALT

### Pieces 6-11

**CONTACTS:** Top contact not observed, except Piece 6 much finer grained and more glassy (replaced by green and blue clays and carbonate) than Piece 5 above. Bottom contact (Piece 11) of very fine-grained, spherulitic textured, dark gray basalt with sparse phenocrysts.
**PHENOCRYSTS:** Observed at basal contact, rarely seen throughout rest of Unit.
Plagioclase - trace; 0.1; Subhedral and unaltered.
Olivine - 2%, <0.1; invariably replaced by green smectite.
**GROUNDMASS:** Fine-grained, hypocrystalline throughout, except mesostasis distribution is patchy. Base of Unit much finer and formed of coalesing plagioclase-bearing spherulites and fan variolites interspersed by green smectite-replaced glass.
**VESICLES:** None observed.
**COLOR:** Speckled medium gray (N5 to N6) throughout, except dark gray at base (N4).
**STRUCTURE:** Thin flow.
**ALTERATION:** Slight. Green and blue clays replacing glassy mesostasis and themselves replaced by carbonate. Pyrite may occasionally be associated with carbonate. Clay and carbonate in veins.
**VEINS/FRACTURES:** 2%; 0.2-3.0 mm; two sets: 20 & 50; typically infilling is dark smectitic clay (saponite?), carbonate and pyrite.
**ADDITIONAL COMMENTS:** Small cooling unit, which could be a section of a pillow lava.

## 129-802A-59R-1 (continued)

## UNIT 9: SPARSELY OLIVINE-PLAGIOCLASE MICROPHYRIC BASALT

### Pieces 12-14

**CONTACTS:** Only top contact observed adjacent to curved basal contact of Unit 8 above. Contact zone of coalesed spherulites and minor interstitial glass, that curves down parallel to green clay vein (Piece 12). Inwards from this quenched zone fan variolites are developed.

**PHENOCRYSTS:** Apparently concentrated in contact zone, although some olivine seen throughout Unit.

Plagioclase - trace; 0.1; very small and rare laths.

Olivine - 2%; <0.1; commonly euhedral and smectite replaced.

**GROUNDMASS:** Fine-grained, hypocrystalline throughout although higher proportion of glass at Unit top with spherulites and fan variolites which decrease downwards to more granular texture.

**VESICLES:** None observed.

**COLOR:** Uniform medium gray (N6).

**STRUCTURE:** Top of thin flow or possibly pillow lava.

**ALTERATION:** Slight. Glassy rim and mesostasis altered to green smectite. Blue-green clays and carbonate in veins.

**VEINS/FRACTURES:** <1%; <0.1 mm; sub-vertical; generally very fine fractures and curving veins infilled with blue-green clay (celadonite?) and carbonate.

**ADDITIONAL COMMENTS:** Base of this Unit seen in 59R-2 (Piece 8).

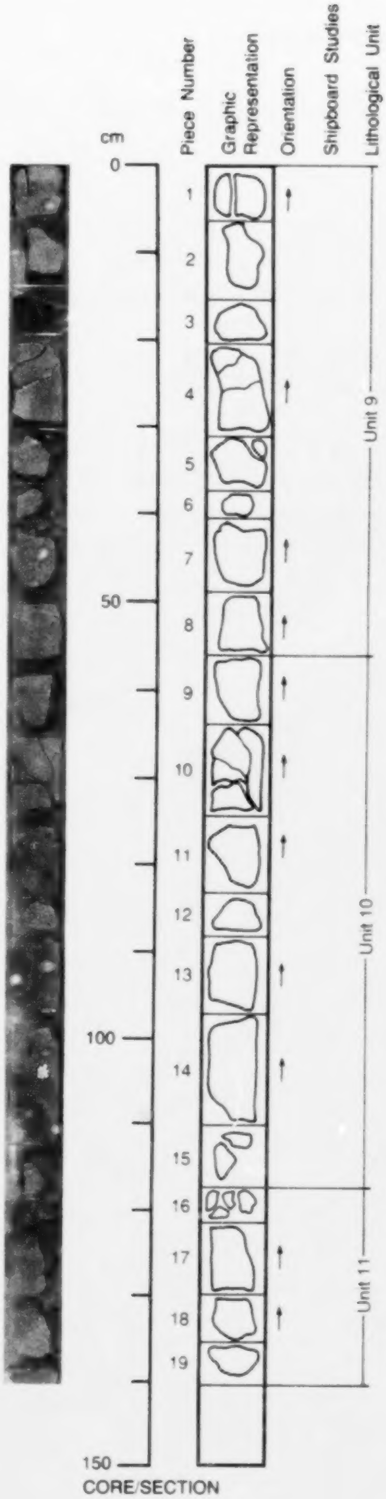

## 129-802A-59R-2

## UNIT 9: SPARSELY OLIVINE-PLAGIOCLASE MICROPHYRIC BASALT

### Pieces 1-8

**CONTACTS:** Only basal contact seen in this section. Grain-size increases in Pieces 1-6 and then decreases in 7 & 8 to the very fine-grained spherulitic basal zone in Piece 8.
**PHENOCRYSTS:** Possibly a few pyroxene microphenocrysts within basal zone.
livine - 2%; <0.1; generally euhedral; smectite replaced.
Plagioclase - 0.5%; 0.1; subhedral
**GROUNDMASS:** Fine-grained, hypocrystalline, except in basal contact zone with spherulitic texture.
**VESICLES:** None observed.
**COLOR:** Uniform medium gray (N6).
**STRUCTURE:** Base of thin flow or possibly pillow lava.
**ALTERATION:** Slight. Glassy mesostasis replaced by green smectite. Blue-green and green clays +/- carbonate in veins.
**VEINS/FRACTURES:** 1%; 0.1 mm; irregular; infilling blue-green and green clays (smectite and celadonite?), sometimes associated with carbonate.
**ADDITIONAL COMMENTS:** Continuation of Unit 9 from 59R-1.

## UNIT 10: SPARSELY OLIVINE-PLAGIOCLASE MICROPHYRIC BASALT

### Pieces 9-15

**CONTACTS:** Top contact not observed, although Piece 9 is fine-grained compared to piece : following. Grain-size increases downwards until base which is very fine-grained, dark and spherulitic (Piece 15).
**PHENOCRYSTS:** Possibly one or two greenish pyroxene microphenocrysts concentrated with others in basal zone.
Plagioclase - trace; 0.1; subhedral
Olivine - 2%; <0.1; some eudral crystals, mostly replaced by green smectite.
**GROUNDMASS:** Fine-grained, hypocrystalline throughout with minor smectite-replaced mesostasis, basal zone with coalesed spherulites that give way to fan-shaped variolites.
**VESICLES:** none observed.
**COLOR:** Speckled medium gray (N6).
**STRUCTURE:** Thin flow.
**ALTERATION:** Slight. Green smectite after glassy mesostasis. Clay +/- carbonate veinlets.
**VEINS/FRACTURES:** 1%; 0.1 mm; irregular; infilled with dark clay (saponite?) +/- carbonate.
**ADDITIONAL COMMENTS:** Drilling rubble (piece 16) and quench textured Pieces 15 and 17 mark boundary between Units 10 and 11.

## UNIT 11: MODERATELY OLIVINE-PLAGIOCLASE MICROPHYRIC BASALT

### Pieces 16-19

**CONTACTS:** Top contact marked by unaltered black glass and spherulitic zone (2 mm) at top of Piece 17. Drilling rubble also marks approximately boundary between Units 10 and 11.
**PHENOCRYSTS:** Apparently concentrated in upper quenched zone.
Plagioclase - 1%; 0.1; Subhedral.
Olivine - 3%; <0.1; often euhedral.
**GROUNDMASS:** Fine-grained, hypocrystalline throughout, except for upper quenched zone with interstitial glass and spherulites.
**VESICLES:** None observed.
**COLOR:** Speckled medium gray (N5).
**STRUCTURE:** Thin flow.
**ALTERATION:** Slight. Green smectite after mesostasis and olivine microphenocrysts.
**VEINS/FRACTURES:** <1%; 0.1 mm; vertical; two minor veinlets normal to quenched margin. Green smectite infilling.
**ADDITIONAL COMMENTS:** Preservation of apparently little altered black glass in quenched rim. Although no curved glassy zones have been observed, the extrusive units in 59R-2 (and previously) are charactereistically thin and could equally represent a series of pillow lava sections, rather than thin flows.

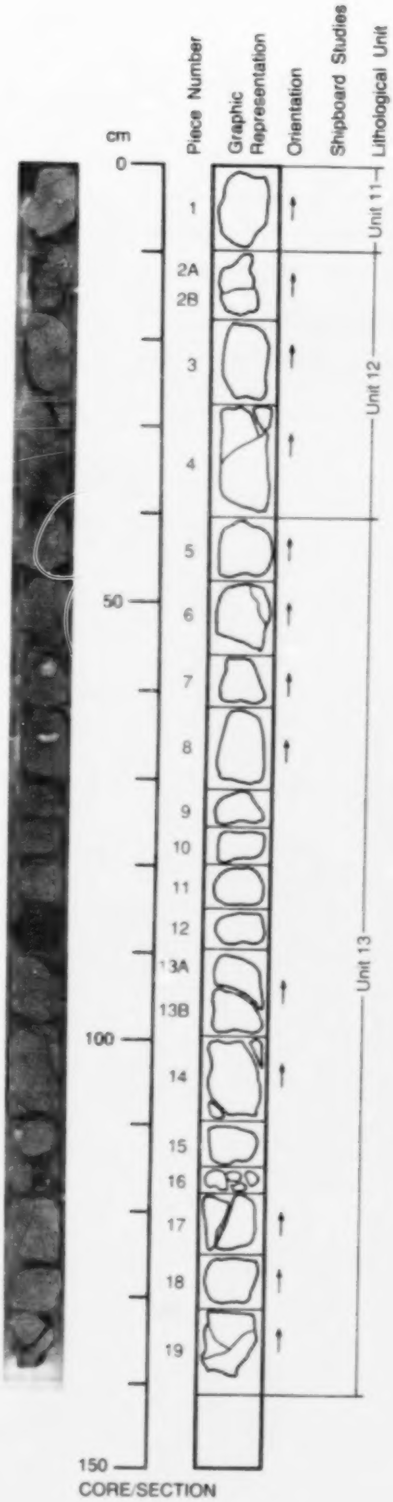

## 129-802A-59R-3

## UNIT 11: APHYRIC BASALT

### Piece 1

**CONTACTS:** None observed; coninuation of Unit 11.
**PHENOCRYSTS:** None observed.
**GROUNDMASS:** Fine-grained, hypocrystalline.
**VESICLES:** None observed.
**COLOR:** Speckled medium gray (N5).
**STRUCTURE:** Possibly fine-grained central portion of thin flow or pillow section.
**ALTERATION:** Slight; minor green smectite in matrix.
**VEINS/FRACTURES:** None.
**ADDITIONAL COMMENTS:** Continuation of Unit 11 from 59R-2.

## 129-802A-59R-3

## UNIT 12: MODERATELY OLIVINE-PLAGIOCLASE-PYROXENE MICROPHYRIC BASALT

### Pieces 2A - 4

**CONTACTS:** None observed, except Piece 2 is very fine-grained and spherulitic and marks approximate position of unit top. Piece 5 has fan variolitic texture and marks either the base of Unit 12 or more likely the top of Unit 13.
**PHENOCRYSTS:** Largely observed within upper spherulitic zone.
Plagioclase - 1%; 0.1-0.3; generally very small, a few larger subhedral laths.
Olivine - 4%; <0.1; smectite-replaced euhedra.
Pyroxene - trace; 0.1; rare subhedral prisms.
**GROUNDMASS:** Fine-grained, hypocrystalline. Coalesed spherulites in part of Piece 2 (contact zone).
**VESICLES:** None observed.
**COLOR:** Speckled, grading from N5 to N6.
**STRUCTURE:** Thin flow or part of pillow.
**ALTERATION:** Slight. Green smectite replacing mesostasis.
**VEINS/FRACTURES:** <1%; 0.2 mm; irregular; infilling of green smectite +/- carbonate.
**ADDITIONAL COMMENTS:** None.

## UNIT 13: MODERATELY OLIVINE-PLAGIOCLASE MICROPHYRIC BASALT

### Pieces 5-19

**CONTACTS:** None observed, except Piece 5 has a fan variolitic texture and possibly marks top of Unit 13, especially as grain-size increases away from this piece downwards.
**PHENOCRYSTS:** Olivine microphenocrysts randomly distributed.
Plagioclase - trace; 0.1-0.3; two size generations.
Olivine - 3%; <0.1; smectite-replaced euhedral.
**GROUNDMASS:** Fine-grained, hypocrystalline. Variable distribution of smectite-replaced mesostasis.
**VESICLES:** None observed.
**COLOR:** Speckled, medium gray (N6).
**STRUCTURE:** Thin flow.
**ALTERATION:** Slight. Mesostasis replaced by green smectite+/- carbonate and rarer pyrite. Clay-carbonate-pyrite veins.
**VEINS/FRACTURES:** 1%; 0.1-1.0 mm; variable; dark green smectite (saponite?) with central part of vein filled with carbonate and sometimes pyrite.
**ADDITIONAL COMMENTS:** None.

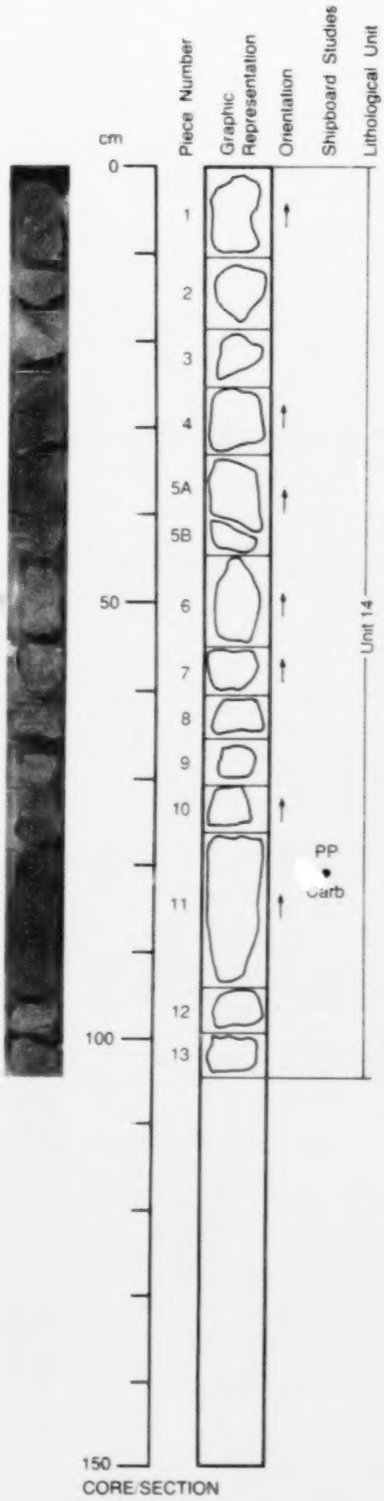
cm
Piece Number
Graphic Representation
Orientation
Shipboard Studies
Lithological Unit
0
50
100
150
1
2
3
4
5A
5B
6
7
8
9
10
11
12
13
PP
Carb
Unit 14
CORE/SECTION

## 129-802A-60R-1

## UNIT 14: SPARSELY PLAGIOCLASE MICROPHYRIC TO APHYRIC BASALT

### Pieces 1-13

**CONTACTS:** None observed, but Piece 1 has a variolitic, very fine-grained texture that increases in grain-size downwards.
**PHENOCRYSTS:** Possibly one or two olivine and pyroxene microphenocrysts also. Plagioclase - 1-2%; 0.1-0.2; few subhedral laths.
**GROUNDMASS:** Generally fine-grained, hypocrystalline throughout, coarsening downwards. Fan variolites in upper quenched zone.
**VESICLES:** None observed.
**COLOR:** Medium gray (5B 5/1) grading downwards to speckled light gray (N6).
**STRUCTURE:** Thin flow.
**ALTERATION:** Slight. Darker gray and green alteration haloes in Pieces 6 and 10, with matrix replaced by green smectite and mesostasis by yellow palagonite (?) and green smectite. Green clay-carbonate veins.
**VEINS/FRACTURES:** 1%; 0.2-1.0 mm; variable; infilled with green smectite-carbonate.
**ADDITIONAL COMMENTS:** None.

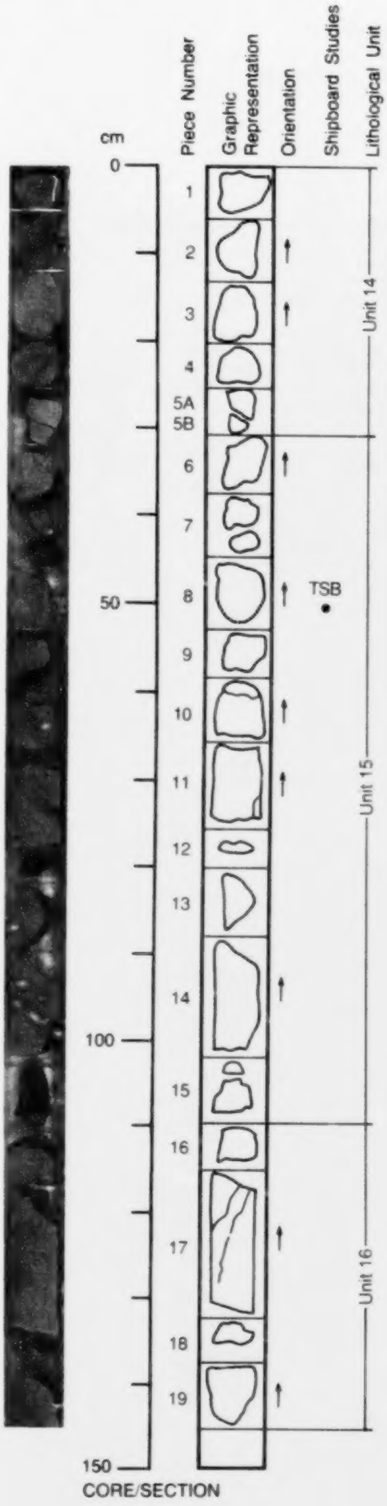

## 129-802A-61R-1

### UNIT 14: APHYRIC BASALT

#### Pieces 1-5B

**CONTACTS:** None observed, although slight decrease in grain-size towards Piece 5A & 5B. Continuation of Unit 14 from 60R-1.
**PHENOCRYSTS:** None observed in this part of Unit.
**GROUNDMASS:** Fine-grained, hypocrystalline.
**VESICLES:** None observed.
**COLOR:** Speckled light gray (N6).
**STRUCTURE:** Possibly lower portion of thin flow.
**ALTERATION:** Slight. Minor smectite in matrix.
**VEINS/FRACTURES:** <1%; 0.2 mm; vertical & horizontal; green smectite infilling.
**ADDITIONAL COMMENTS:** Possibly nearing basal portion of Unit 14.

### UNIT 15: SPARSELY OLIVINE MICROPHYRIC BASALT

#### Pieces 6-15

**CONTACTS:** Not observed, except top 2 mm of piece is quenched with plume and fan variolites. Rest of pieces coarsen downwards and texture becomes more granular.
**PHENOCRYSTS:** Apparently concentrated within top portion of Unit. One or two possible pyroxene microphenocrysts.
Olivine - 1%; 0.1; replaced by green smectite.
**GROUNDMASS:** Mainly fine-grained, hypocrystalline with randomly distributed and smectite-replaced mesostasis.
**VESICLES:** None observed.
**COLOR:** Medium gray (N5 to N6).
**STRUCTURE:** Thin flow.
**ALTERATION:** Slight. Olivine microphenocrysts and mesostasis replaced by green smectite and minor carbonate.
**VEINS/FRACTURES:** 1-2%; 0.1 mm; irregular; infilled with green smectite +/- carbonate.
**ADDITIONAL COMMENTS:** None.

### UNIT 16: MODERATELY OLIVINE-PLAGIOCLASE MICROPHYRIC BASALT

#### Pieces 16-19

**CONTACTS:** None observed, but Pieces 16 & 17 are finer grained than Pieces 18 & 19.
**PHENOCRYSTS:** None.
Plagioclase - trace; 0.1; variably altered laths.
Olivine - ~2%; <0.1; Euhedral-subhedral; slightly altered.
**GROUNDMASS:** Fine-grained; hypohyaline top grading to hypocrystalline bottom. Quenched textures typical.
**VESICLES:** None observed.
**COLOR:** Speckled gray (N6).
**STRUCTURE:** Perhaps top of thin flow.
**ALTERATION:** Slight. Olivine microphenocrysts altered to green clays, traces of carbonate along some crystal margins. Occasional pyrite grains.
**VEINS/FRACTURES:** <1%; 0.1-1.0 mm; very irregular; infilled with green smectite +/- carbonate.
**ADDITIONAL COMMENTS:** This unit is recognized by a fine-grained top that coarsens towards the bottom.

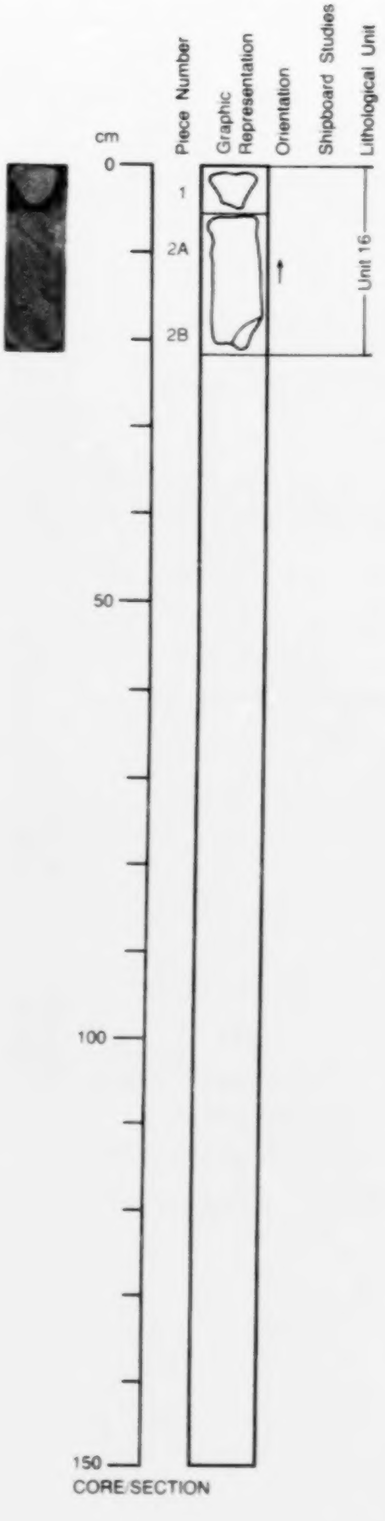
cm
Piece Number
Graphic Representation
Orientation
Shipboard Studies
Lithological Unit
0
1
2A
2B
Unit 16
50
100
150
CORE/SECTION

## 129-802A-61R-2

## UNIT 16: SPARSELY OLIVINE-PLAGIOCLASE MICROPHYRIC BASALT

### Pieces 1-2B

**CONTACTS:** None observed.
**PHENOCRYSTS:** Proportion and distribution of olivine relatively uniform throughout but groundmass becomes more granular.
Plagioclase - trace; <0.1; Subhedral laths
Olivine - 1%; <0.1; Euhedral to subhedral; some alteration.
**GROUNDMASS:** Fine-grained, hypocrystalline with quench textures.
**VESICLES:** None observed.
**COLOR:** Speckled gray (N5).
**STRUCTURE:** Probably portion of thin flow (Unit 16 continued from 61R-1).
**ALTERATION:** Slight. Olivine altered to green smectite, trace of carbonate.
**VEINS/FRACTURES:** 0.5%; <0.1 mm; irregular; irregular sub-vertical branching veinlets, none cross-cutting. Infilled with green smectite and carbonate.
**ADDITIONAL COMMENTS:** None.

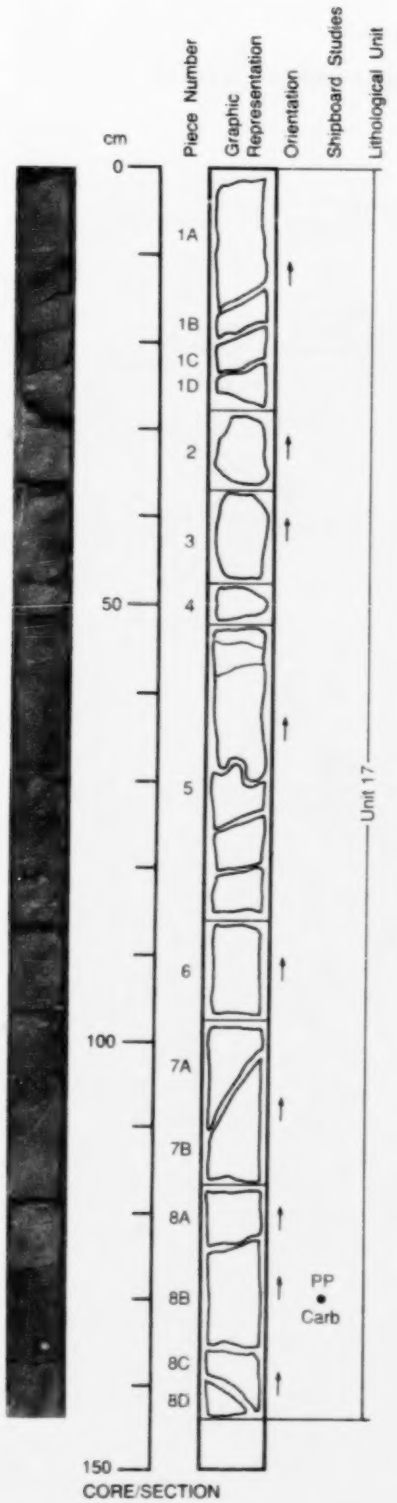
cm
Piece Number
Graphic Representation
Orientation
Shipboard Studies
Lithological Unit
0
50
100
150
1A
1B
1C
1D
2
3
4
5
6
7A
7B
8A
8B
8C
8D
PP
Carb
Unit 17
CORE/SECTION

## 129-802A-62R-1

## UNIT 17: SPARSELY OLIVINE MICROPHYRIC BASALT

### Pieces 1A-8D

**CONTACTS:** None observed and no systematic grain-size distribution.
**PHENOCRYSTS:** None
Olivine - 1%; <0.1; Slightly altered Euhedral and Subhedral grains.
**GROUNDMASS:** Fine-grained, hypocrystalline to slightly holocrystalline. Quenched textures.
**VESICLES:** Generally none observed, except piece 3 contains a few very irregular, green clay infilled miaroles.
**COLOR:** Fine-speckled gray (N5-N6)
**STRUCTURE:** Perhaps a lava flow.
**ALTERATION:** Slight. Olivine altered to green clays. Fractured boundary between pieces 5C and 5D is moderately altered with mesostasis changed to green clays.
**VEINS/FRACTURES:** <0.5%; <0.1-5.0 mm; Very irregular; infilled with green clays, pyrite and traces of carbonate and quartz. A sharp fracture in Piece 1B is filled with dark green clays.
**ADDITIONAL COMMENTS:** Although still fine-grained, this is the most holocrystalline and massive of all previous Units (see next two sections) and perhaps more representative of a lava flow rather than a pillow lava.

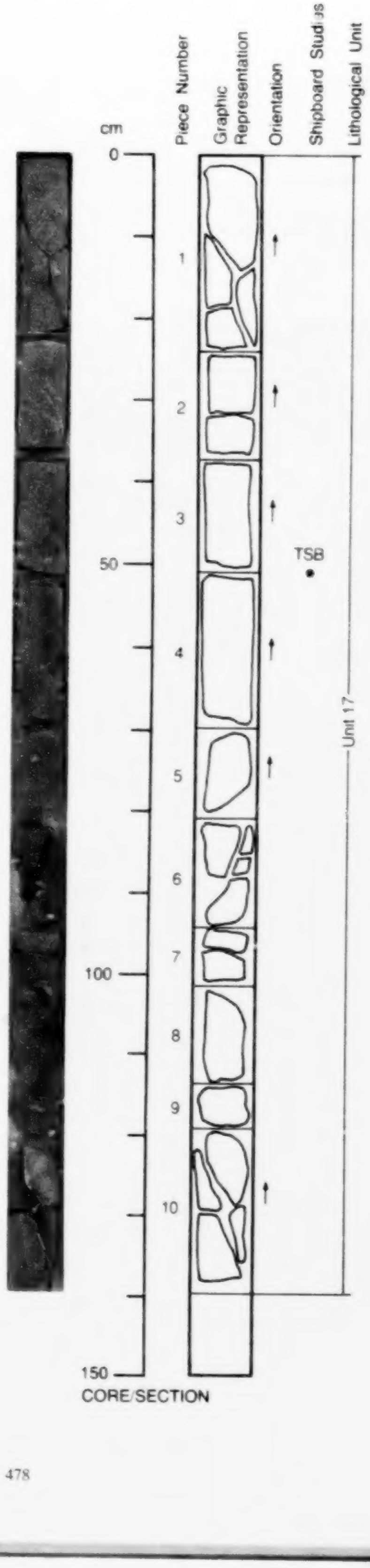
cm
Piece Number
Graphic Representation
Orientation
Shipboard Studies
Lithological Unit
0
50
100
150
1
2
3
4
5
6
7
8
9
10
TSB
Unit 17
CORE/SECTION

## 129-802A-62R-2

## UNIT 17: SPARSELY OLIVINE MICROPHYRIC BASALT

### Pieces 1 - 10

**CONTACTS:** None observed.
**PHENOCRYSTS:** None.
Olivine - 1%; <0.1; slightly altered, Euhedral to Subhedral.
**GROUNDMASS:** Fine-grained, hypocrystalline to holocrystalline, with quench-textured crystal morphologies.
**VESICLES:** None observed.
**COLOR:** Fine-speckled gray (N5 to N6).
**STRUCTURE:** Perhaps a portion of a lava flow.
**ALTERATION:** Slight. Olivine altered to green smectite.
**VEINS/FRACTURES:** 0.5%; <0.1-5.0 mm; irregular; branching common, but little cross-cutting relationships. Pieces 10A and 10B are separated by a 5 mm wide fracture infilled with calcite and green clays. Pyrite in trace amounts may also be present as infill.
**ADDITIONAL COMMENTS:** Fairly uniform grain size throughout the section.

## 129-802A-62R-3

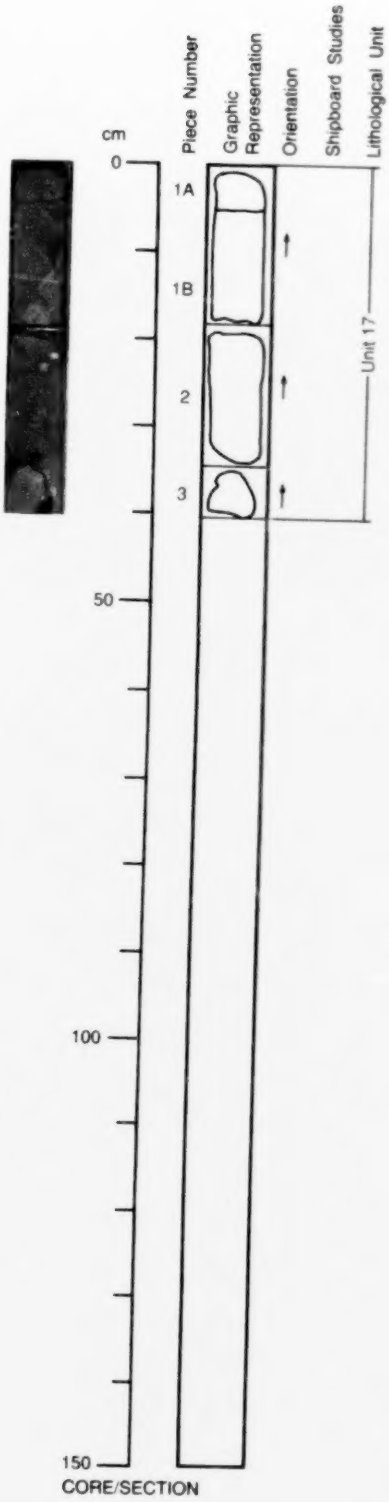
cm
0
50
100
150
CORE/SECTION
Piece Number
Graphic Representation
Orientation
Shipboard Studies
Lithological Unit
1A
1B
2
3
Unit 17

## UNIT 17: SPARSELY OLIVINE MICROPHYRIC BASALT

### Pieces 1A-3

**CONTACTS:** None observed, but Piece 3 is finer-grained than other pieces and may represent beginning of the lower margin of the unit.

**PHENOCRYSTS:** None.

Olivine - 1%; <0.1; Slightly altered euhedral and subhedral grains.

**GROUNDMASS:** Fine-grained, hypocrystalline with quenched textures in Piece 3.

**VESICLES:** None observed.

**COLOR:** Fine speckled gray (N5 to N6).

**STRUCTURE:** Perhaps bottom part of Unit 17 flow.

**ALTERATION:** Slight. Olivine altered to green smectite. Carbonate grains present in matrix, together with some Fe staining.

**VEINS/FRACTURES:** <1%; 0.1-1.0 mm; irregular; infilled with green smectite, pyrite and calcite.

**ADDITIONAL COMMENTS:** Abrupt change in grain-size and texture from Piece 2 to 3 and assumed that later piece represents basal portion of Unit 17 with intervening section not recovered.

# SECTION 4: POLICY

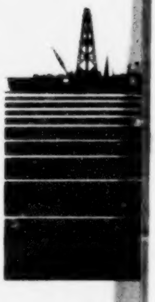

# JOIDES ADVISORY GROUPS*

**Executive Committee (EXCOM)**

Charles E. Helsley
*University of Hawaii*

Roger N. Anderson (Wireline Logging Services liaison)
*Columbia University*

D. James Baker, Jr. (JOI liaison)
*Joint Oceanographic Institutions, Inc.*

Bernard Biju-Duval
*IFREMER (France)*

James C. Briden
*Natural Environment Research Council (U.K.)*

Douglas R. Caldwell
*Oregon State University*

Craig E. Dorman
*Woods Hole Oceanographic Institution*

Robert A. Duce
*University of Rhode Island*

Hans-J. Dürbaum
*Bundesanstalt für Geowissenschaften und Rohstoffe*

David Falvey
*Bureau of Mineral Resources, Geology and Geophysics (Australia)*

Edward A. Frieman
*University of California, San Diego*

G. Ross Heath
*University of Washington*

Donald F. Heinrichs (NSF liaison)
*National Science Foundation (U.S.)*

Dennis V. Kent
*Columbia University*

Arthur E. Maxwell
*University of Texas at Austin*

William J. Merrell, Jr.
*Texas A&M University at Galveston*

Ralph Moberly (PCOM liaison)
*University of Hawaii*

Takahisa Nemoto
*University of Tokyo*

Philip D. Rabinowitz (Science Operator liaison)
*Texas A&M University*

Bruce Rosendahl
*University of Miami*

Jan H. Stel
*Stichting Onderzoek der Zee*

*Membership at time of cruise.

**Planning Committee (PCOM)**

Ralph Moberly
*University of Hawaii*

James A. Austin, Jr.
*University of Texas at Austin*

Garrett W. Brass
*University of Miami*

Maria Bianca Cita-Sironi
*Università degli Studi di Milano*

Darrel S. Cowan
*University of Washington*

Robert A. Duncan
*Oregon State University*

Louis E. Garrison (Science Operator liaison)
*Texas A&M University*

Richard D. Jarrard (Wireline Logging Services liaison)
*Columbia University*

Hugh C. Jenkyns
*Oxford University*

Miriam Kastner
*University of California, San Diego*

Yves P. Lancelot
*Université Pierre et Marie Curie*

Marcus G. Langseth
*Columbia University*

Margaret Leinen
*University of Rhode Island*

Bruce Malfait (NSF liaison)
*National Science Foundation (U.S.)*

John Malpas
*Memorial University*

Thomas E. Pyle (JOI liaison)
*Joint Oceanographic Institutions, Inc.*

Asahiko Taira
*University of Tokyo*

Brian E. Tucholke
*Woods Hole Oceanographic Institution*

Ulrich von Rad
*Bundesanstalt für Geowissenschaften und Rohstoffe*

Joel Watkins
*Texas A&M University*

**Central and Eastern Pacific Detailed Planning Group (CEPDPG)**

David K. Rea
*University of Michigan*

Helmut Beiersdorf
*Bundesanstalt für Geowissenschaften und Rohstoffe*

Earl E. Davis
*Geological Survey of Canada*

André W. Droxler (OHP liaison)
*Rice University*

Martin F.J. Flower
*University of Illinois, Chicago*

Peter A. Floyd
*University of Keele*

Jean Francheteau
*Université Pierre et Marie Curie*

Loren W. Kroenke
*University of Hawaii*

Margaret Leinen (PCOM liaison)
*University of Rhode Island*

Ralph Moberly (PCOM liaison)
*University of Hawaii*

Hakuyu Okada
*Kyushu University*

Robin P. Riddihough
*Geological Survey of Canada*

Constance A. Sancetta
*Columbia University*

Seymour O. Schlanger
*Northwestern University*

Hans Joachim Schrader
*University of Bergen*

William V. Sliter
*U.S. Geological Survey*

Roy H. Wilkens (DMP liaison)
*University of Hawaii*

**Downhole Measurements Panel (DMP)**

Paul F. Worthington
*British Petroleum Company, Ltd.*

Keir Becker (LITHP liaison)
*University of Miami*

Bobb Carson
*Lehigh University*

Darrel S. Cowan (PCOM liaison)
*University of Washington*

Hugh Crocker
*Crocker Data Processing Pty., Ltd.*

Andrew Fisher (Science Operator liaison)
*Texas A&M University*

Jean-Paul Foucher
*IFREMER (France)*

Joris M. Gieskes
*University of California, San Diego*

Xenia Golovchenko (Wireline Logging Services liaison)
*Columbia University*

Eddie P. Howell
*Arco Oil and Gas Company*

Daniel E. Karig
*Cornell University*

Hajimu Kinoshita
*Chiba University*

Marcus G. Langseth (PCOM liaison)
*Columbia University*

Peter Lysne
*Sandia National Laboratories*

Jürgen Mienert (SGPP liaison)
*GEOMAR (F.R.G.)*

Roger H. Morin
*U.S. Geological Survey*

Carl Sondergeld
*Amoco Production Company*

Ove Stephansson
*University of Luleå*

Heinrich Villinger
*Alfred Wegener Institute for Polar and Marine Research*

Roy H. Wilkens
*University of Hawaii*

### Fluid Processes in Accretionary Prisms Working Group (FPAPWG)

Graham K. Westbrook
*University of Birmingham*

Keir Becker
*University of Miami*

Joris M. Gieskes
*University of California, San Diego*

Roy D. Hyndman
*Pacific Geoscience Centre (Canada)*

Daniel E. Karig
*Cornell University*

Xavier Le Pichon
*Ecole Normale Supérieure*

J. Casey Moore
*University of California, Santa Cruz*

E. Nuti
*Istituto Internationale de Geotermia*

Thomas H. Shipley
*University of Texas at Austin*

Erwin Suess
*GEOMAR (F.R.G.)*

Roland von Huene
*GEOMAR (F.R.G.)*

### Information Handling Panel (IHP)

Ted C. Moore, Jr.
*University of Michigan*

James A. Austin, Jr. (PCOM liaison)
*University of Texas at Austin*

Cristina Broglia (Wireline Logging Services liaison)
*Columbia University*

Brian M. Funnell
*University of East Anglia*

Raymond V. Ingersoll
*University of California, Los Angeles*

Yves P. Lancelot (PCOM liaison)
*Université Pierre et Marie Curie*

Chao-Shing Lee
*Bureau of Mineral Resources, Geology and Geophysics (Australia)*

Michael S. Loughridge
*National Geophysical Data Center (U.S.)*

Russell B. Merrill (Science Operator liaison)
*Texas A&M University*

Judit Nowak
*Bundesanstalt für Geowissenschaften und Rohstoffe*

William R. Riedel
*University of California, San Diego*

William W. Sager
*Texas A&M University*

John B. Saunders
*Naturhistorisches Museum (Basel, Switzerland)*

André Schaaf
*Université Claude Bernard*

Henry Spall
*U.S. Geological Survey*

Kensaku Tamaki
*University of Tokyo*

### Lithosphere Panel (LITHP)

Rodey Batiza
*University of Hawaii*

Keir Becker
*University of Miami*

Lawrence M. Cathles
*Cornell University*

Sierd Cloetingh
*Vrije Universiteit*

Robert A. Duncan (PCOM liaison)
*Oregon State University*

Jorg Erzinger
*Universität Giessen*

James M. Franklin
*Geological Survey of Canada*

Toshitsugu Fujii
*University of Tokyo*

Martin B. Goldhaber (SGPP liaison)
*U.S. Geological Survey*

Susan E. Humphris
*Woods Hole Oceanographic Institution*

John Malpas (PCOM liaison)
*Memorial University*

Catherine Mevel
*Université Pierre et Marie Curie*

John C. Mutter
*Columbia University*

Julian A. Pearce
*University of Newcastle upon Tyne*

Michael R. Perfit
*University of Florida*

W. Jason Phipps-Morgan
*Massachusetts Institute of Technology*

Guy M. Smith
*St. Louis University*

### Ocean History Panel (OHP)

Nicholas J. Shackleton
*Cambridge University*

Eric J. Barron
*Pennsylvania State University*

Wolfgang H. Berger
*University of California, San Diego*

William A. Berggren
*Woods Hole Oceanographic Institution*

Garrett W. Brass (PCOM liaison)
*University of Miami*

Peter J. Davies
*Bureau of Mineral Resources, Geology and Geophysics (Australia)*

Margaret Lois Delaney
*University of Southern California, Santa Cruz*

André W. Droxler
*Rice University*

Philip N. Froelich (SGPP liaison)
*Columbia University*

Eystein Jansen
*University of Bergen*

Hugh C. Jenkyns (PCOM liaison)
*Oxford University*

Dennis V. Kent
*Columbia University*

Alan C. Mix
*Oregon State University*

Tsunemasa Saito
*Yamagata University*

Ruediger Stein
*Universität Giessen*

Edith Vincent
*Université Pierre et Marie Curie*

**Pollution Prevention and Safety Panel (PPSP)**

Mahlon M. Ball
*U.S. Geological Survey*

Yutaka Aoki
*Japex Geoscience Institute, Inc.*

Carl Brenner (Databank liaison)
*Columbia University*

Emanuela Cassano
*AGIP S.p.A. (Italy)*

George E. Claypool
*Mobil Oil Company*

Claude Delas
*Total Compagnie Française des Pétroles*

Mimi Fortier
*Canadian Oil and Gas Lands Administration*

Louis E. Garrison (Science Operator liaison)
*Texas A&M University*

Arthur R. Green
*Exxon Production Research Company*

Paul Haseldonckx
*Deminex (F.R.G.)*

Stephen D. Lewis (SSP liaison)
*U.S. Geological Survey*

David B. MacKenzie
*Littleton, Colorado*

Ralph Moberly (PCOM liaison)
*University of Hawaii*

David G. Roberts
*British Petroleum Company, Ltd.*

**Sedimentary and Geochemical Processes Panel (SGPP)**

Erwin Suess
*GEOMAR (F.R.G.)*

Jacques J. Boulègue
*Université Pierre et Marie Curie*

Lawrence M. Cathles (LITHP liaison)
*Cornell University*

Nicholas Christie-Blick
*Columbia University*

Shirley Dreiss
*University of California, Santa Cruz*

André W. Droxler (OHP liaison)
*Rice University*

Henry Elderfield
*Cambridge University*

Philip N. Froelich
*Columbia University*

Martin B. Goldhaber
*U.S. Geological Survey*

Makoto Ito
*Chiba University*

Noel P. James
*Queen's University at Kingston*

Miriam Kastner (PCOM liaison)
*University of California, San Diego*

Judith A. McKenzie
*Eidgenossische Technische Hochschule (Switzerland)*

Lawrence Mayer
*Dalhousie University*

Jürgen Mienert
*GEOMAR (F.R.G.)*

William R. Normark
*U.S. Geological Survey*

Frederick Prahl
*Oregon State University*

Dorrik A.V. Stow
*University of Southampton*

Ulrich von Rad (PCOM liaison)
*Bundesanstalt für Geowissenschaften und Rohstoffe*

Graham K. Westbrook (TECP liaison)
*University of Birmingham*

**Sedimented Ridges Detailed Planning Group (SRDPG)**

Robert S. Detrick
*University of Rhode Island*

Harald Bäcker
*GEOMAR (F.R.G.)*

Keir Becker
*University of Miami*

Wilfred B. Bryan
*Woods Hole Oceanographic Institution*

David Chapman
*University of Utah*

Earl E. Davis
*Geological Survey of Canada*

John R. Delaney
*University of Washington*

Craig B. Forster
*University of Utah*

Jean Francheteau
*Université Pierre et Marie Curie*

James M. Franklin
*Geological Survey of Canada*

Hiromi Fujimoto
*University of Tokyo*

Jan Hertogen
*Katholieke Universiteit Leuven*

Steven P. Howard
*Texas A&M University*

Marcus G. Langseth (PCOM liaison)
*Columbia University*

Mitchell W. Lyle
*Columbia University*

Kenneth C. MacDonald
*University of California, Santa Barbara*

Catherine Mevel
*Université Pierre et Marie Curie*

Michael J. Mottl
*University of Hawaii*

Michael R. Perfit
*University of Florida*

Bernd R. Simoneit
*Oregon State University*

Ralph A. Stephen
*Woods Hole Oceanographic Institution*

Robert A. Zierenberg
*U.S. Geological Survey*

**Shipboard Measurements Panel (SMP)**

Kate Moran
*Bedford Institute of Oceanography*

Maria Bianca Cita-Sironi (PCOM liaison)
*Universitá degli Studi di Milano*

Ian L. Gibson
*University of Waterloo*

Joris M. Gieskes (DMP liaison)
*University of California, San Diego*

John W. King
*University of Rhode Island*

Margaret Leinen (PCOM liaison)
*University of Rhode Island*

Michael J. Mottl
*University of Hawaii*

J. Michael Rhodes
*University of Massachusetts*

Adrian F. Richards
*Adrian Richards Company (Netherlands)*

Ellen Thomas
*Wesleyan University*

Hidekazu Tokuyama
*University of Tokyo*

Jean-Pierre Valet
*Université Pierre et Marie Curie*

Robert B. Whitmarsh
*Institute of Oceanographic Sciences (U.K.)*

### Site Survey Panel (SSP)

Robert B. Kidd
*University College of Swansea*

Mahlon M. Ball (PPSP liaison)
*U.S. Geological Survey*

Carl Brenner (Databank liaison)
*Columbia University*

Frederick K. Duennebier
*University of Hawaii*

James D. Hedberg
*Exxon Exploration, Inc.*

Kim A. Kastens
*Columbia University*

Yves P. Lancelot (PCOM liaison)
*Université Pierre et Marie Curie*

Birger Larsen
*Danmarks Geologiske Undersogelse*

Stephen D. Lewis
*U.S. Geological Survey*

Keith E. Louden
*Dalhousie University*

Audrey W. Meyer (Science Operator liaison)
*Texas A&M University*

Heinrich Meyer
*Bundesanstalt für Geowissenschaften und Rohstoffe*

Kate Moran (SMP liaison)
*Bedford Institute of Oceanography*

Guy Pautot
*IFREMER (France)*

Thomas E. Pyle (JOI liaison)
*Joint Oceanographic Institutions, Inc.*

Kiyoshi Suyehiro
*University of Tokyo*

Richard P. Von Herzen
*Woods Hole Oceanographic Institution*

Joel Watkins (PCOM liaison)
*Texas A&M University*

### Technology and Engineering Development Committee (TEDCOM)

Charles Sparks
*Institut Français du Pétrole*

Jean Bonnasse-Gahot
*Elf-Aquitaine*

Garrett W. Brass (PCOM liaison)
*University of Miami*

William R. Cotten
*Chevron Services Company*

Bert R. Dennis
*Los Alamos National Laboratories*

Hiromi Fujimoto
*University of Tokyo*

Barry W. Harding (Science Operator liaison)
*Texas A&M University*

Archie R. McLerran
*Solana Beach, California*

Keith Manchester
*Bedford Institute of Oceanography*

Claus Marx
*Institut für Tiefbohrkunde und Erdolgewinnung*

Keith Millheim
*Amoco Production Company*

Alan J. Milton
*British Petroleum Company, Ltd.*

Heinrich Rischmüller
*Bundesanstalt für Geowissenschaften und Rohstoffe*

Frank J. Schuh
*Intertech Operations Technology, Inc.*

Paul N. Stanton
*Exxon Production Research Company*

Harald Strand
*Norsk Hydro*

Alexander Sutherland (NSF liaison)
*National Science Foundation (U.S.)*

Walter W. Svendsen
*Longyear Company*

Paul F. Worthington (DMP liaison)
*British Petroleum Company, Ltd.*

### Tectonics Panel (TECP)

Ian W.D. Dalziel
*University of Texas at Austin*

Sebastian Bell (DMP liaison)
*Geological Survey of Canada*

Jacques Bourgois
*Université Pierre et Marie Curie*

Roger Buck
*Columbia University*

Dan M. Davis
*State University of New York, Stony Brook*

David C. Engebretson
*Western Washington University*

Michael A. Etheridge
*Australian National University*

Karl Hinz
*Bundesanstalt für Geowissenschaften und Rohstoffe*

Hans-Christian Larsen
*Greenland Geological Survey*

Gregory F. Moore (WPDPG liaison)
*University of Hawaii*

E. M. Moores
*University of California, Davis*

Yujiro Ogawa
*Kyushu University*

Dale S. Sawyer
*Rice University*

Asahiko Taira (PCOM liaison)
*University of Tokyo*

Brian E. Tucholke (PCOM liaison)
*Woods Hole Oceanographic Institution*

Anthony B. Watts
*Columbia University*

Graham K. Westbrook
*University of Birmingham*

### Western Pacific Detailed Planning Group (WPDPG)

James B. Gill
*University of California, Santa Cruz*

Kent Brooks
*Kobenhavns Universitet*

David S. Cronan
*University of London, Imperial College*

James V. Eade
*CCOP/SOPAC (Fiji)*

Neville Exon
*Bureau of Mineral Resources, Geology and Geophysics (Australia)*

Philippe Huchon
*Ecole Normale Supérieure*

Roy D. Hyndman
*Pacific Geoscience Centre (Canada)*

H. R. Kudrass
*Bundesanstalt für Geowissenschaften und Rohstoffe*

Gregory F. Moore
*University of Hawaii*

James Natland
*University of California, San Diego*

Steven D. Scott
*University of Toronto*

Asahiko Taira (PCOM liaison)
*University of Tokyo*

Kensaku Tamaki
*University of Tokyo*

Brian Taylor
*University of Hawaii*

# SAMPLE-DISTRIBUTION POLICY[1]

Distribution of Ocean Drilling Program (ODP) and Deep Sea Drilling Project (DSDP) samples is undertaken in order to (1) provide support to shipboard scientists in achieving the scientific objectives of their cruise and to support shore-based investigators who are preparing contributions to ODP reports, (2) provide individual investigators with materials to conduct detailed studies beyond the scope of ODP reports, (3) provide micropaleontological reference centers with samples for reference and comparison purposes, and (4) provide educators with samples for teaching purposes.

Funding for sample-related activities must be secured by the investigator independently of requesting the samples.

The Ocean Drilling Program Curator is responsible for distributing samples and for preserving and conserving core material. The Curator, who may accept advice from chairmen of the appropriate JOIDES advisory panels, is responsible for enforcing the provisions of this Sample-Distribution Policy. He is responsible for maintaining a record of all samples that have been distributed, both on board ship and subsequently from the repositories, indicating the recipients and the nature of investigations proposed. This information is available to interested investigators on request.

Every sample distributed from the ship or from a repository is labeled with a standard identifier, which includes leg number, hole number, core and section numbers, and interval within the section from which the sample was removed. It is imperative that this standard identifier be associated with all data reported in the literature, and that residues of the sample remain labeled throughout their lives, so that later workers can relate the data to the cores.

Distribution of sample materials is made directly from the repositories (Lamont-Doherty Geological Observatory, Scripps Institution of Oceanography, and Texas A&M University) by the Curator or his designated representative.

1. *Distribution of Samples for Research Leading to Contributions to ODP Reports*

Any investigator who wishes to contribute to the reports of a scheduled cruise may write to the Curator, Ocean Drilling Program, 1000 Discovery Drive, College Station, Texas 77845-9547, U.S.A., in order to request samples from that cruise. Requests for a specific cruise must be received by the Curator at least TWO MONTHS in advance of the departure of that cruise, in order to allow time for review of the request in conjunction with other requests, so that a suitable shipboard sampling program can be assembled. The request should include a statement of the nature of the proposed research, the size and approximate number of samples required to complete the study, and any particular sampling technique or equipment which may be required. Requests will be reviewed by the Staff Representative and co-chief scientists of the cruise and by the Curator. Approval/disapproval will be based on the scientific requirements of the cruise as determined by the appropriate JOIDES advisory panel(s). The scope of a request must be such that samples can be processed, that proposed research can be completed, and that the paper can be written in time for submission to the relevant ODP cruise report.

Except for rare, specific instances involving ephemeral properties, the total volume of samples removed during a cruise-related sampling program will not exceed one-quarter of the volume of core recovered, and no interval will be depleted. One-half of all recovered materials will be retained in the archives in as pristine a condition as is practicable. Investigators requesting shipboard samples of igneous materials may receive a maximum of 100 igneous samples per cruise.

Because many sample requests are received for shipboard work and because the time of the shipboard party is at a premium, co-chief scientists are strongly urged to limit shipboard sampling to the minimum necessary to accomplish the cruise objectives. Shore-based investigators whose requests for cruise-related samples are approved should expect that they will receive the samples after the cores are returned to the repository, and should schedule research activities accordingly.

Co-chief scientists may invite investigators who are not cruise participants to perform special studies of selected core samples in direct support of shipboard activities. If this occurs, the names and addresses of these investigators and details of all samples loaned or distributed to them must be forwarded to the Curator, via the ODP Staff Representative to that cruise, immediately after the cruise. These investigators are expected to contribute to the cruise reports as though they had been cruise participants. All requirements of the Sample-Distribution Policy apply.

Any publication of results other than in ODP reports within twelve (12) months of completion of the cruise must be approved and authored by the whole shipboard party and, where appropriate, shore-based investigators. After twelve (12) months, individual investigators may submit related papers for open publication, provided they have already submitted their contributions to ODP reports and had them accepted. Investigations which are not completed in time for inclusion in the ODP reports for a specific cruise may be published in a later edition of the ODP reports; however, they may not appear in another journal until the report for which they were intended has been published.

2. *Distribution of Samples for Research Leading to Publication Outside of the ODP Reports*

   A. Researchers who wish to use samples for studies beyond the scope of the ODP reports should obtain sample-request forms from the Curator, Ocean Drilling Program, 1000 Discovery Drive, College Station, Texas 77845-9547, U.S.A. Requestors are required to specify the quantities and intervals of core required, to make a clear statement of the nature of the proposed research, to state the time which will be required to complete the work and to submit results for publication, and to specify funding status and the availability of equipment and space for the research.

   Additionally, if the requestor has received samples from ODP or from DSDP previously, he/she will be required to account for the disposition of those samples by citing published works, four (4) copies of which must be sent to the Curator. If no report has been published, this requirement can be fulfilled by sending a brief (two- or three-page) report of the status of the research.

   If the requestor has never before received samples from ODP or DSDP, he/she will be required to show that the samples will be used for responsible research. This requirement can be met by providing the Curator with a copy of the requestor's résumé and bibliography. If the requestor is a student working on a higher degree, he/she can meet this requirement by sending a copy of his/her dissertation or research proposal endorsed by the student's advisor.

   Unused and residual samples should be returned and data should be sent to the Curator if the project has terminated. Paleontological materials may be returned either to the Curator at ODP or to one of the designated micropaleontological reference centers. If material is returned to a reference center, notify the Curator when it is sent.

   Requests for samples from researchers in industrial laboratories will be honored in the same manner as those from academic organizations. Industrial investigators have the same obligations as other investigators to publish all results promptly in the open literature and to provide the Curator with copies of all reports published and of all data acquired in their research.

   In order to ensure that all requests for highly desirable but limited samples can be considered together, approval of requests and distribution of samples will be delayed until twelve (12) months after completion of the cruise or two (2) months after official publication of the core descriptions, whichever occurs earlier. The only exceptions to this policy will be made for specific requests involving ephemeral properties. Requests for samples may be based on core descriptions published in ODP reports produced by the shipboard party, copies of which are on file at various institutions throughout the world. Copies of original core logs and data are kept on open file at ODP, and at the repositories at Lamont-Doherty Geological Observatory and Scripps Institution of Oceanography.

   B. Most investigations can be accomplished handily with sample volumes of 10 mL or less. Investigators must provide explicit justification of requests for larger sample sizes or for frequent intervals within a core. Requests which exceed reasonable size or frequency limits will require more time to process and are unlikely to be granted in their entirety.

---

[1] Revised October 1988.

Requests for samples from thin layers, from stratigraphically important boundaries, or from sections which are badly depleted or in unusually high demand may be delayed in order to coordinate requests from several investigators or while the Curator seeks advice from the community. Investigators who submit such requests may expect to receive suggestions for alternative sampling programs or for joining with a research consortium which will share the samples. In any event, such exceptional requests will require more time for processing than will more routine requests.

Investigators who wish to study ephemeral properties may request a waiver of the twelve-month waiting period; however, such requests will be referred automatically to the relevant co-chiefs. If such a request is approved, the investigator will join the shore-based contributors to the shipboard science effort, and will incur the obligations thereof (see section 1).

C. Samples will not be provided until the requestor assures the Curator that funding for the proposed research is available or unnecessary. If a sample request is dependent in any way on proposed funding, the Curator is prepared to provide the proposed funding organization with information on the availability (or potential availability) of suitable samples.

D. Investigators who receive samples incur the following obligations:

(1) To publish significant results promptly; however, no contribution may be submitted for publication prior to twelve (12) months following the termination of the relevant leg unless it is approved and authored by the entire shipboard party.

(2) To acknowledge in all publications that the samples were supplied through the assistance of the international Ocean Drilling Program and others as appropriate.

(3) To submit four (4) copies of reprints of all published works to the Curator, Ocean Drilling Program, 1000 Discovery Drive, College Station, Texas 77845-9547, U.S.A. These reprints will be distributed to the repositories and to the ship. All reprints received will be logged in an on-line bibliographic data base.

(4) To submit all final analytical data obtained from the samples to the Data Librarian, Ocean Drilling Program, 1000 Discovery Drive, College Station, Texas 77845-9547, U.S.A. Please consult announcements in the *JOIDES Journal* or call (409–845-2673) for information on acceptable data formats. Investigators should be aware that they may have other data obligations under the National Science Foundation's Ocean Science Data Policy or under relevant policies of other funding agencies which require submission of data to national data centers.

(5) To return all unused or residual samples, in good condition and with a detailed explanation of any processing they may have undergone, upon termination of the proposed research. In particular, all thin sections and smear slides manufactured on board the vessel or in the repositories are to be returned to the Curator. Paleontological materials may be returned either to the Curator at ODP or to one of the designated micropaleontological reference centers.

Failure to honor these obligations will prejudice future applications for samples.

E. Cores are available for examination by interested parties at the repositories. Investigators are welcome to visit the repositories in order to inspect cores and to specify sample locations when that is required for their research; however, time and space in the workrooms are limited, so advance appointments are required. Occasionally, the space may be fully booked several weeks in advance, so investigators are urged to call for appointments well ahead in order to avoid disappointment. Only the Curator or his delegate may actually remove samples from the cores.

F. A reference library of thin sections, smear slides, and archive photographs is maintained in the repositories for the use of visiting investigators. All thin sections and smear slides produced on board the ship or in repositories belong to this library.

### 3. *Distribution of Samples to Micropaleontological Reference Centers*

As a separate and special category of repository activity, selected samples are distributed to micropaleontological reference centers, where the prepared material may be studied by visitors. Foraminifers, calcareous nannofossils, and diatoms can be viewed; radiolarians will be prepared in the future. The present centers are (1) U.S. East Coast: Lamont-Doherty Geological Observatory, Palisades, NY 10964 (Ms. Rusty Lotti; telephone, 914–359-2900; telex, 7105762653 LAMONTGEO); (2) U.S. National Museum: Smithsonian Institution, Washington, D.C. 20560 (Dr. Martin Buzas; telephone, 202–357-1390; telex, 264729); (3) U.S. Gulf Coast: Texas A&M University, Department of Oceanography, College Station, TX 77843 (Dr. Stefan Gartner; telephone, 409–845-8479; telex, 792779/ODP TAMU); (4) U.S. West Coast: Scripps Institution of Oceanography, La Jolla, CA 92093 (Dr. William Riedel; telephone, 619–534-4386); telex, 910337127 IUC WWD SIOSDG); (5) Western Europe: Natural History Museum, CH-4001 Basel, Switzerland (Mr. J. B. Saunders; telephone, 061-29-55-64); (6) U.S.S.R.: Institute of the Lithosphere, Staromonet 22, Moscow 109180, U.S.S.R. (Dr. Ivan Basov; telephone, 231-48-36); (7) Japan: National Science Museum, Department of Geology, 3-23-1 Hyakunio-cho, Shinjuku-ku, Tokyo 160, Japan (Dr. Y. Tanimura; telephone, 03-364-2311; telemail, 03-364-2316); (8) New Zealand: New Zealand Geological Survey, P.O Box 30368, Lower Hutt, New Zealand (Dr. Tony Edwards; telephone, (04) 699059).

Further details concerning the micropaleontological reference centers are reported periodically in the *JOIDES Journal*.

### 4. *Distribution of Samples for Educational Purposes*

Samples may be available in limited quantities to college-level educators for teaching purposes. Interested educators should request application forms from the Curator, Ocean Drilling Program, 1000 Discovery Drive, College Station, Texas 77845-9547, U.S.A. Requestors are required to specify preferred sample size and location, to make a very clear statement of the nature of the course work in which the samples will be used, to explain how the samples will be prepared and how they will be used in the classroom, to explain in detail why similar materials derived from outcrops or dredge hauls cannot be used (it is NOT acceptable to argue that it requires less effort for the requestor to obtain samples from ODP than to assemble them from other sources), and to certify that funds are available to prepare the materials for classroom use. In general, only samples of materials which are abundant in the collection and which are in little demand for research purposes should be requested for educational purposes. The Curator will not approve requests for materials which are limited in supply or for which demand (real or potential) is great, including most paleontological materials.

### 5. *Distribution of Data*

The Deep Sea Drilling Project and the Ocean Drilling Program have routinely captured much of the data generated on board ship and published in Program reports. Additionally, data supplied by investigators who have received samples are incorporated into the data bases, so data sets which are larger than can be published are available to investigators. Magnetic, downhole-logging, seismic-reflection, bathymetric, and other data collected by the drilling vessel become available for distribution to investigators at the same time as core samples.

Requests for ODP and DSDP data should be addressed to the Data Librarian, Ocean Drilling Program, 1000 Discovery Drive, College Station, Texas 77845-9547, U.S.A. Many varieties of DSDP data are included in ODP data bases. Information on sources of DSDP data is available from the ODP Data Librarian.

A charge will be made to recover material expenses greater than $25.00 incurred in filling individual requests. If required, estimates of charges can be furnished before the work is performed.

Formation microscanner images for Leg 129, Holes 800A, 801B, 802A

## Drilling locations

| Leg | Location | Sites |
|---|---|---|
| Phase 1 1968–1970 | | |
| 1 | North Atlantic | 1–7 |
| 2 | North Atlantic | 8–12 |
| 3 | South Atlantic | 13–22 |
| 4 | Central Atlantic | 23–31 |
| 5 | North Pacific | 32–43 |
| 6 | North Pacific | 44–60 |
| 7 | Central Pacific | 61–67 |
| 8 | Central Pacific | 68–75 |
| 9 | Central Pacific | 76–84 |
| Phase 2 1970–1972 | | |
| 10 | Gulf of Mexico | 85–97 |
| 11 | North Atlantic | 98–108 |
| Re-entry trials | | 109–110 |
| 12 | North Atlantic | 111–119 |
| 13 | Mediterranean | 120–134 |
| 14 | Central Atlantic | 135–144 |
| 15 | Caribbean | 146–154 |
| 16 | Central Pacific | 155–163 |
| 17 | Central Pacific | 164–171 |
| 18 | North Pacific | 172–182 |
| 19 | North Pacific | 183–193 |
| 20 | North Pacific | 194–202 |
| 21 | Coral Sea | 203–210 |
| 22 | Indian Ocean | 211–218 |
| 23 | Arabian Sea | 219–230 |
| 24 | Indian Ocean | 231–238 |
| 25 | Indian Ocean | 239–249 |
| Phase 3 1972–1975 | | |
| 26 | Indian Ocean | 250–258 |
| 27 | Indian Ocean | 259–263 |
| 28 | Antarctic | 264–274 |
| 29 | Tasman Sea | 275–284 |
| 30 | South Pacific | 285–289 |
| 31 | North Pacific | 290–302 |
| 32 | North Pacific | 303–313 |
| 33 | North Pacific | 314–318 |
| 34 | South Pacific | 319–321 |
| 35 | South Pacific | 322–325 |
| 36 | South Atlantic | 326–331 |
| 37 | North Atlantic | 332–335 |
| 38 | Arctic | 336–352 |
| 39 | Atlantic | 353–359 |
| 40 | South Atlantic | 360–365 |
| 41 | South Atlantic | 366–370 |
| 42A | Mediterranean | 371–378 |
| 42B | Black Sea | 379–381 |
| 43 | North Atlantic | 382–387 |
| 44 | North Atlantic | 388–392 |
| 44A | North Atlantic | 393–394 |
| IPOD 1 1975–1983 | | |
| 45 | North Atlantic | 395–396 |
| 46 | North Atlantic | 396A–396B |
| 47 | North Atlantic | 397–398 |
| 48 | North Atlantic | 399–406 |
| 49 | North Atlantic | 407–414 |
| 50 | North Atlantic | 415–416 |
| 51A | North Atlantic | 417–417A |
| 51B | North Atlantic | 417B–417D |
| 52 | North Atlantic | 417D–418A |
| 53 | North Atlantic | 418A–418B |
| 54 | Central Pacific | 419–429 |
| 55 | North Pacific | 430–433 |
| 56 | North Pacific | 434–437 |
| 57 | North Pacific | 438–441 |
| 58 | North Pacific | 442–446 |
| 59 | North Pacific | 447–451 |
| 60 | North Pacific | 452–461 |
| 61 | Central Pacific | 462 |
| 62 | North Pacific | 463–466 |
| 63 | North Pacific | 467–473 |
| 64 | Gulf of California | 474–481 |
| 65 | Gulf of California | 482–485 |
| 66 | Central Pacific | 486–493 |
| 67 | Central Pacific | 494–500 |
| 68 | Central Pacific | 502–503 |
| 69 | Central Pacific | 504–505, 501 |
| 70 | Central Pacific | 506–510, 504B |
| 71 | South Atlantic | 511–514 |
| 72 | South Atlantic | 515–518 |
| 73 | South Atlantic | 519–524 |
| 74 | South Atlantic | 525–529 |
| 75 | South Atlantic | 530–532 |
| 76 | North Atlantic | 533–534 |
| 77 | Caribbean | 535–540 |
| 78 | North Atlantic | 541–543, 395A, B |
| 79 | North Atlantic | 544–547 |
| 80 | North Atlantic | 548–551 |
| 81 | North Atlantic | 552–555 |
| 82 | North Atlantic | 556–564 |
| 83 | Central Pacific | 504B |
| 84 | Central Pacific | 565–570 |
| 85 | Central Pacific | 571–575 |
| 86 | North Pacific | 576–581 |
| 87 | North Pacific | 582–584 |
| 88 | North Pacific | 581 |
| 89 | Central Pacific | 585–586, 462A |
| 90 | South Pacific | 587–594 |
| 91 | Central Pacific | 595–596 |
| 92 | Central Pacific | 597–602, 504B |
| 93 | North Atlantic | 603–605 |
| 94 | North Atlantic | 606–611 |
| 95 | North Atlantic | 612–613, 603 |
| 96 | Gulf of Mexico | 614–624 |

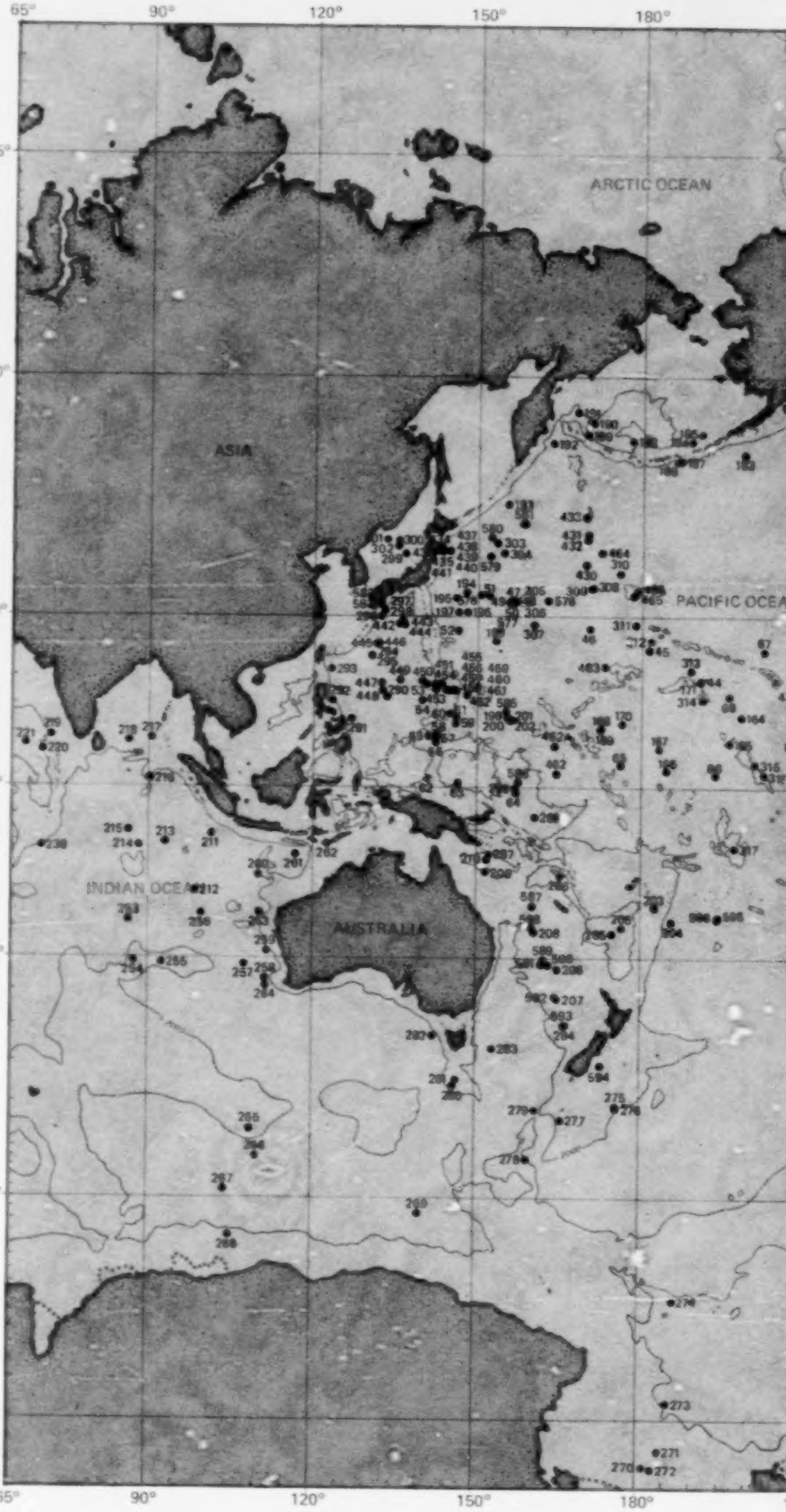

D

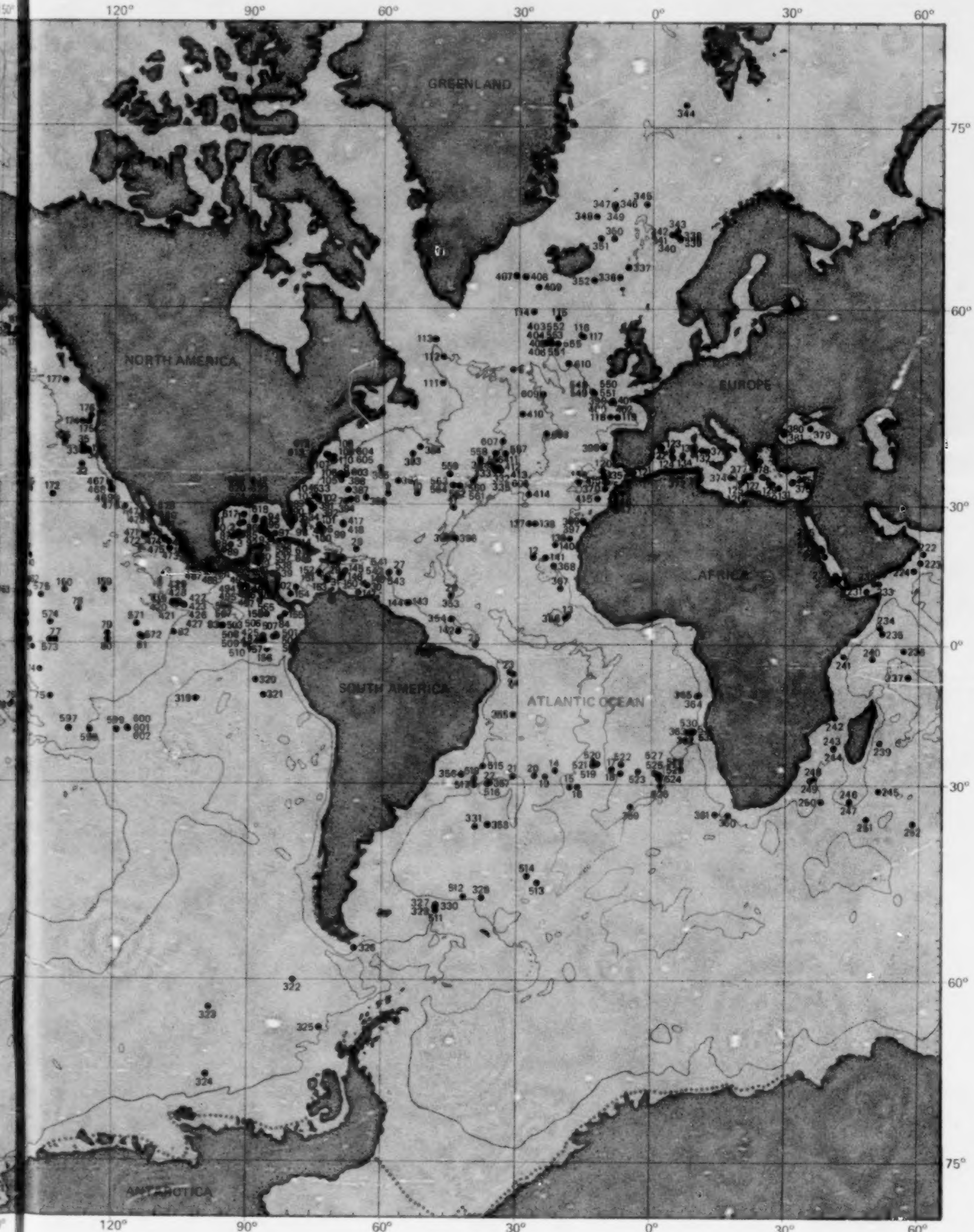
120°
90°
60°
30°
0°
30°
60°
75°
60°
30°
0°
30°
60°
75°
GREENLAND
NORTH AMERICA
EUROPE
AFRICA
SOUTH AMERICA
ATLANTIC OCEAN
ANTARCTICA

SEA DRILLING PROJECT